Onkar N. Tripathi
T. Alexander Quinn
Ursula Ravens *Editors*

Heart Rate and Rhythm

Molecular Basis, Pharmacological Modulation and Clinical Implications

Second Edition

Springer

Heart Rate and Rhythm

Onkar N. Tripathi • T. Alexander Quinn •
Ursula Ravens
Editors

Heart Rate and Rhythm

Molecular Basis, Pharmacological Modulation and Clinical Implications

Second Edition

Springer

Editors
Onkar N. Tripathi
Cardiac Electrophysiology Division,
Ion Channel Study Center
Life Science Academy
Lucknow, India

T. Alexander Quinn
Department of Physiology and
Biophysics
Dalhousie University
Halifax, Canada

Ursula Ravens
Institute for Experimental
Cardiovascular Medicine
University Heart Center and Faculty
of Medicine, University of Freiburg
Freiburg, Germany

ISBN 978-3-031-33587-7 ISBN 978-3-031-33588-4 (eBook)
https://doi.org/10.1007/978-3-031-33588-4

© Springer Nature Switzerland AG 2011, 2023
This work is subject to copyright. All rights are reserved by the Publisher, whether the whole or part of the material is concerned, specifically the rights of translation, reprinting, reuse of illustrations, recitation, broadcasting, reproduction on microfilms or in any other physical way, and transmission or information storage and retrieval, electronic adaptation, computer software, or by similar or dissimilar methodology now known or hereafter developed.

The use of general descriptive names, registered names, trademarks, service marks, etc. in this publication does not imply, even in the absence of a specific statement, that such names are exempt from the relevant protective laws and regulations and therefore free for general use.

The publisher, the authors, and the editors are safe to assume that the advice and information in this book are believed to be true and accurate at the date of publication. Neither the publisher nor the authors or the editors give a warranty, expressed or implied, with respect to the material contained herein or for any errors or omissions that may have been made. The publisher remains neutral with regard to jurisdictional claims in published maps and institutional affiliations.

This Springer imprint is published by the registered company Springer Nature Switzerland AG
The registered company address is: Gewerbestrasse 11, 6330 Cham, Switzerland

I dedicate this book to my son, late Pranav (Vibhu) who left for his heavenly abode on 16th of June 2020 and was always a great inspiration for me to complete this volume having supported me in all my activities.
–Onkar N. Tripathi

I would like to dedicate this to those, who for me, make everything possible: Renae, Freida, and Eiler.
–T. Alexander Quinn

I would like to dedicate it to Günther, the person most patient with me.
–Ursula Ravens

Preface to 2nd Edition of *Heart Rate and Rhythm: Molecular Basis, Pharmacological Modulation and Clinical Implications*

Since the first edition of *Heart Rate and Rhythm* appeared more than a decade ago, considerable progress has been made in diagnosing and treating cardiovascular diseases. Nevertheless, cardiovascular diseases in general, and arrhythmic events in particular, are still major causes of mortality in Western societies. Worldwide, sudden cardiac death and arrhythmias account for an estimated 15–20% of deaths and continue to inflict a heavy burden on the health care systems. Despite enormous research efforts to unravel the molecular mechanisms of cardiac disorders and search for better cardiac therapeutic substances during the last decade, recent surveys indicate continued increase in disability and death due to cardiac disorders necessitating further research. In order to effectively prevent and treat cardiac arrhythmias, there is an urgent need to unravel the underlying pathophysiological drivers. Heart Rate and Rhythm was originally designed to serve as a reference for current knowledge regarding the complicated molecular and cellular mechanisms that underlie normal and pathophysiological cardiac rhythms. The rapid progress in the field has called for an update to the book.

The second edition of *Heart Rate and Rhythm* has maintained its established structure. Some of the distinguished authors of the first Edition have reached retirement or did not wish to contribute again, so the respective chapters have been updated by their co-authors. We have also included new, emerging topics, which we expect will determine directions of future basic and biomedical research: a section including two new chapters dealing with the neurocardiac axis in arrhythmia, and chapters in other sections discuss the role of optogenetics and epigenetics in arrhythmia research.

Publication of this second edition has seen unprecedented Covid-19 epidemic seriously compromising the working of most of the contributors to this book. The tenacity and commitment of authors to submit their chapters under these trying conditions made publication of this volume possible. The editors of the book express gratitude to the chapter contributors for their unstinted support in making this endeavor a success.

We hope that our readers will find this update to *Heart Rate and Rhythm* useful for their scientific work to unravel the molecular and cellular mechanisms responsible for cardiac rate and rhythms in health and disease.

Lucknow, Uttar Pradesh, India Onkar N. Tripathi
Dalhousie, Canada T. Alexander Quinn
Freiburg im Breisgau, Germany Ursula Ravens

Contents

Part I Normal Cardiac Rhythm and Pacemaker Activity

1 Cardiac Ion Channels and Heart Rate and Rhythm 3
Onkar Nath Tripathi

2 A Historical Perspective on the Development of Models of Rhythm in the Heart 27
Penelope J. Noble and Denis Noble

3 Ionic Basis of the Pacemaker Activity of SA Node Cell Revealed by the Lead Potential Analysis 43
Yukiko Himeno, Akira Amano, and Akinori Noma

4 The "Funny" Pacemaker Current 63
Andrea Barbuti, Mirko Baruscotti, and Annalisa Bucchi

5 Cardiac Pacemaking Is an Emergent Property of Complex Synchronized Signaling on Multiple Scales 89
Oliver Monfredi, David Kim, Victor A. Maltsev, and Edward G. Lakatta

6 Unique Features of the Human Sinoatrial Node Structure, Function, and Arrhythmias: Mechanistic Insights from Integrated 3D Mapping Approaches 109
Anuradha Kalyanasundaram, Ning Li, and Vadim V. Fedorov

7 Mechano-Electric Coupling in the Heart: Effects on Heart Rate and Rhythm 131
T. Alexander Quinn, Rebecca A. Capel, and Peter Kohl

Part II Neurocardiac Axis and Arrhythmias

8 Fundamental Neurocardiology: The Intracardiac Nervous System 151
Frank M. Smith

9 The Neuro-cardiac Axis in Arrhythmogenesis: Role and Impact of Autonomic Modulation 187
Shui Hao Chin and G. André Ng

Part III Role of Specific Channels and Subcellular Structures in Arrhythmia

10 L-Type Ca^{2+} Channels and Cardiac Arrhythmias 227
Elza Kuzmenkina, Sarah Salamon, Patrick Despang, and Jan Matthes

11 Kv11.1 (hERG1) Channels and Cardiac Arrhythmia 255
Michael C. Sanguinetti

12 TRPC Channels in Cardiac Arrhythmia: Their Role during Purinergic Activation Induced by Ischemia 275
Julio L. Alvarez and Julio Alvarez-Collazo

13 Role of NCX1 and NHE1 in Ventricular Arrhythmia 293
András Tóth and András Varró

14 Gap Junctions and Cardiac Impulse Propagation. New Aspects of Arrhythmogenesis and Antiarrhythmic Agents Targeting Gap Junctions 309
Stefan Dhein and Aida Salameh

15 Role of the T-Tubules in the Control of Cellular Calcium and Inotropic Interventions in Cardiac Ventricular Myocytes 329
Andrew F. James and Clive H. Orchard

16 Structure of Transverse (T)-Tubules in Health and Disease . . 347
Eva A. Rog-Zielinska

17 Enlightening Cardiac Arrhythmia with Optogenetics 359
Tobias Bruegmann, Patrick M. Boyle, and Franziska Schneider-Warme

Part IV Mechanisms of Acquired Arrhythmia

18 An Overview of Spiral- and Scroll-Wave Dynamics in Mathematical Models for Cardiac Tissue 377
Mahesh Kumar Mulimani, Soling Zimik, Jaya Kumar Alageshan, Rupamanjari Majumder, Alok Ranjan Nayak, and Rahul Pandit

19 The Role of Intracellular Ca^{2+} in Arrhythmias in the Postmyocardial Infarction Heart 399
Wen Dun and Penelope A. Boyden

20 Implications of Sarcolemmal Ca^{2+}-Handling Proteins in Heart Function in Health and Disease 415
Paramjit S. Tappia, Sukhwinder K. Bhullar, Anureet K. Shah, and Naranjan S. Dhalla

21 Characteristics of Intracellular Ca^{2+} Handling Proteins in Heart Function in Health and Disease 429
Naranjan S. Dhalla, Mohamad Nusier, Anureet K. Shah, and Paramjit S. Tappia

22 Calmodulin Kinase II Regulation of Heart Rhythm and Disease 443
Drew M. Nassal and Thomas J. Hund

23 Pathways in Human Arrhythmias: Impact of Post-translational Modifications 459
Aaron D. Argall, Sara N. Koenig, and Peter J. Mohler

24 Viral Myocarditis 475
Stefan Peischard, Huyen Tran Ho, and Guiscard Seebohm

25 Epigenetic Influences of Air Pollution-Induced Cardiac Arrhythmias 493
Devin R. O'Piela, Jacob A. Grimmer, Neill A. Schwieterman, Matthew J. Mears, Matthew W. Gorr, and Loren E. Wold

Part V Mechanisms of Inherited Arrhythmia

26 The Short QT Syndrome 517
Jules C. Hancox, Mark J. McPate, Aziza El Harchi, Andrew S. Butler, Yihong Zhang, Dominic G. Whittaker, Christopher E. Dempsey, Harry J. Witchel, Ismail Adeniran, Alan G. Stuart, and Henggui Zhang

27 Defects in Ankyrin-based Protein Targeting Pathways in Human Arrhythmia 539
Emma K. Dudley, Holly C. Sucharski, Sara N. Koenig, and Peter J. Mohler

Part VI Novel Antiarrhythmic Approaches

28 Ion Channels as Drug Targets in Atrial Fibrillation 551
Ursula Ravens and Rémi Peyronnet

29 K Channel Openers as New Antiarrhythmic Agents 567
Nathalie Strutz-Seebohm and Guiscard Seebohm

Index 579

Contributors

Ismail Adeniran Biological Physics Group, School of Physics and Astronomy, University of Manchester, Manchester, UK

Jaya Kumar Alageshan Centre for Condensed Matter Theory, Department of Physics, Indian Institute of Science, Bangalore, Karnataka, India

Julio L. Alvarez Laboratorio de Electrofisiología. Instituto de Cardiología y Cirugía Cardiovascular, La Habana, Cuba

Julio Alvarez-Collazo Data Sciences International, Harvard Bioscience Incorporation, Holliston, MA, USA

Akira Amano Faculty of Bioinformatics, College of Life Sciences, Ritsumeikan University, Kusatsu, Japan

Aaron D. Argall Dorothy M. Davis Heart and Lung Research Institute and Frick Center for Heart Failure and Arrhythmia Research, Wexner Medical Center, Columbus, OH, USA
Departments of Physiology and Cell Biology and Internal Medicine, Division of Cardiovascular Medicine, The Ohio State University College of Medicine and Wexner Medical Center, Columbus, OH, USA

Andrea Barbuti Department of Biomolecular Sciences and Biotechnology, University of Milano, Milano, Italy

Mirko Baruscotti Department of Biosciences, University of Milano, Milano, Italy

Sukhwinder K. Bhullar Institute of Cardiovascular Sciences, St. Boniface Hospital Albrechtsen Research Centre, and Department of Physiology and Pathophysiology, College of Medicine, Rady Faculty of Health Sciences, University of Manitoba, Winnipeg, Canada

Penelope A. Boyden Department of Pharmacology, Columbia College of Physicians and Surgeons, New York, NY, USA

Patrick M. Boyle Department of Bioengineering, Center for Cardiovascular Biology, and Institute for Stem Cell and Regenerative Medicine, University of Washington, Seattle, USA

Tobias Bruegmann Institute of Cardiovascular Physiology, University Medical Center, and DZHK e.V. (German Center for Cardiovascular Research), Partner Site Göttingen, Göttingen, Germany

Annalisa Bucchi Department of Biomolecular Sciences and Biotechnology, University of Milano, Milano, Italy

Andrew S. Butler Department of Physiology and Pharmacology, School of Medical Sciences, University Walk, Bristol, UK

Rebecca A. Capel Department of Pharmacology, British Heart Foundation Centre of Research Excellence, University of Oxford, Oxford, UK

Shui Hao Chin Neurocardiology Group, Department of Cardiovascular Sciences, University of Leicester, and University Hospitals of Leicester NHS Trust, Leicester, UK

Chris E. Dempsey School of Biochemistry, School of Biomedical Sciences, University Walk, Bristol, UK

Patrick Despang Center of Pharmacology, University of Cologne, Köln, Germany

Naranjan S. Dhalla Institute of Cardiovascular Sciences St. Boniface Hospital Albrechtsen Research Centre, Winnipeg, Manitoba, Canada
Department of Physiology, Faculty of Medicine, University of Manitoba, Winnipeg, MB, Canada

Stefan Dhein Institute of Pharmacology and Toxicology, University of Leipzig, Leipzig, Germany

Emma K. Dudley Dorothy M. Davis Heart and Lung Research Institute and Frick Center for Heart Failure and Arrhythmia Research, Wexner Medical Center, Columbus, OH, USA
Departments of Physiology and Cell Biology and Internal Medicine, Division of Cardiovascular Medicine, The Ohio State University College of Medicine and Wexner Medical Center, Columbus, OH, USA

Wen Dun Department of Cardiovascular Medicine Columbia University, New York, NY, USA

Aziza El Harchi Department of Physiology and Pharmacology, School of Medical Sciences, University Walk, Bristol, UK

Vadim V. Fedorov Department of Physiology and Cell Biology, and Bob and Corrine Frick Center for Heart Failure and Arrhythmia, and Davis Heart & Lung Research Institute, The Ohio State University Wexner Medical Center, Columbus, OH, USA

Matthew W. Gorr Department of Physiology and Cell Biology, The Ohio State University College of Medicine, Columbus, OH, USA

Jacob A. Grimmer College of Nursing, The Ohio State University, 603 Davis Heart and Lung Research Institute, Columbus, OH, USA

Jules C. Hancox Department of Physiology and Pharmacology, School of Medical Sciences, University Walk, Bristol, UK

Yukiko Himeno Faculty of Bioinformatics, College of Life Sciences, Ritsumeikan University, Kusatsu, Japan

Huyen Tran Ho Department for Myocellular Electrophysiology and Molecular Biology, Institute for Genetics of Heart disease (IfGH), University Muenster, Münster, Germany

Thomas J. Hund The Frick Center for Heart Failure and Arrhythmia, Dorothy M. Davis Heart and Lung Research, Institute, The Ohio State University Wexner Medical Center, Columbus, OH, USA

Andrew F. James School of Physiology, Pharmacology and Neuroscience, Biomedical Sciences Building, University of Bristol, Bristol, UK

Anuradha Kalyanasundaram Department of Physiology and Cell Biology, and Bob and Corrine Frick Center for Heart Failure and Arrhythmia, and Davis Heart & Lung Research Institute, The Ohio State University Wexner Medical Center, Columbus, OH, USA

David Kim University of Virginia Medical Center, Charlottesville, VA, USA

Sara N. Koenig Dorothy M. Davis Heart and Lung Research Institute and Frick Center for Heart Failure and Arrhythmia Research, Wexner Medical Center, Columbus, OH, USA
Departments of Physiology and Cell Biology and Internal Medicine, Division of Cardiovascular Medicine, The Ohio State University College of Medicine and Wexner Medical Center, Columbus, OH, USA

Peter Kohl Institute for Experimental Cardiovascular Medicine, University Heart Center Freiburg • Bad Krozingen, Freiburg, Germany
Faculty of Medicine, University of Freiburg, Freiburg, Germany

Elza Kuzmenkina Center of Pharmacology, University of Cologne, Köln, Germany

Edward G. Lakatta Laboratory of Cardiovascular Science, NIA (IRP), NIH, Baltimore, MD, USA

Ning Li Department of Physiology and Cell Biology, and Bob and Corrine Frick Center for Heart Failure and Arrhythmia, and Davis Heart & Lung Research Institute, The Ohio State University Wexner Medical Center, Columbus, OH, USA

Rupamanjari Majumder Max-Planck-Institute of Dynamics and Self-Organization, Göttingen, Germany

Victor A. Maltsev Laboratory of Cardiovascular Science, NIA (IRP), NIH, Baltimore, MD, USA

Jan Matthes Center of Pharmacology, University of Cologne, Köln, Germany

Mark J. McPate Department of Physiology and Pharmacology, School of Medical Sciences, University Walk, Bristol, UK

Matthew J. Mears Department of Physiology and Cell Biology, The Ohio State University College of Medicine, Columbus, OH, USA

Peter J. Mohler Dorothy M. Davis Heart and Lung Research Institute and Frick Center for Heart Failure and Arrhythmia Research, Wexner Medical Center, Columbus, OH, USA
Departments of Physiology and Cell Biology and Internal Medicine, Division of Cardiovascular Medicine, The Ohio State University College of Medicine and Wexner Medical Center, Columbus, OH, USA

Oliver Monfredi Laboratory of Cardiovascular Science, NIA (IRP), NIH, Baltimore, MD, USA
University of Virginia Medical Center, Charlottesville, VA, USA

Mahesh Kumar Mulimani Centre for Condensed Matter Theory, Department of Physics, Indian Institute of Science, Bangalore, India

Drew M. Nassal The Frick Center for Heart Failure and Arrhythmia, Dorothy M. Davis Heart and Lung Research, Institute, The Ohio State University Wexner Medical Center, Columbus, OH, USA

Alok Ranjan Nayak International Institute of Information Technology (IIIT-Bhubaneswar), Bhubaneswar, India

G. André Ng Neurocardiology Group, Department of Cardiovascular Sciences, University of Leicester, and University Hospitals of Leicester NHS Trust, NIHR Leicester Biomedical Research Centre, Leicester, UK

Penelope J. Noble Department of Physiology, Anatomy and Genetics, Oxford University, Oxford, UK

Denis Noble Department of Physiology, Anatomy and Genetics, Oxford University, Oxford, UK

Akinori Noma Faculty of Bioinformatics, College of Life Sciences, Ritsumeikan University, Kusatsu, Japan

Mohamad Nusier Institute of Cardiovascular Sciences, St. Boniface Hospital Albrechtsen Research Centre, Winnipeg, Canada

Devin R. O'Piela Department of Physiology and Cell Biology, The Ohio State University College of Medicine, Columbus, OH, USA

Clive H. Orchards School of Physiology and Pharmacology, Medical Sciences Building, University of Bristol, Bristol, UK

Rahul Pandit Centre for Condensed Matter Theory, Department of Physics, Indian Institute of Science, Bangalore, Karnataka, India

Stefan Peischard Department for Myocellular Electrophysiology and Molecular Biology, Institute for Genetics of Heart disease (IfGH), University Muenster, Muenster, Germany

Rémi Peyronnet Institute for Experimental Cardiovascular Medicine, University Heart Center Freiburg • Bad Krozingen, Freiburg, Germany
Faculty of Medicine, University of Freiburg, Freiburg, Germany

T. Alexander Quinn Department of Physiology and Biophysics and the School Biomedical Engineering, Dalhousie University, Halifax, Canada

Ursula Ravens Department of Pharmacology and Toxicology, Medical Faculty Carl Gustav Carus, Dresden University of Technology, Dresden, Germany
Institute for Experimental Cardiovascular Medicine, University Heart Center Freiburg • Bad Krozingen, Freiburg, Germany
Faculty of Medicine, University of Freiburg, Freiburg, Germany

Eva Rog-Zielinska Institute for Experimental Cardiovascular Medicine, University Heart Center Freiburg • Bad Krozingen, Freiburg, Germany
Faculty of Medicine, University of Freiburg, Freiburg, Germany

Aida Salameh Clinic of Pediatric Cardiology, Heart Centre Leipzig, University of Leipzig, Leipzig, Germany

Sarah Salamon Center of Pharmacology, University of Cologne, Köln, Germany

Michael C. Sanguinetti Department of Internal Medicine, University of Utah, Salt Lake City, UT, USA

Franziska Schneider-Warme Institute for Experimental Cardiovascular Medicine, University Heart Center Freiburg • Bad Krozingen, Freiburg, Germany
Faculty of Medicine, University of Freiburg, Freiburg, Germany

Neill A. Schwieterman Department of Physiology and Cell Biology, The Ohio State University College of Medicine, Columbus, OH, USA

Guiscard Seebohm Department for Myocellular Electrophysiology and Molecular Biology, Institute for Genetics of Heart Disease (IfGH), University Muenster, Münster, Germany

Anureet K. Shah Department of Kinesiology and Nutritional Sciences, California State University, Los Angeles, USA

Frank M. Smith Department of Medical Neuroscience, Faculty of Medicine, Dalhousie University, Halifax, Nova Scotia, Canada

Nathalie Strutz-Seebohm AG Rezeptorstruktur und Funktion, IfGH - Abteilung Zelluläre Elektrophysiologie und Molekularbiologie, Westfälische Wilhelms-Universität Münster, Münster, Germany

Alan G. Stuart National Institute for Health Research (NIHR), Cardiovascular Biomedical Research Centre, Congenital Heart Unit, Bristol Heart Institute, Bristol, UK

Holly C. Sucharski Dorothy M. Davis Heart and Lung Research Institute and Frick Center for Heart Failure and Arrhythmia Research, Wexner Medical Center, Columbus, OH, USA
Departments of Physiology and Cell Biology and Internal Medicine, Division of Cardiovascular Medicine, The Ohio State University College of Medicine and Wexner Medical Center, Columbus, OH, USA

Paramjit S. Tappia Asper Clinical Research Institute, St. Boniface Hospital, Winnipeg, Canada

András Tóth Department of Pharmacology and Pharmacotherapy, University of Szeged, Szeged, Hungary

Onkar Nath Tripathi Cardiac Electrophysiology Division, Ion Channel Study Center, Life Sciences Academy, Lucknow, India

Gioia Turitto New York Presbyterian-Brooklyn Methodist Hospital, Brooklyn, New York, NY, USA

András Varró Department of Pharmacology and Pharmacotherapy, University of Szeged, Szeged, Hungary
Division of Cardiovascular Pharmacology, Hungarian Academy of Sciences, Szeged, Hungary

Dominic G. Whittaker Biological Physics Group, School of Physics and Astronomy, University of Manchester, Manchester, UK

Harry J. Witchel Medical Research Building, Brighton and Sussex Medical School, University of Sussex, Brighton, UK

Loren E. Wold Department of Physiology and Cell Biology, The Ohio State University College of Medicine, Columbus, OH, USA

Henggui Zhang Biological Physics Group, School of Physics and Astronomy, University of Manchester, Manchester, UK

Yihong Zhang Department of Physiology and Pharmacology, School of Medical Sciences, University Walk, Bristol, UK

Soling Zimik Centre for Condensed Matter Theory, Department of Physics, Indian Institute of Science, Bangalore, India

Part I

Normal Cardiac Rhythm and Pacemaker Activity

Cardiac Ion Channels and Heart Rate and Rhythm

1

Onkar Nath Tripathi

Abstract

The excitability of the heart is a prerequisite for its function as a pump distributing blood throughout the body. Initiated in the sinoatrial node, cardiac action potentials spread throughout the heart and trigger a coordinated contraction. The current chapter describes the molecular basis of cardiac excitability. It provides a brief overview of the various ion channels and transporters that give rise to the ionic currents underlying the characteristic shapes of action potentials in the various parts of the heart. Understanding the ionic mechanisms underlying electrical activity during a cardiac cycle in health and disease is the prerequisite for identifying potential drug targets for novel therapeutic strategies.

Keywords

Voltage-gated Na, K, and Ca channels · Ca^{2+}- and Na^{+}-activated K channels (K_{Ca}/K_{Na}) · Leak K channels (K_{2P}/4 TM) · Inwardly rectifying K channels (2 TM) · Cyclic nucleotide-regulated channels · Transient receptor potential channels · Stretch-activated channels · Ryanodine receptor channels · SR · inositol trisphosphate receptor channels · Mitochondrial and nuclear channels

1.1 Introduction

The heart beat originates in the form of the spontaneous electrical activity of the primary pacemaker cells of the sino-atrial node (SAN). Efficient propagation of the electrical waveform initiated by this spontaneous electrical activity (action potentials, AP) to the atria and, via the cardiac conduction system, viz., atrioventricular node (AVN), Bundle of His, Bundle branches, and Purkinje fiber network, to the rest of the heart brings about a highly coordinated rhythmic mechanical activity characterized by synchronized contraction and relaxation of different regions of the heart. The cardiac cycle repeats itself throughout an organism's life with a high-efficiency level and determines the heart rate and rhythm.

The classical work of Carl Wiggers [1] on the cardiac cycle identified the correlation between the electrical activity (electrocardiogram, ECG) and different parameters of mechanical activity, making it evident that the electrical cycle initiates the mechanical cycle. Excitation–contraction (E–C) coupling plays a crucial role in this process through the influx of Ca ions (Ca^{2+}), facilitating the conversion of the electrical energy into chemical energy required for myocardial contraction [2]. The two phases of the electrical cycle, viz. electrical systole and diastole, are clinically examined to assess the cardiac functions in the normal and diseased heart. The electrical cycle, recorded with an ECG, begins with the P wave,

O. N. Tripathi (✉)
Cardiac Electrophysiology Division, Ion Channel Study Center, Life Sciences Academy, Lucknow, India

© Springer Nature Switzerland AG 2023

O. N. Tripathi et al. (eds.), *Heart Rate and Rhythm*, https://doi.org/10.1007/978-3-031-33588-4_1

reflecting the atrial depolarization (Fig. 1.1). The PR interval, the time taken for atrial depolarization to reach the AVN and beyond, is characteristically well preserved in different mammals. The PR interval is only one order of magnitude longer in humpback whales, the largest mammal, compared to the mouse, even though the body mass differs by six orders of magnitude ([3]; Table 1.1). The QRS complex represents the entry of the wave of excitation via the cardiac conduction system into the ventricles and the depolarization of ventricular myocytes. Subsequent repolarization of the ventricles is reflected in the T wave, which is often followed by the U wave, the cause of which is still unclear [4]. The QT interval is the time required for repolarization of the ventricles and corresponds roughly to the duration of ventricular APs. It serves as an important indicator for the arrhythmogenic propensity of the heart associated with congenital or acquired long QT syndrome.

The cardiac electrical cycle is initiated and maintained by the transmembrane flux of ions via ion channels, exchangers, and pumps (Fig. 1.2). The specific tissue and subcellular distribution of a wide spectrum of ion channel types determine the AP shape and spread of the wave of excitation in the heart. Notable advances in the molecular basis of cardiac excitation and conduction are well covered in several reviews [5–8]. This chapter provides an overview of some basic features of ion channels expressed in the heart, their likely contributions to ionic currents and APs, and their proposed role in cardiac activity.

1.2 Molecular Basis of Cardiac Electrical Activity

The cardiac AP is typically described with five distinct phases, namely phase 0 (upstroke, depolarization), phase 1 (early repolarization—notch), phase 2 (plateau), phase 3 (repolarization), and phase 4 (resting potential or pacemaker potential or diastolic depolarization). Ionic currents through electrogenic membrane ion transport proteins form the basis of the different phases of the AP (Fig. 1.3). These proteins are heterogeneously distributed in different types of heart cells endowed with specific functions, and their superbly orchestrated activity determines the characteristic configuration of the AP. Ion channels allow passive flux of Na^+, K^+, Ca^{2+}, and Cl^- in a direction dictated by their concentration gradient across the membrane, and the resulting ion currents contribute to the maintenance of resting potential and generation and conduction of APs (Fig. 1.2).

Palettes of ion channels in sarcolemma (SL) and sarcoplasmic reticular (SR), mitochondrial (MT), and nuclear (NUC) membranes differ significantly in the same cell and in different types of heart cells. The SL electrogenic proteins primarily determine the shape of cardiac APs. However, the SR ion transport proteins are crucial in cardiac pacemaker activity, E–C coupling, and intracellular Ca^{2+} homeostasis. MT ion channels contribute to the metabolic state of heart cells via excitation–metabolism coupling. NUC ion channels contribute to the transcriptional regulation of SL and MT ion transport and signaling proteins (excitation–transcription coupling), thereby contributing indirectly to heart rate and rhythm.

Altered ion channel activity is frequently associated with arrhythmias, and mutations in ion channel genes, in particular, cause several cardiac channelopathies. On the basis of the primary gating (activating) factor, two major groups of ion channels have been identified: voltage-gated (VGIC) and ligand-gated (LGIC) ion channels. The VGICs are activated by a change in membrane potential and contribute maximally to cardiac APs. Information on their genes, amino acid residues, conductance, kinetics, etc., is presented concerning adult heart cells [9–11].

1.3 Sarcolemmal Ion Channels

1.3.1 Voltage-Gated Na Channels

Nine different types of mammalian voltage-gated sodium channels (VGSCs) have been identified and are named after their α-subunits as $Na_V1.1$–$Na_V1.9$. The heart primarily expresses $Na_V1.5$

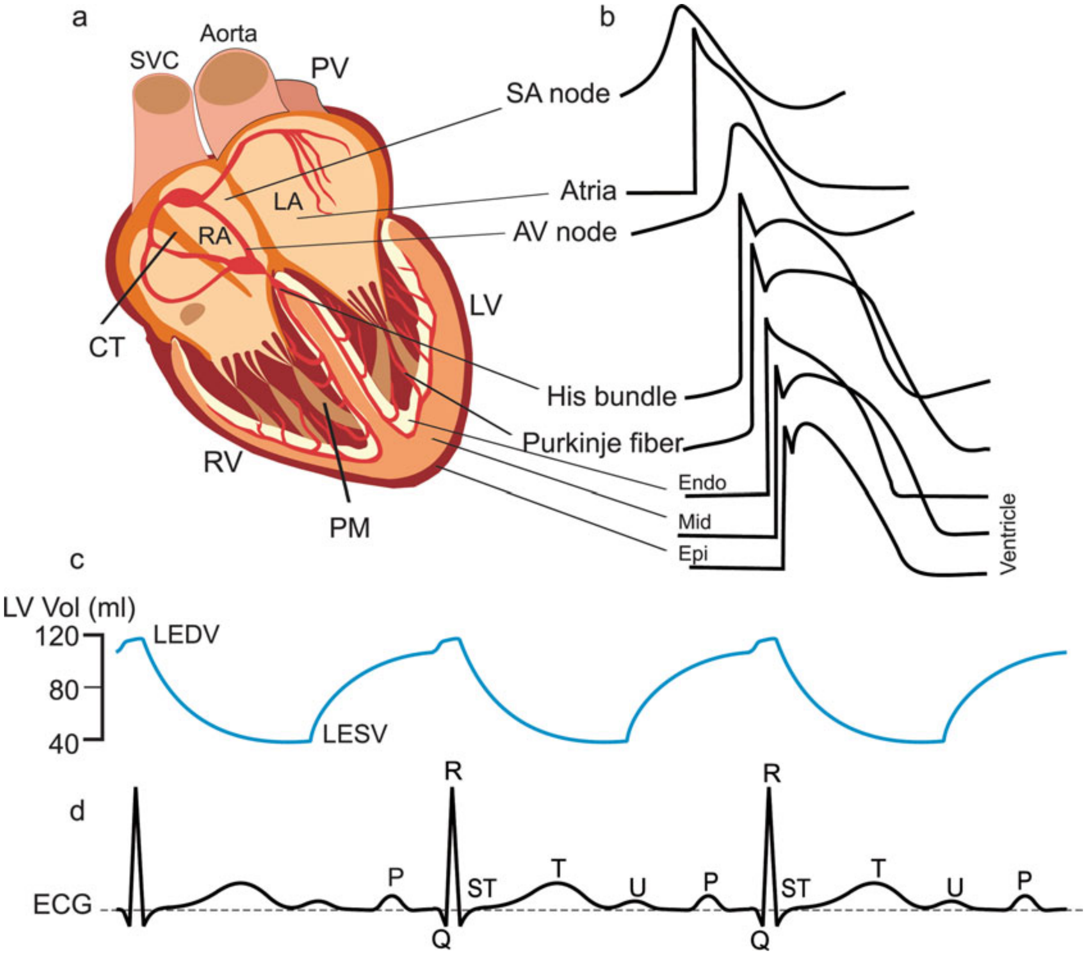

Fig. 1.1 Diagrammatic representation of the salient electrical events in different regions of heart during a cardiac cycle. (**a**) Heart showing SA node, conducting system, and the working cardiac tissues. SVC, superior vena cava; PV, pulmonary vein; CT, crista terminalis; RA, right atrium, LA, left atrium; RV, right ventricle; LV, left ventricle; Endo, endocardium; Epi, epicardium; Mid, midmyocardium; PM, papillary muscle. (**b**) APs in the cells of different heart regions roughly correspond to different phases of ECG. (**c**) Left ventricular volume (LV) indicating left ventricular contraction and relaxation; LEDV, Left ventricular end-diastolic volume; LESV, Left ventricular end-systolic volume. (**d**) Surface ECG showing the classical P, Q, R, S, T, and U waves; ST indicates the end of S and beginning of T wave

(cardiac type), but is also reported to express the brain-type Na channels, $\mathrm{Na_V1.1}$, $\mathrm{Na_V1.3}$, and $\mathrm{Na_V1.6}$ [12, 13]. The VGSCs carry a fast inward $\mathrm{Na^+}$ current, I_{Na}, that underlies the fast upstroke (phase 0) of AP in most cardiac cells. VGSCs are hetero-multimeric membrane proteins composed of four subunits: α, β, γ, and δ. The α-subunit is the primary functional unit and contains the pore, ion selectivity filter, voltage sensor, and the drug and toxin binding sites. An α-subunit has four

Table 1.1 Heart rate and PR interval vary as a function of body size in mammals (values taken from [3])

Species	Heart rate (beats per minute)	PR interval (ms)	Heart weight (g)	Body weight (kg)
Mouse	376 ± 49	43 ± 4	0.192	0.029 ± 0.04
Human (male)	80	164 ± 0.16	390	66 ± 3
Humpback whale	30	400	180,000	30,000

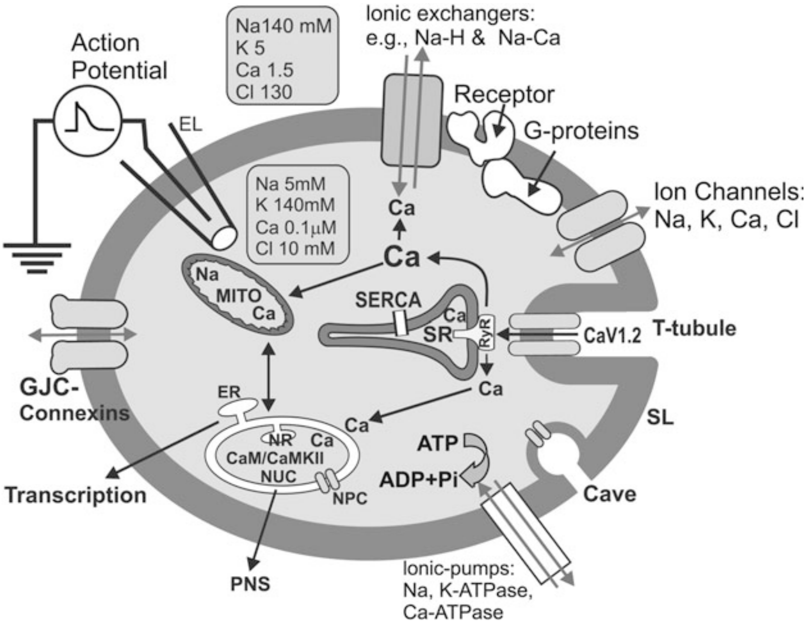
Action Potential
Na140 mM
K 5
Ca 1.5
Cl 130
Ionic exchangers:
e.g., Na-H & Na-Ca
Receptor
G-proteins
EL
Na 5mM
K 140mM
Ca 0.1μM
Cl 10 mM
Ca
Ca
Ion Channels:
Na, K, Ca, Cl
Na
MITO
Ca
SERCA
Ca
SR
RyR
CaV1.2
T-tubule
GJC-
Connexins
ER
Ca
Ca
SL
NR
Ca
CaM/CaMKII
NUC
ATP
ADP+Pi
Transcription
NPC
Cave
PNS
Ionic-pumps:
Na, K-ATPase,
Ca-ATPase

Fig. 1.2 Cartoon diagram of a cardiac myocyte depicting various categories of ion transporters in the sarcolemma and intracellular organelles. Extracellular and cytosolic concentrations of Na^+, K^+, Ca^{2+}, and Cl, which offer passive electrochemical gradients for the flow of ion currents through ion channels, are shown. The ion currents underlie APs which can be recorded using classical glass microelectrode (El) techniques. SL, sarcolemma; Cave, caveolae; SR, sarcoplasmic reticulum; MITO, mitochondria; NUC, nucleus; ER, endoplasmic reticulum; PNS, perinuclear space; NR, nuclear reticulum; NPC, nuclear pore complex; GJC, gap junction channel; RyR, ryanodine receptor; SERCA, SR Ca^{2+}-ATPase

domains (DI–DIV), each comprising of six TM segments (S1–S6). The four domains are arranged concentrically to collectively form a water-filled, open-ended central cavity. An inverted loop (P) between the extracellular ends of S5 and S6 of each domain forms the channel's selectivity filter and outer vestibule. S4 acts as the voltage sensor due to its many positively charged amino acids. A short intracellular loop between DIII and DIV serves as an inactivation gate that is proposed to occlude the inner vestibule. The N and C termini of α-subunits are intracellular. Four β-subunits, β1–β4, are reported for VGSCs and are formed of one TM segment. The β1-subunit regulates the subcellular localization and functions of α-subunits. The β-subunits interact with the extracellular matrix, cytosolic linker proteins, and cell adhesion molecules (CAM). The following VGSCs have been identified in heart.

Na_V1.1 (Brain I, Gene - *SCN1A*, 1998 amino acids (aa)) is expressed in ventricular myocytes [12] and SAN cells [13] and conducts a small or negligible I_{Na}. Two auxiliary subunits, β1 and β2, are identified for this channel. The macroscopic $I_{NaV1.1}$ has a voltage of half-maximum ($V_{0.5}$) activation of -19.6 to -13.7 mV and a $V_{0.5}$ of inactivation of -41.9 to -37.9 mV. Na_V1.1 is localized in the T-tubules of ventricular myocytes and is involved in E–C coupling in ventricles [12]. In SAN, it is homogeneously distributed on SL and is associated with AP firing frequency [13, 14]. Na_V1.1 is blocked by tetrodotoxin (TTX) with high sensitivity and is activated by β scorpion toxin, CssIV [13].

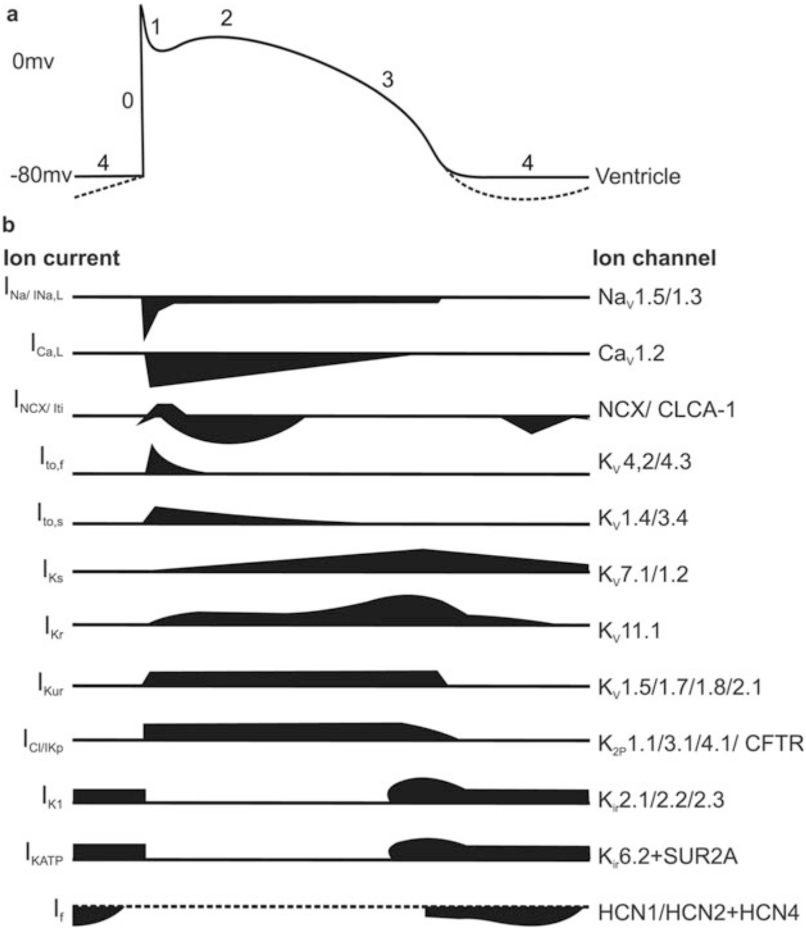

Fig. 1.3 Diagram showing different phases of ventricular AP and the underlying ion currents. (**a**) AP showing rapid depolarization (upstroke-phase 0) followed by rapid repolarization (notch-phase 1), slow repolarization (plateau phase 2) and then faster final repolarization (phase 3) terminating into resting potential (phase 4). The cells of SAN, AVN, and Purkinje fiber exhibit slow diastolic depolarization (DD, dotted lines). (**b**) Various inward and outward ion currents depicted by downward and upward deflections, respectively, relative to the baseline, are shown along with the ion channels/ transporters generating the currents. The bottom recording shows inward (dotted line) pacemaker current, I_f/I_h, that contributes to DD in the pacemaker cells of SAN, AVN, and Purkinje fiber

$Na_V1.3$ (Brain III, Gene - *SCN3A*, 2000 aa) is expressed in fetal and adult hearts, ventricular myocytes [12], and in SAN cells [13]. It is reported to have two auxiliary subunits, β1 and β3. $Na_V1.3$ carries a small macroscopic $I_{NaV1.3}$ having a $V_{0.5}$ of activation of −12 mV and $V_{0.5}$ of inactivation of −47.5 mV. $Na_V1.3$ is also localized on T-tubules and plays a role in E–C coupling in ventricles [12] and mediates AP firing in SAN cells [13]. It is blocked by TTX with high sensitivity and is stimulated by CssIV.

$Na_V1.5$ (h1, cardiac, Gene - *SCN5A*, 2016 aa, ~20 pS) is the cardiac-specific VGSC and has four auxiliary subunits, β1, β2, β3, and β4. $Na_V1.5$ is localized on the intercalated discs in ventricles [12] and has an important role in the cell-to-cell conduction of impulse in the heart. $Na_V1.5$ is also present in peripheral cells of SAN and is involved in the conduction of SAN APs to atria [14]. A fast, transient inward Na^+ current, I_{Na}, with rapid kinetics of activation ($V_{0.5}$ −44 mV) and inactivation ($V_{0.5}$ −87 mV) is mediated by $Na_V1.5$ and contributes significantly to the fast upstroke of AP in atria, ventricles, and Purkinje fibers. $Na_V1.5$ is reported to contribute significantly to the late Na current, I_{NaL} [15]. $Na_V1.5$ is relatively insensitive to the blocking effect of TTX and is more sensitive to saxitoxin (STX). Class I antiarrhythmic drugs, e.g., lidocaine, procainamide, flecainide, propafenone, etc., act by blocking $Na_V1.5$. Ranolazine, an antiarrhythmic drug, targets I_{NaL} [15]. $Na_V1.5$ is implicated in sick sinus syndrome, Brugada syndrome, and other cardiac arrhythmias [16]. Gain of function mutations in *SCN5A* cause type 3 long QT syndrome (LQTS).

$\mathbf{Na_V}$1.6 (Gene - *SCN8A*, 1980 aa) is expressed in the T-tubules of ventricular myocytes [12]. It mediates a small current with $V_{0.5}$ of activation of −28.7 mV and $V_{0.5}$ of inactivation of −71.9 mV [17]. All four β subunits, β1–β4, are associated with Na_V1.6. It is activated by β scorpion toxins and blocked by TTX. Na_V1.6 is suggested to be involved in E–C coupling [12]. Interestingly, TTX is a potent inhibitor of the chick and fish heart $I_{Na,}$ as evident from studies on isolated fish ventricular myocytes and isolated chick ventricular tissue, which indicates a predominant role of other TTX-sensitive isoforms of VGSCs in the nonmammalian heart [18, 19].

1.3.2 Voltage-Gated Ca Channels

The voltage-gated calcium channels (VGCCs) conduct an inward Ca^{2+} current (I_{Ca}), which leads to the elevation of intracellular Ca^{2+}, a second messenger necessary for a large variety of cellular functions including cardiac contraction, impulse generation, secretion, neurotransmission, gene expression, development, and differentiation etc. VGCCs facilitate the conversion of electrical energy into chemical energy for the execution of cellular functions.

Three families of VGCCs are identified and generally grouped under two categories depending on their activation voltage, viz. high voltage-activated (HVA) and low voltage-activated (LVA) Ca channels. The HVA Ca channels are activated at higher membrane voltages (i.e., more depolarized potentials) and include Ca_V1.x (L, N, and P/Q type) and Ca_V2.x (R-type) VGCCs. The LVA Ca channels, Ca_V3.x (T-type) VGCCs, are activated at low membrane voltages (i.e., more negative potentials). VGCCs are hetero-multimeric membrane protein complexes of four to five subunits, viz. α1, α2, β, γ, and δ. The α1 (Ca_V) subunits of 150–250 kDa have essentially the same structure as $Na_{V,}$ containing the pore, the voltage sensor, and binding sites for most of the pharmacological modulators [20]. The auxiliary subunits of VGCCs, α2, β, γ, and δ, are smaller proteins compared to α1; α2 is a 140 kDa extracellular protein, and δ a 27 kDa TM glycoprotein. The β subunits, β1–β4, are located intracellularly, have specific tissue distribution, and play important regulatory roles in surface expression and activation/inactivation kinetics of α1 subunit. The γ subunit, formed of 4TM segments, is involved in the assembly and surface expression of α1 subunit and other membrane signaling proteins. Some of the salient features of the VGCCs expressed in the heart are described below.

$\mathbf{Ca_V}$1.2 (Cardiac L-type Ca channel, α1C, Gene - *CACNA1C*, 2138 aa, 8 pS with Ca^{2+}) is strongly expressed in all regions of heart and is localized in the T-tubules of ventricular myocytes [20]. A cardiac-specific isoform, Ca_V1.2α, has been identified [21]. β1–β4 accessory subunits are differentially distributed at the subcellular level. Four α2δ isoforms are also reported as the auxiliary subunits of Ca_V1.2 [22]. Ca_V1.2 current, $I_{Ca,L}$, contributes to the plateau phase (phase 2) of ventricular APs and plays a key role in E–C coupling [2]. In SAN, $I_{Ca,L}$ underlies the slow upstroke of APs and is also considered to contribute to pacemaker potential [23]. The ventricular macroscopic $I_{Ca,L}$ has a $V_{0.5}$ of activation of −4.8 mV and τ of 5–7 ms; the $V_{0.5}$ of inactivation is −20.4 mV and τ_f and τ_s are 20.4 ms and 61–133 ms, respectively [9, 11].

The organic Ca channel blockers (CCBs), dihydropyridines (DHP; e.g., nifedipine), phenylalkylamines (e.g., verapamil), diphenylalkylamines (e.g., fendiline), and benzothiazepines (e.g., diltiazem), inhibit Ca_V1.2 activity. Several Ca channel activators (CCA), e.g., Bay K 8644 and FPL 64176, activate Ca_V1.2 [24]. Ca_V1.2 is strongly modulated by phosphorylation via the β-adrenergic receptor-induced increase in cAMP level and PKA activation, which is terminated by PP2A [25]. This β-AR pathway has an important role in sympathetic nerve-induced positive chronotropy and inotropy invoked during the "fight-or-flight" response of the heart. $Ca_V1.2$ and its auxiliary subunits are associated with inherited (Timothy syndrome-LQT8) and acquired cardiac arrhythmias. Calmodulin and CaMKII, which regulate the activity of L-type Ca channels, are suggested to contribute to arrhythmogenesis [26, 27].

Ca_V1.3 (α1D, L-type Ca channel, Gene - *CACNA1D*, 2181 aa) is expressed in SAN, AVN, and right atrial cells [28–30]. $Ca_V1.3$ is reported to have two auxiliary subunits, β and α2δ. The macroscopic $I_{CaV1.3}$ has activation $V_{0.5}$ -12.9 mV and τ 0.5–2.5 ms and inactivation $V_{0.5}$ -42.7 mV and τ 3.8–74 ms [31]. It contributes to normal pacemaking in SAN and is implicated in SAN dysfunction [28, 29, 32]. Channel phosphorylation following β-AR stimulation brings about positive chronotropy accounting for part of the effects of increased sympathetic discharge. The CCBs and Ca channel activators (CCAs) have profound effects on $Ca_V1.3$.

Ca_V2.3 (α1E, R-type Ca channel, Gene - *CACNA1E*, 2270 aa, 20 pS) is associated with β and α2δ subunits. $Ca_V2.3$ channel allows the flow of a residual inward Ca^{2+} current ($I_{Ca,R}$) at high membrane voltages when $I_{Ca,L}$ is blocked by CCBs. The macroscopic $I_{Ca,R}$ has an activation $V_{0.5}$ of -29 mV, τ 2.4 ms, and inactivation $V_{0.5}$ of -54 mV and τ 16–655 ms [9]. $Ca_V2.3$ is expressed in atrial cells [33]. It is insensitive to CCBs and CCAs and is inhibited by Ni^{2+} and Cd^{2+} [9].

Ca_V3.1 (α1G, T-type Ca channel, Gene - *CACNA1G*, 2377 aa, 7.3 pS) is expressed predominantly in the conduction system, viz. SAN, AVN, and Purkinje fibers [34]. $Ca_V3.1$ elicits $I_{Ca,T}$, a transient inward Ca^{2+} current activated at low (more negative) membrane voltages, suggested to play a key role in the pacemaker activity of SAN and in AVN conduction [29, 34]. The macroscopic $I_{Ca,T}$ exhibits a $V_{0.5}$ of activation of -50 mV, τ 1–7 ms, $V_{0.5}$ of inactivation -68 mV, and τ 15–40 ms [35]. $Ca_V3.1$ is insensitive to CCBs and CCAs and is blocked by Ni^{2+} and mibefradil [9, 36].

Ca_V3.2 (α1H, T-type Ca channel, gene- - *CACNA1H*, 2353 aa, 9.1 pS) are most abundant in the conduction system of the heart and are not expressed in adult mammalian ventricles [34, 37]. The macroscopic $I_{CaV3.2}$ shows $V_{0.5}$ of activation of -41.9 mV and τ of 2–10 ms. The $V_{0.5}$ of inactivation is -50.9 mV and τ is in the range of 20–120 ms [9]. $I_{CaV3.2}$ is inhibited by mibefradil, Ni^{2+}, pimozol, and anandamide [9, 36]. $Ca_V3.2$ is expressed in atria and ventricles during cardiac pathologies such as heart failure (HF) and cardiac hypertrophy and is associated ventricular arrhythmias [34, 38].

1.3.3 Voltage-Gated K Channels (K_V)

K channels contribute to the maintenance of resting membrane potential and repolarization of cardiac APs and, therefore, determine excitability, AP duration, and refractoriness of the myocardium. K channels are the most diverse groups of ion channels encoded by about 70 genes in mammals. The channels consist of 4 α-subunits each with six TM segments in voltage-gated (K_v), with 6/7 TM segments Ca^{2+}- and Na^+-activated (K_{Ca}, K_{Na}), and with two TM segments in inwardly rectifying (K_{ir}), and of two α-subunits each with four TM segments, but two pore-forming loops in the two-pore (K_{2p}) K channel families [9].

Voltage-gated potassium channels (VGPCs) are the largest family of K channels encoded by 40 genes in the human genome and are, therefore, extremely diverse. VGPCs are comprised of four primary pore-forming α-subunits, each with six TM segments. α-subunits co-assemble to form homo- or hetero-tetramers that have the pore for K^+ flux, the selectivity filter, voltage sensor, activation and inactivation gates, and sites for interaction with pharmacological agents. Presently

12 subfamilies of VGPCs are identified and are named $K_V1.x$–$K_V12.x$.

The members of $K_V5.x$, $K_V6.x$, $K_V8.x$, and $K_V9.x$ form “modifiers” and are nonfunctional ion channels upon formation of homotetramers. Auxiliary β-subunits, $K_V\beta1.x$, $K_V\beta2.x$, and $K_V\beta3.x$, and other associated proteins are also identified for several VGPCs and modulate their functions.

$K_V1.1$ (Gene - *KCNA1*, 495 aa, 10 pS) is associated with two heteromeric pore-forming subunits, $K_V\beta1$ and $K_V\beta2$ [9]. $K_V1.1$ mediates an outward I_K contributing to delayed rectifier K current, which maintains the resting potential and cellular excitability [39, 40]. The kinetics of macroscopic $I_{KV1.1}$ is characterized by $V_{0.5}$ of activation of −29.7 mV and τ 15.5 ms, and $V_{0.5}$ of inactivation of −47 mV and τ 83.4 ms [39]. SA node is reported to over-express $K_V1.1$ in mice exhibiting chronic bradycardia [41].

$K_V1.2$ (Gene - *KCNA2*, 499 aa, 14–18 pS) has two heteromeric pore-forming units, $K_V\beta1$ and $K_V\beta2$, and co-assembles with other K_V channels. The outward $I_{KV1.2}$ contributes to delayed rectifier I_K and restores resting potential and excitability [42, 43]. The macroscopic $I_{KV1.2}$ has a $V_{0.5}$ of activation of 5–27 mV and τ of 6 ms, and $V_{0.5}$ of inactivation of −15 mV [43]. It is expressed in SAN, atria, and ventricles [44] and is associated with right ventricular hypertrophy [45].

$K_V1.4$ (Gene - KCNA4, 653 aa, 5 pS) forms heteromeric pore with $K_V\beta$ and co-assembles with other K_V channels. They are expressed in SAN, AVN, Purkinje fibers, and ventricles [40, 46–49]. $K_V1.4$ is responsible for the slow transient outward K^+ current, $I_{to,s}$, involved in early repolarization that shapes the configuration of APs in different types of heart cells [50, 51] and is altered in postmyocardial infarction (MI) ventricular myocardium in a differential manner [52]. $K_V1.4$ is associated with cardiac hypertrophy and heart failure (HF) [51, 53].

$K_V1.5$ (Gene - *KCNA5*, 613 aa, 8 pS) forms heteromeric channel with $K_V\beta1$ and $K_V\beta2$. It is expressed in SAN, AVN, atria, and ventricles, being more predominant in atria [40, 46, 54, 55] and is a major contributor to ultra-rapidly activating delayed rectifier outward K^+ current (I_{Kur}). The macroscopic $I_{Kv1.5}$ shows a $V_{0.5}$ of activation of −14 mV and τ of 23 ms which is in the range of those for I_{Kur}. I_{Kur} participates in repolarization and maintenance of resting potential [56, 57]. $K_V1.5$ expression levels and I_{Kur} are associated with cardiac rhythm disorders like atrial fibrillation (AF) and with ventricular hypertrophy [53, 57].

$K_V1.7$ (Gene - *KCNA7*, 456 aa, 21 pS) co-assembles with other K_V1 channels. It is expressed in heart [58] and is responsible for an I_{Kur} like current. The macroscopic $I_{KV1.7}$ has a $V_{0.5}$ of activation of −4.3 mV and a $V_{0.5}$ of inactivation of −21 mV and τ of 181.8 ms [59]. $K_V1.7$ is suggested to contribute significantly to I_{Kur} and facilitates repolarization. *KCNA7* is considered a candidate gene for inherited cardiac disorders [60].

$K_V1.8$ (Gene - *KCNA10*, 511 aa, 11 pS) co-assembles with other $K_V1.x$ and KCNA4B acts as a novel β subunit of this channel to form a heteromeric channel [61]. $K_V1.8$ is activated by cGMP and not by cAMP [62]. $K_V1.8$ is expressed in heart, contributes to I_{Kur}, and facilitates repolarization and restoration of resting potential and has a potential role in acquired arrhythmias [62, 63].

$K_V2.1$ (Gene - *KCNB1*, 858 aa, 8 pS) is associated with several “modifier” heteromeric pore-forming subunits, viz. $K_V5.1$, $K_V6.1$–$K_V6.3$, $K_V8.1$, and $K_V9.1$–$K_V9.3$. The expression level of $K_V2.1$ is high in ventricles and atria [49, 55]. $K_V2.1$ causes a delayed rectifier outward current $I_{K,slow2}$ and contributes significantly to I_{Kur}, facilitating repolarization [49, 64]. It is associated with arrhythmias and left ventricular remodeling [49, 65].

K_V3.4 (Gene - *KCNC4*, 635 aa, 14 pS) co-assembles with the auxiliary subunit MiRP2. It is expressed in Purkinje fibers and ventricles [55, 66] and mediates a K^+ outward current that facilitates repolarization. K_V3.4 is associated with conduction abnormalities in congestive HF [66].

K_V4.1 (Gene - *KCND1*, 647 aa, 6 pS) forms a K channel co-assembling with KChiP1 and DPPX [9]. It is differentially expressed in the heart [47, 67].

K_V4.2 (Gene - *KCND2*, 630 aa, 7.5 pS) forms heteromeric ion channels with the β-subunits KChIP1, 2, 3, and 4 and $K_V\beta$. It is asymmetrically expressed in heart and is localized in the T-tubules in ventricles [68]. K_V4.2 contributes to $I_{to,f}$ and participates in repolarization during phase 1 of cardiac AP [51]. However, its expression level is low in the ventricles of higher mammals allowing the appearance of prominent notch phase of AP [64]. K_V4.2 is implicated in diabetic cardiomyopathy [69, 70].

K_V4.3 (Gene - *KCND3*, 655 aa, 5 pS) is associated with KChIP2. K_V4.3 is expressed in heart with profound differences in regional distribution and between different species [64, 71]. It also mediates a transient outward K^+ current and contributes to $I_{to,f,}$ which determines AP duration in different types of heart cells. K_V4.3 is associated with several cardiac rhythm disorders [51, 70, 72, 73].

K_V7.1 (KvLQT1, Gene - *KCNQ1*, 676 aa; 5.8 pS) has several auxiliary subunits, viz. MinK (KCNE1), and MiRP1–MiRP4 [74]. It is expressed in atria and ventricles and mediates the slowly activating delayed rectifier outward K^+ current, I_{Ks}, contributing to repolarization during the “plateau” phase of the AP [75]. Mutation in K_V7.1 is the most common cause of LQTS [76] and, very rarely, SQT syndrome [76, 77] and is associated with AF.

K_V11.1 (Gene - *KCNH2* or *HERG*, 1159 aa; 12 pS) is proposed to co-assemble with the accessory subunit MiRP1 [78]. These channels are abundantly and asymmetrically expressed in SAN, atria and ventricles [79, 80]. K_V11.1 channel underlies the rapidly activating delayed rectifier outward K^+ current, I_{Kr}, having strong inwardly rectifying properties [80]. I_{Kr} determines the time course of the late phase of repolarization of the AP. hERG channels are associated with both inherited (LQTS and SQTS) and acquired (drug-induced) arrhythmia [80]. Several chemically unrelated drugs, and several of those intended for noncardiac use, are reported to block the hERG channel causing ventricular arrhythmias, torsades de pointes (TDP), and sudden cardiac death (SCD) (see Chap. 11).

1.3.4 Ca^{2+}- and Na^+-Activated K Channels (K_{Ca}/K_{Na})

Five families of K_{Ca} channels (including K_{Na} channels), namely, K_{Ca}1.x, K_{Ca}2.x, K_{Ca}3.x, K_{Ca}4.x, and K_{Ca}5.x have been identified [9]. The K_{Ca} channels are activated by intracellular Ca^{2+}, and are grouped as small conductance (SK), intermediate conductance (IK), and big conductance (BK) channels on the basis of their conductance and pharmacological sensitivity. K_{Ca}1.x has one member, i.e., K_{Ca}1.1 (BK, slo1), and belongs to the BK group. K_{Ca}5.x also has one member (K_{Ca}5.1, slo3) and is related to K_{Ca}1.x. K_{Ca}2.x has three members, viz. K_{Ca}2.1, K_{Ca}2.2, and K_{Ca}2.3, and belongs to the SK group. K_{Ca}3.1 is the only member of K_{Ca}3.x (IK) group.

The Na^+-activated K (K_{Na}) channels are named K_{Ca}4.x by IUPHAR and have two members, i.e., K_{Ca}4.1 (slack, slo2.2) and K_{Ca}4.2 (slick, slo2.1), hence K_{Ca}4.x channels are activated by intracellular Na^+, but not by Ca^{2+}. The following K_{Ca} and K_{Na} channels are reported to be expressed in heart.

K_{Ca}2.1 (SK1, Gene - *KCNN1*, 543 aa, 9.2 pS) is formed of six TM segments. Calmodulin serves as its auxiliary subunit. They are activated by intracellular Ca^{2+} and are voltage-dependent. K_{Ca}2.1 is reported in atria and ventricles [81], and is blocked by apamin and leiurotoxin I [9, 82].

K_{Ca}2.2 (SK2, Gene - *KCNN2*, 579 aa, 9.5 pS) has no auxiliary subunits and is present in heart its expression being higher in atria than in ventricles [83–85]. K_{Ca}2.2 is voltage-independent and facilitates repolarization in atrial cells; their deletion in mice results in AF [85]. Apamin and leiurotoxin I are its pore blockers [9, 82].

K_{Ca}2.3 (SK3, Gene - *KCNN3*, 731 aa) is voltage-independent, and no auxiliary subunits are reported. K_{Ca}2.3 is equally expressed in atria and ventricles [84]. Apamin and leiurotoxin I are its pore blockers [9, 82].

K_{Ca}4.2 (Slick/Slo2.1/K_{Na}, Gene - *KCNT2*, 1138 aa, 141 pS [86], and 220 pS [87]). First reported in guinea pig ventricular myocytes, these channels are widely distributed in the heart [88]. K_{Na} channels in ventricular myocytes show complex bursting behavior [87] with several stable subconductance levels [89]. K_{Ca}4.2 is reported to form heteromers with K_{Ca}4.1 in neurones [90]. K_{Ca}4.2 channels are believed to protect from hypoxic insults [91]. They are blocked by several antiarrhythmic drugs [92] and activated (Slo2.1) by niflumic acid [93].

1.3.5 Leak K Channels (K_{2P}/4 TM)

Leak K channels, in part, mediate a background leak of K^+ across the SL and maintain the membrane potential at subthreshold resting levels, thus modulating cellular excitability [94, 95]. The primary pore-forming α-subunits of these K channels have two pore-forming loops each, arranged within four TM segments, usually as homodimers or heterodimers. Fifteen types of K_{2P} channels have been identified [9]. K_{2P} channels remain open in the range of resting potential and carry time- and voltage-independent outward K^+ currents. A variety of factors are known to modulate the activity of K_{2P} channels, including temperature, pO_2, pH, lipids, neurotransmitters, G-protein-coupled receptors, and mechanical stimuli. The cardiac K_{2P} family members underlie K^+ currents somewhat similar to the "plateau current" and steady-state K^+ current, ISS [95, 96], and are described below:

K_{2P}1.1 (TWIK-1, Gene - *KCNK1*-336 aa, 34 pS) is expressed more abundantly in ventricles and Purkinje fibers than in atria [97, 98]. These channels conduct an inwardly rectifying outward K^+ current and have been implicated in cardiac arrhythmias, e.g., Brugada syndrome and right ventricular arrhythmia [73].

K_{2P}2.1 (TREK-1, Gene - *KCNK2*, 426 aa, 100 pS) [99, 100] is a TWIK-related channel and is expressed differentially in the three layers of left ventricle, being higher in the epicardium than in the endocardium [94]. It is present in longitudinal stripes in the SL of ventricular myocytes [100]. K_{2P}2.1 channel underlies an outward K^+ current with weak inward rectification and exhibits mechano-sensitivity [100]. The transmural gradient of K_{2P}2.1 has been proposed to contribute to AP duration and dispersion of repolarization [94, 100].

K_{2P}3.1 (TASK-1, Gene - *KCNK3*, 394 aa, 14 pS) is a TWIK-related acid-sensitive K channel that is expressed strongly in heart. The outward K^+ current mediated by these channels facilitates repolarization [99]. K_{2P}3.1 level in left ventricular mycocytes is increased in experimental left ventricular hypertrophy [65]. I_{TASK-1} is suggested to mediate α_1-adrenergic receptor-mediated prolongation of cardiac repolarization that is inhibited by A293 [101].

1.3.6 Inwardly Rectifying K Channels (2 TM)

The inwardly rectifying K channels allow larger inward currents at potentials negative to E_K than outward currents positive to E_K. They are comprised of four pore-forming α-subunits, K_{ir}, each of which consists of two TM-spanning segments. The K channels form homo-tetramers, although some members also form hetero-tetramers. Seven subfamilies of Kir channels have been identified: $K_{ir}1.x$–$K_{ir}7.x$.

$K_{ir}2.x$ families have four subfamilies, $K_{ir}2.1$–$K_{ir}2.4$, and their inwardly rectifying K^+ currents contribute significantly to I_{K1} [102]. $K_{ir}3.x$ family has four channel types identified as $K_{ir}3.1$, $K_{ir}3.2$, $K_{ir}3.3$, and $K_{ir}3.4$, also called GIRK1, GIRK2, GIRK3, and GIRK4, respectively. The $K_{ir}3$ channels are coupled to G-proteins. $K_{ir}6.x$ (K_{ATP}) family has two members, $K_{ir}6.1$ and $K_{ir}6.2$. Functional $K_{ir}6.x$ channels form hetero-multimers of octameric conformation with four auxiliary subunits, the sulfonylurea receptors (SUR) binding sites for glibenclamide and diazoxide. The following K_{ir} family members are expressed in the heart.

K_{ir}2.1 (IRK1, Gene - *KCNJ2*, 427 aa, 21 pS) has a higher expression in ventricles than in atria. Other $K_{ir}2.x$ members and $K_{ir}4.1$ serve as its heteromeric pore-forming domain. $K_{ir}2.1$ channel K^+ outward current is the major contributor to I_{K1} and contributes to the repolarization phase of the AP and maintenance of resting potential in ventricles and atria [103, 104]. $K_{ir}2.1$ is associated with several rhythm disorders, including AF, left ventricular hypertrophy, and Andersen–Tawil syndrome (LQT7) [65, 66, 105] and SQT3.

K_{ir}2.2 (IRK2, Gene - *KCNJ12*, 433 aa, 34.2 pS) is expressed in ventricles and atria [9, 103, 106]. $K_{ir}2.1$ serves as a heteromeric pore-forming subunit for $K_{ir}2.2$. K^+ outward current due to $K_{ir}2.2$ contributes partly to I_{K1} and facilitates repolarization of AP and maintenance of resting potential [103].

K_{ir}2.3 (IRK3, Gene - *KCNJ4*, 445 aa, 13 pS) forms complexes with other $K_{ir}2.x$ subunits [9, 107–109]. It also contributes to I_{K1} and, thus, to repolarization phase and resting potential. $K_{ir}2.3$ is associated with several types of cardiac arrhythmias including Andersen's syndrome [102, 108].

K_{ir}3.1 (GIRK1, Gene - *KCNJ3*, 501 aa, 42 pS) is abundant in SA node, AV node, and atria [110, 111]. $K_{ir}3.1$ is electrically silent and forms functional heteromers with the pore-forming subunits, $K_{ir}3.2$, $K_{ir}3.3$, or $K_{ir}3.4$, with virtually identical conductances, kinetics, and Gβγ sensitivities [111]. M_2R stimulation leads to Gβ-γ-mediated activation of heteromeric $K_{ir}3.1$ channel, causing an outward K^+ current (I_{KACh}), which brings about SA nodal cellular hyperpolarization, AV conduction delay, atrial hyperpolarization, and negative chronotropy [112].

K_{ir}3.2 (GIRK2. Gene - *KCNJ6*, 423 aa, 30 pS) is primarily a brain-type channel but its splice variants are also reported in SA node and atria [113]. $K_{ir}3.2$ is activated by M_2R-mediated Gβγ and RGS4 pathways and induces $I_{KACh,}$ causing bradycardia due to the hyperpolarization of SAN cells [113].

K_{ir}3.4 (GIRK4, Gene - *KCNJ5*, 419 aa, 15–30 pS) can form homomeric channels but usually forms heteromers with $K_{ir}3.1$, $K_{ir}3.2$, and $K_{ir}3.3$. It assembles in heart as hetero-tetramers with $K_{ir}3.1$ [114]. The $K_{ir}3.4/K_{ir}3.1$ heteromeric channels are strongly activated by Gβγ subunits of G protein that mediate the M_2 receptor stimulation by ACh, resulting in the activation of I_{KACh} [111]. A decrease in I_{KACh} prevents, while its increase favors the occurrence of AF in GIRK4 knock-out mice [57, 115–117]. It is, therefore, suggested that I_{KACh} has a potential role in clinical AF ([118], See Chap. 28).

K_{ir}6.1 (KATP, Gene - *KCNJ8*, 424 aa, 33 pS) forms hetero-multimeric complex with four auxiliary subunits, SUR2B. These channels are activated by low ($<10^{-5}$ M) concentrations of intracellular ATP but inhibited by its higher ($>10^{-4}$ M) concentrations [119]. $K_{ir}6.1$ channels are reported in atria and ventricles, they are distributed in the sarcolemma of cardiac myocytes and are associated with maladaptive cardiac remodeling [120].

$K_{ir}6.2$ (KATP, Gene - *KCNJ11*, 390 aa, 79 pS) forms hetero-multimers with SUR2A in the heart and causes the repolarizing I_{KATP} [121]. $K_{ir}6.2$ and SUR2A subunits predominate in the sarcolemma of ventricular and atrial myocytes [122]. While $K_{ir}6.2$ is the K channel, SUR2A acts as the sensor for intracellular ATP and ADP levels and modulates the activity of the former, thereby determining the amplitude of I_{KATP}, the membrane potential, and APD. K_{ATP} channels play important roles in normal myocardial function and in several acquired and inherited cardiac disorders, viz. AF, cardiomyopathy, HF, and poor adaptability to stress-induced cardiac dysfunction [123]. The sarcolemmal $K_{ir}6.2$/SUR2A is reported to facilitate protection from ischemia–reperfusion cardiac injury [124].

1.3.7 Cyclic Nucleotide-Regulated Channels

Two groups of channels belong to the superfamily of cyclic nucleotide-regulated (CNG) channels: (1) cyclic nucleotide-gated (CNG) channels and (2) hyperpolarization-activated, cyclic nucleotide-gated (HCN) channels [9].

CNG Channels: These cation channels are expressed as hetero-tetramers comprised of homologous six TM A subunits (CNGA1–CNGA4) with six TM B subunits (CNGB1 and CNGB3). A cyclic nucleotide-binding domain (CNBD) located on the cytosolic C terminal serves as the site for activation by cAMP or cGMP. CNG channels are permeable to monovalent cations Na^+ and K^+ and also to Ca^{2+}. CNGA2 (Gene - *CNGA2*, 664 aa, 35 pS) is expressed, though feebly, in myocardial sarcolemma [125]. CNGA2 is permeable to $Ca^{2+,}$ but its physiological significance is unknown.

HCN channels: Four types of HCN channels, HCN1–HCN4, are identified in cardiac and neuronal tissues [126]. HCN channels are homo- or hetero-tetramers of subunits comprised of six TM segments, S1–S6, with S4 acting as the voltage sensor. The four monomeric subunits are arranged around a central pore lined by their S6 TM segments. The N and C termini of the subunits are cytosolic, the latter having a crucial role in channel regulation by cAMP. A cyclic nucleotide-binding domain on the C terminus serves as the binding site for cAMP and has a key role in the channel activity. Membrane potentials in the hyperpolarized range (negative to resting potential) activate these channels. HCN channels are permeable to monovalent cations, K^+ and Na^+, which upon channel opening, carry an inward depolarizing cation current, contributing to funny (I_f) or hyperpolarizing (I_h) currents. I_f contributes significantly to diastolic depolarization in the pacemaker cells of SAN, AVN, and Purkinje fibers and modulates heart rate and rhythm. Therefore, HCN channels are often called “pacemaker channels”. Sympathetic neurotransmitters, epinephrine, and norepinephrine, stimulate the activity of HCN channels through β-AR-mediated increase in intracellular cAMP level and induce positive chronotropy. The parasympathetic neurotransmitter, ACh, is reported to cause negative chronotropy partly by inhibiting HCN channel activity. Several specific blockers of I_f (bradycardiac agents) have been discovered, exemplified by ivabradine, offering new therapeutic agents to treat sinus tachycardia.

HCN1 (Gene - *HCN1*, 890 aa, 12.9 pS) is expressed feebly in SAN and embryonic ventricular myocytes [9, 126]. MiRP1 serves as an auxiliary subunit.

HCN2 (Gene - *HCN2*, 889 aa, 1.5–35 pS) is also expressed feebly in SAN and is considered to be complimentary to HCN4. HCN2 channels contribute up to 20% to I_f current in mice SAN cells [126, 127]. HCN2 channels are permeable to Na^+ and K^+. Dysfunction of HCN2 is associated with sinus dysrhythmia [127].

HCN4 (Gene - *HCN4*, 1203 aa, 17.5 pS) is expressed predominantly in SAN [128]. MiRP1 is a potential auxiliary subunit. HCN4 has a $V_{0.5}$ of activation of -82 mV and τ of ~2 s when expressed in HEK293 cells [9]. HCN4 contributes up to 80% to I_f in SAN. HCN4 is associated with sick sinus syndrome and other disorders of SAN and AVN and has also been implicated in AF, ventricular tachycardia (VT), and HF [129–132]. The HCN channels are extensively covered in Chap. 4. Mathematical modeling of the role of HCN channels in pacemaker activity of SAN cells is also covered extensively in Chaps. 2 and 3.

1.3.8 Transient Receptor Potential Channels

The mammalian transient receptor potential (TRP) ion channel superfamily is comprised of six protein families, the classical TRP (TRPC), vallinoid receptor (TRPV), melastatin (TRPM), mucolipin (TRPML), polycystin (TRPP), and ankyrin (TRPA1) protein channels. TRP channel α-subunits consist of six α-helical TM segments (S1–S6), the loops between S5 and S6 form the pore. Although S4 in these ion channels lacks classical voltage sensors, several members of the TRP family show voltage-dependent gating [10, 133]. Most of the TRP channels are nonselectively cation permeant, except TRPV5 and TRPV6, which are Ca^{2+} selective, and TRPM4 and TRPM5, which are monovalent cation selective. TRP channels, when in an open state, allow an increase in cytosolic Ca^{2+} and Na^{+} concentrations and depolarize the cell; they are also considered to act as store-operated Ca channels (SOCCs), contribute significantly to cellular Ca^{2+} homeostasis and are implicated in hypertrophy [134]. Several TRP channels are activated by stretch and contribute to mechanoelectrical feedback [135]. Chapter 12 covers the TRP channel in detail.

1.3.9 Chloride Channels

The chloride channels are functionally and structurally diverse, with ubiquitous distribution both on the plasma membrane as well as on intracellular organelles [10, 136, 137]. A surge of research on Cl channels during the past decade has led to the identification of a large variety of these anion channels and their prospective roles in various cellular functions in health and disease. As a consequence, Cl channels are emerging as important targets for new drug discovery for a number of diseases. The mammalian Cl channels identified so far are grouped into five families: Voltage-sensitive Cl channels (ClC), Cystic fibrosis transmembrane conductor regulator (CFTR), Ca^{2+}-activated Cl channels (CaCC), Maxi Cl channels (Maxi Cl), and Volume-regulated Cl channels (VRC, VRAC) [10].

Several types of Cl channels have been described in heart cells, and their special features and roles in cardiac activity are well described in a review [136]. Some salient features of these channels and their relevance to cardiac electrical activity and heart rate and rhythm are discussed below.

ClC-2 channels are responsible for a voltage-activated inwardly rectifying chloride current, $I_{\mathrm{Cl,ir}}$, and are likely to contribute to cell swelling. ClC-2 is expressed in SAN pacemaker cells, Purkinje fibers and atrial and ventricular myocytes [137].

ClC-3 channels elicit a volume-regulated outwardly rectifying Cl^{-} current, $I_{\mathrm{Cl,vol}}$, with two components, the swelling-activated one, $I_{\mathrm{Cl,swell}}$, and the basally activated one, $I_{\mathrm{Cl,b}}$. ClC-1, -2, and -3 channels are expressed in atria and ventricles and $I_{\mathrm{Cl,Swell}}$ is reported in SAN, and atrial and ventricular myocytes [136, 138, 139]. $I_{\mathrm{Cl,Swell}}$ is stretch-sensitive and is thought to play a role in regulating membrane potential, APD, and excitability and has arrhythmogenic potential [139]. They are implicated in VF dynamics in isolated guinea pig heart and exert a protective role in cardiac hypertrophy and HF [140].

CFTR channels are expressed in atria and ventricles and give rise to slightly outwardly rectifying currents named after their activators, namely $I_{\mathrm{Cl,PKA}}$, $I_{\mathrm{Cl,PKC}}$, and $I_{\mathrm{Cl,ATP}}$ [141]. The cAMP/PKA-induced current, $I_{\mathrm{Cl,PKA}}$, was the first Cl channel current recorded in heart cells. The PKC-activated current, $I_{\mathrm{Cl,PKC}}$, has been recorded from ventricular myocytes [142–144]. The extracellular ATP-activated [136] CFTR current, $I_{\mathrm{Cl,ATP}}$, has also been recorded from atria and ventricles. CFTR responsible for $I_{\mathrm{Cl,PKA}}$ are clustered on the z-groove but are not seen on the mouth of T-tubules [144].

I_{CFTR} is associated with early afterdepolarizations (EAD) [139] and is reported to modulate ventricular myocyte contraction rate and is associated with changes in HF [145]. An epicardium-to-endocardium gradient is suggested to exist for CFTR ($I_{\mathrm{Cl,PKA}}$), which is lost in cardiac hypertrophy [146]. The channel is blocked by the scorpion toxin GaTx-1 and activated by nicorandil [10, 147].

CLCA-1 channel-mediated current, $I_{\mathrm{Cl,Ca}}$, has been recorded from ventricular myocytes [148]. $I_{\mathrm{Cl,Ca}}$ has a role in determining membrane potential and membrane excitability in heart cells and contributes to I_{ti} in addition to I_{NCX} (Fig. 1.3). An increase in $I_{\mathrm{Cl,Ca}}$ is reported to be associated with delayed afterdepolarization (DAD) in ventricular myocytes [148] and with left ventricular hypertrophy exhibiting APD prolongation, AP alternans, and T wave alternans, indicating a role of CLCA-1 in arrhythmogenesis [149]. Bestrophin, a member of CaCC group, has several homologues, expressed in a wide variety of cells including myocardium [136, 150] where Best-3 is more predominant than Best-1 and Best-2 [151]. mBest-3 is widely distributed in mouse heart and has a sarcolemmal localization [151]. It is shown to have a putative pore domain and to function like a channel. The bestrophin-induced $I_{\mathrm{Cl,Ca}}$ is time- and voltage-independent and displays slight outward rectification. It is inhibited by niflumic acid and DIDS [10, 151].

THEM16 (anoctamin, ANO), another member of Ca^{2+}-activated Cl channels, has 10 homologues, and THEM16A is expressed in heart [136, 152]. VDAC1, the voltage-dependent anion channel 1, having very high conductance (280–430 pS; [10]) and normally localized on the outer mitochondrial membrane in ventricular myocytes, is also expressed on SL [136].

Acid-activated Cl channels, $I_{\mathrm{Cl,acid}}$, activated by acidic extracellular pH [153], has also been reported in atrial and ventricular myocytes showing outward rectification. Its activation is independent of $[Ca^{2+}]_i$. Since high extracellular pH increases APD and extracellular acidosis accompanies MI-induced arrhythmias, it is likely that $I_{\mathrm{Cl,acid}}$ has a role in the pathophysiology of such arrhythmias [154].

1.3.10 Stretch-Activated Channels

Mechano-sensitive (MSC), mechano-gated (MGC), or stretch-activated (SAC) channels are activated primarily by mechanical stress (mechanical tension) in the membrane [155]. The membrane cytoskeleton is considered to mediate the mechanical stress to the channel protein bringing about the required changes in channel conformation to induce channel opening. Although several members of VGIC and LGIC superfamilies do respond to mechanical stress, they are not categorized as SACs. However, a few members of TRPC and K_{2P} (TWIK) families indeed respond to primary mechanical stimulus and are, therefore, identified as SACs. In the strict sense of SACs, no specific protein has yet been identified as a representative of these channels [155]. It is well recognized that mechano-electric feedback has important roles in the cardiac cycle and is involved in maintaining the heart rate and rhythm under physiological conditions and cardiac rhythm disturbances (see Chap. 7). The mechano-sensitive channels include TREK-1, TRPC1, and TRPV2. These SACs are implicated in AF, DADs, cardiomyopathy, and ventricular arrhythmia [100, 156]. Gadolinium and streptomycin inhibit the activity of SACs, but GsMTx4, a peptide isolated from tarantula venom, is a more specific blocker of SACs and inhibits stretch-induced AF [155].

1.3.11 Gap Junction Channels

The intercalated discs (ICD) on SL between adjacent cardiac myocytes connect the two neighboring cells. Gap junction (GJ) channels are one of the three components of ICDs, the other two being fascia adherens and desmosomes, and provide electrical coupling between adjacent cells (see also Chap. 14). GJ channels are composed of two hemichannels, each one, called connexons, inserted in the SL of two adjoining cells. Each connexon comprises of six domains of connexins arranged concentrically to form a central pore. The connexins themselves are made up of four TM segments, M1–M4 with their N and C termini located intracellularly. Two loops connecting M1 with M2, and M3 with M4 are extracellular, while an intracellular loop connects M2 to M3. Normally GJ channels are located at the terminal poles of myocardial cells and bring about cell-to-cell electrical coupling facilitating impulse conduction along cardiac fibers. GJ channels allow passive diffusion of molecules <1 kDa, e.g., anions, cations, nutrients, metabolites, and second messengers (IP_3). Connexins, e.g., Cx43, have a short half-life that may have implications in myocardial excitability [157]. GJ channels are named after their constituent connexin (Cx) followed by numerals that denote its molecular weight, e.g., Cx40 meaning connexin of 40 kDa. Twenty-one connexins are expressed in humans, only four being expressed in the heart, viz. Cx30, Cx40, Cx43, and Cx45 [158, 159]. Cx30 is weakly expressed in SAN central cells and contributes to the regulation of pacemaker activity and heart rate [160]. Cx40 is expressed in the SAN peripheral cells and atrial myocytes [157–159]. Cx43 is a protein expressed mainly in the ventricles, but also to alesser extent in the atria and the periphery of SAN [158, 159]. Cx45 is expressed in AVN cells and in the SAN peripheral cells. Cx30.2, Cx40, and Cx45 are expressed in AVN and His-bundle and contribute to supra-Hisian and infra-Hisian impulse conduction in mice, as evident from ECG changes in Cx30.2/Cx40 deficient animals [161].

Connexins play a key role in impulse conduction in the entire heart, maintaining specific regional conduction requirements necessary for a coordinated cardiac contraction underlying a normal heart rate. Alterations in the expression pattern of specific connexins herald several cardiac rhythm disorders including AF, ischemia–reperfusion injury, and congestive heart failure (CHF) [66]. Chapter 14 provides an account of GJ channels in cardiac disorders.

1.4 Sarcoplasmic Reticulum Membrane Ion Channels

SR membrane is endowed with the capability of contributing to fine maintenance of cytosolic free Ca^{2+} concentration and to make free Ca^{2+} available at strategic locations necessary for the performance of cellular functions. To this end, the SR membrane possesses two major types of Ca^{2+}-release channels, ryanodine receptor channels (RyR) and inositol trisphosphate receptor channels (InsP3R). The SR membrane Ca^{2+}-ATPase (SERCA2) takes up excess Ca^{2+} from cytosol and fills the SR Ca stores. This topic is covered in Chap. 21.

1.4.1 Ryanodine Receptor Channels

The RyRs are ubiquitously distributed. Three types of RyRs have been identified, namely RyR1, RyR2, and RyR3, which represent large (~558 kDa) structurally related tetrameric membrane-spanning proteins, which co-assemble with four calstabin (FKBP12) proteins [10, 162]. The RyR channels form a mushroom-like structure and the bulk of their protein lies on the cytosolic surface of SR. Significant advances have been made in resolving the pore structure of RyRs using high-resolution cryo-electron microscopy [163]. RyR2, the main cardiac Ca^{2+} release channel, plays a key role in E–C coupling by releasing the required amount of Ca^{2+} in the cytosol following SL influx of Ca^{2+} through $Ca_V1.2$ channels localized in T-tubules (Fig. 1.2). RyR2 and RyR3 are also expressed in SAN and Purkinje fiber cells, contributing to the pacemaker activity of the former [164, 165], and impulse conduction in the latter, thereby contributing to regulation of heart rate and rhythm. RyR2 is implicated in several acquired and inherited cardiac rhythm disorders, e.g., arrhythmogenic right ventricular cardiomyopathy type 2 (ARVC2), CPVT, AF, and abnormal sinus rhythm [166, 167]. It is suggested that changes in RyR2 in the His-Purkinje system underlie CPVT [165]. RyR2 channels are blocked by ryanodine, dantrolene, ruthenium red, tetracaine, and lidocaine and are activated by caffeine. Treatability of CPVT-like condition by tetracaine in mice shows that RyR2 is a promising target for developing novel antiarrhythmic drugs [165, 168]. Chapter 5 describes the role of RyRs in the pacemaker activity of the SA node.

1.4.2 SR Inositol Trisphosphate Receptor Channels

Out of several isoforms of $InsP_3R$, heart expresses $InsP_3R2$, a 300 kDa protein that co-assembles to form a tetrameric channel. $InsP_3R2$ is expressed in atria, ventricles, and Purkinje fibers albeit at a lower density than RyR2. $InsP_3R2$ is suggested to fine-tune the perinuclear Ca and activate CaMKII to modulate transcription mechanisms of nucleus [27, 169]. Such a role of $InsP_3R2$ in excitation–transcription coupling may be involved in gene expression alterations during cardiac disorders like ventricular hypertrophy and HF. RyR2 and $InsP_3R2$ have distinct functions to perform in heart and modulate heart rhythm via altogether different mechanisms (see also Chap. 21).

1.5 Mitochondrial and Nuclear Channels

Mitochondria serve as the energy center of heart cells and also regulate cardiac electrical activity by modulating the SL ion channel kinetics. The mitochondrial membranes express several ion channels with crucial roles in normal and pathological cardiac activity including arrhythmogenesis [170]. Given below are some of the predominant mitochondrial and nuclear ion channels (see also Chap. 21).

K_{Ca}1.1 (Slo, BK, Gene - *KCNMA1*, 1182 aa, 200–220 pS) has Slack as its heteromeric pore-forming subunit and β1–β4 serve as auxiliary subunits [9]. It is activated both by voltage and intracellular Ca^{2+} and is blocked by TEA, charybdotoxin, and iberiotoxin. K_{Ca}1.1 is expressed in inner mitochondrial membrane in heart and plays a significant role in myocardial energetics. Openers of K_{Ca}1.1 are reported to protect the ventricles from ischemia–reperfusion injury and open the possibility of developing new drugs to treat cardiac disorders [170].

K_{ir}6.1, K_{ir}6.2 (K_{ATP}), and SUR2A Subunits are expressed in mitochondria and are associated with protection from ischemia–reperfusion injuries [124]. In addition, voltage-dependent anion channels, VDAC, are expressed prominently in the mitochondrial outer membrane.

The nucleus in cardiomyocytes serves as the seat of transcription, and the nuclear membrane and nucleoplasmic reticulum have key roles in excitation–transcription coupling [169]. Both the nuclear membrane and the nucleoplasmic reticulum express several ion channels, including RyR, InsP3R, R-type Ca channels, and K channels [171].

1.6 Conclusions

Our present knowledge of the molecular basis of the heart's electrical activity owes greatly to the analytical approach in identifying the ion channels and other transport proteins expressed at mRNA and protein levels in the sarcolemma of different types of heart cells. The roles of SR, mitochondrial, and nuclear membrane ion transport proteins in cardiac cellular activity during normal and abnormal cardiac rhythm are also better understood now. Future research on analytical and integrative aspects of “ion channels, ion transporters, signaling cascades, mechanical function, energy metabolism, transcription, translation and targeting” [172] (Fig. 1.2) is expected to provide a better picture of the molecular basis of ionic mechanisms underlying electrical activity during a cardiac cycle in health and disease. Because most of the studies on cardiac ion channels in SR, mitochondria, and nucleus have been carried out on ventricular myocytes, the need for research on these aspects of cells from other regions of heart cannot be overemphasized. An important problem, however, concerns differences in the ion channel compliments of the same type of cardiac tissue in different mammalian species limiting extrapolation of data from laboratory animals to humans. It is hoped that future research will overcome this issue by identifying the entire compliment of human cardiac ion channel signature and also establish their role in arrhythmias including channelopathies. The other problem concerns reported disparities between the ion channel mRNA and protein expression levels in different regions of heart and functional aspects of the expressed channel proteins. Thus, for example, we do not yet fully know about the molecular components of all the ionic currents recorded in different types of heart cells in mammals, including humans, let alone their precise contributions to AP configuration and ECG waveform. Ongoing research is expected to provide a better understanding of these important aspects. This will also help identify and validate new target molecules that could be explored by employing the newly developed ion channel-high throughput screening and related technologies to discover novel and better antiarrhythmic drugs.

Acknowledgments The author is thankful to the generous financial support from Life Sciences Academy, Lucknow, India, for the preparation of this manuscript.

References

1. Landes EM. Carl John Wiggers: a biographical memoir. Washington DC: National Academy of Sciences; 1976.
2. Trautwein W, McDonald TF, Tripathi O. Calcium conductance and tension in mammalian ventricular muscle. Pflugers Arch. 1975;354:55–74.
3. Noujaim SF, Lucca E, Munoz V, Persaud D, Berenfeld O, Meijler FL, et al. From mouse to whale: a universal scaling relation for the PR interval of the electrocardiogram of mammals. Circulation. 2004;110:2802–8.
4. Postema PG, Ritsema van Eck HJ, Opthof T, van Herpen G, van Dessel PF, Priori SG, et al. IK1 modulates the U-wave: insights in a 100-year-old enigma. Heart Rhythm. 2009;6:393–400.
5. Nerbonne JM, Kass RS. Molecular physiology of cardiac repolarization. Physiol Rev. 2005;85(4): 1205–53.
6. Gaborit N, Le Bouter S, Szuts V, Varro A, Escande D, Nattel S, et al. Regional and tissue specific transcript signatures of ion channel genes in the non-diseased human heart. J Physiol. 2007;582(Pt 2): 675–93.
7. Amin AS, Tan HL, Wilde AA. Cardiac ion channels in health and disease. Heart Rhythm. 2010;7(1): 117–26.
8. Varró A, Tomek J, Nagy N, Virag L, Passini E, Rodriguez B, et al. Cardiac transmembrane ion channels and action potentials: cellular physiology and arrhythmogenic behavior. Physiol Rev. 2020;101(3):1083–176.
9. IUPHAR database of G protein coupled receptors and ion channels (2009). http://www.iuphar-db.org/DATABASE/
10. Alexander SP, Mathie A, Peters JA. Guide to receptors and channels (GRAC), 5th edn. Br J Pharmacol. 2011;164(Suppl 1):S1–324.
11. Alexander SP, Mathie A, Peters JA, Veale EL, Striessnig J, Kelly E, et al. The concise guide to pharmacology 20/21: ion channels. Br J Pharmacol. 2021;178(Suppl 1):S157–245.
12. Maier SK, Westenbroek RE, Schenkman KA, Feigl EO, Scheuer T, Catterall WA. An unexpected role for brain-type sodium channels in coupling of cell surface depolarization to contraction in the heart. Proc Natl Acad Sci USA. 2002;99(6):4073–8.
13. Maier SK, Westenbroek RE, Yamanushi TT, Dobrzynski H, Boyett MR, Catterall WA, Scheuer T. An unexpected requirement for brain-type sodium channels for control of heart rate in the mouse sinoatrial node. Proc Natl Acad Sci USA. 2003;100(6): 3507–12.
14. Lei M, Jones SA, Liu J, Lancaster MK, Fung SS, Dobrzynski H, et al. Requirement of neuronal- and cardiac-type sodium channels for murine sinoatrial node pacemaking. J Physiol. 2004;559:835–48.
15. Maltsev VA, Kyle JW, Undrovinas A. Late Na+ current produced by human cardiac Na+ channel isoform Nav1.5 is modulated by its beta1 subunit. J Physiol Sci. 2009;59(3):217–25.
16. Lei M, Huang CL, Zhang Y. Genetic Na+ channelopathies and sinus node dysfunction. Prog Biophys Mol Biol. 2008;98:171–8.
17. Burbidge SA, Dale TJ, Powell AJ, Whitaker WR, Xie XM, Romanos MA, et al. Molecular cloning, distribution and functional analysis of the NaV1.6. Voltage-gated sodium channel from human brain. Brain Res Mol Brain Res. 2002;103:80–90.
18. Prakash P, Tripathi O. Verapamil and TTX inhibit +Vmax but differentially alter the duration of action potential of adult chicken ventricular myocardium. Indian J Biochem Biophys. 1998;35(2):123–30.
19. Haverinen J, Hassinen M, Vornanen M. Fish cardiac sodium channels are tetrodotoxin sensitive. Acta Physiol. 2007;191(3):197–204.

20. Hofmann F, Biel M, Flockerzi V. Molecular basis for Ca2+ channel diversity. Annu Rev Neurosci. 1994;17:399–418.
21. Murakami M, Ohba T, Takahashi Y, Watanabe H, Miyoshi I, Nakayama S, et al. Identification of a cardiac isoform of the murine calcium channel alpha1C (Cav1.2-a) subunit and its preferential binding with the beta2 subunit. J Mol Cell Cardiol. 2006;41(1):115–25.
22. Foell JD, Balijepalli RC, Delisle BP, Yunker AM, Robia SL, Walker JW, et al. Molecular heterogeneity of calcium channel beta-subunits in canine and human heart: evidence for differential subcellular localization. Physiol Genomics. 2004;17(2):183–200.
23. Irisawa H, Brown HF, Giles W. Cardiac pacemaking in the sinoatrial node. Physiol Rev. 1993;73(1):197–227.
24. McDonald TF, Pelzer S, Trautwein W, Pelzer DJ. Regulation and modulation of calcium channels in cardiac, skeletal, and smooth muscle cells. Physiol Rev. 1994;74(2):365–507.
25. Dai S, Hall DD, Hell JW. Supramolecular assemblies and localized regulation of voltage-gated ion channels. Physiol Rev. 2009;89(2):411–52.
26. Wu Y, Temple J, Zhang R, Dzhura I, Zhang W, Trimble R, et al. Calmodulin kinase II and arrhythmias in a mouse model of cardiac hypertrophy. Circulation. 2002;106:1288–93.
27. Prakash O, Gupta N, Milburn A, McCormick L, Deugi V, Fisch P, et al. Calmodulin variant E140G associated with long QT syndrome impairs CaMKIIδ autophosphorylation and L-type calcium channel inactivation. J Biol Chem. 2023;299(1):102777.
28. Zhang Z, Xu Y, Song H, Rodriguez J, Tuteja D, Namkung Y, et al. Functional roles of Cav1.3 (alpha(1D)) calcium channel in sinoatrial nodes: insight gained using gene-targeted null mutant mice. Circ Res. 2002;90(9):981–7.
29. Mangoni ME, Nargeot J. Genesis and regulation of the heart automaticity. Physiol Rev. 2008;88(3):919–82.
30. Qu Y, Baroudi G, Yue Y, El-Sherif N, Boutjdir M. Localization and modulation of {alpha} 1D (CaV1.3) L-type Ca channel by protein kinase A. Am J Physiol Heart Circ Physiol. 2005;288(5):H2123–30.
31. Singh A, Gebhart M, Fritsch R, Sinnegger-Brauns MJ, Poggiani C, Hoda JC, et al. Modulation of voltage- and Ca2+-dependent gating of CaV1.3 L-type calcium channels by alternative splicing of a C-terminal regulatory domain. J Biol Chem. 2008;283(30):20733–44.
32. Platzer J, Engel J, Schrott-Fischer A, Stephan K, Bova S, Chen H, et al. Congenital deafness and sinoatrial node dysfunction in mice lacking class D L-type Ca2+ channels. Cell. 2000;102(1):89–97.
33. Mitchell JW, Larsen JK, Best PM. Identification of the calcium channel alpha 1E (CaV2.3) isoform expressed in atrial myocytes. Biochim Biophys Acta. 2002;1577(1):17–26.
34. Ono K, Iijima T. Cardiac T-type Ca2+ channels in the heart. J Mol Cell Cardiol. 2010;48(1):65–70.
35. EmerickMC SR, Kunze R, McNultyMM RMR, Hanck DA, et al. Profiling the array of CaV3.1 variants from the human T-type calcium channel gene CACNA1G: alternative structures, developmental expression, and biophysical variations. Proteins. 2006;64(2):320–42.
36. McGivern JG. Pharmacology and drug discovery for T-type calcium channels. CNS Neurol Disord Drug Targets. 2006;5(6):587–603.
37. Cribbs LL, Lee JH, Yang J, Satin J, Zhang Y, Daud A, et al. Cloning and characterization of alpha1H from human heart, a member of the T-type Ca2+ channel gene family. Circ Res. 1998;83(1):103–9.
38. Maturana A, Lenglet S, Python M, Kuroda S, Rossier MF. Role of the T-type calcium channel CaV3.2 in the chronotropic action of corticosteroids in isolated rat ventricular myocytes. Endocrinology. 2009;150(8):3726–34.
39. Stühmer W, Ruppersberg JP, Schröter KH, Sakmann B, Stocker M, Giese KP, et al. Molecular basis of functional diversity of voltage-gated potassium channels in mammalian brain. EMBO J. 1989;8(11):3235–44.
40. Roberds SL, Tamkun MM. Cloning and tissue-specific expression of five voltage-gated potassium channel cDNAs expressed in rat heart. Proc Natl Acad Sci USA. 1991;88(5):1798–802.
41. Leoni AL, Marionneau C, Demolombe S, Le Bouter S, Mangoni ME, Escande D, et al. Chronic heart rate reduction remodels ion channel transcripts in the mouse sinoatrial node but not in the ventricle. Physiol Genomics. 2005;24(1):4–12.
42. Matsubara H, Liman ER, Hess P, Koren G. Pretranslational mechanisms determine the type of potassium channels expressed in the rat skeletal and cardiac muscles. J Biol Chem. 1991;266(20):13324–8.
43. Grissmer S, Nguyen AN, Aiyar J, Hanson DC, Mather RJ, Gutman GA, et al. Pharmacological characterization of five cloned voltage-gated K+ channels, types Kv1.1, 1.2, 1.3, 1.5, and 3.1, stably expressed in mammalian cell lines. Mol Pharmacol. 1994;45(6):1227–34.
44. Brahmajothi MV, Morales MJ, Rasmusson RL, Campbell DL, Strauss HC. Heterogeneity in K+ channel transcript expression detected in isolated ferret cardiac myocytes. Pacing Clin Electrophysiol. 1997;20(2 Pt 2):388–96.
45. Lee JK, Nishiyama A, Kambe F, Seo H, Takeuchi S, Kamiya K, et al. Downregulation of voltage-gated K + channels in rat heart with right ventricular hypertrophy. Am J Physiol. 1999;277(5 Pt 2):H1725–31.
46. Tamkun MM, Knoth KM, Walbridge JA, Kroemer H, Roden DM, Glover DM. Molecular

cloning and characterization of two voltage-gated K+ channel cDNAs from human ventricle. FASEB J. 1991;5(3):331–7.

47. Brahmajothi MV, Morales MJ, Liu S, Rasmusson RL, Campbell DL, Strauss HC. In situ hybridization reveals extensive diversity of K+ channel mRNA in isolated ferret cardiac myocytes. Circ Res. 1996;78 (6):1083–9.
48. Han W, Wang Z, Nattel S. A comparison of transient outward currents in canine cardiac Purkinje cells and ventricular myocytes. Am J Physiol Heart Circ Physiol. 2000;279(2):H466–74.
49. O'Connell KM, Whitesell JD, Tamkun MM. Localization and mobility of the delayed-rectifer K+ channel Kv2.1 in adult cardiomyocytes. Am J Physiol Heart Circ Physiol. 2008;294(1): H229–37.
50. Roberds SL, Knoth KM, Po S, Blair TA, Bennett PB, Hartshorne RP, et al. Molecular biology of the voltage-gated potassium channels of the cardiovascular system. J Cardiovasc Electrophysiol. 1993;4(1): 68–80.
51. Niwa N, Nerbonne JM. Molecular determinants of cardiac transient outward potassium current (Ito) expression and regulation. J Mol Cell Cardiol. 2010;48(1):12–25.
52. Huang B, Qin D, El-Sherif N. Spatial alterations of Kv channels expression and K+ currents in post-MI remodeled rat heart. Cardiovasc Res. 2001;52(2): 246–54.
53. Matsubara H, Suzuki J, Inada M. Shaker-related potassium channel, Kv1.4, mRNA regulation in cultured rat heart myocytes and differential expression of Kv1.4 and Kv1.5 genes in myocardial development and hypertrophy. J Clin Invest. 1993;92: 1659–66.
54. Dobrzynski H, Rothery SM, Marples DD, Coppen SR, Takagishi Y, Honjo H, et al. Presence of the Kv1.5 K+ channel in the sinoatrial node. J Histochem Cytochem. 2000;48(6):769–80.
55. Ordög B, Brutyó E, Puskás LG, Papp JG, Varró A, Szabad J, et al. Gene expression profiling of human cardiac potassium and sodium channels. Int J Cardiol. 2006;111(3):386–93.
56. Snyders DJ, Tamkun MM, Bennett PB. A rapidly activating and slowly inactivating potassium channel cloned from human heart. Functional analysis after stable mammalian cell culture expression. J Gen Physiol. 1993;101(4):513–43.
57. Van Wagoner DR, Pond AL, McCarthy PM, Trimmer JS, Nerbonne JM. Outward K+ current densities and Kv1.5 expression are reduced in chronic human atrial fibrillation. Circ Res. 1997;80(6):772–81.
58. Kalman K, Nguyen A, Tseng-Crank J, Dukes ID, Chandy G, Hustad CM, et al. Genomic organization, chromosomal localization, tissue distribution, and biophysical characterization of a novel mammalian Shaker-related voltage-gated potassium channel, Kv1.7. J Biol Chem. 1998;273(10):5851–7.
59. Finol-Urdaneta RK, Strüver N, Terlau H. Molecular and functional differences between heart mKv1.7 channel isoforms. J Gen Physiol. 2006;128(1): 133–45.
60. Bardien-Kruger S, Wulff H, Arieff Z, Brink P, Chandy KG, Corfield V. Characterisation of the human voltage-gated potassium channel gene, KCNA7, a candidate gene for inherited cardiac disorders, and its exclusion as cause of progressive familial heart block I (PFHBI). Eur J Hum Genet. 2002;10(1):36–43.
61. Tian S, Liu W, Wu Y, Rafi H, Segal AS, Desir GV. Regulation of the voltage-gated K+ channel KCNA10 by KCNA4B, a novel beta-subunit. Am J Physiol Renal Physiol. 2002;283(1):F142–9.
62. Yao X, Liu Y, Tung F, Desir GV. Genomic structure and regulation of Kcn1, a cGMP-gated potassium channel. Am J Physiol. 1996;271(1 Pt 2):F37–41.
63. Iwasa H, Kurabayashi M, Nagai R, Nakamura Y, Tanaka T. Genetic variations in five genes involved in the excitement of cardiomyocytes. J Hum Genet. 2001;46(9):549–52.
64. Rosati B, Dong M, Cheng L, Liou SR, Yan Q, Park JY, et al. Evolution of ventricular myocyte electrophysiology. Physiol Genomics. 2008;35:262–72.
65. Marionneau C, Brunet S, Flagg TP, Pilgram TK, Demolombe S, Nerbonne JM. Distinct cellular and molecular mechanisms underlie functional remodeling of repolarizing K+ currents with left ventricular hypertrophy. Circ Res. 2008;102(11): 1406–15.
66. Maguy A, Le Bouter S, Comtois P, Chartier D, Villeneuve L, Wakili R, et al. Ion channel subunit expression changes in cardiac Purkinje fibers: a potential role in conduction abnormalities associated with congestive heart failure. Circ Res. 2009;104(9): 1113–22.
67. Suzuki H, Momoi N, Ono T, Maeda S, Shikama Y, Matsuoka I, Suzuki H, Kimura J, et al. Inhibitory effect of thiopental on ultra-rapid delayed rectifier K + current in H9c2 cells. J Pharmacol Sci. 2005;99(2): 177–84.
68. Takeuchi S, Takagishi Y, Yasui K, Murata Y, Toyama J, Kodama I. Voltage-gated K+ channel, Kv4.2, localizes predominantly to the transverse-axial tubular system of the rat myocyte. J Mol Cell Cardiol. 2000;32(7):1361–9.
69. Postma AV, Bezzina CR, de Vries JF, Wilde AA, Moorman AF, Mannens MM. Genomic organisation and chromosomal localisation of two members of the KCND ion channel family, KCND2 and KCND3. Hum Genet. 2000;106(6):614–9.
70. Birnbaum SG, Varga AW, Yuan LL, Anderson AE, Sweatt JD, Schrader LA. Structure and function of Kv4-family transient potassium channels. Physiol Rev. 2004;84(3):803–33.
71. Dilks D, Ling HP, Cockett M, Sokol P, Numann R. Cloning and expression of the human kv4.3 potassium channel. J Neurophysiol. 1999;81(4):1974–7.

72. Kääb S, Dixon J, Duc J, Ashen D, Näbauer M, Beuckelmann DJ, et al. Molecular basis of transient outward potassium current downregulation in human heart failure: a decrease in Kv4.3 mRNA correlates with a reduction in current density. Circulation. 1998;98(14):1383–93.
73. Gaborit N, Wichter T, Varro A, Szuts V, Lamirault G, Eckardt L, et al. Transcriptional profiling of ion channel genes in Brugada syndrome and other right ventricular arrhythmogenic diseases. Eur Heart J. 2009;30(4):487–96.
74. Abbott GW, Xu X, Roepke TK. Impact of ancillary subunits on ventricular repolarization. J Electrocardiol. 2007;40(6 Suppl):S42–6.
75. Sanguinetti MC, Curran ME, Zou A, Shen J, Spector PS, Atkinson DL, et al. Coassembly of K(V)LQT1 and minK (IsK) proteins to form cardiac IKs potassium channel. Nature. 1996;384(6604):80–3.
76. Keating MT, Sanguinetti MC. Molecular and cellular mechanisms of cardiac arrhythmias. Cell. 2001;104 (4):569–80.
77. Bellocq C, van Ginneken AC, Bezzina CR, Alders M, Escande D, Mannens MM, et al. Mutation in the KCNQ1 gene leading to the short QT-interval syndrome. Circulation. 2004;109(20):2394–7.
78. Abbott GW, Sesti F, Splawski I, Buck ME, Lehmann MH, Timothy KW, et al. MiRP1 forms IKr potassium channels with HERG and is associated with cardiac arrhythmia. Cell. 1999;97(2):175–87.
79. Jones EM, Roti Roti EC, Wang J, Delfosse SA, Robertson GA. Cardiac IKr channels minimally comprise hERG 1a and 1b subunits. J Biol Chem. 2004;279(43):44690–4.
80. Sanguinetti MC, Tristani-Firouzi M. hERG potassium channels and cardiac arrhythmia. Nature. 2006;440(7083):463–9.
81. Tuteja D, Xu D, Timofeyev V, Lu L, Sharma D, Zhang Z, et al. Differential expression of small-conductance Ca2+-activated K+ channels SK1, SK2, and SK3 in mouse atrial and ventricular myocytes. Am J Physiol Heart Circ Physiol. 2005 Dec;289(6):H2714–23.
82. Wulff H, Kolski-Andreaco A, Sankaranarayanan A, Sabatier JM, Shakkottai V. Modulators of small- and intermediate-conductance calcium-activated potassium channels and their therapeutic indications. Curr Med Chem. 2007;14(13):1437–57.
83. Xu Y, Tuteja D, Zhang Z, Xu D, Zhang Y, Rodriguez J, et al. Molecular identification and functional roles of a Ca2+-activated K+ channel in human and mouse hearts. J Biol Chem. 2003;278(49): 49085–94.
84. Chen MX, Gorman SA, Benson B, Singh K, Hieble JP, Michel MC, et al. Small and intermediate conductance Ca2+-activated K+ channels confer distinctive patterns of distribution in human tissues and differential cellular localisation in the colon and corpus cavernosum. Naunyn Schmiedebergs Arch Pharmacol. 2004;369(6):602–15.
85. Li N, Timofeyev V, Tuteja D, Xu D, Lu L, Zhang Q, et al. Ablation of a Ca2+-activated K+ channel (SK2 channel) results in action potential prolongation in atrial myocytes and atrial fibrillation. J Physiol. 2009;587(Pt 5):1087–100.
86. Bhattacharjee A, Joiner WJ, Wu M, Yang Y, Sigworth FJ, Kaczmarek LK. Slick (Slo2.1), a rapidly-gating sodium-activated potassium channel inhibited by ATP. J Neurosci. 2003;23(37): 11681–91.
87. Mistry DK, Tripathi O, Chapman RA. Kinetic properties of unitary Na+-dependent K+ channels in inside-out patches from isolated guinea-pig ventricular myocytes. J Physiol. 1997;500(Pt 1):39–50.
88. Kameyama M, Kakei M, Sato R, Shibasaki T, Matsuda H, Irisawa H. Intracellular Na+ activates a K+ channel in mammalian cardiac cells. Nature. 1984;309(5966):354–6.
89. Mistry DK, Tripathi O, Chapman RA. The occurrence of stable subconductance levels in Na+-activated K+ channels in excised membrane patches from guinea-pig ventricular myocytes. Exp Physiol. 1996;81(6):899–907.
90. Chen H, Kronengold J, Yan Y, Gazula VR, Brown MR, Ma L, et al. The N-terminal domain of Slack determines the formation and trafficking of Slick/Slack heteromeric sodium-activated potassium channels. J Neurosci. 2009;29(17):5654–65.
91. Yuan A, Santi CM, Wei A, Wang ZW, Pollak K, Nonet M, et al. The sodium-activated potassium channel is encoded by a member of the Slo gene family. Neuron. 2003;37(5):765–73.
92. Mori K, Kobayashi S, Saito T, Masuda Y, Nakaya H. Inhibitory effects of class I and IV antiarrhythmic drugs on the Na+-activated K+ channel current in guinea pig ventricular cells. Naunyn Schmiedebergs Arch Pharmacol. 1998;358(6):641–8.
93. Dai L, Garg V, Sanguinetti MC. Activation of Slo2.1 channels by niflumic acid. J Gen Physiol. 2010;135 (3):275–95.
94. Tan JH, Liu W, Saint DA. Differential expression of the mechanosensitive potassium channel TREK-1 in epicardial and endocardial myocytes in rat ventricle. Exp Physiol. 2004;89(3):237–42.
95. Gurney A, Manoury B. Two-pore potassium channels in the cardiovascular system. Eur Biophys J. 2009;38(3):305–18.
96. Charpentier F. Understanding the cardiac role of K2P channels: a new TASK for electro-physiologists. Cardiovasc Res. 2007;75(1):5–6.
97. Lesage F, Guillemare E, Fink M, Duprat F, Lazdunski M, Romey G, et al. TWIK-1, a ubiquitous human weakly inward rectifying K+ channel with a novel structure. EMBO J. 1996;15(5):1004–11.
98. Wang Z, Yue L, White M, Pelletier G, Nattel S. Differential distribution of inward rectifier potassium channel transcripts in human atrium versus ventricle. Circulation. 1998;98(22):2422–8.

99. Lesage F, Lazdunski M. Molecular and functional properties of two-pore-domain potassium channels. Am J Physiol Renal Physiol. 2000;279(5):F793–801.
100. Li XT, Dyachenko V, Zuzarte M, Putzke C, Preisig-Müller R, Isenberg G, et al. The stretch-activated potassium channel TREK-1 in rat cardiac ventricular muscle. Cardiovasc Res. 2006;69(1):86–97.
101. Putzke C, Wemhöner K, Sachse FB, Rinné S, Schlichthörl G, Li XT, et al. The acid-sensitive potassium channel TASK-1 in rat cardiac muscle. Cardiovasc Res. 2007;75(1):59–68.
102. Dhamoon AS, Jalife J. The inward rectifier current (IK1) controls cardiac excitability and is involved in arrhythmogenesis. Heart Rhythm. 2005;2(3):316–24.
103. Zaritsky JJ, Redell JB, Tempel BL, Schwarz TL. The consequences of disrupting cardiac inwardly rectifying K+ current (IK1) as revealed by the targeted deletion of the murine Kir2.1 and Kir2.2 genes. J Physiol. 2001;533(Pt 3):697–710.
104. Hibino H, Inanobe A, Furutani K, Murakami S, Findlay I, Kurachi Y. Inwardly rectifying potassium channels: their structure, function, and physiological roles. Physiol Rev. 2010;90(1):291–366.
105. Ma D, Tang XD, Rogers TB, Welling PA. An Andersen-Tawil syndrome mutation in Kir2.1 (V302M) alters the G-loop cytoplasmic K+ conduction pathway. J Biol Chem. 2007;282(8):5781–9.
106. Takahashi N, Morishige K, Jahangir A, Yamada M, Findlay I, Koyama H, et al. Molecular cloning and functional expression of cDNA encoding a second class of inward rectifier potassium channels in the mouse brain. J Biol Chem. 1994;269(37):23274–9.
107. Périer F, Radeke CM, Vandenberg CA. Primary structure and characterization of a small-conductance inwardly rectifying potassium channel from human hippocampus. Proc Natl Acad Sci USA. 1994;91(13): 6240–4.
108. Preisig-Müller R, Schlichthörl G, Goerge T, Heinen S, Brüggemann A, Rajan S, et al. Heteromerization of Kir2.x potassium channels contributes to the phenotype of Andersen's syndrome. Proc Natl Acad Sci USA. 2002;99(11): 7774–9.
109. Dhamoon AS, Pandit SV, Sarmast F, Parisian KR, Guha P, Li Y, et al. Unique Kir2.x properties determine regional and species differences in the cardiac inward rectifier K+ current. Circ Res. 2004;94(10): 1332–9.
110. Dascal N, Schreibmayer W, Lim NF, Wang W, Chavkin C, DiMagno L, et al. Atrial G protein-activated K+ channel: expression cloning and molecular properties. Proc Natl Acad Sci USA. 1993;90 (21):10235–9.
111. Krapivinsky G, Gordon EA, Wickman K, Velimirovic B, Krapivinsky L, Clapham DE. The G-protein-gated atrial K+ channel IKACh is a heteromultimer of two inwardly rectifying K+-channel proteins. Nature. 1995;374(6518):135–41.
112. Kurachi Y. G protein regulation of cardiac muscarinic potassium channel. Am J Physiol. 1995;269 (4 Pt 1):C821–30.
113. Lignon JM, Bichler Z, Hivert B, Gannier FE, Cosnay P, del Rio JA, et al. Altered heart rate control in transgenic mice carrying the KCNJ6 gene of the human chromosome 21. Physiol Genomics. 2008;33: 230–9.
114. Corey S, Clapham DE. Identification of native atrial G-protein-regulated inwardly rectifying K+ (GIRK4) channel homomultimers. J Biol Chem. 1998;273(42): 27499–504.
115. Wickman K, Nemec J, Gendler SJ, Clapham DE. Abnormal heart rate regulation in GIRK4 knockout mice. Neuron. 1998;20(1):103–14.
116. Kovoor P, Wickman K, Maguire CT, Pu W, Gehrmann J, Berul CI, et al. Evaluation of the role of IKACh in atrial fibrillation using a mouse knockout model. J Am Coll Cardiol. 2001;37(8):2136–43.
117. Ehrlich JR, Nattel S. Atrial-selective pharmacological therapy for atrial fibrillation: hype or hope? Curr Opin Cardiol. 2009 Jan;24(1):50–5.
118. Dobrev D, Wettwer E, Kortner A, Knaut M, Schüler S, Ravens U. Human inward rectifier potassium channels in chronic and postoperative atrial fibrillation. Cardiovasc Res. 2002;54(2):397–404.
119. Yamada M, Isomoto S, Matsumoto S, Kondo C, Shindo T, Horio Y, et al. Sulphonylurea receptor 2B and Kir6.1 form a sulphonylurea-sensitive but ATP-insensitive K+ channel. J Physiol. 1997;499 (Pt 3):715–20.
120. Kane GC, Lam CF, O'Cochlain F, Hodgson DM, Reyes S, Liu XK, et al. Gene knockout of the KCNJ8-encoded Kir6.1 K(ATP) channel imparts fatal susceptibility to endotoxemia. FASEB J. 2006;20(13):2271–80.
121. Inagaki N, Gonoi T, Clement JP, Wang CZ, Aguilar-Bryan L, Bryan J, et al. A family of sulfonylurea receptors determines the pharmacological properties of ATP-sensitive K+ channels. Neuron. 1996;16(5): 1011–7.
122. Morrissey A, Rosner E, Lanning J, Parachuru L, Dhar Chowdhury P, Han S, et al. Immuno-localization of KATP channel subunits in mouse and rat cardiac myocytes and the coronary vasculature. BMC Physiol. 2005;5(1):1.
123. Olson TM, Terzic A. Human KATP channelopathies: diseases of metabolic homeostasis. Pflugers Arch. 2010;460(2):295–306.
124. Suzuki M, Sasaki N, Miki T, Sakamoto N, Ohmoto-Sekine Y, Tamagawa M, et al. Role of sarcolemmal K(ATP) channels in cardioprotection against ischemia/reperfusion injury in mice. J Clin Invest. 2002;109(4):509–16.
125. Ruiz ML, London B, Nadal-Ginard B. Cloning and characterization of an olfactory cyclic nucleotide-gated channel expressed in mouse heart. J Mol Cell Cardiol. 1996;28(7):1453–61.

126. Moosmang S, Stieber J, Zong X, Biel M, Hofmann F, Ludwig A. Cellular expression and functional characterization of four hyperpolarization-activated pacemaker channels in cardiac and neuronal tissues. Eur J Biochem. 2001;268(6):1646–52.
127. Ludwig A, Budde T, Stieber J, Moosmang S, Wahl C, Holthoff K, et al. Absence epilepsy and sinus dysrhythmia in mice lacking the pacemaker channel HCN2. EMBO J. 2003;22(2):216–24.
128. Shi W, Wymore R, Yu H, Wu J, Wymore RT, Pan Z, et al. Distribution and prevalence of hyperpolarization-activated cation channel (HCN) mRNA expression in cardiac tissues. Circ Res. 1999;85(1):e1–6.
129. Dobrev D, Ravens U. Remodeling of cardiomyocyte ion channels in human atrial fibrillation. Basic Res Cardiol. 2003;98(3):137–48.
130. Stieber J, Hofmann F, Ludwig A. Pacemaker channels and sinus node arrhythmia. Trends Cardiovasc Med. 2004;14(1):23–8.
131. Stillitano F, Lonardo G, Zicha S, Varro A, Cerbai E, Mugelli A, et al. Molecular basis of funny current (If) in normal and failing human heart. J Mol Cell Cardiol. 2008;45:289–99.
132. Chandler NJ, Greener ID, Tellez JO, Inada S, Musa H, Molenaar P, et al. Molecular architecture of the human sinus node: insights into the function of the cardiac pacemaker. Circulation. 2009;119(12): 1562–75.
133. Watanabe H, MurakamiM OT, Ono K, Ito H. The pathological role of transient receptor potential channels in heart disease. Circ J. 2009;73(3):419–27.
134. Wu X, Eder P, Chang B, Molkentin JD. TRPC channels are necessary mediators of pathologic cardiac hypertrophy. Proc Natl Acad Sci USA. 2010;107 (15):7000–5.
135. Yamaguchi Y, Iribe G, Nishida M, Naruse K. Role of TRPC3 and TRPC6 channels in the myocardial response to stretch: linking physiology and pathophysiology. Prog Biophys Mol Biol. 2017;130 (Pt B):264–72.
136. Duan D. Phenomics of cardiac chloride channels: the systematic study of chloride channel function in the heart. J Physiol. 2009;587(Pt 10):2163–77.
137. Huang ZM, Prasad C, Britton FC, Ye LL, Hatton WJ, Duan D. Functional role of CLC-2 chloride inward rectifier channels in cardiac sinoatrial nodal pacemaker cells. J Mol Cell Cardiol. 2009;47(1):121–32.
138. Choi BR, Hatton WJ, Hume JR, Liu T, Salama G. Low osmolarity transforms ventricular fibrillation from complex to highly organized, with a dominant high-frequency source. Heart Rhythm. 2006;3(10): 1210–20.
139. Hiraoka M, Kawano S, Hirano Y, Furukawa T. Role of cardiac chloride currents in changes in action potential characteristics and arrhythmias. Cardiovasc Res. 1998;40(1):23–33.
140. Xiong D, Heyman NS, Airey J, Zhang M, Singer CA, Rawat S, et al. Cardiac-specific, inducible ClC-3 gene deletion eliminates native volume-sensitive chloride channels and produces myocardial hypertrophy in adult mice. J Mol Cell Cardiol. 2010;48(1):211–9.
141. Hume JR, Duan D, Collier ML, Yamazaki J, Horowitz B. Anion transport in heart. Physiol Rev. 2000;80(1):31–81.
142. Walsh KB, Long KJ. Properties of a protein kinase C-activated chloride current in guinea pig ventricular myocytes. Circ Res. 1994;74(1):121–9.
143. Collier ML, Hume JR. Unitary chloride channels activated by protein kinase C in guinea pig ventricular myocytes. Circ Res. 1995;76(2):317–24.
144. James AF, Sabirov RZ, Okada Y. Clustering of protein kinase A-dependent CFTR chloride channels in the sarcolemma of guinea-pig ventricular myocytes. Biochem Biophys Res Commun. 2010;391(1): 841–5.
145. Sellers ZM, De Arcangelis V, Xiang Y, Best PM. Cardiomyocytes with disrupted CFTR function require CaMKII and Ca2+-activated Cl- channel activity to maintain contraction rate. J Physiol. 2010;588(Pt 13):2417–29.
146. Wong KR, Trezise AE, Vandenberg JI. Developmental regulation of the gradient of cftr expression in the rabbit heart. Mech Dev. 2000;94: 195–7.
147. Nishimura N, Reien Y, Matsumoto A, Ogura T, Miyata Y, Suzuki K, et al. Effects of nicorandil on the cAMP-dependent Cl- current in guinea-pig ventricular cells. J Pharmacol Sci. 2010;112(4):415–23.
148. Zygmunt AC, Goodrow RJ, Weigel CM. INaCa and IClCa contribute to isoproterenol-induced delayed after depolarizations in midmyocardial cells. Am J Physiol. 1998;275(6 Pt 2):H1979–92.
149. Guo D, Young L, Patel C, Jiao Z, Wu Y, Liu T, et al. Calcium-activated chloride current contributes to action potential alternations in left ventricular hypertrophy rabbit. Am J Physiol Heart Circ Physiol. 2008;295(1):H97–104.
150. Kunzelmann K, Kongsuphol P, Aldehni F, Tian Y, Ousingsawat J, Warth R, et al. Bestrophin and TMEM16-Ca2+ activated Cl- channels with different functions. Cell Calcium. 2009;46(4):233–41.
151. O'Driscoll KE, Hatton WJ, Burkin HR, Leblanc N, Britton FC. Expression, localization, and functional properties of Bestrophin 3 channel isolated from mouse heart. Am J Physiol Cell Physiol. 2008;295 (6):C1610–24.
152. Galietta LJ. The TMEM16 protein family: a new class of chloride channels? Biophys J. 2009;97(12): 3047–53.
153. Lambert S, Oberwinkler J. Characterization of a proton-activated, outwardly rectifying anion channel. J Physiol. 2005;567(Pt 1):191–213.
154. Komukai K, Brette F, Orchard CH. Electrophysiological response of rat atrial myocytes to acidosis. Am J Physiol Heart Circ Physiol. 2002;283(2):H715–24.

155. Sachs F. Stretch-activated ion channels: what are they? Physiology. 2010;25(1):50–6.
156. Watanabe H, Murakami M, Ohba T, Ono K, Ito H. The pathological role of transient receptor potential channels in heart disease. Circ J. 2009;73(3): 419–27.
157. Saffitz JE, Laing JG, Yamada KA. Connexin expression and turnover: implications for cardiac excitability. Circ Res. 2000;86(7):723–8.
158. Boyett MR, Inada S, Yoo S, Li J, Liu J, Tellez J, et al. Connexins in the sinoatrial and atrioventricular nodes. Adv Cardiol. 2006;42:175–97.
159. Lin X, Gemel J, Glass A, Zemlin CW, Beyer EC, Veenstra RD. Connexin40 and connexin43 determine gating properties of atrial gap junction channels. J Mol Cell Cardiol. 2010;48(1):238–45.
160. Gros D, Théveniau-Ruissy M, Bernard M, Calmels T, Kober F, Söhl G, et al. Connexin 30 is expressed in the mouse sino-atrial node and modulates heart rate. Cardiovasc Res. 2010;85(1):45–55.
161. Schrickel JW, Kreuzberg MM, Ghanem A, Kim JS, Linhart M, Andrié R, et al. Normal impulse propagation in the atrioventricular conduction system of Cx30.2/Cx40 double deficient mice. J Mol Cell Cardiol. 2009;46(5):644–52.
162. Zalk R, Lehnart SE, Marks AR. Modulation of the ryanodine receptor and intracellular calcium. Annu Rev Biochem. 2007;76:367–85.
163. Hamilton SL, Serysheva II. Ryanodine receptor structure: progress and challenges. J Biol Chem. 2009;284(7):4047–51.
164. Marionneau C, Couette B, Liu J, Li H, Mangoni ME, Nargeot J, et al. Specific pattern of ionic channel gene expression associated with pacemaker activity in the mouse heart. J Physiol. 2005;562(Pt 1):223–34.
165. Kang G, Giovannone SF, Liu N, Liu FY, Zhang J, Priori SG, et al. Purkinje cells from RyR2 mutant mice are highly arrhythmogenic but responsive to targeted therapy. Circ Res. 2010;107(4):512–9.
166. Thomas NL, George CH, Williams AJ, Lai FA. Ryanodine receptor mutations in arrhythmias: advances in understanding the mechanisms of channel dysfunction. Biochem Soc Trans. 2007;35(Pt 5): 946–51.
167. Eisner DA, Kashimura T, Venetucci LA, Trafford AW. From the ryanodine receptor to cardiac arrhythmias. Circ J. 2009;73(9):1561–7.
168. Mackrill JJ. Ryanodine receptor calcium channels and their partners as drug targets. Biochem Pharmacol. 2010;79(11):1535–43.
169. Wu X, Zhang T, Bossuyt J, Li X, McKinsey TA, Dedman JR, et al. Local InsP3-dependent perinuclear Ca2+ signaling in cardiac myocyte excitation-transcription coupling. J Clin Invest. 2006;116(3): 675–82.
170. Aon MA, Cortassa S, Akar FG, Brown DA, Zhou L, O'Rourke B. From mitochondrial dynamics to arrhythmias. Int J Biochem Cell Biol. 2009;41(10): 1940–8.
171. Bkaily G, Avedanian L, Jacques D. Nuclear membrane receptors and channels as targets for drug development in cardiovascular diseases. Can J Physiol Pharmacol. 2009;87(2):108–19.
172. Rudy Y, Ackerman MJ, Bers DM, Clancy CE, Houser SR, London B, et al. Systems approach to understanding electromechanical activity in the human heart: a national heart, lung, and blood institute workshop summary. Circulation. 2008;118(11): 1202–11.

2

A Historical Perspective on the Development of Models of Rhythm in the Heart

Penelope J. Noble and Denis Noble

Abstract

The chapter provides a comprehensive account of biophysical models of cardiac pacemaker action potentials and how they have been improved over time by including additional components as they were discovered. Starting with ionic currents conducted via sodium, potassium and 'leak' channels, the addition of further selective ion channels, sodium-calcium exchangers or other transporters and calcium oscillations led to more sophisticated models with better predictive potential. This development culminated when the 'funny' pacemaker current I_f was discovered. Today, all mathematical models are made available for research on the CellML repository (https://models.cellml.org/cellml/electrophysiology). Finally, we briefly introduce the *Physiome Project* which will ensure that published models are fully tested.

Keywords

Pacemaker action potentials · Biophysical models · Conductance · Ionic currents · Sodium channels · Potassium channels · Sodium-calcium-exchanger · 'Funny' current I_f · *Physiome* project

2.1 Introduction

Models of cardiac rhythm have a long history, starting with the van der Pol equations in 1928 [1]. These equations were based on the idea of a relaxation oscillator involving a threshold for activation of a rapid change to a different range of potentials, followed by a relatively slow relaxation towards a reverse threshold for return to the original range. Models of this type (including the Bonhoeffer modification in Bonhoeffer-van der Pol (BVP) models) have their uses, particularly in mathematical analysis of rhythm, but they are not based on biophysically detailed experiments. In the 1960s, 22 biophysically detailed models were developed, of which 5 are Purkinje, 16 SA nodes and 1 AV node. Three of the Purkinje models are mammalian, one canine and one human; seven of the SA node models are mammalian, eight are rabbit and one mouse, and finally, the AV node model is rabbit. In this chapter, we simply explore the progress in model development, providing the reader with a comprehensive list of models and how they fit into the history of modelling of cardiac rhythm. In cases where the authors' comments on the models seem to provide the best description, we have quoted from the original paper as indicated. The development of these models over time is illustrated in Table 2.1.

P. J. Noble · D. Noble (✉)
Department of Physiology, Anatomy and Genetics,
Oxford University, Oxford, UK
e-mail: denis.noble@dpag.ox.ac.uk

© Springer Nature Switzerland AG 2023

O. N. Tripathi et al. (eds.), *Heart Rate and Rhythm*, https://doi.org/10.1007/978-3-031-33588-4_2

Table 2.1 Historical development of cardiac models of rhythm

A. By model species and cell type

1962	1975	1980	1984	1985	1989	1993	1994–2004	2006	2009
First cardiac mammalian Purkinje cell (model A)	Model A develop	First SAN Model	SAN model B from model A	Model A develop	Model B develop	First network model atria and SAN	Eight (mostly Rabbit) SAN models	Mouse SAN model	Human and canine Purkinje models
									First AV node model (rabbit)

B. By model (Author) name

1962	1975	1980	1984	1985	1989	1993	1994–2004	2006	2009
Noble	MNT	Yanagihara	Noble–Noble	DFN	Noble	Winslow	Demir et al. [2]	Mangoni	Stewart
							Dokos [3]		Aslanidi
							Endresen [4]		
							Demir et al. [5]		
							Zhang [6]		
							Sarai [7]		
							Garny [8]		
							Lovell [9]		
									Inada

2.2 The Models and Their Key Features

2.2.1 Noble [10, 11]

The first model to be based on actual measurements of transmembrane ionic currents was that of Noble in 1962 [10], published in a preliminary form as a letter to *Nature* in 1960 [11].

Figure 2.1 shows the 1962 model run using COR. The top trace shows the cell voltage changes, while the bottom traces show the changes in ionic conductance in the sodium and potassium channels. The conductance scale has been chosen to reveal the main changes during the plateau and pacemaker potential variations. The peak sodium conductance (at 12,000 μS) is way off the scale.

This model of a Purkinje fibre was developed using the Hodgkin–Huxley (1952) squid giant axon model [12] as a base. In fact, the sodium current equations were largely taken over from that model since Weidmann in 1956 [13] had shown great similarity between heart and nerve, while the potassium current equations were based on early membrane current measurements in sodium-deficient solutions. The classification of K current equations into inward and delayed rectifiers is still used today. The main success of the model was that it provided a counter-intuitive explanation of resistance changes during the action and pacemaker potentials, particularly for the phenomenon of all-or-nothing repolarisation. This was inherent in the van de Pol equations, so this property is a very general one in the case of oscillators of the relaxation type. The existence of inward rectifier K current, I_{K1}, also provided a mechanism for energy conservation during the long plateau of the cardiac action potential.

Components: I_{Na}, I_K and I_{leak}.

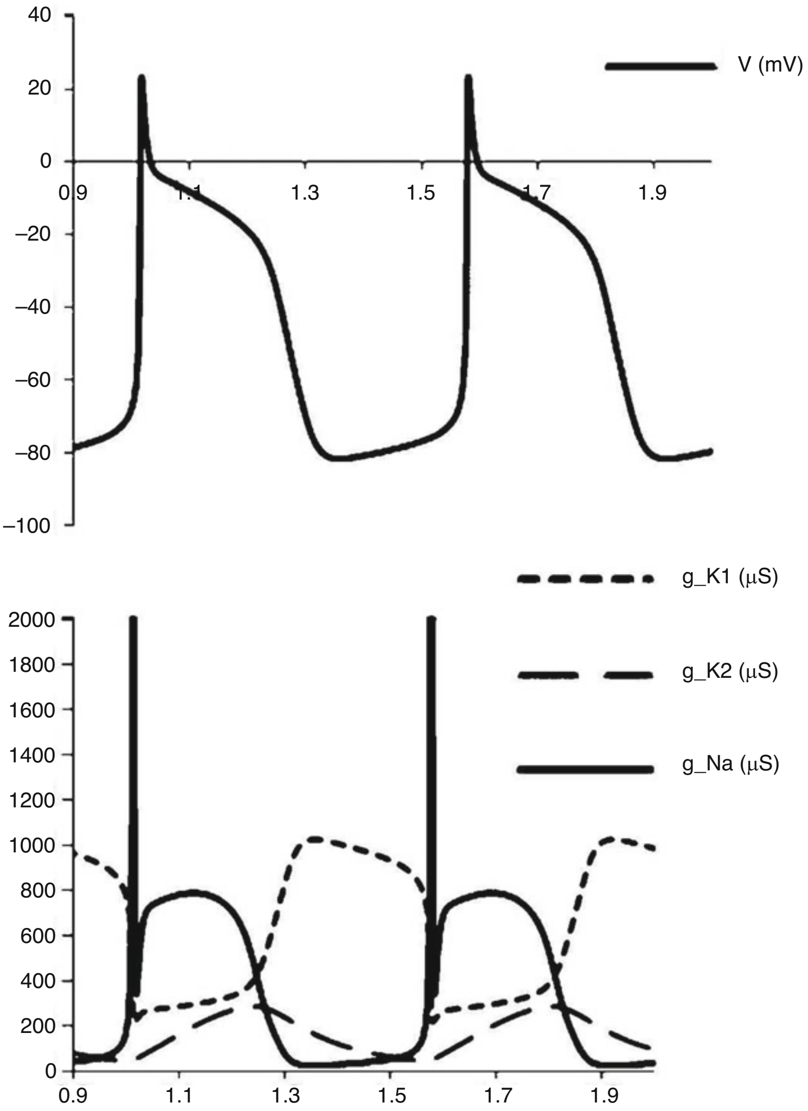

Fig. 2.1 *The Noble 1962 model* shows the role of the potassium conductances on the action potential profile. Note: gNa peaks up to around 12,000 μS

2.2.2 McAllister–Noble–Tsien (MNT) [14]

This model was developed by Noble (1962) and is also a Purkinje fibre model. It was the first complete model to be based on the voltage clamp analyses of individual ionic current components performed over the 10 years leading up to the date of the model. The main advances in knowledge of ionic currents included the multiple components of the delayed rectifier K current. Noble and Tsien [15] were the first to identify the components I_{x1} and I_{x2}, now referred to as I_{Kr} and I_{Ks}. It succeeded in reproducing slow action potentials in the absence of I_{Na}, so presaging the development of sinus node models, it established the independence of plateau and pacemaker mechanisms and reproduced the notch separating spike and plateau phases of repolarisation. The main deficiency of the model was that the main contributor to the pacemaker depolarisation (I_{K2}) was interpreted as a pure potassium current. This is the current now known to be the hyperpolarising-activated current, I_f, carrying both sodium and potassium ions.

Components: I_{Na}, I_{si}, I_{K2}, I_{x1}, I_{x2}, I_{qr}, I_{K1}, I_{Nab}, I_{Clb}.

2.2.3 Yanagihara–Noma–Irisawa [16]

The first sinus node model was developed by Yanagihara, Noma and Irisawa in 1980. They were the first to succeed in difficult voltage clamp experiments in sinus node preparations (then multicellular), so this model based on their careful experimental measurements was a major step forward. In this model, the calcium current (called I_{si} in those days) is responsible for the upstroke and oscillation; changing the maximum value for this current changes the frequency of oscillation (see Fig. 2.2); an increase in frequency with an increase in value of I_{max}.

Components: I_{si}, I_K, I_f, I_{Na}, I_b.

2.2.4 Bristow–Clark [17]

This model is a modification of the MNT model to give SA node behaviour.

Components: I_{K1}, I_{K2}, I_{si}, I_K, I_{Na}, I_{bNa}, I_{bK}, I_{bsi}.

2.2.5 Noble–Noble [18]

2.2.5.1 Multicellular (100 Cells)

The first sinus node model to incorporate currents generated by Na-K and Na-Ca exchange processes and to reconstruct variations in intracellular and extracellular ion concentrations was that of Noble and Noble in 1984. It was developed from DFN even though DFN was actually published afterwards! This was simply attributable to the different time schedules of the two Royal Society journals involved. The method used was to change parameters from DFN to reflect data for the SA node, which had been obtained by Brown et al. [19, 20]. Both peripheral and central models were developed, but these were speculative because of a lack of data.

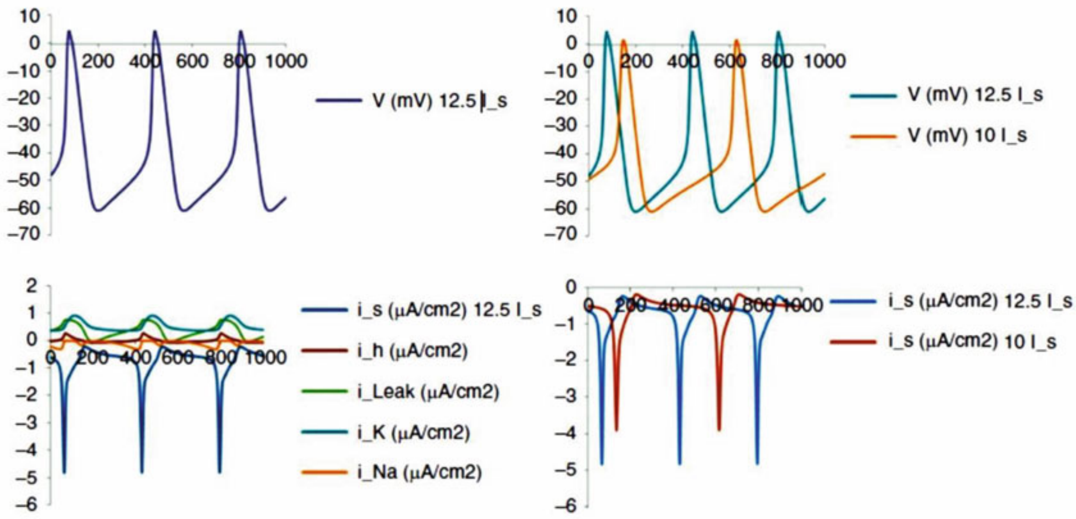

Fig. 2.2 *The Yanagihara 1980 model* shows the cell voltage (*top left*) and all underlying ionic currents in the model (*bottom left*). A lower maximum calcium current (I_s) reduces automaticity

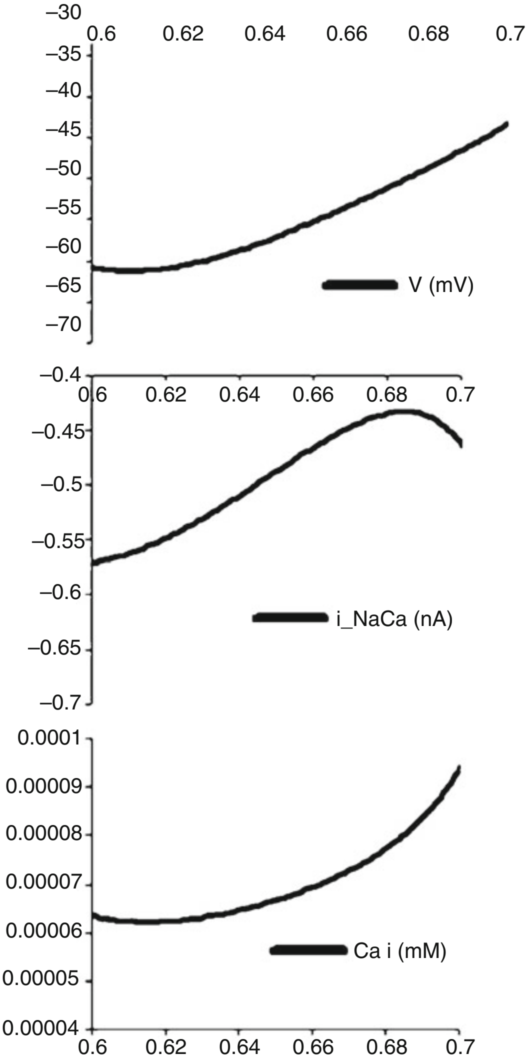

Fig. 2.3 *The Noble–Noble 1984 model*. Role of calcium dynamics and NCX in depolarisation

The really important development that this model established is that it was the first to highlight the role of Na-Ca exchange (NCX) and Ca^{2+} oscillations in pacemaker activity. It can therefore be seen as a forerunner of models developed more recently by Lakatta's team [21]. Figure 2.3 shows the key result that NCX can be activated towards the end of the pacemaker depolarisation by release of calcium from the sarcoplasmic reticulum occurring before the action potential upstroke. Only models reproducing variations in intracellular sodium and calcium can incorporate this property, as explained in the next section.

Components: I_f, I_K, I_{K1}, I_{Nab}, I_{Cab}, I_{NaK}, I_{NaCa}, I_{Na}, I_{si}, Na_i, Na_o, K_i, K_o, Ca_i, Ca_o.

2.2.6 DiFrancesco-Noble (DFN) [22]

2.2.6.1 Multicellular (100 Cells)

This Purkinje fibre model was the first cardiac cell model to incorporate currents generated by Na–K and Na-Ca exchange processes and to reconstruct variations in intracellular and extracellular ion concentrations. As such, it is the generic model from which nearly all the subsequent models have been derived. It also incorporated the reinterpretation of I_{K2} (the pacemaker current in the MNT model) as I_f. In addition, intracellular calcium sequestration and release by the sarcoplasmic reticulum were modelled, an aspect that was greatly improved in the Hilgemann-Noble [23] model of the atrial action potential by incorporating calcium buffers and the essential details of Fabiato's [24] work on calcium-induced calcium release. That model is not dealt with here since it does not concern pacemaker activity.

The incorporation of NCX into this model was originally quite controversial. Following its discovery in the heart by Reuter [25] in 1967, the exchanger had been thought to be electrically neutral, with a stoichiometry of two sodium ions for each calcium ion transported. But, with the known values for intracellular and extracellular sodium concentrations and external calcium concentration, this stoichiometry was found to be insufficient to drive resting calcium levels down to below those known to activate the contractile proteins. DiFrancesco and Noble, therefore, experimented with higher possible stoichiometries, including 4:1 (that favoured by Lorin Mullins [26], from whom the equations for sodium-calcium exchange were derived) and 3:1. The results were quite clear. Only 3:1 worked. The consequence, however, was the prediction that the exchanger must carry an electric current during the action potential. The middle curves in Fig. 2.4 show the predicted current as a function of membrane potential at different levels of external sodium ion concentration. The lower figure shows a fairly large inward current predicted to occur during the plateau of the action potential. These results were mostly speculative until, in 1986 and 1987, Kimura, Myamae and Noma [27] published their experimental results. The top curves in Fig. 2.4 show some of their results and how closely they correspond to the predicted curves (middle). The main difference is that the experimental results do not curve as strongly at very negative potentials, an effect that could be attributable to the saturation of the carrier mechanism. It is not often that theoretical work leads to predictions as close as this to the experimental results! But it secured the main advance of the DiFrancesco-Noble model in incorporating not only successful representations of ion concentration changes but also in making correct predictions of the consequences for ion current flow during normal rhythmic electrical activity.

Components: I_f, I_K, I_{K1}, I_{to}, I_{Nab}, I_{Cab}, I_{NaK}, I_{NaCa}, I_{Na}, I_{si}, Na_i, Na_o, K_i, K_o, Ca_i, Ca_o.

2.2.7 Reiner–Antzelevitch [29]

2.2.7.1 SA Node

This model is a modification of Bristow–Clark.

Components: I_{K1}, I_f, I_{si}, I_K, I_{Na}, I_{bNa}, I_{bK}, I_{bsi}.

2.2.8 Noble et al. [30]

2.2.8.1 SA Node

This model is based on Noble–Noble, modified to be appropriate to a single cell. The I_f and I_K

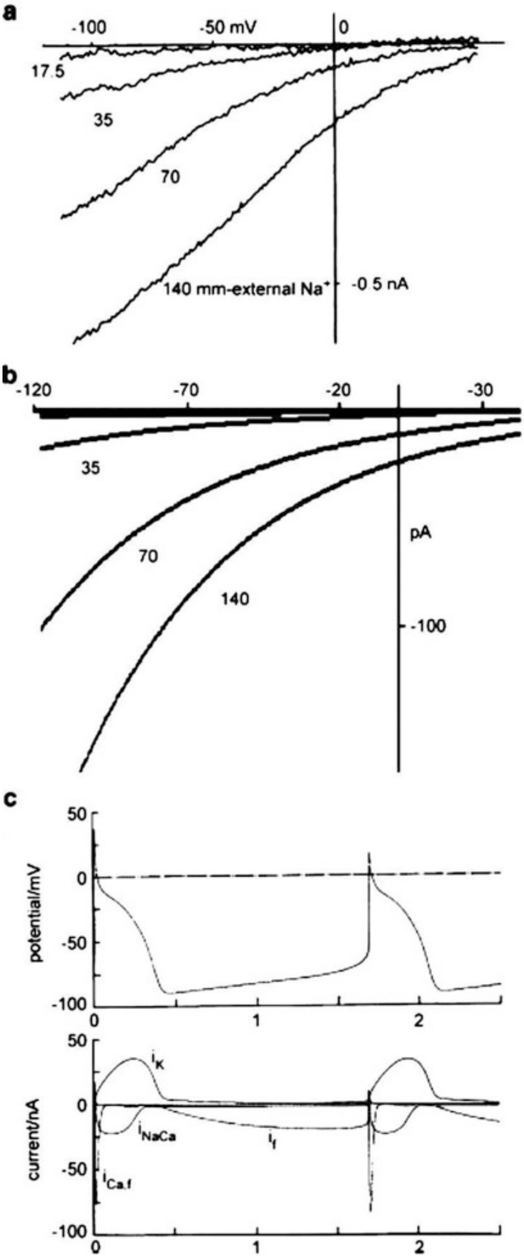

Fig. 2.4 *The DiFrancesco-Noble 1985 model.* (**a**) Experimental results obtained by Kimura et al. [27]. (**b**) Current–voltage relations are given by the equations for sodium-calcium exchange used in the DiFrancesco-Noble model. The curves show the relations at various external sodium concentrations. (**c**) Action and pacemaker potentials computed from the DiFrancesco-Noble modelling highlight the roles played by activation of I_f during the pacemaker depolarisation and of I_{NaCa} during the action potential. Reproduced from Noble [28] with permission

equations were replaced by those from fits to more recent experimental data.

Components: I_f, I_K, I_{K1}, I_{Nab}, I_{Cab}, I_{NaK}, I_{NaCa}, I_{Na}, I_{si}, Na_i, Na_o, K_i, K_o, Ca_i, Ca_o.

2.2.9 Wilders et al. [31]

2.2.9.1 SA Node

Wilders et al. compared Bristow–Clark (1982), Irisawa–Noma (1980) and Noble–Noble (1984) models and found "drawbacks" that he aimed to correct in this model. In particular, he introduced I_{CaT}. Another major difference is that "in contrast to the other models only small amount of background current contributes to the overall electrical charge flow."

Components: I_{CaL}, I_{CaT}, I_f, I_K, I_{NaK}, I_{NaCa}, I_{bCa}, I_{bNa}, Na_i, Na_o, K_i, K_o, Ca_i, Ca_o

2.2.10 Winslow et al. [32]

These were the first network models simulating atria and SA node together using Noble–Noble (1984) and Noble et al. (1989) models. They also represent the first use of massively parallel computers in cardiac electrophysiology. The computer used was the 64,000 processor Connection Machine at the University of Minnesota.

2.2.11 Demir et al. [2]

SA node: this was the first model specifically for rabbit. It used new equations for I_f and assessment of the role of I_{CaT} during pacemaker depolarisation modifying pacemaker potential (while I_{CaL} is important in upstroke and plateau). It incorporated I_{Na} based on recent experimental data and assessed the possible influence of pump, exchanger and background currents on pacemaker rate. The model incorporated the buffers troponin, calmodulin and calsequestrin and modified HN formulation for Ca dynamics.

Components: I_{Na}, I_{CaT}, I_{CaL}, I_K, I_f, I_B, I_{NaK}, I_{NaCa}, I_{CaP}, Na_i, Na_o, K_i, K_o, Ca_i, Ca_o.

2.2.12 Dokos et al. [3]

2.2.12.1 Rabbit SA Node

This model mentioned the Wilders et al. (1991) model. The authors provided a review and update of existing formulations—derived from a wide range of data from literature. The update included a significantly new formulation for NCX—not Mullins [26], but the E4 translocation model of Matsuoka and Hilgemann [33]. They found I_{bNa} to be the dominant mechanism underlying pacemaker depolarisation; I_K is insignificant in this phase in contrast to other models, I_f is not essential to pacemaker activity. A previous suggestion that net background current is outward during the pacemaker range of potentials was not found in this model. The AP overshoot is based on the reversal potential of I_{CaL}. The MDP is based on the reversal potential of I_K. The AP is sustained by incomplete deactivation of I_{CaL} and NCX. The model uses a square-root formula for inactivation of all K currents by $[K^+]_o$—but is unable to reproduce the correct response to elevated $[K^+]_o$.

Components: I_{CaL}, I_{CaT}, I_{Na}, I_K, I_f, I_{NaK}, I_{NaCa}, I_{bNa}, I_{bK}, Na_i, Na_o, K_i, K_o, Ca_i, Ca_o.

2.2.13 Endresen [4]

2.2.13.1 SA Node

This is a very simple model compared to previous models. It is modified from Morris and Lecar [34] barnacle giant muscle fibre model. The model is composed of two nonlinear first-order ODEs with ten constant parameters. Endresen stated that it perfectly reproduces experimentally recorded APs. A model of two coupled cells was developed. Vagal stimulation was simulated.

Components: I_s, I_K, I_{KACh}, I_j.

2.2.14 Demir et al. [5]

2.2.14.1 Rabbit SA Node

This model was an extension of the previous Demir et al. model to include responses to bath ACh and isoprenaline as well as neuronally released ACh; this was achieved via three types of muscarinic receptors. It was the first unified approach to modelling adrenergic and cholinergic effects on SAN pacemaker activity.

Components: I_{Na}, I_{CaT}, I_{CaL}, I_K, I_f, I_B, I_{NaK}, I_{NaCa}, I_{CaP}, I_{KACh}, Na_i, Na_o, K_i, K_o, Ca_i, Ca_o, cAMP.

2.2.15 Zhang et al. [6]

2.2.15.1 SA Node

This work included the development of separate models of peripheral and central rabbit SA node cells based on experimental data. "The model-generated peripheral action potential has a more negative takeoff potential, faster upstroke, more positive peak value, prominent phase 1 repolarization, greater amplitude, shorter duration, and more negative maximum diastolic potential than the model-generated central action potential. In addition, the model peripheral cell shows faster pacemaking". These results are consistent with experimental recordings. The model responds as in experiments to block of TTX-I_{Na}, I_{CaL}, I_{CaT}, I_{to}, I_{Kr}, I_{Ks} and I_f. "A one-dimensional model of a string of SA node tissue, incorporating regional heterogeneity, coupled to a string of atrial tissue has been constructed to simulate the behavior of the intact SA node".

Components: I_{Na}, I_{CaL}, I_{CaT}, I_{to}, I_{sus}, I_{Kr}, I_{Ks}, I_f, I_{bNa}, I_{bCa}, I_{bK}, I_{NaCa}, I_{NaK}, I_{Cap} (concentrations constant).

2.2.16 Kurata et al. [35]

2.2.16.1 Rabbit SA Node

This is an "improved mathematical model for a single primary pacemaker cell of the rabbit sinoatrial node (SAN)." "Original features of our model include (1) incorporation of the sustained inward current (I_{st}) recently identified in primary pacemaker cells, (2) reformulation of voltage- and Ca^{2+}-dependent inactivation of the L-type Ca^{2+} channel current ($I_{Ca,L}$), (3) new expressions for activation kinetics of the rapidly activating delayed rectifier Kr channel current (I_{Kr}) and (4) incorporation of the subsarcolemmal space as a diffusion barrier for Ca^{2+}." This model was found to more accurately mimic the effects of channel blockers and Ca^{2+} buffers on pacemaker activity than previous models.

Components: I_{CaL}, I_{CaT}, I_{Kr}, I_{Ks}, I_{to}, I_{sus}, I_h, I_{st}, I_{bNa}, I_{KACh}, I_{NaK}, I_{NaCa}, Na_i, Na_o, K_i, K_o, Ca_i, Ca_{sub}, Ca_o.

2.2.17 Sarai et al. [7, 36]

2.2.17.1 SA Node and Ventricular Cell

This model uses a common set of equations to describe SAN pacemaker [7] and ventricular [36] cells. The authors produced new kinetics for I_{K1}, I_K and I_{st}. Combined with the NL contraction model, it can reproduce the staircase phenomenon. They showed modulation by varying Ca_o and K_o to be well simulated and that the Ca gain agreed with experimental data. "Increasing the amplitude of L-type Ca^{2+} current (I_{CaL}) prolongs the duration of the action potential and thereby slightly decreases the spontaneous rate. On the other hand, a negative voltage shift of I_{CaL} gating by a few milliVolt markedly increases the spontaneous rate. When the amplitude of sustained inward current (I_{st}) is increased, the spontaneous rate is increased irrespective of the I_{CaL} amplitude. Increasing $[Ca^{2+}]_o$ shortens the action potential and increases the spontaneous rate. When the spontaneous activity is stopped by decreasing I_{CaL} amplitude, the resting potential is nearly constant (−35 mV) over 1–15 mM $[K^+]_o$ as observed in the experiment. This is because the conductance of the inward background nonselective cation current balances with the outward $[K^+]_o$-dependent K^+ conductance. The unique role of individual voltage- and time-dependent ion channels is clearly demonstrated and distinguished from that of the background current by calculating an instantaneous zero current potential ('lead potential') during the course of the spontaneous activity."

They included a comparison with other models: Wilders, Demir, "Oxsoft98".

Components: I_{Na}, I_{CaL}, I_{CaT}, I_{K1}, I_{Kr}, I_I, I_{NaK}, I_{NaCa}, I_{st}, I_{ha}, I_{KACh}, I_{bNSC}, I_{Cab}, I_{Kpl}, I_{lCa}, I_{KATP}, Na_i, Na_o, K_i, K_o, Ca_i, Ca_o, ATP, NL contraction.

2.2.18 Garny et al. [8]

In 2002, Garny et al. [37] compared the Noble et al. [30], Demir et al. [2], Dokos et al. [3] and Zhang et al. [6] SA node models, finding that according to current experimental data of that time, the Zhang et al. (2000) model was the best model to use for incorporation into multicellular models of the atrium as it includes regional differences in SA node cells as well as responding correctly to interventions such as block of specific ionic currents.

This development was a "thorough overhaul" of Zhang et al. [6]. The authors "investigated the effects of intercellular coupling on SAN-atrial function. We reconfirm that removal of SAN to atrial connections causes a pacemaker shift from SAN center to its periphery, and show that (1) low dimensional multicellular models such as 1D SAN-atrial cell strands require larger, than experimentally established, coupling between individual cell pairs (to compensate for the lack in anatomic 3D spatial connectivity); (2) the increase in cell coupling from the center to the periphery of the SAN is a crucial feature for rhythm entrainment and (3) the electrotonic effect of the atrium on SAN periphery is best described as opposing depolarization rather than hyperpolarizing".

"Thus, 1D models of the origin and spread of cardiac excitation, while limited by spatial parameter restrictions, can be a valuable tool for theoretical assessment of cardiac SAN atrial electrophysiology".

Figure 2.5 shows central and peripheral action potentials overlayed with the largest differences in currents: I_{sus} and I_{Kr}.

Components: I_{Na}, I_{CaL}, I_{CaT}, I_{to}, I_{sus}, I_{Kr}, I_{Ks}, I_f, I_{bNa}, I_{bCa}, I_{bK}, I_{NaCa}, I_{NaK}, I_{Cap} (concentrations constant).

2.2.19 Lovell et al. [9]

The authors said, "We have formulated a spatial-gradient model of action potential heterogeneity within the rabbit SAN, based on cell-specific ionic models of electrical activity from its central and peripheral regions. The ionic models are derived from a generic cell model, incorporating five background and exchange currents, and seven time-dependent currents based on three- or four-state Markov schemes. State transition rates are given by nonlinear sigmoid functions of membrane potential."

"Using a custom least squares parameter optimisation routine, we have constructed a

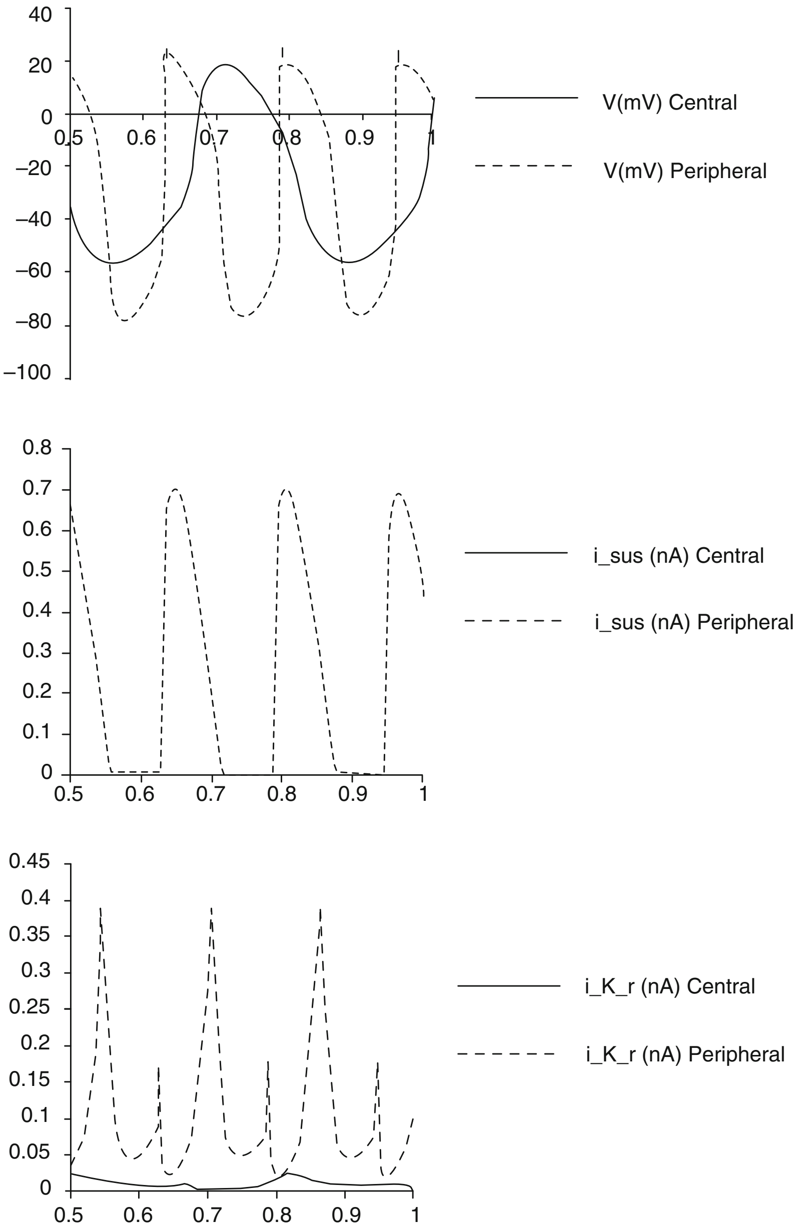

Fig. 2.5 *The Garny 2003 model* shows central and peripheral versions. The conductances of many currents are higher in peripheral than central; most significantly, I_{CaL} and I_{to} are ~10 times, I_{Kr} 20 times and I_{sus} 171 times

spatially-varying gradient model that exhibits a smooth transition in action potential characteristics from the central to the peripheral region, whilst ensuring individual membrane currents remain physiologically accurate. The gradient model is suitable for developing higher dimensional models of the right atrium, in which action potential heterogeneity within nodal tissue may be readily incorporated.”

Components: I_f, I_{Kr}, I_{Ks}, I_{bNa}, I_{Na}, I_{NaK}, I_{NaCa}, I_{to}, I_{CaL}, I_{CaT}, I_{bK}, I_{bCl}, Na_i, Na_o, K_i, K_o, Ca_i, Ca_o, Cl_i, Cl_o.

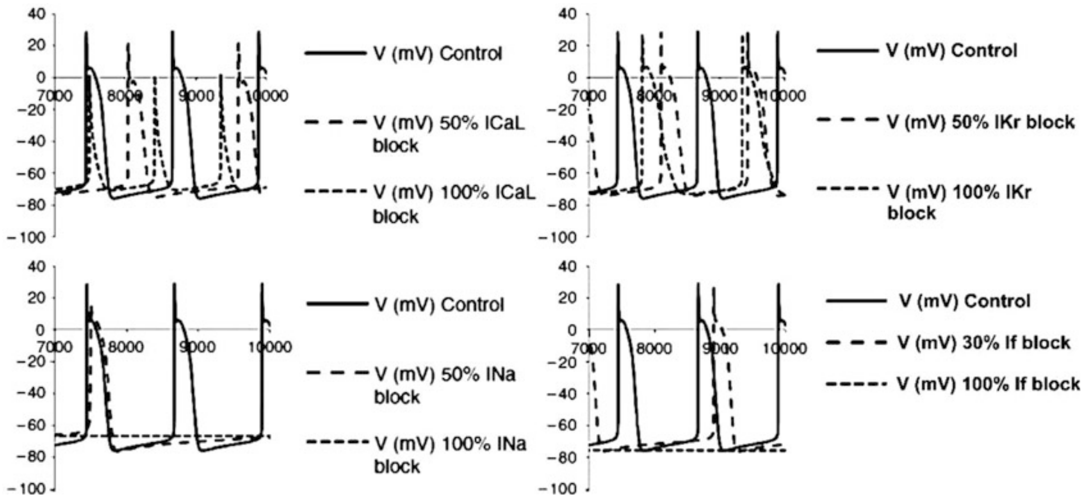

Fig. 2.6 *The Stewart 2009 model* shows the effects of block of ionic currents on autorhythmicity. 100% block of I_{CaL} increases automaticity while 50% block of I_{CaL}, I_{Na} or I_{Kr} and 30% block of I_{f} slow the rate. Hundred per cent block of I_{Na} or I_{f} abolish automaticity. I_{Ks} and I_{to} 50 and 100% blocks have minimal effects on rate (not shown)

2.2.20 Mangoni et al. [38]

2.2.20.1 Mouse SA Node

This model emphasised the importance of calcium channels in pacemaking, because they substantially influence pacemaker rate. It dealt with knockout mice. This model is important as a mouse model and to illustrate different channel subtypes.

Cardiac and neuronal Na channels. Cardiac and pacemaker L-type Ca channels.

Components: I_{Na}, I_{Nas}, I_{CaD}, I_{CaL}, I_{CaT}, I_{to}, I_{sus}, I_{K1}, I_{Kr}, I_{Ks}, I_{f}, I_{bNa}, I_{bCa}, I_{bK}, I_{NaCa}, I_{NaK}, I_{st} (concentrations constant).

2.2.21 Stewart et al. [39]

It is interesting to note that, although the Purkinje fibre was the first cardiac tissue to be modelled, for two decades development of Purkinje fibre models had been neglected. This article introduced a human Purkinje fibre model and included validation against experimental data.

Figure 2.6 illustrates the effects of blocked ionic currents on autorhythmic APs and suggests that I_{CaL}, I_{Na} and I_{f} have important roles in automaticity.

Components: I_{K1}, I_{to}, I_{sus}, I_{Kr}, I_{Ks}, I_{CaL}, I_{NaK}, I_{Na}, I_{bNa}, I_{NaCa}, I_{bCa}, I_{pK}, I_{pCa}, I_{f}, $\mathrm{Na_i}$, $\mathrm{Na_o}$, $\mathrm{K_i}$, $\mathrm{K_o}$, $\mathrm{Ca_i}$, $\mathrm{Ca_o}$.

2.2.22 Aslanidi et al. [40]

This work developed a structurally and electrophysiologically detailed model of the canine Purkinje-ventricular junction and varied heterogeneity parameters to determine the relationships between tissue structure, wave conduction velocity and safety through the nonuniform junction. The investigators note that slow and discontinuous wave conduction are considered to be arrythmogenic, hence their interest in investigating these features using their model.

Components: I_{Na}, I_{NaI}, I_{CaL}, I_{CaT}, I_{to1}, I_{to2}, I_{Kr}, I_{Ks}, I_{K1}, I_{NaCa}, I_{NaK}, I_{Nab}, I_{Kb}, I_{Cab}, I_{Clb}, I_{Cap}, I_{Kp}, Na_i, Na_o, K_i, K_o, Ca_i, Ca_o, Cl_i, Cl_o.

2.2.23 Inada et al. [41]

This is the first AV node model. Separate action potential models were developed for single atrio-nodal, nodal and nodal-His cells. A 1D multicellular model including SAN and AVN was also created.

The models were found to show typical physiological and pathophysiological behaviour of the tissue.

Figure 2.7 illustrates the ability of the model to reproduce potential action propagation from sinoatrial node to the atrio-ventricular node.

Components: I_{Na}, I_{CaL}, I_{to}, I_{Kr}, I_f, I_{st}, I_{K1}, I_{NaCa}, I_{NaK}, I_b, Ca_i, Ca_{sub} (other concentrations constant).

2.3 Conclusions

In this chapter, we have given a systematic summary of all the known models of cardiac rhythm, while highlighting some of the most important milestones in the development of models in this field. It is clear that the range of species and types of cardiac cells have greatly expanded in recent years. It is also clear to us that different models, even those of the same cell type and species, concentrate on different applications. The idea that we could have a definitive set of models is elusive. Perhaps this is a reflection of the difficulty of dealing with the complexity of nature. A common experience in modelling is that when one aspect is improved in relation to fits to experimental data, other aspects of the model can “deteriorate” by this criterion. This is sometimes represented as a criticism of modelling. It seems to us rather to be an indication of the inevitably partial nature of all models. Models have range of applications. Outside that range, they can be misleading.

We hope that this chapter, through being systematic, will help researchers in this field to find their way through the large range of models available to choose carefully those most appropriate to their applications. Used thoughtfully and with good physiological insight, models can be a very helpful tool in physiology. After all, models are simply quantitative mathematical versions of what otherwise would be mere hand-waving “ideas” on how cells work. It is better to be quantitative and precise than to hope to understand nature simply by reflecting on one’s experimental data in an armchair!

2.4 Addendum (2021)

2.4.1 Improved Availability and Reliability of Physiological Models

This chapter summarises all the relevant models when the previous edition of this book was published. It is no longer necessary to do that since, as we note at the beginning of the chapter, all the models we reviewed are available on the CellML repository (https://models.cellml.org/cellml/electrophysiology), where they are annotated and can be downloaded for research. Furthermore, a major development of this approach to curating and making useful models readily available has now taken place. This is the launch of the *Physiome* journal in 2020 (https://journal.physiomeproject.org), which is dedicated to the curation and ready availability of physiological models.

Physiome will ensure that published models are fully tested so that simple instructions for reproducing any of the figures in those papers will be available. Anyone, anywhere in the world and from whatever speciality, should then be able to run a model to obtain any published results and then alter any parameters to investigate the model's behaviour under new conditions,

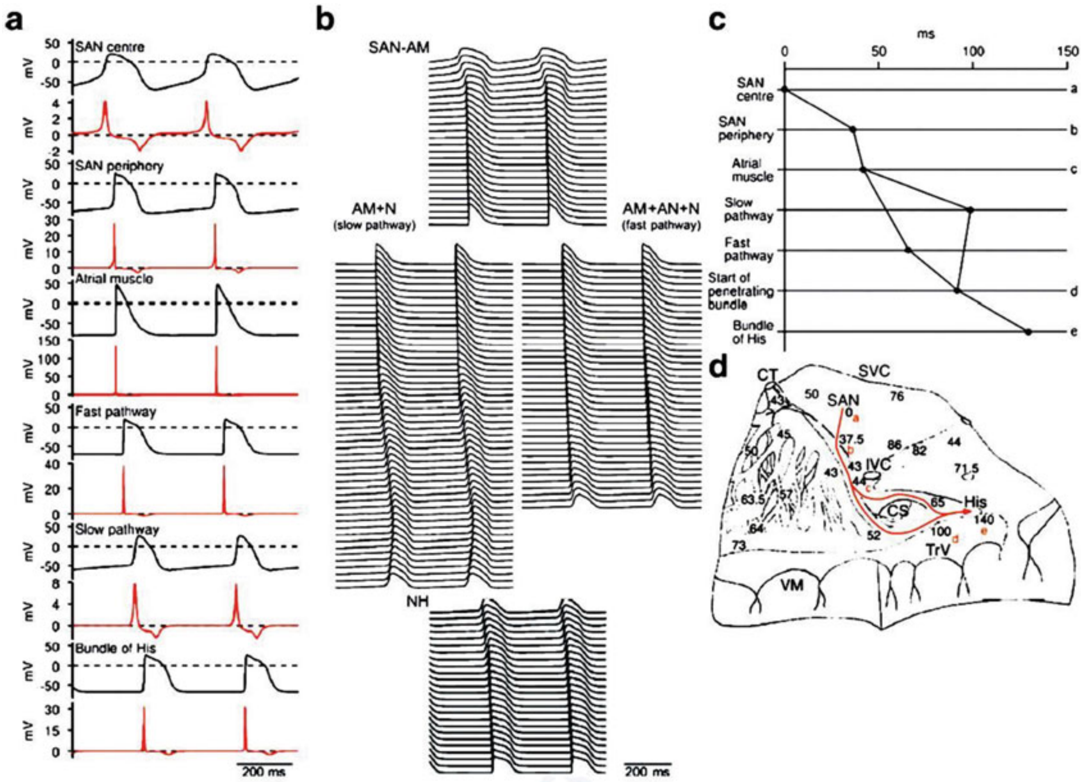

Fig. 2.7 *The Inada 2009 model* Action potential propagation from SAN to AVN. (**a**) Simulated action potentials and the first derivative of membrane potential from centre and periphery of SAN, atrial muscle and AN, N and NH cells. (**b**) Action potentials from many cells along the length of 1D multicellular model. Action potentials from consecutive cells are displaced downward. (**c**) Activation times at the centre and periphery of SAN, atrial muscle at the start of fast and slow pathways into AVN, middle of fast and slow pathways, the start of penetrating bundle and bundle of His (middle of the penetrating bundle). (**d**) Activation times (in metre/second) were recorded experimentally in rabbit right atrial preparation including SAN and AVN during sinus rhythm (from DeCarvalho et al. [42]). *Red* or *grey* line is approximately equivalent to the multicellular model. Letters a–e identify points along the conduction pathway from SAN to AVN at which activation time was measured in simulation: a, centre of SAN; b, periphery of SAN; c, atrial muscle at the start of fast and slow pathways into AVN; d, the start of penetrating bundle; e, bundle of His. *AM* atrial muscle, *CS* coronary sinus, *CT* crista terminalis, *His* bundle of His, *IVC* inferior vena cava, *SVC* superior vena cava, *TrV* tricuspid valve, *VM* ventricular muscle. Reproduced from Inada et al. [37] with permission

including changes in gene expression and gene knockouts.

Physiome models are also annotated with semantic terms so that, if appropriate, a mathematical component always has both a biological meaning and a biophysical meaning. This should make it easier to link models that contain a description of the physiological phenotype for a particular protein to the accession number for that protein in a bioinformatic database. As models of gene expression are developed, this will also facilitate the connection with a corresponding DNA and RNA sequence and the presence of epigenetic markers that may be included in the model.

One of the key aims of *Physiome* is to provide a library of CellML modules that will allow a modeller to build a new model by importing some pre-existing components from the library. For example, if a new model requires a sodium-potassium ATPase ion channel pump, a well-validated model of that ion exchanger will be available for import into OpenCOR as a CellML module. Wherever possible, these protein-level models will be available in bond graph form [43] to ensure that appropriate biophysical laws are obeyed.

2.4.2 Physiological Models and GWAS

The early expectations of genome-wide sequencing were that, within a decade or two, we would find cures for most intractable diseases including heart disease. This has not happened on the scale expected. We have not found many strong correlations between particular genes, their protein products and the probability of particular diseases. On the contrary, most of the association scores are remarkably small, so much so that many genome scientists now favour multi-genic or even omnigenic theories to explain the results [44]. The exceptions include some of the genes whose mutations are involved in cardiac arrhythmias.

One of the successful applications of sinus node models was the demonstration that the presence of multiple mechanisms by which rhythm can be generated ensures the robustness of function. Removing components that have strong functionality may not abolish rhythm [45]. As one component is removed, the rhythmic function continues to be served by alternative pathways of interactions. Noble and Hunter (2020) [46] have pointed out that explaining low association scores could be a valuable contribution of physiological models, and they outlined some of the ways in which that may be achieved.

2.4.3 The Surprising Heart Revisited

One of the most surprising developments in the history of modelling cardiac rhythm was the sudden switch in 1980 from the old I_{K2} interpretation [14] to the "funny" current—a mixed sodium-potassium channel—formed by HCN proteins. The key researcher in that development was Dario DiFrancesco, who recently retired from his chair in Milan. A special issue of *Progress in Biophysics and Molecular Biology* is devoted to celebrating the "funny" current discovery. The opportunity was taken to revisit the Surprising Heart review of 1985 [47]. Readers interested in the early development of pacemaker models will find much new material in the updated Surprising Heart review [47].

2.4.4 Celebration of the DiFrancesco-Noble Model and the Discovery of HCN Channels

After this book was first published in 2011, research on heart rhythm received a further accolade. In 2015, The Royal Society celebrated 350 years of the publication of *Philosophical Transactions,* the longest-running scientific journal in the world. It did so by selecting just a few historic articles from its physical and biological sciences sides. Potential authors were then selected to explain the significance of each article. To the widely revered historic names of Leeuwenhoek and Medawar, amongst biologists, Newton and Faraday amongst physicists, the DiFrancesco-Noble 1985 model [22] was chosen and was set in context in a full-length article [48]. Readers are therefore referred to that article for an update on research today, as well as an assessment of the significance of the first cardiac modelling to incorporate ion concentration changes and ion pumps, as well as the "funny" current HCN channel.

References

1. Van der Pol B, Van der Mark J. The heartbeat considered as a relaxation oscillation and an electrical model of the heart. Philos Mag Suppl. 1928;6:763–75.
2. Demir SS, Clark JW, Murphey CR, Giles WR. A mathematical model of a rabbit sinoatrial node cell. Am J Physiol. 1994;266:C832–52.

3. Dokos S, Celler B, Lovell N. Ion currents underlying sinoatrial node pacemaker activity: a new single cell mathematical model. J Theor Biol. 1996;181:245–72.
4. Endresen LP. Chaos in weakly-coupled pacemaker cells. J Theor Biol. 1997;184:41–50.
5. Demir SS, Clark JW, Giles WR. Parasympathetic modulation of sinoatrial node pacemaker activity in rabbit heart: a unifying model. Am J Physiol. 1999;276:H2221–44.
6. Zhang H, Holden AV, Kodama I, Honjo H, Lei M, Varghese T, et al. Mathematical models of action potentials in the periphery and center of the rabbit sinoatrial node. Am J Physiol. 2000;279:H397–421.
7. Sarai N, Matsuoka S, Kuratomi S, Ono K, Noma A. Role of individual ionic current systems in the SA node hypothesized by a model study. Jpn J Physiol. 2003;53:125–34.
8. Garny A, Kohl P, Hunter PJ, Boyett MR, Noble D. One-dimensional rabbit sinoatrial node models: benefits and limitations. J Cardiovasc Electrophysiol. 2003;14:S121–32.
9. Lovell NH, Cloherty SL, Celler BG, Dokos S. A gradient model of cardiac pacemaker myocytes. Prog Biophys Mol Biol. 2004;85:301–23.
10. Noble D. A modification of the Hodgkin–Huxley equations applicable to Purkinje fibre action and pace-maker potentials. J Physiol. 1962;160:317–52.
11. Noble D. Cardiac action and pacemaker potentials based on the Hodgkin–Huxley equations. Nature. 1960;188:495–7.
12. Hodgkin AL, Huxley AF. A quantitative description of membrane current and its application to conduction and excitation in nerve. J Physiol. 1952;117:500–44.
13. Weidmann S. Elektrophysiologie der Herzmuskelfaser. Bern: Huber; 1956.
14. McAllister RE, Noble D, Tsien RW. Reconstruction of the electrical activity of cardiac Purkinje fibres. J Physiol. 1975;251:1–59.
15. Noble D, Tsien RW. Outward membrane currents activated in the plateau range of potentials in cardiac Purkinje fibres. J Physiol. 1969;200:205–31.
16. Yanagihara K, Noma A, Irisawa H. Reconstruction of the sino-atrial node pacemaker potential based on voltage clamp experiments. Jpn J Physiol. 1980;30:841–57.
17. Bristow DG, Clark JW. A mathematical model of primary pacemaking cell in SA node of the heart. Am J Physiol. 1982;243:H207–18.
18. Noble D, Noble SJ. A model of sino-atrial node electrical activity based on a modification of the DiFrancesco-Noble (1984) equations. Proc R Soc Lond B. 1984;222:295–305.
19. Brown HF, Kimura J, Noble D, Noble SJ, Taupignon A. The ionic currents underlying pacemaker activity in rabbit sino-atrial node: experimental results and computer simulations. Proc R Soc Lond B. 1984;222:329–47.
20. Brown HF, Kimura J, Noble D, Noble SJ, Taupignon A. Mechanisms underlying the slow inward current, isi, in the rabbit sino-atrial node investigated by voltage clamp and computer simulation. Proc R Soc Lond B. 1984;222:305–28.
21. Maltsev VA, Lakatta EG. Synergism of coupled subsarcolemmal Ca^{2+} clocks and sarcolemmal voltage clocks confers robust and flexible pacemaker function in a novel pacemaker cell model. Am J Physiol. 2009;286:H594–615.
22. DiFrancesco D, Noble D. A model of cardiac electrical activity incorporating ionic pumps and concentration changes. Philos Trans R Soc B. 1985;307:353–98.
23. Hilgemann DW, Noble D. Excitation–contraction and extracellular calcium transients in rabbit atrium: reconstruction of basic cellular mechanisms. Proc R Soc Lond B. 1987;230:163–205.
24. Fabiato A. Calcium-induced release of calcium from the cardiac sarcoplasmic reticulum. Am J Physiol. 1983;243:C1–14.
25. Reuter H. The dependence of slow inward current in Purkinje fibres on the extracellular calcium-concentration. J Physiol. 1967;192:479–92.
26. Mullins LJ. Na/Ca exchange. In: Ion transport in the heart. New York: Raven Press; 1981. p. 20–43.
27. Kimura J, Miyamae S, Noma A. Identification of sodium–calcium exchange current in single ventricular cells of guinea-pig. J Physiol. 1987;384:199–222.
28. Noble D. Hodgkin–Huxley–Katz prize lecture: from the Hodgkin–Huxley axon to the virtual heart. J Physiol. 2007;580:15–22.
29. Reiner VS, Antzelevitch C. Phase resetting and annihilation of a mathematical model of sinus node. Am J Physiol. 1985;249:H1143–53.
30. Noble D, DiFrancesco D, Denyer JC. Ionic mechanisms in normal and abnormal cardiac pacemaker activity. In: Jacklet JW, editor. Cellular and neuronal oscillators; 1989. p. 59–85.
31. Wilders R, Jongsma HJ, van Ginneken ACG. Pacemaker activity of the rabbit sinoatrial node. A comparison of mathematical models. Biophys J. 1991;60: 1202–16.
32. Winslow RL, Kimball AL, Varghese A, Noble D. Simulating cardiac sinus and atrial network dynamics on the connection machine. Physica D. 1993;64: 281–98.
33. Matsuoka S, Hilgemann DW. Steady-state and dynamic properties of cardiac sodium–calcium exchange: ion and voltage dependencies of the transport cycle. J Gen Physiol. 1992;100:963–1001.
34. Morrris C, Lecar H. Voltage oscillations in the barnacle giant muscle fiber. Biophys J. 1981;35:193–213.
35. Kurata Y, Hisatome I, Imanishi S, Shibamoto T. Dynamical description of sinoatrial node pacemaking: improved mathematical model for primary pacemaker cell. Am J Physiol. 2002;283:H2074–101.
36. Matsuoka S, Sarai N, Kuratomi S, Ono K, Noma A. Role of individual ionic current systems in ventricular cells hypothesized by a model study. Jpn J Physiol. 2003;53:105–23.

37. Garny A, Noble PJ, Kohl P, Noble D. Comparative study of rabbit sino-atrial node cell models. Chaos Solitons Fractals. 2002;13:1623–30.
38. Mangoni ME, Couette B, Marger L, Bourinet E, Striessnig J, Nargeot J. Voltage-dependent calcium channels and cardiac pacemaker activity: from ionic currents to genes. Prog Biophys Mol Biol. 2006;90: 38–63.
39. Stewart P, Aslanidi OV, Noble D, Noble PJ, Boyett MR, Zhang H. Mathematical models of electrical action potential of Purkinje fibre cells. Philos Trans R Soc A. 2009;367:2225–55.
40. Aslanidi OV, Stewart P, Boyett MR, Zhang H. Optimal velocity and safety of discontinuous conduction through the heterogeneous Purkinje-ventricular junction. Biophys J. 2009;97:20–39.
41. Inada S, Hancox JC, Zhang H, Boyett MR. One-dimensional mathematical model of the atrioventricular node including atrio-nodal, nodal and nodal-His cells. Biophys J. 2009;97:2117–27.
42. De Carvalho AP, Mello WC, Hoffman BF. Electrophysiological evidence for specialized fiber types in rabbit atrium. Am J Physiol. 1959;196: 483–8.
43. Gawthrop PJ, Cursons J, Crampin EJ. Hierarchical bond graph modeling of biochemical networks. Proc R Soc A Math Phys Eng Sci. 2015;471:(2184).
44. Boyle EA, Li Y, Pritchard JK. An expanded view of complex traits: from polygenic to omnigenic. Cell. 2017;169:1177–86.
45. Noble D. Differential and integral views of genetics in computational systems biology. Interface Focus. 2011;1:7–15.
46. Noble D, Hunter P. How to link genomics to physiology through epigenomics. Epigenomics. 2020;12: 285–7.
47. Noble D. The surprising heart revisited: an early history of the funny current with modern lessons. Progr Biophys Mol Biol. 2020;166:3–11.
48. Dibb K, Trafford A, Zhang H, Eisner D. A model: a commentary on DiFrancesco and Noble (1985) A model of cardiac electrical activity incorporating ionic pumps and concentration changes. Philos Trans R Soc Lond B Biol Sci. 2015;370(1666):20140316.

3

Ionic Basis of the Pacemaker Activity of SA Node Cell Revealed by the Lead Potential Analysis

Yukiko Himeno, Akira Amano, and Akinori Noma

Abstract

Ionic mechanisms of spontaneous action potential (AP) in sinoatrial (SA) node pacemaker cells have been discussed for decades. Although several theoretical studies have proposed different mathematical models, no scientific consensus has been achieved yet, because of the complexity and variations in experimental findings used for developing models. Here, we introduce a theoretical method in simulation study, the lead potential (V_L) analysis, which enabled us to isolate the contribution of individual currents from the secondary effect of modified channel activities. We compared three models suggesting different ionic mechanisms (Himeno et al. model, Kurata et al. model, and Maltsev and Lakatta model), and contributions of Ca^{2+} through activation of I_{NaCa} are estimated. Finally, the primary mechanisms of the SA node pacemaker activity were examined by the V_L analysis and confirmed by the bifurcation analysis using a simple minimal cardiac action potential model.

Keywords

Sinoatrial node · Pacemaker activity · Mathematical model · Lead potential · Diastolic depolarization

3.1 Introduction

The ionic mechanisms underlying SA node pacemaker activity have been discussed for decades based on findings of voltage-clamp experiments using the isolated single pacemaker cells as well as the SA node tissue preparation. It is now well established that there is no single "pacemaker current," instead multiple ion channels and electrogenic ion transporter currents generate the pacemaker potential. Thus, although technically challenging, the key issue is to clarify the quantitative as well as qualitative role of individual ionic currents in the pacemaker potential generation. In experiments, a given current of interest is often blocked or depressed using a channel-specific drug. The interpretation of the results or quantitative measure of the contribution is largely interfered with secondary changes in other current systems via modified time course of membrane potential change or ionic concentrations within a cell. This difficulty is largely solved by the recent progress in developing the electrophysiological cardiac cell model. Indeed the pacemaker activity has been well reproduced by a variety of

Y. Himeno (✉) · A. Amano · A. Noma
Faculty of Bioinformatics, College of Life Sciences, Ritsumeikan University, Kusatsu, Japan
e-mail: hime@fc.ritsumei.ac.jp

© Springer Nature Switzerland AG 2023

O. N. Tripathi et al. (eds.), *Heart Rate and Rhythm*, https://doi.org/10.1007/978-3-031-33588-4_3

mathematical cell models which integrate experimental findings [1].

In this chapter, we will introduce an analytical tool, the V_L analysis, to estimate the quantitative contribution of each ionic current and ion exchanger to the pacemaker potential based on mathematical SA node cell models. We will apply this new method to six mathematical models published by Wilders et al. [2], Demir et al. [3], Kurata et al. [4], Sarai et al. [5], Himeno et al. [6] and Maltsev and Lakatta [7]. This analysis allows us to indicate common mechanisms shared by all these models. Further analyses are used to clarify the reasons for discrepancies among these models.

3.2 The Lead Potential (V_L) Analysis

The concept of the V_L analysis has been refined to measure the contribution of individual currents to changes in membrane potential [8]. To facilitate understanding of this method, we first explain the preliminary version of the method introduced by Sarai et al. in 2003 [5] before describing the later version.

3.2.1 The Primary Concept of V_L

The ionic mechanisms underlying the spontaneous action potential (AP) in SA node cells can be explained as follows. The rising phase of the AP is mainly due to the rapid activation of the L-type Ca^{2+} current (I_{CaL}). A positive feedback mechanism is well established that the depolarization by the activation of inward I_{CaL} causes more activation of I_{CaL} itself, culminating in the overshoot potential. The resulting membrane depolarization and Ca^{2+} influx cause inactivation of I_{CaL} and activation of the delayed rectifier K^+ currents (I_{Kr} and I_{Ks}), which together promote repolarization of the cell to the maximum diastolic potential (MDP). Then, the negative potential progressively deactivates I_{Kr} and I_{Ks} in the presence of background inward currents, resulting in the gradual depolarization during the early diastolic period that finally triggers the next AP through the activation of I_{CaL}. The slow diastolic depolarization (DD) is also influenced by Na^+/Ca^{2+} exchanger current (I_{NaCa}) and Na^+/K^+ pump current (I_{NaK}) to the extent that depends on the concentrations of intracellular Ca^{2+} and Na^+, respectively.

In general, the spontaneous changes of the membrane potential are generated by variations in the conductance of individual channel currents by membrane potential, the chemical gating, or the intracellular ion concentrations, and also in the transporter currents. Accordingly, the development of the V_L analysis method started by reducing the membrane system consisting of more than ten ion channels into a single whole-cell membrane conductance (G_m). Irrespective of the conductance properties of each channel, G_m is defined as a sum of the whole cell conductance of K^+ (G_K), Na^+ (G_{Na}), Ca^{2+} (G_{Ca}) and Cl^- (G_{Cl}) (Fig. 3.1a)

$$G_m = G_K + G_{Na} + G_{Ca} + G_{Cl}, \tag{3.1}$$

$$G_K = \frac{I_K}{V_m - E_K} = \frac{I_{net}K - 2I_{NaK}}{V_m - E_K}, \tag{3.2}$$

$$G_{Na} = \frac{I_{Na}}{V_m - E_{Na}} = \frac{I_{net}Na + 3I_{NaK}}{V_m - E_{Na}}, \tag{3.3}$$

$$G_{Ca} = \frac{I_{Ca}}{V_m - E_{Ca}} = \frac{I_{net}Ca + I_{PMCA}}{V_m - E_{Ca}}, \tag{3.4}$$

$$G_{Cl} = \frac{I_{Cl}}{V_m - E_{Cl}} = \frac{I_{net}Cl}{V_m - E_{Cl}}. \tag{3.5}$$

Here, V_m is the membrane potential, and E_x stands for the reversal potential for ion X, which can be defined by the Nernst equation. $I_{net}X$, the whole cell net current for ion X, is calculated according to the ion species irrespective of the passage through specific channel types. For example, the Ca^{2+}, $Na^{+,}$ and K^+ current components through the L-type Ca^{2+} channel were involved in $I_{net}Ca$, $I_{net}Na$, and $I_{net}K$, respectively. The Na^+ and Ca^{2+} fluxes through the Na^+/Ca^{2+} exchanger are included in $I_{net}Na$ and $I_{net}Ca$, since this ion exchange is driven by the passive electrochemical driving force similar to the ion

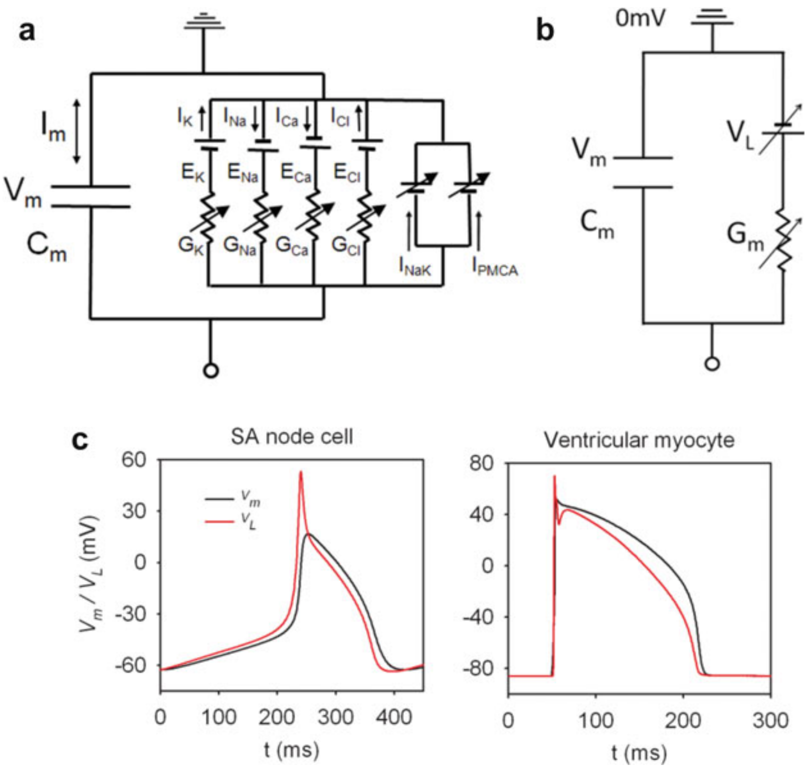

Fig. 3.1 The equivalent electrical circuit of a pacemaker cell membrane excitation (**a**) and a reduced circuit (**b**). C_m, cell membrane capacitance; V_m, membrane potential; G_m, membrane conductance; I_m, total membrane current; I_X, current carried by ion X; E_x, reversal potential for ion X; G_x, conductance for ion X; V_L, lead potential, which is the replacement of E_0 in Eq. (3.8). (**c**): The time course of V_L (red curve, old V_L analysis) superimposed on V_m (black) in the SA node cell (left) and ventricular cell model (right)

channel flux. On the other hand, for the ion fluxes through active transporters, such as I_{NaK} and the plasma membrane Ca^{2+}-ATPase (PMCA) current (I_{PMCA}), are excluded from $I_{net}X$ because the energy drives them through ATP hydrolysis. Although I_{NaK} and I_{PMCA} are not supposed to make substantial contributions to DD, they are essential to maintain the Ca^{2+} homeostasis of the cell [9, 10] and indispensable in the integrative model.

The electrical property of the model can then be reduced to an equivalent circuit consisting of a capacitor, a single variable resistor, and a battery, as shown in Fig. 3.1b. The battery is defined as a zero current potential E_0, which satisfies the following equation

$$I_{\text{net}}K + I_{\text{net}}\text{Na} + I_{\text{net}}\text{Ca} + I_{\text{net}}\text{Cl} = 0. \qquad (3.6)$$

E_0 is solved by substituting net ionic currents in Eqs. (3.2)–(3.5) into Eq. (3.6);

In the reduced circuit, the membrane current is driven by the difference between V_m and E_0. Thus, the time-dependent change in V_m is given by,

$$\frac{dV_m}{dt} = -\frac{I_m}{C_m} = -\frac{G_m \times (V_m - E_0)}{C_m}. \qquad (3.8)$$

Eq. (3.8) indicates thatV_m always moves toward E_0 with a time constant given by C_m/G_m. In Fig. 3.1c, the time course of E_0 is superimposed on that of V_m. Indeed, E_0 is always more positive than V_m during the depolarizing phase and vice versa during the hyperpolarizing phase. E_0 continuously changes in SA node cell and V_m crosses E_0 when $dV_m/dt = 0$ at the MDP and at the peak of AP. In the ventricular myocyte model, V_m remains constant at the resting

---

$$E_0 = \frac{G_K \times E_K + G_{Na} \times E_{Na} + G_{Ca} \times E_{Ca} + G_{Cl} \times E_{Cl} - I_{NaK} - I_{PMCA}}{G_K + G_{Na} + G_{Ca} + G_{Cl}} \qquad (3.7)$$

membrane potential, but once AP is triggered, E_0 changes in advance of V_m in the repolarizing phase. Since E_0 leads the change in V_m, we named E_0 as lead potential (V_L).

Note that the spontaneous change in V_L is caused by the time-dependent changes in ion channel conductance or time-dependent change in the electrogenic ion pumps. If changes in these membrane conductances are all stopped, the time-dependent changes in V_m level off at V_L, and the spontaneous activity disappears. The nongating background ion currents scarcely contribute to the time-dependent changes in V_L because their conductance remains constant.

3.2.2 Contribution of each Ionic Current Estimated Using the Primary V_L Analysis

The application of the preliminaryV_L method to the Sarai et al. model [5], Wilders et al. model [2], and Demir et al. model [3] provided a clear general view of ionic mechanisms as seen in Fig. 3.2. In this method, p(o) of a given channel was suddenly fixed at the MDP. In all models, fixation of p(o) of I_{Kr} almost suppresses DD in V_L, indicating that the time-dependent deactivation of I_{Kr} is the basal mechanism to drive the DD. Fixing p(o) of I_{CaL} results in a slight downward deflection of V_L in the late diastolic phase, indicating that the activation of I_{CaL} is responsible for initiating the next AP. It is obvious that the deactivation of I_{Kr} and the activation of I_{CaL} are the primary mechanisms of the pacemaker depolarization in all three models.

Differences among these three models are observed in the contributions of the hyperpolarization-activated current (I_h or I_f), the sustained inward current (I_{st}) and the T-type calcium current (I_{CaT}). Fixing p(o) of these currents hinders the DD, but the effects are rather small if compared to that of I_{Kr} in these three models. In this respect, these currents might be categorized as ‘supplemental’ currents. Namely, fixing p(o) of I_h is modest in the Sarai et al. model and Demir et al. model. On the other hand, fixing p(o) of I_f in the Wilders model caused a significant downward deflection throughout the DD as if it substitutes the effects of I_{st} in the Sarai et al. model [5] or I_{CaT} in the Demir et al. model [3]. It is evident that the difference among currents in these three models is caused by the different experimental findings used for developing the model, as described below.

I_{CaT} is the low voltage-activated “transient” Ca^{2+} current, but its window current acts as a sustained current in the Demir et al. model. Steady-state activation and inactivation curves in the two models are shown and compared in Fig. 3.3. In the Sarai et al. model, the description of the current is based on data obtained by Hagiwara et al. [11]. On the other hand, Demir et al. modeled the current based on experimental data obtained by Fermini and Nathan [12], whose inactivation was slower and occurred at more positive voltage range. It might be noted that the experimental data points suggest even larger window current than the activation curve used for I_{CaT} modeling (Fig. 3.3a, right panel). In contrast, the fast inactivation kinetics hinders I_{CaT} to exhibit an obvious contribution in the Sarai et al. model. These differences in the inactivation kinetics resulted in an obvious difference in the I_{CaT} contributions between the two models. It should be finally clarified if a different subgroup of cells in the SA node region or different experimental protocols caused different results in each study.

The I_{st} assumed in Sarai et al.’s model is not always used in other SA node modeling but plays a substantial role in the pacemaker depolarization, especially in the late phase of the DD (Fig. 3.2a). I_{st} is a sustained inward current, whose reversal potential ranges between +10 and + 30 mV. It was first reported by Guo et al. in rabbit [13] and then in guinea pig [14, 15] (Fig. 3.4), mouse [16], and rat [17] SA node cells. This nicardipine-sensitive single channel current as well as whole cell current, has been recorded as shown in Fig. 3.4 [14, 15]. Furthermore, its physiological response to autonomic agonists is also observed in guinea pig [18]. Recently, $Ca_V1.3$ channel has been identified as one of the essential molecular components of I_{st} in the SA node cell [19], and its molecular basis has become clearer in some population of SA node cells.

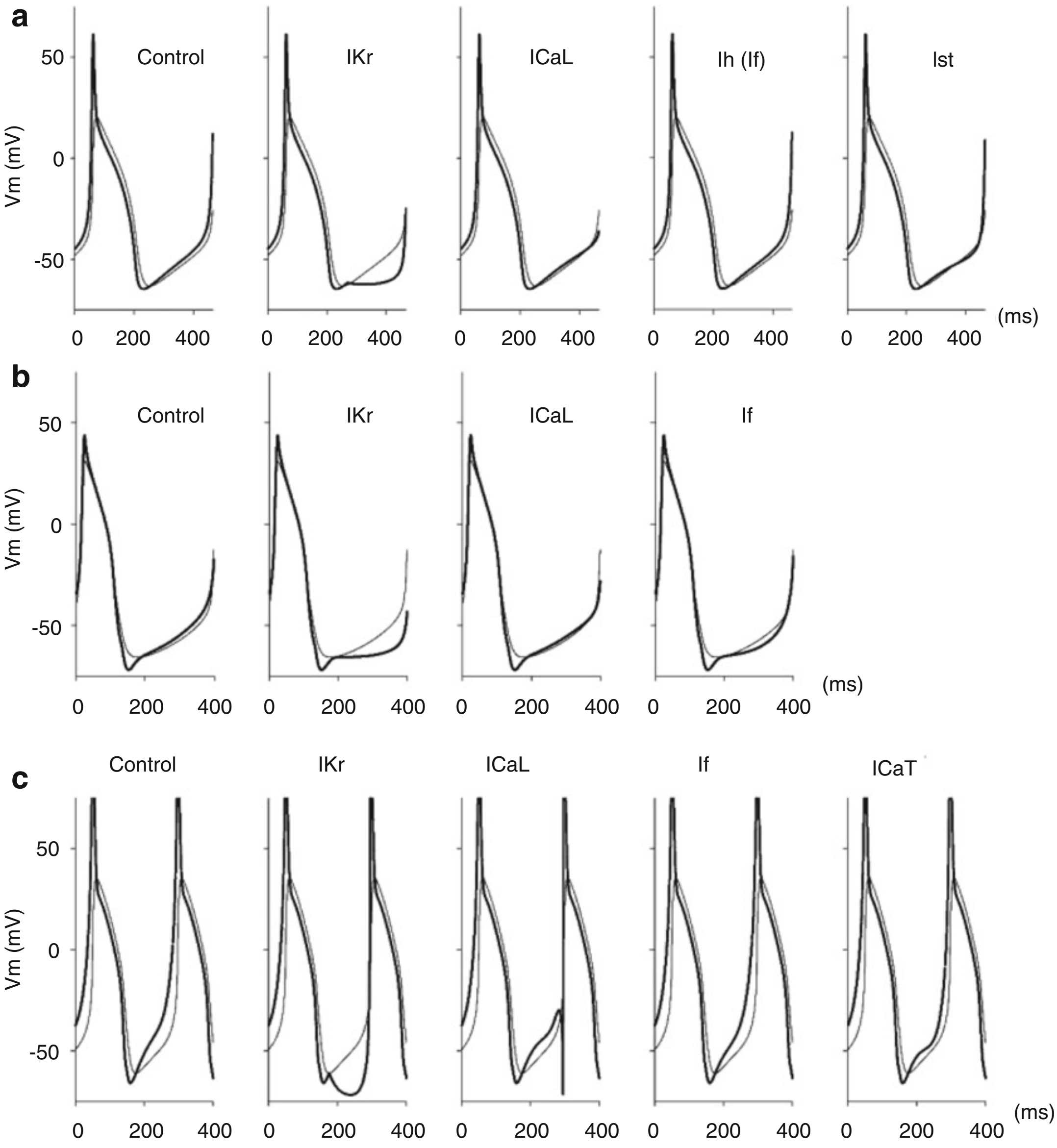

Fig. 3.2 Contribution of each current component to time-dependent changes in V_L examined by the old V_L analysis. (**a**): Sarai et al. model (Kyoto model), (**b**): Wilders et al. model and (**c**): Demir et al. model. The thin trace is the V_m record, and the thick trace is V_L, which is calculated during the interval from the maximum diastolic potential to the beginning of the upstroke of AP. In calculating V_L, the *p*(o) of indicated current was fixed at the value obtained at the maximum diastolic potential

3.3 Sophistication of the V_L Analysis

Although the original V_L analysis enabled us to conclude which ionic channel has relatively large or small contribution to pacemaker activity, it was still intuitive and qualitative. The goal of improving the V_L analysis method was to perform quantitative measurement of the contribution of individual current components during the time

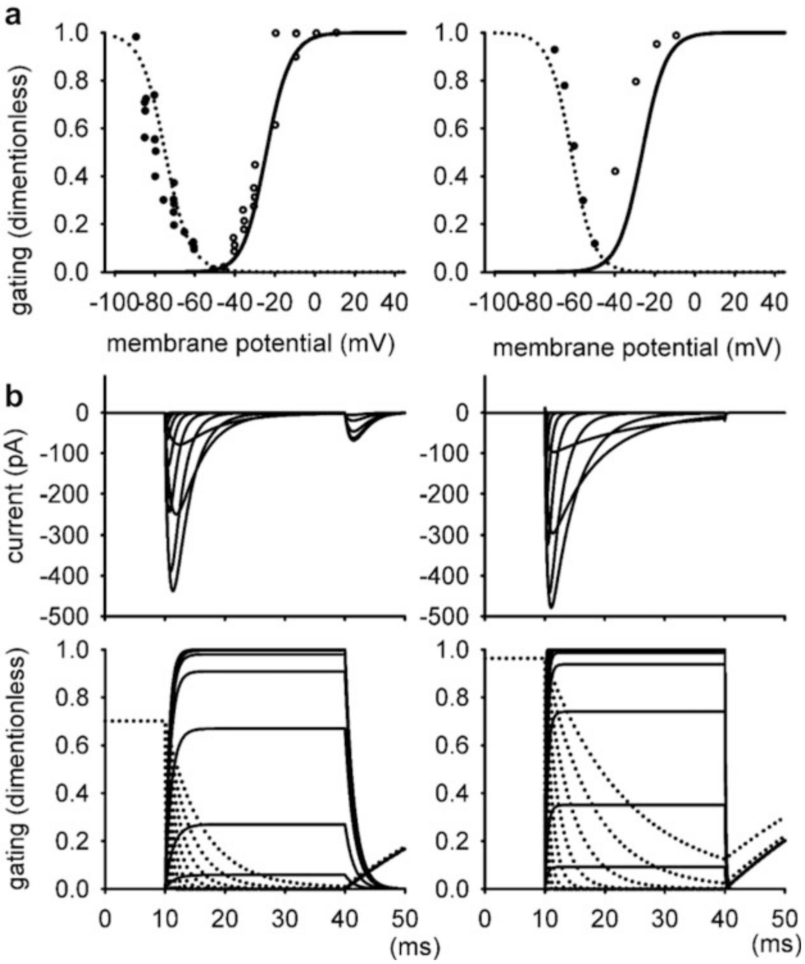

Fig. 3.3 A comparison between the two I_{CaT} models in Sarai et al. (left) and in Demir et al. (right). (**a**): Steady-state voltage dependence of the models (continuous curves). Filled circles and open circles indicate experimental data of steady-state inactivation and activation, respectively, taken from Hagiwara et al. [9] (left) and Fermini and Nathan [10] (right). (**b**): Superimposed traces of simulated currents activated by various test pulses to the range between −40 and 50 mV from a holding potential of −80 mV (top). Time courses of inactivation (dotted lines) and activation (solid lines) gating parameters are shown at the bottom

course of the DD. Toward this end, we refined the mathematical derivation of V_L.

3.3.1 Derivation of the Refined V_L

The temporal change of V_m is described with the following fundamental equation in a single cell:

$$\frac{dV_m}{dt} = -\frac{I_m}{C_m}, \tag{3.9}$$

where C_m is the whole cell membrane capacitance, and I_m is the sum of membrane currents through all ion channels and electrogenic transporters in a single cell. In most mathematical models, current conducted by a channel X (I_X) is described by Ohm's law;

$$I_X = g_{max} \times p(o) \times (V_m - E_{rev}), \tag{3.10}$$

or the Goldman-Hodgkin-Katz (GHK) current equation with a constant field approximation,

$$\begin{aligned} I_X &= p_{max} \times p(o) \times \frac{V_m z_s^2 F^2}{RT} \frac{[S]_i - [S]_o \exp(-z_s FV_m/RT)}{1-\exp(-z_s FV_m/RT)} \\ &= p_{max} \times p(o) \times f(V_m). \end{aligned} \tag{3.11}$$

E_{rev} is the reversal potential for the channel in Eq. (3.10) and f(V_m) is the nonlinear part of the GHK equation in Eq. (3.11). g_{max}, the maximum conductance in Eq. (3.10) and p_{max}, the maximum permeability in Eq. (3.11), are defined as constant parameters. [S] is the concentration of ion S, and F, R, T, and z_s are the Faraday constant, gas constant, absolute temperature and the valence of

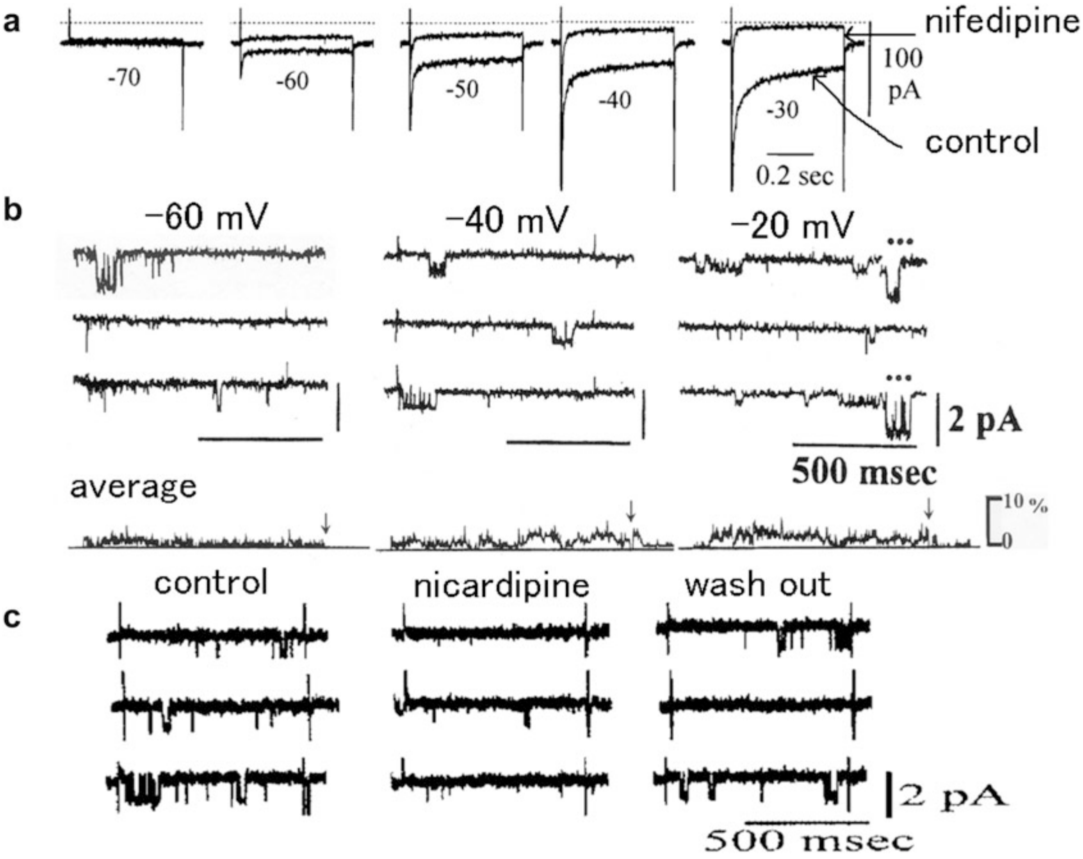

Fig. 3.4 Recordings of I_{st}. (**a**): Whole cell current traces elicited by depolarization pulses in 10 mV steps from −70 to −30 mV from a holding potential of −80 mV. Superimposed traces were recorded with and without 1 μM nicardipine [12]. (**b**): Single channel current (i_{st}) traces (cell-attached patches) evoked by sequential test pulses to −60, −40 and −20 mV from a holding potential of −100 mV and their averages of 70–120 sequential sweeps. (**c**): i_{st} recordings before, during and after the application of 5 μM nicardipine [13]

ion S. p(o) stands for the open probability of the channel, which is a time- and voltage-dependent variable determined by V_m- and/or ligand-dependent gating of the channel. For example, pore block of the inward rectifier K$^+$ (I_{K1}) channel by polyamines or Mg^{2+} [20], or unspecified mechanisms underlying the rectifying properties of the plateau K$^+$ current (I_{Kpl}) were attributed to changes in p(o) in this V_L analysis.

When aiming at quantitatively determining the contribution of ionic systems to the pacemaker depolarization, neglecting nonlinearity of $f(V_m)$ in the old V_L method is a fatal weakness. The new V_L method solves this problem by restricting the following argument only at the moment of observation ($t = t_{ob}$). That is, $f(V_m)$ can be described as a tangential line at $t = t_{ob}$ as follows:

$$f(V_m) \simeq f'(V_m) \times (V_m - E), \qquad (3.12)$$

where E is the value of the intersection of the tangential line with the voltage axis. Then, all the channel currents can be expressed in the common form of $G_X \times (V_m - E_X)$, where

$G_X = g_{max} \times p(o)$ in Eq. (3.10),

and

$G_X = p_{max} \times p(o) \times f'(V_m)$ in Eq. (3.11).

Thus, Eq. (3.9) can be described and rearranged as follows:

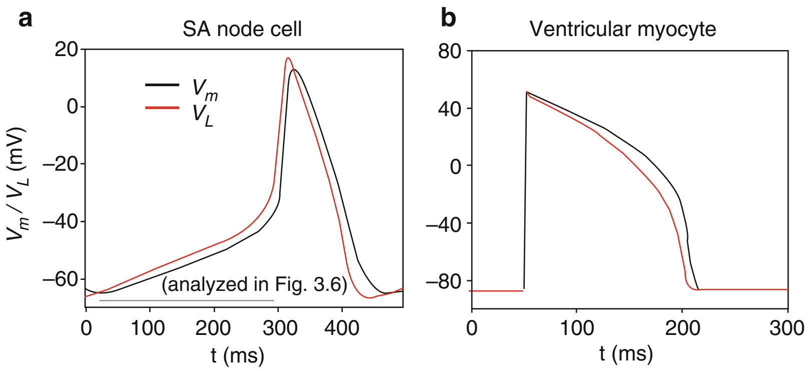

Fig. 3.5 V_L (red) obtained by the new V_L analysis method superimposed on V_m (black) in SA node cell model (**a**) and ventricular myocyte model (**b**). The gray bar in A indicates the time spans analyzed in Fig. 3.6

$$\begin{aligned}\frac{dV_m}{dt} &= -\frac{1}{C_m}\times\left(\sum_X G_X\times(V_m-E_X)+\sum_Y I_Y\right)\\ &= -\frac{1}{C_m}\times\left(V_m\times\sum_X G_X-\sum_X G_X\times E_X+\sum_Y I_Y\right)\\ &= -\frac{\sum_X G_X}{C_m}\times\left(V_m-\frac{\sum_X G_X\times E_X-\sum_Y I_Y}{\sum_X G_X}\right),\end{aligned} \tag{3.13}$$

where X and Y are labels for a channel current and an ion transporter current, respectively, thus, an individual channel is expressed with one battery (E_X) and one conductance (G_X), and each transporter is represented by a current source (I_Y).

Therefore, Eq. (3.13) is described as

$$\frac{dV_m}{dt} = -\frac{1}{\tau}\times(V_m-V_L), \tag{3.14}$$

then,

$$V_L = \frac{\sum_X G_X\times E_X-\sum_Y I_Y}{\sum_X G_X}, \tag{3.15}$$

$$\tau = \frac{C_m}{\sum_X G_X}. \tag{3.16}$$

Until the derivation for Eqs. (3.9) to (3.16), we fixed all the time-dependent variables by the values at $t = t_{ob}$. Now, if we consider V_m as a free variable, Eq. (3.15) corresponds to Fig. 3.1b. Therefore, V_m tends to approach V_L with a time constant τ at each time point. Figure 3.5a and b show temporal changes of V_L and V_m during an AP in SA node cell [6] and ventricular myocyte [21] models obtained by calculating Eq. (3.16) at every moment. Note that the V_L of the new version (Fig. 3.5a) is slightly different from the old one (Fig. 3.1c, left).

3.3.2 Estimation of Contributions of Each Ionic Component

According to Fig. 3.1b and Eq. (3.15), it can be interpreted that the automatic change of V_m is driven by the time-dependent change in V_L, and τ represents the passive property of the membrane. Therefore, automaticity can be expressed in terms of "dV_L/dt" with complete exclusion of τ.

$$\frac{dV_L}{dt} = \frac{\left(\sum_X \dot{G}_X\times E_X+\sum_X G_X\times\dot{E}_X-\sum_Y \dot{I}_Y\right)\times\sum_X G_X-\left(\sum_X G_X\times E_X-\sum_Y I_Y\right)\times\sum_X \dot{G}_X}{\left(\sum_X G_X\right)^2}. \tag{3.17}$$

Here, we will calculate the extent to which a component of interest affects $\mathrm{d}V_\mathrm{L}/\mathrm{dt}$. To evaluate the contribution of a single component, we determine $\mathrm{d}V_\mathrm{L\_Fix}/\mathrm{dt}$ after eliminating its time-dependent change (i.e. $\dot{G}_\mathrm{i} = 0$, $\dot{E}_\mathrm{i} = 0$, or $\dot{I}_\mathrm{i} = 0$), leaving all the other components intact. We refer to this process of eliminating the time-dependent change as "fixing." For example, when we fix G_i, we set $\dot{G}_i = 0$ in Eq. (3.18):

$$\frac{\mathrm{d}V_{L\_\mathrm{Fix}}}{\mathrm{dt}} = \frac{\left(\sum\limits_{\mathrm{X}\neq i}\dot{G}_\mathrm{X}\times E_\mathrm{X} + \sum\limits_{\mathrm{X}} G_\mathrm{X}\times\dot{E}_\mathrm{X} - \sum\limits_{\mathrm{Y}}\dot{I}_\mathrm{Y}\right)\times\sum\limits_{\mathrm{X}} G_\mathrm{X} - \left(\sum\limits_{\mathrm{X}} G_\mathrm{X}\times E_\mathrm{X} - \sum\limits_{\mathrm{Y}} I_\mathrm{Y}\right)\times\sum\limits_{\mathrm{X}\neq i}\dot{G}_\mathrm{X}}{\left(\sum\limits_{\mathrm{X}} G_\mathrm{X}\right)^2}. \quad (3.18)$$

The relative contribution of each component, r_c is defined as follows:

$$r_\mathrm{c} = \frac{\frac{\mathrm{d}V_\mathrm{L}}{\mathrm{dt}} - \frac{\mathrm{d}V_\mathrm{L\_Fix}}{\mathrm{dt}}}{\frac{\mathrm{d}V_\mathrm{L}}{\mathrm{dt}}} \qquad \left(\text{when } \frac{\mathrm{d}V_\mathrm{L}}{\mathrm{dt}} \neq 0\right), \quad (3.19)$$

and r_c satisfies the following equation:

$$\sum r_\mathrm{c} = 1, \quad (3.20)$$

for all components. An r_c of positive sign means that the component is operating to drive $\mathrm{d}V_\mathrm{L}/\mathrm{dt}$ in the same direction as the control $\mathrm{d}V_\mathrm{L}/\mathrm{dt}$. On the other hand, an r_c of negative sign means that the component interferes with the change of V_L by inclining $\mathrm{d}V_\mathrm{L}/\mathrm{dt}$ in the opposite direction.

3.3.3 Contribution of Each Ionic Component to the Pacemaker Potential Quantified by the V_L Analysis

Using the refined V_L method, the description of the contribution of each ionic component has been improved dramatically. Figure 3.6 shows the result of the V_L analysis performed on the same SA node model illustrated in Fig. 3.5a. Transition of the relative contribution is shown along the time axis, and the mechanisms of contribution are explained based on the time-dependent variations of $p(o)$ and the current amplitude shown in Fig. 3.6b. The magnitude of $\mathrm{d}V_\mathrm{L}/\mathrm{dt}$ remained nearly constant at around 0.09 mV/ms during the initial 200 ms after MDP and increased exponentially thereafter, as shown in Fig. 3.6a. At the beginning of depolarization, $\mathrm{d}V_\mathrm{L}/\mathrm{dt}$ is largely determined by the deactivation of the outward I_Kr (i.e., the decrease in p(o) of I_Kr in Fig. 3.6b). As r_c of I_Kr decreases, it is substituted by those of the inward currents, I_st and I_CaL, via depolarization-dependent activation. r_c of I_st reached a peak of ~0.63 and then decreased after 220 ms, which is simply biased by the much larger increase in r_c of I_CaL. Although the increase of p(o) in I_CaL is tiny (<0.002) during the late diastolic period, it is the main current in the upstroke of AP and also affects $\mathrm{d}V_\mathrm{L}/\mathrm{dt}$. Inward I_h also plays a positive role at the early stage with an r_c of ~0.1. This is relatively small because the increase of p(o) saturates around 220 ms, and the amplitude of I_h is small. Similarly, the relatively small contribution of I_Ks is explained by a little change in p(o) (~0.002), which is attributable to a limited activation during the preceding AP. The V_L analysis clearly separates the role of the nonselective cation current (I_bNSC) from that of V_m-gated channel currents. It has been reported that I_bNSC, the largest inward current of ~−25 pA, plays a role in DD by driving V_m toward its reversal potential of ~0 mV [22]. However, r_c of I_bNSC is zero because I_bNSC has neither gating nor rectification.

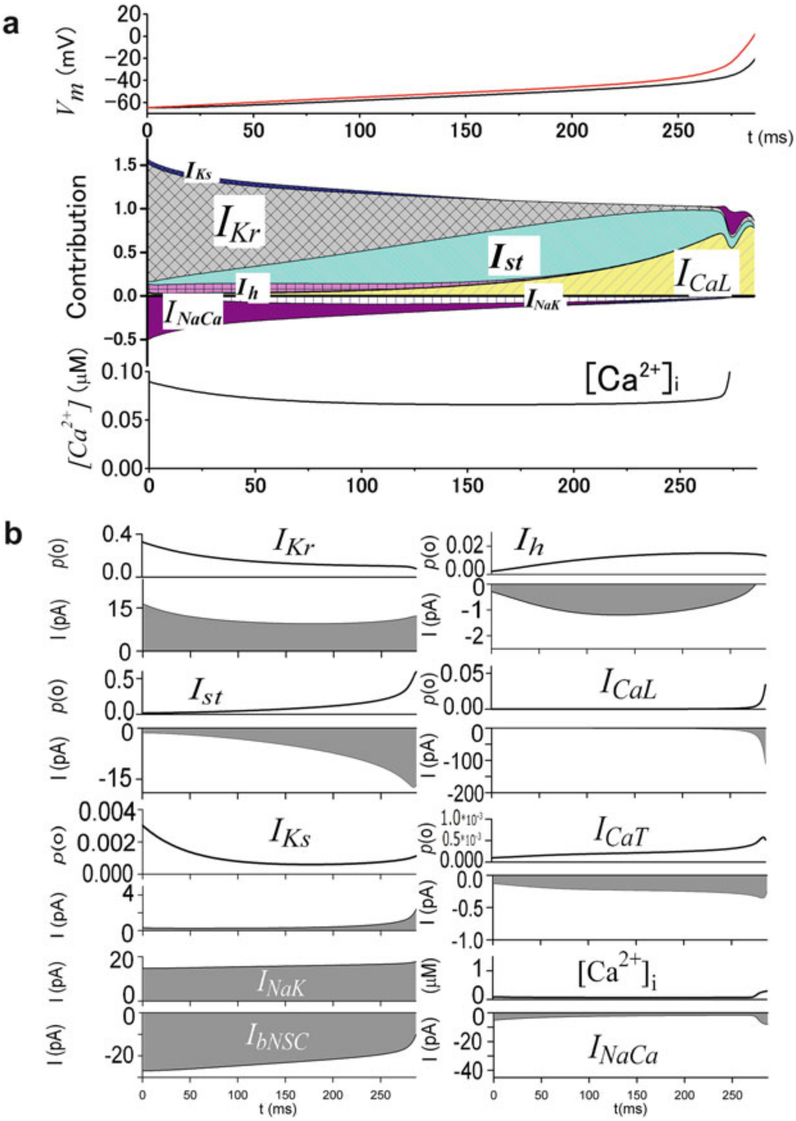

Fig. 3.6 The time profile of r_c (defined by Eqs. (3.2)–(3.9)) during DD in the Himeno et al. model. (**a**). The time-dependent changes of r_c of the major current components during changes of V_L (red) and V_m (black) are shown at the top and $[Ca^{2+}]_i$ at the bottom. The analyzed section of AP is shown by the gray bar in Fig. 3.5a. (**b**). changes of p (o)s or amplitudes of individual currents indicated in the graph, and $[Ca^{2+}]_i$

The amplitude of inward-going I_{NaCa} gradually decreases during DD due to a decrease of $[Ca^{2+}]_I$ in the first 2/3 of the depolarization phase and a continuous increase in V_m. Thereby, r_c of I_{NaCa} is negative for DD. I_{NaK} also has a negative r_c because the outward I_{NaK} increases with depolarizing V_m. Because of these negative contributions of I_{NaCa} and I_{NaK}, the sum of positive contributions in the profile is larger than 1.0 in this model. As far as we are aware, the concept of this negative contribution is introduced for the first time in this V_L analysis and is clearly defined by Eq. (3.19).

3.4 Variations in the Ionic Mechanisms Hypothesized by Different Mathematical Pacemaker Cell Models

It has long been suggested that the configuration of the spontaneous APs shows variations according to the recording location within the SA node regions. This issue has been thoroughly investigated by Mark Boyett’s group by examining the ion channel expression in the different types of cells isolated from different locations within SA node [23]. This kind of variation may partly correspond to the variable weight of individual channel current contribution among different mathematical models, as demonstrated in Fig. 3.2.

Variations in the ionic mechanisms have also been explained by modifying the model structure. Especially the intracellular Ca^{2+} distribution within the cell has been examined in the pacemaker mechanism by assuming a subsarcolemmal space. It might be noted that SA node cells have no transverse tubules within the cell, and therefore the EC coupling may occur at the junction of subsarcolemmal cisterna of sarcoplasmic reticulum (SR) with the surface membrane [24]. For the sake of simplicity, a uniform subsarcolemmal space was first assumed in the SA node cell model [4]. Later this model was further modified and used by Maltsev and Lakatta [7], focusing on the contribution of intracellular Ca^{2+} concentration to the pacemaker mechanisms. In the following section, we will apply the V_L method to the Kurata et al. model and the Maltsev and Lakatta model to compare with the Himeno et al. model.

3.4.1 Contribution of I_{NaCa} Intensified by the Localized Ca^{2+} in Kurata Model

In the Kurata model, a subsarcolemmal space of 20 nm in depth is introduced underneath the surface membrane and occupies only 1% of the cytosolic space. Since it is assumed that the Ca^{2+} flux through both the I_{CaL} channel as well as the ryanodine receptor (RyR) channel on the sarcoplasmic reticulum (SR) is directed into this limited subsarcolemmal space, the transient increase in subsarcolemmal Ca^{2+} ($[Ca^{2+}]_{sub}$) is much larger than that in intracellular bulk Ca^{2+} ($[Ca^{2+}]_i$) in other SA node cell models, where $[Ca^{2+}]_i$ is assumed to be homogeneous throughout the cell. Figure 3.7a shows the results of V_L analysis as well as Ca^{2+} concentrations ($[Ca^{2+}]_{sub}$ and $[Ca^{2+}]_i$) in the Kurata et al. model. Except for the Ca^{2+}-related events, the general view of the mechanism is in good agreement with Himeno et al. model. Namely, the successive shift of the major role from I_{Kr} to I_{st} and the following significant increase in the contribution of I_{CaL} is essentially the same in the other pacemaker cell models described previously. A gradual decrease in the negative contribution of I_{NaCa} caused by dissipation of the Ca^{2+} transient is also a common mechanism observed in other models. The prominent difference is the timing of conversion of the sign of I_{NaCa} contribution from negative to positive in the last 1/3 of the diastolic period in this model. This conversion is caused by voltage-dependent activation of I_{CaT} as well as I_{CaL} over the corresponding time period in Kurata et al.'s model. $[Ca^{2+}]_{sub}$ increased twice as much as that in myoplasm at 125 ms and yielded a peak of ~1.8 μM at its maximum as reported by Glukhovsky et al. [25] and Snyder et al. [26] in their simulation studies. The activation of I_{CaT} starts soon after the MDP, and thereby favors the early contribution of I_{NaCa} through the Ca^{2+} accumulation in the subsarcolemmal space. The r_c of I_{NaCa}, which is accelerated by the Ca^{2+} released from the SR is still minor (27%) in this model at the end of the V_L profile. The r_c of I_{CaT} is enlarged in this model (22%) compared to that in Himeno et al.'s model (12%). The maximum amplitude of I_{CaT} reached to ~ − 7 pA in late DD in the Kurata et al. model (Fig. 3.7), whereas it is only −0.2 pA in Himeno et al.'s model (Fig. 3.6). The difference is attributable to the different experimental data referred to in each model as explained in Sect. 3.2.1 above and Fig. 3.3. Kurata et al. assumed a larger contribution of I_{CaT} to the pacemaker depolarization based on an experimental observation by Doerr et al. [27] and adopted equations from a model by Demir et al. [3].

3.4.2 Intracellular Ca^{2+} Clock in Maltsev and Lakatta Model

A new pacemaker mechanism was proposed by Edward Lakatta's group: the intracellular "Ca^{2+} clock" [28–30]. This mechanism is quite comparable to the 'triggered activity,' which is well established in the ventricular myocytes. If ventricular myocytes are superfused with a solution containing moderate concentrations of cardiotonic

Fig. 3.7 The time profile of r_c during DD in the Kurata et al. model. (**a**) and (**b**) are shown in the same style as in Fig. 3.6 except for the presence of blue line, which represents $[Ca^{2+}]_{sub}$

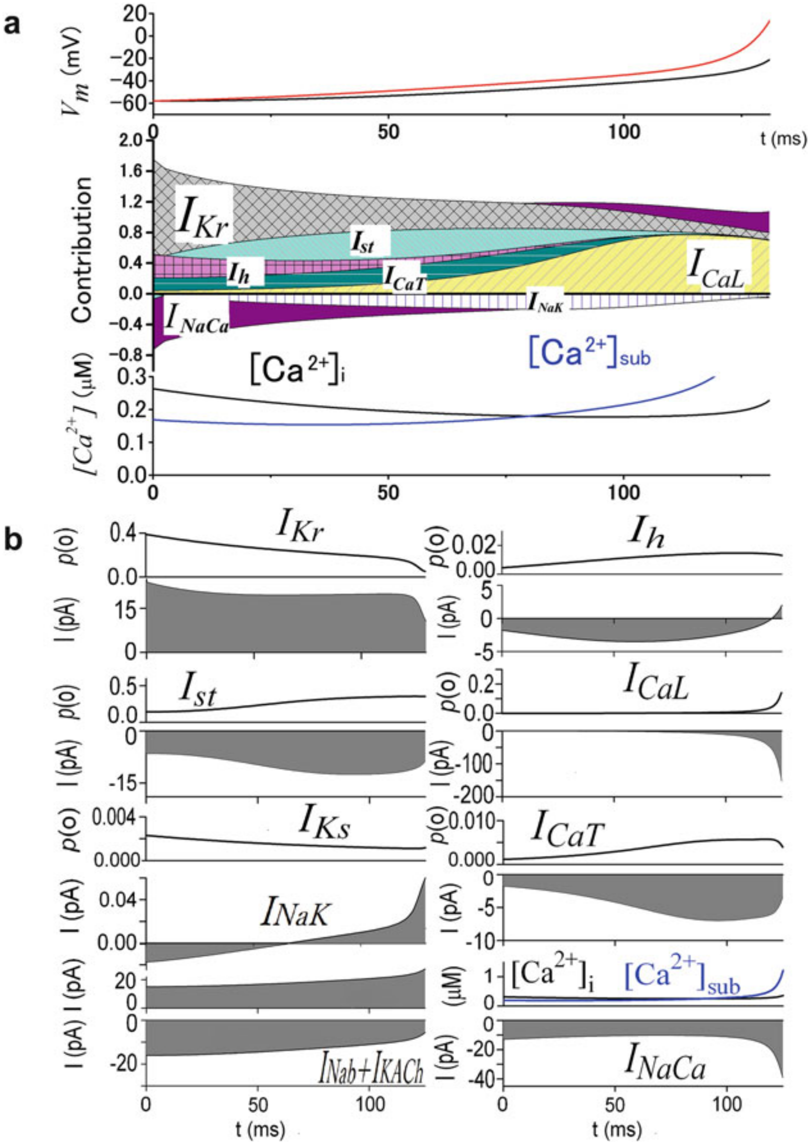

steroids and a high concentration of extracellular Ca^{2+} (75–200 ng/ml acetylstrophanthidin and 2.5 mM Ca^{2+} in Ferrier [31]; and 2–10 μM ouabain and 5.4 mM Ca^{2+} in Matsuda et al. [32]), the Ca^{2+} content in the SR is increased and the spontaneous Ca^{2+} release is accelerated. By applying conditional depolarizing pulses under voltage-clamp conditions, this spontaneous Ca^{2+} release can be detected by the oscillatory transient inward current, I_{NaCa}. Without voltage-clamp, repetitive Ca^{2+} transients or inward I_{NaCa} are evoked after conditional repetitive electrical stimulation. When the increase in the amplitude of transient depolarization was sufficient to bring the membrane potential to the threshold, a spontaneous full-amplitude AP was elicited, especially with β-adrenergic stimulation. This triggered activity disappears if the ventricular myocytes are relieved from the Ca^{2+} overload. Healthy myocytes do not show transient depolarization or such an inward current.

In SA node pacemaker cells, repetitive Ca^{2+} transients were recorded by Edward Lakatta's group when the spontaneous AP was stopped by voltage-clamp, even under normal physiological conditions. Vinogradova et al. [28] observed repetitive spontaneous inward currents, largely dependent on the spontaneous Ca^{2+} release from SR. This hypothesis provoked much discussion and was finally explained with a concrete SA node pacemaker cell model [7]. The significant modifications from the Kurata et al. model [4] were reductions of conductance in major inward currents, g_{CaL}, g_{CaT}, $g_{h,}$ and g_{st}, by 20%, 60%, 60%, and 80%, respectively, which interfered with spontaneous generation of AP by plasma membrane currents. In addition, the Ca^{2+}-dependent mechanisms were enhanced by increasing the maximum amplitude of I_{NaCa} by 50% and increasing the background Ca^{2+} influx (I_{Cab}). Parameters for the SR Ca^{2+} dynamics, such as the time constant of Ca^{2+} transfer from the network SR (uptake site) to junctional SR (release site) and rate constant for Ca^{2+} uptake by Ca^{2+} pump and Ca^{2+} release flux via RyR, are also modified to strengthen the effect of SR based on their experimental results [27]. Consequently, it is noted that $[Ca^{2+}]_{sub}$ starts increasing almost from the beginning of the DD and activates I_{NaCa} significantly to contribute to V_m change throughout DD, as revealed by the V_L analysis (Fig. 3.8).

3.5 Mechanisms of the Cardiac Pacemaker Activity

To sustain the Ca^{2+} clock mechanism, it was theoretically suggested using a mathematical model that the concentration of Ca^{2+} in the junctional SR should be high enough (more than 0.5 mM) at least in the SA node cell model developed by Stern et al. [33] and refilled by Ca^{2+} influx through Ca^{2+} channels beat by beat for the regenerative Ca^{2+}-induced Ca^{2+} release (CICR). In addition, the whole cell Ca^{2+} concentration level including not only bulk free Ca^{2+} but also buffered Ca^{2+} in the intracellular bulk space as well as in the SR, needs to be kept high enough to induce spontaneous CICR [34, 35]. It is true that there are some types of cardiomyocytes in which the Ca^{2+} clock mechanism may play a major role in inducing automaticity, such as in pulmonary vein cardiomyocytes under the effect of catecholamine, for example [36, 37]. However, it was experimentally revealed that the pacemaker activity remained almost intact after fixing the intracellular Ca^{2+} concentration to zero level by injecting a high concentration (10 mM) of strong Ca^{2+} chelator, BAPTA, into the cell in the guinea pig SA node [38]. In this section, the essential key feature of the membrane clock mechanism in the cardiac pacemaker will be explained using a model composed of a minimum number of factors required for the rhythmic membrane oscillations.

3.5.1 The Minimal Model of the Spontaneous AP in a Cardiac Pacemaker Cell

To understand the basic mechanism underlying the spontaneous AP in the cardiac pacemaker cell, a radically simplified model composed of four current components was created, as shown in Fig. 3.9. The model is represented by the electrical equivalent circuit superimposed on the cell scheme.

The membrane capacitance (C_m) is connected to a simplified K^+ channel, Ca^{2+} channel, and two Ohmic background channels. The current I_K is calculated by using a gating parameter n and the current I_{Ca} with an activation gate d and inactivation gate f. The remaining two channels, I_{Nabg} and I_{Kbg}, use constant conductance parameters: G_{Nabg} and G_{Kbg}, respectively

$$I_K = G_{Kmax} \cdot n \cdot (V_m - E_K) \tag{3.21}$$

$$I_{Ca} = G_{Camax} \cdot d \cdot f \cdot (V_m - E_{Ca}) \tag{3.22}$$

$$I_{Nabg} = G_{Nabg} \cdot (V_m - E_{Na}) \tag{3.23}$$

$$I_{Kbg} = G_{Kbg} \cdot (\mathrm{V_m} - \mathrm{E_K}) \tag{3.24}$$

The instantaneous equilibrium potential (E_m) is determined at the equilibrium, $\mathrm{d}V_m/\mathrm{dt} = 0$

$$I_K + I_{Ca} + I_{Nabg} + I_{Kbg} = 0 \tag{3.25}$$

By substituting each current component of Eq. (3.14) by Eqs. (3.10)–(3.13), the instantaneous equilibrium potential (E_m) is given as a sum of each channel element of V_L [8]

Fig. 3.8 The time profile of r_c during DD in the Maltsev and Lakatta model. (**a**) and (**b**) are shown in the same style as in Fig. 3.7

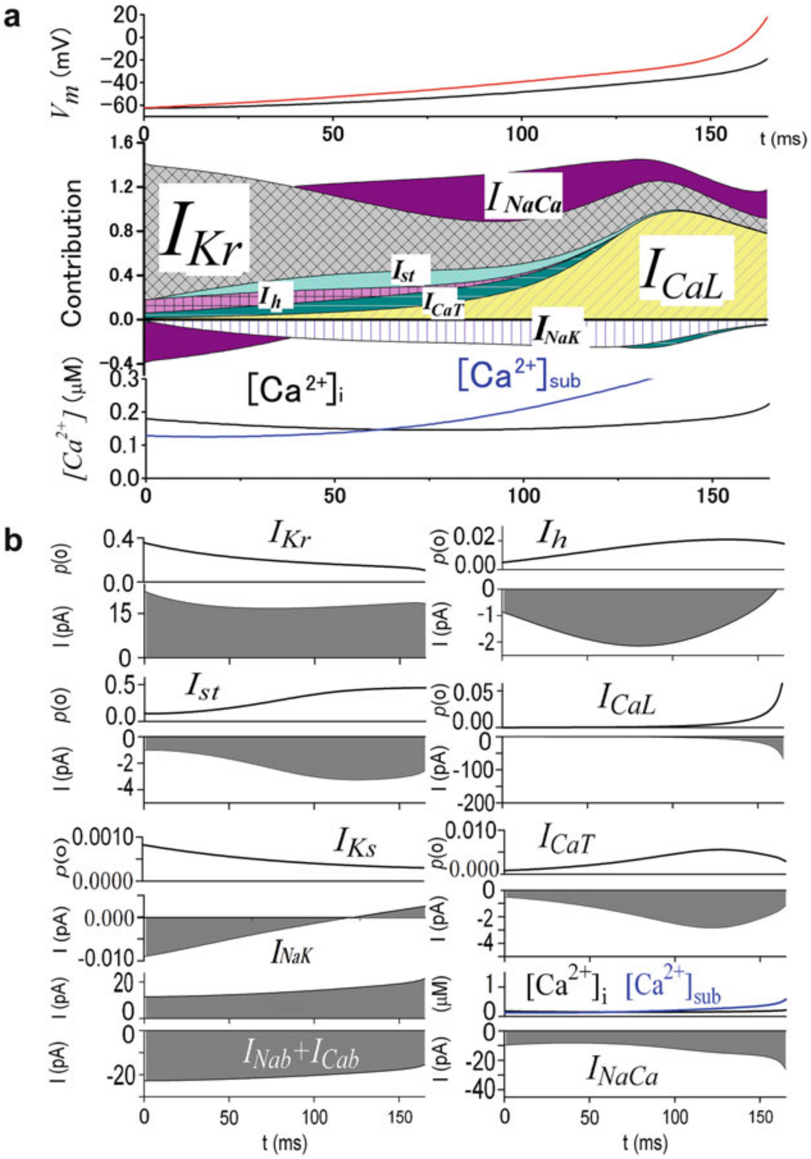

$$E_m = \frac{G_K E_K + G_{Ca} E_{Ca} + G_{Kbg} E_K + G_{Nabg} E_{Na}}{G_K + G_{Ca} + G_{Kbg} + G_{Nabg}} \tag{3.26}$$

The gating parameters of the K$^+$ and Ca^{2+} channels are calculated by assuming a two-state transition scheme with the forward and backward rate constants, α and β which are dependent on V_m

$$\alpha_n = \frac{1}{28 \cdot \exp\left(-\frac{V_m}{10}\right) + 20 \cdot \exp\left(-\frac{V_m}{80}\right)} \tag{3.27}$$

$$\beta_n = \frac{1}{500 \cdot \exp\left(\frac{V_m}{9}\right) + 300 \cdot \exp\left(\frac{V_m}{50}\right)} \tag{3.28}$$

$$\alpha_d = \frac{1}{0.35 \cdot \exp\left(-\frac{V_m}{7}\right) + 2 \cdot \exp\left(-\frac{V_m}{30}\right)} \tag{3.29}$$

$$\beta_d = \frac{1}{9 \cdot \exp\left(\frac{V_m}{8}\right) + 2 \cdot \exp\left(\frac{V_m}{50}\right)} \tag{3.30}$$

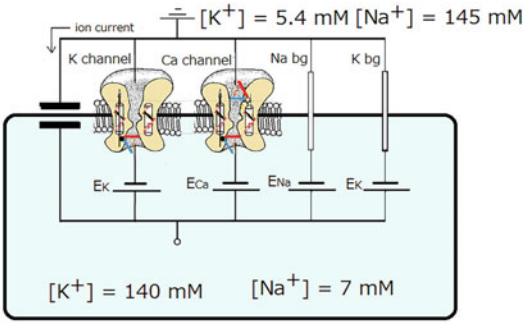

Fig. 3.9 The schematic representation of the minimal pacemaker model circuit. The default parameters of the model are, $C_m = 1$ pF, $G_{\text{Camax}} = 2.7$ nS/pF, $G_{\text{Kmax}} = 0.078$ nS/pF, $G_{\text{Kbg}} = 0.05$ nS/pF, $G_{\text{Nabg}} = 0.02$ nS/pF, $E_{\text{Ca}} = +40$ mV, $E_K = -87$ mV, $E_{\text{Na}} = +81$ mV. E_{Ca} was approximated by the experimental reversal potential of I_{CaL} (+40 mV)

$$\alpha_f = \frac{1}{1500 \cdot \exp\left(\frac{V_m}{7}\right) + 50 \cdot \exp\left(\frac{V_m}{4000}\right)} \tag{3.31}$$

$$\beta_f = \frac{1}{0.8 \cdot \exp\left(-\frac{V_m}{8}\right) + 25 \cdot \exp\left(-\frac{V_m}{4000}\right)} \tag{3.32}$$

In the electric circuit in Fig. 3.9, V_c always follows E_m, which corresponds to V_L, with a time constant τ, when the gating variables are continuously changing during the AP

$$\frac{dV_c}{dt} = -\frac{V_c - V_L}{\tau} \tag{3.33}$$

$$\tau = \frac{C_m}{G_{\text{tot}}} \tag{3.34}$$

$$G_{\text{tot}} = G_K + G_{\text{Ca}} + G_{\text{Kbg}} + G_{\text{Nabg}} \tag{3.35}$$

The Eq. (3.26) is reformatted as,

$$V_L = \frac{\sum_X G_X E_X}{\sum_X G_X}. \tag{3.36}$$

Differentiating Eq. (3.36) gives,

$$\frac{dV_L}{dt} = \frac{\left(\sum_X \dot{G}_X E_X + \sum_X G_X \dot{E}_X\right) \cdot \sum_X G_X + \left(\sum_X G_X E_X\right) \cdot \sum_X \dot{G}_X}{\left(\sum_X G_X\right)^2}, \tag{3.37}$$

$$\frac{dV_L}{dt} = \frac{\sum_X \dot{G}_X E_X + \sum_X G_X \dot{E}_X}{\sum_X G_X} - V_L \cdot \frac{\sum_X \dot{G}_X}{\sum_X G_X}, \tag{3.38}$$

$$\frac{dV_L}{dt} = \frac{\sum_X \dot{G}_X (E_X - V_L) + \sum_X G_X \dot{E}_X}{\sum_X G_X}. \tag{3.39}$$

In the minimal model, E_X is fixed.

$$\dot{E}_X = \frac{dE_X}{dt} = 0 \tag{3.40}$$

Then,

$$\dot{G}_K = G_{\text{Kmax}} \cdot \frac{dn}{dt}, \tag{3.41}$$

$$\dot{G}_{\text{Ca}} = G_{\text{Camax}} \cdot \frac{d(\text{df})}{dt}, \tag{3.42}$$

$$\frac{dV_L}{dt} = \frac{\frac{dn}{dt}(E_K - V_L) + \frac{d(\text{df})}{dt}(E_{\text{Ca}} - V_L)}{n \cdot G_{\text{Kmax}} + d \cdot f \cdot G_{\text{Camax}} + G_{\text{Kbg}} + G_{\text{Nabg}}}, \tag{3.43}$$

$$\frac{dV_L}{dt} = \frac{\frac{dn}{dt}(E_K - V_L)}{n \cdot G_{\text{Kmax}} + d \cdot f \cdot G_{\text{Camax}} + G_{\text{Kbg}} + G_{\text{Nabg}}} + \frac{\frac{d(\text{df})}{dt}(E_{\text{Ca}} - V_L)}{n \cdot G_{\text{Kmax}} + d \cdot f \cdot G_{\text{Camax}} + G_{\text{Kbg}} + G_{\text{Nabg}}}. \tag{3.44}$$

Each component of the right side of Eq. (3.44) defines each contribution of K^+ channel and Ca^{2+} channel to dV_L/dt, respectively.

3.5.2 Results of the V_L Analysis

The simulation results of the minimal model are demonstrated in Fig. 3.10.

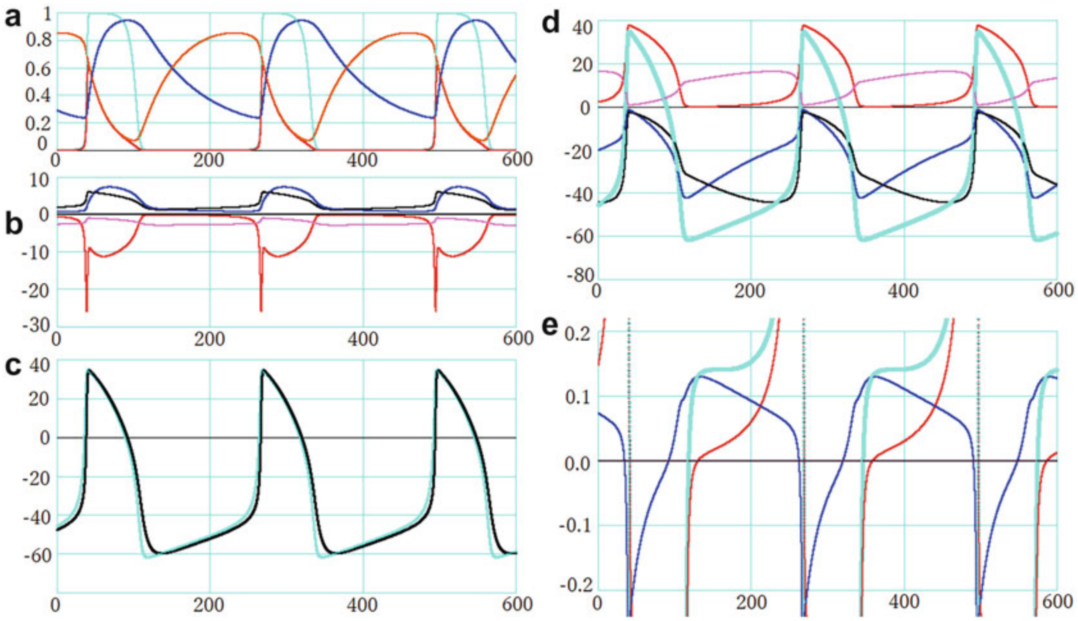

Fig. 3.10 Simulation results using the minimal AP model. Panel (**a**) shows time-dependent changes in *n* (blue), df (red), Panel (**b**) shows I_K (blue), I_{Kbg} (black), I_{Ca} (red) and I_{Nabg} (pink), and Panel (**c**) shows the action potential (black) superimposed with V_L (cyan). Panel (**d**) shows changes in V_L, as well as V_L elements of I_K (blue), I_{Ca} (red), I_{Kbg} (black), I_{Nabg} (pink). Panel (**e**) shows changes in dV_L/dt, as well as dV_L/dt elements of I_K (blue), I_{Ca} (red)

The dV_L/dt elements of I_{Kbg} (black) and I_{Nabg} (pink) are zero, because G_X as well as E_X are constant, therefore, their contribution to the numerator of dV_L/dt in Eq. 3.39 is zero. The variations in the V_L element of I_{Kbg} and I_{Nabg} (in Fig. 3.10d) are caused by a change in the denominator G_{tot} in Eq. (3.36).

Note that the slope of the DD is determined as a sum of decremental I_K conductance and incremental I_{Ca} conductance as clearly shown by the large positive dV_L/dt elements of I_K (blue) and I_{Ca} (red) in Fig. 3.10e.

3.5.3 The Application of the Bifurcation Analysis (Equilibrium Point Analysis) to the Minimal Model

As we have seen in the previous sections, the mathematical models of the SA node cell are composed of many ordinary differential equations, which describe the time-varying changes in the function of molecular components of the cell. The time-dependent changes in the cell function observed in experimental studies can be reconstructed by the numerical methods for the simultaneous multiple lines of differential equations in good approximation. Separately, analytical solutions can be obtained as an equilibrium point or oscillatory solution by applying the bifurcation analysis. For example, the resting membrane potential is defined by the stable equilibrium point and the steady cycle of action potential generation by the stable limit cycle.

Taking advantage of the simplified model, we applied the bifurcation analysis to get a deeper insight into the mechanisms underlying the rhythmic discharge of AP in the minimal model.

Figure 3.11 shows the basic influence of the background inward (I_{Nabg}) or outward (I_{Kbg}) background conductance to the generation of the spontaneous AP.

When G_{Nabg} was increased from 0, the equilibrium point, that was exactly equal to the resting potential, was continuously obtained until the

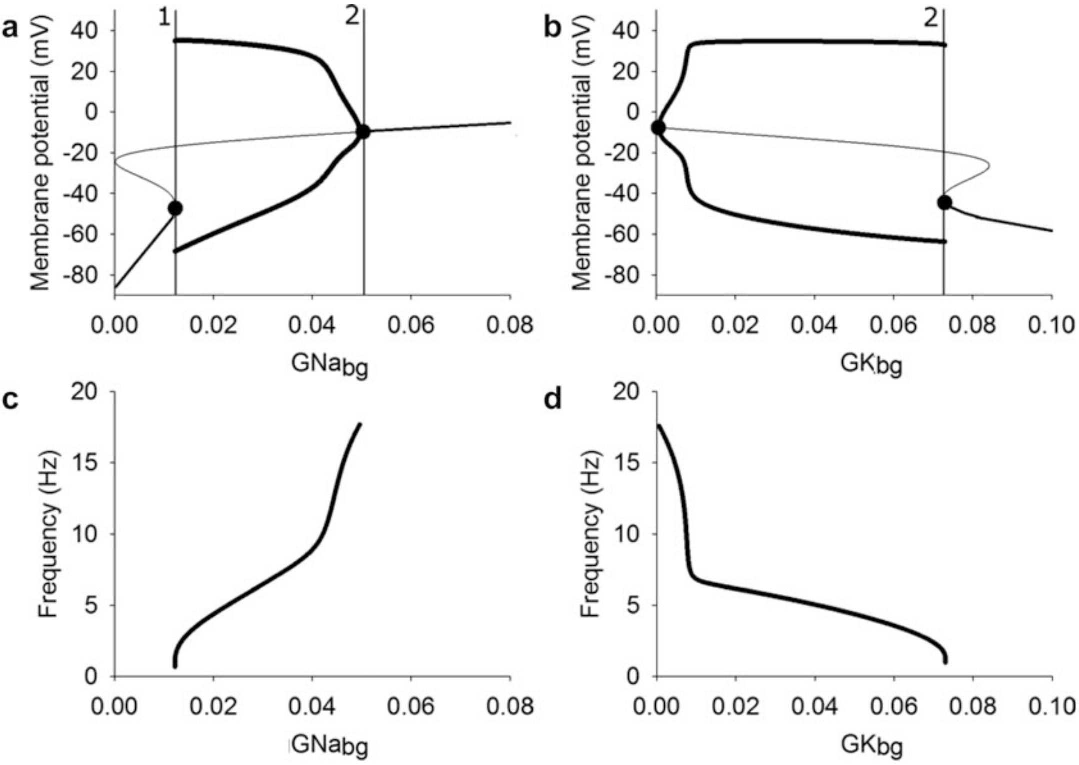

Fig. 3.11 The stable equilibrium point and limit cycle revealed by applying the bifurcation analysis to the minimal model. (**a**, **b**): the bifurcation diagram are obtained by varying the conductance of I_{Nabg} (**a**) or I_{Kbg} (**b**) on the abscissa, and the equilibrium state of the membrane potential is plotted on the ordinate. The bold lines between the two vertical lines 1 and 2 in (**a**) or vertical axis and line 2 in (**b**)) indicate the upper and lower limit of the stable limit cycle with the unstable equilibrium point represented by the thinner line. In the outside of the range bracketed by the two vertical lines, the thicker line indicates the stable equilibrium point, and the thinner line shows the unstable equilibrium points. The frequencies of the limit cycles in (**a**) and (**b**) are shown in (**c**) and (**d**), respectively

vertical line 1. Within the range of G_{Nabg} indicated by vertical lines 1 and 2, the spontaneous APs with varying discharge frequencies were observed with the overshoot potential and the MDP, which also well corresponded to the upper and lower boundaries of the limit cycle, respectively. The frequency of discharge was also in good agreement. Beyond the line 2, the membrane oscillation ceased in the numerical integration and the stable equilibrium point appeared in Fig. 3.11a, which corresponded to the depolarized resting potential at high Na^+ background conductance in the numerical integration. The influence of G_{Kbg} was just opposite to that of G_{Nabg} as evident in B and D. The smaller the G_{Kbg}, the higher the frequency of AP generation becomes. The steep slope of the frequency in the panels C and D both indicate the small and fast oscillatory activity of the membrane potential near Hopf bifurcation points at the high and the low ends of the stable limit cycles of G_{Nabg} and G_{Kbg}, respectively.

3.6 Conclusions

The V_{L} analysis revealed a common profile of contributions of ionic channels and transporters among variety of pacemaker cell model. That is, the transition of the main contributor current from I_{Kr} to I_{CaL} transmitted by a set of inward currents, such as I_{st}, $I_{\mathrm{h}}/I_{f,}$ and I_{CaT}. As to the role of I_{NaCa}, although the extent of the contribution may differ, the contribution of I_{NaCa} is no more than the substitution of some contribution of the set of inward currents. It should be noted that the variations among models arise from the different weights of each ionic current in the set of inward currents, leaving the common feature intact. Lastly, the essential feature of the pacemaker activity of the SA node cells was summarized by V_{L} analysis and bifurcation analysis using a minimal mathematical model composed of four idealized ionic current components; two voltage-gated channel currents, I_{Kr} and I_{CaL}, and two background currents, I_{Kbg} and I_{Nabg}.

Acknowledgments This work was supported by JSPS Grant-in-Aid for Young Scientists (B) (JP16K18996), the Research Promotion Program for Acquiring Grants in-Aid for Scientific Research (KAKENHI) and Individual Research Allowance at Ritsumeikan University to Y. H.

References

1. Wilders R. Computer modelling of the sinoatrial node. Med Biol Eng Comput. 2007;45:189–207.
2. Wilders R, Jongsma HJ, van Ginneken AC. Pacemaker activity of the rabbit sinoatrial node. A comparison of mathematical models. Biophys J. 1991;60:1202–16.
3. Demir SS, Clark JW, Murphey CR, Giles WR. A mathematical model of a rabbit sinoatrial node cell. Am J Phys. 1994;266:C832–52.
4. Kurata Y, Hisatome I, Imanishi S, Shibamoto T. Dynamical description of sinoatrial node pacemaking: improved mathematical model for primary pacemaker cell. Am J Physiol Heart Circ Physiol. 2002;283:H2074–101.
5. Sarai N, Matsuoka S, Kuratomi S, Ono K, Noma A. Role of individual ionic current systems in the SA node hypothesized by a model study. Jpn J Physiol. 2003;53:125–34.
6. Himeno Y, Sarai N, Matsuoka S, Noma A. Ionic mechanisms underlying the positive chronotropy induced by beta1-adrenergic stimulation in Guinea pig sinoatrial node cells: a simulation study. J Physiol Sci. 2008;58:53–65.
7. Maltsev VA, Lakatta EG. Synergism of coupled subsarcolemmal Ca2+ clocks and sarcolemmal voltage clocks confers robust and flexible pacemaker function in a novel pacemaker cell model. Am J Physiol Heart Circ Physiol. 2009;296:H594–615.
8. Cha CY, Himeno Y, Shimayoshi T, Amano A, Noma A. A novel method to quantify contribution of channels and transporters to membrane potential dynamics. Biophys J. 2009;97:3086–94.
9. Takeuchi A, Tatsumi S, Sarai N, Terashima K, Matsuoka S, Noma A. Ionic mechanisms of cardiac cell swelling induced by blocking Na+/K+ pump as revealed by experiments and simulation. J Gen Physiol. 2006;128:495–507.
10. Sarai N, Kobayashi T, Matsuoka S, Noma A. A simulation study to rescue the Na+/Ca2+ exchanger knockout mice. J Physiol Sci. 2006;56:211–7.
11. Hagiwara N, Irisawa H, Kameyama M. Contribution of two types of calcium currents to the pacemaker potentials of rabbit sino-atrial node cells. J Physiol. 1988;395:233–53.
12. Fermini B, Nathan RD. Removal of sialic acid alters both T- and L-type calcium currents in cardiac myocytes. Am J Phys. 1991;260:H735–43.
13. Guo J, Ono K, Noma A. A sustained inward current activated at the diastolic potential range in rabbit sino-atrial node cells. J Physiol. 1995;483:1–13.
14. Guo J, Mitsuiye T, Noma A. The sustained inward current in sino-atrial node cells of Guinea-pig heart. Pflugers Arch. 1997;433:390–6.
15. Mitsuiye T, Guo J, Noma A. Nicardipine-sensitive Na+−mediated single channel currents in Guinea-pig sinoatrial node pacemaker cells. J Physiol. 1999;521:69–79.
16. Cho HS, Takano M, Noma A. The electrophysiological properties of spontaneously beating pacemaker cells isolated from mouse sinoatrial node. J Physiol. 2003;550:169–80.
17. Shinagawa Y, Satoh H, Noma A. The sustained inward current and inward rectifier K+ current in pacemaker cells dissociated from rat sinoatrial node. J Physiol. 2000;523:593–605.
18. Toyoda F, Ding WG, Matsuura H. Responses of the sustained inward current to autonomic agonists in Guinea-pig sino-atrial node pacemaker cells. Br J Pharmacol. 2005;144:660–8.
19. Toyoda F, Mesirca P, Dubel S, et al. CaV1.3 L-type Ca2+ channel contributes to the heartbeat by generating a dihydropyridine-sensitive persistent Na+ current. Sci Rep. 2017;7:7869.
20. Ishihara K, Yan DH, Yamamoto S, Ehara T. Inward rectifier K(+) current under physiological cytoplasmic conditions in Guinea-pig cardiac ventricular cells. J Physiol. 2002;540:831–41.
21. Matsuoka S, Sarai N, Kuratomi S, Ono K, Noma A. Role of individual ionic current systems in ventricular cells hypothesized by a model study. Jpn J Physiol. 2003;53:105–23.
22. Hagiwara N, Irisawa H, Kasanuki H, Hosoda S. Background current in sino-atrial node cells of the rabbit heart. J Physiol. 1992;448:53–72.
23. Tellez JO, Dobrzynski H, Greener ID, et al. Differential expression of ion channel transcripts in atrial muscle and sinoatrial node in rabbit. Circ Res. 2006;99:1384–93.
24. Irisawa A, editor. Fine structure of the small sinoatrial node specimen used for voltage clamp experiment,

vol. 26. The Hague: Martinus Nijihoff Medical Division; 1978. p. 311–9.

25. Glukhovsky A, Adam DR, Amitzur G, Sideman S. Mechanism of Ca++ release from the sarcoplasmic reticulum: a computer model. Ann Biomed Eng. 1998;26:213–29.
26. Snyder SM, Palmer BM, Moore RL. A mathematical model of cardiocyte Ca(2+) dynamics with a novel representation of sarcoplasmic reticular Ca(2+) control. Biophys J. 2000;79:94–115.
27. Doerr T, Denger R, Trautwein W. Calcium currents in single SA nodal cells of the rabbit heart studied with action potential clamp. Pflugers Arch. 1989;413:599–603.
28. Vinogradova TM, Zhou YY, Maltsev V, Lyashkov A, Stern M, Lakatta EG. Rhythmic ryanodine receptor Ca2+ releases during diastolic depolarization of sinoatrial pacemaker cells do not require membrane depolarization. Circ Res. 2004;94:802–9.
29. Lyashkov AE, Juhaszova M, Dobrzynski H, et al. Calcium cycling protein density and functional importance to automaticity of isolated sinoatrial nodal cells are independent of cell size. Circ Res. 2007;100:1723–31.
30. Maltsev VA, Lakatta EG. Dynamic interactions of an intracellular Ca2+ clock and membrane ion channel clock underlie robust initiation and regulation of cardiac pacemaker function. Cardiovasc Res. 2008;77:274–84.
31. Ferrier GR. The effects of tension on acetylstrophanthidin-induced transient depolarizations and aftercontractions in canine myocardial and Purkinje tissues. Circ Res. 1976;38:156–62.
32. Matsuda H, Noma A, Kurachi Y, Irisawa H. Transient depolarization and spontaneous voltage fluctuations in isolated single cells from Guinea pig ventricles. Calcium-mediated membrane potential fluctuations. Circ Res. 1982;51:142–51.
33. Stern MD, Maltseva LA, Juhaszova M, et al. Hierarchical clustering of ryanodine receptors enables emergence of a calcium clock in sinoatrial node cells. J Gen Physiol. 2014;143:577–604.
34. Himeno Y, Asakura K, Cha CY, Memida H, Powell T, Amano A, Noma A. A human ventricular myocyte model with a refined representation of excitation-contraction coupling. Biophys J. 2015;109:415–27.
35. Asakura K, Cha CY, Yamaoka H, Horikawa Y, Memida H, Powell T, Amano A, Noma A, et al. EAD and DAD mechanisms analyzed by developing a new human ventricular cell model. Prog Biophys Mol Biol. 2014;116:11–24.
36. Okamoto Y, Takano M, Ohba T, Ono K. Arrhythmogenic coupling between the Na+ -Ca2+ exchanger and inositol 1,4,5-triphosphate receptor in rat pulmonary vein cardiomyocytes. J Mol Cell Cardiol. 2012;52:988–97.
37. Umehara S, Tan X, Okamoto Y, Ono K, Noma A, Amano A, Himeno Y. Mechanisms underlying spontaneous action potential generation induced by catecholamine in pulmonary vein cardiomyocytes: a simulation study. Int J Mol Sci. 2019;20:2913.
38. Himeno Y, Toyoda F, Satoh H, Amano A, Cha CY, Matsuura H, Noma A. Minor contribution of cytosolic Ca2+ transients to the pacemaker rhythm in Guinea pig sinoatrial node cells. Am J Physiol Heart Circ Physiol. 2011;300:H251–61.

The “Funny” Pacemaker Current

4

Andrea Barbuti, Mirko Baruscotti, and Annalisa Bucchi

Abstract

When isolated from the body, the heart continues beating for some time, suggesting an intrinsic pacemaker mechanism, the nature of which is still debated. In this chapter, we will summarize the evidence in favor of the “funny” current I_f being responsible for initiating the heartbeat in the specialized pacemaker cells of the sinoatrial node (SAN). The basic biophysical properties of I_f include activation upon hyperpolarization, a reversal potential much less negative than a pure K^+ current, and modulation by cyclic nucleotides. After cloning the genes for the molecular correlates of I_f, the α-subunits of the channel were termed *H*yperpolarization-activated *C*yclic *N*ucleotide-gated (HCN) channels. HCN channels are regulated by kinases (PI3K, Src-kinases), localized in caveolar lipid rafts, and interact with several activity-modifying proteins. In addition, the effects of multiple hormones, i.e., thyroid, parathyroid, and sex hormones, of physical training or of microRNAs on SAN function can be explained by HCN channel modulation. HCN channels play a role in cardiac development and are found in spontaneously active, pluripotent stem cell-derived cardiomyocytes. Targeting HCN channels with selective f-channel blockers strongly affects heart rate. Moreover, genetics of HCN channels have revealed that several mutations in the coding sequence of the *hHCN4* gene are associated with alterations of cardiac rhythm and other pathological cardiac phenotypes. HCN channels have also been exploited for biological pacemakers. Taken together, we conclude that there is compelling evidence for the importance of I_f in the SAN pacemaker.

Keywords

*H*yperpolarization-activated *C*yclic *N*ucleotide-gated (HCN) channels · Sinus node pacemaker · Regulation · Kinases · Sex hormones · Thyroid hormones

4.1 Introduction: The Mechanism of Cardiac Pacemaking

The spontaneous activity of the heart has been known for a long time. In the second century AD, the physician Claudius Galenus (Galen of Pergamum AD ca 130–ca 200) realized that the heart keeps beating for a long period when extracted from the chest. However, several more centuries were necessary for Keith and Flack to discover, in 1907, a structure responsible for initiating the heartbeat, the sinoatrial node

---

A. Barbuti (✉) · M. Baruscotti · A. Bucchi
Cell Physiology Lab, Department of Biosciences and Department of Biomolecular Sciences and Biotechnology, University of Milano, Milano, Italy
e-mail: andrea.barbuti@unimi.it

© Springer Nature Switzerland AG 2023

O. N. Tripathi et al. (eds.), *Heart Rate and Rhythm*, https://doi.org/10.1007/978-3-031-33588-4_4

(SAN) [1, 2]. More than 100 years later, the electrical and molecular mechanisms responsible for the intrinsic automaticity of the SAN are still debated [3].

The shape and duration of action potentials (APs) of SAN cells are different from those of atrial and ventricular myocytes, most notably for the presence of the diastolic phase (pacemaker or diastolic depolarization, DD), which drives the membrane potential from the maximum diastolic potential (MDP, around −60 mV) up to the threshold for another AP (around −40 mV), thus generating autorhythmicity.

The pacemaker phase is the result of a concerted interplay of several mechanisms comprising ionic currents, pumps, and exchangers. Activation of the "funny" current (I_f or "pacemaker" current) drives early DD up to a point where Ca^{2+}-dependent mechanisms, involving first the T-type calcium current and the Na-Ca exchanger and then the L-type Ca^{2+} current, kick in to determine the late fraction of DD and help reaching the threshold of a new AP. The events leading to the discovery of the funny current and its main properties in SAN tissue/cells are described below.

4.1.1 Historical Background and Basic Biophysical Properties of I_f

In 1979, a new pacemaking mechanism was proposed, to explain the spontaneous activity of SAN myocytes. This mechanism was based on the activation, upon membrane hyperpolarization to the diastolic (pacemaker) voltage range (Fig. 4.1a), of an inward current responsive to stimulation by noradrenaline (Fig. 4.1b–d). The current was dubbed "funny" (I_f) because of its unusual properties [4]. Prior to the discovery of I_f, pacemaking had been largely investigated in Purkinje fibers and attributed to a completely different mechanism, i.e., the decay of a K^+ current (I_{K2}). However, some I_{K2} properties, such as a strong dependence on external Na^+ and a very negative reversal potential, did not reconcile with those of a pure K^+ current. The pacemaking mechanism proposed for SAN myocytes based on I_f was actually opposite to that involving I_{K2} deactivation suggested for Purkinje fibers. This puzzle was indeed solved in 1981, with the demonstration that I_{K2} was the same I_f current just discovered in the SAN [5]. The I_f current had several unusual features: (1) it was the first voltage- and time-dependent current found to be activated on membrane hyperpolarization rather than on depolarization; (2) it had a reversal potential around −10/−20 mV, due to a mixed Na^+ and K^+ permeability [5–8]. Although the Na^+/K^+ permeability ratio is about 0.27–0.33, implying a preferential permeability of K^+ over Na^+, Na^+ permeation is functionally important because it renders the current inward and depolarizing at diastolic voltages (about −40 to −60 mV in the SAN); (3) I_f had a dual modulation by voltage and cyclic nucleotides [9].

4.1.2 Voltage Dependence of f-Channel Activation

According to data from the literature, the voltage range of activation of I_f in the SAN has a large variability with threshold values ranging between −32 and −70 mV and half-activation voltages ($V_{1/2}$) in the range −50/−120 mV [10]. These differences can be explained partly by the different experimental conditions and partly by the high sensitivity of this channel to the cellular "environment." For example, cAMP concentration and "run-down" can influence the open probability of f-channels [11]. Run-down causes a rapid negative shift of the f-channel activation curve during whole-cell patch clamp recordings and can induce a substantial underestimation of the I_f contribution [12], which might explain the highly negative threshold or $V_{1/2}$ values reported in some studies. Other mechanisms modulating f-channel function include phosphorylation [13, 14], interaction with auxiliary subunits [15–19], and interaction with lipids and/or structural proteins [20, 21].

The variability in the activation range of I_f becomes even greater when considering that f-channels are also expressed in other

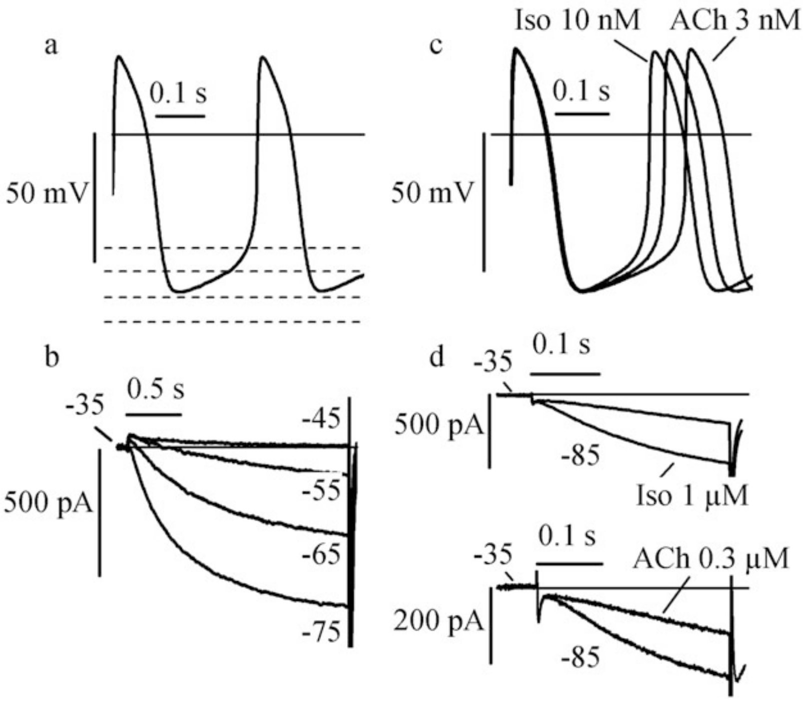

Fig. 4.1 Properties of the funny current. **a**, **b**: action potentials (**a**) and I_f current recorded during steps to the voltages indicated (**b**) from a rabbit SAN cell; the same voltages are indicated in (**a**) by broken lines. (**c**) low doses of isoprenaline and acetylcholine accelerate and slow rate, respectively, of a SAN cell by changing the rate of diastolic depolarization. (**d**) these changes are due to I_f increase/decrease caused by Iso/ACh, respectively

autorhythmic cardiac regions, such as the atrioventricular node (AVN) and the His-Purkinje system [22], where I_f activates at more negative voltages compared to SAN myocytes [23, 24].

f-Channels have also been found in working myocardium (atrial and ventricular muscle), although their physiological relevance is negligible due to both a low expression and a too-negative range of activation [25, 26]. Interestingly, pathological conditions such as cardiac hypertrophy may lead to an increased f-channel expression in the working myocardium with an associated increased propensity to ventricular arrhythmias [27].

4.1.3 I_f-Mediated Autonomic Modulation of Cardiac Rate

The heart rate needs to be promptly adjusted to match the metabolic needs depending on the physical and emotional state of the organism. Since the duration of DD is a main determinant of heart rate, its fine modulation is achieved by precise control of the steepness of DD by autonomic neurotransmitters (Fig. 4.1c). Sympathetic stimulation accelerates, and parasympathetic stimulation slows heart rate through the activation of β-adrenoceptor (β-ARs) and muscarinic M2 receptors, respectively. β-ARs (coupled to stimulatory G-protein, Gαs) and M2 receptors (coupled to inhibitory G-proteins, Gαi) exert opposite effects on adenylyl cyclase, thus controlling, together with cAMP-activated phosphodiesterase, the cytosolic concentration of cAMP.

cAMP directly binds to f-channels and shifts their activation curve toward more positive potentials [28]. This mechanism increases the net inward current flowing during the DD, and results in the steepening of DD slope and consequent cardiac acceleration [29]; slowing of heart rate is obtained by an opposite set of events initiated by M2-receptor-mediated decrease in cAMP.

Both β1 and β2 subtypes of β-ARs are expressed in the heart, and although β1-ARs are predominant, the SAN has the highest expression of β2-ARs among cardiac tissues [30]. Interestingly, in rabbit SAN myocytes, stimulation of β2-ARs causes a larger shift of I_f activation curve and a more pronounced positive chronotropic effect than β1-AR stimulation. This is due to the co-localization of β2-ARs and f-channels into specific membrane microdomains (caveolae, see also Sects. 4.2 and 4.3) [21].

4.2 Molecular Structure of Pacemaker Channels

The genes encoding the molecular correlates of f-channels were cloned in the late 1990s [31]. Based on structural homology, the f-channel α-subunits, termed Hyperpolarization-activated Cyclic Nucleotide-gated (HCN) channels, were included in the superfamily of voltage-dependent K^+ and Cyclic Nucleotide-Gated (CNG) channels. HCN channels have been cloned from vertebrates, invertebrates, and urochordates; in mammals, four different isoforms were found (HCN1–4) [32, 33].

HCN isoforms are widely expressed both in excitable (heart and nervous system, and also smooth muscle) and nonexcitable tissues (testes, pancreatic β-cells) [33]. Moreover, the various subunits can assemble to form functional homomeric and/or heteromeric channels (with the exception of HCN2–HCN3 heteromers), which are tetramers [33, 34].

The overall structure of HCN channels includes a conserved core region formed by six transmembrane (S1–S6) domains, with a positively charged S4 segment, a pore (P) region involving S5, S6, and their connecting loop; a relatively short intracellular N-terminus and a relatively long intracellular C-terminus which are less conserved among isoforms. All HCN isoforms exhibit, within the permeation pathway, a selectivity filter including the GYG triplet typical of K^+ channels, although partially hydrated Na^+ ions can also accommodate in the not-too-rigid structure of the inner pore of HCN channels [35].

The N-terminus contains a sequence, which appears to be important in mediating channel trafficking to the plasma membrane [36, 37]. In the C-terminus, three separate structural elements can be recognized: the C-linker, organized in 6 α-helices, the Cyclic Nucleotide Binding Domain (CNBD), and the proper C-terminus. The CNBD and the C-linker act as functional unit that modulates the open probability of a pacemaker channel. When cAMP is bound the α-helices of the C-linker of one subunit interact with the α-helices of the adjacent subunit, a conformation favoring the open state of the channel. The removal of cAMP favors a rearrangement of the structure leading to channel closing [38–40].

The overall molecular structure confers to all HCN isoforms the specific functional properties typical of f-channels described above; there are nonetheless important differences in channel opening/closing rates and cAMP sensitivities. HCN1 is by far the fastest activating/deactivating isoform, followed by HCN2 and HCN3, while HCN4 has the slowest kinetics [41, 42]. HCN1 is weakly affected by cAMP (4.3–5.8 mV maximal shift), and HCN2 and HCN4 display a larger response (shifts of 16.9 to 19.2 and 11 to 23 mV, respectively); curiously, the activation curve of HCN3 is shifted to the negative direction by cAMP (from −2.9 to −5 mV) [40, 43]. The voltage dependence of activation also varies: HCN1 has the most positive $V_{1/2,}$ followed by HCN4, HCN3, and HCN2 [42]. Finally, the functional properties of these channels depend on several factors, referred to as “context dependence” (see Sect. 4.3), which can significantly offset the position of the activation curve [44].

4.2.1 HCN Composition of Native Pacemaker Channels

The existence of four different HCN isoforms was initially seen as a possible basis for tissue-specific differences in I_f properties. However, none of the four isoforms, when heterologously expressed as homomeric channels, could generate currents with properties identical to those of native I_f current in specific cardiac tissues. This finding raised the question of whether native pacemaker channels could be heteromers of different subunits, and prompted the study of the distribution of HCN channels in different cardiac regions.

Analysis of HCN distribution indicated that the HCN4 isoform represents the major component of pacemaker channels in the SAN (Table 4.1). In fact, from early cardiac development up to adulthood, HCN4 expression delineates the pacemaker region/conduction system of the heart [55, 56, 62, 63]. Species-dependent expression of HCN1 and HCN2 has been reported in the SAN; in particular, in human SAN, all three isoforms are expressed at the protein levels [53]. In the working myocardium, HCN2 is the predominant isoform even though at a low level of expression compared to SAN and the conduction system. The HCN3 mRNA has been found both in mouse SAN and ventricle, with higher expression during embryogenesis. HCN3 protein expression has never been shown [34].

As a consequence of the finding that more than one HCN subunits are co-expressed in a specific cardiac region, the ability of the various subunits to co-assemble in heterotetramers was evaluated. Co-expression of various subunits often results in functional channels displaying kinetic and modulatory characteristics intermediate between those of the individual components; nevertheless, heterotetramers often fail to fully recapitulate native I_f [33, 64, 65].

4.3 Regulation of HCN Channels

When HCN2 channels are heterologously expressed in neonatal and adult ventricular myocytes, they generate similar currents, but the voltage range of activation in neonatal cells is some 18 mV more positive than in the adult [66]. A 22 mV difference is also found when comparing native I_f activation curves in newborn and adult ventricular myocytes [67]. These differences cannot be readily explained in terms of different channel-bound cAMP concentrations. Indeed HCN channels are also regulated by several other factors such as Src-kinases [13, 68], membrane phospholipids (phosphatidylinositol 4,5-bisphosphate PI(4,5)P_2) [69, 70], cholesterol [20], cyclic dinucleotides [71], and by interaction with transmembrane/intracellular proteins (KCNE2, caveolin-1 and -3, KCR1, SAP97) [15, 16, 18, 19, 21, 72, 73]. As mentioned above, these and perhaps other modulatory factors generate the “context dependence” of funny channels.

4.3.1 PI3-Kinase and Src-Kinases

4.3.1.1 Phosphoinositide 3-Kinase

Recent studies have identified an interesting and novel modulatory mechanism of pacemaker rate and pacemaker HCN channels [74, 75]. The authors demonstrated that inhibition of the phosphoinositide 3-kinase (PI3K) enzyme ultimately leads to a negative shift of the activation curve of the I_f current and to bradycardia. In physiological conditions, the PI3K activity determines the generation of the second messenger phosphatidylinositol 3,4,5-trisphosphate (PI(3,4,5)P_3) and the activation of the Akt kinase. Perfusion of the PI3K inhibitor (PI-103) on ex-vivo mouse hearts and on in vitro canine SAN reduced the rate by ~10% (from 418 to 377 bpm) and by ~17% (from 100 to 83 bpm), respectively. The effects were reversible in all cases, and the autonomic modulation was fully preserved. The preservation of an intact autonomic modulation and the evidence that PI3K actions required up to 2 h to reach a stable level strongly suggest that such a mechanism is involved in tonic control of basal heart rate.

When the effects of PI3K inhibition were tested on the I_f current recorded from SAN rabbit myocytes, a negative shift of the activation curve (−15.9 mV) was observed. Noticeably, this effect was robustly reversed (+11.7 mV) by the additional presence of the PI3K second messengers PI(3,4,5)P_3.

The authors further investigated the molecular basis of the PI3K effect and carried out specific experiments on the mouse HCN2 isoform [74, 75]. These experiments nicely confirmed the functional importance of Akt since delivery of the active form of Akt kinase or PI(3,4,5)P_3 was able to rescue the HCN2 alteration induced by PI3K inhibition and identified the mHCN2 serine residue in position 861 as the specific phosphorylation target.

Table 4.1 HCN isoform distribution in different cardiac regions: SAN, sinoatrial node; PF, Purkinje Fibers; AVN, atrioventricular node; NM not measured, – below detection level; +/– very low expression at the limit of detection; from + to ++++ increasing levels of expression

Tissue		Species	Method(s)	HCN1	HCN2	HCN3	HCN4	Ref
SAN	mRNA	Human	qPCR	++	+	–	++++	[45]
		Human	RT-PCR	+	+	–	++++	[46]
		Dog	C RT-PCR	–	++	NM	+++	[47]
		Rabbit	RNase PAs	++	+	–	++++	[48]
		Rabbit	NB, isH	+	NM	NM	NM	[49]
		Mouse	qRT-PCR	++	+	+/–	++++	[50]
		Mouse	isH	+	++	NM	++++	[51]
		Rat	qRT-PCR	–	+	–	+	[52]
	Protein	Human	Immuno	NM	NM	NM	++	[45]
		Human	WB	+++	++	NM	++	[53]
		Dog	WB/immuno	NM	++	NM	+++	[47]
		Rabbit	WB/immuno	+	NM	NM	NM	[49]
		Rabbit	WB/immuno	+/–	–	NM	++	[54]
		Mouse	Immuno	–	–	NM	+	[55]
		Rat	Immuno	NM	NM	NM	+	[56]
Atrium	mRNA	Human	qPCR	+	+++	–	++	[45]
		Human	rt RT-PCR	++	+++	–	++++	[57]
		Human	C RT-PCR	+	+	NM	++	[50]
		Dog	C RT-PCR	–	+	NM	++	[47]
		Mouse	qRT-PCR	+	+	–	+	[50]
	Protein	Human	Immuno	NM	NM	NM	–	[45]
		Human	WB	–	+	NM	++	[58]
		Dog	WB/immuno	NM	+	NM	++	[47]
		Rabbit	Immuno	NM	NM	NM	–	[59]
		Mouse	Immuno	–	–	NM	–	[55]
		Rat	Immuno	NM	NM	NM	–	[56]
Ventricle	mRNA	Human	rt RT-PCR	+	++	–	+++	[57]
		Human	C RT-PCR	–	++	NM	+	[58]
		Dog	C RT-PCR	–	++	NM	–	[60]
		Rabbit	RNase PAs	–	+	–	–	[48]
		Mouse	qRT-PCR	+	++	–	+	[50]
		Rat	RNase PAs	–	++++	NM	+	[48]
		Rat	qRT-PCR	–	+	NM	+	[61]
	Protein	Human	WB	–	++	NM	+	[58]
		Dog	WB	–	+	NM	–	[60]
		Rabbit	Immuno	NM	NM	NM	–	[59]
PF	mRNA	Human	rt RT-PCR	+	+	+	++	[57]
		Dog	C RT-PCR	+/–	++	NM	+++	[60]
		Rabbit	RNase PAs	–	+	–	–	[48]
	Protein	Dog	WB	–	++	–	+++	[60]
AVN	mRNA	Rabbit	NB, isH	–	NM	NM	NM	[49]
		Mouse	qRT-PCR	+	+	–	+	[50]
	Protein	Rabbit	Immuno	–	NM	NM	+	[59]
		Rat	Immuno	NM	NM	NM	+	[56]

The + symbols do not refer to absolute values and can be compared only within the same group. qPCR, quantitative Polymerase chain reaction (PCR); RT-PCR, reverse transcriptase PCR; C RT-PCR, competitive RT-PCR; rt RT-PCR, real-time RT-PCR; NB, Northern Blot; WB, Western Blot; immuno, immunolabeling; isH, in situ hybridization; RNase PAs, RNase Protection Assays

However, when the effect of Akt inhibition was tested on rabbit SAN pacemaker channels (mostly contributed by the HCN4 isoform), no effect was found, thus leading to the conclusion that in the SAN, a still undefined PI3K-dependent but Akt-independent pathway must be at work.

4.3.1.2 Src-Kinases

Src forms complexes with HCN2 and HCN4 channels and phosphorylates HCN4 in at least two different highly conserved tyrosine residues in the C-linker (Tyr 531 and Tyr 554) [13, 14]; this increases channel open probability and speeds activation kinetics [13].

4.3.2 Cholesterol and Membrane Phospholipids

Phospholipids are not uniformly distributed in the membrane but form distinct microdomains, called lipid rafts, enriched in cholesterol and sphingolipids [76]. In rabbit SAN myocytes, HCN4 localizes in caveolar lipid rafts, and their disruption strongly affects f-channel kinetics, shifting the activation curve toward more positive potentials and slowing deactivation kinetics, which leads to the acceleration of spontaneous activity [20].

Funny channels are also modulated by PI(4,5) P_2, whose depletion can partially explain the I_f run-down phenomenon [70]. Furthermore, the increase of PI(4,5)P_2 mediated by activation of phospholipase C-coupled receptors (bradykinin BK2 receptor and muscarinic M1 receptor) can modulate channel gating; specifically, stimulation of BK2 receptors induces a large positive shift of the activation curve of HCN2, HCN1 and SAN f-channels [69].

4.3.3 Protein–Protein Interactions

A well-established function of lipid rafts is to confine in a discrete membrane domain proteins involved in the same signal transduction pathway, so as to favor their functional interaction [76]. Functional interactions that are able to alter channel properties have been demonstrated between cardiac HCN channels and caveolin-3, MiRP1, KCR1, and SAP97 (Fig. 4.2).

4.3.3.1 Caveolin-3

Caveolae are a type of lipid raft characterized by the presence of the scaffold protein caveolin. In rabbit SAN cells, particularly rich in caveolae [77], HCN4 co-localizes and interacts with caveolin-3 and caveolin-1 [21, 73]. Disorganization of caveolae strongly affects f-channel kinetics, by shifting the activation curve toward more positive potentials, slowing deactivation kinetics, and altering adrenergic modulation [20, 21]. Interaction of HCN channels with caveolins is mediated by the caveolin-binding domain (CBD) located at the N-terminus just prior to the S1 transmembrane domain. Disruption of the CBD induces a rightward shift of the HCN4 activation curve, a slowing of deactivation time constants, and a severe impairment of channel trafficking to the plasma membrane [78].

4.3.3.2 MiRP1

Mink-related protein 1 (MiRP1 or *KCNE2*) is a single transmembrane domain protein that acts as a β-subunit of hERG and HCN channels. It has been shown that MiRP1 interacts with HCN2 channels in SAN and ventricular myocytes. In heterologous expression systems, MiRP1 increases HCN1, HCN2, and HCN4 current densities and alters activation kinetics; however, this latter effect depends on the specific isoform tested and on the expression system used [15–17].

4.3.3.3 KCR1

This is another membrane-spanning protein shown to interact in heterologous expression systems with HCN2 channels. It causes a significant decrease in current density and a negative shift of the activation curve when both proteins are co-expressed in CHO cells. Exogenous expression of KCR1 in neonatal ventricular myocytes decreased current density, while downregulation of KCR1 by specific siRNA (small interfering RNA) increased current density. Interestingly, in pig and rat hearts, SAN has

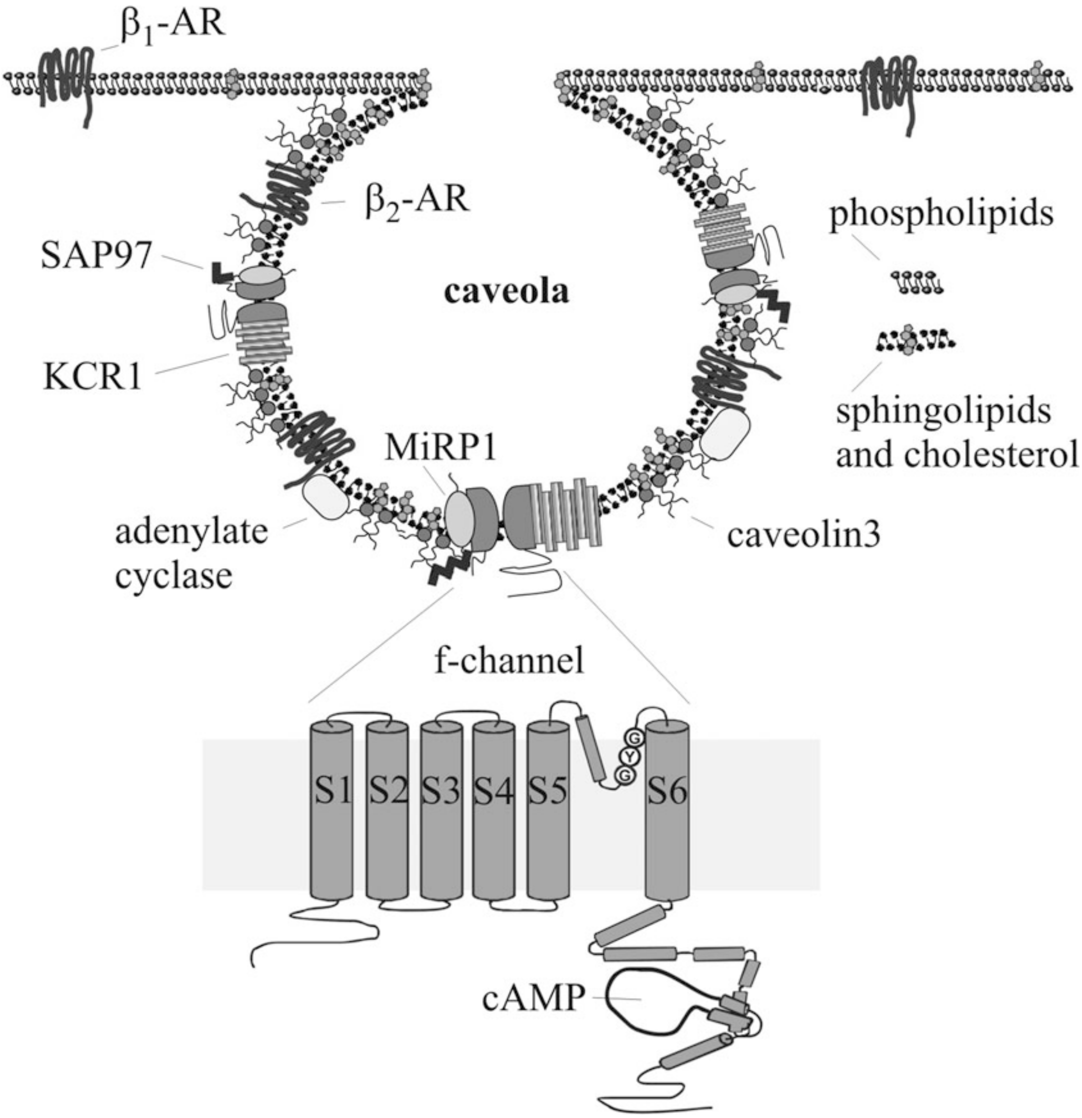
β_1-AR
β_2-AR
caveola
phospholipids
SAP97
KCR1
sphingolipids and cholesterol
MiRP1
adenylate cyclase
caveolin3
f-channel
S1
S2
S3
S4
S5
G
Y
G
S6
cAMP

Fig. 4.2 Cartoon illustrating the caveolar localization of f-channels and other elements of the f-channel modulatory pathway. Further explanation in the text

the lowest level of KCR1 mRNA, in agreement with the relevant role of I_f in this tissue [18].

4.3.3.4 SAP97

In rabbit SAN, HCN2 and HCN4 channels co-localize with the Synapse Associated Protein-97 (SAP97), a scaffold protein that clusters proteins at the cell membrane. In heterologous expression systems, SAP97 functionally interacts with HCN2 and HCN4 channels through a PDZ domain and alters the current density, though in a context (in CHO cells but not in HEK cells) and isoform-specific manner (increases HCN2 and decreases HCN4 current) [19].

While a general picture of all the relative interactions among these proteins is still lacking, the above data, together with evidence that in heart MiRP1, SAP97, and other voltage-gated ion channels are also associated with caveolin3-rich membrane microdomains [79, 80], suggest the formation of a macromolecular complex important for the proper activity and modulation of HCN channels and correct electrical function of SAN pacemaker myocytes.

4.3.4 Epigenetic Modulation of f/HCN Channels

4.3.4.1 Hormones

The SAN activity is strongly modulated by humoral stimuli, and the I_f current has been shown to be one of the targets for some of them [81]. In particular, the effects of thyroid, parathyroid, and sex hormones are summarized below.

Thyroid hormones (THs). It is well documented that these biogenic amines (T3 and T4) can strongly influence cardiovascular function including heart rate, as evident from the increase/decrease of the HR due to hyperthyroidism/ hypothyroidism in humans. This modulation has been attributed, at least in part, to the ability of T3 to increase the I_f current density (and HCN4 and HCN2 mRNA) via activation of the Thyroid Receptors α1 (TRα1), the main isoform of TR receptors expressed in the heart [82, 83]. T3 influence I_f expression also during development; indeed, treatment of differentiating mouse embryonic stem cells (mES) with T3 induce a twofold increase of I_f current density, a positive shift of the activation curve, and consequently an acceleration of the beating rate. This is likely due to an epigenetic modulation of Tbx3, a transcription factor known to influence HCN4 channel expression (see Sect. 4.4.1 below) [84].

Parathyroid hormone (PTH) released by the parathyroid gland has positive chronotropic effects along with its main function in the regulation of calcium homeostasis. In isolated rabbit SAN cells and canine Purkinje fibers, PTH increases the spontaneous activity of these cells and the I_f current. A similar action was shown for the PTH-related protein, an autocrine/paracrine hormone produced by cardiomyocytes [85, 86].

Sex hormones: involvement of I_f current with estrogen level is associated with higher resting HR during pregnancy [87]. El Khoury et al. [88] have shown that SAN cells isolated from late (18–19 gestation days) pregnant mice exhibited both higher automaticity and I_f density. These effects have been attributed to the activation of the estrogen receptor α by 17β-estradiol (E2), the predominant estrogen released during pregnancy, which seems to regulate HCN2 channels expression [88, 89]. In addition, the increase in the I_f current could also be favored by an E2-mediated increase in the expression of the MinK-related peptide 1 (MiRP1; see Sect. 4.3.3 above [90]).

To date, there is no data showing an effect of testosterone on either I_f or SAN cell rate; however, during mouse embryonic stem cell differentiation, testosterone induces a dose-dependent upregulation of HCN4 by recruiting the androgen receptor to its gene locus [91].

4.3.4.2 Training

The origin of the bradycardia induced by endurance athletes has been quite debated [92]. The classical view that training-induced bradycardia dependent upon an increased vagal tone was recently challenged by new pieces of evidence in human and animal models. Indeed, D’Souza and colleagues have shown that endurance athletes under complete autonomic block have an intrinsic heart rate significantly lower than nonathletes [93]. In trained mice and rats, these authors have also shown that sinus bradycardia primarily results from a reversible, training-induced remodeling of the sinus node. In particular, it has been shown that training-induced bradycardia in mice can be attributed, at least in part, to downregulation of HCN4 expression, with a consequent decrease in the density of I_f. The epigenetic mechanism linking exercise to sinoatrial bradycardia seems to involve the decrease of Tbx3 expression, the increase of NRSF (both known to modulate HCN4 expression), and a specific increase in few miRNAs (see Sect. 4.3.4.3 below) [93, 94]. Another important player in this modulatory process is the AMP-activated protein kinase (AMPK), a known regulator of cellular energy homeostasis; indeed, in mice lacking the ability to activate AMPK (γ2 AMPK KO mice), the I_f current is no more regulated by endurance exercise and mice do not develop exercise-induced intrinsic bradycardia [95].

4.3.4.3 miRNA

miRNA is a class of noncoding RNA that has gained a prominent role in the last two decades as a posttranscriptional modulator of protein expression. The role of miRNA on HCN channels has been studied mainly in relation to pathological cardiac remodeling and exercise-induced bradycardia.

The first indirect evidence of a possible role of miRNA on HCN expression came from studying the effect of chronic treatment with ivabradine on the I_f/HCN upregulation in the working myocardium of a rat model of myocardial infarction. In this model, the I_f blocker ivabradine (see Sect. 4.5) induced downregulation of HCN2 and HCN4 and a parallel upregulation of miR-1, miR-133a, and miR-133b [96]. Similarly, spironolactone, an aldosterone blocker, decreased the overexpression of HCN4 due to myocardial infarction by acting on miR-1 levels, as demonstrated by the lack of spironolactone effect on HCN4 when an antagomir-1 was employed [97]. A possible interaction of HCN channels and miRNA has also been reported by Li et al. [98], who reported that cardiac samples obtained from aged patients with atrial fibrillation showed higher levels of HCN2 and HCN4 mRNA and proteins with a parallel downregulation of miR-1 and miR-133. Very recently, Yanni and collaborators [99] demonstrated that the I_f current, and particularly the HCN4 subunit, was significantly downregulated in a mouse model of pressure overload heart failure. Although heart failure induced modulation of many miRNAs, among these, miR-370-3p and miR-139-3p were selected for further analysis since they were able to modulate HCN4 expression in vitro, and miR370-3p was also found upregulated specifically in the sinus node of patients with heart failure [94, 99]. Interestingly, in vitro, upregulation of either miR-370-3p or miR-139-3p in the sinus node caused bradycardia and decreased HCN4 (and I_f) expression. In in vivo experiments, systemic injection of an antimiR-370-3p, reversed both bradycardia and the first-degree conduction block observed in the heart failure mice and restored HCN4 levels and I_f density toward control levels.

miRNAs have also been implicated in the I_f (and HCN4)-dependent bradycardia associated with endurance training [93, 94]. Endurance-trained rats and mice displayed bradycardia and a decreased sinoatrial expression of I_f (and HCN4) accompanied by a significant upregulation of miR-1 [94]. However, a direct causative relation was not reported. In subsequent work, the same group demonstrated a sinus node-specific upregulation of miR-423-5p in swimming-trained animals. In this case, however, the authors demonstrated that in vivo injection of an antimiR targeting specifically miR-423-5p reverted the effects on I_f (and HCN4) and on heart rate [93].

4.4 Pacemaker Channels in Cardiac Development

In the chick embryonic heart, pacemaker activity initiates from the sinus venosus (the prospective SAN) before the first contraction takes place [100–102]. In mice, the first cardiac contraction is visible around embryonic day 8.5 (E8.5) when the heart is a linear tube; at this stage, all cardiomyocytes, when isolated, are autorhythmic and express the I_f current [103]. Toward the end of gestation (E18), the number of spontaneously active myocytes decreases to 33%. Interestingly this occurs in parallel with an 82% decrease of I_f current density and a concomitant large downregulation of HCN1 and HCN4 mRNAs, by far the predominant HCN isoforms at early stages of development [103].

4.4.1 f/HCN Channels During Embryonic Cardiac Development

A detailed analysis of HCN4 localization during mouse cardiac development by in situ hybridization indicates that HCN4 mRNA is expressed as early as E6 and E7 in the mesoderm, representing progenitors of the first heart field (FHF). These cells display the spontaneous rhythmic activity that starts the peristaltic contraction as soon as the heart tube is formed [104–106]. The fact that these HCN4+ progenitors give rise to part of the left ventricle and atria later in the development (E19.5) starting from E8.5, HCN4 is upregulated in the Tbx18+ progenitors that will give rise to autorhythmic cells of the sinus venous and SAN [106], indicates that HCN4 expression represents a functional requirement for pacemaking. However, it is important to remember that HCN4 starts to become functionally indispensable only when its expression coincides with the perspective SAN. Indeed mice with either global or cardiac-specific knockout of HCN4 die in utero between E9.5-E11.5 [107], a time corresponding to the development of the sinoatrial node [104].

The expression of HCN4 is maintained by a precise interplay of various transcription factors that together delineate the cardiac region in which the SAN develops [108]. Lineage tracing studies have elucidated the critical role of some important transcription factors that either directly or indirectly sustain the expression of HCN4 and inhibit genes responsible for its repression. Tbx18, Shox-2, and Isl-1 concur to induce expression of Tbx3 that represses atrial differentiation of primary pacemaker myocardium, thus limiting downregulation of HCN4. In parallel, Shox2 influences HCN4 expression by inhibiting Nkx2.5, whose expression limits that of HCN4. Interestingly, constitutive deletion of the transcription factor Shox2 prevents the expression of both Tbx3 and HCN4 and causes the formation of an underdeveloped and bradycardic SAN that leads to embryonic death at mid-gestation (E11.5) [109]. These data show that pacemaker activity, development of the SAN and expression of HCN4 are strictly related and, together with the evidence of embryonic lethality of *Hcn4* and *Shox2* knockout mice at comparable developmental stages, strongly support the essential role of HCN4 in the correct development of SAN [107].

4.4.2 f/HCN Channels in Pluripotent Stem Cell-Derived Cardiomyocytes

An alternative approach to studying either early events in cardiac development or alterations in cardiomyocyte function leading to pathological conditions involves in vitro differentiation of pluripotent stem cells (PSCs). The main sources of PSC are mouse and human embryonic stem cells (mESC and hESC) and induced pluripotent stem cells (iPSC, mostly of human origin). PSC can be differentiated into beating cardiomyocytes either spontaneously through the formation of tridimensional aggregates called embryoid bodies (EBs) [110] or following induction with specific molecules [111].

4.4.2.1 mESC-Derived Cardiomyocytes

Several reports indicate that mESC-derived cardiomyocytes express all HCN channels [112, 113], even with some variability in the isoforms. This variability likely arises from the heterogeneity in terms of the cardiac subtype composition of the culture. When SAN-like precursors are selected on the basis, for example, of CD166 expression during a specific developmental window, the resulting SAN cells have molecular and functional characteristics very similar to native mouse SAN cells and, indeed express mainly HCN4 and HCN1 [114].

mESC-derived autorhythmic cardiomyocytes display SAN-like APs and exhibit I_f [112, 113, 115]. Involvement of I_f in the generation and modulation of rate in this cellular system has been confirmed using specific I_f inhibitors. 3 μM ivabradine, for example, slowed the beating rate by 25% and reduced I_f by about 50% [113]; these effects are quantitatively similar to those reported in SAN myocytes. ZD7288 (0.3 μM) also slowed the beating rate by about 50% and reduced I_f by 15% [112].

4.4.2.2 hESC- and hiPSC-Derived Cardiomyocytes

The first study showing the expression of the HCN channel in hESC-derived cardiomyocytes reported the expression of HCN2 with no expression of HCN4 [116]. Later works displayed the expression of also HCN1 and HCN4 in variable proportion [117]. In hiPSC cardiac differentiation, it has been reported that HCN2 levels increase with time in culture [118, 119], while HCN4 levels have been reported either to increase or decrease with time in culture [120, 121]. Again, the variability arises from the heterogeneity of the culture, and indeed, when the culture is enriched in SAN-like cardiomyocytes, HCN1 and HCN4 are the prevalent isoform expressed [122, 123], in line with data from human SAN tissue [45, 53].

I_f current has been repeatedly reported in hESC and hiPSC-CMs, however, in these cases, the comparison with native cells is complicated by the fact that up to date, only one study reported I_f current in pacemaker cells isolated from a diseased human sinus node [124]. In hESC-derived cardiomyocytes, Satin et al. [116] and Bosman et al. [125] found I_f density in the range 5 to 12 pA/pF at fully activating potentials (around −120 mV). In hiPSC, however, the recorded current density is more consistently around 4–5 pA/pF [126–128]. These values agree with those observed in highly-selected SAN-like cardiomyocytes by Protze et al. [122].

Others have also reported smaller current densities, especially after longer differentiation times, in the range of 1 pA/pF, but these values may simply reflect an enrichment in ventricular-like cells, rather than nodal-like cells, where the I_f density is within this range [122].

We have recently found that when single spontaneously beating hiPSC-derived cardiomyocytes are chosen for electrophysiological analysis, the I_f current density remains constant around 4–5 pA/pF independently of the time in culture (from day 15 to 60; Giannetti et al. Pflügers Archiv - European Journal of Physiologyhttps://doi.org/10.1007/s00424-021-02571-w).

Furthermore, the rate of spontaneously beating hES-derived cardiomyocytes, which express a robust I_f current, is slowed by zatebradine, another I_f blocker [117, 130].

Together these reports indicate that I_f and the underlying HCN channels contribute significantly to cardiac cellular autorhythmicity (Fig. 4.3).

4.5 f-Channels Blockers

Given the importance of I_f in generation of pacemaker activity, it is not surprising that f-channels have been considered as a main target in the search for drugs able to control heart rate specifically. The underlying reason is that a specific (and moderate) reduction of I_f will affect only the slope of DD and thus cardiac rate without undesired effects on AP duration and/or inotropism associated with altered K^+ and/or Ca^{2+} channel activities.

Drugs able to selectively reduce I_f have, therefore, been long regarded as important tools in the search for a novel therapeutic approach to ischemic heart disease (IHD), normally due to unbalanced myocyte oxygen demand and supply. Slowing heart rate is beneficial under these conditions because it causes both a reduction in oxygen consumption and an increase in the duration of diastole and coronary perfusion. Unfortunately, β-blockers, Ca^{2+}-channel inhibitors, and nitrates reduce heart rate and cause side effects such as reduced cardiac inotropism and are, therefore, not entirely satisfactory in terms of efficacy and tolerance.

Substances able to reduce specifically heart rate, initially termed “specific bradycardic” and later “pure heart rate-reducing” agents, were developed in the late 1970s, starting with a clonidine derivative (alinidine, ST 567) [10]. This family includes falipamil (AQ-A39), zatebradine (UL-FS49), cilobradine (DK-AH26), ZD-7288, and ivabradine (S16257) [10, 34]. Investigation in Purkinje fibers and SAN revealed that these substances reduce the slope of DD and slow heart rate by blocking the I_f current [131, 132]. Except for ivabradine, clinical use of these drugs was hampered by the presence of side effects at therapeutic concentrations (i.e., concentrations blocking I_f) caused by partial block of K^+ and/or Ca^{2+} channels, and by block of the neuronal I_h current (equivalent to the cardiac I_f). Undesired visual effects were reported in patients treated with zatebradine due to block of I_h in photoreceptors [10].

Ivabradine is the only member of this family of compounds presently available on the market and

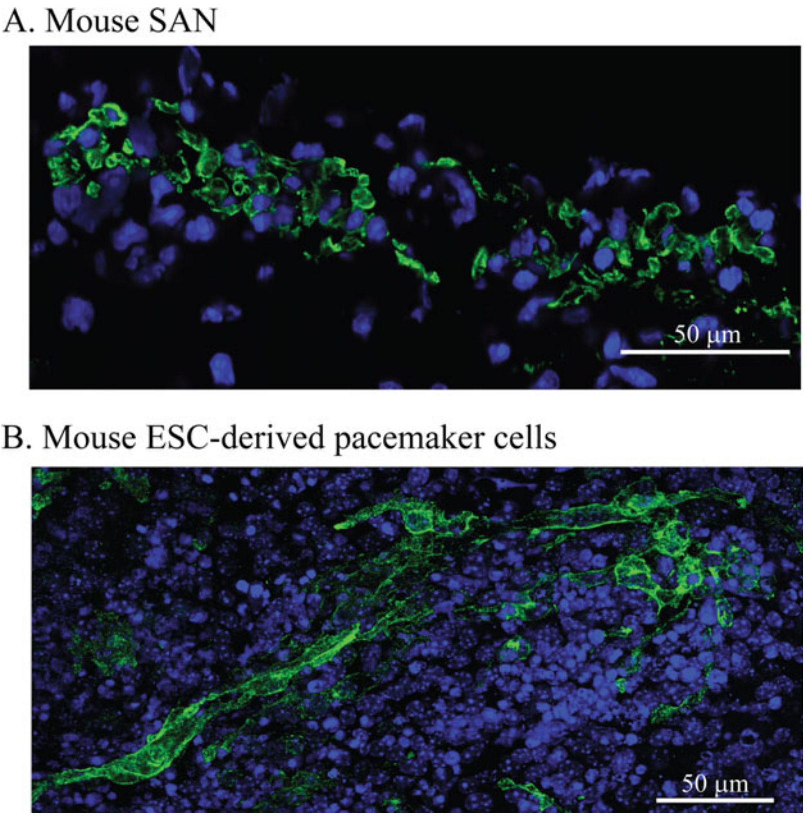

Fig. 4.3 Confocal images showing HCN4 expression (green) in the central part of the mouse SAN tissue (**a**) and in ESC-derived cardiac myocytes in culture (**b**); nuclei stained with DAPI (blue)

is used for the treatment of chronic stable *angina* and to reduce hospitalization from worsening heart failure [133].

At low/moderate doses, ivabradine is a highly specific I_f inhibitor (Fig. 4.4). In rabbit SAN, 3 μM ivabradine decreased spontaneous firing by 24%, mainly by reducing DD slope (−67%) with only a minor effect on AP duration (+9%) [134]. Studies in isolated rabbit SAN myocytes showed that ivabradine (3 μM) blocks I_f substantially (about 60%) without altering neither T- nor L-type Ca^{2+} currents or delayed outward rectifying K^+ currents [135]. Additional studies showed that ivabradine acts from the cytoplasmic side [135] and that drug binding/ unbinding to f-channels was constrained to open channel states [136]; also, the block has the unique feature of being determined by the direction of current flow (current dependence). According to this mechanism, drug molecules are “kicked-in” their blocking site within the pore by the outward ion flow during depolarization and “kicked off” during hyperpolarization [136]. The overall block properties determine use-dependence, implying that the block is favored by frequent cycling between open and closed states [137].

The bradycardic action of ivabradine has been confirmed in both preclinical and clinical studies [34, 138, 139]. In healthy volunteers, a single oral dose of ivabradine (20 mg) induced a decrease of heart rate by 18 ± 6% during physical exercise [140]. Trials in patients with stable *angina* showed that the anti-anginal effects of ivabradine are comparable to those of β-blockers but without side effects such as sexual disturbances, respiratory problems, and rebound phenomena; the only adverse events linked to ivabradine treatment were a limited reduction of blood pressure and mild, well tolerated visual symptoms (phosphenes). The visual disturbances are due to the action of ivabradine on HCN channels expressed in the retina [141, 142].

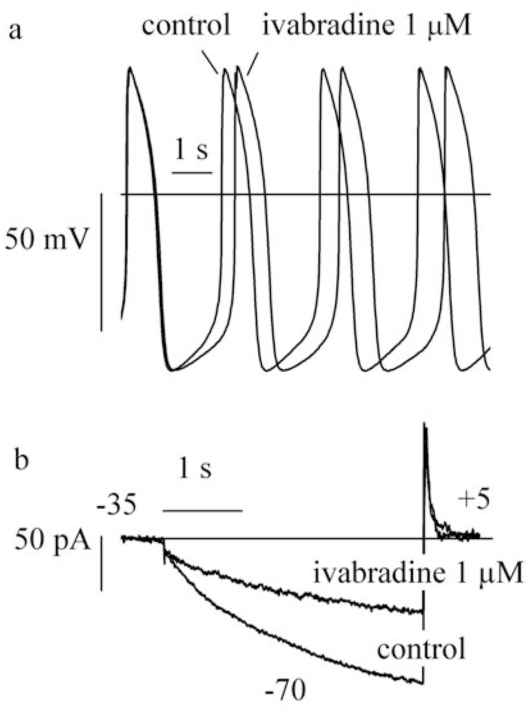

Fig. 4.4 Ivabradine slows heart rate by partial block of I_f. (**a**) spontaneous activity recorded from a SAN cell before and during perfusion with ivabradine 1 μM. Note that slowing is due to a reduced steepness of the diastolic depolarization. (**b**) inhibition by ivabradine 1 μM of I_f recorded from a SAN cell during steps to −70 mV

4.5.1 Effects of Heart Rate-Reducing Agents on HCN Isoforms

All the pure heart rate-reducing agents listed so far do not show any isoform specificity: in HEK293 cells, cilobradine, ivabradine, and zatebradine block HCN1, HCN2, and HCN4 homomeric channels with a similar IC_{50} (close to 1 μM) and Hill slope factors close to 1; these values are similar to those reported for native f-channels in SAN [10]. Ivabradine blocks HCN4 and HCN1 differently; it is an open-channel blocker of HCN4 channels and a closed-channel blocker of HCN1 channels [143]. Some of the knowledge gained so far in relation to molecular interactions between heart rate-reducing agents and HCN channels can be summarized as follows: (1) binding of ZD7288 to the mHCN1 isoform was shown to depend critically on residues Y355, M357, and V359 in the S6 domain [10]; (2) residues A425 and I432 in the S6 domain of mHCN2 were found to be critical for ZD7288 and cilobradine binding [144]; residues Y506, F509, and I510 in the S6 domain of hHCN4 were found to be critical for ivabradine binding [145].

The wide distribution of HCN proteins in different tissues, and their involvement in various cardiac and noncardiac pathological conditions (arrhythmias, pain associated with nerve injury, epileptic seizure disorders, and others) [146–148] led to the development of new isoform-specific compounds, [149]: (1) zatebradine derivatives dubbed EC18 and MEL57A showed higher selectivity for hHCN4 and mHCN1, respectively, and this selectivity was maintained when they were tested in various tissues expressing different HCN isoforms [150, 151]; (2) Compound 12m, an f 2,2-di-substituted indane-derivative, showed higher selectivity for hHCN1 with respect to hHCN2 and hHCN4, and, in in vivo experiment, it showed analgesic effects without affecting heart rate [152].

4.6 Genetics of HCN Channels

In a large-scale screen for mutations that affect the development of the heart in the embryo of zebrafish *Danio rerio*, a mutant (*slow-mo*) showed a substantially reduced heart rate compared to wild-type animals [153]. The bradycardic phenotype was also evident in the isolated heart and patch clamp experiments showing that the only current greatly reduced (85%) was I_f. The *slow-mo* mutant was the first genetic model showing the importance of I_f for generating cardiac pacemaker activity in vivo.

4.6.1 Transgenic Animal Models

In recent years, four HCN4 knockout mouse models have been developed to evaluate in vivo the functional contribution of this isoform to pacemaking [107, 154, 155]. Both global and cardiac-specific constitutive knockouts of the

HCN4 gene cause premature death of mice at mid-gestation (E9.5–E11.5), a developmental stage when regular contractile activity normally develops [107]. SAN myocytes isolated from knockout embryos at day E9.5 showed reduced spontaneous rate (−36.7%) and I_f current (−85%) compared with controls. The knockout process also led to the complete loss of cAMP-mediated β-adrenergic modulation, suggesting that the residual I_f current might be carried by the HCN1 and HCN3 isoforms which are almost insensitive to cAMP stimulation [42, 43, 49]. These data show that HCN4 expression is necessary for proper embryonic heart development, although they do not provide evidence for the role of the HCN4 current in adult animals.

To avoid the limitations due to constitutive HCN4 knockout, inducible knockout animals were generated [154, 155]. In one model, ECGs recorded from freely moving knockout animals showed sinus pauses followed by normal rhythmic activity; β-modulation of rate was not lost, and any acceleration in heart rate reduced sinus pauses [154]. In another model, the induction of the HCN4 knockout was under the control of a regulatory region of the HCN4 gene. ECG recordings from these animals also showed sinus pauses (mean frequency 16.1 per minute) [155]. Since 90% of the global knockout-derived and 50% of the HCN4-targeted knockout-derived SAN myocytes were quiescent and the I_f current was reduced by about 75–80% [154, 155], further investigation will be required to understand the difference between the effects of the knockout process on SAN automaticity in in vivo and in vitro conditions.

4.6.2 Pathologies Associated with HCN Dysfunctions

Several mutations in the coding sequence of the *hHCN4* gene associated with alterations in cardiac rhythm and other pathological cardiac phenotypes have been identified in humans (Table 4.2). The majority of the mutations have been classified as loss-of-function (l.o.f.) since in vitro functional studies revealed a decreased contribution of the current to cell excitability. Although sinus bradycardia is the most frequently observed arrhythmic manifestation in patients presenting with these l.o.f. mutations, several other pathological features have been described.

A convincing and robust example of the causative chain of events linking the presence of a single point *HCN4* gene mutation, the altered HCN4/pacemaker current features, and the clinical manifestation is represented by the S672R mutation. The functional correlation between the defective HCN4 and arrhythmias was reported in 2006 [166] during a study on a large Italian family spanning three generations. The S672R point mutation, located in a highly conserved residue within the Cyclic Nucleotide Binding Domain, was found to be associated with the presence of an inherited asymptomatic sinus bradycardia according to an autosomal dominant pattern. The heart rate of family members carrying the mutation was significantly slower (52.2 ± 1.4 bpm, $n = 15$) than that measured in wild-type members (73.2 ± 1.6 bpm, $n = 12$). Co-segregation of bradycardia with the *hHCN4* gene was strong, as shown by the high LOD score value (5.47). In vitro electrophysiological analysis of S672R channels showed a more negative activation curve (−4.9 mV shift) and faster deactivation kinetics than the wild-type. The effect of the S672R mutation, in heterozygosis, is, therefore, analogous to a mild vagal stimulation corresponding to a low concentration of acetylcholine (about 20 nM); this action leads to a reduced net inward current during DD and negative chronotropy.

An opposite functional consequence has been observed in the *HCN4* R524Q gain-of-function (g.o.f.) mutation, which was identified in family siblings affected by Inappropriate Sinus Tachycardia (IST) [162]. IST is a type of sinus node dysfunction associated with higher than normal resting SAN rate; clinical symptoms are variable and include palpitations, activity intolerance, recurrent syncopes, lightheadedness, and orthostatic intolerance. The R524Q mutation is located in the C-linker, in close proximity to the S6 segment, a region known to couple cAMP binding to channel activation. Patch clamp experiments

Table 4.2 Mutations of the pacemaker (HCN4) channels associated with nodal and more general cardiac dysfunctions

↑ G-O-F ↓ L-O-F	Mutation	Associated phenotypes	Ref
↓	P257S	Atrial fibrillation	[156]
↓	R378C	Sinus bradycardia	[157]
↓	A414G	Sinus bradycardia, left ventricular noncompaction, atrial fibrillation, atrial standstill	[158]
↓	G480R	Sinus bradycardia	[159]
↓	Y481H	Sinus Bradycardia, left ventricular noncompaction, atrial fibrillation, degeneration of the mitral valve; polymorphic ventricular extrasystoles during exercise	[158]
↓	*G482R*	Sinus bradycardia, I° atrioventricular block, impaired chronotropic capacity, left ventricular noncompaction, intermittent ectopic atrial rhythms, mitral valve prolapse, out-of-hospital cardiac arrest	[158, 160]
↓	*A485V*	Sinus Bradycardia, out-of-hospital cardiac arrest during extreme exercise, inducible and paroxysmal atrial fibrillation	[161]
↑	*R524Q*	Inappropriate sinus tachycardia	[162]
↓	*K530N*	Sinus bradycardia, sinus pauses, tachycardia-bradycardia syndrome, Persistent, Atrial Fibrillation	[163]
↓	*R550H*	Sinus bradycardia	[157]
↓	*D553N*	Sinus bradycardia, QT prolongation; torsade de pointes, cardiac arrest for 40 s followed by polymorphic ventricular tachycardia	[164]
↓	*573X*	SBS, chronotropic incompetence during exercise, intermittent atrial fibrillation	[165]
↓	*S672R*	Sinus Bradycardia	[166]
↓	*695X*	Sinus bradycardia, episodes of distinctive sinus arrhythmia linked to adrenergic stress, left ventricular noncompaction, susceptibility to atrial and ventricular premature beats, mitral valve prolapse	[160, 167]
↑	*P883R*	Bradycardia-tachycardia syndrome, paroxysmal atrial fibrillation	[168]
↓	*G1097W*	Atrioventricular block	[169]
↓	*E1193Q*	Sinus bradycardia, atrial fibrillation, Brugada syndrome restrictive cardio	[157]

In many cases, the phenotypic features of the mutations listed in the table have been investigated in heterologous expression studies with the patch clamp technique. Symptoms listed were identified in the proband and/or in siblings carrying the mutation.

revealed that mutant HCN4 channels exhibit a higher than normal cAMP affinity, and this feature provides the logical molecular and functional framework to explain both the tachycardic resting condition due to exaggerated response to basal cAMP level and the increased response to sympathetic stimuli, which is also observed in mutant carriers.

Additional “non-SAN related” pathological conditions have been variously found in association with different types of *HCN4* mutations, and among them, it is important to cite atrial fibrillation, noncompaction cardiomyopathy, and mitral valve degeneration. While the causative relation between *HCN4* mutations and sinus arrhythmias is straightforward, the mutation-specific connections with non-SAN pathological manifestations are challenging and represent an incredible window into the future of the research. Indeed, unraveling the associative link between these pathologies and pacemaker channels will add a still-missing and fundamental knowledge of the biology of these channels.

In conclusion, the identification of *HCN4* mutations represents a genetic and molecular paradigm that highlights the importance of these channels in cardiac rhythm generation and disturbances as well as in other cardiac diseases.

4.7 Biological Pacemaker

Normal generation and propagation of heart rhythm can be affected by several cardiac diseases such as Sick Sinus Syndrome, AV block, and severe bradycardia, requiring implantation of an electronic pacemaker. Therefore there is an increasing interest in biological pacemakers, which consist of cellular substrates able to spontaneously drive a quiescent but excitable tissue and to respond to autonomic modulation. The first attempts to induce autorhythmic activity in a quiescent substrate used viruses to over-express β2-adrenoceptors or to inhibit inwardly rectifying K^+ currents [170]. HCN channels, however, are more suitable candidates for gene transfer technology because (1) they are active only during, and thus contribute solely to, the diastolic phase of APs, and (2) they are responsive to autonomic regulation [11, 28]. An exhaustive description of all the strategies used to create the biological pacemaker are reviewed in Cingolani et al. (2018) [171]; here, only HCN and stem cell-based strategies are summarized.

4.7.1 HCN-Gene Strategies

“Proof of principle” evidence that HCN overexpression can induce spontaneous activity was provided by experiments showing that in vitro infection of primary cultures of neonatal rat myocytes with adenoviruses carrying the mouse HCN2 channel leads to a significant increase in their beating rate (83%) [66]. Further, in vivo, overexpression of HCN2 in the left atrium or in the left bundle branch of dogs increased the I_f current density and generated stable, spontaneous activity following sinus arrest or AV block [170]. Similar strategies using HCN1 and HCN4 isoforms also successfully induced stable ectopic rhythm in an animal model [172]. To overcome the limitation of the low rate at which these biological pacemakers drove the heart, either mutated HCN2 constructs, with a more depolarized activation curve and faster kinetics, or HCN1–HCN2 chimeric constructs characterized by fast activation kinetics (provided by HCN1) and cAMP modulation (provided by HCN2) were used. In vivo experiments showed that the former construct improves catecholamine sensitivity but not basal heart rate, and the latter construct causes episodes of ventricular tachycardia interrupted by pauses of variable length [170].

In an alternative approach, a synthetic HCN channel, obtained by mutating human Kv1.4 channels in four specific residues, was used. In vivo expression of the engineered channel in guinea pig ventricle generated an HCN-like inward current and an ectopic rhythm [170].

In a hybrid approach, human mesenchymal stem cells (hMSCs) or fibroblasts, engineered to provide an HCN channels-mediated depolarizing current, were delivered to specific regions of the heart to produce cardiac automaticity. These approaches were based on the ability of hMSCs to electrically couple with cardiomyocytes through gap-junctions [173], and on the ability of fibroblasts to fuse with cardiomyocytes [174].

In the last two decades, the elucidation of the genetic program driving the embryonic differentiation of the SAN has paved the road to a novel type of gene-based approach to biological pacemaking. Tbx18, Shox2, and Tbx3 have been shown to play a critical role in SAN specification [108]. This evidence has rushed researchers to test the hypothesis that ectopic expression of one of these transcription factors may transdifferentiate the working myocardium into pacemaker cells. Hoogaars et al. in 2007 showed that ectopic expression of Tbx3 in atrial cells leads to repression of working myocardium genes and activation of HCN4 [175, 176]. In 2013, Kapoor and colleagues demonstrated that both in vitro and in vivo expression of TBX18 convert murine ventricular cardiomyocytes into pacemaker cells morphologically similar to SAN cardiomyocytes and expressing *HCN4*/I_f current [177].

4.7.2 Stem Cell-Based Biological Pacemakers

Because of teratogenic risk, viral vectors, even if efficient, are unlikely to be the choice delivery system for HCN channels. Cell-based biological pacemakers have therefore been considered with growing interest. Progress in this direction came from the use of human adult mesenchymal stem cells (MSCs) over-expressing the mouse *HCN2* gene [178]. MSCs express endogenously gap-junctions, and when electrically coupled to ventricular myocytes, their membrane hyperpolarizes, leading to large activation of the HCN2 channels and spontaneous rhythm generation in the surrounding tissue [178]. MSCs engineered with HCN4 channels also effectively paced ventricular substrate [179]. A different approach was based on HCN1-expressing fibroblasts induced to fuse (by PolyEthylene Glycol; PEG) with guinea pig ventricular myocytes. The heterokaryons displayed spontaneous APs with slow depolarization phase and expressed I_f-like pacemaker current sensitive to the I_f blocker ZD7288. Surprisingly, heterokaryons were responsive to β-adrenergic but not to cholinergic agonists [170].

Embryonic stem cells (ESCs), known to differentiate into spontaneously beating SAN-like cells expressing I_f have also been used to develop a cell-based biological pacemaker [112–115, 117, 180]. Two separate studies have demonstrated that spontaneously beating ESC-derived myocytes can pace cultures of neonatal rat cardiac myocytes and generate an ectopic rhythm when injected in the ventricle of animal models after AV ablation [130, 180]. Although the presence of f/HCN channels was not directly addressed in these studies, their involvement in the generation of the rhythmic activity was apparent, based on evidence for rate increase by β-adrenergic activation and rate decrease by f-channel blocker ZD7288 [130, 180].

More recently, human iPSC-derived autorhythmic cells were proven to be a suitable cell model for generating patient-specific biological pacemakers. Chauveau et al. have demonstrated that spontaneously beating EBs generated from iPSC, expressing a prominent I_f current, are able to pace the heart of a canine model of conduction block, when injected into the anterobasal left ventricle, and are responsive to adrenergic stimulation [182]. However, the ectopic rate resulted to be quite low, probably because EBs are a heterogeneous cell system containing only a minor number of sinoatrial-like cells. Of note, Protze and collaborators have published a method for selecting a highly pure subpopulation of sinoatrial-like cardiomyocytes that are able to pace in vitro ventricular-like cardiomyocytes [122].

4.8 Conclusions

Although the biophysical properties of the “funny” current fit well with an important role in pacemaking, the idea of this bizarre but essentially simple mechanism having a relevant part in the governance of cardiac rhythm took time to be accepted and is still hotly debated [3, 183–185]. In the late 1990s, after the cloning of the *HCN* genes, strong evidence in favor of f/HCN channels as key players in the pacemaking process was gathered. Analysis of HCN isoform distribution highlighted the selective expression of HCN4 channels in SAN and the conduction system of various species including humans. While embryological studies on mice showed the early onset of HCN4 expression, specifically in the prospective SAN and conduction system, the evidence that transgenic mice lacking the HCN4 gene die early during embryogenesis strengthened the functional role of f-channels in the generation of cardiac pacemaker activity. Finally, the development of f-channel blockers for the therapeutic control of heart rate in humans and the discovery of HCN4 mutations in patients affected by rhythm disturbances has further established the importance of f-channels in pacemaking.

References

1. Silverman ME, Grove D, Upshaw CB Jr. Why does the heart beat? The discovery of the electrical system of the heart. Circulation. 2006;113(23):2775–81.
2. Keith A, Flack M. The form and nature of the muscular connections between the primary divisions of the vertebrate heart. J Anat Physiol. 1907;41(Pt 3): 172–89.
3. Lakatta EG, DiFrancesco D. What keeps us ticking: a funny current, a calcium clock, or both? J Mol Cell Cardiol. 2009;47(2):157–70.
4. Brown HF, DiFrancesco D, Noble SJ. How does adrenaline accelerate the heart? Nature. 1979;280 (5719):235–6.
5. DiFrancesco D. A new interpretation of the pacemaker current in calf Purkinje fibres. J Physiol. 1981;314:359–76.
6. DiFrancesco D. A study of the ionic nature of the pace-maker current in calf Purkinje fibres. J. Physiol. 1981;314:377–93.
7. Frace AM, Maruoka F, Noma A. External K+ increases Na+ conductance of the hyperpolarization-activated current in rabbit cardiac pacemaker cells. Pflugers Arch. 1992;421(2-3):97–9.
8. Wollmuth LP, Hille B. Ionic selectivity of Ih channels of rod photoreceptors in tiger salamanders. J Gen Physiol. 1992;100(5):749–65.
9. DiFrancesco D. Dual allosteric modulation of pacemaker (f) channels by cAMP and voltage in rabbit SA node. J Physiol. 1999;515(2):367–76.
10. Baruscotti M, Bucchi A, DiFrancesco D. Physiology and pharmacology of the cardiac pacemaker (“funny”) current. Pharmacol Ther. 2005;107(1): 59–79.
11. DiFrancesco D, Ferroni A, Mazzanti M, Tromba C. Properties of the hyperpolarizing-activated current (if) in cells isolated from the rabbit sino-atrial node. J Physiol. 1986;377:61–88.
12. DiFrancesco D. The contribution of the ‘pacemaker’ current (if) to generation of spontaneous activity in rabbit sino-atrial node myocytes. J Physiol. 1991;434:23–40.
13. Arinsburg SS, Cohen IS, Yu HG. Constitutively active Src tyrosine kinase changes gating of HCN4 channels through direct binding to the channel proteins. J Cardiovasc Pharmacol. 2006;47(4): 578–86.
14. Li CH, Zhang Q, Teng B, Mustafa SJ, Huang JY, Yu HG. Src tyrosine kinase alters gating of hyperpolarization-activated HCN4 pacemaker channel through Tyr531. Am. J. Physiol. Cell. Physiol. 2008;294(1):C355–62.
15. Qu J, Kryukova Y, Potapova IA, Doronin SV, Larsen M, Krishnamurthy G, et al. MiRP1 modulates HCN2 channel expression and gating in cardiac myocytes. J Biol Chem. 2004;279(42):43497–502.
16. Decher N, Bundis F, Vajna R, Steinmeyer K. KCNE2 modulates current amplitudes and activation kinetics of HCN4: influence of KCNE family members on HCN4 currents. Pflugers Arch. 2003;446(6):633–40.
17. Brandt MC, Endres-Becker J, Zagidullin N, Motloch LJ, Er F, Rottlaender D, et al. Effects of KCNE2 on HCN isoforms: distinct modulation of membrane expression and single channel properties. Am J Physiol Heart Circ Physiol. 2009;297(1):H355–63.
18. Michels G, Er F, Khan IF, Endres-Becker J, Brandt MC, Gassanov N, et al. K+ channel regulator KCR1 suppresses heart rhythm by modulating the pacemaker current If. PLoS One. 2008;3(1):e1511.
19. Peters CJ, Chow SS, Angoli D, Nazzari H, Cayabyab FS, Morshedian A, et al. In situ co-distribution and functional interactions of SAP97 with sinoatrial isoforms of HCN channels. J Mol Cell Cardiol. 2009;46(5):636–43.
20. Barbuti A, Gravante B, Riolfo M, Milanesi R, Terragni B, DiFrancesco D. Localization of pacemaker channels in lipid rafts regulates channel kinetics. Circ Res. 2004;94(10):1325–31.
21. Barbuti A, Terragni B, Brioschi C, DiFrancesco D. Localization of f-channels to caveolae mediates specific beta2-adrenergic receptor modulation of rate in sinoatrial myocytes. J Mol Cell Cardiol. 2007;42 (1):71–8.
22. DiFrancesco D. Cardiac pacemaker: 15 years of “new” interpretation. Acta Cardiol. 1995;50(6): 413–27.
23. Munk AA, Adjemian RA, Zhao J, Ogbaghebriel A, Shrier A. Electrophysiological properties of morphologically distinct cells isolated from the rabbit atrioventricular node. J Physiol. 1996;493(Pt 3):801–18.
24. Yuill KH, Hancox JC. Characteristics of single cells isolated from the atrioventricular node of the adult guinea-pig heart. Pflugers Arch. 2002;445(3): 311–20.
25. Yu H, Chang F, Cohen IS. Phosphatase inhibition by calyculin A increases i(f) in canine Purkinje fibers and myocytes. Pflugers Arch. 1993;422(6):614–6.
26. Cerbai E, Barbieri M, Mugelli A. Characterization of the hyperpolarization-activated current, I(f), in ventricular myocytes isolated from hypertensive rats. J Physiol. 1994;481(Pt 3):585–91.
27. Cerbai E, Barbieri M, Mugelli A. Occurrence and properties of the hyperpolarization-activated current If in ventricular myocytes from normotensive and hypertensive rats during aging. Circulation. 1996;94 (7):1674–81.
28. DiFrancesco D, Tortora P. Direct activation of cardiac pacemaker channels by intracellular cyclic AMP. Nature. 1991;351:145–7.
29. Barbuti A, Baruscotti M, DiFrancesco D. The pacemaker current: from basics to the clinics. J Cardiovasc Electrophysiol. 2007;18(3):342–7.
30. Rodefeld MD, Beau SL, Schuessler RB, Boineau JP, Saffitz JE. Beta-adrenergic and muscarinic cholinergic receptor densities in the human sinoatrial node: identification of a high beta 2-adrenergic receptor

density. J Cardiovac Electrophysiol. 1996;7(11): 1039–49.

31. Santoro B, Grant SG, Bartsch D, Kandel ER. Interactive cloning with the SH3 domain of N-src identifies a new brain specific ion channel protein, with homology to eag and cyclic nucleotide-gated channels. Proc Natl Acad Sci USA. 1997;94(26):14815–20.
32. Jackson HA, Marshall CR, Accili EA. Evolution and structural diversification of hyperpolarization-activated cyclic nucleotide-gated channel genes. Physiol Genomics. 2007;29(3):231–45.
33. Biel M, Wahl-Schott C, Michalakis S, Zong X. Hyperpolarization-activated cation channels: from genes to function. Physiol. Rev. 2009;89(3): 847–85.
34. Baruscotti M, Barbuti A, Bucchi A. The cardiac pacemaker current. J Mol Cell Cardiol. 2010;48(1): 55–64.
35. Giorgetti A, Carloni P, Mistrik P, Torre V. A homology model of the pore region of HCN channels. Biophys J. 2005;89(2):932–44.
36. Proenza C, Tran N, Angoli D, Zahynacz K, Balcar P, Accili EA. Different roles for the cyclic nucleotide binding domain and amino terminus in assembly and expression of hyperpolarization-activated, cyclic nucleotide-gated channels. J Biol Chem. 2002;277 (33):29634–42.
37. Tran N, Proenza C, Macri V, Petigara F, Sloan E, Samler S, et al. A conserved domain in the NH2 terminus important for assembly and functional expression of pacemaker channels. J Biol Chem. 2002;277(46):43588–92.
38. Wainger BJ, DeGennaro M, Santoro B, Siegelbaum SA, Tibbs GR. Molecular mechanism of cAMP modulation of HCN pacemaker channels. Nature. 2001;411(6839):805–10.
39. Craven KB, Zagotta WN. Salt bridges and gating in the COOH-terminal region of HCN2 and CNGA1 channels. J Gen Physiol. 2004;124(6):663–77.
40. Zagotta WN, Olivier NB, Black KD, Young EC, Olson R, Gouaux E. Structural basis for modulation and agonist specificity of HCN pacemaker channels. Nature. 2003;425(6954):200–5.
41. Accili EA, Proenza C, Baruscotti M, DiFrancesco D. From funny current to HCN channels: 20 years of excitation. News Physiol Sci. 2002;17:32–7.
42. Stieber J, Stockl G, Herrmann S, Hassfurth B, Hofmann F. Functional expression of the human HCN3 channel. J Biol Chem. 2005;280(41): 34635–43.
43. Mistrik P, Mader R, Michalakis S, Weidinger M, Pfeifer A, Biel M. The murine HCN3 gene encodes a hyperpolarization-activated cation channel with slow kinetics and unique response to cyclic nucleotides. J Biol Chem. 2005;280(29):27056–61.
44. Qu J, Altomare C, Bucchi A, DiFrancesco D, Robinson RB. Functional comparison of HCN isoforms expressed in ventricular and HEK 293 cells. Pflugers Arch. 2002;444(5):597–601.
45. Chandler NJ, Greener ID, Tellez JO, Inada S, Musa H, Molenaar P, et al. Molecular architecture of the human sinus node: insights into the function of the cardiac pacemaker. Circulation. 2009;119(12): 1562–75.
46. Thollon C, Bedut S, Villeneuve N, Coge F, Piffard L, Guillaumin JP, et al. Use-dependent inhibition of hHCN4 by ivabradine and relationship with reduction in pacemaker activity. Br J Pharmacol. 2007;150 (1):37–46.
47. Zicha S, Fernandez-Velasco M, Lonardo G, L'Heureux N, Nattel S. Sinus node dysfunction and hyperpolarization-activated (HCN) channel subunit remodeling in a canine heart failure model. Cardiovasc Res. 2005;66(3):472–81.
48. Shi W, Wymore R, Yu H, Wu J, Wymore RT, Pan Z, et al. Distribution and prevalence of hyperpolarization-activated cation channel (HCN) mRNA expression in cardiac tissues. Circ Res. 1999;85(1):e1–6.
49. Moroni A, Gorza L, Beltrame M, Gravante B, Vaccari T, Bianchi ME, et al. Hyperpolarization-activated cyclic nucleotide-gated channel 1 is a molecular determinant of the cardiac pacemaker current I(f). J Biol Chem. 2001;276(31):29233–41.
50. Marionneau C, Couette B, Liu J, Li H, Mangoni ME, Nargeot J, et al. Specific pattern of ionic channel gene expression associated with pacemaker activity in the mouse heart. J Physiol. 2005;562(Pt 1):223–34.
51. Moosmang S, Stieber J, Zong X, Biel M, Hofmann F, Ludwig A. Cellular expression and functional characterization of four hyperpolarization-activated pacemaker channels in cardiac and neuronal tissues. Eur J Biochem. 2001;268(6):1646–52.
52. Huang X, Yang P, Du Y, Zhang J, Ma A. Age-related down-regulation of HCN channels in rat sinoatrial node. Basic Res Cardiol. 2007;102(5):429–35.
53. Li N, Csepe TA, Hansen BJ, Dobrzynski H, Higgins RS, Kilic A, et al. Molecular mapping of sinoatrial node HCN channel expression in the human heart. Circ Arrhythm Electrophysiol. 2015;8(5):1219–27.
54. Brioschi C, Micheloni S, Tellez JO, Pisoni G, Longhi R, Moroni P, et al. Distribution of the pacemaker HCN4 channel mRNA and protein in the rabbit sinoatrial node. J Mol Cell Cardiol. 2009;47(2): 221–7.
55. Liu J, Dobrzynski H, Yanni J, Boyett MR, Lei M. Organisation of the mouse sinoatrial node: structure and expression of HCN channels. Cardiovasc Res. 2007;73(4):729–38.
56. Yamamoto M, Dobrzynski H, Tellez J, Niwa R, Billeter R, Honjo H, et al. Extended atrial conduction system characterised by the expression of the HCN4 channel and connexin45. Cardiovasc Res. 2006;72 (2):271–81.
57. Gaborit N, Le Bouter S, Szuts V, Varro A, Escande D, Nattel S, et al. Regional and tissue

specific transcript signatures of ion channel genes in the non-diseased human heart. J Physiol. 2007;582 (Pt 2):675–93.

58. Stillitano F, Lonardo G, Zicha S, Varro A, Cerbai E, Mugelli A, et al. Molecular basis of funny current (If) in normal and failing human heart. J Mol Cell Cardiol. 2008;45(2):289–99.
59. Dobrzynski H, Nikolski VP, Sambelashvili AT, Greener ID, Yamamoto M, Boyett MR, et al. Site of origin and molecular substrate of atrioventricular junctional rhythm in the rabbit heart. Circ Res. 2003;93(11):1102–10.
60. Han W, Bao W, Wang Z, Nattel S. Comparison of ion-channel subunit expression in canine cardiac Purkinje fibers and ventricular muscle. Circ Res. 2002;91(9):790–7.
61. Fernandez-Velasco M, Goren N, Benito G, Blanco-Rivero J, Bosca L, Delgado C. Regional distribution of hyperpolarization-activated current (If) and hyperpolarization-activated cyclic nucleotide-gated channel mRNA expression in ventricular cells from control and hypertrophied rat hearts. J Physiol. 2003;553(Pt 2):395–405.
62. Garcia-Frigola C, Shi Y. Evans SM Expression of the hyperpolarization-activated cyclic nucleotide-gated cation channel HCN4 during mouse heart development. Gene Expr Patterns. 2003;3(6):777–83.
63. Mommersteeg MT, Hoogaars WM, Prall OW, Gier-de Vries C, Wiese C, Clout DE, et al. Molecular pathway for the localized formation of the sinoatrial node. Circ Res. 2007;100(3):354–62.
64. Ishii TM, Takano M, Ohmori H. Determinants of activation kinetics in mammalian hyperpolarization-activated cation channels. J Physiol. 2001;537:93–100.
65. Xue T, Marban E, Li RA. Dominant-negative suppression of HCN1- and HCN2-encoded pacemaker currents by an engineered HCN1 construct: insights into structure-function relationships and multimerization. Circ Res. 2002;90(12):1267–73.
66. Qu J, Barbuti A, Protas L, Santoro B, Cohen IS, Robinson RB. HCN2 overexpression in newborn and adult ventricular myocytes: distinct effects on gating and excitability. Circ Res. 2001;89(1):E8–14.
67. Robinson RB, Yu H, Chang F, Cohen IS. Developmental change in the voltage-dependence of the pacemaker current, if, in rat ventricle cells. Pflugers Arch. 1997;433(4):533–5.
68. Zong X, Eckert C, Yuan H, Wahl-Schott C, Abicht H, Fang L, et al. A novel mechanism of modulation of hyperpolarization-activated cyclic nucleotide-gated channels by Src kinase. J Biol Chem. 2005;280(40):34224–32.
69. Pian P, Bucchi A, Decostanzo A, Robinson RB, Siegelbaum SA. Modulation of cyclic nucleotide-regulated HCN channels by PIP(2) and receptors coupled to phospholipase C. Pflugers Arch. 2007;455(1):125–45.
70. Pian P, Bucchi A, Robinson RB, Siegelbaum SA. Regulation of gating and rundown of HCN hyperpolarization-activated channels by exogenous and endogenous PIP2. J Gen Physiol. 2006;128(5): 593–604.
71. Lolicato M, Bucchi A, Arrigoni C, Zucca S, Nardini M, Schroeder I, et al. Cyclic dinucleotides bind the C-linker of HCN4 to control channel cAMP responsiveness. Nat Chem Biol. 2014;10(6):457–62.
72. Yu H, Wu J, Potapova I, Wymore RT, Holmes B, Zuckerman J, et al. MinK-related peptide 1: a beta subunit for the HCN ion channel subunit family enhances expression and speeds activation. Circ Res. 2001;88(12):E84–7.
73. Ye B, Balijepalli RC, Foell JD, Kroboth S, Ye Q, Luo YH, et al. Caveolin-3 associates with and affects the function of hyperpolarization-activated cyclic nucleotide-gated channel 4. Biochemistry. 2008;47 (47):12312–8.
74. Lu Z, Wang HZ, Gordon CR, Ballou LM, Lin RZ. Cohen IS regulation of HCN2 current by PI3K/ Akt signaling. Front Physiol. 2020;11:587040.
75. Lin RZ, Lu Z, Anyukhovsky EP, Jiang YP, Wang HZ, Gao J, et al. Regulation of heart rate and the pacemaker current by phosphoinositide 3-kinase signaling. J Gen Physiol. 2019;151(8):1051–8.
76. Simons K, Toomre D. Lipid rafts and signal transduction. Nat Rev Mol Cell Biol. 2000;1(1):31–9.
77. Masson-Pevet M, Gros D, Besselsen E. The caveolae in rabbit sinus node and atrium. Cell Tissue Res. 1980;208(2):183–96.
78. Barbuti A, Scavone A, Mazzocchi N, Terragni B, Baruscotti M, DiFrancesco D. A caveolin-binding domain in the HCN4 channels mediates functional interaction with caveolin proteins. J Mol Cell Cardiol. 2012;53(2):187–95.
79. Folco EJ, Liu GX, Koren G. Caveolin-3 and SAP97 form a scaffolding protein complex that regulates the voltage-gated potassium channel Kv1.5. Am J Physiol Heart Circ.Physiol. 2004;287(2):H681–90.
80. Balijepalli RC, Delisle BP, Balijepalli SY, Foell JD, Slind JK, Kamp TJ, et al. Kv11.1 (ERG1) K+ channels localize in cholesterol and sphingolipid enriched membranes and are modulated by membrane cholesterol. Channels (Austin). 2007;1(4): 263–72.
81. MacDonald EA, Rose RA, Quinn TA. Neurohumoral control of sinoatrial node activity and heart rate: insight from experimental models and findings from humans. Front Physiol. 2020;11:170.
82. Renaudon B, Lenfant J, Decressac S, Bois P. Thyroid hormone increases the conductance density of f-channels in rabbit sino-atrial node cells. Receptors Channels. 2000;7(1):1–8.
83. Gassanov N, Er F, Endres-Becker J, Wolny M, Schramm C, Hoppe UC. Distinct regulation of cardiac I(f) current via thyroid receptors alpha1 and beta1. Pflugers Archiv Eur J Physiol. 2009;458(6): 1061–8.

84. Re A, Nanni S, Aiello A, Granata S, Colussi C, Campostrini G, et al. Anacardic acid and thyroid hormone enhance cardiomyocytes production from undifferentiated mouse ES cells along functionally distinct pathways. Endocrine. 2016;53(3):681–8.
85. Ogino K, Burkhoff D, Bilezikian JP. The hemodynamic basis for the cardiac effects of parathyroid hormone (PTH) and PTH-related protein. Endocrinology. 1995;136(7):3024–30.
86. Hara M, Liu YM, Zhen L, Cohen IS, Yu H, Danilo P Jr, et al. Positive chronotropic actions of parathyroid hormone and parathyroid hormone-related peptide are associated with increases in the current, I(f), and the slope of the pacemaker potential. Circulation. 1997;96(10):3704–9.
87. Hollier LM, Martin JN, Connolly H, Turrentine M, Hameed A, Arendt KW, et al. Pregnancy and heart disease. Obstet Gynecol. 2019;133(5):e320–56.
88. El Khoury N, Mathieu S, Marger L, Ross J, El Gebeily G, Ethier N, et al. Upregulation of the hyperpolarization-activated current increases pacemaker activity of the sinoatrial node and heart rate during pregnancy in mice. Circulation. 2013;127(20): 2009–20.
89. Long V, Fiset C. Contribution of estrogen to the pregnancy-induced increase in cardiac automaticity. J Mol Cell Cardiol. 2020;147:27–34.
90. Kundu P, Ciobotaru A, Foroughi S, Toro L, Stefani E, Eghbali M. Hormonal regulation of cardiac KCNE2 gene expression. Mol Cell Endocrinol. 2008;292(1-2):50–62.
91. Al Madhoun AS, Voronova A, Ryan T, Zakariyah A, McIntire C, Gibson L, et al. Testosterone enhances cardiomyogenesis in stem cells and recruits the androgen receptor to the MEF2C and HCN4 genes. J Mol Cell Cardiol. 2013;60:164–71.
92. D'Souza A, Sharma S, Boyett MR. Rebuttal from Alicia D'Souza, Sanjay Sharma and Mark R. Boyett. J Physiol. 2015;593(8):1755.
93. D'Souza A, Pearman CM, Wang Y, Nakao S, Logantha S, Cox C, et al. Targeting miR-423-5p reverses exercise training-induced HCN4 channel remodeling and sinus bradycardia. Circ Res. 2017;121(9):1058–68.
94. D'Souza A, Bucchi A, Johnsen AB, Logantha SJ, Monfredi O, Yanni J, et al. Exercise training reduces resting heart rate via downregulation of the funny channel HCN4. Nat Commun. 2014;5:3775.
95. Yavari A, Bellahcene M, Bucchi A, Sirenko S, Pinter K, Herring N, et al. Mammalian gamma2 AMPK regulates intrinsic heart rate. Nat Commun. 2017;8(1):1258.
96. Suffredini S, Stillitano F, Comini L, Bouly M, Brogioni S, Ceconi C, et al. Long term treatment with ivabradine in post-myocardial infarcted rats counteracts f-channel overexpression. Br J Pharmacol. 2011;165(5):1457–66.
97. Yu HD, Xia S, Zha CQ, Deng SB, Du JL, She Q. Spironolactone regulates HCN protein expression through micro-RNA-1 in rats with myocardial infarction. J Cardiovasc Pharmacol. 2015;65(6):587–92.
98. Li YD, Hong YF, Yusufuaji Y, Tang BP, Zhou XH, Xu GJ, et al. Altered expression of hyperpolarization-activated cyclic nucleotide-gated channels and microRNA-1 and -133 in patients with age-associated atrial fibrillation. Mol Med Rep. 2015;12(3):3243–8.
99. Yanni J, D'Souza A, Wang Y, Li N, Hansen BJ, Zakharkin SO, et al. Silencing miR-370-3p rescues funny current and sinus node function in heart failure. Sci Rep. 2020;10(1):11279.
100. DeHaan RL. Development of pacemaker tissue in the embryonic heart. Ann NY Acad Sci. 1965;127(1): 7–18.
101. Van Mierop LH. Location of pacemaker in chick embryo heart at the time of initiation of heartbeat. Am J Physiol. 1967;212(2):407–15.
102. Pennisi DJ, Rentschler S, Gourdie RG, Fishman GI. Mikawa T induction and patterning of the cardiac conduction system. Int J Dev Biol. 2002;46(6): 765–75.
103. Yasui K, Liu W, Opthof T, Kada K, Lee JK, Kamiya K, et al. I(f) current and spontaneous activity in mouse embryonic ventricular myocytes. Circ. Res. 2001;88(5):536–42.
104. Christoffels VM, Smits GJ, Kispert A, Moorman AF. Development of the pacemaker tissues of the heart. Circ Res. 2010;106(2):240–54.
105. Liang X, Wang G, Lin L, Lowe J, Zhang Q, Bu L, et al. HCN4 dynamically marks the first heart field and conduction system precursors. Circ Res. 2013;113(4):399–407.
106. Spater D, Abramczuk MK, Buac K, Zangi L, Stachel MW, Clarke J, et al. A HCN4+ cardiomyogenic progenitor derived from the first heart field and human pluripotent stem cells. Nat Cell Biol. 2013;15(9):1098–106.
107. Stieber J, Herrmann S, Feil S, Loster J, Feil R, Biel M, et al. The hyperpolarization-activated channel HCN4 is required for the generation of pacemaker action potentials in the embryonic heart. Proc. Natl. Acad. Sci. USA. 2003;100(25):15235–40.
108. Barbuti A, Robinson RB. Stem cell-derived nodal-like cardiomyocytes as a novel pharmacologic tool: insights from sinoatrial node development and function. Pharmacol. Rev. 2015;67(2):368–88.
109. Espinoza-Lewis RA, Yu L, He F, Liu H, Tang R, Shi J, et al. Shox2 is essential for the differentiation of cardiac pacemaker cells by repressing Nkx2-5. Dev Biol. 2009;327(2):376–85.
110. Hescheler J, Fleischmann BK, Lentini S, Maltsev VA, Rohwedel J, Wobus AM, et al. Embryonic stem cells: a model to study structural and functional properties in cardiomyogenesis. Cardiovasc Res. 1997;36(2):149–62.
111. Paige SL, Osugi T, Afanasiev OK, Pabon L, Reinecke H, Murry CE. Endogenous Wnt/beta-catenin signaling is required for cardiac

differentiation in human embryonic stem cells. PloS One. 2010;5(6):e11134.

112. Qu Y, Whitaker GM, Hove-Madsen L, Tibbits GF, Accili EA. Hyperpolarization-activated cyclic nucleotide-modulated 'HCN' channels confer regular and faster rhythmicity to beating mouse embryonic stem cells. J Physiol. 2008;586(3):701–16.
113. Barbuti A, Crespi A, Capilupo D, Mazzocchi D, Baruscotti M, DiFrancesco D. Molecular composition and functional properties of f-channels in murine embryonic stem cell-derived pacemaker cells. J Mol Cell Cardiol. 2009;46:343–51.
114. Scavone A, Capilupo D, Mazzocchi N, Crespi A, Zoia S, Campostrini G, et al. Embryonic stem cell-derived CD166+ precursors develop into fully functional sinoatrial-like cells. Circ Res. 2013;113(4):389–98.
115. Abi-Gerges N, Ji GJ, Lu ZJ, Fischmeister R, Hescheler J, Fleischmann BK. Functional expression and regulation of the hyperpolarization activated non-selective cation current in embryonic stem cell-derived cardiomyocytes. J Physiol. 2000;523(Pt 2):377–89.
116. Satin J, Kehat I, Caspi O, Huber I, Arbel G, Itzhaki I, et al. Mechanism of spontaneous excitability in human embryonic stem cell derived cardiomyocytes. J Physiol. 2004;559(Pt 2):479–96.
117. Sartiani L, Bettiol E, Stillitano F, Mugelli A, Cerbai E, Jaconi ME. Developmental changes in cardiomyocytes differentiated from human embryonic stem cells: a molecular and electrophysiological approach. Stem Cells. 2007;25(5):1136–44.
118. Zwi L, Caspi O, Arbel G, Huber I, Gepstein A, Park IH, et al. Cardiomyocyte differentiation of human induced pluripotent stem cells. Circulation. 2009;120(15):1513–23.
119. Mehta A, Chung YY, Ng A, Iskandar F, Atan S, Heming W, et al. Pharmacological response of human cardiomyocytes derived from viral-free induced pluripotent stem cells. Cardiovasc Res. 2011;91(4):577–86.
120. Lundy SD, Zhu WZ, Regnier M, Laflamme MA. Structural and functional maturation of cardiomyocytes derived from human pluripotent stem cells. Stem Cells Dev. 2013;22(14):1991–2002.
121. van den Heuvel NH, van Veen TA, Lim B, Jonsson MK. Lessons from the heart: mirroring electrophysiological characteristics during cardiac development to in vitro differentiation of stem cell derived cardiomyocytes. J Mol Cell Cardiol. 2014;67:12–25.
122. Protze SI, Liu J, Nussinovitch U, Ohana L, Backx PH, Gepstein L, et al. Sinoatrial node cardiomyocytes derived from human pluripotent cells function as a biological pacemaker. Nat Biotechnol. 2017;35(1):56–68.
123. Schweizer PA, Darche FF, Ullrich ND, Geschwill P, Greber B, Rivinius R, et al. Subtype-specific differentiation of cardiac pacemaker cell clusters from human induced pluripotent stem cells. Stem Cell Res. Ther. 2017;8(1):229.
124. Verkerk AO, Wilders R, van Borren MM, Peters RJ, Broekhuis E, Lam K, et al. Pacemaker current (I(f)) in the human sinoatrial node. Eur Heart J. 2007;28(20):2472–8.
125. Bosman A, Sartiani L, Spinelli V, Del Lungo M, Stillitano F, Nosi D, et al. Molecular and functional evidence of HCN4 and caveolin-3 interaction during cardiomyocyte differentiation from human embryonic stem cells. Stem Cells Dev. 2013;22(11):1717–27.
126. Ma J, Guo L, Fiene SJ, Anson BD, Thomson JA, Kamp TJ, et al. High purity human-induced pluripotent stem cell-derived cardiomyocytes: electrophysiological properties of action potentials and ionic currents. Am J Physiol Heart Circ Physiol. 2011;301(5):H2006–17.
127. Weisbrod D, Peretz A, Ziskind A, Menaker N, Oz S, Barad L, et al. SK4 Ca2+ activated K+ channel is a critical player in cardiac pacemaker derived from human embryonic stem cells. Proc Natl Acad Sci USA. 2013;110(18):E1685–94.
128. Benzoni P, Campostrini G, Landi S, Bertini V, Marchina E, Iascone M, et al. Human iPSC modelling of a familial form of atrial fibrillation reveals a gain of function of If and ICaL in patient-derived cardiomyocytes. Cardiovasc. Res. 2020;116(6):1147–60.
129. Giannetti F, Benzoni P, Campostrini G, Milanesi R, Bucchi A, Baruscotti M, et al. A detailed characterization of the hyperpolarization-activated "funny" current (I_f) in human-induced pluripotent stem cell (iPSC)–derived cardiomyocytes with pacemaker activity. Pflugers Arch - Eur J Physiol. 2021;473:1009–21. https://doi.org/10.1007/s00424-021-02571-w.
130. Kehat I, Khimovich L, Caspi O, Gepstein A, Shofti R, Arbel G, et al. Electromechanical integration of cardiomyocytes derived from human embryonic stem cells. Nat Biotechnol. 2004;22(10):1282–9.
131. Bogaert V, Goethals M. Pharmacological influence of specific bradycardic agents on the pacemaker current of sheep cardiac Purkinje fibres. A comparison between three different molecules. Eur Heart J. 1987;8(Suppl L):35–42.
132. DiFrancesco D. Some properties of the UL-FS 49 block of the hyperpolarization-activated current (i(f)) in sino-atrial node myocytes. Pflugers Arch. 1994;427(1-2):64–70.
133. DiFrancesco D, Camm JA. Heart rate lowering by specific and selective I(f) current inhibition with ivabradine: a new therapeutic perspective in cardiovascular disease. Drugs. 2004;64(16):1757–65.
134. Thollon C, Cambarrat C, Vian J, Prost JF, Peglion JL, Vilaine JP. Electrophysiological effects of S 16257, a novel sino-atrial node modulator, on rabbit and

guinea-pig cardiac preparations: comparison with UL-FS 49. Br J Pharmacol. 1994;112(1):37–42.

135. Bois P, Bescond J, Renaudon B, Lenfant J. Mode of action of bradycardic agent, S 16257, on ionic currents of rabbit sinoatrial node cells. Br J Pharmacol. 1996;118(4):1051–7.
136. Bucchi A, Baruscotti M, DiFrancesco D. Current-dependent block of rabbit sino-atrial node I (f) channels by ivabradine. J Gen Physiol. 2002;120 (1):1–13.
137. Bucchi A, Baruscotti M, Robinson RB, DiFrancesco D. I(f)-dependent modulation of pacemaker rate mediated by cAMP in the presence of ryanodine in rabbit sino-atrial node cells. J Mol Cell Cardiol. 2003;35(8):905–13.
138. Borer JS, Heuzey JY. Characterization of the heart rate-lowering action of ivabradine, a selective I (f) current inhibitor. Am J Ther. 2008;15(5):461–73.
139. Lopez-Bescos L, Filipova S, Martos R. Long-term safety and efficacy of ivabradine in patients with chronic stable angina. Cardiology. 2007;108(4): 387–96.
140. Ragueneau I, Laveille C, Jochemsen R, Resplandy G, Funck-Brentano C, Jaillon P. Pharmacokinetic-pharmacodynamic modeling of the effects of ivabradine, a direct sinus node inhibitor, on heart rate in healthy volunteers. Clin Pharmacol Ther. 1998;64(2):192–203.
141. Cervetto L, Demontis GC, Gargini C. Cellular mechanisms underlying the pharmacological induction of phosphenes. Br J Pharmacol. 2007;150(4): 383–90.
142. Demontis GC, Gargini C, Paoli TG, Cervetto L. Selective Hcn1 channels inhibition by ivabradine in mouse rod photoreceptors. Invest Ophthalmol Vis Sci. 2009;50(4):1948–55.
143. Bucchi A, Tognati A, Milanesi R, Baruscotti M, DiFrancesco D. Properties of ivabradine-induced block of HCN1 and HCN4 pacemaker channels. J Physiol. 2006;572(Pt 2):335–46.
144. Cheng L, Kinard K, Rajamani R, Sanguinetti MC. Molecular mapping of the binding site for a blocker of hyperpolarization-activated, cyclic nucleotide-modulated pacemaker channels. J Pharmacol Exp Ther. 2007;322(3):931–9.
145. Bucchi A, Baruscotti M, Nardini M, Barbuti A, Micheloni S, Bolognesi M, et al. Identification of the molecular site of ivabradine binding to HCN4 channels. PloS One. 2013;8(1):e53132.
146. Cerbai E, Mugelli A. I(f) in non-pacemaker cells: role and pharmacological implications. Pharmacol Res. 2006;53(5):416–23.
147. Jiang YQ, Sun Q, Tu HY, Wan Y. Characteristics of HCN channels and their participation in neuropathic pain. Neurochem Res. 2008;33(10):1979–89.
148. Reid CA, Berkovic SF, Petrou S. Mechanisms of human inherited epilepsies. Prog Neurobiol. 2009;87(1):41–57.
149. Novella Romanelli M, Sartiani L, Masi A, Mannaioni G, Manetti D, Mugelli A, et al. HCN channels modulators: the need for selectivity. Curr Top Med Chem. 2016;16(16):1764–91.
150. Del Lungo M, Melchiorre M, Guandalini L, Sartiani L, Mugelli A, Koncz I, et al. Novel blockers of hyperpolarization-activated current with isoform selectivity in recombinant cells and native tissue. Br J Pharmacol. 2012;166(2):602–16.
151. Resta F, Micheli L, Laurino A, Spinelli V, Mello T, Sartiani L, et al. Selective HCN1 block as a strategy to control oxaliplatin-induced neuropathy. Neuropharmacology. 2018;131:403–13.
152. McClure KJ, Maher M, Wu N, Chaplan SR, Eckert WA 3rd, Lee DH, et al. Discovery of a novel series of selective HCN1 blockers. Bioorg Med Chem Lett. 2011;21(18):5197–201.
153. Baker K, Warren KS, Yellen G, Fishman MC. Defective "pacemaker" current (Ih) in a zebrafish mutant with a slow heart rate. Proc Natl Acad Sci USA. 1997;94(9):4554–9.
154. Herrmann S, Stieber J, Stockl G, Hofmann F, Ludwig A. HCN4 provides a 'depolarization reserve' and is not required for heart rate acceleration in mice. EMBO J. 2007;26(21):4423–32.
155. Hoesl E, Stieber J, Herrmann S, Feil S, Tybl E, Hofmann F, et al. Tamoxifen-inducible gene deletion in the cardiac conduction system. J Mol Cell Cardiol. 2008;45(1):62–9.
156. Macri V, Mahida SN, Zhang ML, Sinner MF, Dolmatova EV, Tucker NR, et al. A novel trafficking-defective HCN4 mutation is associated with early-onset atrial fibrillation. Heart Rhythm. 2014;11(6):1055–62.
157. Moller M, Silbernagel N, Wrobel E, Stallmayer B, Amedonu E, Rinne S, et al. In vitro analyses of novel HCN4 gene mutations. Cell Physiol Biochem. 2018;49(3):1197–207.
158. Milano A, Vermeer AM, Lodder EM, Barc J, Verkerk AO, Postma AV, et al. HCN4 mutations in multiple families with bradycardia and left ventricular noncompaction cardiomyopathy. J Am Coll Cardiol. 2014;64(8):745–56.
159. Nof E, Luria D, Brass D, Marek D, Lahat H, Reznik-Wolf H, et al. Point mutation in the HCN4 cardiac ion channel pore affecting synthesis, trafficking, and functional expression is associated with familial asymptomatic sinus bradycardia. Circulation. 2007;116(5):463–70.
160. Schweizer PA, Schroter J, Greiner S, Haas J, Yampolsky P, Mereles D, et al. The symptom complex of familial sinus node dysfunction and myocardial noncompaction is associated with mutations in the HCN4 channel. J Am Coll Cardiol. 2014;64(8):757–67.
161. Laish-Farkash A, Glikson M, Brass D, Marek-Yagel-D, Pras E, Dascal N, et al. A novel mutation in the HCN4 gene causes symptomatic sinus bradycardia in

Moroccan Jews. J Cardiovasc Electrophysiol. 2010;21(12):1365–72.

162. Baruscotti M, Bucchi A, Milanesi R, Paina M, Barbuti A, Gnecchi-Ruscone T, et al. A gain-of-function mutation in the cardiac pacemaker HCN4 channel increasing cAMP sensitivity is associated with familial inappropriate sinus tachycardia. Eur Heart J. 2017;38(4):280–8.
163. Duhme N, Schweizer PA, Thomas D, Becker R, Schroter J, Barends TR, et al. Altered HCN4 channel C-linker interaction is associated with familial tachycardia-bradycardia syndrome and atrial fibrillation. Eur Heart J. 2013;34(35):2768–75.
164. Ueda K, Nakamura K, Hayashi T, Inagaki N, Takahashi M, Arimura T, et al. Functional characterization of a trafficking-defective HCN4 mutation, D553N, associated with cardiac arrhythmia. J Biol Chem. 2004;279(26):27194–8.
165. Schulze-Bahr E, Neu A, Friederich P, Kaupp UB, Breithardt G, Pongs O, et al. Pacemaker channel dysfunction in a patient with sinus node disease. J Clin Invest. 2003;111(10):1537–45.
166. Milanesi R, Baruscotti M, Gnecchi-Ruscone T, DiFrancesco D. Familial sinus bradycardia associated with a mutation in the cardiac pacemaker channel. N Engl J Med. 2006;354(2):151–7.
167. Schweizer PA, Duhme N, Thomas D, Becker R, Zehelein J, Draguhn A, et al. cAMP sensitivity of HCN pacemaker channels determines basal heart rate but is not critical for autonomic rate control. Circ Arrhythm Electrophysiol. 2010;3(5):542–52.
168. Weigl I, Geschwill P, Reiss M, Bruehl C, Draguhn A, Koenen M, et al. The C-terminal HCN4 variant P883R alters channel properties and acts as genetic modifier of atrial fibrillation and structural heart disease. Biochem Biophys Res Commun. 2019;519(1): 141–7.
169. Zhou J, Ding WG, Makiyama T, Miyamoto A, Matsumoto Y, Kimura H, et al. A novel HCN4 mutation, G1097W, is associated with atrioventricular block. Circ J. 2014;78(4):938–42.
170. Rosen MR, Brink PR, Cohen IS, Robinson RB. Cardiac pacing: from biological to electronic ... to biological? Circ Arrhythm Electrophysiol. 2008;1 (1):54–61.
171. Cingolani E, Goldhaber JI, Marban E. Next-generation pacemakers: from small devices to biological pacemakers. Nat Rev Cardiol. 2018;15 (3):139–50.
172. Cai J, Yi FF, Li YH, Yang XC, Song J, Jiang XJ, et al. Adenoviral gene transfer of HCN4 creates a genetic pacemaker in pigs with complete atrioventricular block. Life Sci. 2007;80(19):1746–53.
173. Plotnikov AN, Shlapakova I, Szabolcs MJ, Danilo P Jr, Lorell BH, Potapova IA, et al. Xenografted adult human mesenchymal stem cells provide a platform for sustained biological pacemaker function in canine heart. Circulation. 2007;116(7):706–13.
174. Cho HC, Kashiwakura Y, Marban E. Creation of a biological pacemaker by cell fusion. Circ Res. 2007;100(8):1112–5.
175. Hoogaars WM, Engel A, Brons JF, Verkerk AO, de Lange FJ, Wong LY, et al. Tbx3 controls the sinoatrial node gene program and imposes pacemaker function on the atria. Genes Dev. 2007;21(9): 1098–112.
176. Bakker ML, Boink GJ, Boukens BJ, Verkerk AO, van den Boogaard M, den Haan AD, et al. T-box transcription factor TBX3 reprogrammes mature cardiac myocytes into pacemaker-like cells. Cardiovasc Res. 2012;94(3):439–49.
177. Kapoor N, Liang W, Marban E, Cho HC. Direct conversion of quiescent cardiomyocytes to pacemaker cells by expression of Tbx18. Nat Biotechnol. 2013;31(1):54–62.
178. Rosen MR, Brink PR, Cohen IS, Robinson RB. The utility of mesenchymal stem cells as biological pacemakers. Congest Heart Fail. 2008;14(3):153–6.
179. Yang XJ, Zhou YF, Li HX, Han LH. Jiang WP Mesenchymal stem cells as a gene delivery system to create biological pacemaker cells in vitro. J Int Med Res. 2008;36(5):1049–55.
180. Yanagi K, Takano M, Narazaki G, Uosaki H, Hoshino T, Ishii T, et al. Hyperpolarization-activated cyclic nucleotide-gated channels and T-type calcium channels confer automaticity of embryonic stem cell-derived cardiomyocytes. Stem Cells. 2007;25(11): 2712–9.
181. Xue T, Cho HC, Akar FG, Tsang SY, Jones SP, Marban E, et al. Functional integration of electrically active cardiac derivatives from genetically engineered human embryonic stem cells with quiescent recipient ventricular cardiomyocytes: insights into the development of cell-based pacemakers. Circulation. 2005;111(1):11–20.
182. Chauveau S, Anyukhovsky EP, Ben-Ari M, Naor S, Jiang YP, Danilo P Jr, et al. Induced pluripotent stem cell-derived cardiomyocytes provide in vivo biological pacemaker function. Circ Arrhyth Electrophysiol. 2017;10(5):e004508.
183. DiFrancesco D. Considerations on the size of currents required for pacemaking. J Mol Cell Cardiol. 2009;48 (4):802–3.
184. Maltsev VA, Lakatta EG. Funny current provides a relatively modest contribution to spontaneous beating rate regulation of human and rabbit sinoatrial node cells. J Mol Cell Cardiol. 2010;48(4):804–6.
185. Verkerk AO, Wilders R. Relative importance of funny current in human versus rabbit sinoatrial node. J Mol Cell Cardiol. 2010;48(4):799–801.

5

Cardiac Pacemaking Is an Emergent Property of Complex Synchronized Signaling on Multiple Scales

Oliver Monfredi, David Kim, Victor A. Maltsev,
and Edward G. Lakatta

Abstract

The generation of automaticity in the sinoatrial node is a multiscale process involving the integration of complex biochemical and biophysical processes, including a membrane clock and a calcium clock operating in a coupled-clock system within single cells and further complex integration of heterogeneous intercellular signaling at the tissue level. Our current understanding of these processes is reviewed in detail. Ground-breaking recent studies in intact SAN have discovered a new paradigm of SAN operation, and this, along with other frontiers in pacemaker research, are addressed.

Keywords

Pacemaking · Calcium · Ion channels · Synchronization · Ignition · Automaticity · Autonomic · Emergence

5.1 Introduction

Intrinsic cardiac automaticity, or "pacemaking," is the fundamental physiological process that sustains zoological life on Earth. The absence of cardiac automaticity is not compatible with life, save for in very few medically supported circumstances (e.g. cardiopulmonary bypass, ventricular assist devices, ECMO). Substantial increases in our understanding of cardiac automaticity have been made over the last century [1], yet significant uncertainties remain, and paradigms continue to shift [2]. Pacemaker cells that lead cardiac automaticity are located in the sinoatrial node (SAN) of the right atrium and spontaneously generate rhythmic changes of their membrane potential, producing relatively periodic (but not metronomic) spontaneous action potential (APs), so-called "sinus rhythm." The essence of cardiac automaticity is diastolic depolarization (DD)—a slow, spontaneous increase in membrane potential toward the membrane excitation threshold, followed by the firing of an all-or-nothing AP.

The initial focus of pacemaker cell research was on sarcolemmal ion currents (review [3]). In

O. Monfredi
Laboratory of Cardiovascular Science, NIA (IRP), NIH, Baltimore, MD, USA

University of Virginia Medical Center, Charlottesville, VA, USA
e-mail: ojm9w@virginia.edu

D. Kim
University of Virginia Medical Center, Charlottesville, VA, USA
e-mail: dk3am@hscmail.mcc.virginia.edu

V. A. Maltsev · E. G. Lakatta (✉)
Laboratory of Cardiovascular Science, NIA (IRP), NIH, Baltimore, MD, USA
e-mail: maltsevvi@mail.nih.gov; LakattaE@grc.nia.nih.gov

© Springer Nature Switzerland AG 2023

O. N. Tripathi et al. (eds.), *Heart Rate and Rhythm*, https://doi.org/10.1007/978-3-031-33588-4_5

silico reconstruction of the ensemble behavior of these currents based on experimental voltage-clamp data is able to generate spontaneous APs, and ultimately the coordinated behavior of these ion channels leading to SAN cell automaticity was dubbed the "membrane clock" (M-clock).

It was with some difficulty that the important role of intracellular Ca cycling in normal automaticity was added to the paradigm. The SAN cell's major intracellular store of Ca is the sarcoplasmic reticulum (SR), which was discovered to generate roughly periodic diastolic Ca releases, dubbed the "Ca clock" (review [4]), whether the cell membrane was present or not. This latterly elucidated clock can impact the M-clock at many "nodes" of interaction between the two, perhaps most importantly through the acceleration of DD via the electrogenic membrane-bound Na/Ca exchanger (NCX) [5, 6]. Further studies suggested that the Ca clock depends on the membrane clock and vice versa, and the functions of both clocks are tightly and synergistically integrated to formulate a coupled oscillator, leading to the coupled-clock theory of normal automaticity [7, 8]. Having coupled clocks ensures both robustness (i.e., "fail safe" operation) and flexibility (i.e., the ability to react to demands for faster or slower AP firing rate) in SAN cells. The coupled-clock paradigm has been intricately numerically modeled [7, 9–11] and extensively reviewed [1, 8, 12]. In this chapter, we review key and novel aspects of this concept. Of particular interest will be challenging the present perspective that SAN output is generated by the collective behavior of loosely coupled SAN cells and is not dominated by the DD of a single cell. Further, the interactive network of mechanisms intrinsic and extrinsic to SAN cells must also interpret and react to signals arising extrinsic to the cell, e.g., stretch, electrotonic impulses, or neurotransmitter or hormonal stimulation of surface membrane receptors. This must result from the timely integration of signaling events at multiple levels within the SAN, including subcellular, cellular (surface membrane), and tissue architecture. This is presently poorly understood, yet extremely important, and represents the current and future frontier of cardiac pacemaker research [13–15].

5.2 The Membrane Clock

Every pacemaker cycle involves the interaction of Ca and membrane clocks via multiple time-, voltage-, and Ca-dependencies of proteins comprising the system. The membrane clock (Fig. 5.1, top) features ion channels, transporters, and pumps. Its key molecules include L-type Ca channels (LCCh) and T-type Ca channels (generating I_{CaL} and I_{CaT}, respectively); K channels; nonselective hyperpolarization-activated cation channels (HCN4), generating I_{f}; and NCX, generating I_{NCX}. NCX is electrogenic—it exchanges 3Na for 1Ca, thereby generating a membrane current, and this operation is both Ca- and voltage-dependent, executing an efficient coupling mechanism between the clocks.

5.3 The Calcium Clock

The Ca clock (Fig. 5.1, bottom) features the SR refilling Ca pump SERCA, and Ca release channels, ryanodine receptors (RyRs), the latter of which generate rhythmic, diastolic local Ca releases (LCRs). LCRs first appear as small Ca spark-like events early in DD, around the time of the maximum diastolic potential (MDP). As membrane depolarization proceeds, LCRs increase in size and develop local propagation attributes (abrupted waves). In late DD, these propagating LCRs merge into the AP-induced whole-cell Ca transient [16]. The LCR period is the period from the peak of the prior AP-induced cytosolic Ca transient and subsequent diastolic LCR emergence. LCR periods inform not only on the RyR activation but also on the kinetics of recharging the SR Ca capacitor [17].

5.4 Clock Coupling During Diastolic Depolarization

Each spontaneous AP is followed by repolarization and the re-establishment of an MDP, from which DD begins due to the removal of K channel

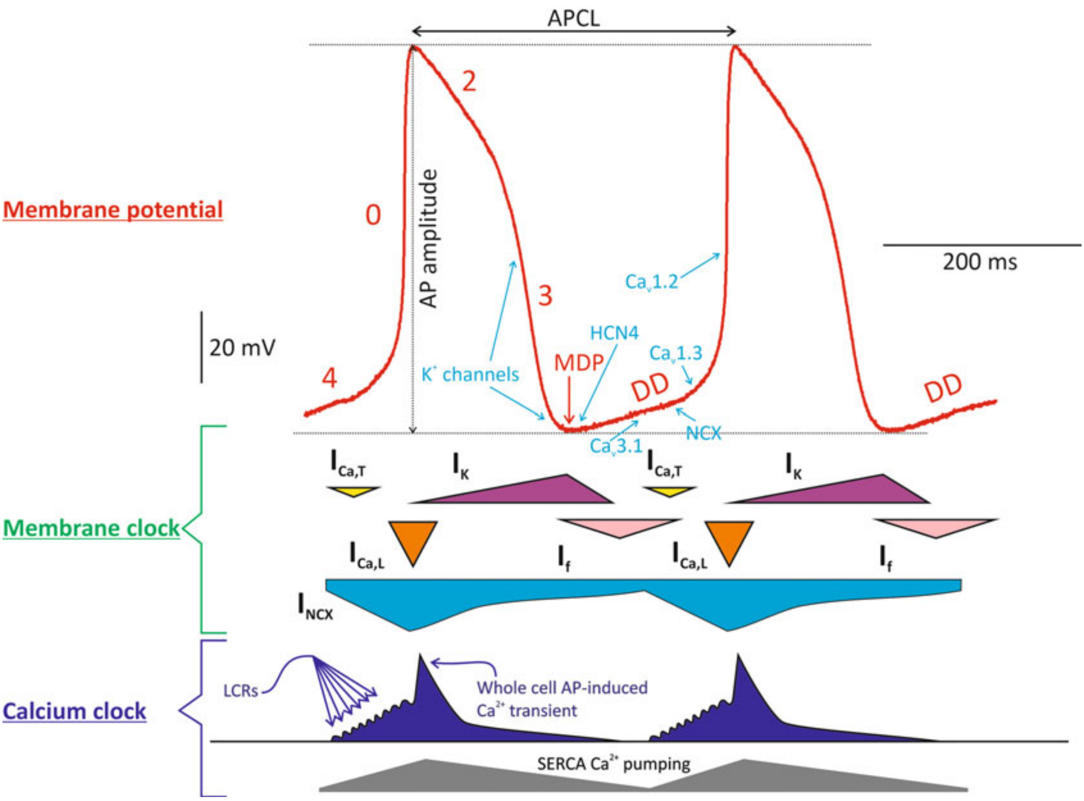
APCL
Membrane potential
0
2
3
4
AP amplitude
20 mV
200 ms
K+ channels
MDP
HCN4
Cav1.2
Cav1.3
Cav3.1
NCX
DD
DD
Membrane clock
ICa,T
IK
ICa,L
If
INCX
Calcium clock
LCRs
Whole cell AP-induced Ca2+ transient
SERCA Ca2+ pumping

Fig. 5.1 The biophysical “engine” of the coupled-clock system

activation, activation of I_f and I_{CaT}, and spontaneous local RyR activation generating multiple submembrane LCRs. Summation of individual LCRs promoted in part by Ca-induced-Ca-release (CICR) [18, 19] produces an ensemble Ca signal that activates electrogenic inward I_{NCX}. Blooming of the LCR ensemble Ca signal, with associated accelerating I_{NCX} activation, initiates an acceleration in DD to the so-called nonlinear phase [20], activating I_{CaL}. The time from MDP to the nonlinear DD informs on the kinetics of LCR generation and synchronization. I_f decreases during late DD as it gets closer to its reversal potential (near –30 mV).

The relative importance of events in early DD continues to be debated. Some believe that LCRs are the key events that initiate APs, based on several fundamental observations, including (1) spontaneous LCRs occur under voltage clamp [21], independent of membrane potential change, (2) LCRs occur as early as AP repolarization reaches the MDP [16], and (3) oscillatory LCRs are observed in membrane-free (i.e., detergent-permeabilized, “skinned”) SAN cells bathed in a physiological [Ca] of 100 nM [21, 22]. These membrane-independent LCRs are generated at rates of 1–5 Hz, i.e., similar to the rates of spontaneous AP firing in SAN cells (in rabbits).

Others favor the importance of low voltage-activated Ca currents, such as I_{CaT} [23] and I_{CaL} generated by Cav1.3 channels ($I_{Cav1.3}$) [24] as primary AP-initiating events. Loss of Cav1.3 function in humans is associated with bradycardia and congenital deafness [25], and Cav1.3 knockout mice have substantially reduced SAN cell Ca dynamics [26].

5.4.1 The Concept of Ignition

A unifying view of the AP ignition process [27] suggests that pacemaker APs are ignited during DD via a feed-forward mechanism that includes membrane potential, LCRs, NCX, I_{CaT}, and I_{CaL}. This ignition phase begins when the magnitude of inward I_{NCX} begins to increase due to its activation by LCRs. I_{NCX}, together with I_{f} and I_{CaT} depolarizes the membrane potential to the $I_{\mathrm{Cav1.3}}$ activation threshold (near –55 mV). During the ignition phase, $I_{\mathrm{Cav1.3}}$ depolarizes cell membrane, and concurrently its mediated Ca influx generates more LCRs via CICR that further activates inward I_{NCX}, implementing a feed-forward control that drives membrane potential to the threshold potential of –40 mV required for activation of I_{CaL} via Cav1.2 channels ($I_{\mathrm{Cav1.2}}$) that generates the AP upstroke.

Because Ca and membrane mechanisms are so tightly linked within the coupled-clock system, perturbations in either clock inevitably affect the other to some degree and together affect the ultimate readout of the coupled system, which is the AP firing rate. LCR period and AP cycle length (APCL) are similarly affected by either selective perturbation of the membrane clock (inhibition of I_{f} by ivabradine) or Ca clock (inhibition of SERCA by cyclopiazonic acid) [28], indicating that the LCR period reports the crosstalk between the clocks. In the case of ivabradine-induced bradycardia, the initial effect on membrane clock funny channels reduces the rate of I_{CaL} activation and respective Ca influx and SR Ca loading. Within the novel concept of AP ignition, whereby LCRs interact with NCX and I_{CaL}, this important result can be re-cast in terms of a “time-to-ignition” phase (when I_{NCX} becomes activated by LCRs), determined by coupled-clock interactions, playing a key role in determining cycle length.

Robustness is rigidly built into AP ignition, as one might expect of such a physiologically critical process—genetically modified mice with knock-down of as much as 80% of NCX molecules have normal resting heart rates [29]. This is not evidence of a lack of importance of NCX; instead, numerical modeling of the coupled-clock system revealed that having as few as 20% NCX molecules is sufficient to keep diastolic I_{NCX} amplitude almost unchanged and the ignition mechanism remaining intact [30]. This is thought to be because, under normal function, LCRs occur only in a small part of the cell, leaving a substantial portion of NCX molecules not yet activated by the LCRs. Those NCX molecules in the LCR-free areas represent a substantial depolarization reserve. NCX-deficient cells exhibit a compensatory increase in the spatial extent of the LCR ensemble to activate almost all remaining NCX molecules. However, such baseline compensation comes at a cost: nearly 100% NCX activation at rest leaves no reserve to support a further I_{NCX} increase, hence no ability to increase the AP firing rate in the fight-or-flight reflex [29].

5.5 The AP Upstroke, Plateau, and Repolarization

The AP upstroke relies on the availability of LCCh (Cav1.2 type). More available channels to respond to a membrane voltage change lead to a greater rate of increase (dV/dt) of the AP upstroke. The resultant Ca influx via activated I_{CaL} partially binds to SR-based RyRs and synchronizes their activation via CICR, resulting in synchronous RyR Ca release to generate the whole cell-engulfing AP-induced Ca transient [31, 32]. This partially depletes Ca in the SR. LCCh also begins to inactivate with time at the depolarized membrane potential. The Ca transient (intracellularly derived Ca) and Ca influx via LCCh (extracellularly derived Ca) activates SERCA2 to pump cytoplasmic Ca into the SR, with the rapid (Ca-dependent) kinetics of this process facilitating efficient and timely replenishment of the Ca store.

Membrane depolarization activates K channels and inactivates forward mode NCX, leading to AP repolarization, whose kinetics inform on the combined actions of K channels, cytosolic [Ca], I_{NCX}, and I_f. K channel activation repolarizes the surface membrane, reactivating forward Na-Ca exchange, which assists in removing the Ca released via the AP-induced Ca release via RyRs. This same Ca also activates repolarizing K channels [33].

Membrane ion channels and transporters regulate the Ca balance of the coupled system not only directly (Ca influx/efflux via LCCh/NCX) but also indirectly, via I_K activation, which repolarizes the membrane and, in doing so, limits Ca influx via LCCh while simultaneously increasing Ca efflux via voltage-dependent activation of forward mode NCX. Even I_f activation indirectly regulates the cell Ca balance by limiting the MDP, thereby limiting voltage-dependent Ca efflux via NCX.

5.6 Intracellular Na Is an Important Modulator of Clock Coupling

The critical role of NCX within the coupled-clock system would naturally suggest a key regulating role for intracellular Na. In SAN cells perturbed by digitonin (blocker of Na/K ATPase, causing intracellular Na accumulation) [34], increases in $[Na]_i$ and $[Ca]_i$ and respective reductions in E_{Na} and E_{Ca} lead to a small reduction in MDP, enhanced LCRs, increased diastolic I_{NCX} and reduced average APCL. As $[Na]_i$ and $[Ca]_i$ continue to increase, MDP, E_{Na}, and E_{Ca} are further reduced; LCR signal becomes reduced, diastolic I_{NCX} decreases, and APCL progressively prolongs, accompanied by increased APCL variability. Numerical modeling reveals that increased $[Na]_i$ causes E_{Na} and E_{Ca} to reduce monotonically and decrease important ionic currents (I_{CaL}, I_{CaT}, I_f, I_{Kr}, and I_{bNa}). Digitonin's ability via a monotonic Na increase to initially increase rate and rhythmicity, followed by a decrease in rate and rhythmicity, followed ultimately by frank arrhythmia, is clear evidence of the fundamental role played by intracellular Na and Ca in the genesis and maintenance of normal heart rhythm (see Fig. 3 in [34]).

5.7 Diastolic Depolarization May Be Regarded as a Phase of Transition

While the membrane clock operates as a limit cycle oscillator, the Ca-clock operates by a completely different mechanism called "criticality" [15]. Ca release channels—RyRs—are organized into and operate in clusters, known as Ca release units in all cardiac cells, including in SAN cells [19]. In vitro experiments and numerical modeling have demonstrated that LCRs emerge via self-organized synchronized activation of Ca release units (driven by explosive CICR), leading to oscillatory, phase-like transitions in SAN cells [18], reinforced in more recent theoretical studies [35, 36] that demonstrate phase transitions (including order-disorder transitions), pointing to the fractal-like functional and structural (hierarchical) organization of RyRs in SAN cells (i.e., within and among Ca release units).

Based on the results of these modeling experiments and the importance of Na (described above), the ignition theory and local interactions during DD can now be viewed in terms of phase transition, criticality, and electrochemical gradient oscillations. As already noted, LCRs begin to occur around the time of the MDP [16], sometimes before. Such early release events are small and stochastic (i.e., disordered), akin to Ca sparks in resting ventricular myocytes. The ensuing simultaneous growth of the diastolic ensemble LCR signal and DD during AP ignition can be viewed as self-organization of the LCRs, interacting with an excitable cell membrane that reaches criticality in late diastole, followed by a phase transition manifest as the rapid AP upstroke that triggers a global systolic Ca transient.

5.8 Emerging Players in the Coupled-Clock System

Several new and relatively unclear mechanisms are increasingly believed to be important in the genesis and maintenance of SAN automaticity.

Store-operated Ca entry (SOCE) via *store-operated Ca channels* may represent an additional pathway for Ca entry into the SR upon Ca store depletion. Murine SAN experiments suggested that store-operated activity was attributable to TRPC expression and that store-operated Ca channels may be involved in regulating pacemaker firing rate [37]. More recently [38], two new proteins, stromal interacting molecule (STIM) (an endoplasmic reticulum Ca sensor) and Orai (surface membrane channel) were implicated in SOCE in pacemaker cells; after store depletion, STIM1 redistributed to the cell periphery and co-localized with surface membrane-linked Orai1, suggesting the involvement of these proteins in SOCE activity and cardiac pacemaker function. The TRPC3 channel is also involved in the SOCE mechanism, and TRPC3(–/–) mice experience sinoatrial arrhythmias [39].

The *inositol 1,4,5-trisphosphate receptor* (IP3R) represents a second mechanism of Ca release from the SR and contributes to the automaticity of SAN cells: pharmacological perturbation of these channels affected automaticity in wild-type mice, but not in transgenic IP3R2 knockout mice [40]. Furthermore, stimulation of IP3Rs accelerates spontaneous beating rate in isolated mouse SAN cells, while inhibition slows the rate [41], and in mice with uncoupled clocks (i.e., in atria-specific NCX knockout mice), IP3R agonists and antagonists modulated the rate of spontaneous Ca waves, suggesting that IP3R-mediated SAN pacemaker regulation is controlled primarily by the Ca clock rather than the membrane clock [41].

SK4 *Ca-activated K channels* generate $I_{K(Ca)}$—inhibition of this current in spontaneously beating human embryonic stem cells depolarized the MDP and suppressed automaticity [42]. All three SK isoforms (SK1, SK2, and SK3) have since been identified in mouse SAN [33]. Inhibition of SK channels with apamin (i) prolonged APs in isolated SAN cells, (ii) slowed diastolic depolarization, and (iii) reduced pacemaker rate in isolated SAN cells and intact SAN tissue. It is proposed that these channels modulate pacemaking via activating a repolarizing Ca-activated current. Intraperitoneal injection of SK4 channel blockers greatly reduced the arrhythmias in CASQ2-D307H knock-in mice and CASQ2 knockout mice at rest and during exercise, demonstrating a role of SK4 channels in adult pacemaker function and suggesting that these channels may be therapeutic targets for the treatment of certain cardiac arrhythmias [43].

5.9 Biochemical Characteristics of the Coupled-Clock System

5.9.1 Enhanced Basal Levels of cAMP and Protein Phosphorylation by PKA and CaMKII Drive SAN Automaticity

Uniquely among cardiac cells, SAN cells express neuronal, Ca-activated adenylate cyclase (AC) types AC1 and AC8 [44, 45]. Under baseline conditions, SAN Ca binds to calmodulin to activate these ACs, leading to a high basal level of cAMP-mediated, protein kinase A (PKA)-dependent phosphorylation of coupled-clock proteins [22, 45, 46].

The critical functional importance of these Ca-dependent ACs has been validated in studies of genetically modified cells and animals. In vivo adenoviral implantation and expression of AC1 into the left bundle branch of dogs with heart block results in highly efficient heart automaticity emanating from the implant site [47]. Along similar lines, drug-induced activation of the AC8 gene substantially increases rate and improves rhythmicity in cardiac pacemaker-like cells differentiated from the genetically modified P19 cell line [48]. Recent studies [49] have also shown that increased cAMP production in mice with heart-targeted expression of AC8 (TG^{AC8}) is accompanied by a marked increase in heart rate with a concurrent reduction in heart rate variability (discussed below), regardless of autonomic innervation.

The challenge of directly measuring PKA activity in SAN cells was eventually met in cultured rabbit SAN cells infected with an adenovirus expressing the FRET sensor AKAR3

[50]. Here, the kinetics and stoichiometry of increased PKA activity matched the increase in AP firing rate in response to β-adrenergic receptor (β-AR) stimulation or phosphodiesterase inhibition. Associated numerical modeling predicted that phospholamban phosphorylation is a potent PKA target to stimulate positive chronotropism.

Phosphorylation of coupled-clock proteins is also achieved via Ca/calmodulin-dependent protein kinase II (CaMKII) [51, 52], which (like AC and LCRs) is highly localized beneath the surface membrane [53]. Mice genetically lacking CaMKII fail to mount a fight-or-flight SAN response [54]. However, experiments in isolated SAN cells subsequently showed twofold greater basal levels of activated (autophosphorylated) CaMKII in SAN cells compared to ventricular myocytes; this high basal CaMKII activation modifies the phosphorylation state of phospholamban, RyR, LCCh (and likely others), affecting LCR period and other LCR characteristics, and ultimately regulates both normal and reserve cardiac pacemaker function [51].

5.9.2 Pumping the Brakes: Mechanisms Intrinsic to the Coupled-Clock System That Restrain Its Basal AP Firing Rate

The coupled-clock system would be perpetually self-amplifying until maximal function was reached (i.e., Ca release begets more Ca release via PKA and CaMKII pathways (Fig. 5.2, green arrows)) were it not for continuous and concurrent mechanisms functioning to drive down SAN cAMP level and phosphorylation levels (Fig. 5.2, red arrows). High basal phosphodiesterase (PDE) activity is one such restraining mechanism [55]. The cAMP-degrading PDE1, PDE3, and PDE4 represent major PDE activities in rabbit SAN cells, with several specific targets (LCCh and phospholamban) being regulated by basal concurrent PDE3 + PDE4 activation [56]. Basal cardiac pacemaker function regulated by concurrent PDE3+PDE4 activation operates in a synergistic manner via a decrease in cAMP/PKA phosphorylation, suppression of LCR activity, and prolongation of the LCR period and APCL [57]. High basal phosphoprotein phosphatase activity also operates in SAN cells [58] to limit PKA and CaMKII-dependent phosphorylation. Other restraining mechanisms include the limitation of Ca influx and cell Ca load by calmodulin-mediated LCCh inactivation.

The net result of these restraining mechanisms is that the cAMP production, protein phosphorylation, basal LCR period, and APCL are maintained near the midpoint of their functional ranges. Compare this with ventricular myocytes, where the basal phosphorylation of Ca-cycling proteins is low to prevent undesirable and potentially arrhythmogenic Ca waves. Forced phosphorylation of SR Ca-cycling proteins in a physiologic Ca milieu unleashes a high-power, rhythmic Ca clock in ventricular myocytes generating LCRs and spontaneous APs, generating a SAN cell phenotype from the ventricular myocyte [60]. These results demonstrated that all cardiomyocytes have the potential for automaticity in the right circumstances but that normal cardiac function relies on suppression of this phenotype in the working myocytes of the atria and ventricles.

5.10 Coupling Biochemical and Biophysical Aspects of the System Yields Functional Flexibility

5.10.1 High Basal Levels of cAMP and Phosphorylation Translate into Powerful LCR Signals

The biochemical and biophysical aspects of the coupled-clock system are tightly linked—spontaneous LCRs are more likely to occur in response to a higher SR Ca load, which is determined by the Ca available for pumping into the SR and the phosphorylation status of the Ca-cycling proteins,

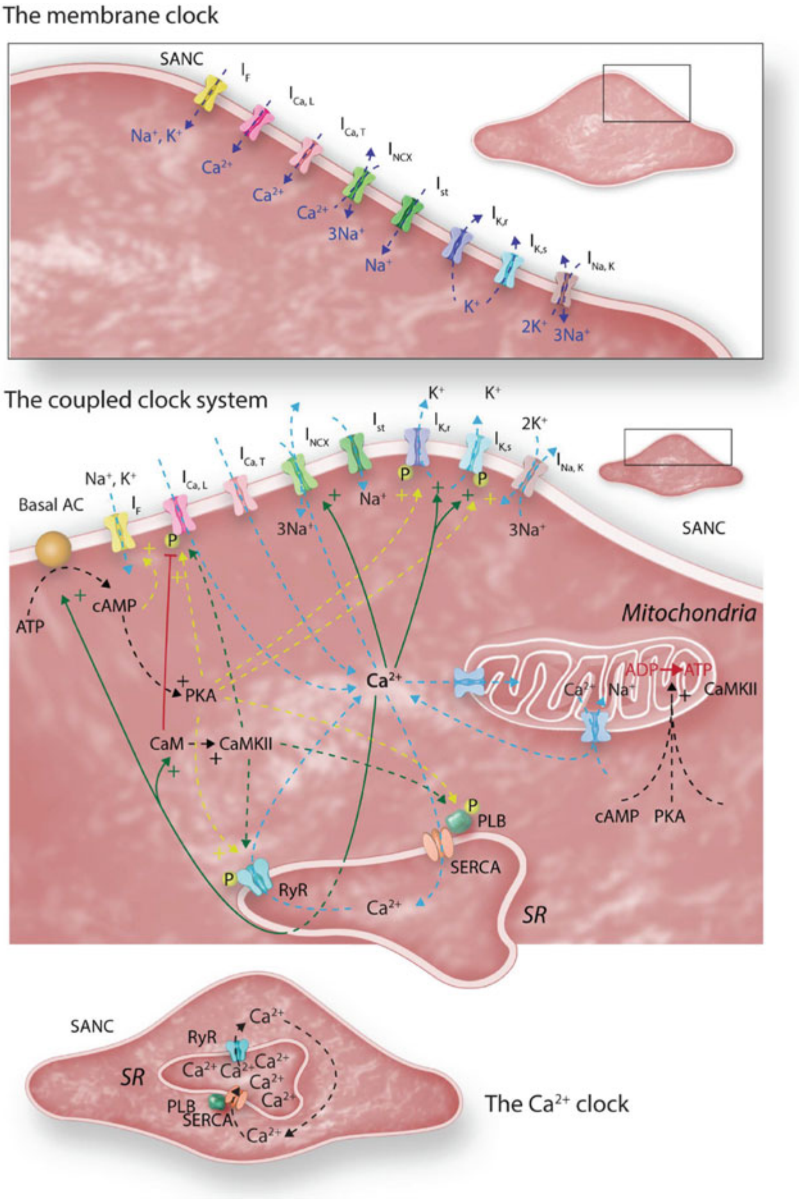
The membrane clock
SANC
I_f
$I_{Ca,L}$
$I_{Ca,T}$
I_{NCX}
I_{st}
$I_{K,r}$
$I_{K,s}$
$I_{Na,K}$
Na⁺, K⁺
Ca²⁺
Ca²⁺
Ca²⁺
3Na⁺
Na⁺
K⁺
2K⁺
3Na⁺
The coupled clock system
K⁺
K⁺
2K⁺
Na⁺, K⁺
Basal AC
ATP
cAMP
P
PKA
CaM
CaMKII
3Na⁺
Na⁺
3Na⁺
SANC
Mitochondria
Ca²⁺
ADP
ATP
Ca²⁺
Na⁺
CaMKII
cAMP
PKA
PLB
SERCA
RyR
Ca²⁺
SR
SANC
SR
RyR
Ca²⁺
Ca²⁺
Ca²⁺
Ca²⁺
Ca²⁺
Ca²⁺
Ca²⁺
PLB
SERCA
The Ca²⁺ clock

Fig. 5.2 The biochemical "engine" of the coupled-oscillator system (from [59])

including phospholamban (major regulator of SERCA activity), RyR, and LCCh. SR Ca refilling kinetics regulate the LCR period and spontaneous beating rate of rabbit SAN cells [17]. PKA- and CaMKII-dependent phosphorylation of Ca-cycling proteins and LCCh synchronizes spontaneous RyR activation. The restitution process that determines the LCR period is regulated by (1) SR Ca-cycling kinetics, i.e., rate of Ca pumping into the SR; and (2) the threshold of SR Ca load required for spontaneous RyR activation. Exquisitely biophysically detailed numeric models support these findings [7, 9, 19, 50, 61].

5.10.2 Autonomic Modulation of AP Firing Rate Occurs via the Same Coupled Biophysical and Biochemical Mechanisms

The coupled-clock system has to function flexibly over the range of rates necessary to sustain life. It does this via variation in G protein-coupled receptor signaling to link both adrenergic and cholinergic receptors (ChR) to the very same critical components of the coupled-clock system that regulate the basal state LCR period [8]. Stimulation of sympathetic β-ARs in SAN cells increases the spontaneous AP firing rate via G_s and further downstream signaling components resulting in a multitude of effects on proteins of both clocks, including ion channels of the membrane clock [3], specifically I_K and I_{CaL} (via PKA-dependent phosphorylation) and I_f (via a direct effect of cAMP). Note that the direct effect of cAMP on I_f has recently been studied in exquisite detail using a knock-in mouse expressing cAMP-insensitive HCN4 channels—these mice showed sinus dysrhythmia, marked sinus bradycardia, sinus pauses, and an inability to increase heart rate appropriately ("chronotropic incompetence") [62].

β-AR stimulation similarly affects the Ca clock, via changes in cAMP/PKA-dependent phosphorylation due to AC activation and phosphatase inhibition, leading to altered SR Ca release via RyR, and Ca sequestration via SERCA [63–65]. The ultimate effect is the generation of stronger and earlier LCR ensemble signals [17, 22, 65], activating stronger and earlier I_{NCX}, accelerating DD toward threshold potential [9]. In addition, CaMKII-dependent phosphorylation of phospholamban and RyR also increases in response to β-AR stimulation (likely, secondary due to changes in cell Ca dynamics and concomitant calmodulin activation, affected primarily by PKA activation). Thus, CaMKII-dependent phosphorylation has an important role as a Ca-calmodulin-dependent "late" amplifier of the initial effect of β-AR stimulation.

ChRs contrastingly acts as a physiological "brake" on heart rate. ChR signaling activates G_i proteins that couple to several downstream targets: (1) G_i-βγ activation of I_{KACh} (see review [3] for details) ; (2) a G_i-α_s coupled reduction in AC activity that limits cAMP/PKA-dependent phosphorylation. Ultimately, in contrast to β-AR stimulation, ChR stimulation decreases the Ca balance of the system, which leads to a reduction in the AP firing rate.

5.10.3 Mitochondria Provide Tailoring of the "Gas" to Fuel the System

Mitochondrial ATP use is unique in SAN cells [66], most being consumed in the synthesis of cAMP and Ca cycling maintenance (rather than in myofilament contraction as in working myocardium) (Fig. 5.2). That cyanide reduces intracellular Ca transient amplitude and AP firing rate in primary pacemaker cells [66, 67] suggests mitochondria have an important role in pacemaking. There is evidence that the Ca-activated-cAMP/PKA signaling cascade not only drives basal ATP consumption but also regulates ATP production [66]. cAMP/PKA signaling can affect ATP production by phosphorylation of several mitochondrial proteins (for review, see [68]), and a decrease in basal cAMP/PKA signaling in SAN cells appears to signal to mitochondria to reduce ATP production. Crosstalk occurs between the SR and the mitochondria through the currency of Ca [69], for example, an increase in mitochondrial Ca by inhibition of mitochondrial NCX decreases the SR Ca load and reduces the ensemble LCR Ca signal. In contrast, a reduction in mitochondrial Ca by inhibition of mitochondrial uniporter increases the SR Ca load and increases the ensemble LCR Ca signal.

5.10.4 Local Signaling in Microdomains

Complex crosstalk of biophysical and biochemical aspects of the coupled system described above is precisely organized and implemented in time and space within subcellular microdomains associated with discrete clusters of different ion channels, transporters, and regulatory receptors (review [70]). Such subcellular microdomains represent an interacting network of various proteins that function locally and efficiently as macromolecular signaling complexes. The spatial organization of essential signaling components makes it possible for different proteins to effectively interact and be tightly controlled by a variety of neurohormonal signaling mechanisms so that a limited pool of protein types and second messengers can generate a large variety of cellular responses commensurate to the current physiological demand. As an example of such local regulation, co-localization of PDE3 and PDE4 beneath the sarcolemma or in striated patterns inside SAN cells strongly suggests that PDE-dependent regulation of cAMP/PKA signaling is locally executed [56].

5.11 The Human Coupled-Clock System

Our historical appreciation of the coupled-clock operational paradigm stems largely from studies in small mammal hearts. Few studies exist focusing on pacemaker cell function in human hearts [71], and until very recently, none had substantiated the coupled-clock theory in human hearts. Tsutsui et al. [72] made this breakthrough, simultaneously measuring LCRs and membrane potential in freshly isolated human SAN cells and demonstrating all of the salient features of the coupled clock previously only seen in experimental animals.

5.11.1 The Workings of Automaticity Are Finely Tuned to Satisfy Physiological Demand in Individual Species

It is well-recognized that major species differences in heart rate exist. For example, baseline APCL in mice is ~100 ms, while in humans is ~1000 ms. The work of Tsutsui et al. referred to in the above paragraph, broadly showed that characteristics of the membrane and calcium clock are similar among mammalian species, including humans [72]. What has remained unclear is the degree and nature of differences in the coupled clock between species. Recent intricate work from Tagirova et al. has demonstrated that parametric Ca and membrane potential kinetic transitions in APCL in SAN cells in vitro, heart rate in vivo, and body mass can be scaled, and demonstrate self-similarity (i.e. obey power laws) across species [73]. They concluded that "In designing optimal heart rate to match widely different body mass and energy requirements from mice to humans, nature did not 'reinvent pacemaker cell wheels', but differentially scaled kinetics of gears that regulate the rates at which the 'wheels spin'." This work represents a frontier in our current trans-species understanding of automaticity and paves the way for the future development of novel therapies and biological pacemakers (see Sect. 5.16 concerning future studies).

5.12 AP Firing Rate and Rhythm Reflect Clock Coupling Determined by Clock Protein Phosphorylation Status

5.12.1 Beat-to-Beat Ca-Dependent Regulation of the Coupled-Clock System

A hallmark of the SAN automaticity is AP firing rate variability, i.e., beat-to-beat changes in spontaneous AP cycle length. Initially, this variability was attributed to the stochastic opening of sarcolemmal ion channels, mainly I_{CaL} and I_K [74]. Latterly, the spotlight fell on the Ca clock, specifically whether Ca signals variably influence the duration of each cycle on a beat-to-beat basis. Vinogradova et al. [21] showed that the LCR period and LCR signal mass remain strongly coupled to APCL, not only in the steady-state AP firing but also in each cycle during the transient state after the removal of the voltage clamp at the MDP. Further experiments clearly demonstrated beat-to-beat Ca-dependent regulation of APCL: acute Ca release from a caged Ca buffer by flash-induced photolysis or from the SR by low concentrations of caffeine acutely reduced APCL via activation of LCRs and NCX in the same cycle that the perturbation was applied [75, 76].

LCRs are stochastically generated by RyRs and demonstrate clear cycle-to-cycle variations in both individual and meantime of LCR occurrence during DD. Because Ca regulates automaticity on a beat-to-beat basis, it follows that LCRs must contribute to the beat-to-beat variability of spontaneous AP firing. This was proven in experiments using high-speed, high-resolution cameras: while individual LCR timing varied, the LCR period averaged for all LCRs in a given cycle closely predicted the time of occurrence of the next AP [16]. Further studies [77] showed that the changes in the average LCR period and its variability in response to chemical perturbation of the coupled-clock system (with cyclopiazonic acid or ivabradine) are correlated with changes in APCL and APCL variability. The study concluded that the stochasticity within the coupled-clock system affects and is affected by the AP firing rate and rhythm via modulation of the effectiveness of clock coupling.

5.12.2 Mechanisms Affecting Clock Coupling

Mechanisms influencing the coupling of the clocks are of critical importance in understanding the SAN's ability to change its rate/rhythm. Yaniv et al. [77] showed that the gradual increase of APCL variability (along with APCL) produced by increasing concentrations of ivabradine is accompanied by gradual decreases in phospholamban phosphorylation at Ser16, pointing to a key role of PKA-dependent phosphorylation in the clock coupling and APCL variability [77].

Moen et al. [49] used mice with heart-targeted expression of AC8 (TG^{AC8}) to demonstrate that increased AC activity in SAN tissue is accompanied by a marked increase in heart rate and a concurrent marked reduction in heart rate variability, both in the absence or presence of dual autonomic blockade, providing further evidence for the importance of the cAMP-PKA-dependent clock-coupling mechanism. Another important result of this study is that variability in spontaneous beating intervals in isolated SAN tissue and single SAN cells, devoid of autonomic neural input, suggests that clocks (and clocks coupling) intrinsic to SAN cells may also contribute to heart rate and heart rate variability in vivo.

5.12.3 Aging Affects Clock Coupling

The full spectrum of mouse SAN AP firing rates requires PKA-dependent Ca signaling [78], but the fidelity of this signaling and, therefore, clock coupling deteriorates with age. Liu et al. [79] reported that the sensitivity of the SAN beating rate responses to both muscarinic and adrenergic receptor activation becomes decreased in advanced age. The sensitivity of the SAN beating rate to cAMP perturbations is also reduced. These compromised clock functions, including a reduced SR Ca load and reduced size, number, and duration of spontaneous LCRs, coincided with decreased expression of crucial SR Ca-cycling proteins (including SERCA, RyR, and NCX). Heart rate variability is also affected by aging due to reduced clock coupling. In the isolated SAN, the sensitivity of the average beating interval and beating interval variability in response to autonomic receptor stimulation or activation of mechanisms intrinsic to pacemaker cells by an increase in cAMP production (by phosphodiesterase inhibition) declines with advanced age [80].

5.12.4 Autonomic Signaling and System "Memory"

Extrinsic factors affecting SAN cells, including mechanical, autonomic, and hormonal factors, modulate the rate and rhythm of spontaneous AP cycles. Extrinsic adrenergic input via β-AR increases the phosphorylation of clock proteins that increases Ca influx in SAN cells. This indirectly and directly increases synchronization of diastolic LCR events, accelerating the kinetics of self-organized growth of the LCR ensemble Ca signal and activating NCX and $I_{CaL,}$ which both ignite the AP *almost simultaneously* in time, increasing rhythmicity and decreasing variability [19, 61]. Contrastingly, external cholinergic inputs and associated low phosphorylation levels leave LCRs small and disordered in time and space (like sparks in ventricular cells). Consequently, the peak of the LCR ensemble signal and attendant AP ignition occurs with substantial variability, decreasing the rhythmicity of AP firing. Other important cues to AP firing are generated by additional members of the coupled-clock system (including HCN4, K channels, SERCA, etc.). This highly complex oscillatory system has memory implemented by the SR Ca load level and phosphorylation states of clock molecules that reflects the history of stimulation and frequency changes in previous cycles; and all cues are interrelated and become recursive in such a system [81]. Both phosphorylation and Ca modulation of K channels in response to βAR stimulation accelerate membrane repolarization, which is required for more rapid AP firing to occur. A more frequent AP firing, ipso facto (via increased Ca influx by I_{CaL}) increases SR Ca load, leading to more robust and synchronized spontaneous LCR signals.

5.13 Increasing Clock Coupling: From Dormancy to Highly Rhythmic Firing

SAN cell experiments have traditionally focused on cells beating spontaneously at an arbitrarily defined “physiological” rate. Other healthy appearing isolated cells were ignored. Kim et al. [82] examined *all* single cells isolated from guinea pig SAN, including rhythmically firing, dysrhythmically firing, and cells without any apparent spontaneous firing activity (“dormant”). LCRs are present in all cell types, indicating that SAN cells can generate subthreshold signals that have never previously been considered in the pacemaker operational paradigm. β-AR stimulation increases LCR size and synchronizes LCR occurrences in all dysrhythmic, and about a third of dormant cells, some of which develop automaticity, and LCRs become coupled to spontaneous AP-induced Ca transients. The majority of dysrhythmic cells become rhythmically firing in response to β-AR stimulation. Biophysical measurements combined with numerical model simulations indicate that the two previously unstudied dysrhythmic and dormant cell populations have intrinsically partially or completely uncoupled clocks and that they can be recruited to fire rhythmically through β-AR stimulation via increased rhythmic LCR activity reflecting increased clock coupling.

Similar findings were made in cells isolated from human SAN [72]. Nonbeating arrested human SAN cells, or those that do not generate spontaneous APs, exhibit extreme clock uncoupling, being relatively depolarized yet still continuing to generate LCRs. Such “dormancy” or “arrest” can be linked to the depolarized membrane potential (near –35 mV), with I_{NCX} being closer to its reversal potential. When LCRs fail to activate I_{NCX}, partial uncoupling of the Ca and membrane clocks occurs, resulting in substantially slower, dysrhythmic AP firing or even AP failure vs. optimal clock coupling in rhythmically firing cells. Extreme clock uncoupling leads to failure of spontaneous AP generation, which is once more restored by recoupling of the clocks by β-AR stimulation.

5.13.1 Self-Similarity Is a Key Characteristic of SAN Cell Automaticity

SAN cells do not beat metronomically, that is to say, the intervals between action potentials are not identical; instead, they vary by varying amounts from beat to beat. Autonomic innervation has a large impact on this in vivo, yet the characteristic remains in denervated preparations, i.e., single cells, isolated SAN preparations, and isolated hearts. One consequence of this variability is that SAN cells and their pacemaker mechanisms never achieve equilibrium during AP firing. But what is the nature of this variability? Yang et al. recently comprehensively studied rabbit SAN cells across the whole range of firing rates affected by autonomic agonists and found that all studied parameters of automaticity (including means and variabilities of APCL, local Ca release kinetics, Ca transient decay times, diastolic depolarization rates, AP repolarization times) demonstrate self-similarity ("concordance") across the physiological spectrum of heart rates [81]. This suggests a hitherto unrecognized degree of protein cooperation and synchronization, whereby each AP represents the most potent integrator/synchronizer of the prior diastolic depolarization and ignition events. This kind of self-similar behavior in pacemaking represents another frontier in our understanding of SAN automaticity and mandates further study.

5.14 Marked Electrophysiological Heterogeneity Exists Among SAN Cells

The importance of cAMP-dependent phosphorylation in clock coupling (or fidelity of coupling) is clear, yet how different degrees of phosphorylation translate in clock coupling and specific cell behaviors (e.g., dormancy) will depend on the expression level of clock proteins in individual cells. This cannot be assumed to be the same from cell to cell—immunocytochemical labeling of the LCCh, NCX, RyR2, and SERCA2 varies widely in SAN cells [83]. SAN cells exhibit a substantial degree of cell-to-cell variability in the functional expression of I_{CaL}, I_f, and I_K [84, 85]. Patch clamp recording of key ion currents in the same cell, relationships between basal beating rate and I_{CaL} and I_f density were found, along with a positive relationship between I_f and I_K; the response to Ca-cycling blockade was also correlated with I_f density [85]. These results demonstrate the existence of SAN cells with substantially different clock-coupling capabilities that could be important to execute specific roles at specific times as dictated by the prevailing physiological milieu.

5.15 The Forefront of SAN Physiology: Time for a New Paradigm?

The SAN exhibits a high degree of structural and functional complexity, and these characteristics seem to be critical for its central role in cardiac physiology—to reliably deliver automaticity, flexibility, and robustness [86]. But how specifically this enormous heterogeneity translates into robust and flexible SAN operation still remains an unsolved mystery of the cardiac pacemaker field. Numerous SAN cell characteristics have been described including diversity in cell shape [85] and protein expression; the arrangement of cells within the SAN tissue (e.g., gradient vs. mosaic [87]); autonomic neuronal input [88]; cell-to-cell electrical and mechanical interactions [89, 90]; and intranodal impulse initiation, spread within, and exit from, the SAN [91–94].

A generalized view of impulse initiation and transmission in the SAN emerged about 40 years ago, in which a dominant or "master" pacemaker cell or leading pacemaker center dictates the excitation rate and rhythm of thousands of other subservient SAN pacemaker cells by overdriving their intrinsic spontaneous excitation rates [91, 95]. Shortly thereafter, the idea of mutual entrainment of coupled oscillators [96] was applied to the coordinated firing of the entire SAN [97, 98], whereby individual SAN cells, loosely connected through low resistance junctions, mutually entrain each other to fire APs with a common period (dubbed the "democratic" process). In this theory, the frequency of impulses that exit the SAN lies somewhere between the fastest and slowest spontaneous intrinsic excitation rates of resident SAN cells, and there can be marked phase differences among spontaneous excitation in individual cells. Rather than mimicking classical electrical conduction by consecutively exciting each other, as in ventricular muscle tissue, according to this theory, SAN cells are instead mutually entrained by phase resetting, and conduction within SAN is only "apparent" [98, 99]. The idea of apparent conduction was supported by later studies that showed that the cardiac impulse could arise from different locations [100]. Then Verheijck et al. [101] performed studies utilizing computer-controlled coupling conductance between individual pacemaker cells and found a critical coupling conductance for 1:1 frequency entrainment of less than 0.5 nS, which could be generated by a few connexin molecules only.

Classic macroscopic imaging of voltage and Ca signals within intact SAN tissue lack the resolution to characterize LCR events occurring within individual cells within SAN tissue [92]. Even though recent studies at higher optical magnification detected LCRs within individual cells of SAN tissue [102, 103], they did not systematically examine their role in impulse initiation and spread across individual cells within the SAN. Therefore, the current paradigm of SAN impulse generation is that full-scale APs of a common frequency are initiated at one site and conducted within the SAN along smooth isochrones yet does not feature fine details of Ca signaling known to be present in isolated SAN cells.

A ground-breaking recent study by Bychkov et al. [2] investigated subcellular Ca signals within and among cells comprising the SAN tissue. The study combined immunolabeling with a novel technique to detect the occurrence of LCRs and AP-induced Ca transients (APCTs) in individual pixels across the entire mouse SAN. At high magnification, Ca signals appear markedly heterogeneous in space, amplitude, frequency, and phase among cells comprising an HCN4$^+$/CX43$^-$ cell meshwork. The signaling exhibits several distinguishable patterns of LCR/APCT interactions within and among cells: in some cells, APCT occurrence is preceded by diastolic LCRs occurring in the same cell (i.e., similar to the coupled-clock operation discovered in isolated cells); other cells do not generate spontaneous APCTs, but have subthreshold LCRs only (like in dormant cells, described above), which precede APCT generation by adjacent cells; APCTs of various frequencies are generated steadily or in bursts. Apparently, conducting rhythmic APCTs of the meshwork are transferred to a truly conducting HCN4$^-$/CX43$^+$ network of striated cells via narrow functional interfaces where different cell types intertwine. At low magnification, the earliest APCT of each cycle occurs within a small area of the HCN4 meshwork, and the subsequent APCT throughout SAN pixels is discontinuous. Similar heterogeneous signaling has also been demonstrated in SAN isolated from human hearts and from genetically manipulated mice (pCAGGS-GCaMP8) in which Ca signals are linked to HCN4 expression [2].

In summary, rhythmic, synchronized APs emerge from heterogeneous, subthreshold Ca signaling not detected in low-resolution macroscopic isochrones. These results require a fundamental paradigm shift in our understanding of SAN function to include complex/multiscale integration of subthreshold Ca signals with full-scale APs (Fig. 5.3), resembling the emergence of organized signals from heterogeneous local signals within neuronal networks, e.g., Bötzinger cells of the brainstem, interstitial cells of Cajal in the gut, and uterine smooth muscle [104–106]. In their associated editorial, Clancy and Santana suggested emergent pacemaking as a complex multiscale process with a possible role of stochastic resonance that can increase the synchronization and robustness of the pacemaking system [14].

Thus, classical SAN pacemaking concepts of driving, pacing, leading, and concentric propagation, associated with biological “dictatorship,” should be replaced with concepts of “emergence and heterogeneity.” While the idea of the “democratic” process within weakly coupled entrained AP oscillators [97, 98] had challenged the old “dictatorship” concept, it considered full-scale AP firing by pacemaker cells at one common frequency via mutual entrainment. Surprisingly, there is no such thing as “*the* pacemaker cell” within the new paradigm. No cell alone or in a cluster initiates the impulse; rather, numerous cells (individually and in clusters) generate heterogeneous complex (partially periodic) signals, both subthreshold LCR and/or full-scale APs of different frequencies, and those signals integrate and synchronize over the cellular meshwork so that the rhythmic output **emerges** from those

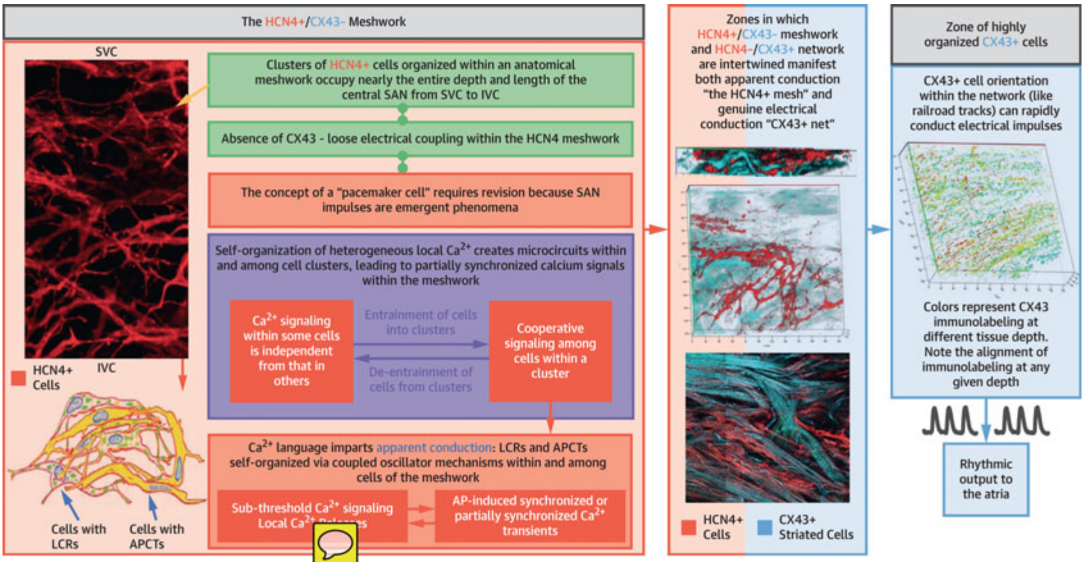
The HCN4+/CX43- Meshwork
SVC
IVC
HCN4+ Cells
Cells with LCRs
Cells with APCTs
Clusters of HCN4+ cells organized within an anatomical meshwork occupy nearly the entire depth and length of the central SAN from SVC to IVC
Absence of CX43 - loose electrical coupling within the HCN4 meshwork
The concept of a "pacemaker cell" requires revision because SAN impulses are emergent phenomena
Self-organization of heterogeneous local Ca^{2+} creates microcircuits within and among cell clusters, leading to partially synchronized calcium signals within the meshwork
Ca^{2+} signaling within some cells is independent from that in others
Entrainment of cells into clusters
De-entrainment of cells from clusters
Cooperative signaling among cells within a cluster
Ca^{2+} language imparts apparent conduction: LCRs and APCTs self-organized via coupled oscillator mechanisms within and among cells of the meshwork
Sub-threshold Ca^{2+} signaling Local Ca^{2+} Releases
AP-induced synchronized or partially synchronized Ca^{2+} transients
Zones in which HCN4+/CX43- meshwork and HCN4-/CX43+ network are intertwined manifest both apparent conduction "the HCN4+ mesh" and genuine electrical conduction "CX43+ net"
HCN4+ Cells
CX43+ Striated Cells
Zone of highly organized CX43+ cells
CX43+ cell orientation within the network (like railroad tracks) can rapidly conduct electrical impulses
Colors represent CX43 immunolabeling at different tissue depth. Note the alignment of immunolabeling at any given depth
Rhythmic output to the atria

Fig. 5.3 A novel SAN structure/function paradigm. Panels illustrate HCN4 meshwork (left panel), intertwining area (central panel), and CX43 network of cells (right panel). Spontaneous signals are generated within the HCN4 meshwork and transmitted to the CX43 network of cells through the intertwining area. AP, action potential; APCT, action potential-induced Ca^{2+} transient; CX43, connexin 43: HCN4+, hyperpolarization-activated cyclic nucleotide-gated channel 4; IVC, inferior vena cava; LCR, local Ca^{2+} release; SAN, sinoatrial node (from [2]). See also online video 9 from the same paper (https://www.jacc.org/cms/asset/aa14ddc8-c5d5-45d0-bcce-d2c0e36c9651/mmc11.mp4)

multiple signals as the result of this complex signal processing. The recent work by Fenske et al. [62, 107] in knock-in mice expressing cAMP-insensitive HCN4 channels has further underlined the likely importance of nonfiring SAN cells—they showed that tonic and mutual interaction (so-called "tonic entrainment") between firing and nonfiring cells slows down pacemaking in the SAN and that cAMP increases the proportion of firing cells, and in doing so increases rate of automaticity, and increases resistance to vagal signaling.

5.16 Summary, Future Studies, and Harnessing the Coupled-Clock Operation for Clinical Applications

Above, we have reviewed contemporary concepts surrounding the generation of automaticity in the SAN—a multiscale process involving the integration of complex biochemical and biophysical processes. The Ca clock generates diastolic LCRs that are small and disordered at about the time of MDP but then self-organize into larger events that initiate AP ignition. The system reaches *criticality* in late diastole and undergoes a *phase transition* culminating in AP generation. The ignition process involves feed-forward local interactions among LCRs, NCX, and I_{CaL}. Clock coupling is biochemically regulated by a complex enzyme network featuring high basal levels of cAMP (produced by Ca-activated AC1 and AC8) and a high basal degree of clock protein phosphorylation via cAMP-dependent PKA and CaMKII. The feed-forward system is checked by highly constitutionally active PDEs and phosphatases, leaving the engine's basal state tuned to operate near the middle of its spectrum. Various degrees of cAMP production and phosphorylation achieved by autonomic receptor modulation increase or decrease clock coupling and hence AP firing rate and rhythm, commensurate to the chronotropic physiologic demand. The degree of clock coupling determines the entire spectrum of APCL and APCL variability, ranging from high coupling (β-AR stimulation) to medium coupling (basal state) to low coupling (ChR-stimulation), extending further to dysrhythmic firing and dormancy. Ground-breaking recent studies in intact SAN discovered a new paradigm of SAN operation: rhythmic cardiac impulses emerge from heterogeneous local signals within and among cells of pacemaker tissue. These signals include both subthreshold LCRs and APs so that the coupled-clock theory translates into SAN tissue to operate within and among cells. How local heterogeneous signals self-organize into signaling patterns in cell clusters (or cell communities) and further synchronize to generate rhythmic cardiac impulses is currently at the frontier of our understanding.

With respect to clinical applications, failure to initiate and conduct electrical activity within the heart is associated with various cardiovascular and noncardiovascular diseases and increases as we age. Current treatment of such sinoatrial node dysfunction involves the implantation of an electronic pacemaker, which is both a costly and imperfect solution. A comprehensive understanding of SAN automaticity helps to expedite the creation of a "biological pacemaker," a superior, more physiological, and potentially less invasive treatment that would reliably and sustainably induce or reinstall cardiac pacemaker cell functions via somatic gene transfer, cell fusion, or cell transplantation [108, 109]. One type of genetically engineered biological pacemakers, based on the coupled-clock theory, activates Ca-stimulated AC1 or AC8 via virus-transfection gene therapy [48]. Indeed, efficient biological pacing has been reported in experiments with dogs in which AC1 was used as single gene therapy and in combination with HCN2 [47]. Other ideas for biological pacing include the transfer of genes encoding transcription factors [109, 110].

Acknowledgments This research was supported by the Intramural Research Program of the National Institutes of Health and the National Institute on Aging.

References

1. Monfredi O, Maltsev VA, Lakatta EG. Modern concepts concerning the origin of the heartbeat. Physiology (Bethesda). 2013;28(2):74–92.
2. Bychkov R, Juhaszova M, Tsutsui K, Coletta C, Stern MD, Maltsev VA, et al. Synchronized cardiac impulses emerge from heterogeneous local calcium signals within and among cells of pacemaker tissue. JACC Clin Electrophysiol. 2020;6(8):907–31.
3. Mangoni ME, Nargeot J. Genesis and regulation of the heart automaticity. Physiol Rev. 2008;88(3): 919–82.
4. Maltsev VA, Vinogradova TM, Lakatta EG. The emergence of a general theory of the initiation and strength of the heartbeat. J Pharmacol Sci. 2006;100 (5):338–69.
5. Yue X, Hazan A, Lotteau S, Zhang R, Torrente AG, Philipson KD, et al. Na/Ca exchange in the atrium: Role in sinoatrial node pacemaking and excitation-contraction coupling. Cell Calcium. 2020;87:102167.
6. Kohajda Z, Loewe A, Toth N, Varro A, Nagy N. The cardiac pacemaker story-fundamental role of the Na (+)/Ca(2+) exchanger in spontaneous automaticity. Front Pharmacol. 2020;11:516.
7. Maltsev VA, Lakatta EG. Synergism of coupled subsarcolemmal Ca^{2+} clocks and sarcolemmal voltage clocks confers robust and flexible pacemaker function in a novel pacemaker cell model. Am J Physiol Heart Circ Physiol. 2009;296(3):H594–615.
8. Lakatta EG, Maltsev VA, Vinogradova TM. A coupled SYSTEM of intracellular Ca^{2+} clocks and surface membrane voltage clocks controls the timekeeping mechanism of the heart's pacemaker. Circ Res. 2010;106:659–73.
9. Maltsev VA, Lakatta EG. A novel quantitative explanation for autonomic modulation of cardiac pacemaker cell automaticity via a dynamic system of sarcolemmal and intracellular proteins. Am J Physiol Heart Circ Physiol. 2010;298:H2010–H23.
10. Maltsev VA, Lakatta EG. Numerical models based on a minimal set of sarcolemmal electrogenic proteins and an intracellular Ca clock generate robust, flexible, and energy-efficient cardiac pacemaking. J Mol Cell Cardiol. 2013;59:181–95.
11. Maltsev VA, Yaniv Y, Maltsev AV, Stern MD, Lakatta EG. Modern perspectives on numerical modeling of cardiac pacemaker cell. J Pharmacol Sci. 2014;125:6–38.
12. Yaniv Y, Lakatta EG, Maltsev VA. From two competing oscillators to one coupled-clock pacemaker cell system. Front Physiol. 2015;6:28.
13. Lakatta EG. Heartbeat music. Heart Rhythm. 2021;18(5):811–2. https://doi.org/10.1016/j.hrthm.2021.01.011.
14. Clancy CE, Santana LF. Evolving discovery of the origin of the heartbeat: a new perspective on sinus rhythm. JACC Clin Electrophysiol. 2020;6(8):932–4.

15. Weiss JN, Qu Z. The sinus node: still mysterious after all these years. JACC Clin Electrophysiol. 2020;6(14):1841–3.
16. Monfredi O, Maltseva LA, Spurgeon HA, Boyett MR, Lakatta EG, Maltsev VA. Beat-to-beat variation in periodicity of local calcium releases contributes to intrinsic variations of spontaneous cycle length in isolated single sinoatrial node cells. PLoS One. 2013;8(6):e67247.
17. Vinogradova TM, Brochet DX, Sirenko S, Li Y, Spurgeon H, Lakatta EG. Sarcoplasmic reticulum Ca^{2+} pumping kinetics regulates timing of local Ca^{2+} releases and spontaneous beating rate of rabbit sinoatrial node pacemaker cells. Circ Res. 2010;107(6):767–75.
18. Maltsev AV, Maltsev VA, Mikheev M, Maltseva LA, Sirenko SG, Lakatta EG, et al. Synchronization of stochastic Ca^{2+} release units creates a rhythmic Ca^{2+} clock in cardiac pacemaker cells. Biophys J. 2011;100:271–83.
19. Stern MD, Maltseva LA, Juhaszova M, Sollott SJ, Lakatta EG, Maltsev VA. Hierarchical clustering of ryanodine receptors enables emergence of a calcium clock in sinoatrial node cells. J Gen Physiol. 2014;143(5):577–604.
20. Bogdanov KY, Maltsev VA, Vinogradova TM, Lyashkov AE, Spurgeon HA, Stern MD, et al. Membrane potential fluctuations resulting from submembrane Ca^{2+} releases in rabbit sinoatrial nodal cells impart an exponential phase to the late diastolic depolarization that controls their chronotropic state. Circ Res. 2006;99(9):979–87.
21. Vinogradova TM, Zhou YY, Maltsev V, Lyashkov A, Stern M, Lakatta EG. Rhythmic ryanodine receptor Ca^{2+} releases during diastolic depolarization of sinoatrial pacemaker cells do not require membrane depolarization. Circ Res. 2004;94(6):802–9.
22. Vinogradova TM, Lyashkov AE, Zhu W, Ruknudin AM, Sirenko S, Yang D, et al. High basal protein kinase A-dependent phosphorylation drives rhythmic internal Ca^{2+} store oscillations and spontaneous beating of cardiac pacemaker cells. Circ Res. 2006;98(4):505–14.
23. Huser J, Blatter LA, Lipsius SL. Intracellular Ca^{2+} release contributes to automaticity in cat atrial pacemaker cells. J Physiol. 2000;524(Pt 2):415–22.
24. Mangoni ME, Couette B, Bourinet E, Platzer J, Reimer D, Striessnig J, et al. Functional role of L-type Cav1.3 Ca^{2+} channels in cardiac pacemaker activity. Proc Natl Acad Sci U S A. 2003;100(9):5543–8.
25. Baig SM, Koschak A, Lieb A, Gebhart M, Dafinger C, Nurnberg G, et al. Loss of Ca(v)1.3 (CACNA1D) function in a human channelopathy with bradycardia and congenital deafness. Nat Neurosci. 2011;14(1):77–84.
26. Torrente AG, Mesirca P, Neco P, Rizzetto R, Dubel S, Barrere C, et al. L-type Cav1.3 channels regulate ryanodine receptor-dependent Ca^{2+} release during sino-atrial node pacemaker activity. Cardiovasc Res. 2016;109(3):451–61.
27. Lyashkov AE, Behar J, Lakatta EG, Yaniv Y, Maltsev VA. Positive feedback mechanisms among local Ca releases, NCX, and ICaL ignite pacemaker action potentials. Biophys J. 2018;114(5):1176–89.
28. Yaniv Y, Sirenko S, Ziman BD, Spurgeon HA, Maltsev VA, Lakatta EG. New evidence for coupled clock regulation of the normal automaticity of sinoatrial nodal pacemaker cells: Bradycardic effects of ivabradine are linked to suppression of intracellular Ca cycling. J Mol Cell Cardiol. 2013;62C:80–9.
29. Gao Z, Rasmussen TP, Li Y, Kutschke W, Koval OM, Wu Y, et al. Genetic inhibition of Na^{+}-Ca^{2+} exchanger current disables fight or flight sinoatrial node activity without affecting resting heart rate. Circ Res. 2013;112(2):309–17.
30. Maltsev AV, Yaniv Y, Stern MD, Lakatta EG, Maltsev VA. RyR-NCX-SERCA local crosstalk ensures pacemaker cell function at rest and during the fight-or-flight reflex. Circ Res. 2013;113(10):e94–e100.
31. Stern MD, Song LS, Cheng H, Sham JS, Yang HT, Boheler KR, et al. Local control models of cardiac excitation-contraction coupling. A possible role for allosteric interactions between ryanodine receptors. J Gen Physiol. 1999;113(3):469–89.
32. Koivumaki JT, Korhonen T, Takalo J, Weckstrom M, Tavi P. Regulation of excitation-contraction coupling in mouse cardiac myocytes: integrative analysis with mathematical modelling. BMC Physiol. 2009;9:16.
33. Torrente AG, Zhang R, Wang H, Zaini A, Kim B, Yue X, et al. Contribution of small conductance K^{+} channels to sinoatrial node pacemaker activity: insights from atrial-specific Na^{+}/Ca^{2+} exchange knockout mice. J Physiol. 2017;595(12):3847–65.
34. Sirenko SG, Maltsev VA, Yaniv Y, Bychkov R, Yaeger D, Vinogradova T, et al. Electrochemical Na^{+} and Ca^{2+} gradients drive coupled-clock regulation of automaticity of isolated rabbit sinoatrial nodal pacemaker cells. Am J Physiol Heart Circ Physiol. 2016;311(1):H251–67.
35. Maltsev AV, Maltsev VA, Stern MD. Clusters of calcium release channels harness the Ising phase transition to confine their elementary intracellular signals. Proc Natl Acad Sci U S A. 2017;114(29):7525–30.
36. Maltsev AV, Stern MD, Maltsev VA. Mechanisms of calcium leak from cardiac sarcoplasmic reticulum revealed by statistical mechanics. Biophys J. 2019;116(11):2212–23.
37. Ju YK, Chu Y, Chaulet H, Lai D, Gervasio OL, Graham RM, et al. Store-operated Ca^{2+} influx and expression of TRPC genes in mouse sinoatrial node. Circ Res. 2007;100(11):1605–14.
38. Liu J, Xin L, Benson VL, Allen DG, Ju YK. Store-operated calcium entry and the localization of STIM1

and Orai1 proteins in isolated mouse sinoatrial node cells. Front Physiol. 2015;6:69.

39. Ju YK, Lee BH, Trajanovska S, Hao G, Allen DG, Lei M, et al. The involvement of TRPC3 channels in sinoatrial arrhythmias. Front Physiol. 2015;6:86.
40. Ju YK, Liu J, Lee BH, Lai D, Woodcock EA, Lei M, et al. Distribution and functional role of inositol 1,4,5-trisphosphate receptors in mouse sinoatrial node. Circ Res. 2011;109(8):848–57.
41. Kapoor N, Tran A, Kang J, Zhang R, Philipson KD, Goldhaber JI. Regulation of calcium clock-mediated pacemaking by inositol-1,4,5-trisphosphate receptors in mouse sinoatrial nodal cells. J Physiol. 2015;593 (12):2649–63.
42. Weisbrod D, Peretz A, Ziskind A, Menaker N, Oz S, Barad L, et al. SK4 Ca^{2+} activated K^+ channel is a critical player in cardiac pacemaker derived from human embryonic stem cells. Proc Natl Acad Sci U S A. 2013;110(18):E1685–94.
43. Haron-Khun S, Weisbrod D, Bueno H, Yadin D, Behar J, Peretz A, et al. SK4 K^+ channels are therapeutic targets for the treatment of cardiac arrhythmias. EMBO Mol Med. 2017;9(4):415–29.
44. Mattick P, Parrington J, Odia E, Simpson A, Collins T, Terrar D. Ca^{2+}-stimulated adenylyl cyclase isoform AC1 is preferentially expressed in guinea-pig sino-atrial node cells and modulates the I_f pacemaker current. J Physiol. 2007;582(Pt 3):1195–203.
45. Younes A, Lyashkov AE, Graham D, Sheydina A, Volkova MV, Mitsak M, et al. Ca^{2+}-stimulated basal adenylyl cyclase activity localization in membrane lipid microdomains of cardiac sinoatrial nodal pacemaker cells. J Biol Chem. 2008;283(21):14461–8.
46. Sirenko S, Yang D, Li Y, Lyashkov AE, Lukyanenko YO, Lakatta EG, et al. Ca^{2+}-dependent phosphorylation of Ca^{2+} cycling proteins generates robust rhythmic local Ca^{2+} releases in cardiac pacemaker cells. Sci Signal. 2012;6(260):ra6.
47. Boink GJ, Nearing BD, Shlapakova IN, Duan L, Kryukova Y, Bobkov Y, et al. Ca^{2+}-stimulated adenylyl cyclase AC1 generates efficient biological pacing as single gene therapy and in combination with HCN2. Circulation. 2012;126(5):528–36.
48. Maltsev VA, Lakatta EG, Zahanich I, Sirenko S, Mikheev M, Vodovotz Y. engineered biological pacemakers patent US9506032B2 granted. 2016. https://patents.google.com/patent/US9506032B2/en
49. Moen JM, Matt MG, Ramirez C, Tarasov KV, Chakir K, Tarasova YS, et al. Overexpression of a neuronal type adenylyl cyclase (type 8) in sinoatrial node markedly impacts heart rate and rhythm. Front Neurosci. 2019;13:615.
50. Yaniv Y, Ganesan A, Yang D, Ziman BD, Lyashkov AE, Levchenko A, et al. Real-time relationship between PKA biochemical signal network dynamics and increased action potential firing rate in heart pacemaker cells: Kinetics of PKA activation in heart pacemaker cells. J Mol Cell Cardiol. 2015;86:168–78.
51. Li Y, Sirenko S, Riordon DR, Yang D, Spurgeon H, Lakatta EG, et al. CaMKII-dependent phosphorylation regulates basal cardiac pacemaker function via modulation of local Ca^{2+} releases. Am J Physiol Heart Circ Physiol. 2016;311(3):H532–44.
52. Yaniv Y, Maltsev VA. Numerical modeling calcium and CaMKII effects in the SA node. Front Pharmacol. 2014;5:58.
53. Vinogradova TM, Zhou YY, Bogdanov KY, Yang D, Kuschel M, Cheng H, et al. Sinoatrial node pacemaker activity requires Ca^{2+}/calmodulin-dependent protein kinase II activation. Circ Res. 2000;87(9): 760–7.
54. Wu Y, Gao Z, Chen B, Koval OM, Singh MV, Guan X, et al. Calmodulin kinase II is required for fight or flight sinoatrial node physiology. Proc Natl Acad Sci U S A. 2009;106(14):5972–7.
55. Vinogradova TM, Sirenko S, Lyashkov AE, Younes A, Li Y, Zhu W, et al. Constitutive phosphodiesterase activity restricts spontaneous beating rate of cardiac pacemaker cells by suppressing local Ca^{2+} releases. Circ Res. 2008;102:761–9.
56. Vinogradova TM, Kobrinsky E, Lakatta EG. Dual activation of phosphodiesterases 3 and 4 regulates basal spontaneous beating rate of cardiac pacemaker cells: role of compartmentalization? Front Physiol. 2018;9:1301.
57. Vinogradova TM, Sirenko S, Lukyanenko YO, Yang D, Tarasov KV, Lyashkov AE, et al. Basal spontaneous firing of rabbit sinoatrial node cells is regulated by dual activation of PDEs (phosphodiesterases) 3 and 4. Circ Arrhythm Electrophysiol. 2018;11(6):e005896.
58. Zahanich I, Li Y, Lyashkov AE, Lukyanenko YO, Vinogradova TM, Younes A, et al. Protein phosphatase 1 regulates normal automaticity of the heart's pacemaker node cells by site-specific modulation of phospholamban phosphorylation that regulates spontaneous subsarcolemmal local Ca^{2+} releases. Circulation. 2010;122:A21546. (Abstract)
59. Monfredi O, Lakatta EG. Complexities in cardiovascular rhythmicity: perspectives on circadian normality, ageing and disease. Cardiovasc Res. 2019;115 (11):1576–95.
60. Sirenko S, Maltsev VA, Maltseva LA, Yang D, Lukyanenko Y, Vinogradova TM, et al. Sarcoplasmic reticulum Ca cycling protein phosphorylation in a physiologic Ca milieu unleashes a high-power, rhythmic Ca clock in ventricular myocytes: Relevance to arrhythmias and bio-pacemaker design. J Mol Cell Cardiol. 2014;66C:106–15.
61. Maltsev AV, Maltsev VA, Stern MD. Stabilization of diastolic calcium signal via calcium pump regulation of complex local calcium releases and transient decay in a computational model of cardiac pacemaker cell with individual release channels. PLoS Comput Biol. 2017;13(8):e1005675.
62. Fenske S, Hennis K, Rotzer RD, Brox VF, Becirovic E, Scharr A, et al. cAMP-dependent

regulation of HCN4 controls the tonic entrainment process in sinoatrial node pacemaker cells. Nat Commun. 2020;11(1):5555.

63. Ju YK, Allen DG. How does beta-adrenergic stimulation increase the heart rate? The role of intracellular Ca^{2+} release in amphibian pacemaker cells. J Physiol. 1999;516(Pt 3):793–804.
64. Rigg L, Heath BM, Cui Y, Terrar DA. Localisation and functional significance of ryanodine receptors during beta-adrenoceptor stimulation in the guinea-pig sino-atrial node. Cardiovasc Res. 2000;48(2):254–64.
65. Vinogradova TM, Bogdanov KY, Lakatta EG. beta-Adrenergic stimulation modulates ryanodine receptor Ca^{2+} release during diastolic depolarization to accelerate pacemaker activity in rabbit sinoatrial nodal cells. Circ Res. 2002;90(1):73–9.
66. Yaniv Y, Juhaszova M, Lyashkov AE, Spurgeon HA, Sollott SJ, Lakatta EG. Ca^{2+}-regulated-cAMP/PKA signaling in cardiac pacemaker cells links ATP supply to demand. J Mol Cell Cardiol. 2011;51(5):740–8.
67. Ju YK, Allen DG. Early effects of metabolic inhibition on intracellular Ca^{2+} in toad pacemaker cells: involvement of Ca^{2+} stores. Am J Physiol Heart Circ Physiol. 2003;284(4):H1087–94.
68. Covian R, Balaban RS. Cardiac mitochondrial matrix and respiratory complex protein phosphorylation. Am J Physiol Heart Circ Physiol. 2012;303(8):H940–H66.
69. Yaniv Y, Spurgeon HA, Lyashkov AE, Yang D, Ziman BD, Maltsev VA, et al. Crosstalk between mitochondrial and sarcoplasmic reticulum Ca^{2+} cycling modulates cardiac pacemaker cell automaticity. PLoS One. 2012;7(5):e37582.
70. Lang D, Glukhov AV. Functional microdomains in heart's pacemaker: a step beyond classical electrophysiology and remodeling. Front Physiol. 2018;9:1686.
71. Verkerk AO, van Borren MM, Peters RJ, Broekhuis E, Lam KY, Coronel R, et al. Single cells isolated from human sinoatrial node: action potentials and numerical reconstruction of pacemaker current. Conf Proc IEEE Eng Med Biol Soc. 2007;2007:904–7.
72. Tsutsui K, Monfredi O, Sirenko-Tagirova SG, Maltseva LA, Bychkov R, Kim MS, et al. A coupled-clock system drives the automaticity of human sinoatrial nodal pacemaker cells. Science signaling. 2018;11:eaap7608.
73. Tagirova S, Tsutsui K, Yang D, Ziman B, Tarasov KV, Yaniv Y, et al. Local calcium signals in pacemaker cells heart rate and body mass are self-similar from mice to humans. BioRxiv. 2021. https://www.biorxiv.org/content/10.1101/2020.10.26.355412v1
74. Wilders R, Jongsma HJ. Beating irregularity of single pacemaker cells isolated from the rabbit sinoatrial node. Biophys J. 1993;65(6):2601–13.
75. Yaniv Y, Maltsev VA, Escobar AL, Spurgeon HA, Ziman BD, Stern MD, et al. Beat-to-beat Ca^{2+}-dependent regulation of sinoatrial nodal pacemaker cell rate and rhythm. J Mol Cell Cardiol. 2011;51(6):902–5.
76. Yaniv Y, Stern MD, Lakatta EG, Maltsev VA. Mechanisms of beat-to-beat regulation of cardiac pacemaker cell function by Ca^{2+} cycling dynamics. Biophys J. 2013;105(7):1551–61.
77. Yaniv Y, Lyashkov AE, Sirenko S, Okamoto Y, Guiriba TR, Ziman BD, et al. Stochasticity intrinsic to coupled-clock mechanisms underlies beat-to-beat variability of spontaneous action potential firing in sinoatrial node pacemaker cells. J Mol Cell Cardiol. 2014;77:1–10.
78. Liu J, Sirenko S, Juhaszova M, Ziman B, Shetty V, Rain S, et al. A full range of mouse sinoatrial node AP firing rates requires protein kinase A-dependent calcium signaling. J Mol Cell Cardiol. 2011;51(5):730–9.
79. Liu J, Sirenko S, Juhaszova M, Sollott SJ, Shukla S, Yaniv Y, et al. Age-associated abnormalities of intrinsic automaticity of sinoatrial nodal cells are linked to deficient cAMP-PKA-Ca^{2+} signaling. Am J Physiol Heart Circ Physiol. 2014;306(10):H1385–97.
80. Yaniv Y, Ahmet I, Tsutsui K, Behar J, Moen JM, Okamoto Y, et al. Deterioration of autonomic neuronal receptor signaling and mechanisms intrinsic to heart pacemaker cells contribute to age-associated alterations in heart rate variability in vivo. Aging Cell. 2016;15(4):716–24.
81. Yang D, Lyashkov A, Morrell CH, Zahanich I, Yaniv Y, Vinogradova T, et al. Self-similar action potential cycle-to-cycle variability of Ca2+ and current oscillators in cardiac pacemaker cells. BioRxiv. 2021. https://www.biorxiv.org/content/10.1101/2020.09.01.277756v1.full
82. Kim MS, Maltsev AV, Monfredi O, Maltseva LA, Wirth A, Florio MC, et al. Heterogeneity of calcium clock functions in dormant, dysrhythmically and rhythmically firing single pacemaker cells isolated from SA node. Cell Calcium. 2018;74:168–79.
83. Musa H, Lei M, Honjo H, Jones SA, Dobrzynski H, Lancaster MK, et al. Heterogeneous expression of Ca^{2+} handling proteins in rabbit sinoatrial node. J Histochem Cytochem. 2002;50(3):311–24.
84. Honjo H, Boyett MR, Kodama I, Toyama J. Correlation between electrical activity and the size of rabbit sino-atrial node cells. J Physiol. 1996;496(Pt 3):795–808.
85. Monfredi O, Tsutsui K, Ziman B, Stern MD, Lakatta EG, Maltsev VA. Electrophysiological heterogeneity of pacemaker cells in the rabbit intercaval region, including the SA node: insights from recording multiple ion currents in each cell. Am J Physiol Heart Circ Physiol. 2018;314(3):H403–H14.
86. Boyett MR, Honjo H, Kodama I. The sinoatrial node, a heterogeneous pacemaker structure. Cardiovasc Res. 2000;47(4):658–87.

87. Zhang H, Holden AV, Boyett MR. Gradient model versus mosaic model of the sinoatrial node. Circulation. 2001;103(4):584–8.
88. Inokaitis H, Pauziene N, Rysevaite-Kyguoliene K, Pauza DH. Innervation of sinoatrial nodal cells in the rabbit. Ann Anat. 2016;205:113–21.
89. Quinn TA, Kohl P. Mechano-sensitivity of cardiac pacemaker function: pathophysiological relevance, experimental implications, and conceptual integration with other mechanisms of rhythmicity. Prog Biophys Mol Biol. 2012;110(2-3):257–68.
90. Iyer R, Monfredi O, Lavorato M, Terasaki M, Franzini-Armstrong C. Ultrastructure of primary pacemaking cells in rabbit sino-atrial node cells indicates limited sarcoplasmic reticulum content. FASEB Bioadv. 2020;2(2):106–15.
91. Bleeker WK, Mackaay AJ, Masson-Pevet M, Bouman LN, Becker AE. Functional and morphological organization of the rabbit sinus node. Circ Res. 1980;46(1):11–22.
92. Efimov IR, Nikolski VP, Salama G. Optical imaging of the heart. Circ Res. 2004;95(1):21–33.
93. Lang D, Petrov V, Lou Q, Osipov G, Efimov IR. Spatiotemporal control of heart rate in a rabbit heart. J Electrocardiol. 2011;44(6):626–34.
94. Li N, Hansen BJ, Csepe TA, Zhao J, Ignozzi AJ, Sul LV, et al. Redundant and diverse intranodal pacemakers and conduction pathways protect the human sinoatrial node from failure. Sci Transl Med. 2017;9(400)
95. Sano T, Sawanobori T, Adaniya H. Mechanism of rhythm determination among pacemaker cells of the mammalian sinus node. Am J Physiol. 1978;235(4): H379–84.
96. Winfree AT. Biological rhythms and the behavior of populations of coupled oscillators. J Theor Biol. 1967;16(1):15–42.
97. Jalife J. Mutual entrainment and electrical coupling as mechanisms for synchronous firing of rabbit sinoatrial pace-maker cells. J Physiol. 1984;356:221–43.
98. Michaels DC, Matyas EP, Jalife J. Mechanisms of sinoatrial pacemaker synchronization: a new hypothesis. Circ Res. 1987;61(5):704–14.
99. Anumonwo JM, Delmar M, Vinet A, Michaels DC, Jalife J. Phase resetting and entrainment of pacemaker activity in single sinus nodal cells. Circ Res. 1991;68(4):1138–53.
100. Schuessler RB, Boineau JP, Bromberg BI. Origin of the sinus impulse. J Cardiovasc Electrophysiol. 1996;7(3):263–74.
101. Verheijck EE, Wilders R, Joyner RW, Golod DA, Kumar R, Jongsma HJ, et al. Pacemaker synchronization of electrically coupled rabbit sinoatrial node cells. J Gen Physiol. 1998;111(1):95–112.
102. Neco P, Torrente AG, Mesirca P, Zorio E, Liu N, Priori SG, et al. Paradoxical effect of increased diastolic Ca^{2+} release and decreased sinoatrial node activity in a mouse model of catecholaminergic polymorphic ventricular tachycardia. Circulation. 2012;126(4):392–401.
103. Torrente AG, Zhang R, Zaini A, Giani JF, Kang J, Lamp ST, et al. Burst pacemaker activity of the sinoatrial node in sodium-calcium exchanger knockout mice. Proc Natl Acad Sci U S A. 2015;112(31): 9769–74.
104. Feldman JL, Kam K. Facing the challenge of mammalian neural microcircuits: taking a few breaths may help. J Physiol. 2015;593(1):3–23.
105. Lee MY, Ha SE, Park C, Park PJ, Fuchs R, Wei L, et al. Transcriptome of interstitial cells of Cajal reveals unique and selective gene signatures. PLoS One. 2017;12(4):e0176031.
106. Bru-Mercier G, Gullam JE, Thornton S, Blanks AM, Shmygol A. Characterization of the tissue-level Ca^{2+} signals in spontaneously contracting human myometrium. J Cell Mol Med. 2012;16(12): 2990–3000.
107. Hennis K, Biel M, Wahl-Schott C, Fenske S. Beyond pacemaking: HCN channels in sinoatrial node function. Prog Biophys Mol Biol. 2021;166:51–60.
108. Rosen MR, Robinson RB, Brink PR, Cohen IS. The road to biological pacing. Nat Rev. 2011;8(11): 656–66.
109. Cingolani E, Goldhaber JI, Marban E. Next-generation pacemakers: from small devices to biological pacemakers. Nat Rev. 2018;15(3):139–50.
110. Kapoor N, Liang W, Marbán E, Cho HC. Direct conversion of quiescent cardiomyocytes to pacemaker cells by expression of Tbx18. Nat Biotechnol. 2013;31(1):54–62.

6

Unique Features of the Human Sinoatrial Node Structure, Function, and Arrhythmias: Mechanistic Insights from Integrated 3D Mapping Approaches

Anuradha Kalyanasundaram, Ning Li, and Vadim V. Fedorov

Abstract

The sinoatrial node (SAN) is the primary pacemaker in mammalian hearts, which generates intrinsic electrical activation to maintain synchronous and rhythmic contractility of the heart. Impairments in SAN structure and function lead to cardiac dysfunction manifesting as tachy-/brady arrhythmias, conduction impediments, and rhythm failure. Identifying and treating SAN dysfunctions requires an in-depth understanding of the complex 3D human SAN structure and function, which has been possible in recent years with the advent of integrated high-resolution 3D mapping techniques. While general electrical activation properties of the SAN have been accepted to be similar across species, recent studies reveal that the human SAN pacemaker-conduction complex may be unique in both structural and electrophysiological aspects required to maintain pacemaking and conduction. The human SAN possesses a compact 3D architecture, unlike the 2D structure of other small mammalian SAN, and is characterized by pacemaker myocytes, fibroblasts, and multiple other cell types enmeshed within a fibrotic extracellular matrix. This structure is further compartmentalized into head, central, and tail compartments characterized by heterogeneous ion channels and proteins necessary to maintain pacemaking and conduction. Furthermore, recent findings utilizing high-resolution near-infrared optical mapping (NIOM) to investigate the 3D human SAN have revealed the existence of several distinct sinoatrial conduction pathways (SACP), which deliver electrical activation from the SAN to the atrial myocardium. NIOM has also revealed several mechanisms involving novel protein targets that contribute to maintaining robust pacemaking and conduction during physiological conditions and dedicated mechanisms that function as backup systems recruited specifically during pathophysiological conditions to prevent SAN arrhythmia and rhythm failure. Furthermore, the altered protein composition of the SAN extracellular matrix (ECM), including the appearance of periostin and increasing intranodal fibrosis, may also contribute to rhythm and conduction abnormalities leading to SAN arrhythmias in failing hearts. Integrated studies in ex vivo human hearts have also greatly expanded our understanding of how cardiac diseases including heart failure,

---

A. Kalyanasundaram · N. Li · V. V. Fedorov (✉)
Department of Physiology and Cell Biology, The Ohio State University Wexner Medical Center, Columbus, OH, USA

Bob and Corrine Frick Center for Heart Failure and Arrhythmia, The Ohio State University Wexner Medical Center, Columbus, OH, USA

Davis Heart and Lung Research Institute, The Ohio State University Wexner Medical Center, Columbus, OH, USA
e-mail: vadim.fedorov@osumc.edu

© Springer Nature Switzerland AG 2023

O. N. Tripathi et al. (eds.), *Heart Rate and Rhythm*, https://doi.org/10.1007/978-3-031-33588-4_6

diabetes, and ischemic cardiomyopathy impact human SAN structure and function, resulting in contractile impairments and arrhythmias. This chapter will discuss many of these unique structural and functional features of the human SAN in the context of both physiological and pathophysiological conditions. We will also present novel perspectives from high-throughput sequencing RNA and proteomics datasets that can identify novel RNA and protein targets and pharmaceutical interventions that can be considered for treating SAN dysfunction and arrhythmias.

Keywords

Near-infrared optical mapping · SAN compartmentation · Conduction pathways · Connexins · Molecular landscape · SAN extracellular matrix · Periostin · Heart failure · Diabetes · Ischemic cardiomyopathy

6.1 Structure and Anatomy of the Mammalian Sinoatrial Node

The SAN is a complex, multi-compartmental structure composed of small clusters of pacemaker myocytes arranged in parallel rows that frequently anastomose [1–4]. It is located at the junction of the superior vena cava and the right atrium. Unlike in small animals, including mouse, the human, and canine SAN structures are complex and more compact, composed of distinct compartments and located at an intramural depth of ~1–3 mm (Fig. 6.1). The mouse SAN [5, 6] is primarily a 2D structure ~0.6–0.9 mm long and ~0.2–0.5 mm wide while the human and canine SAN are 3D structures ~12–29 mm long, ~2–6 mm wide, 1–3 mm deep, banana-shaped structure [3, 5]. The human SAN 3-dimensional (3D) structure is normally tilted such that the SAN head (superior third) is subepicardial while the SAN tail (inferior third) is more subendocardial. The human SAN is centered on the SAN artery, which is an important anatomical landmark of the SAN complex [1–3]. The SAN artery arises from the right coronary artery in 55% of humans, or from the left circumflex artery in the other 45%. In contrast, SAN arteries in canine arise primarily from the right coronary artery and run along the SAN borders rather than within the SAN. Mammalian SAN is composed of not only pacemaker cardiomyocytes but also other multiple cell types including fibroblasts, endothelial cells, immune cells, neurons and adipose cells [1, 2, 6]. SAN pacemaker cells are striated similar to other cardiomyocytes; however, they are typically skinny, long [7], and twisted with other cells into small clusters. These clusters of specialized pacemaker cardiomyocytes are enmeshed and electrically insulated within strands of dense connective tissue, nerve fibers, and capillaries to create a distinct SAN pacemaker complex [1–4]. These specialized SAN pacemaker cell clusters serve as leading pacemakers that initiate electrical activation. Based on canine and human functional-structural mapping studies, three intranodal pacemaker compartments have been defined [4, 5, 8], the superior third of the SAN as the head, the middle third as the center, and the inferior third as the tail intranodal pacemaker regions (Fig. 6.1). The location of the leading pacemaker is primarily detected within the central SAN compartment of human or canine SAN; however, optical mapping studies clearly show that the leading pacemaker can shift to either the head or tail compartments in response to many stimuli including autonomic triggers [4, 9, 10]. For instance, in mouse SAN, isoproterenol can accelerate sinus rhythm and cause a superior intranodal shift of the leading pacemaker, while acetylcholine causes inferior shifts and slowed rhythm (Fig. 6.1c). Similarly, adenosine has been shown to slow sinus rhythm and shift leading pacemakers from the central to either head or tail compartments. In canine SAN, adenosine-induced inferior pacemaker shifts inside the SAN complex [8] while in human SAN, it could shift pacemaker locations in both superior and inferior directions [4].

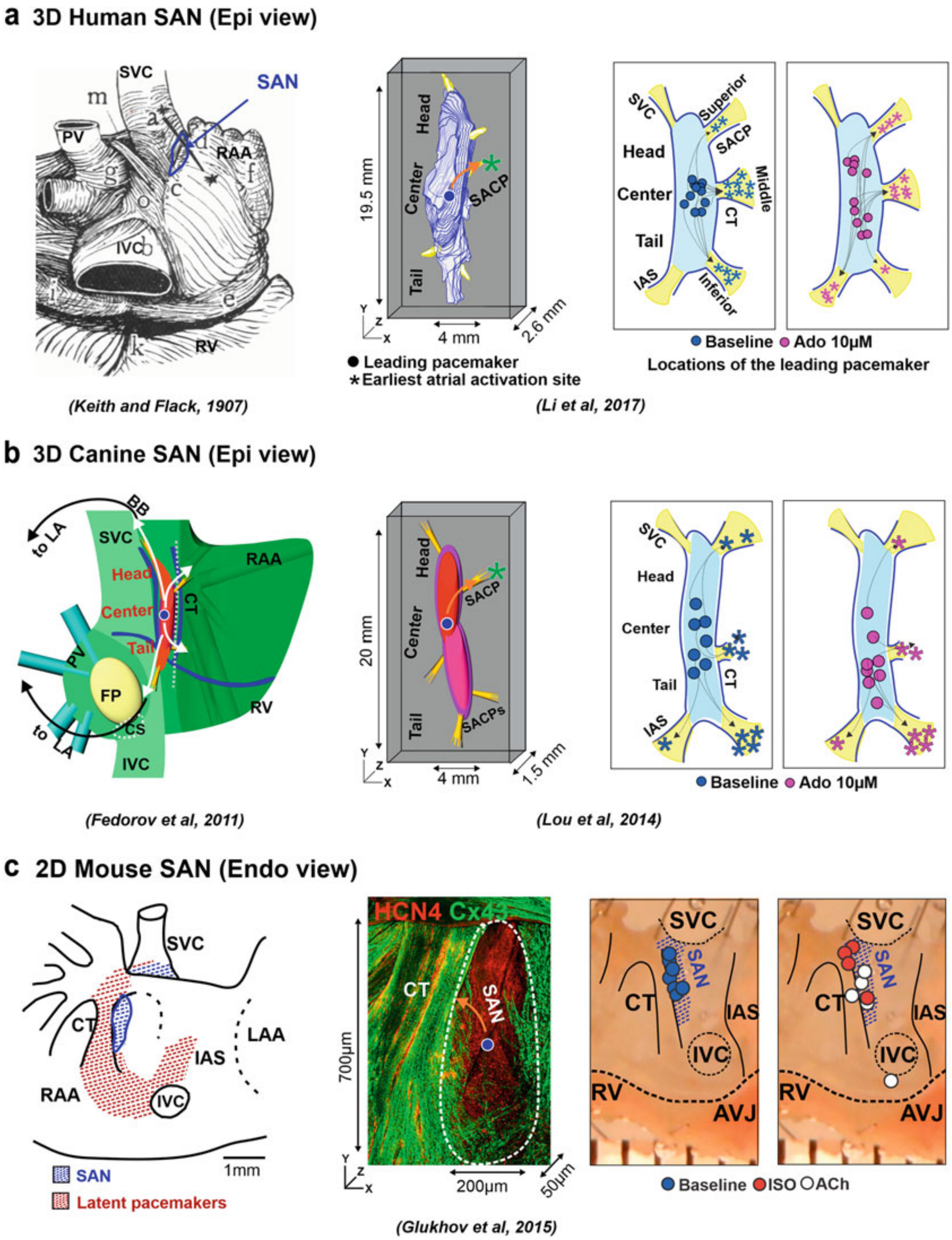
a 3D Human SAN (Epi view)
SVC
SAN
m
PV
a
d
RAA
g
c
f
o
IVC
b
i
e
k
RV
(Keith and Flack, 1907)
19.5 mm
Head
Center
Tail
SACP
4 mm
2.6 mm
Y
Z
X
● Leading pacemaker
* Earliest atrial activation site
SVC
Superior
SACP
Head
Center
Middle
CT
Tail
IAS
Inferior
● Baseline ● Ado 10μM
Locations of the leading pacemaker
(Li et al, 2017)
b 3D Canine SAN (Epi view)
BB
to LA
SVC
Head
Center
Tail
CT
RAA
PV
FP
CS
to LA
IVC
RV
(Fedorov et al, 2011)
20 mm
Head
Center
Tail
SACP
SACPs
4 mm
1.5 mm
Y
Z
X
SVC
Head
Center
Tail
CT
IAS
● Baseline ● Ado 10μM
(Lou et al, 2014)
c 2D Mouse SAN (Endo view)
SVC
CT
LAA
IAS
RAA
IVC
1mm
▨ SAN
▨ Latent pacemakers
HCN4 Cx43
CT
SAN
700μm
200μm
50μm
Y
Z
X
SVC
SAN
CT
IAS
IVC
RV
AVJ
SVC
SAN
CT
IAS
IVC
RV
AVJ
● Baseline ● ISO ○ ACh
(Glukhov et al, 2015)

Fig. 6.1 3D structure of SAN pacemaker complex. (**a**–**c**) Anatomical view of the Human, Canine, and Mouse SAN pacemaker complex, respectively. Panels show 3D human and canine and 2D mouse SAN structure and locations of the leading pacemaker at baseline and in response to adenosine (Ado) or isoproterenol (Iso) and acetylcholine (ACh). BB, Bachmann's bundle; Cx43, connexin 43; CS, coronary sinus; CT, crista terminalis; Endo, endocardium; Epi, epicardium; FP, fat pad; IAS, interatrial septum; HCN4, hyperpolarization-activated channel 4; IVC, inferior vena cava; LA, left atria; PV, pulmonary veins; RAA, right atrial appendage; RV, right ventricle; SACP, sinoatrial conduction pathway; SAN, sinoatrial node; SVC, superior vena cava (data modified from Human: Keith and Flack [49]; Li et al. [4]; Canine: Fedorov et al. [10]; Lou et al. [5]. Mouse: Glukhov et al. [56])

6.2 The Redundant and Robust Human SAN Complex: Intranodal Leading Pacemaker and Conduction in the Human SAN Revealed by Near-Infrared Optical Mapping Ex Vivo

The first important steps in the investigation of SAN excitation and conduction were made by microelectrode studies in small mammalian hearts including rabbit SAN [11]. However, the SAN in small mammals, such as rabbit or mouse, are essentially two-dimensional 2D structures [11, 12], raising concerns about its relevance to the 3D structure of the human [1, 13] SAN, where it is practically impossible to utilize the same microelectrode techniques. Despite numerous detailed direct microelectrode studies of the leading pacemaker and conduction in the SAN of many animal species, only indirect measurements of SAN conduction have been recorded in humans until recently [4, 14].

Both surface epicardial [13] or endocardial [15–17] and recent epi-endo multielectrode mapping studies [18] have demonstrated anatomically widespread but discreet sites of earliest atrial activation (EAS) during sinus rhythm (SR) and postpacing recovery (Fig. 6.1). Furthermore, even multifocal atrial activation started simultaneously during normal SR in humans in 2–5 EASs located >1 cm apart which suggest dynamic changes in leading pacemaker sites and preferential sinoatrial conduction pathways (SACPs).

Pioneering studies of atrial epicardial multielectrode mapping in canine and humans by the Schuessler and Boineau groups reported that EAS or atrial breakthroughs over a region of 7.5 cm along the CT [13, 16] as that region is significantly larger than the length of the human anatomical SAN body (11–29 mm) [1, 19] two possible mechanisms were suggested. The first mechanism proposed that the multifocal activity of atria may be caused by a widely distributed system of pacemaker clusters, which may have similar pacemaker cycle length. The alternative mechanism proposed the existence of “...a unique form of specialized conduction within the intramural layers of the crista terminalis...” which can potentially deliver depolarization waves simultaneously to the different areas of atrial myocardium. However, due to the inability of surface electrode recordings to define intramural activation within SAN pacemaker structure, the role of multiple intranodal SAN pacemakers and SACPs in the robust regulation of human SR and how this system fails, leading to SAN dysfunction (SND) remained an enigma in the human heart until recent developments in 3D optical mapping with voltage-sensitive dyes [20], particularly with the nontoxic near-infrared dye di-4-ANBDQBS [21] or NIOM (Fig. 6.2) [3, 4].

NIOM is currently the only reliable method to delineate activation and conduction within the intramural human [4, 14] or canine [5] SAN complex that is obscured to clinical surface electrode mapping by the surrounding atrial fat and fibrotic tissues (Fig. 6.2). Importantly, Optical action potentials (OAPs) recorded with near-infrared shifted voltage-sensitive dyes represent a weighted average of transmembrane potentials through fluorescent signals from myocardium reaching a depth of several millimeters [22]. As such, SAN OAPs have specific morphological criteria: slow diastolic depolarization and upstrokes with multiple components corresponding to activation in SAN and atrial tissue layers [20] (Fig. 6.2). Analytical approaches allow the separation [20] and/or the extraction [8] of the slow SAN upstroke components from the fast atrial activation and resolves subsurface intramural SAN conduction separately from epicardial and/or endocardial atrial activation [5, 23]. Figure 6.2 shows SAN activation patterns and OAPs recorded in human, canine, rabbit, and mouse atria during baseline SR. In our recent NIOM studies, at baseline, all coronary-perfused human hearts exhibited stable intrinsic sinus rhythm (55–101 bpm) with cycle length 819 ± 173 ms, which are within the range of “intrinsic” rates measured during autonomic blockade with propranolol and atropine from adult human subjects with diseased hearts (range 57–126 bpm) [24] and for healthy patients (69–128 bpm) [25]. Figure 6.2 (top panel)

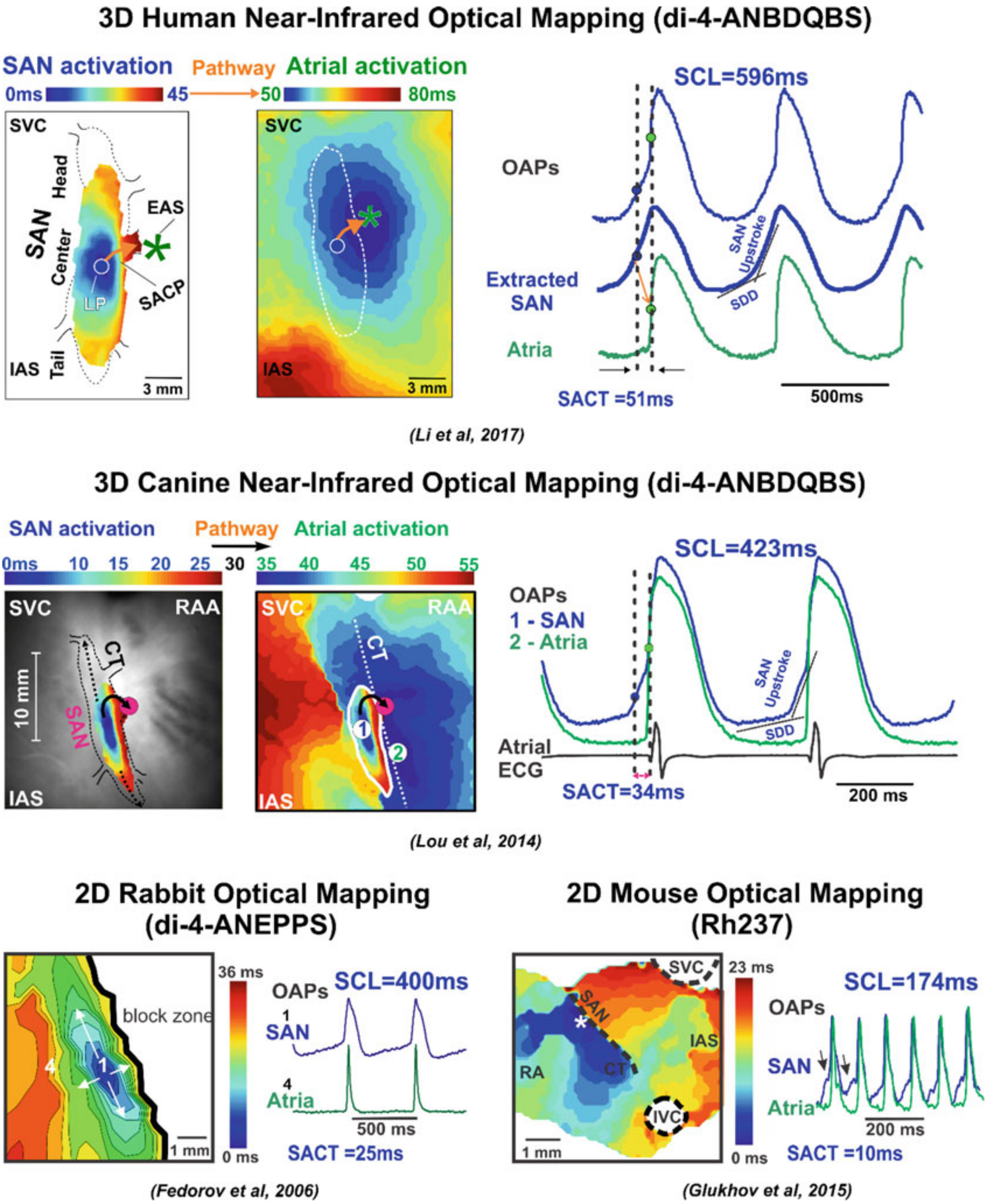

Fig. 6.2 Activation maps and optical action potentials recorded from ex vivo optical mapping experiments. Optical action potentials (OAPs) from the SAN exhibit the slow diastolic depolarization (SDD), slowly rising upstroke of the SAN (SAN component), and rapidly rising upstroke of the atrial myocardium (atrial component). SAN activation time (SACT) is the delay between SAN and earliest atrial activation. CT, crista terminalis; IAS, interatrial septum; RAA, right atrial appendage; RAFW, right atrial free wall; SACP, sinoatrial conduction pathway; SVC, superior vena cava (data modified from Human: Li et al. [4]; Canine: Lou et al. [8]; Rabbit: Fedorov et al. [12]; and Mouse: Glukhov et al. [56])

shows an example of NIOM of the explanted coronary-perfused human SAN during stable SR [4]. SAN activation originated from the leading pacemaker in the SAN center-tail region, preferentially propagated superiorly, and exited the SAN through the lateral SACP to excite the atria in the superior CT after 58 ± 35 ms by direct SACT measurement [4]. While additional septal and inferior lateral SACPs were also observed, the superior lateral SACP and corresponding atrial breakthrough was the primary excitation pattern during normal SR, which is consistent with previous clinical and experimental observations [21, 26]. Human and canine intranodal SAN conduction velocities, ranging from 1 to 16 cm/s [3, 14], are significantly slower compared to CT and right atrial conduction (70–160 cm/s). Similar significant differences between SAN and RA conduction persist across all properly mapped mammalian species including rabbit and mouse.

6.3 SAN Conduction Pathways

Studies using small animal models have proposed a long-held multifocal hypothesis that SAN excitation is delivered to the atrial myocardium by a widely distributed system of pacemakers. However, recent canine and human studies have clarified that distinct SACPs structurally and functionally connect the SAN with the atria. SACPs were functionally identified in NIOM experiments as the preferential conduction path between the SAN border and the EAS, which could only be defined using SAN and atrial activation maps (Fig. 6.3). Intramural NIOM mapping studies [4, 20] revealed that the SAN is functionally insulated from the atria except for the two to five discrete SACPs, which transmit electrical impulses to the atrial myocardium and correspond to the discrete EAS. Recent clinical simultaneous epi-endo Multi-electrode mapping (MEM) mapping studies by Kalman and Sanders group [18] confirmed these ex vivo observations in patients with structural heart disease. SACPs are identified based on their general anatomic locations (lateral superior/middle/inferior, superior vena cava, and septal pathways) (Fig. 6.1). During normal sinus rhythm, excitation originating in one of the pacemaker compartments, and the excitation is preferentially delivered to the atria via either superior or inferior SACPs resulting in atrial activation. An intranodal leading pacemaker could activate one or more preferential SACPs simultaneously [10]. It could also be possible that two distinct SACPs are present in the same anatomic region. The same SACP may serve for both exit and entrance conduction or preferentially serve as an exit SACP (lateral pathways) or an entrance SACP (superior vena cava and septal pathways) [9, 10]. In the human SAN pacemaker complex, 3–5 SACPs are formed by 200–400 μm thick branching myofiber tracts, providing discrete, insulated, and continuous electrical connections between the SAN pacemakers and atria. Similar to intranodal pacemaker shifts, perfusion with isoproterenol and acetylcholine also generally results in preferential use of superior and inferior SACPs, respectively. This could be due to the intranodal pacemaker shifts and/or different conduction properties and sensitivities to autonomic stimulations including adenosine. Integrated mapping studies of ex vivo human hearts have revealed the existence of redundant pacemakers that were specifically revealed in response to the adenosine challenge. These data suggest that there may be more SACPs, which could be revealed under different conditions. As discussed later, such redundancies in available SACPs may exist to maintain conduction when disease-induced stress may suppress some pathways.

New clinical epi-endo multielectrode mapping studies of patients with cardiac diseases and AF from two independent groups, de Groot [27] and Kalman [18], confirmed ex vivo NIOM observations of several discrete SACPs: Variations in activation patterns of the SAN observed in these studies highlight the complex three-dimensional SAN-atria geometry and indicate the presence of inter-individual differences in SACPs. During intra-operative Electrophysiological (EP) studies, the de Groot group found in patients with a history of AF, EASs during activity occurred more caudally compared to cranial

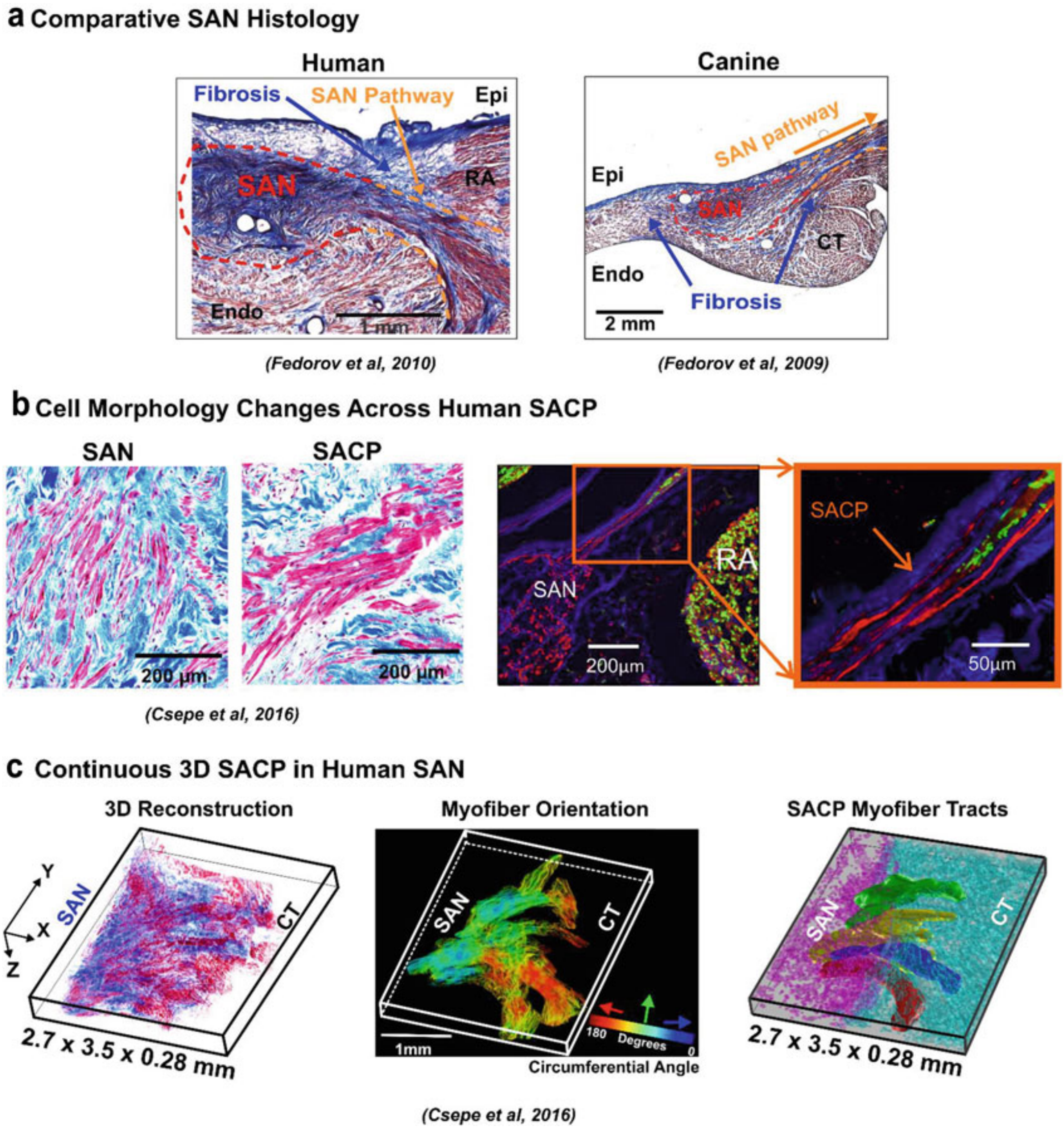
a Comparative SAN Histology
Human
Fibrosis
SAN Pathway
Epi
SAN
RA
Endo
1 mm
(Fedorov et al, 2010)
Canine
SAN pathway
Epi
SAN
CT
Endo
Fibrosis
2 mm
(Fedorov et al, 2009)
b Cell Morphology Changes Across Human SACP
SAN
SACP
200 μm
200 μm
(Csepe et al, 2016)
SAN
RA
200μm
SACP
50μm
c Continuous 3D SACP in Human SAN
3D Reconstruction
Y
X
Z
SAN
CT
2.7 x 3.5 x 0.28 mm
Myofiber Orientation
SAN
CT
1mm
180 Degrees 0
Circumferential Angle
SACP Myofiber Tracts
SAN
CT
2.7 x 3.5 x 0.28 mm
(Csepe et al, 2016)

Fig. 6.3 Structure and morphology of the SAN-SACPs. (**a**) Masson's Trichrome stained SAN from human and canine, identifying the SAN and SACP. (**b**) Cell morphology and protein expression (red-αActinin and green-connexin 43) transitions across the SACP and (**c**) 3D reconstruction of SACP showing myofiber orientation and tracts continuing into the atrial myocardium (data modified from (**a**) Fedorov et al. [9], Fedorov et al. [20]; (**b**, **c**) Csepe et al. [3])

EASs in non-AF patients, which indicates disease-induced changes in preferential SACPs [27]. Kalman group, during simultaneous endo-epi mapping of the SAN regions, also confirmed redundancy of EAS or SACPs with postoverdrive shift in EAS and epi-endo dissociation of SAN EAS.

Reconstruction of serial high-resolution histology sections of optically mapped SANs allowed defining structural features of the functionally identified SACPs [3]. In nondiseased hearts, several discrete branching myofiber tracts are found to form the SACP structure, resulting in continuous, uninterrupted physical connections between the SAN and atria. Microstructural analyses further reveal a smooth transition along these tracts of increasing cell diameter (Fig. 6.3b) from SAN to atria in selected SACP regions, unlike the abrupt increase in non-SACP regions. Structural studies of the human SAN also show continuous myofibers of similar orientation coalescing into several tracts crossing the SAN border, creating continuous physical connections between the SAN and atria. 3D analysis with a novel fiber-tracking approach (Fig. 6.3c) showed continuous myofibers in functional SACP but discontinuous myofibers in nonfunctional SACPs, which can lead to exit blocks and SND. Furthermore, immunolabeling for connexin 43 (Cx43), a gap junction protein, showed a progressive transition from Cx43 negative SAN pacemaker cells to intermediate expression in the SACP region and high Cx43 gap junction expression in the atria (Fig. 6.3). This continuous myofibrillar structure of the SACP is hypothesized to support the normal function of the SAN by maintaining the source-sink relationship between the SAN leading pacemaker and atria. The SAN is a relatively weak source of current since the pacemaker cell clusters are small and rely on a relatively weak action potential, while the atrial cells are much larger with a more negative resting potential. This apparent source-sink mismatch may be overcome by the specialized branching myofiber structure of SACPs. The slow conduction through branching myofiber tracts of SACPs with weak Cx43 expression is also suggested to allow the SAN enough time to build up a sufficient charge to excite the large atria in both canine and human SAN [3].

In contrast to human and canine SAN 3D SAN structure, such distinct pathways that conduct SAN excitation have not been identified in small animal models such as mouse and rabbit. In mouse [28], a complex interface between the SAN and surrounding atrial muscle has been suggested, which may be important for conducting the action potential from the SAN to the atria. Such structural differences between large and small SANs can potentially be due to the smaller surrounding atria and the simpler 2D-like SAN pacemaker structures, which may not require sophisticated specialized pathways to conduct activation from the SAN.

6.4 Molecular Profiling of the SAN

The SAN complex is distinguished from the surrounding atria by a unique composition of ion channels and Ca^{2+}-handling proteins, which maintain SAN pacemaker automaticity and conduction (Fig. 6.4). In keeping with the intranodal shifts of the leading pacemaker, recent findings show that the expression and composition of ion channels and receptors vary between SAN compartments [4, 14]. This variation allows each compartment to respond differently to metabolic and pathologic stimuli, which is functionally critical in preventing complete SAN arrest. SAN pacemaker cells exhibit a characteristic slow diastolic depolarization which leads to the spontaneous generation of the SAN pacemaker action potential driven by both membrane and Ca^{2+} clock components [29]. Importantly, central SAN pacemaker cells lack the fast Na^{+} current I_{Na} responsible for the fast depolarization and conduction in atrial and ventricular cells. Instead, SAN conduction is very slow [11, 20, 21] as action potential upstroke is generated by small, slow Ca^{2+} current $I_{Ca,L}$ [30] which is modulated by sympathetic and parasympathetic stimulation. The membrane voltage clock is driven by the hyperpolarization-activated funny current (I_f), whose molecular alpha-subunits are represented by hyperpolarization-activated cyclic nucleotide-gated channels (HCN1, HCN2, and HCN4). Synergistically, the Ca^{2+} clock contributes to SAN diastolic depolarization by activating the Na^{+}/Ca^{2+} exchanger current through spontaneous localized Ca^{2+} release from the sarcoplasmic reticulum via type 2 ryanodine receptors.

The SAN complex has a unique expression of gap junction proteins [31], which contributes to slow intranodal conduction. Unlike the atrial working myocardium, the SAN lacks high

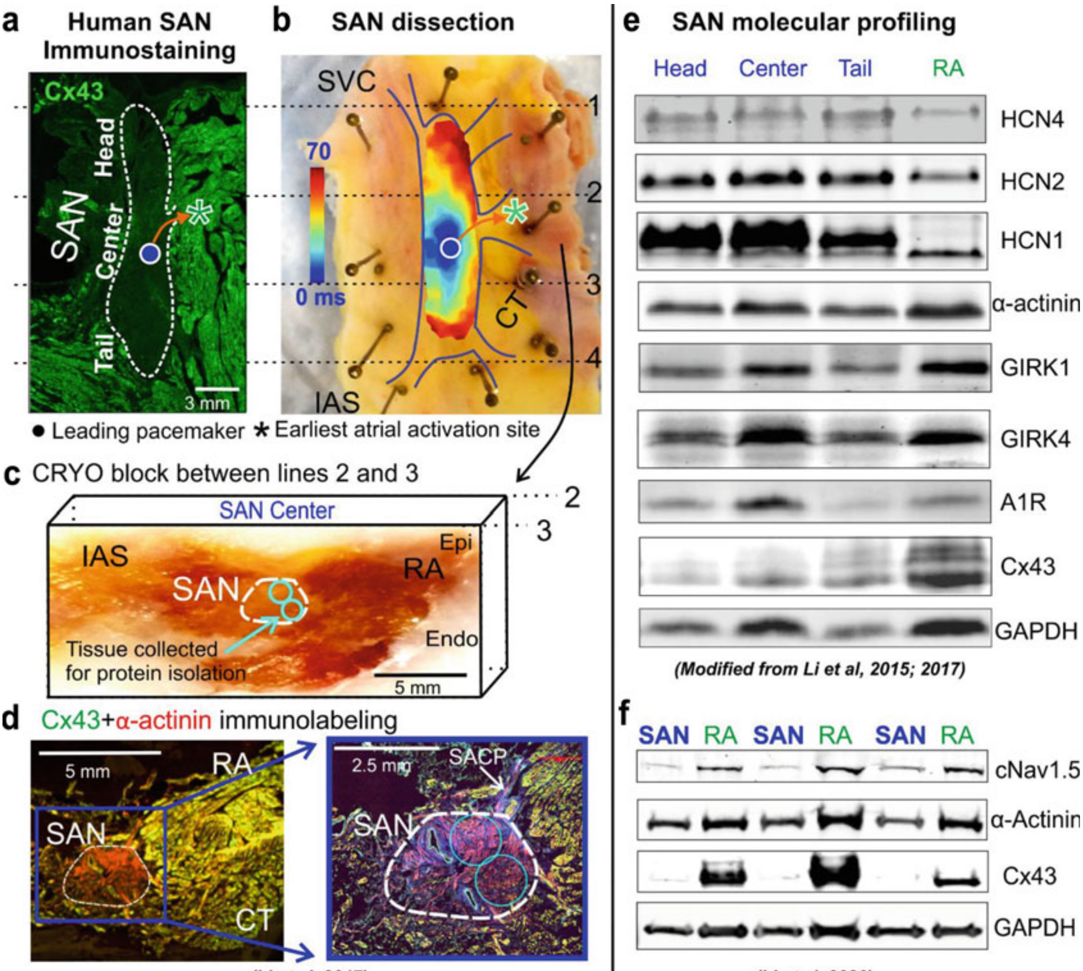
a Human SAN Immunostaining
Cx43
SAN
Head
Center
Tail
3 mm
b SAN dissection
SVC
70
0 ms
CT
IAS
1
2
3
4
● Leading pacemaker * Earliest atrial activation site
c CRYO block between lines 2 and 3
SAN Center
IAS
SAN
RA
Epi
Endo
Tissue collected for protein isolation
5 mm
2
3
d Cx43+α-actinin immunolabeling
5 mm
RA
SAN
CT
2.5 mm
SACP
SAN
e SAN molecular profiling
Head
Center
Tail
RA
HCN4
HCN2
HCN1
α-actinin
GIRK1
GIRK4
A1R
Cx43
GAPDH
f
SAN
RA
SAN
RA
SAN
RA
cNav1.5
α-Actinin
Cx43
GAPDH

(Modified from Li et al, 2015; 2017)

(Li et al, 2017)

(Li et al, 2020)

Fig. 6.4 Molecular profile of the human SAN pacemaker complex. (**a**) Immunostaining defines borders in human SAN based on connexin43 (Cx43) negativity in SAN and high Cx43 expression in atrial myocardium. (**b**) Representative photograph of the human SAN tissue superimposed with the intramural activation map showing the direction of activation from the leading pacemaker (blue circle) in the central compartment and exiting from the mid-lateral SACP and the demarcations of the head, center, and tail compartments dissected for molecular studies. (**c**) Transmural CRYO block of SAN tissue through line #3 (from panel **b**) indicates the exact location of SAN and RA tissues (blue circles) that were micro-dissected using biopsy needles for molecular studies. (**d**) CRYO sections of the SAN were used to identify the exact locations of the SAN (blue circles also shown in **c**) and SACPs by immunostaining for Cx43 and α-actinin. (**e**, **f**) Representative immunoblotting images of various proteins examined: (**e**) SAN head, center, and tail compartments and RA from the same heart and (**f**) SAN center and RA from three different human hearts. A1R, adenosine A1 receptor; CT, crista terminalis; GAPDH, glyceraldehyde 3-phosphate dehydrogenase; HCN, hyperpolarization-activated cyclic nucleotide-gated ion channel; IAS, interatrial septum; IVC, inferior vena cava; cNav1.5, cardiac isoform of sodium channel 1.5; RA, right atrium; SACP, sinoatrial conduction pathway; SAN, sinoatrial node; SVC, superior vena cava (data modified from **a**–**d**, Li et al. [4]; (**e**) Li et al. [33] and Li et al. [4]; (**f**) Li et al. [14])

conductance gap junction proteins Cx43 and Cx40, responsible for myocardial electrical coupling, but expresses Cx45, a low conductance connexin that provides weak electrical coupling. In fact, the specialized SAN structure, connexin distribution, and combination of other ion channels that contribute to SAN automaticity are often used as molecular markers to distinguish the SAN from surrounding atrial tissue [7, 32] (Fig. 6.4a). A recent molecular mapping study [33] of HCN isoform distribution in the human heart revealed that HCN1 was found to be exclusively expressed in the SAN pacemaker compartment, which can also be used as a new specific molecular marker of the human SAN.

In keeping with the shifting locations of the leading pacemaker, studies show that protein expression can vary significantly across different compartments of the SAN (head vs. center vs. tail). These unique compartment-specific ratios are known to predetermine the leading pacemaker locations [4, 5, 33]. The adenosine receptor (A1R) mediated pathway, along with its downstream components, the G-protein-coupled inward rectifying potassium channel ($_{\mathrm{IK.Ado/ACh}}$) subunits, GIRK1 and GIRK4 [34, 35], impacts human SAN [36] function via its heterogeneous expression pattern across the SAN. Adenosine, an endogenous metabolite of the heart [37], has been shown to directly affect SAN function through negative chronotropic depression, especially in patients with SND. It is known to cause excessive bradycardic response and atrial pauses (2–23 s) in response to adenosine bolus [38, 39]. Recent NIOM studies [4] have revealed heterogenous adenosine-induced inhibition of pacemaking and conduction across the human SAN complex. The central intranodal pacemaker compartment consistently demonstrates a high sensitivity to adenosine and a profound bradycardic response compared to the other intranodal pacemakers [4], which corresponds to high expression of A1R and GIRK4 in the central compartment than in the head and tail regions. As shown in Fig. 6.1, in addition to defining pacemaker locations, the differential expression patterns of A1R and GIRK4 subunits also define sensitivity to adenosine. Hence, while regions such as the central compartment may be depressed due to higher sensitivity to adenosine, other compartments may still be functional due to lower expression of A1R and function as backup pacemakers.

Voltage-gated sodium channels (Nav) are major contributors to cardiac and neuronal excitability; however, their contributions have remained controversial in human SAN pacemaking and conduction. Studies from animal models have shown that the expression of cardiac isoform (cNav) Nav 1.5 is significantly lower in the SAN versus atria [40, 41]. However, loss-of-function mutations in the *SCN5A* gene [42] (encodes cNav1.5 α-subunit) are found in some symptomatic SND patients suggesting that the voltage-gated I_{Na} may also be required for human SAN function. Recent studies [14] in ex vivo human hearts show that cNav as well as neuronal isoforms (nNav), are heterogeneously expressed within the human SAN and they perform isoform-specific distinct functions. The study [14] showed that cNav might be important for both SAN pacemaking and conduction, especially during conditions of metabolic or pacing-induced stress, while cNav1.5 was found to be highly expressed in the atria relative to the SAN (Fig. 6.4f). In contrast, nNav1.6 was highly expressed in the SAN relative to the atria, which were recruited specifically to preserve intranodal conduction and to prevent SAN exit blocks. Interestingly, diseases including heart failure, hypertrophy, and life-style factors including alcohol consumption can alter nNav expression in human SAN, which could lead to SAN arrhythmias.

6.5 Advanced Insights from High-Throughput Sequencing into the Cellular and Molecular Landscape of the SAN

Studies at the cellular and molecular levels in the SAN have always been challenging. The main hurdles have been identifying and delineating the SAN and the technical ability to dissect the SAN with minimal atrial contamination for further analyses including cell isolation and molecular studies. Recent studies have made tremendous progress in characterizing the transcriptomic signatures of SAN cells using animal models as well as in human SAN. Precise dissection techniques including laser capture micro-dissection have aided in accurately collecting pure SAN tissue even from mouse hearts [43]. The human SAN has also been accurately dissected and used to quantify connective tissue content and identify expression patterns of SAN-specific proteins and RNA levels in nondiseased and heart failure (HF) hearts (Fig. 6.4). Similarly, high-throughput large-scale analyses including RNA sequencing have been used to identify and characterize the unique molecular signature of SAN tissue which has not been possible previously. Transcriptomic studies have revealed SAN enriched developmental gene programs including TBX3, SHOX2, ISL1 and HOX family members are evolutionarily conserved between human and mouse [44]. Goodyer et al. [45] used single-cell RNA sequencing to identify gene signatures across the developing conduction system and specifically showed that the head and tail compartments of the mouse SAN reveal different gene signatures. Large-scale high-throughput omics studies have also been able to provide insights into the functional parameters of the SAN. Linscheid et al. [46] combined proteomics and single-nucleus RNA sequencing and identified significant differences in ion channels responsible for the membrane clock in mouse SAN but not in Ca^{2+} clock proteins and suggested that the membrane clock underpins pacemaking in the mouse SAN. Liang et al. [47] conducted single-cell RNA sequencing of the mouse SAN and identified four distinct cell clusters, which revealed novel insights into the cellular composition of the SAN. Their results revealed that Cluster 1 highly expressed genes involved in calcium ion transport, regulation of heart rate, and membrane depolarization of SAN cells. Cluster 2 and Cluster 3 also revealed enrichment of genes associated with cell adhesion and extracellular matrix organization, respectively. Cluster 4 was shown to highly express classical markers of pacemaker cells and the basic electrogenic genes involved in SAN pacemaker activity including ion channels, transporters, calcium regulators, and autonomic nerve signaling. More recently, Kalyanasundaram et al. [48] have studied SAN fibroblasts isolated from nonfailing and HF human hearts. They used high-resolution studies to generate a comprehensive atlas of proteomic and whole transcriptomic signatures of SAN fibroblasts, which suggest increased SAN fibrosis and stiffer SAN ECM composition in human HF. These large-scale, fibroblast-specific datasets have not only offered previously unknown molecular insights into human SAN connective tissue content as well as disease-induced structural remodeling but have also introduced new human SAN cellular models that can effectively be utilized to study SAN fibrosis and its role in SND (Figs. 6.5 and 6.7).

6.6 Unique Structure and Functional Role of the Human SAN Extracellular Matrix

The SAN is characterized by high levels of dense connective tissue [49, 50], which has been used as a landmark to identify the SAN (Fig. 6.5). Traditionally, connective tissue content within the SAN is quantified using standard histological methods including Masson's trichrome staining. In recent years, contrast-enhanced cardiovascular magnetic resonance (CE-CMR) has advanced the field by accurately quantifying fibrotic content, which has also helped identify the human 3D SAN structure in vivo and ex vivo. These high-resolution imaging techniques have opened new avenues to study the structure and contribution of the 3D collagenous matrix to the human SAN function in normal and diseased hearts. The normal adult SAN structure consists of dense 40–55% fibrotic connective tissue, which creates a honeycomb-like matrix mostly composed of collagen sheaths [50, 51]. This fibrotic content has been found to increase within the SAN in aging and diseased hearts [50].

The fibrotic scaffolding houses the specialized SAN myocytes and provides mechanical protection to the SAN. Biomechanical properties of the porcine SAN [52] showed that the SAN ECM is stiffer than in the ventricle and composed of fibrillar collagens, which can withstand high tensile strength along with regions rich in elastin,

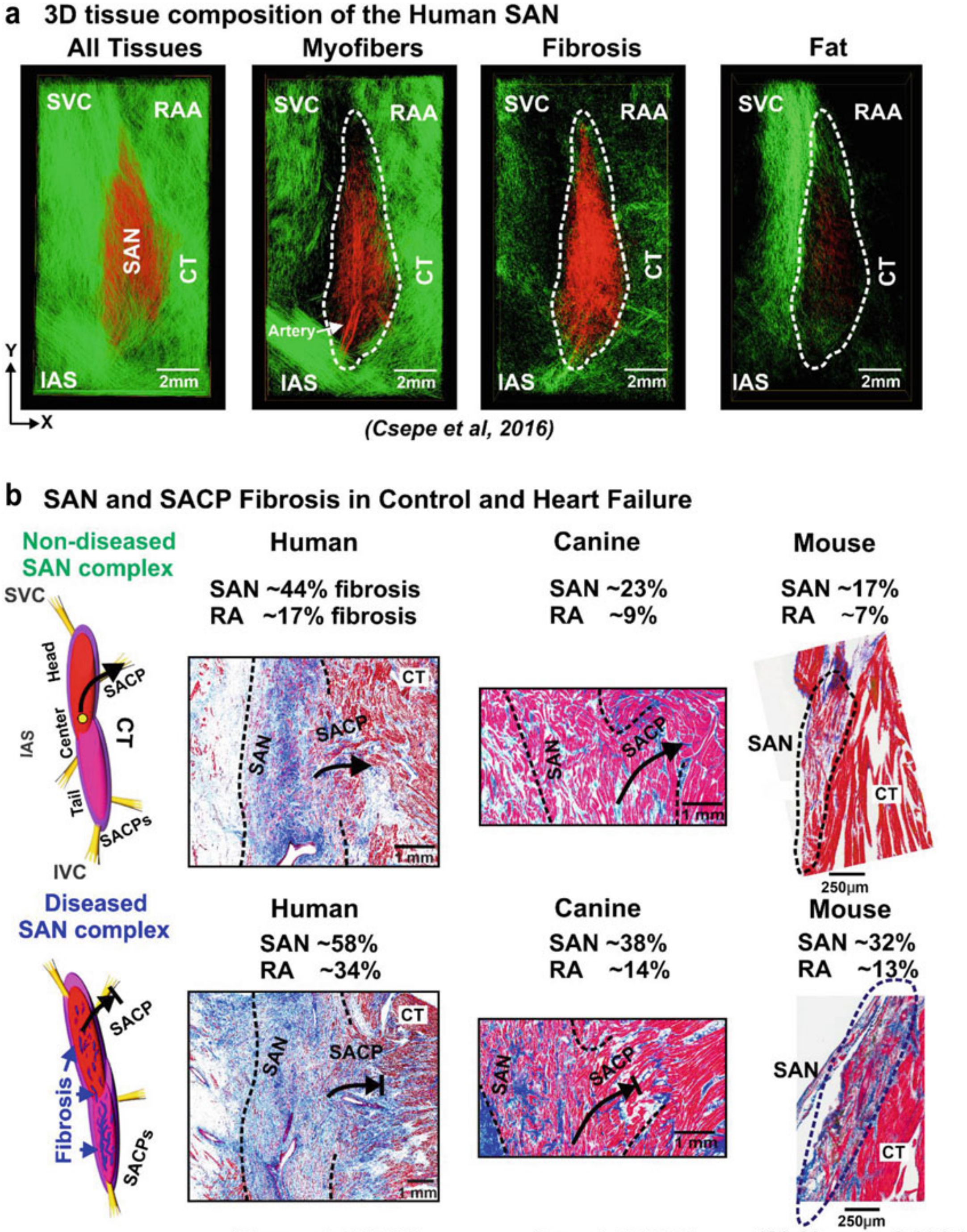
a 3D tissue composition of the Human SAN
All Tissues
Myofibers
Fibrosis
Fat
SVC
RAA
SAN
CT
IAS
Artery
2mm
Y
X
b SAN and SACP Fibrosis in Control and Heart Failure
Non-diseased SAN complex
SVC
Head
Center
Tail
SACP
SACPs
IAS
CT
IVC
Human
SAN ~44% fibrosis
RA ~17% fibrosis
Canine
SAN ~23%
RA ~9%
Mouse
SAN ~17%
RA ~7%
SAN
SACP
CT
1 mm
250μm
Diseased SAN complex
Fibrosis
Human
SAN ~58%
RA ~34%
Canine
SAN ~38%
RA ~14%
Mouse
SAN ~32%
RA ~13%

(Csepe et al, 2016)

(Csepe et al, 2016) (Lou et al, 2014) (Glukhov et al, 2015)

Fig. 6.5 Fibrotic tissue composition in normal and diseased human and animal SAN. (**a**) 3D myofiber, fibrotic tissue and fat composition in and around human SAN: 3D computational analysis by a fiber-tracking approach with seeding in different textures displays microstructure of all tissue types including myofibers, fibrotic tissue, and fat in the SAN complex (red) and surrounding atrial tissue (green). (**b**) SAN models depicting increased fibrosis within the SAN; histology sections from nondiseased and diseased human, canine, and mouse SAN shows intranodal fibrosis and fibrosis extending into the SACP region with myofibers branching off from the compact nodal tissue. CT, crista terminalis; IAS, interatrial septum; SACP, sinoatrial conduction pathway; SVC, superior vena cava; RAA, right atrial appendage (data modified from Human: Csepe et al. [3]; Canine: Lou et al. [5]. Mouse: Glukhov et al. [56])

which can undergo deformation to reduce the mechanical strain on the myocytes. A structural border composed of fibrotic, fatty tissue, and/or discontinuous myofibers is found around the SAN, penetrated only by the SACPs that exit the SAN. This structural border is known to electrically insulate the SAN pacemaker cells from the hyperpolarizing effects of the surrounding atrial myocardium, thereby protecting normal sinus rhythm (SR) [4, 10, 14, 21]. Furthermore, in addition to the significant amount of fibrotic tissue within the SAN, 3D computational analysis using a fiber-tracking approach identifies microstructure of several tissue types including myofibers, fibrotic tissue, and fat within the human SAN complex [3] (Fig. 6.5a). Cardiac diseases, including heart failure (HF), atrial arrhythmia, myocardial infarction, and genetic mutations, can significantly increase fibrosis heterogeneously across the SAN pacemaker complex leading to pacemaker-conduction impairments, SND and SAN reentrant arrhythmias (Fig. 6.5b). In addition, an increase in fibrosis, specifically within the SACPs, can cause exit blocks whereby impulses generated in the SAN cannot be delivered to the atria. Our recent study [48] revealed that a significant increase in fibrosis in failing human SAN is associated with the presence of myofibroblasts, cartilage intermediate layer protein 1 (CILP1), and periostin-positive interstitial fibrosis. This study suggests that in addition to increasing intranodal fibrosis, HF can also alter the composition of human SAN ECM toward increased stiffness, which may impair pacemaking and intranodal conduction.

6.7 Arrhythmias and Disease Mechanisms in the Mammalian and Human SAN

SND is largely a disease of the elderly, and its incidence increases exponentially with age [53]. Importantly, patients with SND usually exhibit combined abnormalities in SAN automaticity and conduction [54]. SND can be induced by a number of different pathophysiological conditions such as autonomic and hormone imbalances, genetic mutations, drug side effects, SAN ischemia, inflammatory conditions, heart failure, and AF [5, 15]. The degenerative loss of SAN pacemaker cells and their replacement with fibrotic tissue is frequently evident upon pathological examination of specimens from aged patients with SND [55]. Animal models of SND [5, 56, 57] also found upregulated fibrosis in the dysfunctional SAN pacemaker complex indicating fibrotic remodeling as a major cause of SND (Fig. 6.5b).

6.8 Tachy–Brady Syndrome and SAN Entrance and Exit Blocks

Tachy–brady syndrome, or tachy–brady arrhythmias, is defined as a pathological heart rate alteration between too fast and too slow, where termination of paroxysmal tachycardia including AF may be followed by long atrial pauses lasting several seconds, which can provoke another tachyarrhythmia paroxysm [50, 58]. These posttachycardia atrial pauses could theoretically result from either sinus arrest and/or SAN exit block (Fig. 6.6). Several clinical studies have demonstrated the presence of SAN exit block by using sinoatrial node electrogram (SNE) [54]. These clinical observations and the optical mapping of canine and human SAN strongly suggest an important role for SAN exit block, rather than sinus pacemaker arrest, in tachy–brady syndrome.

SACPs normally conduct the excitation activity from the SAN to the atria [9], but during AF or atrial pacing excitation waves can also enter and slowly propagate into the SAN center. Canine SAN studies [4, 8, 9] have shown that the central intranodal pacemakers cannot be paced faster than 10–50% above their intrinsic spontaneous rate, although the surrounding atrial rate could be 5–10 times faster than normal SR. Similarly, the occurrence of SAN entrance blocks could be limited by pacing at lower rates (500 ms) in human hearts, while faster pacing rates or AF induced entrance blocks in SACPs. Moreover, in

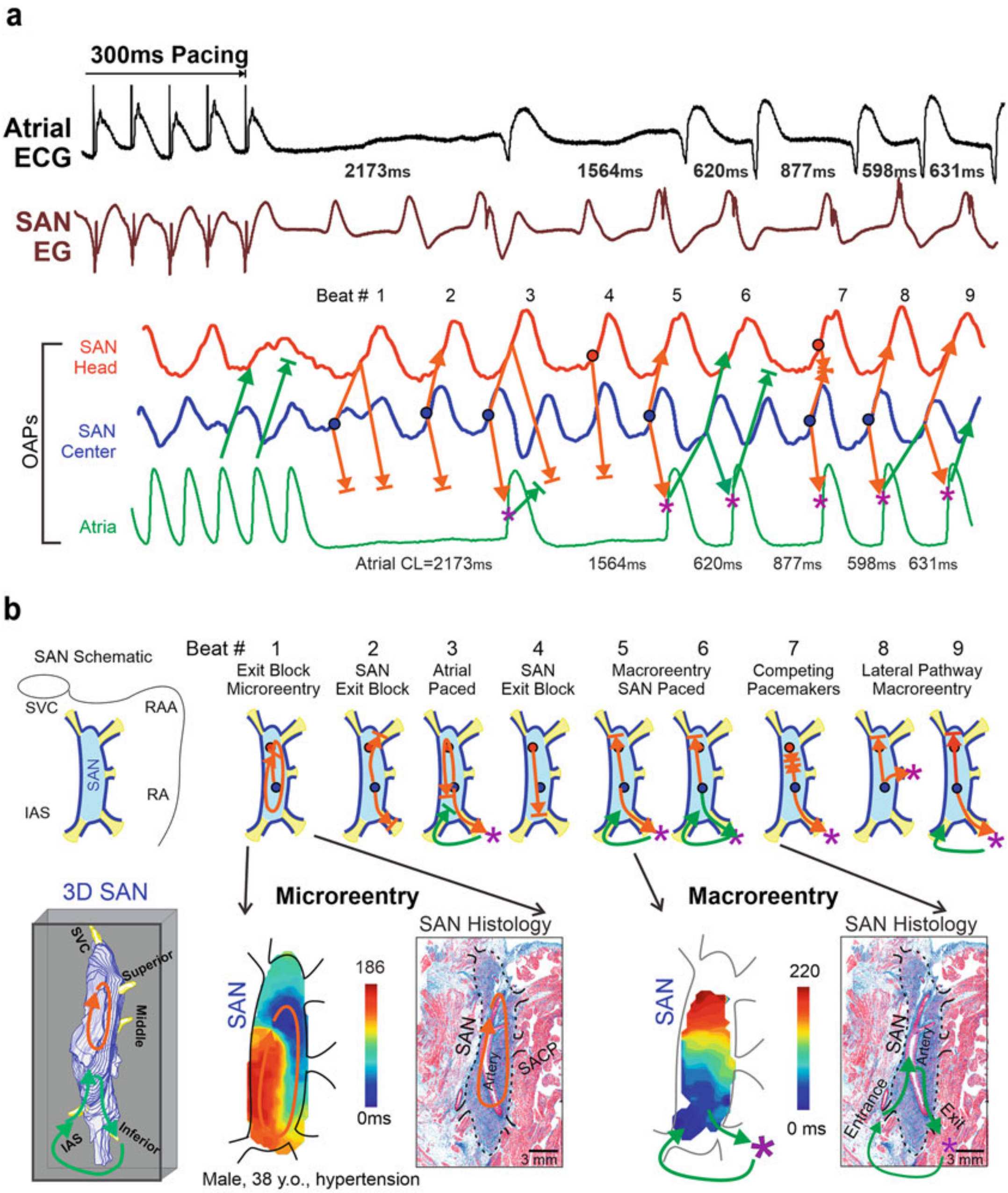

(Li et al, 2017)

Fig. 6.6 SAN arrhythmias in SND patients and in ex vivo human SAN. **A**. Top to bottom, atrial ECG, SAN electrogram (EG), SAN, and atrial OAPs show atrial pause, irregular sinus rhythm, and arrhythmia after 300 ms atrial pacing in the ex vivo human heart; SAN activation and conduction patterns revealed by high-resolution optical mapping; **B**. Top, schematic of the SAN pacemaker complex representing SAN activation pattern for nine postpacing arrhythmic beats. Bottom, SAN activation maps and corresponding histology sections show locations of micro-reentry and macro-reentrant pathways within the SAN complex structure. Colored dots indicate the positions of SAN leading pacemaker OAPs presented in panel A. Orange arrows show the conduction direction within the SAN, and green arrows indicate conduction between SAN and atrium; asterisk indicates the earliest atrial activation site. IAS, interatrial septum; RA(A), right atrial (appendage); SVC, superior vena cava; SAN, sinoatrial node (data modified from Li et al. [4])

the human SAN, the left superior, and septal SACPs are usually used as the preferential entrance pathways rather than lateral SACPs, which usually serve only as exit pathways. These studies revealed that SACPs may play a crucial role not only in SR regulation but also in protecting SAN pacemakers from overdrive suppression during atrial pacing and atrial arrhythmias. The SACPs may act like a low-pass filter for atrial waves by creating an entrance block during atrial pacing. Furthermore, rapid stimulation is filtered more in the SACPs, which prevents overdrive suppression of the SAN-leading pacemaker. The mechanism responsible for SAN entrance block during AF or tachypacing is likely related to differences in refractoriness and excitability between the SAN pacemaker complex and surrounding atria [5].

Despite the protective effect of the SAN entrance block, the effects of overdrive suppression can still impact the SAN automaticity and intranodal conduction. Atrial tachycardia has been shown to directly depress the excitability of the SAN pacemaker cells by inactivation of the $I_{\mathrm{Ca,L}}$ current [59]. The filtering conduction properties of the SACPs would cause the pacemaker cells near the SACPs to experience more overdrive suppression than the central SAN compartment. The leading pacemaker located in the SAN center may recover before cells in other compartments or the SACPs and manifest as an exit block after cessation of tachycardia. Importantly, acetylcholine and adenosine may potentiate pacing-induced depression of excitability of SACPs cells, leading to a postpacing-induced exit block and, consequently, tachy–brady syndrome [8].

Postpacing recovery time of SR (SAN recovery time or SNRT) is widely used in clinical electrophysiology labs to evaluate the SAN pacemaker and diagnose SND. However, clinical atrial electrograms can only measure the time between the last paced atrial beat and the first spontaneous atrial beat, which provides only an indirect measurement of SNRT (or SNRTi) (Fig. 6.6). Moreover, results can be normal despite the patient having SND, as it significantly depends on autonomic tone. The presence of entrance block can also significantly affect SNRTi results and may even lead to a falsely short SNRTi if the last paced atrial beat measured does not pace the SAN [8]. Importantly, when presented with an extended pause after pacing is stopped, SNRTi cannot differentiate between exit block and automaticity failure as the cause. These long postpacing pauses are frequent in diseased hearts, and clinical studies with SNE and or experimental NIOM are necessary to elucidate the mechanism because these methods allow for the measurement of direct SNRT (SNRTd), the time from the last paced atrial beat to the first spontaneous SAN upstroke. NIOM studies in both canine and human hearts [3–5, 8, 60] showed that pacing-induced atrial pauses (>1.5 s) are attributable to exit block, which is consistent with the majority of clinical studies with SNE [54].

6.9 SAN Reentrant Arrhythmias and Fibrosis

SAN arrhythmias including SAN macro-reentry tachyarrhythmia involving the SAN and surrounding atrial tissue, may account for up to 17% of atrial arrhythmias [61, 62]. The electrocardiographic similarity of the P-wave during SAN reentry and normal rhythm may lead to an underdiagnosis of these arrhythmias in clinics [61]. Using transmural NIOM, we were able to unmask the mechanisms of SAN reentrant arrhythmias in canine failing models [60] and in the human-diseased SAN [14] (Fig. 6.6). Depending on the excitable state of SAN pacemaker complex compartments, SAN macro-reentry and/or micro-reentry could be observed. SAN macro-reentry: the initial SAN wave could propagate through one SACP and then excite atria and re-excite SAN pacemaker compartments via another SACP and thus form a macro-reentry circuit with two main pathways: a slow intranodal and a fast atrial pathway located between exit and entrance SACPs [60]. By using this concept, a recent clinical study [62] demonstrated the high efficiency and safety of targeted ablation of the entrance SACP for successful SAN reentry treatment. In SAN micro-reentry, pivot waves anchored to the longitudinal conduction block can produce not only tachycardia but even paradoxical bradycardia (due to the exit block) [60].

An example of complex human SAN arrhythmias is shown in Fig. 6.6, that mediated by impairment of Nav channels and fibrotic remodeling [14]. These SAN arrhythmias may result from a perfect storm of several dysfunctions including stochastic SAN exit block, competing intranodal pacemakers, and SAN micro- and macro-reentry. Heterogeneous slowing of SAN conduction by Na_V blockade could lead to intranodal unidirectional blocks and initiated SAN micro-reentry or macro-reentry. Due to the extensive interstitial fibrotic strands and the SAN artery (Fig. 6.6). Importantly, the phenomena of SAN reentry were not observed in human hearts without structural remodeling. Histological analysis revealed that these arrhythmias required intranodal fibrotic strands, which were not present in healthy hearts, indicating a critical role of a structural substrate for SAN macro- and micro-reentry [4, 5].

6.10 SAN Dysfunctions

As discussed above, upregulated interstitial fibrosis may lead to disruption of electrical coupling between intranodal pacemaker clusters and SACP myofiber tracks, thereby disrupting SAN automaticity and slowing conduction, particularly in SACPs and ultimately leading to exit block (Fig. 6.5b) and/or reentrant arrhythmias (Fig. 6.6). Importantly, SAN impaired by fibrotic remodeling may still generate physiologically adequate pacemaker rhythm. Still, it would be vulnerable to exit block in the SACPs when exposed to a physiological or pathophysiological stimulus that may depress SAN or atrial excitability [5, 60].

Moreover, many genetic mutations and disease-induced remodeling of ion channels (e.g., HCN4 [63] and Na_V [14, 42]), structural proteins (ankyrin-B [64]), autonomic and metabolic receptors (A1 [4]), G proteins/GIRK channels [65, 66] gap junctions (Cx40 [67]), and Ca^{2+} handling proteins [32] may also alter the excitability and conduction of the pacemaker complex and disrupt the delicate source-sink relationship and ultimately lead to a variety of heart rhythm disorders. Moreover, the expression gradient of key proteins including A1R and GIRK subunits [4] across the SAN combined with fibrosis remodeling may exacerbate region-specific conduction abnormalities and incapacitate the fail-safe mechanisms of robust heart rhythm protection, which can predispose to SND. Similarly, when cardiac and neuronal Na_V channels are not available as in diseased hearts, specifically in the SACPs, susceptibility to SAN conduction blocks increases since the source-sink balance cannot be maintained [14].

6.11 Therapeutic Advances and Novel Strategies to Treat Human SND

Currently, pacemaker implantation is the primary treatment option for human SND. Very few studies have addressed mechanisms of human SND, which has greatly limited our understanding of disease-causing mechanisms in the human SAN (Fig. 6.7). This limitation translates into the lack of direct treatment modalities including pharmacological interventions to treat underlying mechanisms of SND in human hearts. Therefore, current treatment options are focused on ameliorating symptoms of SND rather than causal mechanisms.

SND is often associated with AF (tachy–brady syndrome) which further complicates treating SND independent of AF. Currently, mechanisms that connect SND and atrial arrhythmias are not completely known. SAN remodeling including prolongation of corrected SNRT and P-wave duration and decreased maximal and intrinsic heart rates was shown in a chronic pacing-induced canine model of AF [68]. Hocini et al. [69] showed that ablation to terminate AF in the absence of medical therapies in patients with prolonged sinus pauses improves heart rate parameters and a decrease in the corrected SNRT, indicating that terminating AF may help

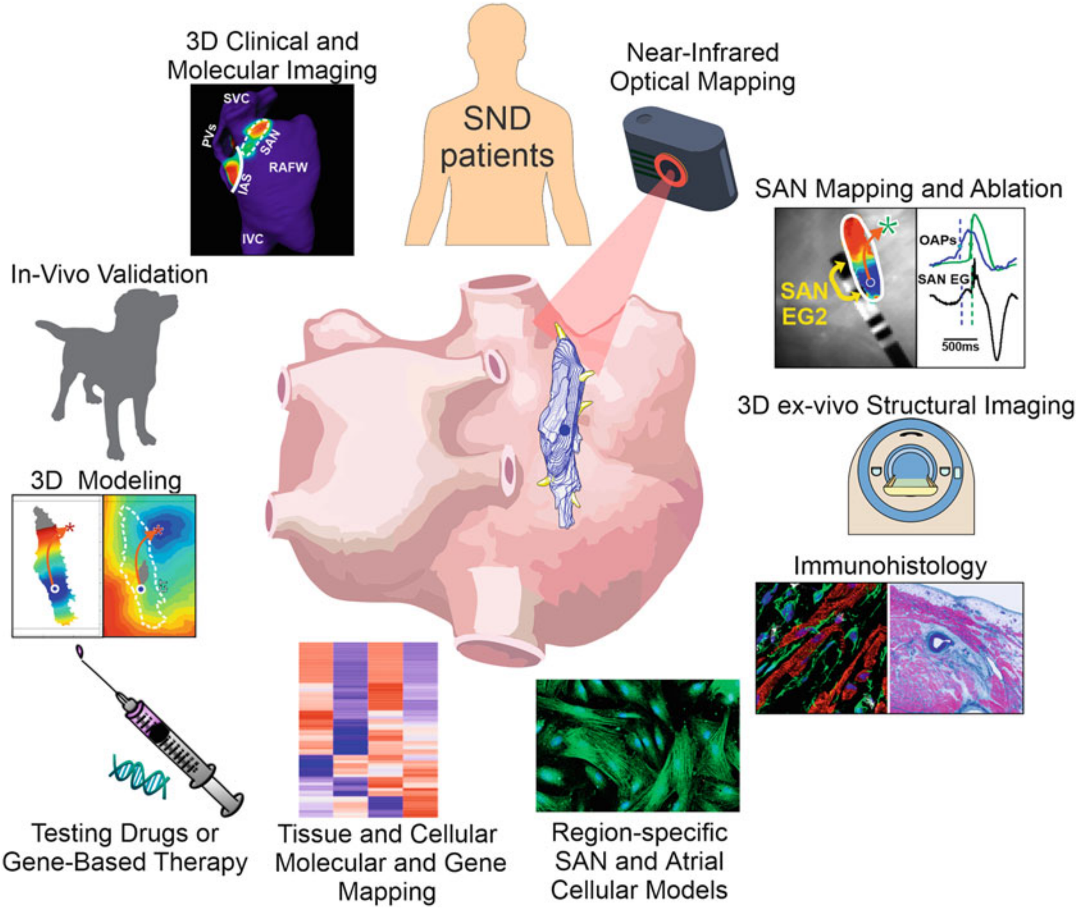
3D Clinical and Molecular Imaging
SVC
PVs
SAN
RAFW
IAS
IVC
SND patients
Near-Infrared Optical Mapping
SAN Mapping and Ablation
OAPs
SAN EG
SAN EG2
500ms
In-Vivo Validation
3D Modeling
3D ex-vivo Structural Imaging
Immunohistology
Testing Drugs or Gene-Based Therapy
Tissue and Cellular Molecular and Gene Mapping
Region-specific SAN and Atrial Cellular Models

Fig. 6.7 Integrated experimental and clinical modalities together with therapeutic interventions to define mechanisms of human sinoatrial (SAN) pacemaker and functional conduction impairments and treat human SAN dysfunction (SND)

improve SAN impairments in some patients. In contrast, many rate-controlling pharmaceuticals, e.g., beta-blockers, nondihydropyridine calcium channel blockers, antiarrhythmic agents, and sodium channel blockers that may benefit AF treatment, can secondarily worsen SND.

Explanted human heart studies have shown that ex vivo NIOM intramural mapping of nondiseased and diseased human SAN can provide critical insights into the disease-causing mechanisms of human SND. As described earlier, NIOM can reveal impairments in pacemaking as well as intranodal conduction, which could suggest both functional and structural sources of SND. Canine models also replicate some of these disease mechanisms identified in the human SAN, indicating that SND mechanisms can be studied in canine models. As we have seen above, human and canine SANs share many structural and functional aspects more than any commonly used small animal models, including mice, which emphasize the need for studying disease mechanisms in canine models that can be translated to human SAN therapies.

Animal studies have identified several molecular targets including proteins and miRNAs that could play important roles in normal as well as diseased SAN function. HCN4 has been shown to be downregulated in human HF SAN, which impacts the membrane ion clock by reducing I_f.

This results in impaired pacemaking and bradycardia associated with HF. Recent studies have identified higher levels of miRNA, miR-370-3p, which targets HCN4, in the human HF SAN. They further showed in a mouse model of HF that is, silencing miR-370-3p with intraperitoneal injection of antimiR-370-3p, blunted, or reversed the downregulation of HCN4 mRNA and protein expression, as well as the density of I_f and bradycardia [70]. They also showed that this treatment partially decreased SAN fibrosis as well as SAN cardiomyocyte hypertrophy. These novel animal findings suggest that SND can be treated by targeting molecular targets that can directly affect SAN function via multiple mechanisms. However, it remains unknown if such experimental approaches can be utilized in humans, where the SAN structure and function are very different from that of mouse models (Figs. 6.1 and 6.2). Furthermore, HF in humans is also more complex and multifactorial, which makes it difficult to directly translate such promising animal findings to treat human SND.

In the absence of suitable animal models that replicate the complexities of human SND, computer modeling can be utilized to accurately model human SND incorporating findings from multiple studies [14, 71]. Many of the ion channels that were found altered in HF and other diseases, including HCN, Na_V isoforms and Ca_V channels can be incorporated into models to study their mechanisms as well as to test suitable therapeutic interventions including pharmaceuticals to treat SND. Structural remodeling due to increased interstitial fibrosis can also be incorporated into these models along with molecular alterations to derive integrated therapeutic strategies to treat human SND. Importantly, these functional and/or structural remodeling can be done within specific SAN compartments and SACPs, which could provide valuable insights into region-specific impairments within the SAN.

Future therapies for human SND will benefit from incorporating novel imaging modalities to diagnose and identify causal mechanisms and develop suitable therapeutics. Late gadolinium-enhanced cardiovascular magnetic resonance (LGE-CMR), originally proposed as a method to visualize ventricular scarring, is now used routinely to visualize many types of fibrosis and scarring in the left and right atria. Recently, LGE-CMR has been used to visualize the fibrotic structure of the human SAN [23], which could help avoid the SAN structure as well as its neurovascular inputs during targeted ablations. As discussed above, recent ex vivo human SAN studies [48] have also addressed molecular profiles, including RNA and protein, in normal vs diseased SAN using high-throughput sequencing studies. Such large-scale studies at the whole tissue as well as at the single-cell level can provide unique databases to identify novel targets to address cell-specific perturbations that may lead to functional and/or structural SAN dysfunctions.

6.12 Conclusion and Future Directions

The human SAN pacemaker complex has a unique molecular profile and 3D structure that consists of several discrete compartments responsible for the spontaneous generation of electrical impulses (pacemaker clusters) and the delivery of these electrical impulses to the atria via the SACPs, which allow for robust physiological regulation of SR. SAN robustness, maintained through functional, structural, and molecular redundancies, is an important property of the human SAN, which allows it to efficiently maintain its automaticity and conduction even during external and internal perturbations. Disease and aging-induced molecular and structural remodeling in the SAN pacemaker complex may decrease its robust function, causing conduction impairments and abnormal impulse propagation, leading to various types of brady- and tachyarrhythmias.

The development of new integrated 3D electro-structural mapping methodologies is warranted to directly measure intramural SAN conduction and link functional results to patient-specific SAN pacemaker complex structure. The knowledge of the realistic human 3D SAN pacemaker complex is critically needed for the successful targeted treatment of SAN tachyarrhythmias [62]. Moreover, 3D computer models of human SAN function and dysfunction incorporating the realistic 3D intramural human SAN pacemaker and SACP structures, specific ion channels, and connexin distribution may shed more light on the exact mechanisms behind normal SR regulation and SND and could aid in the development of biological pacemakers [72]. Eventually, the field may move toward the development of new therapies focused on restoring the robustness of the SAN complex where a dysfunctional compartment (e.g., SACPs impaired by fibrosis) can be defined and selectively treated by gene/cell interventions.

Acknowledgements National Institutes of Health (HL115580, HL135109), Leducq Foundation (TNE FANTASY 19CVD03), the Bob and Corrine Frick Center for Heart Failure and Arrhythmia at the Ohio State University.

References

1. James TN. Anatomy of the human sinus node. Anat Rec. 1961;141:109–39.
2. Sanchez-Quintana D, Cabrera JA, Farre J, Climent V, Anderson RH, Ho SY. Sinus node revisited in the era of electroanatomical mapping and catheter ablation. Heart. 2005;91:189–94.
3. Csepe TA, Zhao J, Hansen BJ, Li N, Sul LV, Lim P, et al. Human sinoatrial node structure: 3D microanatomy of sinoatrial conduction pathways. Prog Biophys Mol Biol. 2016;120:164–78.
4. Li N, Hansen BJ, Csepe TA, Zhao J, Ignozzi AJ, Sul LV, et al. Redundant and diverse intranodal pacemakers and conduction pathways protect the human sinoatrial node from failure. Sci Transl Med. 2017;9:eaam5607.
5. Lou Q, Hansen BJ, Fedorenko O, Csepe TA, Kalyanasundaram A, Li N, et al. Upregulation of adenosine A1 receptors facilitates sinoatrial node dysfunction in chronic canine heart failure by exacerbating nodal conduction abnormalities revealed by novel dual-sided intramural optical mapping. Circulation. 2014;130:315–24.
6. James TN. Anatomy of the sinus node of the dog. Anat Rec. 1962;143:251–65.
7. Chandler NJ, Greener ID, Tellez JO, Inada S, Musa H, Molenaar P, et al. Molecular architecture of the human sinus node: insights into the function of the cardiac pacemaker. Circulation. 2009;119:1562–75.
8. Lou Q, Glukhov AV, Hansen B, Hage L, Vargos-Pinto P, Billman GE, et al. Tachy-brady arrhythmias: The critical role of adenosine-induced sino-atrial conduction block in post-tachycardia pauses. Heart Rhythm. 2013;10:110–8.
9. Fedorov VV, Chang R, Glukhov AV, Kostecki G, Janks D, Schuessler RB, et al. Complex interactions between the sinoatrial node and atrium during reentrant arrhythmias in the canine heart. Circulation. 2010;122:782–9.
10. Fedorov VV, Glukhov AV, Chang R. Conduction barriers and pathways of the sinoatrial pacemaker complex: their role in normal rhythm and atrial arrhythmias. Am J Physiol Heart Circ Physiol. 2012;302:H1773–83.
11. Bleeker WK, Mackaay AJ, Masson-Pevet M, Bouman LN, Becker AE. Functional and morphological organization of the rabbit sinus node. Circ Res. 1980;46: 11–22.
12. Fedorov VV, Hucker WJ, Dobrzynski H, Rosenshtraukh LV, Efimov IR. Postganglionic nerve stimulation induces temporal inhibition of excitability in the rabbit sinoatrial node. Am J Physiol. 2006;291: H612–23.
13. Boineau JP, Canavan TE, Schuessler RB, Cain ME, Corr PB, Cox JL. Demonstration of a widely distributed atrial pacemaker complex in the human heart. Circulation. 1988;77:1221–37.
14. Li N, Kalyanasundaram A, Hansen BJ, Artiga EJ, Sharma R, Abudulwahed SH, et al. Impaired neuronal sodium channels cause intranodal conduction failure and reentrant arrhythmias in human sinoatrial node. Nat Commun. 2020;11:512.
15. Sanders P, Morton JB, Kistler PM, Spence SJ, Davidson NC, Hussin A, et al. Electrophysiological and electroanatomic characterization of the atria in sinus node disease: evidence of diffuse atrial remodeling. Circulation. 2004;109:1514–22.
16. Cosio FG, Martin-Penato A, Pastor A, Nunez A, Montero MA, Cantale CP, et al. Atrial activation mapping in sinus rhythm in the clinical electrophysiology laboratory: observations during Bachmann's bundle block. J Cardiovasc Electrophysiol. 2004;15:524–31.
17. Joung B, Hwang HJ, Pak HN, Lee MH, Shen C, Lin SF, et al. Abnormal response of superior sinoatrial node to sympathetic stimulation is a characteristic finding in patients with atrial fibrillation and symptomatic bradycardia. Circ Arrhythm Electrophysiol. 2011;4:799–807.
18. Parameswaran R, Lee G, Morris GM, Royse A, Goldblatt J, Larobina M, et al. Simultaneous epicardial-endocardial mapping of the sinus node in humans with structural heart disease: Impact of overdrive suppression on sinoatrial exits. Heart Rhythm. 2020;17:2154–63.
19. Truex RC, Smythe MQ, Taylor MJ. Reconstruction of the human sinoatrial node. Anat Rec. 1967;159:371–8.
20. Fedorov VV, Schuessler RB, Hemphill M, Ambrosi CM, Chang R, Voloshina AS, et al. Structural and functional evidence for discrete exit pathways that

connect the canine sinoatrial node and atria. Circ Res. 2009;104:915–23.

21. Fedorov VV, Glukhov AV, Chang R, Kostecki G, Aferol H, Hucker WJ, et al. Optical mapping of the isolated coronary-perfused human sinus node. J Am Coll Cardiol. 2010;56:1386–94.
22. Macianskiene R, Martisiene I, Navalinskas A, Vosyliute R, Treinys R, Vaidelyte B, et al. Evaluation of excitation propagation in the rabbit heart: optical mapping and transmural microelectrode recordings. PLoS One. 2015;10:e0123050.
23. Csepe TA, Zhao J, Sul LV, Wang Y, Hansen BJ, Li N, et al. Novel application of 3D contrast-enhanced CMR to define fibrotic structure of the human sinoatrial node in vivo. Eur Heart J Cardiovasc Imaging. 2017;18: 862–9.
24. Jose AD, Taylor RR. Autonomic blockade by propranolol and atropine to study intrinsic myocardial function in man. J Clin Invest. 1969;48:2019–31.
25. Jose AD, Collison D. The normal range and determinants of the intrinsic heart rate in man. Cardiovasc Res. 1970;4:160–7.
26. Stiles MK, Brooks AG, Roberts-Thomson KC, Kuklik P, John B, Young GD, et al. High-density mapping of the sinus node in humans: Role of preferential pathways and the effect of remodeling. J Cardiovasc Electrophysiol. 2010;21:532–9.
27. Kharbanda RK, Wesselius FJ, van Schie MS, Taverne Y, Bogers A, de Groot NMS. Endo-epicardial mapping of in vivo human sinoatrial node activity. JACC Clin Electrophysiol. 2021;7(6):693–702.
28. Liu J, Dobrzynski H, Yanni J, Boyett MR, Lei M. Organisation of the mouse sinoatrial node: structure and expression of HCN channels. Cardiovasc Res. 2007;73:729–38.
29. Lakatta EG, DiFrancesco D. What keeps us ticking: a funny current, a calcium clock, or both? J Mol Cell Cardiol. 2009;47:157–70.
30. Kodama I, Nikmaram MR, Boyett MR, Suzuki R, Honjo H, Owen JM. Regional differences in the role of the Ca2+ and Na+ currents in pacemaker activity in the sinoatrial node. Am J Physiol. 1997;272: H2793–806.
31. Boyett MR, Inada S, Yoo S, Li J, Liu J, Tellez J, Greener ID, et al. Connexins in the sinoatrial and atrioventricular nodes. Adv Cardiol. 2006;42:175–97.
32. Dobrzynski H, Anderson RH, Atkinson A, Borbas Z, D'Souza A, Fraser JF, et al. Structure, function and clinical relevance of the cardiac conduction system, including the atrioventricular ring and outflow tract tissues. Pharmacol Ther. 2013;139:260–88.
33. Li N, Csepe TA, Hansen BJ, Dobrzynski H, Higgins RS, Kilic A, et al. Molecular mapping of sinoatrial node HCN channel expression in the human heart. Circ Arrhythm Electrophysiol. 2015;8:1219–27.
34. Krapivinsky G, Gordon EA, Wickman K, Velimirovic B, Krapivinsky L, Clapham DE. The G-protein-gated atrial K+ channel IKACh is a heteromultimer of two inwardly rectifying K(+)-channel proteins. Nature. 1995;374:135–41.
35. Belardinelli L, Giles WR, West A. Ionic mechanisms of adenosine actions in pacemaker cells from rabbit heart. J Physiol. 1988;405:615–33.
36. Watt AH. Sick sinus syndrome: an adenosine-mediated disease. Lancet. 1985;325:786–8.
37. Headrick JP, Peart JN, Reichelt ME, Haseler LJ. Adenosine and its receptors in the heart: regulation, retaliation and adaptation. Biochim Biophys Acta. 2011;1808:1413–28.
38. Burnett D, Abi-Samra F, Vacek JL. Use of intravenous adenosine as a noninvasive diagnostic test for sick sinus syndrome. Am Heart J. 1999;137:435–8.
39. Fragakis N, Antoniadis AP, Korantzopoulos P, Kyriakou P, Koskinas KC, Geleris P. Sinus nodal response to adenosine relates to the severity of sinus node dysfunction. Europace. 2012;14:859–64.
40. Protas L, Oren RV, Robinson CCE, RB. Age-dependent changes in Na current magnitude and TTX-sensitivity in the canine sinoatrial node. J Mol Cell Cardiol. 2010;48:172–80.
41. Lei M, Jones SA, Liu J, Lancaster MK, Fung SS, Dobrzynski H, et al. Requirement of neuronal- and cardiac-type sodium channels for murine sinoatrial node pacemaking. J Physiol. 2004;559:835–48.
42. Benson DW, Wang DW, Dyment M, Knilans TK, Fish FA, Strieper MJ, et al. Congenital sick sinus syndrome caused by recessive mutations in the cardiac sodium channel gene (SCN5A). J Clin Invest. 2003;112:1019–28.
43. Vedantham V, Galang G, Evangelista M, Deo RC, Srivastava D. RNA sequencing of mouse sinoatrial node reveals an upstream regulatory role for Islet-1 in cardiac pacemaker cells. Circ Res. 2015;116:797–803.
44. van Eif VWW, Stefanovic S, van Duijvenboden K, Bakker M, Wakker V, de Gier-de Vries C, et al. Transcriptome analysis of mouse and human sinoatrial node cells reveals a conserved genetic program. Development. 2019;146(8):dev173161.
45. Goodyer WR, Beyersdorf BM, Paik DT, Tian L, Li G, Buikema JW, et al. Transcriptomic profiling of the developing cardiac conduction system at single-cell resolution. Circ Res. 2019;125:379–97.
46. Linscheid N, Logantha S, Poulsen PC, Zhang S, Schrolkamp M, Egerod KL, et al. Quantitative proteomics and single-nucleus transcriptomics of the sinus node elucidates the foundation of cardiac pacemaking. Nat Commun. 2019;10:2889.
47. Liang D, Xue J, Geng L, Zhou L, Lv B, Zeng Q, et al. Cellular and molecular landscape of mammalian sinoatrial node revealed by single-cell RNA sequencing. Nat Commun. 2021;12:287.
48. Kalyanasundaram A, Li N, Gardner ML, Artiga EJ, Hansen BJ, Webb A, et al. Fibroblast-Specific proteo-transcriptomes reveal distinct fibrotic signatures of human sinoatrial ode in non-failing and failing hearts. Circulation. 2021;144:126–43.

49. Keith A, Flack M. The form and nature of the muscular connections between the primary divisions of the vertebrate heart. J Anat Physiol. 1907;41:172–89.
50. Csepe TA, Kalyanasundaram A, Hansen BJ, Zhao J, Fedorov VV. Fibrosis: a structural modulator of sinoatrial node physiology and dysfunction. Front Physiol. 2015;6:37.
51. Shiraishi I, Takamatsu T, Minamikawa T, Onouchi Z, Fujita S. Quantitative histological analysis of the human sinoatrial node during growth and aging. Circulation. 1992;85:2176–84.
52. Gluck JM, Herren AW, Yechikov S, Kao HKJ, Khan A, Phinney BS, et al. Biochemical and biomechanical properties of the pacemaking sinoatrial node extracellular matrix are distinct from contractile left ventricular matrix. PLoS One. 2017;12:e0185125.
53. Jensen PN, Gronroos NN, Chen LY, Folsom AR, deFilippi C, Heckbert SR, et al. Incidence of and risk factors for sick sinus syndrome in the general population. J Am Coll Cardiol. 2014;64:531–8.
54. Wu DL, Yeh SJ, Lin FC, Wang CC, Cherng WJ. Sinus automaticity and sinoatrial conduction in severe symptomatic sick sinus syndrome. J Am Coll Cardiol. 1992;19:355–64.
55. Thery C, Gosselin B, Lekieffre J, Warembourg H. Pathology of sinoatrial node. Correlations with electrocardiographic findings in 111 patients. Am Heart J. 1977;93:735–40.
56. Glukhov AV, Kalyanasundaram A, Lou Q, Hage LT, Hansen BJ, Belevych AE, et al. Calsequestrin 2 deletion causes sinoatrial node dysfunction and atrial arrhythmias associated with altered sarcoplasmic reticulum calcium cycling and degenerative fibrosis within the mouse atrial pacemaker complex. Eur Heart J. 2015;36:686–97.
57. Hao X, Zhang Y, Zhang X, Nirmalan M, Davies L, Konstantinou D, et al. TGF-beta1-mediated fibrosis and ion channel remodeling are key mechanisms in producing the sinus node dysfunction associated with SCN5A deficiency and aging. Circ Arrhythm Electrophysiol. 2011;4:397–406.
58. Moss AJ, Davis RJ. Brady-Tachy syndrome. Prog Cardiovasc Dis. 1974;16:439–54.
59. Watanabe EI, Honjo H, Boyett MR, Kodama I, Toyama J. Inactivation of the calcium current is involved in overdrive suppression of rabbit sinoatrial node cells. Am J Physiol. 1996;271:H2097–107.
60. Glukhov AV, Hage LT, Hansen BJ, Pedraza-Toscano-A, Vargas-Pinto P, Hamlin RL, et al. Sinoatrial node reentry in a canine chronic left ventricular infarct model: role of intranodal fibrosis and heterogeneity of refractoriness. Circ Arrhythm Electrophysiol. 2013;6:984–94.
61. Gomes JA, Hariman RJ, Kang PS, Chowdry IH. Sustained symptomatic sinus node reentrant tachycardia: incidence, clinical significance, electrophysiologic observations and the effects of antiarrhythmic agents. J Am Coll Cardiol. 1985;5:45–57.
62. Yamabe H, Orita Y. Demonstration of the anatomical tachycardia circuit in sinoatrial node reentrant tachycardia: analysis using the entrainment method. J Am Heart Assoc. 2020;9:e014472.
63. Schweizer PA, Schroter J, Greiner S, Haas J, Yampolsky P, Mereles D, et al. The symptom complex of familial sinus node dysfunction and myocardial noncompaction is associated with mutations in the HCN4 channel. J Am Coll Cardiol. 2014;64:757–67.
64. Le SS, Bhasin N, Vieyres C, Hund TJ, Cunha SR, Koval O, et al. Dysfunction in ankyrin-B-dependent ion channel and transporter targeting causes human sinus node disease. Proc Natl Acad Sci U S A. 2008;105:15617–22.
65. Veerman CC, Mengarelli I, Koopman CD, Wilders R, van Amersfoorth SC, Bakker D, et al. Genetic variation in GNB5 causes bradycardia by augmenting the cholinergic response via increased acetylcholine-activated potassium current (I K,ACh). Dis Model Mech. 2019;12:dmm037994.
66. Stallmeyer B, Kuss J, Kotthoff S, Zumhagen S, Vowinkel K, Rinne S, et al. A Mutation in the G-protein gene GNB2 causes familial sinus node and atrioventricular conduction dysfunction. Circ Res. 2017;120:e33–44.
67. Bagwe S, Berenfeld O, Vaidya D, Morley GE, Jalife J. Altered right atrial excitation and propagation in connexin40 knockout mice. Circulation. 2005;112: 2245–53.
68. Elvan A, Wylie K, Zipes DP. Pacing-induced chronic atrial fibrillation impairs sinus node function in dogs. Electrophysiological remodeling. Circulation. 1996;94:2953–60.
69. Hocini M, Sanders P, Deisenhofer I, Jais P, Hsu LF, Scavee C, et al. Reverse remodeling of sinus node function after catheter ablation of atrial fibrillation in patients with prolonged sinus pauses. Circulation. 2003;108:1172–5.
70. Yanni J, D'Souza A, Wang Y, Li N, Hansen BJ, Zakharkin SO, et al. Silencing miR-370-3p rescues funny current and sinus node function in heart failure. Sci Rep. 2020;10:11279.
71. Fabbri A, Fantini M, Wilders R, Severi S. Computational analysis of the human sinus node action potential: model development and effects of mutations. J Physiol. 2017;595:2365–96.
72. Cingolani E, Goldhaber JI, Marban E. Next-generation pacemakers: from small devices to biological pacemakers. Nat Rev Cardiol. 2018;15:139–50.

Mechano-Electric Coupling in the Heart: Effects on Heart Rate and Rhythm

7

T. Alexander Quinn, Rebecca A. Capel, and Peter Kohl

Abstract

Cardiac electrical and mechanical activity are closely interrelated, not only via the chain of events commonly referred to as 'excitation-contraction coupling' that links electrical excitation to contraction, but equally via feedback from the heart's mechanical environment to the origin and spread of cardiac excitation. The latter has been termed mechano-electric coupling and complements excitation-contraction coupling to form an intracardiac electro-mechanical regulatory loop. This chapter will explore the relevance of mechano-electric coupling in the heart by reviewing its pro- and anti-arrhythmic effects on heart rate and rhythm, and the underlying mechanisms that may account for clinical and experimental observations.

Keywords

Mechano-electric feedback · Sinoatrial node · Arrhythmia · Atrial dilation · Ventricular fibrillation · *Commotio cordis* · Precordial thump · Stretch-activated channel · Computational modelling

7.1 Introduction

The heart is a remarkably dynamic organ, whose efficient function depends on well-coordinated excitation and contraction, and their beat-by-beat adjustment to continuously fluctuating haemodynamic conditions. Incredibly, this autoregulatory coordination and acute adaption to systemic requirements occur in the absence of neuro-muscular junctions (which are required for steering skeletal muscle activity) and continues to function after the removal of extracardiac neuro-hormonal inputs (for instance, when the heart is removed from the body).

This intracardiac autoregulation is driven by 'feedforward' and 'feedback' interactions between the heart's electrical and mechanical activity. In what is generally thought of as the

T. A. Quinn (✉)
Department of Physiology and Biophysics, Dalhousie University, Halifax, NS, Canada

School Biomedical Engineering, Dalhousie University, Halifax, NS, Canada
e-mail: alex.quinn@dal.ca

R. A. Capel
Department of Pharmacology, British Heart Foundation Centre of Research Excellence, University of Oxford, Oxford, UK
e-mail: rebecca.capel@pharm.ox.ac.uk

P. Kohl
Institute for Experimental Cardiovascular Medicine, University Heart Center Freiburg Bad Krozingen, Freiburg, Germany

Faculty of Medicine, University of Freiburg, Freiburg, Germany
e-mail: peter.kohl@uniklinik-freiburg.de

© Springer Nature Switzerland AG 2023

O. N. Tripathi et al. (eds.), *Heart Rate and Rhythm*, https://doi.org/10.1007/978-3-031-33588-4_7

forward direction, electrical excitation of the heart, which originates in the sinoatrial node (SAN) and spreads through the myocardium via intracellular coupling and specialised conducting pathways (atrioventricular node, bundles of His, Purkinje fibres), results in cellular contraction through a process known as 'excitation-contraction coupling (ECC)' [1, 2]. In the opposite direction, the heart's mechanical state, determined by internal and external parameters, affects cardiac electrical activity. This acute feedback is known as 'mechano-electric feedback' (when considering only the effects of the mechanical activity of the heart itself), or more broadly, 'mechano-electric coupling' (MEC, which includes responses to extracardiac mechanical inputs). MEC is thought to act through stretch-activated ion channels (SAC, which are directly gated by a mechanical stimulus) [3], as well as through stretch-modulated ion channels (whose normal activity is modulated by mechanical stimulation), changes in calcium (Ca^{2+}) handling, and mechano-sensitive second messenger systems (Fig. 7.1) [5, 6].

In this chapter, we will present the most striking clinical and experimental evidence for MEC and explore molecular mechanisms underlying these (patho-)physiological observations.

7.2 Mechanical Modulation of Heart Rate

7.2.1 Background

Modulation of heart rate (HR) by changes in venous return was reported over a century ago by Francis Bainbridge, who attributed HR acceleration upon venous fluid injection in anaesthetised dogs to a predominantly vagal autonomic reflex [7, 8]. His experiments established a correlation between HR response and central venous pressure (CVP) but not arterial pressure. Reconfirmation of this response in humans proved difficult, as most non-invasive interventions that change CVP also tend to affect arterial pressure. The latter may trigger dominant baroreceptor responses that stimulate contrasting HR effects (e.g., via the depressor reflex). Donald and Shepherd finally circumvented this problem and established the equivalent of a 'Bainbridge response' in humans, using passive leg-elevation of volunteers in the supine position to favour venous blood return to the trunk of the body. This raised CVP without measurably affecting arterial pressure, revealing a positive chronotropic effect on HR in human [9].

Since then, the Bainbridge response has also been observed in isolated hearts, right atrial preparations [10], sinoatrial node (SAN) tissue [11], and even single cardiac pacemaker cells [12]. Thus, local MEC mechanisms contribute to mechanical modulation of HR, beyond the originally-implied neural reflex response.

7.2.2 Clinical Observations

Human studies of the Bainbridge response have focussed on the assessment of respiratory sinus arrhythmia (RSA) in normal subjects and in heart transplant recipients.

RSA is a 'physiological arrhythmia', where HR is modulated during the respiratory cycle, increasing during inspiration (when low intrathoracic pressure aids not only air intake but also venous return) and decreasing during expiration (when output from the chest is favoured). RSA is reported to reduce pulmonary shunt effects and increase oxygen uptake, when compared to stable HR [13], indicating a possible role for mechanical HR modulation in normal physiology. RSA can be measured non-invasively by establishing respiratory rate-related frequency oscillations in the R-R intervals of the electrocardiogram. Two major peaks in HR frequency oscillations appear in healthy subjects at rest. A so-called high-frequency (HF) peak (0.15–0.3 Hz) is correlated with the respiratory cycle and is usually attributed to oscillations in 'vagal tone'. It is this peak which is considered to represent RSA. A second, low-frequency (LF) peak (~0.1 Hz), attributed to changes in 'sympathetic tone', is not modulated with each respiratory cycle.

As expected, transplant recipients (whose hearts no longer receive nervous system inputs) tend to lack the LF peak. A distinct HF peak is

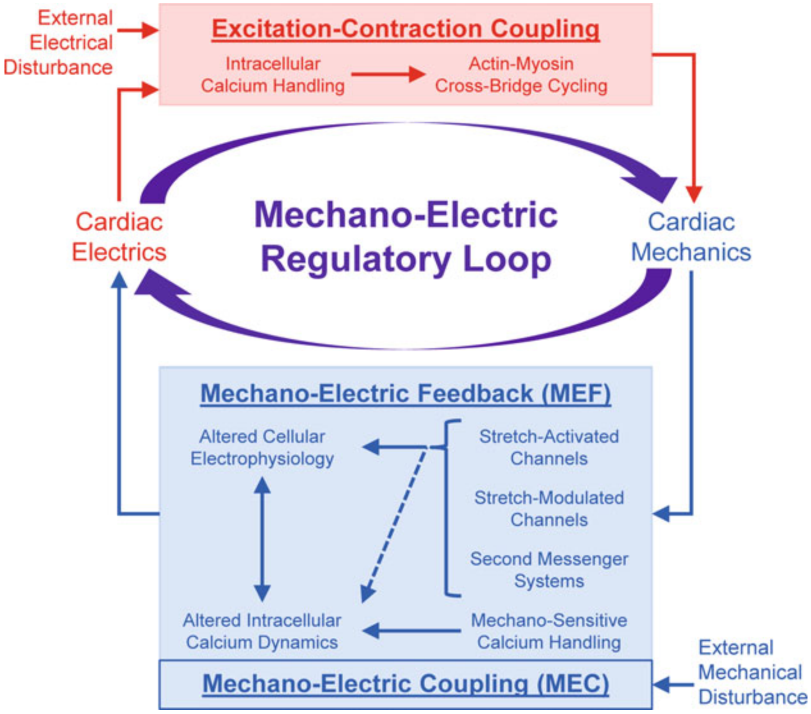
External
Electrical
Disturbance
Excitation-Contraction Coupling
Intracellular
Calcium Handling
Actin-Myosin
Cross-Bridge Cycling
Cardiac
Electrics
Mechano-Electric
Regulatory Loop
Cardiac
Mechanics
Mechano-Electric Feedback (MEF)
Altered Cellular
Electrophysiology
Stretch-Activated
Channels
Stretch-Modulated
Channels
Second Messenger
Systems
Altered Intracellular
Calcium Dynamics
Mechano-Sensitive
Calcium Handling
External
Mechanical
Disturbance
Mechano-Electric Coupling (MEC)

Fig. 7.1 The feedforward and feedback links between cardiac electrophysiology and mechanics forming an intracardiac mechano-electric regulatory loop. The feedforward between electrical excitation and mechanical contraction involving intracellular Ca^{2+} handling and actin-myosin cross-bridge cycling, is a process known as 'Excitation-Contraction Coupling' (top). Feedback (bottom) from myocardial deformation to cell electrophysiology and intracellular Ca^{2+} dynamics occurs via multiple interdependent mechano-sensitive mechanisms, which in turn affect the origin and spread of excitation, a phenomenon known as 'Mechano-Electric Feedback' (considering only cardiac mechanical activity as an input signal) or more broadly 'Mechano-Electric Coupling' (encompassing mechanical perturbations of the heart irrespective of their origin). (From [4], with permission)

still discernible, albeit at a reduced magnitude, suggesting that mechanisms intrinsic to the heart may contribute to RSA [14]. In support of this suggestion, tidal volume (and, therefore, venous return) modulates HR variability in these patients to a greater extent than changes in breathing rate.

Intrinsic HR modulation is not unique to transplant recipients. In normal subjects, the magnitude of both LF and HF oscillations is reduced during early exercise. As workload increases, the LF component diminishes and all but disappears at maximal workloads, whereas the HF peak increases in magnitude, despite the loss of 'vagal tone' associated with physical work [15]. This can be observed even after additional ganglion block [16], again suggesting intracardiac contributions to RSA. Interestingly, the delay between respiratory and HF oscillation peaks drops with exercise in normal subjects, rendering it similar to that in transplant recipients (in whom it remains unchanged), perhaps suggesting a switch from normally dominant longer-latency reflex loops to intrinsic cellular/tissue-level control [15].

Human studies, therefore, point towards the existence of an intracardiac mechano-sensitive HR control mechanism contributing to HR modulation through fluctuations in venous return. Elucidation of the stimulus for, and mechanisms of, this response requires experimental manipulation that would be impractical and/or unethical in humans.

7.2.3 Experimental Studies

The HR changes observed in humans have been reproduced in intact anaesthetised dogs, where SAN-specific stretch (applied via a weight and pulley system in open-chest experiments) can elicit instantaneous HR acceleration by >20%, which is not abolished by denervation or adrenergic and cholinergic block [17].

In the isolated rabbit heart, responses similar to those in intact preparations were described by Blinks, who observed that progressive increases in atrial pressure (up to ~100 mmHg) are accompanied by instantaneous HR acceleration in rabbit [10]. This response appears rapidly (within the first minute), plateaus by 2–3 min, and can be maintained for several hours. Interestingly, further atrial pressure increases beyond this (already supra-physiological) range result in HR deceleration.

Adrenergic or cholinergic block, sufficient to alter HR by 50% from baseline, have no effect on the HR response to changes in filling pressure in rat [18]. Neither do application of tetrodotoxin (a fast sodium [Na^+] channel blocker) or neonatal capsaicin injections (ablation of intracardiac neurons). This suggests that neither external autonomic nor intracardiac neuronal signalling is necessary for the intrinsic HR response to stretch. Finally, the high solution flow rates used in atrial preparations [10] and the speed of HR response suggest that humoral factors are unlikely to be key contributors.

In the 1960s, Deck observed beating rate (BR) changes during the distension of cat and rabbit isolated atrial tissue containing the SAN. Measuring the trans-membrane potential (V_m) of SAN pacemaker cells and the contractile behaviour of the tissue during uni-axial or equi-biaxial stretch [11], he observed a 15–20% BR acceleration upon stretch. This was accompanied by an instantaneous reduction in absolute amplitudes of both maximum systolic and maximum diastolic potentials (MSP and MDP, respectively), giving rise to a reduction in SAN action potential (AP) amplitude and in the duration of the spontaneous diastolic depolarisation phase. These direct electrophysiological observations of V_m changes in SAN tissue help to narrow down the range of plausible molecular mechanisms involved, as their effect would appear to be linked to an electrophysiological mechanism with a net reversal potential (E_{rev}) between the MDP and MSP of SAN pacemaker cells.

7.2.4 Underlying Mechanisms

Early single-cell studies into the mechanisms underlying mechanical modulation of HR used cell swelling as a mechanical stimulus. This was shown to activate a chloride current ($I_{Cl,swell}$), whose E_{rev} near 0 mV could conceivably confer the capacity to augment pacemaker frequency in response to mechanical stimulation [19]. However, $I_{Cl,swell}$ activates with a lag time of over 30 s in cardiac myocytes, rendering it too slow for acute beat-by-beat changes in HR. Furthermore, cell swelling is associated with an increase in cell diameter and negligible axial elongation (or even shortening). Micromechanically, this is fundamentally different from axial stretch, where lengthening at constant cell volume is associated with a reduction in cell diameter. In addition to these biophysical differences in stimulus, hypo-osmotic swelling of rabbit spontaneously beating SAN pacemaker cells actually reduces spontaneous BR [20]. Cell swelling is not an ideal approach, therefore, to probe acute mechanical modulation of cardiomyocyte electrophysiology in normal physiological conditions, where cardiomyocyte cell volume is not assumed to change. That said, acute cell swelling mimics certain aspects of cell behaviour in ischaemia and reperfusion which, together with pathologically remodelled cells (e.g., in hypertrophy, where $I_{Cl,swell}$ can be persistently activated in working myocardium [21]), may constitute meaningful research targets for this technique.

Axial stretch can be applied to single myocytes using a range of techniques to attach probes for mechanical stimulation. One approach is to use carbon fibres, which adhere to single cells without the need for gluing, tying, or suction [22]. Using this technique, Cooper et al. observed a significant increase in BR of rabbit single SAN cells during 5–10% stretch. This was accompanied by a reduction in absolute values of MSP and MDP [12], reproducing previous SAN tissue results [11]. Voltage clamp studies revealed that stretch-activated a 6 nS/pF whole-cell current with an E_{rev} of –11 mV [12].

The properties of the stretch-activated current measured by Cooper et al. [12] are similar to the mechanically induced cation non-selective current ($\mathrm{SAC_{NS}}$) reported in many other eukaryotic cells [3]. $\mathrm{SAC_{NS}}$ is carried by rapidly activating channels with E_{rev} approximately halfway between MDP and MSP [23]. $\mathrm{SAC_{NS}}$ opening will therefore depolarise diastolic, and re-polarise systolic V_{m}, potentially explaining the observed changes in SAN cell and tissue MSP and MDP during stretch.

A point of contention has been the observation that HR responses may differ between species. Most medium and large mammals (and other classes of animals, such as fish [24, 25]) respond to SAN stretch with HR acceleration, while smaller mammals have shown HR deceleration [26]. Interestingly, this discrepancy is not incompatible with a major contribution of $\mathrm{SAC_{NS}}$ to both responses. Larger animals (as well as fish) tend to have a more slowly beating SAN, with AP shapes that are characterised by a slow AP upstroke (carried by $\mathrm{Ca^{2+}}$ influx) and a prominent plateau-like phase, while smaller mammals with faster HR show a faster upstroke (with a significant contribution from fast $\mathrm{Na^{+}}$ channels) and swift initial repolarisation, giving rise to a more triangular AP shape (Fig. 7.2). Thus, 'slow' SAN AP waveforms spend the majority of each cycle moving their V_{m} from MDP (or MSP) *towards* the E_{rev} of $\mathrm{SAC_{NS}}$. Their faster counterparts spend a larger proportion of time moving their V_{m} *away* from E_{rev} of $\mathrm{SAC_{NS}}$. Thus, one and the same mechanism—activation of $\mathrm{SAC_{NS}}$ by SAN stretch—may speed up slow HR *and* reduce already fast ones. This notion has been supported recently by experiments involving stretch of mouse-isolated SAN, in which lengthening of the AP plateau by block of rapidly activating potassium currents with 4-aminopyridine shifted the stretch-induced change in BR from slowing to acceleration [28].

Ideally, the insight obtained by the reduction of a problem from whole animal to tissue, cells and channels is complemented by re-integration, from putative mechanisms to systemic response [29]. This can be achieved using conceptual consideration, or better, quantitative mathematical models [30] and experimental investigation (e.g., via application of selective pharmacological probes). Computational modelling of stretch effects on SAN cell activity has confirmed the *plausibility* of $\mathrm{SAC_{NS}}$ contributions as a key to stretch-induced BR changes [12]. Experimental proof calls for selective inhibition (or activation) of $\mathrm{SAC_{NS}}$. At present, available pharmacological tools are limited. Gadolinium ions are potent $\mathrm{SAC_{NS}}$ blockers, but they also affect other ion channels and precipitate in physiological buffers. At low concentrations (<50 μM), streptomycin is both potent and reasonably selective when used on isolated cells, but its utility for acute $\mathrm{SAC_{NS}}$ block in multicellular preparations has been called into question (if streptomycin did act as an acute $\mathrm{SAC_{NS}}$ blocker in situ, we could probably not prescribe it to patients) [26]. The most specific $\mathrm{SAC_{NS}}$ blocker, *Grammostola spatulata* mechanotoxin-4 (GsMTx-4), is a peptide isolated from a tarantula toxin [31]. It has been found to reversibly block stretch-induced BR changes in guinea pig and mouse SAN tissue, without affecting background force [26]. One should remember, however, that quantitative plausibility is no substitute for experimental validation [32], and mechano-sensitivity of other currents involved in pacemaking, or changes in intracellular signalling, may also contribute to SAN stretch responses [33–36].

The magnitude of mechanical effects on HR appears to increase with the structural complexity of the biological model (isolated SAN cells ~5%, whole-heart/SAN tissue ~15%, intact dog up to 30% [26]). Probable explanations include: (1) the increasing loss of structures involved in the transmission of mechanical stimuli to molecular effectors as one reduces the biological model system [28]; (2) increasing deprivation of possible paracrine effects, such as may be mediated by

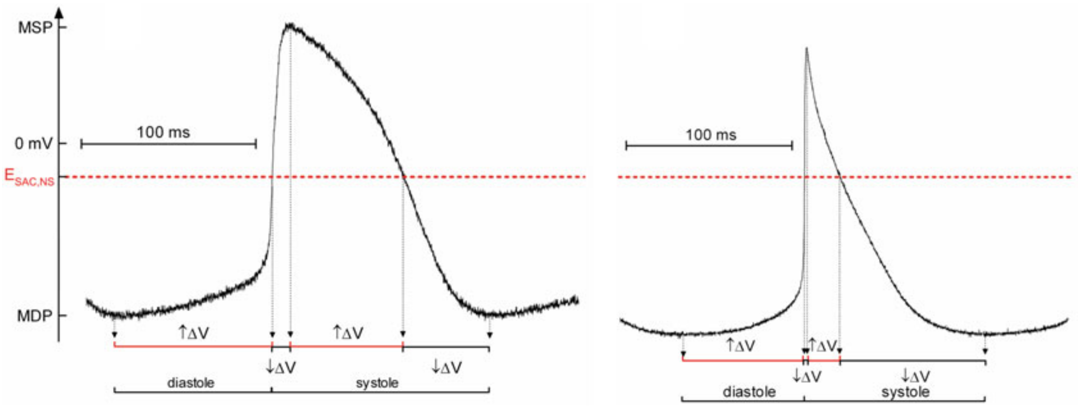

Fig. 7.2 Species differences in the theoretical effects of SAC_{NS} on the SAN cell AP. Membrane potential recordings illustrate the interrelation of cell electrophysiological parameters (MSP and MDP) and the SAC_{NS} reversal potential ($E_{SAC,NS}$). Time periods during which SAC_{NS} activation would either accelerate (↑ΔV) or slow (↓ΔV) intrinsic changes in SAN cell membrane potential are labelled. Left: rabbit SAN cell; right: mouse SAN cell. The rabbit SAN cell spends ~71% of cycle duration in ↑ΔV, whereas in the mouse, this phase accounts for just ~46%. (From [27], with permission)

endothelial cells, which are prone to suffer from tissue isolation and are removed by cell separation; or (3) removal of inter-cellular electrotonic coupling between identical and/or different cell populations. For instance, human fibroblasts have been found to contain SAC_{NS} [37], and functional electrotonic coupling has been shown to exist between fibroblasts and myocytes in native cardiac tissue [38, 39], including the SAN [40]. The possibility that fibroblasts may be important for stretch-induced changes in HR is supported by computational modelling, which predicts that stretch-modulation of fibroblast V_m could accelerate diastolic depolarisation in electrotonically coupled SAN myocytes by >20% [41]. Similar considerations may apply for macrophages, which have also been shown to be mechano-sensitive [42] and can electrotonically couple to cardiomyocytes, affecting their electrical activity [43, 44].

Finally, intrinsic cellular MEC responses could be amplified in vivo by interaction with autonomic signalling. Atrial pressure increases of just 2 mmHg, for example, induce both HR acceleration and a significant reduction in the percentage response to vagal stimulation in intact rabbit [45], effectively reducing the influence of underlying vagal tone. Thus, local and systemic HR modulation occur in conjunction and may amplify, or dampen, each other's effect.

7.2.5 Summary

The intrinsic HR response to stretch, such as caused by changes in venous return, is demonstrable at physiologically-relevant levels of mechanical stimulation, over multiple spatial scales. Intrinsic control has been estimated to contribute >30% of RSA during exercise in healthy individuals [16]. The evolutionary advantage of such a mechanism has been speculated to arise from earlier beat induction in response to cardiac filling (haemodynamic benefit), from improving cardiac pump function (which is more mechanically efficient when working at smaller radii), and/or from maximising pulmonary gas exchange (with reduced shunt volume) [13]. Alternatively, stretch effects on HR could be a side-effect of mechanisms that underlie mechanical modulation of contractile force [46].

Future investigations should consider the mounting evidence suggesting that SAN pacemaker rate depends not only on trans-sarcolemmal ion fluxes but involves an intracellular Ca^{2+} redistribution, driven by the release of

Ca^{2+} from the sarcoplasmic reticulum, followed by trans-sarcolemmal inward currents such as via the Na^+/Ca^{2+} exchanger [47]. Of note, stretch has been shown to increase sarcoplasmic reticulum Ca^{2+} release in ventricular cells [48–50], which—if present in SAN—could be relevant for the mechanical modulation of heart rate.

7.3 Pro-arrhythmic Effects of Mechanical Stimulation

7.3.1 Background

First observations that perturbation of the heart's mechanical status may initiate deadly cardiac arrhythmias were published nearly 150 years ago, with reports of sudden cardiac death associated with non-penetrating impact to the precordium (*Commotio cordis*, CC; for review, see [51]). More recently, rhythm disturbances due to internal mechanical stimulation during cardiac catheterisation have been observed [52]. It is now also believed that cardiac tachyarrhythmias, encountered in pathologies associated with non-uniform contraction, tissue remodelling, and/or volume or pressure overload are, in part, caused by electrophysiological responses to the altered mechanical environment [4, 5]. Arrhythmogenic effects of stretch on cardiac electrophysiology have been investigated in isolated whole heart, tissue and cellular models, helping to elucidate underlying mechanisms [5, 53].

7.3.2 Clinical Observations

Reports about pro-arrhythmic effects of acute external mechanical stimulation by CC [51], occasionally occurring during chest compressions soon after electrical defibrillation [54], together with cases of ectopy induction upon intracardiac catheter contact [52], suggest that heart rhythm disturbances can be related to intracardiac MEC effects. In vivo evidence also indicates that arrhythmogenic mechanical stimulation can be local or global. For instance, an increase in ventricular load by transient aortic occlusion during cardiac surgery has been shown to reduce longitudinal shortening and increase mechanical dispersion, which is associated with AP shortening and a pro-arrhythmic increase in local dispersion of AP duration [55], while balloon inflation during pulmonary valvuloplasty is associated with the induction of ventricular ectopy [56]. The same is true for the atria, where acute changes in volume loading have been found to increase the incidence and sustenance of arrhythmias [57]. Changes in atrial electrophysiology have also been seen with acute drops in atrial pressure during balloon commissurotomy for mitral stenosis and atrial flutter, as well as with short-term dual chamber pacing [57].

Effects of chronic stretch are usually observed in patients with sustained ventricular pressure or volume overload. Hypertension, congestive heart failure, and dilated cardiomyopathy are all associated with a high incidence of arrhythmias [58, 59]. It is difficult to assess, in these cases, whether mechanical stimulation directly contributes to rhythm disturbances or whether it acts via structural and functional tissue remodelling [60]. However, the observations that average daily blood pressure is highly correlated with the risk of ventricular tachyarrhythmias in heart failure patients [61], and that acute temporary removal of ventricular overload (e.g., by the Valsalva manoeuvre) can terminate chronic ventricular tachycardia [62], suggest that mechanical factors may play a role in the chronic setting.

7.3.3 Experimental Studies

Depolarisation of V_m by acute diastolic stretch has been demonstrated in isolated hearts, as well as in ventricular and atrial tissue and cell preparations [5]. In isolated hearts, a transient increase of intraventricular volume during diastole results in membrane depolarisation, which, if sufficiently large and rapid, can trigger premature ventricular excitation [63] and short periods of ventricular tachycardia (VT) [64].

The effects of acute systolic stretch are more complex. Both shortening and prolongation of the AP have been observed, along with early afterdepolarisation-like events, both in isolated cardiomyocytes and multicellular experimental preparations [5]. In the setting of CC, non-penetrating precordial impacts can induce rhythm disturbances in the absence of structural damage to the heart. The severity of arrhythmias, including ventricular fibrillation (VF), changes in an impact magnitude- and timing-dependent manner. This was first investigated experimentally some 90 years ago by Schlomka et al., who found that impacts to the precordial region of anaesthetised rabbits, cats, and dogs result in ectopic excitation and, in 20% of cases, VF [65, 66]. Importantly, they showed that mechanical induction of arrhythmias is not affected by bilateral vagotomy, indicating that arrhythmogenesis is not a result of a parasympathetic reflex. Furthermore, arrhythmia induction depends on the region of impact (mid and lower sternum are the most susceptible areas, especially for VF), the size of the contact area (smaller impact areas result in more severe rhythm disturbances), and the duration of the impact (rapid impacts are most arrhythmogenic). More recently, in a swine model of CC, Link et al. confirmed the importance of impact site, size, and severity and showed that only impacts during the early T-wave result in VF, while impacts at other times of the cardiac cycle produce various other transient rhythm disturbances [67]. A similar response has been demonstrated with a rapid increase in intraventricular volume in isolated rabbit hearts [68]. Acute volume loading has been shown to decrease conduction velocity, both in ventricles [69] and atria [57], which can contribute to the initiation and maintenance of arrhythmias. With volume loading of the atria, a reduction in AP duration and refractoriness, and an increase in dispersion of refractoriness, have been demonstrated, increasing the vulnerability to atrial fibrillation [57]. This can be prevented by acute atrial unloading [70]. Interestingly, it has been shown (by one of the editors of this book under her maiden name Theophile) that stretch of Purkinje fibres speeds up their rate of spontaneous diastolic depolarisation [71], while increasing conduction velocity [72], potentially leading to stretch-induced ectopy [71]. Other cardiac cell types, such as fibroblasts [41], pulmonary vein muscle cells [73], valve cells [74], chondrocytes, smooth muscle and endothelial cells [75], macrophages [42], and intracardiac neurons [76] are also mechano-sensitive, suggesting that the interplay between different cell types in the heart may be relevant for stretch-induced arrhythmogenesis, an important concept that has been insufficiently explored.

The similarity of effects of precordial impact and rapid intraventricular pressure increase raises an interesting question about the relative contribution of local versus global stretch to electrophysiological responses. This is highlighted by the large change in intraventricular pressure (brief spikes of more than 500 mmHg seen with precordial impact in the swine model), whose magnitude has been correlated with the probability of VF induction in vivo (maximum effects between 250 and 450 mmHg) [77]. Myocardial compliance varies throughout the ventricle (which may also be affected by regional differences in coronary vascular pressure), so gross changes in intraventricular pressure or volume will result in a heterogeneous distribution of tissue stretch. This is supported by the observation that intraventricular volume changes yield non-uniform depolarisation, with the origin of any stretch-induced excitation most often in the posterolateral region of the left ventricle, typically an area of high compliance [63]. The only published data of intraventricular activation sequence during extracorporeal CC impacts from a single pig experiment suggests focal excitation of the ventricle right underneath the impact site. This suggests a more directly impact site-related mechanism and reemphasises the question of the relative causal contributions of global and local stretch to arrhythmogenesis [78].

In isolated heart models, large intraventricular pressure pulses (between 200 and 280 mmHg) have been used to trigger VF [68]. At the same time, local low-energy non-traumatic impacts, timed with the early T-wave, can induce VF in isolated guinea pig [79] and rabbit hearts [80]. Epicardial optical mapping revealed the presence of deformation-magnitude-dependent focal activation [80, 81]. This results in VF only when there is spatiotemporal overlap of the mechanical stimulus with the trailing wave of repolarisation [80], as predicted in prior modelling work (see next section) [82].

The idea that the structural heterogeneity of ventricular tissue modulates globally applied stretch to create heterogeneous strain distributions and focal sites of excitation that lead to initiation of re-entrant arrhythmias is further supported by a study that used optical mapping with stretch applied across a right ventricular tissue flap [83]. This demonstrated that focal excitation originates at the point of largest strain differences, which can result in sustained re-entrant tachyarrhythmias. Similarly, an increase in the probability of mechanically induced excitation in areas showing paradoxical segment lengthening has been observed in diseases with heterogeneous changes in ventricular compliance, such as regional ischaemia [84] and infarction [85]. In acute regional ischaemia, the degree of dilation of the acutely ischaemic tissue is a strong predictor of the probability of arrhythmogenesis, including VF [86]. The role of heterogeneous stretch in VF induction is further supported by experiments showing that acute localised stretch increases the complexity of VF activation maps, with more areas of conduction block and breakthrough patterns [87]. Such heterogeneities in stress-strain distribution would result in significant differences in mechanical stimulation of cells, which could give rise to local ectopic foci and regions of functional block.

7.3.4 Underlying Mechanisms

Pro-arrhythmic effects of myocardial stretch can be explained, in part at least, by SAC activation. Two sub-categories of SAC can be distinguished in myocardium: SAC_{NS}, which allow passage of various cations (E_{rev} usually between 0 and –20 mV), and potassium-selective SAC_K (E_{rev} near –90 mV; for review see [88]). During diastolic stretch, V_m tends to show depolarisation (Fig. 7.3), which can be explained by a predominant contribution of SAC_{NS} (SAC_K would cause diastolic hyperpolarisation, which is not seen in cardiac cells). Systolic stretch primarily accelerates AP repolarisation, which could be caused by either SAC sub-type [90].

A predominant contribution to stretch-induced changes in V_m by SAC_{NS} is further supported by the observation that MEC effects can be eliminated in ventricles [80, 91] and atria [57] by pharmacological block of this channel. In turn, activation of SAC_{NS} is sufficient to trigger AP generation in isolated cardiomyocytes [92]. Interestingly, SAC_{NS} blockers do not prevent the reduction in refractory period seen with atrial pressure-loading of the isolated heart, suggesting that SAC_K may contribute to responses in that setting [93].

Relative contributions of SAC_{NS} and SAC_K to impact-induced VF have remained controversial. The vulnerable window for VF induction coincides with a period of pronounced heterogeneity in ventricular V_m and refractoriness. Mechanical stimulation, in this setting, depolarises cells that have regained excitability (presumably a SAC_{NS} effect, potentially giving rise to ectopic foci), while in other cells that are still more depolarised the time-course of repolarisation is altered (possibly through both SAC_{NS} and/or SAC_K effects, increasing heterogeneity in refractoriness). The former may provide the trigger, and the latter a sustaining mechanism for arrhythmias, including VF. Among experimentally proposed contributors is the ATP-dependent potassium channel (K_{ATP}), whose open probability is also modulated by stretch [94]. In the presence of glibenclamide (to block K_{ATP}), the incidence of VF upon precordial impact is significantly reduced in pig. At the same time, impacts during the T-wave still trigger premature ventricular contractions, highlighting the continued ability to mechanically induce an arrhythmogenic trigger [95]. Application of streptomycin in the same animal model did not affect VF inducibility [96], but as mentioned before there is potential for false-negative interpretation of data obtained with systemic streptomycin application (as it doesn't block SAC_{NS} well in intact tissue). In rabbit isolated hearts, block of SAC_{NS} with GsMTx-4 was indeed effective in preventing mechanically induced VF [80]. Thus, activation of SAC_{NS} seems to be a necessary contributor to CC.

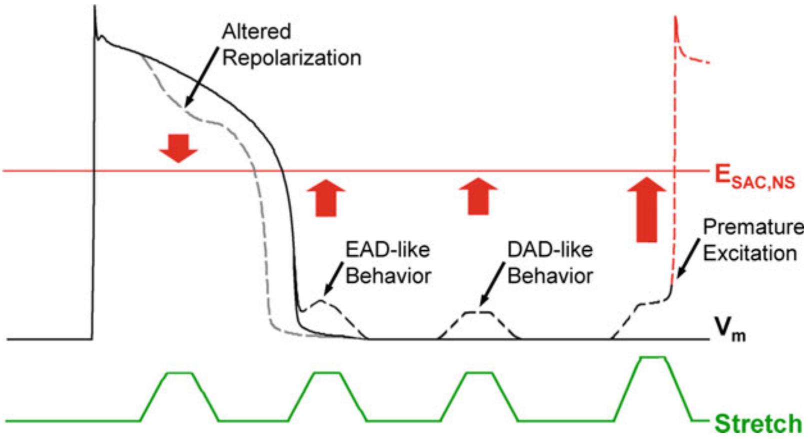

Fig. 7.3 Schematic representation of transient stretch effects on whole-cell V_m. SAC_{NS} have a reversal potential ($E_{SAC,NS}$) about halfway between plateau and resting potentials. Depending on the timing of mechanical stimuli (bottom curve), SAC_{NS} activation may shorten AP duration, cause early or delayed after-depolarisation-like behaviour, or—if strong enough—trigger excitation (top curve). The reversal potential of SAC_K is negative to resting V_m. Their activation, during *any* part of the cardiac cycle, would tend to re- or hyperpolarise cardiac cells, in particular during the AP plateau (when their electrotonic driving force is largest). Given that diastolic stretch, if it causes any change in V_m at all, tends to depolarise resting cells, thus this response appears to be dominated by SAC_{NS} under normal circumstances. (From [89], with permission)

The principal electrophysiological consequences of cardiac MEC have been reproduced in various computational models of cardiomyocyte SAC effects [97]. These formulations have been integrated into two- [82] and three-dimensional models [98] of ventricular tissue, which suggest that sustained re-entry is observed only if a mechanical stimulus (1) encounters tissue that has regained excitability (so that a mechanically-induced ectopic focus can arise), (2) overlaps with the trailing wave of repolarisation (so that local AP prolongation gives rise to an area of the functional block at the intersection of the preceding and new excitation wave), and (3) extends into tissue that is still at more positive V_m levels (so that regional AP shortening may help to sustain the arrhythmia). This would explain why the most severe expression of CC, sudden cardiac death from VF, is rare in real life. The view that ischaemic segment lengthening may be responsible for mechanically induced excitation and re-entry has also been supported by three-dimensional computational modelling, suggesting that premature ventricular excitation originates from the ischaemic border because of mechanically induced depolarisation [99]. These computational predictions form interesting targets for further experimental assessment.

7.3.5 Summary

Stretch of the myocardium, whether acute or chronic, has pronounced effects on cardiac electrophysiology. This can contribute to induction and sustenance of cardiac arrhythmias. Experimental models have reproduced the effects of stretch on heart rhythm in single cells, tissue preparations, isolated hearts and whole animals, demonstrating that a significant proportion of mechanically induced changes in heart rate and rhythm can be explained by intracardiac MEC. Experimental and computational work strongly suggests a role for SAC in these responses. In addition to mechanically *gated* SAC, most ion channels in the heart can be *modulated* by the mechanical environment [100], which complicates the picture, in particular as longer-term responses mediated via altered intracellular ion concentrations are concerned. In addition, effects of heterogeneous stretch on myocardial Ca^{2+} handling have been shown to independently act as sources of ectopic excitation (for a review, see [101]). The molecular mechanisms by which ion channels (and Ca^{2+} handling proteins) sense mechanical changes, as well as their individual roles in the generation of arrhythmias, may, in the long run, help to devise new pharmacological and device therapies to treat diseases associated with stretch-induced changes in cardiac electrophysiology.

7.4 Anti-arrhythmic Effects of Mechanical Stimulation

7.4.1 Background

Schott's observation that a forceful blow to the chest wall (precordial thump, PT) could restore a palpable pulse of a patient in ventricular standstill during a Stokes-Adams attack, published in 1920, is believed to have been the first report on anti-arrhythmic effects of mechanical stimulation in the Western medical literature [102]. Since then, mechanical resuscitation has been attempted using a range of interventions. However, even though PT has been a documented part of European clinical practice for much of the past century, there is little agreement on the mechanisms and clinical utility of mechanical cardioversion.

7.4.2 Clinical Observations

Anti-arrhythmic mechanical stimulation has been observed in various clinical settings [103]. In his studies of 'intracardiac therapy' in the 1930s, Hyman found that the mechanical interaction of a needle with the myocardium could induce contractile activity [104]. Similarly, direct myocardial contact with catheters can cause ectopic excitation, with case reports illustrating termination of VT, ventricular bradycardia [52], and even atrial fibrillation [105]. Cardiac mechano-sensitivity is also exploited by cardiac surgeons when weaning the heart from cardiopulmonary bypass, where finger tapping of the heart may serve to restore rhythmic contractile activity, in particular after failed electrical defibrillation. Extracorporeal mechanical stimuli can trigger contractions in ventricular standstill [106], for example, to maintain consciousness in cardiac arrest victims [107] and (although less reliably) terminate VT and VF [108]. Several reports have also found a link between an abrupt increase in intra-thoracic pressure (due to coughing [109] or the Valsalva manoeuvre [62]) and termination of tachyarrhythmias, although contributions by the nervous system and/or improved coronary perfusion have not been differentially assessed.

7.4.3 Experimental Studies

The use of cardiac catheterisation to terminate sustained cardiac arrhythmias was systematically explored in patients by Befeler [52], who showed that catheter tip stimulation of atrial and ventricular muscle is effective in reverting various rhythm disturbances (24% of atrial tachycardia cases, 60% of junctional tachycardias, and 14% of VT).

The success rate of PT has been studied with highly variable results. In the report by Befeler, 27% of VT cases were successfully treated with PT [52], while other investigations have shown success rates exceeding 40% [110]. Only a handful of prospective studies on PT effects have been published, all of which demonstrated vanishingly low success rates of tachyarrhythmia termination by PT (below 2%) [111–114]. However, the use of PT may be more promising in the asystolic heart, where PT-induced restoration of spontaneous circulation was found in 50% of asystolic cardiac arrest victims (although this study suffers from low n-numbers, so extrapolation to practice should be done with care) [114].

The (limited) clinical utility of PT in the setting of VF [115] appears to be related to time-since-collapse, as all reported successful cases of PT-induced cardioversion occurred very early during the development of VF, either at the verge of VT deterioration [116] or within the first few seconds of VF [52]. Animal models of PT have shown a similar disparity of results, with success rates ranging from 0% in an asphyxiated dog model [117] to 95% in a post-infarction pig model [118], suggesting that the utility of PT may be inversely related to myocardial tissue energy supply. Also, in keeping with clinical data, repetitive extracorporeal mechanical stimuli in a pig model of cardiac standstill have been shown to be an effective means to mechanically pace the heart [119].

7.4.4 Underlying Mechanisms

The mechanisms underlying mechanical induction of ectopic excitation in the asystolic heart have been discussed above, and similar mechanisms may underlie PT pacing of patients in ventricular standstill. The dynamic interaction of SAC effects with ectopic foci and/or re-entrant excitation in the tachycardiac heart is more complex.

During mechanical stimulation in VT and VF, cells in the excitable gap(s) will be near the resting V_m, while others will be at various stages of the AP (somewhat like in the setting of CC, only that there will be multiple waves that co-exist in the tissue). Stretch of resting cells, if of sufficient amplitude, may cause excitation and obliterate the excitable gap. In cases where no re-entrant circles survive and no new ones are created by the intervention, this may terminate the arrhythmia. Computational simulations have shown that this conceptual view is biophysically plausible, using two- [97] and three-dimensional models [120]. Interestingly, these simulations also highlight how reduced availability in energy substrates may render PT less efficient. This is mediated via an ATP-reduction induced ‘pre-conditioning’ of K_{ATP} channels, which activate more readily upon mechanical stimulation in ischaemic conditions [121]. In the models, mechanical co-activation of K_{ATP} channels shifts the whole-cell ‘net’ E_{rev} towards more negative potentials, compared to what would be encountered with SAC_{NS} activation alone. This shortens AP duration and reduces the ability of mechanical stimulation to obliterate excitable gaps by depolarisation, with eventual failure to terminate re-entry, as observed in the setting of severe hypoxia [117].

7.4.5 Summary

The anti-arrhythmic effects of mechanical stimulation in various settings have been known to medical practitioners for over a century. PT can be utilised to pace the asystolic heart or, less successfully, to terminate tachyarrhythmias. These beneficial effects have been attributed to SAC_{NS} activation. However, reported success rates vary drastically, and even though PT can be quickly and easily applied, recent international resuscitation guidelines have de-emphasised PT as an emergency intervention in cardiac arrest [122, 123]. There is a concern, also, regarding the timing of PT, due to potential pro-arrhythmic effects of mechanical stimulation. The idea, however, that ill-timed PT would easily convert VT to VF has not been confirmed in most studies, except in the setting of pre-existing severe hypoxia [117]. Overall, reported PT side effects have been rare and minor. The variable success rates of PT may be related to a lack of training and/or variability in energy delivery by individuals applying PT. The scarcity of prospective study data calls for further research, to help identify the clinical utility of PT, and to explore the potential for more sophisticated mechanical interventions in emergency medicine and anti-arrhythmic therapy.

7.5 Conclusion

The heart is an integrated electro-mechanical system. Firmly established mechanisms underlying cardiac MEC effects include mechanical modulation of trans-sarcolemmal ion fluxes and intracellular Ca^{2+}handling. MEC affects heart rate and rhythm, from venous return-mediated changes in SAN pacemaker rate, to stretch-induced induction or termination of arrhythmias.

What is less clear is the physiological relevance of MEC [124]. Of course, from a regulation theory point of view, ECC *should* be complemented by an intracardiac feedback pathway from mechanics to electrics [125]. But perhaps many of the 'most striking' examples of MEC effects on electrophysiology are, in fact, secondary to mechanisms involved in the mechanical modulation of contractility. Strategies successfully employed in skeletal muscle force grading, such as spatial recruitment or temporal summation of muscle fibre contractility, are ill-suited for the heart, where all cells contract during every cardiac cycle, where long AP plateaus cover most or all of the period during which cytosolic free Ca^{2+} is elevated, and where neuro-muscular junctions for individual cells are missing. Thus, cardiac myocytes must be able to actively adjust their own contractility to locally prevailing, and dynamically changing, mechanical demands. If this involved mechanisms (such as SAC) that—in response to distension (or reduced active cell shortening)—allowed a cardiomyocyte to preserve or gain Ca^{2+} (whether directly or indirectly via Na^+ influx with knock-on effects on Na^+/Ca^{2+} exchanger flux balance), then that would offer an evolutionary advantage. This advantage for autoregulation of *mechanics* may well be more important than the associated 'side-effect' on *electrics* of inward currents, which carry a risk of triggering ectopic excitation or of contributing to the sustenance of tachyarrhythmias.

Clearly, cardiac bi-directional electro-mechanical cross-talk is an area for further study. What is without question is that the heart is an exquisitely mechano-sensitive organ, and that this mechano-sensitivity has direct effects on heart rate and rhythm.

Acknowledgements Work in the authors' laboratories is supported by the Canadian Institutes of Health Research (MOP 342562 to TAQ), the Natural Sciences and Engineering Research Council of Canada (RGPIN-2016-04879 to TAQ), the Heart and Stroke Foundation of Canada (G-18-0022185 and National New Investigator Award to TAQ), and the German Research Foundation (Collaborative Research Centre 'SFB 1425' #422681845; PK). RAC was supported by the Wellcome Trust and Royal Society (109371/Z/15/Z).

References

1. Bers DM. Cardiac excitation-contraction coupling. Nature. 2002;415:198–205.
2. Eisner DA, Caldwell JL, Kistamas K, Trafford AW. Calcium and excitation-contraction coupling in the heart. Circ Res. 2017;121:181–95.
3. Peyronnet R, Nerbonne JM, Kohl P. Cardiac mechano-gated ion channels and arrhythmias. Circ Res. 2016;118:311–29.
4. Quinn TA. The importance of non-uniformities in mechano-electric coupling for ventricular arrhythmias. J Interv Card Electrophysiol. 2014;39: 25–35.
5. Quinn TA, Kohl P. Cardiac mechano-electric coupling: acute effects of mechanical stimulation on heart rate and rhythm. Physiol Rev. 2021;101:37–92.
6. Quinn TA, Kohl P, Ravens U. Cardiac mechano-electric coupling research: fifty years of progress and scientific innovation. Prog Biophys Mol Biol. 2014;115:71–5.
7. Bainbridge FA. The influence of venous filling upon the rate of the heart. J Physiol. 1915;50:65–84.
8. Quinn TA, Kohl P. The Bainbridge effect: stretching our understanding of cardiac pacemaking for more than a century. J Physiol. 2022;600:4377–9.
9. Donald DE, Shepherd JT. Reflexes from the heart and lungs: physiological curiosities or important regulatory mechanisms. Cardiovasc Res. 1978;12:446–69.
10. Blinks JR. Positive chronotropic effect of increasing right atrial pressure in the isolated mammalian heart. Am J Physiol. 1956;186:299–303.
11. Deck KA. Dehnungseffekte am spontanschlagenden, isolierten Sinusknoten. Pflugers Arch Gesamte Physiol Menschen Tiere. 1964;280:120–30.
12. Cooper PJ, Lei M, Cheng LX, Kohl P. Selected contribution: axial stretch increases spontaneous pacemaker activity in rabbit isolated sinoatrial node cells. J Appl Physiol. 2000;89:2099–104.
13. Yasuma F, Hayano J. Respiratory sinus arrhythmia: why does the heartbeat synchronize with respiratory rhythm? Chest. 2004;125:683–90.
14. Bernardi L, Keller F, Sanders M, Reddy PS, Griffith B, Meno F, et al. Respiratory sinus arrhythmia in the denervated human heart. J Appl Physiol. 1989;67:1447–55.
15. Bernardi L, Salvucci F, Suardi R, Solda PL, Calciati A, Perlini S, et al. Evidence for an intrinsic mechanism regulating heart rate variability in the transplanted and the intact heart during submaximal dynamic exercise? Cardiovasc Res. 1990;24:969–81.
16. Casadei B, Moon J, Johnston J, Caiazza A, Sleight P. Is respiratory sinus arrhythmia a good index of cardiac vagal tone in exercise? J Appl Physiol. 1996;81:556–64.
17. Brooks CM, Lu HH, Lange G, Mangi R, Shaw RB, Geoly K. Effects of localized stretch of the sinoatrial

node region of the dog heart. Am J Physiol. 1966;211:1197–202.

18. Wilson SJ, Bolter CP. Do cardiac neurons play a role in the intrinsic control of heart rate in the rat? Exp Physiol. 2002;87:675–82.
19. Hagiwara N, Masuda H, Shoda M, Irisawa H. Stretch-activated anion currents of rabbit cardiac myocytes. J Physiol. 1992;456:285–302.
20. Lei M, Kohl P. Swelling-induced decrease in spontaneous pacemaker activity of rabbit isolated sino-atrial node cells. Acta Physiol Scand. 1998;164:1–12.
21. Clemo HF, Stambler BS, Baumgarten CM. Persistent activation of a swelling-activated cation current in ventricular myocytes from dogs with tachycardia-induced congestive heart failure. Circ Res. 1998;83: 147–57.
22. Le Guennec JY, Peineau N, Argibay JA, Mongo KG, Garnier D. A new method of attachment of isolated mammalian ventricular myocytes for tension recording: length dependence of passive and active tension. J Mol Cell Cardiol. 1990;22:1083–93.
23. Craelius W, Chen V, el-Sherif N. Stretch activated ion channels in ventricular myocytes. Biosci Rep. 1988;8:407–14.
24. MacDonald EA, Stoyek MR, Rose RA, Quinn TA. Intrinsic regulation of sinoatrial node function and the zebrafish as a model of stretch effects on pacemaking. Prog Biophys Mol Biol. 2017;130: 198–211.
25. Baillie JS, Gendernalik A, Garrity DM, Bark D Jr, Quinn TA. The in vivo study of cardiac mechano-electric and mechanomechanical coupling during heart development in zebrafish. Front Physiol. 2023;14:1086050.
26. Cooper PJ, Kohl P. Species- and preparation-dependence of stretch effects on sino-atrial node pacemaking. Ann N Y Acad Sci. 2005;1047:324–35.
27. Cooper PJ, Kohl P. Mechanical modulation of sino-atrial node pacemaking. In: Kohl P, Franz MR, Sachs F, editors. Cardiac mechano-electric feedback and arrhythmias: from pipette to patient. Philadelphia: Saunders (Elsevier); 2005. p. 72–82.
28. MacDonald EA, Madl J, Greiner J, Ramadan AF, Wells SM, Torrente AG, et al. Sinoatrial node structure, mechanics, electrophysiology and the chronotropic response to stretch in rabbit and mouse. Front Physiol. 2020;11:809.
29. Kohl P, Crampin EJ, Quinn TA, Noble D. Systems biology: an approach. Clin Pharmacol Ther. 2010;88: 25–33.
30. Quinn TA, Kohl P. Combining wet and dry research: experience with model development for cardiac mechano-electric structure-function studies. Cardiovasc Res. 2013;97:601–11.
31. Suchyna TM, Johnson JH, Hamer K, Leykam JF, Gage DA, Clemo HF, et al. Identification of a peptide toxin from *Grammostola spatulata* spider venom that blocks cation-selective stretch-activated channels. J Gen Physiol. 2000;115:583–98.
32. Quinn TA, Kohl P. Systems biology of the heart: hype or hope? Ann N Y Acad Sci. 2011;1245:40–3.
33. Jansen HJ, Quinn TA, Rose RA. Cellular sinoatrial node and atrioventricular node activity in the heart. In: Vasan RS, Sawyer DB, editors. Encyclopedia of cardiovascular research and medicine. Amsterdam: Elsevier; 2018. p. 576–92.
34. MacDonald EA, Quinn TA. What keeps us ticking? Sinoatrial node mechano-sensitivity: the grandfather-clock of cardiac rhythm. Biophys Rev. 2021;13:707–16.
35. MacDonald EA, Rose RA, Quinn TA. Neurohumoral control of sinoatrial node activity and heart rate: insight from experimental models and findings from humans. Front Physiol. 2020;11:170.
36. Quinn TA, Kohl P. Mechano-sensitivity of cardiac pacemaker function: pathophysiological relevance, experimental implications, and conceptual integration with other mechanisms of rhythmicity. Prog Biophys Mol Biol. 2012;110:257–68.
37. Stockbridge LL, French AS. Stretch-activated cation channels in human fibroblasts. Biophys J. 1988;54: 187–90.
38. Quinn TA, Camelliti P, Rog-Zielinska EA, Siedlecka U, Poggioli T, O'Toole ET, et al. Electrotonic coupling of excitable and nonexcitable cells in the heart revealed by optogenetics. Proc Natl Acad Sci U S A. 2016;113:14852–7.
39. Rubart M, Tao W, Lu XL, Conway SJ, Reuter SP, Lin SF, et al. Electrical coupling between ventricular myocytes and myofibroblasts in the infarcted mouse heart. Cardiovasc Res. 2018;114:389–400.
40. Camelliti P, Green CR, LeGrice I, Kohl P. Fibroblast network in rabbit sinoatrial node: structural and functional identification of homogeneous and heterogeneous cell coupling. Circ Res. 2004;94:828–35.
41. Kohl P, Kamkin AG, Kiseleva IS, Noble D. Mechanosensitive fibroblasts in the sino-atrial node region of rat heart: interaction with cardiomyocytes and possible role. Exp Physiol. 1994;79:943–56.
42. Atcha H, Jairaman A, Holt JR, Meli VS, Nagalla RR, Veerasubramanian PK, et al. Mechanically activated ion channel Piezo1 modulates macrophage polarization and stiffness sensing. Nat Commun. 2021;12: 3256.
43. Simon-Chica A, Fernández MC, Wülfers EM, Lother A, Hilgendorf I, Seemann G, et al. Novel insights into the electrophysiology of murine cardiac macrophages: relevance of voltage-gated potassium channels. Cardiovasc Res. 2022;118:798–813.
44. Hulsmans M, Clauss S, Xiao L, Aguirre AD, King KR, Hanley A, et al. Macrophages facilitate electrical conduction in the heart. Cell. 2017;169:510–22.
45. Bolter CP, Wilson SJ. Influence of right atrial pressure on the cardiac pacemaker response to vagal stimulation. Am J Physiol. 1999;276:R1112–7.

46. Quinn TA, Kohl P. Rabbit models of cardiac mechano-electric and mechano-mechanical coupling. Prog Biophys Mol Biol. 2016;121:110–22.
47. Lakatta EG, Maltsev VA, Vinogradova TM. A coupled SYSTEM of intracellular Ca^{2+} clocks and surface membrane voltage clocks controls the timekeeping mechanism of the heart's pacemaker. Circ Res. 2010;106:659–73.
48. Cameron BA, Kai H, Kaihara K, Iribe G, Quinn TA. Ischemia enhances the acute stretch-induced increase in calcium spark rate in ventricular myocytes. Front Physiol. 2020;11:289.
49. Iribe G, Ward CW, Camelliti P, Bollensdorff C, Mason F, Burton RA, et al. Axial stretch of rat single ventricular cardiomyocytes causes an acute and transient increase in Ca^{2+} spark rate. Circ Res. 2009;104: 787–95.
50. Prosser BL, Ward CW, Lederer WJ. X-ROS signaling: rapid mechano-chemo transduction in heart. Science. 2011;333:1440–5.
51. Nesbitt AD, Cooper PJ, Kohl P. Rediscovering *Commotio cordis*. Lancet. 2001;357:1195–7.
52. Befeler B. Mechanical stimulation of the heart: its therapeutic value in tachyarrhythmias. Chest. 1978;73:832–8.
53. Quinn TA, Kohl P. Mechanical triggers and facilitators of ventricular tachy-arrhythmias. In: Kohl P, Sachs F, Franz M, editors. Cardiac mechano-electric coupling and arrhythmias. Oxford: Oxford University Press; 2011. p. 160–7.
54. Berdowski J, Tijssen JG, Koster RW. Chest compressions cause recurrence of ventricular fibrillation after the first successful conversion by defibrillation in out-of-hospital cardiac arrest. Circ Arrhythm Electrophysiol. 2010;3:72–8.
55. Orini M, Taggart P, Bhuva A, Roberts N, Di Salvo C, Yates M, et al. Direct in-vivo assessment of global and regional mechano-electric feedback in the intact human heart. Heart Rhythm. 2021;18(8):1406–13.
56. Levine JH, Guarnieri T, Kadish AH, White RI, Calkins H, Kan JS. Changes in myocardial repolarization in patients undergoing balloon valvuloplasty for congenital pulmonary stenosis: evidence for contraction-excitation feedback in humans. Circulation. 1988;77:70–7.
57. Ninio DM, Saint DA. The role of stretch-activated channels in atrial fibrillation and the impact of intracellular acidosis. Prog Biophys Mol Biol. 2008;97: 401–16.
58. Kohl P, Hunter P, Noble D. Stretch-induced changes in heart rate and rhythm: clinical observations, experiments and mathematical models. Prog Biophys Mol Biol. 1999;71:91–138.
59. Cameron BA, Kohl P, Quinn TA. Cellular and subcellular mechanisms of ventricular mechano-arrhythmogenesis. In: Hecker M, Duncker DJ, editors. Cardiac mechanobiology in physiology and disease. Cham: Springer; 2023. p. 256–98.
60. Sutherland GR. Sudden cardiac death: the pro-arrhythmic interaction of an acute loading with an underlying substrate. Eur Heart J. 2017;38:2986–94.
61. Reiter MJ, Stromberg KD, Whitman TA, Adamson PB, Benditt DG, Gold MR. Influence of intracardiac pressure on spontaneous ventricular arrhythmias in patients with systolic heart failure: insights from the REDUCEhf trial. Circ Arrhythm Electrophysiol. 2013;6:272–8.
62. Waxman MB, Wald RW, Finley JP, Bonet JF, Downar E, Sharma AD. Valsalva termination of ventricular tachycardia. Circulation. 1980;62:843–51.
63. Franz MR, Cima R, Wang D, Profitt D, Kurz R. Electrophysiological effects of myocardial stretch and mechanical determinants of stretch-activated arrhythmias. Circulation. 1992;86:968–78.
64. Hansen DE, Craig CS, Hondeghem LM. Stretch-induced arrhythmias in the isolated canine ventricle. Evidence for the importance of mechanoelectrical feedback. Circulation. 1990;81:1094–105.
65. Schlomka G, Hinrichs A. Experimentelle Untersuchungen über den Einfluß stumpfer Brustkorbverletzungen auf das Elektrokardiogramm. Z Ges Exp Med. 1932;81:43–61.
66. Schlomka G, Hinrichs A. Untersuchungen über den Einfluß stumpfer Brustkorbtraumen auf das Elektrokardiogramm (II. Mitteilung). Z Ges Exp Med. 1932;83:779–91.
67. Link MS, Wang PJ, Pandian NG, Bharati S, Udelson JE, Lee MY, et al. An experimental model of sudden death due to low-energy chest-wall impact (*Commotio cordis*). N Engl J Med. 1998;338:1805–11.
68. Bode F, Franz M, Wilke I, Bonnemeier H, Schunkert H, Wiegand U. Ventricular fibrillation induced by stretch pulse: implications for sudden death due to *Commotio cordis*. J Cardiovasc Electrophysiol. 2006;17:1011–7.
69. Sung D, Mills RW, Schettler J, Narayan SM, Omens JH, McCulloch AD. Ventricular filling slows epicardial conduction and increases action potential duration in an optical mapping study of the isolated rabbit heart. J Cardiovasc Electrophysiol. 2003;14:739–49.
70. Ishikawa K, Watanabe S, Lee P, Akar FG, Lee A, Bikou O, et al. Acute left ventricular unloading reduces atrial stretch and inhibits atrial arrhythmias. J Am Coll Cardiol. 2018;72:738–50.
71. Kaufmann R, Theophile U. Automatie-fördernde Dehnungseffekte an Purkinje-Fäden, Papillarmuskeln und Vorhoftrabekeln von Rhesus-Affen. Pflugers Arch Gesamte Physiol Menschen Tiere. 1967;297:174–89.
72. Dominguez G, Fozzard HA. Effect of stretch on conduction velocity and cable properties of cardiac Purkinje fibers. Am J Physiol. 1979;237:C119–24.
73. Chang SL, Chen YC, Chen YJ, Wangcharoen W, Lee SH, Lin CI, et al. Mechanoelectrical feedback

regulates the arrhythmogenic activity of pulmonary veins. Heart. 2007;93:82–8.

74. Al-Shammari H, Latif N, Sarathchandra P, McCormack A, Rog-Zielinska EA, Raja S, et al. Expression and function of mechanosensitive ion channels in human valve interstitial cells. PLoS One. 2020;15:e0240532.
75. Wang JH, Thampatty BP. Mechanobiology of adult and stem cells. Int Rev Cell Mol Biol. 2008;271:301–46.
76. Beaumont E, Salavatian S, Southerland EM, Vinet A, Jacquemet V, Armour JA, et al. Network interactions within the canine intrinsic cardiac nervous system: implications for reflex control of regional cardiac function. J Physiol. 2013;591:4515–33.
77. Link MS, Maron BJ, Wang PJ, VanderBrink BA, Zhu W, Estes NA 3rd. Upper and lower limits of vulnerability to sudden arrhythmic death with chest-wall impact (*Commotio cordis*). J Am Coll Cardiol. 2003;41:99–104.
78. Alsheikh-Ali AA, Akelman C, Madias C, Link MS. Endocardial mapping of ventricular fibrillation in *Commotio cordis*. Heart Rhythm. 2008;5:1355–6.
79. Cooper PJ, Epstein A, Macleod IA, Schaaf ST, Sheldon J, Boulin C, et al. Soft tissue impact characterisation kit (STICK) for ex situ investigation of heart rhythm responses to acute mechanical stimulation. Prog Biophys Mol Biol. 2006;90:444–68.
80. Quinn TA, Jin H, Lee P, Kohl P. Mechanically induced ectopy *via* stretch-activated cation-nonselective channels is caused by local tissue deformation and results in ventricular fibrillation if triggered on the repolarization wave edge (*Commotio cordis*). Circ Arrhythm Electrophysiol. 2017;10:e004777.
81. Quinn TA, Kohl P. Comparing maximum rate and sustainability of pacing by mechanical vs. electrical stimulation in the Langendorff-perfused rabbit heart. Europace. 2016;18:iv85-iv93.
82. Garny A, Kohl P. Mechanical induction of arrhythmias during ventricular repolarization: modeling cellular mechanisms and their interaction in two dimensions. Ann N Y Acad Sci. 2004;1015: 133–43.
83. Seo K, Inagaki M, Nishimura S, Hidaka I, Sugimachi M, Hisada T, et al. Structural heterogeneity in the ventricular wall plays a significant role in the initiation of stretch-induced arrhythmias in perfused rabbit right ventricular tissues and whole heart preparations. Circ Res. 2010;106:176–84.
84. Parker KK, Lavelle JA, Taylor LK, Wang Z, Hansen DE. Stretch-induced ventricular arrhythmias during acute ischemia and reperfusion. J Appl Physiol. 2004;97:377–83.
85. Lu F, Jun-Xian C, Rong-Sheng X, Jia L, Ying H, Li-Qun Z, et al. The effect of streptomycin on stretch-induced electrophysiological changes of isolated acute myocardial infarcted hearts in rats. Europace. 2007;9:578–84.
86. Barrabes JA, Garcia-Dorado D, Padilla F, Agullo L, Trobo L, Carballo J, et al. Ventricular fibrillation during acute coronary occlusion is related to the dilation of the ischemic region. Basic Res Cardiol. 2002;97:445–51.
87. Chorro FJ, Trapero I, Guerrero J, Such LM, Canoves J, Mainar L, et al. Modification of ventricular fibrillation activation patterns induced by local stretching. J Cardiovasc Electrophysiol. 2005;16: 1087–96.
88. Sachs F. Mechanical transduction by membrane ion channels: a mini review. Mol Cell Biochem. 1991;104:57–60.
89. Kohl P. Cardiac stretch-activated channels and mechano-electric transduction. In: Zipes DP, Jalife J, editors. Cardiac electrophysiology: from cell to bedside. Philadelphia: Saunders; 2009. p. 115–26.
90. Zabel M, Koller BS, Sachs F, Franz MR. Stretch-induced voltage changes in the isolated beating heart: importance of the timing of stretch. Cardiovasc Res. 1996;32:120–30.
91. Hansen DE, Borganelli M, Stacy GP, Taylor LK. Dose-dependent inhibition of stretch-induced arrhythmias by gadolinium in isolated canine ventricles. Evidence for a unique mode of antiarrhythmic action. Circ Res. 1991;69:820–31.
92. Craelius W. Stretch-activation of rat cardiac myocytes. Exp Physiol. 1993;78:411–23.
93. Bode F, Sachs F, Franz MR. Tarantula peptide inhibits atrial fibrillation. Nature. 2001;409:35–6.
94. Van Wagoner DR. Mechanosensitive gating of atrial ATP-sensitive potassium channels. Circ Res. 1993;72:973–83.
95. Link MS, Wang PJ, VanderBrink BA, Avelar E, Pandian NG, Maron BJ, et al. Selective activation of the K^+(ATP) channel is a mechanism by which sudden death is produced by low-energy chest-wall impact (*Commotio cordis*). Circulation. 1999;100: 413–8.
96. Garan AR, Maron BJ, Wang PJ, Estes NA 3rd, Link MS. Role of streptomycin-sensitive stretch-activated channel in chest wall impact induced sudden death (*Commotio cordis*). J Cardiovasc Electrophysiol. 2005;16:433–8.
97. Kohl P, Bollensdorff C, Garny A. Effects of mechanosensitive ion channels on ventricular electrophysiology: experimental and theoretical models. Exp Physiol. 2006;91:307–21.
98. Li W, Kohl P, Trayanova N. Induction of ventricular arrhythmias following mechanical impact: a simulation study in 3D. J Mol Histol. 2004;35:679–86.
99. Jie X, Gurev V, Trayanova N. Mechanisms of mechanically induced spontaneous arrhythmias in acute regional ischemia. Circ Res. 2010;106:185–92.
100. Morris CE, Juranka PF, Lin W, Morris TJ, Laitko U. Studying the mechanosensitivity of voltage-gated channels using oocyte patches. Methods Mol Biol. 2006;322:315–29.

101. Ter Keurs HE, Wakayama Y, Miura M, Shinozaki T, Stuyvers BD, Boyden PA, et al. Arrhythmogenic Ca^{2+} release from cardiac myofilaments. Prog Biophys Mol Biol. 2006;90:151–71.
102. Schott E. On ventricular standstill (Adam-Stokes attacks) together with other arrhythmias of temporary nature. Deutsches Archiv klinischer Medizin. 1920;131:211–29.
103. Quinn TA. Non-optogenetic approaches for leadless cardiac pacing: mechanically-induced excitation for extracorporeal control of cardiac rhythm. In: Nussinovitch U, editor. Emerging technologies for heart diseases: Volume 2: Treatments for myocardial ischemia and arrhythmias. Amsterdam: Elsevier; 2020. p. 891–905.
104. Hyman AS. Resuscitation of the stopped heart by intracardiac therapy. Arch Intern Med. 1930;46: 553–68.
105. Lee HT, Cozine K. Incidental conversion to sinus rhythm from atrial fibrillation during external jugular venous catheterization. J Clin Anesth. 1997;9:664–7.
106. Scherf D, Bornemann C. Thumping of the precordium in ventricular standstill. Am J Cardiol. 1960;5:30–40.
107. Don Michael TA, Lond MB, Stanford RL. Precordial percussion in cardiac asystole. Lancet. 1963;699
108. Kohl P, King AM, Boulin C. Antiarrhythmic effects of acute mechanical stimulation. In: Kohl P, Franz MR, Sachs F, editors. Cardiac mechano-electric feedback and arrhythmias: from pipette to patient. Philadelphia: Saunders (Elsevier); 2005. p. 304–14.
109. Criley JM, Blaufuss AH, Kissel GL. Cough-induced cardiac compression: self-administered form of cardiopulmonary resuscitation. JAMA. 1976;236:1246–50.
110. Rajagopalan RS, Appu KS, Sultan SK, Jagannadhan TG, Nityanandan K, Sethuraman S. Precordial thump in ventricular tachycardia. J Assoc Physicians India. 1971;19:725–9.
111. Amir O, Schliamser JE, Nemer S, Arie M. Ineffectiveness of precordial thump for cardioversion of malignant ventricular tachyarrhythmias. Pacing Clin Electrophysiol. 2007;30:153–6.
112. Caldwell G, Millar G, Quinn E. Simple mechanical methods for cardioversion: Defence of the precordial thump and cough version. BMJ. 1985;291:627–30.
113. Haman L, Parizek P, Vojacek J. Precordial thump efficacy in termination of induced ventricular arrhythmias. Resuscitation. 2009;80:14–6.
114. Pellis T, Kette F, Lovisa D, Franceschino E, Magagnin L, Mercante WP, et al. Utility of pre-cordial thump for treatment of out of hospital cardiac arrest: A prospective study. Resuscitation. 2009;80:17–23.
115. Smith J, Judge B. BET 1: Effectiveness of the precordial thump in restoring heart rhythm following out-of-hospital cardiac arrest. Emerg Med J. 2016;33: 366–7.
116. Baderman H, Robertson NR. Thumping the precordium. Lancet. 1965;2:1293.
117. Yakaitis RW, Redding JS. Precordial thumping during cardiac resuscitation. Crit Care Med. 1973;1:22–6.
118. Gertsch M, Hottinger S, Mettler D, Leupi F, Gurtner HP. Conversion of induced ventricular tachycardia by single and serial chest thumps: a study in domestic pigs 1 week after experimental myocardial infarction. Am Heart J. 1989;118:248–55.
119. Wada T, Ohara H, Nakamura Y, Cao X, Izumi-Nakaseko H, Ando K, et al. Efficacy of precordial percussion pacing assessed in a cardiac standstill microminipig model. Circ J. 2017;81:1137–43.
120. Li W, Kohl P, Trayanova N. Myocardial ischemia lowers precordial thump efficacy: an inquiry into mechanisms using three-dimensional simulations. Heart Rhythm. 2006;3:179–86.
121. Van Wagoner DR, Lamorgese M. Ischemia potentiates the mechanosensitive modulation of atrial ATP-sensitive potassium channels. Ann N Y Acad Sci. 1994;723:392–5.
122. Brooks SC, Anderson ML, Bruder E, Daya MR, Gaffney A, Otto CW, et al. Part 6: alternative techniques and ancillary devices for cardiopulmonary resuscitation: 2015 American Heart Association guidelines update for cardiopulmonary resuscitation and emergency cardiovascular care. Circulation. 2015;132:S436–43.
123. Link MS, Berkow LC, Kudenchuk PJ, Halperin HR, Hess EP, Moitra VK, et al. Part 7: adult advanced cardiovascular life support: 2015 American Heart Association guidelines update for cardiopulmonary resuscitation and emergency cardiovascular care. Circulation. 2015;132:S444–64.
124. Quinn TA. Cardiac mechano-electric coupling: a role in regulating normal function of the heart? Cardiovasc Res. 2015;108:1–3.
125. Kaufmann RL, Lab MJ, Hennekes R, Krause H. Feedback interaction of mechanical and electrical events in the isolated mammalian ventricular myocardium (cat papillary muscle). Pflugers Arch. 1971;324:100–23.

Part II

Neurocardiac Axis and Arrhythmias

Fundamental Neurocardiology: The Intracardiac Nervous System

8

Frank M. Smith

Abstract

Cardiac output is controlled by the autonomic nervous system to meet continually changing demands for the perfusion of systemic vascular beds. Dysfunction of autonomic control can contribute to a range of cardiopathies; conversely, robust autonomic function can help maintain a failing myocardium as heart diseases progress. Understanding the structure and operation of the intracardiac nervous system is thus essential to guide the formation of novel neuronally-directed cardiac therapies. Neural control of the heart operates through a hierarchy of interconnected reflex loops at the levels of the intracardiac neural network, the extracardiac intrathoracic ganglia and medullary and spinal autonomic nuclei. Within this hierarchy, the intracardiac nervous system represents the final common pathway for local cardiac control, capable of modulating chronotropy, dromotropy and inotropy on a fast, beat-by-beat basis. Intracardiac neurons constitute a series of interconnected ganglionated plexi distributed throughout the atrial walls and around the atrioventricular border; plexus nerves innervate all regions of the heart. This chapter reviews the position of the intracardiac nervous system in the autonomic control hierarchy and summarizes current knowledge of the neuroanatomy, physiology and potential roles of neuronal populations in cardiac control. Opportunities for future research to address remaining gaps in knowledge of this system are discussed in terms of the application of new tissue imaging technologies, genetic manipulations and novel experimental models.

Keywords

Autonomic innervation of the heart · Cardiac ganglia · Postganglionic neurons · Parasympathetic and sympathetic efferent neurons · Neuroanatomy · Cardiac neurochemical transmitters · Neuronal heart rate control

8.1 Introduction and Scope

This chapter considers the role of the autonomic nervous system in controlling cardiac output to maintain cardiovascular homeostasis, a role that has been recognized at least since the middle of the nineteenth century. Modern concepts of the anatomy and organization of the autonomic nervous system were crystallized by Gaskell [1], Langley [2], and Cannon [3], whose works carried forward earlier ideas of the innervation and control of the viscera by the cranial and spinal nerves. These concepts were developed

---

F. M. Smith (✉)
Department of Medical Neuroscience, Faculty of Medicine, Dalhousie University, Halifax, NS, Canada
e-mail: fsmith@dal.ca

© Springer Nature Switzerland AG 2023
O. N. Tripathi et al. (eds.), *Heart Rate and Rhythm*, https://doi.org/10.1007/978-3-031-33588-4_8

principally from the seventeenth century on (see [4] for a historical review). In the last four decades, the relationship between the nervous system and the heart has become a fertile area of research in which the interests of basic scientists and clinicians have converged. This convergence has led to the formation of the discipline of neurocardiology. A core tenet of this discipline is that in healthy individuals, normal control of the heart involves autonomic reflexes that drive rapid variations in cardiac output to meet changing demands for vascular perfusion under different physiological conditions such as exercise, arousal and sleep. Furthermore, in a wide variety of cardiovascular disease states, dysfunction of the neurocardiac axis can parallel or even precede the deterioration of the pumping capability of the heart. Therefore changes in neural and myocardial components must be considered together in developing many cardiac diseases [5]. It is thus essential to establish a clear understanding of the fundamental principles of the structure and operation of the autonomic network controlling the heart to guide the evolution of effective, neurally based therapies for managing cardiovascular diseases.

Progress in neurocardiology has been comprehensively represented in a series of review articles, book chapters and books covering both clinical and basic aspects of this field. In a landmark volume on neurocardiology edited by J. A. Armour and J. L. Ardell [6], the opening chapter by Dr W. Randall succinctly describes its genesis [5]. Dr Randall, with whom both of these investigators had worked, was a pioneer in the field and his article continues to reward the reader with valuable insights into major issues still driving research in neurocardiology. A second, expanded edition of that book [7] updated progress made in the decade after the publication of the first edition; both of those volumes remain essential reading. In a 2008 review by Armour, summarizing more than two decades of work from his and others' laboratories, codified the proposition that the portion of the autonomic nervous system lying within the heart, the intracardiac nervous system (ICNS), comprised a "little brain on the heart", that provides fast, local processing of responses to intracardiac events [8]. In 2016, special issues on neurocardiology were published in the Journal of Physiology [9] and in Autonomic Neuroscience [10]. These issues included articles that comprehensively summarized work on basic, translational and clinical aspects of autonomic control of the heart. Osteraas and Lee [11], Durães Campos et al. [12], Wake and Brack [13] and others have also recently reviewed aspects of neurocardiology. Together these reviews give a wide-ranging perspective of the state of this field at both central and peripheral levels of organization.

At the level of the mammalian central nervous system, nuclei involved in determining autonomic output to the heart and other viscera extend along the neuraxis from the insular cortex through the basal ganglia, hypothalamus, midbrain, medulla and spinal cord (see for example [14, 15]). These nuclei process inputs from generalized and specific visceral afferents conveying information to the central nervous system about changes in cardiorespiratory status. Cardiovascular-specific afferent information projecting to the central nervous system arises from two general populations of receptors, those with their somata in the petrosal and nodose ganglia of the vagus nerve, targeting secondary neurons in the nucleus of the tractus solitarius [16, 17] and receptors with their somata in the dorsal root ganglia associated with the lower cervical and upper thoracic segments of the spinal cord, targeting the dorsal horn of the cord [16, 18]. These inputs drive a wide range of reflexes generated by central autonomic nuclei that modify the heart to maintain cardiovascular homeostasis. The outputs of these reflexes are conveyed to the heart by the parasympathetic and sympathetic limbs of the autonomic nervous system through populations of peripheral neurons located in intrathoracic and intracardiac ganglia, connected in networked circuitry that modulates the activity of effectors within the heart to modify cardiac output.

The operating principles of those peripheral circuits are beginning to emerge from studies of the properties of their individual elements, the neurons in the intrathoracic and intracardiac ganglia. In this system, the ICNS represents the final common pathway for cardiac control. In the present chapter, I consider current knowledge of the physiological properties, patterns of synaptic connectivity, neurotransmitter phenotypes, receptor complements and cardio-modulatory influences of neurons in the ICNS and summarize the evidence for the operation of the circuitry in which they are embedded. Ultimately, clarifying the properties and functions of these neurons will have profound implications for the development of evidence-based therapies for cardiovascular diseases that target the intracardiac component of the autonomic nervous system. Clinical aspects of neurocardiology are considered elsewhere in this volume (see Chap. 9).

8.2 Hierarchical and Distributed: An Overview of Autonomic Innervation of the Heart

Autonomic neurons within the thoracic and intracardiac ganglia form a network coordinating the activities of myocardial effector cell populations that collectively determine cardiac output. This network innervates pacemaker cells in the sinoatrial and atrioventricular nodes, myocytes in the atrial and ventricular walls, the ventricular conducting system and the coronary vasculature. In the normal heart, the ongoing activity of effector cells is modulated by tonic influences and phasic fluctuations of inputs from this neural network to precisely match cardiac output with vascular perfusion demands.

A major theme running through many of the reviews of neurocardiology cited in Sect. 8.1 is that the organization of autonomic neurons in the network controlling the heart is hierarchical, comprising several nested levels. This theme is embodied in a series of schematic diagrams that have evolved over time to encompass more and more elements as investigators became increasingly aware of the complexity of the system and as additional information became available about the details at each level in the hierarchy. One of the earliest of these schematics is shown in Fig. 8.1 [19]. A more recent version of Fig. 8.1 is shown in Fig. 8.2 [20] to illustrate the development of this concept. Broad acceptance of the principle of hierarchical organization and its usefulness as a conceptual framework for thinking about cardiac control has provided a focus for the rapid expansion of the field of neurocardiology in recent decades. This framework will be used here to structure the discussion of cardiac-associated neurons and how they may be organized into networks for control of the heart.

The "classical" concept of efferent cardiac innervation consists of a parallel series of simple, two-neuron pathways from the central nervous system to the target organ, in accord with the general plan of dual sympathetic and parasympathetic efferent autonomic outflow to the viscera proposed by Langley [2] and Cannon [3]. In this scheme, sympathetic cardiac preganglionic neurons are located in the intermediolateral cell column of the spinal cord in the caudal cervical and cranial thoracic segments [14, 21]. Axons arising from these neurons exit the cord via the white rami to synapse on somata of postganglionic neurons located predominantly in intrathoracic ganglia (middle cervical and stellate ganglia) of the sympathetic paravertebral ganglion chain. Neurons in these ganglia in turn project axons via cardiac nerves [22] to target virtually all regions of the heart [23], acting to accelerate pacemaker cell discharge, increase contractility of atrial and ventricular myocytes, enhance activity in conducting tissues and induce changes in radius of the cardiac vasculature. Parasympathetic preganglionic neurons, located in the nucleus ambiguus, the dorsal vagal motor nucleus and areas between these in the medulla, give rise to axons coursing peripherally via the vagosympathetic trunks and cardiac vagal branches to target postganglionic neurons in intracardiac ganglia distributed in subepicardial tissue. In turn, axons from intracardiac parasympathetic neurons innervate the same groups of cardiac effector cells as do sympathetic postganglionic axons [19], influencing the activity of these cells in the opposite direction to the actions of sympathetic innervation. Thus, in this "classical" view of autonomic cardiac control, sympathetic and parasympathetic drive is conveyed

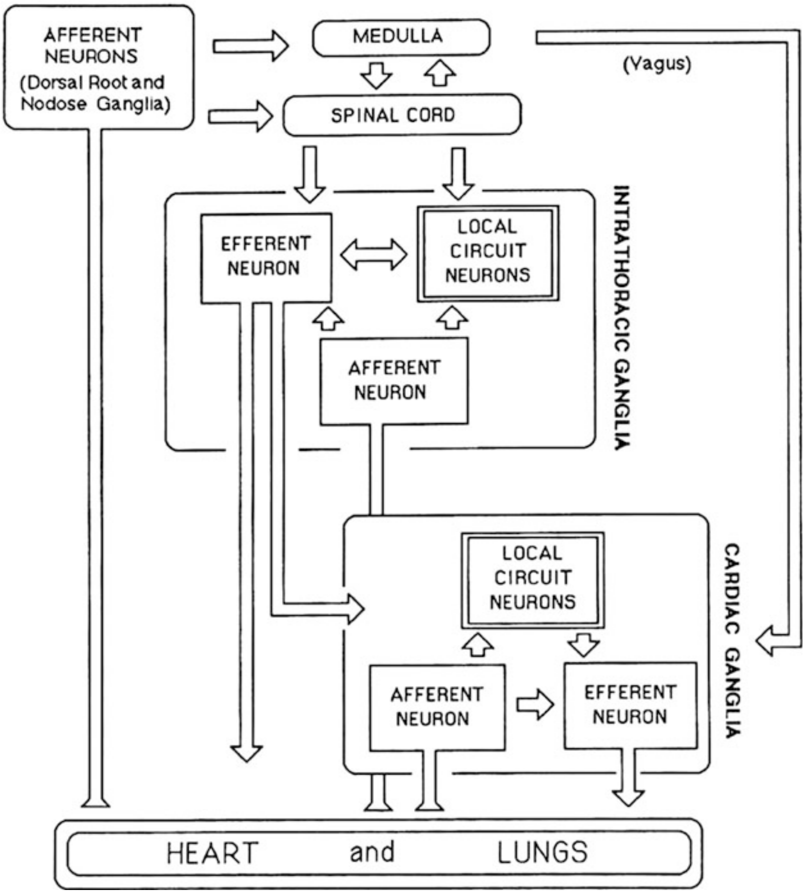
AFFERENT NEURONS (Dorsal Root and Nodose Ganglia)
MEDULLA
SPINAL CORD
(Vagus)
EFFERENT NEURON
LOCAL CIRCUIT NEURONS
AFFERENT NEURON
INTRATHORACIC GANGLIA
LOCAL CIRCUIT NEURONS
AFFERENT NEURON
EFFERENT NEURON
CARDIAC GANGLIA
HEART and LUNGS

Fig. 8.1 Schematic representation of a proposed hierarchical organization for populations of autonomic neurons involved in control of the heart and their interconnections. Three levels of hierarchy are shown: intracardiac neurons ("cardiac ganglia"); neurons within the thorax ("intrathoracic ganglia") and central neurons ("medulla" and "spinal cord") ([19] used by permission)

from the brain to the heart by pre- to postganglionic synapses functioning as basic 1:1 relays. In this view, it was also considered that these autonomic divisions acted antagonistically on the heart such that when sympathetic drive was elevated, parasympathetic activity was withdrawn and vice versa [24]. The elements of this simple innervation scheme can be readily identified in the schematics in Figs. 8.1 and 8.2.

This simplistic view of cardiac innervation has been belied by the results of studies in the last four decades using a variety of experimental models including open-chest, anesthetized mammalian preparations in which the heart was accessed in situ. The outcomes of these studies have driven the continued revision of our concepts of neural control of the heart, as demonstrated by (1) the addition of components representing populations of local-circuit neurons (LCN) and (2) afferent somata and their interconnections with the intrathoracic and intracardiac levels of the hierarchy, as shown in the schematic of Fig. 8.1. As more information became available about the operation of these components, the schematic was modified to reflect the increasing complexity of the system (Fig. 8.2).

According to the "classical" view of operation of the neurocardiac axis, all neuronal activity within intrathoracic and intracardiac ganglia should result from the activation of efferent postganglionic neurons by inputs from the central nervous system. However, recordings of neuronal activity in these ganglia during electrical stimulation of preganglionic axons showed that only a proportion of neurons were activated at the short latencies consistent with a monosynaptic pathway. Other neurons responded indirectly

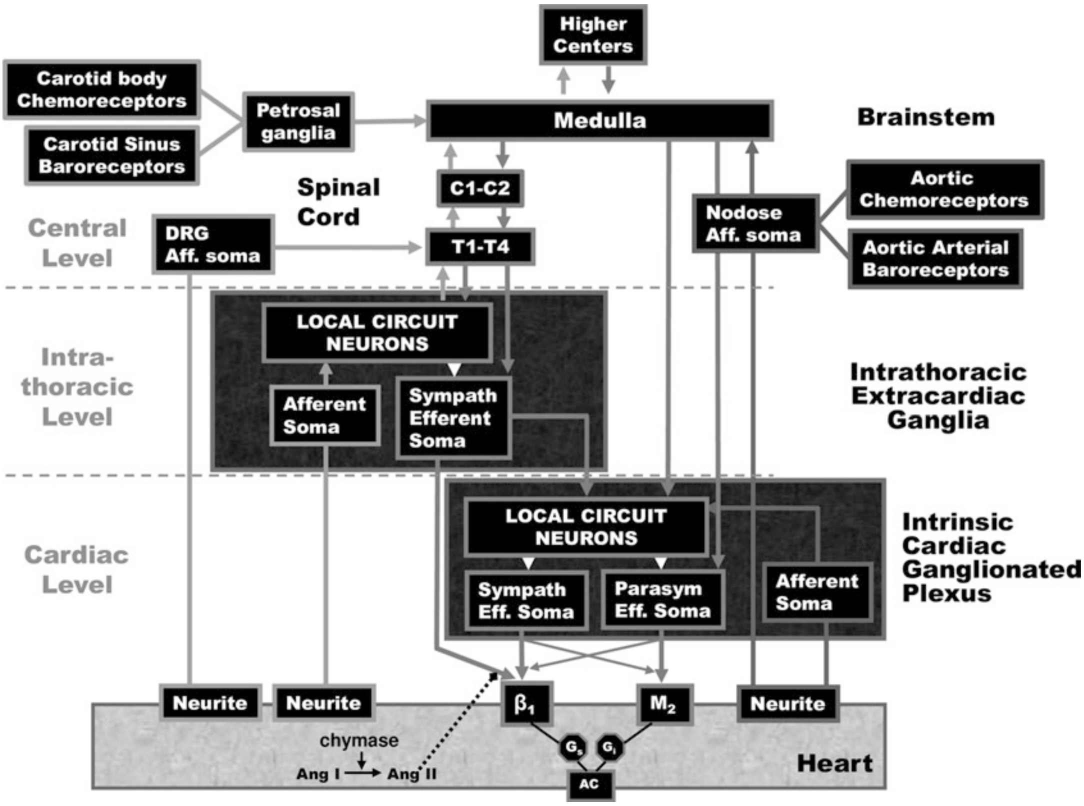
Higher Centers
Carotid body Chemoreceptors
Carotid Sinus Baroreceptors
Petrosal ganglia
Medulla
Brainstem
Spinal Cord
C1-C2
T1-T4
Nodose Aff. soma
Aortic Chemoreceptors
Aortic Arterial Baroreceptors
Central Level
DRG Aff. soma
Intra-thoracic Level
LOCAL CIRCUIT NEURONS
Afferent Soma
Sympath Efferent Soma
Intrathoracic Extracardiac Ganglia
Cardiac Level
LOCAL CIRCUIT NEURONS
Sympath Eff. Soma
Parasym Eff. Soma
Afferent Soma
Intrinsic Cardiac Ganglionated Plexus
Neurite
Neurite
β1
M2
Neurite
chymase
Ang I
Ang II
Gs
Gi
AC
Heart

Fig. 8.2 Advanced hierarchical model for neural control of the heart showing the elaboration of known interconnections between levels in the hierarchy, derived from studies undertaken since the schematic in Fig. 8.1 was proposed ([20] used by permission)

(presumably through multisynaptic pathways with varying degrees of latency) to such stimulations, or had activity patterns not correlated with the stimuli (summarized by Armour [19, 25]). These observations led to the concept of a population of neurons in peripheral cardiac ganglia that did not receive direct preganglionic inputs but were instead involved in processing information originating either from within the ganglia or, more distally, from cardiac afferents [8, 19]. This concept was expressed by the incorporation of LCN at the levels of the intrathoracic and intracardiac ganglia in schematic diagrams (Figs. 8.1 and 8.2).

A critical question in determining the origin of spontaneous neuronal activity within extra- and intracardiac ganglia was whether this activity could have arisen from events in the periphery rather than originating from the central nervous system. This question was investigated by disconnecting these peripheral ganglia from the central nervous system by surgical means aimed at severing preganglionic inputs (decentralization), leaving all other connections intact. In a landmark paper, Armour, Randall and coworkers [26] established that spontaneous activity in intracardiac ganglia, much of which was phase-related to events in the cardiac cycle, continued after decentralization, although the overall frequency of this activity was reduced. Likewise, spontaneous neuronal activity in decentralized stellate and middle cervical ganglia also survived decentralization [27, 28]. These observations led to the proposal that afferent neurons, transducing chemical or mechanical events in the heart, provided local inputs to LCN or directly to efferent postganglionic neurons, thus engendering cardio-cardiac reflexes that operated independently of the central nervous system. These inputs may have arisen as intraganglionic collaterals of cardiac sensory axons with their somata in the dorsal root [16, 18, 29] or vagal nodose [30, 31] ganglia or from somata of afferent neurons located within the intracardiac or intrathoracic ganglia themselves [8]. This concept was illustrated by representing afferent neurons at the levels of the intrathoracic and intracardiac ganglia in the cardiac control hierarchy (Figs. 8.1 and 8.2).

The presence within intracardiac ganglia of afferent neuronal somata (or collateral branching within these ganglia from axons of nodose or dorsal root cardiac afferents), along with LCN, together provide the necessary components for local, short-latency (on the order of <20–40 ms) cardio-cardiac reflexes that operate within the ICNS. Reflexes of slightly longer latency (100–200 ms) would involve projections through the intrathoracic ganglia [8]. Such reflexes are presumably capable of operating well within the duration of systole of a single cardiac cycle. Cardio-cardiac reflexes with the longest latencies (up to 350 ms [8]) would involve feedback from the heart originating from mechano- or chemosensitive afferents with their receptors in the atria or ventricles and their somata in the nodose ganglion or dorsal root ganglia. These would project to cardiomotor circuits in the central nervous system, indicated in the schematic diagrams at the "central" level of the network hierarchy (Figs. 8.1 and 8.2).

8.3 Elements of Intracardiac Neuronal Circuitry

To date, the vast majority of data on the organization and principles of control of the heart by the intrathoracic and intracardiac neural networks has resulted from studies recording spontaneous or evoked axonal or ganglion cell activity along with the behavior of cardiac functional indices (e.g., heart rate, atrial and ventricular chamber pressures, regional chamber wall tension). This work has been done in a variety of experimental models in which the beating heart (in vivo, in situ or in vitro) and components of the ICNS and extracardiac nerves are accessible for manipulation. These studies have provided major advances in our understanding of the principles of cardiac control at the systems level and are the subject of a number of recent reviews to which the reader is referred (e.g., [11, 12, 32–34]). While many of the issues addressed in the present chapter arise from aspects of this work, this material will not be covered in depth here.

Extracellular recordings of action potential discharge in the peripheral cardiac nervous system (particularly when multiple recording electrodes are used to increase the regional scope of data recovery; see, e.g., [35]) and the changes in neuronal activity evoked by electrical, mechanical and chemical stimulation in this system are effective tools for enabling analysis of the behavior of populations of neurons. In that type of study, it may, however, be problematic to discern the ongoing activity pattern of a particular neuron from others recorded simultaneously at the same electrode site. Furthermore, the connectivity and physiological type of neuron from which such extracellular recordings are made may only be deduced indirectly from circumstantial evidence. In contrast, intracellular recordings or whole-cell patch recordings provide direct access to membrane properties, firing behavior and postsynaptic responses of single neurons, usually in reduced preparations of isolated tissues. Such recordings leave no doubt about the physiological type and the nature of synaptic inputs for each cell sampled. However, in those reduced preparations, the connections of the sampled neurons with extracardiac and distant intracardiac neurons have been disrupted. It is thus difficult to determine, based on single-cell recordings, what the roles and contributions of the sampled neurons might have been in the system in which they were originally embedded. Yet the determination of functional properties and input patterns of individual autonomic neurons in the intrathoracic and intracardiac ganglia is essential in understanding how neuronal networks are built from these basic elements.

A major principle of autonomic control of the viscera is that the sympathetic and parasympathetic limbs of this system are organized into "function-specific pathways" that precisely target visceral organs and specific tissues performing particular functions (hence "function-specific") within those organs [36–40]. Understanding the properties, characteristics and connections of individual neurons in the networks controlling the heart enables a fundamental step to be taken in unraveling the integrative capabilities of this network. Neurons subserving various functions (motor neurons, afferents and those that integrate and process information locally) form the basic elements of a variety of local reflex arcs, the organization and operating principles of which will emerge from investigations of the properties and connectivity of these elements. In the following sections, I focus on the characteristics of intracardiac neurons and what is known of their connections to see how these neurons might work in combination to create function-specific pathways within the heart.

8.3.1 Overview of the Intracardiac Nervous System

Among the vertebrates autonomic innervation of the heart is phylogenetically ancient, with sympathetic and parasympathetic pathways employing the same basic operating principles in all extant orders from Teleostei [41] to mammals [42–44]. Interest in the gross innervation of the heart has been strong for centuries (see [4] for historical aspects). In the last century, works by Nonidez [45], Mizeres [22] and others have clarified the anatomical pathways of cardiac nerves into the heart in a number of mammalian species. It was recognized from the late 1800s that the ICNS consisted of collections of ganglia, associated with the epicardium, that were connected together into ganglionated plexi [46], but the details of this organization have only become clear relatively recently. The neuroanatomy of the ganglia and interganglionic plexi has now been well-established in both small and large mammals commonly used as experimental models in cardiovascular research. Among small mammals, the ICNS has been characterized in the mouse (estimated ~1000–1800 intracardiac neurons [47, 48]), rat (~4000 [49–51]) and guinea pig (~1500 [52–54]). Comparative studies of the neuroanatomy of the ICNS have also been done between rat and guinea pig [55, 56]. In larger mammals, the neuroanatomy of the ICNS has been analyzed in the pig (~3000 [57]), sheep (700–800 [58]) and dog (~20,000 [59]). Several studies have examined the innervation of the human heart and patterns of occurrence of ganglionated plexi (~40,000 [56, 60, 61]). Pauza et al. [56] presented a quantitative, comparative study of neurons in ganglionated plexi in rat, guinea pig, dog and human specimens, finding that the morphology of neuronal somata was similar across species and that the numbers of ganglia and the total numbers of neurons per heart scaled positively with body and heart size.

In mammalian hearts, the ganglionated plexi are associated with the external walls of both atria, the region adjacent to the atrioventricular border and within the interatrial septum. The occurrence of ganglionated plexi in the human heart is illustrated in Fig. 8.3 [34], where major plexi have been named for their proximate cardiac regions. This example clearly shows the distributed nature of the ICNS: ganglionated plexi are located close to the pacemaker loci in the right atrium (sinoatrial and atrioventricular nodes), the ostia of the inferior and superior vena cavae, adjacent to the pulmonary vein-atrial wall junctions and near the roots of the pulmonary artery and aorta. These ganglionated plexi are connected together into a network by numerous interganglionic nerves, so that there is communication among populations of neurons located in all regions of the heart [62].

Once details of the neuroanatomy of the ICNS became available, these were used to design a variety of physiological studies to electrically and chemically stimulate specific loci within the system to map the relationships between local neurons and cardiac effectors. As a general organizing principle for the ICNS, it is tempting to assume that most, if not all, neurons adjacent to a particular cardiac effector tissue, for instance,

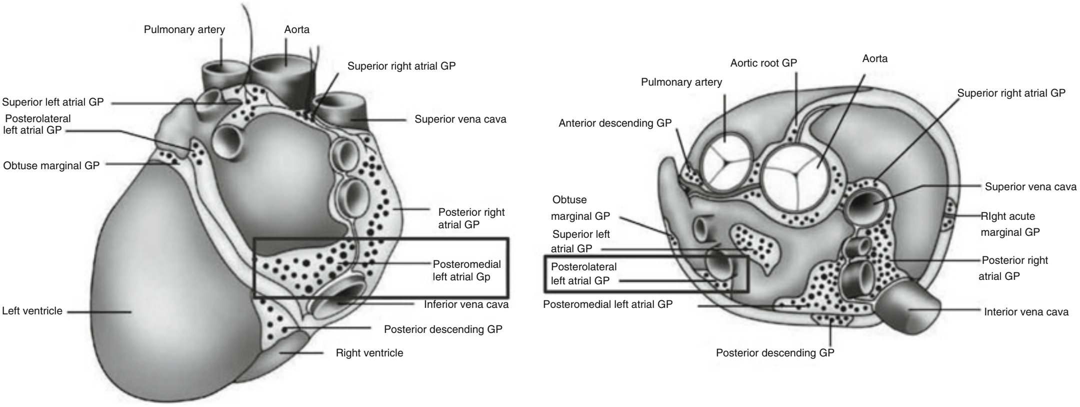
Pulmonary artery
Aorta
Superior right atrial GP
Superior left atrial GP
Posterolateral left atrial GP
Superior vena cava
Obtuse marginal GP
Posterior right atrial GP
Posteromedial left atrial Gp
Inferior vena cava
Left ventricle
Posterior descending GP
Right ventricle
Aortic root GP
Aorta
Pulmonary artery
Superior right atrial GP
Anterior descending GP
Superior vena cava
Obtuse marginal GP
RIght acute marginal GP
Superior left atrial GP
Posterior right atrial GP
Posterolateral left atrial GP
Posteromedial left atrial GP
Interior vena cava
Posterior descending GP

Fig. 8.3 Illustrations of distribution of major ganglionated plexi (dots) in the mammalian heart (left panel, dorsal view; right panel, superior view with dorsal aspect of heart toward the bottom of panel) ([34] used by permission)

the SAN, would be involved in the control of that tissue (e.g., pacemaker discharge rate [63]). However, this assumption has proven to be an oversimplification [64]. Certainly, neurons exist in right atrial ganglionated plexi near the SAN that do in fact affect heart rate, but subpopulations of neurons with their somata in most other ganglionated plexi in the heart can also modify heart rate via axons coursing in the plexus nerves to the SAN region. More generally, it has been firmly established that the ICNS constitutes a functionally as well as anatomically distributed system, with neurons in all ganglionated plexi projecting to effector tissues in the atria and the ventricles [62, 65–68].

8.3.1.1 Properties of Intracardiac Neurons

8.3.1.1.1 Electrophysiological Properties

The first recordings of transmembrane potential in intracardiac neurons were made from cells in the cardiac ganglion in the interatrial septum of amphibian hearts in vitro [69, 70]. Those studies investigated the synaptophysiology of inputs to the neurons from vagal preganglionic axons. Two categories of neurons were described: (1) large principal cells projecting axons to the myocardium and to other nearby principal cells, releasing acetylcholine from their terminals; and (2) a population of catecholamine-containing intercalated cells with somata smaller than those of principal cells and with processes that terminate exclusively on nearby principal cells [71, 72]. Principal cells from the cardiac ganglion of mudpuppy, studied in an isolated tissue preparation, exhibited repetitive action potential (AP) firing behavior when depolarized by long-duration intracellular current injection [73, 74]. A major advantage of such reduced preparations of the amphibian heart is that cardiac ganglia are readily visualized in the thin wall of the interatrial septum and can be easily accessed for electrical recording and stimulation. In contrast, in the mammalian ICNS, it has proven difficult to obtain intracellular recordings from ICN somata in situ since these are embedded in subepicardial tissue throughout both atria and near the atrioventricular border. Two general approaches have been taken to solve this problem. In the first, tissue containing atrial ganglionated plexi are removed from the heart and the neurons are enzymatically dissociated and cultured in preparations in which sharp intracellular microelectrodes or patch pipettes are used to record membrane potentials and ion channel currents. In the second approach, atrial tissues containing ganglionated plexi are isolated and dissected to expose individual ganglia for the impalement of neurons with sharp electrodes.

Both of these approaches have yielded insights into the properties of individual ICN, but the scope of information obtainable from each type of preparation is limited.

Dissociated and cultured ICN are free of associated connective tissue and are not subject to movement artifacts resulting from the contraction of substrate cardiomyocytes; however, these cells no longer have synaptic connections. This type of preparation has been used extensively to analyze passive and active membrane voltage properties as well as ion channel currents, AP firing behavior and membrane receptor-mediated responses to neurotransmitters, agonists and antagonists (see [75] for review). A key electrophysiological property in understanding neuronal function is AP firing behavior during long-duration current pulses (usually 0.2–1 s), delivered through the recording electrode to depolarize the membrane above the threshold for AP initiation. This type of stimulation at least partially mimics the effect of strong excitatory synaptic drive on neurons in situ and has been used to classify cells into functional categories. Based on this test, cultured neurons from a variety of mammalian models display three main classes of AP discharge in response to prolonged depolarization, illustrated in the example from guinea pig intracardiac neurons shown in Fig. 8.4 [76]. The most common neuronal type (65–75% of neurons sampled) typically discharged one AP at the start of prolonged (>1 s duration) depolarization (Fig. 8.4a, right panel). Furthermore, this type of neuron, when depolarized with a short (5 ms duration) intrasomal stimulus pulse, displayed a high-amplitude, prolonged afterhyperpolarization (AHP) following the AP (Fig. 8.4a, left panel), so was designated "AHs" after these characteristics. A second neuron type also displayed a prolonged AHP following single APs (Fig. 8.4b, left panel), but when challenged with long-duration depolarizing current injection, these cells produced multiple APs, initially at a high frequency but accommodating to a lower discharge rate as the stimulus continued (Fig. 8.4b, right panel). This type, making up 10–15% of the neurons, was designated "AHm" to reflect a prolonged AHP along with multiple AP discharges. The third type of neuron (10–15%) displayed continuous, high-frequency AP discharge during sustained depolarization (Fig. 8.4c, right panel) but had a short-duration AHP following a single AP (Fig. 8.4c, left panel). This type was classed as "M," reflecting its multiple and rapidly repeating AP discharge. Similar results were obtained by Xu and Adams [77] in neurons dissociated and cultured from the neonatal rat heart; those authors described neurons with two patterns of AHP time course and AP firing behavior that resembled those of the guinea pig AHs and M type neurons shown in Fig. 8.4. In cultured guinea pig and neonatal rat intracardiac neurons, the distinct AHP time courses and firing behaviors of the different neuron types were shown to result from differential membrane ion channel complements, thus establishing the ionic basis for the functional differences among these types [75].

Cultured neurons lack the interconnections present in intact ganglia, so studies such as those cited above cannot address questions concerning the organization and properties of synaptic connections between cells. These questions and others have been addressed using isolated, perfused preparations of atrial ganglionated plexi in vitro, taken from the hearts of a variety of mammalian species. Electrophysiological properties of ICN in these studies show trends generally similar to those in cultured ICN. Passive membrane properties (transmembrane potential, whole-cell input resistance, membrane capacitance and characteristics of evoked APs) of ICN in vitro (summarized in [78]) appear to be within the range of those of autonomic neurons in other peripheral ganglia (summarized in [79]), so these characteristics may not be particularly useful in distinguishing between functional neuron types (or their roles) in the heart. However, by extension, from studies in cultured ICN, properties such as the time course and amplitude of AHP and AP firing behavior appear to provide distinctions among neuronal types in the heart that may be correlated with their functions. When analysis of these electrophysiological properties is combined with investigation of other neuronal features, such as sources of synaptic input or neurochemical phenotype of axon

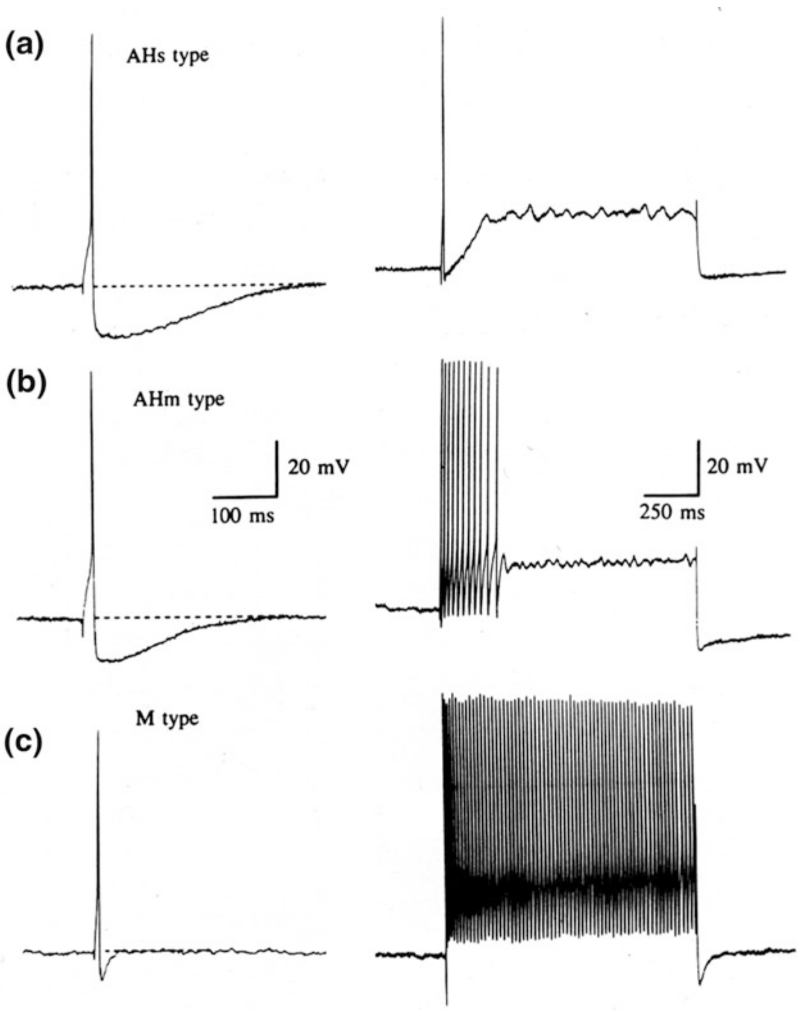

Fig. 8.4 Intracellular recordings of action potential firing properties of identified intracardiac neurons dissociated from guinea pig heart and cultured. In **a**, **b** and **c**, left panels show responses to single, short intrasomally injected depolarizing current pulse; right panels show responses to 1 s duration current pulses. (**a**) Responses of AHs neuron subclass. (**b**) Responses of AHm subclass. (**c**) Responses of M subclass (see text for explanation of subclasses) ([75] used by permission)

terminals and somata, a clearer picture of the role of specific classes of neurons in intracardiac function-specific pathways may result. To address progress on this issue, I focus on several schemes for classifying ICN based on data from cells in ganglia with intact synaptic connections and what these schemes may contribute to a unified perspective relating the properties of neurons to their network functions.

Figure 8.5 shows examples typical of the classification schemes that have been proposed based on active membrane properties of ICN from in vitro studies of intact ganglion preparations in four mammalian species. In the adult rat heart, Selyanko [80] proposed two general neuronal types: Type I and Type II (Fig. 8.5a). Type I neurons had relatively short AHP duration following a single brief stimulus that evoked an AP (Fig. 8.5a, trace designated "a"). These neurons were further categorized into two subtypes, I_b and I_m, based on responses to long-duration depolarizing intracellular current injection (Fig. 8.5a, traces designated "b" and "c"). Type I_b neurons generated a short burst of APs only at the start of this depolarization, while I_m displayed multiple but frequency-decrementing APs for the duration of depolarization. Type II neurons had a relatively long-duration AHP following a single

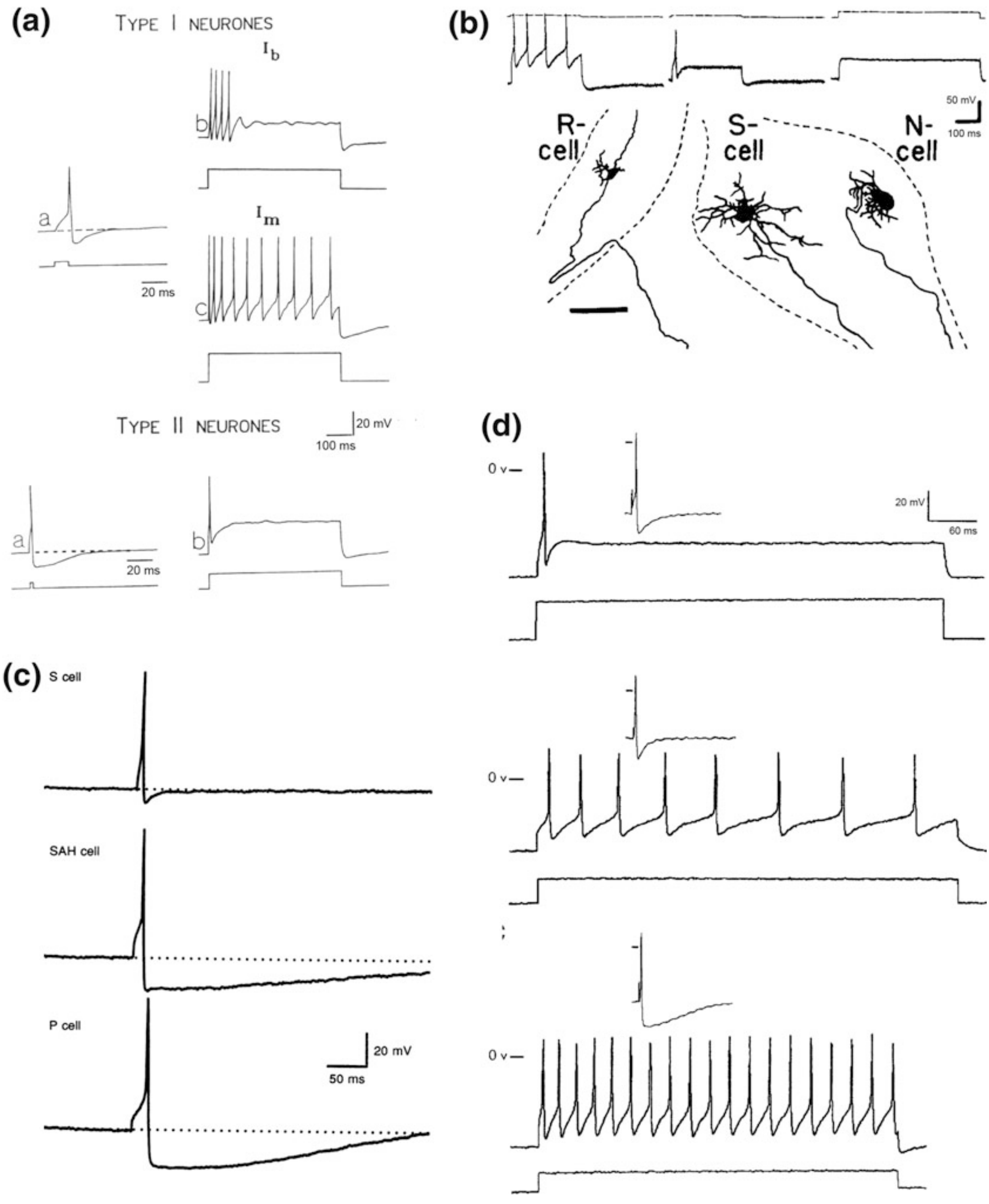

Fig. 8.5 Comparison of classification systems for intracardiac neurons based on intracellular recordings of membrane potentials from in vitro preparations of mammalian hearts (see text for details). Action potentials were evoked by intracellular stimulus protocols similar to those used in Fig. 8.4. (**a**) Rat (after [80]). (**b**) Canine [82]. (**c**) Guinea pig [84]. (**d**) Pig [85] (all images used by permission)

AP and produced one or a few low-frequency APs during long-duration depolarization (Fig. 8.5a, traces designated "a" and "b" respectively, bottom panels). No information, however, was provided on synaptic inputs to any of these neuron types.

Xi et al. [81, 82] identified R, S and N neurons in the canine right atrial ganglionated plexus based on AP firing behavior during long-duration depolarization (Fig. 8.5b; note, no data on AHP were given). Type R ("repetitive") neurons fired APs for the duration of depolarization (Fig. 8.5b, upper left), usually with an accommodating firing pattern (decrementing in frequency), but a few cells maintained a high firing frequency throughout. The authors indicated that nearly two-thirds of R neurons also generated spontaneous APs (that is, APs appearing in the absence of external stimulation). Type S ("single AP") neurons generated one AP at the start of depolarization (Fig. 8.5b, center traces, top); half of these neurons showed spontaneous APs. Type N ("nonresponding") neurons (Fig. 8.5b, traces at top right) did not respond to hyperpolarizing or depolarizing currents injected intracellularly at any intensity. These authors noted that, overall, AP discharge patterns of these classes of neurons paralleled those reported in other peripheral autonomic ganglia [83], such that type R neuronal discharge resembled that of tonic neurons, type S resembled that of phasic neurons, and the lack of responses of type N neurons was also found in other ganglia. Xi et al. [82] also injected a neuromarker into some of the cells they sampled to determine if there was any correlation between electrophysiological class and morphology of ICN. Examples of the typical somatic morphology and patterns of processes of each cell type are shown in Fig. 8.5b under their respective membrane response traces. Some differences in somatic morphology were reported among these types, but the processes of some samples of each cell type were observed either to terminate entirely within the ganglion under study, or to leave the ganglion.

In the guinea pig, Edwards et al. [84] also reported three classes of neurons, S, SAH, and P cells (Fig. 8.5c). S cells (Fig. 8.5c, upper trace) had a relatively short AHP and displayed frequent spontaneously arising postsynaptic depolarizations (hence the designation). These cells were reported to respond with only a single AP at the start of long-duration intracellular depolarization (responses not illustrated in their article). They described this cell type as discharging phasically. S cells displayed ongoing, spontaneous postsynaptic depolarizations, some of which exceeded the threshold for AP generation. All of these cells responded synaptically to electrical stimulation of local interganglionic nerves attached to the sampled ganglion, but very few of these cells were even weakly responsive to stimulation of the vagosympathetic trunk. SAH cells had long AHPs (Fig. 8.5c) and maintained AP discharge throughout the duration of long intracellular depolarizing pulses. These cells showed strong postsynaptic depolarizations and AP discharge from vagosympathetic trunk stimulation. P cells had long AHPs (Fig. 8.5c) and displayed repetitive AP discharges under long-duration depolarization, as well as showing spontaneous and rhythmic AP discharge without apparent postsynaptic depolarizations. No postsynaptic responses could be elicited by stimulating the vagosympathetic trunk or local nerves in this cell type.

In pigs, ICN have been classified into three categories: phasic, accommodating, and tonic (Fig. 8.5d [85]). Phasic neurons, constituting 40% of the neurons sampled, showed only one AP at the start of long-duration depolarization and had a relatively short-duration AHP after the AP (Fig. 8.5d, top panel, main trace and insert). These neurons all received cholinergic synaptic inputs from vagal preganglionic axons; some also received adrenergic inputs from postganglionic axons in cardiopulmonary nerves. Accommodating neurons (33%) displayed multiple AP firing that decremented during long-duration depolarization and had short AHPs following the AP (Fig. 8.5c, middle panel, main trace and insert). Few of these neurons received inputs from either the vagosympathetic trunk or the cardiopulmonary nerves. Tonically discharging neurons (27%) showed long AHP duration and fired APs continuously at a high frequency throughout the duration of long depolarizing pulses (Fig. 8.5d, bottom main trace and insert). These cells had neither vagosympathetic nor cardiopulmonary inputs.

The above data begs the question: are there common features among these schemes that may be used to determine what the roles of the identified neurons might be in controlling the heart? First, it appears that different AP firing characteristics during prolonged depolarization are determined by specific membrane ion channel compositions that vary among the neuron types (see [75] for discussion), so a categorization founded on AP discharge patterns likely has a physiological basis. Second, neurons that could be identified with "phasic," "accommodating" (equivalent to "adapting") or "tonic" firing behaviors occur in all of the classification schemes discussed here. Third, there are large variations among these schemes in terms of correlations between neuronal firing behavior and accompanying characteristics such as patterns of synaptic input or AHP duration, within each neuronal class. Regarding synaptic connectivity, all neuron types in the classification system of Xi et al. [82] and Smith [85] appeared to have synaptic inputs. However, while SAH and P neurons in the scheme of Edwards et al. [84] had mixed accommodating and tonic firing patterns, only SAH neurons received synaptic inputs. There was thus no clear correlation between the source of synaptic drive and AP discharge behavior in that study. In the scheme of Smith [85], phasic neurons predominantly received inputs from extracardiac nerves while accommodating and tonic neurons were innervated primarily by axons of intracardiac origin. Conversely, in the scheme of Edwards et al. [84], S (phasic) neurons received primarily intracardiac inputs, while SAH (accommodating or tonic) neurons received inputs from the vagosympathetic trunk. It is likely that at least some of the differences in connectivity of ICN among these schemes resulted from interspecies variations in the organization of the ICNS, given that data were derived from four different species. Additionally, many details of the features of ICN and their integration into the ICNS are still unexplored within each of these experimental models.

In the ongoing quest for a consistent neuronal classification scheme, more recent studies of the properties of ICN at the cellular level in both cultured cells and intact ganglia preparations have used AP firing behavior as a primary characteristic in categorizing cells. In cultured rat ICN, Xu and Adams [86] found that the majority of neurons sampled were phasic (85%), and the rest were tonic. Cuevas et al. [87], also working with cultured rat ICN, reported that while more than 90% of neurons were accommodating (termed "multiple adaptive firing") at room temperature, when the temperature was increased to 37 °C more than a third of the accommodating neurons were converted to phasic discharge. The temperature of the preparation is thus a factor in the firing behavior of ICN, so should be considered in experimental designs. In in vitro studies of ICN in rat atria by Rimmer and Harper [88] and Dyavanapalli et al. [89] phasic, accommodating and tonic neurons were identified, all with synaptic inputs from both extracardiac and intracardiac sources. In a refinement of the technique of recording from ICN in situ, McAllen et al. [90] used a working heart-brainstem preparation in the rat to record intracellularly from ICN in the innervated heart. They identified neurons responding to activation of centrally-mediated cardiorespiratory reflexes that displayed either tonic or phasic discharge characteristics. Tonic neurons, which they termed "principal cells," responded predominantly to reflex-driven vagal inputs; these neurons were proposed to be the major intracardiac relays from preganglionic neurons in the medulla to cardiac effectors. Phasic neurons had synaptic inputs from intracardiac sources but not from the vagus; these ICN were proposed to represent "interneurons" that fulfill the role of LCN [8]. One potential limitation of this study was that intracellular recordings were made only from a limited subset of cardiac ganglia located near the sinoatrial node, so generalizing these results to the whole ICNS may be problematic. In a recent study by Ashton et al. [91] in atrial tissue isolated from rat, ICN with intact synaptic connections were accessed through whole-cell patch electrodes to record synaptic currents. No phasic cells were found; all voltage-clamp records were made from tonic neurons that received synaptic inputs. The authors reported that there was considerable ongoing, spontaneous synaptically driven activity in these ICN but were unable to identify the source of the activity.

It is thus clear from the studies cited above that knowledge of the basic AP discharge properties of ICN is an important component of the overall characterization of the roles of these neurons in the intracardiac network. Inherent AP firing patterns of specific neuron types will control the frequency-dependent properties of information throughput by the network. However, while this component is a necessary factor, it is not sufficient to evaluate how ICN work in function-specific pathways in the heart. In addition to the inherent membrane properties of ICN, their synaptic connections, axonal projections, neurotransmitter phenotype and receptor complement remain to be established to complete the profile of these neuron types.

8.3.1.1.2 Neurochemical Complexity

In the peripheral autonomic nervous system, parasympathetic postganglionic neurons generally employ acetylcholine as their main excitatory neurotransmitter at neuroeffector terminals while sympathetic postganglionic neurons release norepinephrine from their terminals (some also release epinephrine). Activation of subtype-specific receptors for these neurotransmitters on effector cells in the visceral organs then determines the nature of the influence of the limbs of the autonomic nervous system on these organs. However, as studies of the neurochemical constitutions of various populations of peripheral autonomic neurons have progressed, it has become clear that there is a wide variety of additional neurotransmitters and neuromodulators that may be expressed by a given population of neurons. In fact, in some systems, these so-called "nonadrenergic, noncholinergic" (NANC) neurochemicals may have a greater influence on visceral effectors than the "main" neurotransmitter [92]. The patterns of co-localization of neurotransmitters or neuromodulators in autonomic neurons (termed "chemical coding" [37, 39, 40, 93]) are thus part of the overall profile identifying discrete populations of these cells with their roles in function-specific pathways.

In the ICNS, primary parasympathetic efferent postganglionic neurons have been identified as cholinergic by the presence of choline acetyltransferase (ChAT), an enzyme in the synthesis pathway for this neurotransmitter, or by the occurrence of vesicular acetylcholine transporter (VAChT), in their somata and processes. Similarly, sympathetic postganglionic efferent neurons are usually identified as adrenergic by their expression of one or more enzymes involved in the synthesis of NE (most commonly tyrosine hydroxylase, TH). Numerous studies over the last three decades have used immunohistochemical detection of these markers to explore the distribution of parasympathetic and sympathetic ICN in a wide variety of mammalian hearts. Immunohistochemical techniques have also been used to detect the coexpression of NANC neurotransmitters and neuromodulators, such as peptides, nitric oxide (NO) and glutamate in these neurons. Much of this work has recently been summarized by Wake and Brack [13].

In all species examined to date, the majority of ICN appears to be cholinergic, and many receive synaptic inputs from cholinergic axon terminals (see for example guinea pig intracardiac ganglia in Fig. 8.6: map, Fig. 8.6a; ChAT immunohistochemistry, Fig. 8.6b [54]). At least a portion of this population appears to represent principal parasympathetic postganglionic neurons in the ICNS. However, many subpopulations of cholinergic ICN display differential coexpression of NANC neurochemicals. For most of these subpopulations, data on their synaptic connectivity, target projections within the heart and the physiological effects of neurochemicals released by these cells are still lacking. The specific details of neurochemicals co-localized in cholinergic neurons also vary greatly depending on the species examined [13]. The most common peptides co-localized in neurons expressing ChAT or VAChT in the ICNS across species are vasoactive intestinal polypeptide (VIP) and neuropeptide Y (NPY); in addition, ICN in many species commonly express neuronal nitric oxide synthetase (nNOS), an enzyme in the synthetic pathway for

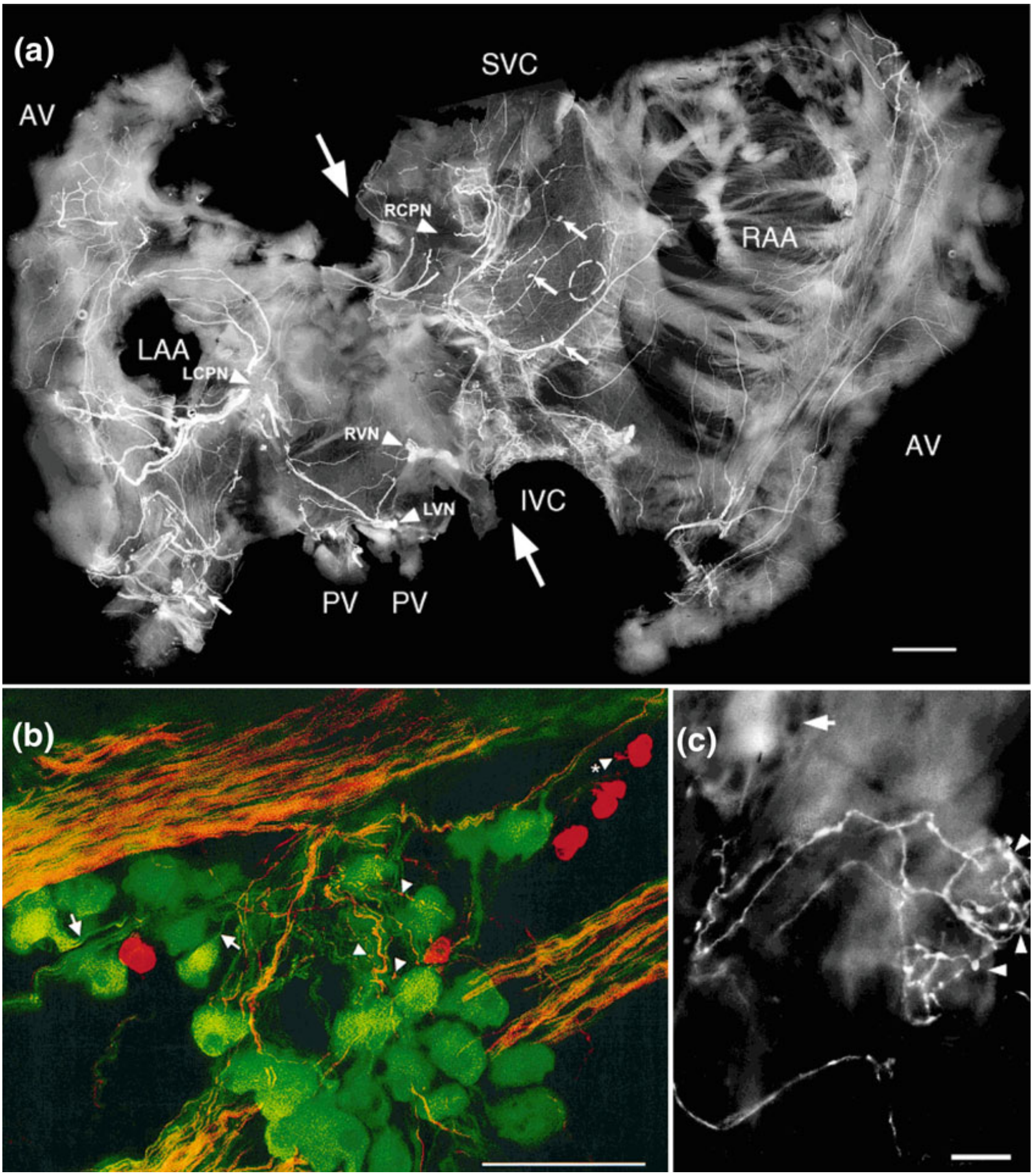

Fig. 8.6 Neuroanatomy of intracardiac nervous system in guinea pig heart. (**a**) Flattened wholemount preparation of both atria; neuronal network identified by antibodies directed against the pan-neuronal marker protein gene product 9.5 (white lines). Edges of tissue mark atrioventricular border (AV), interrupted by areas labeled PV (pulmonary veins), IVC (inferior vena cava) and SVC (superior vena cava). LAA and RAA: left and right atrial appendages; LVN, RVN: left and right vagosympathetic nerve trunks (arrowheads); LCPN, RCPN: left and right cardiopulmonary nerves (arrowheads). Small arrows indicate ganglia containing intracardiac neuronal cell bodies; dotted oval shows the location of sinoatrial node pacemaker. A line taken between the large arrows at top and bottom of the tissue marks the position of the junction of the external atrial wall with the interatrial septum (not shown). (**b**) Ganglion with labeled neuronal somata (oval-shaped cells; protein gene product 9.5) adjacent to two interganglionic nerves. Smaller, lighter-staining cells and processes expressing tyrosine hydroxylase (arrows and arrowheads) are also shown; these do not overlap with the neuronal label. (**c**) Catecholamine-containing processes with varicosities (arrowheads) associated with ganglion neurons (diffuse background staining). Scale bars represent 2.5 mm in **a**, 50 μm in **b**, 25 μm in **c** ([54] with permission)

generating NO, a gaseous transmitter with widespread effects on many visceral organs. In the ICNS of some mammals, cholinergic neurons have been shown to express multiple neuropeptides, thus defining a series of subpopulations with distinct neurochemical profiles. For instance, in the guinea pig ICNS Steele and coworkers reported that neurons expressing combinations of the peptides somatostatin, dynorphin, substance P, NPY and VIP constituted at least seven neuronal subclasses; this picture is further complicated by the fact that many but not all of these cells also expressed nNOS [52, 94]. Furthermore, in an extensive immunohistochemical study, Steele et al. [95] established the axonal termination patterns within the heart of multiple peptide-expressing subpopulations of ICN, showing that the sinoatrial node, the atrioventricular node and the cardiac valves were each innervated by several of these subpopulations. In human ICN, the most common somatic phenotype was cholinergic, with the majority of cells expressing nNOS. However, none of the somata in humans showed labeling for VIP, SP or calcitonin gene-related peptide (CGRP, commonly associated with the somata of sensory neurons), but these peptides were abundant in axons and terminals throughout the ganglia [96]. The latter finding suggests that these peptide-containing elements were derived from neurons with their somata extrinsic to the heart.

The number of neurons (<10–15% of the total number) in the ICNS that express TH is relatively small. Members of that population should have the capability for synthesizing and releasing NE (and possibly epinephrine) [53, 97–101] so they may represent sympathetic postganglionic neurons with their somata located in the ICNS. Certainly, when intracardiac ganglia in most parts of the mammalian heart are stimulated chemically to activate neuronal somata (but not axons that may be of extracardiac origin), cardioaugmentation occurs similar to the effects of activating sympathetic postganglionic neurons in the intrathoracic ganglia via axons projecting to the heart [32]. On the basis of these findings, sympathetic efferent neurons have been represented at the intracardiac level of the schematic diagrams of neuronal hierarchy for cardiac control (Figs. 8.1 and 8.2). Putative sympathetic postganglionic efferent neurons in the ICNS have also been shown to co-express peptides such as NPY [53].

Many reports have also identified TH-positive cells in the ganglia of the ICNS that do not express markers typical of neurons; such cells have a smaller average soma size than ICN and may release catecholaminergic neurotransmitters [54]. The function of these cells in the heart is not known, but it is possible that they may represent a form of “interneuron” as proposed by Parsons et al. [102] in the cardiac ganglion of the amphibian. In some studies of the mammalian heart, these cells are reported to have pericellular baskets of cholinergic axon terminals. They also give rise to short projections that appear to contact nearby cholinergic ganglion neurons (Fig. 8.6), reinforcing the idea that these cells could release catecholamines under the influence of cholinergic synaptic input. There is also the possibility that these TH-positive cells may be a type of “small, intensely fluorescent cell” (SIF cell), common in other peripheral autonomic ganglia (for instance, pelvic ganglia [103]).

There is a small subpopulation of ICN in which individual somata may contain both cholinergic and adrenergic neuromarkers, reported in several species (guinea pig [53]; mouse [47, 99]; human [98]; rats, mice and human [104]). As yet, it is unclear what the function of such neurons might be, since ACh and NE have different influences (i.e., inhibitory versus excitatory) on those effectors expressing receptors for both neurotransmitters. It has been proposed that the function of such neurons may be switched, perhaps by fluctuating local concentrations of neurotrophic factors that control neurotransmitter gene expression, to work in either sympathetic or parasympathetic pathways at different times and under different physiological conditions [98, 104]. However, the connectivity and physiology of these neurons have not been established and their roles in the control of the heart are still unknown, leaving an intriguing gap in our knowledge of this system.

Nerve fibers containing neuropeptides (SP, CGRP) that are expressed by visceral afferent neuronal populations with their somata in the nodose and petrosal ganglia and the dorsal root ganglia (DRG) have also been reported within the ICNS [13, 34, 47, 99, 105, 106]. In addition, DRG neurons express markers for glutamate-handling biochemistry and there are numerous intracardiac plexus components containing these markers [107]. Furthermore, mechanical and chemical manipulation of most parts of the myocardium evoke rapid changes in ICNS activity that correlate with changes in the behavior of cardiac effectors. It has been proposed that collaterals of afferent axons within the heart terminate on some ICN, constituting local sensory feedback to intracardiac circuitry about the dynamic state of the heart [20, 32, 33]. There is also evidence that the somata of some ICN contain sensory neuronal markers (CGRP, SP [53]; glutamate [107]). These neurons may thus serve as intracardiac afferent neurons with their processes entirely within the ICNS [32] (see Sect. 8.3.1.2.2 for further discussion). Such afferent neurons are therefore represented within the ICNS in the hierarchy for cardiac control (Figs. 8.1 and 8.2).

8.3.1.2 Functional Roles

At the level of individual neurons within the ICNS, what practical criteria might be used during experimental studies to identify the cell types labeled "efferent," "local circuit" and "afferent" in Figs. 8.1 and 8.2? This question is considered in the discussion of function-specific neuronal types below.

8.3.1.2.1 Efferent Neurons

(i) Parasympathetic Postganglionic Efferent Neurons

There is no doubt that cholinergic ICN are the primary parasympathetic postganglionic neurons in the two-neuron pathway for signaling from medullary preganglionic neurons to the cardiac effectors. However, as a number of studies have shown over the last four decades, not all, and perhaps not even the majority of ICN (depending at least partly on species) subserve this function. Even determining how many neurons are in this category in any species is still problematic. What would constitute a reasonable set of necessary and sufficient characteristics to define parasympathetic efferent ICN, and what is the evidence for neurons that would fit this set?

1. ***Axonal projection pattern***. Each neuron in this category should project an axon directly to at least one class of cardiac effector cell (pacemaker, conducting system, myocytes, smooth muscle of vasculature) in a region of the heart (or multiple regions if the axon branches) that may lie adjacent to, or more distant from, the location of the ganglion in which the soma is located. There is anatomical and physiological evidence in every species examined so far indicating that all regions of the heart receive parasympathetic postganglionic innervation [13, 34, 95, 108] and that stimulation of ICN in ganglia located in all of the major intracardiac plexi can affect cardiac function via activation of effector cells both adjacent to and remote from the stimulated ganglia [62, 65–68]. To date, there have been few attempts to analyze the intracardiac axonal projection patterns of ICN with the use of neurotracers. In an intracellular study of the morphology-function relationships of physiologically identified ICN [82], a neurotracer was injected through the recording microelectrode into the somata of sampled neurons. The processes of some of these neurons exited the ganglion under study via interganglionic nerves, but the distal targets of these projections could not be determined. In the reverse experiment, in which the neurotracer cholera toxin subunit B (CTB) was applied to the right or left atrial wall of the canine heart, the tracer was transported from axonal terminals to neuronal somata in both local and remotely located ganglia. In some cases, individual somata were labeled by CTB transport from axonal branches innervating multiple, well-separated injection sites [109]. However, somata in this study were not characterized on the basis of their physiological properties. While these findings

reinforce the general idea of the distributed nature of ICN projections to local and distant cardiac effectors, it is not clear what the specific pattern of "fanout" of axonal projections of specific efferent parasympathetic neurons may be within the heart.

2. ***Transmitter release at neuroeffector junctions***. Parasympathetic efferent neurons release ACh from axon terminals in the vicinity of cardiac effectors, representing the fulcrum for parasympathetic control of cardiac functions. Endogenously released ACh acts postjunctionally at primarily M_2-type muscarinic receptors, with consequent negative chronotropic, inotropic and dromotropic effects. In addition to cholinergic neuroeffector transmission, these neurons may also release one or more of a constellation of neurotransmitters and neuromodulators (e.g., NO, VIP and NPY) from their axonal terminals (Sect. 8.3.1.1.2), which can modify the postjunctional effects of muscarinic receptor activation. However, there have as yet been no definitive studies in functioning cardiac preparations on the nature of neuroeffector transmission from cholinergic efferent neurons identified either by their neurochemical profiles or by their specific axonal projection patterns to particular cardioeffectors.
3. ***Convergence of synaptic inputs***. Some efferent postganglionic parasympathetic neurons receive direct synaptic input from one (or more) vagal preganglionic axons coursing into the heart from extrinsic nerves, although the proportion of neurons receiving such inputs is known to be only a small fraction of the total number of ICN [26, 110]. Vagal preganglionic axon terminals release ACh, causing excitatory postsynaptic potentials (EPSPs) in the postsynaptic membrane via activation of nicotinic receptors. The simplest arrangement for information transfer in this system, assuming that preganglionic input is represented by one axon terminating on a single postganglionic cell, would therefore consist of strong synaptic drive (one AP arriving at the preganglionic terminal evoking a high-amplitude EPSP) that is suprathreshold for AP generation in the postganglionic neuron. This would fit the "classical" concept of the two-neuron peripheral autonomic pathway from central neurons to the viscera. However, data from studies recording extracellular AP discharge within the ICNS in the in situ heart show that this condition is rare: trains of high-frequency, high-intensity stimuli delivered to vagal preganglionic nerves are normally required to evoke even minimal AP discharge in ICN in efferent pathways [26, 110]. The major implication of this is that the majority of postganglionic parasympathetic efferent ICN do not receive direct synaptic inputs from extracardiac preganglionic axons. Other investigations using intracellular recordings from ICN in isolated atrial preparations in vitro have identified a population of neurons with preganglionic vagal inputs [85, 111]. Some of these neurons display high-strength, unitary synaptic excitation, but most show evidence of polysynaptic innervation, requiring summation of inputs from multiple presynaptic terminals to reach the threshold for AP generation. In contrast, McAllen et al. [90] have reported that vagal preganglionic inputs to individual ICN, driven both by cardiorespiratory reflexes and vagosympathetic trunk stimulation, usually evoke strong, unitary postsynaptic responses and APs in these neurons. However, it was not possible in any of these studies to identify where in the intracardiac control pathways the sampled neurons resided so their identity as potential parasympathetic postganglionic neurons could not be confirmed.

While details of the number, source and neurochemical phenotypes of synaptic terminals on efferent ICN remain unknown, it is likely that most, if not all, of these cells, will receive inputs from several different populations of ICN involved in local processing and possibly from cardiac afferent axon collaterals or axons from afferent ICN. These inputs may originate from cells within the ganglion in which the efferent neuron resides or from neurons in other intracardiac ganglia. In any case, given the potential complexity of convergence of inputs onto efferent ICN, if there are specific subsets of these inputs forming differentiable patterns, these have not yet been established (see further discussion in Sect. 8.3.1.2.3 below).

4. ***AP discharge properties***. The separation of ICN into discrete populations based on their AP firing behaviors (Sect. 8.3.1.1.1) was originally done in the hope that these behaviors would correlate with other characteristics such as input pattern or output projection to enable the identification of neurons in each category with a particular functional pathway. So far, however, this has not proven to be the case. While there appears to be general consensus that neurons with phasic and multiple-firing (accommodating or tonic) behaviors actually represent physiologically distinct subtypes (based on discrete sets of membrane ion channel complements), there are as yet no straightforward correlations between the firing behavior of a neuron and its position within a specific pathway or its functional role in cardiac control. This may partly be due to interspecies differences and partly to the fact that the anatomical identification of efferent neurons is still lacking in any species (see above). Therefore studies in which the somata of neurons are retrogradely labeled with neurotracers applied to various cardioeffectors, combined with intracellular recordings to determine the firing properties of such neurons, would represent the most direct way to address the question of physiological to pathway-position correlation. Such studies have been performed in investigations of the enteric nervous system to help establish the functional characteristics of myenteric and submucosal neuronal populations (see [112]), but these techniques have not yet been applied to the heart.
5. ***Integrative properties***. The capability of a single efferent parasympathetic postganglionic ICN to generate APs that modulate the activity of a cardiac effector will be determined by integration of the combination of factors discussed above pertaining to that particular neuron: the origins of synaptic input and postsynaptic receptor types present, synaptic strength of different inputs and the firing behavior of the cell. Given that some of these characteristics can also be modified by ongoing changes in the cardiac milieu (such as metabolite levels, extracellular ion concentrations, availability of nutritive substrates, local ischemia and pH [33]), the role of any efferent neuron will likely also adapt at least in the degree of its effectiveness if not in principle, during such variations.

(ii) Sympathetic Postganglionic Efferent Neurons

While the somata of the vast majority of sympathetic neurons in the peripheral autonomic innervation targeting the heart are located in the extracardiac intrathoracic ganglia [101], there is evidence that some somata lie within the ICNS [32, 101]. These neurons may have been displaced from the intrathoracic ganglia into the heart during development, so they could have the same operating characteristics as those in the thoracic ganglia, or they may represent a different subpopulation of sympathetic postganglionic neurons with their own set of characteristics. This has not been established. There is in fact very little known about these neurons at the cellular level. Their neuroeffector terminals contain catecholamines (chiefly NE), so these cells should be distinguishable as a distinct subpopulation from the other neuron types in the ICNS by their expression of amine-synthesizing enzymes, capability for storing and releasing adrenergic neurotransmitters and affinity for pan-neuronal markers.

1. ***Axonal projection pattern***. By analogy with parasympathetic efferent neurons in the heart (Sect. 8.3.1.2.1, i(1)), sympathetic efferent ICN should project axons to neuroeffectors in one or more regions of the heart (diverging through axonal branching) and their axon terminals will release NE at neuroeffector junctions to augment effector function. Physiological experiments support this supposition. Activation of these ICN with focal application of small volumes of excitatory neurochemicals

to individual ganglia located in all parts of the heart evokes neurally mediated increases in cardiac indices [67, 113]. Those results demonstrate that sympathetic postganglionic ICN are present and project axons to a range of neuroeffectors throughout the heart. It thus appears that, while sympathetic postganglionic neurons within the ICNS appear to be much more rare than parasympathetic neurons, adrenergic ICN also constitute a distributed control system capable of driving local and remote cardio-augmentatory responses. However, despite several studies that have identified ICN somata with adrenergic characteristics, thus making them likely candidates for sympathetic postganglionic ICN [53, 98, 100], there have been no studies of the neuroanatomy of the axonal projections of these neurons.

2. ***Transmitter release at neuroeffector junctions***. Sympathetic postganglionic neurons with their somata located in the ICNS will likely have axon terminal-cardiac effector relationships similar to those of postganglionic neurons with their somata in the intrathoracic ganglia. Release of NE from the terminals of sympathetic ICN would thus be expected to augment chronotropic, dromotropic and inotropic cardiac functions. The neuropeptide NPY is co-localized with the adrenergic marker TH in the somata and terminals of some sympathetic ICN [53] and release of this peptide can modulate the effects of NE on cardiac myocytes [114] as well as reduce the negative chronotropic effect of parasympathetic cholinergic inputs to the pacemaker [115].
3. ***Convergence of synaptic inputs***. The major synaptic input on sympathetic postganglionic ICN, as for postganglionic neurons in the intrathoracic ganglia, is likely from preganglionic neurons with their cell bodies in the intermediolateral column of the spinal cord. Preganglionic terminals release ACh at the synaptic junction, acting at nicotinic cholinergic receptors on the postsynaptic membrane (Sect. 8.3.1.2.1, i(1)). The cardiac augmentation that results from chemical activation of these neurons was eliminated by propranolol, a β-adrenergic antagonist that blocks postjunctional effects of NE, as well as by the application of hexamethonium, a nicotinic cholinergic channel blocker that interrupts cholinergic neurotransmission to these cells [67].

   There is as yet no information about noncholinergic synapses on sympathetic postganglionic neurons in the ICNS. Studies identifying putative sympathetic ICN by their primary expression of TH [53, 99] have not provided details of the neurotransmitter phenotypes of synaptic terminals on these cells.
4. ***AP discharge properties***. No intracellular records have yet been made from cells identified as intracardiac sympathetic postganglionic neurons, so the firing behavior of these neurons is not established.
5. ***Integrative properties***. Given that sympathetic postganglionic ICN will have synaptic inputs from one or more sympathetic preganglionic axons and that the neurochemical profiles of any additional synaptic contacts on these cells remain unclear, it is tempting to speculate that their capability for integration at the level of the soma may be limited. In the simplest case, these cells may receive only one strong synaptic preganglionic input, thus acting as simple relays from the autonomic motor neurons in the spinal cord to the cardiac effectors. However, intracellular studies of sympathetic postganglionic neurons in the intrathoracic ganglia have shown that neurons here typically integrate multiple preganglionic inputs and may receive additional inputs from afferent axons and possibly from intraganglionic processing neurons [8, 29, 116]. The capability for processing information through the network of intracardiac sympathetic postganglionic neurons is, therefore, likely to be no less complex than that for their counterparts in the intrathoracic ganglia.

8.3.1.2.2 Afferent Neurons

Primary afferent neurons associated with the heart may be defined as those that respond to one or more sensory modalities (mechanical stretch or change in the local chemical environment) with a receptive field limited to a restricted cardiac region [117]. Some of these afferent neurons can transduce both mechanical and chemical stimuli [32]. The somata of such neurons may be located outside the heart in the DRG, vagal sensory ganglia, intrathoracic ganglia or within the ICNS [8, 33]. Thus, within the heart, there are two apparent sources of sensory signaling: (1) afferent neurons with their somata in extracardiac ganglia with axons that give rise to intracardiac collaterals terminating on neurons within the ICNS; and (2) afferent neurons with their somata resident within the ICNS and with axons that project intracardially. Activation of receptor endings of either of these neuron types by an adequate stimulus of the correct modality results in the generation of trains of APs. These in turn activate other ICN involved in a variety of integrative processes that eventually contribute to cardiac command signals by which the heart responds to the original stimulus [20]. Such afferent input into LCN and efferent neurons within the ICNS would thus provide the necessary drive for short-latency intracardiac reflexes [33].

The observation of ongoing, spontaneous intracardiac neuronal activity, recorded in the absence of inputs from the central nervous system or intrathoracic ganglia (heart decentralized), was the first convincing physiological evidence that afferent neurons could be driving activity within the ICNS [26, 110, 118]. The fact that spontaneous activity could be recorded in the hearts of dogs up to a year after cardiac transplant (in those animals that did not show signs of regrowth of extracardiac nerves into the heart) further indicated that afferent neurons resident in the ICNS were driving this activity [119]. In these, and in virtually all other studies of ICN in the beating heart, neuronal activity was recorded extracellularly. It has thus not been possible to determine whether the source of afferent discharge was the primary afferent neurons themselves or activity that was induced in secondary or higher-order neurons entrained by such primary afferent inputs [110]. The characteristics of primary afferent ICN at the level of individual cells have not been established.

Primary cardiac afferent neurons with their somata in the DRG that project to the dorsal horn of the spinal cord express CGRP and SP along with markers for the synthesis of glutamate [107, 120] and have a stereotypical bipolar morphology [55, 105]. Cardiac afferent information is also conveyed to the nucleus solitarius in the medulla via primary afferent neurons with their somata in the nodose and petrosal ganglia of the vagus. The occurrence and distribution of the axons of these afferent neurons within the heart are identifiable by the patterns of expression of their sensory neuromarkers. It is reasonable to suppose that resident cardiac afferent ICN would have similar profiles of neuromarkers; in fact, cell bodies expressing neuromarkers typical of afferent neurons have been identified within the ICNS [53], although these are relatively rare. Some afferent terminals and axons in the heart also express the transient receptor potential vanilloid 1 (TRPV1) ion channel [121–124]; these terminals are activated by a variety of chemical stimuli including capsaicin and bradykinin [121, 122, 125]. Recently the TRPV1 agonist resiniferatoxin has been used to overstimulate and thus partially deplete these channels, providing a method to selectively impair some intracardiac afferent terminals [121, 123]. This has allowed the contribution of these receptors to cardio-cardiac reflexes to be evaluated [123, 124]. It is, therefore, possible that the characteristics typical of vagal and DRG afferent neurons may also apply to resident afferent ICN.

There is physiological evidence for the presence of intracardiac afferent neurons in multiple mammalian species. Spontaneous, ongoing activity from ICN in isolated atrial tissues in vitro has been reported during intracellular recording by several authors [84, 126, 127]. This activity generally consists of EPSPs occurring either irregularly or in rhythmic trains; some of these depolarizations exceeded the threshold for AP discharge. In this situation, it is not clear whether these neurons are themselves primary sensory cells or are responding to activity in a primary neuron with a synapse on the sampled neuron. In some cells, APs rose directly from the baseline membrane potential without a preceding EPSP. Such activity may represent ongoing discharge of primary afferent neurons, perhaps responding to small contractions of the underlying myocardial substrate.

An attempt to correlate the firing pattern of ICN with other indicators of a potential afferent function was made by Edwards et al. [84], who recorded intracellularly from several classes of neurons in the guinea pig heart (see Sect. 8.3.1.1.1 for details). They described one class, P-type neurons, that had no synaptic inputs, showed bipolar or pseudounipolar morphology after labeling with neurotracer injected via the recording electrode and displayed multiple AP discharges in response to long intracellular depolarizing current injection. P-type neurons also had consistent patterns of spontaneous, frequent short depolarizations that were subthreshold for AP generation and occasionally discharged APs that rose rapidly from the baseline membrane potential without a preceding EPSP. Selyanko [80] also reported that some ICN with the firing properties of type Im (Fig. 8.5) showed regular spontaneous AP discharges that rose directly from the baseline membrane potential without evidence of preceding EPSPs. This author discounted the possibility that injury potentials resulting from poor cell impalement were responsible, suggesting that this activity was "intrinsic in origin". Such activity may well have arisen from the transduction of mechanical stimuli from elements of the myocardium underlying the ganglia containing the sampled neurons.

Given the attributes of extracardiac afferent neurons innervating the atria and ventricles, it would be appropriate to speculate that afferent neurons with their somata within the ICNS had similar attributes, as a starting point for identifying these cells. The most useful criteria for this may be: (1) somata and processes that exhibit immunohistochemistry for one or more of the neuropeptides associated with extracardiac afferent cells (CGRP and SP) with markers of glutamate expression also a possibility; (2) expression of TRPV family channels or stretch-activated channels in the cell membrane; (3) lack of synaptic inputs; (4) pseudounipolar or possibly bipolar cell morphology; (5) receptor terminals associated with the myocardium or cardiac connective tissue; (6) membrane potential depolarization in response to activation of chemosensory or mechanosensory transduction mechanisms (or both), with such depolarizations reaching the threshold for AP discharge upon delivery of an adequate stimulus to the membrane; (7) capability for firing APs repetitively under strong sensory stimulation (some of these neurons may show adaptation of AP firing rate); (8) synaptic transmission, with a high safety factor, to one or more secondary neurons. It is possible, in regard to item 8, that those afferent neurons make connections with nearby secondary neurons or with those in more distant ganglia; ultimately, such afferents may even project axons centripetally via extracardiac nerves.

8.3.1.2.3 Local-Circuit Neurons

Evidence from numerous studies employing extracellular recordings of ICN activity in in situ hearts indicates that the majority of activity originates from neither principal postganglionic efferent neurons nor primary afferent neurons [32]. Instead, such activity is proposed to result from the potentially very large number of interactions between neurons of as yet indeterminate function within the intracardiac ganglia; these neurons are represented in the hierarchical schematics of the ICNS as LCN (Figs. 8.1 and 8.2).

Beaumont et al. [110] showed that, in spontaneously beating hearts in the open-chest, anesthetized canine, many ICN discharged APs spontaneously at varying rates. Their activity could be modulated by manipulations including mechanical stimulation of the myocardium, short periods of left ventricular ischemia, great vessel occlusion, induction of atrial arrhythmia or extracardiac nerve stimulation. However, it is salutary that none of the neurons sampled in that study responded directly to extracardiac inputs. Instead, approximately half of the neurons responded indirectly to electrical stimulation of either vagal or sympathetic extracardiac nerves. A proportion of these ICN showed responses to stimulation of both extrinsic input pathways. The authors interpreted these results as showing that most ICN with responses to extrinsic inputs was located in intracardiac processing pathways that were involved in integrating information from central neurons but were not directly driven by those inputs. Many of the sampled ICN, whether or not they received extrinsic inputs, showed spontaneous activity that was locked to specific phases of the cardiac cycle, implying that this aspect of their activity originated from intracardiac afferent neurons or axon collaterals innervating the myocardium. In keeping with this, about one-quarter of neurons sampled in this study responded to mechanical manipulation of the myocardium or to multiple cardiac stressors.

Given the apparent complexity of neuronal pathways within the ICNS and the finding that the majority of ICN within this system appears to consist of subpopulations of LCN that presumably perform a variety of functions within these pathways, it has been proposed that LCN be subdivided into three classes on the basis of experimental evidence [110, 128].

(i) ***Secondary afferent local-circuit neurons***. These neurons are defined as receiving inputs from one or more primary afferents mediating mechanosensory or chemosensory modalities (or both). The designation “secondary” refers to ICN contacted either monosynaptically or through a multisynaptic pathway by primary afferents. In the study of Beaumont et al. [110], the majority of neurons that preferentially received afferent inputs certainly belonged to this class, as they commonly responded to multimodal sensory signals and had broad receptive fields.

(ii) ***Secondary efferent local-circuit neurons***. Neurons of this type would be entrained in the cardiomotor pathways between extrinsic vagal or sympathetic preganglionic inputs and cardiac effectors. They would process inputs derived from extracardiac sources, and their activity would presumably be subject to modification by intracardiac integrative processes controlling the routing of cardiomotor information through these pathways.

(iii) ***Convergent local-circuit neurons***. These neurons are perhaps the least well-defined of the three LCN categories but may be the largest population in the ICNS. A substantial portion of ICN responding indirectly to extrinsic nerve stimulation was activated by more than one input source. These ICN could respond to inputs from the right or left vagus, the right or left sympathetic nerves, or from both sets of nerves [110, 128]. These findings are corroborated by intracellular microelectrode studies in isolated atrial tissue in vitro, in which membrane potential responses of single ICN were recorded during electrical stimulation of the proximal ends of extracardiac nerves [85, 111].

In the rat heart stimulation of the stump of the vagosympathetic trunk attached to the preparation evoked EPSPs and APs in ICN (Fig. 8.7a, top panel [111]); bath application of mecamylamine, a nicotinic cholinergic antagonist, eliminated the nicotinic component of the EPSP, revealing a small noncholinergic postsynaptic depolarization (Fig. 8.7a, bottom panel). In this context, it is important to note that the stimulated nerve branch contains both vagal preganglionic (cholinergic) and sympathetic postganglionic (adrenergic) axons. In the pig heart, more than one-third of the neurons sampled responded with EPSPs to vagosympathetic trunk stimulation; depolarizations usually appeared at latencies of 20–40 ms or longer from the stimulation pulse ([85]; Fig. 8.7b, top trace). Some of those inputs exceeded the threshold for AP discharge (not shown). Roughly half of the ICN responding to vagosympathetic trunk input also responded to cardiopulmonary nerve stimulation with EPSPs (Fig. 8.7b, second trace from the top; none of these reached the threshold for AP discharge). In

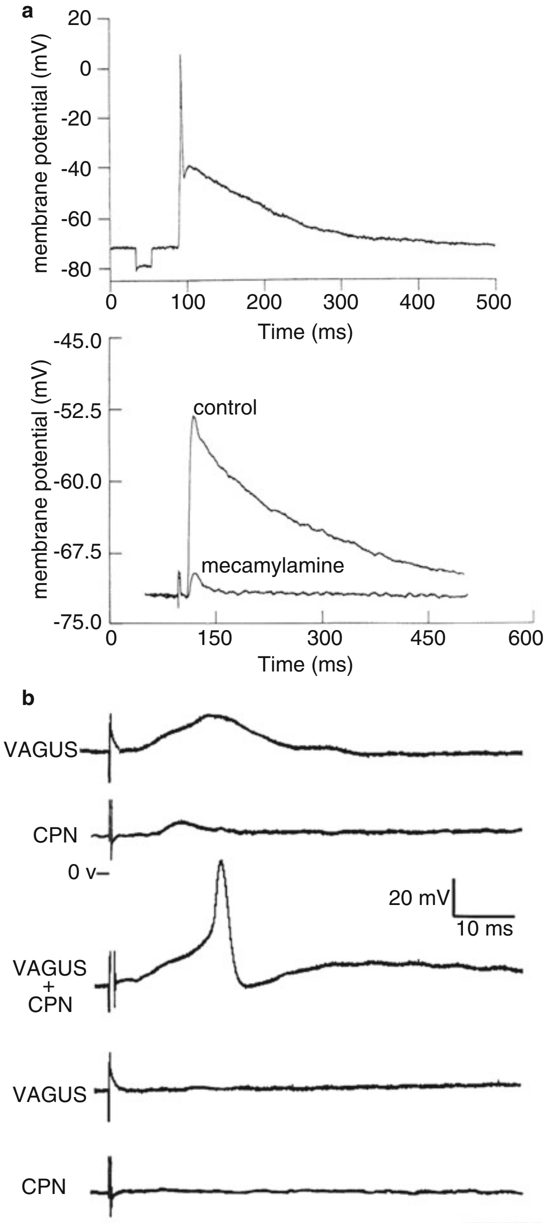

Fig. 8.7 Intracellular postsynaptic responses of intracardiac neurons to electrical stimulation of extrinsic cardiac nerves. (**a**) Isolated heart of neonatal rat. Upper panel: neuron responds with action potential to single presynaptic stimulus. Lower panel: upper trace ("control") shows excitatory postsynaptic response in another neuron to single presynaptic stimulus; response did not reach threshold for action potential discharge. Lower trace ("mecamylamine") shows that depolarizing response to a repeated presynaptic stimulus was eliminated by exposure to this nicotinic cholinergic antagonist. (**b**) Isolated heart of pig. From top of panel downward: Postsynaptic depolarizing responses of the same neuron to single-pulse stimuli delivered to attached stumps of extrinsic cardiac nerves ("VAGUS," upper trace) and cardiopulmonary nerve ("CPN," second trace). Stimulation of either nerve alone evoked excitatory postsynaptic potentials (EPSPs) that did not reach the threshold for action potential discharge. Middle trace, simultaneous stimulation of both nerves ("VAGUS+CPN") evoked multiple EPSPs that summated to exceed threshold for action potential. Second trace from bottom: hexamethonium, a nicotinic antagonist, blocked postsynaptic responses from vagosympathetic trunk stimulation ("VAGUS"). Bottom trace: timolol, a B-adrenergic antagonist, blocked responses from stimulating the cardiopulmonary nerve ("CPN"). In **a** and **b**, the stimulus artifact is represented by small pulse on baseline trace preceding responses (**a**: [111]; **b**: [85] with permission)

the example shown here, when both nerves were stimulated together, the combined EPSP exceeded the threshold for the AP (Fig. 8.7b, third trace from top). Bath application of hexamethonium, a nicotinic cholinergic antagonist, eliminated the effect of vagosympathetic trunk stimulation (Fig. 8.7b, second trace from bottom) and application of timolol, a β-adrenergic antagonist, blocked depolarizations from cardiopulmonary nerve stimulation (Fig. 8.7b, bottom trace). In both studies, ICN were identified that responded to extrinsic nerve stimulation over a range of latencies, and in many of these cells, increasing the stimulus amplitude recruited multiple temporally- and spatially-summated EPSP components. It is, therefore, arguable that the ICN recorded in these intracellular studies could be examples of convergent LCN. Unfortunately, in neither study was a response to local, interganglionic nerve stimulation tested, so whether these neurons received synaptic inputs from intracardiac sources is not known.

The concept of classification of LCN by a combination of (1) their responses to events transduced by primary afferent inputs; (2) their connectivity (or lack of it) with extrinsic autonomic inputs; and (3) their spontaneous discharge profiles entrained by the process of integrative network signal processing as proposed by Beaumont et al. [110] makes a compelling framework to begin to understand how information may be processed in the ICNS. Furthermore, it appears that there is some evidence of support for this system at the level of single ICN, at least for the category of convergent LCN, as in the examples above. However, the characteristics of potential LCN of all types must be further investigated at the level of the single cell.

8.4 Future Directions in Analysis of Intracardiac Neuronal Circuitry

A critical factor in the anatomical and functional analysis of circuitry within the ICNS is access to the system for visualization and experimental manipulation in preparations in which in vivo levels of integration are maintained. In most mammalian models studied to date, the ICNS is embedded in relatively thick cardiac walls, so not accessible in its entirety. Functional studies on the physiology and synaptic interconnections of ICN have thus largely been done in explanted cardiac segments studied in vitro. This has limited the scope for gleaning information about the circuitry in which individual ICN are involved. Similarly, anatomical studies of the ICNS have been hindered by the lack of capability for visualizing labeled neuronal elements in relatively thick, nontransparent cardiac tissue. The development of new tools for tissue clearance to facilitate visualization of the three-dimensional organization of cardiac innervation in whole mammalian hearts with relatively low volumes, such as the mouse heart, has begun to solve the problem of lack of tissue transparency at depth. There are new techniques becoming available for identifying neurotransmitter-specific populations of ICN in whole, spontaneously beating hearts in situ and in vitro. Furthermore, enabling the membrane expression of light-activated channels in identified neuronal subpopulations of the ICNS will allow these populations to be selectively stimulated and their effects on cardioeffectors assessed with high precision. In addition, exploration of the ICNS is being extended to encompass alternative, nonmammalian experimental models, such as zebrafish, that provide advantages for analyzing the fundamental principles of neural control in hearts that are dually innervated by sympathetic and parasympathetic nerves, representing archetypes for control of the mammalian heart. Such “simple” hearts face the same basic challenges of controlling cardiac output as mammalian hearts.

8.4.1 “Low-Volume” Mammalian Hearts

The development of genetically engineered animal models in which defined lines of neurons are identified by their expression of specific neurotransmitters has begun to clarify our understanding of function-specific pathways within the

ICNS. This approach has been facilitated by the advent of the parallel development of advanced tissue-clearing protocols so that fluorescent markers genetically incorporated into neuronal somata and processes can be visualized at the single-cell level in whole organs [129–132]. Recent advances in microscopy techniques, such as light-sheet microscopy [133] and improvements in laser confocal microscopy, are also contributing to the process of visualizing details of the ICNS in three dimensions in the whole heart [34]. A prime example of the recent use of these techniques is the publication of an atlas of the ICNS in the whole rat heart: this study has, for the first time, provided a detailed three-dimensional map of the intracardiac neuroanatomy in the mammalian heart as well as elaborating the organization and distribution of neurotransmitter-specific neuronal populations at the single-cell level [51]. The rich detail provided by such advances is now facilitating the analysis of the functional roles of specific populations of ICN in cardiac control.

A very powerful tool for identifying and genetically manipulating specific neuronal populations is the use of recombinant adenoassociated viruses (AAV) as vectors for delivering genetic material into these populations [134, 135]. Such techniques have been used for inducing neurons to express fluorescent marker proteins, optogenetic actuators such as channelrhodopsins (ChR, see below) and a variety of cytosolic calcium indicators and membrane voltage-sensitive agents. These viruses can be used to deliver genetic material into adult organs and tissues including the heart, and once delivered, the resulting expression of the cellular products is long-lasting. This technique raises the possibility of identifying and manipulating whole populations of neurotransmitter-identified ICN to help define the circuitry in which these neurons are embedded.

A recent example of the use of a combination of these new techniques to explore the wiring of the ICNS is a study by Rajendran et al. [136] in the mouse heart. Here these authors have mapped the broad outlines of sympathetic and parasympathetic intracardiac and intrathoracic circuitry controlling pacemaker and other cardioeffector functions using neuroanatomical and optogenetic techniques. In the ICNS, they first defined the detailed three-dimensional distribution of ganglia and nerves using a pan-neuronal, fluorescently-tagged marker, whole-organ tissue-clearing procedure [130, 132] and visualization with confocal and light-sheet microscopy. They then used AAV-based labeling of cholinergic ICN to identify parasympathetic efferent neurons projecting to the SAN, the AVN and the conducting system, thus anatomically defining a portion of the function-specific neuronal pathway controlling heart rate and conduction (Fig. 8.8). To evaluate the function of this neuronal circuitry the authors developed a transgenic mouse line expressing ChR in the cell membrane of cholinergic ICN. Neurons expressing ChR, when exposed to pulses of light of the correct wavelength to open these channels, become depolarized and generate APs. Light-associated opening of ChR channels thus emulates excitation of these neurons by suprathreshold synaptic input. In an isolated preparation of the spontaneously beating heart, light application to the inferior pulmonary ganglionated plexus, adjacent to the SAN, evoked varying degrees of bradycardia that depended on the light intensity (Fig. 8.9). Activation of these ganglionic neurons also altered the electrocardiogram waveform (prolonging the P-wave) and caused ectopic atrial beats. These results illustrate the potential for the use of genetic engineering and optogenetic techniques to dissect the circuitry of the ICNS to unravel the roles of defined subpopulations of neurons in cardiac control. The authors were thus able to explore the cardiac effects of activating a population of cells that could represent primary efferent parasympathetic neurons, thus defining the output segment of one of the function-specific reflex pathways within the heart that controls rate. It is anticipated that the combination of such new circuitry-defining techniques with established intracellular and patch-clamp recording methodology will allow the next step to be taken in understanding the organization and physiology of intracardiac reflexes.

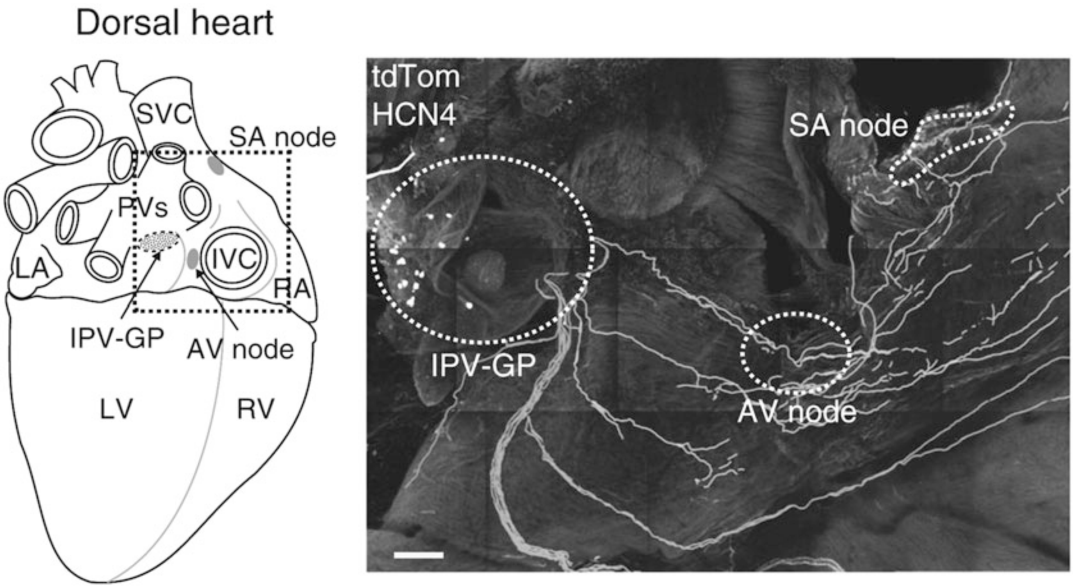

Fig. 8.8 Intracardiac nervous system in transgenic mouse heart. Left panel: schematic of dorsal aspect of heart showing the location of major cardiac ganglionated plexi. AV node, atrioventricular node; IVC, inferior vena cava; IPV-GP, inferior pulmonary vein ganglionated plexus; LA, left atrium; LV, left ventricle; PVs, pulmonary veins; RA, right atrium; RV, right ventricle; SA node, sinoatrial node; SVC, superior vena cava. Right panel shows enlarged image of region in dotted box in left panel. Cholinergic neurons in the IVP-GP and their processes were labeled using an adenovirus-associated vector-based system (see text for details) showing cholinergic axons innervating the SA and AV nodes (dotted circles, nodal tissue identified with antibodies against hyperpolarization-activated, cyclic nucleotide-gated ion channel 4, HCN4). Scale bar in the photomicrograph represents 200 μm ([136] with permission)

8.4.2 Ancestral Vertebrate Hearts: Alternative Models for Neurocardiology

The ICNS in several amphibian and teleost fish species has been studied using a variety of in vitro experimental approaches. The earliest studies of vertebrate ICN were done in amphibians to determine the nature of synaptic inputs from vagal preganglionic neurons (see discussion in Sect. 8.3.1.1.1). At approximately the same time, Saito and Tenma [137] evaluated the vagal control of pacemaker discharge in the heart of the carp, a cyprinid teleost fish, demonstrating that the principles of neural control of pacemaker discharge rate were broadly similar to those in the mammalian heart. The fish heart has one atrium and one ventricle, while the amphibian heart has a divided atrium supplying blood to a single ventricle; these organisms thus represent different evolutionary stages in progress toward the four-chambered hearts of mammals. Yet even the most ancestral version of the vertebrate heart, that of teleosts, is governed by dual sympathetic and parasympathetic autonomic inputs and has broadly distributed postganglionic innervation of the myocardium [42–44]. The single atrium and ventricle, operating in series in these hearts, face the same issues in controlling cardiac output to perfuse the vascular beds in the body as do mammalian hearts. The fish heart also has several advantages for neuroanatomical and structure-function studies of the heart, including the hardiness of explanted, perfused hearts and ready access to the entire ICNS in spontaneously beating in vitro preparations.

The most powerful nonmammalian model emerging for investigating many fundamental research questions is the zebrafish, a cyprinid teleost. Studies into a broad range of questions

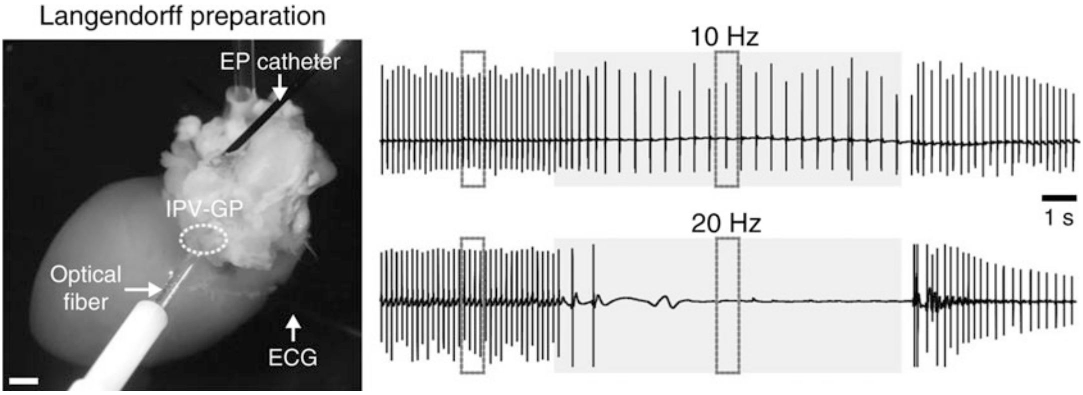

Fig. 8.9 Chronotropic effects of light activation of channelrhodopsin-expressing intracardiac neurons. Left panel: photograph of Langendorff preparation of mouse heart: light pulses from optical fiber were directed toward inferior pulmonary vein ganglionated plexus (IVP-GP, dotted oval). ECG, bath electrodes placed for surface electrocardiogram recording; EP (electrophysiology) catheter site for recording intracardiac ECG. Right panel: bradycardia resulting from the application of light pulses to IVP-GP neurons. Upper trace: light pulses delivered at 10 Hz; lower trace, 20 Hz. Scale bar in the left panel represents 1 mm ([136], with permission)

have burgeoned over the last three decades, and a number of reviews have covered the use of zebrafish in these investigations (i.e., [138] and works cited therein). This model was originally employed for studies of the genetics and molecular biology of embryonic development and organogenesis [139, 140] and the effects of mutagenesis (see the special issue of the journal *Development* 123 [1996]) as well as organ function in adults [141]. The zebrafish genome has been sequenced and is highly conserved to that of humans; there may be one or more orthologues in zebrafish for about 70% of human genes [142]. There is now extensive literature on studies taking advantage of zebrafish to investigate many aspects of basic cardiac function (e.g., [138, 143, 144]). This model has many applications in studies of organ function: zebrafish are readily available and have modest breeding and upkeep requirements; fertilization is external and animals in early developmental stages are transparent; they reproduce quickly and plentifully and form an ideal platform for mutagenesis studies [145]. Moreover, the physiological range of normal heart rate, operation of the pacemaker, cardiac electrophysiology, myocyte AP morphology, contractile protein function and some aspects of calcium handling strongly resemble those of human hearts [146–150]. Transgenic lines of zebrafish have been created with modified orthologues of human genes that are responsible for many heart defects ranging from channelopathies to cardiac conduction. These transgenics have provided clear and profound insights into the physiological mechanisms underlying such defects [144, 151–155] .

Given these factors, our research group has investigated the possibility that the zebrafish ICNS could illuminate fundamental questions of organization and operation of this system. We have shown that all parts of the zebrafish heart are innervated, neurons in the ICNS are mainly localized at the venous pole within a plexus surrounding the sinoatrial valves and the vast majority of neuronal somata are cholinergic with some adrenergic and nitrergic somata also present (Fig. 8.10 [156]). There are approximately 200 ICN somata within the zebrafish heart. Application of a neuronal tracer to the ends of the left and right vagosympathetic trunks attached to the heart showed that axons in these nerves merge with the sinoatrial plexus. Extrinsic adrenergic axons terminate either on ICN somata within the plexus or continue through the plexus into the heart, diverging to innervate targets at the junction of the sinoatrial valve leaflets with the atrium

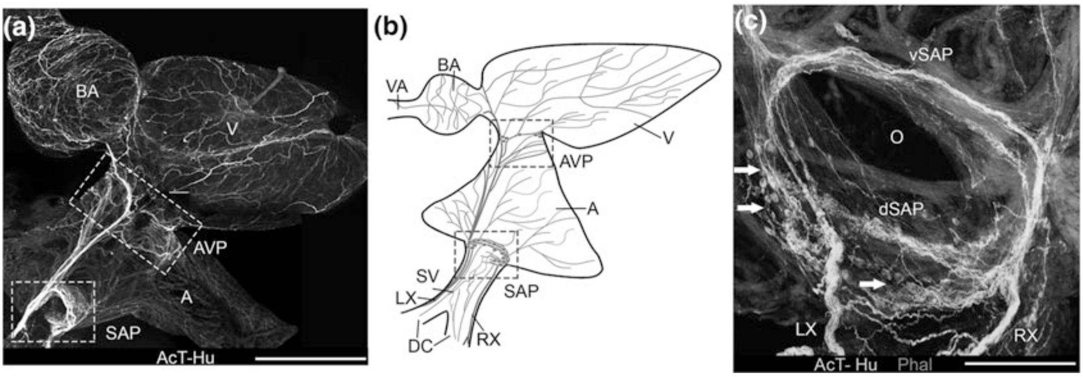

Fig. 8.10 Image (panel **a**) and schematic (panel **b**) of wholemount preparation of zebrafish heart; intracardiac nervous system labeled with pan-neuronal markers acetylated tubulin (Act, axons) and human neuronal protein C/D (Hu, somata). A, atrium; AVP, atrioventricular plexus; BA, bulbus arteriosus; SAP, sinoatrial plexus; V, ventricle. (**c**) Enlarged view of SAP region surrounding sinoatrial valve leaflets. Arrows indicate the locations of some of the ganglia containing intracardiac neurons. dSAP, vSAP: dorsal and ventral components of the plexus; LX, RX: entry into the plexus of left and right vagosympathetic trunks; O: ostium of sinoatrial valve between its leaflets. Scale bar in **a** represents 1 mm; in **c**, 100 μm ([156] with permission)

and throughout the atrial and ventricular walls. Extrinsic cholinergic axons terminate extensively on the somata of ICN throughout the plexus. An intriguing finding from the application of neurotracer to extrinsic nerves was that a few neuronal somata were labeled within the sinoatrial plexus. These somata potentially represent afferent neurons with their axons projecting cardiofugally. Axons arising from some plexus ICN expressing the cholinergic phenotype terminated proximal to cells that were immunoreactive for antibodies against hyperpolarization-activated, cyclic nucleotide-gated ion channel 4 (HCN4, a marker for pacemaker cells in mammalian hearts [157]). These cells were located at the junctions of the sinoatrial valve leaflets with the atrium, forming a ring around the valve ostium, and were adjacent to plexus ICN (Fig. 8.10). This study shows that the ICNS can be visualized in the whole heart, that this system is neurochemically complex, that separate populations of ICN express markers indicating cholinergic, adrenergic or NANC phenotypes, that there may be afferent ICN present and that postganglionic axons from both parasympathetic and sympathetic limbs of the autonomic nervous system innervate all cardiac regions. Our results thus provide details of the neuroanatomical substrate involved in control of cardiac function in the zebrafish.

We developed an isolated preparation of the spontaneously beating, perfused zebrafish heart to study the relationship between the ICNS and pacemaker function (Fig. 8.11 [158]). This preparation provides access to both extrinsic and intrinsic neural elements to dissect their roles in the control of heart rate. Electrical stimulation of attached vagosympathetic trunks activated parasympathetic preganglionic axons evoking bradycardia during the duration of stimulation (Fig. 8.11b). Blockade of cholinergic drive to the pacemaker with atropine eliminated the bradycardia. A delayed, adrenergically mediated tachycardia occurred following the cessation of nerve stimulation (Fig. 8.11b), produced by activation of sympathetic postganglionic axons also present in the vagosympathetic trunks. Blockade of β-adrenergic neurotransmission eliminated this response. Optical imaging of the spread of electrical activity in the myocardium demonstrated that excitation originated in the region of the sinoatrial valve, confirming anatomical results showing that the HCN4-positive cells clustered in this area likely constitute the primary pacemaker. These cells express both β_2-adrenergic and muscarinic cholinergic receptors on their

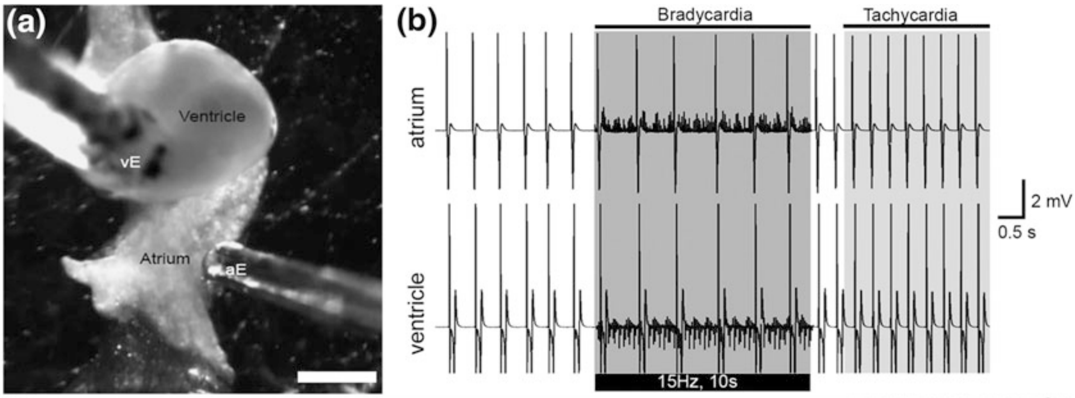

Fig. 8.11 Effects of vagosympathetic trunk electrical stimulation on cardiac chronotropy in isolated zebrafish heart. (**a**) Photograph of preparation showing placement of electrocardiogram electrodes on atrial (aE) and ventricular (vE) walls. Nerve stimulation electrode is not shown. (**b**) Simultaneous electrical stimulation of both attached vagosympathetic trunks (0.5 ms, 300 μA pulses, 15 Hz pulse rate in 10 s train) evoked bradycardia during stimulation, followed by poststimulus tachycardia. Scale bar in **a** represents 1 mm ([158] with permission)

membranes, consistent with the influence of sympathetic and parasympathetic activation on pacemaker discharge rate.

Our results from studies of the neuroanatomy and activation of the ICNS in the isolated zebrafish heart indicate that this preparation has the capability to provide additional insight into the principles governing neural control of the heart. The easy accessibility of the ICNS in this preparation for physiological experiments, as well as the tractability of the zebrafish for genetic manipulation, provides an opportunity to use the same advanced techniques for analyzing ICNS properties already in use for studies in mammalian hearts. Studies designed to identify neurotransmitter-specific neuron populations in whole, living zebrafish hearts and to insert genes coding for light-activated ion channels into the membranes of these neurons to demonstrate the effects of optically activating ICN would begin to clarify the circuitry of intracardiac reflexes, leading to an improved understanding of the operating principles of the ICNS.

8.5 Conclusions

The neural control of the heart has been proposed to depend upon a set of feedback loops involving populations of neurons in the central and peripheral compartments of the autonomic nervous system, illustrated in Figs. 8.1 and 8.2. At the level of the heart, the ICNS is the final common pathway for cardiac control. Intracardiac neurons integrate inputs from higher levels in the hierarchy along with a range of afferent signals from within the heart to generate motor outputs to the effector cells that determine cardiac output on a beat-by-beat basis. The ICNS appears to be composed of collections of locally driven reflex circuits whose activity is constantly and rapidly being modified by changes sensed by local afferents to modulate motor outputs. These reflex circuits are subject to modulation over longer time scales by higher-order reflexes relayed through intrathoracic and central loops. It is thus not surprising that the majority of the ICNS appears to consist of populations of LCN involved in the integration of information that ultimately sets the discharge rates of efferent neurons controlling the cardiac effectors. This, coupled with the distributed nature of intracardiac ganglia throughout the heart and the capability for ICN to influence both local and remote cardiac regions, provides this system with a highly flexible control capability. However, at the level of individual ICN, there remain large gaps in our knowledge related to their physiological types and membrane properties, connectivity, neurotransmitter phenotypes and organization into local reflexes. New technologies for analyzing the neuroanatomical organization of this system combined with novel and established methodologies for studying neuronal circuitry within the heart will ultimately yield a better understanding of the integrated function of the ICNS in controlling cardiac output in the face of varying demands for whole-body perfusion. This understanding is essential to guide the development of effective, neurally based therapies for managing cardiovascular diseases.

References

1. Gaskell W. The involuntary nervous system. London, UK: Longmans; 1916.
2. Langley G. The autonomic nervous system. Cambridge: Cambridge University Press; 1921.
3. Cannon W, Rosenblueth A. Autonomic effector systems. New York: The MacMillan Company; 1937.
4. Sheehan D. Discovery of the autonomic nervous system. Arch Neurol Psychiatry. 1936;35:1081–115.
5. Randall WC. Changing perspectives concerning neural control of the heart. In: Armour JA, Ardell JL, editors. Neurocardiology. New York: Oxford University Press; 1994. p. 3–17.
6. Armour JA, Ardell JL, editors. Neurocardiology. New York: Oxford University Press; 1994.
7. Armour JA, Ardell JL, editors. Basic and clinical neurocardiology. New York: Oxford University Press; 2004.
8. Armour JA. Potential clinical relevance of the “little brain” the mammalian heart. Exp Physiol. 2008;93 (2):165–76.
9. Shivkumar K, Ardell JL. Cardiac autonomic control in health and disease. J Physiol. 2016;594(14): 3851–2.
10. Coote JH, Gilbey MP. Special issue, ‘Central and peripheral nerve influence on cardiac function in health and disease’. Auton Neurosci Basic Clin. 2016;199:1–2.
11. Osteraas ND, Lee VH. Neurocardiology. In: Wijdicks EFM, Kramer AH, editors. Handbook of Clinical Neurology vol 140 (3rd series): Critical care neurology, Part 1. Edinburgh: Elsevier; 2017. p. 49–65.
12. Durães Campos I, Pinto V, Sousa N, Pereira VH. A brain within the heart: A review on the intracardiac nervous system. J Mol Cell Cardiol. 2018;119:1–9.
13. Wake E, Brack K. Characterization of the intrinsic cardiac nervous system. Auton Neurosci. 2016;199: 3–16.
14. Loewy A, Spyer K, editors. Central regulation of autonomic functions. New York: Oxford University Press; 1990.
15. Taggart P, Critchley H, van Duijvendoden S, Lambiase PD. Significance of neuro-cardiac control mechanisms governed by higher regions of the brain. Auton Neurosci. 2016;199:54–65.
16. Hopkins DA, Armour JA. Ganglionic distribution of afferent neurons innervating the canine heart and cardiopulmonary nerves. J Auton Nerv Syst. 1989;26(3):213–22.
17. Armour JA, Huang MH, Pelleg A, Sylvén C. Responsiveness of in situ canine nodose ganglion afferent neurones to epicardial mechanical or chemical stimuli. Cardiovasc Res. 1994;28(8):1218–25.
18. Vance WH, Bowker RC. Spinal origins of cardiac afferents from the region of the left anterior descending artery. Brain Res. 1983;258(1):96–100.
19. Armour JA. Anatomy and function of the intrathoracic neurons regulating the mammalian heart. In: Zucker I, Gilmore J, editors. Reflex control of the circulation. Boca Raton, FL: CRC Press; 1991. p. 1–37.
20. Kember G, Ardell JL, Shivkumar K, Armour JA. Recurrent myocardial infarction: mechanisms of free-floating adaptation and autonomic derangement in networked cardiac neural control. PLoS One. 2017;12(7):e0180194.
21. Norris JE, Foreman RD, Wurster RK. Responses of the canine heart to stimulation of the first five ventral thoracic roots. Am J Physiol. 1974;227(1):9–12.
22. Mizeres NJ. The anatomy of the autonomic nervous system in the dog. Am J Anat. 1955;96(2):285–318.
23. Hopkins DA, Armour JA. Localization of sympathetic postganglionic and parasympathetic preganglionic neurons which innervate different regions of the dog heart. J Comp Neurol. 1984;229(2):186–98.
24. Levy MN. Sympathetic-parasympathetic interactions in the heart. Circ Res. 1971;29(5):437–45.
25. Armour JA. Anatomy and function of thoracic cardiac neurons. In: Ciriello J, Calaresu F, Renaud L, Polosa C, editors. Organization of the autonomic nervous system: central and peripheral mechanisms. New York: Alan R Liss; 1987. p. 67–77.
26. Gagliardi M, Randall WC, Bieger D, Wurster RD, Hopkins DA, Armour JA. Activity of in vivo canine cardiac plexus neurons. Am J Physiol. 1988;255(4): H789–800.
27. Armour JA. Activity of in situ stellate ganglion neurons of dogs recorded extracellularly. Can J Physiol Pharmacol. 1986;64(2):101–11.

28. Armour JA. Neuronal activity recorded extracellularly in chronically decentralized in situ canine middle cervical ganglia. Can J Physiol Pharmacol. 1986;64(7):1038–46.
29. Bosnjak ZJ, Kampine JP. Intracellular recordings from the stellate ganglion of the cat. J Physiol. 1982;324:273–83.
30. Kalia M, Mesulam MM. Brain stem projections of sensory and motor components of the vagus complex in the cat: I. The cervical vagus and nodose ganglion. J Comp Neurol. 1980;193(2):435–65.
31. Kalia M, Mesulam MM. Brain stem projections of sensory and motor components of the vagus complex in the cat: II. Laryngeal, tracheobronchial, pulmonary, cardiac, and gastrointestinal branches. J Comp Neurol. 1980;193(2):467–508.
32. Ardell JL, Armour JA. Neurocardiology: structure-based function. Compr Physiol. 2016;6(4):1635–53.
33. Shivkumar K, Ajijola OA, Anand I, Armour JA, Chen P-S, Esler M, et al. Clinical neurocardiology defining the value of neuroscience-based cardiovascular therapeutics. J Physiol. 2016;594(14):3911–54.
34. Hanna P, Rajendran PS, Ajijola OA, Vaseghi M, Andrew Armour J, Ardell JL, et al. Cardiac neuroanatomy—imaging nerves to define functional control. Auton Neurosci. 2017;207:48–58.
35. Rajendran PS, Nakamura K, Ajijola OA, Vaseghi M, Armour JA, Ardell JL, et al. Myocardial infarction induces structural and functional remodelling of the intrinsic cardiac nervous system. J Physiol. 2016;594(2):321–41.
36. Jänig W. The integrative action of the autonomic nervous system: neurobiology of homeostasis. Cambridge: Cambridge University Press; 2006.
37. Jänig W, McLachlan EM. Specialized functional pathways are the building blocks of the autonomic nervous system. J Auton Nerv Syst. 1992;41(1–2):3–13.
38. Jänig W, McLachlan EM. Neurobiology of the autonomic nervous system. In: Mathias C, Bannister R, editors. Autonomic failure: a textbook of clinical disorders of the autonomic nervous system. 5th ed. Oxford: Oxford University Press; 2013. p. 21–34.
39. Jänig W, McLachlan EM. Characteristics of function-specific pathways in the sympathetic nervous system. Trends Neurosci. 1992;15(12):475–81.
40. Jänig W. Neurocardiology: a neurobiologist's perspective. J Physiol. 2016;594:3955–62.
41. Farrell A, Smith F. Cardiac form, function and physiology. In: Gamperl A, Gillis T, Farrell A, Brauner C, editors. The cardiovascular system: morphology, control and function. Cambridge, MA: Academic; 2017. p. 155–264.
42. Nilsson S. Autonomic nerve function in the vertebrates. Berlin: Springer; 1983.
43. Nilsson S. Comparative anatomy of the autonomic nervous system. Auton Neurosci. 2011;165:3–9.
44. Nilsson S, Holmgren S, editors. Comparative physiology and evolution of the autonomic nervous system. Chur, Switzerland: Harwood Academic Publishers; 1994.
45. Nonidez J. Studies on the innervation of the heart: 1. Distribution of the cardiac nerves, with special reference to the identification of the sympathetic and parasympathetic postganglionics. Am J Anat. 1939;65(3):361–413.
46. King TS, Coakley JB. The intrinsic nerve cells of the cardiac atria of mammals and man. J Anat. 1958;92(3):353–76.
47. Rysevaite K, Saburkina I, Pauziene N, Noujaim SF, Jalife J, Pauza DH. Morphologic pattern of the intrinsic ganglionated nerve plexus in mouse heart. Heart Rhythm. 2011;8(3):448–54.
48. Pauza DH, Saburkina I, Rysevaite K, Inokaitis H, Jokubauskas M, Jalife J, et al. Neuroanatomy of the murine cardiac conduction system: a combined stereomicroscopic and fluorescence immunohistochemical study. Auton Neurosci. 2013;176(1–2):32–47.
49. Pardini BJ, Patel KP, Schmid PG, Lund DD. Location, distribution and projections of intracardiac ganglion cells in the rat. J Auton Nerv Syst. 1987;20(2):91–101.
50. Richardson RJ, Grkovic I, Anderson CR. Immunohistochemical analysis of intracardiac ganglia of the rat heart. Cell Tissue Res. 2003;314(3):337–50.
51. Achanta S, Gorky J, Leung C, Moss A, Robbins S, Eisenman L, et al. A comprehensive integrated anatomical and molecular atlas of rat intrinsic cardiac nervous system. iScience. 2020;23(6):101140.
52. Steele PA, Gibbins IL, Morris JL, Mayer B. Multiple populations of neuropeptide-containing intrinsic neurons in the guinea-pig heart. Neurosci. 1994;62(1):241–50.
53. Horackova M, Armour JA, Byczko Z. Distribution of intrinsic cardiac neurons in whole-mount guinea pig atria identified by multiple neurochemical coding. A confocal microscope study. Cell Tissue Res. 1999;297(3):409–21.
54. Leger J, Croll RP, Smith FM. Regional distribution and extrinsic innervation of intrinsic cardiac neurons in the guinea pig. J Comp Neurol. 1999;407(3):303–17.
55. Pauza DH, Skripkiene G, Skripka V, Pauziene N, Stropus R. Morphological study of neurons in the nerve plexus on heart base of rats and guinea pigs. J Auton Nerv Syst. 1997;62(1–2):1–12.
56. Pauza DH, Pauziene N, Pakeltyte G, Stropus R. Comparative quantitative study of the intrinsic cardiac ganglia and neurons in the rat, guinea pig, dog and human as revealed by histochemical staining for acetylcholinesterase. Ann Anat. 2002;184(2):125–36.
57. Arora RC, Waldmann M, Hopkins DA, Armour JA. Porcine intrinsic cardiac ganglia. Anat Rec Part A Discov Mol Cell Evol Biol. 2003;271(1):249–58.
58. Saburkina I, Rysevaite K, Pauziene N, Mischke K, Schauerte P, Jalife J, et al. Epicardial neural

ganglionated plexus of ovine heart: anatomic basis for experimental cardiac electrophysiology and nerve protective cardiac surgery. Heart Rhythm. 2010;7(7): 942–50.

59. Yuan BX, Ardell JL, Hopkins DA, Losier AM, Armour JA. Gross and microscopic anatomy of the canine intrinsic cardiac nervous system. Anat Rec. 1994;239(1):75–87.
60. Armour JA, Murphy DA, Yuan BX, Macdonald S, Hopkins DA. Gross and microscopic anatomy of the human intrinsic cardiac nervous system. Anat Rec. 1997;247(2):289–98.
61. Pauza DH, Skripka V, Pauziene N, Stropus R. Morphology, distribution, and variability of the epicardiac neural ganglionated subplexuses in the human heart. Anat Rec. 2000;259(4):353–82.
62. Randall DC, Brown DR, McGuirt AS, Thompson GW, Armour JA, Ardell JL. Interactions within the intrinsic cardiac nervous system contribute to chronotropic regulation. Am J Physiol Regul Integr Comp Physiol. 2003;285(5):R1066–75.
63. Gatti PJ, Johnson TA, Phan P, Jordan IK 3rd, Coleman W, Massari VJ. The physiological and anatomical demonstration of functionally selective parasympathetic ganglia located in discrete fat pads on the feline myocardium. J Auton Nerv Syst. 1995;51(3):255–9.
64. Armour JA. Cardiac neuronal hierarchy in health and disease. Am J Physiol Regul Integr Comp Physiol. 2004;287(2):R262–71.
65. Butler CK, Smith FM, Cardinal R, Murphy DA, Hopkins DA, Armour JA. Cardiac responses to electrical stimulation of discrete loci in canine atrial and ventricular ganglionated plexi. Am J Physiol. 1990;259(5 Pt 2):H1365–73.
66. Butler CK, Smith FM, Nicholson J, Armour JA. Cardiac effects induced by chemically activated neurons in canine intrathoracic ganglia. Am J Physiol. 1990;259(4 Pt 2):H1108–17.
67. Yuan BX, Ardell JL, Hopkins DA, Armour JA. Differential cardiac responses induced by nicotine sensitive canine atrial and ventricular neurones. Cardiovasc Res. 1993;27(5):760–9.
68. Cardinal R, Pagé P, Vermeulen M, Ardell JL, Armour JA. Spatially divergent cardiac responses to nicotinic stimulation of ganglionated plexus neurons in the canine heart. Auton Neurosci. 2009;145(1–2): 55–62.
69. Dennis MJ, Harris AJ, Kuffler SW. Synaptic transmission and its duplication by focally applied acetylcholine in parasympathetic neurons in the heart of the frog. Proc Roy Soc London Ser B Biol Sci. 1971;177 (1049):509–39.
70. Harris AJ, Kuffler SW, Dennis MJ. Differential chemosensitivity of synaptic and extrasynaptic areas on the neuronal surface membrane in parasympathetic neurons of the frog, tested by microapplication of acetylcholine. Proc Roy Soc London Ser B Biol Sci. 1971;177(1049):541–53.
71. McMahan UJ, Purves D. Visual identification of two kinds of nerve cells and their synaptic contacts in a living autonomic ganglion of the mudpuppy (*Necturus maculosus*). J Physiol. 1976;254(2): 405–25.
72. Hartzell HC, Kuffler SW, Stickgold R, Yoshikami D. Synaptic excitation and inhibition resulting from direct action of acetylcholine on two types of chemoreceptors on individual amphibian parasympathetic neurones. J Physiol. 1977;271(3):817–46.
73. Konopka LM, McKeon TW, Parsons RL. Galanin-induced hyperpolarization and decreased membrane excitability of neurones in mudpuppy cardiac ganglia. J Physiol. 1989;410:107–22.
74. Parsons RL, Barstow KL, Scornik FS. Spontaneous miniature hyperpolarizations affect threshold for action potential generation in mudpuppy cardiac neurons. J Neurophysiol. 2002;88(3):1119–27.
75. Allen T, Hassall C, Burnstock G. Mammalian intrinsic cardiac neurons in cell culture. In: Armour JA, Ardell JL, editors. Neurocardiology. New York: Oxford University Press; 1994. p. 115–38.
76. Allen TG, Burnstock G. Intracellular studies of the electrophysiological properties of cultured intracardiac neurones of the guinea-pig. J Physiol. 1987;388: 349–66.
77. Xu ZJ, Adams DJ. Voltage-dependent sodium and calcium currents in cultured parasympathetic neurones from rat intracardiac ganglia. J Physiol. 1992;456:425–41.
78. Adams DJ, Cuevas J. Electrophysiological properties of intrinsic cardiac neurons. In: Armour JA, Ardell JL, editors. Basic and clinical neurocardiology. New York: Oxford University Press; 2004. p. 1–60.
79. Adams DJ, Harper AA. Electrophysiological properties of autonomic ganglion neurons. In: McLachlan EM, editor. Autonomic ganglia. London: Harwood Academic Publishers; 1995. p. 153–212.
80. Selyanko AA. Membrane properties and firing characteristics of rat cardiac neurones in vitro. J Auton Nerv Syst. 1992;39(3):181–9.
81. Xi XH, Thomas JXJ, Randall WC, Wurster RD. Intracellular recordings from canine intracardiac ganglion cells. J Auton Nerv Syst. 1991;32(2): 177–82.
82. Xi X, Randall WC, Wurster RD. Morphology of intracellularly labeled canine intracardiac ganglion cells. J Comp Neurol. 1991;314(2):396–402.
83. Griffith WH 3rd, Gallagher JP, Shinnick-Gallagher P. An intracellular investigation of cat vesical pelvic ganglia. J Neurophysiol. 1980;43(2):343–54.
84. Edwards FR, Hirst GD, Klemm MF, Steele PA. Different types of ganglion cell in the cardiac plexus of guinea-pigs. J Physiol. 1995;486(2): 453–71.
85. Smith FM. Extrinsic inputs to intrinsic neurons in the porcine heart in vitro. Am J Physiol. 1999;276(2): R455–67.

86. Xu ZJ, Adams DJ. Resting membrane potential and potassium currents in cultured parasympathetic neurones from rat intracardiac ganglia. J Physiol. 1992;456:405–24.
87. Cuevas J, Harper AA, Trequattrini C, Adams DJ. Passive and active membrane properties of isolated rat intracardiac neurons: regulation by H- and M-currents. J Neurophysiol. 1997;78(4): 1890–902.
88. Rimmer K, Harper AA. Developmental changes in electrophysiological properties and synaptic transmission in rat intracardiac ganglion neurons. J Neurophysiol. 2006;95(6):3543–52.
89. Dyavanapalli J, Rimmer K, Harper AA. The action of high K+ and aglycaemia on the electrical properties and synaptic transmission in rat intracardiac ganglion neurones in vitro. Exp Physiol. 2009;94(2):201–12.
90. McAllen RM, Salo LM, Paton JFR, Pickering AE. Processing of central and reflex vagal drives by rat cardiac ganglion neurones: an intracellular analysis. J Physiol. 2011;589(Pt 23):5801–18.
91. Ashton JL, Argent L, Smith JEG, Jin S, Sands GB, Smaill BH, et al. Evidence of structural and functional plasticity occurring within the intracardiac nervous system of spontaneously hypertensive rats. Am J Physiol Heart Circ Physiol. 2020;318(6): H1387–400.
92. Gibbins IL. Chemical neuroanatomy of sympathetic ganglia. In: McLachlan EM, editor. Autonomic Ganglia. Luxembourg: Harwood Academic Publishers; 1995. p. 73–122.
93. Morris JL, Gibbins IL, Holmgren S. Galanin is more common than NPY in vascular sympathetic neurons of the brush-tailed possum. Regul Pept. 1992;37(2): 101–9.
94. Steele PA, Choate JK. Innervation of the pacemaker in guinea-pig sinoatrial node. J Auton Nerv Syst. 1994;47(3):177–87.
95. Steele PA, Gibbins IL, Morris JL. Projections of intrinsic cardiac neurons to different targets in the guinea-pig heart. J Auton Nerv Syst. 1996;56(3): 191–200.
96. Hoover DB, Tompkins JD, Parsons RL. Differential activation of guinea pig intrinsic cardiac neurons by the PAC1 agonists maxadilan and pituitary adenylate cyclase-activating polypeptide 27 (PACAP27). J Pharmacol Exp Ther. 2009;331(1):197–203.
97. Hoard JL, Hoover DB, Mabe AM, Blakely RD, Feng N, Paolocci N. Cholinergic neurons of mouse intrinsic cardiac ganglia contain noradrenergic enzymes, norepinephrine transporters, and the neurotrophin receptors tropomyosin-related kinase A and p75. Neurosci. 2008;156(1):129–42.
98. Hoover DB, Isaacs ER, Jacques F, Hoard JL, Pagé P, Armour JA. Localization of multiple neurotransmitters in surgically derived specimens of human atrial ganglia. Neurosci. 2009;164(3):1170–9.
99. Rysevaite K, Saburkina I, Pauziene N, Vaitkevicius R, Noujaim SF, Jalife J, et al. Immunohistochemical characterization of the intrinsic cardiac neural plexus in whole-mount mouse heart preparations. Heart Rhythm. 2011;8(5):731–8.
100. Singh S, Johnson PI, Javed A, Gray TS, Lonchyna VA, Wurster RD. Monoamine- and histamine-synthesizing enzymes and neurotransmitters within neurons of adult human cardiac ganglia. Circulation. 1999;99(3):411–9.
101. Coote JH, Chauhan RA. The sympathetic innervation of the heart: important new insights. Auton Neurosci. 2016;199:17–23.
102. Parsons RL, Neel DS, McKeon TW, Carraway RE. Organization of a vertebrate cardiac ganglion: a correlated biochemical and histochemical study. J Neurosci. 1987;7(3):837–46.
103. de Groat WC, Booth AM. Inhibition and facilitation in parasympathetic ganglia of the urinary bladder. Fed Proc. 1980;39(12):2990–6.
104. Weihe E, Schütz B, Hartschuh W, Anlauf M, Schäfer MK, Eiden LE. Coexpression of cholinergic and noradrenergic phenotypes in human and nonhuman autonomic nervous system. J Comp Neurol. 2005;492(3): 370–9.
105. Hoover DB, Shepherd AV, Southerland EM, Armour JA, Ardell JL. Neurochemical diversity of afferent neurons that transduce sensory signals from dog ventricular myocardium. Auton Neurosci. 2008;141 (1–2):38–45.
106. Hardwick JC, Mawe GM, Parsons RL. Evidence for afferent fiber innervation of parasympathetic neurons of the guinea-pig cardiac ganglion. J Auton Nerv Syst. 1995;53(2–3):166–74.
107. Wang T, Miller KE. Characterization of glutamatergic neurons in the rat atrial intrinsic cardiac ganglia that project to the cardiac ventricular wall. Neurosci. 2016;329:134–50.
108. Pauza DH, Rysevaite K, Inokaitis H, Jokubauskas M, Pauza AG, Brack KE, et al. Innervation of sinoatrial nodal cardiomyocytes in mouse. A combined approach using immunofluorescent and electron microscopy. J Mol Cell Cardiol. 2014;75:188–97.
109. Lee S-R, Cho Y, Cha M-J, Choi E-K, Seo J-W, Oh S. Atrial innervation patterns of intrinsic cardiac autonomic nerves. J Korean Med Sci. 2018;33(39):e253.
110. Beaumont E, Salavatian S, Southerland EM, Vinet A, Jacquemet V, Armour JA, et al. Network interactions within the canine intrinsic cardiac nervous system: implications for reflex control of regional cardiac function. J Physiol. 2013;591(18):4515–33.
111. Seabrook GR, Fieber LA, Adams DJ. Neurotransmission in neonatal rat cardiac ganglion in situ. Am J Physiol. 1990;259(4 Pt 2): H997–1005.
112. Furness JB, Callaghan BP, Rivera LR, Cho H-J. The enteric nervous system and gastrointestinal innervation: integrated local and central control. Adv Exp Med Biol. 2014;817:39–71.
113. Huang MH, Smith FM, Armour JA. Modulation of in situ canine intrinsic cardiac neuronal activity by

nicotinic, muscarinic, and beta-adrenergic agonists. Am J Physiol. 1993;265(3):R659–69.

114. Masliukov PM, Moiseev K, Emanuilov AI, Anikina TA, Zverev AA, Nozdrachev AD. Development of neuropeptide Y-mediated heart innervation in rats. Neuropeptides. 2016;55:47–54.
115. Herring N, Paterson DJ. Neuromodulators of peripheral cardiac sympatho-vagal balance. Exp Physiol. 2009;94(1):46–53.
116. Bosnjak ZJ, Seagard JL, Kampine JP. Peripheral neural input to neurons of the stellate ganglion in dog. Am J Physiol. 1982;242(3):R237–43.
117. Brown AM. Cardiac reflexes. In: Berne RM, Sperelakis N, Geiger SR, editors. Handbook of physiology, section 2: The cardiovascular system Vol 1, The heart. Washington, DC: American Physiological Society; 1979. p. 677–89.
118. Ardell JL, Butler CK, Smith FM, Hopkins DA, Armour JA. Activity of in vivo atrial and ventricular neurons in chronically decentralized canine hearts. Am J Physiol. 1991;260(3):H713–21.
119. Murphy DA, Thompson GW, Ardell JL, McCraty R, Stevenson RS, Sangalang VE, et al. The heart reinnervates after transplantation. Ann Thorac Surg. 2000;69(6):1769–81.
120. Spencer NJ, Kyloh M, Beckett EA, Brookes S, Hibberd T. Different types of spinal afferent nerve endings in stomach and esophagus identified by anterograde tracing from dorsal root ganglia. J Comp Neurol. 2016;524(15):3064–83.
121. Wang H-J, Rozanski GJ, Zucker IH. Cardiac sympathetic afferent reflex control of cardiac function in normal and chronic heart failure states. J Physiol. 2017;595(8):2519–34.
122. Lázár BA, Jancsó G, Oszlács O, Nagy I, Sántha P. The insulin receptor is colocalized with the TRPV1 nociceptive ion channel and neuropeptides in pancreatic spinal and vagal primary sensory neurons. Pancreas. 2018;47(1):110–5.
123. Yoshie K, Rajendran PS, Massoud L, Kwon O, Tadimeti V, Salavatian S, et al. Cardiac vanilloid receptor-1 afferent depletion enhances stellate ganglion neuronal activity and efferent sympathetic response to cardiac stress. Am J Physiol. 2018;314(5):H954–66.
124. Shanks J, de Morais SDB, Gao L, Zucker IH, Wang H-J. TRPV1 (transient receptor potential vanilloid 1) cardiac spinal afferents contribute to hypertension in spontaneous hypertensive rat. Hypertension. 2019;74(4):910–20.
125. Liu X, Zhang Q, Han M, Du J. Intrapericardial capsaicin and bradykinin induce different cardiac-somatic and cardiovascular reflexes in rats. Auton Neurosci. 2016;198:28–32.
126. Xi X, Randall WC, Wurster RD. Intracellular recording of spontaneous activity of canine intracardiac ganglion cells. Neurosci Lett. 1991;128(1):129–32.
127. Smith FM, Vermeulen M, Cardinal R. Long-term spinal cord stimulation modifies canine intrinsic cardiac neuronal properties and ganglionic transmission during high-frequency repetitive activation. Physiol Rep. 2016;4(13):e12855.
128. Salavatian S, Beaumont E, Longpré J-P, Armour JA, Vinet A, Jacquemet V, et al. Vagal stimulation targets select populations of intrinsic cardiac neurons to control neurally induced atrial fibrillation. Am J Physiol. 2016;311(5):H1311–20.
129. Treweek JB, Gradinaru V. Extracting structural and functional features of widely distributed biological circuits with single cell resolution via tissue clearing and delivery vectors. Curr Opin Biotechnol. 2016;40:193–207.
130. Renier N, Wu Z, Simon DJ, Yang J, Ariel P, Tessier-Lavigne M. iDISCO: a simple, rapid method to immunolabel large tissue samples for volume imaging. Cell. 2014;159(4):896–910.
131. Richardson DS, Lichtman JW. Clarifying tissue clearing. Cell. 2015;162(2):246–57.
132. Treweek JB, Chan KY, Flytzanis NC, Yang B, Deverman BE, Greenbaum A, et al. Whole-body tissue stabilization and selective extractions via tissue-hydrogel hybrids for high-resolution intact circuit mapping and phenotyping. Nat Protoc. 2015;10(11):1860–96.
133. Mano T, Albanese A, Dodt H-U, Erturk A, Gradinaru V, Treweek JB, et al. Whole-brain analysis of cells and circuits by tissue clearing and light-sheet microscopy. J Neurosci. 2018;38(44):9330–7.
134. Bedbrook CN, Deverman BE, Gradinaru V. Viral strategies for targeting the central and peripheral nervous systems. Annu Rev Neurosci. 2018;41:323–48.
135. Chan KY, Jang MJ, Yoo BB, Greenbaum A, Ravi N, Wu W-L, et al. Engineered AAVs for efficient noninvasive gene delivery to the central and peripheral nervous systems. Nat Neurosci. 2017;20(8):1172–9.
136. Rajendran PS, Challis RC, Fowlkes CC, Hanna P, Tompkins JD, Jordan MC, et al. Identification of peripheral neural circuits that regulate heart rate using optogenetic and viral vector strategies. Nat Commun. 2019;10(1):1944.
137. Saito T, Tenma K. Effects of left and right vagal stimulation on excitation and conduction of the carp heart (*Cyprinus carpio*). J Comp Physiol. 1976;111:39–53.
138. Gut P, Reischauer S, Stainier DYR, Arnaout R. Little fish, big data: zebrafish as a model for cardiovascular and metabolic disease. Physiol Rev. 2017;97(3):889–938.
139. Woo K, Shih J, Fraser SE. Fate maps of the zebrafish embryo. Curr Opin Genet Dev. 1995;5(4):439–43.
140. Kimmel CB, Ballard WW, Kimmel SR, Ullmann B, Schilling TF. Stages of embryonic development of the zebrafish. Dev Dyn. 1995;203(3):253–310.
141. Briggs JP. The zebrafish: a new model organism for integrative physiology. Am J Physiol. 2002;282(1):R3–9.
142. Howe K, Clark MD, Torroja CF, Torrance J, Berthelot C, Muffato M, et al. The zebrafish reference

genome sequence and its relationship to the human genome. Nature. 2013;496(7446):498–503.

143. Genge CE, Lin E, Lee L, Sheng X, Rayani K, Gunawan M, et al. The zebrafish heart as a model of mammalian cardiac function. Rev Physiol Biochem Pharmacol. 2016;171:99–136.
144. Shrestha R, Lieberth J, Tillman S, Natalizio J, Bloomekatz J. Using zebrafish to analyze the genetic and environmental etiologies of congenital heart defects. Adv Exp Med Biol. 2020;1236:189–223.
145. Rafferty SA, Quinn TA. A beginner's guide to understanding and implementing the genetic modification of zebrafish. Prog Biophys Mol Biol. 2018;138:3–19.
146. Vornanen M, Hassinen M. Zebrafish heart as a model for human cardiac electrophysiology. Channels. 2016;10(2):101–10.
147. Nemtsas P, Wettwer E, Christ T, Weidinger G, Ravens U. Adult zebrafish heart as a model for human heart? An electrophysiological study. J Mol Cell Cardiol. 2010;48(1):161–71.
148. Brette F, Luxan G, Cros C, Dixey H, Wilson C, Shiels HA. Characterization of isolated ventricular myocytes from adult zebrafish (*Danio rerio*). Biochem Biophys Res Commun. 2008;374(1): 143–6.
149. Ravens U. Ionic basis of cardiac electrophysiology in zebrafish compared to human hearts. Prog Biophys Mol Biol. 2018;38:38–44.
150. Rayani K, Lin E, Craig C, Lamothe M, Shafaattalab S, Gunawan M, et al. Zebrafish as a model of mammalian cardiac function: optically mapping the interplay of temperature and rate on voltage and calcium dynamics. Prog Biophys Mol Biol. 2018;138:69–90.
151. Dvornikov AV, de Tombe PP, Xu X. Phenotyping cardiomyopathy in adult zebrafish. Prog Biophys Mol Biol. 2018;138:116–25.
152. Haverinen J, Hassinen M, Korajoki H, Vornanen M. Cardiac voltage-gated sodium channel expression and electrophysiological characterization of the sodium current in the zebrafish (*Danio rerio*) ventricle. Prog Biophys Mol Biol. 2018;138:59–68.
153. Hull CM, Genge CE, Hobbs Y, Rayani K, Lin E, Gunawan M, et al. Investigating the utility of adult zebrafish ex vivo whole hearts to pharmacologically screen hERG channel activator compounds. Am J Physiol. 2019;317(6):R921–31.
154. Verkerk AO, Remme CA. Zebrafish: a novel research tool for cardiac (patho)electrophysiology and ion channel disorders. Front Physiol. 2012;3:255.
155. Lin E, Shafaattalab S, Gill J, Al-Zeer B, Craig C, Lamothe M, et al. Physiological phenotyping of the adult zebrafish heart. Mar Genomics. 2020;49: 100701.
156. Stoyek MR, Croll RP, Smith FM. Intrinsic and extrinsic innervation of the heart in zebrafish (*Danio rerio*). J Comp Neurol. 2015;523(11):1683–700.
157. Christoffels VM, Smits GJ, Kispert A, Moorman AFM. Development of the pacemaker tissues of the heart. Circ Res. 2010;106(2):240–54.
158. Stoyek MR, Quinn TA, Croll RP, Smith FM. Zebrafish heart as a model to study the integrative autonomic control of pacemaker function. Am J Physiol. 2016;311(3):H676–88.

9

The Neuro-cardiac Axis in Arrhythmogenesis: Role and Impact of Autonomic Modulation

Shui Hao Chin and G. André Ng

Abstract

The autonomic nervous system consisting of two limbs, the sympathetic and parasympathetic nervous system, plays a key role in the modulation of various cardiac arrhythmias. Neurotransmitters, including catecholamines and acetylcholine, as well as other co-transmitters mediate supraventricular and ventricular arrhythmogenesis through distinctive electrophysiologic mechanisms. The intricate autonomic interplay depicts that most arrhythmias arise from sympathetic overactivity and parasympathetic attenuation, with the sympathetic nervous system mitigating the effects of antiarrhythmic drugs. While this remains true for adrenergic-driven arrhythmias such as atrial fibrillation, post-infarct ventricular tachycardia, and some long QT syndromes 1 and 2, parasympathetic nervous overactivity may act as a trigger for vagotonic arrhythmias including Brugada syndrome, long QT syndrome 3, and idiopathic ventricular fibrillation. Knowledge of the neuro-cardiac hierarchies and awareness of different methods for assessment of autonomic tone, combined with promising results from animal studies, has established a clear rationale for clinical trials of various autonomic neuromodulatory interventions, which have had varying success for defined arrhythmias. Whereas cardiac sympathetic denervation imparts clear therapeutic benefits in patients with long QT syndrome 1 and polymorphic catecholaminergic ventricular tachycardia, the impact of vagus nerve stimulation in heart failure patients is less defined. Sustainable and relatable therapeutic outcomes from future clinical trials of neuromodulatory interventions dictate conscientious patient selection, optimized study protocols, and the use of reproducible biomarkers. Novel tools such as optogenetics present an exciting direction in the future for noninvasive neuromodulatory interventions.

Keywords

Autonomic neuromodulatory interventions · Arrhythmogenesis · Autonomic neurotransmitters · Neuro-cardiac axis

---

S. H. Chin
Neurocardiology Group, Department of Cardiovascular Sciences, University of Leicester, Glenfield Hospital, Leicester, UK

University Hospitals of Leicester NHS Trust, Leicester, UK

G. A. Ng (✉)
Neurocardiology Group, Department of Cardiovascular Sciences, University of Leicester, Glenfield Hospital, Leicester, UK

University Hospitals of Leicester NHS Trust, Leicester, UK

NIHR Leicester Biomedical Research Centre, Leicester, UK
e-mail: andre.ng@leicester.ac.uk

© Springer Nature Switzerland AG 2023
O. N. Tripathi et al. (eds.), *Heart Rate and Rhythm*, https://doi.org/10.1007/978-3-031-33588-4_9

9.1 Introduction

The autonomic nervous system (ANS) is composed of two limbs, the sympathetic (SNS) and parasympathetic nervous system (PNS), each exerting opposing effects in modulating arrhythmogenesis [1]. The ANS contributes to various supraventricular and ventricular arrhythmias through distinctive pro- and antiarrhythmic mechanisms. Intricate interaction occurs between the SNS and PNS at each anatomical hierarchy, from the central nervous system (brain and spinal cord) and intrathoracic extracardiac ganglia (stellate ganglia, dorsal root ganglia) to intrinsic cardiac nerves and ganglia, thereby enabling the many possibilities for autonomic interventions to modulate arrhythmogenesis in both atria and ventricles. The effect of arrhythmic triggers by the SNS and PNS are unique to each type of arrhythmia. At the atrial level, atrial fibrillation (AF) can be triggered by both the SNS and PNS [2]. At the ventricular level, SNS overactivation is the hallmark of most arrhythmias that occur with myocardial ischemia and myocardial infarction (MI), long QT syndrome (LQTS), and catecholaminergic polymorphic ventricular tachycardia (CPVT), including benign ventricular premature beats, whereas the PNS confers protective effects against such arrhythmias [3]. On the other hand, the PNS contributes to ventricular arrhythmias in certain cardiac channelopathies (Table 9.1).

In this chapter, the pathophysiological properties of SNS and PNS neurotransmitters will be discussed, linking their effects with various supraventricular and ventricular arrhythmias through distinctive mechanisms. The chapter proceeds to describe each of these arrhythmias, followed by discussion of up-to-date evidence-driven autonomic interventions applicable to the relevant arrhythmias. This is followed by outlining the current tools available for assessment of autonomic tone. And finally challenges of current autonomic interventions and potential future directions will be considered.

9.2 Autonomic Neurotransmitters and Their Electrophysiological Properties

9.2.1 Role of Autonomic Neurotransmitters in Arrhythmogenesis

The ANS exerts its effect on inducing and maintaining arrhythmias through the now well-known neurotransmitters, catecholamines (SNS) and acetylcholine (PNS). Briefly, SNS and PNS exert opposing effects on heart rate (chronotropy) and conduction through the atrioventricular node (dromotropy). While SNS stimulation leads to positive chronotropy and dromotropy, PNS stimulation results in negative chronotropy and dromotropy (i.e., slowing of sinus rate and atrioventricular (AV) node conduction). Sympatho-vagal interaction studies, however, revealed a phenomenon known as *accentuated antagonism* characterized by vagal dominance in both chronotropy and dromotropy [4]. In contrast, this phenomenon was absent at the ventricular level in terms of ventricular repolarization and ventricular fibrillation (VF) threshold during direct sympatho-vagal stimulation [5].

Recently SNS co-transmitters, notably neuropeptide Y (NPY) and galanin, were identified in association with certain arrhythmic states and play an important role in attenuating the chronotropic effect of the PNS. Both NPY and galanin reduce acetylcholine release, thereby attenuating vagal bradycardia through their corresponding receptors (NPY2, GalR1) located on the postganglionic vagal neurons projecting to the sinus node [6, 7]. At the ventricular level, NPY1 receptors found on cardiomyocytes exert pro-arrhythmic effects through the putative mechanism of increasing calcium transient amplitude and diastolic calcium sparks [7]. Indeed, in a study comprising 78 patients who underwent percutaneous coronary interventions, 8% experienced ventricular arrhythmias within 48 h, all of whom had noticeably elevated levels of NPY [8]. In an experimental ischemic and reperfusion model, NPY reduced VF threshold, leading to an

Table 9.1 Autonomic nervous system-modulated supraventricular and ventricular arrhythmias

	ANS	
	SNS	PNS
Supraventricular arrhythmias	AF SVT (AT, AVNRT, AVRT) IST POTS	AF Sinus bradycardia Cardioinhibitory NCS
Ventricular arrhythmias	Normal heart VT – OTVA Structural heart disease – Ischemic VT – Post-infarct VT – ARVC Channelopathies – CPVT – LQTS (LQT1, LQT2)	LQT3 Brugada syndrome

AF, atrial fibrillation; ANS, autonomic nervous system; ARVC, arrhythmogenic right ventricular cardiomyopathy; AT, automatic tachycardia; AVNRT, atrioventricular nodal reentry tachycardia; AVRT, atrioventricular reentry tachycardia; CPVT, catecholaminergic polymorphic ventricular tachycardia; IST, inappropriate sinus tachycardia, LQTS, long QT syndrome; NCS, neurocardiogenic syncope; OTVA, outflow tract ventricular arrhythmias; PNS, parasympathetic nervous system; POTS, postural orthostatic tachycardia syndrome; SNS, sympathetic nervous system; SVT, supraventricular tachycardia; VT, ventricular tachycardia

increased incidence of ventricular tachycardia (VT, 60%) and VF (10%), the effect of which was nullified by an NPY1-receptor antagonist. Elsewhere, NPY receptors were also found in coronary vessels, mediating a vasoconstrictor effect via NPY5 receptors.

9.2.2 SNS-Mediated Arrhythmic Triggers

SNS and its circulating catecholamines (i.e., epinephrine and norepinephrine) account for the induction and triggering of many arrhythmias (Table 9.1) via different electrophysiological mechanisms (Table 9.2). SNS overactivity is accountable for most ventricular arrhythmias, notably LQTS, CPVT, and those associated with myocardial ischemia, mediated through beta-adrenoreceptors and cyclic-AMP/protein-kinase-dependent signaling pathways. On one hand, circulating catecholamines increase the rate of spontaneous depolarization, resulting in autonomic tachyarrhythmias. On the other hand, the heterogenous spatial distribution of sympathetic nerve endings may result in non-uniform repolarization, promoting reentrant tachycardias. Under certain conditions such as ischemia, hypoxia, or electrolyte imbalance, cardiomyocytes become more susceptible to the pro-fibrillatory effect of catecholamines [9]. It has been postulated that occurrence of VF in early ischemia is driven by the local metabolic effect of norepinephrine as opposed to a centrally induced effect [9]. In this respect, pharmacological agents with a beta-blockade effect are effective in antagonizing some of these arrhythmias precipitated by SNS overactivity. In certain refractory cases, cervical sympathetic denervation (CSD) presents an effective therapeutic option [10]. Table 9.3 outlines other physiological states, medical conditions, and drugs associated with SNS overactivity.

9.2.2.1 Physical Stress/Exercise

The health-enhancing effect of regular moderate exercise is well established in both normal individuals and those with cardiovascular diseases. A strategy of gradual increments in exercise intensity may enhance the predominance of the PNS, conferring cardioprotection. Conversely, SNS overactivity occurs during intense and strenuous exercise, conferring potentially adverse or even detrimental effects in provocation and exacerbation of potentially malignant arrhythmias in individuals with evident or occult

Table 9.2 Cardiac electrophysiologic properties of the autonomic nervous system contributing to various arrhythmogenic mechanisms

Arrhythmogenic mechanisms/EP parameters		ANS		EP properties of neurotransmitters
		SNS	PNS	
Reentry	APD/ERP	↓	↑[a]	SNS: NE release, BAR activation PNS: ACh release, antagonizes NE, MR activation
	Repolarization dispersion	↑	↓	SNS: ↑ spatial and temporal heterogeneity PSNS: ↓ spatial and temporal heterogeneity
	VFT	↓	↑[b]	SNS: NE ± NPY release PNS: ACh release
Triggered activity	EADs	↑	↓	SNS: Ca^{++} overload PNS: ↓ Ca^{++} influx
	DADs			
Automaticity	Physiological	↑	↓	SNS: NE release, BAR activation, ↑ L-type Ca^{++} and I_f currents with ↑ SAN phase 4 slope PNS: ACh release, MR activation/ ↑ K^+ current with ↓ SAN phase 4
	Pathological	↑	↓	SNS: NE release, BAR activation; NPY release PNS: ACh release, MR activation

ACh, acetylcholine; ANS, autonomic nervous system; APD, action potential duration; BAR, beta adrenoreceptor; DADs, delayed afterdepolarizations; EADs, early afterdepolarizations; EP, electrophysiology; ERP, effective refractory period; MR, muscarinic receptor; NE, norepinephrine; NPY, neuropeptide Y; PNS, parasympathetic nervous system; SAN, sinoatrial node; SNS, sympathetic nervous system; VFT, ventricular fibrillation threshold

[a] Shorten atrial ERP and contribute to triggering AF

[b] Reduce VFT in Brugada syndrome and idiopathic VF

underlying cardiovascular abnormalities. Given the pro-arrhythmic effects of the acute surge of SNS activity and its circulating catecholamines, acute bouts of vigorous exercise should be avoided in these individuals. When high-intensity exercise is entertained in these cases, appropriate screening is recommended beforehand to avoid unnecessary risks of adverse cardiovascular and arrhythmic events [11].

9.2.2.2 Emotional Stress

SNS overactivity is an autonomic profile typified in acute and chronic psychological or mental stress among individuals with cardiovascular diseases, including various cardiac arrhythmias. It is associated with increased frequency and malignancy of ventricular arrhythmias. Anger, anxiety, sadness, and stress have been found to be precipitants for ventricular arrhythmias and AF in patients with implantable cardioverter-defibrillators (ICDs). In contrast, happiness

Table 9.3 Physiological and non-physiological triggers of autonomic nervous system overactivation

Sympathetic nervous system	Parasympathetic nervous system
Physical stress Emotional/mental stress Sleep disorders Acute coronary syndrome Heart failure Metabolic syndrome Phaeochromocytoma/paraganglioma Hypoglycemia Surgery Other medical illness Drugs (sympathomimetics, amphetamines, cocaine)	Sleep Regular athletic activity Bezold–Jarisch reflex • Orthostasis • Hypovolemia • Infero-posterior myocardial ischemia/reperfusion • Neurocardiogenic syncope (cardioinhibitory response) Reflex syncope • Increased intrathoracic pressure (cough, sneeze, weight-lifting) • Gastrointestinal stimulation (swallowing, defecation, endoscopy) • Genito-urinary stimulation (micturition) • Glossopharyngeal neuralgia Drugs (pilocarpine, neostigmine, pyridostigmine, arecoline)

appears to be protective against such arrhythmias [12]. It remains inconclusive whether psychological interventions, such as in the form of cognitive-behavioral therapy, may alleviate stress-induced arrhythmias in this context [13, 14].

9.2.2.3 Sleep Disorders

An optimal sleep duration of ~7 h/night may contribute to a balanced ANS profile. Disturbed sleep in the form of reduced sleep duration, low sleep efficiency, sleep-disordered breathing, and insomnia are associated with attenuated PNS tone and/or elevated SNS tone, thereby increasing susceptibility to arrhythmias [15–17]. Sleep disruptions have been associated with both AF and ventricular arrhythmias [17]. While acute sleep deprivation modifies ANS activity by increased SNS, chronic sleep deprivation produces a constant hyperadrenergic state associated with pro-arrhythmic consequences. In individuals with sleep-disordered breathing, sympathetic overactivity may be one of the pathological drivers for increased incidence of arrhythmias [15, 16].

9.2.3 PNS-Mediated Arrhythmic Triggers

Parasympathetic nerve fibers form synapses with ganglionic plexuses (GPs) on the epicardial surface of the heart, facilitating adaptive changes in neuronal activity, i.e., neuroplasticity to fine-tune the neuro-cardiac status [18]. However, maladaptive changes of PNS overactivity or attenuation are a source of arrhythmogenesis [19]. One classical example is vagally induced AF due to spatially heterogeneous shortening of atrial refractoriness (Table 9.2), forming the rationale for certain ablation strategies that constitute a degree of autonomic intervention [10]. Furthermore, Brugada syndrome and LQT3 have been attributed to vagotonia (Table 9.1). Yet, vagus nerve stimulation (VNS) was shown to reduce VT/VF inducibility in the setting of myocardial ischemia and infarct.

The contribution to arrhythmias by ANS goes beyond the balance between SNS and PNS activity. On its own, VNS exerts differential effects on the heart based on its tonic (resting) and phasic activation pattern [18, 20]. For example, resting sinus bradycardia is common and thought to be normal among the athletes due to high vagal tone. Whereas in individuals suffering from neurocardiogenic syncope (NCS), the vagus nerve activation pattern is phasic, provoking cardioinhibitory and/or vasodepressor response under certain conditions [21]. AF in athletes, however, may not be solely due to vagus nerve overactivity as other factors such as atrial stretch, inflammation, and fibrosis have been implicated [11]. Finally, the different hierarchy of SNS and PNS at the neuro-cardiac axis provides a recipe for spatial heterogeneity in the interaction between the two arms of ANS with the temporal variation in this interaction providing additional mechanistic intricacies in precipitating different arrhythmias [22, 23].

9.2.3.1 Neurocardiogenic Syncope (NCS)

NCS is the most common form of syncope manifesting as profound slowing of heart rate (cardioinhibitory component, Type II) and/or hypotension from vasodilation (vasodepressor component, Type III) [24]. In spite of potential manifestations as isolated asystole/bradycardia vs. hypotension, most NCS is in fact a mixed response (i.e., Type I). Type II NCS is precipitated by cardio-inhibition by increased vagal input to the sinus and/or AV node, contributing to profound bradycardia (<40 bpm for >10 s) or even asystole (Type IIb). Type III NCS characterized by a vasodepressor response is attributed to a decrease in sympathetically mediated peripheral vasoconstriction. NCS have several well-identified triggers including emotional stress and upright posture, as well as specific activity triggers such as cough, micturition, deglutition, and pain (i.e., situational syncope). Post-exercise rebound vagotonia has been described in healthy individuals whereby exercise-induced sympathetic activation is swiftly followed by a neuro-cardiac interaction of sympathetic withdrawal coupled with excessive parasympathetic overdrive at the end of the exercise [25].

Cardio-neuroablation aiming to eliminate postganglionic parasympathetic neurons in atrial wall and GPs has been advocated as an alternative to pacemaker intervention for patients with medically refractory NCS with dominant cardioinhibitory component [26].

9.2.3.2 Bradyarrhythmias with Long-Short Sequence

A resting sinus bradycardia is generally a reflection of a favorable autonomic profile with a dominant parasympathetic state, as observed in athletes. However, excessive parasympathetic activity has been implicated in debilitating arrhythmias, including extreme sinus bradycardia, sinus exit blocks, sinus and AV blocks, and cardioinhibitory NCS, all of which can lead to pre-syncopal and syncopal episodes with a risk of head injury [24].

Vagotonia-induced bradycardia has, in addition, been associated with certain extrasystole-induced arrhythmias through the mechanism of long-short sequence. These have been found in patients with paroxysmal AF, LQTS, and VT/VF [27]. The underlying arrhythmogenic mechanism of long-short sequence is functional conduction block and/or slowed conduction, resulting in functional reentry when there is differential transmural repolarization, typically with a greater degree of refractoriness at midmyocardial and endocardial sites compared to epicardial sites [27]. This phenomenon has been observed in patients with cardiac implantable electronic devices (CIEDs) when an overzealous lowering of the pacing rate leads to bradycardia, which facilitates pause-dependent VT/VF in addition to polymorphic VT in the context of *Torsades-de-pointes* (TdP) [28]. This insight forms the basis of a higher programmed pacing rate in the first few weeks following AV node ablation for rate control in drug-refractory fast AF. In patients presenting with complete heart block, the possibility of polymorphic VT sometimes necessitates insertion of a temporary pacemaker for overdrive pacing until a definitive permanent pacemaker is inserted [29]. Similarly, overdrive ventricular pacing also effectively prevents arrhythmia recurrences in patients with LQTS by abolishing VT/VF induced by long-short sequence. On the other hand, continuous atrial pacing at 75–80 bpm anecdotally prevents recurrence of AF in patients with CIEDs [30].

As such, parasympathetic-modulated bradycardias are not all benign, especially in view of potential bradycardia/pause-dependent VT/VFs. Although pacing interventions may circumvent these bradyarrhythmias, ANS modulatory interventions may avoid the use of pacemakers [26, 31]. It should be emphasized that bradycardia/pause-dependent arrhythmias are not exclusive to ANS dysfunction but can occur independently [28, 29].

9.3 Tachyarrhythmogenic States Associated with Autonomic Imbalance

The two limbs of ANS modulates various supraventricular and ventricular arrhythmias (Table 9.1) either through the dominant effect of one of the limbs or the convergent effect of autonomic interaction via different electrophysiologic effects (Table 9.2).

9.3.1 Supraventricular Arrhythmias

Supraventricular tachycardia (SVT) associated with SNS overactivity can be induced by abnormal automaticity or triggered activity, typically under physical and/or emotional stress (atrial tachycardia, AF), upright postures (postural orthostatic tachycardia syndrome), or in some cases without any obvious precipitant (inappropriate sinus tachycardia) [32]. Other SVTs (atrioventricular nodal reentrant tachycardia, atrioventricular reentrant tachycardia, atrial tachycardia), especially those involving the ANS-innervated AV node, rely on a reentrant mechanism when catecholamines expose differential conduction velocities in the critical part of the reentrant circuit [33].

9.3.1.1 Inappropriate Sinus Tachycardia (IAST) and Postural Orthostatic Tachycardia Syndrome (POTS)

IAST is a clinical condition characterized by nonparoxysmal palpitation manifesting as a sinus rate of >100 bpm at rest, and/or a mean 24-h heart rate of >95 bpm without any obvious cause, out of proportion to physiological need [21]. This condition is generally regarded as a reflection of a hypersympathetic state, leading to the concept of beta-blockade as the mainstay of treatment to achieve sympatholysis. In some cases, ivabradine, a selective HCN channel (I_f current) blocker—largely considered to be without any other cardiovascular effect apart from chronotropy—is an effective adjunct or alternative [34]. Other more invasive therapeutic interventions involving sinus-node modification through catheter ablation of atrial GPs or sympathetic denervation are not recommended for treatment of IAST [21].

POTS is a clinical syndrome manifesting with a myriad of symptoms including lightheadedness, palpitations, tremor, fatigue, general weakness, exercise intolerance, and visual blurring when sinus rate increases by ≥30 bpm upon standing (≥40 bpm in individuals aged 12–19 years) [21]. The underpinning mechanisms of POTS are complex and have been postulated to include peripheral autonomic denervation, hyperadrenergic stimulation, deconditioning, hypovolemia, and/or hypervigilance. Management of POTS overlaps with that of IAST encompassing lifestyle modifications (increased fluid and salt intake, avoidance of certain drugs and dehydration, compression stockings, structured exercise) and pharmacological approaches (fludrocortisone, midodrine, propranolol, ivabradine, central sympatholytic agents) [21].

9.3.1.2 Atrial Tachycardia

ANS imbalance with hyperadrenergic state contributes to neural triggers of atrial tachycardia. This is supported by the observation that paroxysmal atrial tachycardia can be abolished with ablation of extrinsic sympatho-vagal nerves akin to the effect of abolishing paroxysmal AF with the same method [23]. Focal atrial tachycardias are catecholamine-sensitive, occurring as a result of increased automaticity and/or triggered activity as opposed to reentrant mechanism in certain atrial tachycardia/flutter [32]. As such, focal atrial tachycardias tend to manifest in catecholamine-driven states, e.g., during exercise and/or stressful conditions. A further corroboration arises from the induction of these atrial tachycardias by infusion of isoproterenol during an electrophysiology study [32].

9.3.1.3 Atrial Fibrillation

The pulmonary veins (PV) are anatomically linked to the left atrium (LA) through myocardial sleeves, the latter being extensions of atrial myocardium over the PVs. These myocardial sleeves are typically more prominent around the superior than the inferior PVs, containing not only cardiac myocytes but also rich innervation of autonomic nerves [35]. Indeed, co-located sympathetic and vagal nerves are at their highest densities within 5 mm of the PV-LA junction [36]. While there is emerging evidence suggesting that histological remodeling at the PV-LA junction contributes to the development of AF, the exact role of neural remodeling in AF initiation remains uncertain [20].

The atria are richly innervated by both intrinsic cardiac nerves and extracardiac autonomic nerves/ganglia, with remodeling potential under various conditions [36, 37]. In particular, the PVs and posterior LA wall demonstrate unique depolarization and repolarization patterns associated with heterogenous vagal activity during autonomic manipulation, contributing to both the triggers and substrate for AF [37]. In a canine model of sustained AF induced by prolonged right atrial pacing, significant nerve sprouting and sympathetic hyperinnervation were observed [38]. As such, selective stimulation or inhibition of these extracardiac autonomic neural structures may form attractive therapeutic targets for autonomic interventions of AF.

While abnormal neuro-cardiac innervation at the PV-LA junction and other parts of LA provide the trigger and substrate for AF, the role of autonomic imbalance in the modulation of AF is far more complex as AF itself may result in autonomic disturbance, thus explaining the maxim “AF begets AF” [22]. Vagotonia is regarded as a classical trigger for AF as seen in young, healthy individuals with lone AF, yet stressful situations like acute mental stress have been shown to induce a transiently adverse LA electrophysiological state and hence provide the perfect substrate for AF [39]. Furthermore, it is thought that the initiation of AF does not rely exclusively on vagal or adrenergic activation, but rather the complex interaction between SNS and PNS to achieve a certain level of autonomic imbalance [1]. It has been postulated that while PNS overactivity is the culprit of spontaneous AF initiation, circulating catecholamines provide the appropriate adrenergic tone to modulate the initiation and maintenance of vagally triggered AF [2].

Neuromodulation via low-level VNS (LLVNS) at voltages below the bradycardia threshold achieved both antiadrenergic and anticholinergic effects [40, 41]. In experimental models of AF [41] and postoperative AF patients [42], LLVNS has been shown to reduce AF inducibility and duration. Chronic LLVNS has been shown to be associated with reduced stellate ganglia activity, leading to improved rate control in persistent AF [40].

Endurance athletes undergoing extreme exercise may have maladaptation of their autonomic tone in addition to development of an arrhythmogenic atrial substrate (i.e., atrial fibrosis), driving the high prevalence of AF in this group of individuals [11]. Indeed, an arrhythmogenic right ventricular cardiomyopathy (ARVC)-like phenotype has been described in these individuals although the role of chronic SNS overactivity in this phenotype remains unestablished [11].

9.3.1.4 Atrioventricular Nodal Reentrant Tachycardia (AVNRT)

The AV node forms a critical part of the reentrant circuit in patients with AVNRT, and is a structure richly innervated by autonomic nerves exerting positive (SNS) or negative (PNS) dromotropic effect. The inducibility of AVNRT by catecholamines is attested by triggering of tachycardia in some patients during exercise and/or emotional stress, in addition to the occasional requirement for isoproterenol infusion during electrophysiology studies and ablation procedures to initiate AVNRT [43]. Furthermore, the reversal effect of antiarrhythmic drugs by adrenergic agents (e.g., isoproterenol) in patients with SVT suggests a key role for adjunctive use of beta-blockers [44].

Interestingly, transient inappropriate sinus tachycardia (IAST) has been noted following ablation of the AV node fast- or slow-pathway due to thermal injury to the parasympathetic fibers at the right septal region. This phenomenon has been postulated to be a consequence of radiofrequency ablation at the anterior, mid, and posterior aspects of the interatrial septum disrupting preganglionic or postganglionic parasympathetic fibers innervating the sinus node, thus producing parasympathetic denervation that accounts for the IAST [45].

9.3.1.5 Atrioventricular Reentrant Tachycardia (AVRT)

In patients with pre-excitation syndromes, including those who are asymptomatic, malignant arrhythmias can occur during states of increased sympathetic activity. Exercise and/or administration of exogeneous catecholamines may unmask high-risk features in patients with Wolff–Parkinson–White (WPW) syndrome (i.e., patients with manifest/antegrade accessory pathway conduction) [46, 47]. Thus, appropriate risk assessment should be performed in these patients including those with purportedly low-risk features at baseline (i.e., intermittent pre-excitation) with isoproterenol/epinephrine administration or an electrophysiology study. Indeed, the use of exercise traditionally as a noninvasive risk assessment tool has been called into question in one study [48]. In extreme cases, increased sympathetic activity such as exercise/emotional stress can accelerate antegrade conduction over the accessory pathway facilitating degeneration of pre-excited atrial tachyarrhythmias (atrial flutter/AF) into VF causing sudden cardiac death (SCD) [49].

Administration of exogeneous catecholamines has also been shown to partially or completely reverse the therapeutic effect of certain antiarrhythmic drugs in patients with pre-excitation syndromes already established on antiarrhythmic drugs, further cementing the requirement for adjunctive use of a beta-blocker in such patients [44, 50].

9.3.2 Ventricular Arrhythmias

ANS dysfunction plays a key role in modulating the initiation and maintenance of ventricular arrhythmias. Sympathetic overdrive and parasympathetic attenuation are the hallmark of increased risk of sudden arrhythmic death in the setting of channelopathies, ARVC, and structural heart diseases (SHD) such as MI and heart failure [1]. SNS overactivity provides the trigger (increased automaticity and triggered activity) and the substrate (reduced action potential duration and refractoriness, reduced VF threshold) necessary for initiation and maintenance of VT/VF. In conjunction, PNS attenuation exacerbates pro-fibrillatory effect through reduced refractoriness, augmentation of dispersion of repolarization, and reduced VF threshold. However, in certain arrhythmic syndromes such as the Brugada syndrome and LQT3, increased PNS is conversely pro-arrhythmic [51].

9.3.2.1 Channelopathies

The underlying arrhythmogenesis of congenital LQT1 and LQT2 is prolongation of the QT interval by sympathetic activation. In these patients, heightened sympathetic activity under certain circumstances leads to increased malignant ventricular arrhythmias with arrhythmogenic events among LQT1 occurring during exercise or stress, while those among LQT2 occur during emotional stress, such as provoked by auditory stimuli (alarm clock, telephone ring, abrupt noises), especially at rest. In comparison, the arrhythmic events among LQT3 patients occur during states of high parasympathetic tone, i.e., at rest or during sleep. CPVT is another channelopathy relying on sympathetic triggers, characterized by the onset of bidirectional VT during exercise [1]. As such, patients with LQT1 and CPVT should be steered away from physical or emotional exertion to avoid potential ventricular arrhythmias.

Similar to LQT3, ventricular arrhythmias in Brugada syndrome tend to manifest during states of high parasympathetic tone, typically during rest or sleep. The vagotonic trigger in combination with an underlying electrophysiologic substrate (e.g., at the epicardial surface of the right ventricular outflow tract [RVOT]) mediates and perpetuates the ventricular arrhythmias [1, 51]. An abrupt surge in PNS activity characteristically occurs before episodes of VF in Brugada syndrome, further supported by the observation of adverse ECG changes enhanced by parasympathomimetic agents and mitigated by sympathomimetic agents [1].

In spite of autonomic imbalance being strongly characterized in these channelopathies, the underlying molecular pathology remains the culprit for the manifestation of malignant ventricular arrhythmias. As such, autonomic interventions remain limited in these conditions with the most success observed in LQT1.

9.3.2.2 Arrhythmogenic Right Ventricular Cardiomyopathy (ARVC)

ARVC is an inherited arrhythmogenic syndrome characterized by abnormal fibrofatty infiltration of the right and/or left ventricular myocardium, progressing from epicardial to endocardial (i.e., out-to-in) aspects. A high incidence of ventricular arrhythmias with potential SCD events tend to occur at times of heighted sympathetic state, e.g., during sports and athletic activities [52]. Both exercise and isoproterenol infusion can lead to an arrhythmogenic response in patients with ARVC [53]. In summary, the role of SNS in ARVC-related arrhythmogenesis is supported by the occurrence of exercise-induced or catecholamine-sensitive VT, as well as the therapeutic effect of beta-blockade. However, the presence of fibrofatty replacement of ventricular myocardium providing the arrhythmogenic substrate should not be neglected. Like most channelopathies, the impact of autonomic modulation is reflected by a lack of concrete autonomic intervention to treat ventricular arrhythmias in ARVC, although patients with ARVC are advised against competitive sports [54].

9.3.2.3 Idiopathic Premature Ventricular Complexes (PVCs), VT, and VF

The relationship between ANS activity and premature ventricular complexes (PVCs) is complex. Although PVCs commonly occur with increased SNS activity, these can occur in the setting of increased PNS activity as previously described [3, 11]. Most of the idiopathic focal VTs (otherwise known as the normal heart VTs) arise from outflow tracts (70% RVOT), but can also arise from other locations (e.g., papillary muscles, left ventricular fascicles, mitral annulus, aortic cusps, and RV moderator band) [55]. The involvement of SNS in arrhythmogenesis is implicated by the inducibility of such tachyarrhythmias during physical and/or mental stress, as well as by catecholamine infusion. Furthermore, the origin of RVOT PVCs and VT has been found to have dense sympathetic innervation, suggesting the impact of sympathetic hyperactivity in the trigger and perpetuation of RVOT PVCs and VT [56]. Prognosis of patients with these idiopathic VTs is generally benign, but life-threating arrhythmic events have been reported [57].

Idiopathic VF is a rare arrhythmic conundrum, comprising 1.2% of out-of-hospital cardiac arrests with a shockable rhythm. However, given its predilection for young individuals and its malignant presentation, it has garnered considerable focus [58]. In particular, idiopathic VF among pediatric patients was noted to occur in situations associated with high adrenergic tone [59]. An implantable cardioverter-defibrillator (ICD) implantation is mandated in all survivors of idiopathic VF. Successful ablation of PVC triggers has been reported in selected cases of idiopathic VF [60]. Interestingly some of these patients were found to have elevated vagal tone, in association with an adverse ECG phenotype of J point elevation, with some similarities seen in Brugada syndrome [61].

9.3.2.4 VT/VF in Structural Heart Disease (SHD)

The left stellate ganglion, an integral component of the cardiac SNS, modulates ventricular electrophysiology in patients with SHD, thereby contributing to initiation and perpetuation of VT/VF. During myocardial ischemia, the myocardium becomes sensitive to the catecholamines from increased sympathetic activity, increasing its susceptibility to VF [9]. Indeed, left stellate ganglionectomy (more commonly known as left cardiac sympathetic denervation, LCSD) has been shown to prevent post-ischemic VF in experimental models [62]. Correction of autonomic imbalance during myocardial ischemia by pharmacologic stimulation of PNS with a muscarinic agonist has also been shown to protect against malignant ventricular arrhythmias [63].

A more elaborate and complex neural phenomenon occurs during MI. Sympathetic denervation occurring at the infarct zone undergoes neural remodeling characterized by nerve sprouting, heterogeneous sympathetic hyperinnervation with subsequent supersensitivity, and increased propensity for ventricular arrhythmogenesis [64]. Upstream autonomic intervention by LCSD, either with surgical or percutaneous approach, has been effective in treating patients with post-infarct ventricular tachyarrhythmias and electrical storm [65].

9.4 Autonomic Neuromodulatory Interventions (ANIs)

Interventions for autonomic neuromodulation have been introduced in neurological practices for over two decades, treating conditions such as epilepsy and depression [66]. As the knowledge of different ANS hierarchy at the neuro-cardiac axis expands [67], there has been a growing interest to develop autonomic neuromodulatory interventions (ANIs) aiming at different targets of the ANS hierarchy to treat a variety of cardiovascular diseases, in particular heart failure and arrhythmias [68]. ANIs may include lifestyle practices, pharmacological agents, and percutaneous and surgical interventions. Lifestyle practices such as habitual moderate aerobic exercise have been shown to improve ANS balance while mind-and-body practices including yoga and meditation may also exert a restorative effect on ANS imbalance [11, 20]. In this section, the antiarrhythmic impact of ANIs in clinical neurocardiology, from drug therapy to invasive approaches, will be discussed, focusing on the different modalities available for supraventricular and ventricular arrhythmias, respectively. Prospective clinical trials of ANIs are summarized in Tables 9.4 and 9.5 for corresponding supraventricular and ventricular arrhythmias.

9.4.1 Fundamental Principles of Autonomic Neuromodulatory Interventions

ANIs, similar to other neuro-stimulatory interventions, exhibit memory, allowing short interventional duration to provide long-lasting therapeutic effects [90, 91]. The physiological phenomenon of long-term potentiation or long-term depression, i.e., stimulatory or inhibitory effects of neuro-stimulation extending beyond the interventional period, is preserved in ANIs [92]. Indeed, cardiac GP has been shown to exhibit synaptic plasticity, a property that allows the neurons to strengthen synaptic communication to achieve long-term potentiation or long-term depression [93].

Different approaches of ANIs acting at either limb of the ANS at various hierarchies have been developed over the years, although the underlying therapeutic mechanisms remain to be fully elucidated. Several mechanisms have been proposed, including restoration of ANS neurotransmitter balance, potentiation of nitric oxide pathways, and inhibition of downstream processes including inflammation, fibrosis, and apoptosis [94–99].

9.4.2 Autonomic Modulation for Supraventricular Arrhythmias

9.4.2.1 Beta-Blocker

Beta-blocker therapy is an established pharmacological agent for all catecholamine-driven and/or exercise-induced arrhythmias. They act as a competitive antagonist for adrenoreceptors, specifically β1-receptors, which constitute 80% of the adrenoreceptors in the heart [100]. By inhibiting the effect of epinephrine and norepinephrine, they effectively counteract the arrhythmogenic effect of SNS activity. Unlike other antiarrhythmic drugs, they are virtually free from pro-arrhythmic effect and therefore present a safe and effective therapeutic option.

In patients with AVNRT or AVRT, which classically are triggered by SNS activity, beta-blocker therapy is a useful adjunctive therapy [44, 50]. In AF, beta-blockers are used primarily for control of ventricular rate, but in a subset of patients with adrenergic AF triggered by anger or stress, beta-blockers have a role in rhythm control, attenuating the SNS response [101]. The rhythm control property of beta-blockers has also been demonstrated in persistent AF following electrical cardioversion [102].

9.4.2.2 Vagus Nerve Stimulation (VNS)

Increased vagal activity with the resultant prolongation of atrial effective refractory period (ERP) is a well-known trigger for atrial fibrillation [103]. As such, the use of VNS in suppressing AF appears counterintuitive. While high-level VNS achieving >60% sinus rate slowing promotes AF inducibility, mild to moderate levels of VNS producing <40% sinus rate slowing do not have an impact on the inducibility of AF [104]. Studies using LLVNS, i.e., at levels 10 or 50% below the bradycardia threshold, in fact exhibit a strong antiarrhythmic effect [40, 41, 105, 106]. The targets of LLVNS appear to be the efferent nerve endings and the GPs. The lack of antiarrhythmic effect on sectioned sympatho-vagal trunks supports the notion that LLVNS mediates its AF suppressive effect at the efferent

Table 9.4 Summary of prospective clinical trials of autonomic neuromodulation for supraventricular arrhythmias in humans

ANI modality	Clinical trial/ first author	Study design	Selection criteria	*N*	Outcome
Vagus nerve stimulation	Stavrakis et al. [42]	Randomized sham-controlled trial	Patients undergoing cardiac surgery	54	↓ postoperative AF incidence
Tragus stimulation	Stavrakis et al. [69]	Randomized sham-controlled trial	Patients with paroxysmal AF undergoing EP study	40	↓ inducible AF duration during EP study
	TREAT-AF [70]	Randomized sham-controlled trial	Paroxysmal AF	53	↓ AF burden at 6 months
Renal denervation	Pokushalov et al. [71]	Randomized open-label trial	Paroxysmal/persistent AF and resistant hypertension	27	↓ recurrence of atrial tachyarrhythmia at 3 months
	AFFORD [72]	Single-arm feasibility trial	Paroxysmal/persistent AF and hypertension	20	↓ AF burden at 12 months
	ERADICATE-AF [73]	Randomized open-label trial	Paroxysmal AF undergoing AF ablation	302	↑ freedom from AF, AFL, or AT recurrence at 12 months
Ganglionated plexus ablation	Kampaktsis et al. [74]	Meta-analysis of 4 randomized controlled trials [75–78]	Paroxysmal/persistent AF undergoing thoracoscopic [75] or catheter-based [76–78] AF ablations	718	↑ freedom from AF/AT recurrence[a]

AF, atrial fibrillation; AFFORD, atrial fibrillation reduction by renal sympathetic denervation; ERADICATE-AF, effect of renal denervation and catheter ablation vs. catheter ablation alone on atrial fibrillation recurrence among patients with paroxysmal atrial fibrillation and hypertension; TREAT-AF, transcutaneous electrical vagus nerve stimulation to suppress atrial fibrillation

[a] Results driven by catheter-based AF ablation trials

nerve endings [107]. In one study, LLVNS suppressed the bradycardic response from anterior right GP stimulation as well as markedly reduced both frequency and amplitude of the neural activity recorded from the anterior right or superior left GPs [105]. In another study, LLVNS of the right vagus nerve alone exerted a profound antiarrhythmic effect sufficient to suppress the neural activity of both adrenergic and cholinergic components of the intrinsic cardiac nerve [41].

In an experimental model of ambulatory dogs, LLVNS of the left vagus nerve suppressed left stellate ganglion neural activity which occurs in the morning as well as decreased tyrosine-hydroxylase positive cells in the left stellate ganglion 1-week post-LLVNS [40]. Importantly, AF inducibility by rapid atrial pacing in these dogs was prevented by left-sided LLVNS [40]. In a follow-up study by the same group of investigators, chronic LLVNS was shown to produce left stellate ganglion damage, resulting in attenuated ganglionic activity [108].

Application of LLVNS in clinical studies is currently limited to its demonstrated effect in the treatment of postoperative AF. One study randomized 54 patients undergoing cardiac surgery to active or sham LLVNS [42]. LLVNS was achieved by suturing a bipolar wire to the preganglionic vagus nerve fibers along the lateral aspect of the superior vena cava, and by delivering a mean 61 h of VNS (20 Hz, 50% bradycardia threshold). At 1-month follow-up, the incidence of postoperative AF was significantly lower in the LLVNS group compared to the sham group.

The electrophysiologic mechanism underlying LLVNS in AF suppression may involve prolongation of atrial and PV ERPs, but the

Table 9.5 Summary of prospective clinical trials of autonomic neuromodulation for ventricular arrhythmias in humans

ANI modality	Clinical trial/ first author	Study design	Selection criteria	*N*	Outcome
Vagus nerve stimulation	De Ferrari et al. [79]	Single-arm open-label trial	Systolic heart failure, NYHA class II or III, LVEF ≤35%	32	Significant improvement in NYHA class, QoL, 6-min walk distance
	ANTHEM-HF [80] ENCORE [81]	Randomized open-label trial	Systolic heart failure, NYHA class II or III, LVEF ≤40%	60	Significant improvement in NYHA class, LVEF, HRV
	INOVATE-HF [82]	Randomized open-label trial	Systolic heart failure, NYHA class II or III, LVEF ≤40%	707	No significant difference in all-cause mortality or worsening heart failure
	NECTAR-HF [83]	Randomized single-blind trial	Systolic heart failure, NYHA class II or III, LVEF ≤35%	96	No significant change in LVESV or LVEF at 6 months
Tragus stimulation	Yu et al. [84]	Randomized sham-controlled trial	Patients with STEMI	95	↓ VAs within 24 hours
Renal denervation	SYMPLICITY HF [85]	Single-arm feasibility trial	Systolic heart failure, NYHA class III, LVEF <40%, renal impairment	39	↓ NT-proBNP at 12 months
Spinal cord stimulation	SCS HEART [86]	Nonrandomized open-label trial	Systolic heart failure, NYHA class III, LVEF ≤35%	22	Improved NYHA class, LVEF, QoL, exercise capacity
	DEFEAT-HF [87]	Randomized single-blind trial	Systolic heart failure, NYHA class III, LVEF ≤35%	66	No difference in incidence of VAs
Baroreceptor activation therapy	HOPEF4HF [88]	Randomized open-label trial	Systolic heart failure, NYHA class III, LVEF ≤35%	146	Improved NYHA class, QoL, exercise capacity, NT-proBNP
	BeAT-HF [89]	Randomized open-label trial	Systolic heart failure, NYHA class II or III, LVEF ≤35%	245	Significant improvement in NYHA class, QoL, 6-min walk distance, exercise capacity, NT-proBNP

ANTHEM-HF, autonomic regulation therapy for the improvement of left ventricular function and heart failure symptoms; BeAT-HF, baroreflex activation therapy for heart failure; DEFEAT-HF, determining the feasibility of spinal cord neuromodulation for the treatment of chronic systolic heart failure; ENCORE, extension of the ANTHEM-HF study evaluating autonomic regulation therapy in reduced ejection fraction heart failure; HOPE4HF, hope for heart failure; HRV, heart rate variability; LVEF, left ventricular ejection fraction; LVESV, left ventricular end-systolic volume; NECTAR-HF, neural cardiac therapy for heart failure; NT-proBNP, N-terminal B-type natriuretic peptide; NYHA, New York Heart Association; QoL, quality of life; SCS HEART, spinal cord stimulation for heart failure as a restorative treatment; SYMPLICITY HF, renal denervation in patients with chronic heart failure and renal impairment

induced structural changes during LLVNS should be highlighted: upregulation of atrial gap junctions by preventing loss of atrial connexins and phenotype-switching between adrenergic and cholinergic nerve fibers [22, 40, 41]. In support of the potential anti-inflammatory role of VNS beyond AF suppression through an antiadrenergic effect, there was a significant effect in peptide neuromodulation and reduction of inflammatory cytokines associated with VNS [109].

9.4.2.3 Tragus Stimulation

In view of the antiarrhythmic effect of VNS, transcutaneous stimulation of the tragus of the ear, where the auricular branch of the vagus nerve is located, has been developed as a method of noninvasive VNS, affirmed by observation of evoked potentials in the brainstem in humans [110].

In a canine model of AF induced by rapid atrial pacing, low-level tragus stimulation

(LLTS) at 80% below the threshold of sinus node or AV node conduction slowing suppressed AF inducibility through attenuation of pacing-induced atrial ERP shortening [111]. In addition, the amplitude and frequency of GP firing, evident from direct neural recordings from the anterior right GP, were reduced. When the vagus nerves were bisected distal to the site of stimulation, the beneficial electrophysiologic effects of LLTS on atrial ERP and AF inducibility were abolished, suggesting that the LLTS effect was mediated through efferent nerve fibers [111].

In humans, a study reported LLTS in 40 patients with paroxysmal AF (20 LLTS, 20 sham) [69]. In the LLTS group, the patients were subjected to 1 h of LLTS (50% lower than voltage to achieve bradycardia threshold) in the right ear using a flat metal clip attached onto the tragus. Under general anesthesia, AF was induced at baseline and after 1 h of either LLTS or sham stimulation. In the LLTS group, pacing-induced AF duration was shorter and atrial ERP was longer compared to baseline, while in the sham group, there was no significant difference. In the same study, LLTS is associated with reduced serum levels of anti-inflammatory cytokines, namely tumor necrosis factor (TNF-α), compared to the sham control. Hence, akin to LLVNS, LLTS exerted its antiarrhythmic effect potentially through both antiadrenergic and anti-inflammatory pathways.

The feasibility and efficacy of LLTS in ambulatory settings has been demonstrated in the TREAT-AF (Transcutaneous Electrical Vagus Nerve Stimulation to Suppress Atrial Fibrillation) study [70]. In this study enrolling 53 patients with paroxysmal AF randomized to LLTS or sham group, LLTS was achieved using ear clip applied to the earlobe (a site devoid of vagal innervation) for 1 h daily over a 6-month study period. At 6 months, AF burden measured by a 14-day ECG performed at baseline, 3 months, and 6 months was 85% lower in the LLTS group compared with sham. Furthermore, the LLTS group also demonstrated a concomitant 23% reduction in TNF-α level. This study has several implications in therapeutic application of tragus stimulation. First, a self-administered noninvasive treatment with little or no risk can have a significant impact on both AF burden and systemic inflammatory response. Second, tragus stimulation preferentially activates afferent vagal nerve fibers with therapeutic potential [112]. Third, tragus stimulation has been shown to activate central vagal projections in humans with resultant decreased sympathetic output [113]. Fourth, tragus stimulation avoids the possibility of concomitant stimulation of sympathetic fibers collocated with vagal fibers in the cervical vagus nerve when compared to the cervical VNS in humans [114].

9.4.2.4 Renal Denervation (RDN)

Renal denervation (RDN) presents an attractive treatment for hypertension, as the proximal renal arteries are richly innervated by a network of sympathetic ganglia, as well as afferent and efferent nerve fibers linking the central nervous system, the kidney, and the cardiovascular system [115]. Although RDN was first proposed as an innovative tool for treatment of resistant hypertension with subsequent disappointing results from the SIMPLICITY HTN-3 trial (A Controlled Trial of Renal Denervation for Resistant Hypertension), several preclinical and clinical studies have demonstrated a beneficial effect of RDN on AF. In particular, the antiarrhythmic effect was suggested to be independent of an improvement in blood pressure in preclinical studies [116, 117]. In a goat model of pacing-induced AF, RDN resulted in reduced atrial sympathetic nerve sprouting and AF complexity [117], whereas in a porcine model of obstructive sleep apnea, RDN attenuated atrial ERP shortening and AF inducibility [116]. The beneficial effect of RDN on AF inducibility is purported to be mediated through favorable electrical (attenuation of atrial ERP shortening) and structural (reduced afferent sympathetic input to the central nervous system, with a resultant decrease in efferent sympathetic output to the heart) remodeling [115].

Small clinical studies in humans involving pulmonary vein isolation (PVI) with adjuvant RDN during AF ablation procedures appear to be supportive of the preclinical findings

[71, 72]. In these studies, an effective RDN response manifested as abolishment of a sudden expected hypertensive response during high-frequency stimulation (HFS) of aortico-renal ganglion. The efficacy of RDN combined with standard PVI was assessed in the large multicenter ERADICATE-AF trial (Effect of Renal Denervation and Catheter Ablation vs. Catheter Ablation Alone on Atrial Fibrillation Recurrence Among Patients with Paroxysmal Atrial Fibrillation and Hypertension) [73]. In total, 302 patients with paroxysmal AF and hypertension on ≥1 antihypertensive drugs were recruited. At 12-month follow-up, the RDN+PVI group enjoyed greater freedom from AF off antiarrhythmic drugs compared to standalone PVI (71.4% vs. 57.8%; hazard ratio: 0.61; 95% confidence interval: 0.41–0.90; $p = 0.011$). Complication rates were comparable between the two groups. Blood pressure control was noted to be better in the RDN+PVI group. Interestingly, only 57% of patients with RDN demonstrated conclusive HFS response. As such, this calls into question whether the beneficial RDN effect on AF recurrence is related to favorable autonomic modulation, improved blood pressure control, or a combination of both mechanisms.

9.4.2.5 Ganglionic Plexi (GP) Ablation

In contrast to the extracardiac location of post-ganglionic sympathetic neurons at the paravertebral ganglia, the parasympathetic post-ganglionic neurons are located in vagal GPs within the epicardial fat pads and the ligament of Marshal [118, 119]. The short axons of these vagal neurons lend themselves to be feasible radiofrequency ablation targets from the endocardial surface. Variable measures have been used to define the GPs location, ranging from HFS associated with a positive vagal response defined as AV block >2 s to spectral analysis through fast Fourier transform analysis or anatomical guidance [118].

Given the parasympathetic contribution to initiation and maintenance of AF through electrophysiologic and structural mechanisms as discussed before, GP ablation has been proposed as an adjunct to PVI during AF ablation procedures [118]. A meta-analysis of four studies ($n = 718$, mean LA size 45.7 mm, mean LV EF 54.8%) comparing the strategy of GP ablation +PVI ($n = 358$) vs. standalone PVI ($n = 360$) demonstrated that adjunctive GP ablation was associated with significantly higher freedom from AF among patients with paroxysmal AF (75.8% vs. 60%; odds ratio [OR] 2.22, $p = 0.001$) [74]. For patients with persistent AF, the antiarrhythmic effect of GP ablation was more modest, with a non-significant trend toward higher rates of freedom from AF (54.7% vs. 43.3%; OR 1.55, $p = 0.08$). This meta-analysis concluded that GP ablation+PVI led to better AF freedom in patients with PAF and without significant SHD.

Ablation of complex fractionated atrial electrograms (CFAE) was employed as an adjunctive ablation strategy in addition to PVI, although no real benefit was demonstratable [120]. Part of the rationale for this approach was attributable to vagal atrial denervation, with these electrograms commonly encountered in areas juxtaposed to GPs [121, 122]. However, a meta-analysis of 14 studies ($n = 1613$ patients) revealed no benefit with adjunctive CFAE ablation compared to adjunctive GP ablation in both short- (OR 1.72; $p = 0.003$) and long-term (OR 2.0, $p = 0.0006$) AF freedom [123].

GP ablation remains a challenging approach to achieve sustainable vagal denervation due to the variable, inconsistent techniques of GP detection (electrical vs functional vs anatomical), assessment of complete GP ablation, and prevention of reinnervation [124]. Of note, denervation of post-ganglionic vagal neurons at the atrial level has been shown to be associated with increased susceptibility to ventricular arrhythmias [125, 126].

9.4.2.6 Spinal Cord Stimulation (SCS)

SCS is currently used to treat patients with refractory, chronic severe pain or angina pectoris by delivering electrical stimuli to the segments of spinal cord through implantable electrodes [127, 128]. Of relevance, SCS can exert electrophysiologic changes through modulation of afferent and efferent connections between the heart and the intrinsic cardiac autonomic nerves

[129]. In a canine model with chronic AF induced by rapid atrial pacing, SCS prolonged atrial ERP as well as reduced AF burden and inducibility [130]. Another postulated mechanism includes direct suppression of neural activity in atrial GP and stellate ganglia [131, 132]. At the molecular level, SCS modulates relevant cytokine levels, reducing the expression of c-fos and nerve growth factor in addition to increasing the expression of the small conductance calcium-activated potassium channels type 2 within the stellate ganglia neurons [132]. However, adoption of SCS beyond pain management into the clinical realm of AF treatment is curtailed by its invasiveness.

9.4.2.7 Baroreceptor Receptor Activation Therapy (BAT)

Baroreceptors in the carotid sinus are an integral component of the neural feedback loop in modulating blood pressure. Elevation in blood pressure activates these baroreceptors, enhancing neural signals to the brainstem and ultimately reducing sympathetic output [133, 134]. Over the last few decades, several medical devices for baroreceptor receptor activation therapy (BAT) have been designed for the treatment of drug-refractory hypertension [135, 136]. In principle, BAT modulates ANS by sympathetic withdrawal and vagal activation [137, 138]. Low-level BAT (80% of threshold for blood pressure reduction) in a canine model invoked atrial electrophysiologic changes in the form of progressive prolongation of atrial ERP, reduction in AF inducibility, and attenuation of GP function, with the latter effect suggesting potential AF suppression through inhibition of atrial GP [139]. Moreover, low-level BAT was noted to attenuate atrial electrical remodeling induced by rapid atrial pacing in another canine AF model [140]. In spite of the promising experimental data hinting at prominent antiarrhythmic potential of BAT in the treatment of AF, the widespread applicability of BAT in clinical practice will be limited by its invasive nature.

9.4.3 Autonomic Modulation for Ventricular Arrhythmias

9.4.3.1 Beta-Blockers

Beta-blockers with their antiadrenergic properties are considered the mainstay therapy in managing patients with inherited channelopathies such as LQTS and CPVT. In patients with SHD, especially those with myocardial ischemia, post-myocardial infarct, or heart failure with reduced left ventricular ejection fraction including ischemic and non-ischemic cardiomyopathies, beta-blockers remain a steadfast therapy in reducing ventricular arrhythmias and sudden arrhythmic death [141].

Although selective β1 adrenoreceptor antagonists (metoprolol, bisoprolol) have been the beta-blockers of choice in a majority of the indicated cardiovascular conditions, non-selective beta-blockers (nadolol, propranolol) are the preferred agents for channelopathies (LQTS, CPVT) [142]. Indeed, propranolol achieved a better QT-shortening effect in LQTS compared to metoprolol and nadolol. While nadolol and propranolol are equally effective, metoprolol trails behind in its cardioprotective effect and should not be used for symptomatic LQTS individuals [142]. In contrast, selective β1-blockers (metoprolol, bisoprolol, carvedilol, nebivolol) are effective in patients with both ischemic and non-ischemic cardiomyopathies, especially in the setting of heart failure with reduced ejection fraction [141].

9.4.3.2 Cardiac Sympathetic Denervation (CSD)

Stellate ganglia serve not only as a key relay station for cardiac sympathetic afferents but also contain the cell bodies of postganglionic sympathetic efferent neurons with direct connections to the myocardium [143]. Importantly, they present an accessible target for ANIs through CSD, the latter aiming to interrupt the sympathetic input to the heart by removal or blockade of the extrinsic sympathetic nerves. In general, CSD involves bisecting the stellate ganglion with removal of the lower half of this ganglion along with a few ganglia below it, thus creating an adequate sympathetic block to the heart. This makes mechanistic sense as the arrhythmogenic sympathetic input has been shown to be more prominent from the caudal spinal segments and on the left [143]. The boundary of bisection is important as to prevent Horner's syndrome when denervation occurs above the level intended. Bilateral or left CSD (LCSD) is regarded as an effective antiadrenergic therapy, disrupting both afferent and efferent sympathetic fibers [144]. The technique of LCSD has matured over the years, progressing from an open surgical approach via thoracotomy or supraclavicular access to a minimally invasive technique of video-assisted thoracic surgery [145, 146]. A percutaneous approach has been described, achieved either through radiofrequency ablation or use of an anesthetic agent for stellate ganglion blockade (SGB) [147].

The efficacy of CSD extends beyond a local antiadrenergic effect, with anti-fibrillatory impact on patients with LQTS, CPVT, and SHD [144, 148]. LCSD was first pioneered by Schwartz et al. for treatment of patients with LQTS refractory to beta-blockers [149]. Although LCSD led to significant reduction in the incidence of aborted sudden death and syncope in high-risk LQTS cohort compared to pre-LCSD period, the risk of sudden cardiac death persisted in the long-term follow-up [150]. As such, LCSD is currently a recommended adjunctive therapy to beta-blockers and ICD in LQTS patients experiencing breakthrough events [151]. Furthermore, the therapeutic effectiveness of LCSD extends to patients with CPVT [152]. In patients with either LQTS or CPVT, improvement in procedural technique enables LCSD to be performed via video-assisted thoracic surgeries [145].

In patients with SHD and refractory ventricular arrhythmias, CSD has proved to be a valuable anti-fibrillatory intervention. A multicenter CSD study involving 121 patients (26% female, mean age 55 ± 13 years, LVEF 30 ± 13%) with SHD and refractory VT/VT storm demonstrated a 1-year composite freedom from sustained VT, ICD shock, transplant, and death of 58% for LCSD and 50% for bilateral CSD [153]. In this study, 120 patients were on antiarrhythmic drugs before CSD with 39 (32%) no longer requiring antiarrhythmic drugs at follow-up. Interestingly, bilateral CSD appears to be more effective than LCSD in this group of patients as those undergoing bilateral CSD were found to have longer VT or ICD shock- and transplant-free survival.

The overall efficacy and safety of CSD was attested by a systematic review of 13 studies comprising 183 patients (70% male, mean age 54.6 years, 28% ischemic cardiomyopathy, 82% bilateral CSD) [148]. Freedom from arrhythmic events was noted to be 58–100% while most complications were transient with no procedural death reported. Complication rate was reported at 28% including transient hypotension (9%), pneumothorax (5%), neuropathic pain (4%), Horner's syndrome (3%), abnormal perspiration pattern (3%), and hemothorax (2%).

Recently, percutaneous SGB has been advocated as a less invasive approach to achieve CSD in patients with refractory ventricular arrhythmias. A systematic review of 23 studies comprising 38 patients (71% male, mean age 52 ± 19.1 years, 45% ischemic cardiomyopathy, mean LVEF 31 ± 10%) presenting with an electrical storm (15 patients with acute MI; 7 patients with QT prolongation) who were refractory to antiarrhythmic drugs and subsequently underwent SGB concluded that SGB with the use of bupivacaine (0.25–0.5%) resulted in a significantly lower burden of ventricular arrhythmias ($p < 0.001$) and number of external and ICD shocks ($p < 0.01$) [65]. More importantly, the survival rate was 80.6% at discharge.

9.4.3.3 Vagus Nerve Stimulation

Ventricular electrophysiology depicts a cardioprotective effect exerted by parasympathetic dominance. Conversely, reduced vagal activity following MI is associated with heightened risks of ventricular arrhythmias [154, 155]. In experimental models, VNS and exogeneous cholinergic agonists prolong the ventricular ERP [156, 157]. Of note, VNS reduced the vulnerability to VF by increasing VF threshold, flattening the restitution curve (i.e., reducing the maximum slope of action potential duration restitution), attenuation of electrical alternans, and increasing ventricular ERP in an in vitro experimental model [158]. In a separate study, VNS was found to mediate these favorable ventricular electrophysiologic effects through a nitric-oxide-dependent pathway [159].

In addition to inducing a protective electrophysiologic profile, VNS in multiple animal models is shown to prevent adverse cardiac remodeling and ventricular arrhythmias [98, 160]. In a rat model of acute MI, VNS prevented the loss of phosphorylated connexin-43 [94]. In a canine model of healed MI, VNS prevented sudden arrhythmic death [161]. In a canine model of pacing-induced heart failure, chronic VNS improved cardiac autonomic control, promoted anti-inflammatory effects, and attenuated heart failure development [97]. Notably, VNS modulates all these beneficial effects independent of a reduction in heart rate [79, 162].

The promising findings in preclinical studies have led to the design of clinical trials of VNS in humans. An initial open-label, non-randomized trial in patients with heart failure demonstrated that VNS produced significant improvement in a multitude of outcomes including New York Heart Association (NYHA) class, quality of life, 6-min walk test, and LV end-systolic volume, without any major side effects [79]. However, three subsequent randomized trials of VNS in heart failure showed inconsistent results, with two trials reporting neutral results [82, 83] and one reporting modest benefits [80]. At present, ANTHEM-HFrEF (Autonomic Regulation Therapy to Enhance Myocardial Function and Reduce Progression of Heart Failure with Reduced Ejection Fraction) pivotal study (NCT03425422) is an ongoing multicenter randomized clinical trial for VNS in heart failure [163]. Its open-label feasibility study comprising 60 patients (ANTHEM-HF) has shown improvement in heart failure parameters at 6 months [80], with results sustained to a 12-month follow-up period (ENCORE [Extension Study of Neural Regulation Therapy on Myocardial Infarction with Heart Failure]) [81].

9.4.3.4 Tragus Stimulation

All clinical trials of VNS in heart failure populations involve an invasive approach of surgical placement of the electrodes around the cervical vagus nerve in the neck, which is not without procedural risk, with 1 death from implantation-related embolic stroke 3 days following the procedure in the ANTHEM-HF trial [80]. Furthermore, there is long-term implication for potential device-related complications, including infections, electrode fracture/displacement/malfunction, and battery depletion [164]. Direct stimulation of the cervical vagus nerve may be associated with such side effects as tinnitus, dysphonia, cough, and nausea [164, 165]. As such, tragus stimulation involving transcutaneous stimulation of the auricular branch of the vagus nerve presents an attractive noninvasive option [110].

Animal studies provided evidence for the effects of tragus stimulation in preventing adverse cardiac remodeling and ventricular arrhythmias. In a canine model of chronic MI, chronic intermittent LLTS 2 h daily for 2 months (80% below the bradycardia threshold) induced neuropeptide modulatory changes including suppression of left stellate ganglion activity, attenuation of cardiac sympathetic nerve sprouting, downregulation of nerve growth factor, and upregulation of small conductance calcium-activated potassium channel type 2. Notably favorable electrophysiological remodeling occurred with suppression of ventricular arrhythmias and a flattening of restitution slope [166]. Chronic intermittent LLTS also attenuated adverse structural remodeling, fibrosis, and inflammation [160]. In a proof-of-concept study, LLTS for 2 hours in humans undergoing primary coronary intervention for ST-segment elevation MI led to reduced ventricular arrhythmias, preserved cardiac function, and reduced biomarkers of myocardial injury/inflammation, suggesting a potential opportunity for noninvasive ANIs as an adjunctive nonpharmacological treatment in ST-segment elevation MI [84].

9.4.3.5 Renal Denervation

Early preclinical studies with RDN achieved using low-energy radiofrequency ablation along the renal arteries demonstrated reduced angiotensin receptor density and improved cardiac output [167]. In the SYMPLICITY HF study, a single-arm feasibility study enrolling 39 patients with mild-moderate symptoms, EF <40%, and renal impairment, RDN resulted in a reduction in NT-pro-brain natriuretic peptide 12 months after treatment without perceived deterioration in both cardiac and renal function [85]. In patients with cardiomyopathy and refractory VT, RDN has been shown to be an effective adjunctive therapy to catheter ablation of VT [168]. In patients with cardiomyopathy and recurrent VT following catheter ablation, RDN was used as an adjunct to CSD, leading to reduced ICD therapies in patients who underwent CSD and RDN as staged procedures [169].

9.4.3.6 Spinal Cord Stimulation (SCS)

In canine post-infarct heart failure models, SCS was consistently associated with reduced ventricular arrhythmias and recovery of left ventricular ejection fraction [170–172]. The improved electrical and structural remodeling mediating the antiarrhythmic effects of SCS was attributable to sympathetic withdrawal and vagal enhancement [171]. Initial case series of two patients with high ventricular arrhythmia burden depicted the same antiarrhythmic effect from SCS [173]. However, the two clinical trials investigating SCS in patients with heart failure, including the randomized controlled trial DEFEAT-HF (Determining the Feasibility of Spinal Cord Neuromodulation for the Treatment of Chronic Systolic Heart Failure), have yielded conflicting results [86, 87]. The conflicting outcomes of the two trials could be accounted for by variation in the duty cycle, intensity of stimulation, and design and position of the electrode, highlighting the need to optimize a systematic stimulation protocol to allow for meaningful translational research from animal studies to large clinical trials.

9.4.3.7 Baroreceptor Activation Therapy (BAT)

BAT has been shown to modulate ventricular electrophysiology through prolongation of ventricular ERP and flattening of the action potential duration restitution slope in canines [174]. At 80% below the voltage threshold for blood pressure lowering, low-level BAT was found to suppress premature ventricular complexes VT and VF in a canine model with acute ischemia induced by occlusion of the left anterior descending artery [175]. Additionally, BAT reversed adverse structural remodeling in canine models of heart failure with improvement in interstitial fibrosis, myocyte hypertrophy, LV end-diastolic pressure, and survival [176, 177].

In the clinical arena, a proof-of-concept, single-center, open-label study demonstrated the safety and efficacy of carotid BAT in improving quality of life and exercise capacity [178]. A small randomized clinical trial of BAT showed improvement in various heart failure markers at 6 months, including 6-min walk test, quality of life, NYHA class, and N-terminal pro-B-type natriuretic peptide level [88]. A large randomized clinical trial (BeAT-HF [Baroreflex Activation Therapy for Heart Failure]) comprising 245 patients (from a pool of 408 randomized patients) with heart failure and reduced ejection fraction (8% female, mean age 62 ± 11 years; LV EF 27 ± 6%) concluded that BAT is not only safe but also efficacious, resulting in significant improvement in quality of life, 6 min walk, exercise capacity, and functional status, as well as significantly lower N-terminal pro-B-type natriuretic peptide [89]. The impact of BAT on hard clinical endpoints is currently pending from this trial.

9.5 Assessment of Autonomic Tone

Distinctive methods have been developed over the years for assessment of specific aspects of sympathetic and parasympathetic nervous systems. These noninvasive and invasive methods can complement one another, contributing to a global picture of autonomic status. While these methods provided key insights into the abnormal autonomic characteristics in arrhythmias and heart failure, they remain rooted in the research arena, each with their unique strength and limitations.

9.5.1 Baroreflex Sensitivity (BRS)

Baroreflex sensitivity (BRS) describes the acuity of arterial baroreceptor control of heart rate in response to blood pressure changes. The heart rate changes in response to acute perturbation in blood pressure are thought to be an indication of reflex vagal response due to the preferential influence of cardiac cycles on the release of acetylcholine as opposed to norepinephrine. The strength of this reflex vagal response can be assessed by three techniques: (1) analysis of bradycardic response following the increase of blood pressure with vasoconstrictors such as phenylephrine; (2) assessment of reflex sympathetic-induced tachycardic response following the reduction of blood pressure by vasodilators such as nitroprusside or nitroglycerin; and (3) direct stimulation of carotid baroreceptors with neck suction or unloading by neck pressure, allowing these neck maneuvers to elicit counter-regulatory responses from aortic arch baroreceptors. These techniques are not without their limitations. Prolonged infusion of vasoactive agents can simulate a steady state, leading to competing sympathetic responses. Additionally, these vasoactive agents may exert a confounding effect on sinoatrial node discharges, baroreceptor nerve endings, and atrial and pulmonary mechanoreceptors [179, 180]. To circumvent these limitations, algorithms have been developed with the ability of identifying spontaneous concordant fluctuations in blood pressure and heart rate within the brief time window from continuous noninvasive or invasive recordings [181].

Central to all these techniques is the utilization of a regression equation correlating changes in pulse interval to changes in systolic blood pressure during the immediately preceding cardiac cycles. The gradient of the resulting graph describes the gain of the arterial baroreflex regulation on heart rate. The final results therefore indicate the sensitivity of vagal response toward stress response in blood pressure changes, allowing this method to be used as a bedside test comparable to the BRS derived from drug-induced changes in blood pressure. This method lacks the ability to identify the cause of autoimmune impairment. Nonetheless, low BRS has been shown to correlate with poor prognostic outcome. Canine models demonstrating reduced BRS after MI were more susceptible to VF [182]. These findings were extrapolated to post-MI human studies, demonstrating that a depressed BRS of <3 ms/mmHg was associated with a high incidence of arrhythmic deaths [183–185]. In heart failure patients receiving optimal medical therapy, the prognostication of BRS has recently been challenged [186].

9.5.2 Heart Rate Variability (HRV)

Beat-to-beat heart rate varies stochastically due to the influence of tonic vagal control of the sinus node, with direct or indirect influence of circadian rhythms, temperature regulations, and changes in autonomic nerve activity [187–189]. The positive chronotropy (increase in sinus rate) induced by catecholamines (epinephrine and norepinephrine) released by the SNS and the negative chronotropy (decrease in sinus rate) by acetylcholine released by the PNS are responsible for the subtle degree of variability in the intervals between consecutive beats [190–192]. Heart rate variability (HRV) is therefore a noninvasive surrogate marker of autonomic balance of the heart, with its analysis being performed in time, frequency, or nonlinear domains.

9.5.2.1 Time-Domain Measures

Time-domain measurements represent the most widely adopted technique to evaluate HRV due to its relatively straightforward computation of parameters derived from the time series of RR intervals. Long-term HRV is deduced from the standard deviation of RR intervals usually computed from 24-h Holter recordings, whereas short-term HRV is reflected by root mean square of successive differences of the RR intervals. Additionally, short-term HRV can also be assessed as the percentage of consecutive RR intervals with >50 ms difference. All these time-domain measures have been verified to be age-dependent, gender-sensitive, and decreased with aging, whereas preservation of HRV is associated with healthy longevity [193, 194].

9.5.2.2 Frequency-Domain Measures

Using fast Fourier transform and wavelet analysis quantifying the spectral and time-frequency content of HRV, the frequency-domain measures serve to complement the time-domain measurements of HRV. High frequencies (0.15–0.5 Hz) are thought to be a representation of the parasympathetic component of the ANS with vagal blockade abolishing oscillations in heart rate within this frequency band [195]. Low frequencies (0.05–0.15 Hz) are mediated by both the PNS and SNS and are affected by BRS. This is supported by observations that the low-frequency spectral power is increased by maneuvers that stimulate central sympathetic output, such as standing up, tilting, and exercising. Conversely the spectral power in this frequency band of 0.05–0.15 Hz is decreased by beta-blockade, clonidine, and during sleep. Very-low frequencies (<0.05 Hz) are under the influence of many in vivo factors including the renin-angiotensin system and thermoregulation [195]. As a rough guide, the ratio of low- to high-frequency power is therefore considered a measure of autonomic balance [189].

In heart failure, the spectral power appears to be markedly reduced and concentrated within the very-low- and low-frequency ranges [196]. Similar to BRS, HRV provides insights into sympathetic and parasympathetic contributions to heart rate modulation and contributes to estimation of prognostic outlook, despite the lack of specificity to the degree of regional sympathetic output. Historically, a depressed HRV demonstrated a high sensitivity and specificity in predicting susceptibility to VF in MI canine models [197]. This is further corroborated by the finding of HRV recovery in low-risk post-MI dogs compared to high-risk dogs with persistent depressed HRV parameters independent of beta-blockade [198]. These preclinical findings were echoed by subsequent human studies involving post-MI patients. In these trials, HRV was a significant predictor of SCD after adjusting for clinical and demographic factors, including ejection fraction [185, 199, 200]. Furthermore HRV improvement over time following MI coincided with decreasing risk of arrhythmic death [201]. In one study, a HRV of <5 ms conferred a hazard relative risk of 5.3 in SCD, compared with low-risk patients with a HRV of >10 ms during a follow-up period of 31 months [200]. Notably a depressed HRV has also been observed in patients with idiopathic dilated cardiomyopathy with a history of SCD compared to those without fatal ventricular arrhythmias [202, 203]. Other conditions in which frequency-domain measures have been utilized to evaluate autonomic balance include sleep apnea and hypertension [204, 205].

The concept of low- to high-frequency ratio as a reflection of autonomic balance has been questioned due to the fact that, in contrast to the previously conceived notion that low-frequency content comprises exclusively SNS activity, low-frequency content is now regarded to be a reflection of combined SNS and PNS inputs [192, 206].

9.5.2.3 Nonlinear Domain Measures

Nonlinear measures have been developed over the past decade to address complex nonlinear autonomic interactions [207–209]. Measurements such as SD1/SD2, Poincare maps, entropy, and detrended fluctuation analysis attempt to quantify the degree of information, disorder, or complexity of HRV.

SD1 and SD2 are measures of short- and long-term HRV, respectively, both based on RR intervals and derived from Poincare maps. SD1 measures immediate beat-to-beat variability, signifying parasympathetic tone, whereas SD2 reflects combined SNS and PNS influences on the heart [209]. The ratio SD1/SD2 therefore serves to indicate underlying autonomic tone, as well as short- and long-term variability in RR intervals. Indeed, intermittent VNS has been demonstrated to increase SD1/SD2 ratio in heart failure patients, suggesting a restorative role of VNS in autonomic balance [208]. In patients with dilated cardiomyopathy, Poincare plot analysis of HRV has been utilized for risk stratification [207]. Furthermore, approximate entropy has been shown to be raised in patients with heart failure compared with healthy subjects, indicating loss of autonomic control in association with more erratic heart rate [210]. Other measures such as sample entropy and detrended fluctuation analysis were used to demonstrate changes in autonomic drive and to assess the neural effects of HRV in both healthy individuals and those with spinal cord injury [211].

9.5.3 Neural Tracer Imaging

Over the last few decades, neural imaging techniques have been developed and employed using several different tracers that allow for direct visualization of sympathetic nervous innervation in the heart. These tracers target molecular landmarks at the presynaptic and postsynaptic side as well as second messenger systems of the sympathetic nervous system and are thereby capable of portraying the overall picture of sympathetic signal transduction. The majority of these radiotracers mimic the structure of norepinephrine and other catecholamines to enable them to target the endogenous reuptake pathway of sympathetic neurons. These tracers are exemplified by labeled neurotransmitters ([^{18}F]-dopamine, [^{11}C]-epinephrine), “false neurotransmitters” serving as substrate analogues ([^{123}I]-MIBG, [^{11}C]-mHED, [^{18}F]-LMI1195, [^{11}C]-phenylephrine, [^{11}C]-phenethylguanidines), and uptake-1 inhibitors ([^{11}C]=methylreboxetine, [^{11}C]-desipramine). Each tracer possesses unique uptake and retention characteristics, contributing information on various aspects of neuronal reuptake, uptake-1 density, vesicular packaging, vesicular release, and norepinephrine metabolism. In heart failure, a chronic state of sympathetic overdrive fuels a decrease in neuronal reuptake, downregulation of uptake-1, and increased synaptic norepinephrine content and regional spillover.

The two most commonly utilized tracers in clinical practice are [^{123}iodine]-metaiodobenzylguanidine ([^{123}I]-MIBG) and [^{11}C]-meta-hydroxyephedrine ([^{11}C]-mHED). The former was first developed to image neuroendocrine tumors, with early studies identifying [^{123}I]-MIBG uptake in myocardium to be in inverse correlation with plasma and urinary catecholamines [212] due to its high affinity to neuronal uptake-1 and extra-neuronal uptake-2 [213, 214]. Using semiquantitative analyses in single-photon emission computed tomography (SPECT), an estimation of sympathetic tone can be inferred from the rate of [^{123}I]-MIBG washout, as well as early and late heart-to-mediastinum ratios [215]. Reduced late heart-to-mediastinum or raised [^{123}I]-MIBG washout in semiquantitative myocardial [^{123}I]-MIBG measurements has been shown to be a poor prognostic marker in a systematic meta-analysis [216]. Conversely beta-blockade and renin–angiotensin–aldosterone inhibition are characterized by an increase in [^{123}I]-MIBG uptake and a reduced myocardial washout. Pertinently large-scale clinical trials have recognized [^{123}I]-MIBG imaging as an independent prognostic tool in the identification of heart failure patients at the greatest risk of disease progression [217–219] and sudden cardiac death independent of left ventricular ejection fraction and B-type natriuretic peptide [216, 220–223]. In patients with ventricular tachycardia without any coronary artery disease, the uptake of [^{123}I]-MIBG was noted to be reduced [224]. Notably, a reduced [^{123}I]-MIBG predicted ventricular arrhythmias requiring ICD therapy in patients with heart failure [218]. Recently, [^{123}I]-MIBG imaging was shown to accurately identify atrial GP locations as verified by HFS [225].

In positron emission tomography (PET), [^{11}C]-mHED is the most widely used radiotracer for sympathetic neuronal imaging. As it is devoid of postsynaptic activity, the retention of [^{11}C]-mHED reflects solely presynaptic function of sympathetic neurons due to its selectivity for uptake-1 over other reuptake transporters [226]. [^{11}C]-mHED has a predilection for tissue retention in organs with complex adrenergic networks including the heart, adrenal glands, and spleen, with gradual accumulation in the liver. This is supported by the findings of selective competitive inhibitors of uptake-1, including true or false neurotransmitters, attenuating myocardial accumulation of [^{11}C]-mHED, with consequent increase in hepatic activity due to the accumulation of metabolites [213, 227–232]. High-speed liquid chromatography further confirmed plasma accumulation of [^{11}C]-mHED metabolites in guinea pigs and rats within 30 min after injection [229, 230, 232], and in human subjects within 10–20 min [233].

In spite of the attractiveness of these imaging modalities to measure autonomic tone noninvasively, complete assessment of autonomic tone is currently confounded by the lack of parasympathetic tracers.

9.5.4 Direct Measurement of Sympathetic Nerve Activity

While neural tracer imaging provides a means of direct visualization of sympathetic innervation, microneurography allows direct multi-fiber or single-fiber microelectrode measurements of postganglionic sympathetic nerve activity, thereby serving as a real-time recording of the dynamic sympathetic nerve and reflex controls [234, 235]. Sympathetic nerve activity is recorded from intraneural microelectrodes inserted percutaneously in a peripheral nerve, typically at the level of the peroneal nerve [236, 237]. Skin (SKNA) and muscle sympathetic nerve activities (MSNA) manifest as distinctive discharge patterns, the former preferentially responding to external acoustic, tactile, or temperature stimuli independent of cardiac cycles while the latter being heavily entrained by input from cardiopulmonary and arterial mechanoreceptors.

MSNA possesses unique pulse synchronicity, firing discharges 1.1–1.3 seconds after the preceding R wave of the electrocardiogram. At rest, MSNA is found to correlate with both cardiac and renal norepinephrine spillover, whereas during isometric exercises there is a concordant increase of sympathetic nerve activity between MSNA and cardiac norepinephrine spillover [238, 239]. This phenomenon is absent in heart failure [240]. Indeed, in heart failure, evidence of sympathetic hyperactivity manifested as increased firing probability and frequency with possible recruitment of otherwise silent sympathetic nerve fibers [235]. Importantly, increased MSNA predicts mortality in patients with heart failure in addition to its association with non-responders of cardiac resynchronization therapy [237, 241].

In view of the invasiveness and time-consuming nature of microneurography, MSNA is not routinely used despite its reproducibility and reliability in assessment of autonomic tone [236]. In contrast, SKNA activity can be measured noninvasively from ECG recordings [242]. SKNA is found to increase in subjects undergoing Valsalva maneuver as well as water pressor test due to increased sympathetic drive [242]. In ambulatory dogs, SKNA correlated well with stellate ganglion activity [243]. In humans, increased SKNA demonstrated a temporal relationship with paroxysmal atrial tachyarrhythmias, preceding the onset and termination of paroxysmal atrial tachycardia and AF [244]. In another study, sustained level of increased SKNA is noted to associate with temporal clustering of AF as well as spontaneous VT and VF in humans [245].

9.5.5 Alternans

Alternans in ventricular repolarization, measured as T-wave alternans (TWA), has been shown to surge in magnitude during elevated sympathetic activity in humans as well as in an end-stage heart failure animal model [246–248]. These surges in TWA amplitude are attenuated by beta-blockers, supporting the concept that sympathetic activity modulates TWA [249, 250]. It is postulated that beta-blockade-mediated attenuation of TWA amplitude occurs by (1) blunting of the exercise-related chronotropic response, thereby preventing patients from reaching the specific heart rate threshold necessary for TWA development, and (2) direct reduction of TWA magnitude [250]. Conversely, VNS was shown in an isolated rabbit heart model to reduce TWA amplitude and to increase the cycle length for VF induction [158].

P-wave alternans (PWA) has been proposed as a novel atrial substrate of electrical instability, predisposing to the development of AF [251]. Using a customized algorithm for PWA estimation [252, 253], LLTS for 1 h/day resulted in lower AF burden and diminished PWA voltage in a single patient compared to baseline and to another patient on a sham protocol [254]. AF and PWA burden for the patient with active LLTS was not increased over 6 months when compared to the sham patient.

9.6 Challenges and Limitations of Autonomic Neuromodulatory Interventions

The conflicting outcome among contemporary clinical trials of VNS in heart failure epitomizes the challenges and limitations of ANIs. In spite of a robust rationale to restore autonomic balance in heart failure supported by favorable preclinical data, the anticipated promising outcome of VNS in clinical populations of heart failure has failed to materialize [255]. The discrepancy between clinical trials is reflected by inconsistency in patient selection, VNS dosing, and stimulation parameters in terms of frequency and intensity. Future studies designed after homogenization of these challenges are imperative to showcase the efficacy of ANIs in various arrhythmias particularly in the heart failure population.

Use of a biomarker to identify appropriate candidates for ANIs is of paramount importance given that heterogeneous characteristics in subjects with heart failure may account for the conflicting results of the VNS clinical trials. This concept is in fact well recognized, aiding appropriate patient selection for AF ablation [251] and for cardiac resynchronization therapy. Furthermore, biomarkers capable of predicting long-term response to ANIs are currently lacking. Although MSNA [256], HRV [256, 257], TNF-α [69], global longitudinal strain [257], and possibly PWA have been shown to change accordingly following acute LLTS in humans, the predictive value of these biomarkers for response to chronic treatment remains elusive. A novel biomarker known as neurotrophic protein S100B, released from cardiac glial cells, appears to correlate with acute cardiac autonomic nerve damage in patients undergoing AF ablation [258]. Importantly, following AF ablation, higher levels of S100B predicted sinus rhythm maintenance during follow-up [258, 259]. Further studies are required to investigate the role of S100B in predicting response of ANIs.

9.7 Future Directions

9.7.1 Optogenetics

Optogenetics refers to the capability of specific cell types for optical imaging and genetic targeting [260]. In principle, illumination of genetically targeted brain circuits can regulate excitable tissue via the expression of opsins (light-sensitive microbial proteins) in the target cells [260]. The various functions of opsins as ion channels, ion pumps, or signaling receptors enable light-sensitive, temporally precise, focused low-energy control at cellular, tissue, and organ levels (see also Chap. 17). Application of optogenetics in cardiovascular research involves the use of viruses and exogenous “donor” cells expressing opsins as a means to create optically sensitive cardiac cells and syncytia [261]. Using this technique, two categories of opsins can be created: (1) excitatory opsins (e.g., channelrhodopsin2), which can provide currents sufficient for triggering action potentials, and (2) inhibitory opsins (e.g., archaerhodopsin, halorhodopsin) which suppresses action potentials [262]. The use of optogenetics at the neural-cardiac axis will allow precise dissection of neuro-cardiac interaction, as well as focused dynamic manipulation of cell signaling, neural feedback loop, and specific gene control through light transmission [263].

In an experimental model, left stellate ganglion was optogenetically silenced by using adenovirus vector to deliver archaerhodopsin T (ArchT, an inhibitory opsin) to the neurons within the left stellate ganglion of 20 male beagles [264]. All dogs successfully expressed ArchT, the latter activated by transient light-emitting diode illumination, resulting in significantly suppressed left stellate ganglion function and neural activity, depressed sympathetic indices of HRV, and prolongation of left ventricular ERP and action potential duration. These effects were enhanced by up to 30-min duration of illumination. Crucially, ischemia-induced ventricular arrhythmias were greatly reduced throughout the duration of illumination. All these observations returned to baseline within 2 h after illumination was turned off.

9.7.2 Transcutaneous Magnetic Stimulation (TCMS)

Although optogenetics presents a noninvasive revenue for autonomic neuromodulation, manipulation of left stellate ganglion activity using this method to reduce sympathetic input to the heart and to suppress ventricular arrhythmias is very much restricted in the preclinical realm [264]. In comparison, transcutaneous magnetic stimulation (TCMS) presents itself as a suitable noninvasive and nondestructive method of neuromodulation [265, 266]. Animal studies demonstrated the feasibility of magnetic stimulation to achieve antiarrhythmic effect in both AF and post-infarct ventricular arrhythmia by targeting cardiac sympathetic activation [267, 268].

Recently the first-in-human TCMS study was performed in five patients with drug-refractory VT storm [269]. In this study, a figure-of-8 TCMS coil was attached to a magnetic stimulation system which was positioned lateral to the C7 spinous process in approximation of the left stellate ganglion. TCMS was conducted at 80% left trapezius motor threshold (0.9 Hz for 60 min). Compared to baseline 24 h preceding TCMS, there was a lower burden of sustained VT in the 48 h ensuing TCMS. Additionally, there were no further external shocks during this period in contrast to an aggregate of 41 shocks prior to TCMS. One patient required subsequent catheter ablation 36 h after enrollment as a result of aborted TCMS from coil overheating. Importantly, no adverse event was reported. Given the promising findings of this case series, a randomized, sham-controlled trial evaluating the safety and efficacy of TCMS in patients with VT storm is currently ongoing (NCT04043312).

9.8 Conclusions

The two divisions of the cardiac ANS, the SNS and the PNS, play a critical role in supraventricular and ventricular arrhythmogenesis. These arrhythmias arise from distinctive electrophysiologic mechanisms, being mediated by SNS and PNS neurotransmitters as well as co-transmitters interacting at various hierarchies of the neurocardiac axis. Knowledge of the intricate autonomic interplay derived from preclinical studies gives rise to exciting clinical application of ANIs in suppression of troublesome atrial arrhythmias and potentially fatal ventricular arrhythmias, albeit with conflicting results, especially in the clinical trials comprising HF patients. Novel methods such as optogenetics and TCMS offer noninvasive ANI tools to modulate arrhythmias. However, clinical trials of various ANIs demonstrating sustainable and meaningful therapeutic outcome in the suppression of various arrhythmias would require conscientious patient selection, optimization of study protocols, as well as utilization of reproducible biomarkers.

Acknowledgments Some of the work discussed here was supported by a British Heart Foundation Clinical Research fellowship (FS/12/52/29629 to S.H.C.) and a British Heart Foundation Programme Grant (RG/17/3/32774 to G.A. N.).

References

1. Shen MJ, Zipes DP. Role of the autonomic nervous system in modulating cardiac arrhythmias. Circ Res.

2014;114(6):1004–21. https://doi.org/10.1161/circresaha.113.302549.

2. Sharifov OF, Fedorov VV, Beloshapko GG, Glukhov AV, Yushmanova AV, Rosenshtraukh LV. Roles of adrenergic and cholinergic stimulation in spontaneous atrial fibrillation in dogs. J Am Coll Cardiol. 2004;43(3):483–90. https://doi.org/10.1016/j.jacc.2003.09.030.
3. Frigy A, Csiki E, Caraşca C, Szabó IA, Moga VD. Autonomic influences related to frequent ventricular premature beats in patients without structural heart disease. Medicine (Baltimore). 2018;97(28):e11489. https://doi.org/10.1097/md.0000000000011489.
4. Levy MN, Martin P. Parasympathetic control of the heart. In: Randall WC, editor. Nervous control of the cardiovascular function. New York: Oxford University Press; 1984. p. 68–94.
5. Chin SH, Allen E, Brack KE, Ng GA. Effects of sympatho-vagal interaction on ventricular electrophysiology and their modulation during beta-blockade. J Mol Cell Cardiol. 2020;139:201–12. https://doi.org/10.1016/j.yjmcc.2020.01.011.
6. Herring N, Cranley J, Lokale MN, Li D, Shanks J, Alston EN, et al. The cardiac sympathetic co-transmitter galanin reduces acetylcholine release and vagal bradycardia: implications for neural control of cardiac excitability. J Mol Cell Cardiol. 2012;52(3):667–76. https://doi.org/10.1016/j.yjmcc.2011.11.016.
7. Tan CMJ, Green P, Tapoulal N, Lewandowski AJ, Leeson P, Herring N. The role of neuropeptide Y in cardiovascular health and disease. Front Physiol. 2018;9:1281. https://doi.org/10.3389/fphys.2018.01281.
8. Kalla M, Hao G, Tapoulal N, Tomek J, Liu K, Woodward L, et al. The cardiac sympathetic co-transmitter neuropeptide Y is pro-arrhythmic following ST-elevation myocardial infarction despite beta-blockade. Eur Heart J. 2020;41(23):2168–79. https://doi.org/10.1093/eurheartj/ehz852.
9. Schömig A, Richardt G. The role of catecholamines in ischemia. J Cardiovasc Pharmacol. 1990;16(Suppl 5):S105–12.
10. Zhu C, Hanna P, Rajendran PS, Shivkumar K. Neuromodulation for ventricular tachycardia and atrial fibrillation: A clinical scenario-based review. J Am Coll Card Clin Electrophysiol. 2019;5(8):881–96. https://doi.org/10.1016/j.jacep.2019.06.009.
11. Manolis AS, Manolis AA. Exercise and arrhythmias: A double-edged sword. Pacing Clin Electrophysiol. 2016;39(7):748–62. https://doi.org/10.1111/pace.12879.
12. Buckley U, Shivkumar K. Stress-induced cardiac arrhythmias: The heart-brain interaction. Trends Cardiovasc Med. 2016;26(1):78–80. https://doi.org/10.1016/j.tcm.2015.05.001.
13. Irvine J, Firestone J, Ong L, Cribbie R, Dorian P, Harris L, et al. A randomized controlled trial of cognitive behavior therapy tailored to psychological adaptation to an implantable cardioverter defibrillator. Psychosom Med. 2011;73(3):226–33. https://doi.org/10.1097/PSY.0b013e31820afc63.
14. Chevalier P, Cottraux J, Mollard E, Sai N, Brun S, Burri H, et al. Prevention of implantable defibrillator shocks by cognitive behavioral therapy: a pilot trial. Am Heart J. 2006;151(1):191. https://doi.org/10.1016/j.ahj.2005.10.007.
15. Yamada S, Suzuki H, Kamioka M, Suzuki S, Kamiyama Y, Yoshihisa A, et al. Sleep-disordered breathing increases risk for fatal ventricular arrhythmias in patients with chronic heart failure. Circ J. 2013;77(6):1466–73. https://doi.org/10.1253/circj.cj-12-0836.
16. Padeletti M, Zacà V, Mondillo S, Jelic S. Sleep-disordered breathing increases the risk of arrhythmias. J Cardiovasc Med (Hagerstown). 2014;15(5):411–6. https://doi.org/10.2459/jcm.0000000000000019.
17. Manolis TA, Manolis AA, Apostolopoulos E, Melita H, Manolis AS. Cardiovascular complications of sleep disorders: A better night's sleep for a healthier heart/from bench to bedside. Curr Vasc Pharmacol. 2020;19(2):210–32. https://doi.org/10.2174/1570161118666200325102411.
18. Armour JA. Potential clinical relevance of the 'little brain' on the mammalian heart. Exp Physiol. 2008;93(2):165–76. https://doi.org/10.1113/expphysiol.2007.041178.
19. Beaumont E, Salavatian S, Southerland EM, Vinet A, Jacquemet V, Armour JA, et al. Network interactions within the canine intrinsic cardiac nervous system: implications for reflex control of regional cardiac function. J Physiol. 2013;591(18):4515–33. https://doi.org/10.1113/jphysiol.2013.259382.
20. Shivkumar K, Ajijola OA, Anand I, Armour JA, Chen PS, Esler M, et al. Clinical neurocardiology defining the value of neuroscience-based cardiovascular therapeutics. J Physiol. 2016;594(14):3911–54. https://doi.org/10.1113/jp271870.
21. Sheldon RS, Grubb BP 2nd, Olshansky B, Shen WK, Calkins H, Brignole M, et al. 2015 heart rhythm society expert consensus statement on the diagnosis and treatment of postural tachycardia syndrome, inappropriate sinus tachycardia, and vasovagal syncope. Heart Rhythm. 2015;12(6):e41–63. https://doi.org/10.1016/j.hrthm.2015.03.029.
22. Scridon A, Şerban RC, Chevalier P. Atrial fibrillation: Neurogenic or myogenic? Arch Cardiovasc Dis. 2018;111(1):59–69. https://doi.org/10.1016/j.acvd.2017.11.001.
23. Tan AY, Zhou S, Ogawa M, Song J, Chu M, Li H, et al. Neural mechanisms of paroxysmal atrial fibrillation and paroxysmal atrial tachycardia in ambulatory canines. Circulation. 2008;118(9):916–25. https://doi.org/10.1161/circulationaha.108.776203.
24. Manolis AS, Linzer M, Salem D, Estes NA 3rd. Syncope: current diagnostic evaluation and

management. Ann Intern Med. 1990;112(11):850–63. https://doi.org/10.7326/0003-4819-112-11-850.

25. van den Berg MP, Crijns HJ, Bouwmeester TR, Smit AJ, Lie KI. Cardiac asystole post-exercise: a report of two cases. Int J Cardiol. 1995;51(3):296–300. https://doi.org/10.1016/0167-5273(95)02432-v.
26. Hu F, Zheng L, Liang E, Ding L, Wu L, Chen G, et al. Right anterior ganglionated plexus: The primary target of cardioneuroablation? Heart Rhythm. 2019;16(10):1545–51. https://doi.org/10.1016/j.hrthm.2019.07.018.
27. El-Sherif N, Caref EB, Chinushi M, Restivo M. Mechanism of arrhythmogenicity of the short-long cardiac sequence that precedes ventricular tachyarrhythmias in the long QT syndrome. J Am Coll Cardiol. 1999;33(5):1415–23. https://doi.org/10.1016/s0735-1097(98)00700-1.
28. Sweeney MO, Ruetz LL, Belk P, Mullen TJ, Johnson JW, Sheldon T. Bradycardia pacing-induced short-long-short sequences at the onset of ventricular tachyarrhythmias: a possible mechanism of proarrhythmia? J Am Coll Cardiol. 2007;50(7):614–22. https://doi.org/10.1016/j.jacc.2007.02.077.
29. Kawasaki R, Machado C, Reinoehl J, Fromm B, Baga JJ, Steinman RT, et al. Increased propensity of women to develop torsades de pointes during complete heart block. J Cardiovasc Electrophysiol. 1995;6(11):1032–8. https://doi.org/10.1111/j.1540-8167.1995.tb00380.x.
30. Manolis AA, Manolis TA, Apostolopoulos EJ, Apostolaki NE, Melita H, Manolis AS. The role of the autonomic nervous system in cardiac arrhythmias: The neuro-cardiac axis, more foe than friend? Trends Cardiovasc Med. 2020;31(5):290–302. https://doi.org/10.1016/j.tcm.2020.04.011.
31. Qin M, Zhang Y, Liu X, Jiang WF, Wu SH, Po S. Atrial ganglionated plexus modification: A novel approach to treat symptomatic sinus bradycardia. J Am Coll Card Clin Electrophysiol. 2017;3(9):950–9. https://doi.org/10.1016/j.jacep.2017.01.022.
32. Brembilla-Perrot B, Terrier de la Chaise A, Pichené M, Aliot E, Cherrier F, Pernot C. Isoprenaline as an aid to the induction of catecholamine dependent supraventricular tachycardias during programmed stimulation. Br Heart J. 1989;61(4):348–55. https://doi.org/10.1136/hrt.61.4.348.
33. Manolis AS, Estes NA 3rd. Supraventricular tachycardia. Mechanisms and therapy. Arch Intern Med. 1987;147(10):1706–16.
34. Cappato R, Castelvecchio S, Ricci C, Bianco E, Vitali-Serdoz L, Gnecchi-Ruscone T, et al. Clinical efficacy of ivabradine in patients with inappropriate sinus tachycardia. A prospective, randomized, placebo-controlled, double-blind, crossover evaluation. J Am Coll Cardiol. 2012;60(15):1323–9. https://doi.org/10.1016/j.jacc.2012.06.031.
35. Ho SY, Cabrera JA, Tran VH, Farré J, Anderson RH, Sánchez-Quintana D. Architecture of the pulmonary veins: relevance to radiofrequency ablation. Heart. 2001;86(3):265–70. https://doi.org/10.1136/heart.86.3.265.
36. Tan AY, Li H, Wachsmann-Hogiu S, Chen LS, Chen PS, Fishbein MC. Autonomic innervation and segmental muscular disconnections at the human pulmonary vein-atrial junction: implications for catheter ablation of atrial-pulmonary vein junction. J Am Coll Cardiol. 2006;48(1):132–43. https://doi.org/10.1016/j.jacc.2006.02.054.
37. Arora R, Ng J, Ulphani J, Mylonas I, Subacius H, Shade G, et al. Unique autonomic profile of the pulmonary veins and posterior left atrium. J Am Coll Cardiol. 2007;49(12):1340–8. https://doi.org/10.1016/j.jacc.2006.10.075.
38. Chang CM, Wu TJ, Zhou S, Doshi RN, Lee MH, Ohara T, et al. Nerve sprouting and sympathetic hyperinnervation in a canine model of atrial fibrillation produced by prolonged right atrial pacing. Circulation. 2001;103(1):22–5. https://doi.org/10.1161/01.cir.103.1.22.
39. O'Neal WT, Hammadah M, Sandesara PB, Almuwaqqat Z, Samman-Tahhan A, Gafeer MM, et al. The association between acute mental stress and abnormal left atrial electrophysiology. J Cardiovasc Electrophysiol. 2017;28(10):1151–7. https://doi.org/10.1111/jce.13295.
40. Shen MJ, Shinohara T, Park HW, Frick K, Ice DS, Choi EK, et al. Continuous low-level vagus nerve stimulation reduces stellate ganglion nerve activity and paroxysmal atrial tachyarrhythmias in ambulatory canines. Circulation. 2011;123(20):2204–12. https://doi.org/10.1161/circulationaha.111.018028.
41. Sha Y, Scherlag BJ, Yu L, Sheng X, Jackman WM, Lazzara R, et al. Low-level right vagal stimulation: anticholinergic and antiadrenergic effects. J Cardiovasc Electrophysiol. 2011;22(10):1147–53. https://doi.org/10.1111/j.1540-8167.2011.02070.x.
42. Stavrakis S, Humphrey MB, Scherlag B, Iftikhar O, Parwani P, Abbas M, et al. Low-level vagus nerve stimulation suppresses post-operative atrial fibrillation and inflammation: A randomized study. J Am Coll Card Clin Electrophysiol. 2017;3(9):929–38. https://doi.org/10.1016/j.jacep.2017.02.019.
43. Yu WC, Chen SA, Chiang CE, Tai CT, Lee SH, Chiou CW, et al. Effects of isoproterenol in facilitating induction of slow-fast atrioventricular nodal reentrant tachycardia. Am J Cardiol. 1996;78(11):1299–302. https://doi.org/10.1016/s0002-9149(96)00607-8.
44. Manolis AS, Katsaros C, Cokkinos DV. Electrophysiological and electropharmacological studies in pre-excitation syndromes: results with propafenone therapy and isoproterenol infusion testing. Eur Heart J. 1992;13(11):1489–95. https://doi.org/10.1093/oxfordjournals.eurheartj.a060091.
45. Kocovic DZ, Harada T, Shea JB, Soroff D, Friedman PL. Alterations of heart rate and of heart rate

variability after radiofrequency catheter ablation of supraventricular tachycardia. Delineation of parasympathetic pathways in the human heart. Circulation. 1993;88(4 Pt 1):1671–81. https://doi.org/10.1161/01.cir.88.4.1671.

46. Kubuš P, Vít P, Gebauer RA, Materna O, Janoušek J. Electrophysiologic profile and results of invasive risk stratification in asymptomatic children and adolescents with the Wolff-Parkinson-White electrocardiographic pattern. Circ Arrhythm Electrophysiol. 2014;7(2):218–23. https://doi.org/10.1161/circep.113.000930.
47. Aleong RG, Singh SM, Levinson JR, Milan DJ. Catecholamine challenge unmasking high-risk features in the Wolff-Parkinson-White syndrome. Europace. 2009;11(10):1396–8. https://doi.org/10.1093/europace/eup211.
48. Escudero CA, Ceresnak SR, Collins KK, Pass RH, Aziz PF, Blaufox AD, et al. Loss of ventricular preexcitation during noninvasive testing does not exclude high-risk accessory pathways: A multicenter study of WPW in children. Heart Rhythm. 2020;17(10):1729–37. https://doi.org/10.1016/j.hrthm.2020.05.035.
49. Timmermans C, Smeets JL, Rodriguez LM, Vrouchos G, van den Dool A, Wellens HJ. Aborted sudden death in the Wolff-Parkinson-White syndrome. Am J Cardiol. 1995;76(7):492–4. https://doi.org/10.1016/s0002-9149(99)80136-2.
50. Manolis AS, Estes NA 3rd. Reversal of electrophysiologic effects of flecainide on the accessory pathway by isoproterenol in the Wolff-Parkinson-White syndrome. Am J Cardiol. 1989;64(3):194–8. https://doi.org/10.1016/0002-9149(89)90456-6.
51. Polovina MM, Vukicevic M, Banko B, Lip GYH, Potpara TS. Brugada syndrome: A general cardiologist's perspective. Eur J Intern Med. 2017;44:19–27. https://doi.org/10.1016/j.ejim.2017.06.019.
52. Thiene G, Nava A, Corrado D, Rossi L, Pennelli N. Right ventricular cardiomyopathy and sudden death in young people. N Engl J Med. 1988;318(3):129–33. https://doi.org/10.1056/nejm198801213180301.
53. Denis A, Sacher F, Derval N, Martin R, Lim HS, Pambrun T, et al. Arrhythmogenic response to isoproterenol testing vs. exercise testing in arrhythmogenic right ventricular cardiomyopathy patients. Europace. 2018;20(Fi1):f30–f6. https://doi.org/10.1093/europace/euy007.
54. Ruwald A-C, Marcus F, Estes NAM III, Link M, McNitt S, Polonsky B, et al. Association of competitive and recreational sport participation with cardiac events in patients with arrhythmogenic right ventricular cardiomyopathy: results from the North American multidisciplinary study of arrhythmogenic right ventricular cardiomyopathy. Eur Heart J. 2015;36(27):1735–43. https://doi.org/10.1093/eurheartj/ehv110.
55. Arya A, Piorkowski C, Sommer P, Gerds-Li JH, Kottkamp H, Hindricks G. Idiopathic outflow tract tachycardias: current perspectives. Herz. 2007;32(3):218–25. https://doi.org/10.1007/s00059-007-2980-5.
56. Chang HY, Lo LW, Chen YR, Chou YH, Lin WL, Lin YJ, et al. The autonomic neural mechanism of right ventricular outflow tract tachycardia. Auton Neurosci. 2018;212:10–6. https://doi.org/10.1016/j.autneu.2018.03.006.
57. Chiladakis JA, Vassilikos V, Maounis T, Cokkinos DV, Manolis AS. Unusual features of right and left idiopathic ventricular tachycardia abolished by radiofrequency catheter ablation. Pacing Clin Electrophysiol. 1998;21(9):1831–4. https://doi.org/10.1111/j.1540-8159.1998.tb00288.x.
58. Conte G, Caputo ML, Regoli F, Marcon S, Klersy C, Adjibodou B, et al. True idiopathic ventricular fibrillation in out-of-hospital cardiac arrest survivors in the Swiss Canton Ticino: prevalence, clinical features, and long-term follow-up. Europace. 2017;19(2):259–66. https://doi.org/10.1093/europace/euv447.
59. Frontera A, Vlachos K, Kitamura T, Mahida S, Pillois X, Fahy G, et al. Long-term follow-up of idiopathic ventricular fibrillation in a pediatric population: Clinical characteristics, management, and complications. J Am Heart Assoc. 2019;8(9):e011172. https://doi.org/10.1161/jaha.118.011172.
60. Haïssaguerre M, Shoda M, Jaïs P, Nogami A, Shah DC, Kautzner J, et al. Mapping and ablation of idiopathic ventricular fibrillation. Circulation. 2002;106(8):962–7. https://doi.org/10.1161/01.cir.0000027564.55739.b1.
61. Kasanuki H, Ohnishi S, Ohtuka M, Matsuda N, Nirei T, Isogai R, et al. Idiopathic ventricular fibrillation induced with vagal activity in patients without obvious heart disease. Circulation. 1997;95(9):2277–85. https://doi.org/10.1161/01.cir.95.9.2277.
62. Puddu PE, Jouve R, Langlet F, Guillen JC, Lanti M, Reale A. Prevention of postischemic ventricular fibrillation late after right or left stellate ganglionectomy in dogs. Circulation. 1988;77(4):935–46. https://doi.org/10.1161/01.cir.77.4.935.
63. De Ferrari GM, Vanoli E, Curcuruto P, Tommasini G, Schwartz PJ. Prevention of life-threatening arrhythmias by pharmacologic stimulation of the muscarinic receptors with oxotremorine. Am Heart J. 1992;124(4):883–90. https://doi.org/10.1016/0002-8703(92)90968-2.
64. Chen PS, Chen LS, Cao JM, Sharifi B, Karagueuzian HS, Fishbein MC. Sympathetic nerve sprouting, electrical remodeling and the mechanisms of sudden cardiac death. Cardiovasc Res. 2001;50(2):409–16. https://doi.org/10.1016/s0008-6363(00)00308-4.
65. Meng L, Tseng CH, Shivkumar K, Ajijola O. Efficacy of stellate ganglion blockade in managing electrical storm: a systematic review. J Am Coll Card Clin Electrophysiol. 2017;3(9):942–9. https://doi.org/10.1016/j.jacep.2017.06.006.

66. Ben-Menachem E. Vagus-nerve stimulation for the treatment of epilepsy. Lancet Neurol. 2002;1(8):477–82. https://doi.org/10.1016/s1474-4422(02)00220-x.
67. Armour JA. Cardiac neuronal hierarchy in health and disease. Am J Physiol Regul Integr Comp Physiol. 2004;287(2):R262–71. https://doi.org/10.1152/ajpregu.00183.2004.
68. Florea VG, Cohn JN. The autonomic nervous system and heart failure. Circ Res. 2014;114(11):1815–26. https://doi.org/10.1161/circresaha.114.302589.
69. Stavrakis S, Humphrey MB, Scherlag BJ, Hu Y, Jackman WM, Nakagawa H, et al. Low-level transcutaneous electrical vagus nerve stimulation suppresses atrial fibrillation. J Am Coll Cardiol. 2015;65(9):867–75. https://doi.org/10.1016/j.jacc.2014.12.026.
70. Stavrakis S, Stoner JA, Humphrey MB, Morris L, Filiberti A, Reynolds JC, et al. TREAT AF (transcutaneous electrical vagus nerve stimulation to suppress atrial fibrillation): A randomized clinical trial. J Am Coll Card Clin Electrophysiol. 2020;6(3):282–91. https://doi.org/10.1016/j.jacep.2019.11.008.
71. Pokushalov E, Romanov A, Corbucci G, Artyomenko S, Baranova V, Turov A, et al. A randomized comparison of pulmonary vein isolation with versus without concomitant renal artery denervation in patients with refractory symptomatic atrial fibrillation and resistant hypertension. J Am Coll Cardiol. 2012;60(13):1163–70. https://doi.org/10.1016/j.jacc.2012.05.036.
72. Feyz L, Theuns DA, Bhagwandien R, Strachinaru M, Kardys I, Van Mieghem NM, et al. Atrial fibrillation reduction by renal sympathetic denervation: 12 months' results of the AFFORD study. Clin Res Cardiol. 2019;108(6):634–42. https://doi.org/10.1007/s00392-018-1391-3.
73. Steinberg JS, Shabanov V, Ponomarev D, Losik D, Ivanickiy E, Kropotkin E, et al. Effect of renal denervation and catheter ablation vs catheter ablation alone on atrial fibrillation recurrence among patients with paroxysmal atrial fibrillation and hypertension: The ERADICATE-AF randomized clinical trial. J Am Med Ass. 2020;323(3):248–55. https://doi.org/10.1001/jama.2019.21187.
74. Kampaktsis PN, Oikonomou EK, Choi DY, Cheung JW. Efficacy of ganglionated plexi ablation in addition to pulmonary vein isolation for paroxysmal versus persistent atrial fibrillation: a meta-analysis of randomized controlled clinical trials. J Interv Card Electrophysiol. 2017;50(3):253–60. https://doi.org/10.1007/s10840-017-0285-z.
75. Driessen AHG, Berger WR, Krul SPJ, van den Berg NWE, Neefs J, Piersma FR, et al. Ganglion plexus ablation in advanced atrial fibrillation: The AFACT study. J Am Coll Card. 2016;68(11):1155–65. https://doi.org/10.1016/j.jacc.2016.06.036.
76. Pokushalov E, Romanov A, Katritsis DG, Artyomenko S, Shirokova N, Karaskov A, et al. Ganglionated plexus ablation vs linear ablation in patients undergoing pulmonary vein isolation for persistent/long-standing persistent atrial fibrillation: a randomized comparison. Heart Rhythm. 2013;10(9):1280–6. https://doi.org/10.1016/j.hrthm.2013.04.016.
77. Katritsis DG, Giazitzoglou E, Zografos T, Pokushalov E, Po SS, Camm AJ. Rapid pulmonary vein isolation combined with autonomic ganglia modification: a randomized study. Heart Rhythm. 2011;8(5):672–8. https://doi.org/10.1016/j.hrthm.2010.12.047.
78. Katritsis DG, Pokushalov E, Romanov A, Giazitzoglou E, Siontis GC, Po SS, et al. Autonomic denervation added to pulmonary vein isolation for paroxysmal atrial fibrillation: a randomized clinical trial. J Am Coll Card. 2013;62(24):2318–25. https://doi.org/10.1016/j.jacc.2013.06.053.
79. De Ferrari GM, Crijns HJ, Borggrefe M, Milasinovic G, Smid J, Zabel M, et al. Chronic vagus nerve stimulation: a new and promising therapeutic approach for chronic heart failure. Eur Heart J. 2011;32(7):847–55. https://doi.org/10.1093/eurheartj/ehq391.
80. Premchand RK, Sharma K, Mittal S, Monteiro R, Dixit S, Libbus I, et al. Autonomic regulation therapy via left or right cervical vagus nerve stimulation in patients with chronic heart failure: results of the ANTHEM-HF trial. J Card Fail. 2014;20(11):808–16. https://doi.org/10.1016/j.cardfail.2014.08.009.
81. Premchand RK, Sharma K, Mittal S, Monteiro R, Dixit S, Libbus I, et al. Extended follow-up of patients with heart failure receiving autonomic regulation therapy in the ANTHEM-HF study. J Card Fail. 2016;22(8):639–42. https://doi.org/10.1016/j.cardfail.2015.11.002.
82. Gold MR, Van Veldhuisen DJ, Hauptman PJ, Borggrefe M, Kubo SH, Lieberman RA, et al. Vagus nerve stimulation for the treatment of heart failure: The INOVATE-HF trial. J Am Coll Cardiol. 2016;68(2):149–58. https://doi.org/10.1016/j.jacc.2016.03.525.
83. Zannad F, De Ferrari GM, Tuinenburg AE, Wright D, Brugada J, Butter C, et al. Chronic vagal stimulation for the treatment of low ejection fraction heart failure: results of the NEural Cardiac TherApy foR Heart Failure (NECTAR-HF) randomized controlled trial. Eur Heart J. 2015;36(7):425–33. https://doi.org/10.1093/eurheartj/ehu345.
84. Yu L, Huang B, Po SS, Tan T, Wang M, Zhou L, et al. Low-level tragus stimulation for the treatment of ischemia and reperfusion injury in patients with ST-segment elevation myocardial infarction: A proof-of-concept study. J Am Coll Card Cardiovasc Interv. 2017;10(15):1511–20. https://doi.org/10.1016/j.jcin.2017.04.036.
85. Hopper I, Gronda E, Hoppe UC, Rundqvist B, Marwick TH, Shetty S, et al. Sympathetic response

and outcomes following renal denervation in patients with chronic heart failure: 12-Month outcomes from the symplicity HF feasibility study. J Card Fail. 2017;23(9):702–7. https://doi.org/10.1016/j.cardfail.2017.06.004.

86. Tse HF, Turner S, Sanders P, Okuyama Y, Fujiu K, Cheung CW, et al. Thoracic spinal cord stimulation for heart failure as a restorative treatment (SCS HEART study): first-in-man experience. Heart Rhythm. 2015;12(3):588–95. https://doi.org/10.1016/j.hrthm.2014.12.014.
87. Zipes DP, Neuzil P, Theres H, Caraway D, Mann DL, Mannheimer C, et al. Determining the feasibility of spinal cord neuromodulation for the treatment of chronic systolic heart failure: The DEFEAT-HF study. J Am Coll Card Heart Fail. 2016;4(2):129–36. https://doi.org/10.1016/j.jchf.2015.10.006.
88. Abraham WT, Zile MR, Weaver FA, Butter C, Ducharme A, Halbach M, et al. Baroreflex activation therapy for the treatment of heart failure with a reduced ejection fraction. J Am Coll Card Heart Fail. 2015;3(6):487–96. https://doi.org/10.1016/j.jchf.2015.02.006.
89. Zile MR, Lindenfeld J, Weaver FA, Zannad F, Galle E, Rogers T, et al. Baroreflex activation therapy in patients with heart failure with reduced ejection fraction. J Am Coll Card. 2020;76(1):1–13. https://doi.org/10.1016/j.jacc.2020.05.015.
90. Salavatian S, Beaumont E, Longpré JP, Armour JA, Vinet A, Jacquemet V, et al. Vagal stimulation targets select populations of intrinsic cardiac neurons to control neurally induced atrial fibrillation. Am J Physiol Heart Circ Physiol. 2016;311(5):H1311–20. https://doi.org/10.1152/ajpheart.00443.2016.
91. Koopman FA, Chavan SS, Miljko S, Grazio S, Sokolovic S, Schuurman PR, et al. Vagus nerve stimulation inhibits cytokine production and attenuates disease severity in rheumatoid arthritis. Proc Natl Acad Sci USA. 2016;113(29):8284–9. https://doi.org/10.1073/pnas.1605635113.
92. Gomes-Osman J, Indahlastari A, Fried PJ, Cabral DLF, Rice J, Nissim NR, et al. Non-invasive brain stimulation: Probing intracortical circuits and improving cognition in the aging brain. Front Aging Neurosci. 2018;10:177. https://doi.org/10.3389/fnagi.2018.00177.
93. Ashton JL, Burton RAB, Bub G, Smaill BH, Montgomery JM. Synaptic plasticity in cardiac innervation and its potential role in atrial fibrillation. Front Physiol. 2018;9:240. https://doi.org/10.3389/fphys.2018.00240.
94. Ando M, Katare RG, Kakinuma Y, Zhang D, Yamasaki F, Muramoto K, et al. Efferent vagal nerve stimulation protects heart against ischemia-induced arrhythmias by preserving connexin43 protein. Circulation. 2005;112(2):164–70. https://doi.org/10.1161/circulationaha.104.525493.
95. Stavrakis S, Scherlag BJ, Fan Y, Liu Y, Mao J, Varma V, et al. Inhibition of atrial fibrillation by low-level vagus nerve stimulation: the role of the nitric oxide signaling pathway. J Interv Card Electrophysiol. 2013;36(3):199–208. https://doi.org/10.1007/s10840-012-9752-8.
96. Zhou L, Filiberti A, Humphrey MB, Fleming CD, Scherlag BJ, Po SS, et al. Low-level transcutaneous vagus nerve stimulation attenuates cardiac remodelling in a rat model of heart failure with preserved ejection fraction. Exp Physiol. 2019;104(1):28–38. https://doi.org/10.1113/ep087351.
97. Zhang Y, Popovic ZB, Bibevski S, Fakhry I, Sica DA, Van Wagoner DR, et al. Chronic vagus nerve stimulation improves autonomic control and attenuates systemic inflammation and heart failure progression in a canine high-rate pacing model. Circ Heart Fail. 2009;2(6):692–9. https://doi.org/10.1161/circheartfailure.109.873968.
98. Beaumont E, Southerland EM, Hardwick JC, Wright GL, Ryan S, Li Y, et al. Vagus nerve stimulation mitigates intrinsic cardiac neuronal and adverse myocyte remodeling postmyocardial infarction. Am J Physiol Heart Circ Physiol. 2015;309(7):H1198–206. https://doi.org/10.1152/ajpheart.00393.2015.
99. Ardell JL, Foreman RD, Armour JA, Shivkumar K. Cardiac sympathectomy and spinal cord stimulation attenuate reflex-mediated norepinephrine release during ischemia preventing ventricular fibrillation. JCI Insight. 2019;4(23):e131648. https://doi.org/10.1172/jci.insight.131648.
100. Martínez-Milla J, Raposeiras-Roubín S, Pascual-Figal DA, Ibáñez B. Role of beta-blockers in cardiovascular disease in 2019. Rev Esp Cardiol (Engl Ed). 2019;72(10):844–52. https://doi.org/10.1016/j.rec.2019.04.014.
101. Lampert R, Burg MM, Jamner LD, Dziura J, Brandt C, Li F, et al. Effect of β-blockers on triggering of symptomatic atrial fibrillation by anger or stress. Heart Rhythm. 2019;16(8):1167–73. https://doi.org/10.1016/j.hrthm.2019.03.004.
102. Plewan A, Lehmann G, Ndrepepa G, Schreieck J, Alt EU, Schömig A, et al. Maintenance of sinus rhythm after electrical cardioversion of persistent atrial fibrillation; sotalol vs bisoprolol. Eur Heart J. 2001;22(16):1504–10. https://doi.org/10.1053/euhj.2000.2546.
103. Liu L, Nattel S. Differing sympathetic and vagal effects on atrial fibrillation in dogs: role of refractoriness heterogeneity. Am J Physiol. 1997;273(2 Pt 2):H805–16. https://doi.org/10.1152/ajpheart.1997.273.2.H805.
104. Zhang Y, Ilsar I, Sabbah HN, Ben David T, Mazgalev TN. Relationship between right cervical vagus nerve stimulation and atrial fibrillation inducibility: therapeutic intensities do not increase arrhythmogenesis. Heart Rhythm. 2009;6(2):244–50. https://doi.org/10.1016/j.hrthm.2008.10.043.
105. Yu L, Scherlag BJ, Li S, Sheng X, Lu Z, Nakagawa H, et al. Low-level vagosympathetic

nerve stimulation inhibits atrial fibrillation inducibility: direct evidence by neural recordings from intrinsic cardiac ganglia. J Cardiovasc Electrophysiol. 2011;22(4):455–63. https://doi.org/10.1111/j.1540-8167.2010.01908.x.

106. Sheng X, Scherlag BJ, Yu L, Li S, Ali R, Zhang Y, et al. Prevention and reversal of atrial fibrillation inducibility and autonomic remodeling by low-level vagosympathetic nerve stimulation. J Am Coll Cardiol. 2011;57(5):563–71. https://doi.org/10.1016/j.jacc.2010.09.034.
107. Li S, Scherlag BJ, Yu L, Sheng X, Zhang Y, Ali R, et al. Low-level vagosympathetic stimulation: a paradox and potential new modality for the treatment of focal atrial fibrillation. Circ Arrhythm Electrophysiol. 2009;2(6):645–51. https://doi.org/10.1161/circep.109.868331.
108. Chinda K, Tsai WC, Chan YH, Lin AY, Patel J, Zhao Y, et al. Intermittent left cervical vagal nerve stimulation damages the stellate ganglia and reduces the ventricular rate during sustained atrial fibrillation in ambulatory dogs. Heart Rhythm. 2016;13(3):771–80. https://doi.org/10.1016/j.hrthm.2015.11.031.
109. Pavlov VA, Chavan SS, Tracey KJ. Molecular and functional neuroscience in immunity. Annu Rev Immunol. 2018;36:783–812. https://doi.org/10.1146/annurev-immunol-042617-053158.
110. Fallgatter AJ, Neuhauser B, Herrmann MJ, Ehlis AC, Wagener A, Scheuerpflug P, et al. Far field potentials from the brain stem after transcutaneous vagus nerve stimulation. J Neural Transm (Vienna). 2003;110(12):1437–43. https://doi.org/10.1007/s00702-003-0087-6.
111. Yu L, Scherlag BJ, Li S, Fan Y, Dyer J, Male S, et al. Low-level transcutaneous electrical stimulation of the auricular branch of the vagus nerve: a noninvasive approach to treat the initial phase of atrial fibrillation. Heart Rhythm. 2013;10(3):428–35. https://doi.org/10.1016/j.hrthm.2012.11.019.
112. Deuchars SA, Lall VK, Clancy J, Mahadi M, Murray A, Peers L, et al. Mechanisms underpinning sympathetic nervous activity and its modulation using transcutaneous vagus nerve stimulation. Exp Physiol. 2018;103(3):326–31. https://doi.org/10.1113/ep086433.
113. Frangos E, Ellrich J, Komisaruk BR. Non-invasive access to the vagus nerve central projections via electrical stimulation of the external ear: fMRI evidence in humans. Brain Stimul. 2015;8(3):624–36. https://doi.org/10.1016/j.brs.2014.11.018.
114. Verlinden TJ, Rijkers K, Hoogland G, Herrler A. Morphology of the human cervical vagus nerve: implications for vagus nerve stimulation treatment. Acta Neurol Scand. 2016;133(3):173–82. https://doi.org/10.1111/ane.12462.
115. Linz D, Ukena C, Mahfoud F, Neuberger HR, Böhm M. Atrial autonomic innervation: a target for interventional antiarrhythmic therapy? J Am Coll Cardiol. 2014;63(3):215–24. https://doi.org/10.1016/j.jacc.2013.09.020.
116. Linz D, Mahfoud F, Schotten U, Ukena C, Neuberger HR, Wirth K, et al. Renal sympathetic denervation suppresses postapneic blood pressure rises and atrial fibrillation in a model for sleep apnea. Hypertension. 2012;60(1):172–8. https://doi.org/10.1161/hypertensionaha.112.191965.
117. Linz D, van Hunnik A, Hohl M, Mahfoud F, Wolf M, Neuberger HR, et al. Catheter-based renal denervation reduces atrial nerve sprouting and complexity of atrial fibrillation in goats. Circ Arrhythm Electrophysiol. 2015;8(2):466–74. https://doi.org/10.1161/circep.114.002453.
118. Aksu T, Güler TE, Mutluer FO, Oto MA. Vagal denervation in atrial fibrillation ablation: A comprehensive review. Anatol J Cardiol. 2017;18(2):142–8. https://doi.org/10.14744/AnatolJCardiol.2017.7788.
119. Chiou CW, Eble JN, Zipes DP. Efferent vagal innervation of the canine atria and sinus and atrioventricular nodes. The third fat pad. Circulation. 1997;95(11):2573–84. https://doi.org/10.1161/01.cir.95.11.2573.
120. Fadahunsi O, Talabi T, Olowoyeye A, Iluyomade A, Shogbesan O, Donato A. Ablation of complex fractionated atrial electrograms for atrial fibrillation rhythm control: A systematic review and meta-analysis. Can J Cardiol. 2016;32(6):791–802. https://doi.org/10.1016/j.cjca.2015.07.008.
121. You DJ, Chang D, Zhang SL, Yang DH, Gao LJ, Yin XM, et al. Substrate of complex fractionated atrial electrograms: evidence by pathologic analysis. Chin Med J (Engl). 2012;125(24):4393–7.
122. Lin J, Scherlag BJ, Zhou J, Lu Z, Patterson E, Jackman WM, et al. Autonomic mechanism to explain complex fractionated atrial electrograms (CFAE). J Cardiovasc Electrophysiol. 2007;18(11):1197–205. https://doi.org/10.1111/j.1540-8167.2007.00976.x.
123. Qin M, Liu X, Wu SH, Zhang XD. Atrial substrate modification in atrial fibrillation: Targeting GP or CFAE? Evidence from meta-analysis of clinical trials. PLoS One. 2016;11(10):e0164989. https://doi.org/10.1371/journal.pone.0164989.
124. Sakamoto S, Schuessler RB, Lee AM, Aziz A, Lall SC, Damiano RJ Jr. Vagal denervation and reinnervation after ablation of ganglionated plexi. J Thorac Cardiovasc Surg. 2010;139(2):444–52. https://doi.org/10.1016/j.jtcvs.2009.04.056.
125. Jungen C, Scherschel K, Eickholt C, Kuklik P, Klatt N, Bork N, et al. Disruption of cardiac cholinergic neurons enhances susceptibility to ventricular arrhythmias. Nat Commun. 2017;8:14155. https://doi.org/10.1038/ncomms14155.
126. Osman F, Kundu S, Tuan J, Jeilan M, Stafford PJ, Ng GA. Ganglionic plexus ablation during pulmonary vein isolation—predisposing to ventricular arrhythmias? Indian Pacing Electrophysiol J. 2010;10(2):104–7.

127. Kemler MA, de Vet HC, Barendse GA, van den Wildenberg FA, van Kleef M. Spinal cord stimulation for chronic reflex sympathetic dystrophy—five-year follow-up. N Engl J Med. 2006;354(22):2394–6. https://doi.org/10.1056/NEJMc055504.
128. Brodison A, Chauhan A. Spinal-cord stimulation in management of angina. Lancet. 1999;354(9192):1748–9. https://doi.org/10.1016/s0140-6736(99)00296-2.
129. Ardell JL. Heart failure: Mechanisms of spinal cord neuromodulation for heart disease. Nat Rev Cardiol. 2016;13(3):127–8. https://doi.org/10.1038/nrcardio.2016.8.
130. Bernstein SA, Wong B, Vasquez C, Rosenberg SP, Rooke R, Kuznekoff LM, et al. Spinal cord stimulation protects against atrial fibrillation induced by tachypacing. Heart Rhythm. 2012;9(9):1426–33.e3. https://doi.org/10.1016/j.hrthm.2012.04.038.
131. Yu L, Huang B, He W, Wang S, Liao K, Zhou X, et al. Spinal cord stimulation suppresses focal rapid firing-induced atrial fibrillation by inhibiting atrial ganglionated plexus activity. J Cardiovasc Pharmacol. 2014;64(6):554–9. https://doi.org/10.1097/fjc.0000000000000154.
132. Wang S, Zhou X, Huang B, Wang Z, Zhou L, Chen M, et al. Spinal cord stimulation suppresses atrial fibrillation by inhibiting autonomic remodeling. Heart Rhythm. 2016;13(1):274–81. https://doi.org/10.1016/j.hrthm.2015.08.018.
133. Scheffers IJ, Kroon AA, de Leeuw PW. Carotid baroreflex activation: past, present, and future. Curr Hypertens Rep. 2010;12(2):61–6. https://doi.org/10.1007/s11906-009-0087-5.
134. Carlsten A, Folkow B, Grimby G, Hamberger CA, Thulesius O. Cardiovascular effects of direct stimulation of the carotid sinus nerve in man. Acta Physiol Scand. 1958;44(2):138–45. https://doi.org/10.1111/j.1748-1716.1958.tb01615.x.
135. Schwartz SI, Griffith LS, Neistadt A, Hagfors N. Chronic carotid sinus nerve stimulation in the treatment of essential hypertension. Am J Surg. 1967;114(1):5–15. https://doi.org/10.1016/0002-9610(67)90034-7.
136. Mohaupt MG, Schmidli J, Luft FC. Management of uncontrollable hypertension with a carotid sinus stimulation device. Hypertension. 2007;50(5):825–8. https://doi.org/10.1161/hypertensionaha.107.099416.
137. Linz D, Mahfoud F, Schotten U, Ukena C, Neuberger HR, Wirth K, et al. Effects of electrical stimulation of carotid baroreflex and renal denervation on atrial electrophysiology. J Cardiovasc Electrophysiol. 2013;24(9):1028–33. https://doi.org/10.1111/jce.12171.
138. Heusser K, Tank J, Engeli S, Diedrich A, Menne J, Eckert S, et al. Carotid baroreceptor stimulation, sympathetic activity, baroreflex function, and blood pressure in hypertensive patients. Hypertension. 2010;55(3):619–26. https://doi.org/10.1161/hypertensionaha.109.140665.
139. Liao K, Yu L, Zhou X, Saren G, Wang S, Wang Z, et al. Low-level baroreceptor stimulation suppresses atrial fibrillation by inhibiting ganglionated plexus activity. Can J Cardiol. 2015;31(6):767–74. https://doi.org/10.1016/j.cjca.2015.01.007.
140. Dai M, Bao M, Liao J, Yu L, Tang Y, Huang H, et al. Effects of low-level carotid baroreflex stimulation on atrial electrophysiology. J Interv Card Electrophysiol. 2015;43(2):111–9. https://doi.org/10.1007/s10840-015-9976-5.
141. Al-Gobari M, El Khatib C, Pillon F, Gueyffier F. β-Blockers for the prevention of sudden cardiac death in heart failure patients: a meta-analysis of randomized controlled trials. BMC Cardiovasc Disord. 2013;13:52. https://doi.org/10.1186/1471-2261-13-52.
142. Ackerman MJ, Priori SG, Dubin AM, Kowey P, Linker NJ, Slotwiner D, et al. Beta-blocker therapy for long QT syndrome and catecholaminergic polymorphic ventricular tachycardia: Are all beta-blockers equivalent? Heart Rhythm. 2017;14(1):e41–e4. https://doi.org/10.1016/j.hrthm.2016.09.012.
143. Herring N, Kalla M, Paterson DJ. The autonomic nervous system and cardiac arrhythmias: current concepts and emerging therapies. Nat Rev Cardiol. 2019;16(12):707–26. https://doi.org/10.1038/s41569-019-0221-2.
144. Olde Nordkamp LR, Driessen AH, Odero A, Blom NA, Koolbergen DR, Schwartz PJ et al. Left cardiac sympathetic denervation in the Netherlands for the treatment of inherited arrhythmia syndromes. Neth Heart J. 2014;22(4):160-166. doi:https://doi.org/10.1007/s12471-014-0523-2.
145. Collura CA, Johnson JN, Moir C, Ackerman MJ. Left cardiac sympathetic denervation for the treatment of long QT syndrome and catecholaminergic polymorphic ventricular tachycardia using video-assisted thoracic surgery. Heart Rhythm. 2009;6(6):752–9. https://doi.org/10.1016/j.hrthm.2009.03.024.
146. Odero A, Bozzani A, De Ferrari GM, Schwartz PJ. Left cardiac sympathetic denervation for the prevention of life-threatening arrhythmias: the surgical supraclavicular approach to cervicothoracic sympathectomy. Heart Rhythm. 2010;7(8):1161–5. https://doi.org/10.1016/j.hrthm.2010.03.046.
147. Hayase J, Vampola S, Ahadian F, Narayan SM, Krummen DE. Comparative efficacy of stellate ganglion block with bupivacaine vs pulsed radiofrequency in a patient with refractory ventricular arrhythmias. J Clin Anesth. 2016;31:162–5. https://doi.org/10.1016/j.jclinane.2016.01.026.
148. Shah R, Assis F, Alugubelli N, Okada DR, Cardoso R, Shivkumar K, et al. Cardiac sympathetic denervation for refractory ventricular arrhythmias in patients with structural heart disease: A systematic

review. Heart Rhythm. 2019;16(10):1499–505. https://doi.org/10.1016/j.hrthm.2019.06.018.
149. Schwartz PJ, Locati EH, Moss AJ, Crampton RS, Trazzi R, Ruberti U. Left cardiac sympathetic denervation in the therapy of congenital long QT syndrome. A worldwide report. Circulation. 1991;84(2):503–11. https://doi.org/10.1161/01.cir.84.2.503.
150. Schwartz PJ, Priori SG, Cerrone M, Spazzolini C, Odero A, Napolitano C, et al. Left cardiac sympathetic denervation in the management of high-risk patients affected by the long-QT syndrome. Circulation. 2004;109(15):1826–33. https://doi.org/10.1161/01.Cir.0000125523.14403.1e.
151. Priori SG, Wilde AA, Horie M, Cho Y, Behr ER, Berul C, et al. HRS/EHRA/APHRS expert consensus statement on the diagnosis and management of patients with inherited primary arrhythmia syndromes: document endorsed by HRS, EHRA, and APHRS in May 2013 and by ACCF, AHA, PACES, and AEPC in June 2013. Heart Rhythm. 2013;10(12):1932–63. https://doi.org/10.1016/j.hrthm.2013.05.014.
152. Wilde AA, Bhuiyan ZA, Crotti L, Facchini M, De Ferrari GM, Paul T, et al. Left cardiac sympathetic denervation for catecholaminergic polymorphic ventricular tachycardia. N Engl J Med. 2008;358(19):2024–9. https://doi.org/10.1056/NEJMoa0708006.
153. Vaseghi M, Barwad P, Malavassi Corrales FJ, Tandri H, Mathuria N, Shah R, et al. Cardiac sympathetic denervation for refractory ventricular arrhythmias. J Am Coll Cardiol. 2017;69(25):3070–80. https://doi.org/10.1016/j.jacc.2017.04.035.
154. Zipes DP, Rubart M. Neural modulation of cardiac arrhythmias and sudden cardiac death. Heart Rhythm. 2006;3(1):108–13. https://doi.org/10.1016/j.hrthm.2005.09.021.
155. Schwartz PJ, Billman GE, Stone HL. Autonomic mechanisms in ventricular fibrillation induced by myocardial ischemia during exercise in dogs with healed myocardial infarction. An experimental preparation for sudden cardiac death. Circulation. 1984;69(4):790–800. https://doi.org/10.1161/01.cir.69.4.790.
156. Martins JB, Zipes DP, Lund DD. Distribution of local repolarization changes produced by efferent vagal stimulation in the canine ventricles. J Am Coll Cardiol. 1983;2(6):1191–9. https://doi.org/10.1016/s0735-1097(83)80350-7.
157. Litovsky SH, Antzelevitch C. Differences in the electrophysiological response of canine ventricular subendocardium and subepicardium to acetylcholine and isoproterenol. A direct effect of acetylcholine in ventricular myocardium. Circ Res. 1990;67(3):615–27. https://doi.org/10.1161/01.res.67.3.615.
158. Ng GA, Brack KE, Patel VH, Coote JH. Autonomic modulation of electrical restitution, alternans and ventricular fibrillation initiation in the isolated heart. Cardiovasc Res. 2007;73(4):750–60. https://doi.org/10.1016/j.cardiores.2006.12.001.
159. Brack KE, Patel VH, Mantravardi R, Coote JH, Ng GA. Direct evidence of nitric oxide release from neuronal nitric oxide synthase activation in the left ventricle as a result of cervical vagus nerve stimulation. J Physiol. 2009;587(Pt 12):3045–54. https://doi.org/10.1113/jphysiol.2009.169417.
160. Wang Z, Yu L, Wang S, Huang B, Liao K, Saren G, et al. Chronic intermittent low-level transcutaneous electrical stimulation of auricular branch of vagus nerve improves left ventricular remodeling in conscious dogs with healed myocardial infarction. Circ Heart Fail. 2014;7(6):1014–21. https://doi.org/10.1161/circheartfailure.114.001564.
161. Vanoli E, De Ferrari GM, Stramba-Badiale M, Hull SS Jr, Foreman RD, Schwartz PJ. Vagal stimulation and prevention of sudden death in conscious dogs with a healed myocardial infarction. Circ Res. 1991;68(5):1471–81. https://doi.org/10.1161/01.res.68.5.1471.
162. Ardell JL, Nier H, Hammer M, Southerland EM, Ardell CL, Beaumont E, et al. Defining the neural fulcrum for chronic vagus nerve stimulation: implications for integrated cardiac control. J Physiol. 2017;595(22):6887–903. https://doi.org/10.1113/jp274678.
163. Konstam MA, Udelson JE, Butler J, Klein HU, Parker JD, Teerlink JR, et al. Impact of autonomic regulation therapy in patients with heart failure: ANTHEM-HFrEF pivotal study design. Circ Heart Fail. 2019;12(11):e005879. https://doi.org/10.1161/circheartfailure.119.005879.
164. Ben-Menachem E. Vagus nerve stimulation, side effects, and long-term safety. J Clin Neurophysiol. 2001;18(5):415–8. https://doi.org/10.1097/00004691-200109000-00005.
165. Spuck S, Tronnier V, Orosz I, Schönweiler R, Sepehrnia A, Nowak G, et al. Operative and technical complications of vagus nerve stimulator implantation. Neurosurgery. 2010;67(2 suppl operative):489–94. https://doi.org/10.1227/NEU.0b013e3181f88867.
166. Yu L, Wang S, Zhou X, Wang Z, Huang B, Liao K, et al. Chronic intermittent low-level stimulation of tragus reduces cardiac autonomic remodeling and ventricular arrhythmia inducibility in a post-infarction canine model. J Am Coll Card Clin Electrophysiol. 2016;2(3):330–9. https://doi.org/10.1016/j.jacep.2015.11.006.
167. Böhm M, Ewen S, Linz D, Reil JC, Schirmer SH, Ukena C, et al. Therapeutic potential of renal sympathetic denervation in patients with chronic heart failure. EuroIntervention. 2013;9 Suppl R:R122–6. https://doi.org/10.4244/eijv9sra21.
168. Remo BF, Preminger M, Bradfield J, Mittal S, Boyle N, Gupta A, et al. Safety and efficacy of renal denervation as a novel treatment of ventricular tachycardia storm in patients with cardiomyopathy. Heart Rhythm. 2014;11(4):541–6. https://doi.org/10.1016/j.hrthm.2013.12.038.

169. Bradfield JS, Hayase J, Liu K, Moriarty J, Kee ST, Do D, et al. Renal denervation as adjunctive therapy to cardiac sympathetic denervation for ablation refractory ventricular tachycardia. Heart Rhythm. 2020;17(2):220–7. https://doi.org/10.1016/j.hrthm.2019.09.016.
170. Southerland EM, Milhorn DM, Foreman RD, Linderoth B, DeJongste MJ, Armour JA, et al. Preemptive, but not reactive, spinal cord stimulation mitigates transient ischemia-induced myocardial infarction via cardiac adrenergic neurons. Am J Physiol Heart Circ Physiol. 2007;292(1):H311–7. https://doi.org/10.1152/ajpheart.00087.2006.
171. Issa ZF, Zhou X, Ujhelyi MR, Rosenberger J, Bhakta D, Groh WJ, et al. Thoracic spinal cord stimulation reduces the risk of ischemic ventricular arrhythmias in a postinfarction heart failure canine model. Circulation. 2005;111(24):3217–20. https://doi.org/10.1161/circulationaha.104.507897.
172. Lopshire JC, Zhou X, Dusa C, Ueyama T, Rosenberger J, Courtney N, et al. Spinal cord stimulation improves ventricular function and reduces ventricular arrhythmias in a canine postinfarction heart failure model. Circulation. 2009;120(4):286–94. https://doi.org/10.1161/circulationaha.108.812412.
173. Grimaldi R, de Luca A, Kornet L, Castagno D, Gaita F. Can spinal cord stimulation reduce ventricular arrhythmias? Heart Rhythm. 2012;9(11):1884–7. https://doi.org/10.1016/j.hrthm.2012.08.007.
174. Liao K, Yu L, He B, Huang B, Yang K, Saren G, et al. Carotid baroreceptor stimulation prevents arrhythmias induced by acute myocardial infarction through autonomic modulation. J Cardiovasc Pharmacol. 2014;64(5):431–7. https://doi.org/10.1097/fjc.0000000000000135.
175. Liao K, Yu L, Yang K, Saren G, Wang S, Huang B, et al. Low-level carotid baroreceptor stimulation suppresses ventricular arrhythmias during acute ischemia. PLoS One. 2014;9(10):e109313. https://doi.org/10.1371/journal.pone.0109313.
176. Sabbah HN, Gupta RC, Imai M, Irwin ED, Rastogi S, Rossing MA, et al. Chronic electrical stimulation of the carotid sinus baroreflex improves left ventricular function and promotes reversal of ventricular remodeling in dogs with advanced heart failure. Circ Heart Fail. 2011;4(1):65–70. https://doi.org/10.1161/circheartfailure.110.955013.
177. Zucker IH, Hackley JF, Cornish KG, Hiser BA, Anderson NR, Kieval R, et al. Chronic baroreceptor activation enhances survival in dogs with pacing-induced heart failure. Hypertension. 2007;50(5):904–10. https://doi.org/10.1161/hypertensionaha.107.095216.
178. Gronda E, Seravalle G, Brambilla G, Costantino G, Casini A, Alsheraei A, et al. Chronic baroreflex activation effects on sympathetic nerve traffic, baroreflex function, and cardiac haemodynamics in heart failure: a proof-of-concept study. Eur J Heart Fail. 2014;16(9):977–83. https://doi.org/10.1002/ejhf.138.
179. Musialek P, Casadei B. Nitrovasodilators and heart rate: more than the arterial baroreflex. Cardiovasc. Res. 2000;47(2):404–5.
180. Casadei B, Paterson DJ. Should we still use nitrovasodilators to test baroreflex sensitivity? J Hyperten. 2000;18(1):3–6.
181. Parati G, Di Rienzo M, Mancia G. How to measure baroreflex sensitivity: from the cardiovascular laboratory to daily life. J Hyperten. 2000;18(1):7–19.
182. Schwartz PJ, Vanoli E, Stramba-Badiale M, De Ferrari GM, Billman GE, Foreman RD. Autonomic mechanisms and sudden death. New insights from analysis of baroreceptor reflexes in conscious dogs with and without a myocardial infarction. Circulation. 1988;78(4):969–79.
183. Taggart P, Sutton P, Chalabi Z, Boyett MR, Simon R, Elliott D, et al. Effect of adrenergic stimulation on action potential duration restitution in humans. Circulation. 2003;107(2):285–9.
184. Schwartz PJ, Zaza A, Pala M, Locati E, Beria G, Zanchetti A. Baroreflex sensitivity and its evolution during the first year after myocardial infarction. J Am Coll Card. 1988;12(3):629–36.
185. La Rovere MT, Bigger JT Jr, Marcus FI, Mortara A, Schwartz PJ. Baroreflex sensitivity and heart-rate variability in prediction of total cardiac mortality after myocardial infarction. ATRAMI (Autonomic Tone and Reflexes After Myocardial Infarction) Investigators. Lancet. 1998;351(9101):478–84.
186. Paleczny B, Olesińska-Mader M, Siennicka A, Niewiński P, Nowak K, Buldańczyk A, et al. Assessment of baroreflex sensitivity has no prognostic value in contemporary, optimally managed patients with mild-to-moderate heart failure with reduced ejection fraction: a retrospective analysis of 5-year survival. Eur J Heart Fail. 2019;21(1):50–8. https://doi.org/10.1002/ejhf.1306.
187. Schwab JO, Eichner G, Schmitt H, Weber S, Coch M, Waldecker B. The relative contribution of the sinus and AV node to heart rate variability. Heart. 2003;89(3):337–8. https://doi.org/10.1136/heart.89.3.337.
188. Stauss HM. Heart rate variability. Am J Physiol Regul Integr Comp Physiol. 2003;285(5):R927–31. https://doi.org/10.1152/ajpregu.00452.2003.
189. Heart rate variability: standards of measurement, physiological interpretation and clinical use. Task Force of the European Society of Cardiology and the North American Society of Pacing and Electrophysiology. Circulation. 1996;93(5):1043–65.
190. Koizumi K, Terui N, Kollai M. Effect of cardiac vagal and sympathetic nerve activity on heart rate in rhythmic fluctuations. J Auton Nerv Syst. 1985;12(2-3):251–9. https://doi.org/10.1016/0165-1838(85)90065-7.
191. Kleiger RE, Stein PK, Bigger JT Jr. Heart rate variability: measurement and clinical utility. Ann Noninvasive Electrocardiol. 2005;10(1):88–101. https://doi.org/10.1111/j.1542-474X.2005.10101.x.

192. Shaffer F, McCraty R, Zerr CL. A healthy heart is not a metronome: an integrative review of the heart's anatomy and heart rate variability. Front Psychol. 2014;5:1040. https://doi.org/10.3389/fpsyg.2014.01040.
193. Zulfiqar U, Jurivich DA, Gao W, Singer DH. Relation of high heart rate variability to healthy longevity. Am J Cardiol. 2010;105(8):1181–5. https://doi.org/10.1016/j.amjcard.2009.12.022.
194. Umetani K, Singer DH, McCraty R, Atkinson M. Twenty-four hour time domain heart rate variability and heart rate: relations to age and gender over nine decades. J Am Coll Cardiol. 1998;31(3):593–601. https://doi.org/10.1016/s0735-1097(97)00554-8.
195. Akselrod S, Gordon D, Ubel FA, Shannon DC, Berger AC, Cohen RJ. Power spectrum analysis of heart rate fluctuation: a quantitative probe of beat-to-beat cardiovascular control. Science. 1981;213(4504):220–2. https://doi.org/10.1126/science.6166045.
196. Butler GC, Ando S, Floras JS. Fractal component of variability of heart rate and systolic blood pressure in congestive heart failure. Clinical science. 1997;92(6):543–50.
197. Hull SS Jr, Evans AR, Vanoli E, Adamson PB, Stramba-Badiale M, Albert DE, et al. Heart rate variability before and after myocardial infarction in conscious dogs at high and low risk of sudden death. J Am Coll Card. 1990;16(4):978–85.
198. Adamson PB, Huang MH, Vanoli E, Foreman RD, Schwartz PJ, Hull SS Jr. Unexpected interaction between beta-adrenergic blockade and heart rate variability before and after myocardial infarction. A longitudinal study in dogs at high and low risk for sudden death. Circulation. 1994;90(2):976–82.
199. Farrell TG, Bashir Y, Cripps T, Malik M, Poloniecki J, Bennett ED, et al. Risk stratification for arrhythmic events in postinfarction patients based on heart rate variability, ambulatory electrocardiographic variables and the signal-averaged electrocardiogram. J Am Coll Card. 1991;18(3):687–97.
200. Kleiger RE, Miller JP, Bigger JT Jr, Moss AJ. Decreased heart rate variability and its association with increased mortality after acute myocardial infarction. Am J Card. 1987;59(4):256–62.
201. Odemuyiwa O, Poloniecki J, Malik M, Farrell T, Xia R, Staunton A, et al. Temporal influences on the prediction of postinfarction mortality by heart rate variability: a comparison with the left ventricular ejection fraction. Br Heart J. 1994;71(6):521–7.
202. Lanza GA, Bendini MG, Intini A, De Martino G, Galeazzi M, Guido V, et al. Prognostic role of heart rate variability in patients with idiopathic dilated cardiomyopathy. Ital Heart J. 2000;1(1):56–63.
203. Hoffmann J, Grimm W, Menz V, Knop U, Maisch B. Heart rate variability and major arrhythmic events in patients with idiopathic dilated cardiomyopathy. Pacing Clin Electrophysiol PACE. 1996;19(11 Pt 2):1841–4.
204. Pagani M, Lombardi F, Guzzetti S, Sandrone G, Rimoldi O, Malfatto G, et al. Power spectral density of heart rate variability as an index of sympatho-vagal interaction in normal and hypertensive subjects. J Hypertens Suppl. 1984;2(3):S383–5.
205. Vanninen E, Tuunainen A, Kansanen M, Uusitupa M, Länsimies E. Cardiac sympathovagal balance during sleep apnea episodes. Clin Physiol. 1996;16(3):209–16. https://doi.org/10.1111/j.1475-097x.1996.tb00569.x.
206. Billman GE. The LF/HF ratio does not accurately measure cardiac sympatho-vagal balance. Front Physiol. 2013;4:26. https://doi.org/10.3389/fphys.2013.00026.
207. Voss A, Fischer C, Schroeder R, Figulla HR, Goernig M. Segmented Poincaré plot analysis for risk stratification in patients with dilated cardiomyopathy. Methods Inf Med. 2010;49(5):511–5. https://doi.org/10.3414/me09-02-0050.
208. Libbus I, Nearing BD, Amurthur B, KenKnight BH, Verrier RL. Quantitative evaluation of heartbeat interval time series using Poincaré analysis reveals distinct patterns of heart rate dynamics during cycles of vagus nerve stimulation in patients with heart failure. J Electrocardiol. 2017;50(6):898–903. https://doi.org/10.1016/j.jelectrocard.2017.06.007.
209. Brennan M, Palaniswami M, Kamen P. Do existing measures of Poincaré plot geometry reflect nonlinear features of heart rate variability? IEEE Trans Biomed Eng. 2001;48(11):1342–7. https://doi.org/10.1109/10.959330.
210. Beckers F, Ramaekers D, Aubert AE. Approximate entropy of heart rate variability: validation of methods and application in heart failure. Cardiovasc Eng. 2001;1(4):177–82. https://doi.org/10.1023/A:1015212328405.
211. Merati G, Di Rienzo M, Parati G, Veicsteinas A, Castiglioni P. Assessment of the autonomic control of heart rate variability in healthy and spinal-cord injured subjects: contribution of different complexity-based estimators. IEEE Trans Biomed Eng. 2006;53(1):43–52. https://doi.org/10.1109/tbme.2005.859786.
212. Nakajo M, Shapiro B, Glowniak J, Sisson JC, Beierwaltes WH. Inverse relationship between cardiac accumulation of meta-[131I] iodobenzylguanidine (I-131 MIBG) and circulating catecholamines in suspected pheochromocytoma. J Nucl Med. 1983;24(12):1127–34.
213. Degrado TR, Zalutsky MR, Vaidyanathan G. Uptake mechanisms of meta-[123I]iodobenzylguanidine in isolated rat heart. Nucl Med Biol. 1995;22(1):1–12.
214. Dae MW, O'Connell JW, Botvinick EH, Chin MC. Acute and chronic effects of transient myocardial ischemia on sympathetic nerve activity, density, and norepinephrine content. Cardiovasc Res. 1995;30(2):270–80.

215. Narula J, Sarkar K. A conceptual paradox of MIBG uptake in heart failure: retention with incontinence! J Nucl Card. 2003;10(6):700–4. https://doi.org/10.1016/j.nuclcard.2003.09.006.
216. Verberne HJ, Brewster LM, Somsen GA, van Eck-Smit BL. Prognostic value of myocardial 123I-metaiodobenzylguanidine (MIBG) parameters in patients with heart failure: a systematic review. Eur Heart J. 2008;29(9):1147–59. https://doi.org/10.1093/eurheartj/ehn113.
217. Kasama S, Toyama T, Sumino H, Kumakura H, Takayama Y, Minami K, et al. Prognostic value of cardiac sympathetic nerve activity evaluated by [123I]m-iodobenzylguanidine imaging in patients with ST-segment elevation myocardial infarction. Heart. 2011;97(1):20–6. https://doi.org/10.1136/hrt.2010.204149.
218. Boogers MJ, Borleffs CJ, Henneman MM, van Bommel RJ, van Ramshorst J, Boersma E, et al. Cardiac sympathetic denervation assessed with 123-iodine metaiodobenzylguanidine imaging predicts ventricular arrhythmias in implantable cardioverter-defibrillator patients. J Am Coll Card. 2010;55(24):2769–77. https://doi.org/10.1016/j.jacc.2009.12.066.
219. Bax JJ, Kraft O, Buxton AE, Fjeld JG, Parizek P, Agostini D, et al. 123 I-mIBG scintigraphy to predict inducibility of ventricular arrhythmias on cardiac electrophysiology testing: a prospective multicenter pilot study. Circ Cardiovasc Imag. 2008;1(2):131–40. https://doi.org/10.1161/CIRCIMAGING.108.782433.
220. Tamaki S, Yamada T, Okuyama Y, Morita T, Sanada S, Tsukamoto Y, et al. Cardiac iodine-123 metaiodobenzylguanidine imaging predicts sudden cardiac death independently of left ventricular ejection fraction in patients with chronic heart failure and left ventricular systolic dysfunction: results from a comparative study with signal-averaged electrocardiogram, heart rate variability, and QT dispersion. JACC. 2009;53(5):426–35. https://doi.org/10.1016/j.jacc.2008.10.025.
221. Kuramoto Y, Yamada T, Tamaki S, Okuyama Y, Morita T, Furukawa Y, et al. Usefulness of cardiac iodine-123 meta-iodobenzylguanidine imaging to improve prognostic power of Seattle heart failure model in patients with chronic heart failure. J Am Coll Card. 2011;107(8):1185–90. https://doi.org/10.1016/j.amjcard.2010.12.019.
222. Kioka H, Yamada T, Mine T, Morita T, Tsukamoto Y, Tamaki S, et al. Prediction of sudden death in patients with mild-to-moderate chronic heart failure by using cardiac iodine-123 metaiodobenzylguanidine imaging. Heart. 2007;93(10):1213–8. https://doi.org/10.1136/hrt.2006.094524.
223. Jacobson AF, Lombard J, Banerjee G, Camici PG. 123I-mIBG scintigraphy to predict risk for adverse cardiac outcomes in heart failure patients: design of two prospective multicenter international trials. J Nucl Card. 2009;16(1):113–21. https://doi.org/10.1007/s12350-008-9008-2.
224. Mitrani RD, Klein LS, Miles WM, Hackett FK, Burt RW, Wellman HN, et al. Regional cardiac sympathetic denervation in patients with ventricular tachycardia in the absence of coronary artery disease. J Am Coll Cardiol. 1993;22(5):1344–53. https://doi.org/10.1016/0735-1097(93)90541-8.
225. Stirrup J, Gregg S, Baavour R, Roth N, Breault C, Agostini D, et al. Hybrid solid-state SPECT/CT left atrial innervation imaging for identification of left atrial ganglionated plexi: Technique and validation in patients with atrial fibrillation. J Nucl Cardiol. 2020;27(6):1939–50. https://doi.org/10.1007/s12350-018-01535-5.
226. Foley KF, Van Dort ME, Sievert MK, Ruoho AE, Cozzi NV. Stereospecific inhibition of monoamine uptake transporters by meta-hydroxyephedrine isomers. J Neural Trans. 2002;109(10):1229–40. https://doi.org/10.1007/s00702-002-0695-6.
227. Tipre DN, Fox JJ, Holt DP, Green G, Yu J, Pomper M, et al. In vivo PET imaging of cardiac presynaptic sympathoneuronal mechanisms in the rat. J Nucl Med. 2008;49(7):1189–95. https://doi.org/10.2967/jnumed.107.050252.
228. Thackeray JT, Renaud JM, Kordos M, Klein R, Dekemp RA, Beanlands RS, et al. Test-retest repeatability of quantitative cardiac 11C-meta-hydroxyephedrine measurements in rats by small animal positron emission tomography. Nucl Med Biol. 2013;40(5):676–81. https://doi.org/10.1016/j.nucmedbio.2013.03.007.
229. Thackeray JT, Beanlands RS, Dasilva JN. Presence of specific 11C-meta-Hydroxyephedrine retention in heart, lung, pancreas, and brown adipose tissue. J Nucl Med. 2007;48(10):1733–40. https://doi.org/10.2967/jnumed.107.043570.
230. Rosenspire KC, Haka MS, Van Dort ME, Jewett DM, Gildersleeve DL, Schwaiger M, et al. Synthesis and preliminary evaluation of carbon-11-meta-hydroxyephedrine: a false transmitter agent for heart neuronal imaging. J Nucl Med. 1990;31(8):1328–34.
231. Law MP, Schafers K, Kopka K, Wagner S, Schober O, Schafers M. Molecular imaging of cardiac sympathetic innervation by 11C-mHED and PET: from man to mouse? J Nucl Med. 2010;51(8):1269–76. https://doi.org/10.2967/jnumed.110.074997.
232. Law MP, Osman S, Davenport RJ, Cunningham VJ, Pike VW, Camici PG. Biodistribution and metabolism of [N-methyl-11C]m-hydroxyephedrine in the rat. Nucl Med Biol. 1997;24(5):417–24.
233. Link JM, Synovec RE, Krohn KA, Caldwell JH. High speed liquid chromatography of phenylethanolamines for the kinetic analysis of [11C]-meta-hydroxyephedrine and metabolites in plasma. J Chromat B, Biomed Sc App. 1997;693(1):31–41.

234. Wallin BG, Fagius J. Peripheral sympathetic neural activity in conscious humans. Ann Rev Physiol. 1988;50:565–76. https://doi.org/10.1146/annurev.ph.50.030188.003025.
235. Elam M, Macefield V. Multiple firing of single muscle vasoconstrictor neurons during cardiac dysrhythmias in human heart failure. J Appl Physiol. 2001;91(2):717–24.
236. Bernardi L, Spallone V, Stevens M, Hilsted J, Frontoni S, Pop-Busui R, et al. Methods of investigation for cardiac autonomic dysfunction in human research studies. Diabetes Metab Res Rev. 2011;27(7):654–64. https://doi.org/10.1002/dmrr.1224.
237. Goldberger JJ, Arora R, Buckley U, Shivkumar K. Autonomic nervous system dysfunction: JACC focus seminar. J Am Coll Card. 2019;73(10):1189–206. https://doi.org/10.1016/j.jacc.2018.12.064.
238. Wallin BG, Thompson JM, Jennings GL, Esler MD. Renal noradrenaline spillover correlates with muscle sympathetic activity in humans. J Physiol. 1996;491(Pt 3):881–7.
239. Wallin BG, Esler M, Dorward P, Eisenhofer G, Ferrier C, Westerman R, et al. Simultaneous measurements of cardiac noradrenaline spillover and sympathetic outflow to skeletal muscle in humans. J Physiol. 1992;453:45–58.
240. Rundqvist B, Elam M, Bergmann-Sverrisdottir Y, Eisenhofer G, Friberg P. Increased cardiac adrenergic drive precedes generalized sympathetic activation in human heart failure. Circulation. 1997;95(1):169–75.
241. Najem B, Unger P, Preumont N, Jansens JL, Houssière A, Pathak A, et al. Sympathetic control after cardiac resynchronization therapy: responders versus nonresponders. Am J Physiol Heart Circ Physiol. 2006;291(6):H2647–52. https://doi.org/10.1152/ajpheart.00373.2006.
242. Doytchinova A, Hassel JL, Yuan Y, Lin H, Yin D, Adams D, et al. Simultaneous noninvasive recording of skin sympathetic nerve activity and electrocardiogram. Heart Rhythm. 2017;14(1):25–33. https://doi.org/10.1016/j.hrthm.2016.09.019.
243. Jiang Z, Zhao Y, Doytchinova A, Kamp NJ, Tsai WC, Yuan Y, et al. Using skin sympathetic nerve activity to estimate stellate ganglion nerve activity in dogs. Heart Rhythm. 2015;12(6):1324–32. https://doi.org/10.1016/j.hrthm.2015.02.012.
244. Uradu A, Wan J, Doytchinova A, Wright KC, Lin AYT, Chen LS, et al. Skin sympathetic nerve activity precedes the onset and termination of paroxysmal atrial tachycardia and fibrillation. Heart Rhythm. 2017;14(7):964–71. https://doi.org/10.1016/j.hrthm.2017.03.030.
245. Kusayama T, Wan J, Doytchinova A, Wong J, Kabir RA, Mitscher G, et al. Skin sympathetic nerve activity and the temporal clustering of cardiac arrhythmias. JCI Insight. 2019;4(4):e125853. https://doi.org/10.1172/jci.insight.125853.
246. Shusterman V, McTiernan CF, Goldberg A, Saba S, Salama G, London B. Adrenergic stimulation promotes T-wave alternans and arrhythmia inducibility in a TNF-alpha genetic mouse model of congestive heart failure. Am J Physiol Heart Circ Physiol. 2010;298(2):H440–50. https://doi.org/10.1152/ajpheart.01024.2008.
247. Verrier RL, Antzelevitch C. Autonomic aspects of arrhythmogenesis: the enduring and the new. Curr Opin Cardiol. 2004;19(1):2–11. https://doi.org/10.1097/00001573-200401000-00003.
248. Lampert R, Shusterman V, Burg MM, Lee FA, Earley C, Goldberg A, et al. Effects of psychologic stress on repolarization and relationship to autonomic and hemodynamic factors. J Cardiovasc Electrophysiol. 2005;16(4):372–7. https://doi.org/10.1046/j.1540-8167.2005.40580.x.
249. Rashba EJ, Cooklin M, MacMurdy K, Kavesh N, Kirk M, Sarang S, et al. Effects of selective autonomic blockade on T-wave alternans in humans. Circulation. 2002;105(7):837–42. https://doi.org/10.1161/hc0702.104127.
250. Klingenheben T, Grönefeld G, Li YG, Hohnloser SH. Effect of metoprolol and d,l-sotalol on microvolt-level T-wave alternans. Results of a prospective, double-blind, randomized study. J Am Coll Card. 2001;38(7):2013–9. https://doi.org/10.1016/s0735-1097(01)01661-8.
251. Katritsis D, Merchant FM, Mela T, Singh JP, Heist EK, Armoundas AA. Catheter ablation of atrial fibrillation the search for substrate-driven end points. J Am Coll Card. 2010;55(21):2293–8. https://doi.org/10.1016/j.jacc.2010.03.016.
252. Smith JM, Rosenbaum DS, Cohen RJ. Variability in surface ECG morphology: signal or noise? Comput Cardiol. 1988;14:257–60.
253. Rosenbaum DS, Jackson LE, Smith JM, Garan H, Ruskin JN, Cohen RJ. Electrical alternans and vulnerability to ventricular arrhythmias. N Engl J Med. 1994;330(4):235–41. https://doi.org/10.1056/nejm199401273300402.
254. Stavrakis S, Kulkarni K, Singh JP, Katritsis DG, Armoundas AA. Autonomic modulation of cardiac arrhythmias: methods to assess treatment and outcomes. J Am Coll Card Clin Electrophysiol. 2020;6(5):467–83. https://doi.org/10.1016/j.jacep.2020.02.014.
255. Byku M, Mann DL. Neuromodulation of the failing heart: lost in translation? J Am Coll Card Basic Transl Sci. 2016;1(3):95–106. https://doi.org/10.1016/j.jacbts.2016.03.004.
256. Clancy JA, Mary DA, Witte KK, Greenwood JP, Deuchars SA, Deuchars J. Non-invasive vagus nerve stimulation in healthy humans reduces sympathetic nerve activity. Brain Stimul. 2014;7(6):871–7. https://doi.org/10.1016/j.brs.2014.07.031.
257. Tran N, Asad Z, Elkholey K, Scherlag BJ, Po SS, Stavrakis S. Autonomic neuromodulation acutely ameliorates left ventricular strain in humans. J

Cardiovasc Transl Res. 2019;12(3):221–30. https://doi.org/10.1007/s12265-018-9853-6.

258. Scherschel K, Hedenus K, Jungen C, Lemoine MD, Rübsamen N, Veldkamp MW, et al. Cardiac glial cells release neurotrophic S100B upon catheter-based treatment of atrial fibrillation. Sci Transl Med. 2019;11(493):eaav7770. https://doi.org/10.1126/scitranslmed.aav7770.
259. Scherschel K, Hedenus K, Jungen C, Münkler P, Willems S, Anwar O, et al. Impact of the ablation technique on release of the neuronal injury marker S100B during pulmonary vein isolation. Europace. 2020;22(10):1502–8. https://doi.org/10.1093/europace/euaa159.
260. Deisseroth K. Optogenetics: 10 years of microbial opsins in neuroscience. Nat Neurosci. 2015;18(9):1213–25. https://doi.org/10.1038/nn.4091.
261. Ambrosi CM, Klimas A, Yu J, Entcheva E. Cardiac applications of optogenetics. Prog Biophys Mol Biol. 2014;115(2-3):294–304. https://doi.org/10.1016/j.pbiomolbio.2014.07.001.
262. Chow BY, Han X, Dobry AS, Qian X, Chuong AS, Li M, et al. High-performance genetically targetable optical neural silencing by light-driven proton pumps. Nature. 2010;463(7277):98–102. https://doi.org/10.1038/nature08652.
263. Konermann S, Brigham MD, Trevino A, Hsu PD, Heidenreich M, Cong L, et al. Optical control of mammalian endogenous transcription and epigenetic states. Nature. 2013;500(7463):472–6. https://doi.org/10.1038/nature12466.
264. Yu L, Zhou L, Cao G, Po SS, Huang B, Zhou X, et al. Optogenetic modulation of cardiac sympathetic nerve activity to prevent ventricular arrhythmias. J Am Coll Card. 2017;70(22):2778–90. https://doi.org/10.1016/j.jacc.2017.09.1107.
265. McClintock SM, Reti IM, Carpenter LL, McDonald WM, Dubin M, Taylor SF, et al. Consensus recommendations for the clinical application of repetitive transcranial magnetic stimulation (rTMS) in the treatment of depression. J Clin Psychiatry. 2018;79(1):16cs10905. https://doi.org/10.4088/JCP.16cs10905.
266. Repetitive transcranial magnetic stimulation for treatment-resistant depression: A systematic review and meta-analysis of randomized controlled trials. Ont Health Technol Assess Ser. 2016;16(5):1–66.
267. Yu L, Dyer JW, Scherlag BJ, Stavrakis S, Sha Y, Sheng X, et al. The use of low-level electromagnetic fields to suppress atrial fibrillation. Heart Rhythm. 2015;12(4):809–17. https://doi.org/10.1016/j.hrthm.2014.12.022.
268. Wang S, Zhou X, Huang B, Wang Z, Zhou L, Wang M, et al. Noninvasive low-frequency electromagnetic stimulation of the left stellate ganglion reduces myocardial infarction-induced ventricular arrhythmia. Sci Rep. 2016;6:30783. https://doi.org/10.1038/srep30783.
269. Markman TM, Hamilton RH, Marchlinski FE, Nazarian S. Case series of transcutaneous magnetic stimulation for ventricular Tachycardia Storm. J Am Med Ass. 2020;323(21):2200–2. https://doi.org/10.1001/jama.2020.3833.

Part III

Role of Specific Channels and Subcellular Structures in Arrhythmia

L-Type Ca^{2+} Channels and Cardiac Arrhythmias

10

Elza Kuzmenkina, Sarah Salamon, Patrick Despang,
and Jan Matthes

Abstract

L-type Ca^{2+} channels (LTCC) are voltage-gated Ca^{2+} channels with particular importance for cardiac function. They mediate Ca^{2+}-induced Ca^{2+} release from the sarcoplasmic reticulum and thus are essential for excitation–contraction coupling. Furthermore, LTCCs play a key role in pacemaker and conductive tissue. Taken together, it is not surprising that LTCCs are associated with cardiac arrhythmias. The members of the family of voltage-gated Ca^{2+} channels differ in coding genes, expression pattern, and physiological as well as pharmacological properties. Cardiac LTCCs are defined by the pore-forming subunits $Ca_V1.2$ and $Ca_V1.3$, respectively. The expression and function of LTCCs is modulated by auxiliary $Ca_V\beta$ and $Ca_V\alpha_2$-δ subunits, which are also encoded by several genes. Furthermore, LTCC subunits are subject to splicing, cleavage, various protein–protein interactions (e.g., with calmodulin), and modulation by phosphorylation (e.g., by protein kinase A). This chapter focuses on the role of LTCCs in congenital and acquired cardiac arrhythmias. We review LTCC mutations associated with rhythm disturbances and LTCC dysregulations caused by pathologic immune system activation. Furthermore, we address the dysfunction of LTCCs involved in the pathogenesis of atrial fibrillation, rhythm disturbances associated with heart failure, and age-related alterations of the heartbeat.

Keywords

Voltage-dependent calcium channels · Arrhythmia · Cardiac disease · Congenital abnormality · Immune system disease · Heart failure · Atrial fibrillation

Abbreviations

ACHB	Autoimmune congenital heart block
AF	Atrial fibrillation
AID	Alpha-interaction domain
AP	Action potential
APD	Action potential duration
AV	Atrioventricular
BrS	Brugada syndrome
CaM	Calmodulin
CC-AAb	Agonistic $Ca_V1.2$ autoantibody
CDI	Ca^{2+}-dependent inactivation
CICR	Ca^{2+}-induced Ca^{2+} release
CPVT	Catecholaminergic polymorphic ventricular tachycardia
DCM	Dilated cardiomyopathy

E. Kuzmenkina · S. Salamon · P. Despang · J. Matthes (✉)
Center of Pharmacology, University of Cologne, Cologne, Germany
e-mail: jan.matthes@uni-koeln.de

© Springer Nature Switzerland AG 2023

O. N. Tripathi et al. (eds.), *Heart Rate and Rhythm*, https://doi.org/10.1007/978-3-031-33588-4_10

EAD	Early after depolarization
ERS	Early repolarization syndrome
HF	Heart failure
HVA	High-voltage activated
LQTS	Long QT syndrome
LTCC	L-type Ca^{2+} channel
LVA	Low-voltage activated
miR	MicroRNA
Na_V	Voltage-gated Na^+ channel
NCX	Na^+/Ca^{2+} exchanger
RyR	Ryanodine receptor
SA	Sinoatrial
SAN	Sinoatrial node
SANDD	SAN Dysfunction and deafness
SCD	Sudden cardiac death
SQTS	Short QT syndrome
SR	Sarcoplasmic reticulum
TS	Timothy syndrome
VDI	Voltage-dependent inactivation
VF	Ventricular fibrillation
VGCC	Voltage-gated Ca^{2+} channel
VT	Ventricular tachycardia
VWA	von Willebrand factor A

10.1 Introduction

L-type voltage-gated Ca^{2+} channels (LTCCs) are voltage-gated Ca^{2+} channels (VGCCs) ubiquitously expressed in cardiac tissue, but also in smooth muscle, pancreas, adrenal gland, or brain tissue. LTCCs mediate entry of calcium ions (Ca^{2+}) into cardiomyocytes, by this initiating excitation–contraction coupling. Furthermore, LTCCs are critically involved in shaping cardiac action potentials (AP) [1]. In sinoatrial and atrioventricular nodes, LTCCs are involved in diastolic depolarization, thereby participating in the AP firing and regulating automaticity [2, 3]. Accordingly, loss-of-function mutations in LTCCs can lead to sinus bradycardia, sick sinus syndrome, and dysfunction of atrioventricular conduction [4–7]. In the working myocardium and Purkinje system, depolarizing L-type Ca^{2+} currents determine the amplitude of the AP plateau, counterbalanced by repolarizing K^+ currents. Overlapping with an increase of K^+ outward-currents, inactivation of LTCCs drives the AP into the repolarizing phase and, thus, affects its duration (APD) [3]. A disturbed interplay of depolarizing and repolarizing currents and its influence on APD may result in susceptibility for life-threatening ventricular [8] and atrial [9] arrhythmias. Correspondingly, mutations in LTCCs are associated with arrhythmic disorders such as long QT, short QT, Brugada, and early-repolarization syndromes [10]. Furthermore, LTCCs are subject to pro-arrhythmic remodeling in diseased and/or aged hearts [11, 12].

This chapter focuses on the role of LTCCs in congenital and acquired cardiac arrhythmias. We review LTCC mutations associated with rhythm disturbances, LTCC dysregulations caused by pathologic immune system activation and dysfunction of LTCCs involved in the pathogenesis of atrial fibrillation (AF), rhythm disturbances associated with heart failure (HF), and age-related alterations of the heart beat (Table 10.1, Fig. 10.1).

10.2 Molecular Properties of LTCCs

VGCCs conduct Ca^{2+} upon surface-membrane depolarization. VGCCs are divided into high-voltage activated (HVA) and low-voltage activated (LVA) channels according to their activation potential thresholds [13]. Furthermore, HVA VGCCs are characterized by higher channel conductance and slower channel inactivation compared to LVA VGCCs [13]. Based on their biophysical and pharmacological properties, HVA VGCCs are further divided into L-, P/Q-, N,- and R-type channels. LTCCs are sensitive to antagonistic drugs classified as 1,4-dihydropyridines (e.g., amlodipine), phenylalkylamines (e.g., verapamil), and 1,5-benzothiazepines (e.g., diltiazem) [13]. LVA VGCCs consist of the subfamily of T-type Ca^{2+} channels, which can pharmacologically be discriminated against LTCCs by the specific LTCC agonist (*S*)-(–)-Bay K 8644 and the T-type preferring antagonist mibefradil [14]. In cardiomyocytes, both L- and T-type VGCCs are

Table 10.1 Synopsis of rhythm disturbances and channelopathies related to L-type Ca^{2+} channels

Gene/protein	Phenotype/ channelopathy	Pathophysiological effects	Exemplifying references
Genetics			
CACNA1C (Ca$_V$1.2)	LQT8 (including TS)	Gain-of-function, I_{CaL} ↑	[86, 91, 92, 293]
	BrS3, BrS3/SQT4	Loss-of-function, I_{CaL} ↓	[129, 130]
	SQT4	Loss-of-function, I_{CaL} ↓	[138]
	ERS2	Loss-of-function, $I_{CaL} \downarrow^{a}$	[130]
	SAN dysfunction	Loss-of-function, $I_{CaL} \downarrow^{a,b}$	[7]
CACNA1D (Ca$_V$1.3)	SANDD syndrome	Loss-of-function, I_{CaL} ↓	[6]
CACNB2b (Ca$_V\beta_{2b}$)	BrS4, BrS4/SQT5	Loss-of-function, I_{CaL} ↓	[129, 130]
	ERS3	Loss-of-function, $I_{CaL} \downarrow^{a}$	[130]
	SNPs in addition to BrS3, BrS4, ERS3 mutations	Gain-of-function, $I_{CaL} \uparrow^{c}$	[130]
CACNA2D1 (Ca$_V\alpha_2\delta$-1)	BrS9	Loss-of-function, $I_{CaL} \downarrow^{a}$	[130]
	SQTS6	Loss-of-function, I_{CaL} ↓	[145]
	ERS4	Loss-of-function, $I_{CaL} \downarrow^{a}$	[130]
CALM1–3 (CaM)	LQT14–16	Loss-of-function of CaM, reduced CDI of I_{CaL}	[68, 123]
Autoimmunity			
Ca$_V$1.2	VT, SCD in DCM	Agonistic antibodies, I_{CaL} ↑	[156, 157]
	Idiopathic cardiac arrest	Antagonistic antibodies, I_{CaL} ↓	[180]
Ca$_V$1.2 and Ca$_V$1.3	ACHB	Ro/SSA antibodies, I_{CaL} ↓	[154, 174]
Inflammation			
Ca$_V$1.2	LQTS^{d}	IL-1, I_{CaL} ↑	[190]
	AF^{d}	IL-1, I_{CaL} ↓	[193, 194]
	LQTS^{d}	IL-6, Ca$_V$1.2 phosphorylation, I_{CaL} ↑	[187]
	AF^{d}	TNFα, I_{CaL} ↓	[195]
	AF^{d}	MIF, I_{CaL} ↓	[196]
Remodeling			
Ca$_V$1.2 and Ca$_V$1.3	Age-related SSS	miR-1976 ↑, I_{CaL} ↓	[200]
Ca$_V$1.2 and Ca$_V$1.3, Ca$_V\beta_1$, Ca$_V\beta_2$, Ca$_V\alpha_2\delta$-1	AF	I_{CaL} ↓	[207, 218]
Ca$_V$1.2, Ca$_V\beta_{2a}$	HF occurrence of rhythm disturbances ↑	Single LTCC activity ↑, channel hyperphosphorylation, reduced number of functional channels	[253, 255, 267, 273]

Data are compiled from human and animal studies

↑ indicates increase/upregulation; ↓, decrease/downregulation; ACHB, autoimmune congenital heart block; AF, atrial fibrillation; BrS, Brugada syndrome; CaM, calmodulin; CDI, Ca^{2+}-dependent inactivation; DCM, dilated cardiomyopathy; ERS, early-repolarization syndrome; HF, heart failure; I_{CaL}, whole-cell L-type Ca^{2+} current/current density; LQT, long QT syndrome (in the disease names); LQTS, long QT syndrome; LTCC, L-type Ca^{2+} channels; miR, microRNA; SAN, sinoatrial node; SANDD, sinoatrial node dysfunction and deafness; SCD, sudden cardiac death; SNP, single-nucleotide polymorphism; SQT, short QT syndrome (in the disease names); SQTS, short QT syndrome; SSS, sick sinus syndrome; TS, Timothy syndrome; VT, ventricular tachycardia

[a] Proposed mechanism, no experimental measurements

[b] Accompanied by a titin mutation

[c] Probably counteracted by a concomitant HERG channel mutation

[d] Proposed related disorder, no/little experimental evidence

expressed at significant levels [15–19]. LTCCs are the predominant VGCCs in the adult human heart [16–19], whereas T-type VGCCs seem to prevail in the early stages of the heart development [16, 19]. Expression of T-type VGCCs in the adult myocardium depends on the species and

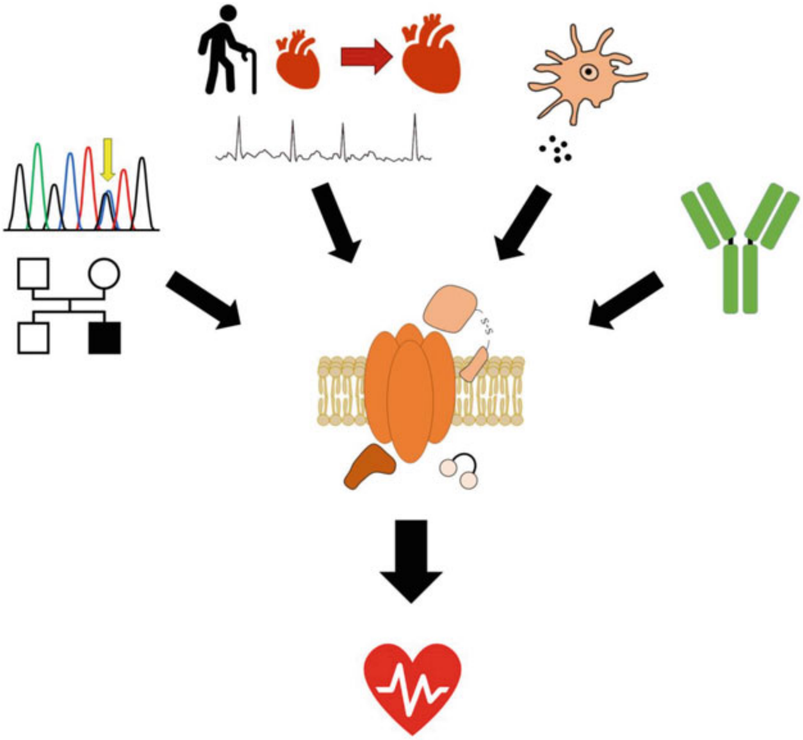

Fig. 10.1 Schematic overview of mechanisms underlying rhythm disturbances associated with L-type Ca^{2+} channel (LTCC) dysfunction. From left to right**: LTCC mutations**, either de novo or hereditary, **aging and age-related diseases** such as heart failure or atrial fibrillation, **inflammatory diseases,** or **(auto-) antibodies** can affect LTCC expression and/or function and lead to alterations in electrical activity of the heart or even to cardiac arrhythmia

strongly decreases with increasing body size in mammals [20]. In diseased hearts, however, T-type VGCCs can be re-expressed [21].

LTCCs are defined by their transmembrane pore-forming subunit, $Ca_V\alpha_1$ ($Ca_V1.X$), which determines most properties of the ion channel complex, which consists of the pore and up to three auxiliary subunits, $Ca_V\alpha_2$-δ, $Ca_V\beta$, and $Ca_V\gamma$ [13, 22]. Auxiliary $Ca_V\alpha_2$-δ and $Ca_V\beta$ subunits are constitutively bound to the $Ca_V\alpha_1$ subunit, although different $Ca_V\beta$ isoforms can dynamically alternate in a competitive manner [23, 24]. $Ca_V\alpha_2$-δ and $Ca_V\beta$ modulate channel trafficking, gating properties, and interaction with other proteins. Cardiac LTCCs can also associate with $Ca_V\gamma$ subunits in heterologous expression systems, but the role of this interaction in native heart tissues remains to be investigated [25]. Multiple genes encoding LTCC subunits and their alternative splicing provide molecular diversity of LTCCs [26]. In addition, the ubiquitous Ca^{2+} sensor protein calmodulin (CaM) can be considered essential for LTCCs [27, 28]. CaM associates with the $Ca_V\alpha_1$ subunit with high affinity and regulates channel activity and Ca^{2+}-dependent feedback, e.g., Ca^{2+}-dependent inactivation (CDI).

10.2.1 $Ca_V\alpha_1$ Subunit

The $Ca_V\alpha_1$ subunit is the primary subunit of VGCCs (Fig. 10.2), which encompasses an ion-conducting pore with a selectivity filter and voltage sensor, as well as activation and inactivation machineries. It provides sites for regulatory interactions and drug binding [1, 29]. Ten phylogenetically related genes encode different $Ca_V\alpha_1$ subunits [1, 29]. Four of them, *CACNA1S*, *CACNA1C*, *CACNA1D*, and *CACNA1F*, encode the LTCC $Ca_V\alpha_1$ subunits, $Ca_V1.1$–$Ca_V1.4$, respectively. While $Ca_V1.1$ ($Ca_V\alpha_{1S}$) is specific for skeletal muscle cells, $Ca_V1.4$ ($Ca_V\alpha_{1F}$) is essential for retinal photoreceptor function. $Ca_V1.2$ ($Ca_V\alpha_{1C}$) and $Ca_V1.3$ ($Ca_V\alpha_{1D}$) are the only LTCCs expressed in cardiac tissue and of particular functional relevance here.

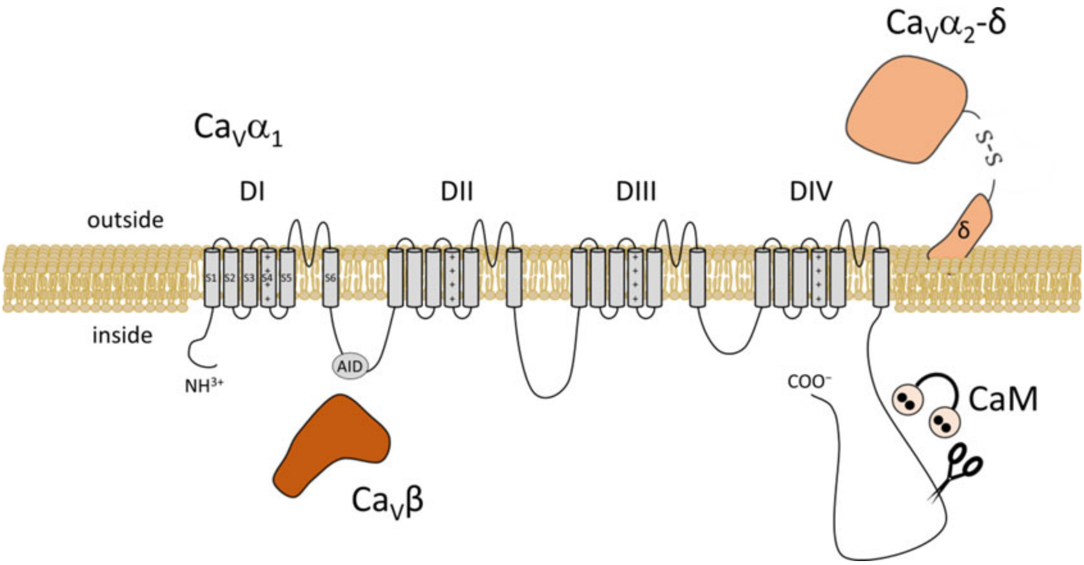

Fig. 10.2 Schematic structure of a $Ca_V\alpha_1$ subunit with associated $Ca_V\beta$, $Ca_V\alpha_2$-δ, and calmodulin. $Ca_V\alpha_1$ consists of four domains (DI–DIV), each comprised of six transmembrane segments (S1–S6). S4 segments are positively charged and serve as voltage sensors. S5 and S6 segments together with S5–S6 loops form the channel's conducting pore. DI–DII loop contains the alpha-interaction domain (AID) enabling high-affinity interaction with $Ca_V\beta$ subunit. The C-terminus of $Ca_V\alpha_1$ can be either post-translationally cleaved ($Ca_V1.2$ channels) or truncated due to alternative splicing ($Ca_V1.3$ channels), as symbolized by the scissors. The proximal part of the full-length C-terminus binds calmodulin (CaM). CaM consists of two lobes, each having two Ca^{2+}-binding sites. The distal part of the full-length C-terminus interacts with the proximal C-terminus and competes with CaM. Of note, the cleaved distal C-terminus of $Ca_V1.2$ can also non-covalently bind to the channel's proximal C-terminus. $Ca_V\alpha_2$-δ subunit is anchored to the membrane through its δ portion and interacts with extracellular loops of $Ca_V\alpha_1$

The $Ca_V\alpha_1$ subunit belongs to the family of four-domain cation channels, which also includes pore-forming subunits of voltage-gated Na^+ channels (Na_Vs) [30]. $Ca_V\alpha_1$ protein with a length of approximately 2000 amino acids consists of four homologous domains (DI–DIV) connected by intracellular loops and having intracellular N- and C-termini [1]. Each domain contains six transmembrane segments (S1–S6). S5 and S6 are connected at their extracellular ends by the reentrant pore loops. Together, S5, S6, and the pore loops of DI to DIV form the ion-conducting pore of $Ca_V\alpha_1$ [1, 31–33]. The lower (intracellular) thirds of S6, which are rich in hydrophobic amino acids, interact with each other, sealing the pore in the non-conducting (closed) state of the channel. The positively charged S4 segments serve as voltage sensors. Their outward movement in response to membrane depolarization allows S6 segments to diverge thus opening the channel [34]. The intracellular DI–DII loop forms the inactivation gate, which docks to the cytoplasmic ends of S6 segments upon channel opening, leading to voltage-dependent inactivation (VDI) [35]. Furthermore, this DI–DII loop of HVA VGCCs contains the alpha-interaction domain (AID) (Fig. 10.2), which enables interaction with $Ca_V\beta$ subunits [36]. The co-localization of AID and the inactivation gate in the DI–DII loop provides structural basis for profound regulation of VDI by $Ca_V\beta$ subunits (see Sect. 10.2.2) [35].

The cytoplasmic C-terminus of $Ca_V\alpha_1$ allows channel regulation by numerous protein–protein interactions [37, 38]. Particularly, it binds CaM and thus permits Ca^{2+}-dependent channel autoregulation [28]. Besides, distal C-termini of LTCC $Ca_V\alpha_1$ contain auto-inhibitory domains [39–42]. However, LTCC $Ca_V\alpha_1$ can exist in the full-length form or in truncated forms, which lack the distal C-terminus. In $Ca_V1.1$ and $Ca_V1.2$ channels, the distal C-terminus can be post-translationally cleaved but remains non-covalently associated with the channel [39, 40]. A dissociated distal C-terminus of $Ca_V1.2$ channels can translocate into the nucleus and regulate transcription [37]. In $Ca_V1.3$ and $Ca_V1.4$ channels, short and long C-termini arise from alternative splicing [42–45].

As mentioned above, from the family of LTCCs, only $Ca_V1.2$ and $Ca_V1.3$ were found in the heart. While $Ca_V1.2$ is ubiquitously expressed in all cardiac tissues, $Ca_V1.3$ is preferentially expressed in sinoatrial (SA) and atrioventricular (AV) nodes, can be found in atria and Purkinje fibers, and is practically absent in ventricles [17–19, 46, 47]. $Ca_V1.2$ and $Ca_V1.3$ channels are often expressed in the same tissues but can have distinct functions due to differences in their gating properties. $Ca_V1.3$ channels activate at more negative potentials than $Ca_V1.2$: the activation threshold of $Ca_V1.3$ channels is at about −50 mV, whereas $Ca_V1.2$ channels open at voltages above −30 mV [13, 46, 48, 49]. The low activation threshold of $Ca_V1.3$ channels, which is slightly more positive than the activation threshold of T-type VGCCs, makes $Ca_V1.3$ channels suitable to support slow conduction and pace-making activity and this correlates with $Ca_V1.3$ expression patterns.

10.2.2 $Ca_V\beta$ Subunit

$Ca_V\beta$ subunits are cytosolic auxiliary subunits of HVA VGCCs (Fig. 10.2) and the main modulator of activation, inactivation, and membrane targeting of these channels [36]. Structurally, $Ca_V\beta$ subunits consist of the so-called functional core flanked by variable N- and C-termini [36]. The $Ca_V\beta$ core comprises conserved SH3 and GK domains, which are linked by a flexible, weakly conserved HOOK region. SH3 and GK domains evolved as interaction sites for protein–protein interactions [50, 51]. The SH3 domain of $Ca_V\beta$s can bind dynamin, promoting channel endocytosis [52]. The GK domain of $Ca_V\beta$s interacts with the family of RGK proteins (Rem, Gem/kir, and Rad), which are strong inhibitors of HVA VGCCs [53]. It also contains a tiny hydrophobic groove, termed α-binding pocket, which interacts with the AID of $Ca_V\alpha_1$ [54]. Both SH3 and GK domains are required to reproduce multiple functional effects of $Ca_V\beta$, with the HOOK region being important for the modulation of VDI of HVA VGCCs [36].

Four $Ca_V\beta$ subfamilies are known, each encoded by a distinct gene (*CACNB1–CACNB4*), but due to alternative splicing several variants of each $Ca_V\beta$ isoform exist [36]. All $Ca_V\beta$ subunits have been found in the mammalian heart, while $Ca_V\beta_2$ is the most prominent. Among these, $Ca_V\beta_{2b,c}$ are the most abundant, while $Ca_V\beta_{2d,e}$ are only robust in young animals, and the expression levels of $Ca_V\beta_{2a}$ seem to be the lowest [55–57]. $Ca_V\beta_2$ isoforms differ in their non-conserved N-terminal region and differentially affect channel activity and inactivation [57]. Besides, cardiac $Ca_V\beta$ subunits can diverge in their subcellular localization: e.g., whereas $Ca_V\beta_{1b}$, $Ca_V\beta_2$ and $Ca_V\beta_3$ were detected in the T-tubule sarcolemma, $Ca_V\beta_{1a}$ and $Ca_V\beta_4$ were found in the surface sarcolemma [58].

10.2.3 $Ca_V\alpha_2$-δ Subunit

$Ca_V\alpha_2$-δ subunits (Fig. 10.2) promote plasma membrane expression of HVA VGCCs, increase Ca^{2+} currents, shift activation to more hyperpolarized potentials, and accelerate inactivation [59–61]. There are four genetic variants, $Ca_V\alpha_2$-δ1–4, encoded by *CACNA2D1–4* genes, respectively [61]. A precursor protein, translated from *CACNA2D*, is cleaved to yield two polypeptides, α_2 and δ, which, however, remain connected by disulfide bridges. $Ca_V\alpha_2$-δ is an extracellularly glycosylated subunit anchored to the plasma membrane by a glycosylphosphatidylinositol attached to the C-terminus of δ. The α_2 portion contains multiple domains, e.g., von Willebrand factor A (VWA) domain, commonly involved in extracellular protein–protein interactions. VWA domain is important for the physical interaction with extracellular loops of LTCCs and the modulation of their biophysical properties [33, 59, 60].

All isoforms $Ca_V\alpha_2$-δ1–4 were found in the heart but only $Ca_V\alpha_2$-δ1 is abundantly expressed in human ventricles [17, 18, 62–64]. In atria, $Ca_V\alpha_2$-δ1 and $Ca_V\alpha_2$-δ2 were found to be expressed at similarly high levels [17, 64].

10.2.4 $Ca_V\gamma$ Subunit

$Ca_V\gamma$ subunits are transmembrane proteins encoded by eight *CACNG* genes. They build a functionally heterogeneous family and can regulate other proteins besides VGCCs [65]. $Ca_V\gamma1$ was identified as a part of the skeletal muscle LTCCs. $Ca_V\gamma4$, $Ca_V\gamma6$, $Ca_V\gamma7$, and $Ca_V\gamma8$ were found in the human heart and they were able to associate with $Ca_V1.2$ and differentially modulate its properties in a heterologous expression system [25]. However, whether $Ca_V\gamma$ regulates native cardiac LTCCs requires further studies. So far, there is no direct evidence of interaction between LTCCs and $Ca_V\gamma$ in cardiomyocytes.

10.2.5 Calmodulin (CaM)

CaM is a universal Ca^{2+}-sensing protein regulating a vast number of proteins [27, 66]. It can be considered as an auxiliary subunit of various ion channels including LTCCs (Fig. 10.2) [27, 28]. In humans, CaM is encoded by three genes, *CALM1–3*, with divergent nucleotide but identical protein sequences [67]. All CaM genes are expressed in the heart, showing expression levels in the rank order *CALM3* > *CALM2* > *CALM1* [68]. CaM consists of two lobes, each composed of two EF hands with high affinity to Ca^{2+} [28]. In LTCCs, CaM is bound to the channel's proximal C-terminus but can be competitively displaced by the distal part of the C-terminus of the channel [41, 69–73]. The competition between CaM and the distal C-terminus is further regulated, e.g., by PKA phosphorylation in response to β-adrenergic stimulation [74]. CaM strongly enhances channel activity in its (Ca^{2+}-free) apo form and is responsible for CDI of the channel upon Ca^{2+} conduction [28]. Furthermore, Ca^{2+} binding to the channels' CaM is involved in internalization of the channels in response to their high activity [75].

10.3 LTCCs and AP

Interplay of various ion currents through the cardiomyocyte membrane regulates generation of cardiac APs [3]. LTCCs open upon membrane depolarization giving rise to inward, depolarizing currents. Activation of LTCCs is slow compared to that of Na_Vs; therefore, LTCCs contribute little to the upstroke (phase 0) of the AP in ventricular, Purkinje, and atrial myocytes [3]. Instead, long-lasting LTCC currents together with opposing outward K^+ currents shape the AP plateau (phase 2) in these cells. In the working myocardium, Ca^{2+} influx through LTCCs activates ryanodine receptors (RyRs) leading to Ca^{2+} release from the sarcoplasmic reticulum (SR). This process is called Ca^{2+}-induced Ca^{2+} release (CICR), and it underlies cardiac excitation–contraction coupling [76, 77]. Subsequent VDI and CDI of LTCCs result in accelerated membrane repolarization (phase 3). Regeneration of depolarizing currents in the case of insufficient repolarization reserve [78] can lead to a new membrane depolarization (early after depolarization, EAD) and thus trigger a premature AP [79, 80]. EADs are associated with fatal arrhythmias, such as Torsades de Pointes tachycardia, a specific form of polymorphic ventricular tachycardia with a high risk of sudden cardiac death (SCD) [79]. Overlap of LTCC activation and inactivation curves results in steady-state currents (so-called window currents, Fig. 10.3). Thus, LTCCs can reactivate and contribute to an increasing (late) inward current [79, 81]. Accordingly, increased LTCC window currents can increase the risk of EADs, while reduced window currents can decrease it.

In SA and AV nodes, LTCCs are essential drivers of the membrane depolarization during pace-making [82]. In the SA node, spontaneous APs are initiated by coupled "membrane-" and "Ca^{2+}-clock" mechanisms, which include depolarizing currents mediated by HCN channels ("funny" currents) and T-type VGCCs as well as

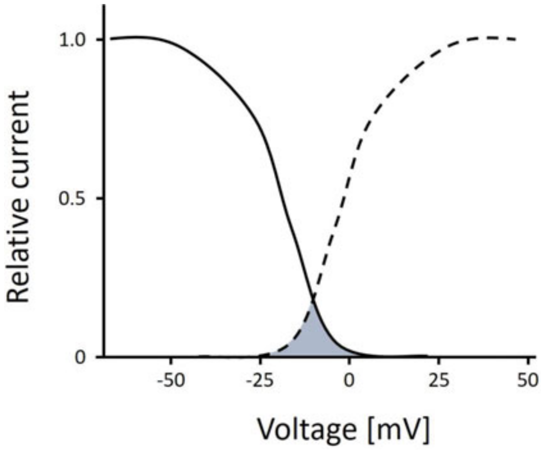

Fig. 10.3 Schematic drawing of a so-called window current. The two curves depict steady-state inactivation (solid line) and activation (dashed line) of Ca^{2+} currents depending on the respective membrane potential. Within the potential range marked in gray ("permissive window of voltage"), a large proportion of the Ca^{2+} channels is in the inactivated state, i.e., non-conducting, while another proportion is just activated. L-type Ca^{2+} channels may reactivate within this voltage range

Na^+/Ca^{2+} exchanger (NCX) activation in response to the spontaneous Ca^{2+} release through RyRs [82, 83] (see also Chaps. 4 and 6). Subsequent activation of $Ca_V1.3$ channels further promotes membrane auto-depolarization. After the membrane potential reaches the activation threshold of $Ca_V1.2$ channels, these LTCCs contribute to the upstroke of the AP. Besides its Ca^{2+}-conducting function, $Ca_V1.3$ channels are an essential molecular determinant of the depolarizing, dihydropyridine-sensitive sustained Na^+ currents in the SA node [84]. $Ca_V1.3$ strongly co-localizes with RyRs in SA node cells [85]. Thus, $Ca_V1.3$ opening here can stimulate RyRs-mediated Ca^{2+} release and further activate depolarizing NCX currents.

10.4 LTCC Mutations Associated with Cardiac Rhythm Disturbance

Ion channel mutations in general account for a variety of hereditary cardiac arrhythmias. For example, a large fraction of sudden unexplained deaths in the young are postmortem attributed to ion-channel mutations which led to cardiac arrhythmias [86]. Primary channelopathies predisposing to sudden cardiac death include long QT syndrome (LQTS), short QT syndrome (SQTS), the Brugada Syndrome (BrS), and the catecholaminergic polymorphic ventricular tachycardia (CPVT) [87]. As discussed below, some LTCC mutations are associated with rhythm disturbances, although the major susceptibility genes revealed so far are *KCNQ1* ($K_V7.1$), *KCNH2* ($K_V11.1$/hERG), *SCN5A* ($Na_V1.5$), and *RYR2* (ryanodine receptor 2) [86, 87].

The report of LTCC mutations causing the Timothy Syndrome (TS) by Splawski et al. in 2004 has highlighted the role of LTCCs for hereditary cardiac arrhythmias and up to now the number of identified mutations in LTCCs affecting cardiac rhythm strongly increased [10, 88–90]. Cardiac LTCC channelopathies can be conditionally classified as gain- or loss-of-function mutations [89]. LQTS mutations in $Ca_V1.2$ channels typically show gain-of-function features, whereas loss-of-function $Ca_V1.2$ mutations were found in BrS, SQTS, and early-repolarization syndrome (ERS) [10, 89]. Furthermore, loss of $Ca_V1.3$ or $Ca_V1.2$ function can lead to sinus node malfunction from bradycardia to sick sinus syndrome [6, 7].

10.4.1 Long QT Syndromes (LQTS)

On the cellular level, LQTS results from a prolongation of the ventricular AP due to an increase of depolarizing Na^+ and Ca^{2+} currents or a decrease of repolarizing K^+ currents [91]. This favors EADs, which can lead to Torsades de Pointes arrhythmia [79]. Three major and at least 14 minor susceptibility genes were identified for congenital LQTS [92].

LQTS caused by mutations in the pore-forming subunit of $Ca_V1.2$ channels (*CACNA1C*-LQTS) is historically termed LQT8. Given the strong expression of $Ca_V1.2$ in various tissues, gain-of-function $Ca_V1.2$ channelopathies can result in multi-organ pathologies. LQT8 was thus subdivided into the multisystem Timothy syndrome (TS) and LQT8 without extra-cardiac symptoms as more and more *CACNA1C* mutations and associated effects became known [10].

TS is a rare multisystem disorder characterized by QT prolongation, cardiac arrhythmias (bradycardia, AV block, ventricular tachyarrhythmia), congenital heart defects, and extra-cardiac manifestations such as syndactyly, facial abnormalities, immune system dysfunction, intermittent hypoglycemia, and neuropsychiatric disorders [88, 93, 94]. TS patients are at high risk of SCD and often die during childhood [88, 93, 95]. TS is a dominant genetic disorder, resulting from de novo *CACNA1C* mutations. However, it can also be inherited from an asymptomatic parent who carries a mosaic *CACNA1C* mutation [88, 96]. The particular phenotype depends on the respective *CACNA1C* mutation and can vary among patients with the same mutation [88, 93–95, 97, 98]. Classical TS (TS-1) is most commonly caused by a recurrent missense mutation (G406R) in the alternatively spliced exon 8a, which is widely expressed and represents approx. 20% of $Ca_V1.2$ transcripts in cardiac and neuronal tissue [88]. The analogous mutation in the mutually exclusive exon 8, responsible for nearly 80% of cardiac $Ca_V1.2$ channels, leads to an atypical TS (TS-2) without syndactyly but a more severe cardiac phenotype [93].

The G406R mutation alters $Ca_V1.2$ activity at various levels: it drastically inhibits channel inactivation (particularly VDI), shifts channel activation to more negative potentials, and promotes a channel gating mode with very long openings [88, 93, 99, 100]. The mutation occurs at the cytoplasmic end of the sixth transmembrane segment of the channel's domain I (DI/S6), which is involved in the voltage-dependent regulation of the channel activation and inactivation and is conserved in VGCCs across various species [34, 35, 93, 101]. Moreover, G406R introduces a new consensus site for CaMKII enabling phosphorylation of S409, which could promote long channel openings ([99]; but: [102]). Furthermore, G406R leads to enhancement of coupled channel gating, by altering the interaction with the scaffolding protein AKAP150 [103, 104].

Some TS cases were reported to be caused by mutations other than the typical G406R mutation. Interestingly, many of them are also located at the cytoplasmic end of an S6 segment similar to G406R, e.g., G402S, G402R, S405R, E407A in DI [93, 95, 105], I1166T in DIII [106, 107], or A1473G in DIV [108]. Besides, a TS-associated mutation was reported in a DII/S4–S5 linker, S643F [109]. Of note, S4–S5 linkers appear to interact with S6 segments [34]. Electrophysiologically, gain of $Ca_V1.2$ function was confirmed for G402S (impairment of inactivation) [93] and I1166T (increased window current due to shifted activation potentials) [106, 107]. S643F mutation showed mixed loss- and gain-of-function features: a reduction of peak current density was opposed by shifting the activation toward more depolarized potentials and increasing late currents due to the drastic reduction of VDI [109].

Although initially LQT8 was equated to TS, later studies expanded the spectrum of phenotypes associated with LQT8 [110–113]. For example, one patient with idiopathic QT prolongation, bradycardia, and autism spectrum disorder carried an E1115K mutation in the selectivity filter in the DIII/S5-S6 loop [113]. When expressed in a recombinant system the mutation caused AP prolongation and turned the LTCC into a dihydropyridine-sensitive but nonselective cation channel.

Some *CACNA1C* mutations result in LQTS without obvious extra-cardiac attributes [10, 90, 107, 110]. A whole-exome sequencing of 102 unrelated “genotype-negative/phenotype-positive” LQTS patients suggested that *CACNA1C* mutations may be responsible for 1% of LQTS cases [110]. *CACNA1C* mutations leading to isolated LQTS were found at various cytoplasmic linkers and both N- and C-terminus and showed gain-of-function features like reduced channel inactivation, increased current density, increased window current, or negative shift of activation potential range [10]. Interestingly, many of the $Ca_V1.2$ mutations concentrate in the DII–DIII linker at a PEST sequence, which serves as a signal for protein degradation [110, 114]. Genetic analyses of several families with multiple cardiac abnormalities, such as LQTS, hypertrophic cardiomyopathy, or congenital heart defects, identified recurrent R581C/H mutations in $Ca_V1.2$ channels [111, 115, 116]. R581C/H mutations lie within the intracellular DI–DII loop, which is responsible for VDI regulation and binding of $Ca_V\beta$ subunits. These mutations show an increase of window and late currents indicating gain of function [111, 117].

LQTS can also be associated with gain of LTCC function due to mutations in the CaM genes *CALM1–3* (LQT14–16, respectively) [68, 118–123]. These CaM mutations led to a reduction of Ca^{2+} affinity to the EF hands in the C-lobe of CaM, resulting in the loss of CDI of $Ca_V1.2$ channels [68, 118, 120, 122, 124, 125]. Crystallographic and NMR investigations suggest that altered interaction between CaM and $Ca_V1.2$ may also be involved [126].

10.4.2 Brugada, Early-Repolarization, and Short QT Syndromes

BrS and ERS belong to the continuous spectrum of so-called J-wave syndromes. They are diagnosed based on the ECG patterns in structurally normal hearts and are associated with an increased risk of SCD due to polymorphic ventricular tachycardia (VT) and ventricular fibrillation (VF) [127]. The mechanisms underlying BrS and ERS are not fully understood [127, 128]. Besides, BrS and ERS appear to be multifactorial rather than pure Mendelian disorders [129].

LTCCs came into focus, when it was observed that the Ca^{2+} channel antagonist verapamil can induce BrS-like patterns in APs and ECGs of canine right ventricular wedges [130]. Subsequent studies revealed that mutations in *CACNA1C* ($Ca_V1.2$), *CACNB2b* ($Ca_V\beta_{2b}$), and *CACNA2D1* ($Ca_V\alpha_2\delta$-1) account for a significant fraction of BrS and ERS cases and are often accompanied by shortening of the QT interval [89, 131, 132].

The latter observation led to reassessment of $Ca_V1.2$ subunit genes as candidate susceptibility genes for SQTS [133]. SQTS is a rare inherited cardiac disease, characterized by a high risk of developing AF and VT leading to syncope or SCD [134, 135]. The short QT interval results from a shortening of APD due to accelerated membrane depolarization. Reduced effective refractory period and increased transmural dispersion predispose to re-entry arrhythmias [91, 136].

In BrS patients, at least eleven *CACNA1C* mutations were identified of which four lead to concomitant BrS/SQTS [131, 132, 137, 138]. Additionally, two ERS-, one SQTS-, and one ERS/SQTS-associated mutations were identified in *CACNA1C* [132, 133, 139, 140]. The majority of the mutations were located in cytoplasmic regions of the channel, particularly in the distal C-terminus. Nine mutations were studied in heterologous expression systems and showed a decrease of Ca^{2+} current density [131, 132, 138–141]. In particular, the splicing-error mutation R632R could be a subject to nonsense-mediated mRNA decay [142]. One BrS patient was shown to carry the missense mutation E1115K [132] converting $Ca_V1.2$ into a nonselective monovalent cation channel associated with LQTS, as discussed above [113]. This BrS patient, however, additionally showed a HERG channel mutation known to be associated with BrS and thus probably compensating for the $Ca_V1.2$ LQTS mutation [132]. *CACNA1C* genetic variants present at low frequencies in the general population may also predispose to BrS and ERS [132, 143]. A T1787M variant, found in 0.8% of an African population, was identified in three unrelated patients with BrS, ERS, or idiopathic VF. T1787M is located in the distal C-terminus and strongly increased its auto-inhibitory effect [143].

Auxiliary $Ca_V\beta$ and $Ca_V\alpha_2$-δ subunits, which modulate surface expression and gating properties of $Ca_V1.2$ channels, are also associated with malignant ventricular arrhythmias. Genetic testing identified nine BrS-related and three ERS-related distinct amino acid changes in the $Ca_V\beta_{2b}$ subunit [131, 132, 144–146]. Among these, one BrS mutation led to concomitant SQTS [131, 132]. Two BrS mutations in the $Ca_V\beta_{2b}$ subunit were studied in whole-cell patch-clamp experiments and showed loss-of-function features such as decreased current density or increased rates of channel inactivation [132, 146]. In the *CACNA2D1* gene, four BrS-, one ERS-, and one SQTS-associated mutations were reported [132, 146, 147]. The SQTS mutation showed reduced current density in patch-clamp experiments [147].

10.4.3 SA and AV Node Dysfunctions

LTCCs are involved in the slow auto-depolarization ($Ca_V1.3$) and in the generation of the upstroke ($Ca_V1.2$ and $Ca_V1.3$) of APs in SA and AV nodes [82]. *CACNA1D* ($Ca_V1.3$)-deficient mice showed SA node (SAN) bradycardia with irregular cellular cycles, disturbed AV conduction, and congenital deafness [4, 5, 46, 148]. Later, a similar phenotype was observed in two consanguineous inbred Pakistani families [6]. The disorder, termed sinoatrial node dysfunction and deafness (SANDD) syndrome, is characterized by severe hearing loss, bradycardia, increased heart-rate variability, and variable degree of AV block [6]. SANDD patients were homozygous carriers of a 3 base pairs insertion in the alternatively spliced exon 8b of *CACNA1D*. The 8b isoform of $Ca_V1.3$ channels is predominant in the SAN [6]. This mutation leads to a glycine insertion (403_404insGly) at the cytoplasmic end of the inner-pore lining helix DI/S6. This region is conserved in human LTCCs, and associated with pathological gain-of-function mutations at homologous position not only in $Ca_V1.3$ (G403R and G403D) but also in $Ca_V1.2$ (G402S known from TS) and $Ca_V1.4$ (G359R) [93, 149, 150]. In contrast, the 403_404insGly mutation results in non-conducting $Ca_V1.3$ channels, although the channels are expressed in the surface membrane and exhibit ON-gating currents, indicating mobility of the voltage sensor [6]. The glycine insertion occurs at the cytoplasmic end of the pore, at the interaction site with S4–S5 linkers, which transmit movements of voltage-sensing S4 segments to the pore-forming S6 segments [34]. Measurements of $Ca_V1.3$ gating currents suggested that the 403_404insGly mutation can disturb this interaction by uncoupling S4 movements from the channel opening [6]. However, it is also possible that the mutation obstructs ion permeation. Recent studies of five supposedly unrelated Pakistani families with SANDD syndrome revealed that four of them were carriers of the 403_404insGly mutation, which was likely inherited from a common distant ancestor [151]. In the fifth family, SANDD syndrome was associated with a homozygous A376V mutation in the exon 8b of *CACNA1D*. A376V is located in the pore loop (DI/S5–S6 linker). The alanine at this position is conserved across LTCCs in various tissues. It was proposed that the substitution by valine could affect the shape of the inner part of the pore and thus affect Ca^{2+} conduction.

$Ca_V1.2$ channels could be involved in familial SAN dysfunction as well [7]. Genetic analysis of a Korean family with sinus bradycardia, early repolarization, and AF revealed compound heterozygosity of *CACNA1C* and titin mutations, predicted to be deleterious and perhaps increasing the severity of early repolarization [7]. Additional age-dependent loss of $Ca_V1.2$ channels in the SAN (see Sect. 10.5.2.1 for more details) imposes a risk of the affected family members to develop sick sinus syndrome [7, 152].

10.5 LTCCs in Acquired Arrhythmias

10.5.1 Autoimmune and Inflammatory LTCC Channelopathies and Cardiac Arrhythmias

The immune system plays an important role in the pathogenesis of cardiac arrhythmias [153–155]. An exemplary mechanism is the production of autoantibodies and inflammatory cytokines which can affect ion channels involved in the generation of cardiac APs [153, 154].

10.5.1.1 Antibodies Activating LTCCs

Autoimmune LTCC channelopathies play an important role in ventricular arrhythmias in dilated cardiomyopathy (DCM) [156]. Agonistic autoantibodies directed against $Ca_V1.2$ channels (CC-AAbs, Ca^{2+} channel autoantibodies) were identified in up to 50% of patients with idiopathic DCM [157–160]. In the prospective studies, patients positive for CC-AAbs had a several-fold higher risk of ventricular tachycardia and SCD than patients without these antibodies [158, 160]. CC-AAbs can bind to the $Ca_V1.2$ N-terminus and increase Ca^{2+} currents [159]. The arrhythmogenicity of CC-AAbs was confirmed in an animal model [158]: in isolated rat hearts, application of the purified CC-AAbs led to ventricular tachycardia and ventricular premature beats. Consistently, on the level of ventricular myocytes, the antibodies led to AP prolongation and occurrence of EADs. Summing up, CC-AAbs are an independent predictor of SCD in DCM resulting from ventricular arrhythmias [158, 160]. CC-AAbs were found in patients with ischemic cardiomyopathy (ICM) at a similar frequency as in DCM patients [160]. In ICM patients, CC-AAbs were associated with a several-fold increased risk of both SCD and non-SCD. Binding of CC-AAbs to the intracellular part of $Ca_V1.2$ and similar prevalence of CC-AAbs in ICM and DCM suggest that CC-AAbs can develop secondary to myocyte damage [154, 158, 161].

Several autoantibodies with targets other than LTCCs have been shown to increase LTCC-mediated currents in DCM. Autoantibodies against adenine nucleotide translocators cross-react with LTCCs, increase Ca^{2+} influx, and lead to progressive cardiomyocyte damage [157]. Monoclonal antibodies against cardiac troponin I can strongly enhance LTCC currents in murine myocytes, likely by an indirect mechanism [162]. However, this effect has not yet been reproduced with human samples [163]. Autoantibodies against β_1 adrenoceptors from DCM patients prolonged APD by increasing LTCC currents via activation of cAMP/PKA signaling [164].

10.5.1.2 Antibodies Inhibiting LTCCs

Inhibition of LTCCs by anti-Ro/SSA autoantibodies plays an important role in autoimmune congenital heart block (ACHB) [154, 156]. Of note, anti-Ro antibodies are present in healthy people, too. Nonetheless, risk for ACHB is significantly enhanced in anti-Ro antibody positive individuals with an incidence of about 5% compared to 1:11,000 in general. ACHB is thought to be caused by transplacental transfer of maternal antibodies, leading to inflammation and eventually fibrosis of the fetal AV node, but also of SAN and His bundle [165–167]. Ro/SSA and La/SSB antigens are intracellular ribonucleoproteins, which become surface exposed in apoptotic cells [168]. Interaction with maternal anti-Ro and anti-La antibodies impairs clearance of fetal apoptotic cardiomyocytes by healthy proliferating cardiomyocytes and provokes inflammation and fibrosis, normally not elicited in physiological apoptosis [169, 170]. However, this hypothesis alone cannot explain many features of ACHB, such as targeting the conduction system [171, 172]. Furthermore, in vitro perfusion of animal or human fetal hearts with Ro/SSA antibodies, which are prevalent antibodies in ACHB, led to sinus bradycardia and AV block within minutes [173–175]. Ro/SSA antibodies directly inhibit L-type ($Ca_V1.2$ and $Ca_V1.3$) and T-type ($Ca_V3.1$ and $Ca_V3.2$) channels in isolated cardiac cells and heterologous expression systems [174–180]. Of note, a study in rabbit SAN cells supported antibody specificity toward VGCCs:

while human antibodies of mothers whose children showed CHB inhibited L- and T-type Ca^{2+} currents, delayed rectifier K^+, and hyperpolarization-activated "funny" currents remained unaffected [177]. Since AP generation in AV and SA nodes depends on inward Ca^{2+} currents, VGCC inhibition explains the acute rhythm disturbances induced by Ro/SSA antibodies. While both $Ca_V1.2$ and $Ca_V1.3$ inhibition may cause AVB, studies on expression patterns, electrophysiological properties, and cellular functions suggest that SAN dysfunction is more likely due to an inhibition of $Ca_V1.3$ channels [5, 156, 181]. The antibody recognition site was identified in the DI/S5-S6 extracellular loop of $Ca_V1.3$ and $Ca_V3.1$ channel pores, respectively [179, 180]. Regarding chronic effects of Ro/SSA antibodies it was proposed that cross-linkage of antibody–antigen complexes leads to channel internalization [156, 171]. As fetal hearts show lower expression of VGCCs and lower SR capacity, particularly here VGCC downregulation can lead to severe Ca^{2+} dysregulation and abnormal apoptosis, initiating inflammation and fibrosis. Translocation of SSA/Ro and SSB/La antigens to the surface of affected cells may play an important role here.

Recently, an observational study identified a novel anti-$Ca_V1.2$ antibody in patients with idiopathic cardiac arrest [182]. The antibody was shown to target the ion selectivity and permeability filter segment in the $Ca_V1.2$ domain DIII and to be pro-arrhythmic by shortening the APD due to Ca^{2+} current inhibition. Of note, it cannot be excluded that antibody generation may be secondary to cardiac arrest rather than being causal for this event.

10.5.1.3 Inflammatory Cytokines and LTCCs

Systemic and cardiac inflammation is associated with development of atrial and ventricular arrhythmias [153, 183, 184]. Higher levels of circulating inflammatory factors are associated with an increased AF risk in the general population as well as in patients after cardiac surgery, AF ablation, or cardioversion [185, 186]. Of note, anti-inflammatory treatments can potentially decrease the risk of postoperative and post-ablation AF [183]. It has also been shown that the risk of ventricular arrhythmias and SCD in apparently healthy subjects and in patients with either cardiac or systemic inflammatory disease correlates with higher serum cytokine levels [184]. Particularly, pro-inflammatory cytokine levels were related to a QT prolongation and cytokine inhibitors shortened QT intervals.

Inflammation promotes structural and electrical remodeling of cardiac tissue. On the cellular level, pro-inflammatory cytokines, such as TNFα, IL-1, and IL-6, can regulate ion channels and Ca^{2+}-handling proteins [187]. For example, they can inhibit depolarizing K^+ currents, thus prolonging ventricular AP [187, 188]. Reported effects of cytokines on LTCCs vary because of different experimental conditions and models. In murine ventricles, IL-6 augmented LTCC currents by SHP2/ERK-mediated phosphorylation of the distal $Ca_V1.2$ C-terminus, thus contributing to the observed APD prolongation [189]. However, no changes in the LTCC current were reported in ventricles of rats and guinea pigs [190, 191]. IL-1 was shown to be able to either stimulate or inhibit LTCC currents via different pathways. It increased LTCC currents by a lipoxygenase pathway in guinea pig ventricular myocytes, and here LTCC upregulation was consistent with the measured prolongation of APD [192]. In other studies on rat and murine ventricular myocytes, IL-1 inhibited LTCCs via G-proteins, NO- (but not cGMP), and ROS/PKC-dependent pathways, respectively [193–195]. TNFα effects on ventricular LTCC currents were studied in various animal models and showed either no effect on LTCCs or current inhibition at TNFα concentrations exceeding those at pathophysiological conditions [187, 195]. Studies of cytokine effects on atrial LTCCs showed channel downregulation, which is consistent with AF pathogenesis (see Sect. 10.5.2.2 for more details). In murine atrial myocytes, IL-1 reduced $Ca_V1.2$ protein levels by inhibiting expression of an mRNA-binding quaking protein [196]. In rabbit cardiomyocytes from pulmonary veins, which are critical in AF initiation, TNFα significantly reduced LTCC currents [197]. Together with the upregulation of atrial K^+ currents by TNFα, this could shorten APD in a pro-arrhythmogenic manner and contribute to AF vulnerability [197]. Similarly, MIF (macrophage migration inhibitory factor), another cytokine associated with the pathogenesis of AF, decreased LTCC current density by lowered $Ca_V1.2$ protein expression, impaired LTCC function, and activation of c-Src kinases [198]. Recombinant MIF reduced LTCC currents in human atrial myocytes from patients with sinus rhythm but not in patients with AF. In contrast, application of an antibody against MIF increased LTCC currents in atrial myocytes from AF but not sinus rhythm patients.

In summary, although the effects of inflammation on LTCCs are poorly understood, it appears that inflammatory cytokines can alter LTCC currents through various mechanisms, so that ventricular (LQTS) and atrial (AF) arrhythmias are promoted.

10.5.2 LTCCs in Age- and Remodeling-Related Arrhythmias

10.5.2.1 SAN Aging and Dysfunction

Decline of SAN function, reflected in the progressive reduction of intrinsic pacemaker activity and maximum heart rates, is an inherent feature of cardiac aging, eventually leading to sinus node dysfunction in some individuals [199]. Besides vital loss of SAN cells and tissue remodeling, reduced excitability of SA myocytes is an intrinsic cause of age-dependent deterioration of SAN function. LTCC currents and subsequently triggered local Ca^{2+} release regulate slow diastolic depolarization and upstroke of SAN AP [82, 181, 200]. In SAN of aged mammals, LTCC expression and consecutive currents were reduced in comparison to younger adults [152, 201, 202]; but: [203]. MicroRNAs (miRs) can post-translationally regulate expression of ion channels. Significant upregulation of circulating miR-1976 was observed in patients with age-related sick sinus syndrome compared to age-matched healthy controls [202]. $Ca_V1.2$ and $Ca_V1.3$ channels were found to be direct targets of miR-1976. In transgenic mice, miR-1976 led to the inhibition of $Ca_V1.2$ and $Ca_V1.3$ expression in SAN and to slowed intrinsic cardiac rhythm. Furthermore, miR-1976 level was progressively increased in blood plasma and SAN tissue of aging rabbits and negatively correlated with protein levels of $Ca_V1.2$ and $Ca_V1.3$ in SAN [202].

10.5.2.2 Atrial Fibrillation

Prevalence of AF depends on age: compared to men aged 65–69 years the AF prevalence is twofold increased at an age of 75–79 years and more than fivefold compared to men aged 55–59 years [204]. While often cardiac diseases like coronary artery disease or heart failure increase the risk of developing AF, there are also genetic and hereditary components [205–207]. Until 2018 over 30 genetic loci have been identified as significantly associated with AF, although none of them were related to genes coding for VGCCs [207]. With regard to aging, $Ca_V1.2$ LTCCs were found to be downregulated in atria of humans, dogs, and sheep, reflected by mRNA, protein, or peak current levels [12, 208]. In patients, downregulation is associated with AF [12, 209], atrial dilation, or other structural diseases predisposing to AF [210, 211]. In animal models of AF, atrial tachypacing reduces LTCC expression and currents in early stages of AF as well as in persistent AF [209]. Downregulation of LTCCs could be initially adaptive to oppose Ca^{2+} overload resulting from atrial tachycardia [212]. Indeed, the Ca^{2+} channel antagonist verapamil prevented atrial contractile dysfunction and attenuated electric remodeling caused by short-term AF in patients and animal models [213–217]. Furthermore, verapamil and other drugs lowering intracellular Ca^{2+} load enhanced cardioversion success in patients with persistent AF [218]. On the other hand, reduction of LTCC currents in AF can be pro-arrhythmic, because it is associated with shortened APD, abolished AP plateau, and attenuation of rate-dependent AP accommodation [219, 220]. A diminished effective refractory period due to shorter APD results in a decreased wavelength of conduction, which permits more re-entrant circuits and thus facilitates AF [221].

Multiple mechanisms may be involved in the regulation of LTCCs in AF. In AF animal models, LTCC currents start to decline within several hours or days of atrial tachypacing, depending on the species [219, 222, 223]. Current reduction paralleled mRNA expression of the pore-forming subunit (*CACNA1C*) as well as $Ca_V\beta$ subunits (*CACNB2a*, *CACNB2b*, and *CACNB3*). In human AF patients, reduced mRNA expression was reported for $Ca_V1.2$ [224–228]; but: [229], $Ca_V1.3$ [227], $Ca_V\beta_1$ [229], $Ca_V\beta_2$ [228], and $Ca_V\alpha_2\delta$-1 [227, 229]. In cultured canine atrial myocytes, it was shown that tachypacing-induced Ca^{2+} load initiated LTCC downregulation by activating Ca^{2+}-dependent calmodulin–calcineurin–NFAT signaling within a few hours of atrial tachypacing [230].

Several studies pointed to the role of miRs in the pathogenesis of AF [231]. MiR-328 was found to be upregulated in canine and murine AF models and human AF patients [232]. Induction of miR-328 expression promoted AF in dogs and mice, and this effect could be antagonized by a specific antisense inhibitor oligonucleotide (AMO-328). In murine atrial myocytes, miR-328 caused APD shortening and reduction of LTCC currents as observed in experimental and clinical AF before. Downregulation of $Ca_V1.2$ and $Ca_V\beta_1$ protein was seen in atria of AF patients, in dogs treated with tachypacing, as well as in murine and neonatal rat atria infected with miR-328. In rats, this effect could be reversed by AMO-328. Other miRs (miR-21 and miR-208b) were also found to be upregulated in AF and to decrease LTCC currents by targeting *CACNA1C* and *CACNB2* expression [228, 233].

Activation of proteolytic mechanisms can decrease LTCC protein expression independent of mRNA reduction [226, 234]. The Ca^{2+}-dependent protease calpain can degrade surface LTCCs on the minute timescale, regulating channel turnover [235]. Expression and activity of atrial calpain was found to be upregulated in AF patients as well as AF animal models and negatively correlated with LTCC protein levels [234, 236].

Phosphorylation of pore and auxiliary LTCC subunits can affect channel gating as well. The role of phosphorylation in chronic human AF, however, is controversial [237]. One group reported unchanged levels of $Ca_V1.2$ and $Ca_V\beta_{2a}$ expression but a more than twofold reduction of LTCC currents, which was associated with the increased activity of protein phosphatases [238]. In contrast, another group observed a reduced $Ca_V1.2$ protein expression, which was accompanied by a compensatory increase in single-channel activity due to higher phosphorylation [239].

Besides $Ca_V1.2$, $Ca_V1.3$ channels may also be involved in AF pathogenesis. Reduction of *CACNA1D* mRNA was reported in atrial samples of patients with persistent AF [227]. $Ca_V1.3$-deficient mice showed significant reduction of LTCC currents in atria but not ventricles and an increased vulnerability to atrial arrhythmias and AF [5, 148, 240]. Although still controversial, several clinical studies observed an association between PR interval prolongation and risk of AF [241]. $Ca_V1.3$-deficient mice showed PR prolongation, too [5, 240]. In atria of AF patients, reduced $Ca_V1.3$ expression was accompanied by decreased levels of ankyrin-B [242]. Using a murine model, the authors showed that ankyrin-B mediates membrane targeting of atrial $Ca_V1.3$ by interacting with its C-terminus and that ankyrin-B deficiency leads to reduced Ca^{2+} current density and enhanced AF vulnerability.

10.5.2.3 Heart Failure

According to the European Society of Cardiology, heart failure (HF) is a clinical syndrome characterized by typical symptoms caused by a structural and/or functional cardiac abnormality, resulting in a reduced cardiac output and/or elevated intracardiac pressures [243]. Of note, there is no agreed single classification of the causes of HF, and many patients have several different pathologies—cardiovascular and non-cardiovascular—underlying this disease. Among the various cardiovascular pathologies are coronary artery disease, myocardial infarction, hypertension, valve disease, AF, and DCM. Prevalence of HF is estimated to be 1–2% among adults in developed countries, but steeply rises with age, reaching 70% and more among persons

>70 years of age. Although treatment options clearly improved during the last few decades, HF is still associated with a high mortality [244]. Data collected in Europe between 2011 and 2013 showed 12-month all-cause mortality rates for hospitalized (acute) and ambulatory (chronic) HF of 24% and 6%, respectively [245]. About a half of the deaths is sudden, with a large fraction of them presumably due to ventricular arrhythmias [246, 247]. AF and HF often coexist, sharing risk factors and promoting development and deterioration of each other [248]. In chronic HF, AF is an independent predictor of mortality [245].

10.5.2.3.1 Alterations of Ventricular LTCCs in HF

Electrophysiological remodeling promoting arrhythmias in HF is manifold, including ion-channel and Ca^{2+}-handling alterations [249–252]. LTCC expression (detected as dihydropyridine binding sites, *CACNA1C* mRNA, or $Ca_V1.2$ protein level) and current density were mostly reported to be unchanged in human failing ventricular myocytes [253–259]. Nonetheless, some studies described reduction of currents or LTCC expression [260–263], although HF etiology and/or stage of HF may play a role [250, 253]. Furthermore, a shift in the expression of $Ca_V1.2$ splice variants was observed in human failing myocytes [264–266]. Expression of the auxiliary $Ca_V\alpha_2$-δ subunit was not altered in human HF [257, 267]. Studies on expression of $Ca_V\beta$ subunits in human HF have been conflicting and inconclusive [268]. In a comprehensive analysis of human specimens from failing ventricles, we found an increased expression of $Ca_V\beta_2$ subunits at both mRNA and protein level, while that of $Ca_V\beta_1$ and $Ca_V\beta_3$ appeared to be unchanged or even reduced ($Ca_V\beta_3$ protein) [257]. Overexpression of $Ca_V\beta_2$ subunits in adult mouse hearts over a period of 6 weeks caused LTCC current alterations similar to those observed in human HF [269]. On the background of constitutive cardiac $Ca_V1.2$ overexpression, this furthermore led to a significantly increased occurrence of cardiac arrhythmias including supraventricular and ventricular extrasystoles and AV block. Expression of the RGK protein Rad was found to be decreased in failing human ventricles both at mRNA and protein levels [270, 271]. Of interest, overexpressing a dominant negative mutant of Rad caused ventricular arrhythmia in mice [272]. Given the inhibitory effect of Rad on $Ca_V1.2$, increased LTCC activity might have been pro-arrhythmic here [272, 273]. Very recently, a study found that Rad inhibits $Ca_V\beta_2$-mediated stimulation of $Ca_V1.2$ [274]. Rad phosphorylation following β-adrenergic stimulation led to a decrease of its affinity for $Ca_V\beta_2$ subunits and by this relieved constitutive inhibition of $Ca_V1.2$. This study sheds new light on the role of β-adrenergic signaling and $Ca_V\beta_2$-$Ca_V1.2$ interaction for LTCC stimulation and thus promotion of probably pro-arrhythmic conditions.

The group of Stefan Herzig found activity of single LTCCs to be significantly increased in human failing ventricular myocytes [275]. Although this was supported by later studies [255, 256], these data are in an apparent contradiction to the abovementioned findings on reduced or rather unchanged $Ca_V1.2$ expression and whole-cell LTCC current density. However, there is loss and remodeling of the T-tubule system, which plays an important role in the pathogenesis and arrhythmogenesis in HF [252, 276]. T-tubule degradation in human and rat HF was accompanied by redistribution of LTCCs from their native positions in T-tubules to the sarcolemma crest [277, 278]. Targeting of LTCCs to T-tubules is controlled by the scaffolding BIN-1 protein [279]. Its downregulation in HF leads to diminished abundance of $Ca_V1.2$ channels in the periphery and, specifically, T-tubules of the failing myocytes despite unchanged overall cellular expression [258]. Besides, BIN-1 organizes dyads formed by LTCCs and RyRs [280]. In HF, the abovementioned microdomain remodeling of LTCCs is related to an increased occurrence of orphaned RyRs, i.e., RyRs not coupled to LTCCs [280–282]. Such RyRs can lead to spontaneous Ca^{2+} release promoting Ca^{2+}-dependent arrhythmias [280]. Dislocated crest LTCCs showed increased single-channel activity in HF, whereas the activity of the remaining T-tubule LTCCs was not changed [275, 278]. The underlying mechanism was proposed to be channel hyper-phosphorylation due to dephosphorylation defects on the one hand and increased phosphorylation on the other hand [255, 256, 275, 278]. An increased expression of $Ca_V\beta_{2a}$ subunits, which are subject to PKA and CaMKII phosphorylation, can also play a role [257, 283, 284]. A channel's basal hyper-phosphorylation is consistent with a compromised ability of β-adrenergic stimulation to (further) augment LTCC activity in HF [255, 256, 262, 275]. Switch to the high-activity gating mode and disorganization with RyRs can result in a slowed inactivation of LTCC currents and thus promote EADs [278]. Accordingly, whole-heart computer simulations demonstrated that this microdomain remodeling of LTCCs promotes EADs in endocardial myocytes, which can trigger reentrant arrhythmias.

So far, research has focused on $Ca_V1.2$ LTCCs in HF. However, recently re-expression of the fetal $Ca_V1.3$ subunit was reported in the human failing ventricles on both mRNA and protein level [263]. The putative role of $Ca_V1.3$ channels in HF and ventricular arrhythmias requires further studies.

10.5.2.3.2 Alterations of Atrial LTCCs in HF

Remodeling of atrial $Ca_V1.2$ LTCCs in HF is similar to that in AF [209]. In HF animal models, atrial LTCC current density was reported to be reduced [285–289]. In human HF, atrial LTCC currents were either decreased [211, 262] or showed no difference compared to control [259, 290, 291]. Besides, disruption of atrial T-tubules in HF can lead to a decreased number of functional LTCCs [292, 293]. Loss of T-tubules caused by HF was more dramatic in atria than in ventricles [292, 293]. Moreover, single-channel current amplitudes of T-tubular LTCCs were largely decreased in HF [294]. Taken together, animal models of HF indicate reduction of functional LTCCs creating substrate for AF [209], while human data are conflicting.

10.6 Conclusion and Limitations

LTCCs are critically involved in shaping cardiac action potentials. By this capability, dysfunction of LTCCs, either congenital or acquired, can lead to life-threatening cardiac rhythm disturbances (Table 10.1, Fig. 10.1). Though LTCC mutations are rare, a growing number of LTCC genetic variants are identified in and related to arrhythmogenic syndromes. While the association between *CACNA1C* mutations and Timothy syndrome is well established, additional research is required to validate causality of arrhythmias by new LTCC mutations, many of them identified in single patients only. Functional studies with cultured cells allow for comparison of mutant and wild-type LTCCs, but limited by the fact that these cells cannot fully reconstitute the conditions in native cardiomyocytes. LTCCs are also involved in the pathogenesis of acquired cardiac diseases. Despite the fact that human data are not easy to obtain and that comparison with animal models is hampered by differences in ion channel expression patterns as well as structural and electrical properties of the myocardium, great progress has been made in understanding LTCC (dys-)regulation in atrial fibrillation, heart failure, and other arrhythmogenic conditions, including aging.

References

1. Catterall WA. Structure and regulation of voltage-gated Ca $^{2+}$ channels. Annu Rev Cell Dev Biol. 2000;16:521–55.
2. Verheijck EE, van Ginneken ACG, Wilders R, Bouman LN. Contribution of L-type Ca $^{2+}$ current to electrical activity in sinoatrial nodal myocytes of rabbits. Am J Physiol-Heart Circ Physiol. 1999;276: H1064–77.
3. Nerbonne JM, Kass RS. Molecular physiology of cardiac repolarization. Physiol Rev. 2005;85:1205–53.
4. Platzer J, Engel J, Schrott-Fischer A, Stephan K, Bova S, Chen H, et al. Congenital deafness and sinoatrial node dysfunction in mice lacking class D L-type Ca2+ channels. Cell. 2000;102:89–97.
5. Matthes J, Yildirim L, Wietzorrek G, Reimer D, Striessnig J, Herzig S. Disturbed atrio-ventricular conduction and normal contractile function in

isolated hearts from Cav1.3-knockout mice. Naunyn Schmiedebergs Arch Pharmacol. 2004;369:554–62.

6. Baig SM, Koschak A, Lieb A, Gebhart M, Dafinger C, Nürnberg G, et al. Loss of Ca(v)1.3 (CACNA1D) function in a human channelopathy with bradycardia and congenital deafness. Nat Neurosci. 2011;14:77–84.
7. Zhu Y, Luo J, Jiang F, Liu G. Genetic analysis of sick sinus syndrome in a family harboring compound CACNA1C and TTN mutations. Mol Med Rep. 2018;17(5):7073–80.
8. Martin CA, Matthews GDK, Huang CL-H. Sudden cardiac death and inherited channelopathy: the basic electrophysiology of the myocyte and myocardium in ion channel disease. Heart. 2012;98:536–43.
9. Franz MR, Jamal SM, Narayan SM. The role of action potential alternans in the initiation of atrial fibrillation in humans: a review and future directions. Europace. 2012;14(Suppl 5):v58–64.
10. Zhang Q, Chen J, Qin Y, Wang J, Zhou L. Mutations in voltage-gated L-type calcium channel: implications in cardiac arrhythmia. Channels. 2018;12:201–18.
11. Nattel S, Maguy A, Le Bouter S, Yeh Y-H. Arrhythmogenic ion-channel remodeling in the heart: Heart failure, myocardial infarction, and atrial fibrillation. Physiol Rev. 2007;87:425–56.
12. Biliczki P, Boon RA, Girmatsion Z, Bukowska A, Ördög B, Kaess BM, et al. Age-related regulation and region-specific distribution of ion channel subunits promoting atrial fibrillation in human left and right atria. Europace. 2019;21:1261–9.
13. Catterall WA, Perez-Reyes E, Snutch TP, Striessnig J. International Union of Pharmacology. XLVIII. Nomenclature and structure-function relationships of voltage-gated calcium channels. Pharmacol Rev. 2005;57:411–25.
14. Michels G, Matthes J, Handrock R, Kuchinke U, Groner F, Cribbs LL, et al. Single-channel pharmacology of mibefradil in human native T-type and recombinant $Ca_v3.2$ calcium channels. Mol Pharmacol. 2002;61:682–94.
15. Bean BP. Two kinds of calcium channels in canine atrial cells. Differences in kinetics, selectivity, and pharmacology. J Gen Physiol. 1985;86:1–30.
16. Qu Y, Boutjdir M. Gene expression of SERCA2a and L- and T-type Ca channels during human heart development. Pediatr Res. 2001;50:569–74.
17. Gaborit N, Le Bouter S, Szuts V, Varro A, Escande D, Nattel S, et al. Regional and tissue specific transcript signatures of ion channel genes in the non-diseased human heart: Regional ion channel subunit gene expression in the human heart. J Physiol. 2007;582:675–93.
18. Chandler NJ, Greener ID, Tellez JO, Inada S, Musa H, Molenaar P, et al. Molecular architecture of the human sinus node: insights into the function of the cardiac pacemaker. Circulation. 2009;119:1562–75.
19. Greener ID, Monfredi O, Inada S, Chandler NJ, Tellez JO, Atkinson A, et al. Molecular architecture of the human specialised atrioventricular conduction axis. J Mol Cell Cardiol. 2011;50:642–51.
20. Ono K, Iijima T. Pathophysiological significance of T-type Ca2+ channels: Properties and functional roles of T-type Ca2+ channels in cardiac pacemaking. J Pharmacol Sci. 2005;99:197–204.
21. Cribbs L. T-type calcium channel expression and function in the diseased heart. Channels. 2010;4:447–52.
22. Bodi I. The L-type calcium channel in the heart: the beat goes on. J Clin Invest. 2005;115:3306–17.
23. Jangsangthong W, Kuzmenkina E, Bohnke AK, Herzig S. Single-channel monitoring of reversible L-type Ca(2+) channel Ca(V)alpha(1)-Ca(V)beta subunit interaction. Biophys J. 2011;101:2661–70.
24. Campiglio M, Di Biase V, Tuluc P, Flucher BE. Stable incorporation versus dynamic exchange of subunits in a native Ca2+ channel complex. J Cell Sci. 2013;126:2092–101.
25. Yang L, Katchman A, Morrow JP, Doshi D, Marx SO. Cardiac L-type calcium channel ($Ca_v1.2$) associates with γ subunits. FASEB J. 2011;25:928–36.
26. Hofmann F, Flockerzi V, Kahl S, Wegener JW. L-Type $Ca_V1.2$ calcium channels: From in vitro findings to in vivo function. Physiol Rev. 2014;94:303–26.
27. Saimi Y, Kung C. Calmodulin as an ion channel subunit. Annu Rev Physiol. 2002;64:289–311.
28. Ben-Johny M, Dick IE, Sang L, Limpitikul WB, Kang PW, Niu J, et al. Towards a unified theory of calmodulin regulation (calmodulation) of voltage-gated calcium and sodium channels. Curr Mol Pharmacol. 2015;8:188–205.
29. Zamponi GW, Striessnig J, Koschak A, Dolphin AC. The physiology, pathology, and pharmacology of voltage-gated calcium channels and their future therapeutic potential. Pharmacol Rev. 2015;67:821–70.
30. Pozdnyakov I, Matantseva O, Skarlato S. Diversity and evolution of four-domain voltage-gated cation channels of eukaryotes and their ancestral functional determinants. Sci Rep. 2018;8(1):3539. https://doi.org/10.1038/s41598-018-21897-7.
31. Zhen X, Xie C, Fitzmaurice A, Schoonover CE, Orenstein ET, Yang J. Functional architecture of the inner pore of a voltage-gated Ca2+ channel. J Gen Physiol. 2005;126:193–204.
32. Stary A, Shafrir Y, Hering S, Wolschann P, Guy HR. Structural model of the $Ca_V1.2$ pore. Channels. 2008;2:210–5.
33. Wu J, Yan Z, Li Z, Qian X, Lu S, Dong M, et al. Structure of the voltage-gated calcium channel Cav1.1 at 3.6 Å resolution. Nature. 2016;537:191–6.
34. Hering S, Zangerl-Plessl E-M, Beyl S, Hohaus A, Andranovits S, Timin EN. Calcium channel gating. Pflüg Arch Eur J Physiol. 2018;470:1291–309.

35. Stotz SC, Jarvis SE, Zamponi GW. Functional roles of cytoplasmic loops and pore lining transmembrane helices in the voltage-dependent inactivation of HVA calcium channels: Calcium-channel inactivation. J Physiol. 2004;554:263–73.
36. Buraei Z, Yang J. The β subunit of voltage-gated Ca^{2+} channels. Physiol Rev. 2010;90:1461–506.
37. Catterall WA. Voltage-gated calcium channels. Cold Spring Harb Perspect Biol. 2011;3:a003947.
38. Striessnig J, Pinggera A, Kaur G, Bock G, Tuluc P. L-type Ca $^{2+}$ channels in heart and brain: L-type Ca $^{2+}$ channels. Wiley Interdiscip Rev Membr Transp Signal. 2014;3:15–38.
39. Hulme JT, Konoki K, Lin TW-C, Gritsenko MA, Camp DG, Bigelow DJ, et al. Sites of proteolytic processing and noncovalent association of the distal C-terminal domain of CaV1.1 channels in skeletal muscle. Proc Natl Acad Sci USA. 2005;102:5274–9.
40. Hulme JT, Yarov-Yarovoy V, Lin TW-C, Scheuer T, Catterall WA. Autoinhibitory control of the Ca $_V$ 1.2 channel by its proteolytically processed distal C-terminal domain: Autoinhibition of Ca $^{2+}$ channel activity by the distal C-terminus. J Physiol. 2006;576: 87–102.
41. Singh A, Hamedinger D, Hoda J-C, Gebhart M, Koschak A, Romanin C, et al. C-terminal modulator controls Ca2+-dependent gating of Cav1.4 L-type Ca2+ channels. Nat Neurosci. 2006;9:1108–16.
42. Singh A, Gebhart M, Fritsch R, Sinnegger-Brauns MJ, Poggiani C, Hoda J-C, et al. Modulation of voltage- and Ca^{2+}-dependent gating of $Ca_V1.3$ L-type calcium channels by alternative splicing of a C-terminal regulatory domain. J Biol Chem. 2008;283:20733–44.
43. Bock G, Gebhart M, Scharinger A, Jangsangthong W, Busquet P, Poggiani C, et al. Functional properties of a newly identified C-terminal splice variant of $Ca_v1.3$ L-type Ca^{2+} channels. J Biol Chem. 2011;286:42736–48.
44. Tan BZ, Jiang F, Tan MY, Yu D, Huang H, Shen Y, Soong TW. Functional characterization of alternative splicing in the C terminus of L-type $Ca_V1.3$ channels. J Biol Chem. 2011;286:42725–35.
45. Tan GMY, Yu D, Wang J, Soong TW. Alternative splicing at C terminus of $Ca_V1.4$ calcium channel modulates calcium-dependent inactivation, activation potential, and current density. J Biol Chem. 2012;287:832–47.
46. Mangoni ME, Couette B, Bourinet E, Platzer J, Reimer D, Striessnig J, et al. Functional role of L-type Cav1.3 Ca2+ channels in cardiac pacemaker activity. Proc Natl Acad Sci USA. 2003;100:5543–8.
47. Dobrzynski H, Anderson RH, Atkinson A, Borbas Z, D'Souza A, Fraser JF, et al. Structure, function and clinical relevance of the cardiac conduction system, including the atrioventricular ring and outflow tract tissues. Pharmacol Ther. 2013;139:260–88.
48. Koschak A, Reimer D, Huber I, Grabner M, Glossmann H, Engel J, et al. α1D (Cav1.3) Subunits can form L-type Ca^{2+} channels activating at negative voltages. J Biol Chem. 2001;276:22100–6.
49. Xu W, Lipscombe D. Neuronal $Ca_V1.3\alpha_1$ L-Type channels activate at relatively hyperpolarized membrane potentials and are incompletely inhibited by dihydropyridines. J Neurosci. 2001;21:5944–51.
50. Zhu J, Shang Y, Chen J, Zhang M. Structure and function of the guanylate kinase-like domain of the MAGUK family scaffold proteins. Front Biol. 2012;7:379–96.
51. Kurochkina N, Guha U. SH3 domains: modules of protein–protein interactions. Biophys Rev. 2013;5: 29–39.
52. Gonzalez-Gutierrez G, Miranda-Laferte E, Neely A, Hidalgo P. The Src homology 3 domain of the β-subunit of voltage-gated calcium channels promotes endocytosis via dynamin interaction. J Biol Chem. 2007;282:2156–62.
53. Buraei Z, Lumen E, Kaur S, Yang J. RGK regulation of voltage-gated calcium channels. Sci China Life Sci. 2015;58:28–38.
54. van Petegem F, Clark KA, Chatelain FC, Minor DL Jr. Structure of a complex between a voltage-gated calcium channel β-subunit and an α-subunit domain. Nature. 2004;429(6992):671–5.
55. Hullin R, Khan IFY, Wirtz S, Mohacsi P, Varadi G, Schwartz A, et al. Cardiac L-type calcium channel β-subunits expressed in human heart have differential effects on single channel characteristics. J Biol Chem. 2003;278:21623–30.
56. Chu P. Distribution and relative expression levels of calcium channel β subunits within the chambers of the rat heart. J Mol Cell Cardiol. 2004;36:423–34.
57. Herzig S, Khan IF, Gründemann D, Matthes J, Ludwig A, Michels G, et al. Mechanism of $Ca_v1.2$ channel modulation by the amino terminus of cardiac β_2-subunits. FASEB J. 2007;21:1527–38.
58. Foell JD, Balijepalli RC, Delisle BP, Yunker AMR, Robia SL, Walker JW, et al. Molecular heterogeneity of calcium channel β-subunits in canine and human heart: evidence for differential subcellular localization. Physiol Genomics. 2004;17:183–200.
59. Bourdin B, Briot J, Tétreault M-P, Sauvé R, Parent L. Negatively charged residues in the first extracellular loop of the L-type $Ca_V1.2$ channel anchor the interaction with the $Ca_V\alpha2\delta1$ auxiliary subunit. J Biol Chem. 2017;292:17236–49.
60. Briot J, Mailhot O, Bourdin B, Tétreault M-P, Najmanovich R, Parent L. A three-way inter-molecular network accounts for the $Ca_V\alpha2\delta1$-induced functional modulation of the pore-forming $Ca_V1.2$ subunit. J Biol Chem. 2018;293:7176–88.
61. Dolphin AC. Voltage-gated calcium channel α2δ subunits: an assessment of proposed novel roles. F1000Research. 2018;7:1830.
62. Qin N, Yagel S, Momplaisir M-L, Codd EE, D'Andrea MR. Molecular cloning and characterization of the human voltage-gated calcium channel

alpha(2)delta-4 subunit. Mol Pharmacol. 2002;62:485–96.

63. Klugbauer N, Marais E, Hofmann F. Calcium channel α2δ subunits: differential expression, function, and drug binding. J Bioenerg Biomembr. 2003;35(6):639–47.
64. Hatano S, Yamashita T, Sekiguchi A, Iwasaki Y, Nakazawa K, Sagara K, et al. Molecular and electrophysiological differences in the L-type Ca^{2+} channel of the atrium and ventricle of rat hearts. Circ J. 2006;70:610–4.
65. Chen R-S, Deng T-C, Garcia T, Sellers ZM, Best PM. Calcium channel γ subunits: a functionally diverse protein family. Cell Biochem Biophys. 2007;47:178–86.
66. Chin D, Means AR. Calmodulin: a prototypical calcium sensor. Trends Cell Biol. 2000;10:322–8.
67. Fischer R, Koller M, Flura M, Mathews S, Strehler-Page MA, Krebs J, et al. Multiple divergent mRNAs code for a single human calmodulin. J Biol Chem. 1988;263:17055–62.
68. Crotti L, Johnson CN, Graf E, De Ferrari GM, Cuneo BF, Ovadia M, et al. Calmodulin mutations associated with recurrent cardiac arrest in infants. Circulation. 2013;127:1009–17.
69. Liu X, Yang PS, Yang W, Yue DT. Enzyme-inhibitor-like tuning of Ca2+ channel connectivity with calmodulin. Nature. 2010;463:968–72.
70. Liu N, Yang Y, Ge L, Liu M, Colecraft HM, Liu X. Cooperative and acute inhibition by multiple C-terminal motifs of L-type Ca2+ channels. eLife. 2017; https://doi.org/10.7554/eLife.21989.
71. Adams PJ, Ben-Johny M, Dick IE, Inoue T, Yue DT. Apocalmodulin itself promotes ion channel opening and Ca2+ regulation. Cell. 2014;159:608–22.
72. Lyu L, Gao Q, Xu J, Minobe E, Zhu T, Kameyama M. A new interaction between proximal and distal C-terminus of Cav1.2 channels. J Pharmacol Sci. 2017;133:240–6.
73. Kuzmenkina E, Novikova E, Jangsangthong W, Matthes J, Herzig S. Single-channel resolution of the interaction between C-terminal Cav1.3 isoforms and calmodulin. Biophys J. 2019;116:836–46.
74. Lei M, Xu J, Gao Q, Minobe E, Kameyama M, Hao L. PKA phosphorylation of Cav1.2 channel modulates the interaction of calmodulin with the C terminal tail of the channel. J Pharmacol Sci. 2018;137:187–94.
75. Hall DD, Dai S, Tseng P-Y, Malik Z, Nguyen M, Matt L, et al. Competition between α-actinin and Ca2+-calmodulin controls surface retention of the L-type Ca2+ channel CaV1.2. Neuron. 2013;78:483–97.
76. Fabiato A. Calcium-induced release of calcium from the cardiac sarcoplasmic reticulum. Am J Physiol-Cell Physiol. 1983;245:C1–C14.
77. Bers DM, Perez-Reyes E. Ca channels in cardiac myocytes: structure and function in Ca influx and intracellular Ca release. Cardiovasc Res. 1999;42:339–60.
78. Roden DM. Taking the “idio” out of “idiosyncratic”: predicting torsades de pointes. Pacing Clin Electrophysiol PACE. 1998;21:1029–34.
79. Weiss JN, Garfinkel A, Karagueuzian HS, Chen P-S, Qu Z. Early afterdepolarizations and cardiac arrhythmias. Heart Rhythm. 2010;7:1891–9.
80. Markandeya YS, Kamp TJ. Rational strategy to stop arrhythmias: Early afterdepolarizations and L-type Ca2+ current. J Gen Physiol. 2015;145:475–9.
81. Markandeya YS, Kamp TJ. Rational strategy to stop arrhythmias: Early afterdepolarizations and L-type Ca2+ current. J Gen Physiol. 2010;145:475–9.
82. Torrente AG, Mesirca P, Bidaud I, Mangoni ME. Channelopathies of voltage-gated L-type Cav1.3/α1D and T-type Cav3.1/α1G Ca2+ channels in dysfunction of heart automaticity. Pflüg Arch Eur J Physiol. 2020;472:817–30.
83. Lakatta EG, Maltsev VA, Vinogradova TM. A coupled SYSTEM of intracellular Ca $^{2+}$ clocks and surface membrane voltage clocks controls the timekeeping mechanism of the heart’s pacemaker. Circ Res. 2010;106:659–73.
84. Toyoda F, Mesirca P, Dubel S, Ding W-G, Striessnig J, Mangoni ME, et al. CaV1.3 L-type Ca2+ channel contributes to the heartbeat by generating a dihydropyridine-sensitive persistent Na+ current. Sci Rep. 2017;7(1):7869. https://doi.org/10.1038/s41598-017-08191-8.
85. Christel CJ, Cardona N, Mesirca P, Herrmann S, Hofmann F, Striessnig J. Distinct localization and modulation of $Ca_v1.2$ and $Ca_v1.3$ L-type Ca^{2+} channels in mouse sinoatrial node: Ca_v1 channels in mouse sinoatrial node. J Physiol. 2012;590:6327–41.
86. Semsarian C, Ingles J, Wilde AAM. Sudden cardiac death in the young: the molecular autopsy and a practical approach to surviving relatives. Eur Heart J. 2015;36:1290–6.
87. Garcia-Elias A, Benito B. Ion Channel disorders and sudden cardiac death. Int J Mol Sci. 2018;19:692.
88. Splawski I, Timothy KW, Sharpe LM, Decher N, Kumar P, Bloise R, et al. CaV1.2 Calcium channel dysfunction causes a multisystem disorder including arrhythmia and autism. Cell. 2004;119:19–31.
89. Betzenhauser M, Pitt G, Antzelevitch C. Calcium channel mutations in cardiac arrhythmia syndromes. Curr Mol Pharmacol. 2015;8:133–42.
90. Gardner RJM, Crozier IG, Binfield AL, Love DR, Lehnert K, Gibson K, et al. Penetrance and expressivity of the R858H *CACNA1C* variant in a five-generation pedigree segregating an arrhythmogenic channelopathy. Mol Genet Genomic Med. 2019;7:e00476.
91. Tse G, Chan YWF, Keung W, Yan BP. Electrophysiological mechanisms of long and short QT syndromes. IJC Heart Vasc. 2017;14:8–13.
92. Giudicessi JR, Wilde AAM, Ackerman MJ. The genetic architecture of long QT syndrome: A critical

reappraisal. Trends Cardiovasc Med. 2018;28:453–64.

93. Splawski I, Timothy KW, Decher N, Kumar P, Sachse FB, Beggs AH, et al. Severe arrhythmia disorder caused by cardiac L-type calcium channel mutations. Proc Natl Acad Sci USA. 2005;102: 8089–96.
94. Han D, Xue X, Yan Y, Li G. Dysfunctional Cav1.2 channel in Timothy syndrome, from cell to bedside. Exp Biol Med. 2019;244:960–71.
95. Dufendach KA, Timothy K, Ackerman MJ, Blevins B, Pflaumer A, Etheridge S, et al. Clinical outcomes and modes of death in Timothy syndrome. JACC Clin Electrophysiol. 2018;4:459–66.
96. Fröhler S, Kieslich M, Langnick C, Feldkamp M, Opgen-Rhein B, Berger F, et al. Exome sequencing helped the fine diagnosis of two siblings afflicted with atypical Timothy syndrome (TS2). BMC Med Genet. 2014;15:48. https://doi.org/10.1186/1471-2350-15-48.
97. Hiippala A, Tallila J, Myllykangas S, Koskenvuo JW, Alastalo T-P. Expanding the phenotype of Timothy syndrome type 2: an adolescent with ventricular fibrillation but normal development. Am J Med Genet A. 2015;167A:629–34.
98. Kosaki R, Ono H, Terashima H, Kosaki K. Timothy syndrome-like condition with syndactyly but without prolongation of the QT interval. Am J Med Genet A. 2018;176:1657–61.
99. Erxleben C, Liao Y, Gentile S, Chin D, Gomez-Alegria C, Mori Y. Cyclosporin and Timothy syndrome increase mode 2 gating of CaV1.2 calcium channels through aberrant phosphorylation of S6 helices. Proc Natl Acad Sci USA. 2006;103:3932–7.
100. Dick IE, Joshi-Mukherjee R, Yang W, Yue DT. Arrhythmogenesis in Timothy syndrome is associated with defects in Ca2+-dependent inactivation. Nat Commun. 2016;7:10370. https://doi.org/10.1038/ncomms10370.
101. Tadross MR, Johny MB, Yue DT. Molecular endpoints of Ca2+/calmodulin- and voltage-dependent inactivation of Cav1.3 channels. J Gen Physiol. 2010;135:197–215.
102. Yarotskyy V, Gao G, Peterson BZ, Elmslie KS. The Timothy syndrome mutation of cardiac CaV1.2 (L-type) channels: multiple altered gating mechanisms and pharmacological restoration of inactivation: Affects of the Timothy syndrome mutation on L-channel gating. J Physiol. 2009;587:551–65.
103. Cheng EP, Yuan C, Navedo MF, Dixon RE, Nieves-Cintrón M, Scott JD, et al. Restoration of normal L-type Ca $^{2+}$ channel function during Timothy syndrome by ablation of an anchoring protein. Circ Res. 2011;109:255–61.
104. Dixon RE, Cheng EP, Mercado JL, Santana LF. L-Type Ca2+ channel function during Timothy syndrome. Trends Cardiovasc Med. 2012;22:72–6.
105. Colson C, Mittre H, Busson A, Leenhardt A, Denjoy I, Fressard V, et al. Unusual clinical description of adult with Timothy syndrome, carrier of a new heterozygote mutation of CACNA1C. Eur J Med Genet. 2019;62:103648.
106. Boczek NJ, Miller EM, Ye D, Nesterenko VV, Tester DJ, Antzelevitch C, et al. Novel Timothy syndrome mutation leading to increase in CACNA1C window current. Heart Rhythm. 2015;12:211–9.
107. Wemhöner K, Friedrich C, Stallmeyer B, Coffey AJ, Grace A, Zumhagen S, et al. Gain-of-function mutations in the calcium channel CACNA1C (Cav1.2) cause non-syndromic long-QT but not Timothy syndrome. J Mol Cell Cardiol. 2015;80:186–95.
108. Gillis J, Burashnikov E, Antzelevitch C, Blaser S, Gross G, Turner L, et al. Long QT, syndactyly, joint contractures, stroke and novel CACNA1C mutation: Expanding the spectrum of Timothy syndrome. Am J Med Genet A. 2012;158A:182–7.
109. Ozawa J, Ohno S, Saito H, Saitoh A, Matsuura H, Horie M. A novel CACNA1C mutation identified in a patient with Timothy syndrome without syndactyly exerts both marked loss- and gain-of-function effects. Hear Case Rep. 2018;4:273–7.
110. Boczek NJ, Best JM, Tester DJ, Giudicessi JR, Middha S, Evans JM, et al. Exome sequencing and systems biology converge to identify novel mutations in the L-type calcium channel, *CACNA1C*, linked to autosomal dominant long QT syndrome. Circ Cardiovasc Genet. 2013;6:279–89.
111. Boczek NJ, Ye D, Jin F, Tester DJ, Huseby A, Bos JM, et al. Identification and functional characterization of a novel *CACNA1C* -mediated cardiac disorder characterized by prolonged QT intervals with hypertrophic cardiomyopathy, congenital heart defects, and sudden cardiac death. Circ Arrhythm Electrophysiol. 2015;8:1122–32.
112. Hennessey JA, Boczek NJ, Jiang Y-H, Miller JD, Patrick W, Pfeiffer R, et al. A CACNA1C variant associated with reduced voltage-dependent inactivation, increased CaV1.2 channel window current, and arrhythmogenesis. PLoS One. 2014;9:e106982.
113. Ye D, Tester DJ, Zhou W, Papagiannis J, Ackerman MJ. A pore-localizing CACNA1C-E1115K missense mutation, identified in a patient with idiopathic QT prolongation, bradycardia, and autism spectrum disorder, converts the L-type calcium channel into a hybrid nonselective monovalent cation channel. Heart Rhythm. 2019;16:270–8.
114. Catalucci D, Zhang D-H, DeSantiago J, Aimond F, Barbara G, Chemin J, et al. Akt regulates L-type Ca2+ channel activity by modulating Cavα1 protein stability. J Cell Biol. 2009;184:923–33.
115. Bagnall RD, Ingles J, Dinger ME, Cowley MJ, Ross SB, Minoche AE, et al. Whole genome sequencing improves outcomes of genetic testing in patients with hypertrophic cardiomyopathy. J Am Coll Cardiol. 2018;72:419–29.
116. Larrañaga-Moreira JM, Quintela-García S, Cárdenas-Reyes IJ, Barbeito-Caamaño C, Monserrat-Iglesias L, Barriales-Villa R. Cardiac-only Timothy syndrome

(COTS): Peripartum cardiomyopathy and long QT syndrome. Rev Esp Cardiol Engl Ed. 2019;72:876–8.

117. Estes SI, Ye D, Zhou W, Dotzler SM, Tester DJ, Bos JM, et al. Characterization of the CACNA1C-R518C missense mutation in the pathobiology of long-QT syndrome using human induced pluripotent stem cell cardiomyocytes shows action potential prolongation and L-type calcium channel Perturbation. Circ Genomic Precis Med. 2019;12(8):e002534. https://doi.org/10.1161/CIRCGEN.119.002534.
118. Makita N, Yagihara N, Crotti L, Johnson CN, Beckmann BM, Roh MS, et al. Novel calmodulin mutations associated with congenital arrhythmia susceptibility. Circ Cardiovasc Genet. 2014;7:466–74.
119. Reed GJ, Boczek NJ, Etheridge SP, Ackerman MJ. CALM3 mutation associated with long QT syndrome. Heart Rhythm. 2015;12:419–22.
120. Boczek NJ, Gomez-Hurtado N, Ye D, Calvert ML, Tester DJ, Kryshtal D, et al. Spectrum and prevalence of *CALM1* -, *CALM2* -, and *CALM3* -encoded calmodulin variants in long QT syndrome and functional characterization of a novel long QT syndrome-associated calmodulin missense variant, E141G. Circ Cardiovasc Genet. 2016;9:136–46.
121. Chaix M-A, Koopmann TT, Goyette P, Alikashani A, Latour F, Fatah M, et al. Novel CALM3 mutations in pediatric long QT syndrome patients support a CALM3 -specific calmodulinopathy. Hear Case Rep. 2016;2:250–4.
122. Pipilas DC, Johnson CN, Webster G, Schlaepfer J, Fellmann F, Sekarski N, et al. Novel calmodulin mutations associated with congenital long QT syndrome affect calcium current in human cardiomyocytes. Heart Rhythm. 2016;13:2012–9.
123. Takahashi K, Ishikawa T, Makita N, Takefuta K, Nabeshima T, Nakayashiro M. A novel de novo calmodulin mutation in a 6-year-old boy who experienced an aborted cardiac arrest. HeartRhythm Case Rep. 2017;3:69–72.
124. Yin G, Hassan F, Haroun AR, Murphy LL, Crotti L, Schwartz PJ, et al. Arrhythmogenic calmodulin mutations disrupt intracellular cardiomyocyte Ca^{2+} regulation by distinct mechanisms. J Am Heart Assoc. 2014;3(3):e000996. https://doi.org/10.1161/JAHA.114.000996.
125. Limpitikul WB, Dick IE, Joshi-Mukherjee R, Overgaard MT, George AL, Yue DT. Calmodulin mutations associated with long QT syndrome prevent inactivation of cardiac L-type Ca2+ currents and promote proarrhythmic behavior in ventricular myocytes. J Mol Cell Cardiol. 2014;74:115–24.
126. Wang K, Holt C, Lu J, Brohus M, Larsen KT, Overgaard MT. Arrhythmia mutations in calmodulin cause conformational changes that affect interactions with the cardiac voltage-gated calcium channel. Proc Natl Acad Sci USA. 2018;115:E10556–65.
127. Antzelevitch C, Yan G-X, Ackerman MJ, Borggrefe M, Corrado D, Guo J, et al. J-Wave syndromes expert consensus conference report: Emerging concepts and gaps in knowledge. Europace. 2017;19:665–94.
128. Skinner JR, Winbo A, Abrams D, Vohra J, Wilde AA. Channelopathies that lead to sudden cardiac death: Clinical and genetic aspects. Heart Lung Circ. 2019;28:22–30.
129. Bezzina CR, Lahrouchi N, Priori SG. Genetics of sudden cardiac death. Circ Res. 2015;116:1919–36.
130. Fish JM, Antzelevitch C. Role of sodium and calcium channel block in unmasking the Brugada syndrome. Heart Rhythm. 2004;1:210–7.
131. Antzelevitch C, Pollevick GD, Cordeiro JM, Casis O, Sanguinetti MC, Aizawa Y, et al. Loss-of-function mutations in the cardiac calcium channel underlie a new clinical entity characterized by ST-segment elevation, short QT intervals, and sudden cardiac death. Circulation. 2007;115:442–9.
132. Burashnikov E, Pfeiffer R, Barajas-Martinez H, Delpón E, Hu D, Desai M, et al. Mutations in the cardiac L-type calcium channel associated with inherited J-wave syndromes and sudden cardiac death. Heart Rhythm. 2010;7:1872–82.
133. Mazzanti A, Kanthan A, Monteforte N, Memmi M, Bloise R, Novelli V, et al. Novel insight into the natural history of short QT syndrome. J Am Coll Cardiol. 2014;63:1300–8.
134. Gussak I, Brugada P, Brugada J, Wright RS, Kopecky SL, Chaitman BR, et al. Idiopathic short QT interval: A new clinical syndrome? Cardiology. 2000;94:99–102.
135. Campuzano O, Sarquella-Brugada G, Cesar S, Arbelo E, Brugada J, Brugada R. Recent advances in short QT syndrome. Front Cardiovasc Med. 2018;5:149.
136. Extramiana F, Antzelevitch C. Amplified transmural dispersion of repolarization as the basis for arrhythmogenesis in a canine ventricular-wedge model of short-QT syndrome. Circulation. 2004;110:3661–6.
137. Fukuyama M, Ohno S, Wang Q, Kimura H, Makiyama T, Itoh H, et al. L-Type calcium channel mutations in Japanese patients with inherited arrhythmias. Circ J. 2013;77:1799–806.
138. Béziau DM, Barc J, O'Hara T, Le Gloan L, Amarouch MY, Solnon A, et al. Complex Brugada syndrome inheritance in a family harbouring compound SCN5A and CACNA1C mutations. Basic Res Cardiol. 2014;109:446.
139. Liu X, Shen Y, Xie J, Bao H, Cao Q, Wan R, et al. A mutation in the CACNA1C gene leads to early repolarization syndrome with incomplete penetrance: A Chinese family study. PLoS One. 2017;12:e0177532.
140. Chen Y, Barajas-Martinez H, Zhu D, Wang X, Chen C, Zhuang R, et al. Novel trigenic CACNA1C/DES/MYPN mutations in a family of hypertrophic cardiomyopathy with early repolarization and short QT syndrome. J Transl Med. 2017;15(1):101. https://doi.org/10.1186/s12967-017-1180-1.
141. Sutphin BS, Boczek NJ, Barajas-Martínez H, Hu D, Ye D, Tester DJ, et al. Molecular and functional

characterization of rare *CACNA1C* variants in sudden unexplained death in the young: Sutphin-CACNA1C variants in SUDY. Congenit Heart Dis. 2016;11:683–92.

142. Fukuyama M, Ohno S, Wang Q, Shirayama T, Itoh H, Horie M. Nonsense-mediated mRNA decay due to a CACNA1C splicing mutation in a patient with Brugada syndrome. Heart Rhythm. 2014;11: 629–34.
143. Blancard M, Debbiche A, Kato K, Cardin C, Sabrina G, Gandjbakhch E, et al. An African loss-of-function CACNA1C variant p.T1787M associated with a risk of ventricular fibrillation. Sci Rep. 2018;8: 14619.
144. Cordeiro JM, Marieb M, Pfeiffer R, Calloe K, Burashnikov E, Antzelevitch C. Accelerated inactivation of the L-type calcium current due to a mutation in CACNB2b underlies Brugada syndrome. J Mol Cell Cardiol. 2009;46:695–703.
145. Kanter RJ, Pfeiffer R, Hu D, Barajas-Martinez H, Carboni MP, Antzelevitch C. Brugada-like syndrome in infancy presenting with rapid ventricular tachycardia and intraventricular conduction delay. Circulation. 2012;125:14–22.
146. Crotti L, Marcou CA, Tester DJ, Castelletti S, Giudicessi JR, Torchio M, et al. Spectrum and prevalence of mutations involving BrS1- through BrS12-susceptibility genes in a cohort of unrelated patients referred for Brugada syndrome genetic testing. J Am Coll Cardiol. 2012;60:1410–8.
147. Templin C, Ghadri J-R, Rougier J-S, Baumer A, Kaplan V, Albesa M, et al. Identification of a novel loss-of-function calcium channel gene mutation in short QT syndrome (SQTS6). Eur Heart J. 2011;32: 1077–88.
148. Zhang Z, He Y, Tuteja D, Xu D, Timofeyev V, Zhang Q, et al. Functional roles of $Ca_v1.3(\alpha_{1D})$ calcium channels in atria: Insights gained from gene-targeted null mutant mice. Circulation. 2005;112:1936–44.
149. Hoda J-C. Congenital stationary night blindness type 2 mutations S229P, G369D, L1068P, and W1440X alter channel gating or functional expression of Cav1.4 L-type Ca2+ channels. J Neurosci. 2005;25: 252–9.
150. Pinggera A, Striessnig J. $Ca_v1.3$ (*CACNA1D*) L-type Ca^{2+} channel dysfunction in CNS disorders: $Ca_v1.3$ Ca^{2+} channel dysfunction in CNS disorders. J Physiol. 2016;594:5839–49.
151. Liaqat K, Schrauwen I, Raza SI, Lee K, Hussain S, Chakchouk I, et al. Identification of CACNA1D variants associated with sinoatrial node dysfunction and deafness in additional Pakistani families reveals a clinical significance. J Hum Genet. 2019;64:153–60.
152. Jones SA, Boyett MR, Lancaster MK. Declining into failure: The age-dependent loss of the L-type calcium channel within the sinoatrial node. Circulation. 2007;115:1183–90.
153. Lazzerini PE, Capecchi PL, Laghi-Pasini F. Systemic inflammation and arrhythmic risk: lessons from rheumatoid arthritis. Eur Heart J. 2017;38:1717–27.
154. Lazzerini PE, Capecchi PL, Laghi-Pasini F, Boutjdir M. Autoimmune channelopathies as a novel mechanism in cardiac arrhythmias. Nat Rev Cardiol. 2017;14:521–35.
155. Swirski FK, Nahrendorf M. Cardioimmunology: the immune system in cardiac homeostasis and disease. Nat Rev Immunol. 2018;18:733–44.
156. Qu YS, Lazzerini PE, Capecchi PL, Laghi-Pasini F, El Sherif N, Boutjdir M. Autoimmune calcium channelopathies and cardiac electrical abnormalities. Front Cardiovasc Med. 2019;6:54. https://doi.org/10.3389/fcvm.2019.00054.
157. Liao YH, Cheng LX, Dai SP, Tu YS. Autoantibodies against ADP/ATP carrier from patients with dilated cardiomyopathy increase activity of voltage-dependent Ca channels in isolated cardiac myocytes. Blood Press Suppl. 1996;3:41–4.
158. Xiao H, Wang M, Du Y, Yuan J, Cheng X, Chen Z, et al. Arrhythmogenic autoantibodies against calcium channel lead to sudden death in idiopathic dilated cardiomyopathy. Eur J Heart Fail. 2011;13:264–70.
159. Xiao H, Wang M, Du Y, Yuan J, Zhao G, Tu D, et al. Agonist-like autoantibodies against calcium channel in patients with dilated cardiomyopathy. Heart Vessels. 2012;27:486–92.
160. Yu H, Pei J, Liu X, Chen J, Li X, Zhang Y, et al. Calcium channel autoantibodies predicted sudden cardiac death and all-cause mortality in patients with ischemic and nonischemic chronic heart failure. Dis Markers. 2014;2014:1–8.
161. Zhou Z, Wang J, Xiao H, Chen Z, Wang M, Cheng X, et al. A novel autoantibody in patients with primary hypertension: antibody against L-type Ca2+ channel. Chin Med J (Engl). 2008;121:1513–7.
162. Okazaki T, Tanaka Y, Nishio R, Mitsuiye T, Mizoguchi A, Wang J, et al. Autoantibodies against cardiac troponin I are responsible for dilated cardiomyopathy in PD-1-deficient mice. Nat Med. 2003;9: 1477–83.
163. Shmilovich H, Danon A, Binah O, Roth A, Chen G, Wexler D, et al. Autoantibodies to cardiac troponin I in patients with idiopathic dilated and ischemic cardiomyopathy. Int J Cardiol. 2007;117:198–203.
164. Christ T, Wettwer E, Dobrev D, Adolph E, Knaut M, Wallukat G, et al. Autoantibodies against the beta1 adrenoceptor from patients with dilated cardiomyopathy prolong action potential duration and enhance contractility in isolated cardiomyocytes. J Mol Cell Cardiol. 2001;33:1515–25.
165. Llanos C, Friedman DM, Saxena A, Izmirly PM, Tseng C-E, Dische R, et al. Anatomical and pathological findings in hearts from fetuses and infants with cardiac manifestations of neonatal lupus. Rheumatology. 2012;51:1086–92.
166. Brito-Zerón P, Izmirly PM, Ramos-Casals M, Buyon JP, Khamashta MA. The clinical spectrum of

autoimmune congenital heart block. Nat Rev Rheumatol. 2015;11:301–12.

167. Clowse MEB, Eudy AM, Kiernan E, Williams MR, Bermas B, Chakravarty E, et al. The prevention, screening and treatment of congenital heart block from neonatal lupus: a survey of provider practices. Rheumatology. 2018;57:v9–v17.
168. Miranda ME, Tseng CE, Rashbaum W, Ochs RL, Casiano CA, Di Donato F, et al. Accessibility of SSA/Ro and SSB/La antigens to maternal autoantibodies in apoptotic human fetal cardiac myocytes. J Immunol. 1998;161:5061–9.
169. Clancy RM, Neufing PJ, Zheng P, O'Mahony M, Nimmerjahn F, Gordon TP, et al. Impaired clearance of apoptotic cardiocytes is linked to anti-SSA/Ro and -SSB/La antibodies in the pathogenesis of congenital heart block. J Clin Invest. 2006;116:2413–22.
170. Briassouli P, Rifkin D, Clancy RM, Buyon JP. Binding of anti-SSA antibodies to apoptotic fetal cardiocytes stimulates urokinase plasminogen activator (uPA)/uPA receptor-dependent activation of TGF-β and potentiates fibrosis. J Immunol. 2011;187:5392–401.
171. Karnabi E, Boutjdir M. Role of calcium channels in congenital heart block. Scand J Immunol. 2010;72:226–34.
172. Ambrosi A, Wahren-Herlenius M. Congenital heart block: evidence for a pathogenic role of maternal autoantibodies. Arthritis Res Ther. 2012;14:208.
173. Garcia S, Nascimento JH, Bonfa E, Levy R, Oliveira SF, Tavares AV, et al. Cellular mechanism of the conduction abnormalities induced by serum from anti-Ro/SSA-positive patients in rabbit hearts. J Clin Invest. 1994;93:718–24.
174. Boutjdir M, Chen L, Zhang ZH, Tseng CE, DiDonato F, Rashbaum W, et al. Arrhythmogenicity of IgG and anti-52-kD SSA/Ro affinity-purified antibodies from mothers of children with congenital heart block. Circ Res. 1997;80:354–62.
175. Boutjdir M, Chen L, Zhang Z-H, Tseng C-E, El-Sherif N, Buyon JP. Serum and Immunoglobulin G from the mother of a child with congenital heart block induce conduction abnormalities and inhibit L-type calcium channels in a rat heart model. Pediatr Res. 1998;44:11–9.
176. Xiao G-Q, Hu K, Boutjdir M. Direct inhibition of expressed cardiac L- and T-type calcium channels by IgG from mothers whose children have congenital heart block. Circulation. 2001;103:1599–604.
177. Hu K, Qu Y, Yue Y, Boutjdir M. Functional basis of sinus bradycardia in congenital heart block. Circ Res. 2004;94:e32–8.
178. Qu Y, Baroudi G, Yue Y, Boutjdir M. Novel molecular mechanism involving alpha1D (Cav1.3) L-type calcium channel in autoimmune-associated sinus bradycardia. Circulation. 2005;111:3034–41.
179. Karnabi E, Qu Y, Wadgaonkar R, Mancarella S, Yue Y, Chahine M, et al. Congenital heart block: Identification of autoantibody binding site on the extracellular loop (domain I, S5–S6) of α1D L-type Ca channel. J Autoimmun. 2010;34:80–6.
180. Strandberg LS, Cui X, Rath A, Liu J, Silverman ED, Liu X, et al. Congenital heart block maternal sera autoantibodies target an extracellular epitope on the α1G T-type calcium channel in human fetal hearts. PLoS One. 2013;8:e72668.
181. Mesirca P, Torrente AG, Mangoni ME. Functional role of voltage gated Ca2+ channels in heart automaticity. Front Physiol. 2015;6:19. https://doi.org/10.3389/fphys.2015.00019.
182. Maguy A, Tardif J-C, Busseuil D, Ribi C, Li J. Autoantibody signature in cardiac arrest. Circulation. 2020;141:1764–74.
183. Korantzopoulos P, Letsas KP, Tse G, Fragakis N, Goudis CA, Liu T. Inflammation and atrial fibrillation: A comprehensive review. J Arrhythmia. 2018;34:394–401.
184. Kouvas N, Kontogiannis C, Georgiopoulos G, Spartalis M, Tsilimigras DI, Spartalis E, et al. The complex crosstalk between inflammatory cytokines and ventricular arrhythmias. Cytokine. 2018;111:171–7.
185. Wu N, Xu B, Xiang Y, Wu L, Zhang Y, Ma X, et al. Association of inflammatory factors with occurrence and recurrence of atrial fibrillation: A meta-analysis. Int J Cardiol. 2013;169:62–72.
186. Yo C-H, Lee S-H, Chang S-S, Lee MC-H, Lee C-C. Value of high-sensitivity C-reactive protein assays in predicting atrial fibrillation recurrence: a systematic review and meta-analysis. BMJ Open. 2014;4:e004418.
187. Kuzmin VS, Abramochkin DV, Mitrochin VM, Tian B, Makarenko EY, Kovalchuk LV, et al. The role of proinflammatory cytokines in regulation of cardiac bioelectrical activity: link to mechanoelectrical feedback. In: Kamkin A, Kiseleva I, editors. Mechanical stretch and cytokines. Dordrecht: Springer; 2012. p. 107–53.
188. Lazzerini PE, Laghi-Pasini F, Boutjdir M, Capecchi PL. Cardioimmunology of arrhythmias: the role of autoimmune and inflammatory cardiac channelopathies. Nat Rev Immunol. 2019;19:63–4.
189. Hagiwara Y, Miyoshi S, Fukuda K, Nishiyama N, Ikegami Y, Tanimoto K, et al. SHP2-mediated signaling cascade through gp130 is essential for LIF-dependent ICaL, [Ca2+]i transient, and APD increase in cardiomyocytes. J Mol Cell Cardiol. 2007;43:710–6.
190. Sugishita K, Kinugawa K, Shimizu T, Harada K, Matsui H, Takahashi T, et al. Cellular basis for the acute inhibitory effects of IL-6 and TNF- alpha on excitation-contraction coupling. J Mol Cell Cardiol. 1999;31:1457–67.
191. Yu X-W, Chen Q, Kennedy RH, Liu SJ. Inhibition of sarcoplasmic reticular function by chronic interleukin-6 exposure via iNOS in adult ventricular myocytes: Chronic exposure to IL-6 decreases cardiac SR function via iNOS. J Physiol. 2005;566:327–40.
192. Li YH, Rozanski GJ. Effects of human recombinant interleukin-1 on electrical properties of guinea pig ventricular cells. Cardiovasc Res. 1993;27:525–30.

193. Liu S, Schreur KD. G protein-mediated suppression of L-type Ca2+ current by interleukin-1 beta in cultured rat ventricular myocytes. Am J Physiol Cell Physiol. 1995;268:C339–49.
194. Tatsumi T, Matoba S, Kawahara A, Keira N, Shiraishi J, Akashi K, et al. Cytokine-induced nitric oxide production inhibits mitochondrial energy production and impairs contractile function in rat cardiac myocytes. J Am Coll Cardiol. 2000;35:1338–46.
195. El Khoury N, Mathieu S, Fiset C. Interleukin-1β reduces L-type Ca2+ current through protein kinase Cϵ activation in mouse heart. J Biol Chem. 2014;289: 21896–908.
196. Sun Z, Zhou D, Xie X, Wang S, Wang Z, Zhao W, et al. Cross-talk between macrophages and atrial myocytes in atrial fibrillation. Basic Res Cardiol. 2016; https://doi.org/10.1007/s00395-016-0584-z.
197. Lee S-H, Chen Y-C, Chen Y-J, Chang S-L, Tai C-T, Wongcharoen W, et al. Tumor necrosis factor-α alters calcium handling and increases arrhythmogenesis of pulmonary vein cardiomyocytes. Life Sci. 2007;80: 1806–15.
198. Rao F, Deng C-Y, Wu S-L, Xiao D-Z, Yu X-Y, Kuang S-J, et al. Involvement of Src in L-type Ca2+ channel depression induced by macrophage migration inhibitory factor in atrial myocytes. J Mol Cell Cardiol. 2009;47:586–94.
199. Peters CH, Sharpe EJ, Proenza C. Cardiac pacemaker activity and aging. Annu Rev Physiol. 2020;82:21–43.
200. Torrente AG, Mesirca P, Neco P, Rizzetto R, Dubel S, Barrere C, et al. L-type Cav1.3 channels regulate ryanodine receptor-dependent Ca2+ release during sino-atrial node pacemaker activity. Cardiovasc Res. 2016;109:451–61.
201. Larson ED, St. Clair JR, Sumner WA, Bannister RA, Proenza C. Depressed pacemaker activity of sino-atrial node myocytes contributes to the age-dependent decline in maximum heart rate. Proc Natl Acad Sci USA. 2013;110:18011–6.
202. Zhang J, Wei F, Ding L, Wang L, Zhang X, Yu L, et al. MicroRNA-1976 regulates degeneration of the sinoatrial node by targeting Cav1.2 and Cav1.3 ion channels. J Mol Cell Cardiol. 2013;134:74–85.
203. Tellez JO, Mczewski M, Yanni J, Sutyagin P, Mackiewicz U, Atkinson A, et al. Ageing-dependent remodelling of ion channel and Ca $^{2+}$ clock genes underlying sino-atrial node pacemaking: Ageing and ion channels in the sino-atrial node. Exp Physiol. 2011;96:1163–78.
204. Chugh SS, Havmoeller R, Narayanan K, Singh D, Rienstra M, Benjamin EJ, et al. Worldwide epidemiology of atrial fibrillation: A global burden of disease 2010 study. Circulation. 2014;129:837–47.
205. Oyen N, Ranthe MF, Carstensen L, Boyd HA, Olesen MS, Olesen S-P, et al. Familial aggregation of lone atrial fibrillation in young persons. J Am Coll Cardiol. 2012;60:917–21.
206. Kirchhof P, Benussi S, Kotecha D, Ahlsson A, Atar D, Casadei B, et al. 2016 ESC Guidelines for the management of atrial fibrillation developed in collaboration with EACTS. Eur Heart J. 2016;37: 2893–962.
207. Campbell HM, Wehrens XHT. Genetics of atrial fibrillation: an update. Curr Opin Cardiol. 2018;33: 304–10.
208. Hamilton S, Terentyev D. Altered intracellular calcium homeostasis and arrhythmogenesis in the aged heart. Int J Mol Sci. 2019;20(10):2386. https://doi.org/10.3390/ijms20102386.
209. Denham NC, Pearman CM, Caldwell JL, Madders GWP, Eisner DA, Trafford AW, et al. Calcium in the pathophysiology of atrial fibrillation and heart failure. Front Physiol. 2018;9:1380. https://doi.org/10.3389/fphys.2018.01380.
210. Le Grand BL, Hatem S, Deroubaix E, Couétil JP, Coraboeuf E. Depressed transient outward and calcium currents in dilated human atria. Cardiovasc Res. 1994;28:548–56.
211. Dinanian S, Boixel C, Juin C, Hulot JS, Coulombe A, Rücker-Martin C, et al. Downregulation of the calcium current in human right atrial myocytes from patients in sinus rhythm but with a high risk of atrial fibrillation. Eur Heart J. 2008;29:1190–7.
212. Sun H, Chartier D, Leblanc N, Nattel S. Intracellular calcium changes and tachycardia-induced contractile dysfunction in canine atrial myocytes. Cardiovasc Res. 2001;49:751–61.
213. Leistad E, Aksnes G, Verburg E, Christensen G. Atrial contractile dysfunction after short-term atrial fibrillation is reduced by verapamil but increased by BAY K8644. Circulation. 1996;93: 1747–54.
214. Goette A, Honeycutt C, Langberg JJ. Electrical remodeling in atrial fibrillation. Time course and mechanisms. Circulation. 1996;94:2968–74.
215. Tieleman RG, De Langen C, Van Gelder IC, de Kam PJ, Grandjean J, Bel KJ, et al. Verapamil reduces tachycardia-induced electrical remodeling of the atria. Circulation. 1997;95:1945–53.
216. Daoud EG, Knight BP, Weiss R, Bahu M, Paladino W, Goyal R, et al. Effect of verapamil and procainamide on atrial fibrillation-induced electrical remodeling in humans. Circulation. 1997;96:1542–50.
217. Daoud EG, Marcovitz P, Knight BP, Goyal R, Man KC, Strickberger SA, et al. Short-term effect of atrial fibrillation on atrial contractile function in humans. Circulation. 1999;99:3024–7.
218. Brandes A, Crijns HJGM, Rienstra M, Kirchhof P, Grove EL, Pedersen KB, et al. Cardioversion of atrial fibrillation and atrial flutter revisited: current evidence and practical guidance for a common procedure. Eur Eur Pacing Arrhythm Card Electrophysiol J Work Groups Card Pacing Arrhythm Card Cell Electrophysiol Eur Soc Cardiol. 2020;22:1149–61.

219. Yue L, Feng J, Gaspo R, Li G-R, Wang Z, Nattel S. Ionic remodeling underlying action potential changes in a canine model of atrial fibrillation. Circ Res. 1997;81:512–25.
220. Van Wagoner DR, Pond AL, Lamorgese M, Rossie SS, McCarthy PM, Nerbonne JM. Atrial L-type Ca^{2+} currents and human atrial fibrillation. Circ Res. 1999;85:428–36.
221. Van Wagoner DR, Nerbonne JM. Molecular basis of electrical remodeling in atrial fibrillation. J Mol Cell Cardiol. 2000;32:1101–17.
222. Yue L, Melnyk P, Gaspo R, Wang Z, Nattel S. Molecular mechanisms underlying ionic remodeling in a dog model of atrial fibrillation. Circ Res. 1999;84:776–84.
223. Bosch RF, Scherer CR, Rüb N, Wöhrl S, Steinmeyer K, Haase H, et al. Molecular mechanisms of early electrical remodeling: transcriptional downregulation of ion channel subunits reduces I (Ca,L) and I(to) in rapid atrial pacing in rabbits. J Am Coll Cardiol. 2003;41:858–69.
224. Lai LP, Su MJ, Lin JL, Lin FY, Tsai CH, Chen YS, et al. Down-regulation of L-type calcium channel and sarcoplasmic reticular Ca(2+)-ATPase mRNA in human atrial fibrillation without significant change in the mRNA of ryanodine receptor, calsequestrin and phospholamban: an insight into the mechanism of atrial electrical remodeling. J Am Coll Cardiol. 1999;33:1231–7.
225. Van Gelder IC, Brundel BJ, Henning RH, Tuinenburg AE, Tieleman RG, Deelman L, et al. Alterations in gene expression of proteins involved in the calcium handling in patients with atrial fibrillation. J Cardiovasc Electrophysiol. 1999;10:552–60.
226. Brundel BJ, Van Gelder IC, Henning RH, Tieleman RG, Tuinenburg AE, Wietses M, et al. Ion channel remodeling is related to intraoperative atrial effective refractory periods in patients with paroxysmal and persistent atrial fibrillation. Circulation. 2001;103:684–90.
227. Gaborit N, Steenman M, Lamirault G, Le Meur N, Le Bouter S, Lande G, et al. Human atrial ion channel and transporter subunit gene-expression remodeling associated with valvular heart disease and atrial fibrillation. Circulation. 2005;112:471–81.
228. Barana A, Matamoros M, Dolz-Gaitón P, Pérez-Hernández M, Amorós I, Núñez M, et al. Chronic atrial fibrillation increases microRNA-21 in human atrial myocytes decreasing L-type calcium current. Circ Arrhythm Electrophysiol. 2014;7:861–8.
229. Grammer JB, Zeng X, Bosch RF, Kühlkamp V. Atrial L-type Ca2+-channel, beta-adrenoreceptor, and 5-hydroxytryptamine type 4 receptor mRNAs in human atrial fibrillation. Basic Res Cardiol. 2001;96:82–90.
230. Qi XY, Yeh Y-H, Xiao L, Burstein B, Maguy A, Chartier D, Villeneuve LR, et al. Cellular signaling underlying atrial tachycardia remodeling of L-type calcium current. Circ Res. 2008;103:845–54.
231. van den Berg NWE, Kawasaki M, Berger WR, Neefs J, Meulendijks E, Tijsen AJ, et al. MicroRNAs in atrial fibrillation: from expression signatures to functional implications. Cardiovasc Drugs Ther. 2017;31:345–65.
232. Lu Y, Zhang Y, Wang N, Pan Z, Gao X, Zhang F, et al. MicroRNA-328 contributes to adverse electrical remodeling in atrial fibrillation. Circulation. 2010;122:2378–87.
233. Cañón S, Caballero R, Herraiz-Martínez A, Pérez-Hernández M, López B, Atienza F, et al. miR-208b upregulation interferes with calcium handling in HL-1 atrial myocytes: Implications in human chronic atrial fibrillation. J Mol Cell Cardiol. 2016;99:162–73.
234. Brundel BJJM, Ausma J, van Gelder IC, Van der Want JJL, van Gilst WH, Crijns HJGM, et al. Activation of proteolysis by calpains and structural changes in human paroxysmal and persistent atrial fibrillation. Cardiovasc Res. 2002;54:380–9.
235. Belles B, Hescheler J, Trautwein W, Blomgren K, Karlsson JO. A possible physiological role of the Ca-dependent protease calpain and its inhibitor calpastatin on the Ca current in guinea pig myocytes. Pflugers Arch. 1988;412:554–6.
236. Xu G-J, Gan T-Y, Tang B-P, Chen ZH, Mahemuti A, Jiang T, et al. Alterations in the expression of atrial calpains in electrical and structural remodeling during aging and atrial fibrillation. Mol Med Rep. 2013;8:1343–52.
237. Heijman J, Ghezelbash S, Wehrens XHT, Dobrev D. Serine/threonine phosphatases in atrial fibrillation. J Mol Cell Cardiol. 2017;103:110–20.
238. Christ T, Boknik P, Wöhrl S, Wettwer E, Graf EM, Bosch RF, et al. L-type Ca2+ current downregulation in chronic human atrial fibrillation is associated with increased activity of protein phosphatases. Circulation. 2004;110:2651–7.
239. Klein G, Schröder F, Vogler D, Schaefer A, Haverich A, Schieffer B, et al. Increased open probability of single cardiac L-type calcium channels in patients with chronic atrial fibrillation. Role of phosphatase 2A. Cardiovasc Res. 2003;59:37–45.
240. Mancarella S, Yue Y, Karnabi E, Qu Y, El-Sherif N, Boutjdir M. Impaired Ca2+ homeostasis is associated with atrial fibrillation in the alpha1D L-type Ca2+ channel KO mouse. Am J Physiol Heart Circ Physiol. 2008;295:H2017–24.
241. Cheng M, Lu X, Huang J, Zhang S, Gu D. Electrocardiographic PR prolongation and atrial fibrillation risk: a meta-analysis of prospective cohort studies. J Cardiovasc Electrophysiol. 2015;26:36–41.
242. Cunha SR, Hund TJ, Hashemi S, Voigt N, Li N, Wright P, et al. Defects in ankyrin-based membrane protein targeting pathways underlie atrial fibrillation. Circulation. 2011;124:1212–22.
243. Ponikowski P, Voors AA, Anker SD, Bueno H, Cleland JGF, Coats AJS, et al. 2016 ESC Guidelines for the diagnosis and treatment of acute and chronic heart failure: The Task Force for the diagnosis and treatment of acute and chronic heart failure of the European Society of Cardiology (ESC)Developed with the special contribution of the Heart Failure

Association (HFA) of the ESC. Eur Heart J. 2016;37: 2129–200.

244. Bui AL, Horwich TB, Fonarow GC. Epidemiology and risk profile of heart failure. Nat Rev Cardiol. 2011;8:30–41.
245. Crespo-Leiro MG, Anker SD, Maggioni AP, Coats AJ, Filippatos G, Ruschitzka F, et al. European Society of Cardiology Heart Failure Long-Term Registry (ESC-HF-LT): 1-year follow-up outcomes and differences across regions. Eur J Heart Fail. 2016;18:613–25.
246. Sweeney MO. Sudden death in heart failure associated with reduced left ventricular function: substrates, mechanisms, and evidence-based management, Part II. Pacing Clin Electrophysiol PACE. 2001;24:1002–22.
247. Lip GY, Heinzel FR, Gaita F, Juanatey JR, Le Heuzey JY, Potpara T, et al. European Heart Rhythm Association/Heart Failure Association joint consensus document on arrhythmias in heart failure, endorsed by the Heart Rhythm Society and the Asia Pacific Heart Rhythm Society. Europace. 2016;18: 12–36.
248. Lee Park K, Anter E. Atrial fibrillation and heart failure: A review of the intersection of two cardiac epidemics. J Atr Fibrillation. 2013;6:751.
249. Tomaselli GF, Zipes DP. What causes sudden death in heart failure? Circ Res. 2004;95:754–63.
250. Nass RD, Aiba T, Tomaselli GF, Akar FG. Mechanisms of disease: ion channel remodeling in the failing ventricle. Nat Clin Pract Cardiovasc Med. 2008;5:196–207.
251. Coronel R, Wilders R, Verkerk AO, Wiegerinck RF, Benoist D, Bernus O. Electrophysiological changes in heart failure and their implications for arrhythmogenesis. Biochim Biophys Acta. 2013;1832:2432–41.
252. Johnson DM, Antoons G. Arrhythmogenic mechanisms in heart failure: Linking β-adrenergic stimulation, stretch, and calcium. Front Physiol. 2018;9:1453.
253. Richard S. Ca2+ currents in compensated hypertrophy and heart failure. Cardiovasc Res. 1998;37:300–11.
254. Mukherjee R, Spinale FG. L-type calcium channel abundance and function with cardiac hypertrophy and failure: a review. J Mol Cell Cardiol. 1998;30: 1899–916.
255. Chen X, Piacentino V, Furukawa S, Goldman B, Margulies KB, Houser SR. L-type Ca^{2+} channel density and regulation are altered in failing human ventricular myocytes and recover after support with mechanical assist devices. Circ Res. 2002;91:517–24.
256. Chen X, Zhang X, Harris DM, Piacentino V, Berretta RM, Margulies KB, et al. Reduced effects of BAY K 8644 on L-type Ca2+ current in failing human cardiac myocytes are related to abnormal adrenergic regulation. Am J Physiol Heart Circ Physiol. 2008;294:H2257–67.
257. Hullin R, Matthes J, von Vietinghoff S, Bodi I, Rubio M, D'Souza K, et al. Increased expression of the auxiliary β2-subunit of ventricular L-type Ca2+ channels leads to single-channel activity characteristic of heart failure. PLoS One. 2007;2:e292.
258. Hong T-T, Smyth JW, Chu KY, Vogan JM, Fong TS, Jensen BC, et al. BIN1 is reduced and Cav1.2 trafficking is impaired in human failing cardiomyocytes. Heart Rhythm. 2012;9:812–20.
259. Ambrosi CM, Yamada KA, Nerbonne JM, Efimov IR. Gender differences in electrophysiological gene expression in failing and non-failing human hearts. PLoS One. 2013;8:e54635.
260. Takahashi T, Allen PD, Lacro RV, Marks AR, Dennis AR, Schoen FJ, et al. Expression of dihydropyridine receptor (Ca2+ channel) and calsequestrin genes in the myocardium of patients with end-stage heart failure. J Clin Invest. 1992;90: 927–35.
261. Gruver EJ, Morgan JP, Stambler BS, Gwathmey JK. Uniformity of calcium channel number and isometric contraction in human right and left ventricular myocardium. Basic Res Cardiol. 1994;89:139–48.
262. Ouadid H, Albat B, Nargeot J. Calcium currents in diseased human cardiac cells. J Cardiovasc Pharmacol. 1995;25:282–91.
263. Srivastava U, Jennings-Charles R, Qu YS, Sossalla S, Chahine M, Boutjdir M. Novel re-expression of L-type calcium channel Cav1.3 in left ventricles of failing human heart. Heart Rhythm. 2020;17:1193–7.
264. Gidh-Jain M, Huang B, Jain P, Battula V, el-Sherif N. Reemergence of the fetal pattern of L-type calcium channel gene expression in non infarcted myocardium during left ventricular remodeling. Biochem Biophys Res Commun. 1995;216:892–7.
265. Yang Y, Chen X, Margulies K, Jeevanandam V, Pollack P, Bailey BA, et al. L-type Ca2+ channel alpha 1c subunit isoform switching in failing human ventricular myocardium. J Mol Cell Cardiol. 2000;32:973–84.
266. Li G, Wang J, Liao P, Bartels P, Zhang H, Yu D, et al. Exclusion of alternative exon 33 of CaV1.2 calcium channels in heart is proarrhythmogenic. Proc Natl Acad Sci USA. 2017;114:E4288–95.
267. Hullin R, Asmus F, Ludwig A, Hersel J, Boekstegers P. Subunit expression of the cardiac L-type calcium channel is differentially regulated in diastolic heart failure of the cardiac allograft. Circulation. 1999;100: 155–63.
268. Matthes J, Herzig S. Auxiliary β-subunits of L-type Ca2+ channels in heart failure. In: Weiss N, Koschak A, editors. Pathologies of calcium channels. Berlin: Springer; 2014. p. 255–75.
269. Beetz N, Hein L, Meszaros J, Gilsbach R, Barreto F, Meissner M, et al. Transgenic simulation of human heart failure-like L-type Ca2+-channels: implications for fibrosis and heart rate in mice. Cardiovasc Res. 2009;84:396–406.
270. Chang L, Zhang J, Tseng Y-H, Xie CQ, Ilany J, Brüning JC, et al. Rad GTPase deficiency leads to cardiac hypertrophy. Circulation. 2007;116:2976–83.

271. Levitan BM, Manning JR, Withers CN, Smith JD, Shaw RM, Andres DA, et al. (2016) Rad-deletion phenocopies tonic sympathetic stimulation of the heart. J Cardiovasc Transl Res. 2016;9:432–44.
272. Yada H, Murata M, Shimoda K, Yuasa S, Kawaguchi H, Ieda M, et al. Dominant negative suppression of Rad leads to QT prolongation and causes ventricular arrhythmias via modulation of L-type Ca2+ channels in the heart. Circ Res. 2007;101:69–77.
273. Manning JR, Yin G, Kaminski CN, Magyar J, Feng HZ, Penn J, et al. Rad GTPase deletion increases L-type calcium channel current leading to increased cardiac contraction. J Am Heart Assoc. 2013;2: e000459.
274. Liu G, Papa A, Katchman AN, Zakharov SI, Roybal D, Hennessey JA, et al. Mechanism of adrenergic CaV1.2 stimulation revealed by proximity proteomics. Nature. 2020;577:695–700.
275. Schröder F, Handrock R, Beuckelmann DJ, Hirt S, Hullin R, Priebe L, et al. Increased availability and open probability of single L-type calcium channels from failing compared with nonfailing human ventricle. Circulation. 1998;98:969–76.
276. Guo A, Zhang C, Wei S, Chen B, Song L-S. Emerging mechanisms of T-tubule remodelling in heart failure. Cardiovasc Res. 2013;98:204–15.
277. Bryant SM, Kong CHT, Watson J, Cannell MB, James AF, Orchard CH. Altered distribution of ICa impairs Ca release at the t-tubules of ventricular myocytes from failing hearts. J Mol Cell Cardiol. 2015;86:23–31.
278. Sanchez-Alonso JL, Bhargava A, O'Hara T, Glukhov AV, Schobesberger S, Bhogal N, et al. Microdomain-specific modulation of L-type calcium channels leads to triggered ventricular arrhythmia in heart failure. Circ Res. 2016;119:944–55.
279. Hong T-T, Smyth JW, Gao D, Chu KY, Vogan JM, Fong TS, et al. BIN1 localizes the L-type calcium channel to cardiac T-tubules. PLoS Biol. 2010;8: e1000312.
280. Fu Y, Shaw SA, Naami R, Vuong CL, Basheer WA, Guo X, et al. Isoproterenol promotes rapid ryanodine receptor movement to bridging integrator 1 (BIN1)-organized dyads. Circulation. 2016;133:388–97.
281. Song L-S, Sobie EA, McCulle S, Lederer WJ, Balke CW, Cheng H. Orphaned ryanodine receptors in the failing heart. Proc Natl Acad Sci USA. 2006;103: 4305–10.
282. Dries E, Santiago DJ, Gilbert G, Lenaerts I, Vandenberk B, Nagaraju CK, et al. Hyperactive ryanodine receptors in human heart failure and ischaemic cardiomyopathy reside outside of couplons. Cardiovasc Res. 2018;114:1512–152.
283. Gerhardstein BL, Puri TS, Chien AJ, Hosey MM. Identification of the sites phosphorylated by cyclic AMP-dependent protein kinase on the beta 2 subunit of L-type voltage-dependent calcium channels. Biochemistry. 1999;38:10361–70.
284. Koval OM, Guan X, Wu Y, Joiner ML, Gao Z, Chen B, et al. CaV1.2 -subunit coordinates CaMKII-triggered cardiomyocyte death and afterdepolarizations. Proc Natl Acad Sci USA. 2010;107:4996–5000.
285. Li D, Melnyk P, Feng J, Wang Z, Petrecca K, Shrier A, et al. Effects of experimental heart failure on atrial cellular and ionic electrophysiology. Circulation. 2000;101:2631–8.
286. Boixel C, Gonzalez W, Louedec L, Hatem SN. Mechanisms of L-type Ca(2+) current downregulation in rat atrial myocytes during heart failure. Circ Res. 2001;89:607–13.
287. Cha T-J, Ehrlich JR, Zhang L, Shi Y-F, Tardif J-C, Leung TK, et al. Dissociation between ionic remodeling and ability to sustain atrial fibrillation during recovery from experimental congestive heart failure. Circulation. 2004;109:412–8.
288. Cha T-J, Ehrlich JR, Zhang L, Nattel S. Atrial ionic remodeling induced by atrial tachycardia in the presence of congestive heart failure. Circulation. 2004;110:1520–6.
289. Clarke JD, Caldwell JL, Horn MA, Bode EF, Richards MA, Hall MC, et al. Perturbed atrial calcium handling in an ovine model of heart failure: potential roles for reductions in the L-type calcium current. J Mol Cell Cardiol. 2015;79:169–79.
290. Cheng TH, Lee FY, Wei J, Lin CI. Comparison of calcium-current in isolated atrial myocytes from failing and nonfailing human hearts. Mol Cell Biochem. 1996;157:157–62.
291. Workman AJ, Pau D, Redpath CJ, Marshall GE, Russell JA, Norrie J, et al. Atrial cellular electrophysiological changes in patients with ventricular dysfunction may predispose to AF. Heart Rhythm. 2009;6:445–51.
292. Dibb KM, Clarke JD, Horn MA, Richards MA, Graham HK, Eisner DA, et al. Characterization of an extensive transverse tubular network in sheep atrial myocytes and its depletion in heart failure. Circ Heart Fail. 2009;2:482–9.
293. Caldwell JL, Smith CER, Taylor RF, Kitmitto A, Eisner DA, Dibb KM, et al. Dependence of cardiac transverse tubules on the BAR domain protein amphiphysin II (BIN-1). Circ Res. 2014;115:986–96.
294. Glukhov AV, Balycheva M, Sanchez-Alonso JL, Ilkan Z, Alvarez-Laviada A, Bhogal N, et al. Direct evidence for microdomain-specific localization and remodeling of functional L-type calcium channels in rat and human atrial myocytes. Circulation. 2015;132:2372–84.

Kv11.1 (hERG1) Channels and Cardiac Arrhythmia

11

Michael C. Sanguinetti

Abstract

The rapid delayed rectifier K$^+$ current (I_{Kr}) is one of several outward currents that mediate repolarization of cardiac action potentials in humans and other vertebrates. In humans, I_{Kr} is conducted by Kv11.1 (hERG1) channels encoded by the gene *KCNH2*. Loss of function mutations in *KCNH2* cause inheritable long QT syndrome, characterized by a prolonged QT interval and an increased risk of ventricular arrhythmia. Gain of function mutations in *KCNH2* cause short QT syndrome and associated arrhythmia. In clinical practice, unintended drug-induced QT prolongation and associated ventricular arrhythmia are most often caused by unintended block of Kv11.1 channels. By contrast, compounds that activate Kv11.1 can shorten the QT interval and thereby have the potential to prevent arrhythmia associated with long QT syndrome. This chapter provides a brief overview of the biophysical properties and physiological and pathophysiological roles of Kv11.1 and a more in-depth description of the structural basis for binding and molecular mechanisms of action of compounds that inhibit or activate these channels.

Keywords

Antiarrhythmic drug · Class III · hERG · I_{Kr} · *KCNH2* · Kv11.1 · Kv11.1 activator · Kv11.1 blocker · Long QT syndrome · Potassium channel · QT interval · Short QT syndrome

11.1 Introduction

Cardiac myocytes express many different types of K$^+$ channels that conduct currents that either maintain the resting potential (e.g., inward rectifier K$^+$ current, I_{K1}) or mediate repolarization of the action potential (e.g., I_{to}, I_{Kur}, I_{Kr}, and I_{Ks}). The relative magnitudes of these outward currents and the two major inward currents that determine the action potential waveform of a typical human ventricular myocyte are depicted in Fig. 11.1. Loss of function mutations in the genes that encode channels that conduct I_{Kr} or I_{Ks} slow the rate of ventricular repolarization and cause inheritable long QT syndrome (LQTS), a cardiac disorder characterized by a prolonged QT interval measured on the body surface ECG and an increased risk of cardiac arrhythmia. LQTS is specifically associated with torsades de pointes (TdP), a ventricular arrhythmia that can degenerate into ventricular fibrillation (VF) and cause sudden cardiac death.

Prolonged QT interval and arrhythmia can also be induced by Class III antiarrhythmic agents that inhibit repolarizing K$^+$ currents with the intention

---

M. C. Sanguinetti (✉)
Department of Internal Medicine, University of Utah, Salt Lake City, UT, USA
e-mail: m.sanguinetti@utah.edu

© Springer Nature Switzerland AG 2023

O. N. Tripathi et al. (eds.), *Heart Rate and Rhythm*, https://doi.org/10.1007/978-3-031-33588-4_11

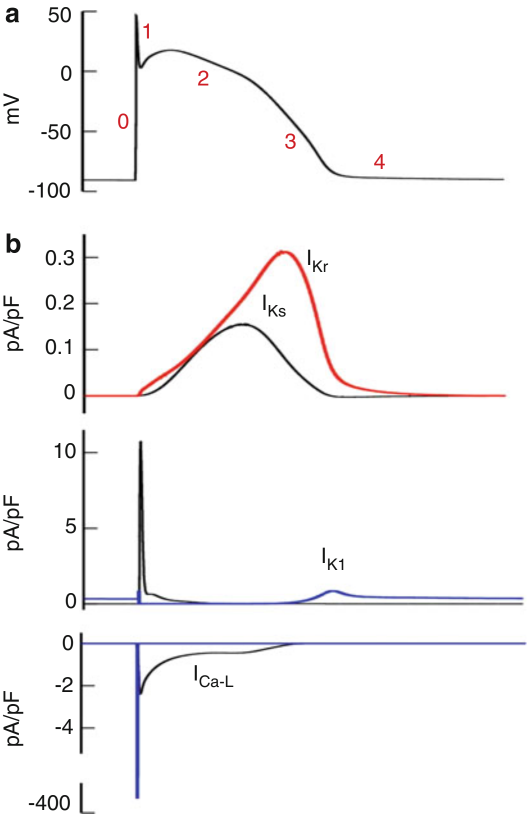

Fig. 11.1 Model of action potential and major ionic currents for a human ventricular myocyte. (**a**) Single action potential. Action potential duration for this cell type is ~280 ms at 1 Hz pacing rate. Numbers refer to different phases of the action potential waveform, including the initial upstroke (0), repolarization (1–3), and the resting membrane potential (4). (**b**) Major ionic currents that underlie action potential shown in panel A. Outward (repolarizing) K^+ currents include the rapid delayed rectifier (I_{Kr}), slow delayed rectifier (I_{Ks}), transient outward (I_{to}) and inward rectifier (I_{K1}). Inward currents include the L-type Ca current (I_{CaL}) and sodium current (I_{Na})

of uniformly prolonging the electrical refractory period of the ventricles. Most potent Class III agents inhibit I_{Kr} as their primary mechanism of action and can prevent ventricular tachycardia (VT) when drug dosing is carefully controlled to prevent excessive QT prolongation. However, excessive inhibition of I_{Kr} by these drugs is associated with a marked dispersion of ventricular repolarization that sometimes leads to TdP and VF. The risk of TdP/VF is especially pronounced when Class III drugs are administered in the setting of other risk factors such as hypokalemia or undiagnosed LQTS. Routine monitoring of adverse drug reactions in the past few decades has also revealed that many noncardiac medications (e.g., some antihistaminic and antibacterial drugs) also prolong the QT interval and are associated with an increased risk of VF.

Drug-induced QT prolongation and arrhythmia, often inappropriately referred to as acquired “long QT syndrome,” by noncardiac medications, is most commonly caused by unintended inhibition of I_{Kr}. In the human heart, I_{Kr} channel α-subunits are encoded by a gene that was initially discovered using a human hippocampus cDNA library to screen for genes homologous to the *Drosophila* K^+ channel gene *eag* (“*ether-a-go-go*”) [1]. The novel cloned gene was named “human *ether-a-go-go-related gene*” (*hERG*), although now the more accepted gene name is *KCNH2* and the International Union of Basic and Clinical Pharmacology (IUPHAR) preferred name for the encoded channel α-subunit protein is Kv11.1. Once inhibition of I_{Kr} was widely recognized as a common mechanism underlying drug-induced arrhythmia, the safety screening of compounds for undesired block of I_{Kr} in isolated cardiomyocytes, or Kv11.1 channels heterologously expressed in mammalian cell lines, became a routine practice early in the drug development process [2]. An unexpected consequence of these safety screening efforts was the discovery of several compounds that activate rather than inhibit Kv11.1 channel activity [3]. Kv11.1 activators shorten the QT interval and thereby have the potential to prevent arrhythmia associated with inherited LQTS or to counteract unintended I_{Kr} inhibition detected in many otherwise useful noncardiac medications. This chapter provides a brief overview of the physiological and pathophysiological roles of Kv11.1 channels, and a more in-depth description of the biophysical properties and the molecular mechanisms of action of compounds that inhibit or activate these channels.

11.2 Physiological Roles of Kv11 Channels

After the initial discovery of the *hERG* gene, further cloning efforts culminated in the description of three families and eight *eag*-related Kv channel α-subunits, including EAG (Kv10.1, Kv10.2), ERG (Kv11.1-Kv11.3) and ELK (Kv12.1-Kv12.3). In the heart, the most prominently expressed *eag*-related Kv channel is Kv11.1, encoded by the gene *KCNH2*. Two closely related genes (*KCNH6* and *KCNH7*) encode hERG2 (Kv11.2) and hERG3 (Kv11.3) channel subunits, respectively, that are expressed in the nervous system but not in cardiac myocytes [4]. Outside the heart, Kv11 channels display a diversity of functions [5], including maintenance of K^+ homeostasis in hippocampal astrocytes [6], regulating spike frequency in glomus cells of the carotid body [7] and cerebellar Purkinje neurons [8], regulation of hormone secretion in anterior pituitary lactotrophs and pancreatic β-cells [9–11], and setting the resting membrane potential of smooth muscle cells in the gastrointestinal tract [12–14]. Kv11 channels are also implicated in cell cycle regulation and apoptosis [15, 16] and the pathogenesis of several cancers [17–19].

In the heart, Kv11.1 channel activity is one of the primary determinants of repolarization during phases 2 (plateau) and 3 (late repolarization) of the action potential waveform (Fig. 11.1a). Similar to other Kv channels, the open probability of Kv11.1 is highly voltage-dependent and thus varies throughout the cardiac cycle. In ventricular myocytes, channels are closed (nonconducting) during diastole (phase 4) when the membrane potential is at its most negative (−90 mV). Although channels open in response to membrane depolarization during the upstroke (phase 0) and initial repolarization phases of the action potential, most channels then rapidly transition to an inactivated (nonconducting) state. This results in a very small net outward current during the onset of the plateau phase. The open probability of Kv11.1 channels (and thus I_{Kr}) progressively increases during the later portion of the plateau phase and even more so during initial phase 3 repolarization, as channels recover from inactivation and re-enter their open state. As the rate of membrane repolarization increases during phase 3, open channels deactivate into a closed state, and I_{Kr} magnitude is reduced. Together, the voltage and time-dependent properties of activation, inactivation, and deactivation gating of Kv11.1 channels results in the whole myocyte I_{Kr} shown in Fig. 11.1b.

11.3 Pathophysiological Roles of Kv11.1 Channels in the Heart

11.3.1 Kv11.1 and Long QT Syndrome

Inherited loss of function mutations in *KCNH2* cause LQTS [20], characterized by a prolonged QT interval and reduced I_{Kr} (Fig. 11.2), an increased risk of TdP, VF and sudden cardiac death. This type of LQTS is called “LQT2” to distinguish it from the many other types of LQTS that are numbered based on the chronology of the gene discovered to underlie the particular LQTS type. LQT1 (*KCNQ1* mutations), LQT2 (*KCNH2* mutations), and LQT3 (*SCN5A* mutations) account for the vast majority of the autosomal dominant inherited LQTS (Romano-Ward syndrome) with an estimated prevalence of 1:2500 live births [21]. In one large study, it was estimated that LQT2 accounts for ~35% of all inherited LQTS [22]. LQT2 is characterized by a prolonged QT_c interval, defined as >440 ms for men and > 460 ms for women, and either a biphasic or notched T wave [23] (Fig. 11.2b). The most common trigger for VT/VF in LQTS is emotional stress, with triggering by sudden auditory stimuli often reported for LQT2 [24].

Multiple mechanisms have been shown to be responsible for the loss of Kv11.1 channel function caused by mutations in *KCNH2*. The most common mechanism is a misfolding and reduced trafficking of channels to the cell membrane [25]. Less common are problems with channel gating that reduce conductance such as a slower rate of activation, faster rate of deactivation or

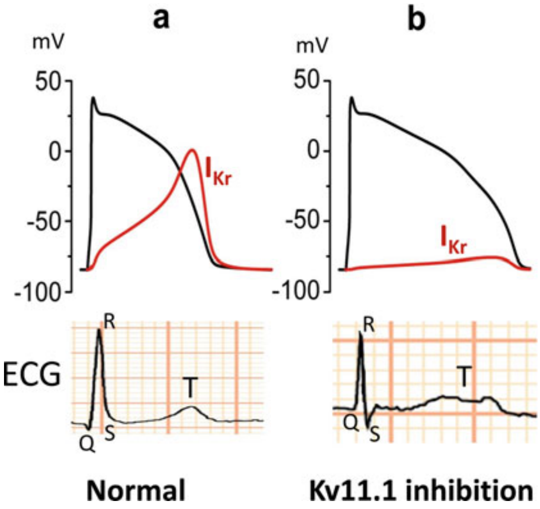

Fig. 11.2 Inhibition of I_{Kr} causes prolongation of action potential in cardiac myocytes and lengthening of QT interval measured on body surface ECG. (**a**) Normal action potential and I_{Kr} (top panel) and normal ECG (bottom panel). (**b**) Action potential duration is lengthened, QT interval is lengthened, and T-wave is typically notched when I_{Kr} is reduced. I_{Kr} reduction can result from the block of Kv11.1 channels by drugs or by a loss of function mutation in the *KCNH2* gene

enhanced inactivation [26]. Transgenic LQT2 rabbits have provided important insights into the cellular and tissue mechanisms of arrhythmia that result from a loss of function mutation (Gly628Ser) in Kv11.1. Isolated cardiac myocytes from LQT2 rabbits have prolonged APD (action potential duration), no measurable I_{Kr} and reduced I_{Ks} [27]. These rabbits have prolonged QTc intervals, exhibit discordant APD alternans, marked dispersion in ventricular effective refractory periods, and when anesthetized with isoflurane develop impaired conduction in the His bundle, block in the infra-His bundle and intermittent, spontaneous second-degree AV (atrioventricular) block [28, 29]. The multiple cardiac defects in LQT2 rabbits result in spontaneous polymorphic VT/VF and a high rate of sudden cardiac death [27].

11.3.2 Kv11.1 and Short QT Syndrome

Gain of function mutations in Kv11.1 channels cause short QT syndrome (SQTS), a rare disorder that hastens cardiac repolarization, increases the risk of VT/VF and atrial fibrillation (AF) that may lead to SCD. SQTS is diagnosed when QTc ≤ 330 ms [30]. The first two point mutations in *KCNH2* reported to cause SQTS (Asn588Lys, Thr618Ile) were shown to increase outward Kv11.1 current ($I_{Kv11.1}$) by shifting the voltage dependence of inactivation gating to more positive potentials. The voltage required to cause 50% of channels to inactivate is dramatically shifted by these mutations, i.e., +102 mV by Asn588Lys [31] and + 50 mV by T618I [32]. Reduced inactivation may increase I_{Kr} more in the ventricle than in Purkinje fibers, and the resulting disparity in APD could create the arrhythmogenic substrate responsible for VF [31]. A transgenic rabbit model of SQTS (with Asn588Lys Kv11.1 mutation) mimics the human phenotype, including reduced atrial and ventricular refractoriness and increased inducibility of VT/VF/AF [33].

11.4 Biophysical and Structural Properties of Kv11.1 Channels

11.4.1 Kv11.1 Channel Subtypes

Like other Kv channels, functional Kv11.1 channels are formed by the coassembly of four α-subunits into a tetramer. Two different Kv11.1 proteins are expressed in the heart – a full-length protein (hERG1a or Kv11.1a) and an N-terminal truncated protein (hERG1b or Kv11.1b) produced by alternative splicing [34, 35]. Homomeric Kv11.1a channels and heteromultimeric Kv11.1a/1b channels are readily trafficked to the plasma membrane, unlike Kv11.1b homotetramers that can be retained in the endoplasmic reticulum [36]. Kv11.1a channels deactivate much slower than Kv11.1b channels. Slow deactivation of Kv11.1a is dependent on an interaction between the cytoplasmic N-terminus of one subunit with the cytoplasmic C-terminus of an adjacent subunit [37–39]. Channels containing Kv11.1b subunits (with a truncated N-terminus) lack the N- to C-terminal interactions and thus deactivate faster than Kv11.1a homotetramers and in fact more closely match the kinetics of native I_{Kr} in the heart. The biophysical properties of heterologously expressed hERG1 channels can be altered when coexpressed with β-subunits such as MinK or MiRP1 [40–42]; however, the physiological relevance of this modulation in the heart is disputed [43].

11.4.2 Biophysical Properties of Kv11.1 Channels

Kv11.1 channels have biophysical properties that are intermediate between a typical Kv channel and an inward rectifier K^+ (Kir) channel. Kv11.1 channels are voltage-gated; i.e., the open probability and rates of activation, inactivation, and deactivation of channels are highly dependent on the transmembrane potential. In contrast, Kir channels lack a voltage sensor, and thus, their open probability is intrinsically voltage-independent. The inward rectification of Kir (outward currents are much smaller than inward currents) results from a voltage-dependent block of outward K^+ flux by intracellular polyamines [44]. Similar to Kir channels, outward $I_{Kv11.1}$ is also diminished at positive transmembrane potentials, but this reduction results from a gating process (inactivation) rather than from pore block by polyamines [45]. Although $I_{Kv11.1}$ (I_{Kr}) is often described as inward rectifying, the more proper biophysical description would be that the fully-activated current-voltage (I-V) relationship for the current exhibits a negative slope conductance at potentials positive to $E_{K,}$ the equilibrium potential for K^+. An example of whole-cell $I_{Kv11.1}$ elicited at physiologically relevant test potentials (−70 to +40 mV) is shown in Fig. 11.3a. At the most negative potentials examined, the currents activate slowly and do not reach a steady-state value during the 2-s pulse. The magnitude of the outward current reaches a peak at about −10 mV. At pulses to more positive potentials, the rate of current activation increases and the current size is decreased. At the end of each 2-s pulse, the membrane potential is returned to −70 mV and the resulting "tail" current exhibits a transient increase in amplitude as channels recover from an inactivated state into an open state. After this initial outward surge, the "tail" current slowly decays in amplitude as channels deactivate (transition from an open to a closed state).

The I-V relationship for peak outward currents, measured at the end of each 2-s test pulse, is bell-shaped and peaks near −10 mV (Fig. 11.3b). The shape of this I-V relationship is determined by the relative dominance of voltage-dependent activation (Fig. 11.3c) at negative voltages versus inactivation (Fig. 11.3d) that dominates at positive voltages. The single channel behavior that underlies the reduced outward $I_{Kv11.1}$ at positive membrane potentials is illustrated in Fig. 11.4. At +40 mV, the probability of a Kv11.1 channel being in the inactivated (nonconducting) state is high and channel openings are rare and brief in duration. Repolarization of the membrane from +40 to −120 mV induces the channel to rapidly recover from its inactivated state into the open state whereupon it

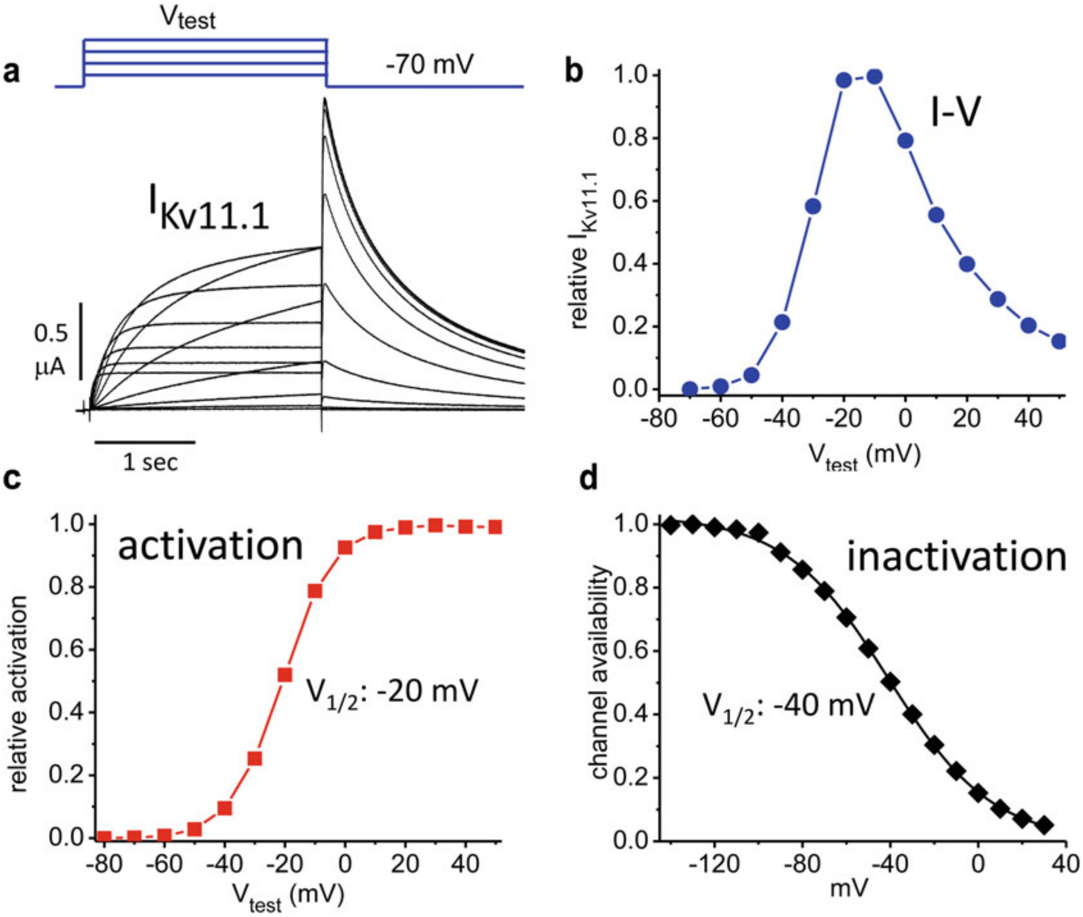

Fig. 11.3 Whole cell $I_{Kv11.1}$ recorded in a *Xenopus* oocyte. (**a**) Voltage clamp protocol (upper panel) and ionic currents were recorded at test potentials applied in 10-mV increments ranging from −70 to +40 mV (lower panel). Tail currents were elicited by repolarization of the membrane potential to −70 mV. (**b**) Current-voltage (I-V) relationship for $I_{Kv11.1}$ was measured at the end of the 2-s test pulse. (**c**) Voltage dependence of $I_{Kv11.1}$ activation was determined by plotting the relative value of tail current amplitude as a function of test potential. The half-point ($V_{1/2}$) for activation is −20 mV. (**d**) Voltage dependence of $I_{Kv11.1}$ inactivation ($V_{1/2} = -40$ mV)

more slowly enters its closed (“resting,” nonconducting) state.

11.4.3 Structural Features of Kv11.1 Channels

Each Kv11.1 subunit has six α-helical transmembrane segments (S1-S6) that are divided into two domains, a voltage-sensing domain (VSD, S1-S4 segments) and a pore domain (S5-S6 segments). The long N-terminus of Kv11.1a is cytosolic and contains a Per Arnt Sim (PAS) domain (absent in Kv11.1b); both α-subunits have a long cytoplasmic C-terminus that contains a cyclic nucleotide-binding homology domain (CNBHD). In 2017, the cryo-EM structure of Kv11.1 (hERG1) channels in an open state was determined (Fig. 11.5a) [46]. Based on the comparison of Kv10 and Kv11.1 channel structures [46], the gating hinge in the S6 segment that mediates the opening and closing of channels is Gly648 (Fig. 11.5b). However, the critical or unique importance of the flexibility afforded to S6 by a Gly in this position seems unlikely since substitution with Ala (Gly648Ala) has little effect

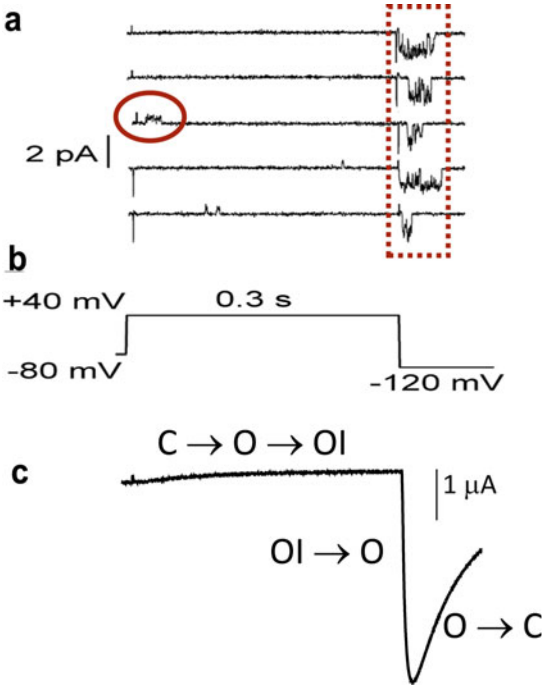

Fig. 11.4 Single channel and whole cell $I_{Kv11.1}$ measured in *Xenopus* oocytes. (**a**) Traces of single Kv11.1 channel activity in a cell-attached patch were recorded during five separate test pulses. At +40 mV, the channel is usually inactivated (nonconducting) and openings are rare (oval). Repolarization of the membrane patch to −120 mV induces the channel to open (dashed box) for a brief time before deactivating into the rested, closed state. $[K^+]_i$ and $[K^+]_o = 140$ mM. (**b**) Voltage pulse protocol used to elicit currents shown in panels a and c. (**c**) Whole-cell $I_{Kv11.1}$. Labeling indicates dominant transitions between different single channel states (*C* closed, *O* open, *OI* open/inactivated) that underlie whole-cell current

on channel gating [47]. Similar to Kv10 channels, the VSD of Kv11.1 channels is packed up against its own pore domain (i.e., not domain-swapped as in many other Kv channels), and each S4 segment connects directly with its adjacent S5 segment, without a long S4-S5 α-helical linker that is commonly found in other Kv channels and previously proposed to play an important role in Kv11.1 channel gating [48–51]. In contrast to the S4-S5 linker acting as a lever that couples movement of the VSD to the gating of the pore domain, the cryo-EM structures suggest instead that the outward movement of the VSD (mainly S4) transmits force required for channel opening via the S5-S6 interface and that inward S4 movement closes the channel by compressing the S5 helices [46].

11.4.4 Structural Basis of Kv11.1 Channel Inactivation

Inactivation of Kv11.1 is normally extremely rapid in onset, but similar to “C-type” inactivation of other Kv channels, can be slowed in the presence of extracellular tetraethylammonium or elevated $[K^+]_e$, and nearly eliminated by point mutations in regions of the pore near the selectivity filter [45, 52–54]. One of these point mutations (Ser631Ala) was found to induce a subtle change in the position of Phe627, a residue in the middle of the Gly-Phe-Gly motif of the K^+ selectivity filter. The altered position of Phe627 closely resembles the position of the residue in the selectivity filter motif of Kv channels that do not exhibit C-type inactivation [46]. The structural basis of C-type inactivation in Kv11.1 is

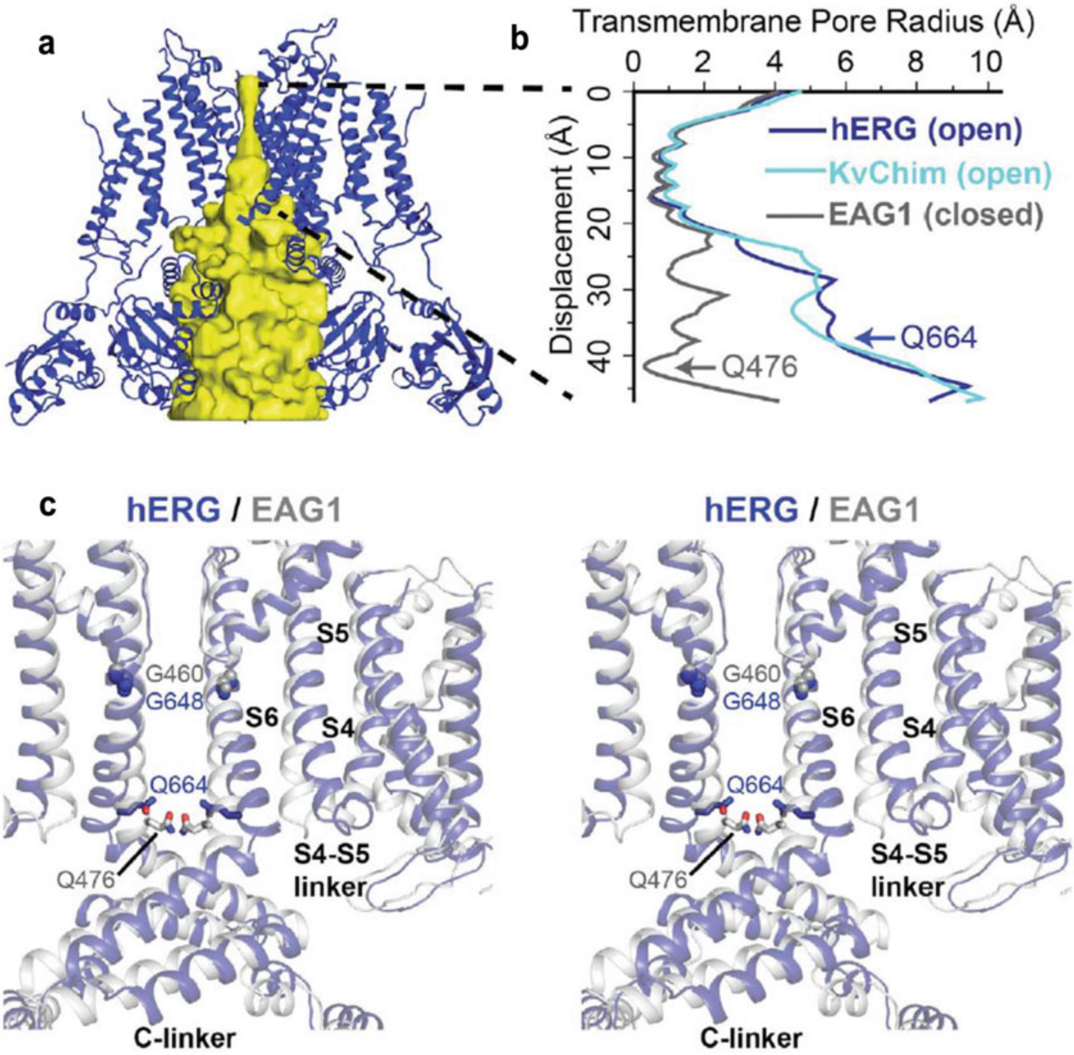
a
b
Transmembrane Pore Radius (Å)
0
2
4
6
8
10
Displacement (Å)
0
10
20
30
40
hERG (open)
KvChim (open)
EAG1 (closed)
Q664
Q476
c
hERG / EAG1
G460
G648
S5
S6
S4
Q664
Q476
S4-S5
linker
C-linker
hERG / EAG1
G460
G648
S5
S6
S4
Q664
Q476
S4-S5
linker
C-linker

Fig. 11.5 Kv11.1 channel structure determined by cryo-EM. (**a**) Side view of the channel in ribbon mode. Yellow surface represents the central pore. (**b**) Pore radius was measured along the S6 segment of Kv11.1 (hERG) in an open state and Kv10.1 (EAG1) in a closed state. (**c**) Comparison of Kv11.1 and Kv10.1 channel structures (two opposing subunits for each channel) in stereo-view. Reprinted from Wang and MacKinnon, 2017 [46] with permission from Elsevier

likely to be quite complex and has been suggested to involve multiple regions of the channel and occur in sequential steps that culminate in a subtle change in the conformation of the selectivity filter [55, 56], perhaps similar to that described for Ser631Ala channels. Inactivation has been studied using concatenated (all four subunits covalently linked) Kv11.1 channels, and findings suggest that the final step in the gating process is mediated by a concerted, all-or-none cooperative interaction [57].

11.5 Drug-Induced QT Prolongation and TdP

Many drugs have been associated with QT prolongation and an increase in the risk of ventricular arrhythmia. Accordingly, the list of drugs that are contraindicated in LQTS is vast [58, 59]. Although the reduction in either I_{Kr} or I_{Ks} can lengthen the cardiac repolarization time, extensive study has led to the general consensus that inhibition of I_{Kr} is by far the more common cause of drug-induced QT prolongation and arrhythmia.

Class III antiarrhythmic drugs were purposely developed for their ability to inhibit I_{Kr}, prolong cardiac refractoriness, and provide protection against arrhythmia initiation mediated by premature excitation. However, because drug-induced changes in the refractory period are not uniform throughout the heart, these drugs can also be proarrhythmic and induce TdP. The proarrhythmic risk of a Class III agent is greater when administered at a high dose or when combined with other conditions that prolong repolarization such as hypokalemia, bradycardia, impaired hepatic or renal function (that can slow metabolism or elimination of drug), or concomitant administration of other drugs that inhibit I_{Kr} [60]. Quinidine was reported to induce TdP in 2–9% of treated patients [61].

Noncardiac medications that block I_{Kr} and prolong the QT interval as an unintended side effect are structurally diverse [62–64] and span a wide spectrum of therapeutic drug classes, including psychiatric, antimicrobial, and antihistaminic compounds [65, 66]. Drug-induced TdP by these compounds is usually a relatively rare event. For example, TdP associated with terfenadine or cisapride treatment is estimated to have occurred in ~1 of 100,000 patients [67]. Of course, this incidence is unacceptable for drugs that are prescribed for the treatment of nonlife-threatening disorders [59]. Cisapride, sertindole, grepafloxacin, terfenadine, and astemizole were removed from the US market, or their use was severely restricted by drug enforcement agencies once a clear association was confirmed between their use and significant QTc prolongation or arrhythmia [65].

11.6 Mechanism of Drug-Induced Kv11.1 Channel Inhibition

The molecular basis of the Kv11.1 channel block has been extensively studied. The main findings can be summarized as follows: (1) Kv11.1 channels are preferentially blocked by most compounds when the channel is in an open or open/inactivated state. (2) Site-directed mutagenesis and functional analysis studies have identified specific amino acid residues in the pore domain that are critical to drug interaction with the channel. Finally, (3) the cryo-EM structure of Kv11.1 provides new clues into the structural basis of drug binding sites, but definitive identification of these site(s) awaits the structural determination of channels bound by specific compounds.

A large number of computational models to predict Kv11.1 channel block has been developed [68–70], including quantitative structure–activity relationship models. These studies have culminated in several pharmacophore models that are summarized elsewhere [71]. While the potency of Kv11.1 channel block by drugs is most commonly defined by an IC_{50} value derived from a fixed voltage clamp protocol, this measure does not always accurately predict the risk of QT prolongation associated with the clinical use of a specific compound. An important component of the disconnect between drug potency and QTc prolongation/arrhythmic risk is the kinetics of drug binding to the channel [72, 73], and it has been demonstrated that dynamic modeling of drug-channel interaction can improve risk assessment of compounds [74].

11.6.1 Open State Channel Block

Voltage clamp studies have provided unequivocal evidence that positively charged drugs require Kv11.1 channels to be in an open state to allow access to their binding site. Even at a high concentration of 10 μM, prolonged incubation with MK-499 (a methanesulfonanilide class III antiarrhythmic drug) does not result in block of Kv11.1

channels in cells that are voltage clamped at a negative membrane potential to ensure that all channels are in the closed state [75]. When the cell is depolarized to a positive potential to activate channels, the initial current magnitude is identical to control (predrug) current, and block develops slowly over a few seconds. Thus, MK-499 only blocks activated Kv11.1 channels, implying that a binding site within a region of the pore (the central cavity) is made accessible only after the activation gate is opened. Slow recovery from channel block by MK-499 appears to be caused by physical trapping of the compound inside the central cavity as the channel deactivates. Recovery from block can be strikingly accelerated when Kv11.1 channels contain a specific mutation (Asp540Lys) that allows the activation gate to reopen in response to membrane hyperpolarization [76]. These characteristics of onset and recovery from pore block are common to several other potent blockers of Kv11.1, including dofetilide, E-4031, and bepridil [77, 78].

11.6.2 Inactivated State Channel Block

Initial studies of state-dependent block of Kv11.1 indicated that compounds preferentially inhibit channels that are in an inactivated state [79–81], although exceptions such as halofantrine were notable [82]. The main evidence for inactivated state block is that inhibition is enhanced when a cell is depolarized to very positive membrane potentials where most channels are forced into an inactivated state and by the finding that inactivation-deficient mutant channels are usually far less susceptible to drug-induced inhibition. More recent studies using concatenated Kv11.1 tetramers, having four subunits (either wild-type or mutant) covalently linked together with defined stoichiometry, have led to a more nuanced interpretation of these experimental results. Kv11.1 channels with specific point mutations (either Ser620Thr or Ser631Ala) do not inactivate [83]. The link between inactivation gating and blocking potency of three compounds (cisapride, dofetilide, MK-499) was assessed using concatenated hERG1 tetramers containing a variable number of wild-type and Ser620Thr or Ser631Ala subunits. The presence of a single Ser620Thr subunit in a concatenated channel removed inactivation just as effectively as a Ser620Thr homotetramer [57], yet the heteromeric channels with only one mutant subunit were much more sensitive to block by the three compounds than the mutant homotetrameric channel [84]. Although Ser631Ala mutant subunits disrupt the inactivation of concatenated channels in a graded fashion, the blocking potency of cisapride was unaltered with up to three Ser631Ala subunits incorporated into the tetramer [84]. Together these findings indicate that inactivation facilitates, but is not an absolute requirement for, high-affinity block of Kv11.1 channels.

11.6.3 Structural Basis of Kv11.1 Blocker Binding Site

Based on the results of binding displacement studies using radiolabeled dofetilide or astemizole [85–87], structurally diverse drugs bind to a common or at least overlapping site on the Kv11.1 channel. Site-directed mutagenesis and functional analysis of mutant channels have provided insights into the structural basis of this binding site. Phe656 of the S6 segment was the first Kv11.1 residue reported to be a critical residue for the binding of dofetilide and quinidine [88]. Additional key amino acid residues that form the drug binding site were identified with more extensive site-directed mutagenesis and MK-499 as a probe [89]. Mutation to Ala of three residues near the pore helix (Thr623, Ser624, and Val625) and several residues in the S6 segment (Gly648, Tyr652, Phe656, and Val659) reduced channel sensitivity to block by MK-499. More recently, Phe557 in the S5 segment was implicated in the binding of Kv11.1 blockers [90]. Compounds that are structurally related to MK-499 such as E4031 and dofetilide have a nearly identical pattern of residue interactions [77]. The locations of these key

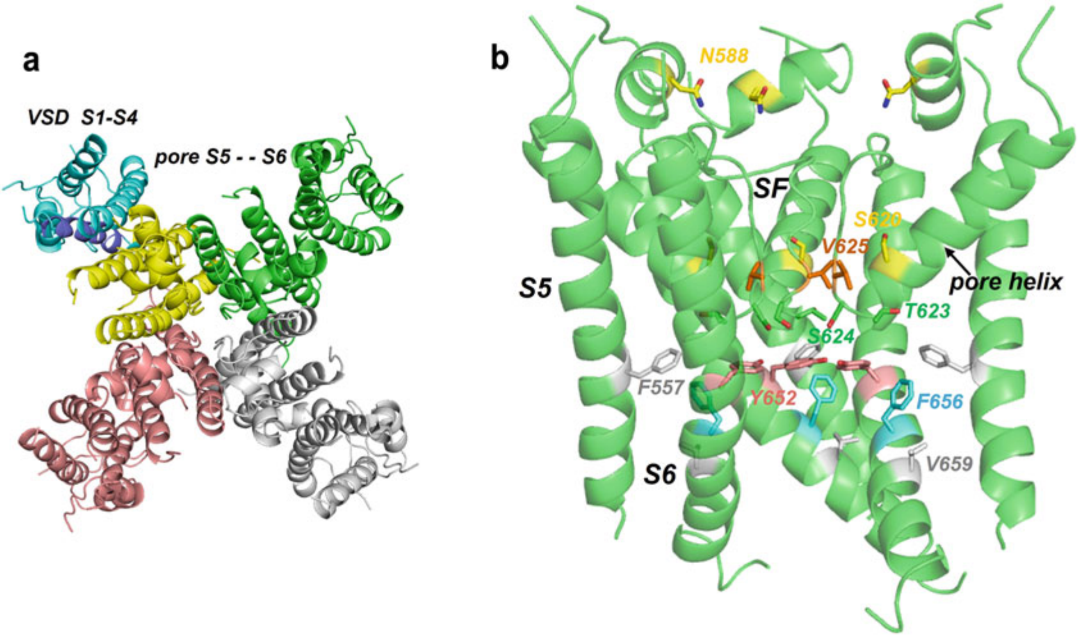

Fig. 11.6 Key residues in Kv11.1 that interact with blockers. (**a**) Top-down view of cryo-EM Kv11.1 structure [46] illustrating fourfold symmetry of the tetrameric channel. For one subunit, the VSD is colored in cyan (S1-S3 segments) and blue (S4 segment), and the pore domain is colored yellow. (**b**) Side view of Kv11.1 channel pore domain with the side chains of key amino acid residues (in stick mode) that comprise the putative blocker binding site indicated. *SF* selectivity filter. Also shown are N588 and S620 (in yellow); mutation of either one of these residues removes inactivation. Figure reproduced from Helliwell et al. 2018 [91]

residues in the Kv11.1 structure are illustrated in Fig. 11.6.

The side chains of Thr623, Ser624, Tyr652, and Phe656 are all orientated toward the central cavity of the closed channel [62], although in the open-state Phe656, sidechains are repositioned and instead face toward Phe557 of the S5 segment. The two-pore helix residues (Thr623 and Ser624) are highly conserved in Kv channels. In contrast, Tyr652 and Phe656 in the S6 segment are not conserved; most Kv channels have an Ile and a Val at these positions. These two aromatic residues have been shown to be of high importance for interaction with many drugs, including chloroquine [92], quinidine [93], halofantrine [82], terfenadine, and cisapride [94], lidoflazine [95], clofilium and ibutilide [96], and cocaine [97]. Further mutagenesis showed that potent Kv11.1 block by MK-499, cisapride, and terfenadine require an aromatic residue in position 652 (either Tyr or Phe), suggesting the possibility of a cation-π interaction. The potency for block by all three drugs was well correlated with the van der Waals hydrophobic surface area of the side chain of residue 656 [94]. Specific residue-drug interactions predicted from site-directed mutagenesis studies have been corroborated by several in silico molecular docking and dynamic simulation studies [98, 99].

A precise understanding of how compounds bind to the pore of Kv11.1 could facilitate design of new drugs devoid of this undesirable molecular interaction [100]. Initial molecular dynamic simulation and docking studies of Kv11.1 blockers such as MK-499 or dofetilide suggested that the orientation of bound compounds was parallel to the longitudinal axis of the central cavity, oftentimes with the basic amine making a cation-π interaction with Tyr652. However, subsequent studies found that compounds could also interact with most of the residues identified by mutagenesis studies when docked perpendicular to this axis and tucked into hydrophobic pockets located beneath each of the pore helices (Fig. 11.7a). These hydrophobic pockets are not found in most other Kv channels and were not revealed until the cryo-EM open-state structure of Kv11.1 was solved [46]. Docking models based on the cryo-EM structure suggest that the basic amine of blockers is positioned in the ion permeation pathway, just below the selectivity filter in a specific location normally occupied by a potassium ion [101] (Fig. 11.7b and c). This mode of docking suggests a more specific mechanism of pore block, interference with ion permeation by inhibiting K^+ coordination at a specific site, rather than a more generalized action (physical plugging of the pore) as was suggested by the parallel orientation docking mode.

11.6.4 Inhibition of hERG Trafficking

Although drug-induced QT prolongation and TdP are most often caused by block of Kv11.1 channels, some drugs reduce I_{Kr} by interference with the process of channel trafficking from the Golgi apparatus to the cell surface. Drug-induced inhibition of Kv11.1 trafficking has been reported for arsenic trioxide [102], pentamidine [103], fluoxetine [104] celastrol [105], and cardiac glycosides [106]. The realization that hERG1 channel function can be reduced by mechanisms other than pore block prompted the development of simple assays to test for drug-induced effects on hERG1 channel trafficking [107, 108].

11.7 Kv11.1 Channel Activators

Pharmacotherapy for LQTS is very limited. β-Adrenergic receptor blockers are the only drugs used commonly to treat LQTS [109]. The most common cause of inherited LQTS is a loss of function mutation in either *KCNH2* or *KCNQ1*. Thus, activators of I_{Kr} or I_{Ks} have been proposed as a potentially useful therapeutic approach to prevent VT/VF associated with prolonged QT intervals [110, 111]. While several compounds with such activity have been discovered and characterized in vitro and in animal models [112–114], none are currently available for clinical use.

11.7.1 Mechanisms of Action of Kv11.1 Activators

Routine screening of compounds for off-target channel activity led to the serendipitous discovery of Kv11.1 channel activators. The first such compound to be discovered and characterized was RPR260243 ((3R,4R)-4-[3-(6-methoxyquinolin-4-yl)-3-oxo-propyl]-1-[3-(2,3,5-trifluorophenyl)-prop-2-ynyl]-piperidine-3-carboxylic acid) in 2005 [3]. A plethora of compounds that activate Kv11.1 by a variety of mechanisms has since been reported, including NS1643 [115, 116], PD-118057 [117], PD-307243 [118], ICA-105574 [119], ML-T531 [120], A-935142 [121], ginsenoside Rg3 [122], AZSMO-23 [123], LUF7244 [124], and HW-0168 [125]. Activation of Kv11.1 is mediated by allosteric modulation of one or more properties of channel gating. The mechanisms of action identified to date include: (1) slowed rate of channel deactivation, (2) attenuation (positive shift in voltage dependence) of C-type inactivation, (3) shift of the voltage dependence of channel activation to more negative potentials, and (4) an increase in channel open probability [111]. RPR260243 (RPR) primarily slows the rate of Kv11.1 deactivation [3], but it also slows the rate of channel activation and enhances current magnitude by attenuation of inactivation [126]. Two compounds, NS1643 [115, 116] and PD-118057 [117], increase the magnitude of outward $I_{Kv11.1}$ but have little or no effect on the rate of channel deactivation. PD-307243 has similar effects on channel gating [118]. Several $I_{K11.1}$ activators markedly inhibit channel inactivation, including ICA-105574 [119], ML-T531 [120], and AZSMO-23 [123]. PD-118057 increases the channel open probability of Kv11.1 and shifts its voltage dependence of inactivation to more positive potentials [127]. NS1643 increases both

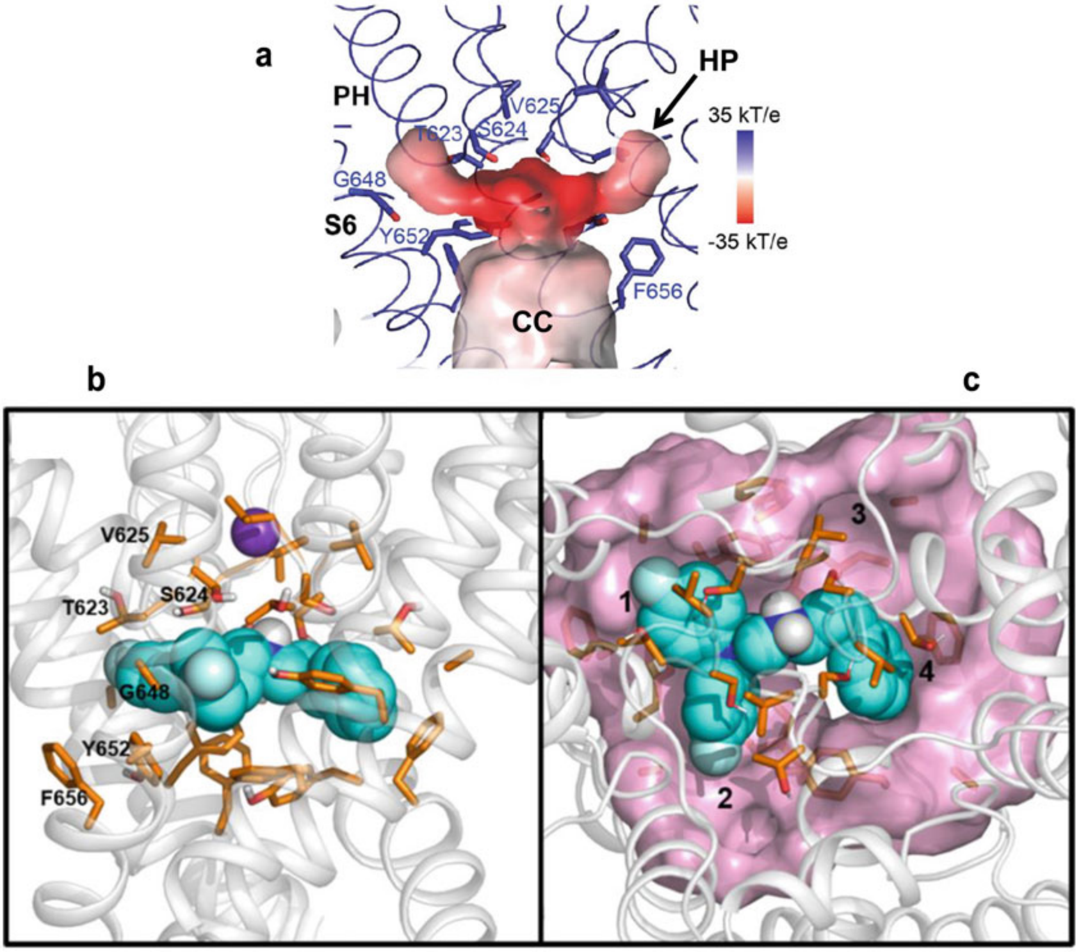

side view

top view

Fig. 11.7 Model of interaction between a potent blocker (Cavalli-6) and hydrophobic pockets located beneath pore helices of Kv11.1. (**a**) Side view of a region of the Kv11.1 channel cryo-EM structure that highlights the upper portion of the central cavity (CC) and lateral hydrophobic pockets (HP) located underneath each pore helix (PH). Structure is shown in ribbon mode, with key drug binding residues shown in stick mode. Figure modified with permission from Wang and MacKinnon [46]. (**b**) Cavalli-6 (in cyan) binds to hydrophobic pockets located beneath the pore helices and selectivity filter of Kv11.1. The key interacting channel residues identified by site-directed mutagenesis studies are labeled and shown in stick mode. (**c**) Top view of Cavalli-6 blocking the ion conduction pathway immediately below the selectivity filter, with its basic amine (in blue) in a location that is normally occupied by a coordinated potassium ion. The hydrophobic pockets illustrated in side view of panel A are numbered 1–4. Panels b and c were reprinted with permission from Dickson et al. 2020 [101]. Copyright 2020 American Chemical Society

$I_{Kv11.1}$ peak and tail currents [116]. Most, if not all, Kv11.1 activators also alter the gating or inhibit channels other than Kv11.1 and, thus, are not ideally suited for testing the specific efficacy or clinical utility of "pure" I_{Kr} activation. In addition, some compounds, especially those that dramatically inhibits inactivation, have the potential to cause excessive QT shortening, essentially mimicking SQTS.

11.7.2 Structural Basis of Kv11.1 Activator Binding Sites

The structural basis of Kv11.1 activation by compounds has been explored by functional analysis of drug response using mutant channels and by molecular modeling. Single residue mutations in the S6 segment (Asn658, Val659) and S5 segment (Leu553, Phe557) attenuate the effects of RPR on deactivation and inactivation, whereas other single mutations (e.g., of Val549, Leu550 in the S4-S5 linker and Ile662, Leu666, Tyr667 in the S6 segment) only affect deactivation [126]. These findings suggest that RPR binds to hydrophobic pockets located between the S5/S6 regions of adjacent subunits to partially inhibit inactivation and the coupling of VSD movement to channel opening. The stoichiometry of RPR activities was characterized using tetrameric Kv11.1 concatemers containing a variable combination of wild-type subunits and subunits containing a mutation (Leu553Ala) that eliminates the drug effect. The slowing of deactivation by RPR was found to be directly proportional to the number of wild-type subunits present in a tetramer, whereas inhibition of inactivation was half-maximal with a single wild-type subunit and maximal in channels with three wild-type subunits [128]. These findings suggest that there are four identical RPR binding sites per channel and that allosteric modulation of deactivation and inactivation are characterized by distinct subunit stoichiometry. Characterization of mutant and chimeric Kv11.1/11.2 channels indicate that the cytoplasmic region of the channel (C-linker and attached cyclic nucleotide-binding homology domain) is the key structural component that mediates the slowing of deactivation by RPR [129]. Based on mutational analyses, other activators, including PD-118057 [127] and ICA-105574 [130, 131] have also been proposed to bind to four symmetrical inter-subunit hydrophobic pockets of the Kv11.1 tetramer. Concatenated tetramer analysis indicates that the increased single-channel open probability induced by PD-118057 (a 2-(phenylamino)-benzoic acid) and the attenuated inactivation induced by ICA-105574 (a substituted benzamide) are mediated by cooperative subunit interactions and that occupancy of all four binding sites in a Kv11.1 channel is required for maximal channel activation by these compounds [132].

Based on analysis of multiple negatively charged activators (e.g., PD-118057) and potassium channel types (including K_2P, BK, and Kv11.1), it has been proposed that channel activators bind to a common site located below the selectivity filter and enhance channel conductance by increasing K^+ occupancy at specific ion coordination sites within the pore and selectivity filter [133]. This binding mode is somewhat analogous to that proposed for Kv11.1 blockers [101], but instead of inhibiting K^+ coordination, this model proposes that activators facilitate ion coordination. Molecular dynamic simulation studies utilizing long periods of sampling (100s of nanoseconds) of the open-state cryo-EM structure of Kv11.1 has revealed refined docking modes for activators, including PD-118057, that are consistent with earlier site-directed mutagenesis studies [101].

11.7.3 Kv11.1 Activators Can Be Proarrhythmic

Some Kv11.1 activators may cause excessively short action potential duration and refractoriness and, therefore, may be proarrhythmic. It is noteworthy that some activators are used to create drug-induced models of SQTS as a short electrical refractory period provides a prime substrate for re-entry-based arrhythmia. Attenuated inactivation by a compound such as ICA-105574 mimics the gain of function Kv11.1 mutations that cause inherited short QT syndrome. In coronary-perfused canine right atria, PD-118057 was reported to increase spatial dispersion of repolarization and a single premature stimulus-induced fibrillation [134]. PD-118057 was also reported to induce polymorphic VT in left ventricular wedge preparations [135]. NS1643 suppressed arrhythmias induced by infusion of dofetilide to methoxamine-sensitized rabbits or by atrioventricular block with ventricular bradypacing in rabbits [136]. However, protection was not observed in a transgenic rabbit model of LQTS; instead, NS1643-induced shortening of QTc was accompanied by an increased incidence of arrhythmia [137].

11.8 Conclusions

Kv11.1 channels conduct a repolarizing K^+ current that is a major determinant of cardiac repolarization in humans. Loss of function mutations in *KCNH2* are a common cause of LQTS. Gain of function mutations in *KCNH2* are a very rare cause of SQTS. In clinical practice, drug-induced QT prolongation is most often caused by block of Kv11.1 channels. The cryo-EM structure of Kv11.1 has been solved, and the molecular determinants of Kv11.1 blockers and activators have been described. Extensive structure–activity relationships for a wide spectrum of compounds are now available and have guided the development of pharmacophore models that facilitate the rational design of medications that are devoid of Kv11.1 channel blocking activity. Further research is warranted to determine if novel Kv11.1 activators can safely prevent arrhythmia associated with congenital LQTS or drug-induced excessive QT prolongation.

References

1. Warmke JW, Ganetzky B. A family of potassium channel genes related to *eag* in *Drosophila* and mammals. Proc Natl Acad Sci U S A. 1994;91:3438–42.
2. Recanatini M, Poluzzi E, Masetti M, Cavalli A, De Ponti F. QT prolongation through hERG K^+ channel blockade: current knowledge and strategies for the early prediction during drug development. Med Res Rev. 2005;25(2):133–66.
3. Kang J, Chen XL, Wang H, Ji J, Cheng H, Incardona J, et al. Discovery of a small molecule activator of the human *ether-à-go-go*-related gene (HERG) cardiac K^+ channel. Mol Pharmacol. 2005;67(3):827–36.
4. Shi W, Wymore RS, Wang H-S, Pan Z, Cohen IS, McKinnon D, et al. Identification of two nervous system-specific members of the *erg* potassium channel gene family. J Neurosci. 1997;17(2–4):9423–32.
5. Babcock JJ, Li M. hERG channel function: beyond long QT. Acta Pharmacol Sin. 2013;34(3):329–35.
6. Emmi A, Wenzel HJ, Schwartzkroin PA, Taglialatela M, Castaldo P, Bianchi L, et al. Do glia have heart? Expression and functional role for *ether-a-go-go* currents in hippocampal astrocytes. J Neurosci. 2000;20(10):3915–25.
7. Overholt JL, Ficker E, Yang T, Shams H, Bright GR, Prabhakar NR. HERG-like potassium current regulates the resting membrane potential in glomus cells of the rabbit carotid body. J Neurophysiol. 2000;83(3):1150–7.
8. Sacco T, Bruno A, Wanke E, Tempia F. Functional roles of an ERG current isolated in cerebellar Purkinje neurons. J Neurophysiol. 2003;90(3):1817–28.
9. Kirchberger NM, Wulfsen I, Schwarz JR, Bauer CK. Effects of TRH on heteromeric rat erg1a/1b K^+ channels are dominated by the rerg1b subunit. J Physiol. 2006;571(Pt 1):27–42.
10. Schledermann W, Wulfsen I, Schwarz JR, Bauer CK. Modulation of rat erg1, erg2, erg3 and HERG K+ currents by thyrotropin-releasing hormone in anterior pituitary cells via the native signal cascade. J Physiol. 2001;532(Pt 1):143–63.
11. Rosati B, Marchetti P, Crociani O, Lecchi M, Lupi R, Arcangeli A, et al. Glucose- and arginine-induced insulin secretion by human pancreatic beta-cells: the role of HERG K^+ channels in firing and release. FASEB J. 2000;14(15):2601–10.
12. Akbarali HI, Thatte H, He XD, Giles WR, Goyal RK. Role of HERG-like K^+ currents in opossum esophageal circular smooth muscle. Am J Phys. 1999;277(6 Pt 1):C1284–90.
13. Farrelly AM, Ro S, Callaghan BP, Khoyi MA, Fleming N, Horowitz B, et al. Expression and function of KCNH2 (HERG) in the human jejunum. Am J Phys. 2003;284(6):G883–95.
14. Shoeb F, Malykhina AP, Akbarali HI. Cloning and functional characterization of the smooth muscle *ether-a-go-go*-related gene K^+ channel. Potential role of a conserved amino acid substitution in the S4 region. J Biol Chem. 2003;278(4):2503–14.
15. Jehle J, Schweizer PA, Katus HA, Thomas D. Novel roles for hERG K^+ channels in cell proliferation and apoptosis. Cell Death Dis. 2011;2:e193.
16. Wang H, Zhang Y, Cao L, Han H, Wang J, Yang B, et al. HERG K^+ channel, a regulator of tumor cell apoptosis and proliferation. Cancer Res. 2002;62(17):4843–8.
17. Bianchi L, Wible B, Arcangeli A, Taglialatela M, Morra F, Castaldo P, et al. *herg* encodes a K^+ current highly conserved in tumors of different histogenesis: a selective advantage for cancer cells? Cancer Res. 1998;58(4):815–22.
18. Lastraioli E, Guasti L, Crociani O, Polvani S, Hofmann G, Witchel H, et al. *herg1* gene and

HERG1 protein are overexpressed in colorectal cancers and regulate cell invasion of tumor cells. Cancer Res. 2004;64(2):606–11.

19. Arcangeli A. Expression and role of hERG channels in cancer cells. Novartis Found Symp. 2005;266: 225–32. discussion 32–4
20. Curran ME, Splawski I, Timothy KW, Vincent GM, Green ED, Keating MT. A molecular basis for cardiac arrhythmia: *HERG* mutations cause long QT syndrome. Cell. 1995;80:795–803.
21. Schwartz PJ, Stramba-Badiale M, Crotti L, Pedrazzini M, Besana A, Bosi G, et al. Prevalence of the congenital long-QT syndrome. Circulation. 2009;120(18):1761–7.
22. Rohatgi RK, Sugrue A, Bos JM, Cannon BC, Asirvatham SJ, Moir C, et al. Contemporary outcomes in patients with long QT syndrome. J Am Coll Cardiol. 2017;70(4):453–62.
23. Schwartz PJ, Crotti L. Long QT and short QT syndromes. In: Zipes D, Jalife J, Stevenson W, editors. Cardiac electrophysiology: from cell to bedside. 7th ed. Philadelphia, PA: Elsevier/Saunders; 2017. p. 893–904.
24. Wilde AA, Jongbloed RJ, Doevendans PA, Duren DR, Hauer RN, van Langen IM, et al. Auditory stimuli as a trigger for arrhythmic events differentiate HERG-related (LQTS2) patients from KVLQT1-related patients (LQTS1). J Am Coll Cardiol. 1999;33(2):327–32.
25. Anderson CL, Delisle BP, Anson BD, Kilby JA, Will ML, Tester DJ, et al. Most LQT2 mutations reduce Kv11.1 (hERG) current by a class 2 (trafficking-deficient) mechanism. Circulation. 2006;113(3): 365–73.
26. Sanguinetti MC, Curran ME, Spector PS, Keating MT. Spectrum of HERG K^+ channel dysfunction in an inherited cardiac arrhythmia. Proc Natl Acad Sci U S A. 1996;93:2208–12.
27. Brunner M, Peng X, Liu GX, Ren XQ, Ziv O, Choi BR, et al. Mechanisms of cardiac arrhythmias and sudden death in transgenic rabbits with long QT syndrome. J Clin Invest. 2008;118(6):2246–59.
28. Odening KE, Kirk M, Brunner M, Ziv O, Lorvidhaya P, Liu GX, et al. Electrophysiological studies of transgenic long QT type 1 and type 2 rabbits reveal genotype-specific differences in ventricular refractoriness and his conduction. Am J Physiol Heart Circ Physiol. 2010;299(3):H643–55.
29. Ziv O, Morales E, Song YK, Peng X, Odening KE, Buxton AE, et al. Origin of complex behaviour of spatially discordant alternans in a transgenic rabbit model of type 2 long QT syndrome. J Physiol. 2009;587(Pt 19):4661–80.
30. Priori SG, Wilde AA, Horie M, Cho Y, Behr ER, Berul C, et al. HRS/EHRA/APHRS expert consensus statement on the diagnosis and management of patients with inherited primary arrhythmia syndromes: document endorsed by HRS, EHRA, and APHRS in may 2013 and by ACCF, AHA, PACES, and AEPC in June 2013. Heart Rhythm. 2013;10(12):1932–63.
31. Cordeiro JM, Brugada R, Wu YS, Hong K, Dumaine R. Modulation of I_{Kr} inactivation by mutation N588K in KCNH2: a link to arrhythmogenesis in short QT syndrome. Cardiovasc Res. 2005;67(3):498–509.
32. Sun Y, Quan XQ, Fromme S, Cox RH, Zhang P, Zhang L, et al. A novel mutation in the KCNH2 gene associated with short QT syndrome. J Mol Cell Cardiol. 2011;50(3):433–41.
33. Odening KE, Bodi I, Franke G, Rieke R, Ryan de Medeiros A, Perez-Feliz S, et al. Transgenic short-QT syndrome 1 rabbits mimic the human disease phenotype with QT/action potential duration shortening in the atria and ventricles and increased ventricular tachycardia/ventricular fibrillation inducibility. Eur Heart J. 2019;40(10):842–53.
34. London B, Trudeau MC, Newton KP, Beyer AK, Copeland NG, Gilbert DJ, et al. Two isoforms of the mouse *ether-a-go-go*-related gene coassemble to form channels with properties similar to the rapidly activating component of the cardiac delayed rectifier K^+ current. Circ Res. 1997;81:870–8.
35. Lees-Miller JP, Kondo C, Wang L, Duff HJ. Electrophysiological characterization of an alternatively processed ERG K^+ channel in mouse and human hearts. Circ Res. 1997;81:719–26.
36. Phartiyal P, Sale H, Jones EM, Robertson GA. Endoplasmic reticulum retention and rescue by heteromeric assembly regulate human ERG 1a/1b surface channel composition. J Biol Chem. 2008;283(7):3702–7.
37. Ng CA, Phan K, Hill AP, Vandenberg JI, Perry MD. Multiple interactions between cytoplasmic domains regulate slow deactivation of Kv11.1 channels. J Biol Chem. 2014;289(37):25822–32.
38. Gianulis EC, Liu Q, Trudeau MC. Direct interaction of eag domains and cyclic nucleotide-binding homology domains regulate deactivation gating in hERG channels. J Gen Physiol. 2013;142(4):351–66.
39. Gustina AS, Trudeau MC. hERG potassium channel gating is mediated by N- and C-terminal region interactions. J Gen Physiol. 2011;137(3):315–25.
40. McDonald TV, Yu Z, Ming Z, Palma E, Meyers MB, Wang K-W, et al. A minK-HERG complex regulates the cardiac potassium current I_{Kr}. Nature. 1997;388: 289–92.
41. Bianchi L, Shen Z, Dennis AT, Priori SG, Napolitano C, Ronchetti E, et al. Cellular dysfunction of LQT5-minK mutants: abnormalities of I_{Ks}, I_{Kr} and trafficking in long QT syndrome. Hum Mol Genet. 1999;8(8):1499–507.
42. Abbott GW, Sesti F, Splawski I, Buck ME, Lehmann MH, Timothy KW, et al. MiRP1 forms I_{Kr} potassium channels with HERG and is associated with cardiac arrhythmia. Cell. 1999;97(2):175–87.
43. Weerapura M, Nattel S, Chartier D, Caballero R, Hebert TE. A comparison of currents carried by HERG, with and without coexpression of MiRP1,

and the native rapid delayed rectifier current. Is MiRP1 the missing link? J Physiol. 2002;540(Pt 1): 15–27.

44. Lopatin AN, Makhina EN, Nichols CG. The mechanism of inward rectification of potassium channels: “long-pore plugging” by cytoplasmic polyamines. J Gen Physiol. 1995;106:923–55.
45. Smith PL, Baukrowitz T, Yellen G. The inward rectification mechanism of the HERG cardiac potassium channel. Nature. 1996;379:833–6.
46. Wang W, MacKinnon R. Cryo-EM structure of the open human *ether-a-go-go*-related K^+ channel hERG. Cell. 2017;169(3):422–30 e10.
47. Hardman RM, Stansfeld PJ, Dalibalta S, Sutcliffe MJ, Mitcheson JS. Activation gating of hERG potassium channels: S6 glycines are not required as gating hinges. J Biol Chem. 2007;282(44):31972–81.
48. Sanguinetti MC, Xu QP. Mutations of the S4-S5 linker alter activation properties of HERG potassium channels expressed in *Xenopus* oocytes. J Physiol. 1999;514(Pt 3):667–75.
49. Tristani-Firouzi M, Chen J, Sanguinetti MC. Interactions between S4-S5 linker and S6 transmembrane domain modulate gating of HERG K^+ channels. J Biol Chem. 2002;277(21):18994–9000.
50. Ferrer T, Rupp J, Piper DR, Tristani-Firouzi M. The S4-S5 linker directly couples voltage sensor movement to the activation gate in the human *ether-a’-go-go*-related gene (hERG) K^+ channel. J Biol Chem. 2006;281(18):12858–64.
51. Ng CA, Perry MD, Tan PS, Hill AP, Kuchel PW, Vandenberg JI. The S4-S5 linker acts as a signal integrator for HERG K^+ channel activation and deactivation gating. PLoS One. 2012;7(2):e31640.
52. Schonherr R, Heinemann SH. Molecular determinants for activation and inactivation of HERG, a human inward rectifier potassium channel. J Physiol. 1996;493(3):635–42.
53. Ficker E, Jarolimek W, Kiehn J, Baumann A, Brown AM. Molecular determinants of dofetilide block of HERG K^+ channels. Circ Res. 1998;82(3):386–95.
54. Wang S, Morales MJ, Liu S, Strauss HC, Rasmusson RL. Time, voltage and ionic concentration dependence of rectification of h-*erg* expressed in *Xenopus* oocytes. FEBS Lett. 1996;389:167–73.
55. Wang DT, Hill AP, Mann SA, Tan PS, Vandenberg JI. Mapping the sequence of conformational changes underlying selectivity filter gating in the K(v)11.1 potassium channel. Nat Struct Mol Biol. 2011;18 (1):35–41.
56. Perry MD, Ng CA, Vandenberg JI. Pore helices play a dynamic role as integrators of domain motion during Kv11.1 channel inactivation gating. J Biol Chem. 2013;288(16):11482–91.
57. Wu W, Gardner A, Sanguinetti MC. Cooperative subunit interactions mediate fast C-type inactivation of hERG1 K^+ channels. J Physiol. 2014;592(Pt 20): 4465–80.
58. Woosley RL, Black K, Heise CW, Romero K. CredibleMeds.org: what does it offer? Trends Cardiovasc Med. 2018;28(2):94–9.
59. Woosley RL, Romero K. Assessing cardiovascular drug safety for clinical decision-making. Nat Rev Cardiol. 2013;10(6):330–7.
60. El-Sherif N, Turitto G, Boutjdir M. Acquired long QT syndrome and electrophysiology of torsade de pointes. Arrhythm Electrophysiol Rev. 2019;8(2): 122–30.
61. Haverkamp W, Breithardt G, Camm AJ, Janse MJ, Rosen MR, Antzelevitch C, et al. The potential for QT prolongation and proarrhythmia by non-antiarrhythmic drugs: clinical and regulatory implications. Report on a policy conference of the European Society of Cardiology. Eur Heart J. 2000;21(15):1216–31.
62. Butler A, Helliwell MV, Zhang Y, Hancox JC, Dempsey CE. An update on the structure of hERG. Front Pharmacol. 2020;10:1572.
63. Vandenberg JI, Perry MD, Perrin MJ, Mann SA, Ke Y, Hill AP. hERG K^+ channels: structure, function, and clinical significance. Physiol Rev. 2012;92 (3):1393–478.
64. Recanatini M, Cavalli A, Masetti M. Modeling HERG and its interactions with drugs: recent advances in light of current potassium channel simulations. ChemMedChem. 2008;3(4):523–35.
65. Fenichel RR, Malik M, Antzelevitch C, Sanguinetti M, Roden DM, Priori SG, et al. Drug-induced torsades de pointes and implications for drug development. J Cardiovasc Electrophysiol. 2004;15 (4):475–95.
66. Sicouri S, Antzelevitch C. Mechanisms underlying the actions of antidepressant and antipsychotic drugs that cause sudden cardiac arrest. Arrhythm Electrophysiol Rev. 2018;7(3):199–209.
67. Vitola J, Vukanovic J, Roden DM. Cisapride-induced torsades de pointes. J Cardiovasc Electrophysiol. 1998;9(10):1109–13.
68. Aronov AM, Goldman BB. A model for identifying HERG K^+ channel blockers. Bioorg Med Chem. 2004;12(9):2307–15.
69. Su BH, Shen MY, Esposito EX, Hopfinger AJ, Tseng YJ. In silico binary classification QSAR models based on 4D-fingerprints and MOE descriptors for prediction of hERG blockage. J Chem Inf Model. 2010;50(7):1304–18.
70. Wang S, Li Y, Wang J, Chen L, Zhang L, Yu H, et al. ADMET evaluation in drug discovery. 12. Development of binary classification models for prediction of hERG potassium channel blockage. Mol Pharm. 2012;9(4):996–1010.
71. Munawar S, Windley MJ, Tse EG, Todd MH, Hill AP, Vandenberg JI, et al. Experimentally validated pharmacoinformatics approach to predict hERG inhibition potential of new chemical entities. Front Pharmacol. 2018;9:1035.

72. DIV GY, Davies MR, Zhang H, Abi-Gerges N, Boyett MR. hERG inhibitors with similar potency but different binding kinetics do not pose the same proarrhythmic risk: implications for drug safety assessment. J Cardiovasc Electrophysiol. 2014;25 (2):197–207.
73. Pearlstein RA, MacCannell KA, Erdemli G, Yeola S, Helmlinger G, Hu QY, et al. Implications of dynamic occupancy, binding kinetics, and channel gating kinetics for hERG blocker safety assessment and mitigation. Curr Top Med Chem. 2016;16(16): 1792–818.
74. Li Z, Dutta S, Sheng J, Tran PN, Wu W, Chang K, et al. Improving the in silico assessment of proarrhythmia risk by combining hERG (human *ether-a-go-go*-related gene) channel-drug binding kinetics and multichannel pharmacology. Circ Arrhythm Electrophysiol. 2017;10(2):e004628.
75. Spector PS, Curran ME, Keating MT, Sanguinetti MC. Class III antiarrhythmic drugs block HERG, a human cardiac delayed rectifier K^+ channel; open channel block by methanesulfonanilides. Circ Res. 1996;78:499–503.
76. Mitcheson JS, Chen J, Sanguinetti MC. Trapping of a methanesulfonanilide by closure of the HERG potassium channel activation gate. J Gen Physiol. 2000;115(3):229–40.
77. Kamiya K, Niwa R, Mitcheson JS, Sanguinetti MC. Molecular determinants of HERG channel block. Mol Pharmacol. 2006;69(5):1709–16.
78. Stork D, Timin EN, Berjukow S, Huber C, Hohaus A, Auer M, et al. State dependent dissociation of HERG channel inhibitors. Br J Pharmacol. 2007;151:1368–76.
79. Numaguchi H, Mullins FM, Johnson JP Jr, Johns DC, Po SS, Yang IC, et al. Probing the interaction between inactivation gating and Dd-sotalol block of HERG. Circ Res. 2000;87(11):1012–8.
80. Tie H, Walker BD, Singleton CB, Valenzuela SM, Bursill JA, Wyse KR, et al. Inhibition of HERG potassium channels by the antimalarial agent halofantrine. Br J Pharmacol. 2000;130(8):1967–75.
81. Ficker E, Jarolimek W, Brown AM. Molecular determinants of inactivation and dofetilide block in ether a- go-go (EAG) channels and EAG-related K+ channels. Mol Pharmacol. 2001;60(6):1343–8.
82. Sanchez-Chapula JA, Navarro-Polanco RA, Sanguinetti MC. Block of wild-type and inactivation-deficient human *ether-a-go-go*-related gene K^+ channels by halofantrine. Naunyn Schmiedeberg's Arch Pharmacol. 2004;370(6): 484–91.
83. Suessbrich H, Schonherr R, Heinemann SH, Lang F, Busch AE. Specific block of cloned Herg channels by clofilium and its tertiary analog LY97241. FEBS Lett. 1997;414(2):435–8.
84. Wu W, Gardner A, Sanguinetti MC. The link between inactivation and high-affinity block of hERG1 channels. Mol Pharmacol. 2015;87(6): 1042–50.
85. Finlayson K, Turnbull L, January CT, Sharkey J, Kelly JS. [3H]dofetilide binding to HERG transfected membranes: a potential high throughput preclinical screen. Eur J Pharmacol. 2001;430(1): 147–8.
86. Diaz GJ, Daniell K, Leitza ST, Martin RL, Su Z, McDermott JS, et al. The [^{3}H]dofetilide binding assay is a predictive screening tool for hERG blockade and proarrhythmia: comparison of intact cell and membrane preparations and effects of altering $[K^+]_o$. J Pharmacol Toxicol Methods. 2004;50(3):187–99.
87. Chiu PJ, Marcoe KF, Bounds SE, Lin CH, Feng JJ, Lin A, et al. Validation of a [^{3}H]astemizole binding assay in HEK293 cells expressing HERG K^+ channels. J Pharmacol Sci. 2004;95(3):311–9.
88. Lees-Miller JP, Duan Y, Teng GQ, Duff HJ. Molecular determinant of high-affinity dofetilide binding to HERG1 expressed in *Xenopus* oocytes: involvement of S6 sites. Mol Pharmacol. 2000;57 (2):367–74.
89. Mitcheson JS, Chen J, Lin M, Culberson C, Sanguinetti MC. A structural basis for drug-induced long QT syndrome. Proc Natl Acad Sci U S A. 2000;97:12329–33.
90. Saxena P, Zangerl-Plessl EM, Linder T, Windisch A, Hohaus A, Timin E, et al. New potential binding determinant for hERG channel inhibitors. Sci Rep. 2016;6:24182.
91. Helliwell MV, Zhang Y, El Harchi A, Du C, Hancox JC, Dempsey CE. Structural implications of hERG K^+ channel block by a high-affinity minimally structured blocker. J Biol Chem. 2018;293(18): 7040–57.
92. Sanchez-Chapula JA, Navarro-Polanco RA, Culberson C, Chen J, Sanguinetti MC. Molecular determinants of voltage dependent HERG K^+ channel block. J Biol Chem. 2002;277:23587–95.
93. Sanchez-Chapula JA, Ferrer T, Navarro-Polanco RA, Sanguinetti MC. Voltage-dependent profile of human *ether-a-go-go*-related gene channel block is influenced by a single residue in the S6 transmembrane domain. Mol Pharmacol. 2003;63(5):1051–8.
94. Fernandez D, Ghanta A, Kauffman GW, Sanguinetti MC. Physicochemical features of the hERG channel drug binding site. J Biol Chem. 2004;279:10120–7.
95. Ridley JM, Dooley PC, Milnes JT, Witchel HJ, Hancox JC. Lidoflazine is a high affinity blocker of the HERG K^+ channel. J Mol Cell Cardiol. 2004;36 (5):701–5.
96. Perry M, de Groot MJ, Helliwell R, Leishman D, Tristani-Firouzi M, Sanguinetti MC, et al. Structural determinants of HERG channel block by clofilium and ibutilide. Mol Pharmacol. 2004;66(2):240–9.
97. Guo J, Gang H, Zhang S. Molecular determinants of cocaine block of human ether-a-go-go-related gene potassium channels. J Pharmacol Exp Ther. 2006;317 (2):865–74.

98. Farid R, Day T, Friesner RA, Pearlstein RA. New insights about HERG blockade obtained from protein modeling, potential energy mapping, and docking studies. Bioorg Med Chem. 2006;14(9):3160–73.
99. Stary A, Wacker SJ, Boukharta L, Zachariae U, Karimi-Nejad Y, Aqvist J, et al. Toward a consensus model of the HERG potassium channel. ChemMedChem. 2010;5(3):455–67.
100. Kalyaanamoorthy S, Barakat KH. Binding modes of hERG blockers: an unsolved mystery in the drug design arena. Expert Opin Drug Discov. 2018;13 (3):207–10.
101. Dickson CJ, Velez-Vega C, Duca JS. Revealing molecular determinants of hERG blocker and activator binding. J Chem Inf Model. 2020;60(1):192–203.
102. Ficker E, Kuryshev YA, Dennis AT, Obejero-Paz C, Wang L, Hawryluk P, et al. Mechanisms of arsenic-induced prolongation of cardiac repolarization. Mol Pharmacol. 2004;66(1):33–44.
103. Kuryshev YA, Ficker E, Wang L, Hawryluk P, Dennis AT, Wible BA, et al. Pentamidine-induced long QT syndrome and block of hERG trafficking. J Pharmacol Exp Ther. 2005;312(1):316–23.
104. Rajamani S, Eckhardt LL, Valdivia CR, Klemens CA, Gillman BM, Anderson CL, et al. Drug-induced long QT syndrome: hERG K^+ channel block and disruption of protein trafficking by fluoxetine and norfluoxetine. Br J Pharmacol. 2006;149(5):481–9.
105. Sun H, Liu X, Xiong Q, Shikano S, Li M. Chronic inhibition of cardiac Kir2.1 and HERG potassium channels by celastrol with dual effects on both ion conductivity and protein trafficking. J Biol Chem. 2006;281(9):5877–84.
106. Wang L, Wible BA, Wan X, Ficker E. Cardiac glycosides as novel inhibitors of human ether-a-go-go-related gene channel trafficking. J Pharmacol Exp Ther. 2007;320(2):525–34.
107. Dennis A, Wang L, Wan X, Ficker E. hERG channel trafficking: novel targets in drug-induced long QT syndrome. Biochem Soc Trans. 2007;35(Pt 5): 1060–3.
108. Wible BA, Hawryluk P, Ficker E, Kuryshev YA, Kirsch G, Brown AM. HERG-lite: a novel comprehensive high-throughput screen for drug-induced hERG risk. J Pharmacol Toxicol Methods. 2005;52 (1):136–45.
109. Schwartz PJ. The congenital long QT syndromes from genotype to phenotype: clinical implications. J Intern Med. 2006;259(1):39–47.
110. Szabo G, Farkas V, Grunnet M, Mohacsi A, Nanasi PP. Enhanced repolarization capacity: new potential antiarrhythmic strategy based on HERG channel activation. Curr Med Chem. 2011;18(24):3607–21.
111. Sanguinetti MC. HERG1 channel agonists and cardiac arrhythmia. Curr Opin Pharmacol. 2014;15:22–7.
112. Qile M, Beekman HDM, Sprenkeler DJ, Houtman MJC, van Ham WB, Stary-Weinzinger A, et al. LUF7244, an allosteric modulator/activator of Kv 11.1 channels, counteracts dofetilide-induced torsades de pointes arrhythmia in the chronic atrioventricular block dog model. Br J Pharmacol. 2019;176(19):3871–85.
113. Asayama M, Kurokawa J, Shirakawa K, Okuyama H, Kagawa T, Okada J, et al. Effects of an hERG activator, ICA-105574, on electrophysiological properties of canine hearts. J Pharmacol Sci. 2013;121(1):1–8.
114. Meng J, Shi C, Li L, Du Y, Xu Y. Compound ICA-105574 prevents arrhythmias induced by cardiac delayed repolarization. Eur J Pharmacol. 2013;718:87–97.
115. Casis O, Olesen SP, Sanguinetti MC. Mechanism of action of a novel human *ether-a-go-go*-related gene channel activator. Mol Pharmacol. 2006;69(2): 658–65.
116. Hansen RS, Diness TG, Christ T, Demnitz J, Ravens U, Olesen SP, et al. Activation of human *ether-a-go-go*-related gene potassium channels by the diphenylurea 1,3-bis-(2-hydroxy-5-trifluoromethyl-phenyl)-urea (NS1643). Mol Pharmacol. 2006;69(1):266–77.
117. Zhou J, Augelli-Szafran CE, Bradley JA, Chen X, Koci BJ, Volberg WA, et al. Novel potent human *ether-à-go-go*-related gene (hERG) potassium channel enhancers and their in vitro antiarrhythmic activity. Mol Pharmacol. 2005;68(3):876–84.
118. Gordon E, Lozinskaya IM, Lin Z, Semus SF, Blaney FE, Willette RN, et al. 2-[2-(3,4-dichloro-phenyl)-2,3-dihydro-1H-isoindol-5-ylamino]-nicotinic acid (PD-307243) causes instantaneous current through human *ether-a-go-go*-related gene potassium channels. Mol Pharmacol. 2008;73(3):639–51.
119. Gerlach AC, Stoehr SJ, Castle NA. Pharmacological removal of human *ether-a-go-go*-related gene potassium channel inactivation by 3-nitro-N-(4-phenoxyphenyl) benzamide (ICA-105574). Mol Pharmacol. 2010;77(1):58–68.
120. Zhang H, Zou B, Yu H, Moretti A, Wang X, Yan W, et al. Modulation of hERG potassium channel gating normalizes action potential duration prolonged by dysfunctional KCNQ1 potassium channel. Proc Natl Acad Sci U S A. 2012;109(29):11866–71.
121. Su Z, Limberis J, Souers A, Kym P, Mikhail A, Houseman K, et al. Electrophysiologic characterization of a novel hERG channel activator. Biochem Pharmacol. 2009;77(8):1383–90.
122. Choi SH, Shin TJ, Hwang SH, Lee BH, Kang J, Kim HJ, et al. Ginsenoside Rg_3 decelerates hERG K^+ channel deactivation through Ser631 residue interaction. Eur J Pharmacol. 2011;663(1–3):59–67.
123. Mannikko R, Bridgland-Taylor MH, Pye H, Swallow S, Abi-Gerges N, Morton MJ, et al. Pharmacological and electrophysiological characterization of AZSMO-23, an activator of the hERG K^+ channel. Br J Pharmacol. 2015;172(12):3112–25.
124. Yu Z, Liu J, van Veldhoven JP, AP IJ, Schalij MJ, Pijnappels DA, et al. Allosteric modulation of Kv11.1 (hERG) channels protects against drug-

induced ventricular arrhythmias. Circ Arrhythm Electrophysiol. 2016;9(4):e003439.

125. Dong X, Liu Y, Niu H, Wang G, Dong L, Zou A, et al. Electrophysiological characterization of a small molecule activator on human *ether-a-go-go*-related gene (hERG) potassium channel. J Pharmacol Sci. 2019;140:284.
126. Perry M, Sachse FB, Sanguinetti MC. Structural basis of action for a human *ether-à-go-go*-related gene 1 potassium channel activator. Proc Natl Acad Sci U S A. 2007;104(34):13827–32.
127. Perry M, Sachse FB, Abbruzzese J, Sanguinetti MC. PD-118057 contacts the pore helix of hERG1 channels to attenuate inactivation and enhance K^+ conductance. Proc Natl Acad Sci U S A. 2009;106 (47):20075–80.
128. Wu W, Gardner A, Sanguinetti MC. Concatenated hERG1 tetramers reveal stoichiometry of altered channel gating by RPR-260243. Mol Pharmacol. 2015;87(3):401–9.
129. Gardner A, Sanguinetti MC. C-linker accounts for differential sensitivity of ERG1 and ERG2 K^+ channels to RPR260243-induced slow deactivation. Mol Pharmacol. 2015;88(1):19–28.
130. Garg V, Stary-Weinzinger A, Sachse F, Sanguinetti MC. Molecular determinants for activation of human *ether-à-go-go*-related gene 1 potassium channels by 3-nitro-N-(4-phenoxyphenyl) benzamide. Mol Pharmacol. 2011;80(4):630–7.
131. Garg V, Stary-Weinzinger A, Sanguinetti MC. ICA-105574 interacts with a common binding site to elicit opposite effects on inactivation gating of EAG and ERG potassium channels. Mol Pharmacol. 2013;83(4):805–13.
132. Wu W, Sachse FB, Gardner A, Sanguinetti MC. Stoichiometry of altered hERG1 channel gating by small molecule activators. J Gen Physiol. 2014;143(4):499–512.
133. Schewe M, Sun H, Mert U, Mackenzie A, Pike ACW, Schulz F, et al. A pharmacological master key mechanism that unlocks the selectivity filter gate in K^+ channels. Science. 2019;363(6429): 875–80.
134. Nof E, Burashnikov A, Antzelevitch C. Cellular basis for atrial fibrillation in an experimental model of short QT1: implications for a pharmacological approach to therapy. Heart Rhythm. 2010;7(2): 251–7.
135. Patel C, Antzelevitch C. Cellular basis for arrhythmogenesis in an experimental model of the SQT1 form of the short QT syndrome. Heart Rhythm. 2008;5(4):585–90.
136. Diness TG, Yeh YH, Qi XY, Chartier D, Tsuji Y, Hansen RS, et al. Antiarrhythmic properties of a rapid delayed-rectifier current activator in rabbit models of acquired long QT syndrome. Cardiovasc Res. 2008;79(1):61–9.
137. Bentzen BH, Bahrke S, Wu K, Larsen AP, Odening KE, Franke G, et al. Pharmacological activation of Kv11.1 in transgenic long QT-1 rabbits. J Cardiovasc Pharmacol. 2011;57(2):223–30.

TRPC Channels in Cardiac Arrhythmia: Their Role during Purinergic Activation Induced by Ischemia

12

Julio L. Alvarez and Julio Alvarez-Collazo

Abstract

Cardiac electrical activity is mainly determined by a set of voltage-dependent channels that control depolarizing currents carried by Na^+ and Ca^{2+} cations and repolarizing currents carried by K^+ and Cl^- ions. Arrhythmia often results from a disorder in these currents or from the occurrence of additional inward currents such as those generated by the transient receptor potential (TRP) channels. In mammals, the TRP family comprises six major subfamilies; TRPC (canonical), TRPV (vanilloid), TRPA (ankyrin), TRPM (melastatin), TRPP (polycystin), and TRPML (mucolipin). In the heart, TRP channels are known to be involved in various diseases, including hypertrophy, heart failure, and arrhythmia. A large part of this chapter focuses on the potential contribution of TRP channels, namely TRPCs and TRPM4, that could carry an inward current at the resting potential to modulate cardiac rhythm, as well as on their potential arrhythmic effects. Specific attention is given to the proarrhythmic effects of ATP as a purinergic agonist. Under ischemia, a burst of ATP is released that stimulates P_2Y_2 receptors, which through phospholipase C activates heterotetrameric TRPC3/TRPC7 channels and, as well, releases Ca^{2+} from the sarcoplasmic reticulum to activate TRPM4. The subsequent inward currents could depolarize the cell and trigger anomalous activity. Furthermore, several other neurotransmitters that all induce through G protein or tyrosine kinase, the formation of DAG could, as well, modulate cardiac rhythm and trigger arrhythmia.

Keywords

Transient receptor potential channels · Background current · Calcium · Cardiac diseases · Purinergic receptors · Cardiac rhythm

Abbreviations

$[Ca^{2+}]_i$	Intracellular Ca^{2+} concentration
AP	Action potential
ATP	Adenosine 5′-triphosphate
DAD	Delayed afterdepolarization
DAG	Diacylglycerol
EAD	Early afterdepolarization
IP_3	Inositol-1,4,5-triphosphate
PIP_2	Phosphatidylinositol 4,5-bisphosphate
PKA	Protein kinase A

J. L. Alvarez (✉)
Laboratorio de Electrofisiología, Instituto de Cardiología y Cirugía Cardiovascular, La Habana, Cuba
e-mail: alvarezj@infomed.sld.cu

J. Alvarez-Collazo
Data Sciences International, Harvard Bioscience Incorporation, Holliston, MA, USA

© Springer Nature Switzerland AG 2023

O. N. Tripathi et al. (eds.), *Heart Rate and Rhythm*, https://doi.org/10.1007/978-3-031-33588-4_12

PKB/Akt	Protein kinase B
PKC	Protein kinase C
PLC	Phospholipase C
RyR_2	Ryanodine receptor (cardiac isoform)
SERCA	Sarcoplasmic/endoplasmic reticulum Ca^{2+}-ATPase
SOCE	Store-operated calcium entry
SR	Sarcoplasmic reticulum
TRP	Transient receptor potential
TRPC	Transient receptor potential "Canonical"
TRPM	Transient receptor potential "Melastatin"
UTP	Uridine 5′-triphosphate

12.1 Introduction

In 1969, Cosens and Manning published a paper demonstrating that in *Drosophila melanogaster*, despite sustained lightening, a mutation induced a transitory response of an ion channel that contributes to phototransduction by conducting Ca^{2+} ions [1]. The corresponding transient receptor potential (*Trp*) gene was cloned in 1989 and led to the identification of a nonspecific cationic channel that is able to conduct Ca^{2+} ions [2]. Since then, TRP channels have been identified in every cell studied, and a huge amount of information about the role of TRP channels in the most diverse functions has emerged [3, 4]. Nowadays, due to their contribution to Ca^{2+} homeostasis, TRP channels are implicated in almost every organ function and are related to many diseases [5–9]. However, most of our knowledge about TRP channel biophysics, pharmacology, and functions, has been achieved by using heterologous expression systems. This is mostly related to the fact that there is still a lack of truly specific activators and inhibitors of TRP channels. Moreover, in every cell function or dysfunction, besides TRP channels, other ion channels or transporters are also involved. In patch-clamp experiments, this complicates the analysis of results and their interpretations and sometimes could limit the conclusions about the role of TRP channels. Although not always recognized, the situation could be even more complex when using fluorescence techniques to study Ca^{2+} signals following the activation of TRP channels. In many cases, TRP channel activity implies activation (under less controlled cellular conditions) of other channels and transporters (especially the Na^+-Ca^{2+} exchanger) making the interpretation of changes in intracellular Ca^{2+} rather complex. Fortunately, genetically-modified animal models have made a great contribution to our knowledge about the roles of TRP channels in health and disease, and generally reasonable schemes about the functioning of many of the TRP family members have emerged. However, there is still much to investigate in this field. In this chapter, we present evidences about the properties of TRP channels that are relevant to their arrhythmogenic effect. In particular, focus is made on the arrhythmogenic potential of "canonical" TRP channel (TRPC) activation following purinergic receptor activation during myocardial infarction. Although other important roles of TRP channels in cardiac physio-pathology (e.g. pacemaking, development of hypertrophy, fibrosis, and diseases of genetic origin) are recognized, they are not fully covered in this chapter. Extensive reviews about these subjects have been published [8–11].

12.2 General Properties of TRP Channels

TRP channels comprise a large super family of nonselective cationic channels. Similar to most voltage-gated channels, each TRP channel subunit contains six transmembrane domains (TM1–TM6) and a pore region formed by a loop between TM5 and TM6 [12]. Like K^+ channels, four subunits are required to constitute functional (conducting) TRP channels which can be assembled as homo- or heterotetramers [13]. According to their functions and amino acid sequences, in mammals, TRP are classified into six large subfamilies: TRPC (canonical; C1-C7; C2 is a pseudogene in humans), TRPM (melastatin;

M1-M8), TRPV (vanilloid; V1-V6), TRPA (ankyrin; A1), TRPP (polycystin; P2, P3, and P5) and TRPML (mucolipin; ML1-ML3) [13–17]. Up to 28 members have been described in mammals [7, 18]. Most of TRP channels lack the typical voltage sensor, i.e., they are not voltage-sensitive [19, 20]. However, they are activated by mechanical stretch, temperature variations and a miscellany of neurohormones, intracellular ligands and various exogenous natural and synthetic ligands such as endothelin-1, thrombin, adenosine 5′-triphoshate (ATP), angiotensin II, bradykinin, diacylglycerol (DAG) and phosphoinositide-4,5-bisphosphate (PIP_2) [21–28]. TRP channels are nonselective for cations, and most of them can conduct Ca^{2+} (except for TRMP4 and TRPM5). The permeability ratio P_{Ca}/P_{Na}, range from ≈ 0.05 in TRPM4 and TRPM5, to ≈ 100 in TRPV5 and TRPV6 [10]. Others, like TRPM6 and TRPM7, are able to conduct Mg^{2+} [29].

12.3 Expression of TRP Channels in the Heart

In cardiomyocytes, intracellular Ca^{2+} cycling is essential for excitation-contraction coupling and relaxation [30]. However, variations in intracellular Ca^{2+} concentration $[Ca^{2+}]_{in}$ are also important in signal transduction pathways that lead to hypertrophy, cardiac remodeling, and heart failure or are essential for cardiac development, energy homeostasis, and even for cell death [31–35]. Ca^{2+} cycling is determined by a complex interplay between L-type Ca^{2+} channels, the Na^+- Ca^{2+} exchanger, the ryanodine receptor (RyR_2), the sarcoplasmic/endoplasmic reticulum Ca^{2+}-ATPase (SERCA) and sarcolemmal Ca^{2+}-ATPases [34]. Pathological processes such as hypertrophy, cardiac remodeling, and development of heart failure are triggered by sustained increases in intracellular Ca^{2+}, which subsequently lead to activation of calcineurin/nuclear factor of activated T cells (NFAT), calmodulin (CaM)-kinase, and protein kinase C (PKC) inducing the development of myocyte growth and cardiac hypertrophy [35]. Although increases in $[Ca^{2+}]_{in}$ can be due to alterations in Ca^{2+} release from and re-uptake by the sarcoplasmic reticulum (SR), variations in the expression or function in L-type Ca^{2+} channels, SERCA, RyR_2, the inositol-1,4,5-trisphosphate(IP_3) receptor, the Na^+-Ca^{2+} exchanger or the Na^+/H^+ exchanger (NHE1) [36–38], other Ca^{2+} entry pathways could also be important. Since TRP channels can conduct Ca^{2+}, they have emerged as another potential source of $[Ca^{2+}]_{in}$ variations in cardiomyocytes [3, 8, 39, 40]. However, the roles of the different TRPs in Ca^{2+} cycling in cardiomyocytes, in physiological and pathological states, are far from being completely understood.

A review of the literature indicates that all 28 members of the TRP superfamily are expressed in heart [10, 11, 29], where the most extensively characterized has been the TRPC subfamily (see below). The eight members of the TRPM subfamily are expressed in the heart, but TRPM2/M4/M7 is specifically expressed in cardiomyocytes [10, 11]. TRPM's influence on cardiac function has been mostly inferred from models of cardiac disorders in pathological states. For example, in failing hearts, expression levels of TRPM2/M3/M8 are reduced [41]. In this sense, it has been suggested that the activity of TRPM2 could favor cardiac protection from ischemia [42]. Likewise, it has been reported that TRPM7 expression is increased in patients suffering from dilated cardiomyopathy [43]. TRPM6/7-like currents have been recorded in isolated ventricular cardiomyocytes from pig, rat, and guinea pig, and their electrophysiological properties correspond to those of the Mg^{2+}-inhibited nonselective cation current. TRPM6/7 currents are modulated by ATP, PIP_2, and nonhydrolysable guanosine 5’triphosphate (GTP) analogs [44–46]. So far, the most studied TRPM channel in cardiomyocytes is TRPM4 which has been involved in normal cardiac electrical activity and arrhythmias [43, 47]. TRPM4 is considered as the molecular counterpart of the nonselective monovalent cationic channel activated by Ca^{2+} (“CNRS channel”) first described in 1981 in cultured cardiac cells [48]. Unitary current-to-voltage relationship of

TRPM4-transfected HEK-293 cells is linear, with a single channel conductance of 20–25 pS, and is similar to TRMP4 currents recorded in cardiomyocytes [49–51]. The TRPM4 channel is equally permeable to Na^+ and K^+, but it is not permeable to Ca^{2+}. Intracellular Ca^{2+} activates the TRPM4 channel with an $EC_{50,}$ depending on the cellular model used. Evidence exists that TRPM4 might be able to activate at physiological $[Ca^{2+}]_{in}$ and that its Ca^{2+} sensitivity is modulated by regulators such as PKC, $PIP_{2,}$ and calmodulin [47]. The TRPM4 channel is inhibited by flufenamic acid, glibenclamide, spermine, quinine, and 9-phenantrol, the latter being considered as more specific to TRPM4 [52, 53]. However, all of these drugs also affect other ion channels as well as protein kinase A (PKA) [47, 54].

As Guinamard's group pointed out [11, 47], three properties of the TRPM4 channels explain their possible influence on cardiomyocyte action potential (AP) duration in normal and pathological conditions: (1) Its probability of being open increases with depolarization; (2) It is activated by intracellular Ca^{2+}, which increases during the AP; and (3) It has a reversal potential at 0 mV or more negative. Although precise measurements of $[Ca^{2+}]_{in}$ variations in sinoatrial node cells are still lacking, it has been considered that TRPM4 contributes to diastolic depolarization in SAN cells. Its activation by local subsarcolemmal Ca^{2+} releases could contribute to membrane depolarization and act "cooperatively" with the pacemaker current I_f, specifically at low heart rates [55–57]. However, there is still a need for studies about in vivo sinus rhythm regulation by pharmacological modulation of TRPM4. Since the TRPM4 channel carries an inward current at potentials negative to 0 mV it can influence cardiac AP duration. This has been confirmed in mice atria with intracellular microelectrode recordings using the TRMP4 inhibitor 9-phenanthrol in wild-type and TRPM4 knockout (KO) animals [58]. However, although some evidence indicates that it could contribute to lengthening the mouse ventricular AP, its participation in the mammalian ventricular AP remains elusive [47].

The biophysical properties of TRPM4 channels suggest that they can also be partially responsible for arrhythmias in several pathological states. During cardiac ischemia and reperfusion, intracellular ATP levels fall drastically, leading to intracellular Ca^{2+} accumulation that can contribute to generating early afterdepolarizations (EAD) [59] at least partially dependent on TRPM4 activation. Based on the fact that 9-phenantrol and flufenamic acid decreased the appearance of EAD in a model of hypoxia-reoxygenation, it was suggested that TRPM4 channels could be at the origin of arrhythmias in this condition [52]. Similarly, a model of ischemic preconditioning in rats seems to support this assumption [53]. Several mutations in the *Trpm4* gene have been identified in inherited cardiac diseases such as atrioventricular (AV) block, Brugada syndrome (BrS), right bundle branch block, and progressive familial heart block type I. Although, in some cases, an increase in TRPM4 current density (e.g., in AV block) or a decreased expression of TRMP4 channel protein (in BrS) have been shown, much remains to be clarified to establish the role of TRPM4 mutations in cardiac inherited diseases and arrhythmias [47]. It has been suggested that TRPM4 could prevent cardiac hypertrophy [60, 61].

TRPV channel expression has been reported in mammalian hearts, most notably TRPV1, TRPV2, and TRPV4 [10, 11]. TRPV1 is mainly expressed in cardiac sensory nerves but also in the myocardium [62–64], where it seems to protect against inflammation and cardiac remodeling during postischemic recovery in infarcted hearts [65]. On the other hand, TRPV2 is overexpressed after myocardial infarction in rats [66]. Its "protective" role was suggested by the results showing a better recovery from myocardial infarction in KO mice [67]. However, other studies suggested a different role for TRPV2 channels since they could serve as a Ca^{2+} entry pathway (and intracellular Ca^{2+} mishandling) in dystrophic cardiomyopathy [68]. Another member of the TRPV family, TRPV4, is highly expressed in the heart and activates during myocardial ischemia and reperfusion, enhancing Ca^{2+} influx and release of reactive oxygen species [69]. Recently, TRPV4 upregulation in cardiomyocytes has also been linked to aging in mice [70].

Information about the roles of other TRP members in heart is scarcer, but certain roles have been suggested [11]. In murine ventricular cardiomyocytes, the TRPA1 agonist allyl isothiocyanate (AITC) produced concentration-dependent transient rises in $[Ca^{2+}]_{in}$ that were not seen in TRPA1-deficient mice or in the presence of the channel antagonist HC-030031 [71]. It has been suggested that TRPA1 activation in cardiac myocytes could be relevant to attenuate ischemia and reperfusion injury [72]. TRPP2-deficient mice die before birth as a result of cardiac malformations [73]. It has been recently published that TRPP2 could be able to regulate autophagy through Ca^{2+} homeostasis in cardiac myocytes [74]. TRPML1–3 have been found in cardiac fibroblasts and are all constitutively active. These channels are necessary for lysosome formation and recycling [13]. However, there is still a need of studies about the roles of these channels in cardiomyocyte function. Several members of the TRPC, TRPV, and TRPM subfamilies are involved in cardiac hypertrophy and failure. Activation of these channels provides a pathway for Ca^{2+} entry into the cardiomyocyte and could contribute to sustained increases in intracellular Ca^{2+}. This leads to the activation of PKC, protein kinase B (PKB/Akt), calcineurin, and NFAT that, finally, involve TRP channel overexpression and the activation of fetal gene reprograming leading to cardiac hypertrophy [9, 10, 29]. More importantly, various TRP channels are activated by stretch, i.e., they are mechanosensitive. In addition to the normal excitation-contraction coupling, there is a feedback system in the heart whereby mechanical stimuli modulates electrical activity. This feedback system is often referred to as mechano-electric feedback [75]. Stretch-induced modulation of electrical activity includes after-depolarization, a decrease of the resting potential, and alteration of the AP duration. In severe cases, these changes are found to be arrhythmogenic as recognized 30 years ago [76]. It was recognized early that major events of mechano-electric feedback were mediated by the activation of stretch-activated channels(SACs) [77–79]. SACs are nonselective to cations and, in most cases, are sensitive to block by Gd^{3+}. Most mammalian TRPC, TRPV, TRPM, TRPA, and TRPP channels are mechanosensitive [80], although the mechanisms underlying mechanosensitivity appear quite divergent and complex. Moreover, myocytes isolated from human failing hearts exhibited enhanced stretch sensitivity with increased density of Gd^{3+}-sensitive currents and arrhythmic electrophysiological features [78, 81].

12.4 TRPC (Canonical) Channels in Cardiomyocytes

TRPC channel primary structure predicts six transmembrane domains (TM1-TM6). The TM4 lacks a voltage sensor and the channel pore is located between domains TM5 and TM6 [82]. TRPC channels have three to four ankyrin repeats at the NH_2-terminus [10, 29]. In TRPCs (and TRPMs), there is a small region that stretches from the COOH terminus to TM6, which is called TRP domain and is involved in PIP_2 regulation of channel activation and desensitization [83]. The seven members of the TRPC subfamily (TRPC1–C7) are widely expressed in heart tissues, all of them localized in the sarcolemma [10, 29]. TRPC3, C6, and C7 channels are gated by DAG or changes in PIP_2 composition after phospholipase C (PLC)-mediated G protein-coupled receptor activation [84]. The mechanism of activation of TRPC1, C4, and C5 is not well defined yet. TRPC channels can also be activated by Ca^{2+} store depletion. It is clear now that TRPC activation contributes to Ca^{2+} influx in several cell types [85]. Particularly in cardiomyocytes, Ca^{2+} influx via TRPC channels can contribute to the Ca^{2+} signaling that initiates and regulates enhanced protein synthesis and an increase infibroblast proliferation typical of cardiac hypertrophy [86]. The most well-known and characterized pathway is that of the calcineurin/nuclear factor of activated T cells (NFAT). Besides this signaling cascade, other pathways are also involved in the development of hypertrophy [35]. The general idea is that Ca^{2+} signaling for these pathways occurs in "Ca^{2+} microdomains" where Ca^{2+} concentration can be extremely high [36, 87]. This might allow the activation of Ca^{2+}-dependent signaling pathways independently from the Ca^{2+} rise that normally occurs during excitation-contraction coupling. However, this entails that the proteins involved in Ca^{2+} signaling pathways, including TRPC channels, must be spatially concentrated into a definite domain [88, 89]. Although much remains to be investigated, it seems possible that TRPC channels could be part of those Ca^{2+} microdomains. For example, Doleschal et al. [90] have shown that TRPC3 channels mediate Ca^{2+} and Na^+ entry in close proximity to the Na^+-Ca^{2+} exchanger and could contribute to an increase in intracellular Ca^{2+} influencing not only cardiac contractility but also arrhythmogenesis.

Several TRPC subtypes seem to be involved in the development of hypertrophy. TRPC1, TRPC3, TRPC4, TRPC6, and TRPC7 are upregulated in different models of hypertrophy and in heart failure patients. Moreover, overexpression of TRPC3, TRPC6-enhanced hypertrophy, and knockdown of TRPC3, TRPC4, and TRPC6 attenuated hypertrophy [91–96]. However, it is still difficult to indicate which TRPC channel is critical for hypertrophic Ca^{2+} signaling.

There is enough evidence that TRPC channels can form heteromers [19, 97]. However, there is no data about heteromeric TRPC channel complexes in cardiac tissues. Also, TRPC channels might interact with the STIM-ORAI signaling complexes that show high selectivity for Ca^{2+} and are activated by the depletion of Ca^{2+} stores after activation of Gq/11 coupled receptors. Interestingly, STIM expression seems to correlate directly with hypertrophic changes [98, 99]. Moreover, it has been suggested that STIM1 can also operate TRPC channels [100, 101]. Yet, a clear picture of how TRPC channels function in cardiomyocytes is still lacking, although a general idea emerges that TRPC channels contribute to a Ca^{2+} influx pathway that will trigger signaling in the calcineurin/NFAT axis [101, 102]. However, it is rather difficult to dissect TRPC currents in cardiomyocytes due to the presence of other important current components and the lack of specific TRP antagonists. The analysis of Ca^{2+} signals in fluorescence experiments is also hampered by similar drawbacks. Therefore, functional studies of TRP channels in cardiomyocytes are difficult to achieve. However, TRPC channels could be related to store-operated Ca^{2+} entry (SOCE). There are evidences that TRPC1, C4, and C5 channels can be activated by intracellular Ca^{2+} store depletion and participate in the SOCE mechanism [103, 104]. Moreover, Domínguez-Rodríguez et al. [99] showed evidences that upregulation of TRPC3/C4 in adult ventricular cardiomyocytes correlated with the enhanced SOCE and proarrhythmic spontaneous Ca^{2+} waves. Camacho-Londoño et al. [105] identified a background Ca^{2+} entry pathway independent of voltage-gated Ca^{2+} channels reduced in *Trpc1/Trpc4*$^{-/-}$ myocytes. This background Ca^{2+} entry was amplified by treatment with isoprenaline and angiotensin II and remained unchanged in *Trpc3/Trpc6*$^{-/-}$ myocytes suggesting that this Ca^{2+} influx pathway contributes to isoprenaline-induced and AngII-induced elevations of intracellular Ca^{2+} concentration in cardiomyocytes and cardiac hypertrophy.

12.5 Activation of TRPC Channels by Purinergic Agonists Released during Myocardial Infarction

Besides its inotropic effect, mostly mediated by an increase in L-type Ca^{2+} current [106–108], extracellular ATP can trigger cardiac automaticity, which results from the activation, following receptor stimulation, of a nonselective cationic current that would appear inward and depolarize. Such appears to be the case during the application of ATP to isolated cardiomyocytes [109–111]. In fact, ATP and UTP (uridine 5′ triphosphate) are known to be released during various pathophysiological conditions, including hypoxia during which they appeared to be associated with arrhythmia in animal models and humans [112, 113]. The diverse range of physiological actions of ATP was recognized very early by Drury and Szent-Györgyi in 1929 [114]. Moreover, the role of ATP as a "nonadrenergic, noncholinergic neurotransmitter" rather than an energy supplier was reported almost 50 years ago by Burnstock [115]. As reviewed by Burnstock and Pelleg [116], our current knowledge of purinergic receptor subtypes, based on cloning, pharmacological characterization, and second messenger systems, shows that in mammals, there are seven P_2X receptor subtypes (P_2X_1–X_7) which are constitutive cationic channels (ionotropic receptors) and eight P_2Y receptors (P_2Y_1, P_2Y_2, P_2Y_4, P_2Y_6, and P_2Y_{11}-Y_{14}) which are G protein-coupled receptors (metabotropic receptors) [117, 118]. All of them play a role in cardiovascular physiology and, more often, in several pathophysiological situations [119].

In cardiomyocytes, ATP was demonstrated to modulate most cellular activities including ionic currents, Ca^{2+} transients, pH, as well as kinases, lipases, and many secondary messengers to control contractile force [119]. Particularly, since the late 1980s and later on, several electrophysiological studies have reported that ATP activates transient nonspecific cationic currents in frog, rat, and guinea pig heart [109, 120, 121]. In a more detailed analysis, ventricular cardiomyocytes isolated from various species revealed that ATP and UTP activate two nonspecific cationic currents (Fig. 12.1). Thus, besides the fast transient nonspecific cationic current that we reported earlier [110], a sustained current ($I_{(ATP)}$) with a lower density is also activated [122]. This current has been characterized in rat, mouse, dog, and human ventricular cardiomyocytes with densities ranging between 1 pA/pF (rat and mouse) and 3 pA/pF (dog and human); the amplitude of $I_{(ATP)}$ was remarkably higher (up to 2 pA/pF) in cardiomyocytes from postmyocardial infarcted rat ventricles. While the activation of the fast transient current requires the presence of Mg^{2+}, suggesting that MgATP is the probable agonist, $I_{(ATP)}$ could be elicited by ATP and UTP, in their free forms, ATP^{-4} and UTP^{-4}. At a constant 300 μM free external Ca^{2+} concentration, the EC_{50} of the ATP^{-4} effect, determined in various ATP-containing (Mg^{2+}-free) solutions, was ≈ 58 μM, a concentration which is well in the range of that reached by released ATP during the early phase of myocardial infarction. We must recall here that lethal ventricular arrhythmias occur in this early phase [112]. Other ATP analogs (Bz-ATP, ATPγS, α,-β-methylene ATP, adenylyl imido-diphosphate, and adenosine 5′-(β,γ-imido) triphosphate) as well as uridine and adenosine diphosphate (UDP, ADP) were ineffective in activating $I_{(ATP)}$. In cells perfused with the nonhydrolyzable GTPγS, $I_{(ATP)}$ was permanently activated. The $I_{(ATP)}$ current reversed near 0 mV, exhibited a weak inward rectification, and was inhibited by increasing external Ca^{2+} concentrations (Fig. 12.2). Its chord conductance was Ca^{2+}-dependent with values around 20 pS/pF and 40 pS/pF at 2 and 0.1 mM extracellular Ca^{2+}, respectively. Furthermore, when $[Ca^{2+}]_{in}$ was increased (by FK-506 or cyclopiazonic acid), $I_{(ATP)}$ was markedly reduced. In the absence of specific inhibitors of TRP channels Alvarez et al. [122] employed a broad pharmacological approach in order to bring to light not only the involved channel (or channels) but also the signaling activation pathway. The pharmacological profile of $I_{(ATP)}$ indicated that a TRPC channel was involved since it was blocked by the general Ca^{2+}-permeable TRPC channel blockers SKF-96365, La^{3+} and Gd^{3+}. Surprisingly, flufenamic acid, known to inhibit TRPC6 (and TRMP4), enhanced current amplitude. Using fluorescence experiments, it was corroborated that channel activity was negligible both in control conditions and in Ca^{2+}-free media since there was no significant Ba^{2+} and Mn^{2+} influx, while ATP triggered marked changes in fluorescence in the presence of one or the other cation.

The nonselective cationic channel related to $I_{(ATP)}$ seems to be a heterotetramer composed of TRPC3 and TRPC7, as evidenced by co-immunoprecipitation. The channel allows cationic flux only in the presence of agonists and at the single channel level, exhibits two main conductance levels of 14 and 23 pS. The intracellular

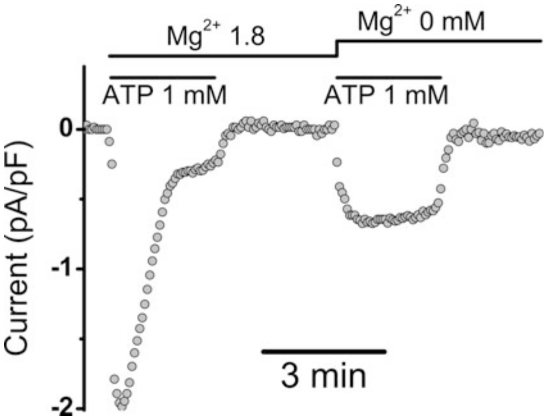

Fig. 12.1 Purinergic activation of ionic currents at resting potential. ATP (1 mM) elicits two inward currents in a rat cardiomyocyte clamped at a holding potential (HP) of −80 mV. The fast transient current requires the presence of Mg^{2+} in the external solution. Reproduced from Alvarez et al. 2008 [122] with permission

application of an anti-TRPC3 antibody, but not of an anti-TRPC6 antibody (Fig. 12.2, markedly inhibits the current [122]. Another pharmacological approach allowed to identify the signaling cascade involved in the activation of $I_{(ATP)}$. Suramin (a P_2Y_1-P_2Y_2 antagonist) markedly reduced $I_{(ATP)}$, whereas strong P_2X inhibitors such as pyridoxal phosphate-6-azo(benzene-2′,4′-disulfonic) acid, oxidized ATP, and brilliant blue did not significantly affect $I_{(ATP)}$. A possible role of P_2X activation by ATP, as a source of $I_{(ATP)}$ was then discarded since, in addition, cardiomyocytes isolated from P_2X_1-KO, P_2X_4-KO as well as from the double KO P_2X_1-P_2X_4 mice, always exhibited both of the transitory and sustained ATP-induced cationic currents recorded in control [122]. These results paved the way in the search of the signaling cascade after the activation of a P_2Y receptor. Inhibitors of phospholipase D (PLD; propranolol), phospholipase A_2(PLA_2; a rachidonyltrifluoromethyl ketone; AACOCF3), PLCγ (LY-294002) as well as the wide-spectrum tyrosine kinase inhibitor genistein had no effect on $I_{(ATP)}$. However, the PLCβ inhibitor U-73122 prevented $I_{(ATP)}$ activation. It was thus concluded that this sustained current results from the activation of the metabotropic P_2Y_2 receptor that leads to the activation of the PLCβ and DAG formation, which, in turn, activates a TRPC3/C7 cationic channel. As a consequence of this signaling cascade, IP_3 formation also triggers Ca^{2+} release from the SR via the activation of the IP_3 receptor. Besides, the local intracellular Na^+ increase due to the activation of TRPC3/C7 channels can also increase $[Ca^{2+}]_{in}$ via the Na^+-Ca^{2+} exchanger. This increase in intracellular Ca^{2+} after purine application could also contribute to the activation of various TRP channels, including TRPM4 which, due to its biophysical properties, is a candidate to contribute to depolarize the cardiomyocyte and trigger EAD or delayed afterdepolarizations (DAD). The signal transduction cascades activated by ATP/UTP and leading to TRP activation are shown in Fig. 12.3. Summarizing, after purinergic activation, the sustained inward current conducted by the TRP channels, together with the Ca^{2+} overload and the subsequent activation of the Na^+-Ca^{2+} exchanger in the reverse mode and probably activation of TRPM4 channels may trigger abnormal electrical activity and arrhythmias.

Due to the presence of interstitial creatine kinase in cardiac muscle, it could be hypothesized that as long as creatine is at a relatively high concentration, transphosphorylation (formation of creatine phosphate) may occur, serving as a buffer for the sudden release of ATP/UTP during the early phase of ischemia. As a result, arrhythmic events [113, 122–125] should decrease. Vassort and co-workers [125] tested the potential preventive effect of creatine by checking its ability to antagonize the arrhythmias that occurred upon left coronary ligature in rats, preinjected or not with creatine, and taking advantage of the fact that creatine kinase is also released together with ATP/ UTP during ischemic injury. A 2 h

Fig. 12.2 Characterization of the sustained current elicited by ATP in rat ventricular cardiomyocytes under whole-cell patch-clamp. (**a**) Current-voltage relationship for the ATP-sensitive current ($I_{(ATP)}$) established during a ramp potential after the application of 300 μM ATP in the absence of Mg^{2+}. (**b**) Concentration-response curve of $I_{(ATP)}$ amplitude elicited by various ATP concentrations at an HP = −80 mV in an Mg^{2+}-free, 300-μM Ca^{2+} solution ($n = 6$). The apparent effective half-maximum ATP concentration, EC_{50}, was 558 μM corresponding to a calculated EC_{50}-ATP^{4-} of 58 μM. (**c**) An anti-TRPC3 antibody (Ab-C3) added to the pipette solution (1:200 dilution) significantly reduced $I_{(ATP)}$ recorded within 5 min after the giga-seal formation. Antibody-induced inhibition was prevented by further adding the TRPC3-antigenic peptide (Ab-C3 + Pep, 1:200) to the pipette solution. Adding the anti-TRPC6 antibody (Ab-C6) to the pipette solution did not significantly affect the ATP-induced current. Number of cells in bars, * $P < 0.05$. Reproduced from Alvarez et al. 2008 [122] with permission

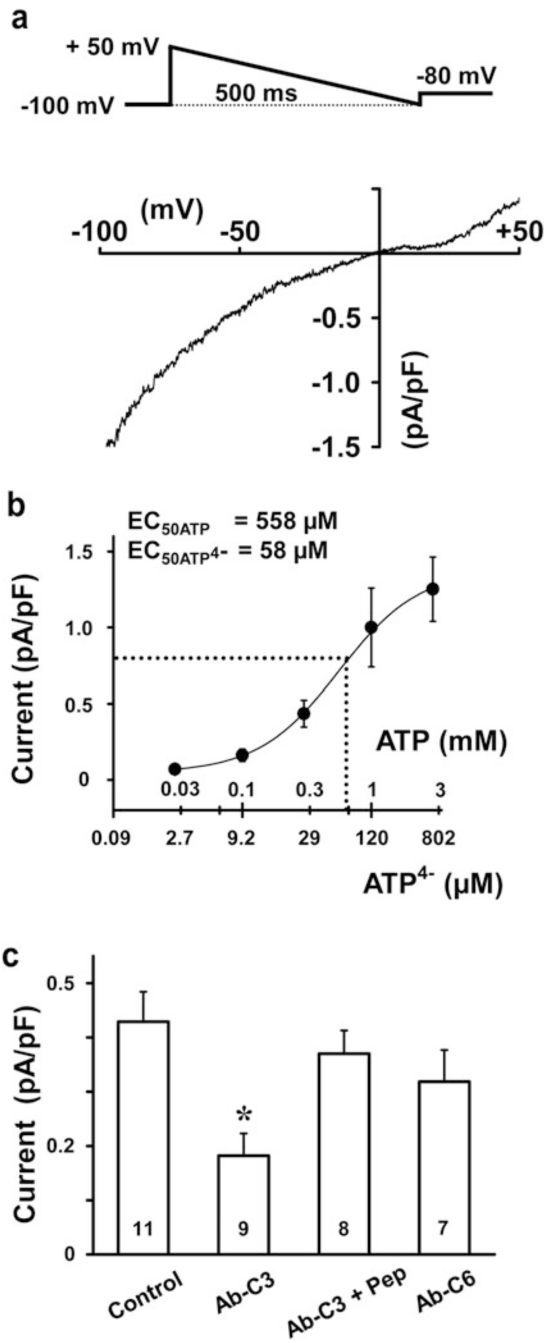

electrocardiogram monitoring revealed that in creatine-injected rats (intraperitoneal injection of creatine at 0.075 g/kg 1 h before surgery), there was a decrease in both ventricular premature beats (40% less events) and particularly in ventricular tachycardia (≈ 60% less events). The creatine effect was even more striking in early deaths. Indeed, while 10% of animals die after coronary ligation in control conditions, no death was observed during the first 2 h following the coronary ligation in creatine-injected rats (more than 30 rats per group). Injection of

Fig. 12.3 Schematic representation of the biochemical pathways involved with ATP or UTP application after their free forms bind to the P_2Y_2 purinoceptors on a cardiomyocyte, leading to activation of TRPC3/7 and TRPM4 channels. Abbreviations are given at the beginning of text

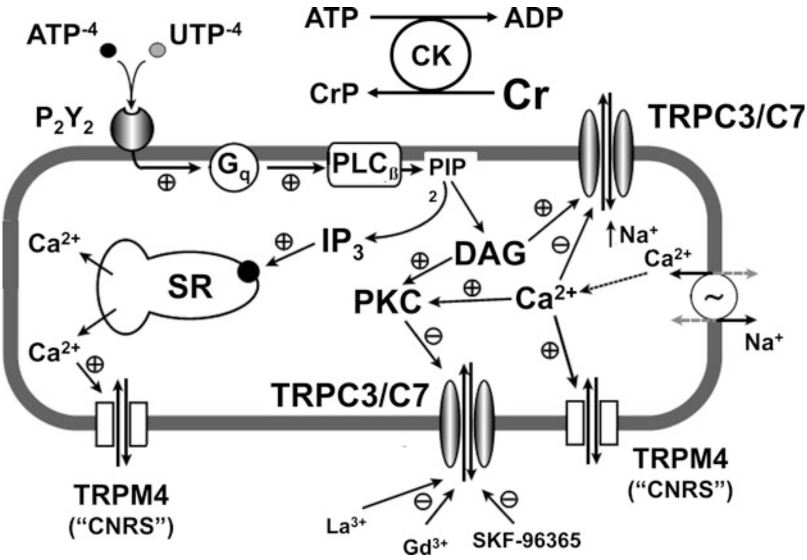

beta-guanidinopropionate, a creatine analog with 1000-fold lower kinetics [126], exerted no significant protective effect. It is to note that the so-far reported electrophysiological effects of creatine phosphate are insufficient to explain such an antiarrhythmic action [124]. Moreover, creatine (3 mM) was able to markedly decrease the ventricular fibrillation threshold in infarcted isolated rat hearts [127] (Fig. 12.4), extending and confirming the results with infarcted rats and strengthening the idea that creatine could have an antiarrhythmic action in the early stages of acute myocardial infarction.

12.6 A Note on the Arrhythmogenicity of $I_{(ATP)}$

One of the major concerns about the contribution of a particular ion channel to the normal cardiac AP or to arrhythmias is whether the experimentally recorded current densities are enough to induce the proposed electrophysiological actions and consequences related to their activity. This can be particularly problematic when referring to cardiac arrhythmias, which are multifactorial in their origin and sustainability. In the case of $I_{(ATP)}$, the experimentally recorded current densities are consistent with a conductance of ≈ 20 pS/pF near the resting potential and at the EC_{50} for $I_{(ATP)}$ activation by extracellular ATP. A current like $I_{(ATP)}$ can easily depolarize the sarcolemma of cardiomyocytes. The addition of a 20 pS/pF linear conductance to a ventricular action potential model [128] generates EADs and significant arrhythmic activity (Fig. 12.5), indicating that a current with the properties of $I_{(ATP)}$ could be able to trigger arrhythmias via the proposed mechanisms. Moreover, $I_{(ATP)}$-induced depolarization is sustained and lasts as far as ATP is acting on the purinergic receptor, a characteristic that makes this current highly arrhythmogenic. One must remember that the signaling cascade activating $I_{(ATP)}$ also releases Ca^{2+} from the SR and could finally activate TRMP4 channels magnifying cell membrane depolarization. Experimentally, at the single cell level or with small multicellular preparations (e. g,, papillary muscle), the arrhythmogenic activity of sudden application of extracellular ATP has been demonstrated [110, 119, 125]. Figure 12.5 shows an example of sustained arrhythmic Ca^{2+} cycling in a nonstimulated quiescent cardiomyocyte suddenly perfused with extracellular ATP.

Another concern could be the concentration range at which $I_{(ATP)}$ is recorded experimentally

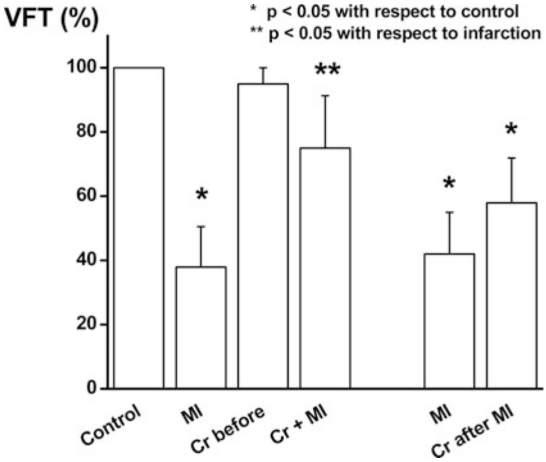

Fig. 12.4 Creatine is able to increase ventricular fibrillation threshold (VFT) during an acute myocardial infarction (AMI) in isolated Langendorff-perfused rat hearts. Ligature of left coronary artery markedly decreased the ventricular fibrillation threshold (VFT). However, when hearts were previously treated with creatine (1–3 mmol/L), VFT, after the AMI, was significantly higher than in untreated hearts. Moreover, in hearts perfused with creatine after coronary ligature, VFT was also increased but to a lesser extent. * $p < 0.05$ with respect to control; ** $p < 0.05$ with respect to infarct. Reproduced from López-Medina et al. 2013 [127] with permission

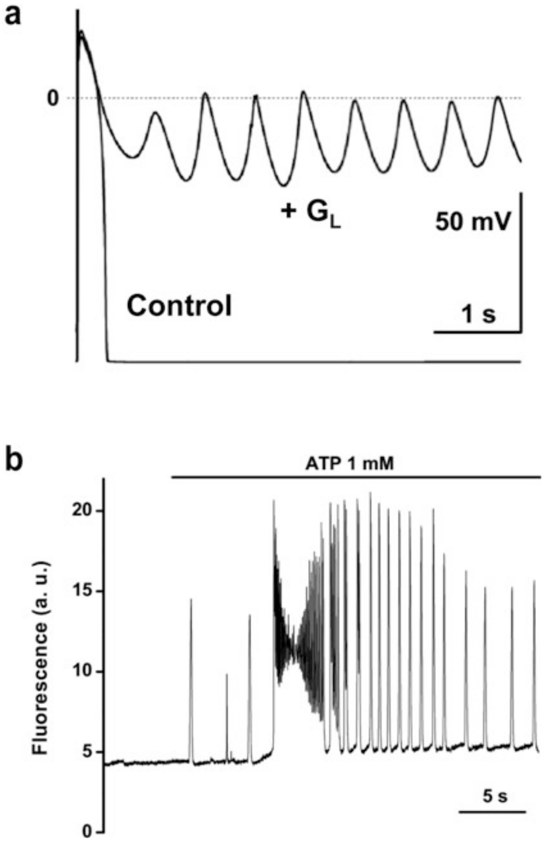

Fig. 12.5 (**a**) Repetitive activity modeled in a ventricular cardiomyocyte. The Ten Tusscher human ventricular AP model [128] was used. “Control” is the AP modeled with the default values for all parameters, and “+ G_L” is the AP after adding a 20 pS/pF time- and voltage-independent linear conductance representative of the TRPC3/7 activated by ATP. The Cellular Open Resource program was used (COR; version 0.9.31.1409, Prof Alan Garny, Oxford). (**b**) Repetitive activity, recorded as intracellular Ca^{2+} fluorescence variations in a rat ventricular cardiomyocyte during extracellular perfusion with ATP (1 mM)

and the possible correspondence with the ATP concentration released in the pathological situation. Kuzmin et al. [112] showed that interstitial ATP could increase up to 0.4 μM range, but there are reports of increases up to 100 μM [129]. However, $I_{(ATP)}$ activation is concentration-dependent, and local ATP concentrations in regions badly perfused (or not perfused at all) during myocardial infarction, could be transiently higher (but hard to determine precisely). Another factor to consider in the pathological scenario in clinics is that often, myocardial infarction occurs in patients with hypomagnesemia related to age, renal damage, or drugs [130]. Moreover, decreases in serum and blood Mg^{2+} concentrations have been reported during myocardial infarction [131, 132], a condition that could facilitate $I_{(ATP)}$, which shows an inverse Mg^{2+} dependence.

Arrhythmias are multifactorial [133], and other players could also be involved in the sustainability of ATP-triggered arrhythmias. Extracellular ATP decreases the fast Na^+ current [107], increase the L-type Ca^{2+} current [106–108, 110], and could affect conduction due to the consequent decrease in gap junction conductance by acidosis and increasing intracellular Ca^{2+} [119]. At this point, it must be remembered that even if a group of cells generate a depolarizing current such as $I_{(ATP)}$ other conditions are important in arrhythmia “propagation” and persistence. A liminal length (or liminal area) must be timely depolarized to ensure the propagation of electrical impulses [134]. In addition, electrical heterogeneity is an essential condition for rhythm disturbances [135]. This latter condition is, however, easily achieved during a myocardial infarction.

12.7 Conclusion

In the cardiovascular system, the specific physiological and pathological roles of each TRP channel are still scarcely known. This results in part due to the multiplicity of the TRP expressed in a single cell, to the fact that they can form heterotetramers with specific properties different from homotetramers, and to the lack of specific pharmacological tools. Often, and not always well recognized, the experimental protocols provoke huge TRP currents that not only compromise voltage control but also, and more importantly, could result in significant intracellular cation concentration variations and activation of other channels and transporters not directly related to the mechanism originally studied. In addition, TRP expression is highly tissue-dependent, and there are large variations in their expression pattern according to species and even strain, age, and pathological status. This emphasizes the necessity to analyze TRP expression in isolated myocytes rather than the whole heart in order to establish some correlation with their specific physiological or pathological function. Despite the present limitations, the discovery of TRP is probably a milestone of similar importance, as was the discovery of voltage-dependent channels in the 1950s, considering the diversity of their physiological and pathological functions presently reported. In the heart, by generating a background inward current at diastolic potential, the TRP channels, whether constitutively opened, or activated under specific conditions by various neuromodulators under control and pathological conditions, are relevant modulators of cardiac rhythm. We must emphasize that in addition to the depolarizing current resulting from TRP activation, the influx of cations might contribute via the electrogenic Na^+-Ca^{2+} exchanger and the Na^+-K^+-ATPase to boost inward depolarizing currents. Despite the weak amplitudes of these sustained currents, relative to the voltage-dependent currents controlling the action potential, their occurrence in a range of membrane potentials could modulate the membrane potential sufficiently to affect cardiac rhythm. Furthermore, there is still a road to go to identify other TRP channels present in cardiac and vascular cells that could also modulate intracellular Ca^{2+} and cardiac electrophysiology on top of the presently reported involvement of TRPCs and TRPM4. Finally, to what extent other agonists such as angiotensin II, norepinephrine, and endothelin that activate the DAG pathway and, thus, TRPC, could favor or induce arrhythmic activities deserves further investigation.

Acknowledgments The idea to investigate the effects of extracellular ATP on cardiomyocytes comes entirely from Professor Guy Vassort (retired). Thirty-five years ago, one of us (JLA) began to work on this passionate subject that evolved, late in the 1990s, to the study of the arrhythmogenic effect of ATP released during early myocardial infarction. By then, Professor Vassort was convinced that TRP channels could be involved in arrhythmogenesis and guided, step by step, all of our research on this subject. The authors wish to express their gratitude to Professor Vassort for his excellent human quality, friendship, and continuous support all along this time.

References

1. Cosens DJ, Manning A. Abnormal electroretinogram from a drosophila mutant. Nature. 1969;224:285–7.
2. Montell C, Rubin GM. Molecular characterization of the drosophila trp locus: a putative integral membrane protein required for phototransduction. Neuron. 1989;2:1313–23.
3. Nilius B, Flockerzi V. Mammalian transient receptor potential (TRP) cation channels, vol. 222. Berlin Heidelberg: Springer; 2014.
4. Rosenbaum Emir TL. Frontiers in neuroscience. Neurobiology of TRP channels. CRC Press; 2017. https://doi.org/10.4324/9781315152837.
5. Firth AL, Remillard CV, Yuan JX-J. TRP channels in hypertension. Biochim Biophys Acta. 2007;1772:895–906.
6. Guinamard R, Bois P. Involvement of transient receptor potential proteins in cardiac hypertrophy. Biochim Biophys Acta. 2007;1772:885–94.
7. Nilius B. TRP channels in disease. Biochim Biophys Acta. 2007;1772:805–12.
8. Smani T, Shapovalov G, Skryma R, Prevarskaya N, Rosado JA. Functional and physiopathological implications of TRP channels. Biochim Biophys Acta. 2015;1853:1772–82.
9. Falcón D, Galeano-Otero I, Calderón-Sánchez E, Del Toro R, Martín-Bórnez M, Rosado JA, et al. TRP channels: current perspectives in the adverse cardiac remodeling. Front Physiol. 2019;10:159.
10. Yue Z, Xie J, Yu AS, Stock J, Du J, Yue L. Role of TRP channels in the cardiovascular system. Am J Physiol Heart Circ Physiol. 2015;308:H157–82.
11. Hof T, Chaigne S, Récalde A, Sallé L, Brette F, Guinamard R. Transient receptor potential channels in cardiac health and disease. Nature Rev Cardiol. 2019;16(6):344–60. https://doi.org/10.1038/s41569-018-0145-2.
12. Pedersen SF, Owsianik G, Nilius B. TRP channels: an overview. Cell Calcium. 2005;38:233–52.
13. Venkatachalam K, Montell C. TRP channels. Annu Rev Biochem. 2007;76:387–417.
14. Montell C, Birnbaumer L, Flockerzi V, Bindels RJ, Bruford EA, Caterina MJ, et al. A unified nomenclature for the superfamily of TRP cation channels. Mol Cell. 2002;9:229–31.
15. Nilius B, Droogmans G. Ion channels and their functional role in vascular endothelium. Physiol Rev. 2001;81:1415–59.
16. Owsianik G, D'hoedt D, Voets T, Nilius B. Structure-function relationship of the TRP channel superfamily. Rev Physiol Biochem Pharmacol. 2006;156:61–90.
17. Peng G, Shi X, Kadowaki T. Evolution of TRP channels inferred by their classification in diverse animal species. Mol Phylogenet Evol. 2015;84:145–57.
18. Clapham DE. TRP channels as cellular sensors. Nature. 2003;426:517–24.
19. Ramsey IS, Delling M, Clapham DE. An introduction to TRP channels. Annu Rev Physiol. 2006;68:619–47.
20. Jardín I, López JJ, Diez R, Sánchez-Collado J, Cantonero C, Albarrán L, et al. TRPs in pain sensation Front Physiol. 2017;8:392.
21. Palazzo E, Rossi F, de Novellis V, Maione S. Endogenous modulators of TRP channels. Curr Top Med Chem. 2013;13:398–407.
22. Ong HL, Ambudkar IS. STIM-TRP pathways and microdomain organization: contribution of TRPC1 in store-operated Ca2+ entry: impact on Ca2+ signaling and cell function. Adv Exp Med Biol. 2017;993:159–88.
23. Vetter I, Lewis RJ. Natural product ligands of TRP channels. Adv Exp Med Biol. 2011;704:41–85.
24. Holzer P, Izzo AA. The pharmacology of TRP channels. Br J Pharmacol. 2014;171:2469–73.
25. Suzuki Y, Kodama D, Goto S, Togari A. Involvement of TRP channels in the signal transduction of bradykinin in human osteoblasts. Biochem Biophys Res Commun. 2011;410:317–21.
26. Albarrán L, López JJ, Dionisio N, Smani T, Salido GM, Rosado JA. Transient receptor potential ankyrin-1 (TRPA1) modulates store-operated ca(2+) entry by regulation of STIM1-Orai1 association. Biochim Biophys Acta. 2013;1833:3025–34.
27. Gerhold KA, Schwartz MA. Ion channels in endothelial responses to fluid shear stress. Physiology (Bethesda). 2016;31:359–69.
28. Sawamura S, Shirakawa H, Nakagawa T, Mori Y, Kaneko S. TRP channels in the brain: what are they there for? In: Sawamura S, Shirakawa H, Nakagawa T, Mori Y, Kaneko S, Rosenbaum Emir TL, editors. Neurobiology of TRP channels. Boca Raton (FL): CRC Press/Taylor & Francis; 2017. p. 16. http://www.ncbi.nlm.nih.gov/pubmed/29356477>.
29. Freichel M, Berlin M, Schürger A, Mathar I, Bacmeister L, Medert R, et al. TRP channels in the

heart. In: Sawamura S, Shirakawa H, Nakagawa T, Mori Y, Kaneko S, Rosenbaum Emir TL, editors. Neurobiology of TRP channels. Boca Raton (FL): CRC Press/Taylor & Francis; 2017. p. 9. http://www.ncbi.nlm.nih.gov/pubmed/29356479>.

30. Bers DM. Cardiac excitation-contraction coupling. Nature. 2002;415:198–205.
31. Frey N, McKinsey TA, Olson EN. Decoding calcium signals involved in cardiac growth and function. Nat Med. 2000;6:1221–7.
32. Frey N, Katus HA, Olson EN, Hill JA. Hypertrophy of the heart: a new therapeutic target? Circulation. 2004;109:1580–9.
33. Roderick H, Higazi D, Smyrnias I, Fearnley C, Harzheim D, Bootman M. Calcium in the heart: when it's good, it's very very good, but when it's bad, it's horrid. Biochem Soc Trans. 2007;35:957–61.
34. Bers DM. Calcium cycling and signaling in cardiac myocytes. Annu Rev Physiol. 2008;70:23–49.
35. Heineke J, Molkentin JD. Regulation of cardiac hypertrophy by intracellular signalling pathways. Nat Rev Mol Cell Biol. 2006;7:589–600.
36. Goonasekera SA, Molkentin JD. Unraveling the secrets of a double life: contractile versus signaling Ca2+ in a cardiac myocyte. J Mol Cell Cardiol. 2012;52:317–22.
37. Makarewich CA, Zhang H, Davis J, Correll RN, Trappanese DM, Hoffman NE, et al. Transient receptor potential channels contribute to pathological structural and functional remodeling after myocardial infarction. Circ Res. 2014;115:567–80.
38. Balijepalli C, Foell JD, Hall DD, Hell JW, Kamp TJ. Localization of cardiac L-type ca(2+) channels to a caveolar macromolecular signaling complex is required for beta(2)-adrenergic regulation. Proc Natl Acad Sci U S A. 2006;103:7500–5.
39. Wu X, Eder P, Chang B, Molkentin JD. TRPC channels are necessary mediators of pathologic cardiac hypertrophy. Proc Natl Acad Sci U S A. 2010;107:7000–5.
40. Freichel M, Tsvilovskyy V, Camacho-Londoño JE. TRPC4- and TRPC4-containing channels. Handb Exp Pharmacol. 2014;222:85–128.
41. Morine KJ, Paruchuri V, Qiao X, Pham DT, Huggins GS, Denofrio D, et al. Endoglin selectively modulates transient receptor potential channel expression in left and right heart failure. Cardiovasc Pathol. 2016;25:478–82.
42. Miller BA, Hoffman NE, Merali S, Zhang XQ, Wang JF, Rajan S, et al. TRPM2 channels protect against cardiac ischemia-reperfusion injury: role of mitochondria. J Biol Chem. 2014;289:7615–29.
43. Hu Y, Duan Y, Takeuchi A, Hai-Kurahara L, Ichikawa J, Hiraishi K, et al. Uncovering the arrhythmogenic potential of TRPM4 activation in atrial-derived HL-1 cells using novel recording and numerical approaches. Cardiovasc Res. 2017;113:1243–55.
44. Gwanyanya A, Amuzescu B, Zakharov SI, Macianskiene R, Sipido KR, Bolotina VM, et al. Magnesium-inhibited, TRPM6/7-like channel in cardiac myocytes: permeation of divalent cations and pH-mediated regulation. J Physiol. 2004;559761–76:761.
45. Gwanyanya A, Sipido KR, Vereecke J, Mubagwa K. ATP and PIP2 dependence of the magnesium-inhibited, TRPM7-like cation channel in cardiac myocytes. Am J Physiol Cell Physiol. 2006;291:C627–35.
46. Macianskiene R, Martisiene I, Zablockaite D, Gendviliene V. Characterization of Mg^{2+}-regulated TRPM7-like current in human atrial myocytes. J Biomed Sci. 2012;19:75.
47. Guinamard R, Bouvagnet P, Hof T, Liu H, Simard C, Sallé L. TRPM4 in cardiac electrical activity. Cardiovasc Res. 2015;108:21–30.
48. Colquhoun D, Neher E, Reuter H, Stevens CF. Inward current channels activated by intracellular Ca in cultured cardiac cells. Nature. 1981;294:752–4.
49. Ehara T, Noma A, Ono K. Calcium-activated non-selective cation channel in ventricular cells isolated from adult Guinea-pig hearts. J Physiol. 1988;403:117–33.
50. Guinamard R, Demion M, Chatelier A, Bois P. Calcium-activated nonselective cation channels in mammalian cardiomyocytes. Trends Cardiovasc Med. 2006;16:245–50.
51. Launay P, Fleig A, Perraud A-L, Scharenberg AM, Penner R, Kinet J-P. TRPM4 is a Ca2+−activated nonselective cation channel mediating cell membrane depolarization. Cell. 2002;109:397–407.
52. Simard C, Sallé L, Rouet R, Guinamard R. Transient receptor potential melastatin 4 inhibitor 9-phenanthrol abolishes arrhythmias induced by hypoxia and re-oxygenation in mouse ventricle. Br J Pharmacol. 2012;165:2354–64.
53. Wang J, Takahashi K, Piao H, Qu P, Naruse K. 9-Phenanthrol, a TRPM4 inhibitor, protects isolated rat hearts from ischemia-reperfusion injury. PLoS One. 2013;8:e70587.
54. Garland CJ, Smirnov SV, Bagher P, Lim CS, Huang CY, Mitchell R, et al. TRPM4 inhibitor 9-phenanthrol activates endothelial cell intermediate conductance calcium-activated potassium channels in rat isolated mesenteric artery. Br J Pharmacol. 2015;172:1114–23.
55. Demion M, Bois P, Launay P, Guinamard R. TRPM4, a Ca2+−activated nonselective cation channel in mouse sino-atrial node cells. Cardiovasc Res. 2007;73:531–8.
56. Bogdanov KY, Maltsev VA, Vinogradova TM, Lyashkov AE, Spurgeon HA, Stern MD, Lakatta EG. Membrane potential fluctuations resulting from submembrane Ca2+ releases in rabbit sinoatrial nodal cells impart an exponential phase to the late diastolic depolarization that controls their chronotropic state. Circ Res. 2006;99:979–87.

57. Hof T, Simard C, Rouet R, Sallé L, Guinamard R. Implication of the TRPM4 nonselective cation channel in mammalian sinus rhythm. Heart Rhythm. 2013;10:1683–9.
58. Simard C, Hof T, Keddache Z, Launay P, Guinamard R. The TRPM4 non-selective cation channel contributes to the mammalian atrial action potential. J Mol Cell Cardiol. 2013;59:11–9.
59. Priori SG, Mantica M, Napolitano C, Schwartz PJ. Early afterdepolarizations induced in vivo by reperfusion of ischemic myocardium. A possible mechanism for reperfusion arrhythmias. Circulation. 1990;81:1911–20.
60. Demion M, Thireau J, Gueffier M, Finan A, Khoueiry Z, Cassan C, et al. Trpm4 gene invalidation leads to cardiac hypertrophy and electrophysiological alterations. PLoS One. 2014;9:e115256.
61. Gueffier M, Zintz J, Lambert K, Finan A, Aimond F, Chakouri N, et al. The TRPM4 channel is functionally important for the beneficial cardiac remodeling induced by endurance training. J Muscle Res Cell Motil. 2017;38:3–16.
62. Zahner MR, Li D-P, Chen S-R, Pan H-L. Cardiac vanilloid receptor 1-expressing afferent nerves and their role in the cardiogenic sympathetic reflex in rats. J Physiol. 2003;551:515–23.
63. Gao Y, Song J, Chen H, Cao C, Lee C. TRPV1 activation is involved in the cardioprotection of remote limb ischemic postconditioning in ischemia-reperfusion injury rats. Biochem Biophys Res Commun. 2015;463:1034–9.
64. Randhawa PK, Jaggi AS. TRPV1 channels in cardiovascular system: a double edged sword? Int J Cardiol. 2017;228:103–13.
65. Wang L, Wang DH. TRPV1 gene knockout impairs postischemic recovery in isolated perfused heart in mice. Circulation. 2005;112:3617–23.
66. Entin-Meer M, Levy R, Goryainov P, Landa N, Barshack I, Avivi C, et al. The transient receptor potential vanilloid 2 cation channel is abundant in macrophages accumulating at the peri-infarct zone and may enhance their migration capacity towards injured cardiomyocytes following myocardial infarction. PLoS One. 2014;9:e105055.
67. Entin-Meer M, Cohen L, Hertzberg-Bigelman E, Levy R, Ben-Shoshan J, Keren G. TRPV2 knockout mice demonstrate an improved cardiac performance following myocardial infarction due to attenuated activity of peri-infarct macrophages. PLoS One. 2017;12:e0177132.
68. Lorin C, Vögeli I, Niggli E. Dystrophic cardiomyopathy: role of TRPV2 channels in stretch-induced cell damage. Cardiovasc Res. 2015;106:153–62.
69. Wu QF, Qian C, Zhao N, Dong Q, Li J, Wang BB, et al. Activation of transient receptor potential vanilloid 4 involves in hypoxia/reoxygenation injury in cardiomyocytes. Cell Death Dis. 2017;8:e2828.
70. Jones JL, Peana D, Veteto AB, Lambert MD, Nourian Z, Karasseva NG, et al. TRPV4 increases cardiomyocyte calcium cycling and contractility yet contributes to damage in the aged heart following hypoosmotic stress. Cardiovasc Res. 2019;115:46–56.
71. Andrei SR, Sinharoy P, Bratz IN, Damron DS. TRPA1 is functionally co-expressed with TRPV1 in cardiac muscle: co-localization at z-discs, costameres and intercalated discs. Channels (Austin). 2016;10:395–409.
72. Lu Y, Piplani H, McAllister SL, Hurt CM, Gross ER. Transient receptor potential Ankyrin 1 activation within the cardiac myocyte limits ischemia-reperfusion injury in rodents. Anesthesiology. 2016;125:1171–80.
73. Pennekamp P, Karcher C, Fischer A, Schweickert A, Skryabin B, Horst J, et al. The ion channel polycystin-2 is required for left-right axis determination in mice. Curr Biol. 2002;12:938–43.
74. Criollo A, Altamirano F, Pedrozo Z, Schiattarella GG, Li DL, Rivera-Mejías P, et al. Polycystin-2-dependent control of cardiomyocyte autophagy. J Mol Cell Cardiol. 2018;118:110–21.
75. Quinn TA, Bayliss RA, Kohl P. In heart rate and rhythm. Berlin, Heidelberg: Springer; 2011. p. 133–51. https://doi.org/10.1007/978-3-642-17575-6_7.
76. Dean JW, Lab MJ. Arrhythmia in heart failure: role of mechanically induced changes in electrophysiology. Lancet (London, England). 1989;1:1309–12.
77. Franz MR, Bode F. Mechano-electrical feedback underlying arrhythmias: the atrial fibrillation case. Prog Biophys Mol Biol. 2003;82:163–74.
78. Kamkin A, Kiseleva I, Isenberg G. Stretch-activated currents in ventricular myocytes: amplitude and arrhythmogenic effects increase with hypertrophy. Cardiovasc Res. 2000;48:409–20.
79. Zhang YH, Youm JB, Sung HK, Lee SH, Ryu SY, Lee SH, et al. Stretch-activated and background non-selective cation channels in rat atrial myocytes. J Physiol. 2000;523(Pt 3):607–19.
80. Liu C, Montell C. Forcing open TRP channels: mechanical gating as a unifying activation mechanism. Biochem Biophys Res Commun. 2015;460: 22–5.
81. Dyachenko V, Husse B, Rueckschloss U, Isenberg G. Mechanical deformation of ventricular myocytes modulates both TRPC6 and Kir2.3 channels. Cell Calcium. 2009;45:38–54.
82. Catterall WA. From ionic currents to molecular mechanisms: the structure and function of voltage-gated sodium channels. Neuron. 2000;2000(26): 13–25.
83. Nilius B, Owsianik G, Voets T. Transient receptor potential channels meet phosphoinositides. EMBO J. 2008;27:2809–16.
84. Yamaguchi Y, Iribe G, Kaneko T, Takahashi K, Numaga-Tomita T, Nishida M, et al. TRPC3 participates in angiotensin II type 1 receptor-dependent stress-induced slow increase in

intracellular Ca2+ concentration in mouse cardiomyocytes. J Physiol Sci. 2018;68:153–64.
85. Gees M, Owsianik G, Nilius B, Voets T. TRP channels Compr Physiol. 2012;2:563–608.
86. Frey N, Olson EN. Cardiac hypertrophy: the good, the bad, and the ugly. Annu Rev Physiol. 2003;65: 45–79.
87. Gomez AM, Mesquita TR, Mercadier J-J, Alvarez J, Benitah J-P. In: Nikolaev V, Zaccolo M, editors. Microdomains in the cardiovascular system. Cham: Springer International Publishing; 2017. p. 361–86. https://doi.org/10.1007/978-3-319-54579-0.
88. Parra V, Rothermel BA. Calcineurin signaling in the heart: the importance of time and place. J Mol Cell Cardiol. 2017;103:121–36.
89. Higazi DR, Fearnley CJ, Drawnel FM, Talasila A, Corps EM, Ritter O, et al. Endothelin-1-stimulated InsP3-induced Ca2+ release is a nexus for hypertrophic signaling in cardiac myocytes. Mol Cell. 2009;33:472–82.
90. Doleschal B, Primessnig U, Wölkart G, Wolf S, Schernthaner M, Lichtenegger M, et al. TRPC3 contributes to regulation of cardiac contractility and arrhythmogenesis by dynamic interaction with NCX1. Cardiovasc Res. 2015;106:163–73.
91. Takahashi Y, Watanabe H, Murakami M, Ohba T, Radovanovic M, Ono K, et al. Involvement of transient receptor potential canonical 1 (TRPC1) in angiotensin II-induced vascular smooth muscle cell hypertrophy. Atherosclerosis. 2007;195:287–96.
92. Brenner JS, Dolmetsch RE. TrpC3 regulates hypertrophy-associated gene expression without affecting myocyte beating or cell size. PLoS One. 2007;2:e802.
93. Satoh S, Tanaka H, Ueda Y, Oyama J-I, Sugano M, Sumimoto H, et al. Transient receptor potential (TRP) protein 7 acts as a G protein-activated Ca2+ channel mediating angiotensin II-induced myocardial apoptosis. Mol Cell Biochem. 2007;294:205–15.
94. Bush EW, Hood DB, Papst PJ, Chapo JA, Minobe W, Bristow MR, et al. Canonical transient receptor potential channels promote cardiomyocyte hypertrophy through activation of calcineurin signaling. J Biol Chem. 2006;281:33487–96.
95. Kuwahara K, Wang Y, McAnally J, Richardson JA, Bassel-Duby R, Hill JA, Olson EN. TRPC6 fulfills a calcineurin signaling circuit during pathologic cardiac remodeling. J Clin Invest. 2006;116:3114–26.
96. Falcón D, Galeano-Otero I, Martín-Bórnez M, Fernández-Velasco M, Gallardo-Castillo I, Rosado JA, et al. Cell. 2020;9:173. https://doi.org/10.3390/cells9010173.
97. Schaefer M. Homo- and heteromeric assembly of TRP channel subunits. Pflugers Arch. 2005;451:35–42.
98. Hulot J-S, Fauconnier J, Ramanujam D, Chaanine A, Aubart F, Sassi Y, et al. Critical role for stromal interaction molecule 1 in cardiac hypertrophy. Circulation. 2011;124:796–805.
99. Domínguez-Rodríguez A, Ruíz-Hurtado G, Sabourin J, Gómez AM, Alvarez JL, Benitah JP. Proarrhythmic effect of sustained EPAC activation on TRPC3/4 in rat ventricular cardiomyocytes. J Mol Cell Cardiol. 2015;87:74–8.
100. Yuan JP, Zeng W, Huang GN, Worley PF, Muallem S. STIM1 heteromultimerizes TRPC channels to determine their function as store-operated channels. Nat Cell Biol. 2007;9:636–45.
101. Lee KP, Yuan JP, So I, Worley PF, Muallem S. STIM1-dependent and STIM1-independent function of transient receptor potential canonical (TRPC) channels tunes their store-operated mode. J Biol Chem. 2010;285:38666–73.
102. Seth M, Zhang Z-S, Mao L, Graham V, Burch J, Stiber J, et al. TRPC1 channels are critical for hypertrophic signaling in the heart. Circ Res. 2009;105: 1023–30.
103. Ong HL, de Souza LB, Ambudkar IS. Role of TRPC Channels in Store-Operated Calcium Entry Adv Exp Med Biol. 2016;898:87–109.
104. Sabourin J, Bartoli F, Antigny F, Gomez AM, Benitah J-P. Transient receptor potential canonical (TRPC)/Orai1-dependent store-operated Ca2+ channels: new targets of aldosterone in cardiomyocytes. J Biol Chem. 2016;291:13394–409.
105. Camacho-Londoño JE, Tian Q, Hammer K, Schröder L, Camacho-Londoño J, Reil JC, et al. A background Ca2+ entry pathway mediated by TRPC1/TRPC4 is critical for development of pathological cardiac remodelling. Eur Heart J. 2015;36: 2257–66.
106. Alvarez JL, Mongo K, Scamps F, Vassort G. Effects of purinergic stimulation on the ca current in single frog cardiac cells. Pflugers Arch. 1990;416:189–95.
107. Scamps F, Vassort G. Effect of extracellular ATP on the Na+ current in rat ventricular myocytes. Circ Res. 1994;74:710–7.
108. Scamps F, Vassort G. Pharmacological profile of the ATP-mediated increase in L-type calcium current amplitude and activation of a non-specific cationic current in rat ventricular cells. Br J Pharmacol. 1994;113:982–6.
109. Friel DD, Bean BP. Two ATP-activated conductances in bullfrog atrial cells. J Gen Physiol. 1988;91:1–27.
110. Scamps F, Vassort G. Mechanism of extracellular ATP-induced depolarization in rat isolated ventricular cardiomyocytes. Pflugers Arch. 1990;417:309–16.
111. Shoda M, Hagiwara N, Kasanuki H, Hosoda S. ATP-activated cationic current in rabbit sino-atrial node cells. J Mol Cell Cardiol. 1997;29:689–95.
112. Kuzmin AI, Lakomkin VL, Kapelko VI, Vassort G. Interstitial ATP level and degradation in control and postmyocardial infarcted rats. Am J Phys. 1998;275:C766–71.
113. Wihlborg A-K, Balogh J, Wang L, Borna C, Dou Y, Joshi BV, et al. Positive inotropic effects by uridine

triphosphate (UTP) and uridine diphosphate (UDP) via P2Y2 and P2Y6 receptors on cardiomyocytes and release of UTP in man during myocardial infarction. Circ Res. 2006;98:970–6.

114. Drury AN, Szent-Gyorgyi A. The physiological activity of adenine compounds with especial reference to their action upon the mammalian heart. J Physiol (L). 1929;68:213–37.
115. Burnstock G, Campbell G, Satchell D, Smythe A. Evidence that adenosine triphosphate or a related nucleotide is the transmitter substance released by non-adrenergic inhibitory nerves in the gut. Br J Pharmacol. 1970;40:668–88.
116. Burnstock G, Pelleg A. Cardiac purinergic signalling in health and disease. Purinergic Signal. 2015;11:1–46.
117. Abbracchio MP, Burnstock G. Purinoceptors: are there families of P2X and P2Y purinoceptors? Pharmacol Ther. 1994;64:445–75.
118. Burnstock G. Physiology and pathophysiology of purinergic neurotransmission. PhysiolRev. 2007;87: 659–797.
119. Vassort G. Adenosine 5′-triphosphate: a P2-purinergic agonist in the myocardium. Physiol Rev. 2001;81:767–806.
120. Matsuura H, Ehara T. Activation of chloride current by purinergic stimulation in Guinea pig heart cells. Circ Res. 1992;70:851–5.
121. Song Y, Belardinelli L. ATP promotes development of afterdepolarizations and triggered activity in cardiac myocytes. Am J Physiol. 1994;267:H2005-11.
122. Alvarez JL, Coulombe A, Cazorla O, Ugur M, Rauzier J-M, Magyar J, et al. ATP/UTP activate cation-permeable channels with TRPC3/7 properties in rat cardiomyocytes. Am J Physiol Heart Circ Physiol. 2008;295:H21–8.
123. Erlinge D, Harnek J, van Heusden C, Olivecrona G, Jern S, Lazarowski E. Uridine triphosphate (UTP) is released during cardiac ischemia. Int J Cardiol. 2005;100:427–33.
124. Hearse DJ, Tanaka K, Crome R, Manning AS. Creatine phosphate and protection against reperfusion-induced arrhythmias in the rat heart. Eur J Pharmacol. 1986;131:21–30.
125. Vassort G, Bideaux P, Alvarez J. Could early ischemic arrhythmia triggered by purinergic activation of the transient receptor potential channels be prevented by creatine? Exp Clin Cardiol. 2010;15:e104–8.
126. Chevli R, Fitch CD. Beta-Guanidinopropionate and phosphorylated beta-guanidinopropionate as substrates for creatine kinase. Biochem Med. 1979;21:162–7.
127. Lopez-Medina AI, Alvarez-Collazo J, Vassort G, Alvarez JL. Antiarrhythmic action of creatine in acute myocardial infarction. Rev Cuba Cardiol Cir Cardiovasc. 2013;19:13–6.
128. ten Tusscher KHWJ, Noble D, Noble PJ, Panfilov AV. A model for human ventricular tissue. AmJ Physiol Heart Circ Physiol. 2004;286:H1573–89.
129. Coade SB, Pearson JD. Metabolism of adenine nucleotides in human blood. Circ Res. 1989;65: 531–7.
130. Shechter M. Magnesium and cardiovascular system. Magnes Res. 2010;23:60–72.
131. Rasmussen HS, Aurup P, Hojberg S, Jensen EK, McNair P. Magnesium and acute myocardial infarction. Transient hypomagnesemia not induced by renal magnesium loss in patients with acute myocardial infarction. Arch Intern Med. 1986;146:872–4.
132. Heesch CM, Eichhorn EJ. Magnesium in acute myocardial infarction. Ann Emerg Med. 1994;24: 1154–60.
133. Qu Z, Weiss JN. Mechanisms of ventricular arrhythmias: from molecular fluctuations to electrical turbulence. Annu Rev Physiol. 2015;77:29–55.
134. Noble D. The relation of Rushton's 'liminal length' for excitation to the resting and active conductances of excitable cells. J Physiol. 1972;226:573–91.
135. Cranefield PF. The conduction of the cardiac impulse: the slow response and cardiac arrhythmias. Mount Kisco, NY: Futura Publishing Co.; 1975. at http://www.ncbi.nlm.nih.gov/pubmed/29356477

Role of NCX1 and NHE1 in Ventricular Arrhythmia

13

András Tóth and András Varró

Abstract

Lethal ventricular arrhythmias are one of the primary causes of high mortality among patients with a variety of cardiac diseases, like acute ischemia-reperfusion injury, chronic ischemic heart disease (IHD), all major forms of heart failure (HF), and congenital cardiomyopathies. Perturbations in intracellular Ca^{2+} and Na^{+} homeostasis leading to massive intracellular Ca^{2+} overload are frequently found in the background of cardiac arrhythmogenesis. Recent data explicitly demonstrate that these perturbations are tightly connected to enhanced function and overexpression of two cardiac sarcolemmal ion transporters, the Na^{+}/Ca^{2+} exchanger (NCX1), a major regulator of the intracellular Ca^{2+} concentration ($[Ca^{2+}]_i$), and the Na^{+}/H^{+} exchanger (NHE1), the primary regulator of intracellular pH. Recent efforts to delineate the real therapeutic value of NCX1 modulation were still hampered by the absence of specific and effective inhibitors and the total absence of specific activators. On the other side, several well-established inhibitors of the NHE1 are already in clinical practice or under evaluation but human data—promising in limiting the size of the ischemic injury—are much less convincing in preventing lethal ventricular arrhythmias. In this chapter, we aim to discuss the involvement of these two ion transporters in the regulation of the $[Ca^{2+}]_i$ homeostasis in the healthy and diseased heart, to underline their principal contribution to the generation of ventricular arrhythmia, and to summarize experimental results obtained in studies in the direction of their antiarrhythmic and cardioprotective modulation.

13.1 Introduction: The Origin and Diversity of Cardiac Arrhythmias

Sudden cardiac death (SCD) is presumed to be related to abnormal generation and propagation of electrical impulses causing lethal cardiac arrhythmias. It may occur in various pathophysiological situations like IHD, major forms of heart failure, atrial fibrillation (AF), and congenital ion channel abnormalities.

The cellular mechanism of cardiac arrhythmias includes (1) enhanced automaticity, (2) reentry, (3) triggered activity, and (4) the combinations of

---

A. Tóth
Department of Pharmacology and Pharmacotherapy,
University of Szeged, Szeged, Hungary

A. Varró (✉)
Department of Pharmacology and Pharmacotherapy,
University of Szeged, Szeged, Hungary

Division of Cardiovascular Pharmacology, Hungarian
Academy of Sciences, Szeged, Hungary
e-mail: a.varro@phcol.szote.u-szeged.hu

© Springer Nature Switzerland AG 2023

O. N. Tripathi et al. (eds.), *Heart Rate and Rhythm*, https://doi.org/10.1007/978-3-031-33588-4_13

these factors. Enhanced normal automaticity can be due to changes in electrophysiological properties of either the SA or the AV nodal cells or the Purkinje fibers under certain conditions, such as largely increased sympathetic tone, ischemia/reperfusion, cardiac hypertrophy, and atrial or ventricular remodeling. Reentry is due to abnormal impulse conduction or changes in refractoriness and often the combination of both. Triggered arrhythmias have been shown to have a rather complex background involving several ion channels, pumps, and exchangers and are manifested as early afterdepolarizations (EAD) and delayed afterdepolarizations (DAD). In this chapter, we focus on the relationship between triggered cardiac activity and upregulation of sarcolemmal ion exchangers, NCX1 and NHE1, clarifying its basic mechanisms at the cellular level.

13.2 NCX1, a Major Regulator of Intracellular Ca^{2+} Balance in Cardiac Cells

The cardiac NCX1 plays a pivotal role in maintaining both the beat-to-beat and the long-term Ca^{2+} balance in cardiomyocytes. The energy used for exchange is normally provided by the sarcolemmal Na^{+}/K^{+}-ATPase (NKA). The molecular properties and physiological functions of NCX have been well explored [1–6]. The primary physiological role of the NCX1 is regulating Ca^{2+} content by beat-to-beat removal of the trigger Ca^{2+} entering the cell during the action potential (AP) via L-type Ca^{2+} channels (LTCC) and the NCX1 itself. However, by doing this—especially when the intracellular Ca^{2+} ([Ca^{2+}]$_i$) homeostasis is severely disturbed—it may result in an arrhythmogenic inward current (I$_{ti}$), primarily responsible for triggered arrhythmias and non-reentrant ventricular tachyarrhythmia [7–12]. Furthermore, since the direction of the Ca^{2+} transport by the NCX1 is fully reversible, beyond its primary (*forward mode)* action of extruding Ca^{2+} from the cells, under certain conditions, Ca^{2+} influx into the cells from the extracellular space by the exchanger (*reverse mode* transport) may substantially contribute to cytoplasmic Ca^{2+} overload—also widely recognized as major inductor of triggered arrhythmogenic activity.

13.2.1 The Significance of NCX1 in Maintaining Intracellular Ca^{2+} Balance

The excitation–contraction (EC) coupling process is explored in detail (reviewed in [13–15]). During depolarization, a relatively small but essential Ca^{2+} flux enters the cell mainly via sarcolemmal LTCCs as the first step in EC coupling. A minor Ca^{2+} influx ($<$10% of total) via “reverse” mode transport of the NCX1 contributes to the influx. The localized [Ca^{2+}] increase in the sub-membrane “fuzzy space” is essential in triggering the release of a larger Ca^{2+} flux via the ryanodine-sensitive Ca^{2+} channels (RyRs) of SR (calcium-induced calcium release, CICR). Integrated Ca^{2+} flux (Ca^{2+} transient) in turn activates myofilaments and generates contractile force. The contribution of the extracellular Ca^{2+} influx to total Ca^{2+} elevation is species dependent (~7% to ~30%). In pathological conditions (e.g. heart failure), it may reach a much higher (50–60%) proportion. For the steady activity of the heart, maintaining the balance between transsarcolemmal and intracellular Ca^{2+} transport systems is critical. In a functional steady state, the exact amount of Ca^{2+} entering the cell during AP should be extruded. Any major and chronic imbalance exceeding functional physiological shifts may result in gradual cellular Ca^{2+} overload, leading to increased arrhythmia propensity, cell injury, and apoptosis, or gradual cellular Ca^{2+} loss compromising cardiac pump function (heart failure). For normal cardiac relaxation, fast dissociation of the activator calcium from the myofilaments and its fast removal from the cytosol is likewise essential. Reduced [Ca^{2+}]$_i$ decay rate might lead to incomplete relaxation, subsequently limiting ventricular refilling. Cellular Ca^{2+} removal mechanisms permanently compete for Ca$^{2+}{}_i$, and their relative contributions dynamically change throughout the cardiac cycle.

The single transporter mechanism to pump back Ca^{2+} to the SR is the sarcoplasmic/endoplasmic reticulum Ca^{2+}-ATPase (SERCA2). Its activity is essential to maintain the Ca^{2+} content of the SR for subsequent Ca^{2+} release. The major transport mechanism extruding the surplus Ca^{2+} from cardiac cells is the *forward mode* activity of the low affinity but high capacity NCX1. Depending on species, 3–47% of the total removed cytosolic Ca^{2+} is extruded from the cell by the NCX1. The plasma membrane Ca^{2+}-ATPase (PMCA) was shown to contribute less than 5% to cytoplasmic Ca^{2+} removal. Nonetheless, PMCA may be more involved in fine-tuning the end-diastolic $[Ca^{2+}]_i$ and also in intracellular Ca^{2+} signaling. A fourth but physiologically insignificant alternative mechanism for cytoplasmic Ca^{2+} removal is uptake into the mitochondria via their Ca^{2+} uniporter. This uptake only occurs when cytoplasmic Ca^{2+} levels are largely elevated (>500 nM) and may represent a safety mechanism that can transiently reduce cellular Ca^{2+} overload. A recently described but practically unexplored alternative of Ca^{2+} removal is into the nuclear envelope. Surprisingly, while NCX function was expected to be essential for normal contraction–relaxation cycling, cardiac-specific (NCX1) KO mice were not only able to survive to adulthood but also with relatively minor cardiac dysfunction. In these animals, the absence of NCX1 was nearly fully compensated by secondary shifts in their Ca^{2+} handling [16, 17].

13.2.2 Physiological Regulation of NCX1 Activity: $[Ca^{2+}]_i$, $[Na^+]_i$, and pH_i Dependence

A rather unique feature of NCX is that its transport substrates also exert important regulatory effects on its transport activity. Indeed, crucial physiological regulation of the direction and rate of the transport is accomplished by Na^+_i (Na^+-dependent inactivation) and Ca^{2+}_i (Ca^{2+}_i-dependent activation). Ca^{2+}_i-dependent activation is an essential mechanism to activate Ca^{2+} extrusion (and subsequent inward current) in forward mode operation. Elevated $[Na^+]_i$ typically activates reverse mode transport, while, in contrast, highly increased $[Na^+]_i$ may completely inactivate $I_{Na/Ca}$. This Na^+-dependent inactivation, however, is abolished by highly elevated $[Ca^{2+}]_i$. These basic NCX1 regulatory mechanisms depend on the practically unknown local Ca^{2+} and Na^+ concentrations in the vicinity of the NCX1 proteins. Indirect estimation of the peak $[Ca^{2+}]$ in the fuzzy space ($[Ca^{2+}]_{sm}$) yielded 3.5 μM, a value substantially higher than any measured $[Ca^{2+}]_i$ [18]. On the other hand, Na^+-dependent inactivation could be observed only at dramatically elevated (> 30 mM) $[Na^+]_i$, thus normally is not likely to be active.

Lowering pH_i inhibits and elevation of pH_i stimulates NCX1 [19]. A moderate decrease in pH_i (0.4 units) may induce its ~90% inhibition. ATP increases the affinity of the exchanger to $[Ca^{2+}]_i$ and $[Na^+]_o$, which may inhibit Na^+-dependent inactivation and stimulate PIP_2 synthesis. The principal action for negatively charged phospholipids is to inhibit Na^+-dependent inactivation. Several regulatory proteins may also have an important role in physiological NCX1 modulation. Phospholemman is an endogenous inhibitor of NCX1 and also has a role in controlling the activity of the NKA. Stimulatory actions by angiotensin-II and endothelin-1 may be mediated by PKC. NCX1 activity is also modulated by local factors, like phosphorylation state or subcellular location. The phosphorylation state of the NCX1 is probably regulated by a large macromolecular complex [20].

13.2.3 The Contribution of NCX1 Currents to AP and the I_{ti}

The net ion transport by NCX1 is not electroneutral. An exchange stoichiometry of 3 $Na^+ \leftrightarrow 1\ Ca^{2+}$ is widely accepted, though higher exchange ratios were also proposed [21]. Uneven charge exchange results in a transmembrane current ($I_{Na/Ca}$) of at least one net charge per transport cycle. The direction of the $I_{Na/Ca}$ is determined by the magnitudes of the membrane potential (E_m) and NCX1 equilibrium potential (E_{NCX}). The latter is defined by local transmembrane gradients of

Na^+ and Ca^{2+} ($E_{NCX} = 3E_{Na} - 2E_{Ca}$). Whenever the difference (E_m - E_{NCX}) is positive, Ca^{2+} entry and Na^+ loss should occur, generating *outward* current. If ($E_m - E_{NCX}$) is negative, Ca^{2+} extrusion and Na^+ gain leading to *inward* current are energetically favored. Consequently, both *depolarizing* and *repolarizing* contribution of $I_{Na/Ca}$ to AP is possible. Depolarization by $I_{Na/Ca}$ may facilitate *arrhythmogenesis* by increasing short-term variability of AP duration (APD). Increased $I_{Na/Ca}$ may have particular importance in *heart failure* when NCX1 expression/function is enhanced [22].

The direction of the $I_{Na/Ca}$ during the different phases of AP is not properly clarified. In the guinea pig, it was found predominantly outward during the plateau phase, while in rat cardiomyocytes, inward $I_{Na/Ca}$ prolonged the APD. Results from rabbit studies suggested that $I_{Na/Ca}$ is mostly inward during AP. In a study based on measurements with buffered $[Ca^{2+}]_i$, elevated $I_{Na/Ca}$ led to APD prolongation [23]. In a complex model [24, 25], NCX1 current was found inward during the plateau phase if $[Na^+]_i$ was normal. In a study based on an integrative model of the canine ventricular myocyte [26] and supposing co-localization between NCX1 and RyR2, a multi-inflection model has been developed [27]. In nodal pacemaker cells, $I_{Na/Ca}$ may significantly contribute to depolarization [28] (see also Chap. 5).

13.3 NHE1: The Major Regulator of $[H^+]_i$ (pH_i) and $[Na^+]_i$ in Cardiomyocytes and an Important Promoter of Cardiac Hypertrophy

The NHE is an integral membrane transport protein playing an essential role in a wide range of cell types in regulating intracellular acid-base balance and cellular electrolyte and volume homeostasis by translocating one intracellular H^+ in exchange for one extracellular Na^+. For its exchange activity, it uses the energy provided by the trans-sarcolemmal Na^+ gradient.

In the mammalian heart, its type 1 isoform (NHE1) is predominant and is expressed in large quantity. Its molecular properties and physiological functions have been well explored [29–32]. Shifts in normal NHE1 activity may also contribute to pathological changes. At physiological pH_i, its activity is low; however, even a moderate decrease in pH_i substantially activates proton extrusion, leading to subsequent Na^+_i accumulation and Ca^{2+}_i overload. Increased NHE1 activity was reported to promote cellular growth leading to cardiac hypertrophy [33, 34]. It also plays a crucial role in the induction of necrotic and/or apoptotic tissue damage and is a major cause of increased arrhythmia generation during/following myocardial infarct (MI) and also in HF. Its activation in *sympathetic nerve endings* leads to significantly increased NE release and decreased reuptake, leading to increased arrhythmia propensity of the heart [35].

There are some important differences between the NCX and NHE. The NCX is electrogenic, and the NHE is electroneutral. However, since their activity is tightly coupled, increased proton extrusion still would induce depolarizing current through co-activation of the NCX1. Another major difference is that in contrast to the NCX1, the Na^+ transport by NHE1 is practically always unidirectional (inward).

13.3.1 The Essential Role of NHE1 in pH_i and $[Na^+]_i$ Regulation and Cellular Growth

The NHE is responsible for pH_i regulation [36]. By removing excess protons, it protects the cells from intracellular acidosis. In hypoxia or acidosis, when excess protons are generated in large quantities (lactacidosis), NHE is several times more effective than other transporters involved in pH_i regulation. By modulating Na^+ uptake, it also participates in the regulation of the transmembrane Na^+ flux and contributes to osmotic cell volume control. In addition, it can be activated by growth factors, and normal NHE activity is essential for cell growth and proliferation. NHE also plays an important role in promoting or inhibiting apoptosis. In cardiomyocytes, NHE1 is restricted to specialized membrane microdomains, and its regulatory function is tightly coupled to the modulation of pH-sensitive membrane proteins. In the transverse tubulus, it is localized in close proximity to the RyRs (consequently in the vicinity of the NCX1; see Chap. 15) and exerts modulatory action on EC coupling. At the intercalated disks, it is localized close to connexin 43 and was shown to modulate cell-to-cell coupling. NHE1 is also present in the caveolae and substantially influences the rate of cAMP-synthesis by its modulatory effect on adenyl-cyclase. It also regulates the cytoskeletal organization and acts as a plasma membrane scaffold assembling regulatory proteins and signaling molecules for enhanced functional interaction [37].

13.3.2 Physiological Regulation of NHE1

In cardiomyocytes, NHE1 activity is regulated by multiple mechanisms [38]. Its primary stimulus is intracellular acidosis. Under normal physiological conditions (i.e. oxidative energy metabolism), its basal activity is practically negligible but is rapidly activated as pH_i decreases [32]. To explain this steep pH_i dependence, NHE1 has been suggested to contain an extra proton binding site for its allosteric regulation.

NHE1 is also regulated through phosphorylation-dephosphorylation, accomplished by cellular signaling protein kinases in response to hormone or growth-factor stimulation or sustained acidosis. Acidosis or ischemia-activated protein kinases are implicated in myocardial NHE1 regulation. Phosphorylation stimulates (by moving its setpoint) the exchanger to be more active at more alkaline pH values. NHE1 activity in response to angiotensin II may be inhibited through its phosphorylation by the p38 MAPK. This kinase inhibits the NHE1 via inhibition of the ERK pathway, but it may also induce alkalization and stimulate NHE1 in a separate, apoptotic pathway. Its modulation by protein kinases C and D is probably indirect. Protein phosphatases 1 and 2A inhibit NHE1 through dephosphorylation, while calmodulin blocks its autoinhibitory region. Further regulatory factors shown to bind to NHE1 are carbonic anhydrase II, PIP_2, HSP70, and CHP (calcineurin homologous protein), but their role is not yet fully clarified. NHE1 expression is also regulated at the transcriptional level [39]. NHE1 expression was induced, and its activity was elevated in isolated cardiomyocytes subjected to chronic external acidosis. In isolated perfused hearts and also in coronary ligated rats, ischemic insult resulted in increased NHE1 mRNA levels [40]. It is important, however, to emphasize that while *acute activation* of the NHE1 usually contributes to the physiological maintenance of the functional integrity of the myocytes, its *sustained activation* and highly *increased* expression results in myocardial injury and structural remodeling, leading to arrhythmogenesis and mechanical dysfunction.

13.4 Role of Altered Exchanger Activities in Cardiac Arrhythmia and Heart Disease

Marked alterations in trans- and intracellular Na^+ and Ca^{2+} transport rates leading to impairment of cellular Na^+ and Ca^{2+} regulation are characteristic of several life-threatening cardiac diseases. Irregular AP morphology commonly caused by cellular Ca^{2+} overload and increased SR Ca^{2+} leakage may result in abnormal EC coupling and increased arrhythmia propensity. In CHF, leaky SR initiates depolarizing currents and may trigger extrasystoles during diastole via the upregulated NCX1, thus substantially increasing the risk of SCD. In sustained ischemia gradual but substantial $[Ca^{2+}]_i$ and $[Na^+]_i$ overload deteriorates normal electrical activity. If acute or chronic focal ischemia is generalized, it may lead to a high probability of SCD.

13.4.1 NCX1-Induced $Ca^{2+}{}_i$ Overload and Its Role in Triggered Arrhythmia

Ca^{2+}-dependent arrhythmias are usually triggered by abnormal membrane potential changes induced by $Ca^{2+}{}_i$ overload, generated either by increased Ca^{2+} influx (caused by the enhanced open probability of LTCCs) or by decreased Ca^{2+} efflux (induced by the elevated $[Na^+]_i$). The sustained rise in $[Ca^{2+}]_i$ increases the SR Ca^{2+} content and subsequently enhances the normally low probability of Ca^{2+} spark generation. If the spark rate is above a threshold, spontaneous Ca^{2+} waves are likely to be induced.

The principal cellular mechanisms leading to triggered focal arrhythmias are EADs and DADs. *Early* EADs arise during the plateau phase of AP due to maintained late Na^+ current [41], increased NCX1 activity, or reactivation of a fraction of LTCCs. *Late* EADs are most likely induced by the activation of Ca^{2+}-dependent inward currents during the end phase of cardiac repolarization. DADs are initiated by spontaneous, generalized SR Ca^{2+} release (multiple Ca^{2+} sparks, Ca^{2+} waves) during diastole through a current carried by the NCX1. EADs are more probable at low heart rates when APs are prolonged. DADs are more likely at high heart rates due to enhanced Ca^{2+} entry despite the shortened APs.

Altered NCX1 activity may play a crucial role in EAD initiation [42], especially in cardiac Purkinje fibers. Inward NCX1 current, generated by the extrusion of the spontaneously released Ca^{2+}, promotes membrane depolarization by enabling window Ca^{2+} currents. Enhanced NCX1 function may also be important in DAD generation through its contribution to elevated cytosolic and highly increased SR Ca^{2+} content [43]. Since SERCA2 is depressed by the high SR Ca^{2+} content, the sudden large elevation in $[Ca^{2+}]_i$ caused by spontaneous Ca^{2+} waves is ultimately removed by the exchanger. Although, during diastole, the membrane potential is at or close to its resting level, sudden release of a large amount of Ca^{2+}—when extruded by the NCX1—may induce sufficiently large depolarizing inward current (I_{ti}) to shift the membrane potential to the threshold of I_{Na}, thus eliciting *propagating* extrasystoles. This is the proposed mechanism in a rare, often lethal genetical disorder, catecholaminergic polymorphic ventricular tachycardia (CPVT), where RyR mutations cause the intermittent abnormal release of Ca^{2+} in response to catecholamine challenge [44].

Thus, cardiac arrhythmia propensity may be attributed to irregular micro- and macroheterogeneities in the generation or propagation of APs, caused by focal, cellular-level disturbances in intracellular Ca^{2+} handling. Abnormally high $[Ca^{2+}]_i$ in a particular cardiomyocyte may easily spread over to the surrounding cells either via membrane depolarization or by direct cell-to-cell diffusion through gap junctions, triggering subsequent secondary intracellular Ca^{2+} release [45].

13.4.2 NHE1-Induced $[Na^+]_i$ Overload, a Generator of Ischemia Induced $[Ca^{2+}]_i$ Overload and Cardiac Hypertrophy

Under physiological conditions, NHE1 removes excess intracellular protons in exchange for extracellular Na^+. Surplus intracellular Na^+ is then removed by the high-capacity NKA and, to a limited extent, the reverse mode activity of NCX1. In hypoxic or ischemic cardiomyocytes—due to the anaerobic shift and largely enhanced glycolysis—proton production is highly elevated. The subsequent acidosis activates NHE1, and intracellular protons are rapidly exchanged for external Na^+. Therefore, a crucial consequence of hypoxic NHE1 activation is increased Na^+ influx. Since, due to the increasing energy deficit, NKA is gradually inhibited, surplus Na^+ content may only be removed by the NCX1, resulting in intracellular Ca^{2+} accumulation. Ca^{2+} overload may trigger various pathways, leading to mechanical dysfunction, arrhythmia generation, and eventually cellular death. The crucial role of NHE1 activation in the induction of ischemia–reperfusion injury is further underlined by the fact that in mice, genetic ablation of NHE1 protects the heart from ischemia-induced injury [46].

NHE1 is also an important factor in inducing cardiac hypertrophy, and its inhibition limits hypertrophy [34, 38]. The hypertrophic effect of norepinephrine, aldosterone, or stretch can, indeed, be prevented by NHE1 inhibition. The details of this mechanism are not fully clarified. Since intracellular alkalosis is *not induced* by NHE1 activation, the actions of NHE1 inhibition are probably *not mediated* through pH_i modulation. Since NHE1 inhibition also limits $Na^+{}_i$ accumulation, the latter may provide a feasible mechanism by which NHE1 modulates hypertrophy [33]. Elevation of $[Na^+]_i$ could act through several alternative mechanisms: increased reverse mode activity of NCX1, increased reactive oxygen species (ROS) generation, or activation of intracellular signaling or phosphorylation pathways. All these pathways were studied in detail, but no final agreement on the role of NHE1 in the induction of hypertrophy has been reached. Enhanced NHE1 expression was also found in hypertrophy, but the significance of this apparently positive feedback mechanism is not fully understood.

13.4.3 NCX1 and Ventricular Arrhythmias in Congestive Heart Failure (CHF)

Perturbations in intracellular Ca^{2+} handling leading to mechanical dysfunction and arrhythmia propensity in HF are summarized in Fig. 13.1. NCX1 mRNA and protein expression and activity are markedly elevated, while SERCA2 activity is depressed, though its expression levels are not always decreased. Decreased SERCA2 activity causes slower and decreased Ca^{2+} reuptake, and slower and reduced decay in systolic $[Ca^{2+}]_i$. Consequently, during relaxation, Ca^{2+} extrusion by NCX1 is increased relative to Ca^{2+} reuptake via SERCA2. Furthermore, in HF, the increased open probability of RyRs leads to marked diastolic Ca^{2+} leak from SR [47]. Phospholamban expression is not necessarily changed, but its phosphorylation level is often lowered. The primary consequences of the inverse shift in NCX1 and SERCA2 activities are: (1) decreased SR Ca^{2+} content and subsequently depressed $[Ca^{2+}]_i$ transients causing *systolic* dysfunction, and (2) largely elevated diastolic $[Na^+]_i$ and $[Ca^{2+}]_i$ leading to *diastolic* dysfunction.

Increased $[Na^+]_i$ due to decreased Na^+ extrusion by NKA or increased Na^+ influx through slowly inactivating Na^+ channels is a typical perturbation in HF. Since $[Ca^{2+}]_i$ and $[Na^+]_i$ are tightly coupled, elevated $[Na^+]_i$ should have important implications for intracellular Ca^{2+} handling. Elevated $[Na^+]_i$ in the fuzzy space shifts the NCX1 reversal potential towards more negative values, leading to larger, prolonged Ca^{2+} influx during systole and shorter, smaller efflux during diastole. Elevated diastolic $[Ca^{2+}]_i$, reduced SR Ca^{2+} content, and subsequently compromised relaxation are the major consequences of downregulated SERCA2, upregulated NCX1 expression, and elevated diastolic $[Na^+]_i$. Since depressed and leaky SERCA2 is the primary cause behind compromised relaxation and subsequent diastolic dysfunction, the enhanced NCX1 expression may be considered a compensatory mechanism. Indeed, in failing hearts, increased Ca^{2+} influx through the NCX1 during systole may partially compensate for decreased SR Ca^{2+} content by increasing SR Ca^{2+} load, elevating Ca^{2+} transients, and enhancing contractile force.

Increased arrhythmia propensity in the failing heart is a consequence of a number of changes in the electrophysiological state of the heart. The results are often diverse and conflicting, depending on the nature of the disease (hypertrophic vs. dilatative), the model applied (pacing vs. valve dysfunction), and species (rat, rabbit, dog). Reduced SA node pacemaker activity is usually accompanied by enhanced automaticity of the AV node and the Purkinje fibers and ventricles (trigger). It may be caused by corresponding shifts in I_f distribution and often lead to enhanced ectopic beat formation (trigger). Furthermore, elevation of the mRNA and protein expression and the current density of I_f channels were also reported in HF [48].

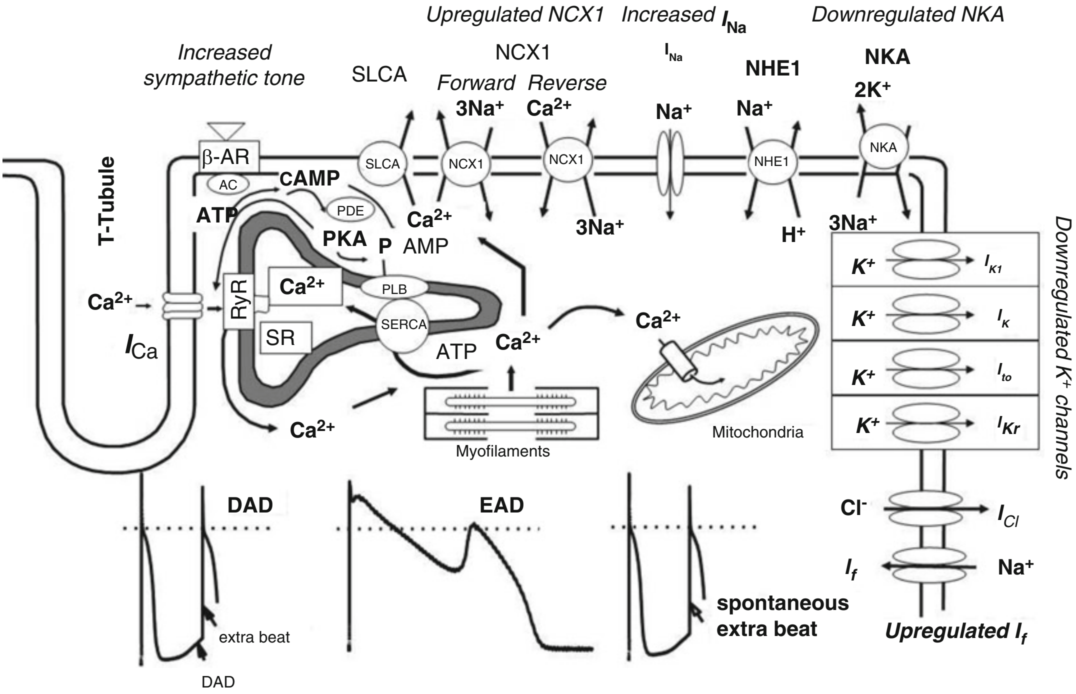
Upregulated NCX1
Increased I_{Na}
Downregulated NKA
Increased sympathetic tone
SLCA
NCX1
Forward
Reverse
I_{Na}
NHE1
NKA
3Na+
Ca2+
Na+
Na+
2K+
T-Tubule
β-AR
AC
CAMP
PDE
ATP
PKA
P
AMP
Ca2+
3Na+
H+
3Na+
SLCA
NCX1
NCX1
NHE1
NKA
Ca2+
RyR
Ca2+
PLB
SERCA
SR
ATP
Ca2+
Ca2+
I_{Ca}
Ca2+
Myofilaments
Mitochondria
K+
I_{K1}
K+
I_K
K+
I_{to}
K+
I_{Kr}
Downregulated K+ channels
Cl-
I_{Cl}
I_f
Na+
Upregulated I_f
DAD
extra beat
DAD
EAD
spontaneous extra beat

Fig. 13.1 Schematics summarizing the principal mechanisms leading to arrhythmogenesis (EAD, DAD, and Ca^{2+} wave generation) in the failing heart (see details in the text)

Since in the failing heart Ca^{2+}-dependent NCX1-mediated depolarizing activity is usually increased and repolarizing K^+ currents (I_{K1}, I_{Ks}, I_{to}) are downregulated, while late Na^+ plateau current (I_{NaL}) is enhanced, APD prolongation and dispersion occurs (substrate), subsequently favoring EAD formation (trigger). Indeed, increased inward exchanger current density during the plateau phase is suggested as a major contributor to electrical instability and delaying the repolarization [49–51]. The probability of EAD initiation and incidence of EADs (trigger) was demonstrated to be increased as a consequence of reduced repolarization reserve due to K^+ channel downregulation and increased inward $I_{Na/Ca}$ generated by the upregulated NCX1. The proarrhythmic effect of the enhanced inward NCX1 current would further be amplified by a reduction in I_{K1}, a current known to stabilize cardiac membrane potential.

Elevated exchanger activity and increased Ca^{2+} leakage from the hyperphosphorylated RyRs promote DAD formation (trigger). While in healthy myocytes, increased SR Ca^{2+} content is a prerequisite for DAD generation, in HF, as a consequence of the decreased K^+ channel expression, the subsequently depressed I_{K1} cannot carry enough repolarizing current to oppose DADs, which may even be generated at lowered SR Ca^{2+} content. The probability of DAD generation may further be increased by cardiac glycosides and β-agonists, commonly used to improve contractile force in the failing heart. HF may also be associated with chronic AF, since in the atria, the enhanced NCX1 has a greater contribution to maintaining AP plateau and duration [52]. Finally, as a consequence of the reduced impulse conduction velocity (substrate), caused by the downregulated connexin 43 density, decreased I_{Na}, and increased APD variability, reentrant activity is substantially increased. Enhanced dispersion of repolarization and cellular refractoriness is a further important factor (substrate) in increasing the probability of reentrant arrhythmias and has been demonstrated in both cardiac hypertrophy and HF.

13.4.4 NHE1-NCX1 Interaction and Ventricular Arrhythmia Generation during Acute Ischemia-Reperfusion Injury and Chronic IHD

Sustained cardiac ischemia is characterized by deprived energy metabolism, acidosis, hypoxia, and elevated extracellular [K^+]. Decreased pH_i (acidosis) exerts severe negative inotropic effects on myocardial contractility (reduced developed force and maximal tension) and depresses Ca^{2+} transport proteins (SERCA2, RyR2, NCX1), while, surprisingly, the amplitude of the $Ca^{2+}{}_i$ transient increases [53, 54]. This contrast suggests that the negative inotropic effect of acidosis is a consequence of the decreased myofilament Ca^{2+} sensitivity and turnover rate and not the depressed Ca^{2+} transport. In acidosis, both $[Ca^{2+}]_i$ and $[Na^+]_i$ are elevated. The latter is caused by increased proton extrusion by NHE1 and depressed NKA activity. In sustained, severe acidosis, the substantial pH_o decrease suppresses Na^+/H^+ exchange, and since Na^+/Ca^{2+} exchange is also inhibited, elevated $[Na^+]_i$ is accompanied by elevated $[Ca^{2+}]_i$. In contrast to acidosis-induced reduction in Ca^{2+} uptake, the SR Ca^{2+} content is usually elevated.

Perturbations in pH_i and Ca^{2+} handling leading to arrhythmia propensity in the ischemic heart are summarized in Fig. 13.2. In acute hypoxia, reactivation of the late Na^+ channel leads to increased Na^+ influx. Na^+ efflux is substantially reduced due to the energy deficit of the NKA. NHE1 activity is significantly enhanced as a consequence of the increased $[Na^+]_i$. During sustained hypoxia, $[Na^+]_i$ may rise to very high levels (> 40 mM). Subsequent activation of the *reverse mode* transport by NCX1 leads to enhanced Ca^{2+} influx and increased $[Ca^{2+}]_i$. Due to the increased K^+ efflux, the transmembrane K^+ gradient also gradually decreases. The decreased K^+ gradient, in combination with a direct effect of hypoxia on K^+ channels, induces depolarization. This further boosts arrhythmogenic reverse mode NCX1 current. *Permanent* elevation of $[Ca^{2+}]_i$ during *lasting* hypoxia inevitably leads to *massive* Ca^{2+} *overload* of both the sarcoplasma and the SR, substantial membrane depolarization, and may initiate triggered arrhythmias.

In acute ischemia, intracellular acidosis activates NHE-1 resulting in elevated $[Na^+]_i$. Increased $[Na^+]_i$ in turn activates *reverse mode* transport of NCX1, leading to increased $[Ca^{2+}]_i$. $Na^+{}_I$ overload is also facilitated by intracellular acidosis, leading to further Na^+ entry through the NHE1. LTCCs are partially inactivated due to gradual membrane depolarization. Therefore, their contribution to enhanced Ca^{2+} influx during late ischemia and early reperfusion is limited. In *prolonged, severe ischemia* unbalanced $Ca^{2+}{}_i$ accumulation leads to gradual cellular Ca^{2+} overload. When $[Ca^{2+}]_i$ reaches a threshold (~ 500 nM) mitochondria begin to accumulate Ca^{2+}. This safety mechanism may transiently decrease the rate of $[Ca^{2+}]_i$ rise [55], but *permanently* increased Ca^{2+} entry during *sustained* ischemia would inevitably lead to a high probability of triggered arrhythmias and permanent mitochondrial and subsequent cellular damage. Interestingly, during the early phase of ischemia, the primary source of $[Ca^{2+}]_i$ increase is the SR, for two important reasons. First, the open probability of RyR2s is increasing when $[Ca^{2+}]_i$ reaches micromolar levels [56]. Second, SERCA2 activity is depressed if ATP delivery is compromised. The initial elevation in $[Ca^{2+}]_i$ further increases the open probability of RyRs, leading to additional Ca^{2+} release from SR. In contrast, during the late phase of ischemia, and especially during reperfusion, $Ca^{2+}{}_i$ accumulation is further accelerated by the uptake of extracellular Ca^{2+} through the reverse mode transport of NCX enhanced by both membrane depolarization and increased $[Na^+]_i$.

Upon reperfusion, $[Ca^{2+}]_i$ may either further increase due to the sustained entry of extracellular Ca^{2+}, invariably leading to cell death, or—if the level of ischemia was moderate—progressively normalize, leading to the survival of the cell. During sustained ischemia, $[Na^+]_i$ gradually increases; however, as NHE1 is temporarily

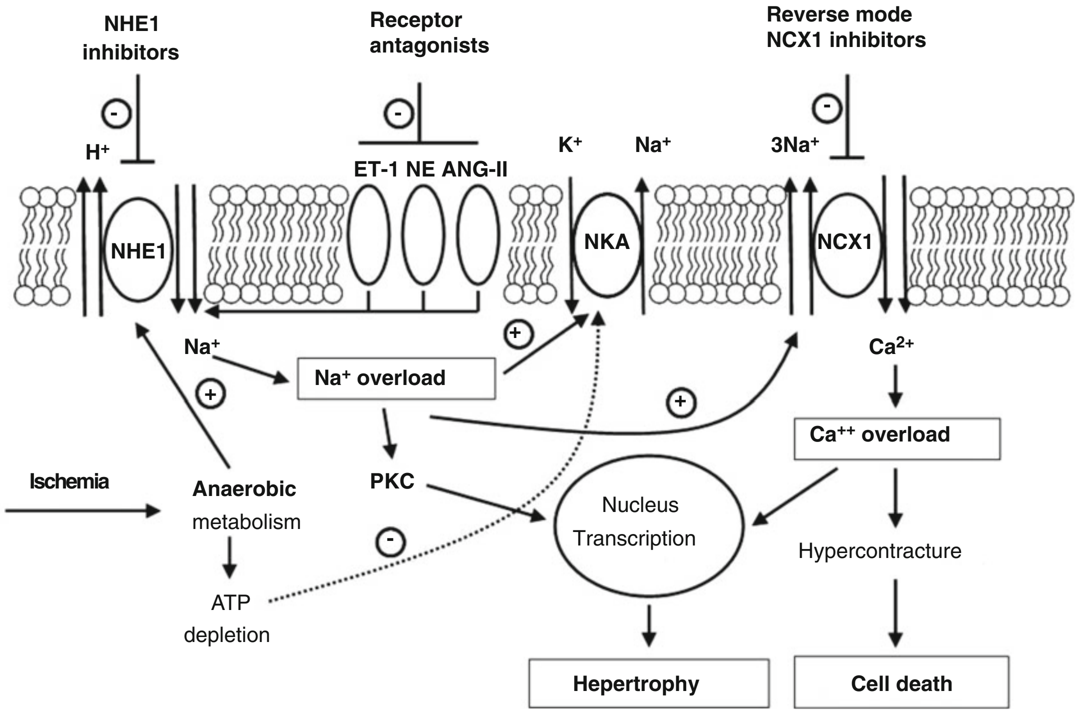
NHE1 inhibitors
Receptor antagonists
Reverse mode NCX1 inhibitors
-
H+
ET-1 NE ANG-II
K+
Na+
3Na+
NHE1
NKA
NCX1
Na+
+
Na+ overload
Ca2+
Ca++ overload
Ischemia
Anaerobic metabolism
PKC
Nucleus Transcription
Hypercontracture
ATP depletion
Hepertrophy
Cell death

Fig. 13.2 Central role of NHE-1 in mediating acute and chronic responses to myocardial ischemia-reperfusion and the three principal preventive strategies to limit ischemia-reperfusion induced tissue injury (see details in the text)

inactivated due to low pH_o, its increase via NCX1 is limited. During the initial phase of reperfusion, pH_o rapidly recovers, while pH_i still remains relatively low. The large pH gradient fully activates NHE1 inducing a second, very rapid increase in $[Na^+]_i$. Since $[Ca^{2+}]_i$ is also high, Na^+-dependent inactivation of NCX1 is not feasible. Indeed, largely elevated $[Na^+]_i$ further accelerates the reverse mode activity of NCX1. The rapid and dramatic gain in $[Ca^{2+}]_i$ may facilitate extreme $Ca^{2+}{}_i$ overload (calcium paradox), often leading to reperfusion-induced cellular injury. The subsequent depolarization enhances arrhythmia propensity.

Another major problem during reperfusion is the rapid induction of a burst of free oxygen radicals. The reason for this is the substantially decreased amount of free radical scavengers combined with markedly elevated ROS production. Oxygen free radicals were shown to significantly participate in the induction of the cellular Ca^{2+} overload, increased I_{ti}, and triggered arrhythmias and were reported to harmfully modulate the activity of all major Ca^{2+} transporters, including NCX1 [57, 58]. Ca^{2+} leak and window Na^+ current may be enhanced during reperfusion, leading to further aggravation of Ca^{2+} overload and substantial depolarization.

Under chronic ischemic conditions (post-infarction myocardial remodeling, IHD), overactivation of endothelin-1 (ET-1), angiotensin II (Ang II), and norepinephrine (NE) signaling pathways promote NHE1 expression and synthesis. Permanent NHE1 activation leads to increased intracellular Ca^{2+} and Na^+ levels. In acute responses, these shifts result in sustained $Ca^{2+}{}_I$ overload, increased arrhythmia propensity, and activation of intracellular necrotic/apoptotic pathways, while chronic over-activation of these signaling pathways leads to transcriptional level changes induced via multiple Ca^{2+} and Na^+-dependent mechanisms promoting ventricular remodeling, hypertrophy and finally heart failure.

13.5 Inhibition of the NCX1 and NHE1 as Possible Pharmacological Strategy in Ventricular Arrhythmias

13.5.1 The Effects of Acute NCX1 Inhibition in Ventricular Arrhythmia Models

Antiarrhythmic effects of NCX1 inhibition are controversial, primarily due to the lack of specific inhibitors. Amran et al. [59] compared the antiarrhythmic efficacy of KB-R7943 and SEA0400 in guinea pigs on aconitine-induced triggered arrhythmias. KB-R7943 suppressed ventricular tachycardia, but SEA-0400 was found ineffective. They concluded that the less specific KB-R7943, in addition to suppressing NCX1, also decreases Na^+_i and Ca^{2+}_i overload by inhibiting Na^+ and Ca^{2+} channels. NCX1 was proposed not to be involved in aconitine-induced triggered activity, and the protective effect of KB-R7943 has been related to a different inhibitory mechanism.

In isolated cardiomyocytes treated with 50 μM/L, strophanthidin KB-R7943 reduced diastolic $[Ca^{2+}]_i$ and abolished spontaneous Ca^{2+} oscillations, without preventing the inotropic action of strophanthidin [60]. In guinea pig papillary muscles 10 μM KB-R7943 decreased the incidence and shortened the duration of reoxygenation-induced arrhythmias [61]. In an in vivo rat model, KB-R7943 suppressed ischemia-reperfusion-induced ventricular fibrillation [62], while in a similar study, it failed to significantly affect coronary ligation- and reperfusion-induced arrhythmias [63]. In a guinea pig arrhythmia model, pretreatment with 3 mg/kg KB-R7943 increased the ouabain dose required to induce ventricular arrhythmias and delayed the onset of arrhythmias and cardiac arrest following ouabain infusion [64]. Other studies in the rat, rabbit, and dog also reported controversial results leaving open the questions of dose-related problems of KB-R 7943 specificity on NCX1.

Postischemic administration of SEA-0400 effectively suppressed the incidence of ventricular fibrillation and mortality induced by coronary ligation and reperfusion in an in vivo rat model [65]. The novel NCX inhibitor, YM-244769, was also effective in the prevention of ischemia-reperfusion-induced ventricular tachycardia and fibrillation in rats [66]. In contrast, neither preischemic nor postischemic administration of SEA0400 could influence the incidence of ischemia-reperfusion-induced arrhythmias in dogs, while the drug was shown to exert a suppressive effect on digitalis-induced tachyarrhythmias [67]. In canine papillary muscles, APD prolongation induced EADs, and in isolated Purkinje fibers, the strophanthin-induced DADs were substantially decreased (Fig. 13.3) following the application of SEA-0400 (1 μM), which fairly selectively inhibits NCX1 [68]. These data argue for the possible antiarrhythmic effect of NCX1 inhibition in triggered arrhythmias.

More recently developed novel inhibitors of NCX-1 exhibit greater selectivity than KB-R7943 and SEA-0400. ORM-11372, for instance, was shown to be effective and safe in human ventricular tissue [69], and ORM-10962 could suppress cardiac alternans [70] to be effective in suppressing cardiac alternans. Although the therapeutic potential of these compounds has not yet been shown, they have helped to validate the close cooperation between I_f and NCX1 in sinusnode pacemaking (see Chaps. 4 and 5).

13.5.2 The Effects of Acute NHE1 Inhibition in Ventricular Arrhythmia Models

Both ischemia and reperfusion can increase the incidence of fatal cardiac arrhythmias. It was suggested long ago that inhibiting NHE1 during ischemia and/or reperfusion may have beneficial effects on myocardium. Numerous investigators have reported that NHE1 inhibitors can abolish ischemia-reperfusion-induced arrhythmias. Even low concentrations of amiloride, a nonselective NHE inhibitor, suppressed sustained ventricular tachyarrhythmia in experimental MI in dogs, in vivo. It was also effective to suppress

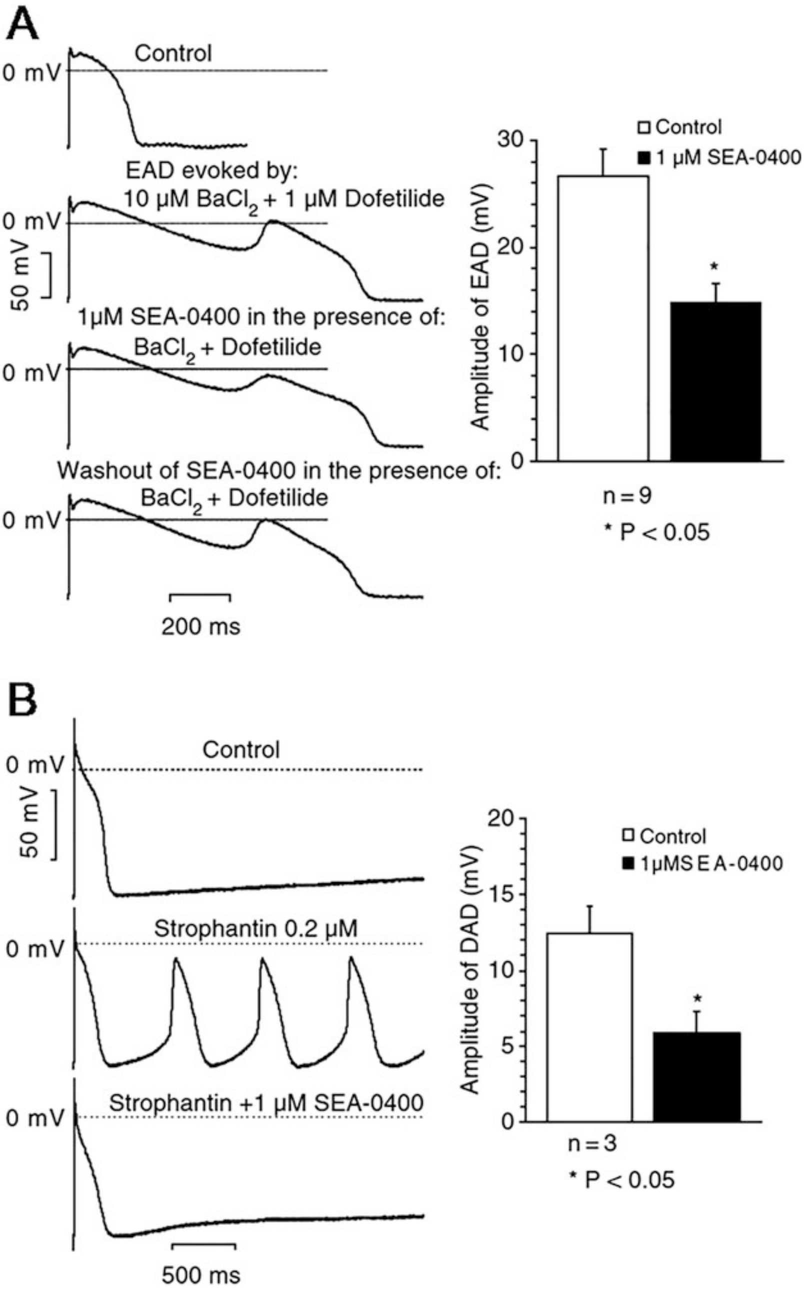

Fig. 13.3 Blocking effect of SEA-0400 on EADs & DADs in canine myocardium. (**a**) The effect of 1 μM SEA-0400 on EADs in right ventricular papillary muscles, stimulated at slow cycle lengths (1500–3000 ms) in the presence of 1 μM dofetilide plus 10 μM $BaCl_2$. On the *left*, the results of a representative experiment are shown, on the *right*, the average values of the amplitude of EADs are presented before (*open bars*) and after (*filled bars*) the administration of SEA-0400. (**b**) The effect of SEA-0400 on the delayed afterdepolarization (DAD) in canine cardiac Purkinje fibers, superfused with 0.2 μM strophanthin. A train of 40 stimuli was applied at a cycle length of 400 ms, followed by a 20-s long stimulation-free period that generated DADs. On the *left*, results of a representative experiment are shown, on the *right*, average values of the amplitude of DADs are given before (*open bars*) and after (*filled bars*) the application of 1 μM SEA-0400. (Reproduced from [68])

symptomatic ventricular tachycardia in humans, but not to the high degree observed in the dog model [71]. In subsequent clinical studies, amiloride suppressed spontaneous ventricular premature beats. If administered before ischemia *and* during reperfusion, EIPA and HOE 694 also afforded substantial protection against reperfusion-induced ventricular fibrillation [72–74]. However, the clinical studies with cariporide derivatives are still controversial and have not fulfilled expectations [22, 75–77]. Nevertheless, a recent study with cariporide in pigs demonstrates a beneficial effect during resuscitation after cardiac arrest [78].

13.6 Conclusions

There is a plethora of experimental evidence that both NCX1 and NHE1 play a vital role in the regulation of the myocardial Ca^{2+} homeostasis, but also in arrhythmogenesis. Nonetheless, our understanding of how these transporters function and how they are regulated is far from being satisfactory. Therefore, further intensive research is needed in these directions. Although clinical data with NHE1 inhibition are not yet satisfactory, a combination of NHE1 blockade with other cardioprotective mechanisms may have improved beneficial effects. For example, a proper combination of NCX1 *and* NHE1 inhibition may be an interesting and important new approach, but to our knowledge, no such experimental work has been done so far. Another promising approach could be enhancing NCX1 activity in the forward mode during the systole in acute Ca^{2+} overload, but subsequent diastolic depolarization and arrhythmia can be a potential risk.

A special potential implication of the NCX1 inhibition is the prevention of triggered arrhythmias in heart failure. Partial blockade of the upregulated NCX1 may decrease the magnitude of EADs and DADs in HF, preventing propagating extrasystoles and enhanced dispersion of repolarization without marked interference with systolic and diastolic Ca^{2+} levels. If the NCX1 block is incomplete and other cardiac Ca^{2+} extrusion mechanisms are functioning, Ca^{2+} overload probably can be avoided. Future work with more specific NCX1 inhibitors is necessary to address this possibility.

References

1. Bers DM. Excitation-contraction coupling and cardiac contractile force. Kluwer Academic Press; 2001.
2. Hryshko LV. Tissue-specific modes of Na/Ca exchanger regulation. Ann N Y Acad Sci. 2002;976: 166–75.
3. Blaustein MP, Lederer WJ. Sodium/calcium exchange: its physiological implications. Physiol Rev. 1999;79(3):763–854.
4. Egger M, Niggli E. Regulatory function of Na-Ca exchange in the heart: milestones and outlook. J Membr Biol. 1999;168(2):107–30.
5. Philipson KD, Nicoll DA. Sodium-calcium exchange: a molecular perspective. Annu Rev Physiol. 2000;62: 111–33.
6. Lytton J. Na+/Ca2+ exchangers: three mammalian gene families control Ca2+ transport. Biochem J. 2007;406(3):365–82.
7. Pogwizd SM, Bers DM. Cellular basis of triggered arrhythmias in heart failure. Trends Cardiovasc Med. 2004;14(2):61–6.
8. Scoote M, Williams AJ. Myocardial calcium signalling and arrhythmia pathogenesis. Biochem Biophys Res Commun. 2004;322(4):1286–309.
9. Sipido KR. Calcium overload, spontaneous calcium release, and ventricular arrhythmias. Heart Rhythm. 2006;3(8):977–9.
10. Homma N, Amran MS, Nagasawa Y, Hashimoto K. Topics on the Na+/Ca2+ exchanger: involvement of Na+/Ca2+ exchange system in cardiac triggered activity. J Pharmacol Sci. 2006;102(1):17–21.
11. Ter Keurs HE, Boyden PA. Calcium and arrhythmogenesis. Physiol Rev. 2007;87(2):457–506.
12. Nattel S, Maguy A, Le Bouter S, Yeh YH. Arrhythmogenic ion-channel remodeling in the heart: heart failure, myocardial infarction, and atrial fibrillation. Physiol Rev. 2007;87(2):425–56.
13. Bers DM, Weber CR. Na/Ca exchange function in intact ventricular myocytes. Ann N Y Acad Sci. 2002;976:500–12.
14. Eisner DA, Choi HS, Diaz ME, O'Neill SC, Trafford AW. Integrative analysis of calcium cycling in cardiac muscle. Circ Res. 2000;87(12):1087–94.
15. Trafford AW, Diaz ME, O'Neill SC, Eisner DA. Integrative analysis of calcium signalling in cardiac muscle. Front Biosci. 2002;7:d843–52.
16. Henderson SA, Goldhaber JI, So JM, Han T, Motter C, Ngo A, et al. Functional adult myocardium in the absence of Na+-Ca2+ exchange: cardiac-specific knockout of NCX1. Circ Res. 2004;95(6):604–11.
17. Pott C, Philipson KD, Goldhaber JI. Excitation-contraction coupling in Na+-Ca2+ exchanger knockout mice: reduced transsarcolemmal Ca2+ flux. Circ Res. 2005;97(12):1288–95.
18. Weber CR, Piacentino V 3rd, Ginsburg KS, Houser SR, Bers DM. Na(+)-Ca(2+) exchange current and submembrane [Ca(2+)] during the cardiac action potential. Circ Res. 2002;90(2):182–9.
19. Doering AE, Lederer WJ. The mechanism by which cytoplasmic protons inhibit the sodium-calcium exchanger in Guinea-pig heart cells. J Physiol. 1993;466:481–99.
20. Schulze DH, Muqhal M, Lederer WJ, Ruknudin AM. Sodium/calcium exchanger (NCX1) macromolecular complex. J Biol Chem. 2003;278(31): 28849–55.
21. Fujioka Y, Komeda M, Matsuoka S. Stoichiometry of Na+-Ca2+ exchange in inside-out patches excised from Guinea-pig ventricular myocytes. J Physiol. 2000;523(Pt 2):339–51.
22. Rupprecht HJ, vom Dahl J, Terres W, Seyfarth KM, Richardt G, Schultheiß HP, et al. Cardioprotective effects of the Na(+)/H(+) exchange inhibitor cariporide

in patients with acute anterior myocardial infarction undergoing direct PTCA. Circulation. 2000;101(25): 2902–8.

23. Janvier NC, Harrison SM, Boyett MR. The role of inward Na(+)-Ca2+ exchange current in the ferret ventricular action potential. J Physiol. 1997;498 (Pt 3):611–25.
24. Weber CR, Ginsburg KS, Bers DM. Cardiac submembrane [Na+] transients sensed by Na+-Ca2+ exchange current. Circ Res. 2003;92(9):950–2.
25. Shannon TR, Bers DM. Integrated Ca2+ management in cardiac myocytes. Ann N Y Acad Sci. 2004;1015: 28–38.
26. Greenstein JL, Hinch R, Winslow RL. Mechanisms of excitation-contraction coupling in an integrative model of the cardiac ventricular myocyte. Biophys J. 2006;90 (1):77–91.
27. Sher AA, Noble PJ, Hinch R, Gavaghan DJ, Noble D. The role of the Na+/Ca2+ exchangers in Ca2+ dynamics in ventricular myocytes. Prog Biophys Mol Biol. 2008;96(1–3):377–98.
28. Sanders L, Rakovic S, Lowe M, Mattick PA, Terrar DA. Fundamental importance of Na+-Ca2+ exchange for the pacemaking mechanism in Guinea-pig sinoatrial node. J Physiol. 2006;571(Pt 3):639–49.
29. Karmazyn M, Gan XT, Humphreys RA, Yoshida H, Kusumoto K. The myocardial Na(+)-H(+) exchange: structure, regulation, and its role in heart disease. Circ Res. 1999;85(9):777–86.
30. Avkiran M. Basic biology and pharmacology of the cardiac sarcolemmal sodium/hydrogen exchanger. J Card Surg. 2003;18(Suppl 1):3–12.
31. Fliegel L. Molecular biology of the myocardial Na+/H + exchanger. J Mol Cell Cardiol. 2008;44(2):228–37.
32. Slepkov ER, Rainey JK, Sykes BD, Fliegel L. Structural and functional analysis of the Na+/H+ exchanger. Biochem J. 2007;401(3):623–33.
33. Cingolani HE, Ennis IL. Sodium-hydrogen exchanger, cardiac overload, and myocardial hypertrophy. Circulation. 2007;115(9):1090–100.
34. Karmazyn M, Kilic A, Javadov S. The role of NHE-1 in myocardial hypertrophy and remodelling. J Mol Cell Cardiol. 2008;44(4):647–53.
35. Dampney RA, Coleman MJ, Fontes MA, Hirooka Y, Horiuchi J, Li YW, et al. Central mechanisms underlying short- and long-term regulation of the cardiovascular system. Clin Exp Pharmacol Physiol. 2002;29 (4):261–8.
36. Vaughan-Jones RD, Spitzer KW, Swietach P. Intracellular pH regulation in heart. J Mol Cell Cardiol. 2009;46(3):318–31.
37. Baumgartner M, Patel H, Barber DL. Na(+)/H(+) exchanger NHE1 as plasma membrane scaffold in the assembly of signaling complexes. Am J Physiol Cell Physiol. 2004;287(4):C844–50.
38. Avkiran M, Cook AR, Cuello F. Targeting Na+/H+ exchanger regulation for cardiac protection: a RSKy approach? Curr Opin Pharmacol. 2008;8(2):133–40.
39. Yang W, Wang H, Fliegel L. Regulation of Na+/H+ exchanger gene expression. Role of a novel poly(dA. dT) element in regulation of the NHE1 promoter. J Biol Chem. 1996;271(34):20444–9.
40. Gan XT, Chakrabarti S, Karmazyn M. Modulation of Na+/H+ exchange isoform 1 mRNA expression in isolated rat hearts. Am J Phys. 1999;277(3 Pt 2): H993–8.
41. Boutjdir M, Restivo M, Wei Y, Stergiopoulos K, el-Sherif N. Early afterdepolarization formation in cardiac myocytes: analysis of phase plane patterns, action potential, and membrane currents. J Cardiovasc Electrophysiol. 1994;5(7):609–20.
42. Volders PG, Vos MA, Szabo B, Sipido KR, de Groot SH, Gorgels AP, et al. Progress in the understanding of cardiac early afterdepolarizations and torsades de pointes: time to revise current concepts. Cardiovasc Res. 2000;46(3):376–92.
43. Fedida D, Noble D, Rankin AC, Spindler AJ. The arrhythmogenic transient inward current iTI and related contraction in isolated Guinea-pig ventricular myocytes. J Physiol. 1987;392:523–42.
44. Marks AR, Priori S, Memmi M, Kontula K, Laitinen PJ. Involvement of the cardiac ryanodine receptor/ calcium release channel in catecholaminergic polymorphic ventricular tachycardia. J Cell Physiol. 2002;190(1):1–6.
45. Miura M, Boyden PA, ter Keurs HE. Ca2+ waves during triggered propagated contractions in intact trabeculae. Am J Phys. 1998;274(1 Pt 2):H266–76.
46. Wang Y, Meyer JW, Ashraf M, Shull GE. Mice with a null mutation in the NHE1 Na+-H+ exchanger are resistant to cardiac ischemia-reperfusion injury. Circ Res. 2003;93(8):776–82.
47. Marx SO, Reiken S, Hisamatsu Y, Jayaraman T, Burkhoff D, Rosemblit N, et al. PKA phosphorylation dissociates FKBP12.6 from the calcium release channel (ryanodine receptor): defective regulation in failing hearts. Cell. 2000;101(4):365–76.
48. Stillitano F, Lonardo G, Zicha S, Varro A, Cerbai E, Mugelli A, et al. Molecular basis of funny current (if) in normal and failing human heart. J Mol Cell Cardiol. 2008;45(2):289–99.
49. Sipido KR, Volders PG, de Groot SH, Verdonck F, Van de Werf F, Wellens HJ, et al. Enhanced Ca(2+) release and Na/Ca exchange activity in hypertrophied canine ventricular myocytes: potential link between contractile adaptation and arrhythmogenesis. Circulation. 2000;102(17):2137–44.
50. Sipido KR, Volders PG, Vos MA, Verdonck F. Altered Na/Ca exchange activity in cardiac hypertrophy and heart failure: a new target for therapy? Cardiovasc Res. 2002;53(4):782–805.
51. Veldkamp MW, Verkerk AO, van Ginneken AC, Baartscheer A, Schumacher C, de Jonge N, et al. Norepinephrine induces action potential prolongation and early afterdepolarizations in ventricular myocytes isolated from human end-stage failing hearts. Eur Heart J. 2001;22(11):955–63.
52. Benardeau A, Hatem SN, Rucker-Martin C, Le Grand B, Mace L, Dervanian P, et al. Contribution of Na+/Ca2+ exchange to action potential of human atrial myocytes. Am J Phys. 1996;271(3 Pt 2):H1151–61.

53. Allen DG, Orchard CH. The effects of changes of pH on intracellular calcium transients in mammalian cardiac muscle. J Physiol. 1983;335:555–67.
54. Hulme JT, Orchard CH. Effect of acidosis on Ca2+ uptake and release by sarcoplasmic reticulum of intact rat ventricular myocytes. Am J Phys. 1998;275(3 Pt 2): H977–87.
55. Duchen MR. Mitochondria and Ca(2+)in cell physiology and pathophysiology. Cell Calcium. 2000;28 (5–6):339–48.
56. Meissner G. Molecular regulation of cardiac ryanodine receptor ion channel. Cell Calcium. 2004;35(6):621–8.
57. Reeves JP, Bailey CA, Hale CC. Redox modification of sodium-calcium exchange activity in cardiac sarcolemmal vesicles. J Biol Chem. 1986;261(11):4948–55.
58. Goldhaber JI. Free radicals enhance Na+/Ca2+ exchange in ventricular myocytes. Am J Phys. 1996;271(3 Pt 2):H823–33.
59. Amran MS, Hashimoto K, Homma N. Effects of sodium-calcium exchange inhibitors, KB-R7943 and SEA0400, on aconitine-induced arrhythmias in Guinea pigs in vivo, in vitro, and in computer simulation studies. J Pharmacol Exp Ther. 2004;310(1):83–9.
60. Satoh H, Ginsburg KS, Qing K, Terada H, Hayashi H, Bers DM. KB-R7943 block of Ca(2+) influx via Na (+)/Ca(2+) exchange does not alter twitches or glycoside inotropy but prevents Ca(2+) overload in rat ventricular myocytes. Circulation. 2000;101(12):1441–6.
61. Mukai M, Terada H, Sugiyama S, Satoh H, Hayashi H. Effects of a selective inhibitor of Na+/Ca2+ exchange, KB-R7943, on reoxygenation-induced injuries in Guinea pig papillary muscles. J Cardiovasc Pharmacol. 2000;35(1):121–8.
62. Nakamura A, Harada K, Sugimoto H, Nakajima F, Nishimura N. Effects of KB-R7943, a novel Na+/Ca2+ exchange inhibitor, on myocardial ischemia/reperfusion injury. Nippon Yakurigaku Zasshi. 1998;111(2):105–15.
63. Lu HR, Yang P, Remeysen P, Saels A, Dai DZ, De Clerck F. Ischemia/reperfusion-induced arrhythmias in anaesthetized rats: a role of Na+ and Ca2+ influx. Eur J Pharmacol. 1999;365(2–3):233–9.
64. Watano T, Harada Y, Harada K, Nishimura N. Effect of Na+/Ca2+ exchange inhibitor, KB-R7943 on ouabain-induced arrhythmias in Guinea-pigs. Br J Pharmacol. 1999;127(8):1846–50.
65. Takahashi K, Takahashi T, Suzuki T, Onishi M, Tanaka Y, Hamano-Takahashi A, et al. Protective effects of SEA0400, a novel and selective inhibitor of the Na+/Ca2+ exchanger, on myocardial ischemia-reperfusion injuries. Eur J Pharmacol. 2003;458 (1–2):155–62.
66. Kuramochi T, Kakefuda A, Yamada H, Tsukamoto I, Taguchi T, Sakamoto S. Discovery of an N-(2-aminopyridin-4-ylmethyl)nicotinamide derivative: a potent and orally bioavailable NCX inhibitor. Bioorg Med Chem. 2005;13(12):4022–36.
67. Nagasawa Y, Zhu BM, Chen J, Kamiya K, Miyamoto S, Hashimoto K. Effects of SEA0400, a Na+/Ca2+ exchange inhibitor, on ventricular arrhythmias in the in vivo dogs. Eur J Pharmacol. 2005;506(3):249–55.
68. Nagy ZA, Virag L, Toth A, Biliczki P, Acsai K, Banyasz T, et al. Selective inhibition of sodium-calcium exchanger by SEA-0400 decreases early and delayed after depolarization in canine heart. Br J Pharmacol. 2004;143(7):827–31.
69. Otsomaa L, Levijoki J, Wohlfahrt G, Chapman H, Koivisto AP, Syrjänen K, et al. Discovery and characterization of ORM-11372, a novel inhibitor of the sodium-calcium exchanger with positive inotropic activity. Br J Pharmacol. 2020;177(24):5534–54.
70. Szlovák J, Tomek J, Zhou X, Tóth N, Veress R, Horváth B, et al. Blockade of sodium-calcium exchanger via ORM-10962 attenuates cardiac alternans. J Mol Cell Cardiol. 2021;153:111–22.
71. Duff HJ, Mitchell LB, Kavanagh KM, Manyari DE, Gillis AM, Wyse DG. Amiloride. Antiarrhythmic and electrophysiologic actions in patients with inducible sustained ventricular tachycardia. Circulation. 1989;79(6):1257–63.
72. du Toit EF, Opie LH. Role for the Na+/H+ exchanger in reperfusion stunning in isolated perfused rat heart. J Cardiovasc Pharmacol. 1993;22(6):877–83.
73. Scholz W, Albus U, Lang HJ, Linz W, Martorana PA, Englert HC, et al. Hoe 694, a new Na+/H+ exchange inhibitor and its effects in cardiac ischaemia. Br J Pharmacol. 1993;109(2):562–8.
74. Sack S, Mohri M, Schwarz ER, Arras M, Schaper J, Ballagi-Pordany G, et al. Effects of a new Na+/H+ antiporter inhibitor on postischemic reperfusion in pig heart. J Cardiovasc Pharmacol. 1994;23(1):72–8.
75. Theroux P, Chaitman BR, Danchin N, Erhardt L, Meinertz T, Schroeder JS, et al. Inhibition of the sodium-hydrogen exchanger with cariporide to prevent myocardial infarction in high-risk ischemic situations. Main results of the GUARDIAN trial. Guard during ischemia against necrosis (GUARDIAN) investigators. Circulation. 2000;102(25): 3032–8.
76. Zeymer U, Suryapranata H, Monassier JP, Opolski G, Davies J, Rasmanis G, et al. The Na(+)/H(+) exchange inhibitor eniporide as an adjunct to early reperfusion therapy for acute myocardial infarction. Results of the evaluation of the safety and cardioprotective effects of eniporide in acute myocardial infarction (ESCAMI) trial. J Am Coll Cardiol. 2001;38(6):1644–50.
77. Mentzer RM Jr, Lasley RD, Jessel A, Karmazyn M. Intracellular sodium hydrogen exchange inhibition and clinical myocardial protection. Ann Thorac Surg. 2003;75(2):S700–8.
78. Gazmuri RJ, Radhakrishnan J, Ayoub IM. Sodium-hydrogen exchanger Isoform-1 inhibition: a promising pharmacological intervention for resuscitation from cardiac arrest. Molecules (Basel, Switzerland). 2019;24(9):1765.

Gap Junctions and Cardiac Impulse Propagation. New Aspects of Arrhythmogenesis and Antiarrhythmic Agents Targeting Gap Junctions

14

Stefan Dhein and Aida Salameh

Abstract

A basic phenomenon of the heart is its regular beating and a directed propagation of the electrical impulse which, during the plateau phase of the action potential, initiates contraction. The heart is a network of inter-communicating cells, allowing such a directed spread of activation. Cardiomyocytes communicate among each other and to a certain degree with non-cardiomyocytes such as fibroblasts. Action potentials are transferred from one cell to the next by intercellular communication channels, the gap junction channels, formed as dodecameric channels from protein subunits called connexins. In the heart, the main connexin isoforms are Cx43 (the 43 kDa connexin; ubiquitous), Cx40 (mostly in the atrium and specific conduction system) and Cx45 (in early developmental states and between fibroblasts and cardiomyocytes). Gap junction channels allow the intercellular transfer of current and small molecules (<1000 Da). Regarding arrhythmia, a specific feature of gap junctions is that they are normally found at the cell poles, thereby contributing to the heart's anisotropic properties, while in cardiac disease, these channels are often found at the lateral borders of the cells. Moreover, a broad number of stimuli can regulate the channels. Thus, ions like H^+, Ca^{++} and Na^+, as well as ATP-loss, acylcarnitines, and lysophosphoglycerides, among others, can close the channels. Since these factors occur during cardiac ischemia, they lead to electrical isolation and silencing of the ischemic area. This alters the current source/sink ratio at the border, which will affect successive conduction.

Antiarrhythmic peptides, such as AAP10 enhance the Cx43-gap junction current by preventing the channels from uncoupling. This effect of AAPs is mediated via PKCα--activation and PKC-dependent phosphorylation of Cx43. The effect of AAP10 is pronounced in areas of increased de-phosphorylation and thereby shows a preference for ischemic tissue. These new agents open novel pharmacological options for prevention of ischemia-associated ventricular fibrillation.

Keywords

Cardiomyocytes · Fibroblasts · Heterocellular communication · Connexins · Lateralisation · Anisotropic conduction · Current source/sink ratio · Ischemia · Antianrhythmic peptide 10

S. Dhein (✉)
Institute of Pharmacology and Toxicology, University of Leipzig, Leipzig, Germany
e-mail: stefan.dhein@medizin.uni-leipzig.de

A. Salameh
Clinic of Pediatric Cardiology, Heart Centre Leipzig, University of Leipzig, Leipzig, Germany

© Springer Nature Switzerland AG 2023

O. N. Tripathi et al. (eds.), *Heart Rate and Rhythm*, https://doi.org/10.1007/978-3-031-33588-4_14

14.1 Introduction

The heart is a rhythmically beating organ serving as a pump. A basic feature of this organ is to maintain a regular rhythm and to adapt the frequency of beating to the actual demands of the organism. The pumping function of the heart requires coordinated contraction of the myocardium, i.e. contraction should start in the lower parts at the apex cordis and proceed to the free walls towards the valves, with a small delay of a few milliseconds between right and left ventricle. This is necessary to allow the directed propulsion of the blood. Any disturbance of this coordination, e.g. dys-synchrony, will lower the efficacy of the pump.

To maintain this feature, electrical activation of the myocardium is coupled to the contraction (electro-mechanical coupling), so that contraction starts after reaching the plateau phase of the action potential, and the working myocardium is activated by the specific conduction system, which ends up in the tree of the Purkinje fibres. From the Purkinje fibre endings in the lower parts of the heart near the apex, the activation wave propagates through the working myocardium from cell to cell.

The working myocardium is organized as a functional syncytium, thus enabling a coordinated response. This feature is realized via intercellular communication channels, which are called gap junction channels. These gap junction channels form intercellular low resistance contacts enabling the transfer of electrical current (for action potential transfer) and the exchange of small molecules (maximum size: about 1000 Da) such as cAMP [1]. These channels function as ohmic resistors for voltage differences of ±50 mV with <200 ms duration [2–5].

The gap junction coupling is highly regulated: the conductance is regulated by a number of factors either enhancing (e.g. PKCα, in certain cases: PKA) or reducing (e.g. H^+, Ca^{++}, Na^+, loss of ATP, PKCε, acylcarnitine) coupling (see below; for review see [6, 7]); moreover, the synthesis of gap junction channel proteins is regulated as well as their insertion into the membrane and their degradation via proteasomal or lysosomal pathways, thus regulating channel density [8]. Interestingly, gap junction proteins possess a relatively short half life time (about 90 min for Cx43) [9–11], which means a rapid turnover of the channels as compared to other integral membrane proteins. The gap junction channels are preferentially situated at the poles of the cells, and only a small part is inserted at the lateral side of the cardiomyocytes [12, 13]. In cardiac diseases such as cardiomyopathy, hypertrophy, post-infarction or atrial fibrillation, however, the amount of lateral gap junction protein often is up-regulated, and it has been speculated that this may change the biophysics of the tissue [14, 15] However, this is still a matter of debate. It seems that certain pathways regulate the trafficking of gap junction proteins and the location of their membrane insertion. However, this process and its regulation is -at present- not well understood. It can be assumed that a permanent adaption of the communication features to the actual situation and actual needs seems to be very important for the cell. Thus, it was shown that 24 h cyclic mechanical stretch can influence the localisation of Cx43 [16, 17].

Gap junction coupling is a prerequisite for the propagation of electrical activation. While the availability of sodium channels for activation determines the propagation velocity along the cell [18], the coupling of gap junctions controls the spreading of excitation from one cell to the next [19]. The sum of both processes gives the final macroscopic conduction velocity resulting in longitudinal velocities of 0.4–0.7 m/s and transverse velocities of approximately 0.1–0.2 m/s [20–22].

Another function related to gap junction coupling is that small differences in the endogenous action potential duration of each cell will be smoothened since each difference in action potential duration results in a voltage gradient between the cells, which will cause a gap junction current between these cells that will equalize the potential durations. Thus, local dispersion or inhomogeneity is kept at a minimum by gap junction coupling.

From the considerations above, it follows that decoupling can lead to slowing of conduction, which will probably affect transverse conduction to a greater extent than longitudinal conduction [21, 22], as well as to enhance local dispersion of action potential duration. Thereby, gap junction decoupling can contribute, facilitate or even cause (in certain situations) cardiac arrhythmia.

14.2 Structure, Function and Regulation of Cardiac Gap Junctions

Cardiac gap junctions are found in clusters located in the intercalated disks. The distance between the two neighbouring membranes is narrowed to about 4 nm and is bridged by the intercellular communicating gap junction channels (outside the intercalated disk, the normal distance between the membranes is about 20 nm) [23]. Each gap junction channel is formed by two neighbouring cells with each cell contributing a hemichannel. These hemichannels dock with each other via their extracellular loops and thus form the intercellular communication channel. A gap junction channel consists of 12 protein subunits, the connexins. Six connexins constitute a connexon or hemichannel.

At present, the connexins represent a protein family with 21 isoforms in humans and 20 isoforms in mice [24, 25] (Table 14.1). A connexin protein has an intracellular C- and N-terminus, four transmembrane domains and two extracellular loops, the latter being stabilized by intramolecular disulfide bonds. The most variable region of these proteins is the C-terminal domain. Its length and molecular weight vary among the isoforms, which are named Cx followed by a number indicating the molecular weight in kDa, i.e. Cx43, the most abundant connexin, has a molecular weight of 43 kDa. Often the name is preceded by a suffix indicating the species, i.e. hCx43 means human connexin43, and rCx40 means the rat connexin40. Two connexons of two neighbouring cells dock to each other via H-bonds (Fig. 14.1). It is possible that the complete dodecameric channel consists of only 1 isoform, and thus is homomeric and homotypic. However, it is also possible that a connexon is formed of two isoforms and thus is heteromeric. Moreover, it is possible that two connexons of different compositions form the channel, which then is heterotypic. Since each isoform has specific biophysical properties with regard to conductance and voltage-dependent inactivation a broad range of channels can be composed.

The process of opening and closing the gap junction channel is commonly considered as realised via a twisting motion. Interestingly, the single channel conductance can vary between several states, a closed state, a residual state, and several conducting states. The preference for a certain state can be regulated by phosphorylation of the C-terminal [26].

Although gap junctions serve as low resistance pathways for spreading the action potentials, an almost 90% reduction in the number of gap junction channels will lower conduction velocity by only 25% [27]. This is however still a matter of debate and might be different in hypoxic or partially depolarised cells within areas of uneven or inhomogeneous current source/sink relationships.

The macroscopic gap junction conductance follows the equation

$$g(\mathrm{GJ}) = N^{*}\gamma^{*}\ P_o$$

(N = number of channels; γ = single channel conductance; P_o = open probability)

Single channel conductance is regulated by phosphorylation processes via PKC (various isoforms have different effects), PKA, PKG, and MAPKs [26, 28], or by ions such as Na^+, H^+ and Ca^{2+} [2]. Whether P_o also might be regulated is under discussion [29]. As a results macroscopic gap junction conductance can be acutely regulated by a number of stimuli (see Table 14.2).

Regulators, such as acidosis (H^+), Na^+ and Ca^{2+}-overload, loss of ATP and acylcarnitines—among other factors play a particular role in

Table 14.1 Cardiovascular connexin isoforms; t½ is indicated for those connexins, if known [24]

Murine Connexin	Human Ortholog (if different)	Organ	Cardiac localisation/Function
Cx 30.2	Human: Cx31.9	Heart	Conduction system (low levels)
Cx37		Endothelium	
Cx40		Heart, vasculature (endothelium and smooth muscle)	Atrium, conduction system
Cx43		Ubiquitous in heart and vessels Many other organs	Working myocardium, atrium, and partially in the conduction system; t½ = ca. 1.5 h
Cx45		Heart	Conduction system and early develop-mental states t½ = ca. 3–4 h
	hCx30.2	Heart	Unknown function
	hCx31.9	Heart	Unknown function
	hCx40.1	Heart	Unknown function
	hCx62	Heart	Unknown function

For the last 4 connexins, there is no murine counterpart [23]

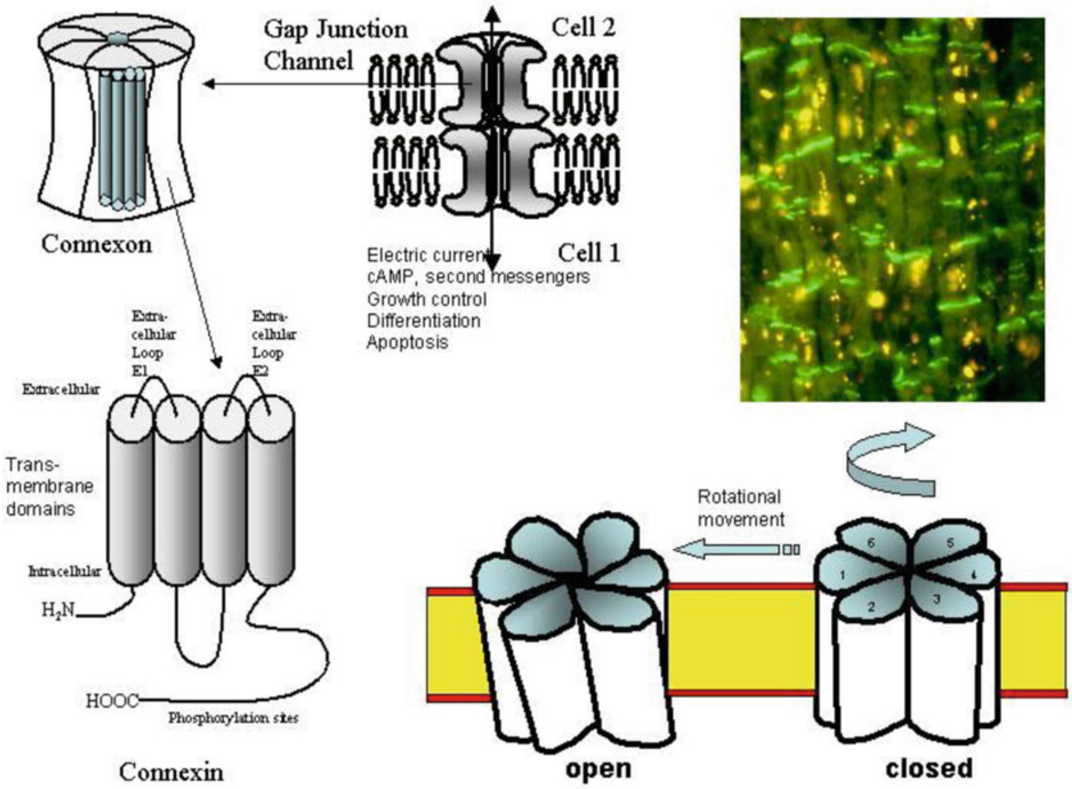
Gap Junction Channel
Cell 2
Connexon
Electric current
Cell 1
cAMP, second messengers
Growth control
Differentiation
Apoptosis
Extra-cellular Loop E1
Extra-cellular Loop E2
Extracellular
Trans-membrane domains
Intracellular
H_2N
HOOC
Phosphorylation sites
Connexin
Rotational movement
6
5
1
4
2
3
open
closed

Fig. 14.1 Cx43 (green) distribution in the human atrium (upper right). Note the location at the cell poles. Gap junction channel (upper middle) made from 2 connexons (upper left), each of which consists of 6 connexins (lower left). Opening and closure is thought to be realized via a rotational movement (lower right)

Table 14.2 Stimuli affecting acute macroscopic gap junction conductance

Stimulus	Opening	Closure	Comment
$H^{+;}$ CO_2		X	Takes 7–10 min.
Na^+, Ca^{++}		X	
Acylcarnitine, lysophosphoglycerides		X	In ischemia/ reperfusion injury
ATP loss		X	In ischema
Arachidonic acid, oleic acid, palmitoleic acid, hepantol, octanol, narcotics (halothane)		X	Via incorporation and/or via altered phosphorylation?
PKC stimulation (e.g. phorbol esters)		X	Depends on PKC isoform
cAMP or cAMP enhancing drugs (isoprenalin, forskolin)	X		Via PKA, in Cx40- or Cx45-coupled cells
PKA	X		In Cx40- or Cx45-coupled cells
Antiarrhythmic peptides, AAP10, rotigaptide	X		Via PKCα

ischemia and contribute to ischemic closure of gap junctions which occurs after about 20 minutes of ischemia [30]. On the one hand, this isolates the ischemic area electrically and thereby reduces oxygen consumption, and, on the other hand, leads to changed geometry of the spread of activation which can initiate or facilitate arrhythmia.

Another possibility to regulate gap junction communication is to affect the number of channels (see Table 14.3). Connexins are synthesized in the SR, then folded and transported to the trans-Golgi network under modulation by low-density lipoprotein receptor-related protein 6 [31], where they are oligomerized to connexons, and thereafter transported to the membrane [32–34], where they move probably on lipid rafts in cholesterol-rich domains until they dock to a hemichannel of a neighbouring cell, typically in regions with N-cadherin and ZO-1 protein [35]. With a short half-life time of around 90 min, they are degraded via phosphorylation, ubiquitinylation and proteasomal degradation, or in some cases via lysosomal degradation [8, 36]. The latter normally is inhibited by the presence of desmoplakin [37].

Finally, the localisation of the channels can be regulated. Thus, it could be shown that mechanical stimuli like stretch can influence whether channels are concentrated at the cellular poles [16, 38]. This process of stretch-dependent Cx-localisation is regulated via focal adhesion kinase FAK [17]

14.3 Propagation of the Cardiac Impulse

14.3.1 Cable Theory

The passive electrical properties of a muscle bundle in a first approximation are similar to passive cable properties: cables formed by cells coupled in series via ohmic resistors with each cell representing a resistor with a parallel capacitor (see Fig. 14.2; for review, see [39]). The change in voltage is a function of distance (x) according to V_x=V_{x0}(exp-x/λ) with the length constant $\lambda = \surd(r_m/r_i)$ (r_m = membrane resistance; r_i = internal longitudinal resistance); the input resistance at $x = 0$ can be described as $r_{\text{input}} = V_{x0}/I = r_i\lambda$. Due to the fibre geometry, the specific membrane resistance R_m equals $2\pi a r_m$ [Ωcm^2] and specific internal resistance $R_i = \pi a^2 r_i$ [Ωcm]. The specific membrane capacitance can be described as $C_m = \tau/R_m$ with τ = time constant. In a multicellular preparation with parallel running fibres the longitudinal resistance of the extracellular space r_o also has to be considered. For these conditions $\lambda = \surd(r_m/(r_i+r_o)))$ and the conduction velocity, $\theta = \surd(1/(T_{\text{foot}}C_m(r_i+r_o)))$. However, this cable theory, originally formulated for nerve axons [40] and later on for Purkinje fibres [41], holds true for a continuous cable.

In the heart, the situation is more complex, and there are discontinuities between the fibres at the cell–cell contact zones, where two membranes are closely neighboured, connected via extracellular fluid and the two cytoplasmata are connected via

Table 14.3 Stimuli regulating the number of cardiovascular gap junction channels

Stimulus	Enhanced number	Enhanced degradation	Comment
Phenylephrine (α-adrenergic stimulator)	Cx43		via PKC, MAPKs (cardiomyocytes)
Isoprenaline (β-adrenergic stimulator)	Cx43		via PKA, MAPKs (cardiomyocytes)
Angiotensin-II	Cx43		via AT_1 receptors (cardiomyocytes)
Endothelin	Cx43		via ET_A-receptors (cardiomyocytes)
Thyroid hormone	Cx40, Cx43		Mechanism unclear
VEGF	Cx43		via TGFβ
bFGF		Cx43	via PKCε
EGF		Cx43	Enhanced internalization
Nicotine		Cx37, Cx43	via nACh-R (endothelium)

a low resistance gap junction channel (Fig. 14.2, lower part). The electrical situation is very complex at the cell–cell border, in particular, because Na channels are probably clustered at these cell-cell contact zones [42, 43], which are supposed to enable ephaptic coupling under certain conditions (see below).

14.3.2 Ephaptic Coupling

Prior to the understanding that gap junctions act as low resistance pathways between cells, the theory of ephaptic (i.e., field effect) coupling was formulated [44, 45] under the assumption that the two neighboured cells can be considered similar to two closely packed capacitors.

Capacitive coupling and electrical field coupling have been proposed as alternative mechanisms of electrical transmission. For several physical reasons ((a) junctional capacitive coupling would be decreased by a factor of 2 since the junction resembles two capacitors in series; (b) if only a small portion of the intercalated disk is involved, the total capacitance would be accordingly smaller; (c) there may be a shunt to ground if the two membranes are not close enough to each other), capacitive coupling may not be operative in normal cardiac tissue [44]. Electrical field coupling [46] means the induction of an action potential in the post-cell by the electrical field arising from the action potential at the intercalated disk of the pre-cell. Accumulation of K^+ in the cleft of the intercalated disk is an important factor allowing the membrane of the pre-cell at the intercalated disk to fire a fraction of a millisecond earlier than the surface membrane, which was necessary for effective coupling. At present, it is uncertain what the contribution of electrical field coupling to electrical transmission is in normal tissue. Computer simulation studies, however, indicate that in certain situations, ephaptic coupling by electrodiffusion may play a role [47]. This is further supported by new investigations demonstrating that the perinexus region at the border of the gap junctions contains voltage-gated sodium channels in sufficiently close proximity to allow ephaptic coupling [48, 49]. In addition, potassium channels in the perinexus region also seem to contribute to this type of coupling [50].

14.3.3 Gap Junction Coupling

If two cells are manipulated into intimate side-to-side contact, initially, there is no transmission of electrotonic potentials or action potentials from one cell to the other [19]. After the cells establish new gap junctions, action potential transfer is possible [19]. This experimental result is contrary to the theory of ephaptic impulse transmission or of electrical field coupling [44]. The time delay at gap junctions has been determined with 0.21–0.27 ms [51]. Taken together, the most

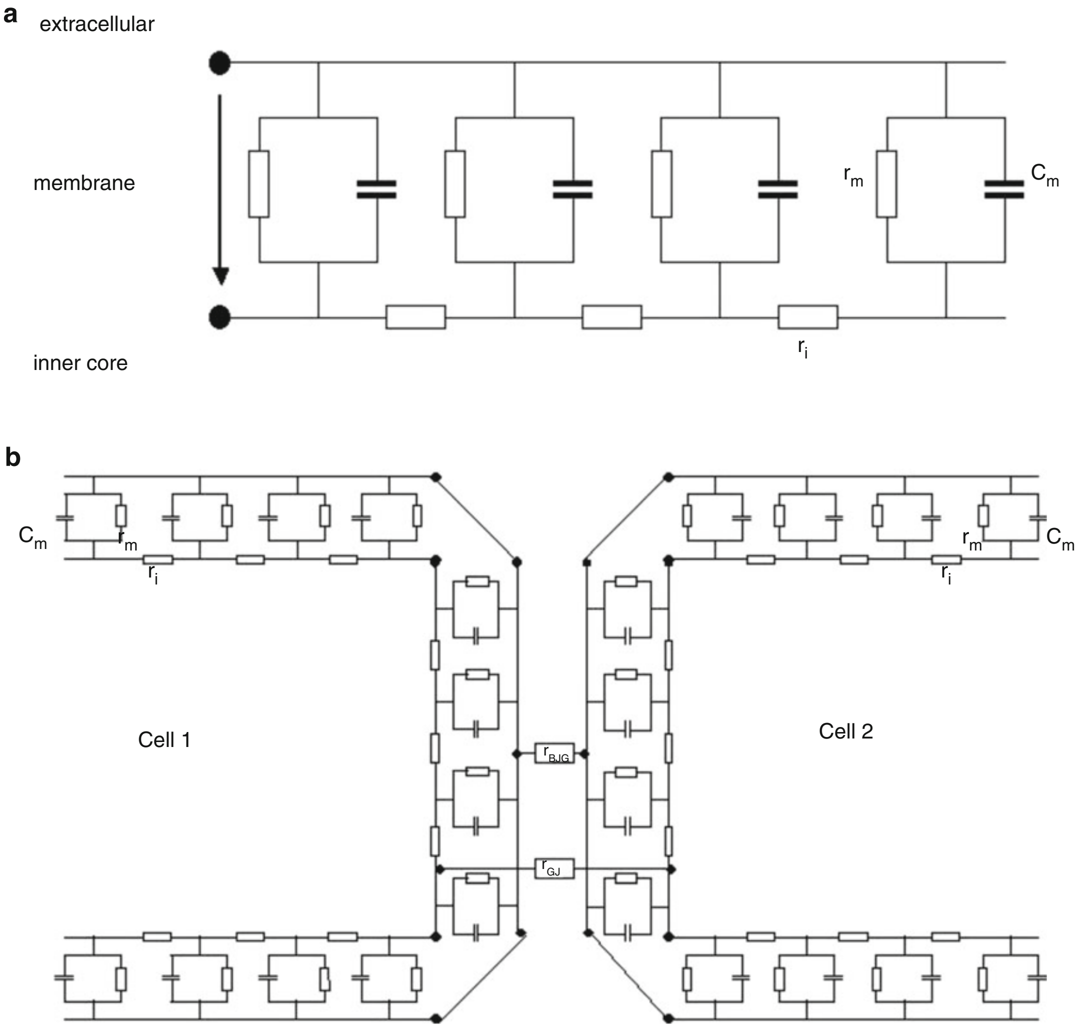

Fig. 14.2 continuous cable (upper part) and discontinuous cable (lower panel), where the two cells are interconnected via (a) an extracellular resistance (extracellular fluid) (r_{exc}) and (b) the cores via gap junction resistances (r_{GJ})

important mechanism under physiological conditions for the transmission of excitation is coupling via the gap junction channels.

14.3.4 Anisotropy and Non-uniformity (Inhomogeneity)

Basic features of cardiac tissue are (a) anisotropy (i.e. longitudinal resistance is lower than transverse resistance), (b) discontinuity (i.e. fibres are separated by intercalated disks (in contrast to continuous cable)), and (c) non-uniformity (i.e. the degree of anisotropy varies from area to area due to variability in morphology and deposition of connective tissue or existence of other non-conducting structures like fat or vessels). The difference between uniform and non-uniform anisotropy has many consequences for the pathophysiology of arrhythmia [52]. In diseased myocardium, the expression of gap junction proteins often is changed. For example, Cx43 levels are decreased in chronic infarction or in heart failure or enhanced in cardiac hypertrophy and in certain forms of atrial fibrillation [12–15, 53, 54]. Moreover, in some of these situations, the ratio Cx43/Cx40 was shifted and, probably most importantly, much of the gap junction protein was not found at the cell poles but at the lateral sides of the cells (lateralization) [14, 15]. These factors probably enhance non-uniformity in cardiac disease. In non-uniform anisotropic tissue, fractionated extracellular waveforms are typically encountered. Such complex waveforms with multiphasic shapes can be interpreted as the reflection of discontinuous propagation, and each of the multiple negative peaks represents the activation of a small group of fibres. With increasing age, there is a general change in the biophysical properties of the cardiac tissue from uniform to non-uniform anisotropy due to the predominant uncoupling of side-to-side connections [52, 55, 56].

14.3.5 Source–Sink Problem

It has been observed that the action potential upstroke velocity and amplitude were greater during transverse propagation, accompanied by a faster foot potential, which led to the hypothesis that longitudinal propagation, although faster, is more vulnerable to block because of its lower upstroke velocity and amplitude. This behaviour can be explained on a theoretical basis: the upstroke velocity increases as a result of reduced coupling [22] since current cannot pass to the neighbouring cells.

Transfer of an action potential principally means that current has to flow from a current source to a sink. This current flow is highly dependent on gap junction conduction; however, the relationship is not trivial, since the dimensions of source and sink have to be taken into account: if a small source, represented by a tiny strand of activated cardiomyocytes, meets a large sink (large area of non-activated cardiomyocytes) current will flow radially to many sites so that the current is divided between many neighbours and in each of these neighbouring cells this current may be too low to allow propagation, resulting in conduction failure [57, 58]. Moreover, this behaviour is critically modulated by gap junction conductance: if in this situation of source–sink mismatch, gap junction conductance is low, this may preserve conduction by limiting fast current loss to many sites. On the other hand, if there is high coupling this might enable conduction failure by current loss.

These phenomena can be mathematically described by the safety factor SF of propagation as $SF = Q_c + Q_{out}/Q_{in}$ (= charge produced/charge consumed) [59, 60]. If coupling is reduced gradually, the safety factor first is enhanced, but, if very low levels of coupling are reached, SF will be reduced until conduction failure if $SF < 1$. In contrast, if I_{Na} is reduced, this will result in a progressive reduction of SF. However, propagation velocity will be reduced in both situations [59, 60].

Situations related to these source-sink problems may be found at the end of a Purkinje fibre or at the border between normal cardiac tissue and an ischemic (electrically silent, depolarised and uncoupled) region.

14.4 Role of Gap Junctions in Arrhythmogenesis

From the considerations above, one can imagine that disturbances of gap junction intercellular communication (GJIC) may result in altered conduction, thereby finally leading or contributing to cardiac arrhythmia. There are several arrhythmias that are –at least in parts – related to changes in gap junction coupling: acute ischemia, digitalis intoxication, aconitine intoxication, acidosis, and remodelling (chronic ischemia; atrial fibrillation, heart failure, cardiac hypertrophy).

14.4.1 Acute Ischemia

During ischemia, Cx43 becomes de-phosphorylated within 30 min [20, 61–63] due to the shortage in ATP [64] and the reduced thermodynamic driving force for phosphorylation

[61]. This de-phosphorylation together with Ca^{2+}-overload [30, 65, 66], intracellular acidosis [65–67] and accumulation of lipid metabolites such as lysophospholipids and arachidonic acid metabolites [68, 69] contributes to acute ischemic gap junction uncoupling. An increase in intracellular Na^+ might also promote uncoupling since it was shown that H^+, Ca^{2+} and Na^+ can uncouple gap junctions [2, 65, 70–73]. The consequences are an acute closure of gap junctions and – via de-phosphorylation – and reduced presence in the membrane probably by removal of gap junctions. This reduction at the membrane can be seen within 30 min of ischemia in the ischemic centre and border [20] and was described as a translocation of Cx43 from the membrane to the cytosol [63, 74]. In addition, Cx43 becomes de-phosphorylated in hypoxia, at least in part by reduced casein kinase-1-dependent phosphorylation [75]. In consequence, the ischemic area becomes uncoupled, and thereby, activation spreading is slowed or ceased so that the ischemic centre becomes electrically isolated, due to gap junction uncoupling and to depolarisation (which results in lower I_{Na} availability). Additionally, since the low resistance shortcuts between the cells are closed, local inhomogeneities in action potential duration cannot be equalized, so that the dispersion is enhanced [20]. These inhomogeneities together with the conduction slowing can lead to a close neighbourhood of still activated cells and already inactivated (excitable) cells, thereby enabling the occurrence of re-entrant arrhythmia. There are two peaks of ventricular fibrillation (VF) in acute ischemia: the first within the first 10 min (type IA VF), which has been ascribed to depolarisation, mechanical factors and catecholamine release, and a second after ca. 20 min (type IB VF), which has been shown to be dependent on gap junction uncoupling [30, 76, 77].

Against the hypothesis of a role for uncoupling, Jongsma and Wilders [27] showed that under normoxic conditions, a 90% decrease in the number of gap junctions is required for a 25% reduction in conduction velocity. It is unclear whether this also holds true for hypoxic conditions. However, heterozygous Cx43 knock-out mice under standard conditions also exhibited only a 25% reduction in conduction velocity [78–80]. Some authors interpret this as a hint for the existence of ephaptic coupling [45]. In simulated ischemia, gap junction coupling of cell pairs remained large enough to equilibrate action potential duration between the coupled cells until inexcitability occurred [81].

On the other hand, there are studies in favour of a role of gap junctions in acute ischemia. For example, the number of hearts exhibiting pacing-induced ventricular tachycardia was significantly higher in $Cx43^{+/-}$ mice than in $Cx43^{+/+}$ [79]. Moreover, we could demonstrate that the antiarrhythmic peptide AAP10 (H_2N-Gly-Ala-Gly-Pro-[4-OH-Pro]-Tyr-$CONH_2$), which enhanced macroscopic gap junction conductance in animals [82–84] and in humans cardiomyocytes [85] without affecting the action potential, could prevent from type IB VF in isolated rabbit hearts [86]. Similar antiarrhythmic effects could also be shown by another group using a chemical derivative of AAP10 (ZP123, now called rotigaptide) [87]. These latter results indicate that gap junction uncoupling probably contributes to type IB ischemic VF. For a detailed review and discussion, see [88].

14.4.2 Intoxications (Digitalis)

Ventricular arrhythmia is the most serious complication of digitalis intoxication. While certainly depolarization caused by Na^+/K^+-ATPase inhibition and enhanced automaticity plays a role, the Na^+/K^+-ATPase inhibition results in increased intracellular $[Na^+]$ and $[Ca^{2+}]$ via altered dynamics of the Na^+/Ca^{++} exchanger. It is known that both intracellular $[Na^+]$ and $[Ca^{2+}]$ can promote cellular uncoupling [5] and that ouabain leads to gap junction uncoupling at 0.68 μM [73], a concentration that is typically reached or exceeded with intoxication. Thus, gap junction uncoupling may play a contributory role in digitalis intoxication.

14.4.3 Acidosis

Gap junctions uncouple in acidotic areas. According to our own experience, pH has to be reduced to values below 6.5 to provoke uncoupling, which develops slowly after a latency of about 7–10 minutes [85], while gap junction conductance (g_j) is nearly constant in a pH range from 7.4 to 6.5 [2]. The pH–g_j-relationship is principally not affected by intracellular pCa. In neonatal rat heart cells, Firek and Weingart [89] found a pK_H of 5.85. One H^+ binding site could be identified as histidine-95 in cardiac connexin 43 [90]. Hermans and colleagues [91] investigated the effects of site-directed mutations in Cx43 transfected SKHep1 cells by exchange of His-126 and His-142 and found an uncoupling effect of acidification related to the position of histidines in the cytoplasmic loop rather than to the total number of histidines. They reported that a fall in pH_i caused a reduction in channel open probability but not in channel conductance. Using a transfection system, it was found that Cx45 channels are more sensitive to pH than Cx43 channels [91]. Regarding the pH sensor, the carboxy tail length has been demonstrated to be a determinant of pH sensitivity [72, 92] and is thought to occlude the channel, comparable to the ball-and-chain-model for N-type inactivation of potassium channels.

14.4.4 Chronic Infarction

After myocardial ischemia, the tissue is submitted to complex remodelling processes starting with increased fibrosis. Among these changes, gap junctions are also remodelled with a decrease in Cx43 and altered distribution of Cx43 and Cx40 [13]. Local contractility is reduced, and the necrosis zone is replaced by connective tissue. Fibroblast growth factor FGF-2, which can be released from cardiomyocytes during contraction and after stimulation with catecholamines, is up-regulated in response to myocardial damage and can decrease intercellular dye coupling in cardiomyocytes, whereas in fibroblasts coupling may be enhanced [93, 94]. It is unclear whether this result from neonatal cardiomyocytes also holds true for adult cardiomyocytes. These changes might be somehow linked to arrhythmias observed after myocardial infarction originating from abnormal conduction of activation in the vicinity of scar areas [95] and slowed anisotropic conduction [96].

The effects seen in the *chronic* phase of ischemia (i.e. infarction) are (a) loss of the common ordered (polarized) distribution of the gap junctions, which was found predominantly in the border zone adjacent to infarct scars and (b) reduction in the quantity of connexin 43 gap junctions in areas distant from the infarct zone [12, 13], which may lead to heterogeneous anisotropic conduction with locally slowed conduction despite nearly normal active properties of cells [96–98]. Gap junctions belong to the most important determinants of these passive conduction properties [95, 99]. In the border zone of healed infarcts (some hundred micrometers from the infarct scar), the distribution of gap junctions is significantly altered, and connexins are scattered over the whole membrane and no longer confined to the cell poles (intercalated disks), although some of the cells show the normal type of distribution, while in the non-ischemic-normal areas there is a regular distribution [12]. In addition, fibroblast/myocyte coupling probably plays an additional pathophysiological role [100]. Interestingly, successful conduction can be established between cardiomyocytes separated by (non-excitable) fibroblasts over a distance of up to 300 μm [58].

Decrease in Cx43, altered Cx43/Cx40 ratio, lateralization in the subcellular gap junction distribution, decrease in gap junction number, and alterations in gap junction size, remodelling processes and fibroblast/myocyte coupling all together initiate a complete change in the biophysical architecture of the tissue with a high degree in heterogeneity and non-uniform anisotropy forming an arrhythmogenic substrate.

14.4.5 Atrial Fibrillation (AF)

In the atrium, Cx43 and Cx40 mediate gap-junctional intercellular communication GJIC. A common finding in AF is an increased heterogeneity in the regional distribution of gap junctions regarding the amounts of Cx43 and Cx40 [14, 101, 102] (with various findings, probably depending on the accompanying diseases (coronary heart disease, heart failure, mitral valve disease, hyperthyreosis or on the disease model or the tissue under investigation (right atrium or left atrium)). Moreover, alterations in the subcellular distribution have been found with enhanced expression of connexins at the lateral side of the cells (lateralization) [14, 15]. Thus, the question arises: what is the specific role of gap junctions in AF?

Regarding *initiation*, AF mostly originates from left atrial sleeves, which protrude from the atrium into the pulmonary veins and form circumferential structures which are coupled by Cx43 and to a lower extent by Cx40 [103]. Among many other factors, this circumferential structure of conducting tissue around the pulmonary veins seems to be necessary for the initiation of a first re-entrant circuit from which AF develops. Obviously, other factors (stretch, heterogeneity, fibrosis, ANF, amyloid, ischemia, age, vagal tone, angiotensin, Ca^{2+}) may also contribute to the initiation of AF. Thus, gap junctions do not seem to be directly/causally involved in AF initiation. However, in some cases, mutations of Cx40 and Cx37 have been described [104, 105]. P88S, G38D and A96S mutations of Cx40 were shown to slow conduction, thereby increasing the propensity for AF induction [106].

Regarding *maintenance of AF*, there is evidence that gap junction remodelling is an important factor leading to the formation of an arrhythmogenic substrate. In lone AF, we found an up-regulation of Cx40, while Cx43 was little affected [14, 107]. Connexin up-regulation was also found in patients suffering from postoperative AF [53]. Moreover, we found that connexins were localized to the lateral sides of the cardiomyocytes (lateralization) [14], which was later verified [15]. Others found also an up-regulation of Cx43 in the right atrium [108]. An additional factor found by Kostin and colleagues [15] is increased heterogeneity in the presence of connexins with the free right atrial wall showing elevated Cx40 but reduced Cx43 expression and the appendage with both connexins being reduced. In another patient population (AF with underlying mitral valve disease), we found Cx43 being up-regulated in the left but not in the right atrium. This up-regulation was accompanied by an elevated expression of AT1-receptors in the left but not right atrium [54]. Since we have also shown that angiotensin-II can up-regulate Cx43 via AT1-receptors [109], and since it is now known clinically that the maintenance of SR after cardioversion is improved if ACE inhibitors are applied, one may suppose that angiotensin-II might be involved in the gap junction remodelling process. Moreover, the perinexal width seems to be greater in AF patients [110].

The findings in humans differ from animal disease models with regard to the expression level of certain connexins [102, 111–113], but a common phenomenon in most species seems to be regional heterogeneity of connexin expression and lateralization. These latter effects will probably change the biophysics of the tissue and may lead to local conduction slowing and to irregular spread of activation, which together with the other factors enable AF to persist. By gap junction remodelling AF becomes structurally fixed. For a detailed review and discussion see [114].

14.4.6 Heart Failure and Cardiac Hypertrophy

If the muscular force of the heart is chronically reduced, compensatory mechanisms lead to cardiac hypertrophy and remodelling processes. A basic mechanism is the activation of the sympathetic nervous system and of the renin-angiotensin-aldosterone cascade and probably of endothelin with stimulation of α_1- and ß-adrenergic receptors as well as AT_1-receptors and ET_A-receptors, which all are known to enhance Cx43 expression [109, 115]. In addition, fibrosis is increased in most types of cardiomyopathy. These changes affect the conducting properties as well. Due to the altered morphology, the cells are larger, which affects both longitudinal and transverse velocity. Fibrotic strands, mostly parallel to the fibres, lead to a transverse separation of the fibres and can reduce transverse propagation. Due to the inhomogeneous nature of fibrosis and the changes in tissue architecture, it is reasonable to assume that the resulting changes in conduction will also be heterogeneous. In addition, it has been shown, that gap junction distribution becomes heterogeneous in de-compensated hypertrophy with areas of tissue with normal, very low or no expression of gap junction [116]. In dilated cardiomyopathy and myocarditis, focal disarrays of gap junctions were found [117]. In compensated hypertrophy, Kostin et al. [116] observed lateralization of Cx43. Thus, heart failure and hypertrophy seem to be associated with a dis-organisation (heterogeneity, lateralization) of gap junctions (= structural remodelling). Lateralization of connexin43 was also seen in patients suffering from hypertrophic obstructive cardiomyopathy (HOCM) [118]. Regarding the level of connexin expression, it was found that Cx43 expression was diminished in patients suffering from congestive or ischemic heart failure [99, 119], or that there was a heterogeneous loss in non-ischemic dilated cardiomyopathy with ventricular tachycardia [120]. In HOCM, however, the Cx43 expression was enhanced [118], as it was in guinea pig hearts with renovascular hypertrophy [121]. It has been hypothetized that the decline in Cx43 expression in manifest heart failure is preceded by an increased expression during the phases of compensated hypertrophy [116]. The up-regulation in hypertrophy was also seen in cell culture models of cardiac hypertrophy and, thus, has been suggested to be possibly related to adrenergic or angiotensinergic stimulation [109, 115]. Interestingly, Yamada et al. [122] reported that Cx45 was up-regulated in heart failure in parallel to decreased Cx43 expression. Cx40 does not seem to be elevated in idiopathic dilated cardiomyopathy, but was found to be elevated in ischemic heart failure [119].

Nevertheless, while the level of connexin expression apparently depend on the phase of the disease [13, 116, 123], a common phenomenon seems to be the changes in the network architecture with lateralization of gap junctions, heterogeneous expression of connexins, and with transverse separation of the fibres by strands of connective tissue. New investigations show that angiotensin II seems to regulate this lateralization via a guanylylcyclase associated with Cx43 [124]. Regarding the functional consequences there is still an ongoing debate about the contribution of cardiomyopathic gap junction remodelling to ventricular arrhythmia. While ventricular arrhythmia and conduction disturbances in cardiomyopathy are clearly present, there is a plethora of factors, which may be involved, and which is out of the scope of the present article. However, the changes described above may lead to local conduction slowing in areas without gap junctions or with very low levels. As stated above, it was argued that reductions below 50% are necessary to affect conduction significantly [27]. However, these considerations did not take into account fibrotic strands, enlarged cells, heterogeneity, together with altered electrophysiology in heart failure. Taken together, these factors may lead to altered source–sink ratios, so that it might be imagined that even lower reductions in connexin level could affect conduction in diseased myocardium (see above). It has been speculated that lateralized gap junctions may enable transverse conduction or may facilitate re-entrant circuits, although this has not been clearly shown in the diseased ventricle until now. It would be a prerequisite that these lateralized gap junctions are functional, and that in such area, the cells are not separated by fibrotic strands. It will be difficult to prove, whether these lateralized gap junctions are functional or not. However, a large reduction in Cx43 expression levels will probably slow conduction, and an up-regulation of Cx45 might result in heteromeric channels with altered electrophysiology. Thus, it is reasonable to assume that the changes seen in connexin expression, and localisation may lead to

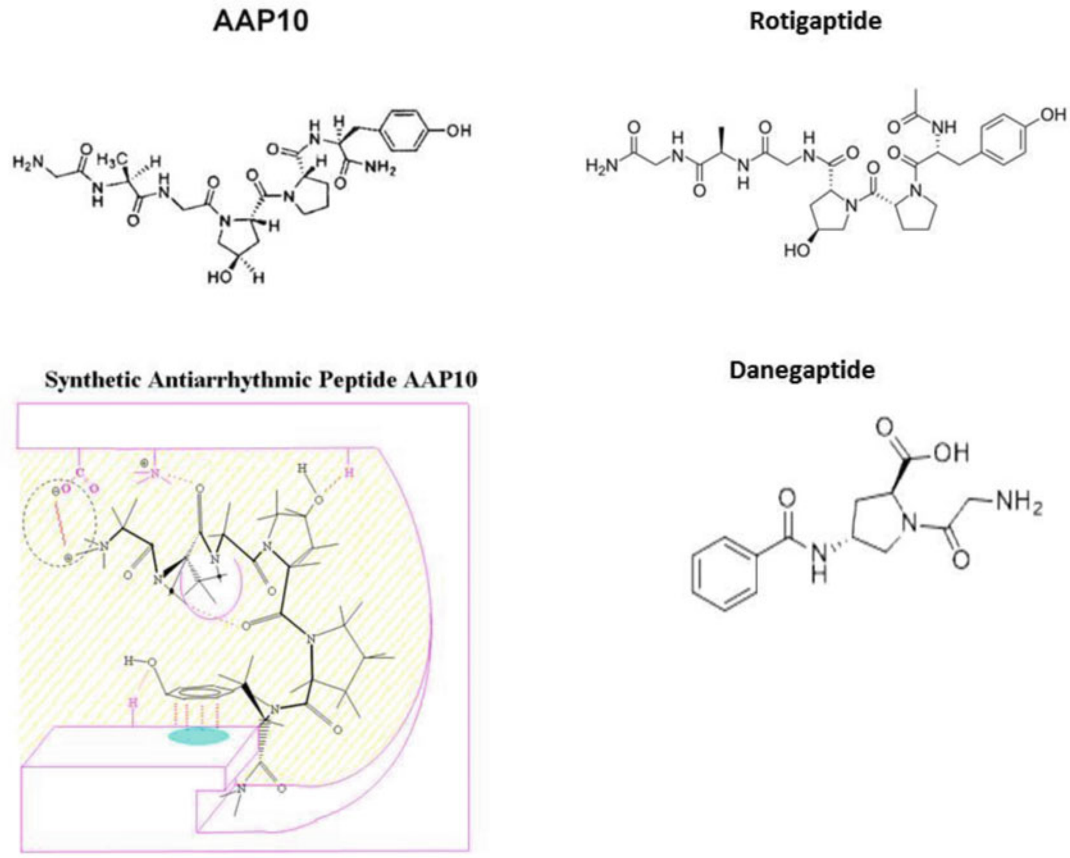

Fig. 14.3 AAP10 and its putative receptor pouch as deduced from [86, 126] together with the AAP10 derivatives rotigaptide and danegaptide

an altered electrical architecture and may contribute to the formation of an arrhythmogenic substrate.

It is necessary to state that there are many other factors contributing to cardiac remodelling in heart failure and to the pathophysiology of this disease, which cannot be mentioned here due to the limitation of space, so that we focus here on a brief description of those processes affecting gap junctions.

14.5 Antiarrhythmic Peptides Targeting Gap Junctions

Regarding therapeutical or pharmacological consequences, in 1994, we developed synthetic antiarrhythmic peptides, among which AAP10 (H_2N-Gly-Ala-Gly-HYP-Pro-Tyr-$CONH_2$) was found to be the most effective [82]. This peptide was found to reduce dispersion with an EC_{50} of 1 nM, to enhance gap junction electrical conductance, and to maintain conduction under hypoxic conditions in papillary muscles [82, 84], and to prevent type IB VF [86]. AAP10 was also effective in the suppression of VF in rabbits with healed myocardial infarction [125].

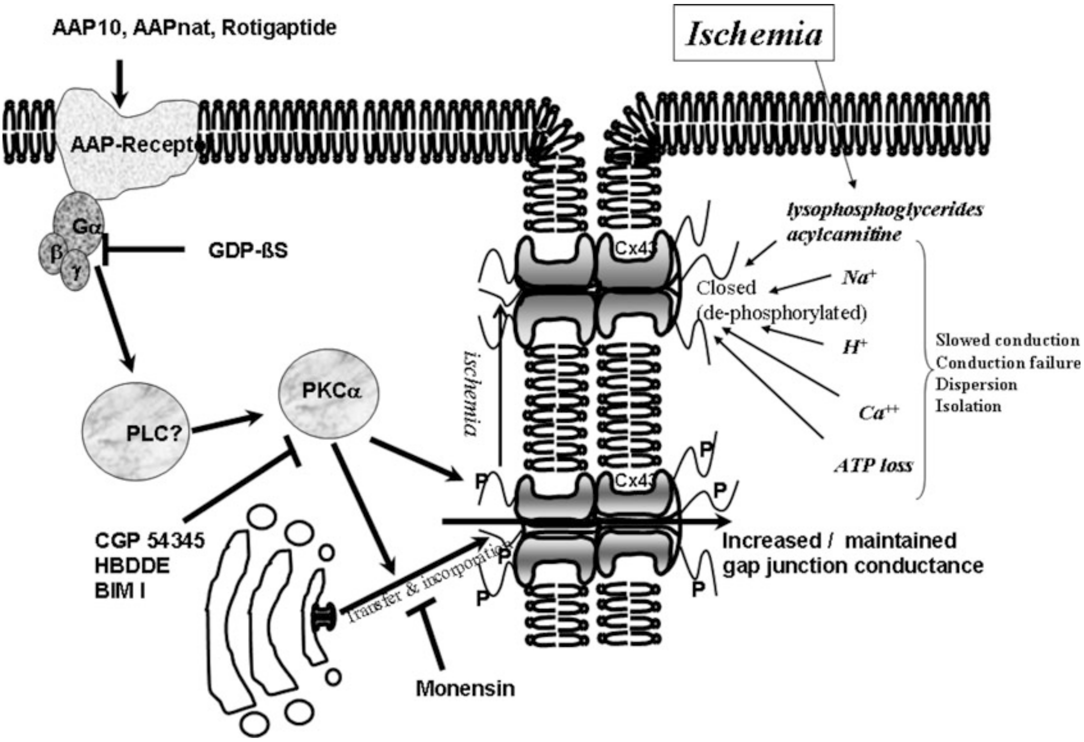
AAP10, AAPnat, Rotigaptide
AAP-Recept
Gα
β
γ
GDP-ßS
PLC?
PKCα
CGP 54345
HBDDE
BIM I
Transfer & incorporation
Monensin
ischemia
Ischemia
lysophosphoglycerides
acylcarnitine
Cx43
Closed
(de-phosphorylated)
Na+
H+
Ca++
ATP loss
Slowed conduction
Conduction failure
Dispersion
Isolation
P
Increased / maintained
gap junction conductance

Fig. 14.4 Present view of the mechanism of action of AAP10 in acute ischemia

The peptide exhibits a semi-cyclic horse-shoe-like spatial structure as evaluated in 2D mass spectroscopy studies ([111]; see Fig. 14.3), so that it was possible to construct an equally effective cyclopeptide cAAP10RG [86, 126], which served as a basis for the development of rotigaptide, a recent AAP10 derivative with certain D-amino acids in reverse order (so that the functional groups are at the same positions as in AAP10). Rotigaptide has also been shown to prevent spontaneous ventricular extrasystoles and ventricular tachycardia during myocardial ischemia/reperfusion [87, 127, 128]. From these peptides, a new small molecule, danegaptide was developed, which seemed to reduce infarct size and lower susceptibility to arrhythmia after infarction [129, 130]. However, a phase 2 clinical trial failed to verify this effect in patients [131].

AAP10 has several mechanisms of action (see Fig. 14.4). It acts via activation of PKCα and phosphorylation of Cx43, probably via a G-protein-coupled membrane receptor [132]. In ischemic rabbit hearts, AAP10 exhibits its inhibitory effect on Cx43-de-phosphorylation preferentially in the ischemic region, as it prevents from Cx43 loss from the cell poles in the ischemic centre and border without affecting the non-ischemic zone [20]. According to these results, Ser368 on the C-terminal of Cx43 is one (but probably not the only) of the phosphorylation sites targeted by AAP10 [20]. Typically, a loss of Cx43 from the cells is observed during ischemia [133]. AAP10 enhances both electric and metabolic coupling and acts on Cx43 and Cx45, but not on Cx40 [85]. Moreover, we showed that AAP10 prevents acidosis-induced uncoupling (pre-treatment), that its effects are significantly larger if cells are partially uncoupled in good accordance with our findings in ischemic hearts (see above) and that it also can reverse acidosis-induced uncoupling (treatment) [85]. Finally, we found that AAP10 acts on human cardiac myocytes [85].

In 1995, we formulated the theory of improvement in gap junction conductance as an antiarrhythmic principle for certain arrhythmia

[134]. However, peptides are pharmacologically critical since they are rapidly degraded. Interestingly, in 2016, a substituted quinolone, PQ1, was described to enhance GJIC and to prevent heptanol-induced dysfunction of sinuatrial node [135].

14.6 Conclusions

Gap junctions play an important role in the conduction properties of cardiac tissues and in arrhythmogenesis. Acute closure of gap junctions is a typical phenomenon in ischemia and acidosis, which is thought to be related to late ischemic ventricular fibrillation. Changes in the expression of connexins, or in the subcellular location (cell pole vs. lateral side of the cells), or in the regional expression level (heterogeneity) have been found in cardiac disease (heart failure, hypertrophy, infarction, atrial fibrillation). The new group of antiarrhythmic peptides that open gap junctions provides a new approach to antiarrhythmic treatment.

References

1. Bedner P, Niessen H, Odermatt B, Willecke K, Harz H. A method to determine the relative cAMP permeability of connexin channels. Exp Cell Res. 2003;291:25–35.
2. Noma A, Tsuboi N. Dependence of junctional conductance on proton, calcium and magnesium ions in cardiac paired cells of Guinea pig. J Physiol Lond. 1987;382:193–211.
3. Spray DC, Harris AL, Bennett MVL. Equilibrium properties of a voltage dependent junctional conductance. J Gen Physiol. 1981;77:77–93.
4. Spray DC, White RL, Mazet F, Bennett MVL. Regulation of gap junction conductance. Am J Phys. 1985;248:H753–64.
5. Weingart R, Maurer P. Cell-to-cell coupling studied in isolated ventricular cell pairs. Experientia. 1987;43:1091–4.
6. Dhein S. Pharmacology of gap junctions in the cardiovascular system. Cardiovasc Res. 2004;62:287–98.
7. Salameh A, Dhein S. Pharmacology of gap junctions. New pharmacological targets for treatment of arrhythmia, seizure and cancer? Biochim Biophys Acta. 2005;1719(1–2):36–58.
8. Salameh A. Life cycle of connexins: regulation of connexin synthesis and degradation. Adv Cardiol. 2006;42:57–70.
9. Fallon RF, Goodenough DA. Five hour half-life of mouse liver gap junction protein. J Cell Biol. 1981;127:343–55.
10. Darrow BJ, Laing JG, Lampe PD, Saffitz JE, Beyer EC. Expression of multiple connexins in cultured neonatal rat ventricular myocytes. Circ Res. 1995;76:381–7.
11. Beardslee AMA, Laing JG, Beyer EC, Saffitz JE. Rapid turnover of connexin43 in the adult rat heart. Circ Res. 1998;83:629–35.
12. Severs NJ. Pathophysiology of gap junctions in heart disease. J Cardiovasc Electrophysiol. 1994;5:462–75.
13. Severs NJ, Dupont E, Thomas N, Kaba R, Rothery S, Jain R, Sharpey K, Fry CH. Alterations in cardiac connexin expression in cardiomyopathies. Adv Cardiol. 2006;42:228–42.
14. Polontchouk L, Haefliger J-A, Ebelt B, Schaefer T, Stuhlmann D, Mehlhorn U, Kuhn-Reignier F, DeVivie ER, Dhein S. Effects of chronic atrial fibrillation on gap junction distribution in human and rat atria. J Am Coll Cardiol. 2001;38:883–91.
15. Kostin S, Klein G, Szalay Z, Hein S, Bauer EP, Schaper J. Structural correlate of atrial fibrillation in human patients. Cardiovasc Res. 2002;54:361–79.
16. Salameh A, Wustmann A, Karl S, Blanke K, Apel D, Rojas-Gomez D, Franke H, Mohr FW, Janousek J, Dhein S. Cyclic mechanical stretch induces cardiomyocyte orientation and polarization of the gap junction protein connexin43. Circ Res. 2010;106:1592–602.
17. Dhein S, Schreiber A, Steinbach S, Apel D, Salameh A, Schlegel F, Kostelka M, Dohmen PM, Mohr FW. Mechanical control of cell biology. Effects of cyclic mechanical stretch on cardiomyocyte cellular organization. Prog Biophys Mol Biol. 2014;115:93–102.
18. Buchanan JW, Saito T, Gettes LS. The effect of antiarrhythmic drugs, stimulation frequency and potassium induced resting membrane potential changes on conduction velocity and dV/dtmax in Guinea pig myocardium. Circ Res. 1985;56:696–703.
19. Weingart R, Maurer P. Action potential transfer in cell pairs isolated from adult rat and Guinea pig ventricles. Circ Res. 1988;63:72–80.
20. Jozwiak J, Dhein S. Local effects and mechanisms of antiarrhythmic peptide AAP10 in acute regional myocardial ischemia: electrophysiological and molecular findings. Naunyn Schmiedebergs Arch Pharmacol. 2008;378:459–70.
21. Dhein S, Krüsemann K, Schaefer T. Effects of the gap junction uncoupler palmitoleic acid on activation and repolarization pattern in isolated rabbit hearts. A mapping study. Br J Pharmacol. 1999;128:1375–84.
22. Delmar M, Michaels DC, Johnson T, Jalife J. Effects of increasing intercellular resistance on transverse

and longitudinal propagation in sheep epicardial muscle. Circ Res. 1987;60:780–5.

23. Unger VM, Kumar NM, Gilula NB, Yeager M. Three-dimensional structure of a recombinant gap junction membrane channel. Science. 1999;283 (5405):1176–80.
24. Cruciani V, Mikalsen SO. Evolutionary selection pressure and family relationships among connexin genes. Biol Chem. 2007;388:253–64.
25. Söhl G, Willecke K. Gap junctions and the connexion protein family. Cardiovasc Res. 2004;62:228–32.
26. Kwak BR, Jongsma HJ. Regulation of cardiac gap junction channel permeability and conductance by several phosphorylating conditions. Mol Cell Biochem. 1996;157:93–9.
27. Jongsma HJ, Wilders R. Gap junctions in cardiovascular disease. Circ Res. 2000;86:1193–7.
28. Kwak BR, Hermanns MMP, De Jonge HR, Lohmann SM, Jongsma HJ, Chanson M. Differential regulation of distinct types of gap junction channels by similar phosphorylating conditions. Mol Biol Cell. 1995;6: 1707–19.
29. Christ GJ, Brink PR. Analysis of the presence and physiological relevance of subconducting states of connxin43-derived gap junction channels in cultured human corporal vascular smooth muscle cells. Circ Res. 1999;85:797–803.
30. Dekker LRC, Fiolet JWT, VanBavel E, Coronel R, Opthof T, Spaan JAE, Janse MJ. Intracellular Ca^{2+}, intercellular electrical coupling and mechanical activity in ischemic rabbit papillary muscle. Effects of preconditioning and metabolic blockade. Circ Res. 1996;79:237–46.
31. Li J, Li C, Liang D, Lv F, Yuan T, The E, Ma X, Wu Y, Zhen L, Xie D, Wang S, Liu Y, Huang J, Shi J, Liu Y, Shi D, Xu L, Lin L, Peng L, Cui J, Zhu W, Chen YH. LRP6 acts as a scaffold protein in cardiac gap junction assembly. Nat Commun. 2016;7:11775. https://doi.org/10.1038/ncomms11775.
32. Musil LS, Goodenough DA. Multisubunit assembly of an integral plasma membrane channel protein, gap junction connexin43, occurs after exit from the ER. Cell. 1993;74:1065–77.
33. Musil LS, Goodenough DA. Biochemical analysis of connexon assembly. In: Kanno Y, Kataoka K, Shiba Y, Shibata Y, Shimazu T, editors. Intercellular communication through gap junctions. Progress in Cell Research Vol.4. Amsterdam: Elesvier Science Publ.; 1995. p. 327–30.
34. Falk MM. Connexin-specific distribution within gap junctions revealed in living cells. J Cell Sci. 2000;113:4109–20.
35. Giepmans BN. Gap junctions and connexin-interacting proteins. Cardiovasc Res. 2004;62:233–45.
36. Berthoud VM, Minogue PJ, Laing JG, Beyer EC. Pathways for degradation of connexins and gap junctions. Cardiovasc Res. 2004;62:256–67.
37. Kam CY, Dubash AD, Magistrati E, Polo S, Satchell KJF, Sheikh F, Lampe PD, Green KJ. Desmoplakin maintains gap junctions by inhibiting Ras/MAPK and lysosomal degradation of connexin-43. J Cell Biol. 2018;217:3219–35.
38. Salameh A, Dhein S. Effects of mechanical forces and stretch on intercellular gap junction coupling. Biochim Biophys Acta. 2013;1828:147–56.
39. Weidmann S. Passive properties of cardiac fibers. In: Rosen MR, Janse MJ, Wit AL, editors. Cardiac electrophysiology. A textbook. Mount Kisco, New York: Futura Publishing Company Inc.; 1990. p. 29–35.
40. Hodgkin AL, Rushton WAH. The electrical constants of a crustacean nerve fibre. Proc R Soc London Ser B. 1946;133:444–79.
41. Weidmann S. The electrical constants of Purkinje fibers. J Physiol Lond. 1952;118:348–60.
42. Kucera J, Rohr S, Rudy Y. Localization of sodium channels in intercalated disks odulates cardiac conduction. Circulation. 2002;91:1176–82.
43. Maier SKG, Westenbroek RE, McCormick KA, Curtis R, Scheuer T, Catterall WA. Distinct subcellular localization of different Sodium Channel α and β subunits in single ventricular myocytes from mouse heart. Circulation. 2004;109:1421–7.
44. Sperelakis N. Propagation mechanisms in the heart. Annu Rev Physiol. 1979;41:441–57.
45. Lin J, Keener JP. Modeling electrical activity of myocardial cells incorporating the effects of ephaptic coupling. Proc Natl Acad Sci U S A. 2010;107: 20935–40.
46. Sperelakis N, Mann JE. Evaluation of electric field changes in the cleft between excitable cells. J Theor Biol. 1977;64:71–96.
47. Mori Y, Fishman GI, Peskin CS. Ephaptic conductin in a cardiac strand model with 3D electrodiffusion. Proc Natl Acad Sci U S A. 2008;105:6463–8.
48. Gourdie RG. The cardiac gap junction has discrete functions in Electrotonic and Ephaptic coupling. Anat Rec (Hoboken). 2019;302:93–100.
49. Veeraraghavan R, Hoeker GS, Alvarez-Laviada A, Hoagland D, Wan X, King DR, Sanchez-Alonso J, Chen C, Jourdan J, Isom LL, Deschenes I, Smyth JW, Gorelik J, Poelzing S, Gourdie RG. The adhesion function of the sodium channel beta subunit (β1) contributes to cardiac action potential propagation. elife. 2018;7:e37610. https://doi.org/10.7554/eLife.37610.
50. Veeraraghavan R, Lin J, Keener JP, Gourdie R, Poelzing S. Potassium channels in the Cx43 gap junction perinexus modulate ephaptic coupling: an experimental and modeling study. Pflugers Arch. 2016;468:1651–61.
51. Hubbard ML, Ying W, Henriquez CS. Effect of gap junction distribution on impulse propagation in a monolayer of myocytes: a model study. Europace. 2007;9(Suppl 6):vi20-8.
52. Spach MS, Dolber PC. Discontinuous anisotropic propagation. In: Rosen MR, Janse MJ, editors.

Wit AL: cardiac electrophysiology: a textbook. Futura Publishing Company Inc, Mount Kisco: New York; 1990. p. 517–34.

53. Dupont E, Ko Y-S, Rothery S, Coppen SR, Bagha M, Haw M, Severs NJ. The gap junctional protein connexin40 is elevated in patients susceptible to postoperative atrial fibrillation. Circulation. 2001;103: 842–9.
54. Boldt A, Wetzel U, Weigl J, Garbade J, Lauschke J, Hindricks G, Kottkamp H, Gummert JF, Dhein S. Expression of angiotensin II receptors in human left and right atrial tissue in atrial fibrillation with and without underlying mitral valve disease. J Am Coll Cardiol. 2003;42:1785–92.
55. Spach MS, Dolber PC. Relating extracellular potentials and their derivatives to anisotropic propagation at a microscopic level in human cardiac muscle. Evidence for electrical uncoupling of side-to-side fiber connections with increasing age. Circ Res. 1986;58:356–71.
56. Dhein S, Hammerrath SB. Aspects of the intercellular communication in aged hearts. Effects of the gap junction uncopler palmitoleic acid. Naunyn Schmiedeberg's Arch Pharmacol. 2001;364:397–408.
57. Rohr S, Kucera JP, Fast VG, Kleber AG. Paradoxical improvement of impulse conduction in cardiac tissue by partial cellular uncoupling. Science. 1997;275 (5301):841–4.
58. Rohr S. Role of gap junctions in the propagation of the cardiac action potential. Cardiovasc Res. 2004;62:309–22.
59. Shaw RM, Rudy Y. (1997a). Electrophysiologic effects of acute myocardial ischemia. A mechanistic investigation of action potential conduction and conduction failure. Circ Res. 1997;80:124–38.
60. Shaw RM, Rudy Y. Ionic mechanisms of propagation in cardiac tissue: roles of the sodium and L-type calcium currents during reduced excitability and decreased gap-junction coupling. Circ Res. 1997;81: 727–41.
61. Beardslee MA, Lerner DL, Tadros PN, Laing JG, Beyer EC, Yamada KA, Kléber AG, Schuessler RB, Saffitz JE. Dephosphorylation and intracellular redistribution of ventricular connexin43 during electrical uncoupling induced by ischemia. Circ Res. 2000;87:656–62.
62. Schulz R, Gres P, Skyschally A, et al. Ischemic preconditioning preserves connexin43 phosphorylation during sustained ischemia in pig hearts in vivo. FASEB J. 2003;17:1355–7.
63. Jain SK, Schuessler RB, Saffitz JE. Mechanisms of delayed electrical uncoupling induced ischemic preconditioning. Circ Res. 2003;92:1138–44.
64. Verecchia F, Duthe F, Duval S, Duchatelle I, Sarrouilhe D, Hervé JC. ATP counteracts the rundown of gap juntional channels of rat ventricular myocytes by promoting protein phosphorylation. J Physiol Lond. 1999;516:447–59.
65. Burt JM. Block of intercellular communication: interaction of intracellular H^+ and Ca^{2+}. Am J Phys. 1987;253:C607–9.
66. White RL, Doeller JE, Verselis VK, Wittenberg BA. Gap junctional conductance between pairs of ventricular myocytes is modulated synergistically by H^+ and Ca^{++}. J Gen Physiol. 1990;95:1061–75.
67. Yan GX, Kléber AG. Changes in extracellular and intracellular pH in ischemic rabbit papillary muscle. Circ Res. 1992;71:460–70.
68. Massey KD, Minnich BN, Burt JM. Arachidonic acid and lipoxygenase metabolites uncouple neonatal rat cardiac myocyte pairs. Am J Phys. 1992;263: C494–501.
69. Wu J, McHowat J, Saffitz JE, Yamada KA, Corr PB. Inhibition of gap junctional conductance by long-chain acylcarnitines and their preferential accumulation in junctional sarcolemma during hypoxia. Circ Res. 1993;72:879–89.
70. Maurer P, Weingart R. Cell pairs isolated from Guinea pig and rat hearts: effects of $[Ca^{++}]_i$ on nexal membrane resistance. Pflüger's Arch. 1987;409:394–402.
71. Reber WR, Weingart R. Ungulate cardiac Purkinje fibers: the influence of intracellular pH on the electrical cell-to-cell coupling. J Physiol Lond. 1982;328: 87–104.
72. Morley GE, Taffet SM, Delmar M. Intramolecular interactions mediate pH regulation of connexin 43 channels. Biophys J. 1996;701294-1302:1294.
73. De Mello WC. Influence of the sodium pump on intercellular communication in heart fibers: effect of intracellular injection of sodium ion on electrical coupling. J Physiol Lond. 1976;263:171–97.
74. Hatanaka K, Kawata H, Toyofuku T, Yoshida K. Down-regulation of Connexin43 in early myocardial ischemia and protective effect by ischemic preconditioning in rat heart in vivo. Jpn Heart J. 2004;45:1007–19.
75. Ek-Vitorín JF, Pontifex TK, Burt JM. Cx43 channel gating and permeation: multiple phosphorylation-dependent roles of the carboxyl terminus. Int J Mol Sci. 2018;19(6):E1659. https://doi.org/10.3390/ijms19061659.
76. Smith WT 4th, Fleet WF, Johnson TA, Engle CL, Cascio WE. The Ib phase of ventricular arrhythmias in ischemic in situ porcine heart is related to changes in cell-to-cell electrical coupling. Experimental Cardiology Group, University of North Carolina. Circulation. 1995;92:3051–60.
77. de Groot JR, Wilms-Schopman FJ, Opthof T, Remme CA, Coronel R. Late ventricular arrhythmias during acute regional ischemia in the isolated blood perfused pig heart. Role of electrical cellular coupling. Cardiovasc Res. 2001;50:362–72.
78. Morley GE, Vaidya D, Samie FH, Lo C, Delmar M, Jalife J. Characterization of conduction in the ventricles of normal and heterozygous Cx43

knockout mice using optical mapping. J Cardiovasc Electrophysiol. 1999;10:1361–75.

79. Lerner DL, Yamada KA, Schuessler RB, Saffitz JE. Accelerated onset and increased incidence of ventricular arrhythmias induced by ischemia in Cx43-deficient mice. Circulation. 2000;101:547–52.
80. Thomas SP, Kucera JP, Bircher-Lehmann L, Rudy Y, Saffitz JE, Kleber AG. Impulse propagation in synthetic strands of neonatal cardiac myocytes with genetically reduced levels of connexin43. Circ Res. 2003;92:1209–16.
81. De Groot JR, Schumacher CA, Verkerk AO, Baartscheer A, Fiolet JWT, Coronel R. Intrinsic heterogeneity in repolarization is increased in isolated failing rabbit cardiomyocytes during simulated ischemia. Cardiovasc Res. 2003;59:705–14.
82. Dhein S, Manicone N, Müller A, Gerwin R, Ziskoven U, Irankhahi A, Minke C, Klaus W. A new synthetic antiarrhythmic peptide reduces dispersion of epicardial activation recovery interval and enhances cellular communication. Antiarrhythmic properties in regional ischemia. Naunyn Schmiedeberg's Arch Pharmacol. 1994;350:174–84.
83. Dhein S, Weng S, Grover R, Tudyka T, Gottwald M, Schaefer T, Polontchouk L. Protein kinase Cα mediates the effect of antiarrhythmic peptide on gap junction conductance. Cell Adh Commun. 2001;8: 257–64.
84. Müller A, Gottwald M, Tudyka T, Linke W, Klaus W, Dhein S. Increase in gap junction conductance by an antiarrhythmic peptide. Eur J Pharmacol. 1997;327:65–72.
85. Hagen A, Dietze A, Dhein S. Human cardiac gap junction coupling: effects of antiarrhythmic peptide AAP10. Cardiovasc Res. 2009;83(2):405–15.
86. Grover R, Dhein S. Structure-activity relationships of novel peptides related to the antiarrhythmic peptide AAP10 which reduce the dispersion of epicardial action potential duration. Peptides. 2001;22:1011–21.
87. Xing D, Kjolbye AL, Nielsen MS, Petersen JS, Harlow KW, Holstein-Rathlou N-H, Martins JB. ZP123 increases gap junctional conductance and prevents reentrant ventricular tachycardia during myocardial ischemia in open chest dogs. J Cardiovasc Electrophysiol. 2003;14:510–20.
88. Dhein S. Cardiac ischemia and uncoupling: gap junctions in ischemia and infarction. Adv Cardiol. 2006;42:198–212.
89. Firek L, Weingart R. Modification of gap junction conductance by divalent cations and protons in neonatal rat heart cells. J Mol Cell Cardiol. 1995;27: 1633–43.
90. Ek JF, Delmar M, Perzova R, Taffet SM. Role of histidine 95 on pH gating of the cardiac gap junction protein connexin43. Circ Res. 1994;74:1058–64.
91. Hermans MMP, Kortekaas P, Jongsma HJ, Rook MB. pH sensitivity of the cardiac gap junction proteins, connexin 45 and 43. Pflüger's Arch. 1995;431:138–40.
92. Liu S, Taffet S, Stoner L, Delmar M, Vallano ML, Jalife J. A structural basis for the unequal sensitivity of the major cardiac and liver gap junctions to intracellular acidification: the carboxy tail length. Biophys J. 1993;64:1422–33.
93. Doble BW, Kardami E. Basic fibroblast growth factor stimulates connexin-43 expression and intercellular communication of cardiac fibroblasts. Mol Cell Biochem. 1995;143:81–7.
94. Doble BW, Chen Y, Bosc DG, Litchfield DW, Kardami E. Fibroblast growth factor-2 decreases metabolic coupling and stimulates phosphorylation as well as masking of connexin43 epitopes in cardiac myocytes. Circ Res. 1996;79:647–58.
95. Saffitz JE, Hoyt RH, Luke RA, Kanter HL, Beyer EC. Cardiac myocyte interconnections at gap junctions: role in normal and abnormal electrical conduction. Trends Cardiovasc Med. 1992;2:56–60.
96. Dillon SM, Allessie MA, Ursell PC, Wit AL. Influences of anisotropic tissue structure on reentrant circuits in the epicardial border zone of subacute canine infarcts. Circ Res. 1988;63:182–206.
97. Spach MS, Dolber PC, Heidlage JF. Influence of the passive anisotropic properties on directional differences in propagation following modification of the sodium conductance in human atrial muscle. A model of reentry based on anisotropic discontinuous propagation. Circ Res. 1988;62:811–32.
98. Ursell PC, Gardner PI, Albala A, Fenoglio JJ, Wit AL. Structural and electrophysiological changes in the epicardial border zone of canine myocardial infarcts during infarct healing. Circ Res. 1985;56: 436–51.
99. Peters NS, Green CR, Poole-Wilson PA, Severs NJ. Reduced content of connexin43 gap junctions in ventricular myocardium from hypertrophied and ischaemic human hearts. Circulation. 1993;88:864–75.
100. Camelliti P, Green CR, Kohl P. Structural and functional coupling of cardiac myocytes and fibroblasts. Adv Cardiol. 2006;42:132–49.
101. Van der Velden HMW, Ausma J, Rook MB, Hellemous AJCGM, Van Veen TAAB, Allessie MA, Jongsma HJ. Gap junctional remodeling in relation to stabilization of atrial fibrillation in the goat. Cardiovasc Res. 2000;46:476–86.
102. Van der Velden HMW, van Kempen MJA, Wijffels MCEF, van Zijverden M, Groenewegen WA, Allessie MA, Jongsma HJ. Altered pattern of connexin40 distribution in persistent atrial fibrillation in the goat. J Cardiovasc Electrophysiol. 1998;9:596–607.
103. Verheule S, Wilson EE, Arora R, Engle SK, Scott LR, Olgin JE. Tissue structure and connexion expression of canine pulmonary veins. Cardiovasc Res. 2002;55:727–38.

104. Noureldin M, Chen H, Bai D. Functional characterization of novel atrial fibrillation-linked GJA5 (Cx40) mutants. Int J Mol Sci. 2018;19(4):E977. https://doi.org/10.3390/ijms19040977.
105. Carballo S, Pfenniger A, Carballo D, Garin N, James RW, Mach F, Shah D, Kwak BR. Differential association of Cx37 and Cx40 genetic variants in atrial fibrillation with and without underlying structural heart disease. Int J Mol Sci. 2018;19(1):E295. https://doi.org/10.3390/ijms19010295.
106. Kanthan A, Fahmy P, Rao R, Pouliopoulos J, Alexander IE, Thomas SP, Kizana E. Human Connexin40 mutations slow conduction and increase propensity for atrial fibrillation. Heart Lung Circ. 2018;27:114–21.
107. Wetzel U, Boldt A, Lauschke J, Weigl J, Schirdewahn P, Dorszewski A, Doll N, Hindricks G, Dhein S, Kottkamp H. Expression of connexins40 and 43 in human left atrium in atrial fibrillation of different aetiologies. Heart. 2005;91:166–70.
108. Yan H, Chen JZ, Zhu JH, Ni YM, Yu GW, Hu SJ, Tao QM. Expression of connexin in atrium of patients with atrial fibrillation and its signal transduction pathway. Zhonghua Yi Xue Za Zhi. 2004;84:209–13.
109. Polontchouk L, Ebelt B, Jackels M, Dhein S. MAP kinases mediate the effects of endothelin-1 and angiotensin-II on the cardiac connexin expression. FASEB J. 2002;16:87–9.
110. Raisch TB, Yanoff MS, Larsen TR, Farooqui MA, King DR, Veeraraghavan R, Gourdie RG, Baker JW, Arnold WS, AlMahameed ST, Poelzing S. Intercalated disk extracellular Nanodomain expansion in patients with atrial fibrillation. Front Physiol. 2018;9:398. https://doi.org/10.3389/fphys.2018.00398.
111. Schotten U, Blaauw Y, Allessie MA. In-vivo models of atrial fibrillation. In: Dhein S, Mohr FW, Delmar M, editors. Practical methods in cardiovascular research. Heidelberg: Springer Verlag; 2005. p. 129–49.
112. Ausma J, Van der Velden HMW, Lenders M-H, van Ankeren EP, Jongsma HJ, Ramaekers FCS, Borgers M, Allessie MA. Reverse structural and gap-junctional remodeling after prolonged atrial fibrillation in the goat. Circulation. 2003;107:2051–8.
113. Elvan A, Huang X-D, Pressler ML, Zipes DP. Radiofrequency catheter ablation of the atria eliminates pacing-induced sustained atrial fibrillation and reduces connexin 43 in dogs. Circulation. 1997;96:1675–85.
114. Dhein S. Role of connexins in atrial fibrillation. Adv Cardiol. 2006;42:161–74.
115. Salameh A, Frenzel C, Boldt A, Rassler B, Glawe I, Schulte J, Muhlberg K, Zimmer HG, Pfeiffer D, Dhein S. Subchronic alpha- and beta-adrenergic regulation of cardiac gap junction protein expression. FASEB J. 2006;20(2):365–7.
116. Kostin S, Dammer S, Hein S, Klövekorn WP, Bauer EP, Schaper J. Connexin 43 expression and distribution in compensated and decompensated cardiac hypertrophy in patients with aortic stenosis. Cardiovasc Res. 2004;62:426–36.
117. Kostin S, Rieger M, Dammer S, Hein S, Richter M, Klövekorn WP, Bauer EP, Schaper J. Gap junction remodeling and altered connexin43 expression in the failing human heart. Mol Cell Biochem. 2003;242:135–44.
118. Salameh A, Mühlberg K, Rahmel A, Dhein S, Pfeiffer D. Änderungen der Connexin expression bei humanen dilatativen und hypertrophen Kardiomyopathien. Z Kardiol. 2005;94(Suppl. 1):V1186.
119. Dupont E, Matsushita T, Kaba RA, et al. Altered connexin expression in human congestive heart failure. J Mol Cell Cardiol. 2001;33:359–71.
120. Kitamura H, Ohnishi Y, Yoshida A, Okajima K, Azumi H, Ishida A, Galeano EJ, Kubo S, Hayashi Y, Itoh H, Yokoyama M. Heterogeneous loss of connexin43 protein in nonischemic dilated cardiomyopathy with ventricular tachycardia. J Cardiovasc Electrophysiol. 2002;13:865–70.
121. Peters NS. New insights into myocardial arrhythmogenesis: distribution of gap junctional coupling in normal, ischaemic and hypertrophied hearts. Clin Sci. 1996;90:447–52.
122. Yamada KA, Rogers JG, Sundset R, Steinberg TH, Saffitz JE. Up-regulation of connexin45 in heart failure. J Cardiovasc Electrophysiol. 2003;14:1205–12.
123. Severs NJ, Coppen SR, Dupont E, Yeh H-I, Ko Y-S, Matsushita T. Gap junction alterations in human cardiac disease. Cardiovasc Res. 2004;62:368–77.
124. Crassous PA, Shu P, Huang C, Gordan R, Brouckaert P, Lampe PD, Xie LH, Beuve A. Newly identified NO-sensor guanylyl cyclase/Connexin 43 association is involved in cardiac electrical function. J Am Heart Assoc. 2017;6(12):e006397. https://doi.org/10.1161/JAHA.117.006397.
125. Ren Y, Zhang CT, Wu J, Ruan YF, Pu J, He L, Wu W, Chen BD, Wang WG, Wang L. The effects of antiarrhythmic peptide AAP10 on ventricular arrhythmias in rabbits with healed myocardial infarction. Zhonghua Xin Xue Guan Bing Za Zhi. 2006;34:825–8.
126. Grover R, Dhein S. Spatial structure determination of antiarrhythmic peptide using nuclear magnetic resonance spectroscopy. Peptides. 1998;19:1725–9.
127. Hennan JK, Swillo RE, Morgan GA, Keith JC Jr, Schaub RG, Smith RP, Feldman HS, Haugan K, Kantrowitz J, Wang PJ, Abu-Qare A, Butera J, Larsen BD, Crandall DL. Rotigaptide (ZP123) prevents spontaneous ventricular arrhythmias and reduces infarct size during myocardial ischemia/reperfusion injury in open-chest dogs. J Pharmacol Exp Ther. 2006;317:236–43.

128. Ng FS, Kalindjian JM, Cooper SA, Chowdhury RA, Patel PM, Dupont E, Lyon AR, Peters NS. Enhancement of gap junction function during acute myocardial infarction modifies healing and reduces late ventricular arrhythmia susceptibility. JACC Clin Electrophysiol. 2016;2:574–82.
129. Skyschally A, Walter B, Schultz Hansen R, Heusch G. The antiarrhythmic dipeptide ZP1609 (danegaptide) when given at reperfusion reduces myocardial infarct size in pigs. Naunyn Schmiedeberg's Arch Pharmacol. 2013;386:383–91.
130. Boengler K, Bulic M, Schreckenberg R, Schlüter KD, Schulz R. The gap junction modifier ZP1609 decreases cardiomyocyte hypercontracture following ischaemia/reperfusion independent from mitochondrial connexin 43. Br J Pharmacol. 2017;174:2060–73.
131. Engstrøm T, Nepper-Christensen L, Helqvist S, Kløvgaard L, Holmvang L, Jørgensen E, Pedersen F, Saunamaki K, Tilsted HH, Steensberg A, Fabricius S, Mouritzen U, Vejlstrup N, Ahtarovski KA, Göransson C, Bertelsen L, Kyhl K, Olivecrona G, Kelbæk H, Lassen JF, Køber L, Lønborg J. Danegaptide for primary percutaneous coronary intervention in acute myocardial infarction patients: a phase 2 randomised clinical trial. Heart. 2018;104:1593–9.
132. Weng S, Lauven M, Schaefer T, Polontchouk L, Grover R, Dhein S. Pharmacological modulation of gap junction coupling by an antiarrhythmic peptide via protein kinase C activation. FASEB J. 2002;16:1114–6.
133. Kaprielian RR, Gunning M, Dupont E, Sheppard MN, Rothery SM, Underwood R, Pennell DJ, Fox K, Pepper J, Poole-Wilson PA, Severs NJ. Down-regulation of immunodetectable connexin43 and decreased gap junction size in the pathogenesis of chronic hibernation in the human left ventricle. Circulation. 1998;97:651–60.
134. Dhein S, Tudyka T. The therapeutic potential of antiarrhythmic peptides. Cellular coupling as a new antiarrhythmic target. Drugs. 1995;49:851–5.
135. Chang CJ, Cheng CC, Chen YC, Kao YH, Chen SA, Chen YJ. Gap junction modifiers regulate electrical activities of the sinoatrial node and pulmonary vein: therapeutic implications in atrial arrhythmogenesis. Int J Cardiol. 2016;221:529–36.

Role of the T-Tubules in the Control of Cellular Calcium and Inotropic Interventions in Cardiac Ventricular Myocytes

15

Andrew F. James and Clive H. Orchard

Abstract

The sarcolemma of mammalian cardiac ventricular myocytes contains a system of invaginations known as transverse (or t-) tubules that arise through openings aligned with the z-lines and connect to a network comprising transverse and axial elements. The detubulation technique, developed more than two decades ago by Orchard and colleagues, physically and functionally uncouples the t-tubules from the surface sarcolemma. Together with electrophysiological and imaging approaches, this technique has provided valuable information regarding the function of the t-tubules. This chapter provides a summary of these studies which highlight the important role of the t-tubules in the control of cardiac excitation–contraction coupling.

Keywords

Cardiac muscle · T-tubules · Calcium · Excitation–contraction coupling · Autoregulation · Inotropic agents · Glycosides · Beta-adrenergic stimulation · Heart failure · Sarcoplasmic reticulum · I_{Ca} · Na/Ca exchange · Protein kinase A · Ca transient

15.1 Introduction

At each heartbeat, the contraction of cardiac muscle is initiated by the depolarisation of the cell membrane (sarcolemma) during the action potential (AP), which causes the opening of L-type Ca^{2+} channels (LTCCs), resulting in Ca^{2+} influx that, in turn, triggers the release of a larger amount of Ca^{2+} from the sarcoplasmic reticulum (SR) by activating ryanodine receptors (RyR) in the adjacent SR membrane by a process known as calcium-induced calcium release (CICR) [1]. The release of Ca^{2+} is localised at the dyad formed by the close juxtaposition of the sarcolemma with the neighbouring junctional SR (jSR) [1–3]. The spatial and temporal summation of such local releases result in a rise in intracellular Ca^{2+} concentration ($[Ca^{2+}]_i$) throughout the cytosol—the systolic Ca^{2+} transient—and it is this that activates the contractile proteins [1]. The localised nature of Ca^{2+} release allows the total amount of Ca^{2+} released from the SR during each action potential to be graded so that the amplitude of the systolic Ca^{2+} transient and, by extension, the strength of the contraction, is controlled by the size of the Ca^{2+} trigger and the SR Ca^{2+} content [1, 3].

Relaxation requires that Ca^{2+} is removed from the cytosol and this is achieved via two main routes: the SR Ca^{2+} ATPase (SERCA), regulated by phospholamban (PLB), pumps Ca^{2+} back into the SR at the expense of the hydrolysis of ATP, while the Na^+/Ca^{2+} exchanger (NCX) is a

---

A. F. James (✉) · C. H. Orchard
School of Physiology, Pharmacology and Neuroscience, Biomedical Sciences Building, University of Bristol, Bristol, UK
e-mail: a.james@bristol.ac.uk

© Springer Nature Switzerland AG 2023
O. N. Tripathi et al. (eds.), *Heart Rate and Rhythm*, https://doi.org/10.1007/978-3-031-33588-4_15

secondarily active transporter that represents the predominant pathway for removal of Ca^{2+} from cardiac myocytes [1]. NCX is an electrogenic antiporter with a stoichiometry of 3 Na^{+} exchanged for each Ca^{2+} transported that can contribute to both Ca^{2+} efflux and influx around the cardiac cycle, depending on the prevailing driving force [4, 5]. The plasmalemmal Ca^{2+} ATPase (PMCA) also makes a minor contribution to Ca^{2+} removal from the cell [1, 6, 7]. The fraction of Ca^{2+} removed from the cytosol at each beat by these pathways depends on their relative activities, but it follows that, in the steady state, the amount of Ca^{2+} extruded from the cell must equal the amount entering the cell at each beat [1].

Transverse (or t-) tubules, invaginations of the cell membrane that form a network with transverse and axial elements, play a critical role in the rapid propagation of the AP throughout the cell, ensuring a synchronised and co-ordinated release of Ca^{2+} to produce the systolic Ca^{2+} transient [2]. As the t-tubules reduce the distance from the cytosol to the cell membrane, in addition to the co-ordination of Ca^{2+} release, the t-tubules play an important role in Ca^{2+} removal from the cell. T-tubules also play a role in cell signalling, as membrane coupling to the cytoskeleton and some G-protein-coupled receptors important to the regulation of cardiac myocyte function are preferentially located here (*e.g* [2, 8, 9].).

15.2 Cardiac T-Tubules

The structure and formation of the t-tubule network is described in greater detail in Chap. 16 by Rog-Zielinska, but points key to this chapter are outlined here. The t-tubules form a highly branched and interconnected network of sarcolemmal invaginations with diameters generally ranging from 50 to 600 nm that penetrate the cell interior [2]. The lipid content of the t-tubule membrane is suggested to be enriched in cholesterol and sphingomyelin compared to the surface sarcolemma [10, 11]. The lumen of the t-tubules is continuous with the extracellular space but represents a space for restricted diffusion within the cell. Constrictions and dilations along the t-tubules, and the presence of glycocalyx within the lumen, affect diffusion and exchange with the extracellular space [12]. The network consists of transverse and axial elements, the transverse elements being located close to the sarcomeric z-disks, while the axial elements can span the sarcomere. The transverse elements of the t-tubules are anchored to the z-disks by costameres comprised of the dystrophin-glycoprotein and vinculin-talin-integrin complexes [2, 13].

Immuno-based imaging studies have been important in demonstrating that many of the proteins involved in EC coupling, Ca^{2+} transport and the regulation of cardiac myocyte function, such as LTCC, RyR and SERCA, are located predominantly at the t-tubules [2, 14, 15]. The development of super-resolution light microscopy and three-dimensional (3D) transmission electron microscopy (TEM) tomography techniques has provided deeper insight at the nanoscale level into the ultrastructure of t-tubules [2, 16–19]. Many of the proteins found predominantly in the t-tubules are localised to membrane microdomains that serve as signalling complexes key to the regulation of cardiac function.

15.2.1 Dyads

The dyads are perhaps the epitome of a membrane domain predominantly located in the t-tubules. At the dyad, LTCC in the sarcolemma are juxtaposed to a cluster of RyR in the jSR membrane, separated by a gap of ~12 nm. The close proximity of LTCC to RyR at the dyad is critical to local control: when an LTCC opens, the local $[Ca^{2+}]_i$ increases abruptly from a diastolic level of ~100 nM to >10 μM, leading to a rapid response from the adjacent RyRs [3]. A proportion of NCX has also been localised close to RyRs and may be present in the dyad [20, 21]. The localisation of the dyads is often identified by immunostaining of the clusters of RyR, and these are predominantly arranged along the transverse elements of the t-tubules at the z-line and the surface sarcolemma [22, 23], although junctions thought to contribute SR Ca^{2+} release during the AP are also found along the axial tubules [24].

15.2.2 Caveolae and Caveolin-3

As outlined in Chap. 16 by Rog-Zielinska, caveolae are 50–100 nm diameter flask-shaped invaginations of the sarcolemma organised in muscle by the cholesterol-binding membrane protein, caveolin-3, that are present in both t-tubules and the surface sarcolemma [2, 17, 25, 26]. While caveolae and caveolin-3 contribute to the genesis of t-tubules [10, 27] and mature t-tubules can clearly be identified by immunostaining for caveolin-3 (e.g [28–30].), there has been some controversy regarding the presence of caveolae at the t-tubule membrane since they are infrequently identified there in 2D TEM [17, 25, 31]. However, caveolar-like structures are present at the t-tubule [26] where they can be more readily observed with 3D imaging techniques [17, 32]. It is noteworthy that knockout of caveolin-3 in mice results in abnormalities to the t-tubule network of isolated ventricular myocytes as well as the loss of cardiac muscle caveolae [33, 34]. Caveolae are dynamic structures that are likely to play important roles in mechanosensation and transduction and membrane trafficking and repair [25, 35, 36]. As a form of lipid raft that concentrate proteins to a microdomain, caveolae play an important role in colocalising signalling molecules [25]. A plethora of proteins have been identified as caveolar cargoes and, due to spatial constraints, it is not feasible that these can all co-exist within the same caveola [37]. Yet little is known of the processes regulating the composition of caveolae, but it seems likely that there is heterogeneity in the composition of caveolae even within the same cell [25, 38]. Notable residents of cardiac caveolae include the LTCC α_1-subunit, $Ca_v1.2$, β-adrenoceptors and elements of cyclic AMP signalling, the α-subunit of the voltage-gated Na^+ channel, $Na_v1.5$, the α1 and α2 catalytic subunits of the Na^+-K^+-ATPase (NKA) and the plasmalemmal Ca^{2+} ATPase (PMCA) [37, 39–43]. It is important to note that while caveolin-3 has been suggested to interact with junctophilin-2 and be involved in the assembly of the dyad [31, 44], caveolin-3 is not thought to be located to the dyad itself [21]. Thus, it is suggested that dyads and caveolae may represent separate pools of LTCC [45, 46]. The concept that caveolin-3 represents a scaffolding protein that tethers proteins to the caveola via a scaffolding domain has been largely discredited due to structural considerations for the putative caveolin binding domain of partner proteins [47, 48]. Nevertheless, peptides based on the caveolin scaffolding domain have been shown to interfere with caveolin-3 signalling [40, 49–51]. Mutations in caveolin-3 have been suggested to cause inherited cardiomyopathies and susceptibility to arrhythmia (long QT syndrome 9), although the pathogenic mechanisms remain unclear [52, 53].

15.2.3 Ankyrin B

Ankyrin B, encoded by the *ANK2* gene, is a cytoskeletal protein originally identified in the brain that attaches integral membrane proteins to the spectrin-actin cytoskeleton [54]. In cardiac myocytes, it colocalises NKA and NCX in the sarcolemma and IP_3 receptors in the SR membrane to a microdomain at the t-tubule [55]. Loss of function mutations in human *ANK2* cause the arrhythmogenic ankyrin B syndromes associated with an increased risk of sudden cardiac death, which can manifest as sick sinus syndrome with bradycardia, atrial fibrillation and long QT syndrome (sometimes referred to as LQT4) [56–58]. Disruption of the ankyrin B microdomain is suggested to cause an increase in the cytosolic $[Na^+]_i$ sensed by NCX, resulting in reduced Ca^{2+} extrusion/increased Ca^{2+} influx and increased frequency of Ca^{2+} sparks and waves and this may be an important pathogenic mechanism in ankyrin B syndrome [59]. While cardiac caveolae are enriched in NKA subunits, ankyrin B does not appear to be a caveolar protein, and it is unclear whether the Na^+/K^+-ATPase exists in multiple membrane domains within the t-tubule [37].

15.2.4 Detubulation

While high- and super-resolution imaging techniques provide important data regarding the localisation of proteins and the structures of microdomains within the t-tubules, they do not provide information about protein function, which depends on membrane insertion, the local environment and the presence and activity of accessory and regulatory proteins. A number of approaches to disrupt t-tubules have been tried to investigate their functional contribution. For example, treatment with methyl-*β*-cyclodextrin (MBCD) to remove cholesterol from the sarcolemma has been suggested to reduce the structural integrity of t-tubules in cardiac myocytes [60]. However, using conditions shown to reduce membrane cholesterol and disrupt caveolae [37, 40, 61, 62], others have reported that the integrity of the t-tubule network was maintained following treatment with MBCD [63, 64]. The reason for the differences between the studies remains unclear, but it can be concluded that cholesterol depletion does not afford a reliable approach to disrupt the t-tubule network. The t-tubule network has been shown to be gradually lost from isolated myocytes maintained in short-term culture, together with changes in membrane currents and their regulation [65–69]. This phenomenon provides a valuable system to examine the mechanisms of t-tubule remodelling and stabilisation (e.g. [31, 44].). However, as it is unclear whether the loss of function seen in short-term culture is due to the loss of t-tubules per se or other aspects of de-differentiation in culture, a more direct experimental approach for the removal of the t-tubules was desirable.

The detubulation technique, developed more than two decades ago by Orchard and colleagues, physically and functionally uncouples the t-tubules from the surface sarcolemma using formamide-induced osmotic shock [70]. The t-tubule membranes remain intact within the cell, disconnected from the surface sarcolemma [71, 72]. The technique has thereby provided insight into the distribution of protein function between the surface and t-tubule membranes [14, 70, 71]. The loss of cell capacitance and membrane currents following detubulation enables the fraction of the cell membrane and the density of membrane currents in the t-tubules and surface sarcolemma to be calculated. For non-electrogenic transporters, the change in relative flux across the membrane on detubulation provides evidence for the distribution of transport between the surface sarcolemma and t-tubules (*e.g.* [73, 74].). The technique was developed in rat ventricular myocytes but has been applied to myocytes from a range of species including, for example, guinea pigs [73], mice [69, 75, 76] and rabbits [77], and has provided considerable insight into the distribution of ion flux pathways in the cardiac sarcolemma. Table 15.1 shows examples of the distribution of activities of key channels and transporters in isolated ventricular myocytes that have been obtained using the detubulation technique.

The concentration of certain transporters and channels to the t-tubule membrane means that ion flux occurs into and out of a restricted diffusion space. Moreover, proteins in the t-tubule membrane are often regulated differently from those in the surface sarcolemma. As we shall see in the remainder of this chapter, these considerations have important implications in the response of cardiac muscle to inotropic interventions.

15.3 Action Potentials and EC Coupling

Detubulation effectively prevents propagation of the AP through the cell [72], resulting in the uncoupling of the RyR in jSR in the transverse and axial tubules from excitation in the sarcolemma so that the synchronous release of Ca^{2+} is lost [71, 83]. Thus, in detubulated cells, Ca^{2+} release is initiated from junctions at the surface sarcolemma and CICR proceeds as a propagating wave towards the cell centre [71, 83]. In comparison to intact myocytes, the time-to-peak of the whole cell Ca^{2+} transient is thereby delayed in detubulated cells [71, 83]. In multicellular preparations, the loss of t-tubules results in slower kinetics of force generation and reduces the

Table 15.1 Distribution between the t-tubules and surface sarcolemma of the key current and transporter activities in ventricular myocytes

Transporter/Current	Percentage in t-tubules	Species	References
I_{Ca}	80	Rat	[78]
	71	Mouse	[79]
$I_{Na,c}$	22	Rat	[80]
$I_{Na,n}$	80	Rat	[80]
I_{NCX}	63	Rat	[81]
	25	Mouse	[79]
I_{NaK}	59	Rat	[81]
	41	Mouse	[75]
NHE	0	Rat	[73]
	0	Guinea pig	[73]
NBC	43*	Rat	[73]
PMCA	100	Rat	[74]
I_{to}	29	Rat	[82]
I_{ss}	71	Rat	[82]
I_K	27	Rat	[82]
I_{K1}	26	Rat	[82]

Transverse tubules typically represent ~30% of the cell membrane. Thus, percentage activity >30% indicates that function is relatively concentrated to the t-tubules. I_{Ca}—L-type Ca^{2+} current, $I_{Na,c}$—cardiac-type voltage-dependent Na^+ current, $I_{Na,n}$—neuronal-type voltage-dependent Na^+ current, I_{NCX}—Na^+/Ca^{2+} exchange current, I_{NaK}—Na^+/K^+-ATPase current, NHE—Na^+/H^+ exchange, NBC—Na^+-HCO_3^- cotransporters, PMCA—plasmalemmal (sarcolemmal) Ca^{2+} ATPase, I_{to}—transient outward current, I_{ss}—steady-state outward current, I_K—delayed rectifier current and I_{K1}—inward rectifier current. *This is an upper estimate taken from the text of Garciarena et al. [73]

energy efficiency of contraction [84, 85]. In isolated myocytes maintained in culture, the partial loss of t-tubules is associated with a loss of synchrony in Ca^{2+} release reminiscent of the effects of t-tubule remodelling in heart failure [68].

The L-type Ca^{2+} current (I_{Ca}) flows predominantly, although not exclusively, across the t-tubule membrane (Table 15.1), consistent with the concentration of LTCC to the dyads. There was no significant difference in the gain of EC coupling between intact and detubulated cells, indicating that I_{Ca} is equally effective in inducing SR Ca^{2+} release at the surface sarcolemma as at the t-tubule membrane [78]. It has been calculated from electron microscopy data and recordings of I_{Ca} in intact and detubulated myocytes that the numbers of LTCC per junction complex (~35) are the same at the surface membrane as at the t-tubule [15, 86, 87]. As Ca^{2+} is a charge carrier, I_{Ca} is important in establishing AP duration (APD). In consequence, detubulation results in considerable shortening of APD, notwithstanding the concomitant loss of (predominantly K^+-selective) steady-state current (Table 15.1) [82, 87, 88]. On the other hand, detubulation had no effect on the resting membrane potential or AP amplitude [87]. The predominant Na^+ channel α_1-subunit in cardiac myocytes, $Na_v1.5$, underlies a current ($I_{Na,c}$) that is relatively insensitive to tetrodotoxin (TTX). $I_{Na,c}$ is comparatively uniformly distributed between the t-tubules and surface sarcolemma (Table 15.1, [80]), consistent with the targeting of $Na_v1.5$ to domains at the intercalated disks and dystrophin-glycoprotein complex [89]. However, neuronal-type Na^+ channels (e.g. $Na_v1.1$–4 and $Na_v1.6$), distinguished by their greater sensitivity to TTX, also contribute to whole cell I_{Na} in cardiac myocytes, underlying a current ($I_{Na,n}$) that is relatively concentrated to the t-tubules (Table 15.1, [80, 90]). The physiological significance of the localisation of Na^+ channels to the t-tubules is not obvious. While it has been suggested that neuronal-type Na^+ channels might contribute to effective excitation of the t-tubule [91], from theoretical considerations, it is not necessary for Na^+ channels to be present in the t-tubule membrane for the depolarisation of the t-tubules during the AP [92].

15.4 Na$^+$ Microdomains and Cardiac Glycosides

Na$^+$ entry early in the AP has been suggested to contribute to the efficiency of Ca^{2+} release through the priming of a microdomain sensed by NCX and RyR, although this idea remains controversial [4]. The suggestion is that the localised increase in cytosolic [Na$^+$]$_i$ results in Ca^{2+} influx to the junction via reverse mode NCX during the AP overshoot; the consequent localised increase in [Ca^{2+}]$_i$ primes the RyR for CICR triggered by the larger Ca^{2+} influx via the relatively slowly gating LTCC. However, the inhibition of $I_{Na,n}$ with 200 nM TTX had no effect on the Ca^{2+} transient amplitude in rat ventricular myocytes, indicating that t-tubule neuronal Na$^+$ channels were not required for normal EC coupling [80]. On the other hand, Na$^+$ influx through neuronal Na$^+$ channels colocalised with RyR and NCX at the t-tubule has been suggested to contribute to diastolic Ca^{2+} release in a mouse model of catecholaminergic polymorphic ventricular tachycardia (CPVT) [93]. The functional significance of colocalization of Na$^+$ transporters at the t-tubule has been illustrated by the arrhythmic syndrome associated with ankyrin B mutation [4, 54, 59]. In rat ventricular myocytes, the t-tubules are enriched in NCX current (I_{NCX}) [20, 81, 94, 95], consistent with the colocalization of NCX with dyads. In contrast, in mouse ventricular myocytes I_{NCX} and NCX staining was greater in the surface sarcolemma than in the t-tubule membranes [79], suggesting the existence of species differences in the sarcolemmal localisation of NCX. Hysteresis in the relationship between I_{NCX} and bulk cytosolic free [Ca^{2+}] recorded during the application of caffeine to unload the SR has been considered as evidence that NCX is sensitive to a Ca^{2+} microdomain controlled by RyR [96, 97]. Interestingly, while detubulation abolished such hysteresis in rat ventricular myocytes, in mouse ventricular myocytes, the hysteresis remained intact following uncoupling of the t-tubules, further suggesting species differences in the colocalization of RyR and NCX [79, 95]. In quiescent rabbit ventricular myocytes, Ca^{2+} spark frequency was increased by inhibition of NCX or by detubulation, indicating a role for NCX at the t-tubule in controlling local [Ca^{2+}]$_i$ at RyR during diastole [77]. In contrast, detubulation of rat ventricular myocytes *reduced* Ca^{2+} spark frequency, an observation also consistent with a role for t-tubule NCX in the regulation of local [Ca^{2+}]$_i$ at RyR, albeit with the direction of Ca^{2+} transport the reverse of that in rabbit ventricular myocytes [83]. The higher resting cytosolic [Na$^+$]$_i$ of rats in comparison to rabbit ventricular myocytes favours Ca^{2+} entry via reverse mode NCX at the resting membrane potential [5, 98].

The positive inotropic effect of inhibition of NKA, or Na$^+$ pump, with cardiac glycosides (e.g. ouabain, strophanthidin) is well known and arises through effects on Ca^{2+} transport via NCX [99]. The t-tubules of both rat and mouse ventricular myocytes are enriched in Na$^+$ pump current (I_{NaK}), although the difference in I_{NaK} density between t-tubules and surface sarcolemma was less marked in the mouse in comparison to the rat [75, 81, 100]. Notably, there was a difference in localisation of the contribution of α_1 and α_2 NKA subunits to I_{NaK} in both rat and mouse ventricular myocytes: while the α_1 subunit predominates in both surface sarcolemma and t-tubules, the majority of the α_2 current is localised to the t-tubules [75, 100]. Although both α_1 and α_2 NKA subunits are present in the t-tubule, the α_2 subunit has been suggested to play a particular role in controlling cytosolic [Na$^+$] concentration in a microdomain sensed by NCX in proximity to RyR [4]. While the strophanthidin-induced change in bulk cytosolic [Na$^+$]$_i$ was blunted in detubulated rat ventricular myocytes, consistent with the concentration of NKA to the t-tubules, the increase in amplitude of the Ca^{2+} transient was preserved, indicating that NCX in the surface sarcolemma contributes to the inotropic action of NKA inhibition [101]. Intriguingly, Na$^+$/H$^+$ exchange (NHE) was found to be largely excluded from the t-tubules, while Na$^+$-bicarbonate co-transporters seemed to be relatively uniformly distributed in the sarcolemma [73]. The compartmentation of Na^+ and H^+ transporters in the sarcolemma is likely to be important in the regulation of cytosolic Ca^{2+} buffering [102].

15.5 The Slow Force Response

Myocardial stretch produces an increase in developed force that has two phases: The rapid response arises through changes in the sensitivity of the myofilaments to Ca^{2+} and is considered to underlie the Frank-Starling mechanism [103]. This is followed by a second phase, thought to underlie the Anrep effect, that takes several minutes to develop and involves an increase in the amplitude of the systolic Ca^{2+} transient [103]. A number of studies have implicated stretch-induced changes in cytosolic $[Na^+]_i$ and changes to the driving force for NCX, often suggesting activation of NHE and an autocrine/paracrine signalling pathway involving angiotensin-II and endothelin-1 [103–105]. The slow force response in rat ventricular trabeculae has recently been shown to be abolished by detubulation, indicating that the t-tubules are essential for this response [85]. As NHE are excluded from the t-tubules, the study indicates that other pathways for stretch-mediated Na^+ entry located in the t-tubules should be considered, such as stretch-sensitive TRPC channels [73, 104, 106].

15.6 Autoregulation

Autoregulation refers to the interdependence of SR Ca^{2+} content, net sarcolemmal Ca^{2+} flux and SR Ca^{2+} release [1]. In the steady state, influx and efflux of Ca^{2+} over the cardiac cycle are equal and the systolic Ca^{2+} transient amplitude is relatively constant from beat to beat [1]. Imbalance in sarcolemmal influx and efflux can occur only transiently as these will result in a change in SR Ca^{2+} release and SR Ca^{2+} content so that, usually, a new steady state is established. Similarly, for a change to the systolic Ca^{2+} transient to be sustained, a change in sensitivity to trigger I_{Ca} of SR Ca^{2+} release must be matched by an increased SR Ca^{2+} uptake [1]. Given the role of the t-tubules in sarcolemmal Ca^{2+} fluxes and Ca^{2+} release, and that a significant proportion of SERCA are localised to the jSR in relative proximity to the t-tubules [107, 108], it might be anticipated that the t-tubules play a significant role in autoregulation and SR Ca^{2+} uptake.

Uncoupling of the t-tubules from the surface sarcolemma in cells from both rat and mouse ventricular myocytes significantly slowed the recovery of the Ca^{2+} transient during successive stimuli following caffeine-induced depletion of the SR, consistent with the t-tubules carrying the majority of Ca^{2+} influx [79, 83], although detubulation had no effect on the steady-state SR Ca^{2+} content in cells from either species [79, 94, 109]. The slowing of SR reloading following caffeine-induced depletion is not as marked as might be expected from the observed decrease in peak I_{Ca}. The inactivation of I_{Ca} was slower in detubulated cells relative to control, indicating faster inactivation of LTCC in the t-tubule membrane relative to LTCC in the surface sarcolemma [78]. As a result, while the surface membrane accounts for only 20% of peak I_{Ca} recorded using conventional rectangular-shaped depolarising pulses (Table 15.1), Ca^{2+} entry across the surface sarcolemma represents ~32% of the total Ca^{2+} entry recorded in voltage-clamp experiments using action potential waveforms (i.e. 1.4 μmol/l cytosol volume at the surface vs 3.0 μmol/l cytosol volume at the t-tubule membrane) [78, 87, 110, 111]. Normalising to junctional area shows relatively greater Ca^{2+} entry per μm^2 of the junctional membrane at the cell surface (1.43 nmol/l cytosol/μm^2) compared with the junctional membrane at the t-tubule (1.06 nmol/l cytosol/μm^2) [87]. In contrast, detubulation of mouse ventricular myocytes had little effect on changes to the influx-to-efflux ratio following the sensitisation of SR Ca^{2+} release to trigger Ca^{2+} using a low concentration (200 μM) of caffeine, possibly reflecting the lack of concentration of NCX to the t-tubules in this species [79].

It is also worth noting that the contribution of the plasmalemmal Ca^{2+} ATPase (PMCA) to Ca^{2+}

extrusion is completely lost in detubulated cells (Table 15.1, [74]). While the PMCA makes little contribution to Ca^{2+} flux balance on a beat-to-beat basis, it seems highly likely that it plays an important role in the longer term regulation of cellular Ca^{2+} load and diastolic $[Ca^{2+}]_i$ [1]. There is evidence of a role for the SR in controlling longer term cellular Ca^{2+} load through store-operated Ca^{2+} entry, although there is much controversy in this area [1, 112]. Store-operated Ca^{2+} entry (SOCE) is a ubiquitous mechanism by which Ca^{2+} depletion of the endoplasmic reticulum/SR (ER/SR) triggers Ca^{2+} entry via non-voltage-gated channels in the plasmalemma/sarcolemma. SOCE involves a protein known as stromal interaction molecule 1 (STIM1), which is a single membrane pass molecule that resides in the ER/SR membrane, sensing luminal $[Ca^{2+}]_{SR}$ and activating Ca^{2+} entry via plasmalemmal channels, particularly Orai channels although TRPC non-selective cation channels may also be regulated by STIM1, when the ER/SR is depleted [112]. Although SOCE can be observed in neonatal cardiac myocytes, which lack a fully developed t-tubule system, there is no consensus as to whether it exists in adult myocytes [1, 112]. It is worth noting that STIM1 is generally localised to the z-lines, so that it seems likely to interact with the t-tubule membrane when present in adult myocytes [112]. As SOCE has been suggested to be important to the development of cardiac hypertrophy and myopathy, it is tempting to speculate that STIM1 is part of the suite of genes expressed early in cardiac development that are recruited in hypertrophy [1, 112]. In any case, the close juxtaposition between the t-tubules and SR implicates a role for the t-tubules in controlling longer term cellular Ca^{2+} load, whether this be via SOCE per se or by adjustment of the Ca^{2+} flux balance via other channels and transporters of the sarcolemma.

15.7 Stimulation Frequency

It has long been recognised that stimulation frequency has a profound effect on the force of contraction [113]. Over the physiological range, force generally increases at a higher frequency, although the mechanisms are complex. The force-frequency relation reflects the balance of positive and negative inotropic effects of shortening the cycle length, and these are mediated through effects on the systolic Ca^{2+} transient [113]. Positive inotropic effects include greater SR Ca^{2+} loading through increased net Ca^{2+} and Na^+ influx due to the greater frequency of APs. As interventions that inhibit Na^+ entry, such as TTX treatment, inhibit the positive inotropic effect, the net accumulation of intracellular Na^+ is likely to be of particular importance to the force-frequency response [114–117]. The change in driving force for Ca^{2+} transport via NCX, together with the shortened diastolic interval, results in reduced Ca^{2+} extrusion from the cell [116, 117]. The frequency-dependent facilitation of I_{Ca} and SR Ca^{2+} uptake by SERCA is also likely to contribute to the positive inotropic effects [118, 119]. Negative inotropic effects result from the filling kinetics of the SR, refractoriness of the release process itself, the Ca^{2+}-dependent inactivation of I_{Ca} and APD shortening [113, 120].

The positive force-frequency relations of rat ventricular myocytes and right ventricular trabeculae were flattened or made negative following detubulation, indicating a particular role for the t-tubules in the positive inotropic effects of increasing stimulation frequency [84, 101]. However, the increase in $[Na^+]_i$ at higher stimulation rates was not significantly altered by detubulation [101]. There are at least three mechanisms by which t-tubules contributed to the positive inotropic effect of increasing pacing rate in these studies: (1) NCX, which translates the increase in $[Na^+]_i$ to a change in cellular Ca^{2+} load is located predominantly to the t-tubule. (2) I_{Ca} is also located predominantly in the t-tubule. While Ca^{2+} influx would be smaller in detubulated cells, the net influx per unit time would still be increased at higher rates. However, frequency-dependent facilitation of I_{Ca} occurs exclusively at the t-tubule so that this positive inotropic effect will be lost in detubulated cells [121]. (3) Modelling suggests that Ca^{2+} influx across the t-tubule membrane (predominantly via I_{Ca}) is greater than Ca^{2+} efflux (predominantly via NCX) so that there is a net loss of Ca^{2+} entry on detubulation. Thus, in detubulated cells, the negative inotropic effects of increased pacing rate may predominate over the positive inotropic effects. The modelling approach also suggests that [Ca^{2+}] within the t-tubule lumen may be decreased below that of the bulk extracellular solution at high stimulation frequencies, an effect that would limit the increase in Ca^{2+} load and protect against pro-arrhythmic activity at high rates [122, 123].

15.8 β-Adrenoceptor Stimulation

β-Adrenergic stimulation of ventricular muscle results in an increase in the amplitude and an abbreviation of the time course of the systolic Ca^{2+} transient [1]. The response involves β_1- and β_2-adrenoceptors, their selective stimulation producing distinct physiological responses although both receptor subtypes are G_s-protein coupled and their inotropic effects are predominantly mediated via the second messenger, cyclic AMP [124]. β_1-adrenoceptor stimulation produces a robust inotropic and lusitropic response, mediated largely by activation of protein kinase A (PKA) but also involving the Ca^{2+}-calmodulin-dependent kinase II (CaMKII) [124, 125]. The major Ca^{2+} flux pathways, LTCC, RyR and SERCA/PLB, are regulated via these two kinases following β_1-adrenoceptor activation, flux balance being required for the inotropic action of β-adrenergic stimulation to be sustained [1]. Note that while NCX may be phosphorylated at consensus sites for PKA, I_{NCX} is not regulated directly by β-adrenoceptor stimulation [126–128]. In contrast to β_1-adrenoceptor stimulation, the selective stimulation of β_2-adrenoceptors is less effective in producing positive inotropy, does not have a lusitropic effect and does not increase phosphorylation of PLB [129]. The β-adrenoceptor-subtype-specific inotropic and lusitropic effects are generally considered to arise largely from the compartmentation of cyclic AMP signalling [124, 125]. Whole-cell recordings from frog ventricular myocytes (that lack t-tubules) provided early evidence of the importance of compartmentation of cyclic AMP signalling in the regulation of I_{Ca} [130]. It was subsequently demonstrated in rat ventricular myocytes that the β_1-adrenoceptor regulation of I_{Ca} is via a cytosolic diffusive pathway, whereas the β_2-adrenoceptor regulation of I_{Ca} is localised to the cell membrane [131]. Fluorescent biosensors reporting cyclic AMP levels in distinct cellular compartments have provided important evidence regarding the compartmentation of cyclic AMP signalling in cardiac myocytes [124, 125, 132].

In mammalian ventricular myocytes, the t-tubules play an important role in the compartmentation of β-adrenoceptor signalling. Detubulation reduced the effectiveness of the non-selective β-adrenoceptor agonist, isoprenaline (isoproterenol, ISO) in increasing I_{Ca}, suggesting that LTCC were better coupled to β-adrenoceptors at the t-tubules than at the surface membrane [109]. Interestingly, the phosphorylation of PLB was not affected by detubulation [109]. The preferential regulation of LTCC at the t-tubule extended to the constitutive regulation by PKA and CaMKII as the inhibition of baseline I_{Ca} by, respectively, H-89 and KN-93 were markedly reduced in detubulated cells [133]. The effects of H-89 and KN-93 on the Ca^{2+} transient were also lost in detubulated cells [133]. The constitutive regulation of I_{Ca} at the t-tubule in rat ventricular myocytes involved caveolin-3 as treatment with a membrane-permeant peptide based on the caveolin-3 scaffolding domain (C3SD) inhibited I_{Ca} in intact but not in detubulated cells [29]. The localised regulation at the t-tubule by caveolin-3 required PKA as (1) the inhibitory effect of H-89 on rat ventricular myocyte I_{Ca} was significantly attenuated by treatment with the C3SD peptide, (2) treatment with the C3SD peptide reduced the fluorescence signal specific for phosphorylated LTCC at the t-tubule in untreated cells but not in cells treated with H-89, and (3) treatment with C3SD did not reduce I_{Ca} density in H-89-treated cells [29]. The β_2-adrenoceptor-mediated response of I_{Ca} to zinterol, which was confined to the t-tubules [134], was also effectively abolished by treatment with the C3SD peptide [29]. The suggestion that caveolin-3 is involved in the localised regulation of I_{Ca} by PKA and β_2-adrenoceptors at the t-tubules is supported by evidence from other approaches. For example, a role for caveolin-3 in the co-ordination of a caveolar signalling complex involving LTCC, PKA, adenylyl cyclase and the β_2-adrenoceptor in adult mouse and canine ventricular myocytes was suggested from data obtained using a combination of biochemical fractionation, electrophysiological recording and immuno-fluorescence imaging techniques [39]. Moreover, Gorelik and co-workers, using a combination of FRET-based probes for cyclic AMP and the scanning ion conductance microscopy system, elegantly demonstrated that cyclic AMP responses to β_2-adrenoceptor stimulation were localised to the t-tubules whereas β_1-adrenoceptor responses could be elicited both at the t-tubules and elsewhere on the cell surface [8, 124, 135].

Studies using mice with global knockout (KO) of the caveolin-3 gene in comparison with wild-type (WT) mice provide further evidence of a role for caveolin-3 in t-tubule I_{Ca} [33, 136]. Knockout of caveolin-3 had no effect on LTCC protein expression on Western blot [33]. However, while I_{Ca} density (current normalised to capacitance as an index of membrane surface area) at the surface membrane was not different between WT and caveolin-3 KO myocytes, I_{Ca} density in the t-tubule was markedly lower in myocytes from KO hearts than in WT cells [33]. Whole-cell I_{Ca} density in ventricular myocytes from WT mice was reduced by treatment with the C3SD peptide, but the peptide had no effect in myocytes from KO mice, indicating that the inhibitory action of the peptide was specific to caveolin-3 [33, 136]. Baseline I_{Ca} density was inhibited by H-89 at the surface and t-tubule membranes in both WT and KO myocytes, indicating that caveolin-3 was not essential for regulating LTCC by constitutive PKA in mouse ventricular myocytes [33]. Moreover, the difference in t-tubule I_{Ca} density between KO and WT myocytes was preserved in cells treated with H-89, indicating the existence of mechanisms independent of PKA in regulating t-tubule LTCC by caveolin-3 [33]. The targeting of an LTCC-blocking Rem protein to caveolar microdomains has led to the suggestion that caveolar I_{Ca} does not contribute to contractility, although hypertrophic signalling to the nucleus was inhibited by the targeting of LTCC in caveolae [46]. The finding that Ca^{2+} release was maintained in caveolin-3 knockout myocytes, despite the reduction in t-tubular I_{Ca} density, appears consistent with this suggestion [33]. It has been suggested that functional redundancy in t-tubule I_{Ca} in triggering Ca^{2+} release could account for the lack of effect of caveolin-3 knockout on the Ca^{2+} transient [33, 137]. On the other hand, the delay in the onset of Ca^{2+} release at the t-tubule following treatment of control myocytes with the C3SD peptide is consistent with a role for caveolin-3-regulated LTCC in EC coupling [136]. Although caveolin-3 is not thought to be present in the dyad itself [21], presumably, it is sufficiently close to control signalling in a microdomain comprising junctional LTCC.

15.9 Heart Failure

Myocytes from failing hearts exhibit a reduction in the amplitude of the systolic Ca^{2+} transient, dis-synchrony and slowing in the onset of Ca^{2+} release, slowing in the recovery phase of the Ca^{2+} transient, increased diastolic Ca^{2+} leak from the SR and a reduced SR Ca^{2+} content [1, 138]. This dysfunction reflects changes to some of the key Ca^{2+} flux pathways in heart failure, including reduced SERCA activity and expression, increased RyR opening probability and increases in NCX expression [1, 138]. Abnormalities in dyadic structure and extensive remodelling of the t-tubule network are important contributors to the pathology [1, 2], and these are considered in greater detail in Chap. 16 by Rog-Zielinska. The remainder of this chapter will consider evidence from recent studies that employed the detubulation technique to produce evidence of the redistribution of I_{Ca} in the sarcolemma and regulation by caveolin-3 in hypertrophy, ageing and heart failure.

Surgical ligation of the left anterior descending coronary artery (CAL) in rats has been shown by Lyon and colleagues to result in chronic heart failure 16 weeks post-surgery, with CAL hearts showing hypertrophy, left ventricular dilatation, and both systolic and diastolic dysfunction compared with heart from Sham-operated controls (Sham) [139]. Myocytes from CAL hearts were hypertrophied relative to Sham cells and imaging of di-8-ANEPPS-stained cells showed significant t-tubule remodelling, with a loss of transverse elements, consistent with the previous report of Lyon et al. [139, 140]. While there was no change in RyR staining at the z-lines, the Ca^{2+} transient amplitude was reduced, there was a slowing in the peak of the transient and this was associated with increased latency and heterogeneity in Ca^{2+} release at the t-tubule [140]. Although there was no difference in total whole-cell I_{Ca} density in CAL compared with Sham myocytes, detubulation revealed that I_{Ca} density was reduced in the t-tubule and increased in the surface membrane of CAL myocytes, indicating an effective redistribution of I_{Ca} from the t-tubule to surface sarcolemma in failing cells [140]. It seems likely that the reduction in t-tubule I_{Ca} contributed to the effects of CAL on local Ca^{2+} release, as these could be mimicked by the treatment of control cells with the LTCC blocker nifedipine at a concentration (200 nM) sufficient to reduce t-tubule I_{Ca} density to the level seen in CAL cells [140]. NCX function was also redistributed from the t-tubule to the surface sarcolemma in failing cells from this model [95]. Notably, hysteresis in the relationship between cytosolic free $[Ca^{2+}]_i$ and I_{NCX} density during the recovery from caffeine-induced unloading of the SR in detubulated CAL myocytes indicated coupling between NCX and RyR at the surface sarcolemma in failing cells that was not evident in Sham myocytes [95].

The inhibitory action of treatment with the C3SD peptide on I_{Ca} density was lost in CAL myocytes, indicating a loss of the localised PKA-dependent regulation of I_{Ca} at the t-tubule by caveolin-3 [134]. In addition, the response of I_{Ca} to zinterol, which was confined to the t-tubules in normal myocytes, could be elicited in both intact and detubulated CAL myocytes [134], consistent with a loss of localisation of signalling to the t-tubule by caveolin-3 and the redistribution β_2-adrenoceptors to the surface membrane in heart failure [8, 124]. The loss of caveolin-3-dependent regulation at the t-tubule in CAL myocytes was associated with a greater fractional decrease in t-tubule I_{Ca} density on treatment with H-89 in CAL myocytes than in Sham myocytes, consistent with the idea that caveolin-3 serves to localise and inhibit cyclic AMP signalling [25, 134, 140]. The reduction of t-tubular I_{Ca} in ventricular myocytes from young adult mice (3 month old) with cardiac-specific transgenic overexpression of caveolin-3 (Cav-3OE) compared with cells from age-matched WT hearts was consistent with the inhibitory action of caveolin-3 at the t-tubule [30]. Taken together, these data suggest a role for caveolin-3 in the localisation of cyclic AMP/PKA/β_2-adrenoceptor signalling to LTCC at the t-tubule in normal myocytes (Fig. 15.1).

In heart failure, I_{Ca} and β_2-adrenoceptors were redistributed to the surface sarcolemma and the localised regulation by caveolin-3 is lost. While the mechanisms underlying this redistribution remain unclear, presumably, the repartitioning of caveolin-3 to noncholesterol-rich membranes in heart failure leads to a loss of caveolin-3 from the t-tubules [141]. I_{Ca} density at the t-tubule was also shown to be reduced with ageing and in a pressure overload model of hypertrophy/heart failure (transverse aortic constriction or TAC) in mice [30, 136]. The reduction of t-tubular I_{Ca} with both ageing and heart failure was associated with reduced expression of caveolin-3 and a loss of sensitivity to the C3SD peptide, consistent with the suggestion that the loss of t-tubular I_{Ca} was attributable to the loss of caveolin-3-dependent regulation of I_{Ca} [30, 136]. Further evidence supporting this contention comes from the transgenic Cav3OE mice, which were protected against the loss of t-tubular I_{Ca} with age and TAC-induced heart failure [30, 142]. On the other hand, the transgenic overexpression of caveolin-3 did not prevent the loss of t-tubules and their remodelling with age and heart failure [30, 142].

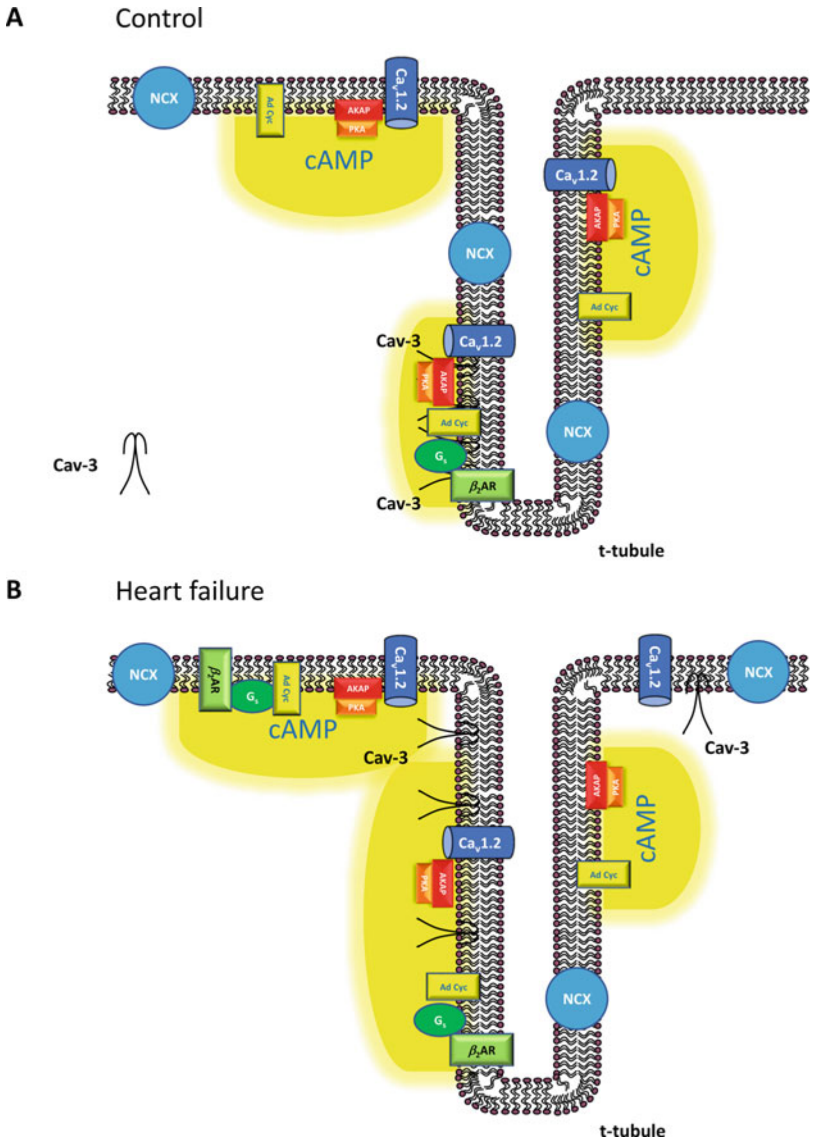
A
Control
NCX
Ad Cyc
AKAP
PKA
Cav1.2
cAMP
Cav1.2
AKAP
PKA
cAMP
NCX
Ad Cyc
Cav-3
Cav1.2
PKA
AKAP
Ad Cyc
NCX
Cav-3
Gs
β2AR
Cav-3
t-tubule
B
Heart failure
NCX
β2AR
Gs
Ad Cyc
AKAP
PKA
Cav1.2
cAMP
Cav1.2
NCX
Cav-3
Cav-3
AKAP
PKA
cAMP
Cav1.2
PKA
AKAP
Ad Cyc
Ad Cyc
NCX
Gs
β2AR
t-tubule

Fig. 15.1 A schematic summarizing the redistribution of I_{NCX}, I_{Ca} and its regulation by β2-adrenoceptors and caveolin-3 (Cav-3) in normal and in failing rat ventricular myocytes. (**a**) I_{NCX} and regulation of I_{Ca} in normal cardiac myocytes. NCX and LTCC density is greatest in the t-tubules, where Cav-3 co-ordinates a signalling domain involving β_2-adrenoceptors (β_2AR), adenylyl cyclase (Ad Cyc), PKA and the LTCC α_{1c}-subunit, $Ca_v1.2$. β_2AR coupled with LTCC are located exclusively in the t-tubules. Ad Cyc, PKA and $Ca_v1.2$ are also located outside of Cav-3 signaling domains, both within and without t-tubules. Activation of Ad Cyc, either via β_2AR or directly, augments LTCC activity through production of cAMP. Note that I_{NCX} is not regulated by β_2-adrenoceptors, cAMP or PKA. (**b**) Remodelling of I_{NCX} and I_{Ca} regulation in heart failure. The Cav-3 signalling complex is disrupted. β_2AR are located both within the t-tubules and on the surface sarcolemma. NCX and LTCC density are more evenly distributed between t-tubules and surface sarcolemma. The role of Cav-3 in the regulation of I_{Ca} is lost in heart failure. Adapted from Bryant et al. [134]

15.10 Conclusions

The use of the formamide-induced detubulation technique has provided considerable insight into the function of t-tubules and continues to be a useful tool in the armoury of the cardiac cellular biologist.

References

1. Eisner DA, Caldwell JL, Kistamás K, Trafford AW. Calcium and excitation-contraction coupling in the heart. Circ Res. 2017;121(2):181–95.
2. Hong T, Shaw RM. Cardiac T-tubule microanatomy and function. Physiol Rev. 2017;97(1):227–52.
3. Cannell MB, Kong CHT. Local control in cardiac E–C coupling. J Mol Cell Cardiol. 2012;52(2):298–303.
4. Shattock MJ, Ottolia M, Bers DM, et al. Na^+/Ca^{2+} exchange and Na^+/K^+-ATPase in the heart. J Physiol. 2015;593(6):1361–82.
5. Bers DM, Barry WH, Despa S. Intracellular Na^+ regulation in cardiac myocytes. Cardiovasc Res. 2003;57(4):897–912.
6. Negretti N, O'Neill SC, Eisner DA. The relative contributions of different intracellular and sarcolemmal systems to relaxation in rat ventricular myocytes. Cardiovasc Res. 1993;27(10):1826–30.
7. Bassani RA, Bassani JW, Bers DM. Mitochondrial and sarcolemmal Ca^{2+} transport reduce $[Ca^{2+}]_i$ during caffeine contractures in rabbit cardiac myocytes. J Physiol. 1992;453(1):591–608.
8. Nikolaev VO, Moshkov A, Lyon AR, et al. β_2-adrenergic receptor redistribution in heart failure changes cAMP compartmentation. Science. 2010;327(5973):1653–7.
9. Robu VG, Pfeiffer ES, Robia SL, et al. Localization of functional endothelin receptor signaling complexes in cardiac transverse tubules. J Biol Chem. 2003;278(48):48154–61.
10. Carozzi AJ, Ikonen E, Lindsay MR, Parton RG. Role of cholesterol in developing T-tubules: analogous mechanisms for T-tubule and caveolae biogenesis. Traffic. 2000;1(4):326–41.
11. Pásek M, Brette F, Nelson A, et al. Quantification of t-tubule area and protein distribution in rat cardiac ventricular myocytes. Progr Biophys Mol Biol. 2008;96(1–3):244–57.
12. Uchida K, Lopatin AN. Diffusional and electrical properties of T-tubules are governed by their constrictions and dilations. Biophys J. 2018;114(2):437–49.
13. Kaprielian RR, Stevenson S, Rothery SM, Cullen MJ, Severs NJ. Distinct patterns of dystrophin organization in myocyte sarcolemma and transverse tubules of normal and diseased human myocardium. Circulation. 2000;101(22):2586–94.
14. Brette F, Orchard C. T-tubule function in mammalian cardiac myocytes. Circ Res. 2003;92(11):1182–92.
15. Orchard C, Brette F. T-tubules and sarcoplasmic reticulum function in cardiac ventricular myocytes. Cardiovasc Res. 2008;77(2):237–44.
16. Rog-Zielinska EA, Johnston CM, O'Toole ET, Morphew M, Hoenger A, Kohl P. Electron tomography of rabbit cardiomyocyte three-dimensional ultrastructure. Progr Biophys Mol Biol. 2016;121(2):77–84.
17. Burton RAB, Rog-Zielinska EA, Corbett AD, et al. Caveolae in rabbit ventricular myocytes: distribution and dynamic diminution after cell isolation. Biophys J. 2017;113(5):1047–59.
18. Rog-Zielinska EA, Moss R, Kaltenbacher W, et al. Nano-scale morphology of cardiomyocyte t-tubule/sarcoplasmic reticulum junctions revealed by ultra-rapid high-pressure freezing and electron tomography. J Mol Cell Cardiol. 2021;153:86–92.
19. Leo-Macias A, Agullo-Pascual E, Sanchez-Alonso JL, et al. Nanoscale visualization of functional adhesion/excitability nodes at the intercalated disc. Nat Commun. 2016;7(1):10342.
20. Thomas MJ, Sjaastad I, Andersen K, et al. Localization and function of the Na^+/Ca^{2+}-exchanger in normal and detubulated rat cardiomyocytes. J Mol Cell Cardiol. 2003;35(11):1325–37.
21. Jayasinghe ID, Cannell MB, Soeller C. Organization of ryanodine receptors, transverse tubules, and sodium-calcium exchanger in rat myocytes. Biophys J. 2009;97(10):2664–73.
22. Hayashi T, Martone ME, Yu Z, et al. Three-dimensional electron microscopy reveals new details of membrane systems for Ca^{2+} signaling in the heart. J Cell Sci. 2009;122(7):1005–13.
23. Soeller C, Crossman D, Gilbert R, Cannell MB. Analysis of ryanodine receptor clusters in rat and human cardiac myocytes. Proc Natl Acad Sci U S A. 2007;104(38):14958–63.
24. Asghari P, Schulson M, Scriven DRL, Martens G, Moore EDW. Axial tubules of rat ventricular myocytes form multiple junctions with the sarcoplasmic reticulum. Biophys J. 2009;96(11):4651–60.
25. Norman R, Fuller W, Calaghan S. Caveolae and the cardiac myocyte. Curr Opin Physiol. 2018;1:59–67.
26. Page E. Quantitative ultrastructural analysis in cardiac membrane physiology. Am J Phys. 1978;235:C147–58.
27. Parton RG, Way M, Zorzi N, Stang E. Caveolin-3 associates with developing T-tubules during muscle differentiation. J Cell Biol. 1997;136(1):137–54.
28. Scriven DRL, Klimek A, Asghari P, Bellve K, Moore EDW. Caveolin-3 is adjacent to a group of Extradyadic ryanodine receptors. Biophys J. 2005;89(3):1893–901.
29. Bryant S, Kimura TE, Kong CHT, et al. Stimulation of I_{Ca} by basal PKA activity is facilitated by caveolin-3 in cardiac ventricular myocytes. J Mol Cell Cardiol. 2014;68(0):47–55.

30. Kong CHT, Bryant SM, Watson JJ, et al. The effects of aging on the regulation of t-tubular I_{Ca} by caveolin in mouse ventricular myocytes. J Gerontol: Series A. 2018;73(6):711–9.
31. Poulet C, Sanchez-Alonso J, Swiatlowska P, et al. Junctophilin-2 tethers T-tubules and recruits functional L-type calcium channels to lipid rafts in adult cardiomyocytes. Cardiovasc Res. 2021;117(1): 149–61.
32. Wagner E, Lauterbach M, Kohl T, et al. Stimulated emission depletion live cell super-resolution imaging shows proliferative remodeling of T-tubule membrane structures after myocardial infarction. Circ Res. 2012;111:402–14.
33. Bryant SM, Kong CHT, Watson JJ, et al. Caveolin-3 KO disrupts t-tubule structure and decreases t-tubular I_{Ca} density in mouse ventricular myocytes. Am J Phys. 2018;315(5):H1101–11.
34. Woodman SE, Park DS, Cohen AW, et al. Caveolin-3 Knock-out mice develop a progressive cardiomyopathy and show hyperactivation of the p42/44 MAPK cascade. J Biol Chem. 2002;277(41): 38988–97.
35. Israeli-Rosenberg S, Chen C, Li R, et al. Caveolin modulates integrin function and mechanical activation in the cardiomyocyte. FASEB J. 2015;29(2): 374–84.
36. Ichikawa Y, Zemljic-Harpf AE, Zhang Z, et al. Modulation of caveolins, integrins and plasma membrane repair proteins in anthracycline-induced heart failure in rabbits. PLoS One. 2017;12(5):e0177660.
37. Wypijewski KJ, Tinti M, Chen W, et al. Identification of caveolar resident proteins in ventricular myocytes using a quantitative proteomic approach: dynamic changes in caveolar composition following adrenoceptor activation. Mol Cell Proteomics. 2015;14(3):596–608.
38. Busija AR, Patel HH, Insel PA. Caveolins and cavins in the trafficking, maturation, and degradation of caveolae: implications for cell physiology. A J Physiol. 2017;312(4):C459–77.
39. Balijepalli RC, Foell JD, Hall DD, Hell JW, Kamp TJ. Localization of cardiac L-type Ca^{2+} channels to a caveolar macromolecular signaling complex is required for β_2-adrenergic regulation. Proc Natl Acad Sci U S A. 2006;103(19):7500–5.
40. MacDougall DA, Agarwal SR, Stopford EA, et al. Caveolae compartmentalise β_2-adrenoceptor signals by curtailing cAMP production and activating phosphatase in the sarcoplasmic reticulum of the adult ventricular myocyte. J Mol Cell Cardiol. 2012;52 (2):388–400.
41. Yarbrough TL, Lu T, Lee H-C, Shibata EF. Localization of cardiac sodium channels in caveolin-rich membrane domains: regulation of sodium current amplitude. Circ Res. 2002;90(4): 443–9.
42. Fujimoto T. Calcium pump of the plasma membrane is localized in caveolae. J Cell Biol. 1993;120(5): 1147–57.
43. Oceandy D, Stanley PJ, Cartwright EJ, Neyses L. The regulatory function of plasma-membrane Ca^{2+}-ATPase (PMCA) in the heart. Biochem Soc Trans. 2007;35(5):927–30.
44. Gross P, Johnson J, Romero CM, et al. Interaction of the joining region in Junctophilin-2 with the L-type Ca^{2+} channel is pivotal for cardiac dyad assembly and intracellular Ca^{2+} dynamics. Circ Res. 2021;128(1): 92–114.
45. Best JM, Kamp TJ. Different subcellular populations of L-type Ca^{2+} channels exhibit unique regulation and functional roles in cardiomyocytes. J Mol Cell Cardiol. 2012;52(2):376–87.
46. Makarewich CA, Correll RN, Gao H, et al. A Caveolae-targeted L-type Ca^{2+} channel antagonist inhibits hypertrophic signaling without reducing cardiac contractility / novelty and significance. Circ Res. 2012;110(5):669–74.
47. Collins Brett M, Davis Melissa J, Hancock John F, Parton RG. Structure-based reassessment of the Caveolin signaling model: do Caveolae regulate signaling through Caveolin-protein interactions? Develop Cell. 2012;23(1):11–20.
48. Byrne DP, Dart C, Rigden DJ. Evaluating caveolin interactions: do proteins interact with the caveolin scaffolding domain through a widespread aromatic residue-rich motif? PLoS One. 2012;7(9):e44879.
49. García-Cardeña G, Martasek P, BSS M, et al. Dissecting the interaction between nitric oxide synthase (NOS) and caveolin: Functional significance of the NOS caveolin binding domain in vivo. J Biol Chem. 1997;272(41):25437–40.
50. Toya Y, Schwencke C, Couet J, Lisanti MP, Ishikawa Y. Inhibition of adenylyl cyclase by caveolin peptides. Endocrinology. 1998;139(4):2025–31.
51. Dewulf M, Köster DV, Sinha B, et al. Dystrophy-associated caveolin-3 mutations reveal that caveolae couple IL6/STAT3 signaling with mechanosensing in human muscle cells. Nat Commun. 2019;10(1):1974.
52. Gazzerro E, Sotgia F, Bruno C, Lisanti MP, Minetti C. Caveolinopathies: from the biology of caveolin-3 to human diseases. E J Hum Genet. 2010;18(2): 137–45.
53. Vaidyanathan R, Reilly L, Eckhardt LL. Caveolin-3 microdomain: arrhythmia implications for potassium inward rectifier and cardiac sodium channel. Front Physiol. 2018;9:1548.
54. Sucharski HC, Dudley EK, Keith CBR, El Refaey M, Koenig SN, Mohler PJ. Mechanisms and alterations of cardiac ion channels leading to disease: role of Ankyrin-B in cardiac function. Biomol Ther. 2020;10(2):211.
55. Mohler PJ, Davis JQ, Bennett V. Ankyrin-B coordinates the Na/K ATPase, Na/ca exchanger, and InsP3 receptor in a cardiac T-tubule/SR microdomain. PLoS Biol. 2005;3(12):e423.
56. Mohler PJ, Schott J-J, Gramolini AO, et al. Ankyrin-B mutation causes type 4 long-QT cardiac arrhythmia and sudden cardiac death. Nature. 2003;421(6923): 634–9.

57. Mohler PJ, Splawski I, Napolitano C, et al. A cardiac arrhythmia syndrome caused by loss of ankyrin-B function. Proc Natl Acad Sci U S A. 2004;101(24):9137–42.
58. Schott JJ, Charpentier F, Peltier S, et al. Mapping of a gene for long QT syndrome to chromosome 4q25-27. Am J Hum Genet. 1995;57(5):1114–22.
59. Skogestad J, Aronsen JM, Tovsrud N, et al. Coupling of the Na^+/K^+-ATPase to Ankyrin B controls Na^+/Ca^{2+} exchanger activity in cardiomyocytes. Cardiovasc Res. 2020;116(1):78–90.
60. Zhu Y, Zhang C, Chen B, et al. Cholesterol is required for maintaining T-tubule integrity and intercellular connections at intercalated discs in cardiomyocytes. J Mol Cell Cardiol. 2016;97:204–12.
61. Calaghan S, Kozera L, White E. Compartmentalisation of cAMP-dependent signalling by caveolae in the adult cardiac myocyte. J Mol Cell Cardiol. 2008;45(1):88–92.
62. Kozera L, White E, Calaghan S. Caveolae act as membrane reserves which limit mechanosensitive $I_{Cl,swell}$ channel activation during swelling in the rat ventricular myocyte. PLoS One. 2009;4(12):e8312.
63. Calaghan S, White E. Caveolae modulate excitation-contraction coupling and β_2-adrenergic signalling in adult rat ventricular myocytes. Cardiovasc Res. 2006;69(4):816–24.
64. Gadeberg HC, Kong CHT, Bryant SM, James AF, Orchard CH. Cholesterol depletion does not alter the capacitance or ca handling of the surface or t-tubule membranes in mouse ventricular myocytes. Physiol Rep. 2017;5(22):e13500.
65. Ellingsen O, Davidoff AJ, Prasad SK, et al. Adult rat ventricular myocytes cultured in defined medium: phenotype and electromechanical function. Am J Physiol - Heart Circ Physiol. 1993;265(2):H747–54.
66. Lipp P, Hüser J, Pott L, Niggli E. Spatially non-uniform Ca^{2+} signals induced by the reduction of transverse tubules in citrate-loaded Guinea-pig ventricular myocytes in culture. J Physiol. 1996;497(3):589–97.
67. Mitcheson JS, Hancox JC, Levi AJ. Action potentials, ion channel currents and transverse tubule density in adult rabbit ventricular myocytes maintained for 6 days in culture. Pflugers Arch. 1996;431:814–27.
68. Louch WE, Bito V, Heinzel FR, et al. Reduced synchrony of Ca^{2+} release with loss of T-tubules—a comparison to Ca^{2+} release in human failing cardiomyocytes. Cardiovasc Res. 2004;62(1):63–73.
69. Pavlovic D, McLatchie LM, Shattock MJ. The rate of loss of T-tubules in cultured adult ventricular myocytes is species dependent. Exp Physiol. 2010;95(4):518–27.
70. Kawai M, Hussain M, Orchard CH. Excitation-contraction coupling in rat ventricular myocytes after formamide-induced detubulation. Am J Phys. 1999;277(2):H603–9.
71. Brette F, Komukai K, Orchard CH. Validation of formamide as a detubulation agent in isolated rat cardiac cells. Am J Phys. 2002;283(4):H1720–8.
72. Sacconi L, Ferrantini C, Lotti J, et al. Action potential propagation in transverse-axial tubular system is impaired in heart failure. Proc Natl Acad Sci U S A. 2012;109(15):5815–9.
73. Garciarena CD, Ma Y-l, Swietach P, Huc L, Vaughan-Jones RD. Sarcolemmal localisation of Na^+/H^+ exchange and Na^+–HCO_3^- co-transport influences the spatial regulation of intracellular pH in rat ventricular myocytes. J Physiol. 2013;591(9):2287–306.
74. Chase A, Orchard CH. Ca efflux via the sarcolemmal ca ATPase occurs only in the t-tubules of rat ventricular myocytes. J Mol Cell Cardiol. 2011;50(1):187–93.
75. Berry RG, Despa S, Fuller W, Bers DM, Shattock MJ. Differential distribution and regulation of mouse cardiac Na^+/K^+-ATPase α_1 and α_2 subunits in T-tubule and surface sarcolemmal membranes. Cardiovasc Res. 2007;73(1):92–100.
76. Horiuchi-Hirose M, Kashihara T, Nakada T, et al. Decrease in the density of t-tubular L-type Ca^{2+} channel currents in failing ventricular myocytes. Am J Phys. 2011;300(3):H978–88.
77. Bovo E, de Tombe PP, Zima AV. The role of dyadic organization in regulation of sarcoplasmic reticulum Ca^{2+} handling during rest in rabbit ventricular myocytes. Biophys J. 2014;106(9):1902–9.
78. Brette F, Sallé L, Orchard CH. Differential modulation of L-type Ca^{2+} current by SR Ca^{2+} release at the T-tubules and surface membrane of rat ventricular myocytes. Circ Res. 2004;95(1):e1–7.
79. Gadeberg HC, Kong CHT, Bryant SM, James AF, Orchard CH. Sarcolemmal distribution of I_{Ca} and I_{NCX} and ca autoregulation in mouse ventricular myocytes. A J Physiol - Heart Circ Physiol. 2017;313(1):H190–9.
80. Brette F, Orchard CH. No apparent requirement for neuronal sodium channels in excitation-contraction coupling in rat ventricular myocytes. Circ Res. 2006;98(5):667–74.
81. Despa S, Brette F, Orchard CH, Bers DM. Na/Ca exchange and Na/K-ATPase function are equally concentrated in transverse tubules of rat ventricular myocytes. Biophys J. 2003;85(5):3388–96.
82. Komukai K, Brette F, Yamanushi TT, Orchard CH. K^+ current distribution in rat sub-epicardial ventricular myocytes. Pflugers Arch. 2002;444:532–8.
83. Brette F, Despa S, Bers DM, Orchard CH. Spatiotemporal characteristics of SR Ca^{2+} uptake and release in detubulated rat ventricular myocytes. J Mol Cell Cardiol. 2005;39(5):804–12.
84. Ferrantini C, Coppini R, Sacconi L, et al. Impact of detubulation on force and kinetics of cardiac muscle contraction. J Gen Physiol. 2014;143(6):783–97.
85. Mellor NG, Pham T, Tran K, et al. Disruption of transverse-tubular network reduces energy efficiency

in cardiac muscle contraction. Acta Physiol. 2021;231(2):e13545.

86. Franzini-Armstrong C, Protasi F, Ramesh V. Shape, size, and distribution of Ca^{2+} release units and couplons in skeletal and cardiac muscles. Biophys J. 1999;77(3):1528–39.
87. Brette F, Salle L, Orchard CH. Quantification of calcium entry at the T-tubules and surface membrane in rat ventricular myocytes. Biophys J. 2006;90(1): 381–9.
88. Jones SA, Morton MJ, Hunter M, Boyett MR. Expression of TASK-1, a pH-sensitive twin-pore domain K^+ channel, in rat myocytes. Am J Phys. 2002;283(1):H181–5.
89. Abriel H, Rougier J-S, Jalife J. Ion channel macromolecular complexes in cardiomyocytes: roles in sudden cardiac death. Circ Res. 2015;116(12): 1971–88.
90. Brette F, Orchard CH. Density and sub-cellular distribution of cardiac and neuronal sodium channel isoforms in rat ventricular myocytes. Biochem Biophys Res Commun. 2006;348(3):1163–6.
91. Maier SKG, Westenbroek RE, Schenkman KA, Feigl EO, Scheuer T, Catterall WA. An unexpected role for brain-type sodium channels in coupling of cell surface depolarization to contraction in the heart. Proc Natl Acad Sci U S A. 2002;99(6):4073–8.
92. Vermij SH, Abriel H, Kucera JP. A fundamental evaluation of the electrical properties and function of cardiac transverse tubules. Biochim Biophys Acta, Mol Cell Res. 2020;1867(3):118502.
93. Radwański PB, Brunello L, Veeraraghavan R, et al. Neuronal Na^+ channel blockade suppresses arrhythmogenic diastolic Ca^{2+} release. Cardiovasc Res. 2015;106(1):143–52.
94. Yang Z, Pascarel C, Steele DS, Komukai K, Brette F, Orchard CH. Na^+-Ca^{2+} exchange activity is localized in the T-tubules of rat ventricular myocytes. Circ Res. 2002;91(4):315–22.
95. Gadeberg HC, Bryant SM, James AF, Orchard CH. Altered Na/Ca exchange distribution and activity in ventricular myocytes from failing hearts. Am J Phys. 2016;310(2):H262–8.
96. Trafford AW, Díaz ME, O'Neill SC, Eisner DA. Comparison of subsarcolemmal and bulk calcium concentration during spontaneous calcium release in rat ventricular myocytes. J Physiol. 1995;488(Pt 3):577–86.
97. Acsai K, Antoons G, Livshitz L, Rudy Y, Sipido KR. Microdomain $[Ca^{2+}]$ near ryanodine receptors as reported by L-type Ca^{2+} and Na^+/Ca^{2+} exchange currents. J Physiol. 2011;589(10):2569–83.
98. Shattock MJ, Bers DM. Rat vs. rabbit ventricle: Ca flux and intracellular Na assessed by ion-selective microelectrodes. Am J Phys. 1989;256:C813–22.
99. Lee CO, Abete P, Pecker M, Sonn JK, Vassalle M. Strophanthidin inotropy: role of intracellular sodium ion activity and sodium-calcium exchange. J Mol Cell Cardiol. 1985;17(11):1043–53.
100. Despa S, Bers DM. Functional analysis of Na^+/K^+-ATPase isoform distribution in rat ventricular myocytes. Am J Phys. 2007;293(1):C321–7.
101. Fowler MR, Dobson RS, Orchard CH, Harrison SM. Functional consequences of detubulation of isolated rat ventricular myocytes. Cardiovasc Res. 2004;62(3):529–37.
102. Swietach P, Leem C-H, Spitzer KW, Vaughan-Jones RD. Pumping Ca^{2+} up H^+ gradients: a Ca^{2+}–H^+ exchanger without a membrane. J Physiol. 2014;592 (15):3179–88.
103. Cingolani HE, Perez NG, Cingolani OH, Ennis IL. The Anrep effect: 100 years later. Am J Phys. 2013;304:H175–82.
104. Calaghan S, White E. Activation of Na^+–H^+ exchange and stretch-activated channels underlies the slow inotropic response to stretch in myocytes and muscle from the rat heart. J Physiol. 2004;559(1): 205–14.
105. Kockskämper J, von Lewinski D, Khafaga M, et al. The slow force response to stretch in atrial and ventricular myocardium from human heart: functional relevance and subcellular mechanisms. Progr Biophys Mol Biol. 2008;97(2):250–67.
106. Jiang Y, Huang H, Liu P, et al. Expression and localization of TRPC proteins in rat ventricular myocytes at various developmental stages. Cell Tissue Res. 2014;355(1):201–12.
107. Jayasinghe ID, Crossman DJ, Soeller C, Cannell MB. Comparison of the organization of t-tubules, sarcoplasmic reticulum and ryanodine receptors in rat and human ventricular myocardium. Clin Exp Pharmacol Physiol. 2012;39(5):469–76.
108. Benson MA, Tinsley CL, Waite AJ, et al. Ryanodine receptors are part of the myospryn complex in cardiac muscle. Sci Rep. 2017;7(1):6312.
109. Brette F, Rodriguez P, Komukai K, Colyer J, Orchard CH. β-Adrenergic stimulation restores the Ca transient of ventricular myocytes lacking t-tubules. J Mol Cell Cardiol. 2004;36(2):265–75.
110. Yuan W, Ginsburg KS, Bers DM. Comparison of sarcolemmal calcium channel current in rabbit and rat ventricular myocytes. J Physiol. 1996;493(Pt 3): 733–46.
111. Grantham CJ, Cannell MB. Ca^{2+} influx during the cardiac action potential in Guinea pig ventricular myocytes. Circ Res. 1996;79:194–200.
112. Rosenberg P, Katz D, Bryson V. SOCE and STIM1 signaling in the heart: timing and location matter. Cell Calcium. 2019;77:20–8.
113. Puglisi JL, Negroni JA, Chen-Izu Y, Bers DM. The force-frequency relationship: insights from mathematical modeling. Adv Physiol Educat. 2013;37(1): 28–34.
114. Frampton JE, Harrison SM, Boyett MR, Orchard CH. Ca^{2+} and Na^+ in rat myocytes showing different force-frequency relationships. Am J Phys. 1991;261 (5):C739–50.

115. Harrison SM, Boyett MR. The role of the Na^+-Ca^{2+} exchanger in the rate-dependent increase in contraction in Guinea-pig ventricular myocytes. J Physiol. 1995;482(3):555–66.
116. Endoh M. Force–frequency relationship in intact mammalian ventricular myocardium: physiological and pathophysiological relevance. Eur J Pharmacol. 2004;500(1–3):73–86.
117. Carmeliet E. Intracellular Ca^{2+} concentration and rate adaptation of the cardiac action potential. Cell Calcium. 2004;35(6):557–73.
118. Tiaho F, Piot C, Nargeot J, Richard S. Regulation of the frequency-dependent facilitation of L-type Ca^{2+} currents in rat ventricular myocytes. J Physiol. 1994;477(2):237–52.
119. DeSantiago J, Maier LS, Bers DM. Frequency-dependent acceleration of relaxation in the heart depends on CaMKII, but not Phospholamban. J Mol Cell Cardiol. 2002;34(8):975–84.
120. Decker KF, Heijman J, Silva JR, Hund TJ, Rudy Y. Properties and ionic mechanisms of action potential adaptation, restitution, and accommodation in canine epicardium. Am J Physiol Heart Circ Physiol. 2009;296(4):H1017–26.
121. Sallé L, Kharche S, Zhang H, Brette F. Mechanisms underlying adaptation of action potential duration by pacing rate in rat myocytes. Prog Biophys Mol Biol. 2008;96(1–3):305–20.
122. Pásek M, Šimurda J, Christé G. The functional role of cardiac T-tubules explored in a model of rat ventricular myocytes. Philos Trans A Math Phys Eng Sci. 2006;364(1842):1187–206.
123. Pásek M, Šimurda J, Christé G, Orchard CH. Modelling the cardiac transverse-axial tubular system. Progr Biophys Mol Biol. 2008;96(1): 226–43.
124. Gorelik J, Wright PT, Lyon AR, Harding SE. Spatial control of the βAR system in heart failure: the transverse tubule and beyond. Cardiovasc Res. 2013;98 (2):216–24.
125. Bers DM, Xiang YK, Zaccolo M. Whole-cell cAMP and PKA activity are epiphenomena, nanodomain signaling matters. Physiology. 2019;34(4):240–9.
126. Lin X, Jo H, Sakakibara Y, et al. β-Adrenergic stimulation does not activate Na^+-Ca^{2+} exchange current in Guinea-pig, mouse and rat ventricular myocytes. Am J Phys. 2006;290(2):C601–8.
127. Barman P, Choisy SCM, Hancox JC, James AF. β-Adrenoceptor/PKA-stimulation, Na^+-Ca^{2+} exchange and PKA-activated Cl^- currents in rabbit cardiomyocytes: a conundrum. Cell Calcium. 2011;49(4):233–9.
128. Barman PP, Cheng H, Hancox JC, James AF. Nickel inhibits β-1 adrenoceptor mediated activation of cardiac CFTR chloride channels. Biochem Biophys Res Commun. 2013;432(1):46–51.
129. Kuschel M, Zhou Y-Y, Spurgeon HA, et al. ß2-adrenergic cAMP signaling is uncoupled from phosphorylation of cytoplasmic proteins in canine heart. Circulation. 1999;99(18):2458–65.
130. Jurevicius J, Fischmeister R. cAMP compartmentation is responsible for a local activation of cardiac Ca^{2+} channels by beta -adrenergic agonists. Proc Natl Acad Sci U S A. 1996;93(1):295–9.
131. Chen-Izu Y, Xiao R-P, Izu LT, et al. Gi-dependent localization of beta 2-adrenergic receptor signaling to L-type Ca^{2+} channels. Biophys J. 2000;79(5): 2547–56.
132. Agarwal SR, Gratwohl J, Cozad M, Yang P-C, Clancy CE, Harvey RD. Compartmentalized cAMP signaling associated with lipid raft and non-raft membrane domains in adult ventricular myocytes. Front Pharmacol. 2018;9:332.
133. Chase A, Colyer J, Orchard CH. Localised Ca channel phosphorylation modulates the distribution of L-type Ca current in cardiac myocytes. J Mol Cell Cardiol. 2010;49(1):121–31.
134. Bryant SM, Kong CHT, Cannell MB, Orchard CH, James AF. Loss of caveolin-3-dependent regulation of I_{Ca} in rat ventricular myocytes in heart failure. Am J Phys. 2018;314:H521–9.
135. Korchev YE, Raval M, Lab MJ, et al. Hybrid scanning ion conductance and scanning near-field optical microscopy for the study of living cells. Biophys J. 2000;78(5):2675–9.
136. Bryant SM, Kong CHT, Watson JJ, et al. Caveolin-3 dependent loss of t-tubular I_{Ca} during hypertrophy and heart failure in mice. Exp Physiol. 2018;103: 652–65.
137. Cannell MB, Berlin JR, Lederer WJ. Effect of membrane potential changes on the calcium transient in single rat cardiac muscle cells. Science. 1987;238: 1419–23.
138. Bers DM. Cardiac sarcoplasmic reticulum calcium leak: basis and roles in cardiac dysfunction. Annu Rev Physiol. 2014;76(1):107–27.
139. Lyon AR, MacLeod KT, Zhang Y, et al. Loss of T-tubules and other changes to surface topography in ventricular myocytes from failing human and rat heart. Proc Natl Acad Sci U S A. 2009;106(16): 6854–9.
140. Bryant SM, Kong CHT, Watson J, Cannell MB, James AF, Orchard CH. Altered distribution of I_{Ca} impairs ca release at the t-tubules of ventricular myocytes from failing hearts. J Mol Cell Cardiol. 2015;86(1):23–31.
141. Ratajczak P, Damy T, Heymes C, et al. Caveolin-1 and -3 dissociations from caveolae to cytosol in the heart during aging and after myocardial infarction in rat. Cardiovasc Res. 2003;57(2):358–69.
142. Kong CHT, Bryant SM, Watson JJ, et al. Cardiac-specific overexpression of caveolin-3 preserves t-tubular I_{Ca} during heart failure in mice. Exp Physiol. 2019;104(5):654–66.

Structure of Transverse (T)-Tubules in Health and Disease

16

Eva A. Rog-Zielinska

Abstract

Transverse (t)-tubules are deep surface membrane invaginations present in mammalian striated muscle cells, including cardiomyocytes (ventricular and, to a lesser extent, atrial). T-tubules allow for close structural and functional coupling of sarcolemma and intracellular compartments, enabling rapid and synchronised excitation–contraction coupling within each muscle cell and—ultimately—uniform and efficient contraction of the whole heart. While continuous with the sarcolemma, t-tubules are structurally and functionally distinct domains whose luminal content, protein composition and lipid composition are tightly regulated. Furthermore, heart failure, even of distinct aetiologies, is commonly associated with adverse t-tubule remodelling. In this chapter, the structure of t-tubules in the healthy and diseased heart, new insights from current research concerning t-tubule remodelling as a therapeutic target in heart failure and, finally, pitfalls commonly encountered when conducting investigations into t-tubule structure will be discussed.

Keywords

Cardiac muscle · T-tubules · Heart failure · Excitation–contraction coupling · Sarcoplasmic reticulum

16.1 Structure of Cardiac T-Tubules in a Healthy Heart

16.1.1 T-Tubules Link Cardiac Electrics and Mechanics

Heart function depends on the coordinated activation of billions of cardiomyocytes. Each individual working cardiomyocyte in turn requires near-synchronous activation of its contractile units. Intracellular membrane systems play a crucial role in the generation of the externally homogenous activity of individual cells [1]. T-tubules form an elaborate, highly polymorphic network of deep tubular invaginations (with diameters ranging between 50 and 600 nm) of the sarcolemma, and are present throughout the entire cardiomyocyte body (Fig. 16.1a, b). T-tubules are electrically continuous with the 'surface' sarcolemma and enable close structural coupling of the plasma membrane with the intracellular calcium stores in the sarcoplasmic reticulum (SR; Fig. 16.1c) [2–4]. Close physical coupling of t-tubules and SR allows the action potential-triggered transmembrane influx of calcium to reach the SR rapidly, triggering

---

E. A. Rog-Zielinska (✉)
Institute for Experimental Cardiovascular Medicine, University Heart Center Freiburg • Bad Krozingen, Freiburg, Germany

Faculty of Medicine, University of Freiburg, Freiburg, Germany
e-mail: eva.rog-zielinska@uniklinik-freiburg.de

© Springer Nature Switzerland AG 2023
O. N. Tripathi et al. (eds.), *Heart Rate and Rhythm*, https://doi.org/10.1007/978-3-031-33588-4_16

much larger SR calcium release and—ultimately—uniform and efficient contraction [1]. This mechanism is further described in detail in Chap. 15 by James and Orchard. The presence of t-tubules ensures that no part of the healthy cardiomyocyte interior (except for nuclear content) is further than ~1 μm away from the sarcolemma.

Historically, the finding that external membrane tubules extend deep into the centre of cardiomyocytes helped to explain how electrical excitation is able to travel through the cardiomyocyte much faster than would be possible based on diffusion alone—with the existence of t-tubules hypothesised long before their first demonstration [5, 6].

While the luminal content of the t-tubular system is extracellular, t-tubules are very much a part of the interior of the cell. This structural duality of t-tubules makes them a fascinating, yet challenging, research target.

16.1.2 Formation of T-Tubules

T-tubules are largely absent during embryonic development. The initial stages of the formation of t-tubules have been reported to involve the appearance and proliferation of initially short, curved membrane invaginations at the cell periphery [7, 8]. These primitive curved domains progressively fuse and extend towards the cell centre. The exact mechanisms and drivers of the progression of t-tubule formation (addition of membrane and proteins, stabilisation of newly formed elements) are still unclear [9]. Plausibly, t-tubule growth may be driven at least partially by motor proteins, cytoskeletal activity, or recruitment of membrane proteins that respond to and regulate membrane curvature [10]. T-tubule biogenesis is concurrent with the maturation of SR and contractile elements, and the three processes are thought to be spatially and temporally linked. T-tubules continue to develop after birth, and in most mammals they achieve their 'adult' appearance within the first few weeks after birth.

Major proteins shown to be involved in the biogenesis of t-tubules are caveolin-3 (Cav-3, contributing to the initial formation of highly curved domains), bridging-integrator-1 (Bin-1, aiding tubulation) and dysferlin (Dysf, involved in membrane maintenance and repair) [11–14]. A further broad repertoire of proteins is involved in the subsequent establishment of the coupling to SR, recruitment of channels, as well as in docking of t-tubules to neighbouring organelles such as sarcomeres [15] and—potentially—mitochondria [16].

Biogenesis and maintenance of t-tubules are highly regulated and dynamic processes, and t-tubules are susceptible to physiological and pathological changes in their mechanical, biochemical, and electrical environment. A comprehensive understanding of t-tubule formation is important not only for basic research, but also in the area of translational medicine. An example is the development of stem cell-derived, cardiomyocyte-based in vitro models, long expected to advance the areas of personalised medicine and high-throughput pharmacology. While indeed promising as a research tool, these models tend to suffer from an immature phenotype (including a lack of t-tubules), limiting translational utility. Recent studies have suggested that the formation of t-tubules can be triggered through genetic manipulation (targeting molecules involved in t-tubule biogenesis), as well as by careful and sustained hormonal, mechanical, and electrical stimulation [17, 18]. The appearance of t-tubules following these interventions, in turn, drives the establishment of mature and functional excitation–contraction coupling machinery. Such approaches have the potential to significantly advance the field of stem cell-based cardiac research towards translational relevance. Similar t-tubule 'enhancing' efforts have also been applied to failing hearts, aimed at restoring disturbed t-tubule networks and—consequently—calcium cycling and contractile function (see Sect. 16.2 below) [19].

16.1.3 Structural Properties of T-Tubules

16.1.3.1 Network Topology

The mature, healthy t-tubular system displays a high order of intrinsic spatial organisation—especially in terms of density, regularity, and

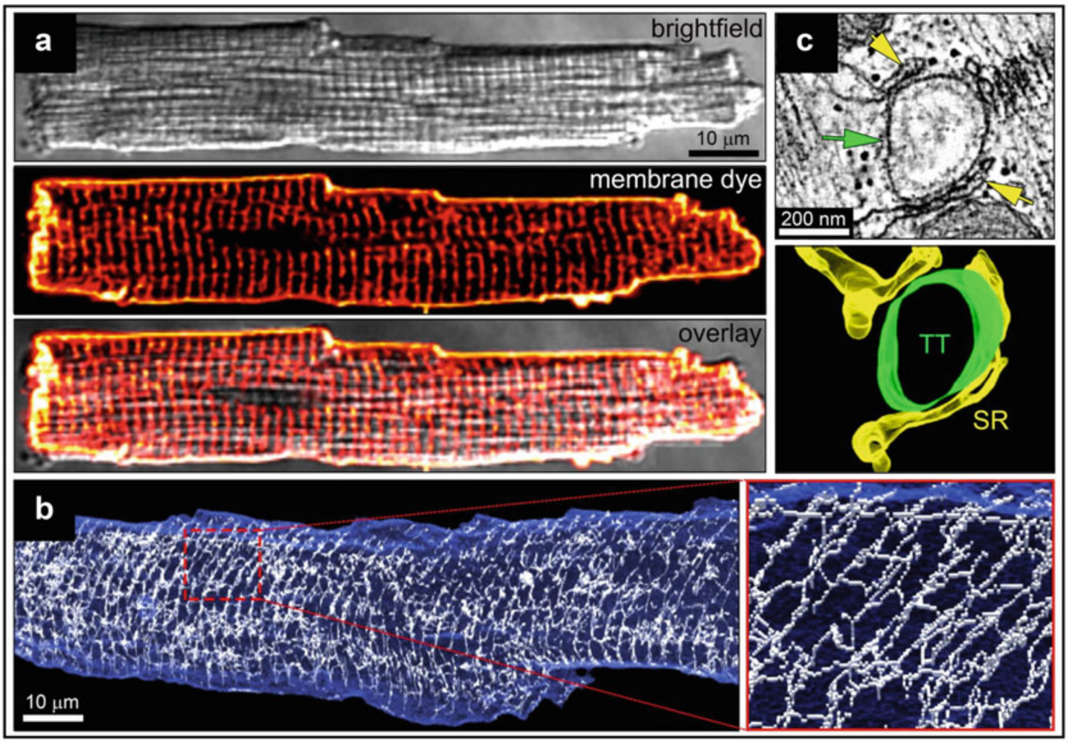

Fig. 16.1 Complex t-tubular structure in healthy cells. (**a**) Murine single ventricular cardiomyocyte, imaged using a combination of brightfield and confocal microscopy; surface and t-tubule membrane (red) visualised using a lipophilic membrane dye (di-8-ANEPPS). (**b**) 3D rendering of rabbit ventricular t-tubular system, segmented and skeletonised (inset) from confocal stacks of ventricular tissue; stained using wheat germ agglutinin to outline cell membranes. Image courtesy of Frédéric Sonak and Joachim Greiner; IEKM Freiburg. (**c**) Electron tomography and 3D segmentation of a single t-tubule (green) and associated SR (yellow) in rabbit ventricular tissue

orientation of individual elements [20]. Depending on the species and developmental stage, t-tubules occupy 1–5% of the total cell volume and contain 20–60% of the total sarcolemma (different estimates are probably due to species differences, as well as experimental differences) [2, 21, 22]. The t-tubule network displays a high degree of regularity, with transverse elements spaced quite evenly and displaying a ‘striation’-like appearance (in longitudinal view) [8, 23]. T-tubules and SR membranes approach each other within 10–20 nm, forming so-called dyads [24, 25]. The precise spatial organisation of the dyad is essential for efficient calcium cycling, and its stability is regulated by specialised proteins, including junctophilin-2 (Jph2) which is thought to ‘hold’ the two membranes closely together and aid in channel recruitment [26].

While generally referred to as ‘t-tubules’, this term is a misnomer, as the system—even under normal conditions—contains a significant proportion of elements that are oriented either axially (longitudinally) or which run diagonally in relation to the long axis of the cell [4]. The two main differently oriented tubule populations (axial and transversal) are believed to be structurally and functionally distinct (in terms of size, extent of coupling to SR, etc.) [27, 28]. The exact relevance of the presence of axial elements is not clear, but may include aiding in mechanical (providing ‘spare’ membrane during stretch) or electrical (aiding calcium diffusion between neighbouring t-tubules) integrity of cardiomyocytes. The presence and contribution of axial elements to excitation–contraction coupling changes with development and during pathological remodelling (see Sect. 16.2 below).

16.1.3.2 Individual T-Tubule Geometry

The topology of individual t-tubule segments introduces an additional level of complexity to the network, as they are not simply straight cylinders of constant diameter, such as usually shown in textbook illustrations. Computer modelling studies strongly support the presence of frequent dilatations and constrictions along the t-tubules, which significantly affect their electrical and diffusive properties [29].

The t-tubule membrane also contains numerous spheroid domains of 50–100 nm diameter, displaying the characteristic 'omega shape' of caveolae often seen in the surface membrane [30]. Caveolae are estimated to occupy as much as 10% of the total t-tubule surface area [31]. The specific role of t-tubule caveolae (beyond compartmentalisation and signal transduction) is not clear; they may aid in buffering membrane tension through the provision of the spare membrane (they get 'flattened' during stretch) [22, 30], and contribute to mechanosensing [32].

Finally, the t-tubule connections with the outer cell surface ('mouth' regions) have been reported to contain additional structural restrictions in certain species—for example, mouse t-tubule mouths form convoluted narrow spaces filled with dense matter, which appears to impede diffusion between the t-tubule lumen and bulk extracellular space [33].

In summary, t-tubule topology is complex and dynamic. The mechanisms governing t-tubule maintenance in the face of continuous beat-by-beat deformation are poorly understood [22]. Several studies have proposed that the stability of individual elements is aided by the presence of an inside and outside scaffold of various curvature-stabilising proteins, adhesion molecules, extracellular matrix components, glycocalyx, and coupling to membrane stores, cytoskeleton, and contractile lattice elements [34]. Exploration of which of these matter, and when and how they matter, will require 'dynamic' 3D ultrastructural studies (see Sect. 16.3 below).

16.1.3.3 Membrane Properties

The passive electrical properties of t-tubule membranes are a subject of ongoing debate. Previous studies have estimated the electrical length constant of t-tubules (a reflection of the electrical propagation capabilities of passive conductors) to be ~200–300 μm, supporting the idea of reliable electrotonic conduction over distances exceeding the size of cardiac myocytes [35]. These values were, however, subsequently suggested to be up to an order of magnitude lower, in particular during electrical excitation, based on computational models that included t-tubule constrictions and a reduced membrane resistivity during the action potential [29].

The t-tubule membrane contains a host of voltage-, ligand-, and mechano-gated ion channels, as well as additional accessory proteins and receptors (e.g. β-adrenergic receptor) [36]. Most crucial for excitation–contraction coupling are calcium, sodium and potassium channels, pumps and transporters—the distribution of which has been shown to be highly regulated and distinct between t-tubules and surface sarcolemma. Previous immunohistochemistry, electrophysiology, and membrane fractionation experiments have indicated that many currents important for excitation–contraction coupling are concentrated in t-tubules and, due to the unique microenvironment of the t-tubule lumen, are subject to potentially differential regulation by signalling molecules, mechanical environment, and pathological remodelling [37]. For more in-depth information, see Chap. 15 by James and Orchard.

Several studies have also shown t-tubule membranes to have a different lipid composition compared to surface sarcolemma, with t-tubules enriched in cholesterol and phospholipids such as phosphatidylserine and sphingomyelin [38, 39]. This unique lipid fingerprint of t-tubules may aid in electrical and mechanical stability and plasticity of the membrane.

16.1.3.4 T-Tubule Content

Another important structural property of t-tubules is their luminal content. While continuous with extracellular space, the t-tubule content exhibits unique characteristics in terms of composition (ions, nutrients, extracellular matrix proteins) and viscosity [40]. The mechanisms underlying such disparities between 'bulk' extracellular and t-tubule content are not well described.

In addition to 'free luminal content', the t-tubule membrane is coated by glycocalyx (also referred to as basal lamina, and extending 30–50 nm from the external membrane surface)—a 'fuzzy' matrix of surface glycoproteins and glycolipids. In addition to protecting the membrane from damage, the glycocalyx is thought to trap and immobilise molecules and ions close to the surface, further shaping the t-tubule microenvironment [41].

16.1.4 Chamber Differences

The extensive t-tubule network is an established feature of adult mammalian ventricular myocytes. In contrast, atrial cells were long believed to not contain t-tubules and rather rely on calcium diffusion from the cell periphery to trigger SR calcium release following membrane depolarisation. This was assumed to be sufficiently fast, given the smaller diameter of atrial compared to ventricular myocytes [42]. More recently, owing to improvements in sample preparation and imaging, atrial myocytes from many species have been reported to contain t-tubule networks, with the networks appearing to become increasingly complex the larger the animal [43, 44].

The atrial t-tubule systems have been shown to contain a comparatively high proportion of axial tubules, and these axial elements have been shown to be major participants in excitation–contraction coupling, able to activate intracellular calcium release and sarcomeric contraction [27].

16.1.5 Species Differences

The topology of the t-tubule system varies between species. In rodents, t-tubules form complex, dense, branched meshes containing a high proportion of axial elements, whereas in larger animals (including humans), t-tubule networks appear less dense and more organised [2, 4, 45, 46]. In addition, there are considerable differences in the diameter of individual elements between species—for example, rabbit t-tubules were shown to be approximately twice the size of mouse t-tubules [2]. Finally, the architecture of t-tubule mouth regions also displays species dependency, being heavily convoluted in mouse, yet fairly open and unobstructed in rat, rabbit, pig, and human [47]. The presence and structure of t-tubules in atrial cells also differ between species (discussed above).

The underlying mechanisms and exact functional consequences of the differences in the appearance of t-tubules between species are unknown. It has been proposed that the complexity and density of the t-tubule system correlate with cell size (larger cells requiring more extensive networks), or heart rate (the higher heart rate in smaller mammals requiring a different degree of 'protection' of t-tubule content from free extracellular fluid).

Significant species differences in t-tubule architecture highlight the importance of a careful choice of appropriate experimental models. Additionally, any experimental data concerning cardiac function should be interpreted with an awareness of species differences in the structure of t-tubules.

16.2 T-Tubules in Diseased Heart

T-tubule network architecture is not static and can be modulated by multiple factors, including biochemical (proteins, signalling molecules) and mechanical cues (cardiac workload, wall stress, changes in the extracellular matrix).

Many studies to date, conducted across a wide range of species including human, have shown various types of heart disease are associated with the pathological remodelling of t-tubules. Among others, multi-aetiology cardiomyopathies (dilated, ischaemic, hypertrophic, diabetic, arrhythmogenic, hypertensive [21, 48–50]), focal injuries (myocardial infarction [51]) and experimentally induced heart failure (e.g. transgenic animal models [52]) have all been shown to be closely associated with disruptions to the t-tubule network.

The most commonly seen pathological phenotypes are a decrease in t-tubule density, the disappearance of regularity with local loss of t-tubules, increases in tortuosity, changes in orientation (from transverse to axial), dilation and sheet-like remodelling, decreased coupling to SR and sarcomeres, and increased collagen deposition within the t-tubule lumen [35, 40, 53–55]. Pathological remodelling of t-tubules is evident not only in ventricular pathologies but also in atrial cells, for example, in the course of atrial fibrillation and atrial overload [42, 56, 57].

Interestingly, t-tubule remodelling may precede disease progression towards detectable functional impairment. Furthermore, deterioration in heart function, once apparent, is paralleled by further progressive t-tubule remodelling, which can spread from the initial area of injury to more remote tissue [58, 59] (see Fig. 16.2). All this suggests that t-tubule remodelling is not merely a secondary modification, but a potentially important driver of heart disease, as well as the final common pathway in heart failure.

A common feature of the development of heart failure is pathological hypertrophy that leads to maladaptive remodelling, including t-tubule loss. However, physiological hypertrophy (resulting, for example, from exercise or pregnancy) is not linked to t-tubule disruption [60]. Several hypotheses have been put forward regarding the significance of t-tubule remodelling during progression from adaptive to maladaptive hypertrophy, proposing that early changes in the t-tubule structure offer a compensatory mechanism that accelerates and/or synchronises excitation–contraction coupling in stressed cells (through an increased number of axial elements) and increases overall cell conductivity (through t-tubule pruning) [36]. The transition point between compensatory and detrimental t-tubule remodelling is currently unknown.

A causative influence of t-tubule loss on cardiac dysfunction has been demonstrated in models of t-tubule removal [61]. Once apparent, pathological t-tubule remodelling has been associated with a host of adverse functional consequences, including loss of calcium transient synchronicity (delays and transient broadening) [62], aberrant membrane proteins function, SR dysfunction [53, 54], decreased contraction kinetics, diminished cardiac output [63], and increased propensity for arrhythmogenesis [64].

T-tubule remodelling, consistently seen in heart failure, highlights t-tubules as an extremely attractive therapeutic target. T-tubule structure in failing hearts has been shown to be improved upon resynchronisation therapy [65], physical exercise [66], genetic [56, 67] and pharmacological [68, 69] interventions, as well as mechanical unloading [70]. Successful recovery of t-tubule structure is closely associated with improved overall cardiac function and continues to be a focus of many pre-clinical and clinical studies.

16.3 Imaging T-Tubules: Challenges and New Approaches

16.3.1 Spatial Considerations

Studying the ultrastructure and function of t-tubules has always been hindered by the fact that even advanced (e.g. confocal) light microscopy methods cannot provide sufficient resolution (optical diffraction limit >200 nm for visible light) for detection and detailed quantitative characterisation of single elements.

Nonetheless, light microscopy studies have provided valuable information regarding pan-cellular t-tubule organisation (including regularity, density, and orientation) [4, 45, 46, 71]. However, the available sub-micrometer scale data are not conducive to the exploration of details, such as cross-sectional shape, membrane topology, or contraction-induced deformation. Super-resolution optical methods can, in

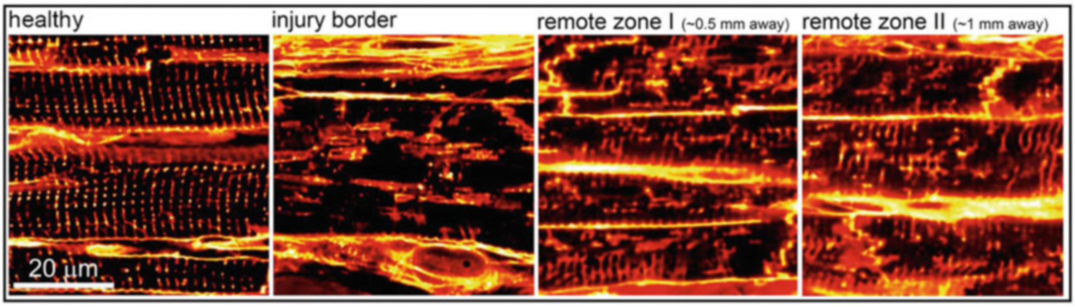

Fig. 16.2 Disrupted t-tubule structure in diseased heart. T-tubules in control (healthy) and in post-myocardial infarction rabbit ventricular tissue; visualised using wheat germ agglutinin to outline cell membrane and fibrotic areas and imaged using confocal microscopy. Pathological t-tubule remodelling (loss, dilation, changes in orientation) is evident both in the immediate vicinity of the injury and in more remote areas. Images courtesy of Joachim Greiner, IEKM Freiburg

certain cases, resolve the lumen of individual t-tubules [72]; these methods, however, often tend to be unsuitable for live-cell imaging and suffer from 'information loss' due to voxel anisotropy (where the X–Y–Z dimensions of the 3D voxel are not equal). Live-cell assessment of t-tubule geometry can be improved using dual t-tubule membrane and lumen staining, followed by post-acquisition image processing, which allows for t-tubule diameter calculation. Such assessments, however, rely on assumptions regarding the relationship between surface area and volume (usually implying a cylindrical tubule model), which would not be suitable for t-tubules with irregular shape (e.g. in diseased or contracting cells) [2].

Transmission electron microscopy-based approaches offer the optimal spatial resolution for imaging individual t-tubules (resolution ~1–10 nm) [24]. The main drawback of these approaches however is their incompatibility with live-cell studies and the inherently 2D nature of conventional electron microscopy, potentially leading to erroneous conclusions regarding t-tubule shape. As most non-perpendicular cuts through a cylinder yield ellipse, for example, it is nearly impossible to determine the cross-section shape of t-tubules or quantify minimum t-tubule-SR distance in 2D images.

Progression of electron microscopy into the 3D domain is offered through several approaches, and the choice of the most appropriate method will inadvertently involve a compromise between imaged volume, resolution, and risk of artefacts. Larger volumes can be imaged by serial sectioning and imaging of the slice [73] or (more frequently) of the remaining block-face using scanning electron microscopy [74], with (in both cases) subsequent image registration. Both approaches allow one to resolve single t-tubules but not finer details of dyadic structures and exact membrane topology. In addition, since both approaches are sample-destructive techniques, additional challenges arise from the 3D integration of inherently deformed 2D sections. Many of these obstacles can be circumvented by the use of electron tomography, which allows for non-destructive imaging of thicker samples with superior resolution (<1 nm) and isotropic voxel dimensions (equal voxel size in X–Y–Z). Electron tomography supports the assessment of the exact shape and topology of t-tubules and their coupling to other organelles; these advantages come at the cost of severely limited imaging volumes [75].

Hybrid methods, combining light and electron microscopic observations, could be employed to first study live cells (for temporal domain and functional information), followed by nano-structural assessments (e.g. protein distribution in specific t-tubule microdomains) by electron microscopy. Furthermore, 'holistic' t-tubule analysis would ideally combine structural and functional imaging and would involve correlating observations of t-tubule structure with measurement of, for example, diffusive or electrical properties [22, 35].

16.3.2 Temporal Considerations

All imaging approaches are essentially based on still images. If taken serially at short enough intervals, these 'stills' turn into movies ('motion pictures'). A problem arises when the dynamics of biological processes are fast compared to frame rates, for example, when objects move. For cardiac imaging, this is often, though incorrectly, referred to as the 'motion artefact'. The fact that physiological motion is rarely incorporated into cardiac cellular studies hinders both light- and electron-based observations. As an example of the latter, earlier studies involving the chemical fixation of cardiac tissue in different steady-state deformation states suggested that t-tubules are subject to significant deformation upon cell stretch and contraction [30]. There, the 'frame rate' (i.e. the time taken between the onset of mechanical deformation and tissue fixation), measured in the minute-range, was far too slow to assess t-tubule deformation dynamics.

More recent work has utilised high-pressure freezing of contracting cardiomyocytes, where cell preservation was timed with millisecond-accuracy relative to the onset of contraction. This confirmed the highly dynamic nature of changes in t-tubule shape, orientation and surface topology—all of which may affect t-tubule function (from adding advection to the previously established diffusive exchange of t-tubule lumen content to beat-by-beat membrane-incorporation of t-tubule caveolae into the cell membrane [22]). In the future, it will be important to further assess changes in t-tubules—individual elements and whole-cell networks—in freely contracting cells, which can be achieved using fast light microscopy of living, stimulated cells, or electron microscopy imaging of samples rapidly preserved at different stages of the contractile cycle [22].

16.3.3 Pitfalls In Sample Preparation

As a final note of caution: structural analysis of t-tubules is prone to artefacts induced by sample preparation. T-tubule structure in living cells is extremely sensitive to changes in the extracellular environment, such as changes in ion concentration, oxygen availability during preparation, solution osmolality, and temperature. T-tubule architecture and surface topology (e.g. the presence of caveolae) have been shown to be affected by cell swelling, shrinking, ischaemia, and prolonged storage prior to preservation [31, 76]. Additionally, careful control of the cells' mechanical state (e.g. preservation in a defined mechanical state, accompanied by an assessment of sarcomere length) should always be conducted to allow for data comparison across studies.

The choice of sample preservation is crucial, particularly for electron microscopy. The conventional method for cardiac sample preservation involves aldehyde-based fixation and subsequent dehydration. This well-established method is associated with pronounced sample shrinkage, altering the structure of biological samples by distortion and displacement of structures—all of which may give rise to erroneous conclusions regarding ultrastructural organisation [25]. This can be avoided by sample vitrification. Vitrification preserves cells by turning water-containing samples into a non-crystalline amorphous solid, and is achieved by ultra-rapid high-pressure freezing. This has been shown to prevent the collapse and distortion of membranous organelles in cardiac samples, such as the SR, that is routinely seen when using aldehyde-based fixation [22, 25, 75]. A drawback of this method is that vitrification can be achieved for relatively small samples only (tissue fragments and cells). For this reason, some studies have combined 'light chemical fixation' of whole hearts with subsequent high-pressure freezing. While avoidance of dehydration prevents much of the tissue shrinkage mentioned above, chemical fixation—even 'light' chemical fixation—distorts cell ultrastructure, and is best avoided when exploring t-tubules and associated cellular compartments.

16.4 Conclusions

T-tubules serve as a crucial link between the heart's electrical and mechanical activity. T-tubule structure is complex and dynamic, changing with developmental stages, with (mal-) adaptation to changing demands in health and disease, and with every single cycle of cardiac filling and ejection. Prevention of pathological t-tubule remodelling may be an attractive therapeutic target, for example, in developing novel strategies to delay and treat heart failure. To achieve this, more research will be required to explore t-tubule structural and functional autoregulation.

Acknowledgements We thank all members of the Institute for Experimental Cardiovascular Medicine (IEKM) for critical discussion of the manuscript, and Dr James O'Reilly for help with editing. This work was supported by the German Research Foundation (DFG; CRC1425 [#4226818459] and the Emmy-Noether Programme [#396913060]).

References

1. Bers DM. Cardiac excitation–contraction coupling. Nature. 2002;415(6868):198–205.
2. Kong CHT, Rog-Zielinska EA, Orchard CH, Kohl P, Cannell MB. Sub-microscopic analysis of t-tubule geometry in living cardiac ventricular myocytes using a shape-based analysis method. J Mol Cell Cardiol. 2017;108:1–7.
3. Orchard CH, Pasek M, Brette F. The role of mammalian cardiac t-tubules in excitation-contraction coupling: experimental and computational approaches. Exp Physiol. 2009;94(5):509–19.
4. Soeller C, Cannell MB. Examination of the transverse tubular system in living cardiac rat myocytes by 2-photon microscopy and digital image-processing techniques. Circ Res. 1999;84(3):266–75.
5. Hill AV. The abrupt transition from rest to activity in muscle. Proc R Soc Lond B Biol Sci. 1949;136(884): 399–420.
6. Lindner E. Die submikroskopische Morphologie des Herzmuskels. Z Zellforsch Mikrosk Anat. 1957;45(6): 702–46.
7. Forbes MS, Sperelakis N. The presence of transverse and axial tubules in the ventricular myocardium of embryonic and neonatal Guinea pigs. Cell Tissue Res. 1976;166(1):83–90.
8. Forbes MS, Hawkey LA, Sperelakis N. The transverse-axial tubular system (TATS) of mouse myocardium: its morphology in the developing and adult animal. Am J Anat. 1984;170(2):143–62.
9. Di Maio A, Karko K, Snopko RM, Mejía-Alvarez R, Franzini-Armstrong C. T-tubule formation in cardiac myocytes: two possible mechanisms? J Muscle Res Cell Motil. 2007;28(4):231–41.
10. Mahapatra A, Uysalel C, Rangamani P. The mechanics and thermodynamics of tubule formation in biological membranes. J Membr Biol. 2021;254:273.
11. Al-Qusairi L, Laporte J. T-tubule biogenesis and triad formation in skeletal muscle and implication in human diseases. Skelet Muscle. 2011;1(1):26.
12. Lee E, Marcucci M, Daniell L, Pypaert M, Weisz OA, Ochoa G-C, et al. Amphiphysin 2 (Bin1) and t-tubule biogenesis in muscle. Science. 2002;297(5584): 1193–6.
13. Hofhuis J, Bersch K, Wagner S, Molina C, Fakuade FE, Iyer LM, et al. Dysferlin links excitation-contraction coupling to structure and maintenance of the cardiac transverse-axial tubule system. Europace. 2020;22(7):1119–31.
14. Parton RG, Way M, Zorzi N, Stang E. Caveolin-3 associates with developing t-tubules during muscle differentiation. J Cell Biol. 1997;136(1):137–54.
15. Ibrahim M, Siedlecka U, Buyandelger B, Harada M, Rao C, Moshkov A, et al. A critical role for Telethonin in regulating t-tubule structure and function in the mammalian heart. Hum Mol Genet. 2013;22(2): 372–83.
16. Rog-Zielinska EA, O'Toole ET, Hoenger A, Kohl P. Mitochondrial deformation during the cardiac mechanical cycle. Anat Rec (Hoboken). 2019;302(1): 146–52.
17. De La Mata A, Tajada S, O'Dwyer S, Matsumoto C, Dixon RE, Hariharan N, et al. BIN1 induces the formation of t-tubules and adult-like Ca^{2+} release units in developing cardiomyocytes. Stem Cells. 2019;37(1): 54–64.
18. Parikh SS, Blackwell DJ, Gomez-Hurtado N, Frisk M, Wang L, Kim K, et al. Thyroid and glucocorticoid hormones promote functional t-tubule development in human-induced pluripotent stem cell-derived cardiomyocytes. Circ Res. 2017;121(12):1323–30.
19. Li J, Richmond B, Hong T. Cardiac t-tubule cBIN1-microdomain, a diagnostic marker and therapeutic target of heart failure. Int J Mol Sci. 2021;22(5):2299.
20. Crossman DJ, Ruygrok PR, Soeller C, Cannell MB. Changes in the organization of excitation-contraction coupling structures in failing human heart. PLoS One. 2011;6(3):e17901.
21. Brette F, Orchard C. T-tubule function in mammalian cardiac myocytes. Circ Res. 2003;92(11):1182–92.
22. Rog-Zielinska EA, Scardigli M, Peyronnet R, Zgierski-Johnston CM, Greiner J, Madl J, et al. Beat-by-beat cardiomyocyte t-tubule deformation drives tubular content exchange. Circ Res. 2021;128(2): 203–15.
23. Sperelakis N, Rubio R. An orderly lattice of axial tubules which interconnect adjacent transverse tubules in guinea-pig ventricular myocardium. J Mol Cell Cardiol. 1971;2(3):211–20.

24. Franzini-Armstrong C, Protasi F, Ramesh V. Shape, size, and distribution of Ca^{2+} release units and couplons in skeletal and cardiac muscles. Biophys J. 1999;77(3):1528–39.
25. Rog-Zielinska EA, Moss R, Kaltenbacher W, Greiner J, Verkade P, Seemann G, et al. Nano-scale morphology of cardiomyocyte t-tubule/sarcoplasmic reticulum junctions revealed by ultra-rapid high-pressure freezing and electron tomography. J Mol Cell Cardiol. 2021;153:86–92.
26. Gross P, Johnson J, Romero CM, Eaton DM, Poulet C, Sanchez-Alonso J, et al. Interaction of the joining region in junctophilin-2 with the L-type Ca^{2+} channel is pivotal for cardiac dyad assembly and intracellular Ca^{2+} dynamics. Circ Res. 2021;128(1):92–114.
27. Brandenburg S, Kohl T, Williams GS, Gusev K, Wagner E, Rog-Zielinska EA, et al. Axial tubule junctions control rapid calcium signaling in atria. J Clin Invest. 2016;126(10):3999–4015.
28. Asghari P, Schulson M, Scriven DRL, Martens G, Moore EDW. Axial tubules of rat ventricular myocytes form multiple junctions with the sarcoplasmic reticulum. Biophys J. 2009;96(11):4651–60.
29. Uchida K, Lopatin AN. Diffusional and electrical properties of T-tubules are governed by their constrictions and dilations. Biophys J. 2018;114(2): 437–49.
30. Kohl P, Cooper PJ, Holloway H. Effects of acute ventricular volume manipulation on in situ cardiomyocyte cell membrane configuration. Prog Biophys Mol Biol. 2003;82(1–3):221–7.
31. Burton RAB, Rog-Zielinska EA, Corbett AD, Peyronnet R, Bodi I, Fink M, et al. Caveolae in rabbit ventricular myocytes: distribution and dynamic diminution after cell isolation. Biophys J. 2017;113(5): 1047–59.
32. Norman R, Fuller W, Calaghan S. Caveolae and the cardiac myocyte. Curr Opin Physiol. 2018;1:59–67.
33. Rog-Zielinska EA, Kong CHT, Zgierski-Johnston CM, Verkade P, Mantell J, Cannell MB, et al. Species differences in the morphology of transverse tubule openings in cardiomyocytes. EP Europace. 2018;20: 120–4.
34. Kostin S, Scholz D, Shimada T, Maeno Y, Mollnau H, Hein S, et al. The internal and external protein scaffold of the t-tubular system in cardiomyocytes. Cell Tissue Res. 1998;294(3):449–60.
35. Scardigli M, Crocini C, Ferrantini C, Gabbrielli T, Silvestri L, Coppini R, et al. Quantitative assessment of passive electrical properties of the cardiac t-tubular system by FRAP microscopy. Proc Natl Acad Sci U S A. 2017;114(22):5737–42.
36. Vermij SH, Abriel H, Kucera JP. A fundamental evaluation of the electrical properties and function of cardiac transverse tubules. Biochim Biophys Acta, Mol Cell Res. 2020;1867(3):118502.
37. Brette F, Orchard C. Resurgence of cardiac t-tubule research. Physiology. 2007;22(3):167–73.
38. Carozzi AJ, Ikonen E, Lindsay MR, Parton RG. Role of cholesterol in developing T-tubules: analogous mechanisms for T-tubule and caveolae biogenesis. Traffic. 2000;1(4):326–41.
39. Pediconi MF, Donoso P, Hidalgo C, Barrantes FJ. Lipid composition of purified transverse tubule membranes isolated from amphibian skeletal muscle. Biochim Biophys Acta. 1987;921(2):398–404.
40. Crossman DJ, Shen X, Jüllig M, Munro M, Hou Y, Middleditch M, et al. Increased collagen within the transverse tubules in human heart failure. Cardiovasc Res. 2017;113(8):879–91.
41. Bers DM, Peskoff A. Diffusion around a cardiac calcium channel and the role of surface bound calcium. Biophys J. 1991;59(3):703–21.
42. Dibb KM, Clarke JD, Horn MA, Richards MA, Graham HK, Eisner DA, et al. Characterization of an extensive transverse tubular network in sheep atrial myocytes and its depletion in heart failure. Circ Heart Fail. 2009;2(5):482–9.
43. Richards MA, Clarke JD, Saravanan P, Voigt N, Dobrev D, Eisner DA, et al. Transverse tubules are a common feature in large mammalian atrial myocytes including human. Am J Physiol Heart Circ. 2011;301 (5):H1996–2005.
44. Smyrnias I, Mair W, Harzheim D, Walker SA, Roderick HL, Bootman MD. Comparison of the T-tubule system in adult rat ventricular and atrial myocytes, and its role in excitation-contraction coupling and inotropic stimulation. Cell Calcium. 2010;47 (3):210–23.
45. Jayasinghe I, Crossman D, Soeller C, Cannell M. Comparison of the organization of T-tubules, sarcoplasmic reticulum and ryanodine receptors in rat and human ventricular myocardium. Clin Exp Pharmacol Physiol. 2012;39(5):469–76.
46. Jayasinghe ID, Clowsley AH, Munro M, Hou Y, Crossman DJ, Soeller C. Revealing t-tubules in striated muscle with new optical super-resolution microscopy techniques. Eur J Transl Myol. 2015;25(1):4747.
47. Rog-Zielinska EA, Kong CHT, Zgierski-Johnston CM, Verkade P, Mantell J, Cannell MB, et al. Species differences in the morphology of transverse tubule openings in cardiomyocytes. Europace. 2018;20:120–4.
48. Guo A, Zhang C, Wei S, Chen B, Song LS. Emerging mechanisms of T-tubule remodelling in heart failure. Cardiovasc Res. 2013;98(2):204–15.
49. Orchard C, Brette F. T-tubules and sarcoplasmic reticulum function in cardiac ventricular myocytes. Cardiovasc Res. 2008;77(2):237–44.
50. Ibrahim M, Gorelik J, Yacoub MH, Terracciano CM. The structure and function of cardiac t-tubules in health and disease. Proc Biol Sci. 2011;278(1719): 2714–23.
51. Louch WE, Mørk HK, Sexton J, Strømme TA, Laake P, Sjaastad I, et al. T-tubule disorganization and reduced synchrony of Ca^{2+} release in murine cardiomyocytes following myocardial infarction. J Physiol. 2006;574(Pt 2):519–33.
52. Swift F, Franzini-Armstrong C, Øyehaug L, Enger UH, Andersson KB, Christensen G, et al. Extreme sarcoplasmic reticulum volume loss and compensatory

t-tubule remodeling after Serca2 knockout. Proc Natl Acad Sci U S A. 2012;109(10):3997–4001.

53. Seidel T, Navankasattusas S, Ahmad A, Diakos NA, Xu WD, Tristani-Firouzi M, et al. Sheet-like remodeling of the transverse tubular system in human heart failure impairs excitation-contraction coupling and functional recovery by mechanical unloading. Circulation. 2017;135(17):1632–45.
54. Song LS, Sobie EA, McCulle S, Lederer WJ, Balke CW, Cheng H. Orphaned ryanodine receptors in the failing heart. Proc Natl Acad Sci U S A. 2006;103(11):4305–10.
55. Pinali C, Bennett H, Davenport JB, Trafford AW, Kitmitto A. Three-dimensional reconstruction of cardiac sarcoplasmic reticulum reveals a continuous network linking transverse-tubules: this organization is perturbed in heart failure. Circ Res. 2013;113(11):1219–30.
56. Brandenburg S, Pawlowitz J, Eikenbusch B, Peper J, Kohl T, Mitronova GY, et al. Junctophilin-2 expression rescues atrial dysfunction through polyadic junctional membrane complex biogenesis. JCI Insight. 2019;4(12):127116.
57. Yue X, Zhang R, Kim B, Ma A, Philipson KD, Goldhaber JI. Heterogeneity of transverse-axial tubule system in mouse atria: remodeling in atrial-specific Na^+-Ca^{2+} exchanger knockout mice. J Mol Cell Cardiol. 2017;108:50–60.
58. Wei S, Guo A, Chen B, Kutschke W, Xie Y-P, Zimmerman K, et al. T-tubule remodeling during transition from hypertrophy to heart failure. Circ Res. 2010;107(4):520–31.
59. Greiner J, Sankarankutty AC, Seemann G, Seidel T, Sachse FB. Confocal microscopy-based estimation of parameters for computational modeling of electrical conduction in the normal and infarcted heart. Front Physiol. 2018;9:239.
60. Kemi OJ, Hoydal MA, MacQuaide N, Haram PM, Koch LG, Britton SL, et al. The effect of exercise training on transverse tubules in normal, remodeled, and reverse remodeled hearts. J Cell Physiol. 2011;226(9):2235–43.
61. Brette F, Despa S, Bers DM, Orchard CH. Spatiotemporal characteristics of SR Ca^{2+} uptake and release in detubulated rat ventricular myocytes. J Mol Cell Cardiol. 2005;39(5):804–12.
62. Crocini C, Ferrantini C, Coppini R, Sacconi L. Electrical defects of the transverse-axial tubular system in cardiac diseases. J Physiol. 2017;595(12):3815–22.
63. Crossman DJ, Young AA, Ruygrok PN, Nason GP, Baddelely D, Soeller C, et al. T-tubule disease: relationship between t-tubule organization and regional contractile performance in human dilated cardiomyopathy. J Mol Cell Cardiol. 2015;84:170–8.
64. Orchard CH, Bryant SM, James AF. Do t-tubules play a role in arrhythmogenesis in cardiac ventricular myocytes? J Physiol. 2013;591(17):4141–7.
65. Sachse FB, Torres NS, Savio-Galimberti E, Aiba T, Kass DA, Tomaselli GF, et al. Subcellular structures and function of myocytes impaired during heart failure are restored by cardiac resynchronization therapy. Circ Res. 2012;110(4):588–97.
66. Stølen TO, Høydal MA, Kemi OJ, Catalucci D, Ceci M, Aasum E, et al. Interval training normalizes cardiomyocyte function, diastolic Ca^{2+} control, and SR Ca^{2+} release synchronicity in a mouse model of diabetic cardiomyopathy. Circ Res. 2009;105(6):527–36.
67. Sikkel MB, Hayward C, MacLeod KT, Harding SE, Lyon AR. SERCA2a gene therapy in heart failure: an anti-arrhythmic positive inotrope. Br J Pharmacol. 2014;171(1):38–54.
68. Lawless M, Caldwell JL, Radcliffe EJ, Smith CER, Madders GWP, Hutchings DC, et al. Phosphodiesterase 5 inhibition improves contractile function and restores transverse tubule loss and catecholamine responsiveness in heart failure. Sci Rep. 2019;9(1):6801.
69. Chen B, Li Y, Jiang S, Xie YP, Guo A, Kutschke W, et al. β-Adrenergic receptor antagonists ameliorate myocyte T-tubule remodeling following myocardial infarction. FASEB J. 2012;26(6):2531–7.
70. Ibrahim M, Navaratnarajah M, Siedlecka U, Rao C, Dias P, Moshkov AV, et al. Mechanical unloading reverses transverse tubule remodelling and normalizes local Ca^{2+}-induced Ca^{2+} release in a rodent model of heart failure. Eur J Heart Fail. 2012;14(6):571–80.
71. Savio-Galimberti E, Frank J, Inoue M, Goldhaber JI, Cannell MB, Bridge JH, et al. Novel features of the rabbit transverse tubular system revealed by quantitative analysis of three-dimensional reconstructions from confocal images. Biophys J. 2008;95(4):2053–62.
72. Wagner E, Lauterbach MA, Kohl T, Westphal V, Williams GS, Steinbrecher JH, et al. Stimulated emission depletion live-cell super-resolution imaging shows proliferative remodeling of T-tubule membrane structures after myocardial infarction. Circ Res. 2012;111(4):402–14.
73. Johnson EA, Sommer JR. A strand of cardiac muscle. Its ultrastructure and the electrophysiological implications of its geometry. J Cell Biol. 1967;33(1):103–29.
74. Pinali C, Kitmitto A. Serial block face scanning electron microscopy for the study of cardiac muscle ultrastructure at nanoscale resolutions. J Mol Cell Cardiol. 2014;76:1–11.
75. Rog-Zielinska EA, Johnston CM, O'Toole ET, Morphew M, Hoenger A, Kohl P. Electron tomography of rabbit cardiomyocyte three-dimensional ultrastructure. Prog Biophys Mol Biol. 2016;121(2):77–84.
76. Vandenberg JI, Rees SA, Wright AR, Powell T. Cell swelling and ion transport pathways in cardiac myocytes. Cardiovasc Res. 1996;32(1):85–97.

Enlightening Cardiac Arrhythmia with Optogenetics

17

Tobias Bruegmann, Patrick M. Boyle, and Franziska Schneider-Warme

Abstract

Cardiac optogenetics offers unprecedented opportunities to study the role of different cell populations in complex biological tissues, such as the heart. To this end, light-emitting sensor proteins or light-inducible effector proteins are expressed in the target cells to either observe or steer their activity with high spatiotemporal resolution. Optogenetic tools to monitor cardiac activity include genetically encoded Ca^{2+} and voltage indicators. In addition, photo-activated ion pumps and channels are used to modulate transmembrane ionic flow and membrane voltage. In cardiac research, optogenetic approaches have been applied successfully for optical pacing, resynchronization, and defibrillation, and they have offered novel insight into cell-specific contributions to arrhythmia formation and termination, as well as simplified automatization of cardiac toxicity screening. Combining optogenetic experiments on intact myocardium with computational modelling allows one to quantitatively assess hypotheses on arrhythmia mechanisms, with the vision of developing novel, targeted approaches to prevent or terminate cardiac arrhythmias. In the following chapter, we summarize principles of optogenetic interrogations of cardiac tissue and present key experiments towards optical control of heart rhythm.

Keywords

Optogenetics · Channelrhodopsin · Optical pacing · Optical defibrillation · Cardiotoxicity screening · Computational modelling

17.1 Introduction

Successful optogenetic experiments require suitable probes, cell-population targeted gene delivery, and optical technologies for spatiotemporally defined, yet minimally invasive light application or collection. Despite the idea of selectively

---

T. Bruegmann
Institute of Cardiovascular Physiology, University Medical Center, Göttingen, Germany

DZHK e.V. (German Center for Cardiovascular Research), Partner Site Göttingen, Göttingen, Germany

P. M. Boyle
Department of Bioengineering, University of Washington, Seattle, USA

Center for Cardiovascular Biology, University of Washington, Seattle, USA

Institute for Stem Cell and Regenerative Medicine, University of Washington, Seattle, USA

F. Schneider-Warme (✉)
Institute for Experimental Cardiovascular Medicine, University Heart Center Freiburg • Bad Krozingen, Freiburg, Germany

Faculty of Medicine, University of Freiburg, Freiburg, Germany
e-mail: franziska.schneider.uhz@uniklinik-freiburg.de

© Springer Nature Switzerland AG 2023

O. N. Tripathi et al. (eds.), *Heart Rate and Rhythm*, https://doi.org/10.1007/978-3-031-33588-4_17

manipulating cellular activity in brain tissue being proposed as early as 1979 [1], and the discovery of light-driven ion pumps in the 1970s [2, 3], only a few optogenetic experiments were reported before the millennium. These include the pioneering work of H. Gobind Khorana expressing bovine rhodopsin in Xenopus oocytes [4] and early studies using fluorescent sensor proteins to image vesicular pH changes, intracellular Ca^{2+} concentrations, and membrane voltage dynamics [5–7]. First optogenetic manipulation of excitable cells was realized by Boris Zemelman and colleagues, co-expressing arrestin-2, rhodopsin, and the α-subunit of the corresponding heterotrimeric G protein in hippocampal neurons to increase action potential firing rate during photostimulation [8]. The breakthrough of optogenetics was the characterization of light-gated ion channels, called channelrhodopsins (ChR), at a time when methods for efficient gene transfer were available. In 2005/2006, several groups used channelrhodopsin-2 (ChR2) to drive depolarizing ion currents in neurons, thereby eliciting action potentials (AP) in vitro and in vivo [7–12]. At the same time, Tallini et al. employed the genetically encoded Ca^{2+} sensor (GCamP2) for measuring Ca^{2+} transients in vivo and for imaging Ca^{2+} signaling in the developing heart [13]. However, the use of ChR2-based tools for cardiac applications was only implemented about five years later [14, 15].

In the following, we introduce commonly applied optogenetic probes (see Figs. 17.1 and 17.2) and summarize strategies for gene targeting and optical measurements, before presenting key studies using optogenetic approaches to monitor and steer cardiac rhythm in vertebrate cells, tissues, and hearts. Furthermore, we highlight how optogenetics will foster our understanding of cardiac arrhythmias, and how we can use it for facilitated cardiotoxicity screening and for dissecting non-myocyte contributions to arrhythmia inducibility and termination.

17.2 Optogenetic Actuators in Cardiac Optogenetics

Optogenetic tools can be divided into light-activated effector proteins, also referred to as optogenetic actuators, and light-emitting sensor proteins [16]. Most commonly used actuators are based on microbial rhodopsins, small heptahelical transmembrane proteins binding all-trans retinal as co-factor for light absorption. More specifically, light-driven proton, chloride, and sodium pumps use the energy provided by visible light for the active transport of ions against the transmembrane gradient (proton and sodium pumps drive outward transport of cations, chloride pumps drive inward transport of anions). When expressed in excitable cells, light-driven pumps will thus mediate hyperpolarizing membrane currents during illumination, which may inhibit AP both in neurons and in cardiomyocytes (Fig. 17.1c). The orange-light activated, inward-directed chloride pump NpHR from Natronomonas pharaonis was first used in zebrafish hearts to induce reversible block of contractions upon global cardiac illumination. Using spatially restricted illumination patterns, it was further utilized to identify the location of pacemaker cells in the developing zebrafish heart and to optically mimic different degrees of atrioventricular conduction block [14]. NpHR-mediated hyperpolarization was also shown to silence or shorten AP in monolayers of neonatal rat ventricular myocytes [17]. Pumping protons out of the cell, the green-light-driven proton pump ArchT shows hyperpolarizing effects on the membrane potential that are comparable to NpHR effects. ArchT-mediated hyperpolarization has been exploited to silence spontaneous excitation of fibroblast–cardiomyocyte co-cultures. Interestingly, in those experiments, ArchT was expressed in fibroblasts, with the resulting hyperpolarization transmitted to cardiomyocytes by electronic coupling [18, 19]. In mouse hearts expressing ArchT in cardiomyocytes,

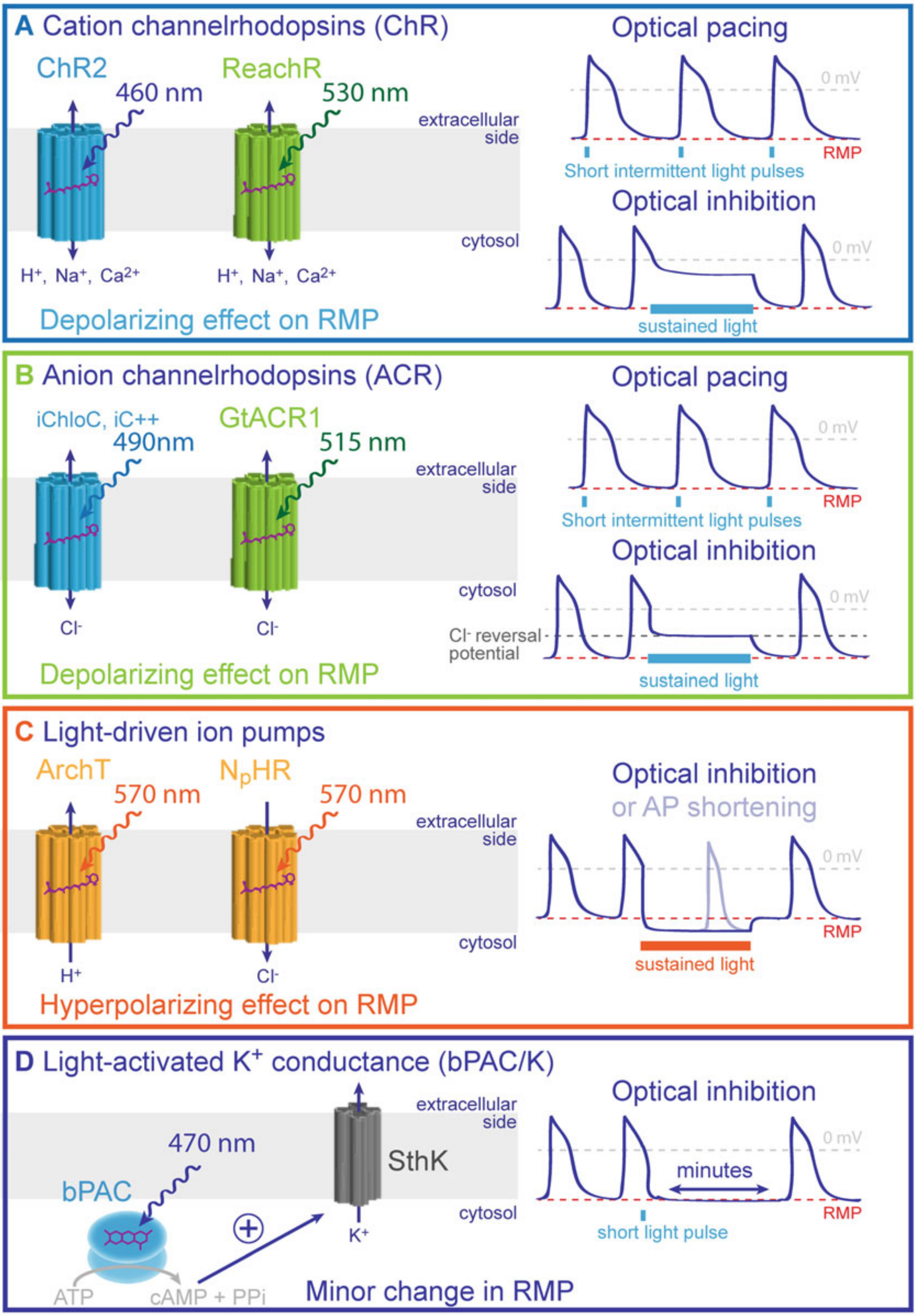
A Cation channelrhodopsins (ChR)
ChR2
460 nm
ReachR
530 nm
extracellular side
cytosol
H+, Na+, Ca2+
H+, Na+, Ca2+
Depolarizing effect on RMP
Optical pacing
0 mV
RMP
Short intermittent light pulses
Optical inhibition
0 mV
sustained light
B Anion channelrhodopsins (ACR)
iChloC, iC++
490nm
GtACR1
515 nm
extracellular side
cytosol
Cl-
Cl-
Depolarizing effect on RMP
Optical pacing
0 mV
RMP
Short intermittent light pulses
Optical inhibition
0 mV
Cl- reversal potential
sustained light
C Light-driven ion pumps
ArchT
570 nm
NpHR
570 nm
extracellular side
cytosol
H+
Cl-
Hyperpolarizing effect on RMP
Optical inhibition
or AP shortening
0 mV
RMP
sustained light
D Light-activated K+ conductance (bPAC/K)
470 nm
bPAC
ATP
cAMP + PPi
+
SthK
K+
extracellular side
cytosol
Minor change in RMP
Optical inhibition
0 mV
minutes
RMP
short light pulse

Fig. 17.1 Optogenetic actuators for membrane potential modulation and their effects in cardiomyocytes. Comparison of common optogenetic actuators and their respective effects on cardiomyocyte resting membrane potential (RMP). Wavelengths of maximal activation are indicated. Abbreviations: *ChR2* channelrhodopsin-2 from *Chlamydomonas reinhardtii, ReachR* red-activatable channelrhodopsin, *iChloC* improved chloride-conducting

hyperpolarizing currents upon green-light exposure were sufficient to terminate ventricular arrhythmia, albeit at low efficiency [20]. This could be explained either by the limited inhibitory effect of hyperpolarization per se or by the high light intensities required, as maximally one ion can be transported per absorbed photon by light-driven ion pumps.

In contrast to pumps, channelrhodopsins (ChR) are light-gated ion channels mediating passive ion flux along the electrochemical gradient upon light activation. ChR can be divided into cation-selective ChR, such as the frequently used channelrhodopsin-2 (ChR2) from *Chlamydomonas reinhardtii*, and the more recently discovered group of anion-conducting channelrhodopsins (ACR), including engineered channels (e.g. iChloC, iC++) and naturally occurring representatives from Guillardia theta (GtACR1, GtACR2) [21–23]. Cation-selective ChR conducts protons, sodium, potassium, calcium, and magnesium ions [24], resulting in depolarizing membrane currents at negative membrane potentials (reversal potential at around 0 mV). Their activation by short light pulses thus leads to short, reversible membrane depolarization of the target cells, sufficient to reliably trigger AP in cardiomyocytes (Fig. 17.1a). Prolonged illumination results in sustained depolarization, preventing repolarization to the resting membrane potential. This precludes recovery from the inactivation of fast sodium channels, thereby suppressing re-excitation of cardiomyocytes [15]. In cardiac optogenetic studies, the blue-light-activated ChR2 and the green-light-activated chimera ReachR [25] have been widely used for modulating cardiac electrophysiology, with applications ranging from cardiac pacing, resynchronization, arrhythmia termination, and drug screening, to studying the role of intracardiac neurons and interstitial non-excitable cells [26].

Anion-selective channelrhodopsins predominantly conduct chloride ions under physiological conditions, thus their reversal potential is determined by the transmembrane gradient for chloride. In cardiomyocytes, ACR activation leads to membrane depolarization, suitable either for optically pacing with short light flashes or for maintaining cells at constant depolarized potentials during prolonged illumination, thereby suppressing further AP (Fig. 17.1b) [27, 28]. Despite high expression levels and large photocurrents of ACR in cardiomyocytes, their use has been restricted to proof-of-principles studies so far. Holding cardiomyocytes at their diastolic membrane potential can be achieved using light-activated K^+-conducting channel systems (Fig. 17.1d). However, currently available systems are either limited by insufficient expression levels in mammalian cells [29] or by slow off-kinetics [30], rendering them unsuitable for applications aiming at beat-by-beat control of cardiac excitation. These challenges might be overcome by the recently discovered class of natural occuring Kalium Rhodopsins, including the potent K^+- selective channel WiChR from Wobblia lunata [31, 32].

In addition to microbial rhodopsin-based tools to control the membrane potential, there is a vast range of other optogenetic actuators, including, but not limited to, light-activated G protein-coupled receptors (GPCR, Fig. 17.2a), photoactivated enzymes, and light-controlled protein interaction systems [16]. Optical control of GPCR signaling is of special interest for understanding intracellular signaling in cardiomyocytes. Suitable GPCR comprise naturally occurring light-sensitive GPCR (visual and non-visual vertebrate rhodopsins and invertebrate

---

Fig. 17.1 (continued) channelrhodopsin, *iC++* improved chloride-conducting chimeric channelrhodopsin, *GtACR1* anion channelrhodopsin-1 from *Guillardia theta, ArchT* proton pump from *Halorubrum sp. TP009, NpHR* halorhodopsin from *Natronomonas pharaonis, AP* action potential, *bPAC* photoactivated cyclase from *Beggiatoa, SthK* cyclic-nucleotide-gated K^+ channel from *Spirochaeta thermophile*

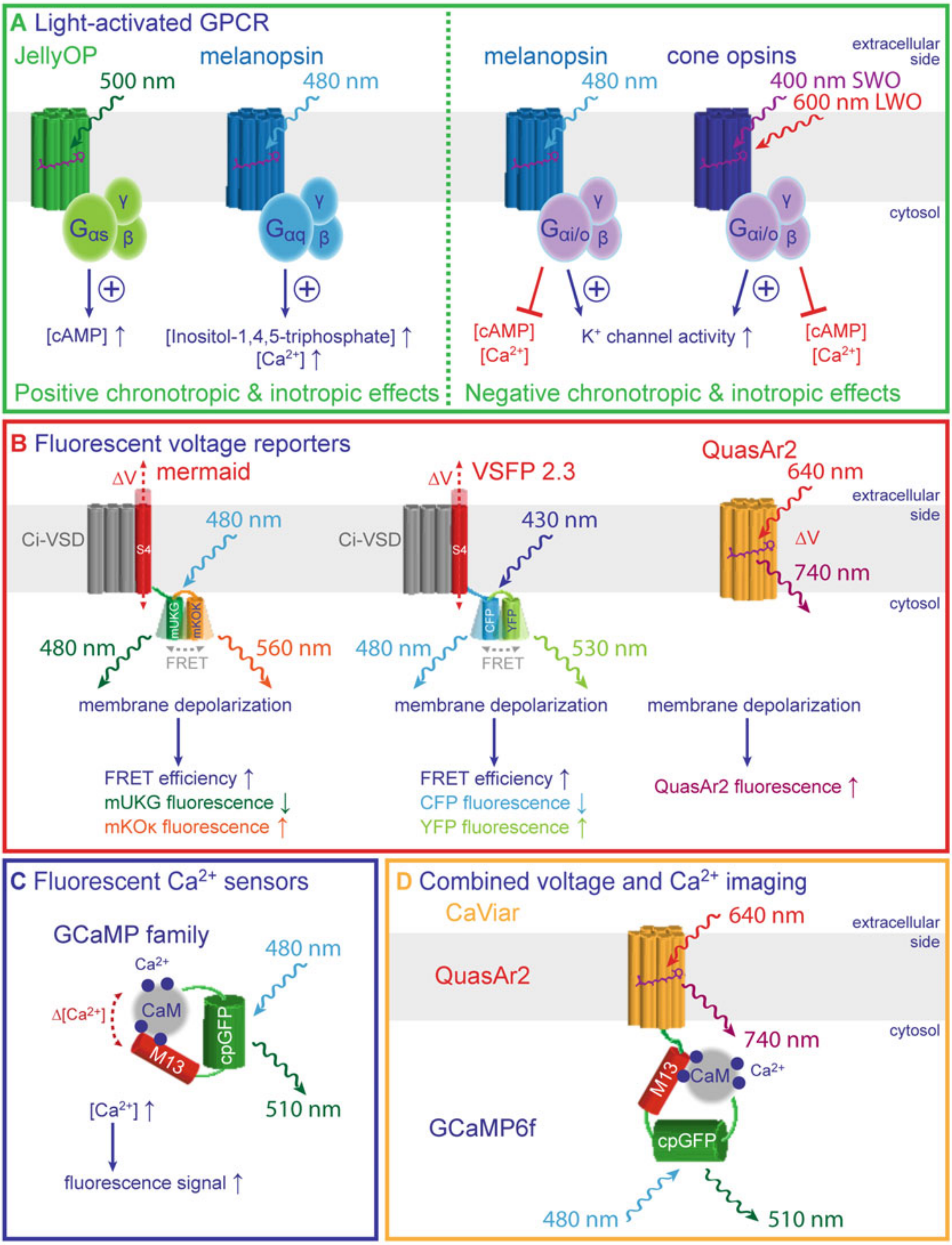
A Light-activated GPCR
JellyOP
500 nm
melanopsin
480 nm
Gαs
γ
β
Gαq
γ
β
[cAMP] ↑
[Inositol-1,4,5-triphosphate] ↑
[Ca2+] ↑
Positive chronotropic & inotropic effects
melanopsin
480 nm
cone opsins
extracellular side
400 nm SWO
600 nm LWO
cytosol
Gαi/o
γ
β
Gαi/o
γ
β
[cAMP]
[Ca2+]
K+ channel activity ↑
[cAMP]
[Ca2+]
Negative chronotropic & inotropic effects
B Fluorescent voltage reporters
ΔV
mermaid
Ci-VSD
S4
480 nm
mUKG
mKOκ
480 nm
FRET
560 nm
membrane depolarization
FRET efficiency ↑
mUKG fluorescence ↓
mKOκ fluorescence ↑
ΔV
VSFP 2.3
Ci-VSD
S4
430 nm
CFP
YFP
480 nm
FRET
530 nm
membrane depolarization
FRET efficiency ↑
CFP fluorescence ↓
YFP fluorescence ↑
QuasAr2
640 nm
extracellular side
ΔV
740 nm
cytosol
membrane depolarization
QuasAr2 fluorescence ↑
C Fluorescent Ca2+ sensors
GCaMP family
Ca2+
Δ[Ca2+]
CaM
M13
cpGFP
480 nm
510 nm
[Ca2+] ↑
fluorescence signal ↑
D Combined voltage and Ca2+ imaging
CaViar
640 nm
extracellular side
QuasAr2
740 nm
cytosol
M13
CaM
Ca2+
GCaMP6f
cpGFP
480 nm
510 nm

Fig. 17.2 Additional optogenetic tools: Light-activated G protein coupled-receptors (GPCR) and fluorescent reporters. (**a**) GPCR used to modulate cardiac activity include JellyOP from *Carybdea rastonii* and murine melanopsin. Of note, by binding a different G_{α} protein, melanopsin can also activate the $G_{i/o}$ signaling pathway, similar to short- and long-wavelength cone opsins (SWO and LWO). (**b**) Fluorescent voltage reporters comprise the Förster-resonance energy transfer (FRET)-based indicators mermaid and VSFP2.3, and rhodopsin-based, single-wavelength indicators such as QuasAr2. In FRET-based reporters, voltage changes are transmitted from the voltage-sensitive domain (VSD) of *Ciona intestinalis* voltage-sensing phosphatase to a FRET pair, thereby

rhodopsins) [33, 34] and custom-engineered rhodopsins referred to as opto-XR.

Light-induced activation of the invertebrate rhodopsin JellyOP allows mimicking β-adrenergic stimulation with unprecedented spatiotemporal precision within the intact heart [35]. Illumination of the right atrium of isolated murine hearts expressing JellyOP leads to an instantaneous increase in spontaneous beating rate. In contrast, illumination of the left posterior atrium at the sites of pulmonary vein insertions results in the generation of supraventricular extrasystoles. Thus, JellyOP activation can be used to look for pathway-specific arrhythmia hotspots within the intact heart. Furthermore, the use of short activating light pulses revealed different on-kinetics of the positive inotropic and lusitropic effects, with the latter being significantly faster. These experiments indicate that optogenetic approaches can facilitate the study of amplification mechanisms and temporal dynamics of G protein signaling cascades, as well as compartment-specific signaling behavior. Importantly, optogenetic control of GPCR activation can mimic physiological responses to pulsatile neurotransmitter release by repeated application of short light flashes.

In embryonic stem-cell-derived cardiomyocytes, heterologous expression of the vertebrate rhodopsin melanopsin enables light-induced G_q protein activation leading to inositol-1,4,5-trisphosphate production and elevation of intracellular Ca^{2+} concentration, thereby enhancing beating frequency of spontaneously beating embryoid bodies [36]. However, melanopsin is a promiscuous receptor also able to activate the G_i signaling cascade [37, 38]. While optogenetic GPCR for specific control of G_i pathways have been identified [39, 40], the optogenetic toolbox currently lacks probes to specifically control G_q signaling – despite the importance of this pathway for acute and chronic adaption of the heart. One possible candidate GPCR could be human Neuropsin (hOPN5), as recently proposed [41].

17.3 Fluorescent Reporters in Cardiac Optogenetics

Complementary to optogenetic actuators, fluorescent sensor proteins can be used for cell-type specific imaging of selected cellular parameters. With respect to cardiac arrhythmias, genetically encoded Ca^{2+} indicators (GECI) and genetically encoded voltage indicators (GEVI) represent the most important tools for imaging cardiac activity (Fig. 17.2b–d). GECI comprise single-fluorophore (e.g. GCaMP family) or FRET-based Ca^{2+} sensors (e.g. Cameleon) that change their fluorescence intensity and/or FRET efficiency upon Ca^{2+} binding [42]. GCaMP2 was first used to image Ca^{2+} dynamics in mouse hearts in vivo and to assess the effects of isoproterenol on diastolic and systolic Ca^{2+} levels as well as kinetics of Ca^{2+} transients in cardiomyocytes. In Langendorff-perfused hearts, GCaMP2 further enabled measurements of the conduction velocity of Ca^{2+} waves, and for combined recordings of Ca^{2+} transients and membrane voltage, the latter using the red-fluorescent voltage dye RH237 [13]. GCaMP2-based imaging also showed functional coupling between engrafted embryonic cardiomyocytes and native myocardium, preventing the risk of post-infarct arrhythmia [43]. To date, a variety of GECI with optimized properties are available, including variants with red-shifted fluorescence spectra [44, 45], fast response times [46, 47], and low-affinity indicators suitable for measuring Ca^{2+} dynamics

Fig. 17.2 (continued) increasing FRET efficiency upon membrane depolarization. Mermaid employs mUKG and mKOκ, VSFP2.3 uses cyan and yellow fluorescent protein (CFP and YFP) as FRET donors and acceptors, respectively. (**c**) Genetically encoded Ca^{2+} sensors of the GCamP family are single-wavelength indicators, wherein Ca^{2+}-induced changes in the interaction of the myosin light chain kinase fragment (M13) and calmodulin (CaM) change fluorescence intensity of a circular permutated green fluorescent protein (cpGFP). (**d**) CaViar can be used for simultaneous imaging of Ca^{2+} and voltage dynamics in intracellular organelles with elevated Ca^{2+} levels such as the sarcoplasmic reticulum [48–50].

GEVI include single-wavelength and ratiometric fluorescent indicators that enable imaging cell-type specific membrane voltage dynamics in real-time [51, 52]. Being expressed under the control of the cardiomyocyte-specific myosin light chain 2 promoter, the ratiometric GEVI mermaid, for example, was used for non-invasive imaging of cardiac activity in embryonic zebrafish hearts, revealing altered cardiac excitation patterns in the presence of the hERG channel blocker astemizole [53]. Similarly, cardiomyocyte-targeted expression of the voltage-sensitive fluorescent protein VSFP2.3 was applied for measuring optical cardiograms, both during sinus rhythm and ventricular tachyarrhythmia in intact mouse hearts [54]. When targeted to cardiac non-myocytes VSFP2.3 was further used to explore electrotonic coupling from cardiomyocytes to non-myocytes in the scar border zone of murine hearts [55]. Additionally, GEVI facilitated rapid phenotyping of stem-cell-derived cardiomyocytes [52, 56]. Improved GEVI comprise variants exhibiting minimized photobleaching and optimized performance for 2-photon imaging, as well as near-IR fluorescent sensors [51, 57], but their utility for cardiac application still needs to be demonstrated.

17.4 Targeted Transgene Delivery

After selecting the appropriate molecular tools for an optogenetic experiment, they need to be targeted to the specific cell population of interest. The four main strategies for targeted transgene delivery to cardiac cells are (1) the generation of knock-in animals expressing the gene of interest under a cell-type specific promoter, (2) the use of recombinatorial animal models (mainly mice) where a cell-type specific driver line (e.g. expressing Cre recombinase) is cross-bred with a driver-dependent line coding for the probe (e.g. Cre-dependent line containing a floxed or flexed transgene) [58–63], (3) viral delivery of genes of interest [64–66], and (4) injection of cells expressing the respective optogenetic probe [67]. The technical details and challenges of the individual methods have been discussed earlier [68, 69]. We would like to strengthen the point that the model generation itself is one of the essential steps towards meaningful optogenetic experiments, which requires thorough controls to exclude off-target expression [70, 71] and side-effects such as cardiotoxicity [72, 73] and immunogenicity [74].

17.5 Ex Vivo Optical Stimulation and Readouts

Another challenge is suitable light delivery and collection for spatiotemporally precise photostimulation and optical readouts of cardiac activity. In principle, for ex vivo experiments, light delivery via conventional light sources for fluorescence microscopy such as shutter-controlled halogen or mercury lamps with suitable bandpass filters, or standard LEDs in combination with microscope/macroscope optics for spatial focusing provide sufficiently high light intensities for optical probe activation. Patterned illumination can be achieved with different optical approaches, e.g. using digital micromirror devices (DMD) from projectors [14, 75], or by rapid scanning of focused excitation light with acousto-optical deflectors [76]. Combining optical stimulation with simultaneous readouts of electrical activity, e.g. via optical mapping, allows one to establish closed-loop systems for real-time adaptation of optical stimulation patterns to observed electrical activation maps. Potential applications for all-optical systems include fast light-controlled restoration of normal electrical activity in hearts showing AV block, and optical termination of ventricular arrhythmias [77, 78].

17.6 Optogenetic Approaches for Controlling Heart Rate and Rhythm

Commonly used devices for heart rhythm control are artificial electrical pacemakers (atrial, ventricular, or dual-chamber pacemakers) and implantable cardioverter defibrillators (ICD), which rely on the application of electrical shocks by electrodes for triggering cardiac excitation and defibrillation, respectively. Pacemakers, on the one hand, have proven extremely useful for long-term maintenance of cardiac activity and come with the advantage that electrical pulses usually remain unnoticeable to patients. ICD shocks, on the other hand, use approximately one thousand times more energy, leading to non-specific tissue excitation of myocardium, nerves, and skeletal muscle. This is associated with adverse effects, including severe pain, chronic anxiety, and structural tissue remodeling [79, 80]. In contrast, optogenetic approaches enable depolarization or hyperpolarization of spatially defined subsets of cardiomyocytes, with minimal effects on other cardiac cell populations. Optogenetic-based systems for external heart rhythm control may thus, in the long term, provide more specific, pain-free, and effective alternatives for heart rhythm management in patients.

17.6.1 Optical Pacing

Depolarizing ChR2-expressing myocytes by short blue-light pulses reliably triggers AP, allowing atrial and ventricular optical pacing in intact hearts from transgenic or virally transduced animals [14, 15, 64, 66]. Furthermore, dual- and multi-site optical stimulation effectively synchronizes ventricular activation, indicating the feasibility of light-driven cardiac resynchronization therapy [66]. Cell-type-specific optogenetic depolarization was also used to assess the number of activated cardiomyocytes or Purkinje cells required for inducing focal ectopic beats, finding that simultaneous depolarization of at least 1300–1800 working cardiomyocytes or 90–160 Purkinje fibers was necessary to trigger extrabeats in murine hearts [58]. Finally, ChR2 activation in human induced pluripotent stem cells in 3D-engineered heart tissue allowed for intermittent tachypacing over the duration of several weeks, providing novel insights into electrical and mechanical remodeling in ventricular and atrial tachycardia, as well as into long-term effects of optogenetic interventions [81, 82].

17.6.2 Optical Defibrillation

Using optogenetic approaches for terminating either atrial or ventricular tachyarrhythmias does not only improve our mechanistic understanding of cardioversion but may also facilitate the development of strategies towards optimized defibrillation therapy, e.g. by testing different locations, geometries, and light levels in a reversible and minimally invasive manner. So far, this relied on ChR2- or ReachR-based depolarization of cardiomyocytes by longer light pulses (hundreds of milliseconds to seconds), thereby suppressing effective repolarization, extending the period of Na^+ channel inactivation and thus inhibiting re-excitation. Bruegmann et al. showed effective termination of ventricular tachycardia by ChR2 activation via blue light application to the anterior ventricular epicardium of Langendorff-perfused mouse hearts, both for healthy hearts and following myocardial infarction [79]. Crocini et al. [76] used a similar experimental approach to terminate induced ventricular tachycardia in ChR2-expressing mouse hearts and showed that a three-barrier pattern of ventricular illumination—based on prior knowledge of the location and geometry of the underlying re-entry pathway—was equally potent to block VT as unfocussed light application on the left ventricular surface, albeit at much lower total irradiation energy (~ 4% of energy). In contrast, single-barrier or point stimulation was insufficient to effectively block arrhythmias in their study [76]. Successful optical defibrillation was also demonstrated on rat hearts expressing the green-light-activated ChR chimera ReaChR [65]. Follow-up studies have since demonstrated the feasibility of optical defibrillation also for terminating atrial fibrillation [83, 84].

Based on experimental studies varying the timing, location and/or intensity of optical stimulation in combination with in silico models, several mechanisms have been suggested for effective optogenetic cardioversion. These include ChR-mediated depolarization and conduction block into illuminated tissue volumes [79]. In this case, transmural depolarization to keep Na^+ channels refractory seems to be mandatory [79, 85]. Alternatively, filling the “excitable gap” can be achieved by pacing the excitable region between wavefronts, promoting the extinction of self-sustained re-entry. While the energy requirements are much lower for this mechanism, filling the excitable gap either relies on spatiotemporal information on rotating wavefronts or requires global illumination of the entire ventricular surface (which obliterates the energetic advantage) [86]. Optogenetic tissue depolarization is also associated with prolonged action potential duration (APD), which has been proposed as a distinct mechanism for terminating VT [65]. Finally, a recent study suggested that low-intensity illumination, leading to sub-threshold depolarization, may be effective for steering rotors towards more depolarized tissue areas, which could be used to terminate cardiac arrhythmias [87]. Interestingly, optogenetic termination of VT is also possible using the light-driven proton pump ArchT, although at lower efficacy compared to depolarizing ChR, potentially via an increased electrical sink mechanism [20]. Light-gated K^+ channels [29, 30] could serve as potent tools for arrhythmia termination if current amplitudes were sufficiently large to counteract the large Na^+ inward currents associated with the propagating wave of excitation, thereby preventing electrical activation and conduction in illuminated tissue areas.

Combining monitoring of heart rhythm and cardiac conduction with optical arrhythmia termination offers the opportunity for automated, real-time correction of rhythm disturbances. Following this idea, Burton et al. implemented light-controlled reversal of spiral wave chirality based on dye-free imaging of contractions in cardiomyocyte monolayers [78]. Scardigli et al. developed a closed-loop system comprising a high-speed sCMOS camera for optical mapping of membrane voltage and a DMD-based projector for optical stimulation, which allowed them to correct for atrioventricular node delay and to optically simulate re-entrant tachycardia [77]. A hybrid bioelectric system with automated ECG-based optogenetic stimulation of the right-atrial epicardial surface was used by Nyns et al. and was shown to be effective in terminating atrial tachyarrhythmias in rats in vivo [84].

The studies described here demonstrate the feasibility of optical rhythm control in select animal models. Further advances in optogenetic proteins (e.g. red-light activated channels with high light sensitivity), methods for safe and targeted gene delivery (ensuring long-lasting, stable protein expression), and software/hardware for optical stimulation (including biocompatible miniature LEDs for photostimulation) will be needed before these concepts may be transferrable to patients in the future [73].

17.7 Using Optogenetics for Cardiotoxicity Screening

Cardiac toxicity and, in particular, drug-induced long QT syndrome are major reasons why newly developed drugs fail to enter or are withdrawn from the market. To avoid life-threatening side effects, as well as the related financial consequences for the pharmaceutical industry, new approaches providing more accuracy and predictive power are required during preclinical drug development [88]. Drug-induced cardiotoxicity is often related to inhibiting Kv11.1 channels, reducing hERG currents, and prolonging APD. Moreover, drugs may also modulate Nav1.5 channels. Inhibition of Nav1.5 channels can induce Brugada-like syndromes, whereas activation of late sodium currents may cause AP prolongation similar to LQT3 syndrome [89–91].

Classically, cardiotoxicity screening of cardiac syncytia relies on spontaneous beating (limited to slow beating rates) or electrical field stimulation (associated with potential stimulation artefacts and/or side effects on stimulated cells) for rate control. In contrast, all-optical approaches provide the unique opportunity for precise external pacing, simultaneous recordings of membrane potential or Ca^{2+} levels, and measurements of myocyte contractility [17, 92, 93]. This further comes with the advantage of potential automatization [94], even if spectral separation can be difficult (i.e. one needs to separate light used for ChR2 and dye excitation from emission light by fluorescent proteins and dyes) [95]. OptoDyce is a platform combining ChR2-mediated stimulation and synthetic dyes for voltage and Ca^{2+} imaging with dye-free video tracking of contractions of cardiomyocyte monolayers. OptoDyce uses short light flashes for optical pacing and temporally separated (intermitted) optical recordings to avoid cross-contamination of the different light signals [92]. In subsequent work, the same group described a quantitative all-optical assay of intercellular connectivity (i.e., OptoGap) [96]; this study also used computational modelling, as discussed in the next section, to show that it may be feasible to scale up this approach to intact human hearts, even after accounting for light attenuation effects. Dempsey et al. used a co-culture of two different, spatially separated transgenic cardiomyocyte lines differentiated from human-induced pluripotent stem cells (a ChR line for optical pacing and a reporter line expressing CaViar; Fig. 17.2d) [93]. Spectral separation was also achieved by employing infrared-compatible dyes for voltage and Ca^{2+} imaging [97]. Alternatively, optical pacing was combined with the recording of electrical field potentials [98]. Global illumination results in near-synchronous activation of all cardiomyocytes, allowing spatial averaging of measured field potentials, as shown with averaging from 60 electrodes within an array [99] and later using one larger electrode [100], thereby simplifying high-throughput screening. Importantly, studies employing optogenetics for cardiotoxicity screening neither reported side effects from overexpression of ChR2, nor acute effects on myocyte electrophysiology. Furthermore, no drug effect on ChR photoactivation has been reported so far. However, chronic optogenetic tachypacing has been shown to be arrhythmogenic by itself [81, 82]. Taken together, combined optogenetic rate control and imaging of cardiomyocyte behaviour provide a unique opportunity for high-throughput cardiotoxicity screening.

17.8 Computational Modelling and Simulation of Cardiac Optogenetics

Multi-scale simulations of cardiac electrophysiology have emerged as a means for investigating mechanistic underpinnings of arrhythmia perpetuation, and for exploring new therapeutic approaches in realistic image-based human atrial or ventricular models [101]. Thanks to the development of robust mathematical representations of light-, voltage-, and time-dependent responses of microbial rhodopsins (e.g., ChR2-H134R) to light stimulation [102], it is possible to simulate optogenetic manipulation of the heart [103, 104]. This involves modifications of existing computational approaches at the cell, tissue, and organ scale to account for the expression of photo-sensitive channels and pumps, spatial distribution of light-sensitized cells resulting from viral gene delivery, and attenuation of light applied to the myocardial surface due to photon scattering and absorption.

Simulations have been used to explore the theoretical possibility of deploying optogenetics in the hearts of larger mammals (e.g., rabbits, dogs, and humans [103]), which thus far cannot be tested in an experimental setting. This work provided proof-of-concept evidence for the feasibility of light-based arrhythmia termination in human atrial [105, 106] and ventricular [79, 107] models. A prominent take-home message has been that the significant attenuation of blue light in the thicker-walled chambers of larger species is expected to be a major hindrance to the translation of approaches from smaller animals, leading to the prediction that optogenetic actuators with red-shifted action spectra would be necessary. Another important finding is that spatially targeted illumination of critical areas to disrupt re-entrant circuits could dramatically reduce the energy needs for optogenetic defibrillation [79, 107], confirming experimental findings in smaller hearts [83]. More recent work has assessed the use of ACR to disrupt re-entrant arrhythmia in human hearts, showing that utilizing these high-efficiency chloride conducting channels may lower the energy required for defibrillation by 2–3 orders of magnitude [108].

A second application of computational cardiac optogenetics research is the use of simulations to enhance the understanding of data from wet lab preparations like tandem cell units [67, 103] or monolayers of cardiomyocytes co-cultured with light-sensitized donor cells [109], or to validate and explore the expansion of methodologies like the OptoGap approach described in the prior section [96]. Likewise, this type of modelling work has been employed to explore completely new applications of optogenetics like the use of subthreshold light-induced depolarization to steer re-entrant drivers towards non-conductive boundaries, ultimately resulting in arrhythmia termination [87]. Notably, while much of the recent interest in computational modelling of cardiac optogenetics has focused on actuator opsins (e.g., ChR2, GtACR1), similar tools have also been developed to realistically simulate light emission from dyes used extensively in optical mapping experiments [110–112].

17.9 Cardiac Optogenetics beyond Cardiomyocytes

Taking advantage of the possibility to selectively target individual cell populations of interest, optogenetic approaches have been extended to cardiac non-myocytes, including cardiac interstitial cells, and intracardiac sympathetic and parasympathetic neurons. While interstitial cells (e.g. fibroblasts and resident immune cells) have traditionally been viewed as electrical insulators, there has been long-standing evidence that cardiac fibroblasts can be electrotonically coupled to cardiomyocytes in vitro, acting as an electrical load and/or interlinking otherwise unconnected cardiomyocytes [113]. Based on fibroblast-specific activation of either ChR2, ArchT, or eNpHR, several optogenetic studies have confirmed electrotonic coupling between (myo) fibroblasts and cardiomyocytes in diverse in vitro systems, with direct effects on cardiomyocyte excitability, AP properties, and conduction velocity [18, 67, 114–116]. In 2016, Quinn et al. showed that fibroblasts expressing VSFP2.3 follow rhythmic depolarizations of cardiomyocytes in scar border zone tissue following ventricular cryoinjury in Langendorff-perfused whole hearts [55]. Similar coupling was subsequently observed by Rubart et al. studying myofibroblasts after myocardial infarction [117]. In 2017, Hulsmans et al. described Cx43-based gap junctions between cardiomyocytes and tissue-resident macrophages and demonstrated that ChR2-mediated macrophage depolarization could facilitate AV node conduction at high atrial stimulation rates [63]. These studies exemplify how cell-type-specific optogenetic manipulation and observation can be applied for unravelling cellular functions that are difficult to assess with classic electrophysiological techniques such as patch-clamp measurements or dye-based optical mapping of membrane voltage.

Another exciting avenue of cardiac optogenetics is the selective photostimulation of intracardiac neurons. Wengrowski et al. established a mouse model expressing ChR2 in murine catecholaminergic sympathetic neurons. In Langendorff-perfused hearts, photostimulation increased both heart rate and developed force of contraction and led to a significant shortening of the AP plateau phase. Moreover, the optogenetic release of norepinephrine increases both the incidence and severity of ventricular arrhythmias following burst pacing [59]. Based on experiments using optogenetic stimulation of sympathetic neurons and FRET-based imaging of cAMP levels, Prando et al. concluded that neurotransmission from sympathetic neurons to cardiomyocytes occurs within spatially (diffusion)-restricted intermembrane domains [60]. In line with the observed chronotropic effects of sympathetic nerve activation, reversible neuronal hyperpolarization by ArchT activation in the left stellate ganglion decreases the amplitude and frequency of nerve activity. This resulted in reduced systolic blood pressure increase upon neuronal stimulation, longer APD and effective refractory periods, decreased heart rate variability, and suppression of ischemia-induced ventricular arrhythmias in an in vivo study using virally transduced beagles [118].

Moreno et al. targeted ChR2 to choline acetyltransferase-expressing neurons; hence, blue-light mediated ChR2 activation induced acetylcholine release from cardiac parasympathetic neurons. Accordingly, illumination slowed the sinus rate and delayed atrioventricular node conduction [119]. When using ChR2-mediated activation of cholinergic neurons of the inferior pulmonary vein ganglionated plexus, Rajendran et al. also observed a light-dependent decrease in the heart rate; however, in their experimental setting, no change in AV node conduction was seen, suggesting that neuronal fibers originating from this plexus may pass the AV node without forming synapses. Photostimulation at higher frequencies further induced ectopic atrial activation and asystole. Finally, the study showed differential effects of optogenetic vs. electrical stimulation of the vagus nerve, enabling authors to dissect the effects of efferent and afferent vagal nerve activation [120]. Taken together, optogenetic interrogation of intracardiac neurons thus represents an elegant method to elucidate the output of defined neuronal subsets on myocyte activity from single-cell to whole-heart level, as selective photostimulation enables superior specificity compared to electrical activation that cannot discriminate well between different neuronal classes, and that may also directly stimulate neighboring myocytes.

17.10 Conclusions

We have summarized the experimental approaches in cardiac optogenetics and how they can be used for studying cardiac electrophysiology and intercellular communication. Moreover, we have highlighted key applications of optical heart rhythm control and cardiotoxicity screening. Computational modelling facilitates the interpretation of experimental data from laboratory-based optogenetic studies and data integration across scales and species.

As cardiac optogenetics opens up a host of new opportunities to tackle basic research questions at present, it may pave the way for cell-type specific anti-arrhythmic therapies in the future. However, proof-of-concept studies are still limited to small animals and major hurdles have to be taken before transfer from bench to patient is realistic, with efficient and safe gene transfer, development of implantable light sources, and prevention of an immune response representing some of the most important challenges. The intrinsic technical advantages of optogenetics compared to pharmacological and unspecific electrical stimulation have already provided important insights into cardiac arrhythmia mechanisms—and we envision further exciting insights to come.

Acknowledgements We thank all members of the Institute for Experimental Cardiovascular Medicine (IEKM) for the critical discussion of the manuscript. This work was supported by the German Centre for Cardiovascular Research (DZHK) and the German Research Foundation (DFG: Priority Program 1926 [#315212873;#315193289], CRC1002 [#193793266], CRC1425 [#4226818459], and the Emmy-Noether Programme [#412853334]). FSW is an associate member of the excellence cluster Centre for Integrated Biological Signalling Studies (CIBSS).

References

1. Crick FHC. Thinking about the brain. Sci Am. 1979;241:219–32.
2. Oesterhelt D, Stoeckenius W. Rhodopsin-like protein from the purple membrane of Halobacterium halobium. Nature. 1971;233:149–52.
3. Matsuno-Yagi A, Mukohata Y. Two possible roles of bacteriorhodopsin; a comparative study of strains of Halobacterium halobium differing in pigmentation. Biochem Biophys Res Commun. 1977;78:237–43.
4. Khorana HG, Knox BE, Nasi E, Swanson R, Thompson DA. Expression of a bovine rhodopsin gene in Xenopus oocytes: demonstration of light-dependent ionic currents. Proc Natl Acad Sci U S A. 1988;85:7917–21.
5. Miesenböck G, de Angelis DA, Rothman JE. Visualizing secretion and synaptic transmission with pH-sensitive green fluorescent proteins. Nature. 1998;394:192–5.
6. Miyawaki A, Llopis J, Heim R, McCaffery JM, Adams JA, et al. Fluorescent indicators for Ca^{2+} based on green fluorescent proteins and calmodulin. Nature. 1997;388:882–7.
7. Siegel MS, Isacoff EY. A genetically encoded optical probe of membrane voltage. Neuron. 1997;19:735–41.

8. Zemelman BV, Lee GA, Ng M, Miesenböck G. Selective photostimulation of genetically chARGed neurons. Neuron. 2002;33:15–22.
9. Ishizuka T, Kakuda M, Araki R, Yawo H. Kinetic evaluation of photosensitivity in genetically engineered neurons expressing green algae light-gated channels. Neurosci Res. 2006;54:85–94.
10. Boyden ES, Zhang F, Bamberg E, Nagel G, Deisseroth K. Millisecond-timescale, genetically targeted optical control of neural activity. Nat Neurosci. 2005;8:1263–8.
11. Li X, Gutierrez DV, Hanson MG, Han J, Mark MD, et al. Fast noninvasive activation and inhibition of neural and network activity by vertebrate rhodopsin and green algae channelrhodopsin. Proc Natl Acad Sci U S A. 2005;102:17816–21.
12. Nagel G, Brauner M, Liewald JF, Adeishvili N, Bamberg E, et al. Light activation of channelrhodopsin-2 in excitable cells of Caenorhabditis elegans triggers rapid behavioral responses. Curr Biol. 2005;15:2279–84.
13. Tallini YN, Ohkura M, Choi B-R, Ji G, Imoto K, et al. Imaging cellular signals in the heart in vivo: cardiac expression of the high-signal Ca^{2+} indicator GCaMP2. Proc Natl Acad Sci U S A. 2006;103: 4753–8.
14. Arrenberg AB, Stainier DYR, Baier H, Huisken J. Optogenetic control of cardiac function. Science. 2010;330:971–4.
15. Bruegmann T, Malan D, Hesse M, Beiert T, Fuegemann CJ, et al. Optogenetic control of heart muscle in vitro and in vivo. Nat Methods. 2010;7: 897–900.
16. Rost BR, Schneider-Warme F, Schmitz D, Hegemann P. Optogenetic tools for subcellular applications in neuroscience. Neuron. 2017;96:572–603.
17. Park SA, Lee S-R, Tung L, Yue DT. Optical mapping of optogenetically shaped cardiac action potentials. Sci Rep. 2014;4:6125.
18. Nussinovitch U, Shinnawi R, Gepstein L. Modulation of cardiac tissue electrophysiological properties with light-sensitive proteins. Cardiovasc Res. 2014;102:176–87.
19. Nussinovitch U, Gepstein L. Optogenetics for suppression of cardiac electrical activity in human and rat cardiomyocyte cultures. Neurophotonics. 2015;2: 031204.
20. Funken M, Malan D, Sasse P, Bruegmann T. Optogenetic hyperpolarization of cardiomyocytes terminates ventricular arrhythmia. Front Physiol. 2019;10:1–7.
21. Wietek J, Beltramo R, Scanziani M, Hegemann P, Oertner TG, et al. An improved chloride-conducting channelrhodopsin for light-induced inhibition of neuronal activity in vivo. Sci Rep. 2015;5:14807.
22. Berndt A, Lee SY, Wietek J, Ramakrishnan C, Steinberg EE, et al. Structural foundations of optogenetics: determinants of channelrhodopsin ion selectivity. Proc Natl Acad Sci U S A. 2016;113:822–9.
23. Govorunova EG, Sineshchekov OA, Janz R, Liu X, Spudich JL. Natural light-gated anion channels: a family of microbial rhodopsins for advanced optogenetics. Science. 2015;349:647–50.
24. Schneider F, Gradmann D, Hegemann P. Ion selectivity and competition in channelrhodopsins. Biophys J. 2013;105:91–100.
25. Lin JY, Knutsen PM, Muller A, Kleinfeld D, Tsien RY. ReaChR: a red-shifted variant of channelrhodopsin enables deep transcranial optogenetic excitation. Nat Neurosci. 2013;16: 1499–508.
26. Entcheva E, Kay MW. Cardiac optogenetics : a decade of enlightenment. Nat Rev Cardiol. 2021;18: 349–67.
27. Govorunova EG, Cunha SR, Sineshchekov OA, Spudich JL. Anion channelrhodopsins for inhibitory cardiac optogenetics. Sci Rep. 2016;6:1–7.
28. Kopton RA, Baillie JS, Rafferty SA, Moss R, Zgierski-Johnston CM, et al. Cardiac electrophysiological effects of light-activated chloride channels. Front Physiol. 2018;9:1806.
29. Alberio L, Locarno A, Saponaro A, Romano E, Bercier V, et al. A light-gated potassium channel for sustained neuronal inhibition. Nat Methods. 2018;15: 969–76.
30. Bernal Sierra YA, Rost BR, Pofahl M, Fernandes AM, Kopton RA, et al. Potassium channel-based optogenetic silencing. Nat Commun. 2018;9:4611.
31. Govorunova EG, Gou Y, Sineshchekov OA, Li H, Lu X et al. Kalium channelrhodopsins are natural light-gated potassium channels that mediate optogenetic inhibition. Nat Neurosci 2022; 25: 967–974.
32. Vierock J, Peter E, Grimm C, Rozenberg A, Chen IW et al. WiChR, a highly potassium-selective channelrhodopsin for lowlight one- and two-photon inhibition of excitable cells. Sci Adv. 2022; 8: eadd7729.
33. Ernst OP, Lodowski DT, Elstner M, Hegemann P, Brown LS, et al. Microbial and animal rhodopsins: structures, functions, and molecular mechanisms. Chem Rev. 2014;114:126–63.
34. Koyanagi M, Terakita A. Diversity of animal opsin-based pigments and their optogenetic potential. Biochim Biophys Acta Bioenerg. 2014;1837:710–6.
35. Makowka P, Bruegmann T, Dusend V, Malan D, Beiert T, et al. Optogenetic stimulation of Gs-signaling in the heart with high spatio-temporal precision. Nat Commun. 2019;10:1281.
36. Beiert T, Bruegmann T, Sasse P. Optogenetic activation of Gq signalling modulates pacemaker activity of cardiomyocytes. Cardiovasc Res. 2014;102:507–16.
37. Tennigkeit SA, Karapinar R, Rudack T, Dreier MA, Althoff P, et al. Design of an ultrafast G protein switch based on a mouse melanopsin variant. Chembiochem. 2019;20:1766–71.

38. Spoida K, Eickelbeck D, Karapinar R, Eckhardt T, Mark MD, et al. Melanopsin variants as intrinsic optogenetic on and off switches for transient versus sustained activation of G protein pathways. Curr Biol. 2016;26:1206–12.
39. Gutierrez DV, Mark MD, Masseck O, Maejima T, Kuckelsberg D, et al. Optogenetic control of motor coordination by Gi/o protein-coupled vertebrate rhodopsin in cerebellar Purkinje cells. J Biol Chem. 2011;286:25848–58.
40. Masseck OA, Spoida K, Dalkara D, Maejima T, Rubelowski JM, et al. Vertebrate cone opsins enable sustained and highly sensitive rapid control of Gi/o signaling in anxiety circuitry. Neuron. 2014;81: 1263–73.
41. Wagdi A, Malan D, Sathyanarayanan U, Beauchamp JS, Vogt M et al. Selective optogenetic control of Gq signaling using human Neuropsin. Nat Commun. 2022; 13: 1765
42. Kaestner L, Scholz A, Tian Q, Ruppenthal S, Tabellion W, et al. Genetically encoded Ca^{2+} indicators in cardiac myocytes. Circ Res. 2014;114: 1623–39.
43. Roell W, Lewalter T, Sasse P, Tallini YN, Choi BR, et al. Engraftment of connexin 43-expressing cells prevents post-infarct arrhythmia. Nature. 2007;450: 819–24.
44. Dana H, Mohar B, Sun Y, Narayan S, Gordus A, et al. Sensitive red protein calcium indicators for imaging neural activity. elife. 2016;5:e12727.
45. Qian Y, Cosio DMO, Piatkevich KD, Aufmkolk S, Su WC, et al. Improved genetically encoded near-infrared fluorescent calcium ion indicators for in vivo imaging. PLoS Biol. 2020;18:e3000965.
46. Chen T-W, Wardill TJ, Sun Y, Pulver SR, Renninger SL, et al. Ultrasensitive fluorescent proteins for imaging neuronal activity. Nature. 2013;499:295–300.
47. Dana H, Sun Y, Mohar B, Hulse BK, Kerlin AM, et al. High-performance calcium sensors for imaging activity in neuronal populations and microcompartments. Nat Methods. 2019;16:649–57.
48. Suzuki J, Kanemaru K, Ishii K, Ohkura M, Okubo Y, et al. Imaging intraorganellar Ca^{2+} at subcellular resolution using CEPIA. Nat Commun. 2014;5:1–13.
49. Henderson MJ, Baldwin HA, Werley CA, Boccardo S, Whitaker LR, et al. A low affinity GCaMP3 variant (GCaMPer) for imaging the endoplasmic reticulum calcium store. PLoS One. 2015;10: 1–17.
50. de Juan-Sanz J, Holt GT, Schreiter ER, de Juan F, Kim DS, et al. Axonal endoplasmic reticulum Ca^{2+} content controls release probability in CNS nerve terminals. Neuron. 2017;93:867–881.e6.
51. Bando Y, Grimm C, Cornejo VH, Yuste R. Genetic voltage indicators. BMC Biol. 2019;17:71.
52. Kaestner L, Tian Q, Kaiser E, Xian W, Müller A, et al. Genetically encoded voltage indicators in circulation research. Int J Mol Sci. 2015;16:21626–42.
53. Tsutsui H, Higashijima S, Miyawaki A, Okamura Y. Visualizing voltage dynamics in zebrafish heart. J Physiol. 2010;588:2017–21.
54. Chang LML, de Boer TP, Mutoh H, Raad N, Richter C, et al. Sensing cardiac electrical activity with a *cardiac* myocyte-targeted optogenetic voltage indicator. Circ Res. 2015;117:401–12.
55. Quinn TA, Camelliti P, Rog-Zielinska EA, Siedlecka U, Poggioli T, et al. Electrotonic coupling of excitable and nonexcitable cells in the heart revealed by optogenetics. Proc Natl Acad Sci U S A. 2016;113:14852–7.
56. Leyton-Mange JS, Mills RW, Macri VS, Jang MY, Butte FN, et al. Rapid cellular phenotyping of human pluripotent stem cell-derived cardiomyocytes using a genetically encoded fluorescent voltage sensor. Stem Cell Reports. 2014;2:163–70.
57. Monakhov MV, Matlashov ME, Colavita M, Song C, Shcherbakova DM, et al. Screening and cellular characterization of genetically encoded voltage indicators based on near-infrared fluorescent proteins. ACS Chem Neurosci. 2020;11:3523–31.
58. Zaglia T, Pianca N, Borile G, Da Broi F, Richter C, et al. Optogenetic determination of the myocardial requirements for extrasystoles by cell type-specific targeting of ChannelRhodopsin-2. Proc Natl Acad Sci U S A. 2015;112:E4495–504.
59. Wengrowski AM, Wang X, Tapa S, Posnack NG, Mendelowitz D, et al. Optogenetic release of norepinephrine from cardiac sympathetic neurons alters mechanical and electrical function. Cardiovasc Res. 2015;105:143–50.
60. Prando V, Da Broi F, Franzoso M, Plazzo AP, Pianca N, et al. Dynamics of neuro-effector coupling at 'cardiac sympathetic' synapses. J Physiol. 2018;596:2055–75.
61. Wang Y, Lin WK, Crawford W, Ni H, Bolton EL, et al. Optogenetic control of heart rhythm by selective timulation of cardiomyocytes derived from Pnmt+ cells in murine heart. Sci Rep. 2017;7:40687.
62. Fernández MC, Kopton RA, Simon-Chica A, Madl J, Hilgendorf I, et al. Channelrhodopsins for cell-type specific illumination of cardiac electrophysiology. Methods Mol Biol. 2021;2191:287–307.
63. Hulsmans M, Clauss S, Xiao L, Aguirre AD, King KR, et al. Macrophages facilitate electrical conduction in the heart. Cell. 2017;169:510–522.e20.
64. Vogt CC, Bruegmann T, Malan D, Ottersbach A, Roell W, et al. Systemic gene transfer enables optogenetic pacing of mouse hearts. Cardiovasc Res. 2015;106:338–43.
65. Nyns ECA, Kip A, Bart CI, Plomp JJ, Zeppenfeld K, et al. Optogenetic termination of ventricular arrhythmias in the whole heart: towards biological cardiac rhythm management. Eur Heart J. 2017;38: 2132–6.
66. Nussinovitch U, Gepstein L. Optogenetics for *in vivo* cardiac pacing and resynchronization therapies. Nat Biotechnol. 2015;33:750–4.
67. Jia Z, Valiunas V, Lu Z, Bien H, Liu H, Wang HZ, et al. Stimulating cardiac muscle by light: cardiac optogenetics by cell delivery. Circ Arrhythm Electrophysiol. 2001;4:753–60.

68. Boyle PM, Karathanos TV, Trayanova NA. “Beauty is a light in the heart”: the transformative potential of optogenetics for clinical applications in cardiovascular medicine. Trends Cardiovasc Med. 2015;25:73–81.
69. Bruegmann T, Sasse P. Optogenetic cardiac pacemakers: science or fiction? Trends Cardiovasc Med. 2015;25:82–3.
70. Johnston CM, Rog-Zielinska EA, Wülfers EM, Houwaart T, Siedlecka U, et al. Optogenetic targeting of cardiac myocytes and non-myocytes: tools, challenges and utility. Prog Biophys Mol Biol. 2017;130:140–9.
71. Prabhakar A, Vujovic D, Cui L, Olson W, Luo W. Leaky expression of channelrhodopsin-2 (ChR2) in Ai32 mouse lines. PLoS One. 2019;14:e0213326.
72. Li Q, Ni RR, Hong H, Gho KY, Rossi M, et al. Electrophysiological properties and viability of neonatal rat ventricular myocyte cultures with inducible ChR2 expression. Sci Rep. 2017;7:1531.
73. Richter C, Bruegmann T. No light without the dark: perspectives and hindrances for translation of cardiac optogenetics. Prog Biophys Mol Biol. 2020;154:39–50.
74. Maimon BE, Diaz M, Revol ECM, Schneider AM, Leaker B, et al. Optogenetic peripheral nerve immunogenicity Sci Rep. 2018;8:14076.
75. Richter C, Christoph J, Lehnart SE, Luther S. Optogenetic light crafting tools for the control of cardiac arrhythmias. Methods Mol Biol. 2016;1408: 293–302.
76. Crocini C, Ferrantini C, Coppini R, Scardigli M, Yan P, et al. Optogenetics design of mechanistically-based stimulation patterns for cardiac defibrillation. Sci Rep. 2016;6:35628.
77. Scardigli M, Müllenbroich C, Margoni E, Cannazzaro S, Crocini C, et al. Real-time optical manipulation of cardiac conduction in intact hearts. J Physiol. 2018;596:3841–58.
78. Burton RAB, Klimas A, Ambrosi CM, Tomek J, Corbett A, et al. Optical control of excitation waves in cardiac tissue. Nat Photonics. 2015;9:813–6.
79. Bruegmann T, Boyle PM, Vogt CC, Karathanos TV, Arevalo HJ, et al. Optogenetic defibrillation terminates ventricular arrhythmia in mouse hearts and human simulations. J Clin Invest. 2016;126: 3894–904.
80. Pedersen SS, van den Broek KC, Theuns DA, Erdman RA, Alings M, et al. Risk of chronic anxiety in implantable defibrillator patients: a multi-center study. Int J Cardiol. 2011;147:420–3.
81. Lemme M, Braren I, Prondzynski M, Aksehirlioglu B, Ulmer BM, et al. Chronic intermittent tachypacing by an optogenetic approach induces arrhythmia vulnerability in human engineered heart tissue. Cardiovasc Res. 2020;116:1487–99.
82. Lemoine MD, Lemme M, Ulmer BM, Braren I, Krasemann S, et al. Intermittent optogenetic tachypacing of atrial engineered heart tissue induces only limited electrical remodelling. J Cardiovasc Pharmacol. 2021;77:291–9.
83. Bruegmann T, Beiert T, Vogt CC, Schrickel JW, Sasse P. Optogenetic termination of atrial fibrillation in mice. Cardiovasc Res. 2017;114:713–23.
84. Nyns ECA, Poelma RH, Volkers L, Plomp JJ, Bart CI, et al. An automated hybrid bioelectronic system for autogenous restoration of sinus rhythm in atrial fibrillation. Sci Transl Med. 2019;11(481):eaau6447.
85. Watanabe M, Feola I, Majumder R, Angsangthong W, Teplenin AS, et al. Optogenetic manipulation of anatomical re-entry by light-guided generation of a reversible local conduction block. Cardiovasc Res. 2017;113:354–66.
86. Quiñonez Uribe RA, Luther S, Diaz-Maue L, Richter C. Energy-reduced arrhythmia termination using global photostimulation in optogenetic murine hearts. Front Physiol. 2018;9:1651.
87. Hussaini S, Venkatesan V, Biasci V, Romero Sepúlveda JM, Quiñonez Uribe RA, et al. Drift and termination of spiral waves in optogenetically modified cardiac tissue at sub-threshold illumination. elife. 2021;10:e59954. https://doi.org/10.7554/eLife.59954.
88. Li X, Zhang R, Zhao B, Lossin C, Cao Z. Cardiotoxicity screening: a review of rapid-throughput in vitro approaches. Arch Toxicol. 2016;90:1803–16.
89. Kannankeril P, Roden DM, Darbar D. Drug-induced long QT syndrome. Pharmacol Rev. 2010;62:760–81.
90. Konstantopoulou A, Tsikrikas S, Asvestas D, Korantzopoulos P, Letsas KP. Mechanisms of drug-induced proarrhythmia in clinical practice. World J Cardiol. 2013;5:175–85.
91. Meyer T, Sartipy P, Blind F, Leisgen C, Guenther E. New cell models and assays in cardiac safety profiling. Expert Opin Drug Metab Toxicol. 2007;3: 507–17.
92. Klimas A, Ambrosi CM, Yu J, Williams JC, Bien H, et al. OptoDyCE as an automated system for high-throughput all-optical dynamic cardiac electrophysiology. Nat Commun. 2016;7:11542.
93. Dempsey GT, Chaudhary KW, Atwater N, Nguyen C, Brown BS, et al. Cardiotoxicity screening with simultaneous optogenetic pacing, voltage imaging and calcium imaging. J Pharmacol Toxicol Methods. 2016;81:240–50.
94. Entcheva E, Bub G. All-optical control of cardiac excitation: combined high-resolution optogenetic actuation and optical mapping. J Physiol. 2016;594: 2503–10.
95. O’Shea C, Holmes AP, Winter J, Correia J, Ou X, et al. Cardiac optogenetics and optical mapping – overcoming spectral congestion in all-optical cardiac electrophysiology. Front Physiol. 2019;10:182.
96. Boyle PM, Yu J, Klimas A, Williams JC, Trayanova NA, et al. OptoGap is an optogenetics-enabled assay for quantification of cell-cell coupling in multicellular cardiac tissue. Sci Rep. 2021;11:9310.
97. Klimas A, Ortiz G, Boggess SC, Miller EW, Entcheva E. Multimodal on-axis platform for all-optical electrophysiology with near-infrared

probes in human stem-cell-derived cardiomyocytes. Prog Biophys Mol Biol. 2020;154:62–70.

98. Yakushenko A, Gong Z, Maybeck V, Hofmann B, Gu E, et al. On-chip optical stimulation and electrical recording from cells. J Biomed Opt. 2013;18:111402.
99. Lapp H, Bruegmann T, Malan D, Friedrichs S, Kilgus C, et al. Frequency-dependent drug screening using optogenetic stimulation of human iPSC-derived cardiomyocytes. Sci Rep. 2017;7:9629.
100. Rehnelt S, Malan D, Juhasz K, Wolters B, Doerr L, et al. Frequency-dependent multi-well cardiotoxicity screening enabled by optogenetic stimulation. Int J Mol Sci. 2017;18:2634.
101. Bifulco SF, Akoum N, Boyle PM. Translational applications of computational modelling for patients with cardiac arrhythmias. Heart 2020, Dec 10: heartjnl-2020-316854. https://doi.org/10.1136/heartjnl-2020-316854.
102. Williams JC, Xu J, Lu Z, Klimas A, Chen X, et al. Computational optogenetics: empirically-derived voltage- and light-sensitive channelrhodopsin-2 model. PLoS Comput Biol. 2013;9(9):e1003220.
103. Boyle PM, Williams JC, Ambrosi CM, Entcheva E, Trayanova NA. A comprehensive multiscale framework for simulating optogenetics in the heart. Nat Commun. 2013;4:2370.
104. Boyle PM, Karathanos TV, Entcheva E, Trayanova NA. Computational modeling of cardiac optogenetics: methodology overview and review of findings from simulations. Comput Biol Med. 2015;65:200–8.
105. Karathanos TV, Boyle PM, Trayanova NA. Optogenetics-enabled dynamic modulation of action potential duration in atrial tissue: feasibility of a novel therapeutic approach. Europace. 2014;16 (Suppl 4):iv69–iv76:iv69.
106. Boyle PM, Murphy MJ, Karathanos TV, Zahid S, Blake RC 3rd, et al. Termination of re-entrant atrial tachycardia via optogenetic stimulation with optimized spatial targeting: insights from computational models. J Physiol. 2018;596:181–96.
107. Karathanos TV, Bayer JD, Wang D, Boyle PM, Trayanova NA. Opsin spectral sensitivity determines the effectiveness of optogenetic termination of ventricular fibrillation in the human heart: a simulation study. J Physiol. 2016;594:6879–91.
108. Ochs AR, Karathanos TV, Trayanova NA, Boyle PM. Optogenetic stimulation using anion channelrhodopsin (GtACR1) facilitates termination of reentrant arrhythmias with low light energy requirements: a computational study. Front Physiol. 2021;12:718622. https://doi.org/10.3389/fphys.2021.718622.
109. Ambrosi CM, Boyle PM, Chen K, Trayanova NA, Entcheva E. Optogenetics-enabled assessment of viral gene and cell therapy for restoration of cardiac excitability. Sci Rep. 2015;5:17350.
110. Bishop MJ, Rodriguez B, Eason J, Whiteley JP, Trayanova N, et al. Synthesis of voltage-sensitive optical signals: application to panoramic optical mapping. Biophys J. 2006;90:2938–45.
111. Bishop MJ, Rodriguez B, Qu F, Efimov IR, Gavaghan DJ, et al. The role of photon scattering in optical signal distortion during arrhythmia and defibrillation. Biophys J. 2007;93:3714–26.
112. Bishop MJ, Rowley A, Rodriguez B, Plank G, Gavaghan DJ, et al. The role of photon scattering in voltage-calcium fluorescent recordings of ventricular fibrillation. Biophys J. 2011;101:307–18.
113. Kohl P, Gourdie RG. Fibroblast-myocyte electrotonic coupling: does it occur in native cardiac tissue? J Mol Cell Cardiol. 2014;70:37–46.
114. Funken M, Bruegmann T, Sasse P. Selective optogenetic stimulation of fibroblasts enables quantification of hetero-cellular coupling to cardiomyocytes in a three-dimensional model of heart tissue. Europace. 2020;22:1590–9.
115. De SSA, Moyle S, Buccarello A, Dellenbach C, Kucera JP, et al. The role of membrane capacitance in cardiac impulse conduction: an optogenetic study with non-excitable cells coupled to cardiomyocytes. Front Physiol. 2020;11:194.
116. Kostecki GM, Shi Y, Chen CS, Reich DH, Entcheva E, et al. Optogenetic current in myofibroblasts acutely alters electrophysiology and conduction of co-cultured cardiomyocytes. Sci Rep. 2021;11:4430.
117. Rubart M, Tao W, Lu X-L, Conway SJ, Reuter SP, et al. Electrical coupling between ventricular myocytes and myofibroblasts in the infarcted mouse heart. Cardiovasc Res. 2018;114:389–400.
118. Yu L, Zhou L, Cao G, Po SS, Huang B, et al. Optogenetic modulation of cardiac sympathetic nerve activity to prevent ventricular arrhythmias. J Am Coll Cardiol. 2017;70:2778–90.
119. Moreno A, Endicott K, Skancke M, Dwyer MK, Brennan J, et al. Sudden heart rate reduction upon optogenetic release of acetylcholine from cardiac parasympathetic neurons in perfused hearts. Front Physiol. 2019;10:16.
120. Rajendran PS, Challis RC, Fowlkes CC, Hanna P, Tompkins JD, et al. Identification of peripheral neural circuits that regulate heart rate using optogenetic and viral vector strategies. Nat Commun. 2019;10:1944.

Part IV

Mechanisms of Acquired Arrhythmia

An Overview of Spiral- and Scroll-Wave Dynamics in Mathematical Models for Cardiac Tissue

18

Study of Arrhythmogenesis in Mathematical Models of Cardiac Tissue and its Elimination Using Defibrillation Techniques

Mahesh Kumar Mulimani, Soling Zimik,
Jaya Kumar Alageshan, Rupamanjari Majumder,
Alok Ranjan Nayak, and Rahul Pandit

Abstract

We provide a brief overview of recent numerical studies of spiral- and scroll-wave dynamics in mathematical models of cardiac tissue. These waves are believed to be important in developing an understanding of life-threatening cardiac arrhythmias like ventricular tachycardia and ventricular fibrillation. In addition to giving a description of how spiral and scroll waves can be initiated in such models, how they evolve, how they interact with conduction and ionic inhomogeneities, and how they may be controlled; we also discuss the relevance of such studies to defibrillation. We give short descriptions of recent studies of (a) early afterdepolarizations (EADs) and their implications for premature ventricular contractions (PVCs) and (b) a deep-learning method for the detection and efficient elimination of spiral waves in mathematical models for ventricular tissue.

Keywords

Ventricular fibrillation · Ionic inhomogeneity · Premature ventricular contractions · Early and delayed afterdepolarization · Impulse conduction · Potassium channel blocker · Late sodium current · Deep learning

18.1 Introduction

Mammalian hearts are among the most efficient electromechanical pumps in the biological world. They sustain pulmonary and systemic circulation by rhythmically pumping roughly 5 L/min and 4.5 L/min of blood in normal adult human males and females, respectively. Aberrancy of normal cardiac rhythm is caused, inter alia, by abnormal rhythmicity of the pacemaker, unusual pathways of impulse propagation through the heart, interim block or the spontaneous generation of abnormal impulses in almost any part of the heart. These lead to conditions that are clinically identified as cardiac arrhythmias and often result in heart failure and sudden death. Cardiac arrhythmias

M. K. Mulimani · S. Zimik · J. K. Alageshan ·
R. Pandit (✉)
Centre for Condensed Matter Theory, Department of Physics, Indian Institute of Science, Bangalore, India
e-mail: rahul@physics.iisc.ernet.in

R. Majumder
Max Planck Institute for Dynamics and Self Organization, Göttingen, DE, Germany

A. R. Nayak
International Institute of Information Technology (IIIT-Bhubaneswar), Bhubaneswar, India

© Springer Nature Switzerland AG 2023
O. N. Tripathi et al. (eds.), *Heart Rate and Rhythm*, https://doi.org/10.1007/978-3-031-33588-4_18

contribute about 50% to the morbidity and mortality in patients with symptomatic heart failure. Approximately 450,000 people in the US, 90,000 in the UK [1], and 60,000 in France [2] die each year as a result of this fatal clinical disorder. It is generally believed that spiral or scroll waves of electrical activation in cardiac tissue play an important role in such arrhythmias. Thus, the development of a detailed understanding of the propagation of waves of electrical activation through cardiac tissue is an interdisciplinary problem of central importance in the biological, physical, and computational sciences.

This chapter provides a concise overview of the initiation, propagation, and break-up of spiral and scroll waves in mathematical models of cardiac tissue. In Sect. 18.2, we begin with an introduction to the biological and experimental background required for our study of spiral- and scroll-wave dynamics in cardiac tissue; this is followed by brief descriptions of some mathematical models of cardiac tissue. Section 18.3 outlines numerical studies of models and presents representative results obtained from single-cell, two-dimensional (2D) sheet, and three-dimensional (3D) slab simulations of these models. In Sect. 18.4, we discuss premature ventricular contractions (PVCs) that arise from early afterdepolarizations (EADs) in the human-ventricular-cell model of O'Hara and Rudy (the ORd model [3]), and the implications of such PVCs for ventricular arrhythmias. In Sect. 18.5, we discuss two control schemes for spiral- and scroll-wave turbulence; these are the mathematical analogs of defibrillation; the second one of these uses a deep-learning method. We end with concluding remarks in Sect. 18.6.

18.2 Experimental Background and Mathematical Models

In the clinic, various forms of cardiac arrhythmias have been observed. Here, we concentrate only on ventricular tachycardia (VT) and ventricular fibrillation (VF), which arise from disorders of impulse formation, impulse conduction, or both. Disorders of impulse formation relate to the abnormal discharge rate of the sino-atrial node (SAN) or premature contraction of the heart resulting from the formation of ectopic foci. Disorders of impulse conduction include conduction delays and blocks that result in bradyarrhythmias and tachyarrhythmias. Tachyarrhythmias, such as VT and VF, occur when delays and blocks produce reentrant excitations.

To develop a mathematical model for cardiac tissue, several experimental inputs are required. Such inputs are obtained principally from patch–clamp experiments that are now capable of providing detailed information about parameters that govern the operation of ion channels in a cardiac cell. Each ion channel is modeled via Hodgkin–Huxley-type equations (Sect. 18.2.1). This requires parameters that include channel conductances and rate constants, which govern the behaviors of gating variables. To go from a single-cell model to a model for cardiac tissue, we need, in addition, the cell's membrane capacitance per unit area and diffusion coefficients along the various directions. These again can be obtained from patch–clamp experiments and a realistic physiological model can then be developed by fitting these parameters in such a way that it can reproduce all the desired experimentally observed physiological properties at cell and tissue levels.

Excitability is an important property of cardiac tissue because it can support various spiral waves of electrical activation like a single spiral or multiple spirals that may annihilate or regenerate by random collision with each other; this has been known since the pioneering studies of Garrey [4, 5], Allessie et al. [6, 7], and Mines [8, 9]; these can arise because of anatomical or functional reentry. A single spiral wave, whose core is stationary, leads to monomorphic VT, whereas a drifting spiral is the cause of polymorphic tachycardia [10]. A drifting spiral or scroll wave occasionally gets attached to a small local inhomogeneity in its path and this leads to a polymorphic-to-monomorphic tachycardia transition [10–14]. Furthermore, the tips of the spiral waves (spiral cores) or, in three dimensions, the lines connecting the spiral tips on all the layers of the scroll waves (scroll filaments) can drift towards the edges of the tissue and get terminated.

In *normal automaticity,* electrical excitations in the heart originate from the sino-atrial node (SAN). In addition, in both normal and diseased cases, electrical signals may originate in the atrial myocardium, the atrio-ventricular (AV) node, and the His-Purkinje network [15] and lead to *ectopic beats*. If this signal frequency is lower than that of excitations from the SAN, then these signals are over-driven by those from the SAN. For example, in *bradycardia* (low-frequency signals from the SAN), these premature excitations can take over from the SAN excitations. Furthermore, mutations in the Na^+ or K^+ channels can lead to early afterdepolarisation (EADs), which may result in PVCs [16, 17] that are implicated in the Long-QT (LQT) and Brugada syndromes [18–22]. An increase in the fibroblast density, which may occur after ischemia, can also lead to PVCs, via the fibroblast–myocyte coupling [17, 23, 24].

Afterdepolarizations in cardiomyocytes are among the leading causes of the triggered activity in cardiac tissue. These abnormal depolarizations occur either (a) in the repolarizing phase (EADs) or (b) in the resting phase (i.e., delayed afterdepolarizations or DADs) of an action potential (AP). If the number of such afterdepolarization-generating cells exceeds a threshold, then such groups of cells can become focal sources of excitations. It has been shown, in a rabbit-heart model, that the threshold numbers are 80 cells in one-dimensional (1D), 7854 cells in two-dimensional (2D), and 817,280 cells in three-dimensional (3D) tissue [25]. Therefore, sufficiently large clusters of such EAD-generating cells, in otherwise homogeneous cardiac tissue, can lead to PVCs. Furthermore, in Ref. [26]**,** it has been shown that (a) irregular EADs are chaotic, (b) the synchronization of EADs occurs at a critical tissue size, and (c) beyond this critical size, partial synchronization occurs and leads to the formation of PVCs, which precipitate multifocal activity and ventricular fibrillation (VF). Such triggered activity depends on (a) the type of EADs, (b) the size of a clump of EAD-generating cells, (c) the reduced coupling between the cells in the EAD clump, and (d) the density of fibroblasts coupled to myocytes in cardiac tissue [16, 25–27].

Drugs can also induce EADs, e.g., dofetilide reduces the K^+ current and anthopleurin-A increases the late I_{Na} current. It has been shown that, in chronic atrio-ventricular block (CAVB) in a dog-heart model, drug-induced EADs are responsible for focal activity that can initiate dangerous arrhythmias such as the Torsade de Pointes (TdP) [28–31]; whether the sustenance of TdP is because of focal activity or re-entrant activity is still a matter of debate [29, 30]. However, in the case of the CAVB dog model, focal activity is the dominant mechanism of TdP, and in simulation studies, it has also been shown that sustenance of TdP arises from focal activity in the presence of large heterogeneities, that result from disease-induced damage that leads to the remodeling of cardiac tissue [30].

18.2.1 Mathematical Models of Cardiac Tissue

Cardiac tissue is excitable in the sense that sub-threshold perturbations decay, whereas super-threshold ones lead to an AP (Fig. 18.1a).

Once excited, the medium cannot be re-excited for a subsequent interval of time known as the refractory period. In general, cardiac tissue is modeled by using a reaction-diffusion equation of the form

$$\frac{\partial V}{\partial t} = \nabla.(D\nabla V) - \frac{I_{\text{ion}} + I_{\text{stimulus}}}{C_m}, \qquad (18.1)$$

where V is the transmembrane potential, D is related to the conductivity of cardiac tissue, I_{ion} is the sum of the currents conducted by all the ion channels, $I_{stimulus}$ is the excitation current, and C_m is the total cell-membrane capacitance per unit surface area. In general, D should be a tensor, but at the simplest level of modeling it is assumed to be a scalar. Different models for cardiac tissue are distinguished by different forms for I_{ion}. Three common models are (a) the Luo-Rudy phase I (LRI) model, (b) the reduced Priebe-

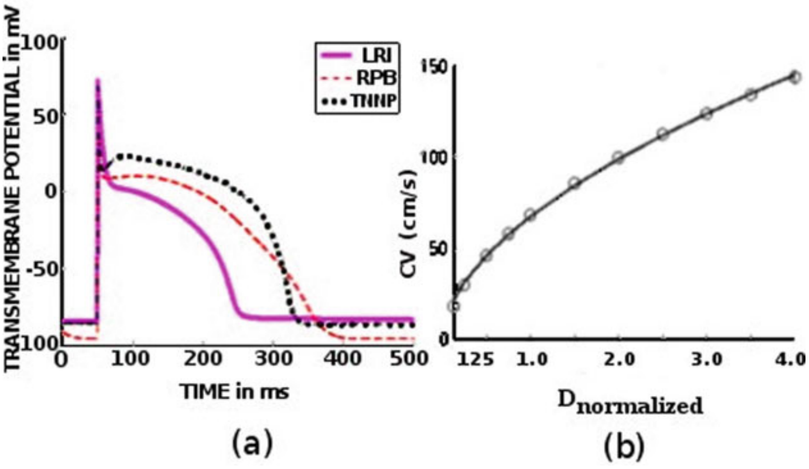

Fig. 18.1 (**a**) Action potentials for realistic ionic models: LRI (solid magenta), RPB (dashed red) and TNNP (dotted black), obtained by applying a current pulse of amplitude $100\ \mu A/cm^2$ for $1\ ms$. (**b**) A plot of conduction velocity CV versus the normalized diffusion coefficient $D_{normalized}$, i.e., the ratio of D and its maximal value $D_{max} = 0.00154\ cm^2/ms$; the solid line indicates a fit of the form $CV = A0 \times D^a$; we find $A0 = 67.3$ and $a = 0.5$, which is consistent with $CV\ \alpha\ \sqrt{D}$

Beuckelmann (RPB) model, and (c) the model of ten Tusscher, Noble, Noble, and Panfilov (TNNP), (d) the human-ventricular-cell model of ten Tusscher and Panfilov (the TP06 model), and (e) the recent human-ventricular-cell model of O'Hara and Rudy model (the ORd model).

The LRI model, based on guinea-pig data, includes ion pumps and has six ionic current components:

$$I_{LR} = I_{Na} + I_{si} + I_K + I_{K1} + I_{Kp} + I_b, \quad (18.2)$$

with current densities I_{Na}, I_{si}, I_K, I_{K1}, I_{Kp}, and I_b for the fast inward Na^+ current, the slow inward (now known as L-$type\ Ca^{2+}$) current, the slow outward time-dependent K^+ current, the time-independent K^+ current, the plateau K^+ current, and the total background current, respectively. Other model parameters and equations are given in [32].

The reduced PB model (RPB) [33] is the reduced version of the original Priebe-Beuckelmann (PB) model [34]. It aims at improving computational efficiency without losing any basic tissue properties such as the AP shape. The reformulated PB model reduces the total number of variables that have to be used. The model has a single delayed rectifier K^+ current, as opposed to individual rapid and slow components. It excludes the dynamics of intracellular ion concentrations by approximating the variables by suitable constants as described by Bernus et al. [33]. The total current is

$$\begin{aligned} I_{RPB} = {} & I_{Na} + I_{Ca} + I_{to} + I_K + I_{K1} \\ & + I_{NaCa} + I_{NaK} + I_{bNa} + I_{bCa}, \end{aligned} \quad (18.3)$$

with I_{Na} the fast inward Na^+ current, I_{Ca} the slow inward Ca^{2+} current, I_{to} the transient outward current, I_K the delayed rectifier K^+ current, I_{K1} the inward rectifier K^+ current, I_{NaK} the Na^+/K^+ pump current, I_{NaCa} the Na^+/Ca^{2+} exchanger current, and I_{bNa} and I_{bCa} the background Na^+ and Ca^{2+} currents, respectively.

The TNNP model fits experimentally recorded AP duration (APD) properties of human myocardium, and is based on experimental data on most of the major ionic currents in human cardiac tissue, and includes simple Ca^{2+} dynamics, which allows for realistic modeling of Ca^{2+} transients, Ca^{2+} current inactivation, and a positive contraction staircase. The total ionic current is

$$\begin{aligned} I_{ion} = & I_{Na} + I_{CaL} + I_{to} + I_{Ks} + I_{Kr} \\ & + I_{K1} + I_{NaCa} + I_{NaK} + I_{pCa} + I_{pK} \\ & + I_{bNa} + I_{bCa}, \end{aligned} \tag{18.4}$$

where I_{CaL} is the *L-type* Ca^{2+} current and I_{pCa} and I_{pK} are the plateau Ca^{2+} and K^{+} currents.

Each current, in the models above, is described by Hodgkin-Huxley-type equations, i.e., for ion channel i the current is

$$I_i(V_m, t) = g_i(V_m - E_i), \tag{18.5}$$

where E_i is the reversal potential for the channel i and g_i its conductance. We must also include differential equations that govern the behaviors of voltage-gated ion channels; these are described in detail in [32].

The TP06 [35] human-ventricular-cell model (of 2006) is based on experimental data on many of the important ionic currents, specifically the Na and Ca currents; this model fits experimental measurements of human-ventricular-myocyte APD restitution, and it includes a more extensive description of intracellular calcium dynamics than does the TNNP model. The instabilities, which lead to spiral-wave breakup because of alternans and APD restitution, appear clearly in the TP06 model that uses the following 12 ionic currents (for the model equations and parameters, see [35]):

$$\begin{aligned} I_{ion} = & I_{Na} + I_{CaL} + I_{to} + I_{Ks} + I_{Kr} \\ & + I_{K1} + I_{NaCa} + I_{NaK} + I_{pCa} + I_{pK} \\ & + I_{bNa} + I_{bCa}, \end{aligned} \tag{18.6}$$

The O'Hara-Rudy (ORd) model (of 2012), for the normal human ventricle, is based on experimental data for (a) the AP, (b) the rate dependences of APD restitution, with and without ion-channel blockers, and (c) the CAMK dependence of many of the ion currents (e.g. I_{Na}, I_{CaL}, I_{to}). This model has realistic Ca^{2+} dynamics, which can reproduce experimentally observed EADs. It has the following 14 ionic currents:

$$\begin{aligned} I_{ion} = & I_{Na} + I_{CaL} + I_{CaNa} + I_{CaK} + I_{to} \\ & + I_{Ks} + I_{Kr} + I_{K1} + I_{NaCa} + I_{NaK} \\ & + I_{pCa} + I_{Kb} + I_{Nab} + I_{Cab}, \end{aligned} \tag{18.7}$$

which are given in Ref. [3] along with the model equations and parameters.

It is often advantageous to use simple, two-variable models with a normalized transmembrane potential e and a slow recovery variable g into which all the essential physics of ion channels is subsumed. One example of such a model is the Panfilov [36, 37] model:

$$\begin{aligned} \frac{\partial e}{\partial t} = \nabla^2 e - f(e) - g; \quad \frac{\partial g}{\partial t} = \varepsilon(e, g) \\ \times (ke - g), \end{aligned} \tag{18.8}$$

Here $f(e) = C_1 e$ when $e < e_1$, $f(e) = -C_2 e + a$ when $e_1 \le e \le e_2$ and $f(e) = C_3(e - 1)$ when $e > e_2$. $\varepsilon(e, g) = \varepsilon_1$ when $e < e_2$, $\varepsilon(e, g) = \varepsilon_2$ when $e > e_2$, $\varepsilon(e, g) = \varepsilon_3$ when $e < e_1$ *and* $g < g_1$, $e_1 = 0.0026$, $e_2 = 0.837$, $C_1 = 20$, $C_2 = 3$, $C_3 = 15$, $a = 0.06$ *and* $k = 3$. The dynamics of the recovery variable is specified by the function $\varepsilon(e, g)$. The recovery time constant for small e and g is specified by ε_3^{-1}. It approximately corresponds to the relative refractory period. The recovery time constant for relatively large g and intermediate e is specified by ε_1^{-1}. Physiologically this corresponds to the wave-front, wave-back and the absolute-refractory periods.

18.3 Numerical Studies and Representative Results

We have performed extensive numerical studies of these four models [32]. Here we give illustrative results from single-cell, 2D, and 3D simulations. For computing single-cell APs (Eq. 18.9 below), a time step $\delta t = 0.01$ *ms* for LRI, RPB, and TNNP models was used. For studies in 2D and 3D, the forward-Euler method for time marching with time steps of *0.11 ms*, *0.01 ms*, *0.02 ms,* and *0.02 ms* for Panfilov, LRI, RPB, and TNNP models, respectively, were used; and the Hodgkin-Huxley-type equations were integrated for the different gating variables (for LRI, RPB, and TNNP models) by using the Rush-Larsen scheme. Furthermore, a finite-difference method with spatial steps of $\delta x = \delta y = 0.5$ for the Panfilov model, $\delta x = \delta y = 0.225$ *mm* for the

LRI model, $\delta x = \delta y = 0.225\ mm$ for the 2D-TNNP model and $\delta x = \delta y = 0.225\ mm$, $\delta z = 0.1\ mm$ for the 3D-TNNP was used. A five-point stencil was used for computing the Laplacian on a square simulation domain in 2D, whereas in 3D we used a seven-point stencil on a rectangular slab. For studies in 2D the domain contains 400 × 400 grid points for the Panfilov and LRI models and 600 × 600 grid points for the TNNP model. For studies in 3D $\delta z = \delta x$ for both Panfilov and LRI models, but $\delta z = 0.01\ cm$ for the TNNP model was employed; we use $N_z = 15$ grid points along the z direction in 3D domains. Neumann (no-flux) boundary conditions (i.e., $\nabla V.\hat{n} = 0$, where $\hat{n}$ is the normal to the surface of the tissue drawn at the boundary) were used and the accuracy of our numerical schemes was tested by varying both the time and space steps [38].

For single-cell simulations of the ORd model, we pace the cell with a pacing cycle length PCL = 1000 ms; and we record the 50th action-potential (AP). We change the repolarization reserve (RR) by changing the conductances of inward and outward currents, such as G_{CaL} and G_{Kr}, multiplicatively by using our scale factors [16, 39]. In our 2D-tissue simulations, we use square domains, with 768 × 768 grid points, a forward-Euler scheme for time stepping ($\delta t = 0.2\ ms$), and a finite-difference method, with a five-point stencil for the Laplacian and $\delta x = \delta y = 0.2\ mm$.

18.3.1 Single Cell

At the single-cell level Eq. (18.1) becomes the ordinary differential equation (ODE)

$$\frac{dV}{dt} = \frac{I_{ion} + I_{stim}}{C_m}, \tag{18.9}$$

with the ionic current given by Eqs. (18.2), (18.3), or (18.4) for LRI, RPB, or TNNP models, respectively. Even though the Panfilov model is extremely simple, compared to the LRI, RPB, and TNNP models, it captures several essential properties of the spatiotemporal evolution of the transmembrane potential; e.g., the AP of the Panfilov model contains both the absolute and relative refractory periods, predominantly seen in advanced models.

The cardiac APs that follow from Eq. (18.7) for the LRI, RPB, and TNNP models are shown in Fig. 18.1(a); to obtain these, a current pulse of $100\ \mu A/cm^2$ for $1\ ms$ was applied to a single cell of each type. From the plots in Fig. 18.1(a), the APD, threshold potential ($V_{threshold}$), resting membrane potential (V_{rest}), maximum plateau potential ($V_{plateau}$), potential at AP notch (V_{notch}), and maximum conduction velocity (CV_{max}) were obtained. These values for all the four models above are listed in Table 18.1. The threshold potential is defined as the minimum voltage that is required for excitation of the cell. Its value is (as listed in Table 18.1) always much higher than the resting-state potential, so that the cells do not get excited because of slight ionic imbalances occurring within them. In other words, the relatively high value of $V_{threshold}$ indicates that proper excitation of a cardiac cell requires a large ionic-concentration drop across the cell wall. For a good review on cardiac propagation, we refer the reader to Kleber and Rudy [40].

18.3.2 Homogeneous Two-Dimensional Sheet of Cells

A 2D sheet of cardiac cells is modeled by Eq. 18.1 in which the cells are coupled via the diffusion term [32]. Given this diffusive coupling, an AP generated from one cell can excite its neighboring cells and thus spread out as an expanding wave. The initial excitation is followed by a refractory period, so a second wave cannot follow the first one immediately. When two waves collide in such a medium, they cannot pass through each other because their wakes (i.e., the part of the medium that has passed into the refractory phase just behind the tail of the excitatory wave) are non-excitable, so they annihilate [32]. It is known that the propagation velocity of a reaction-diffusion-type equation is directly proportional to the square root of the diffusion coefficient D [41]. To observe such a

Table 18.1 Comparison between single cell behaviors of four mathematical models of cardiac tissue

Model	APD *(ms)*	$V_{threshold}$ *(mV)*	V_{rest} *(mV)*	$V_{plateau}$ *(mV)*	V_{notch} *(mV)*	CV_{max} *(cm/s)*
Panfilov	330	–	−80	–	–	–
LRI	366	−60	−84	17.7	12.4	–
RPB	357.2	−60.2	−90.2	~13	~8.5	70.4
TNNP	286.8	−62.8	−86.2	22.6	13.6	68.8

relation in the TNNP model of cardiac tissue, *CV* was measured by using different values of *D* and by injecting a plane wave into the homogeneous domain via a stimulation current of $150\ \mu A/cm^2$ for *3 ms* at the left boundary. The data in Fig. 18.1 (b) are consistent with$CV \propto \sqrt{D}$. We also observed that *CV* and the wavelength λ, which is roughly the product of the refractory period and the *CV*, are *68.28 cm/s* and *13.2 cm*, respectively.

Generally, two methods are used to initiate spiral waves in simulations [10, 32, 33, 42] and experiments [10, 11], namely, (a) the S1-S2 cross-field protocol and (b) the S1-S2 parallel-field protocol. In the cross-field method a super-threshold stimulus S2 is applied at the boundary that is perpendicular to the S1 stimulus. In the parallel-field method, S2 is applied parallel to the refractory tail of the S1 stimulus but not over the entire length of the domain. We used the parallel-field protocol.

To initiate a spiral wave in the TNNP model in a homogeneous domain, a plane wave was injected into the domain via an S1 stimulus of strength $100\ \mu A/cm^2$ for *3 ms* at the left boundary. *D* was chosen to be $0.000385\ cm^2/ms$ (approximately one fourth of its original value, *0.00154*) in the beginning of our simulation to initiate a spiral wave. An S2 stimulus of strength $450\ \mu A/cm^2$ for *3 ms* after *560 ms* and just behind the refractory tail of S1 ($x = 360,\ 1 \le y \le 550$) was then applied. The conductivity was then reset to its original value after *880 ms*. This procedure yielded the fully developed spiral wave as shown in Fig. 18.2(a) at $t = 976\ ms$; and this state was used as the initial condition for subsequent studies. This procedure forms a stable spiral wave in a homogeneous domain [32]; its period of rotation is *263 ms* as shown in Fig. 18.2 (b). However, it can also evolve to a state with spatiotemporal chaos. Whether it does so or not, depends on the conductance of specific ion channels.

18.3.3 Two-Dimensional Sheet of Cells with Inhomogeneities

Cardiac tissue contains various types of heterogeneities that can arise because of (a) genetic disorders, (b) scar tissue formed after a myocardial infarction, (c) major blood vessels, (d) connective tissue, (e) cells other than myocytes (e.g., fibroblasts), or (f) inter-cellular coupling. Therefore, it is important to understand the role of such heterogeneities on spiral- and scroll-wave dynamics in both experimental and numerical settings. We give illustrative studies for the TNNP model.

Conduction inhomogeneities, like scar tissues or major blood vessels, can affect spiral waves in several ways. In some cases such inhomogeneities can anchor a spiral wave or eliminate it completely [12, 14]; the larger the obstacle the more likely is the anchoring; however, even if the obstacle is large, the wave might not attach to it. Furthermore, an obstacle can convert multiple spirals to a single anchored spiral [13]. Such behavior has also been seen in numerical simulations of spiral-wave turbulence in models for cardiac tissue [32, 43, 44].

We introduced inhomogeneities in our 2D simulation domain by setting $D = 0$ at the location of the obstacles. The obstacles were square or circular in shape. Furthermore, Neumann (i.e., no-flux) boundary conditions on the boundaries of the obstacle were used.

Our systematic study of spiral-wave dynamics in the presence of an obstacle [32, 44] shows that the initial condition of Fig. 18.2(a), which evolved to the stable rotating spiral of Fig. 18.2

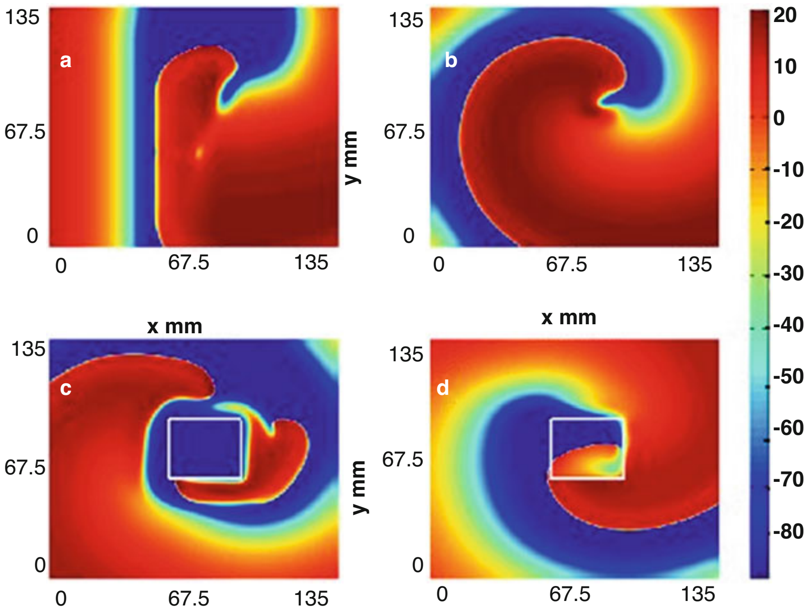

Fig. 18.2 Pseudocolor plots of the transmembrane potential V from 2D simulations of the TNNP model: (**a**) a fully developed spiral wave at time $t = 976\ ms$ that is used as an initial condition to study spiral-wave dynamics in this model; (**b**) stable rotating spiral state in a homogeneous domain at time $t = 2.4\ s$; (**c**) spiral turbulence (ST) state with broken spirals at time $t = 2.4\ s$, in the presence of a square conduction inhomogeneity (obstacle) of side length $l = 3.375\ cm$, whose bottom-left corner is placed at $(56.25\ mm, 56.25\ mm)$; (**d**) single-spiral state with complex periodic behavior in the same system at time $t = 2.4\ s$, in the presence of a square ionic inhomogeneity of side length $l = 3.375\ cm$, whose bottom-left corner is placed at $(56.25\ mm, 56.25\ mm)$

(b) in the absence of an obstacle, can give rise to one of the following results: (a) the spiral wave can continue to rotate, without being anchored to the obstacle, and eventually break down to yield the spiral-wave turbulence state (ST); (b) the tip of the spiral wave can get anchored to the obstacle to give the rotating state (RS) in which the anchored spiral rotates around the obstacle; (c) all spiral waves can be absorbed by the boundaries so that the system evolves into the quiescent state (Q). A representative pseudocolor plot of V, for the ST case in the presence of a square obstacle, is shown in Fig. 18.2(c). We also obtained similar results if the initial condition is a broken-spiral-wave state rather than one in which we have a single rotating spiral wave.

By changing the position of the obstacle, it was found that spiral-wave dynamics depends sensitively on the position of an obstacle [32, 44]: small changes in the position of the obstacle can change the final state of the system from, say, ST to RS or Q. We have suggested [32, 44] that this arises because of an underlying fractal-type basin boundary between the domains of attraction of ST, RS, and Q states. We also observed similar sensitive dependence of spiral-wave dynamics on the position of an obstacle, if we use a circular obstacle; for details, please see [32, 44].

Cardiac tissue can contain other types of inhomogeneities that originate from changes in single-cell properties, which are caused in turn by changes in the chemical environment or metabolic modifications [45]. Collections of such cells are referred to as ionic inhomogeneities; some of their properties, like the conductance of ion channels, are slightly modified relative to those of normal cardiac cells.

The ionic inhomogeneities can also have dramatic effects on spiral-wave dynamics. In particular, they can eliminate spiral waves, or anchor a spiral wave, but with richer dynamics than that in the case of a conduction inhomogeneity. For example, our ionic-inhomogeneity studies in the Panfilov model [32, 44] show that such inhomogeneities can lead to the coexistence of the following types of behaviors: (a) ST outside the inhomogeneity and quasiperiodic behavior inside it; (b) an unbroken RS outside the inhomogeneity and broken spiral waves (ST) inside it; and (c) a spiral anchored to the inhomogeneity with different quasiperiodic temporal evolution of V outside and inside the inhomogeneity. We have observed such complex behaviors in our numerical studies of ionic inhomogeneities in LRI, RPB, and TNNP models [32]. Here we restrict ourselves to representative results for the TNNP model. We introduce square ionic inhomogeneities by changing the *L-type* Ca^{2+} conductance G_{CaL} or the *plateau*-Ca^{2+} conductance G_{pCa}. The initial condition shown in Fig. 18.2(a) was used, which evolves into a stable rotating spiral (Fig. 18.2b) in the absence of an ionic inhomogeneity. Our numerical studies for the TNNP model show that this inhomogeneity can cause the elimination of spiral waves or give rise to breaking up of spiral wave or complex periodic behaviors or have no significant effect on the spiral waves. Precisely which one of these behaviors is obtained depends on the position of the inhomogeneity. In Fig. 18.2(c), we show that the inhomogeneity can break the spiral wave and can possibly lead to ST. A representative case of the coexistence of spiral waves with different quasiperiodic behaviors inside and outside the inhomogeneity is shown in Fig. 18.2(d). Similar results were also obtained if the initial condition was a broken-spiral-wave state rather than a rotating spiral. Complex periodic oscillations and coexistence of the said nature have also been reported in experiments [46]; however, it has been suggested that the oscillations observed in these experiments are caused by the interplay of conduction inhomogeneities and partial conduction blocks [32, 44]. For more information on studies in 2D, we refer the reader to Refs. [47, 48].

18.3.4 Homogeneous Three-Dimensional Slab of Tissue

In this section, we compare 3D simulations of Panfilov, LRI, and TNNP models. In the 3D slab geometry, sheets of cells are stacked one on top of the other with an inter-layer coupling. Furthermore, D is taken to be a tensor with elements $D_{ij} \neq 0$ for any value of j. In the isotropic case, we have $D_{ij} = 0$ for $(i \neq j)$, $D_{xx} = D_{yy} = D_{\|}$ and $D_{zz} = D_2$. $D_{\|}$ is the coefficient of diffusion along and perpendicular to, but in the plane of, the axis of cardiac muscle fibers; its value is the same as the value of D in the homogeneous 2D case. D_2 is different from $D_{\|}$ because of the difference in conduction velocities in the longitudinal and transmural directions in cardiac tissue. Typically we use the values 0.001 $\mathrm{cm}^2\mathrm{s}^{-1}$ and 0.0002$\mathrm{cm}^2\mathrm{s}^{-1}$ for $D_{\|}$ and D_2 respectively [45]. Representative isosurface and volume plots of V from our simulations for homogeneous 3D Panfilov and TNNP models are shown in Figs. 18.3a and c).

The effects of cardiac-muscle-fiber rotation in 3D have been studied for LRI and RPB models. We discuss briefly the effects of such fiber rotation on Panfilov, LRI, and TNNP models; the diffusion tensor now has the form [49], $D_{11} = D_{\|}\cos^2\theta(z) + D_1\sin^2\theta(z), D_{22} = D_{\|}\sin^2\theta(z) + D_1\cos^2\theta(z)$, $D_{33} = D_2$, $D_{13} = D_{31} = D_{23} = D_{32} = 0, D_{12} = D_{21} = (D_{\|} - D_1) \sin\theta(z) \cos\theta(z)$. $D_{\|}$ is the diffusivity for propagation parallel to the fiber axis, D_1 the diffusivity perpendicular to this axis but in-plane, and D_2 the diffusivity perpendicular to the fiber axis in the transmural direction; $\theta(z)$ is the twist angle along the transmural direction. The total fiber rotation from the endocardium to the epicardium is $\theta(z) = \alpha L_z$, where α is the fiber-rotation rate. We assumed that $\delta(z)$ changes continuously [49] from $-\theta_{endocardial\ wall}$ to $+\theta_{epicardial\ wall}$. For 3D studies on the Panfilov and TNNP models, we use slabs of dimensions *20 cm* × *20 cm* × *4 mm.* and *9 cm* × *9 cm* × *2 mm,* respectively.

To study the effect of an initial filament twist on a scroll wave [45], we begin with a stack of 2D spiral waves; spirals in successive planes in the

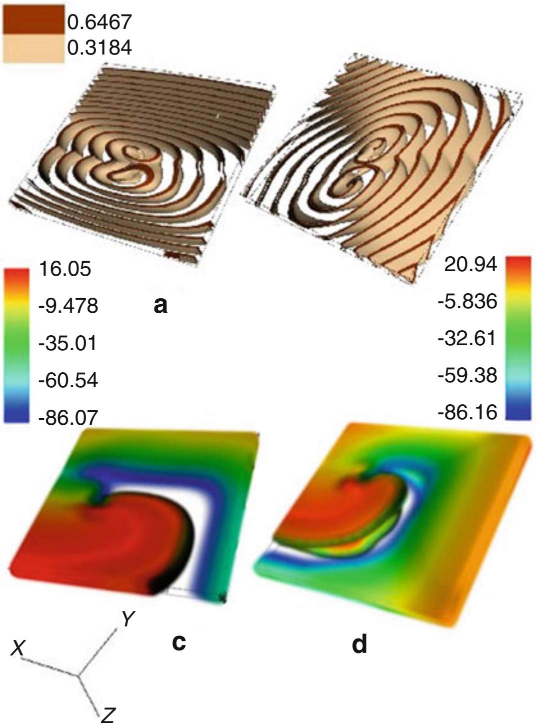

Fig. 18.3 (**a**) Isosurface plot of the transmembrane potential *V* in the homogeneous 3D Panfilov model at time $t = 1.6\ s$; (**b**) the analog of (**a**) but for the 3D Panfilov model with fiber rotation and a rotation angle *40*°; (**c**) a volume plot of the transmembrane potential *V* in the homogeneous 3D TNNP model at time $t = 0.92\ s$; (**d**) the analog of (**c**) but for the 3D TNNP model with fiber rotation and for a rotation angle *40*°

z direction are twisted with respect to each other; this is done by evolving a spiral wave in a 2D simulation and then using the spiral waves, separated by time intervals of, say, $50\delta t$, for successive planes. Thus the initial condition is a scroll wave that is twisted transmurally. For the homogeneous Panfilov and LRI models [45], with parameters belonging to the weak (stable) meander regimes of the corresponding spirals in 2D, the initially twisted scroll is seen to unwind and finally ends up with a straight filament. For the LRI model, this phenomenon occurs for initial twist angles of over 300°, from the top of the filament to its bottom, in 9 mm thick slabs as well as for twist angles of 300°, i.e., two rotations [50]. We obtain analogous results for the Panfilov model.

The analogs of the calculations described in the previous paragraph can also be carried out with fiber rotation; we give illustrative results from our studies of the Panfilov and TNNP models in 3D. We begin with a straight scroll wave and observe that the mere introduction of fiber rotation stimulates bending and twisting of the scroll filament. For fixed tissue thickness, we varied the rate of fiber rotation. The wave developed a complex toroid-like structure as illustrated in Fig. 18.3(b) for the Panfilov model; this structure was unusually stable against both weak and strong perturbations [50]. A representative result from our simulations for the fiber-rotated 3D TNNP model is shown in Fig. 18.3(d).

Scroll-wave break-up has been observed in the LRI model [45, 51–53]. With an initial twist in the scroll filament, a scroll wave in the strong-meander regime breaks up if the angle of twist is greater than a critical value; it then forms a small, less twisted filament along with a scroll ring whose radius shrinks as time increases. The scroll ring ultimately disappears and its counterpart exhibits behavior similar to its parent, depending on its initial twist. For details, we refer the reader to Refs. [51–53]. For more information regarding the dynamics of scroll waves in 3D cardiac tissue, we refer the reader to Ref. [54].

18.4 EADs and the Arrhythmogenesis in the TP06 and ORd Models

We give a brief overview of our *in-silico* studies of a cluster of EAD-generating cells, which can form a substrate of re-entrant excitations that can lead to arrhythmias [39, 55]. We first show that a reduction in the repolarization reserve (RR), achieved by increasing the inward currents (e.g., I_{CaL}) or decreasing the outward currents (e.g., I_{Kr}) or both, leads to EADs in the single-cell AP in the ORd model (see [39] for a similar result for the TP06 model). Figures 18.4(a–d) show the four different types of EADs that we observe by changing the RR in these models: In Fig. 18.4 (a), there is only a marginal effect on the normal repolarization, and the cell returns to its resting-membrane state; in Fig. 18.4(b), the normal repolarization is reversed, depolarization is observed in the form of a bump in the AP, and the cell later comes back to its resting state; in Fig. 18.4(c), the normal repolarization is replaced by oscillations in *V;* in Fig. 18.4(d), the normal repolarization gives way to oscillations in *V* and the cell ends up in a new resting state. In Fig. 18.5, we show, in the G_{CaL}–G_{Kr} plane, the regions in which these four types of EADs occur for different values of PCL; black, red, cyan, and blue colors indicate the regions in which the model shows EADs of the types in Figs. 18.4(a), (b), (c), and (d), respectively. Clearly, EADs appear predominantly for large values of PCL.

We now discuss the implications of these single-cell results for *in-silico* studies of 2D tissue. We observe three different kinds of spiral or broken-spiral waves in the oRd model: Na-Ca-mediated, Ca-mediated, and phase waves, which we illustrate in Fig. 18.6 by representative pseudocolor plots of *V*, I_{Na}, and I_{CaL} (for the following parameter sets: Na-Ca-mediated wave: $G_{CaL} = 4$ and $G_{Kr} = 0.37$; Ca-mediated wave: $G_{CaL} = 4$ and $G_{Kr} = 0.275$; phase wave: $G_{CaL} = 4$ and $G_{Kr} = 0.2$; see Ref. [39] for details). We show in Fig. 18.7, via a representative stability diagram in the G_{CaL}–- G_{Kr} plane (Fig. 18.5 top left panel), the types of waves that occur in different regions (yellow and magenta circles indicate phase waves, yellow-filled triangles Ca-mediated waves, open squares Na-Ca-mediated waves, and yellow-filled squares waves mediated by $I_{Na.}$). We recall that phase waves are pseudo-traveling waves that are not obstructed by impenetrable obstacles, and they are mediated by I_{CaL}. We show in Fig. 18.8 that the defibrillation scheme of Ref. [56] eliminates Na and Na-Ca mediated waves, but it fails to suppress phase waves.

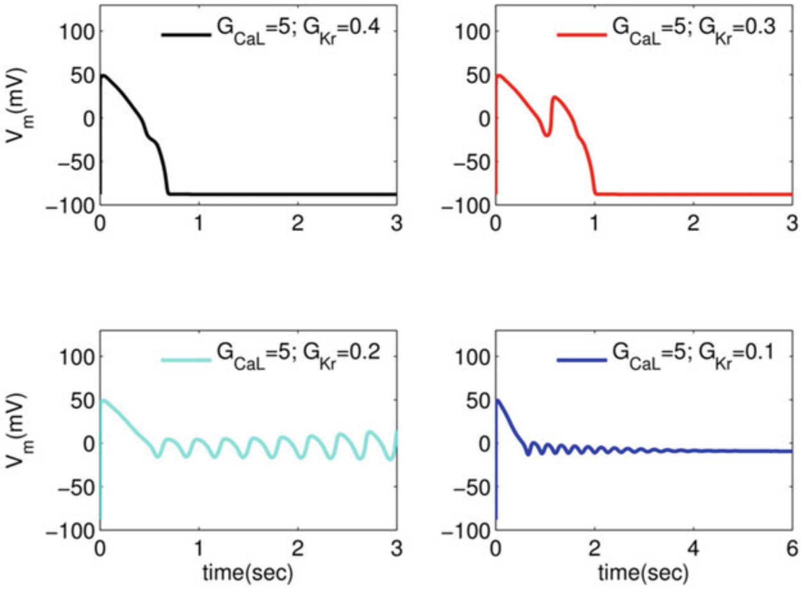

Fig. 18.4 Illustrative action potentials, showing four different types of EADs; (**a**) black colored curve- an AP with marginal change in repolarisation, (**b**) red colored curve- an AP with one EAD, (**c**) cyan colored curve- an AP that has EAD oscillations, and (**d**) blue colored curve- an AP that has EAD oscillations and eventually settles to new resting membrane potential, for different representative values of G_{CaL} and G_{Kr} in the ORd model (see Fig. 2 of Ref. [39] for details)

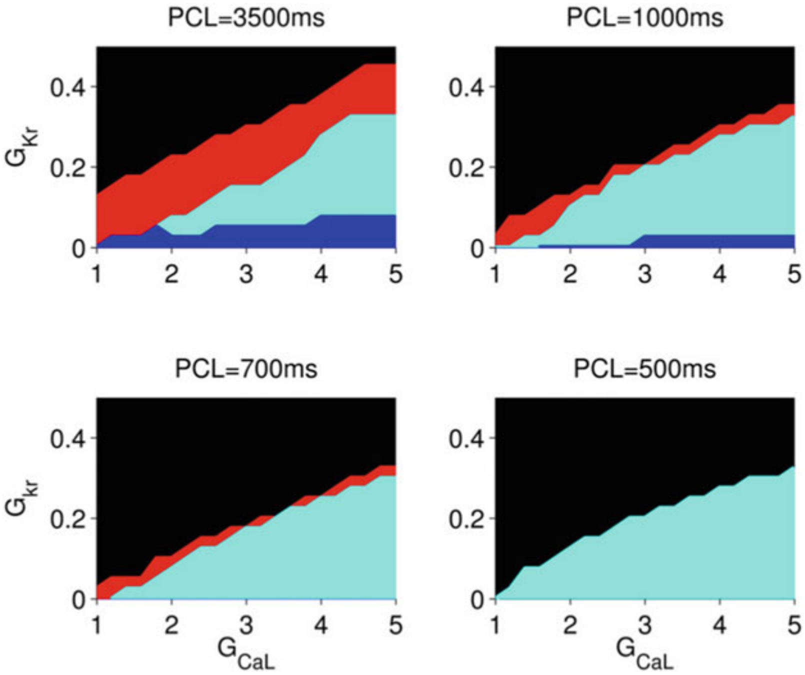

Fig. 18.5 Regions of stability in the G_{CaL}—G_{Kr} plane for the four types of EADs shown in Fig. 18.4 for the ORd model (black: no EADs; red a single EAD; cyan: oscillating EADs which comes back to the resting state; blue: oscillating EADs that shift to a new resting state); different panels show the dependence of these stability regions on the PCL (from Fig. 3 of Ref. [39])

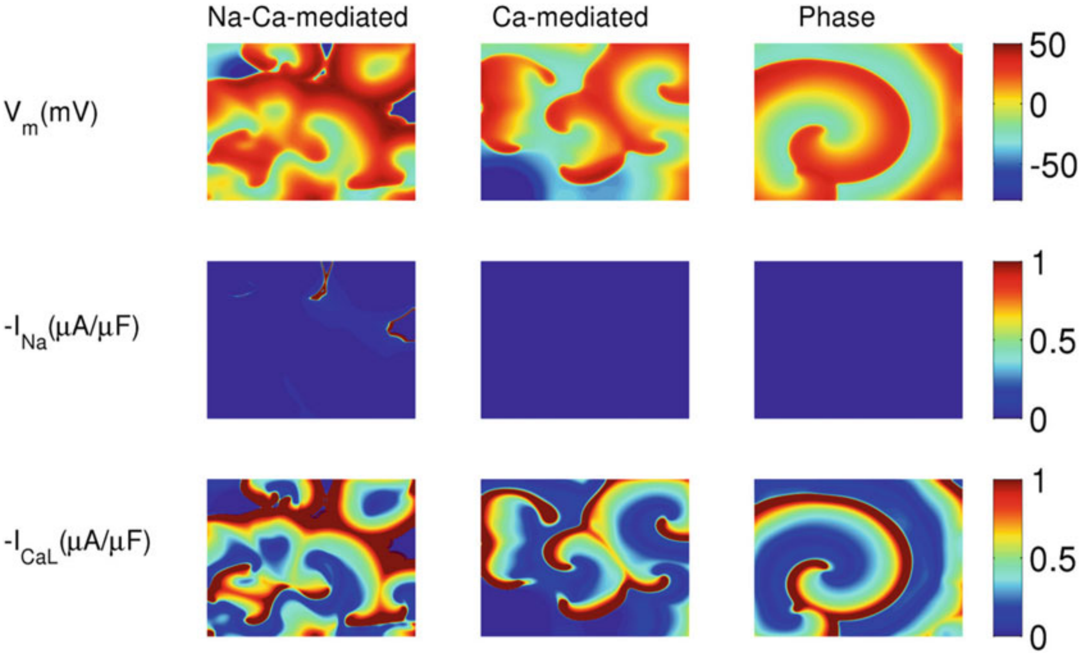

Fig. 18.6 Na-Ca-mediated, Ca-mediated, and phase waves in the ORd model illustrated by representative pseudocolor plots of V, I_{Na}, and I_{CaL} (from Fig. 18.5 in Ref. [39])

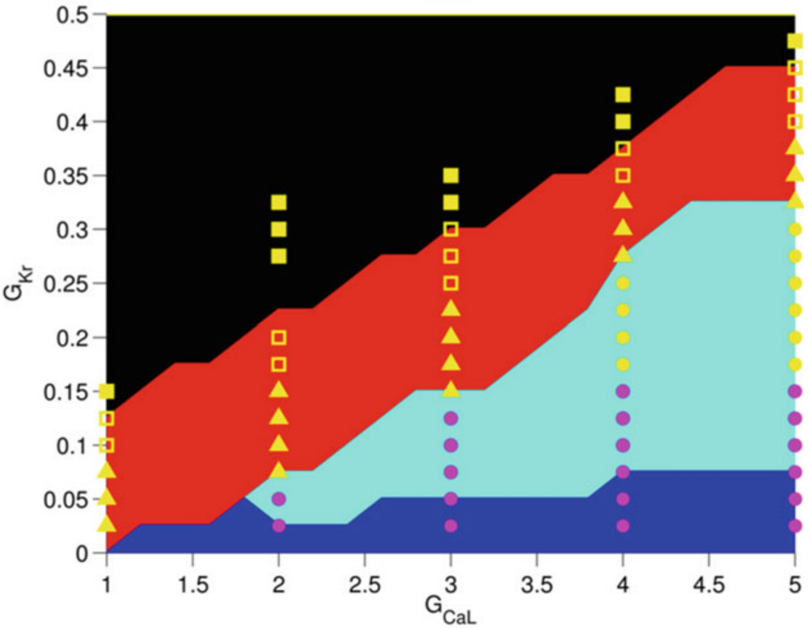

Fig. 18.7 The stability diagram in the G_{CaL}—G_{Kr} plane (top left panel of Fig. 18.6) showing the types of waves that occur in different regions: yellow and magenta circles indicate phase waves; yellow-filled triangles Ca-mediated waves; open squares Na-Ca-mediated waves, and yellow-filled squares waves mediated by $I_{Na.}$ (from Fig. 5 of Ref. [39])

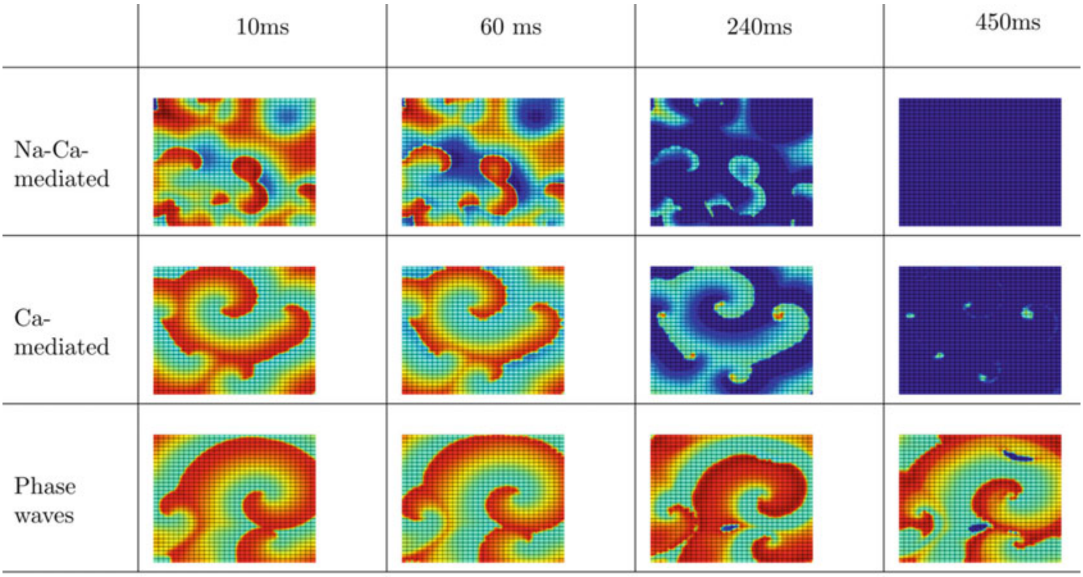

Fig. 18.8 This illustrative plot shows that the defibrillation scheme of Ref. [56] eliminates Na and Na-Ca mediated waves, but it fails to suppress phase waves (from Fig. 18.6 in Ref. [39])

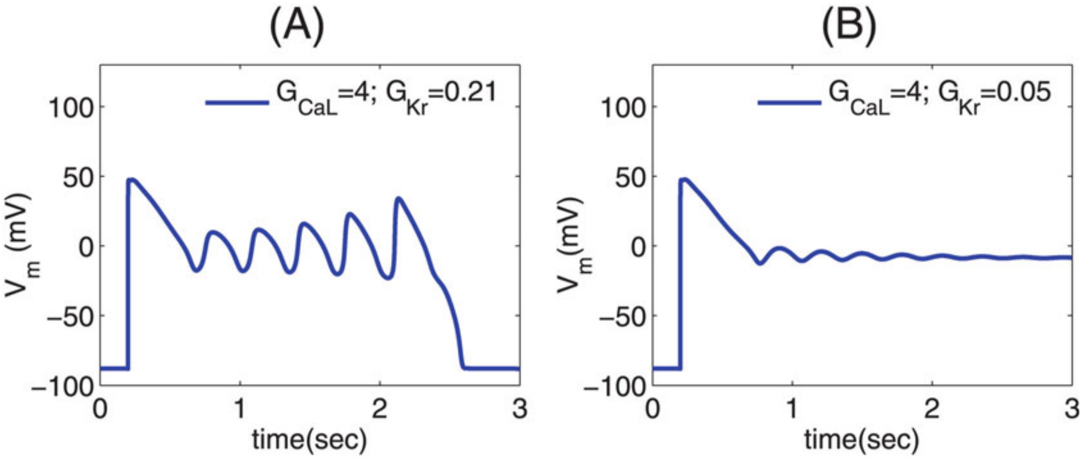

Fig. 18.9 Plots of ORd-model APs showing EADs of (**a**) Type I, with oscillations, increasing with time until the cell repolarizes to the resting membrane potential, and (**b**) Type II, with decaying oscillations, finally relax to a potential that is higher than the normal resting membrane potential (from Fig. 2 of Ref. [16])

18.4.1 Triggered Activity by the EAD Cells in a 2D Cardiac Tissue ORd Model

The role of two different types of EADs in triggered activity that leads to PVCs in the ORd model was investigated by us [16], and the principal results of this study are summarised below: We show that not all EADs, obtained at the single-cell level, are capable of inducing PVCs. We present in Figs. 18.9 (a and b) EADs of types I and II, respectively; we generate these by reducing G_{Kr}. We now consider circular clusters, of radius R, with cells that lead to EADs either of type I or of type II; and we examine wave dynamics with such a circular cluster, of type I or II, in an otherwise homogeneous simulation domain (for the pacing protocol, see Ref. [16]). We show in Fig. 18.10 that type-I EADs are capable of triggered activity, whereas type-II EADs fail in such triggering, because of the low amplitude of EAD oscillations (compare Figs. 18.9 (a) and (b)). In Fig. 18.11, we illustrate how the triggering of PVCs occurs only if the radius R of the EAD-generating cluster is large. Next, we demonstrate in Fig. 18.12 that, as we decrease D by reducing the gap-junctional coupling strength between the EAD-generating cells within the cluster, the propensity of the cluster to yield PVCs is enhanced, because the reduction of D allows the excitations to overcome the source-sink mismatch at the boundaries of the EAD cluster. Finally, we investigate the effects of introducing fibroblasts (caused, e.g., by collagen deposits), which we model as inexcitable obstacles, into the EAD cluster; if this cluster does not generate PVCs on its own, then it can do so as the percentage concentration P_f of fibroblasts increases (see Fig. 18.13), although, for sufficiently large P_f PVCs are suppressed (Fig. 18.14).

For the dependence of of such PVCs on other parameters we refer the reader to [16].

18.5 The Control of Spiral-Wave Turbulence

The efficient control of arrhythmogenic waves has been one of the outstanding goals in clinical cardiology. Specifically, the challenge is the termination of rotors or spiral and scroll waves, especially of those that are broken. This can be achieved by the following two different approaches: (a) the therapeutic approach in which suitable medication is administered (see,

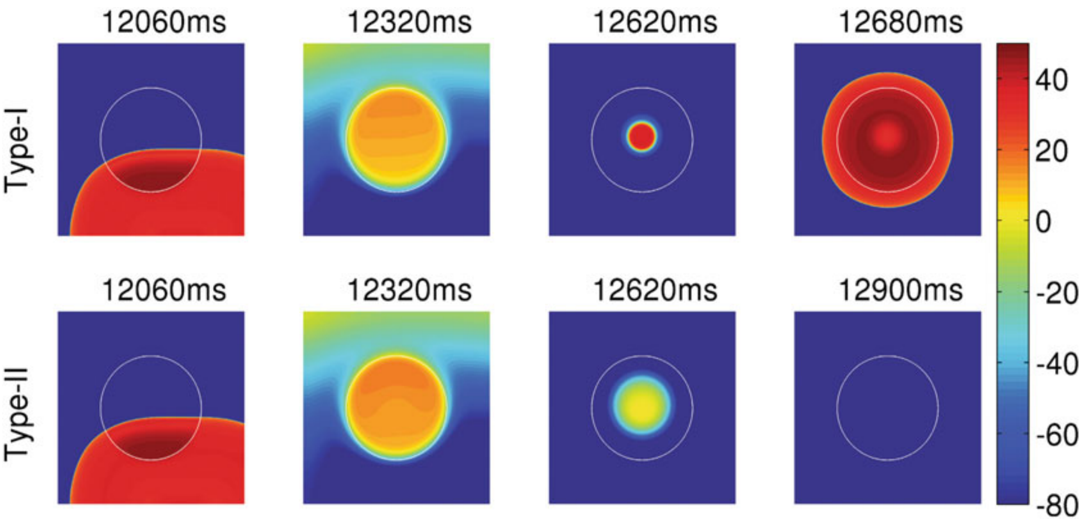

Fig. 18.10 Representative ORd-model tissue simulations showing, via pseudocolor plots of the transmembrane potential, that not all types of EADs can trigger PVCs: Type-I EADs can, after assymetric pacing, but Type-II EADs fail to do so (from Fig. 3 of Ref. [16]); the boundary of the cluster of EAD cells is indicated by a white curve

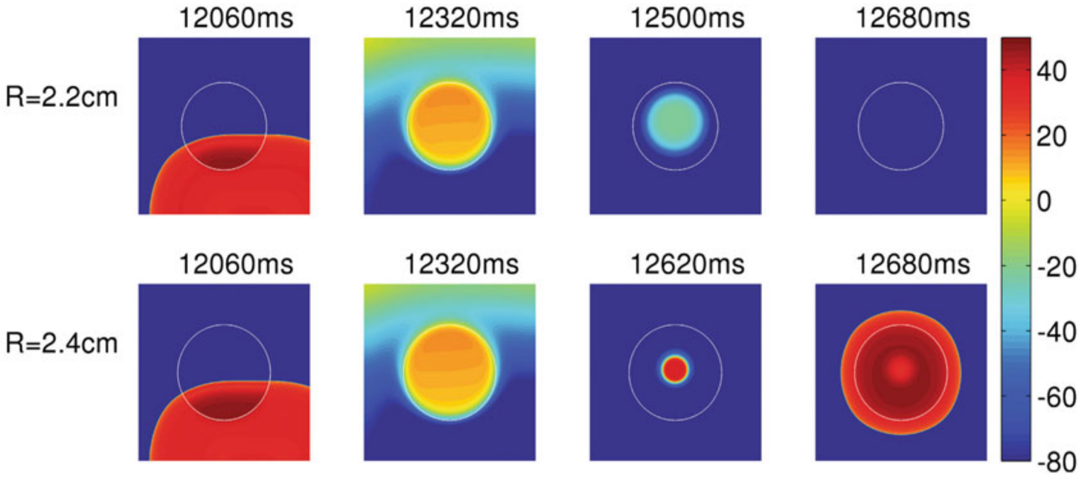

Fig. 18.11 Representative ORd-model tissue simulations showing, via pseudocolor plots of the transmembrane potential, that small (large) size Type-I EAD clusters cannot (can) trigger PVCs after assymetric pacing (from Fig. 4 of Ref. [16]); the boundary of the cluster of EAD cells is indicated by a white curve

e.g., [18, 19]) and (b) defibrillation, i.e., the application of electric fields or low-amplitude currents (see, e.g., [56, 58, 59]).

Defibrillation is the application of electrical shocks to control the fibrillating heart and to restore its normal rhythm. The success rate of defibrillation is variable and sometimes it can also leave the heart damaged [1]. In external defibrillation, one applies electrical shocks ($5\ kV$) across the patient's chest to depolarize all cardiac cells simultaneously. This silences the ventricles electrically and forces all the cardiac

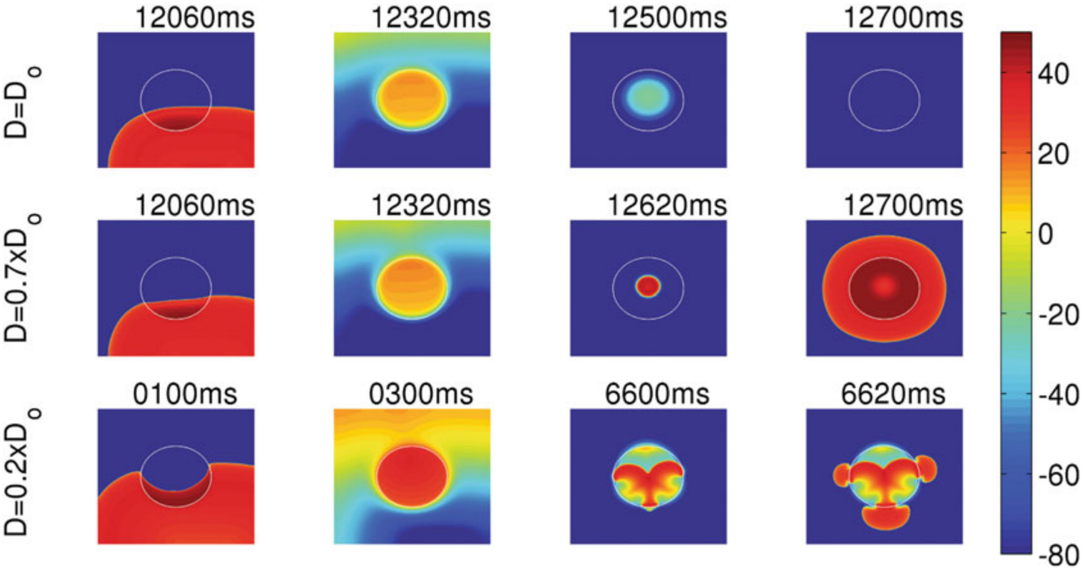

Fig. 18.12 Representative ORd-model tissue simulations showing, via pseudocolor plots of the transmembrane potential, that, as we decrease *D* by reducing the gap-junctional coupling strength between the EAD-generating cells within the cluster, the propensity of the cluster to yield PVCs is enhanced (from Fig. 5 of Ref. [16]); the boundary of the cluster of EAD cells is indicated by a white curve

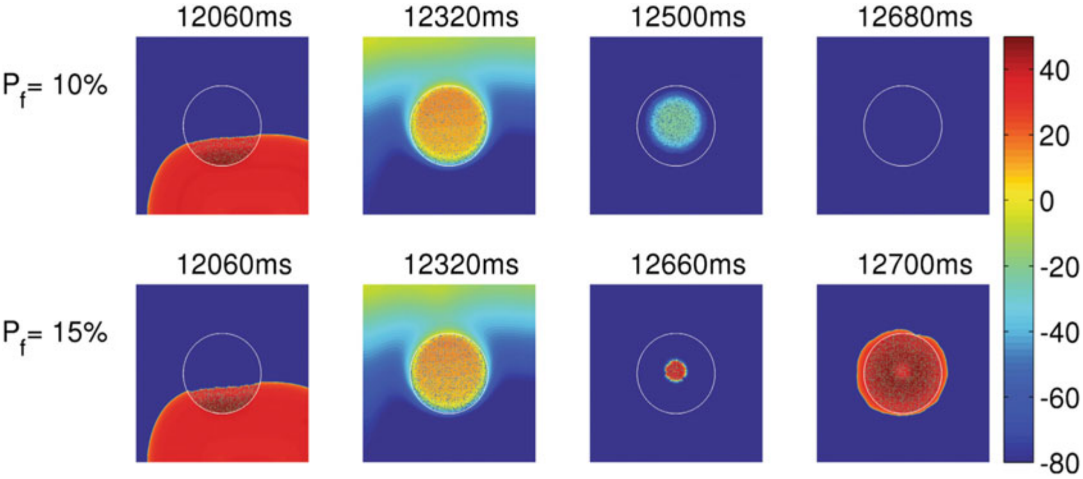

Fig. 18.13 Representative ORd-model tissue simulations showing, via pseudocolor plots of the transmembrane potential, PVC triggering with $P_f = 15\%$ (bottom panel) but not with $P_f = 10\%$ fibrosis (top panel) in an EAD cluster with $R = 2$ cm; here, P_f the percentage of inexcitable cells (fibrosis) within the cluster (from Fig. 7 in Ref. [16]); the boundary of the cluster of EAD cells is indicated by a white curve

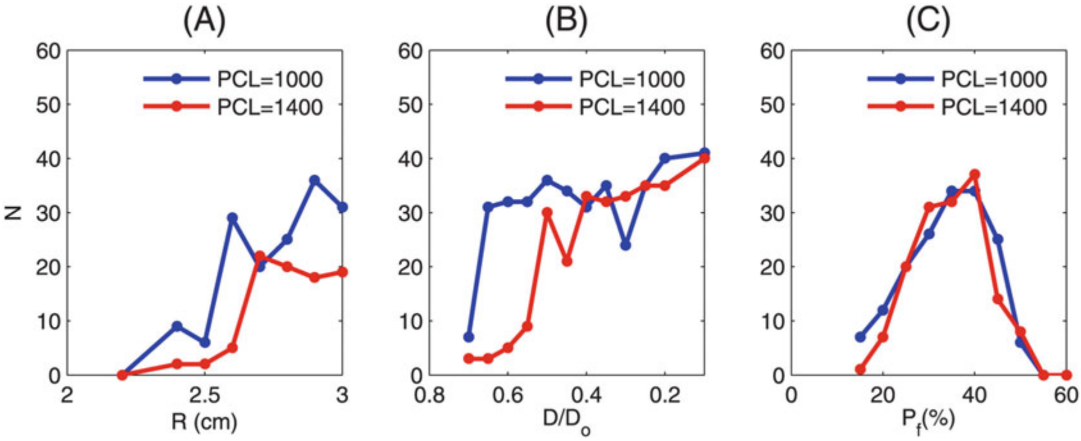

Fig. 18.14 The dependence on P_f (as in Fig. 18.13) of the number N of triggered PVCs (from Fig. 6 in Ref. [16])

cells, including the sino-atrial node (SAN) and the atrio-ventricular node (AVN), to reset and resume normal electrophysiological activity [2].

The analog of defibrillation in mathematical models of cardiac tissue is the control of spiral-wave activity, preferably with low-amplitude voltage pulses. Several schemes have been suggested; here, we discuss the control scheme proposed by Sinha et al. [56] for the Panfilov model. This uses very low-amplitude pulses (of order *mV*) for a brief duration (of order *100 ms*) and over a coarse mesh of lines on the model ventricle [56]. This scheme, if realized in an internal defibrillator, would constitute a significant advance in these devices, because it would lead to the development of low-amplitude defibrillation, which is a major challenge.

In the Panfilov model, the analog of VF arises when the system evolves to a transient state in which large spirals break down [56]. The lifetime τ_L of this state increases rapidly with L, the linear size of the system. Qualitatively, this agrees with the experimental finding that hearts of small mammals are less prone to fibrillation than those of large mammals. For time scales longer than τ_L, a quiescent state is established with $e = g = 0$. In the 2D control scheme, the simulation domain (size $L \times L$) is divided into K^2 smaller blocks bounded by a mesh of lines. A super-threshold pulse is applied to the e-field on the selected mesh of lines. This pulse, applied for a short length of time τ_c, effectively simulates Neumann boundary conditions (for the block bounded by the mesh) because the region near the mesh lines becomes refractory. The mesh lines then absorb the spiral waves formed inside each block and spiral-wave turbulence is eliminated. For a generalization of the 3D case and for the details of the control protocol, we refer the reader to Ref. [56]. We have extended this control scheme to the LRI, RPB, and TNNP models [32] both for homogeneous simulation domains and domains with inhomogeneities. We give representative results for this control scheme for the 2D TNNP model both with and without inhomogeneities in Figs. 18.15(a–d).

We have discussed our earlier proposal for a low-amplitude defibrillation scheme (Ref. [56]). We now summarize our recent suggestion for the defibrillation scheme, which we realize by using a deep-learning approach; this eliminates both unbroken and broken spiral waves. In particular, we develop a convolution neural network (CNN) that we train (see Ref [57]) to classify and distinguish between spiral [S] and non-spiral (N S) wave patterns (Fig. 18.16), which we obtain from pseudocolor plots of the transmembrane potential that result from our *in-silico* studies of different PDE models for cardiac tissue [3, 35, 57, 60–62]. Our CNN (Fig. 18.17) has one *input layer* and three sets of *convolution layers*, ReLU and Max pool layers, and a final fully-connected layer [57, 63]. We train this CNN by employing (a) a stochastic-gradient decent technique and a

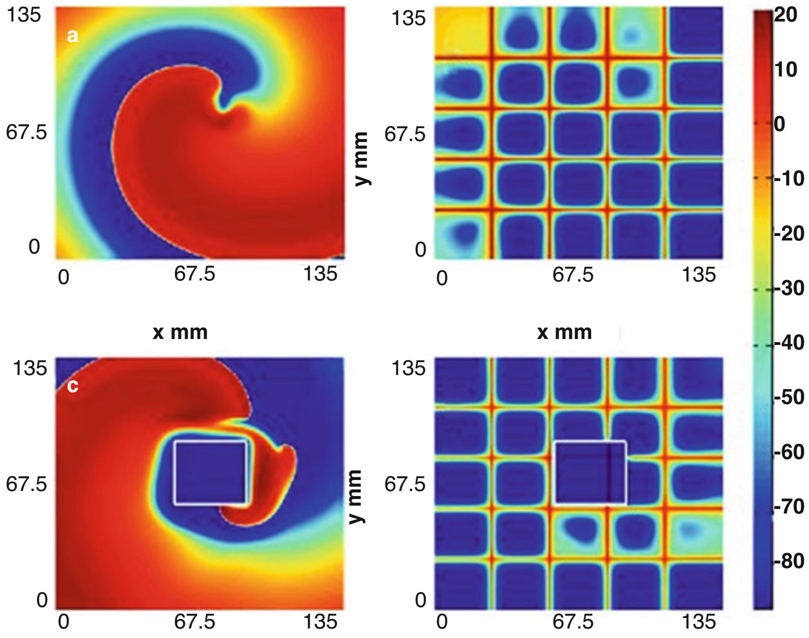

Fig. 18.15 Spiral-wave control in the 2D TNNP model by the application of a control pulse of amplitude $27.75\ A/cm^2$ for $t = 20\ ms$ over a square mesh with each block of size $L/K = 27\ mm$, i.e., the simulation domain is divided into 5^2 square blocks. Figures (**a**) and (**b**) are pseudocolor plots of V for the homogeneous case at time $t = 0\ ms$ and $t = 280\ ms$, respectively. Figures (**c**) and (**d**) are the analogs of (**a**) and (**b**) but in the presence of a square inhomogeneity of side length $l = 33.75\ mm$, whose bottom-left corner is placed at $(56.25\ mm, 56.25\ mm)$

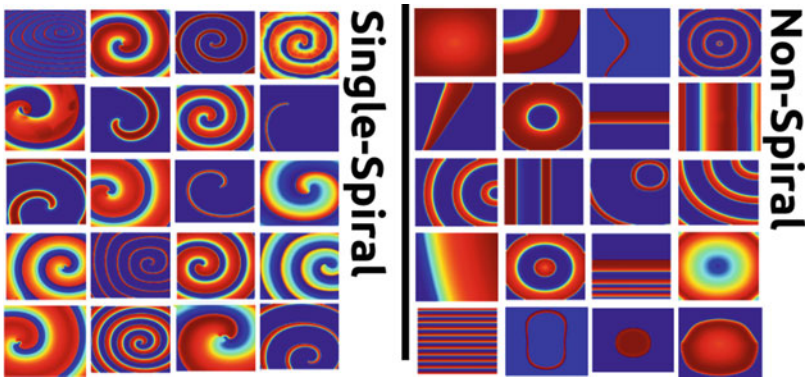

Fig. 18.16 Pseudocolor plots (from Fig. 1 of Ref. [57]) of the transmembrane potential showing spiral (S) and non-spiral (N S) wave patterns, which we obtain from our *in-silico* studies of different PDE models for cardiac tissue Ref. [3, 35, 57, 60–62]

cross-entropy energy function and (b) 100,000 S and N S patterns [57, 63]. Our trained CNN distinguishes between S and N S patterns with an accuracy of 99.6%.

Broken-spiral patterns, in pseudocolor plots of the transmembrane potential, contain multiple spiral waves of different sizes. We use our trained CNN to scan over such images, with a range of scanning sizes, to obtain a heatmap H, which provides the positions of the spiral cores, as is schematically shown in Fig. 18.18. We find that an unbroken spiral wave can be eliminated by targeting the spiral core and the spiral arms by applying a current pulse with a 2D Gaussian profile, with its center at the spiral core [57]. Therefore, in the case of the broken-spiral waves, we use a 2D lattice of such Gaussian current pulses, each one centered at the spiral cores that we identify via the heatmap H. Strictly speaking, this requires the Hadamard product of H and the 2D lattice of Gaussian current pulses; we give illustrative plots in Fig. 18.19 and refer the reader to Mulimani et al. [57] for details.

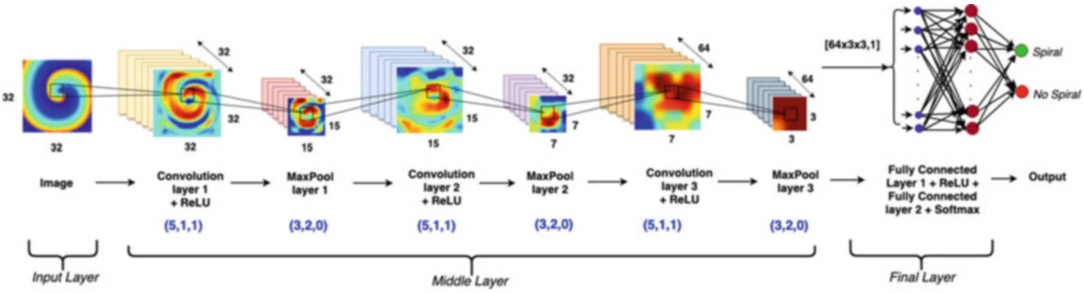
32
32
Image
32
32
32
Convolution layer 1 + ReLU
(5,1,1)
32
15
15
MaxPool layer 1
(3,2,0)
32
15
15
Convolution layer 2 + ReLU
(5,1,1)
32
7
7
MaxPool layer 2
(3,2,0)
64
7
7
Convolution layer 3 + ReLU
(5,1,1)
64
3
3
MaxPool layer 3
(3,2,0)
[64x3x3,1]
Spiral
No Spiral
Fully Connected Layer 1 + ReLU + Fully Connected layer 2 + Softmax
Output
Input Layer
Middle Layer
Final Layer

Fig. 18.17 A schematic diagram (from Fig. 2 of Ref. [57]) of the convolutional neural network (CNN) that we use to identify spiral (S) and non-spiral (N S) wave patterns

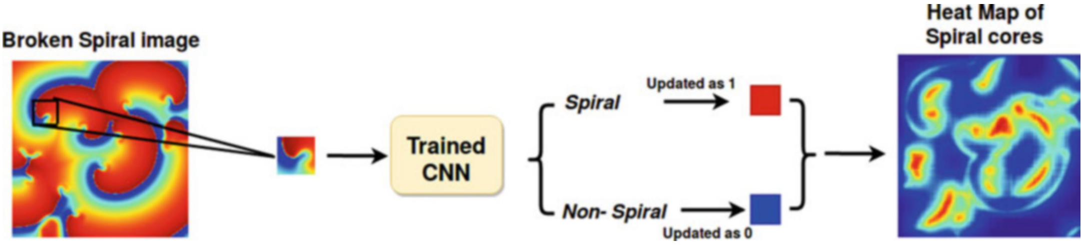
Broken Spiral image
Trained CNN
Spiral
Updated as 1
Non- Spiral
Updated as 0
Heat Map of Spiral cores

Fig. 18.18 Pseudocolor plots (from Fig. 3 of Ref. [57]) of the transmembrane potential (left panel) with multiple spiral waves of different sizes. We use our trained CNN to scan over such images to obtain the heatmap H (right panel); this provides the positions of the spiral cores

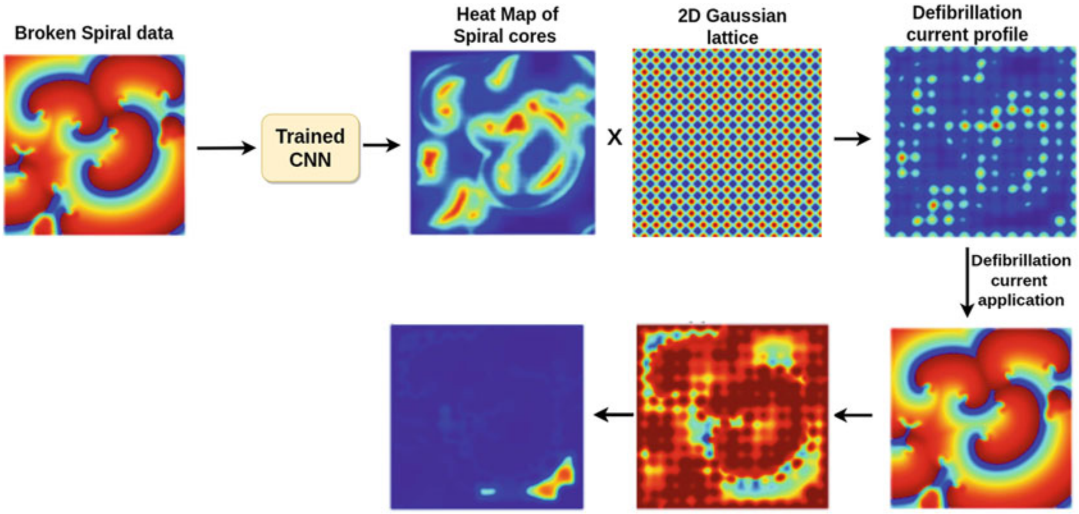
Broken Spiral data
Trained CNN
Heat Map of Spiral cores
X
2D Gaussian lattice
Defibrillation current profile
Defibrillation current application

Fig. 18.19 Pseudocolor plots (from the top two rows of Fig. 7 of Ref. [57]) illustrating the use of the heatmap H (Fig. 18.18) and its use in developing a defibrillation current profile, with Gaussian current pulses at spiral cores; this eliminates broken-spiral waves (see Ref. [57] for details)

18.6 Conclusions

We have provided a brief overview of recent studies of spiral- and scroll-wave dynamics in mathematical models of cardiac tissue. These are believed to be important in developing an understanding of life-threatening cardiac arrhythmias like VT and VF. In addition to giving a summary of Panfilov, LRI, RPB, TNNP, TP06, and ORd models, we have described how spiral and scroll waves can be initiated in such models, how they evolve subsequently, how they interact with conduction and ionic inhomogeneities, how they are affected by the rotation of muscle fibers, and how they may be controlled. We have also given an overview of our recent numerical studies of PVC triggering in models with cells that give rise to EADs.

This sets the stage for systematic numerical studies of the analogs of low-amplitude defibrillation schemes in realistic mathematical models of cardiac tissue like the TNNP, TP06, and ORd models in the presence of inhomogeneities. We have also demonstrated how to use our large computational data sets to train a CNN to distinguish between spiral (S) and non-spiral (N S) wave patterns, obtain heat maps H for broken-spiral-wave patterns, and use these heatmaps to develop an efficient, low-amplitude scheme for the elimination of these pathological waves [57].

In future studies, we plan to explore such schemes with even more features than we have discussed here. In particular, we expect to extend our studies to anatomically realistic simulation domains, to bidomain models, and to models that include the effects of fibroblasts and their coupling to myocytes. Our eventual goal is to bring our in silico studies as close as possible to their in vitro and in vivo counterparts. We hope that our introduction to this challenging interdisciplinary field will stimulate further studies, especially ones that bring together techniques from physics, nonlinear dynamics, and biology.

Acknowledgments We thank T. K. Shajahan and P. Perlekar for discussions, DST, UGC, CSIR (India), and Microsoft Research for support, and SERC (IISc) for computational resources.

References

1. Latest cardiac devices treat arrhythmias while promoting natural heart function: [News release on the Internet]; [cited: 2010 May] Available at http://wwwp.medtronic.com/Newsroom/NewsReleaseDetails.do?itemId=1121166620748&lang=en_UK
2. Zhou H, Hou KMN, Ponsonnaille J, Gineste L, De Vaulx C. A real-time continuous cardiac arrhythmias detection system: RECAD. Proceedings of the 27th IEEE Annual Conference on Engineering in Medicine and Biology. 2005.
3. O'Hara T, Virág L, Varró A, Rudy Y. Simulation of the undiseased human cardiac ventricular action potential: model formulation and experimental validation. PLoS Comput Biol. 2011;7(5):e1002061.
4. Garrey WE. Auricular fibrillation. Physiol Rev. 1924;4:214.
5. Jalife J, Delmar M, Davidenko J, Anumonwo JMB. Basic cardiac electrophysiology for the clinician. Armonk, NY: Futura; 1999.
6. Allessie MA, Bonke FIM, Schopman FJC. Circus movement in rabbit atrial muscle as a mechanism of tachycardia. Circ Res. 1973;33:54.
7. Allessie MA, Bonke FIM, Schopman FJC. Circus movement in rabbit atrial muscle as a mechanism of tachycardia. III. The "leading circle" concept: a new model of circus movement in cardiac tissue without the involvement of an anatomical obstacle. Circ Res. 1977;41:9.
8. Mines GR. On dynamic equilibrium in the heart. J Physiol. 1913;46:349.
9. Mines GR. On circulating excitations in heart muscles and their possible relation to tachycardia and fibrillation. Trans R Soc Can. 1914;IV:43.
10. Pertsov AM, Davidenko JM, Salomonsz R, Baxter WT, Jalife J. Spiral waves of excitation underlie reentrant activity in isolated cardiac muscle. Circ Res. 1993;72:631.
11. Davidenko JM, Perstov AV, Salomonsz R, Baxter W, Jalife J. Stationary and drifting spiral waves of excitation in isolated cardiac muscle. Nature. 1992;355:349.
12. Ikeda T, Yashima M, Uchida T, Hough D, Fishbein MC, et al. Attachment of meandering reentrant wave fronts to anatomic obstacles in the atrium. Circ Res. 1997;81:753.
13. Valderrabano M, Kim YH, Yashima M, Wu TJ, Karagueuzian HS, et al. Obstacle- induced transition from ventricular fibrillation to tachycardia in isolated swine right ventricles. J Am Coll Cardiol. 2000;36: 2000.
14. Lim ZY, Maskara B, Aguel F, Emokpae R, Tung L. Spiral wave attachment to millimeter- sized obstacles. Circulation. 2006;114:2113.
15. Nayak AR, Panfilov AV, Pandit R. Spiral-wave dynamics in a mathematical model of human ventricular tissue with myocytes and Purkinje fibers. Physic Rev E. 2017;95(2):022405.

16. Zimik S, Nayak AR, Pandit R. A computational study of the factors influencing the PVC-triggering ability of a cluster of early afterdepolarization-capable myocytes. PLoS One. 2015;10(12):e0144979.
17. Alonso S, dos Santos RW, Bär M. Reentry and ectopic pacemakers emerge in a three-dimensional model for a slab of cardiac tissue with diffuse microfibrosis near the percolation threshold. PLoS One. 2016;11(11):e0166972.
18. Moreno JD, Yang PC, Bankston JR, Grandi E, Bers DM, Kass RS, et al. Ranolazine for congenital and acquired late INa-linked arrhythmias: in silico pharmacological screening. Circ Res. 2013;113(7):e50–61.
19. Moreno JD, Zhu ZI, Yang C, Bankston JR, Jeng MT, Kang C, et al. A computational model to predict the effects of class I anti-arrhythmic drugs on ventricular rhythms. Sci Transl Med. 2011;3(98):98ra83.
20. Nuss HB, Kääb S, Kass DA, Tomaselli GF, Marbán E. Cellular basis of ventricular arrhythmias and abnormal automaticity in heart failure. Am J Physiol - Heart Circ Physiol. 1999;277(1):H80–91.
21. Clancy CE, Rudy Y. Linking a genetic defect to its cellular phenotype in a cardiac arrhythmia. Nature. 1999;400(6744):566–9.
22. Clancy CE, Rudy Y. Na+ channel mutation that causes both Brugada and long-QT syndrome phenotypes: a simulation study of mechanism. Circulation. 2002;105(10):1208–13.
23. Zimik S, Pandit R. Reentry via high-frequency pacing in a mathematical model for human-ventricular cardiac tissue with a localized fibrotic region. Sci Rep. 2017;7(1):1–4.
24. Nayak AR, Shajahan TK, Panfilov AV, Pandit R. Spiral-wave dynamics in a mathematical model of human ventricular tissue with myocytes and fibroblasts. PLoS One. 2013;8(9):e72950.
25. Xie Y, Sato D, Garfinkel A, Qu Z, Weiss JN. So little source, so much sink: requirements for afterdepolarizations to propagate in tissue. Biophys J. 2010;99(5):1408–15.
26. Sato D, Xie LH, Sovari AA, Tran DX, Morita N, Xie F, et al. Synchronization of chaotic early afterdepolarizations in the genesis of cardiac arrhythmias. Proc Nat Acad Sciences. 2009;106(9):2983–8.
27. Vandersickel N, Van Nieuwenhuyse E, Seemann G, Panfilov A. Spatial patterns of excitation at tissue and whole organ level due to early afterdepolarizations. Fronti Physiol. 2017;8:404.
28. Belardinelli L, Antzelevitch C, Vos MA. Assessing predictors of drug-induced torsade de pointes. Trends Pharmacol Sci. 2003;24(12):619–25.
29. Boulaksil M, Jungschleger JG, Antoons G, Houtman MJ, de Boer TP, Wilders R, et al. Drug-induced torsade de pointes arrhythmias in the chronic AV block dog are perpetuated by focal activity. Circulation: Arrhyth Electrophysiol. 2011;4(4):566–76.
30. Vandersickel N, de Boer TP, Vos MA, Panfilov AV. Perpetuation of torsade de pointes in heterogeneous hearts: competing foci or re-entry? J Physiol. 2016;594(23):6865–78.
31. Asano Y, Davidenko JM, Baxter WT, Gray RA, Jalife J. Optical mapping of drug-induced polymorphic arrhythmias and torsade de pointes in the isolated rabbit heart. J Am Coll of Cardiol. 1997;29(4):831–42.
32. Shajahan TK, Nayak AR, Pandit R. Spiral-wave turbulence and its control in the presence of inhomogeneities in four mathematical models of cardiac tissue. PLoS One. 2009; 4(3):e4738. [cited 2009, September] Available from http://www.plosone.org/article. https://doi.org/10.1371/journal.pone.0004738.
33. Bernus O, Wilders R, Zemlin CW, Versschelde H, Panfilov AV. A computationally efficient electrophysiological model of human ventricular cells. Am J Physiol Heart Circ Physiol. 2002;282:H2296.
34. Priebe L, Beuckelmann J. Simulation study of cellular electric properties in heart failure. Circ Res. 1998;82:1206.
35. Ten Tusscher KH, Panfilov AV. Alternans and spiral breakup in a human ventricular tissue model. Am J Physiol - Heart Circ Physiol. 2006;291(3):H1088–100.
36. Panfilov AV, Hogeweg P. Spiral breakup in a modified FitzHughNagumo model. Phys Lett A. 1993;176 No. 5 (295299):295.
37. Panfilov AV. Spiral breakup as a model of ventricular fibrillation. Chaos. 1998;8(1):57–64.
38. Clayton R, Panfilov A. A guide to modeling cardiac electrical activity in anatomically detailed ventricles. Progr Biophys Mol Biol. 2008;96:14.
39. Zimik S, Vandersickel N, Nayak AR, Panfilov AV, Pandit R. A comparative study of early afterdepolarization-mediated fibrillation in two mathematical models for human ventricular cells. PLoS One. 2015;10(6):e0130632.
40. Kleber AG, Rudy Y. Basic mechanisms of cardiac impulse propagation and associated arrhythmias. Physiol Rev. 2004;84:431–88.
41. Smith NP, Hunter PJ, Pullan AJ, Nash MP. An Anatomically Realistic Cardiac Model. Proceedings of the 11th Conference of the ESB. July 8–11, vol. 31. France: Toulouse; 1998. p. 140.
42. ten Tusscher KHWJ, Noble D, Noble PJ, Panfilov AV. A model for human ventricular tissue. Am J Physiol Heart Circ Physiol. 2004;286:1073–89.
43. Xie F, Qu Z, Garfinkel A. Dynamics of reentry around a circular obstacle in cardiac tissue. Phys Rev E. 1998;58:6355.
44. Shajahan TK, Sinha S, Pandit R. Spiral-wave dynamics depends sensitively on inhomogeneities in mathematical models of ventricular tissue. Phys Rev E. 2007;75:011429.
45. Qu Z, Kil J, Xie F, Garfinkel A, Weiss JN. Scroll wave dynamics in a three-dimensional cardiac tissue model: roles of restitution, thickness, and fiber rotation. Biophys J. 2002;78:2761–75.
46. Hwang SM, Kim TY, Lee KJ. Complex-periodic spiral waves in confluent cardiac cell cultures induced by

localized inhomogeneities. Proc Nat Acad Sciences. 2005;102:10363.

47. Panfilov AV. Theory of reentry. In: Zipes DP, Jalife J, editors. Cardiac electrophysiology: from cell to bedside. 5th ed. Elsevier; 2009. p. 329–37.
48. Qu Z, Xie F, Garfinkel A, Weiss JN. Origins of spiral wave meander and breakup in a two-dimensional cardiac tissue model. Ann Biomed Eng. 2000;28:755–71.
49. Fenton F, Karma A. Vortex dynamics in three-dimensional continuous myocardium with fiber rotation: filament instability and fibrillation. Chaos. 1998;8 (1):20.
50. Aranson IS, Bishop AR. Instability and stretching of vortex lines in the three- dimensional complex Ginzburg-Landau equation. Phys Rev Lett. 1997;79 (21):4174–7.
51. Qu Z, Xie F, Garfinkel A. Diffusion-induced vortex filament instability in 3-dimensional excitable media. Phys Rev Lett. 1999;83(13):2668–71.
52. Ding M, Yang W. Stability of synchronous chaos and on-off intermittency in coupled map lattices. Phys Rev E. 1997;56(4):4009–16.
53. Yang P, Deng T, Zhao D, Feng P, Pine D, Chmelka BF, Whitesides GM, et al. Hierarchically ordered oxides. Science. 1998;282(5397):2244–6.
54. Clayton RH, Zhuchkova EA, Panfilov AV. Phase singularities and filaments: simplifying complexity in computational models of ventricular fibrillation. Prog Biophys Mol Biol. 2006;90:378–98.
55. Vandersickel N, Kazbanov IV, Nuitermans A, Weise LD, Pandit R, Panfilov AV. A study of early afterdepolarizations in a model for human ventricular tissue. PLoS One. 2014;9(1):e84595.
56. Sinha S, Pande A, Pandit R. Defibrillation via the elimination of spiral turbulence in model for ventricular fibrillation. Phys Rev Lett. 2001;86:3678.
57. Mulimani MK, Alageshan JK, Pandit R. Deep-learning-assisted detection and termination of spiral and broken-spiral waves in mathematical models for cardiac tissue. Physic Rev Res. 2020;2(2):023155.
58. Luther S, Fenton FH, Kornreich BG, Squires A, Bittihn P, Hornung D, et al. Low-energy control of electrical turbulence in the heart. Nature. 2011;475 (7355):235–9.
59. Otani NF. Termination of reentrant cardiac action potential propagation using far-field electrical pacing. IEEE Transact Biomed Engin. 2011;58(7):2013–22.
60. Barkley D. A model for fast computer simulation of waves in excitable media. Physica D: Nonlinear Phenomena. 1991;49(1–2):61–70.
61. Aliev RR, Panfilov AV. A simple two-variable model of cardiac excitation. Chaos, Solitons Fractals. 1996;7 (3):293–301.
62. Luo CH, Rudy Y. A model of the ventricular cardiac action potential. Depolarization, repolarization, and their interaction. Circ Res. 1991;68(6):1501–26.
63. Nielsen MA. Neural networks and deep learning. San Francisco, CA: Determination Press; 2015 Sep 25.

The Role of Intracellular Ca^{2+} in Arrhythmias in the Postmyocardial Infarction Heart

19

Wen Dun and Penelope A. Boyden

Abstract

Abnormalities in intracellular Ca^{2+} handling occur in Purkinje and ventricular cells that have survived in the infarcted heart. Such abnormalities are presented and contrasted in this chapter. Interestingly, these changes differ depending on the cell type (IZPC vs. IZ) and contribute differently to the arrhythmogenicity of the postmyocardial infarction (MI) substrate. Thus, it is reasonable to assume that rational drug design could derive compounds against these intracellular Ca^{2+} changes that would be specific not only for the cell type but also for the type of arrhythmias occurring post-MI.

Keywords

Purkinje Cell · Sarcoplasmic Reticulum · Release Channel · Infarcted Heart · Ventricular Cell

19.1 Introduction

19.1.1 Excitation–Contraction Coupling (ECC)

During the action potential (AP), calcium ions enter the cell through L-type Ca^{2+} channels. In ventricular cells, the number of Ca^{2+} channels is estimated to be 15 per μm^2, and yet only 3% are open at peak currents (for review, see [1]). However, the amount of Ca^{2+} entering a cell per second depends on AP duration and the number of APs/min. L-type Ca^{2+} influx occurs at both T-tubular and cell surfaces, but in ventricular cells from normal hearts, more Ca^{2+} entry occurs per μm^2 at the cell surface than at T-tubules [2]. This Ca^{2+} influx begins ECC by triggering the release of Ca^{2+} from the sarcoplasmic reticulum (SR) via the ryanodine (RyR) sensitive Ca^{2+} release channels located in the SR membranes. In the rat [3], the ratio of RyR to L-type Ca^{2+} channels is 7:1 and would fit spatially with a random coupling of the L-type Ca^{2+} channel to Ca^{2+} release via RyR [4]. Based on labeling studies, the ratio of cell surface L-type Ca^{2+} channels vs. T-tubular channels is 1:3 [5].

Intracellular Ca^{2+}-induced Ca^{2+} release (CICR) is proportional to the free intra-SR Ca^{2+} content and dictates the force of the cardiac contraction. Free Ca^{2+} in the SR has been spatially resolved [6], and these data show that intra-SR Ca^{2+} diffusion is rapid and local Ca^{2+} in SR in normal ventricular cells is only partially depleted with a contraction. Ca^{2+}-activated contraction of the sarcomere is short-lived due to the rapid elimination of Ca^{2+} ions from the cytosol. About two-thirds of the Ca^{2+} is resequestered by the SR [7], while the remainder leaves the cell, mostly via the low affinity, high capacity, Na/Ca exchanger transport (NCX) protein. In the steady

W. Dun · P. A. Boyden (✉)
Department of Pharmacology, Center for Molecular Therapeutics, Columbia University, New York, NY, USA
e-mail: pab4@columbia.edu

© Springer Nature Switzerland AG 2023

O. N. Tripathi et al. (eds.), *Heart Rate and Rhythm*, https://doi.org/10.1007/978-3-031-33588-4_19

state, the sum of the Ca^{2+} efflux through the membrane balances the influx during the AP.

It takes time for the RyR-Ca^{2+} release process to recover completely from the last release so that sequestered Ca^{2+} can again be released from the SR. It is known that electrical refractoriness is clearly related to the time course of action potential (AP) repolarization as well as the status of the sodium channel. In forward mode ECC, after the cellular AP evoked Ca^{2+} transient due to SR Ca^{2+} release, time is needed before a second Ca^{2+} release occurs of similar amplitude. Thus, there is a recovery process of Ca^{2+} release in cardiac cells that is independent of membrane voltage. In the electrically stimulated cell, the recovery of the SR Ca^{2+} release process or refractoriness is determined by the recovery of the influx via L-type Ca^{2+} channel as well as the time course of the SR refilling. The latter can be examined by assessing the interval between spontaneous Ca^{2+} sparks occurring at the same release site. Ca^{2+} spark termination is due to the local depletion of Ca^{2+} within junctional SR. The time of one spark to another is related to the sensitivity of the RyR or threshold for Ca^{2+} release. How fast junctional SR refills after depletion is important for the recovery of both spark amplitude and CICR or Ca^{2+} wave formation [8]. Shortened refractoriness of this process has been seen in both acquired (post MI [9]) and genetic diseases [10]. For example, there is a loss of calsequestrin (CASQ) in SR of cells in some patients with catecholaminergic polymorphic ventricular tachycardia (CVPT), that produce fast SR refilling and a greater likelihood of a trigger for re-release [11] and Ca^{2+} waves.

It is possible to load the SR excessively with Ca^{2+}. This may occur following damage to cardiac cells or after exposure to interventions that increase intracellular Ca^{2+} levels (digitalis, high $[Ca^{2+}]_o$, high pacing rate). The SR membrane-associated channel proteins release Ca^{2+} spontaneously into the cytosol by spontaneous activation of RyR due to luminal Ca^{2+} overload or local depolarization. Spontaneous uncoordinated Ca^{2+} release between paced beats can be observed as spontaneous contractions of small groups of sarcomeres in myocardium cells and gives rise to fluctuations of the light scattering properties of the muscle [12, 13]. Spontaneous Ca^{2+} release increases the diastolic force generated by the contractile filaments and, in so doing, reduces Ca^{2+} release during the next heartbeat [14, 15]. In turn, the spontaneous release of Ca^{2+} ions can lead to cell depolarization due to activation of Ca^{2+}-modulated channels and by electrogenic NCX (the current generated has been called I_{ti} [16]).

19.1.2 ECC in Purkinje Cells from Normal Hearts

As a result of the different structures of the Purkinje cell (e.g., lacking T-tubuli) [17], the coupling of excitation of the cell membrane with Ca^{2+} release in the core of these cells differs substantially from that of myocytes. Immunostaining experiments in rabbit Purkinje cells show that RyRs are subsarcolemmal (SSL) in location and are also present within the cell (core) consistent with earlier reports [18, 19]. In fact, canine Purkinje cells contain both RyR3 and RyR2 isoforms, with the RyR3 protein being located predominantly in the SSL area. The implication here is that the normal Purkinje cell contains both junctional and nonjunctional release channels. The AP of the Purkinje cell precedes rapid Ca^{2+} entry into the SSL space, which in turn induces Ca^{2+} release that, in some species, propagates into the core of the cell [20]. In rabbit Purkinje cells, experiments with ryanodine suggest that Ca^{2+} changes in the core of cells are best explained by simple buffered Ca^{2+} diffusion and not Ca^{2+} wave propagation. However, in rabbit Purkinje cells, evoked Ca^{2+} transients are only seen to originate at peripheral cellular components, suggesting that RyRs in the cell center of this type of cell are "silent". However, in canine Purkinje cells, electrically evoked Ca^{2+} transients are multiphasic [20, 21]. In some Purkinje cells from normal hearts, if electrically evoked peripheral release is spatially and temporally inhomogeneous, a local Ca^{2+} wave is produced and can propagate as a traveling cell-wide Ca^{2+} wave along the length of the aggregate as well as towards the cell's core [19, 20]. While a propagating electrical wave utilizes the energy stored in the myocyte, electrical waves rely on the activation of certain ion channels for forward propagation. Propagation of Ca^{2+} waves also depends on stored cellular energy. In this case, the energy comes from Ca^{2+} stored in the SR. The stored Ca^{2+} ions are released when the SR-ligand operated Ca^{2+} channel, the RYR channel, is opened.

19.1.3 Reversal of Excitation–Contraction Coupling

In 2001 [22], Ter Keurs and Boyden defined the term reverse excitation–contraction coupling (RECC) to mean that in any cardiac cell, intracellular Ca^{2+} could feedback onto the cell surface membrane Ca^{2+}-dependent proteins to produce electrical signals. In this way, the released Ca^{2+} drives the membrane excitation. The RECC could occur in both ventricular and Purkinje cells and has gained recent attention as it underlies the mechanism of triggered beats in RyR and CASQ gene mutations arrhythmias [23, 24].

19.2 Ca^{2+} Homeostasis in Subendocardial Purkinje Cells during the Subacute Healing Phase-Postmyocardial Infarction

Rapid ventricular arrhythmias after total coronary artery occlusion in the canine heart arise from ectopic foci (triggered or automatic) within the Purkinje fiber network located in the subendocardium of the infarct zone in the left ventricle [25]. These spontaneously occurring arrhythmias predictably occur between 24 and 48 h after occlusion. We have shown that the density and function of several sarcolemmal ion channels are altered in the Purkinje cells dispersed from the subendocardium of the infarct zone (IZPCs) [26]. Further, we have shown that Ca^{2+} transients in cell aggregates from Purkinje tissues of normal LV subendocardium (NZPCs) consist of a membrane-linked Ca^{2+} transient that occurs in response to an AP. This initial Ca^{2+} transient usually leads to a Ca^{2+} transient that propagates to the cell core. Paced global Ca^{2+} transients of NZPCs are reasonably normal in amplitude, with often a secondary plateau (asterisks in Fig. 19.1a) that occurs during the maintained AP plateau of the Purkinje cell [20]. In time as the cell completes repolarization, a slower decay of the global transient occurs. Cell-wide Ca^{2+}waves (CWW) that propagate along an aggregate occur spontaneously during the inter-stimulus interval and can give rise to nondriven electrical activity [20]. Because abnormal impulse initiation in the subendocardial Purkinje network is the cause of the infarction-related arrhythmias [25], we have gone on to determine whether electrically evoked Ca^{2+} transients and the incidence of spontaneous Ca^{2+} waves are altered in IZPCs.

19.2.1 Purkinje Cell Ca^{2+} Currents

Peak L-type Ca^{2+} channel current (I_{CaL}) density is significantly reduced in subendocardial Purkinje myocytes dispersed from the 48-h infarcted heart as compared to control and to those from the 24-h infarcted heart [27]. This current density reduction is not accompanied by a shift in the current–voltage relationship or a change in the time course of I_{CaL} decay, but by a hyperpolarizing shift in the steady-state availability of the channel. Peak T-type Ca^{2+} channel current (I_{CaT}) density is also decreased in subendocardial Purkinje myocytes that survive in the 24-h infarcted heart, and further reduction occurs by 48 h. The loss in Ca^{2+} channel function could contribute to the depressed and triangular plateau phase of the APs of these arrhythmogenic IZPCs [28].

19.2.2 Intracellular Ca^{2+} Cycling

One of the cellular mechanisms of triggered activity is delayed after depolarization (DAD). We have shown that nonuniform Ca^{2+} transients in

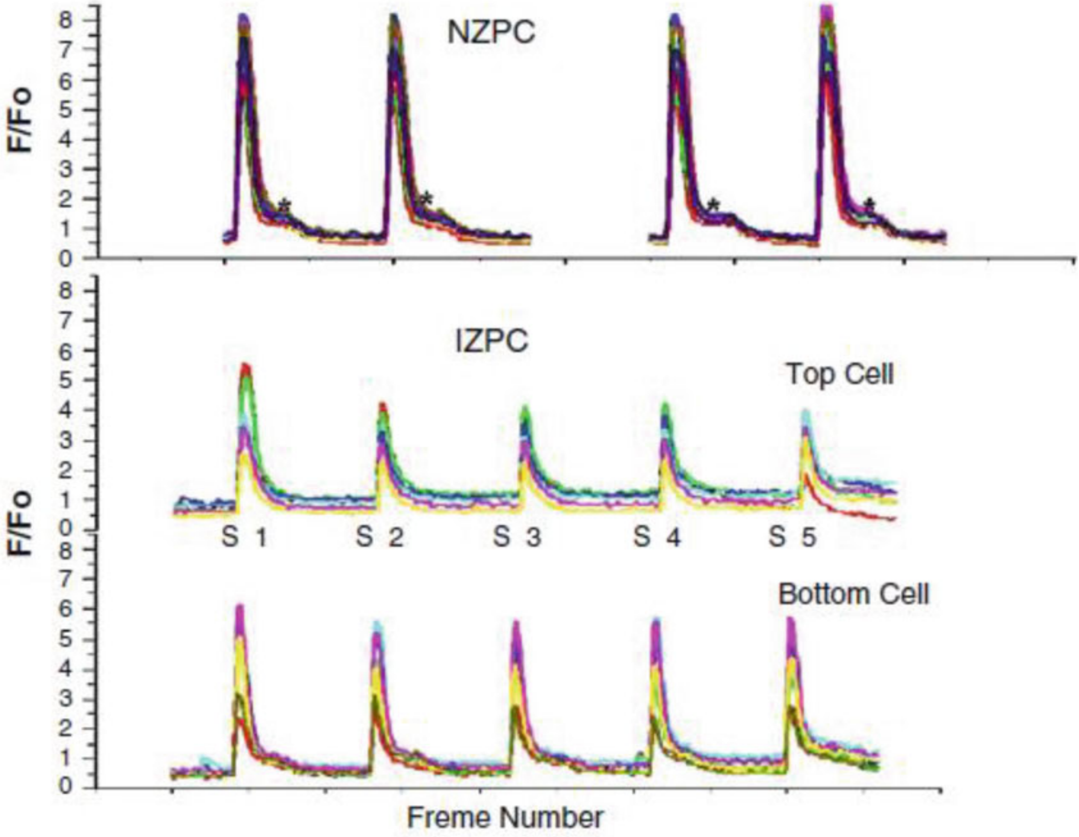

Fig. 19.1 Upper row: Change in intensity (F/F_0) of fluorescence at various regions of interest (ROIs) during pacing in an NZPC aggregate. Note action potential-evoked Ca^{2+} transients are robust and synchronous in the NZPC. *Asterisk* indicates a secondary plateau of Ca^{2+} which coincides with the terminal phase of repolarization. Lower row: Change in intensity (F/F_0) of fluorescence at various ROIs during five paced beats (S1…S5) in two IZPCs (*top* and *bottom*). Note the action potential-evoked Ca^{2+} transients are nonuniform in IZPCs

Purkinje cells that have survived the infarct underlie spontaneous membrane depolarizations, and both the *amplitude* of the Ca^{2+} waves that are present and their number and spatial extent predict the membrane depolarization [21]. Further, electrically evoked Ca^{2+} transients in IZPCs arise faster than those in normal Purkinje cell aggregates but show substantial spatiotemporal nonuniformity within an IZPC aggregate as well as between IZPC aggregates (Fig. 19.1b). Reduced Ca^{2+} influx via I_{CaL} may be partially responsible for the abnormal AP-evoked global Ca^{2+} transients observed in IZPCs [26]. Importantly, IZPCs showed low amplitude, spontaneously occurring micro-Ca^{2+} transients at a fivefold higher incidence than in normal Purkinje aggregates. The μCa^{2+} transients meander over short distances and reduce the local Ca^{2+} transient of the next paced beat (Fig. 19.2). Finally, spontaneous micro-Ca^{2+} transients preceded CWWs (Fig. 19.3). The CWWs, in turn, clearly cause membrane depolarization and elicit spontaneous APs. Thus, the high incidence of micro-Ca^{2+} transients in IZPCs is fundamental to the abnormal Ca^{2+} handling of the diseased Purkinje cells, underlying the arrhythmias originating in the subendocardial Purkinje network after a myocardial infarct.

Recently, we evaluated the reasons for the increased incidence of μCa^{2+} transients in

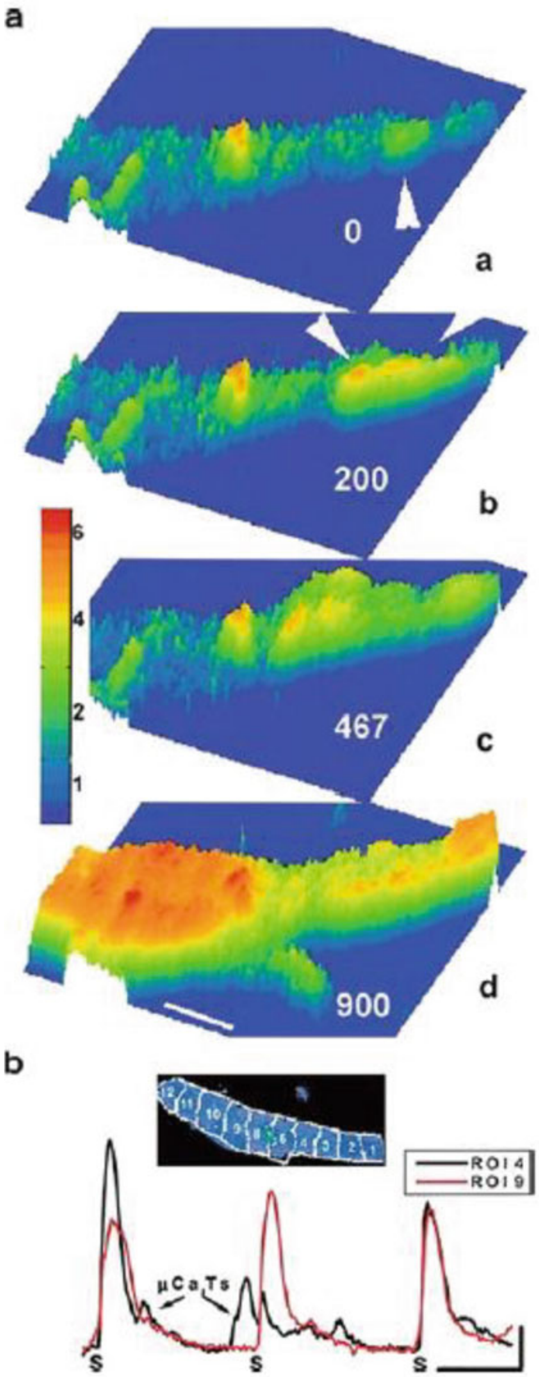

Fig. 19.2 Nonuniformly occurring micro-Ca^{2+} transients (*arrowheads*) cause nonuniformity of the action potential-evoked Ca^{2+} response in a canine IZPC aggregate. Panel (**a**) 3D surface plots of IZPC just preceding and during one electrically evoked Ca^{2+} transient [denoted by S in Panel (**b**)]. [Ca^{2+}] are denoted by both the color and height of the surface. *White numbers* (**b**, upper panel) indicate time of frame relative to $t = 0$ (**a**,a). The aggregate was stimulated just before $t = 900$ ms (**a**,d). Note the presence of micro-Ca^{2+} waves (*arrowheads*), which propagate over short distances ($t = 0$ to 467 ms) meandering from the right section of the aggregate toward the core. Subsequent stimulation causes a nonuniform electrically evoked local Ca^{2+} transients ($t = 900$ ms) particularly in regions where

IZPCs. The μCa^{2+} transients are not affected by verapamil [29] and abnormal electrical rhythms in Purkinje cells that have survived in the infarcted heart are insensitive to the T-type Ca^{2+} channel blocker, mibefradil [30]. Finally, because Ca^{2+} waves and the resultant membrane depolarizations in Purkinje cells are ryanodine sensitive [29], we sought to determine whether the increased incidence of Ca^{2+} waves in IZPCs is due to *enhanced* spontaneous Ca^{2+} release secondary to altered activity of SR Ca^{2+} release channels.

Using 2D confocal microscopy, we found that the amplitude of Ca^{2+} release events, i.e., the Ca^{2+} sparks, was significantly increased in IZPCs compared to NZPCs. In addition, the event rate of Ca^{2+} release in cell regions just below the sarcolemma (SSL, subsarcolemmal) of IZPCs is also increased. Importantly, SR Ca^{2+} content did not differ between NZPCs and IZPCs in all cell regions, which suggested that there was an enhanced sensitivity of SR Ca^{2+} release channels in IZPCs. In fact, permeabilized IZPCs showed an increased Ca^{2+} release event rate in both SSL and core regions, confirming this idea [31]. Other Ca^{2+} release events, such as wide, long-lasting Ca^{2+} release events [32], micro-Ca^{2+} transients, and cell-wide Ca^{2+} waves, show an accelerated decay after Ca^{2+} release in IZPCs. These results suggest that there is an enhanced Ca^{2+} sequestration by SERCA2 by phosphorylation of phospholamban with SERCA pumps [33]. These properties would lower the threshold of Ca^{2+} release channels, setting the stage for the highly frequent arrhythmogenic cell-wide Ca^{2+} waves and DADs in Purkinje cells that survive in the infarcted heart.

19.2.3 Structural Remodeling in Purkinje Cells that Survive in the Infarcted Heart

Our functional data are consistent with the multiple Ca^{2+} release compartments in NZPCs, which we hypothesized to exist based on our immunocytochemistry data using specific RyR antibodies. Frequency analysis was then used to determine whether RyR2 staining was regularly organized in the two cell types (Fig. 19.4). We identified three different types of Purkinje cells. Type I cells showed regular periodicity of RyR2 staining [NZPCs 89% of total cells (31); IZPCs 38% of total ((24), Fig. 19.4, left)]; type II cells lacked some periodicity [NZPCs (11%), IZPCs (42%)], while some IZPCs (21%) showed regions of disorder (Fig. 19.4, right) almost throughout the cell. In NZPCs, IP_3R1 staining was as before [19], showing sarcolemmal and not core gap junctional and nuclear envelope but not intranuclear staining. In IZPCs (42% of total $n = 19$), we found that IP_3R1 signals appear to be shifted from discrete sarcolemma regions to the core, but they retain strong gap signals. IP_3R1s in the nuclear area were markedly changed in that most of the signals now appeared as ribbons within the nucleus.

19.3 Ca^{2+} Homeostasis in Epicardial Border Zone Cells of Healing Phase Post-MI (4–5 Days)

After several days post coronary artery occlusion (4-5 days), spontaneous arrhythmias subside in this canine model. At this time, long-lasting

Fig. 19.2 (continued) micro-Ca^{2+} transients had been. *Horizontal bar* indicates 50 μm. *Color bar* indicates ratio range. Panel (**b**) Changes in intensity of fluorescence (F/F_0) at two selected ROIs in IZPC aggregate of panel (**a**). Stimuli are indicated (S). Each ROI is represented by a different color and location is noted in *upper image*. Note that when the micro-Ca^{2+} transients observed in ROI4 (see *arrowheads* of panel (**a**)) precede S, the subsequent Ca^{2+} transient of S is diminished compared to that of the previous S. Note that in ROIs where micro-Ca^{2+} transients were absent (e.g., ROI 9), response to stimulation was constant. *Vertical* and *horizontal lines* are 1 F/F_0 units and 1.58 s, respectively. From [21]

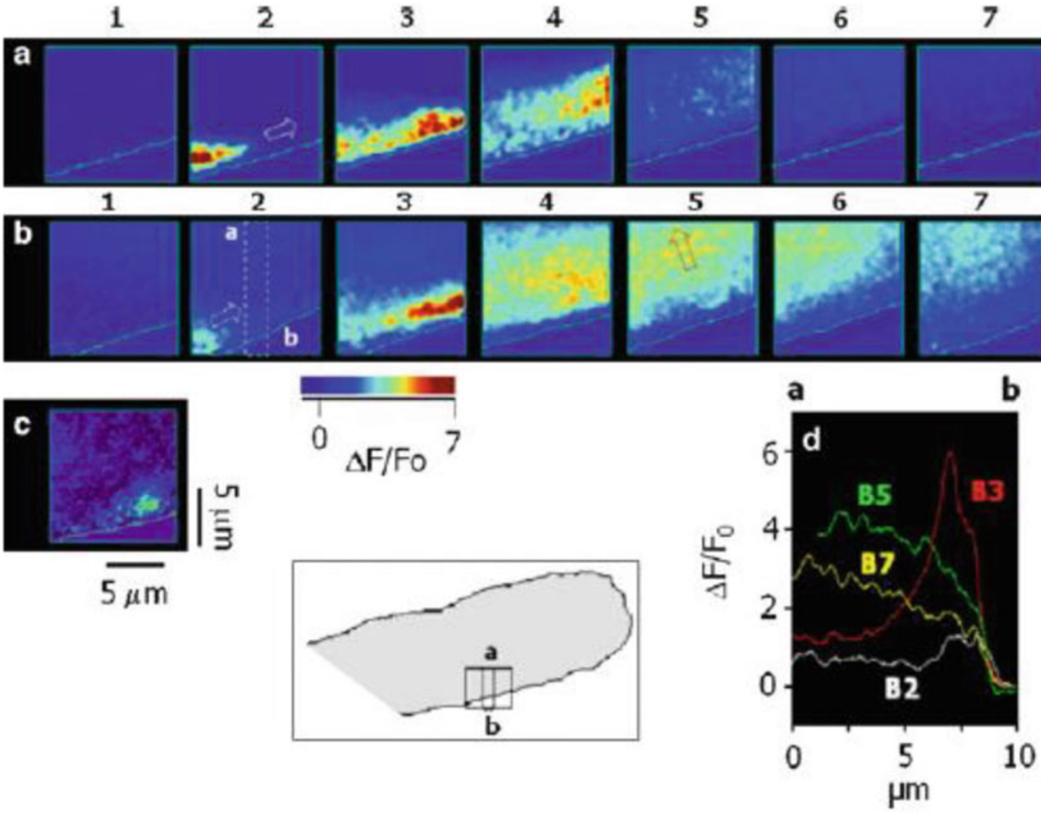

Fig. 19.3 Two-dimensional confocal Ca^{2+} images of the subsarcolemmal events in an NZPC. Panels (**a**) and (**b**) show two series of consecutive 2D frames constructed from *x*/*y* scanning (100 scan lines, 10 µm/line, 1.2 ms/line) of cell region covering sarcolemma (SL), Sub-SL, and a small region of the cell center (see *bottom inset*). $[Ca^{2+}]_i$ is expressed in relative variation of F/F_0 ($\Delta F/F_0 = (F - F_0)/F_0$). Panel (**a**) A wavelet propagates from the left to the right within $a \approx 6$ µm wide region under the sarcolemma (Sub-SL). Panel (**b**) A similar wavelet in the same aggregate initiates (frame **b**4) a wave that propagates to the cell center (see *arrow* in **b**5). The *green line*, superimposed to the frames, underlines the position of the sarcolemma as the boundary between intracellular fluorescence and extracellular milieu. Panel (**c**) Sub-SL nonpropagating Ca^{2+} transient in the same aggregate and spatiotemporal Ca^{2+} profiles (indicated by corresponding frame number: **b**2, **b**3, **b**5, **b**7) of wave generation shown in panel (**b**). From [19]

reentrant tachycardias are easily inducible. These arrhythmias arise from epicardial border zone (EBZ) cells [34] and provide the substrate for reentrant arrhythmias. The APs of these EBZ cells are triangular, having lost their plateau [35, 36]. Just a triangularization of the AP could cause abnormal global Ca^{2+} transients.

19.3.1 EBZ Ca^{2+} Currents

The peak I_{CaL} density of IZ cells dispersed from the 5-day EBZ of the infarcted heart is significantly reduced by 36% compared to control [37]. This reduction is not due to a decrease in steady-state availability or a prolonged time course of recovery of I_{CaL}. However, the time course of decay of these currents is significantly faster than control cells. These findings may be related to a decrease in the number of functioning channels, as well as an acceleration of the inactivation of the remaining channels. Unlike the findings in the subendocardial Purkinje myocytes studies (see above), no significant differences were found between peak density and frequency of T-type Ca^{2+} currents in IZ myocytes vs. control

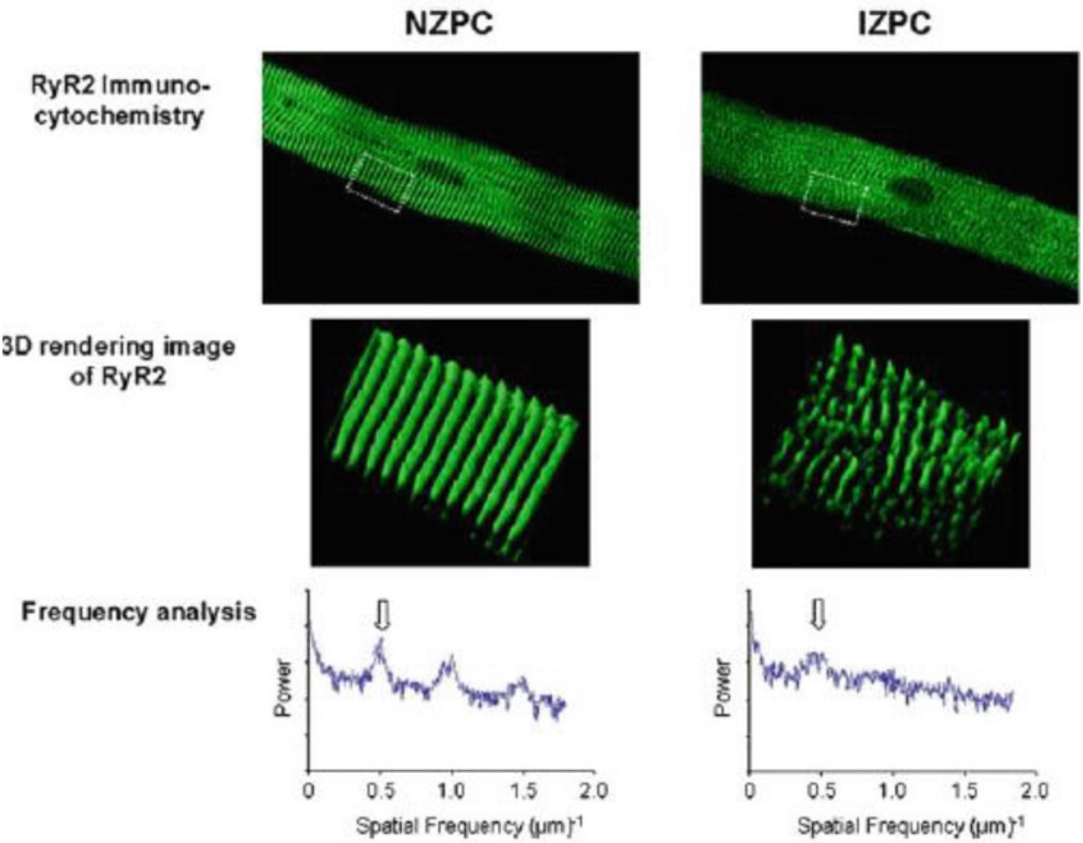

Fig. 19.4 A comparison of RyR2 staining in one NZPC and one IZPC. *Top panel* shows RyR2 staining in 2D representation in NZPC (*left*) and IZPC (*right*). *Middle panel* shows 3D rendering images of RyR2 in NZPC and IZPC. The image areas are marked as the *white squares* in the *top panel*. *Bottom panel* shows the frequency analysis of RyR2 staining in the NZPC and IZPC. Note that RyR2 staining was regularly organized in the NZPC while RyR2 staining was regionally disordered in the IZPC

epicardial myocytes from normal hearts (NZs). Our knowledge of altered sensitivity to transmitters of the autonomic system in diseased myocytes is derived from comparisons of the effects of adrenergic agonists on specific ionic currents. Commonly, adrenergic sensitivity is assessed by the effects of the adrenergic agonist, isoproterenol, on I_{CaL}. In NZs, isoproterenol depolarizes the resting membrane potential by inhibiting I_{K1} [38] and prolongs the AP by increasing I_{CaL} [39, 40]. Mimicry of isoproterenol effects using forskolin and cAMP has provided information regarding additional defects in the adrenergic complex.

Sympathetic stimulation produces minimal AP shortening in areas overlying the infarct and the border zone, whereas in areas remote from the arrhythmia substrate pronounced AP shortening occurs [41]. Furthermore, catecholamine-induced increase of the AP plateau phase is absent in the fibers of the EBZ of the 5- and 14-day infarcted heart [36]. Similar abbreviated responses to catecholamines have been documented in the ischemic human ventricle [42]. From voltage clamp data and in comparison with NZs, isoproterenol produces a smaller increase in I_{CaL} in cells from the 5-day- and 2-month-old infarct, independent of Ca^{2+}-dependent inactivation

Fig. 19.5 Mathematical model of infarct border zone myocyte. Panel (**a**) Remodeling changes incorporated into the model include decreased $I_{Ca(L)}$, I_{Na}, and I_{to} densities and acute effects of CaMKII hyperactivity on downstream substrates. Panel (**b**) Simulated basal CaMKII activity compared to experimentally measured autophosphorylation levels in NZ (*black bars*) and BZ (*gray bars*). Panel (**c**) Simulated action potentials and Panel (**d**) calcium transients (*right panel*) in NZ (control HRd model, *black line*) and BZ (*gray line*) models for steady-state pacing at CL = 2000 ms [48]

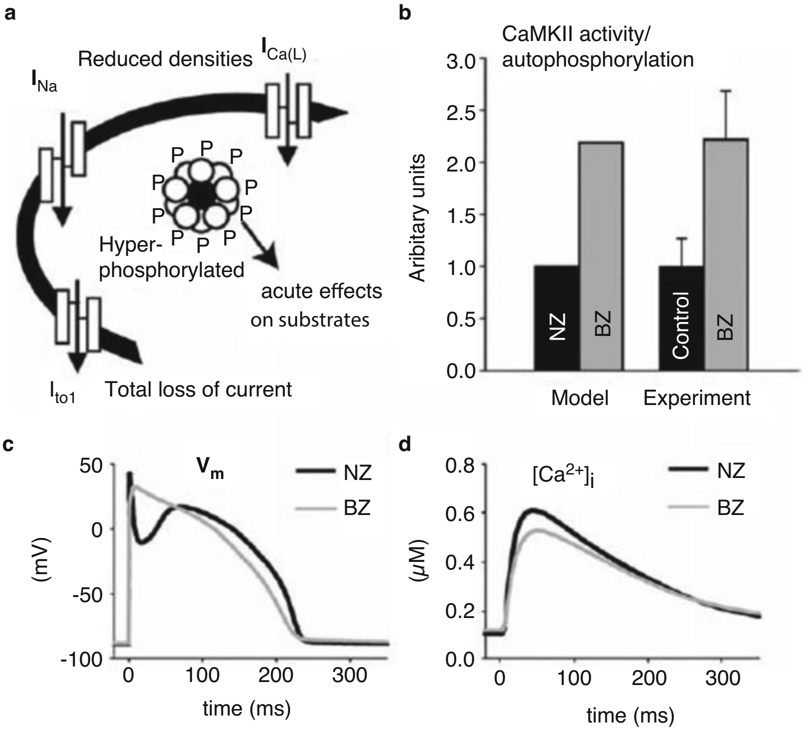

[43, 44]. This is consistent with multiple defects in components of the adrenergic receptor complex in IZ cells of the 5-day-old infarct, including (1) decreases in adrenergic receptor density; (2) diminished basal, guanine nucleotide, isoproterenol, forskolin, and manganese-dependent adenylyl cyclase activities; (3) increases in the EC_{50} for isoproterenol-dependent activation of adenylate cyclase; (4) diminished levels of the subunit of the Gs protein; and (5) elevated levels of the subunit of the Gi protein [45]. Therefore, an interesting question put forward is whether other signaling pathways are involved in the remodeled basal Ca^{2+} currents and isoproterenol-stimulated Ca^{2+} current function in IZs. Protein tyrosine kinases (PTKs) have been shown to modulate basal as well as β-adrenergic-stimulated Ca^{2+} current function in cardiac cells from normal hearts [46]. Our study showed that PKA activity contributes to I_{CaL} in both NZ and IZ cells, but dysregulation of PTK activity cannot account for the reduced basal Ca^{2+} currents or hyporesponsiveness of I_{CaL} to isoproterenol in the IZs [47].

Additional data point to a critical role for calcium–calmodulin (CaM)-dependent protein kinase II (CaMKII) in adverse Ca^{2+} remodeling after myocardial infarction [48]. First, the level of CaMKII autophosphorylation is increased in the EBZ. Second, the results of computer simulations reveal that Ca^{2+} leak from the SR is due to CaMKII hyperphosphorylation. This then depletes SR Ca^{2+} content and contributes to depressed Ca^{2+} transients. Simulations (Fig. 19.5) also display the abnormal rate dependence of IZ Ca^{2+} transients seen experimentally [49].

19.3.2 Remodeling of Ankyrin-B-Associated Proteins Following Myocardial Infarction

Ankyrin-B is an adapter protein required for targeting and stabilizing ion channels, exchangers, and pumps in excitable cells. While it is known that ankyrin-B gene mutations can give rise to LQTS type 4 in patients [50], little is known about ankyrin-B in common forms of acquired human disease. Mice lacking ankyrin-B phenocopy type 4 LQTS and ankyrin-B-deficient cardiomyocytes display abnormal calcium homeostasis due to abnormal targeting of key membrane proteins, resulting in cellular afterdepolarization. We were the first to present a report of ankyrin-B regulation in the EBZ post-MI [51] and showed that ankyrin-B protein levels are reduced in the EBZ (Fig. 19.6). We found no significant difference in expression levels of the IP_3R and NCX in EBZ at 5 or 14+ days postocclusion compared to normal. However, Na–K pump (NKA) protein expression was dramatically reduced in the EBZ 5 days postocclusion compared to normal, consistent with the reduction in ankyrin-B expression. Interestingly, NKA expression remained significantly reduced even at 14+ days, revealing a time course of recovery that follows the recovery of ankyrin-B. Immunoblots indicated that, more specifically, NKA expression remains depressed at 14 days postocclusion but recovers to normal by 2 months.

While we measured decreased expression of NKA by immunoblot in the EBZ, we detected no

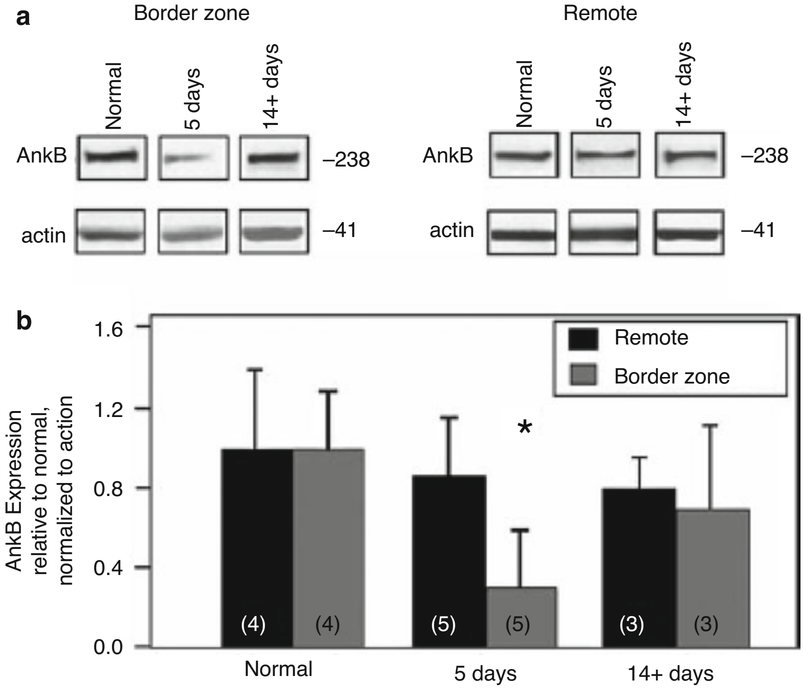

Fig. 19.6 Ankyrin-B (AnkB) protein levels decrease in the border zone 5 days postocclusion. Panel (**a**) Representative immunoblots and Panel (**b**) densitometry measurements (normalized to actin and expressed relative to normal levels) of AnkB from remote and BZ regions of normal and infarcted hearts. *Error bars* designate standard deviation (*$P < 0.01$ compared with normal BZ or remote, $n = 4$ for normal, $n = 5$ for 5-day, and $n = 3$ for 14+ day infarct). Densitometry measurements were made from all samples analyzed on same gel and normalized to the corresponding actin levels from the same blot. Equal protein loading was ensured by BCA assay and verified by analysis of Coomassie and Ponceau stains of gel and blots [51]

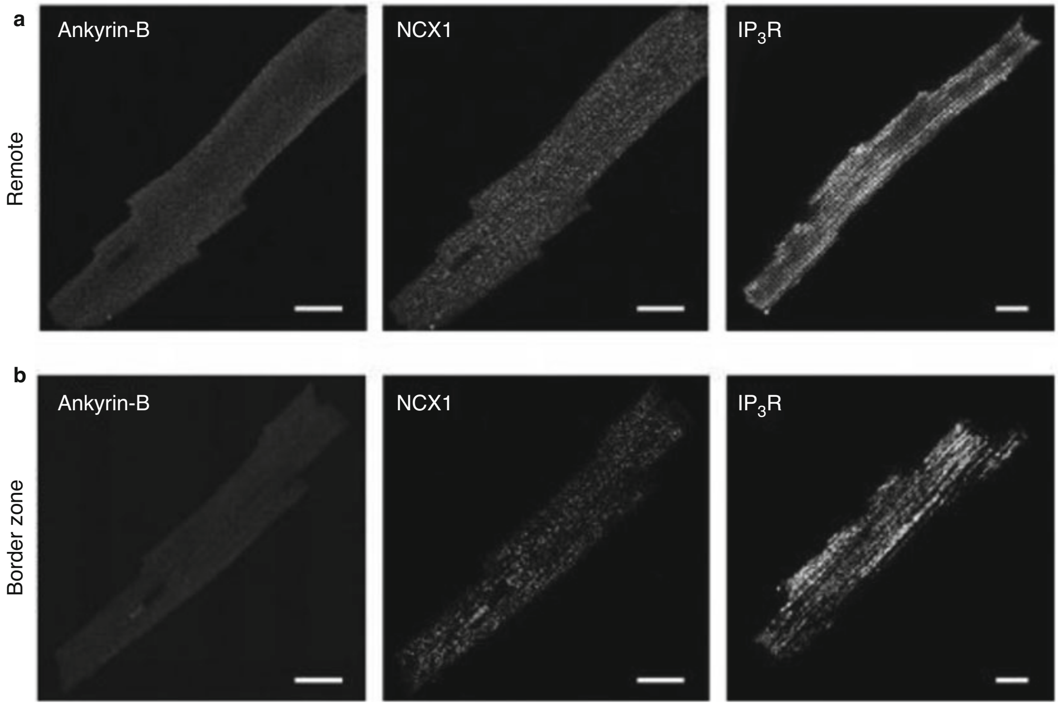

Fig. 19.7 Cellular redistribution of NCX and IP_3R in border zone myocytes. Isolated myocytes from remote and IZ regions of 5-day infarcted hearts were immunoassayed using antibodies against AnkB (*left*), NCX1 (*middle*), and IP_3R (*right*). Localization of NCX1 and IP_3R in BZ myocytes (Panel b) is less pronounced at T-tubules in BZ myocytes (Panel a), where AnkB expression is reduced. *Scale bars*, 10 μm [51]

difference in protein levels of NCX or IP_3R [51]. As it is known that ankyrin helps to target ion channels to specific subcellular domains, we went on to determine whether subcellular redistribution of NCX and IP_3R occurred in 5-day postocclusion IZ myocytes. Immunofluorescence studies revealed cellular redistribution of both IP_3R and NCX in IZ myocytes 5 days postocclusion (Fig. 19.7). Specifically, while NCX and IP_3R show prominent localization at T-tubules in remote noninfarcted myocytes, their intracellular distribution is not uniform in IZs. Thus, cellular distribution but not total protein levels of NCX and IP_3R change in the cells from 5-day EBZ.

Recent studies have also demonstrated that ankyrin-B directly associates with the targeting subunit of the protein phosphatase PP2A. Therefore, we determined whether expression and/or distribution of PP2A was altered in the EBZ. Interestingly, by 5-days postocclusion, expression of the PP2A catalytic subunit (constituent of the core enzyme) increased to more than three times its normal level (Fig. 19.8). These changes in protein expression were paralleled by increased membrane expression of PP2A in IZ myocytes 5-days postocclusion. By 14+ days postocclusion, PP2A protein levels in the EBZ returned to normal levels following a time course similar to that of changes in ankyrin-B expression. Thus, ion channel transporter remodeling post-MI seems to be downstream from ankyrin-B remodeling.

19.3.3 Intracellular Ca^{2+} Cycling

In the pacing studies using fura2 AM loaded, nondialyzed cells, we found that the response of the amplitude of the global Ca^{2+} transient to a

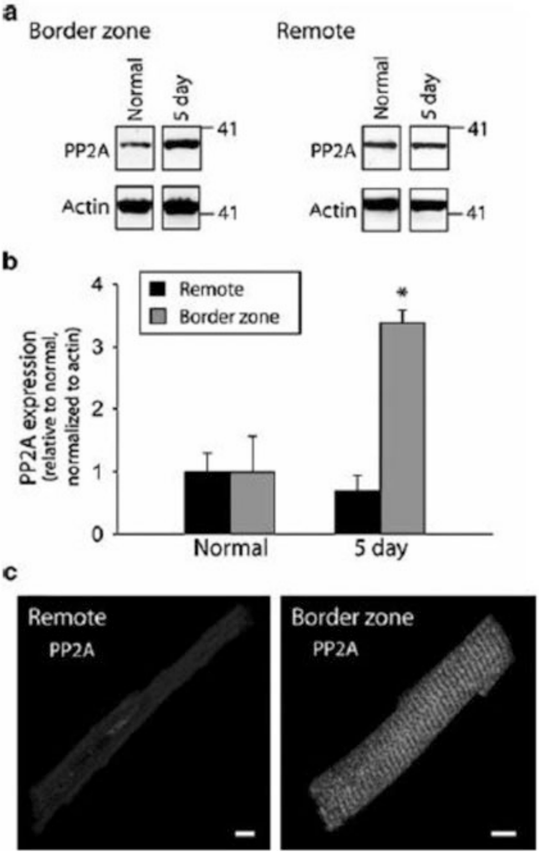

Fig. 19.8 Altered PP2A expression in the border zone 5 days postocclusion. Panel (**a**) Representative immunoblots and Panel (**b**) densitometry measurements (normalized to actin and expressed relative to normal levels) of PP2A catalytic subunit from remote and BZ regions of normal and 5-day infarcted hearts. *Error bars* designate standard deviation ($n = 4$ for each group). Panel (**c**) Isolated myocytes from remote and BZ regions of 5-day infarcted hearts were immunoassayed using antibody against the PP2A catalytic subunit. *Scale bars*, 10 μm [51]

change with pacing rate in IZs is opposite to that which occurs in the normal epicardial cells [49]. In the NZs, an increase in rate is associated with an increase in Ca_i transient amplitude, whereas in IZs, the rate causes a decrease in Ca^{2+} transient amplitude. In addition, the recovery of the amplitude of the AP-evoked Ca_i transient (restitution) is markedly slowed in the IZ cells (Fig. 19.9a; [49]), yet there is marked rest potentiation of Ca_i transients in IZ cells vs. rest depression of the Ca_i transients in the normal cells. Presumably, the alteration in Ca^{2+} influx (see above) in IZ cells may alter ECC coupling in such a way that it results in less SR Ca^{2+} accumulation with the increase in the pacing rate. While these fura2 experiments indicated an elevation of diastolic Ca^{2+} in IZ cells, precise determination of Ca^{2+} using fura2 in the patch pipette showed that at a holding voltage of −50 mV, IZ cells have a 47% increase in resting ratio over NZ values [52].

Importantly, despite the reasonable, albeit smaller, amplitude Ca_i transients in the IZs, little or no cell shortening existed, which suggests that the lack of cell shortening in the IZs may be related to dramatic alterations in excitation–contraction coupling at the level of contractile element activation and/or to an altered production of microtubules. In any case, the alteration in the Ca^{2+} transient in IZs would directly impact on the amplitude of several Ca^{2+}-dependent currents such as I_{to2} [53]. Despite the relatively low Ca^{2+} sensitivity of this channel, they can conduct significant current transiently or in a sustained manner depending on Ca^{2+} and time course of the subplasmalemmal Ca^{2} transient. Thus, IZ cells,

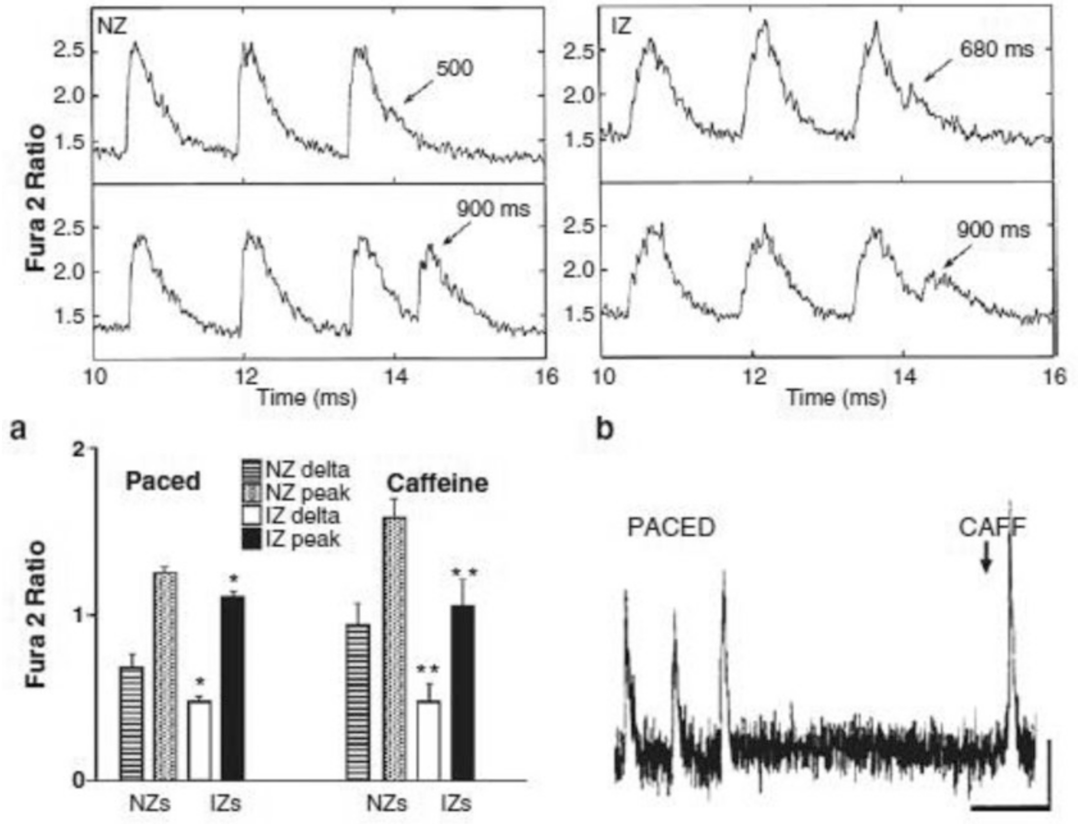

Fig. 19.9 Upper row: Fura-2 tracings from NZ (*left*) and IZ (*right*) during restitution stimulation protocols. For each myocyte, both a short and long S1–S2 coupling interval are illustrated. Note that with a S1–S2 interval of 900 ms in the NZ, a large Ca$_i$ transient is easily evoked while in the IZ a much smaller Ca$_i$ transient is elicited. Lower row: Panel (**a**) Average Fura-2 ratio changes during six paced beats (Vh = −70 to +10 mV) and after exposure to caffeine (10 mM) in a subset of NZs and IZs. Height of *bar* indicates both peak ratio (*solid bars*) or delta ratio (*grey bars*) for each cell type during paced beats and caffeine. $*P < 0.05$ vs. NZ paced values, $**P < 0.05$ vs. NZ caffeine. (**b**) Typical ratio changes in a cell during the last three paced clamp steps and caffeine exposure. Horizontal calibration bar equals 5 s while vertical bar equals 0.25 units. Holding voltage throughout protocol = −70 mV. From [49]

which have highly remodeled I_{CaL} and Ca^{2+} transients, show I_{to2} currents which vary in size [53].

When IZ cells were clamped with a transmembrane voltage similar to an AP profile, we found that abnormal Ca$_i$ transients in the voltage-clamped IZ cells persisted [52]. In the NZs, Ca$_i$ transients showed the expected voltage relationship to I_{CaL} while IZ cells did not. Thus, the abnormalities in [Ca]$_i$ handling in the IZ cells do not appear to arise secondary to changes in AP configuration nor do they appear to be due to disease-induced alterations in NCX function (see below). Interestingly, the abnormal Ca$_i$ transients in IZ cells recover when cells are superfused with the L-type calcium channel agonist, Bay5959 [54]. This effect on the remodeled cells may underlie Bay5959 antiarrhythmic effect in this arrhythmia model [55]. When caffeine was used to compare amounts of SR Ca^{2+} in IZ vs. normal cells, we found that in IZ cells caffeine induced less Ca^{2+} release (Fig. 19.9b). Thus, while Ca^{2+} entry in normal epicardial NZs may not release all SR Ca^{2+} available for release, the smaller Ca^{2+}

amplitudes of paced IZ cells appear to result from Ca^{2+} influx releasing most SR Ca^{2+} that is available for release.

19.3.4 Na–Ca Exchanger Currents

In NZs with normal Ca_i cycling, it is well established that currents generated by NCX play an important role in the electrical activity of a myocyte [56]. The NCX current is either outward (normal mode) as the transporter protein exchanges one internal Ca^{2+} for three external Na^+ or inward (reverse mode) as the transporter causes Ca^{2+} influx by exchanging external Ca^{2+} for internal Na^+. Therefore, the time course of the exchanger current is related to the time course of Ca_i cycling. There have been several reports of abnormal internal Ca^{2+} cycling in cells that have survived in the infarcted heart [57–60]. In myocytes dispersed from the EBZ of the 5-day infarcted heart, both non-clamp [52] and voltage clamp studies [52] show that the diminished globally assessed Ca^{2+} transient of the IZ cell has a slow relaxation (decay) phase. Furthermore, these cells have an altered phase 3 of their APs. These changes are consistent with changes in the NCX current. However, when studied under strict conditions that isolate only Ca_i and ionic current changes secondary to NCX, both Ca^{2+} entry (via the reverse exchanger) and Ni^{2+}-sensitive IZ currents as well as Ca^{2+} extrusion (via normal mode exchanger) in IZs are similar to those of NZs, no matter what the Na_i load [49]. Thus, in these cells where L-type Ca^{2+} channels are downregulated (see above), the NCX has a reserve efficiency and continues to contribute current to the transmembrane AP.

19.4 Conclusions

Abnormalities in intracellular Ca^{2+} handling occur in Purkinje and ventricular cells that have survived in the border zones of the infarcted heart. Interestingly, these changes differ depending on the cell type (IZPC vs. IZ) and contribute differently to the arrhythmogenicity of the post-MI substrate. Thus, it is reasonable to assume that rational drug design could derive compounds against these intracellular Ca^{2+} changes that would be specific not only for the cell type but also for the type of arrhythmias occurring post-MI. For example, for Purkinje cells that survive in the infarcted heart, molecular targets may include Ca^{2+}-release channels, while targets in epicardial cells that survive in the EBZ may include Ca^{2+} channel agonists.

Acknowledgments This work was supported by grant HL58860 from the National Heart Lung and Blood Institute Bethesda, Maryland.

References

1. Ter Keurs HEDJ, Boyden PA. Calcium and arrhythmogenesis. Physiol Rev. 2007;87:457–506.
2. Brette F, Salle L, Orchard CH. Quantification of calcium entry at the T-tubules and surface membrane in rat ventricular myocytes. Biophys J. 2006;90:381–9.
3. Bers DM, Stiffel VM. Ratio of ryanodine to dihydropyridine receptors in cardiac and skeletal muscle and implications for EC coupling. Am J Phys. 1993;264:C1587–93.
4. Cannell MB, Cheng H, Lederer WJ. Spatial nonuniformities in Cai during excitation contraction coupling in cardiac myocytes. Biophys J. 1994;67:1942–56.
5. Wibo M, Bravo G, Godfraind T. Postnatal maturation of excitation contraction coupling in rat ventricle in relation to the subcellular localization and surface density of 1,4 dihydropyridine and ryanodine receptors. Circ Res. 1991;68:662–73.
6. Shannon TR, Guo T, Bers DM. Ca^{2+} scraps: local depletions of free Ca^{2+} in cardiac sarcoplasmic reticulum during contractions leave substantial Ca^{2+} reserve. Circ Res. 2003;93:40–5.
7. Bers DM. Excitation–contraction coupling and cardiac contractile force, vol. 1. 1st ed. Dordrecht: Kluwer; 1991. p. 45.
8. Ramay HR, Liu OZ, Sobie EA. Recovery of cardiac calcium release is controlled by sarcoplasmic reticulum refilling and ryanodine receptor sensitivity. Cardiovasc Res. 2011;91:598–605.
9. Belevych AE, Terentyev D, Terentyeva R, Ho HT, Gyorke I, Bonilla IM, Carnes CA, Billman GE, Györke S. Shortened Ca^{2+} signaling refractoriness underlies cellular Arrhythmogenesis in a Postinfarction model of sudden cardiac death. Circ Res. 2012;110:569–77.
10. Brunello L, Slabaugh JL, Radwanski PB, Ho HT, Belevych AE, Lou Q, et al. Decreased RyR2 refractoriness determines myocardial synchronization of

aberrant Ca^{2+} release in a genetic model of arrhythmia. PNAS. 2013;110:10312–7.

11. Liu N, Denegri M, Dun W, Boncompagni S, Lodola F, Protasi F, et al. Abnormal propagation of calcium waves and ultrastructural remodeling in recessive Catecholaminergic polymorphic ventricular tachycardia. Circ Res. 2013;113:142–52.
12. Kort AA, Lakatta EG. Calcium-dependent mechanical oscillations occur spontaneously in unstimulated mammalian cardiac tissues. Circ Res. 1984;54:396–404.
13. Lakatta EG, Lappe DL. Diastolic scattered light fluctuation, resting force and twitch force in mammalian cardiac muscle. J Physiol. 1981;315:369–94.
14. Lakatta EG, Jewell BR. Length dependent activation. Its effect in the length tension relation in cat ventricular muscle. Circ Res. 1977;40:251–7.
15. Stern MD, Capogrossi MC, Lakatta EG. Spontaneous calcium release from the sarcoplasmic reticulum in myocardial cells: mechanisms and consequences. Cell Calcium. 1988;9:247–56.
16. Lederer WJ, Tsien RW. Transient inward current underlying arrhythmogenic effects of cardiotonic steroids in Purkinje fibers. J Physiol. 1976;263:73–100.
17. Di Maio A, Ter Keurs HEDJ, Franzini-Armstrong C. T-tubular profiles in Purkinje fibres of mammalian myocardium. J Muscle Res Cell Motil. 2007;28:115–21.
18. Sommer JR, Johnson EA. Cardiac muscle. A comparative study of Purkinje fibers and ventricular fibers. J Cell Biol. 1968;36:497–526.
19. Stuyvers BD, Dun W, Matkovich SJ, Sorrentino V, Boyden PA, Ter Keurs HEDJ. Ca^{2+} sparks and Ca^{2+} waves in Purkinje cells: a triple layered system of activation. Circ Res. 2005;97:35–43.
20. Boyden PA, Pu J, Pinto JMB, Ter Keurs HEDJ. Ca^{2+} transients and Ca^{2+} waves in Purkinje cells. Role in action potential initiation. Circ Res. 2000;86:448–55.
21. Boyden PA, Barbhaiya C, Lee T, Ter Keurs HEDJ. Nonuniform Ca^{2+} transients in arrhythmogenic Purkinje cells that survive in the infarcted canine heart. Cardiovasc Res. 2003;57:681–93.
22. Boyden PA, Ter Keurs HEDJ. Reverse excitation–contraction coupling: Ca^{2+} ions as initiators of arrhythmias. J Cardiovasc Electrophysiol. 2001;12:382–5.
23. Cerrone M, Noujaim SF, Tolkacheva EG, Talkachou A, O'Connell R, Berenfeld O, et al. Arrhythmogenic mechanisms in a mouse model of catecholaminergic polymorphic ventricular tachycardia. Circ Res. 2007;101:1039–48.
24. Viatchenko-Karpinski S, Terentyev D, Gyorke I, Terentyeva R, Volpe P, Priori SG, et al. Abnormal calcium signaling and sudden cardiac death associated with mutation of calsequestrin. Circ Res. 2004;94:471–7.
25. Janse MJ, Wit AL. Electrophysiological mechanisms of ventricular arrhythmias resulting from myocardial ischemia and infarction. Physiol Rev. 1989;69:1049–169.
26. Pinto JMB, Boyden PA. Electrophysiologic remodeling in ischemia and infarction. Cardiovasc Res. 1999;42:284–97.
27. Boyden PA, Pinto JMB. Reduced calcium currents in subendocardial Purkinje myocytes that survive in the 24 and 48 hour infarcted heart. Circulation. 1994;89:2747–59.
28. Friedman PL, Stewart JR, Fenoglio JJ Jr, Wit AL. Survival of subendocardial Purkinje fibers after extensive myocardial infarction in dogs. Circ Res. 1973;33:597–611.
29. Boyden PA, Dun W, Barbhaiya C, Ter Keurs HEDJ. 2APB- and JTV519(K201) sensitive micro Ca^{2+} waves in arrhythmogenic Purkinje cells that survive in infarcted canine heart. Heart Rhythm. 2004;1:218–26.
30. Pinto JMB, Sosunov EA, Gainullin RZ, Rosen MR, Boyden PA. The effects of mibefradil a T type calcium channel current antagonist on the electrophysiology of Purkinje fibers that have survived in the infarcted heart. J Cardiovasc Electrophysiol. 1999;10:1224–35.
31. Hirose M, Stuyvers BD, Dun W, Ter Keurs HED, Boyden PA. Function of Ca^{2+} release channels in Purkinje cells that survive in the infarcted canine heart; a mechanism for triggered Purkinje ectopy. Circ Arrhythm Electrophysiol. 2008;1:387–95.
32. Hirose M, Stuyvers BD, Dun W, Ter Keurs HEDJ, Boyden PA. Wide long lasting perinuclear Ca^{2+} release events generated by an interaction between ryanodine and IP3 receptors in canine Purkinje cell. J Mol Cell Cardiol. 2008;45:176–84.
33. Stuyvers BD, Daniels R, Haq KT, Kelly C, Dun W, Boyden PA, et al. Alterations of Regional SR Ca^{2+} Transport in Purkinje cells of the canine heart post infarction. (submitted 2020).
34. Wit AL, Janse MJ. The ventricular arrhythmias of ischemia and infarction. Electrophysiological mechanisms. Mount Kisco, NY: Futura Publishing; 1993.
35. Ursell PC, Gardner PI, Albala A, JJ F Jr, Wit AL. Structural and electrophysiological changes in the epicardial border zone of canine myocardial infarcts during infarct healing. Circ Res. 1985;56:436–51.
36. Boyden PA, Gardner PI, Wit AL. Action potentials of cardiac muscle in healing infarcts: response to norepinephrine and caffeine. J Mol Cell Cardiol. 1988;20:525–37.
37. Aggarwal R, Boyden PA. Diminished calcium and barium currents in myocytes surviving in the epicardial border zone of the 5 day infarcted canine heart. Circ Res. 1995;77:1180–91.
38. Koumi SI, Backer CL, Arentzen CE, Sato R. Beta-adrenergic modulation of the inwardly rectifying potassium channel in isolated human ventricular myocytes. J Clin Invest. 1995;96:2870–81.

39. Kameyama M, Hofmann F, Trautwein W. On the mechanism of beta-adrenergic regulation of the ca channel in the Guinea-pig heart. Pflugers Arch. 1985;405:285–93.
40. Tsien RW, Bean BP, Hess P, Lansman JB, Nilius B, Nowycky MC. Mechanisms of calcium channel modulation by beta adrenergic agents and dihydropyridine calcium agonist. J Mol Cell Cardiol. 1986;18:691–710.
41. Gaide MS, Myerburg RJ, Kozlovskis PL, Bassett AL. Elevated sympathetic response of epicardial proximal to healed myocardial infarction. Am J Phys. 1983;245:H646–52.
42. Mubagwa K, Flameng W, Carmeliet E. Resting and action potentials of nonischemic and chronically ischemic human ventricular muscle. J Cardiovasc Electrophysiol. 1994;5:659–71.
43. Pinto JMB, Yuan F, Wasserlauf BJ, Bassett AL, Myerburg RJ. Regional gradation of L-type calcium currents in the feline heart with a healed myocardial infarct. J Cardiovasc Electrophysiol. 1997;8:548–60.
44. Aggarwal R, Boyden PA. Altered pharmacologic responsiveness of reduced L-type calcium currents in myocytes surviving in the infarcted heart. J Cardiovasc Electrophysiol. 1996;7:20–35.
45. Steinberg SF, Zhang H, Pak E, Pagnotta G, Boyden PA. Characteristics of the beta-adrenergic receptor complex in the epicardial border zone of the 5-day infarcted canine heart. Circulation. 1995;91:2824–33.
46. Davis MJ, Wu X, Nurkiewicz TR, Kawasaki J, Gui P, Hill MA, et al. Regulation of ion channels by protein tyrosine phosphorylation. Am J Physiol Heart Circ Physiol. 2001;281:H1835–62.
47. Yagi T, Boyden PA. The function of protein tyrosine kinases and L type Ca^{2+} currents in cells that have survived in the canine infarcted heart. J Cardiovasc Pharmacol. 2002;40:669–77.
48. Hund TJ, Decker KF, Kanter E, Mohler PJ, Boyden PA, Schuessler RB, et al. Role of activated CaMKII in abnormal calcium homeostasis and I_{Na} remodeling after myocardial infarction: insights from mathematical modeling. J Med Cell Cardiol. 2008;45:420–8.
49. Licata A, Aggarwal R, Robinson RB, Boyden PA. Frequency dependent effects on Cai transients, cell shortening in myocytes that survive in the infarcted heart. Cardiovasc Res. 1997;33:341–50.
50. Mohler PJ, Schott JJ, Gramolini AO, Dilly K, Guatimosim S, DuBell WH, et al. Ankyrin-B mutation causes type 4 long-QT cardiac arrhythmia and sudden cardiac death. Nature. 2003;421:634–9.
51. Hund TJ, Wright PJ, Dun W, Snyder JS, Boyden PA, Mohler PJ. Regulation of the ankyrin-B-based targeting pathway following myocardial infarction. Cardiovasc Res. 2009;81:742–9.
52. Pu J, Robinson RB, Boyden PA. Abnormalities in Cai handling in myocytes that survive in the infarcted heart are not just due to alterations in repolarization. J Med Cell Cardiol. 2000;32:1509–23.
53. Aggarwal R, Pu J, Boyden PA. Ca^{2+} dependent outward currents in myocytes from the epicardial border zone of the 5 day infarcted heart. Am J Phys. 1997;273:H1386–94.
54. Pu J, Ruffy F, Boyden PA. Effects of bay Y5959 on Ca^{2+} currents and intracellular Ca^{2+} in cells that have survived in the epicardial border zone of the infarcted canine heart. J Cardiovasc Pharmacol. 1999;33:929–37.
55. Cabo C, Schmitt H, Wit AL. New mechanism of antiarrhythmic drug action: increasing inward L type calcium current prevents reentrant tachycardia in the infarcted canine heart. Circulation. 2000;102:2417–25.
56. Janvier NC, Boyett MR. The role of Na-ca exchange current in the cardiac action potential. Cardiovasc Res. 1996;32:69–84.
57. Zhang X-Q, Moore RL, Tenhave T, Cheung JY. (ca^{++}) i transients in hypertensive and postinfarction myocytes. Am J Phys. 1995;269:C632–40.
58. Zhang X-Q, Tillotson DL, Moore RL, Cheung JY. Na/ca exchange currents and SR Ca^{2+} contents in postinfarction myocytes. Am J Phys. 1996;271:C1800–7.
59. Cheung JY, Musch TI, Misawa H, Semanchick A, Elensky M, Yelamarty RV, et al. Impaired cardiac function in rats with healed myocardial infarction: cellular vs. myocardial mechanisms. Am J Phys. 1994;266:C29–36.
60. Litwin SE, Bridge JH. Enhanced Na^{+}-Ca^{2+} exchange in the infarcted heart. Implications for excitation contraction coupling. Circ Res. 1997;81:1083–93.

Implications of Sarcolemmal Ca^{2+}-Handling Proteins in Heart Function in Health and Disease

20

Paramjit S. Tappia, Sukhwinder K. Bhullar, Anureet K. Shah, and Naranjan S. Dhalla

Abstract

A small amount of Ca^{2+} enters the cell through the sarcolemmal membrane, releases an additional amount of Ca^{2+} from the sarcoplasmic reticulum, and initiates myocardial contraction. The contraction process is terminated upon lowering the cytosolic Ca^{2+} by accumulation in the sarcoplasmic reticulum as well as removal into the extracellular space through the sarcolemmal membrane. This article describes sarcolemmal L-type Ca^{2+} channel, Na^+–Ca^{2+} exchanger, store-operated Ca^{2+} channels, Ca^{2+}-pump ATPase, Ca^{2+}/Mg^{2+}-ecto-ATPase, Na^+-H^+ exchanger, and Na^+-K^+ ATPase, which directly or indirectly regulate the movements of Ca^{2+} in cardiomyocytes. The pharmacological modulation of these Ca^{2+}-handling proteins has been indicated to gain information regarding the regulation of intracellular Ca^{2+} in cardiomyocytes. Furthermore, alterations in the sarcolemmal Ca^{2+}-handling proteins in different cardiovascular pathologies have been identified to emphasize the Ca^{2+}-handling abnormalities in cardiomyocytes during the development of cardiac dysfunction in heart disease.

Keywords

Heart · Sarcolemma · Sarcoplasmic reticulum · Ca^{2+} handling proteins · Myocyte · Contraction · L-type Ca^{2+} channel, store-operated Ca^{2+} channel · Na^+-Ca^{2+} exchanger · Na^+-H^+ exchanger · Na^+-K^+ ATPase · Sarcolemmal Ca^{2+}-pump ATPase

20.1 Introduction

Contraction of the heart is regulated by changes in intracellular Ca^{2+} concentration ($[Ca^{2+}]_i$); normal function requires that $[Ca^{2+}]_i$ be sufficiently high (1×10^{-5} M) in systole and low (1×10^{-7} M) in diastole [1]. The essential role of Ca^{2+} in cardiac contraction was first discovered by Sydney Ringer in 1885, when he began his research with an isolated frog heart suspended in a 0.75% solution of NaCl. He then introduced additional substances such as blood and albumin to the solution and observed the effects on the beating

---

P. S. Tappia
Asper Clinical Research Institute, St. Boniface Hospital, Winnipeg, Canada

S. K. Bhullar
Institute of Cardiovascular Sciences, St. Boniface Hospital Albrechtsen Research Centre, Winnipeg, Canada

A. K. Shah
School of Kinesiology, Nutrition and Food Science, California State University, Los Angeles, USA

N. S. Dhalla (✉)
Institute of Cardiovascular Sciences, St. Boniface Hospital Albrechtsen Research Centre and Department of Physiology and Pathophysiology, College of Medicine, Rady Faculty of Health Sciences, University of Manitoba, Winnipeg, Canada
e-mail: nsdhalla@sbrc.ca

© Springer Nature Switzerland AG 2023
O. N. Tripathi et al. (eds.), *Heart Rate and Rhythm*, https://doi.org/10.1007/978-3-031-33588-4_20

heart. He demonstrated that the abnormally prolonged ventricular dilation induced by pure NaCl solution was reversed by both blood and albumin. He then showed that a small amount of Ca^{2+} in the perfusing solution was necessary for the maintenance of a normal heartbeat, a discovery he made after realizing that instead of distilled water, his technician was actually using tap water containing Ca^{2+} at nearly the same concentration as the blood [2]. Since then, the role of Ca^{2+} in the process of excitation–contraction coupling, myocardial metabolism, and maintenance of cardiac cell integrity has been examined extensively [3–11].

Within a single beat of a cardiomyocyte, there is a 100-fold increase in the cytosolic free Ca^{2+} level, which must be returned to its original low concentration in order to maintain the normal physiological function of the cell [12]. Depolarization activates the L-type Ca^{2+} channels in sarcolemma (SL), leading to an influx of a small amount of Ca^{2+}. This Ca^{2+} then activates Ca^{2+}-release channels in the sarcoplasmic reticulum (SR) and results in a massive Ca^{2+} release to raise the cytosolic Ca^{2+} from the resting level of 100 nM to 1–10 μM. As a consequence, Ca^{2+} binds to troponin, relieves the inhibitory effect of the troponin complex on the actin and myosin filaments, and initiates the contraction of myofibrils. Most of the cytosolic Ca^{2+} is rapidly pumped into the SR by the ATP-dependent Ca^{2+}-pump ATPase, while the SL Ca^{2+}-pump ATPase and Na^+–Ca^{2+} exchanger remove the rest out of the cell leading to relaxation. Various cation channels, pumps, and exchangers directly or indirectly involved in the excitation–contraction coupling process are shown in Fig. 20.1.

Although most of the Ca^{2+} that activates contraction is released from the SR, up to 30% enters from outside the cell and is pumped out at the end of systole [13]. In addition, while some of the Ca^{2+} influx is required to trigger Ca^{2+} release from the SR, the bulk of it serves to reload the SR with Ca^{2+} that was pumped out of the cell [13]. Accordingly, it has been suggested that the large SL Ca^{2+} fluxes facilitate rapid changes in contractility in the processes of cardiac contraction and relaxation. It should also be mentioned that in the heart, intracellular Na^+ concentration is a key modulator of Ca^{2+} cycling, contractile activity, and cardiomyocyte metabolism [14].

This chapter describes the characteristics of SL Ca^{2+} channels, Na^+–Ca^{2+} exchanger (NCX), and Ca^{2+}-pump ATPase, which participate in raising and lowering the intracellular concentration of Ca^{2+} in cardiomyocytes. Some information regarding SL store-operated Ca^{2+} channels (SOCC) that participate in the Ca^{2+} entry is also provided. In addition, biochemical features of SL Na^+–K^+ ATPase and SL Na^+–H^+ exchanger (NHE), which regulate the intracellular concentration of Ca^{2+}, are discussed. Pharmacological modulation of SL Ca^{2+}-handling proteins for the regulation of intracellular Ca^{2+} in cardiomyocytes as well as SL Ca^{2+}-handling abnormalities during the development of cardiac dysfunction in heart disease is also described. The involvement of changes in the activities of SL Ca^{2+}-handling proteins has been indicated in the cardiac rate and rhythm disturbances under various pathological conditions.

20.2 Sarcolemmal L-Type Ca^{2+} Channel

L-type Ca^{2+} channels, also referred to as voltage-gated Ca^{2+} channels, are embedded in the cardiac SL membrane, including the T-tubules facing the SR junction [15], and play a critical role in excitation–contraction coupling. Following depolarization, L-type Ca^{2+} channels are opened to allow the entry of a small amount of Ca^{2+}, which activates SR Ca^{2+}-release channels. Soon after the increase in cytoplasmic Ca^{2+}, L-type Ca^{2+} channels undergo inactivation in order to terminate the Ca^{2+} entry. There are several isoforms of L-type Ca^{2+} channels, but cardiomyocytes mainly express the Cav1.2 isoform. The L-type Ca^{2+}- channel pore-forming unit (α-subunit) is composed of four homologous domains, each having six transmembrane segments [16]. The accessory subunits, β_2 and α_2–δ, of the L-type Ca^{2+} channel are also expressed in the heart ([17]; see also Chaps. 2 and 10). There are several modulators of SL Ca^{2+} channels; the most important are calmodulin

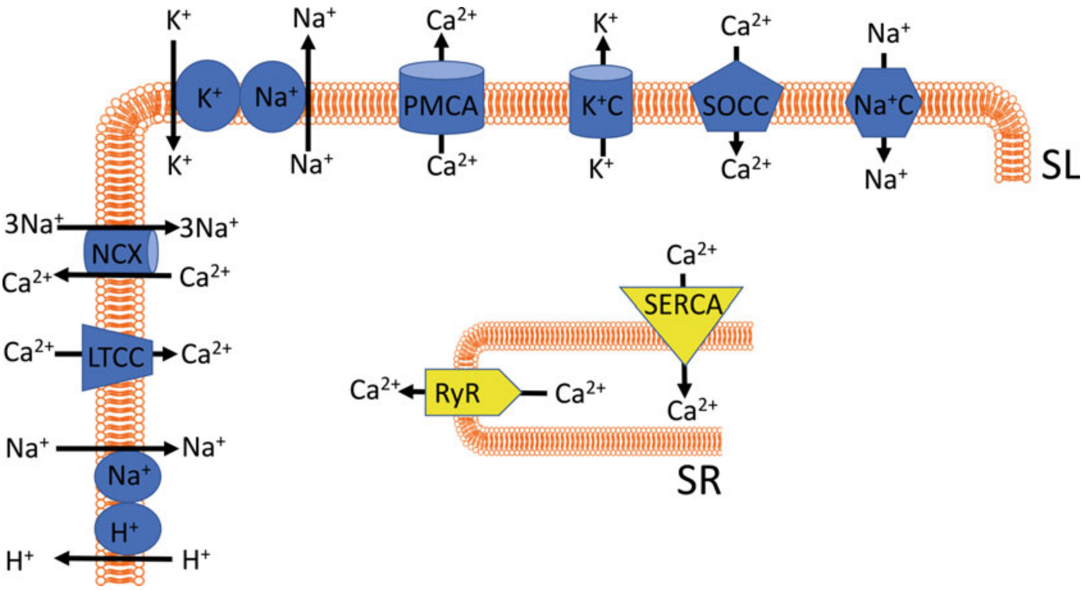

Fig. 20.1 Schematic representation of the cellular components in the excitation-contraction coupling process. In the cardiomyocyte, Na^+ entry through the voltage gated Na^+ channels (Na^+C) in the sarcolemma (SL) membrane leads to cellular depolarization, which then activates the L-type Ca^{2+}-channels (LTCC) causing a small amount of Ca^{2+} influx. This entry of Ca^{2+} activates the sarcoplasmic reticulum (SR) Ca^{2+}-release channels or ryanodine receptors (RyR) and results in the release of additional Ca^{2+} that results in cardiac contraction. The high level of Ca^{2+} in the cytoplasm is taken up by the Ca^{2+}-pump ATPase (SERCA) in the SR. The cytosolic Ca^{2+} is also extruded through the Na^+-Ca^{2+} exchanger (NCX) and the SL Ca^{2+}-pump ATPase (PMCA). Since both cardiac contraction and relaxation processes are intimately associated with hydrolysis of ATP and stimulation of metabolism, the resulting H^+ is removed by Na^+-H^+ exchanger. Thus, Na^+ entering into the cell through Na^+-H^+ exchanger, Na^+ channels and NCX is extruded by the Na^+-K^+ ATPase. The store-operated Ca^{2+}-channels (SOCC) are only active when the SR is depleted of Ca^{2+}, whereas K^+ is removed from the cell by K^+-channels (K^+C)

(CaM) and β-adrenoceptors. CaM was found to be associated with the COOH terminus of the voltage-gated Ca^{2+} channels and can both activate and inactivate the channel in a Ca^{2+}-dependent manner. This mechanism prevents excessive channel activation when Ca^{2+} is high and facilitates channel inactivation when Ca^{2+} is low [18]. On the other hand, stimulation of β-adrenoceptors increases channel current, thus increasing the contractile force development, which is mediated through phosphorylation of this channel via protein kinase A (PKA). L-type Ca^{2+} channels are actually associated with β-adrenoceptors in a multimeric protein complex that may also include heterotrimeric G-proteins, adenylate cyclase, PKA, phosphatases, and PKA binding proteins. This conglomerate of proteins in neurones has been called a signalosome [19].

Mutations in the gene encoding the cardiac L-type Ca^{2+} channels leading to a loss of their function have been associated with short QT syndrome, which may result in atrial fibrillation, syncope, and sudden death [20]. SL L-type voltage-gated Ca^{2+}-channel blockers are used for the treatment of angina pectoris, high blood pressure, and arrhythmias. Voltage-gated Ca^{2+}-channel blockers belong to three chemical entities. The dihydropyridines such as amlodipine are used mainly for their effect on the vascular smooth muscle as a vasodilator for the treatment of stable and vasospastic angina. The second class, phenyalkylamines (verapamil), reduce cardiac oxygen demand and alleviate coronary vasospasm; these drugs are used for the treatment of angina pectoris. The third class, benzothiazepines (diltiazem), are intermediate in their selectivity between the myocardium and the vascular smooth muscles and reduce arterial pressure without depressing the heart muscle. Both verapamil and diltiazem are also used for the treatment of arrhythmias, mainly by blocking L-type Ca^{2+}-channels in the heart pacemaker system [21].

20.3 Sarcolemmal Store-Operated Ca^{2+} Channel (SOCC)

The threshold attribute of SR Ca^{2+} loading tightly controls Ca^{2+} release through RyR, which affects muscle contraction. Both excitable and non-excitable cells need Ca^{2+} in the endoplasmic reticulum for proper protein folding and thus emptying the intracellular Ca^{2+} stores. Measuring Ca^{2+} current that enters the cell upon depletion of intracellular Ca^{2+} stores has helped to identify a group of cation channels that respond to Ca^{2+} depletion from intracellular stores (SOCC) [22]. These cation channels belong to the large family of transient receptor potential (TRP) channels originally discovered in *Drosophila* and consist of six transmembrane (TM) spanning helices and a pore region that exists between TM5 and TM6. The channels are gated by a variety of stimuli that include the binding of intracellular and extracellular messengers, changes in temperature as well as chemical and mechanical pressures [23]. The SOCCs are activated either by agonists such as inositol trisphosphate (IP_3) and PKC or by depletion of the internal Ca^{2+} store [22]. Similar to other cation channels, the SOCCs are modulated by phosphorylation. The phosphorylation of SOCCs due to PKC inhibits Ca^{2+} entry in Jurkat cells (immortalized human T lymphocyte cells) and lymphocytes [24], whereas phosphorylation by PKA activates these channels. Inhibitors of serine/threonine phosphatase A (calyculin A and okadaic acid) have also been reported to reduce the activation of SOCCs [25]. In addition, thiol oxidation and cADP-ribose inhibition were found to reduce the channel activity in isolated pulmonary artery rings and human smooth muscle, respectively [26, 27].

Ca^{2+} influx through SOCC was implicated during protein kinase D and MAPK activation that may be a target of physiological agents such as decosahexanoic acid in Jurkat T-cells [28]. In addition to PKA and PKC, SOCCs are modulated by CaMKII [29]. Acidic pH and hydrogen peroxide were also found to inhibit the SOCCs in cultured human microglia [30, 31]. It should be pointed out that the activity of SOCCs was increased in arterial myocytes as they progressed from a contractile to a proliferative phenotype in tissue culture [32]. These channels were also shown to contribute to the increase of intracellular Ca^{2+} in cardiomyocytes upon inhibition of the Na^+–K^+ ATPase [33]. In cardiomyocytes, Ca^{2+} entry through SOCC has been linked to the activation of calcineurin and the development of hypertrophy [34]. Thus, it is evident that the role of SOCCs in cardiovascular biology is being explored, and the potential for the development of therapies associated with SOCCs in apoptosis, hypertrophy, and arrhythmias has been suggested [35, 36].

Substantial evidence exists that the molecular components of SOCCs (e.g., Stim, Orai, and TRPC channels) are expressed in cardiomyocytes from embryo to adult. Moreover, these proteins have been shown to contribute to disease including pathological hypertrophy and thus reducing their expression can attenuate hypertrophic growth [37]. In addition, the targeting of Orai proteins may treat atherosclerosis and restenosis [38]. The role of SOCC in the pathogenesis of hypertension is now beginning to emerge [39]. In conjunction, a novel role of store-operated Ca^{2+} entry (SOCE) as a by modulator in Ang II-induced cardiac fibrosis by mediating Ca^{2+}-influx has been reported [40]. Interestingly, the expression of STIM1 and Orai 1 increased following Ang II. Elevated intracellular calcium is a factor in the development of pathological cardiac hypertrophy, which leads to the activation of intracellular signaling pathways [41]. SOCE and the activation of the calcineurin—NFAT pathway in the development of pathological hypertrophy has also been reported [41] to be regulated by the TRPM4 channel. In addition, phenylephrine-induced myocardial hypertrophy has been suggested to occur through the activation of SOCE and upregulation of CaMkIIδ [42].

On the other hand, a pro-arrhythmic SOCE-like activity in adult rat ventricular cardiomyocytes has been reported, which may play an important role in the development of cardiac disease [43]. Similarly, an increase in SOCE following endothelin-1 treatment of neonatal rat cardiomyocytes has also been reported [44]. Interestingly, the beneficial role of mineralocorticoid receptor signaling blockade in heart failure and arrhythmias has been suggested because aldosterone is considered to be a key regulator of cardiomyocyte Ca^{2+} influx [45]. Indeed, aldosterone promotes TRPC1 and Orai1-mediated SOCE in cardiomyocytes, which can be blunted by store-operated channel inhibitors, blockade of Orai1, TRPC1, and Orai1 dominant negative mutants or TRPC5 siRNA [45].

20.4 Sarcolemmal Na^{+}–Ca^{2+} Exchanger (NCX)

NCX is the major mechanism for Ca^{2+} efflux and thus plays a critical role in regulating ventricular cardiomyocyte Ca^{2+} content and contractility [46]. In fact, the NCX connects cardiac Ca^{2+} and Na^{+} transport leading to Na^{+}-dependent regulation of EC-coupling [47, 48]. The SL NCX is mainly responsible for lowering the increased level of cytosolic Ca^{2+} due to activation of the voltage-gated Ca^{2+} channel [3, 4]. The cardiac SL NCX operates in either forward mode, where it removes cytosolic Ca^{2+} in exchange for extracellular Na^{+}, or in reverse mode, in which excess Ca^{2+} is transported into the cytosol while Na^{+} is extruded. The reverse exchange mechanism is relevant to conditions of ischemia-reperfusion where the rise in Na^{+} ions is high enough to trigger the reverse activity of NCX [5]. The reverse mode of NCX can also be active in heart failure, where an increase in intracellular [Na^{+}] leads to Ca^{2+} influx via the NCX [5]. Another important function of the NCX is related to the action of cardiac glycosides whereby inhibition of the plasma membrane Na^{+}–K^{+} ATPase leads to Na^{+} accumulation which then triggers NCX reverse mode [3], leading to an increase in cytosolic Ca^{2+} and positive inotropic effect. At resting diastolic levels of 100 nM Ca^{2+}, the cardiac isoform NCX1 is completely activated. In addition, NCX1 is activated by phosphatidyl inositol biphosphate and ATP [49]. SL NCX is also modulated by a cytosolic protein phospholemman, whereas PKA and PKC phosphorylation inhibited this NCX1 activity [50].

The cardiac NCX plays a crucial role in ischemia-reperfusion injury. During ischemia, accumulation of H^{+} in the cell leads to the activation of NHE that creates intracellular Na^{+} overload. This change triggers the activation of NCX1 to extrude intracellular Na^{+} in exchange for extracellular Ca^{2+} and results in the development of intracellular Ca^{2+} overload. As a consequence, there occurs a depression in cardiac contractility as well as apoptotic cell death [51]. It has been documented that NCX is involved in β-adrenergic stimulated Ca^{2+} entry in addition to SL L-type Ca^{2+} channels. This is evident from the inhibition of the catecholamine-induced increase in Ca^{2+} in cardiomyocytes by both NCX and Ca^{2+}-channel antagonists [52]. An increase in the reverse mode activity of SL NCX due to β-adrenergic stimulation may contribute to arrhythmias in the failing heart [53]. On the other hand, NCX activity is also reduced in heart failure, and this effect is mitigated by angiotensin-converting enzyme inhibitors [54]. Several drugs have been developed to inhibit the reverse mode of NCX due to its involvement in ischemia-reperfusion injury [55]. The role of NCX in cardiomyocyte Ca^{2+} homeostasis is well established; however, it has also been reported to contribute to electrical instability and atrial fibrillation (AF) [56]. While elevated NCX activity occurs in AF, SEA0400, an inhibitor of NCX activity, has been reported to be ineffective in attenuating Ni^{2+}-sensitive current in human atrial cells unless it is under unphysiological conditions and thus it has been suggested that blockade of NCX with SEA0400 depends on intracellular Na^{+} concentration [57].

SEA0400 is the most specific inhibitor for the cardiac NCX1, because it is less sensitive towards the brain and skeletal isoforms [58]. It has been shown to be protective against the ischemia-reperfusion-induced injury in the heart [59]. In this regard, it should be mentioned that SEA0400 exerts no effect on the action potential under normal conditions and during ischemia. However, recovery of action potential duration after reperfusion has been observed [59]. The recovery of contractile function during reperfusion by SEA0400 was also demonstrated when SEA0400 treatment was done before and during the ischemic period and when it was used during reperfusion. Taken together, it was suggested that inhibition of NCX activity either during ischemia or during reperfusion exerts cardioprotective effects and improves recovery of the contractile function of the heart [59].

20.5 Sarcolemmal Na^+–H^+ Exchanger (NHE)

The Na^+–H^+ exchanger isoform 1 (NHE1) is an integral membrane protein ubiquitously expressed in mammalian cells. It is made up of two domains: a 500-amino acid membrane domain that is responsible for transport and removes protons, and a regulatory intracellular cytosolic domain made up of 315 amino acids. NHE1 is the major isoform found in the myocardium where it plays an important role in regulating intracellular pH by exchanging one intracellular proton for one extracellular sodium [60, 61]. In fact, NHE clears more than 50% of the cytosolic H^+ load produced by stimulation of metabolism [51, 62]. Although NHE1 normally fulfills this important physiological role, aberrant regulation and overactivation of NHE1 contribute to heart disease, including acute ischemia-reperfusion (I-R) damage and cardiac hypertrophy [60].

The NHE and intracellular pH are regulated by several intracellular modulators such as phosphatidyl inositol 4,5-bisphosphate (PIP_2) [63]. The phosphatase, calcineurin B homologous protein 3, was found to boost the production of mature NHE1 protein, as well as cell surface transport and longevity [64]. CaM has also been observed to modulate NHE1 activity; CaM and Ca^{2+} complex bind to NHE1 and activate the exchanger by interfering with its autoinhibitory mechanism [65, 66]. Another important modulator of NHE1 is carbonic anhydrase, which increases its activity; this increase in activity is dependent on the phosphorylation of NHE upstream of the carbonic anhydrase binding site [67]. The phosphorylation of NHE1 may be useful for the removal of H^+ produced by carbonic anhydrase [68]. On the other hand, dephosphorylation inhibits the NHE1 activity [68, 69]. There are several extracellular activators of NHE such as thrombin, phorbol esters, and serum, which activate NHE through CaMKII, the mitogen-activated protein kinases (MAPK) and extracellular-regulated kinases 1 and 2 (ERK 1/2). Activation of NHE1 by insulin may be mediated via the ERK1/2/MAPK pathway and the PKC pathway [68]. In vascular smooth muscles, angiotensin II may lead to the phosphorylation of NHE through a downstream target of ERK 1/2 and the ribosomal protein S6 kinase (P90RSK) [70, 71].

As indicated earlier, NHE is known to play a central role together with the NCX in I-R injury. Activation of the NHE by the accumulation of H^+ under ischemic conditions leads to a massive influx of Na^+ that in turn activates the NCX [51]. Cariporide, a specific and effective NHE inhibitor was suggested as a potential drug for the prevention of I-R injury [72]. Cariporide was mainly beneficial in patients undergoing coronary artery bypass when administered before the operation to avoid the consequences of I-R injury [73]. Despite the fact that cariporide protected against I-R injury in experimental animals, a paradoxical increase in death due to brain hemorrhage in phase III clinical trials discouraged the development of other NHE blockers [74].

It should be noted that out-of-hospital sudden cardiac arrest is a major public health problem with an overall survival of less than 5%. Cardiac arrest leads to a cessation of coronary blood flow rapidly, resulting in a powerful ischemia and activation of the SL NHE-1. NHE-1 activation drives Na^+ into cardiomyocytes in exchange for H^+ with its exchange rate intensified upon reperfusion during the resuscitation effort. Na^+ accumulates in the cytosol driving Ca^{2+} entry through the NCX, eventually causing cytosolic and mitochondrial Ca^{2+} overload and worsening myocardial injury by compromising mitochondrial bioenergetic function [75]. Therefore, inhibition of NHE-1 may represent a promising target for resuscitation from cardiac arrest [75].

Myocardial NHE1 is activated by a variety of stimuli, including neurohormonal factors and mechanical stress, leading to intracellular Na$^+$-overload and activation of pro-hypertrophic cascades. In this regard, endothelin −1 and norepinephrine stimulate a signaling cascade that leads to ERK1/2 and P90RSK activation and phosphorylation of NHE1 [76]. In fact, NHE1 overexpression/hyperactivity constitutes a “switch on/off” for the pathological phenotype during the development of cardiac hypertrophy and heart failure [77, 78]. Thus, strategies that circumvent NHE-1 hyperactivity may constitute a novel approach to improve cardiovascular health or prevent maladaptive cardiac hypertrophy and heart failure.

20.6 Sarcolemmal Na$^+$–K$^+$ ATPase

The plasma membrane Na$^+$–K$^+$ ATPase was first described in 1957 by Skou [79], and was shown to establish the electrochemical gradient of cells by driving an active exchange of Na$^+$ and K$^+$ ions while consuming ATP in order to maintain the resting membrane potential ([80, 81], see Chap. 2). This functional pump is composed of two major subunits; the α-subunit, which has approximately 10 TM domains, and 3 large intracellular loops. The loop between TM 4 and 5 contains the phosphorylation and the nucleotide-binding domains [82]. The α-subunit also contains the binding site for Na$^+$, K$^{+,}$ and cardiac glycosides [83]. The second subunit, the β-subunit, is essential for the maturation and targeting of the pump, whereas a third subunit, the γ-subunit, has no known function. Among the four α-isoforms, the α1 isoform is ubiquitously expressed, whereas the α2-isoform is specifically expressed in skeletal and cardiac muscles, brain, and adipose tissue [83]. Primate and canine myocardium express the α1 and α3 isoforms, whereas only the α1 isoform is found in sheep and guinea pig myocardium [84]. Prostaglandins (GE2, GF2, and GI2) have been shown to reduce the Na$^+$–K$^+$ ATPase activity [85]. On the other hand, insulin was found to stimulate Na$^+$–K$^+$ ATPase [86]. Interestingly, a cholesterol-enriched membrane showed high Na$^+$–K$^+$ pump activity [87]. Caffeine also appears to increase the efficiency of the pump [88]. Likewise, catecholamine-induced stimulation of PKA and PKC activities was shown to increase the Na$^+$–K$^+$ ATPase activity in cardiomyocytes [89]. On the other hand, we have earlier reported a mechanism for the regulation of cardiac Na$^+$–K$^+$ ATPase through phosphorylation by a Ca^{2+}/calmodulin-dependent protein kinase (CaM kinase) present in the SL membrane. It was demonstrated that phosphorylation of the α-subunit of Na$^+$–K$^+$ ATPase by an endogenous CaM kinase might lead to an inhibition of its catalytic activity [90].

The expression and activity of the Na$^+$–K$^+$ ATPase are significantly enhanced or reduced by a variety of disease states and physiological modulators. In heart failure, a characteristic change in the expression pattern of the α-subunit has been observed where both the mRNA and protein levels of both α1, α2, and β1 isoforms were reduced while α-3 isoform was increased in a rat model of congestive heart failure. These changes were prevented by treatment with imidapril, an angiotensin-converting enzyme inhibitor [54, 91]. The reduction of the expression and activity of Na$^+$–K$^+$ ATPase in congestive heart failure was also shown to be due to the activation of the renin–angiotensin system [92]. The activity of Na$^+$–K$^+$ ATPase was reduced due to ischemia-reperfusion; this change was found to be caused by a reduction in the expression of the specific isoforms of the pump component, namely α2, α3, and β1 subunits [93–95]. Antioxidants such as superoxide dismutase plus catalase or ischemic preconditioning have been reported to prevent these changes

[96, 97]. Indeed, in recent years, the Na^+–K^+ ATPase/ROS amplification loop is a key event in several oxidative stress-related diseases, including obesity, atherosclerosis, heart failure, uremic cardiomyopathy, and hypertension [98].

Cardiac glycosides (CGs) are compounds found in plants and amphibians and are widely distributed in nature with potential cardiovascular action. Their mechanism of action is based on the blockade of Na^+–K^+ ATPase, resulting in an increase in cytosolic Ca^{2+} and thereby exerting a positive inotropic effect [99, 100]. The field of Na^+–K^+ ATPase modulators, including CGs has attracted much interest because of their clinical implication to treat congestive heart failure [100]. In human heart, all Na^+–K^+ ATPase α-subunit isoforms, namely α1, α2, and α3, have shown a high affinity for CGs [101]. The α2–β subunit combination exhibits faster association and dissociation for the cardiac glycoside ouabain than the α1–β subunit, due to a difference in specific amino acids in their extracellular domains. The beneficial effects of CGs on cardiac function in chronic heart failure are believed to be twofold: firstly, the accumulation of Na^+ inside the cell triggers the reverse mode of NCX, leading to Ca^{2+} influx, which causes a positive inotropic effect [102], and secondly, due to signaling to the nucleus, which affects membrane protein trafficking and protein kinase activity [103]. The human body has also been reported to produce cardiac glycoside-like compounds [104] by the adrenal cortex and medulla [105]. These endogenous cardiac glycosides have been shown to be involved in the proliferation of smooth muscles, kidney cells, and endothelial cells [89]. There is also evidence of the existence of endogenous digoxin and the structurally related bufadienolides in human urine [106]. It should be pointed out that marked inhibition of SL Na^+–K^+ ATPase by high doses of CGs is well known to be associated with cardiac arrhythmias; however, the mechanisms of this cardiotoxicity are not fully understood. The activity of the Na^+–K^+ ATPase has also been reported to be depressed in diabetic and genetic cardiomyopathies [107–110].

20.7 Sarcolemmal/Plasma Membrane Ca^{2+}-ATPase (PMCA)

The PMCA activity of the plasma membrane is critical for fine-tuning the cytosolic Ca^{2+}. SL PMCA, a P-type ATPase ([111]; see Chap. 2), has more than 20 splice variants belonging to four isoforms. PMCA1 and 4 are expressed in most tissues, while the expression of PMCA2 and 3 is limited to brain and excitable tissues. PMCA is believed to have 10 transmembrane segments with a large central loop that contains the ATP binding site and a large C-terminal loop that contains the CaM binding domain [112]. CaM is the main protein regulator of the pump [113] because, in the absence of CaM, the pump is auto-inhibited by a mechanism that involves binding of the C-terminal tail to the two major intracellular loops. The activation of PMCA requires the binding of Ca^{2+} with CaM to the C-terminal tail and conformational changes that displace the auto-inhibitory tail from the major catalytic domain. The release of the auto-inhibitory tail may be facilitated by acidic phospholipids as well as PKA- or PKC-mediated phosphorylations of specific (Ser/Thr) residues in the C-terminal. On the other hand, the activity of PMCA is depressed by partial proteolytic cleavage of the tail, which is catalyzed by proteases such as calpain and caspases [114].

The cardiac PMCA is considered to play a minor role as a mechanism for lowering the intracellular concentration of Ca^{2+} in comparison to NCX and SERCA; however, there is growing evidence for the role of PMCA as a signaling center and housekeeping molecule [15, 112]. The critical role of PMCA1 as a housekeeping gene has been demonstrated in a gene knockout study [115]. This study showed that complete knockout of PMCA1 led to embryonic lethality, while heterozygous animals did not show any defect. Interestingly, although PMCA4 is widely expressed, PMCA4 null mutants exhibited no embryonic lethality and appeared outwardly normal. PMCA4 null male mice were infertile but had normal spermatogenesis and mating behavior. In contrast to the minor effect obtained by ablating the PMCA4 gene, overexpression of PMCA4 in arterial smooth muscles had dramatic effects on cardiovascular function and provided evidence of its involvement in cellular signaling [116].

Cardiac overexpression of PMCA attenuates endothelin-1 stimulated early induction of cardiac gene expression, suggesting that PMCA may modulate myocardial growth responses. In fact, cardiomyocytes from rats overexpressing PMCA4b displayed a higher growth rate [117]. Likewise, blood pressure in these animals was increased, indicating a direct involvement of PMCA in Ca^{2+} cycling; however, no significant changes in Ca^{2+} content were found. The effect on blood pressure can be explained by the reduction of nNOS (neuronal nitric oxide synthetase), suggesting a role for PMCAb in nNOS function. Another study showed that overexpression of PMC4b leads to a reduced inotropic effect in response to β-adrenergic stimulation, probably through an nNOS-mediated effect [115]. These mice also showed an increased hypertrophic response under continuous β-adrenergic stimulation. PMCA down regulates the nNOS activity, whereas its inhibition increased the nNOS activity. It seems that this regulation is beneficial for increasing cardiac contractility. Mouse hearts lacking nNOS have a reduced adrenergic and force-frequency response [118].

20.8 Conclusion

From the foregoing discussion, it is evident that Ca^{2+} movements across the SL membrane in cardiomyocytes involve L-type Ca^{2+} channels, NCX, NHE, PMCA, SOCC and Na^{+}–K^{+} ATPase. These cation channels and transporters participate in Ca^{2+} movements, either directly or indirectly, and are highly regulated by the phosphorylation/dephosphorylation system [119]. Any defect in one or more of these Ca^{2+}-handling proteins, which may occur in congestive heart failure [120], appears to result in loss of their coordinated function for the development of abnormalities in the rate and rhythm of the heart. There seem to be three areas of investigation that are becoming the center of attention in cardiovascular research. First, as the classical view of the channels, transporters and pumps with respect to the cation conducting pathway has evolved, more emphasis is being placed on the role of the cation channels as signaling molecules, particularly the signaling mediated by SL Na^{+}-K^{+} ATPase and Ca^{2+}-pump ATPase. The second is the challenging task of finding correlations between the activities of different Ca^{2+}-handling proteins. An example of the influence of one channel on another is the SOCC, where emptying of the SR Ca^{2+} store activates the SOCC in the cell to permit the entry of more Ca^{2+}. Another example is the study of the interaction between the L-type Ca^{2+} channel and RyR. The mechanism of such an interaction in cardiac muscles has revealed that Ca^{2+} influx through the L-type Ca^{2+} channel activates RyR without any physical interaction of the SL and SR channels. Last but not least, developing novel therapeutic approaches to treat heart disease where a drug such as ranolzine specifically targets the late or persistent Na^{+} current [121], or a specific current in a specific type of cell, such as targeting the ultra-rapid K^{+} current in atrial myocytes for correction of arrhythmias [122]. In addition, the control of defective or mutated channels can be achieved before they are translated. In a recent study, silencing micro-RNA was used to downregulate the expression of a mutant K^{+}-channel, thus averting its arrhythmogenic action [123]. Although great progress on work related to the role of Ca^{2+} in heart function in health and disease has been carried out over 150 years, there is still scope for further investigation in order to completely understand the role of different sarcolemmal Ca^{2+}—handling proteins in heart function in health and disease.

Acknowledgements The infrastructural support for this article was provided by the St. Boniface Hospital Research Foundation.

References

1. Eisner DA, Caldwell JL, Kistamás K, Trafford AW. Calcium and excitation-contraction coupling in the heart. Circ Res. 2017;121:181–95.
2. Sternbach G. Sydney ringer: water supplied by the New River water company. J Emerg Med. 1988;6: 71–4.
3. Dhalla NS, Ziegelhoffer A, Harrow JA. Regulatory role of membrane systems in heart function. Can J Physiol Pharmacol. 1977;55:1211–34.
4. Dhalla NS, Pierce GN, Panagia V, Singal PK, Beamish RE. Calcium movements in relation to heart function. Basic Res Cardiol. 1982;77:117–39.
5. Dhalla NS, Saini HK, Tappia PS, Sethi R, Mengi SA, Gupta SK. Potential role and mechanisms of subcellular remodeling in cardiac dysfunction due to ischemic heart disease. J Cardiovasc Med. 2007;8:238–50.
6. Gordon AM, Homsher E, Regnier M. Regulation of contraction in striated muscle. Physiol Rev. 2000;80: 853–924.
7. Cheng H, Lederer WJ. Calcium sparks. Physiol Rev. 2008;88:1491–545.
8. Dulhunty AF. Excitation-contraction coupling from the 1950s into the new millennium. Clin Exp Pharmacol Physiol. 2006;33:763–72.
9. Eisner D. Calcium in the heart: from physiology to disease. Exp Physiol. 2014;99:1273–82.
10. Santulli G, Lewis DR, Marks AR. Physiology and pathophysiology of excitation contraction coupling: the functional role of ryanodine receptor. J Muscle Res Cell Motil. 2017;38:37–45.
11. Santulli G, Marks AR. Essential roles of intracellular calcium release channels in muscle, brain, metabolism, and aging. Curr Mol Pharmacol. 2015;8:206–22.
12. Cartwright EJ, Schuh K, Neyses L. Calcium transport in cardiovascular health and disease –the sarcolemmal calcium pump enters the stage. J Mol Cell Cardiol. 2005;39:403–6.
13. Eisner DA, Trafford AW. What is the purpose of the large sarcolemmal calcium flux on each heartbeat? Am J Physiol Heart Circ Physiol. 2009;297:H493–4.
14. Despa S, Bers DM. Na^+ transport in the normal and failing heart - remember the balance. J Mol Cell Cardiol. 2013;61:2–10.
15. Benitah JP, Alvarez JL, Gómez AM. L-type Ca^{2+} current in ventricular cardiomyocytes. J Mol Cell Cardiol. 2010;48:26–36.
16. Catterall WA, Perez-Reyes E, Snutch TP, Striessnig J. Nomenclature and structure-function relationships of voltage-gated calcium channels. Pharmacol Rev. 2005;57:411–25.
17. Colecraft HM, Alseikhan B, Takahashi SX, Chaudhuri D, Mittman S, Yegnasubramanian V, et al. Novel functional properties of Ca^{2+} channel beta subunits revealed by their expression in adult rat heart cells. J Physiol. 2002;541:435–52.
18. Halling DB, Aracena-Parks P, Hamilton SL. Regulation of voltage-gated Ca2+ channels by calmodulin. Sci STKE. 2006 Jan 17;2006(318):er1.
19. Davare MA, Avdonin V, Hall DD, Peden EM, Burette A, Weinberg RJ, et al. A beta2 adrenergic receptor signaling complex assembled with the Ca^{2+} channel Cav1.2. Science. 2001;293:98–101.
20. Splawski I, Timothy KW, Sharpe LM, Decher N, Kumar P, Bloise R, et al. Ca(V)1.2 calcium channel dysfunction causes a multisystem disorder including arrhythmia and autism. Cell. 2004;119:19–31.
21. Hockerman GH, Peterson BZ, Johnson BD, Catterall WA. Molecular determinants of drug binding and action on L-type calcium channels. Annu Rev Pharmacol Toxicol. 1997;37:361–96.
22. Parekh AB, Putney JW Jr. Store-operated calcium channels. Physiol Rev. 2005;85:757–810.
23. Montell C, Birnbaumer L, Flockerzi V. The TRP channels, a remarkably functional family. Cell. 2002;108:595–8.
24. Parekh AB, Penner R. Depletion-activated calcium current is inhibited by protein kinase in RBL-2H3 cells. Proc Natl Acad Sci. 1995;USA.92:7907–11.
25. Evans NE, Forth MK, Simpson AK, Mason MJ. Inhibition by calyculin a and okadaic acid of the Ca^{2+} release-activated Ca^{2+} entry pathway in rat basophilic leukemia cells: evidence for regulation by type 1/2A serine/threonine phosphatase activity. Biochim Biophys Acta. 2005;1718:32–43.
26. Schach C, Xu M, Platoshyn O, Keller SH, Yuan JX. Thiol oxidation causes pulmonary vasodilation by activating K^+ channels and inhibiting store-operated Ca^{2+} channels. Am J Physiol Lung Cell Mol Physiol. 2007;292:L685–98.
27. Thompson M, White T, Chini EN. Modulation of store-operated Ca^{2+} entry by cyclic- ADP-ribose. Braz J Med Biol Res. 2006;39:739–48.
28. Denys A, Aires V, Hichami A, Khan NA. Thapsigargin-stimulated MAP kinase phosphorylation via CRAC channels and PLD activation: inhibitory action of docosahexaenoic acid. FEBS Lett. 2004;564:177–82.
29. Machaca K. Ca^{2+}-calmodulin-dependent protein kinase II potentiates store-operated Ca^{2+} current. J Biol Chem. 2003;278:33730–7.
30. Khoo C, Helm J, Choi HB, Kim SU, McLarnon JG. Inhibition of store-operated Ca^{2+} influx by acidic extracellular pH in cultured human microglia. Glia. 2001;36:22–30.
31. Tornquist K, Vainio PJ, Bjorklund S, Titievsky A, Dugue B, Tuominen RK. Hydrogen peroxide attenuates store-operated calcium entry and enhances calcium extrusion in thyroid FRTL-5 cells. Biochem J. 2000;351:47–56.
32. Berra-Romani R, Mazzocco-Spezzia A, Pulina MV, Golovina VA. Ca^{2+} handling is altered when arterial myocytes progress from a contractile to a proliferative phenotype in culture. Am J Physiol Cell Physiol. 2008;295:C779–90.

33. Saini HK, Dhalla NS. Sarcolemmal cation channels and exchangers modify the increase in intracellular calcium in cardiomyocytes on inhibiting Na^+-K^+ ATPase. Am J Physiol Heart Circ Physiol. 2007;293:H169–81.
34. Onohara N, Nishida M, Inoue R, Kobayashi H, Sumimoto H, Sato Y, et al. TRPC3 and TRPC6 are essential for angiotensin II-induced cardiac hypertrophy. EMBO J. 2006;25:5305–16.
35. Inoue R, Jensen LJ, Shi J, Morita H, Nishida M, Honda A, et al. Transient receptor potential channels in cardiovascular function and disease. Circ Res. 2006;99:119–31.
36. Watanabe H, Murakami M, Ohba T, Takahashi Y, Ito H. TRP channel and cardiovascular disease. Pharmacol Ther. 2008;118:337–51.
37. Bootman MD, Rietdorf K. Tissue specificity: store-operated Ca^{2+} entry in cardiac myocytes. Exp Med Biol. 2017;993:363–87.
38. Ruhle B, Trebak M. Emerging roles for native ORAI Ca^{2+} channels in cardiovascular disease. Curr Top Membr. 2013;71:209–35.
39. Bhullar SK, Shah AK, Dhalla NS. Store-operated calcium channels: potential target for the therapy of hypertension. Rev Cardiovasc Med. 2019;20:139–51.
40. Zhang B, Jiang J, Yue Z, Liu S, Ma Y, Yu N, et al. Store-operated Ca^{2+} entry (SOCE) contributes to angiotensin II-induced cardiac fibrosis in cardiac fibroblasts. J Pharmacol Sci. 2016;132:171–80.
41. Kecskés M, Jacobs G, Kerselaers S, Syam N, Menigoz A, Vangheluwe P, et al. The Ca^{2+-}activated cation channel TRPM4 is a negative regulator of angiotensin II-induced cardiac hypertrophy. Basic Res Cardiol. 2015;110:43.
42. Ji Y, Guo X, Zhang Z, Huang Z, Zhu J, Chen QH, et al. CaMKIIδ meditates phenylephrine induced cardiomyocyte hypertrophy through store-operated Ca^{2+} entry. Cardiovasc Pathol. 2017;27:9–17.
43. Domínguez-Rodríguez A, Ruiz-Hurtado G, Sabourin J, Gómez AM, Alvarez JL, Benitah JP. Proarrhythmic effect of sustained EPAC activation on TRPC3/4 in rat ventricular cardiomyocytes. J Mol Cell Cardiol. 2015;87:74–8.
44. Ohba T, Watanabe H, Murakami M, Takahashi Y, Iino K, Kuromitsu S, et al. Upregulation of TRPC1 in the development of cardiac hypertrophy. J Mol Cell Cardiol. 2007;42:498–507.
45. Sabourin J, Bartoli F, Antigny F, Gomez AM, Benitah JP. Transient receptor potential canonical (TRPC)/Orai1-dependent store-operated Ca^{2+} channels: new targets of aldosterone in cardiomyocytes. J Biol Chem. 2016;291:13394–409.
46. Ottolia M, Torres N, Bridge JH, Philipson KD, Goldhaber JI. Na/ca exchange and contraction of the heart. J Mol Cell Cardiol. 2013;61:28–33.
47. Aronsen JM, Swift F, Sejersted OM. Cardiac sodium transport and excitation contraction coupling. J Mol Cell Cardiol. 2013;61:11–9.
48. Shattock MJ, Ottolia M, Bers DM, Blaustein MP, Boguslavskyi A, Bossuyt J, et al. Na^+/Ca^{2+} exchange and Na^+/K^+-ATPase in the heart. J Physiol. 2015;593:1361–82.
49. Hilgemann DW, Yaradanakul A, Wang Y, Fuster D. Molecular control of cardiac sodium homeostasis in health and disease. J Cardiovasc Electrophysiol. 2006;17:S47–56.
50. Cheung JY, Rothblum LI, Moorman JR, Tucker AL, Song J, Ahlers BA, et al. Regulation of cardiac Na^+/Ca^{2+} exchanger by phospholemman. Ann N Y Acad Sci. 2007;1099:119–34.
51. Karmazyn M, Gan XT, Humphreys RA, Yoshida H, Kusumoto K. The myocardial Na^+-H^+ exchange: structure, regulation, and its role in heart disease. Circ Res. 1999;85:777–86.
52. Saini HK, Tripathi ON, Zhang S, Elimban V, Dhalla NS. Involvement of Na^+/Ca^{2+} exchanger in catecholamine-induced increase in intracellular calcium in cardiomyocytes. Am J Physiol Heart Circ Physiol. 2006;290:H373–80.
53. Wei SK, Ruknudin AM, Shou M, McCurley JM, Hanlon SU, Elgin E, et al. Muscarinic modulation of the sodium-calcium exchanger in heart failure. Circulation. 2007;115:1225–33.
54. Shao Q, Ren B, Elimban V, Tappia PS, Takeda N, Dhalla NS. Modification of sarcolemmal Na^+-K^+-ATPase and Na^+/Ca^{2+} exchanger expression in heart failure by blockade of renin-angiotensin system. Am J Physiol Heart Circ Physiol. 2005;288:H2637–46.
55. Iwamoto T. Forefront of Na^+/Ca^{2+} exchanger studies: molecular pharmacology of Na^+/Ca^{2+} exchange inhibitors. J Pharmacol Sci. 2004;96:27–32.
56. Fong SPT, Agrawal S, Gong M, Zhao J. Modulated calcium homeostasis and release events under atrial fibrillation and its risk factors: a meta-analysis. Front Cardiovasc Med. 2021;8:662914.
57. Christ T, Kovács PP, Acsai K, Knaut M, Eschenhagen T, et al. Block of Na^+/Ca^{2+} exchanger by SEA0400 in human right atrial preparations from patients in sinus rhythm and in atrial fibrillation. Eur J Pharmacol. 2016;788:286–93.
58. Iwamoto T, Kita S, Uehara A, Imanaga I, Matsuda T, Baba A, et al. Molecular determinants of Na^+/Ca^{2+} exchange (NCX1) inhibition by SEA0400. J Biol Chem. 2004;279:7544–53.
59. Namekata I, Nakamura H, Shimada H, Tanaka H, Shigenobu K. Cardioprotection without cardiosuppression by SEA0400, a novel inhibitor of Na^+-Ca^{2+} exchanger, during ischemia and reperfusion in Guinea-pig myocardium. Life Sci. 2005;77: 312–24.
60. Fliegel L. Regulation of myocardial Na^+/H^+ exchanger activity. Basic Res Cardiol. 2001;96: 301–5.
61. Odunewu-Aderibigbe A, Fliegel L. The Na^+/H^+ exchanger and pH regulation in the heart. IUBMB Life. 2014;66:679–85.

62. Slepkov ER, Rainey JK, Sykes BD, Fliegel L. Structural and functional analysis of the Na^+/H^+ exchanger. Biochem J. 2007;401:623–33.
63. Aharonovitz O, Zaun HC, Balla T, York JD, Orlowski J, Grinstein S. Intracellular pH regulation by Na^+/H^+ exchange requires phosphatidylinositol 4,5-bisphosphate. J Cell Biol. 2000;150:213–24.
64. Zaun HC, Shrier A, Orlowski J. Calcineurin B homologous protein 3 promotes the biosynthetic maturation, cell surface stability, and optimal transport of the Na^+/H^+ exchanger NHE1 isoform. J Biol Chem. 2008;283:12456–67.
65. Bertrand B, Wakabayashi S, Ikeda T, Pouyssegur J, Shigekawa M. The Na^+/H^+ exchanger isoform 1 (NHE1) is a novel member of the calmodulin-binding proteins. Identification and characterization of calmodulin-binding sites. J Biol Chem. 1994;269: 13703–9.
66. Wakabayashi S, Bertrand B, Ikeda T, Pouyssegur J, Shigekawa M. Mutation of calmodulin-binding site renders the Na^+/H^+ exchanger (NHE1) highly H^+-sensitive and Ca^{2+} regulation-defective. J Biol Chem. 1994;269:13710–5.
67. Li X, Alvarez B, Casey JR, Reithmeier RA, Fliegel L. Carbonic anhydrase II binds to and enhances activity of the Na^+/H^+ exchanger. J Biol Chem. 2002;277:36085–91.
68. Malo ME, Fliegel L. Physiological role and regulation of the Na^+/H^+ exchanger. Can J Physiol Pharmacol. 2006;84:1081–95.
69. Sardet C, Counillon L, Franchi A, Pouyssegur J. Growth factors induce phosphorylation of the Na^+/H^+ antiporter, glycoprotein of 110 kD. Science. 1990;247:723–6.
70. Phan VN, Kusuhara M, Lucchesi PA, Berk BC. A 90-kD Na^+-H^+ exchanger kinase has increased activity in spontaneously hypertensive rat vascular smooth muscle cells. Hypertension. 1997;29:1265–7122.
71. Takahashi E, Abe J, Berk BC. Angiotensin II stimulates p90rsk in vascular smooth muscle cells. A potential Na^+-H^+ exchanger kinase. Circ Res. 1997;81:268–73.
72. Scholz W, Albus U, Counillon L, Gogelein H, Lang HJ, Linz W, et al. Protective effects of HOE642, a selective sodium-hydrogen exchange subtype 1 inhibitor, on cardiac ischaemia and reperfusion. Cardiovasc Res. 1995;29:260–8.
73. Chaitman BR. A review of the GUARDIAN trial results: clinical implications and the significance of elevated perioperative CK-MB on 6-month survival. J Card Surg. 2003;18(Suppl 1):13–20.
74. Mentzer J, Lasley RD, Jessel A, Karmazyn M. Intracellular sodium hydrogen exchange inhibition and clinical myocardial protection. Ann Thorac Surg. 2003;75:S700–8.
75. Gazmuri RJ, Radhakrishnan J, Ayoub IM. Sodium-hydrogen exchanger isoform-1 inhibition: A promising pharmacological intervention for resuscitation from cardiac arrest. Molecules. 24 pii: E1765, 2019.
76. Fliegel L. Molecular biology of the myocardial Na^+/H^+ exchanger. J Mol Cell Cardiol. 2008;44:228–37.
77. Nakamura TY, Iwata Y, Arai Y, Komamura K, Wakabayashi S. Activation of Na^+/H^+ exchanger 1 is sufficient to generate Ca^{2+} signals that induce cardiac hypertrophy and heart failure. Circ Res. 2008;103:891–9.
78. Yeves AM, Ennis IL. Na^+/H^+ exchanger and cardiac hypertrophy. Hipertens. Riesgo. Vasc. pii: S1889–183730055-8, 2019.
79. Skou JC. The influence of some cations on an adenosine triphosphatase from peripheral nerves. Biochim Biophys Acta. 1957;23:394–401.
80. Liu CC, Fry NA, Hamilton EJ, Chia KK, Garcia A, et al. Redox-dependent regulation of the Na^+-K^+ pump: new twists to an old target for treatment of heart failure. J Mol Cell Cardiol. 2013;61:94–101.
81. Kryvenko V, Vagin O, Dada LA, Sznajder JI, Vadász I. Maturation of the Na,K-ATPase in the endoplasmic reticulum in health and disease. J Membr Biol. 2021;10:1–11.
82. Takeyasu K, Okamura H, Yasuhara JC, Ogita Y, Yoshimura SH. P-type ATPase diversity and evolution: the origins of ouabain sensitivity and subunit assembly. Cell Mol Biol. 2001;47:325–33.
83. Blanco G, Mercer RW. Isozymes of the Na^+-K^+-ATPase: heterogeneity in structure, diversity in function. Am J Phys. 1998;275:F633–50.
84. Sweadner KJ, Herrera VL, Amato S, Moellmann A, Gibbons DK, Repke KR. Immunologic identification of Na^+-K^+-ATPase isoforms in myocardium. Isoform change in deoxycorticosterone acetate-salt hypertension. Circ Res. 1994;74:669–78.
85. Karmazyn M, Tuana BS, Dhalla NS. Effect of prostaglandins on rat heart sarcolemmal ATPases. Can J Physiol Pharmacol. 1981;59:1122–7.
86. Pierce GN, Ganguly PK, Dzurba A, Dhalla NS. Modification of the function of cardiac subcellular organelles by insulin. Adv Myocardiol. 1985;6: 113–25.
87. Moffat MP, Dhalla NS. Heart sarcolemmal ATPase and calcium binding activities in rats fed a high cholesterol diet. Can J Cardiol. 1985;1:194–200.
88. Gupta MP, Makino N, Takeo S, Kaneko M, Dhalla NS. Cardiac sarcolemma as a possible site of action of caffeine in rat heart. J Pharmacol Exp Ther. 1990;255:1188–94.
89. Tian J, Xie ZJ. The Na-K-ATPase and calcium-signaling microdomains. Physiology. 2008;23:205–11.
90. Netticadan T, Kato K, Tappia P, Elimban V, Dhalla NS. Phosphorylation of cardiac Na^+-K^+ ATPase by Ca^{2+}/calmodulin dependent protein kinase. Biochem Biophys Res Commun. 1997;238:544–8.
91. Dixon IM, Hata T, Dhalla NS. Sarcolemmal calcium transport in congestive heart failure due to

myocardial infarction in rats. Am J Physiol Heart Circ Physiol. 1992;262:H1387–94.

92. Guo X, Wang J, Elimban V, Dhalla NS. Both enalapril and losartan attenuate sarcolemmal Na^{+}-K^{+}-ATPase remodeling in failing rat heart due to myocardial infarction. Can J Physiol Pharmacol. 2008;86:139–47.
93. Dhalla NS, Panagia V, Singal PK, Makino N, Dixon IM, Eyolfson DA. Alterations in heart membrane calcium transport during the development of ischemia-reperfusion injury. J Mol Cell Cardiol. 1988;20(Suppl 2):3–13.
94. Ostadal P, Elmoselhi AB, Zdobnicka I, Lukas A, Chapman D, Dhalla NS. Ischemia- reperfusion alters gene expression of Na^{+}-K^{+}-ATPase isoforms in rat heart. Biochem Biophys Res Commun. 2003;306: 457–62.
95. Ostadal P, Elmoselhi AB, Zdobnicka I, Lukas A, Elimban V, Dhalla NS. Role of oxidative stress in ischemia-reperfusion-induced changes in Na^{+}-K^{+}-ATPase isoform expression in rat heart. Antioxid Redox Signal. 2004;6:914–23.
96. Elmoselhi AB, Lukas A, Ostadal P, Dhalla NS. Preconditioning attenuates ischemia-reperfusion-induced remodeling of Na^{+}-K^{+}-ATPase in hearts. Am J Physiol Heart Circ Physiol. 2003;285:H1055–63.
97. Shao Q, Matsubara T, Bhatt SK, Dhalla NS. Inhibition of cardiac sarcolemma Na^{+}-K^{+}-ATPase by oxyradical generating systems. Mol Cell Biochem. 1995;147:139–44.
98. Srikanthan K, Shapiro JI, Sodhi K. The role of Na/K-ATPase signaling in oxidative stress related to obesity and cardiovascular disease. Molecules. 21. pii: E1172, 2016.
99. Botelho AFM, Pierezan F, Soto-Blanco B, Melo MM. A review of cardiac glycosides: structure, toxicokinetics, clinical signs, diagnosis and antineoplastic potential. Toxicon. 2019;158:63–8.
100. Wang HY, O’Doherty GA. Modulators of Na/K-ATPase: a patent review. Expert Opin Ther Pat. 2012;22:587–605.
101. Crambert G, Hasler U, Beggah AT, Yu C, Modyanov NN, Horisberger JD, et al. Transport and pharmacological properties of nine different human Na, K-ATPase isozymes. J Biol Chem. 2000;275:1976–86.
102. Hilgemann DW, Ball R. Regulation of cardiac Na^{+}, Ca^{2+} exchange and KATP potassium channels by PIP2. Science. 1996;273:956–9.
103. Schoner W, Scheiner-Bobis G. Endogenous and exogenous cardiac glycosides and their mechanisms of action. Am J Cardiovasc Drugs. 2007;7:173–89.
104. Hamlyn JM, Ringel R, Schaeffer J, Levinson PD, Hamilton BP, Kowarski AA, et al. A circulating inhibitor of (Na^{+}-K^{+}) ATPase associated with essential hypertension. Nature. 1982;300:650–2.
105. Hamlyn JM, Lu ZR, Manunta P, Ludens JH, Kimura K, Shah JR, et al. Observations on the nature, biosynthesis, secretion and significance of endogenous ouabain. Clin Exp Hypertens. 1998;20:523–33.
106. Qazzaz HM, Cao Z, Bolanowski DD, Clark BJ, Valdes R Jr. De novo biosynthesis and radiolabeling of mammalian digitalis-like factors. Clin Chem. 2004;50:612–20.
107. Golfman L, Dixon IM, Takeda N, Lukas A, Dakshinamurti K, Dhalla NS. Cardiac sarcolemmal Na^{+}-Ca^{2+} exchange and Na^{+}-K^{+} ATPase activities and gene expression in alloxan-induced diabetes in rats. Mol Cell Biochem. 1998;188:91–101.
108. Kato K, Chapman DC, Rupp H, Lukas A, Dhalla NS. Alterations of heart function and Na^{+}-K^{+}-ATPase activity by etomoxir in diabetic rats. J Appl Physiol. 1999;86:812–8.
109. Kato K, Lukas A, Chapman DC, Dhalla NS. Changes in the expression of cardiac Na^{+}-K^{+} ATPase subunits in the UM-X7.1 cardiomyopathic hamster. Life Sci. 2000;67:1175–83.
110. Kato K, Lukas A, Chapman DC, Rupp H, Dhalla NS. Differential effects of etomoxir treatment on cardiac Na^{+}-K^{+} ATPase subunits in diabetic rats. Mol Cell Biochem. 2002;232:57–62.
111. Axelsen KB, Palmgren MG. Evolution of substrate specificities in the P-type ATPase superfamily. J Mol Evol. 1998;46:84–101.
112. Strehler EE, Filoteo AG, Penniston JT, Caride AJ. Plasma-membrane Ca^{2+} pumps: structural diversity as the basis for functional versatility. Biochem Soc Trans. 2007;35:919–22.
113. Strehler EE, Caride AJ, Filoteo AG, Xiong Y, Penniston JT, Enyedi A. Plasma membrane Ca^{2+} ATPases as dynamic regulators of cellular calcium handling. Ann N Y Acad Sci. 2007;1099:226–36.
114. Carafoli E, Stauffer T. The plasma membrane calcium pump: functional domains, regulation of the activity, and tissue specificity of isoform expression. J Neurobiol. 1994;25:312–24.
115. Okunade GW, Miller ML, Pyne GJ, Sutliff RL, O'Connor KT, Neumann JC, et al. Targeted ablation of plasma membrane Ca^{2+}-ATPase (PMCA) 1 and 4 indicates a major housekeeping function for PMCA1 and a critical role in hyperactivated sperm motility and male fertility for PMCA4. J Biol Chem. 2004;279:33742–50.
116. Gros R, Afroze T, You XM, Kabir G, Van WR, Kalair W, et al. Plasma membrane calcium ATPase overexpression in arterial smooth muscle increases vasomotor responsiveness and blood pressure. Circ Res. 2003;93:614–21.
117. Piuhola J, Hammes A, Schuh K, Neyses L, Vuolteenaho O, Ruskoaho H. Overexpression of sarcolemmal calcium pump attenuates induction of cardiac gene expression in response to ET-1. Am J Physiol Regul Integr Comp Physiol. 2001;281: R699–705.
118. Oceandy D, Buch MH, Cartwright EJ, Neyses L. The emergence of plasma membrane calcium pump as a

novel therapeutic target for heart disease. Mini Rev Med Chem. 2006;6:583–38.

119. Lakatta EG, Vinogradova TM, Maltsev VA. The missing link in the mystery of normal automaticity of cardiac pacemaker cells. Ann N Y Acad Sci. 2008;1123:41–57.
120. Dhalla NS, Saini-Chohan HK, Rodriguez-Leyva D, Elimban V, Dent MR, Tappia PS. Subcellular remodelling may induce cardiac dysfunction in congestive heart failure. Cardiovasc Res. 2008;81: 429–38.
121. Undrovinas A, Maltsev VA. Late sodium current is a new therapeutic target to improve contractility and rhythm in failing heart. Cardiovasc Hematol Agents Med Chem. 2008;6:348–59.
122. Sanguinetti MC, Bennett PB. Antiarrhythmic drug target choices and screening. Circ Res. 2003;93: 491–9.
123. Yang B, Lin H, Xiao J, Lu Y, Luo X, Li B, et al. The muscle-specific microRNA miR-1 regulates cardiac arrhythmogenic potential by targeting GJA1 and KCNJ2. Nat Med. 2007;13:486–91.

21

Characteristics of Intracellular Ca^{2+} Handling Proteins in Heart Function in Health and Disease

Naranjan S. Dhalla, Mohamad Nusier, Anureet K. Shah, and Paramjit S. Tappia

Abstract

In view of its ability to release and accumulate Ca^{2+}, the sarcoplasmic reticulum (SR) plays a major role in cardiomyocyte excitation–contraction coupling. Since Ca^{2+} is important in the functions of both mitochondria and nucleus, it appears that these organelles are involved in excitation–metabolism coupling and excitation–transcription coupling. This brief article discusses some of the characteristics of the SR, mitochondria, and nucleus with respect to their Ca^{2+} transport systems in cardiomyocytes and the role of Ca^{2+} in different coupling processes. In addition, the influence of fluctuations in the cytoplasmic Ca^{2+} concentration on cardiomyocyte contractile activity, metabolism, and gene expression in heart disease is presented. The potential of the SR and the mitochondria and nucleus as therapeutic targets for the treatment of heart disease is also highlighted.

Keywords

Heart · Excitation–contraction coupling · Excitation–metabolism coupling · Excitation–transcription coupling · Intracellular Ca^{2+} handling · Mitochondria · Nucleus · Sarcoplasmic reticulum · SERCA · Ryanodine receptors · Inositol trisphosphate receptor

21.1 Introduction

The precise control of intracellular Ca^{2+} cycling depends on the relationships among various channels and pumps that are involved in different membranous systems of cardiomyocytes. Accordingly, two significant aspects have been proposed: (a) structural coupling in which the transporters are organized within the dyad, linking the transverse tubule and sarcoplasmic reticulum and ensuring proximity of Ca^{2+} entry to sites of release and (b) functional coupling, where the fluxes across all membranes must be balanced such that, in the steady state, Ca^{2+} influx equals Ca^{2+} efflux on every beat [1]. Depolarization of the cardiomyocyte causes Ca^{2+} influx through the sarcolemmal membrane (SL) L-type Ca^{2+} channels (LTCCs), which subsequently elicits a greater release of Ca^{2+} upon activation of the sarcoplasmic reticulum (SR), ryanodine

---

N. S. Dhalla (✉) · M. Nusier
Institute of Cardiovascular Sciences, St. Boniface Hospital Albrechtsen Research Centre & Department of Physiology and Pathophysiology, College of Medicine, Rady Faculty of Health Sciences, University of Manitoba, Winnipeg, MB, Canada
e-mail: nsdhalla@sbrc.ca

A. K. Shah
Department of Kinesiology and Nutritional Sciences, California State University, Los Angeles, CA, USA

P. S. Tappia
Asper Clinical Research Institute, St. Boniface Hospital, Winnipeg, MB, Canada

© Springer Nature Switzerland AG 2023
O. N. Tripathi et al. (eds.), *Heart Rate and Rhythm*, https://doi.org/10.1007/978-3-031-33588-4_21

receptors (RyR), or Ca^{2+}-release channels. This increase in Ca^{2+} in the cytosol is rapidly dissipated by four mechanisms: (a) Ca^{2+} binding by proteins such as calmodulin and troponin [2], (b) Ca^{2+} efflux through SL or plasma membrane Ca^{2+}-pump ATPase (PMCA) and SL Na^{+}–Ca^{2+} exchanger (NCX), (c) storage in the SR by SR Ca^{2+}-pump ATPase (SERCA), and (d) Ca^{2+} buffering by intracellular organelles such as mitochondria and nucleus [3]. In this regard, the uptake of Ca^{2+} by the mitochondria occurs mainly through the mitochondrial Ca^{2+} uniporter (mCUP), while the nucleoplasmic reticulum serves as a Ca^{2+} storing site in the nucleus [4].

It is now well known that the process of cardiac contraction is initiated by the release of Ca^{2+} from the SR, whereas the process of relaxation is associated with Ca^{2+} uptake by the SR in cardiomyocytes. Furthermore, SR is also known to possess inositol trisphosphate receptors (IP$_3$R), the activation of which is considered to release Ca^{2+} in the cardiomyocyte [5, 6]. Fluctuations in the cytosolic levels of Ca^{2+} affect mitochondrial metabolism that may contribute to the pathogenesis of congestive heart failure (CHF) and ischemic heart disease (IHD) [5]. Cytosolic Ca^{2+} is also considered to regulate myocardial gene expression during subcellular remodeling in ischemia-reperfusion (I-R) injury, cardiac hypertrophy, and CHF [6, 7]. Accordingly, this chapter is intended to discuss the major characteristics of the Ca^{2+}-handling and regulatory proteins such as SR RyR, SR Ca^{2+}-pump ATPase, and IP$_3$R. Furthermore, the coupling of Ca^{2+} to the cardiac contraction–relaxation cycle, Ca^{2+} to mitochondrial metabolism, and Ca^{2+} to nuclear transcription is described following the excitation of cardiomyocytes. In addition, their role in the pathophysiology of different myocardial diseases will be briefly discussed, and the potential of the SR, mitochondria, and nucleus as therapeutic targets for heart disease will be highlighted.

21.2 Excitation–Contraction Coupling

The excitation–contraction (E–C) unit comprises synergistic lines of communication between the SL and SR [8]. Since the major functions of the SR are the release of Ca^{2+} for cardiac contraction upon excitation and uptake of Ca^{2+} for cardiac relaxation, it is planned to describe the characteristics as well as the role of SR Ca^{2+}-release channel, SR Ca^{2+}-pump ATPase and SR IP$_3$R (Fig. 21.1) in Ca^{2+} handling and regulation of the intracellular concentration of Ca^{2+} ([Ca^{2+}]$_i$) in cardiomyocytes.

21.2.1 SR Ca^{2+}-release Channel

The SR RyR or Ca^{2+}-release channel is a 564 kDa tetrameric protein consisting of at least four transmembrane segments and a large cytoplasmic domain. Three isoforms have been identified, namely, RyR1 and RyR3 in skeletal muscle and RyR2 in cardiac muscle; these isoforms share up to 60% sequence homology. RyR in cardiac muscle is organized in groups of approximately 20 receptors each. It has been suggested that the close approximation of these receptors is required

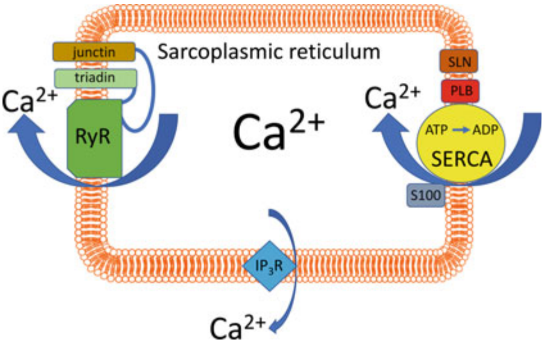

Fig. 21.1 Schematic representation of SR Ca^{2+}-handling proteins involved in the regulation of the intracellular concentration of Ca^{2+} in cardiomyocytes. *RyR* ryanodine receptor, *PLB* phospholamban, *SERCA* sarcoplasmic reticulum Ca^{2+}- pump ATPase, *IP$_3$R* inositol trisphoshate receptor

for orchestrated opening and closing of the Ca^{2+}-release channels [9]. Ca^{2+} has a biphasic effect on RyR; submicromolar Ca^{2+} concentrations activate RyR, whereas higher Ca^{2+} concentrations (>1 μM) inhibit the channel. RyR is inhibited by cytosolic Mg^{2+} but an increase in cytosolic Ca^{2+} relieves the Mg^{2+} inhibition [10]. RyR is also modulated by several cytosolic proteins; however, the most thoroughly studied modulators are calmodulin (CaM), calmodulin kinase (CaMKII), protein kinase A (PKA), and protein phosphatases. CaM binding to RyR is Ca^{2+} dependent, where Ca^{2+} binding increases the sensitivity of RyR to CaM. CaM binding inhibits the cardiac RyR in the presence of high concentration of Ca^{2+} (10 μM). Several kinases have been shown to affect the activity of cardiac RyR. These include protein kinase A, C, and G in addition to the CaM-activated CaMKII [6, 10]. The RyR phosphorylation is of great importance in the pathogenesis of heart failure and arrhythmias [11]. Hyperphosphorylation of RyR in heart failure leads to the dissociation of "calstabin", an accessory protein that stabilizes the closed conformation of the channel [12]. Phosphorylation of RyR cannot be interpreted in isolation from other SR proteins such as the Ca^{2+}-pump ATPase (SERCA) and phospholamban (PLB). PLB phosphorylation activates SERCA and increases the SR Ca^{2+} load, which then stimulates RyR [13]. While the overall effect of phosphorylation is stimulatory, protein phosphatases are inhibitory [10]. In addition to kinases and phosphatases, several other cytoplasmic proteins are considered to modulate the activity of cardiac RyR. These include the transmembrane proteins, junctin and triadin, and the cytosolic proteins, S100, sorcin, glutathione transferase as well as intracellular chloride ion channels, glycolytic enzymes, and the accessory protein, calstabin [14].

Mutations in cardiac RyR have been linked to the development of premature heartbeats. A "leaky" RyR promotes the buildup of Ca^{2+} in the cytosol and subsequently triggers the SL NCX to remove the excess Ca^{2+} in exchange for Na^{+}; this then depolarizes the cell membrane leading to extrasystolic depolarizations and premature beats. On the other hand, adrenergic stimulation leading to the phosphorylation of RyR can cause fatal arrhythmias such as catecholaminergic polymorphic ventricular tachycardia (CPVT) in susceptible individuals. Susceptibility to CPVT was linked mainly to autosomal dominant mutations of RyR2; these mutations destabilize the channel or impair the binding to calstabin that stabilizes RyR [15, 16]. Recently, a mutation linked to the development of CPVT (R2474S) was found to produce "leaky" RyR in the heart and to the development of CPVT in transgenic mice. It has been shown that these RyRs could be stabilized by a novel compound, S107, for averting fatal arrhythmias [17]. Interestingly, the expression of RyR is reduced in heart failure due to the development of myocardial infarction (MI); this change is believed to be mediated through angiotensin receptors because it is inhibited by angiotensin-converting enzymes (ACE) inhibitors such as imidapril and in fact, close involvement of the SR RyR in the cellular remodeling process has been suggested [18]. In addition to suppressing cardiac hypertrophy, ACE inhibitor therapy has been shown to decrease the hyperadrenergic state associated with heart failure, resulting in a reduction of PKA activity, which abolishes the phosphorylation of RyR. Furthermore, ACE inhibitors have been reported to promote the interaction of RyR with the accessory protein calstabin, which stabilizes the channel and reduces the RyR leak [19].

21.2.2 SR Ca^{2+}-Pump ATPase

Most of the Ca^{2+} released from SR stores is rapidly taken up again via the SR Ca^{2+}-pump ATPase (SERCA), while the rest is extruded from the cell by the PMCA and SL NCX. The SERCA transports two Ca^{2+} ions for the hydrolysis of a single ATP molecule [19]. SERCA is organized into three interacting domains: the cytosolic nucleotide-binding domain, the phosphorylation domain containing Asp351, and the transmembrane translocation domain. The cytosolic and transmembrane domains consist of

10 transmembrane segments, which are connected by the stalk domain [20]. At least six isoforms of SERCA have been identified belonging to three different gene families, namely, SERCA1, 2, and 3; cardiomyocytes express the SERCA2a isoform [21]. The SERCA activity is regulated by SR-associated phospholamban (PLB). In this regard, the dephosphorylated form of PLB inhibits the pump by interacting with the enzyme phosphorylation site, which is needed for ATP binding, whereas phosphorylation of PLB by PKA or CaMK relieves this inhibition [22]. During adrenergic stimulation, PKA reduces the affinity of Ca^{2+}-pump ATPase for Ca^{2+} and thus enhances cardiac muscle relaxation. The adrenergic stimulation of the heart enhances the SERCA activity and such a regulatory action has been suggested to be a compensatory mechanism to improve cardiac performance.

Sarcolipin is another modulator of SERCA activity [23]. Sarcolipin is a shorter homologue (31 amino acids) of PLB, which inhibits SERCA. However, unlike PLB, the level of expression of sarcolipin determines its interaction with SERCA rather than its phosphorylation level. It has been found that sarcolipin modulates SERCA in a Ca^{2+}-dependent manner; at low Ca^{2+} levels, sarcolipin reduces its affinity for Ca^{2+} and thus inhibits its activity, whereas at high Ca^{2+} levels, it increases its affinity for Ca^{2+} by increasing the maximum turnover rate [24]. Sarcolipin and PLB both synergistically inhibit SERCA; coexpression of sarcolipin in HEK cells leads to a very strong inhibition of the SERCA activity, whereas a sarcolipin knockout leads to enhanced SERCA activity [25]. On the other hand, the S100 protein, which is abundantly expressed in the heart and skeletal muscle, is believed to stimulate Ca^{2+} uptake by SERCA2a through a direct protein–protein interaction [26].

In cardiac hypertrophy and heart failure, the levels of SERCA expression as well as the SERCA activity have been found to be reduced, leading to compromised SR function [27]. In fact, overexpression of SERCA can improve cardiac functional defects [28]. In heart failure, a reduction in the SERCA activity by about 50% was evident without any changes in the creatine kinase activity and mitochondrial functions [29]. While several studies have indicated a role for SERCA in heart function, heterozygous loss of function of the SERCA2a and 2b in Darier disease was not associated with any defects in cardiac performance [30, 31].

21.2.3 SR Inositol Trisphosphate Receptors

Although IP_3R plays a minor role in EC coupling compared to the RyR in ventricular cardiomyocytes [32, 33], the higher (3.5–10 fold) IP_3R expression in atrial myocytes vs. ventricular myocytes, is suggestive of a greater role of IP_3R in atrial contraction [34]. There are several isoforms of the IP_3R in both excitable and non-excitable tissues; the heart expresses the 300 KDa IP_3R2 isoform that co-assembles to form a tetrameric channel. The channel is predicted to have six transmembrane segments and a large regulatory cytoplasmic domain [35]. IP_3R1 is regulated by Ca^{2+} in a biphasic pattern similar to the RyR. In fact, it is activated by submicromolar concentration of Ca^{2+} (<300 nM) and inhibited by micromolar concentrations of Ca^{2+} (>1 μM). The cardiac IP_3R2 is resistant to inhibition by high Ca^{2+}, as it remains active in the presence of high Ca^{2+} concentration (>100 μM) [36, 37]. The IP_3R is modulated by cytosolic proteins such as calstabin, PKA, and CaM [38]. The most significant interaction of IP_3R is with CaM, because Ca^{2+}-free CaM inhibits the cardiac IP_3R2 in a Ca^{2+}-independent manner, indicating a permanent inhibition of these receptors by CaM in the absence of Ca^{2+} [39]. The development and progression of cardiac hypertrophy have been linked to increases in the phospholipase C-IP_3R expression levels leading to a stimulation of hypertrophic gene transcription. IP_3R2 has been shown to be upregulated, while, in contrast, a reduction in RyR2 expression and activity has been reported in heart failure [34]. In addition, the relative abundance of IP_3R in Purkinje fibers suggests its potential participation in ventricular arrhythmias

[40], however; the precise role of IP_3R in the generation of ventricular arrhythmias remains to be fully elucidated.

In addition to the role of SR in Ca^{2+}-handling in cardiomyocytes, other cellular structures can also be seen to participate in the process of excitation–contraction–relaxation cycle. It should be mentioned that induced pluripotent stem cell-derived cardiomyocytes (iPSC-CMs) hold enormous potential in many fields of cardiovascular research. Overcoming many of the limitations of their embryonic counterparts, the application of iPSC-CMs ranges from facilitating the investigation of familial cardiac disease and pharmacological toxicity screening to personalized medicine and autologous cardiac cell therapies. The main factor preventing the full realization of this potential is the limited maturity of iPSC-CMs, which display a number of substantial differences in comparison to adult cardiomyocytes. E–C coupling, a fundamental property of cardiomyocytes, is often described in iPSC-CMs as being more analogous to neonatal than adult cardiomyocytes. With Ca^{2+}-handling linked, directly or indirectly to almost all other properties of cardiomyocytes, a solid understanding of this process will be crucial to fully realizing the potential of human iPSC-CMs [41].

21.3 Excitation–Metabolism Coupling

E–C coupling consumes a large amount of energy through myosin ATPase, the SL Na^+-K^+ ATPase, and SERCA activities [6]. On the other hand, the mitochondria are the main source of energy production. Mitochondria take up to 30% of the myocyte volume and are present in close proximity to the contractile machinery where energy is most required [42]. Indeed, $[Ca^{2+}]_i$ concentration in different cellular compartments is intimately linked to cell metabolism, because (a) ATP production requires low Ca^{2+}, (b) Ca^{2+} homeostatic systems consume ATP, and (c) Ca^{2+} signals in mitochondria stimulate ATP synthesis, being an essential part of excitation-metabolism (E-M) coupling [43]. The regulation of mitochondrial metabolism by Ca^{2+} is attributed to three key enzymes in the citric acid cycle, namely pyruvate dehydrogenase, isocitrate dehydrogenase, and α-ketoglutarate dehydrogenase, which are activated by low concentrations of Ca^{2+} [44]; in addition, Ca^{2+} also activates the mitochondrial F_1/F_0 ATPase [45].

Mitochondria in cardiac muscles also possess the molecular components for efficient uptake and release of Ca^{2+}. In this regard, Ca^{2+} enters the mitochondrial membrane through the mitochondrial Ca^{2+} uniporter (mCUP), a low affinity (10–20 μM Ca^{2+}) and highly selective ion channel, which accumulates Ca^{2+} in the mitochondria using the potential difference across the mitochondrial membrane; the mCUP is Ca^{2+}-gated and requires calmodulin for its activation [46]. Although mitochondria are generally considered to serve as a Ca^{2+} sink, mitochondrial Ca^{2+} uptake is inhibited by high concentrations of cytosolic Ca^{2+} [47]. Ca^{2+} is extruded from mitochondria through the activity of mitochondrial Na^+-Ca^{2+} exchanger (mNCX), which is believed to possess a stoichiometry similar to that of the SL NCX of three Na^+ to one Ca^{2+} [48]. Since the Ca^{2+} extrusion mechanism is slower relative to the rate of Ca^{2+} entry, this leads to the accumulation of Ca^{2+} in the mitochondria [49]. Ca^{2+} and mitochondria may also be intimately linked to cardiac function as Ca^{2+} is central to cardiac excitation–contraction coupling and stimulates mitochondrial energy production to fuel contraction. It should be mentioned that under conditions of dysregulated Ca^{2+} cycling, mitochondrial Ca^{2+} overload activates cell death pathways [50]. Indeed, excessive accumulation of Ca^{2+} in the mitochondria may induce the translocation of cytochrome C as well as other pro-apoptotic factors [51]. Thus, taken together, the mitochondrial Ca^{2+} microdomain is where contraction, energy, and cardiomyocyte death converge [50, 52].

Studies have shown that increases in mitochondrial $[Ca^{2+}]$ occur simultaneously with the increase in cytosolic $[Ca^{2+}]$ in response to an increase in cardiomyocyte pacing or β-adrenergic stimulation [53, 54]. The rise of mitochondrial $[Ca^{2+}]$ was shown to be dependent on the rise of cytosolic Ca^{2+} in the proximity of the SR, suggesting that mitochondria may also accumulate some of the Ca^{2+} released by the SR [55]. The ability of mitochondria to sense Ca^{2+} in a microdomain rather than the whole cytosol is predicted in modeling studies [56] and can explain the high threshold for Ca^{2+} uptake by the mCUP (1–3 μM). Indeed, localized Ca^{2+} sparks (synchronous coordinated activity of 30–100 RyR) elicit miniature mitochondrial matrix Ca^{2+} signals that last less than 500 ms [55]. The rapid buffering of cytosolic Ca^{2+} by mitochondria may be due to mCUP activity [57] or may be due to some other mechanism, which remains to be investigated.

E-M coupling is modulated by two messengers, ADP and NADH. The ADP production activates the mitochondrial F_1/F_0 ATPase to generate more ATP, which consequently leads to the reduction of inner membrane potential. This drop in potential activates NADH production (the second messenger) to supply electrons to compensate for the electron loss and maintain the inner mitochondrial membrane potential [58]. The other modulatory control of mitochondrial metabolism occurs through the mNCX, which is needed to maintain the intramitochondrial Ca^{2+} concentration. A study examining the influence of cytoplasmic Na^+ and mitochondrial potential on mNCX activity has confirmed the role of mNCX as a Ca^{2+} extrusion mechanism for the mitochondria [59]. In addition, it was demonstrated that mNCX is electrogenic and that depolarization of the mitochondrial membrane activates the mNCX to shuffle Ca^{2+} into the mitochondria rather than eliminating Ca^{2+}; this seems to be a potential protective mechanism against loss of mitochondrial potential that follows ATP depletion [58]. A third potential mechanism modulating E–M coupling is mediated by ATP-sensitive potassium (K_{ATP}) channels. These channels are activated by ADP and inhibited by ATP. It has been shown that K_{ATP} channels can be imported into the mitochondria and localize to the inner mitochondrial membrane following phosphorylation by protein kinase C. K_{ATP} are believed to have a protective effect against I-R-induced increase in cellular Ca^{2+} [60].

A rise in mitochondrial Ca^{2+} is associated with an increase in metabolism [61]. Cardiac pathologies, including CHF, IHD, or potential arrhythmias, lead to an increase in cytosolic Ca^{2+} and have a deleterious effect on mitochondrial metabolism [5]. In fact, a higher Na^+ concentration in the cytosol stimulates the mitochondrial NCX (mNCX), leading to reduced Ca^{2+} accumulation and reduced activity of mitochondrial function [49]. In cardiomyopathies, the reduced cytoplasmic Ca^{2+} negatively affects the mitochondrial Ca^{2+} transient, which is expected to inhibit mitochondrial function. Furthermore, a reduced rate of glycolysis, resulting in reduced availability of pyruvate, contributes to energy starvation in cardiomyopathy [62]. Thus, the mitochondria appear to be a therapeutic target in I-R injury and cardiomyopathies. It has been suggested that inhibition of the mNCX could be beneficial in cases of heart failure as well as during I-R injury.

In heart failure, the increase in cytosolic Na^+ activates the forward mode of mNCX to release mitochondrial Ca^{2+}. On the other hand, an increase in the cytosolic Ca^{2+} will trigger the reverse mode of mNCX and promote the accumulation of excess cytosolic Ca^{2+} in the mitochondria. As a consequence of its effect, the inhibition of mNCX has been shown to improve Ca^{2+} accumulation and mitochondrial energetics in isolated cardiomyocytes [62, 63]. Maintaining a delicate balance in mitochondrial Ca^{2+} content depends on the activities of mCUP and mNCX, where the balance between Ca^{2+} uptake and Ca^{2+} extrusion directly affects mitochondrial metabolism. Thus, inhibition of mNCX may be beneficial in preventing I-R injury and heart failure [5]. In addition, various interventions such as trimetazidine, ranolazine, dichloroacetate, carnitine palmitoyl transferase, and coenzyme Q10 have been proposed to prevent ischemic injury via mitochondrial modulation [63].

It is pointed out that current therapies for patients with stable systolic heart failure are largely limited to treatments that interfere with neurohormonal activation. Critical pathophysiological hallmarks of heart failure are an energetic deficit and oxidative stress, and both may be the result of mitochondrial dysfunction. This

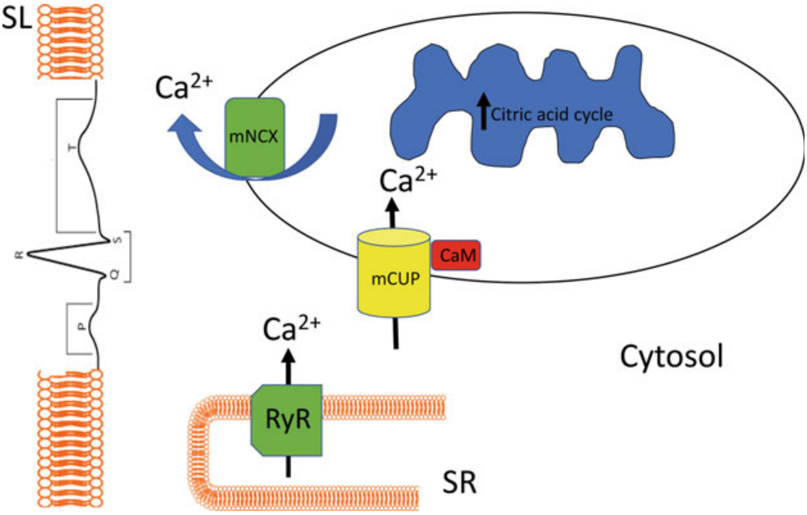

Fig. 21.2 Scheme depicting the role of mitochondria in the excitation-metabolism coupling in cardiomyocytes. *mCUP* mitochondrial Ca^{2+} uniporter, *CaM* calmodulin, *mNCX* mitochondrial Na^+-Ca^{2+} exchanger, *RyR* ryanodine receptor, *SL* Sarcolemma, *SR* sarcoplasmic reticulum

dysfunction is not only the result of a defect within mitochondria per se, but is in particular related to defects in intermediary metabolism. The regulatory interplay between excitation–contraction coupling and mitochondrial energetics, where defects of cytosolic Ca^{2+} and Na^+ handling in failing hearts may play important roles [64]. The contribution and mechanisms of cardiomyocyte mitochondrial Ca^{2+} handling in E-C/E-M coupling as well as how mitochondrial Ca^{2+} regulates physiological mitochondrial and cellular functions in cardiac muscles in health and disease remain to be fully understood [65]. Figure 21.2 summarizes the major components of the E-M coupling process.

21.4 Excitation–Transcription Coupling

Ca^{2+} is a universal regulator of various cellular functions. In cardiomyocytes, Ca^{2+} is the central element of E–C coupling, but it also exerts a great impact on diverse signaling cascades and influences the regulation of gene expression, referred to as excitation–transcription (E–T) coupling. Disturbances in cellular Ca^{2+} handling and alterations in Ca^{2+}-dependent gene expression patterns are pivotal characteristics of failing cardiomyocytes, with several -E–T coupling pathways shown to be critically involved in structural and functional remodeling [66]. Electrical activity initiates a program of selective gene expression in excitable cells. Although such transcriptional activation is commonly attributed to depolarization-induced changes in intracellular Ca^{2+} [67], it should be noted that the specific and localized elevations of Ca^{2+} that are converted into changes in gene expression can be taken as long-term effects on the adaptation of the heart to a sustained stimulus [68].

The role of Ca^{2+} in controlling nuclear signaling has been established in some studies [69, 70]. In cardiomyocytes, nuclei are closely associated with SR; the nucleus of adult cardiomyocytes is reported to possess a nucleoplasmic reticulum, a nuclear Ca^{2+} store that is continuous with SR and the nuclear envelope [33]. The nucleoplasmic reticulum is loaded from cytosolic Ca^{2+} microdomains [71–74]. This organelle expresses functional IP_3R and RyR. There is evidence that the nucleus contains key components of the phosphoinositide-PLC signaling cascade, where the production of IP_3 has been speculated. It is suggested that the nucleus is able to control the effect of Ca^{2+} on gene expression, allowing nuclear Ca^{2+} to regulate cellular functions independently of the cytosolic Ca^{2+} increase [75]. Likewise, IP_3 can trigger the release of Ca^{2+} directly into the nucleoplasm, which may have an important impact on the excitation–

transcription process [75]. An increase in nuclear Ca^{2+} concentration is reported to control the Ca^{2+}-activated gene expression mediated by the cAMP response element [76]. Moreover, cytoplasmic and nuclear Ca^{2+} signals activate transcription through different pathways. Cytoplasmic Ca^{2+} signal activates transcription through the serum response element (SRE) transcription factor and does not require an increase in nuclear Ca^{2+} [77]. Similar to SR, the nucleoplasmic reticulum seems to possess counter-ion channels such as K^+ channels [78]; it is plausible that channels control the change in the potential across the nucleoplasm. This would be particularly important as the nucleoplasmic reticulum contains the voltage-gated R-type Ca^{2+} channels [78]. In addition, there is evidence that the nuclear membrane contains both NCX and NHE that may contribute to nuclear potential and cellular homeostasis.

CaMKII signaling regulates diverse cellular processes in a spatiotemporal manner including excitation–contraction and excitation–transcription coupling, mechanics and energetics in cardiac myocytes. Chronic activation of CaMKII results in cellular remodeling and ultimately arrhythmogenic alterations in Ca^{2+} handling, ion channels, cell-to-cell coupling, and metabolism [79]. Specific alterations in nuclear Ca^{2+} handling via altered excitation–transcription coupling contribute to the development and progression of heart failure. During cardiac remodeling, early changes of cardiomyocyte nuclei cause altered nuclear Ca^{2+} signaling implicated in hypertrophic gene program activation. Normalization of nuclear Ca^{2+} regulation may therefore be a novel therapeutic approach to prevent adverse cardiac remodeling [80].

The increase in nuclear Ca^{2+} signal has been closely associated with cardiac hypertrophy. The most well-characterized mechanism is via Ca^{2+}–CaM. This pathway is under the influence of Ca^{2+}–CaM–CaMK on histone deactylase (HDAC) or the effect of Ca^{2+}–CAM on the protein phosphatase calcineurin (CaN); the two ways may act in parallel, contributing to cardiac hypertrophy [51, 81, 82]. It has been shown that depolarization-mediated Ca^{2+} influx occurs through CaMKII to inhibit the HDAC5, thereby sustaining high activity of the cerebellar granule neuron maintained under myocyte enhancer factor 2 (MEF2) depolarizing conditions. In adult rabbit and mouse cardiomyocytes, phenylephrine and endothelin-1-induced nuclear export of HDAC5 depends not only on CaMK II but also on protein kinase D (PKD) [82]. The nuclear export required type II IP_3R, Ca^{2+} release from stores, CaM, HDAC5 phosphorylation but was completely insensitive to Ca^{2+} transients associated with both nuclear and cytosolic Ca^{2+} and PKC inhibition [51, 82]. HDAC class II is expressed in the heart and possesses a unique extension to bind MEF2, repressing its transcription activation; the relief of MEF2 repression by HDAC comes mainly through phosphorylation of HDAC by CaMK [83]. The latter argues for local control of Ca^{2+} release in the nuclear region, where local activation of nuclear IP_3R releases Ca^{2+} locally that activates CaMKII to phosphorylate HDAC and relieves transcription inhibition. This novel local Ca^{2+} signaling in excitation–transcription coupling is analogous to, but separate from, that involved in excitation–contraction coupling [51]. It is pointed out that MEF2 activation is strongly implicated in cardiac hypertrophy; this has been shown in transgenic animals overexpressing CaMKII and IV [83]. The link between MEF2 and CaMK is through HDAC [84].

Interestingly, acute activation of exchange protein activated by cyclic-AMP (Epac) has been shown to increase Ca^{2+} sparks and diastolic $[Ca^{2+}]_i$ but decrease systolic $[Ca^{2+}]_i$. Epac preferentially increases intranuclear Ca^{2+} concentration ($[Ca^{2+}]_n$) during both diastole and systole, correlating with the perinuclear expression pattern of Epac. Moreover, Epac activation induces HDAC5 nuclear export, with consequent activation of the prohypertrophic transcription factor MEF2. The cAMP-binding protein Epac modulates cardiac nuclear Ca^{2+} signaling by increasing $[Ca^{2+}]_n$ through PLC, IP_3R, and CaMKII activation and initiates a prohypertrophic program via HDAC5 nuclear export and subsequent activation of the transcription factor MEF2 [85].

Other transcription factors that are regulated by CaMK include activating protein (AP1), activating transcription factor (ATF-1), serum response factor (SRF), cyclic AMP response element (CREB), and the myocyte enhancing factor (MEF-2) [86]. While CREB can be phosphorylated by CaMKII, transgenic mice overexpressing CaMKII or CaMKIV that develop hypertrophy did not show an enhanced level of CREB phosphorylation [84, 87]. MEF2 activation is strongly implicated in hypertrophy; this has been shown in transgenic animals overexpressing CaMKII and IV [88]. The other mechanism by which Ca^{2+}–CaM controls transcription is through CaN, a Ca^{2+}-CaM binding phosphatase (500 times more sensitive to Ca^{2+} than CaM), allowing CaN to be more sensitive to small sustained Ca^{2+} transients [89]. CaN dephosphorylates NFAT, which leads to its translocation into the nucleus, where it binds to the transcription factor GATA4 to activate hypertrophic gene transcription [90]. In some studies, a sustained global rise in Ca^{2+} is needed to activate NFAT [91], whereas in others, Ca^{2+} oscillations were more efficient NFAT activators [92]. In neurons, the C-terminal fragment of LTCCs was found to be proteolytically cleaved as it translocated into the nucleus; this is then bound to a transcriptional regulator, Ca^{2+} channel associated transcription (CCAT) factor, leading to an increase in the length of neurites [93, 94]. The latter leads to an increase in some genes such as connexins, regulators of G-protein and catenin, while other proteins such as K^+ channel (Kcn3), NCX, myosin, NMDA receptor, serine-threonine kinase, and glucokinase are down-regulated.

While the role of this catalytic fragment in cardiomyocytes remains to be examined, the potential for developing specific inhibitors of nuclear Ca^{2+} signaling is unlimited. The control of such a mechanism could provide treatments for heart failure and cardiac hypertrophy as well as other conditions where Ca^{2+} oscillations affect gene expression and consequently the expression of signaling molecules that modulate Ca^{2+} cycling. It is now well recognized that CaMKII and a Ca-calmodulin-dependent phosphatase calcineurin are major Ca^{2+}-dependent mediators of transcriptional regulation. Moreover, these pathways contribute to changes in the gene expression of proteins involved in the HF phenotype, including some of the ion channels and Ca^{2+} transporters that are acutely involved in systolic dysfunction and arrhythmias [95]. In fact, the development of intracellular Ca^{2+} overload in the heart has been demonstrated to depress cardiac gene expression for SL Na^+–K^+ ATPase isoforms, SR RyR and SERCA2 proteins as well as α- and β-myosin [96] Fig. 21.3 summarizes the role of Ca^{2+} in E–T coupling in the cardiomyocyte.

21.5 Conclusions

From the aforementioned, it is evident that novel therapeutic interventions will continue to target ion channels; however, the focus may now also be on mitochondrial channels and exchangers in order to influence cellular metabolism and nuclear ion channels to control cell proliferation and growth. Targeting intracellular ion channels for the control of E-C, E-M and E-T coupling has emerged as an attractive new area of cardiovascular research that constitutes novel and exciting approaches for the treatment of IHD, cardiac hypertrophy, and heart failure.

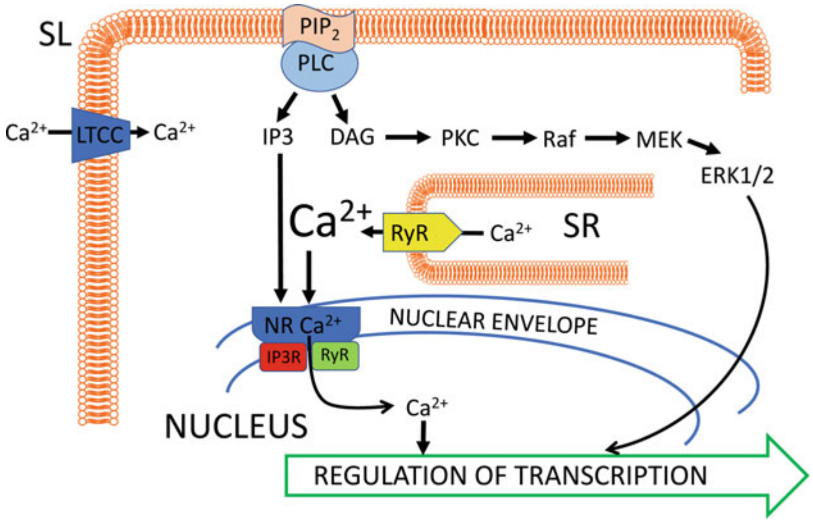

Fig. 21.3 Scheme showing the role of Ca^{2+} in excitation-transcription coupling in the cardiomyocyte. *NR* nucleoplasmic reticulum, *RyR* ryanodine receptor, *IP$_3$R* inositol trisphosphate receptor, *SL* sarcolemma, *LTCC* L-type Ca^{2+}-channel, *SR* sarcoplasmic reticulum, *PIP$_2$* phosphatidylinositol-bisphosphate, *PLC* phospholipase C, *DAG* diacylglycerol, *IP3* inositol trisphosphate, *PKC* protein kinase C, *Raf* Rapidly accelerated fibrosarcoma, *MEK* Mitogen-activated protein kinase kinase, *ERK1/2* extracellular signal-regulated kinase 1/2

Acknowledgements The infrastructural support for the work presented in this article was provided by the St. Boniface Hospital Research Foundation. Dr. Nusier is a Visiting Professor from Jordan University of Science and Technology, School of Medicine, Department of Physiology and Biochemistry, Jordan.

References

1. Eisner DA, Caldwell JL, Kistamás K, Trafford AW. Calcium and excitation-contraction coupling in the heart. Circ Res. 2017;121:181–95.
2. Berlin JR, Bassani JW, Bers DM. Intrinsic cytosolic calcium buffering properties of single rat cardiac myocytes. Biophys J. 1994;67:1775–87.
3. Dhalla NS. Excitation-contraction coupling in heart. I. Comparison of calcium uptake by the sarcoplasmic reticulum and mitochondria of the rat heart. Arch Int Physiol Biochim. 1969;77:916–34.
4. Alonso MT, Villalobos C, Chamero P, Alvarez J, Garcia-Sancho J. Calcium microdomains in mitochondria and nucleus. Cell Calcium. 2006;40: 513–25.
5. Dhalla NS, Saini-Chohan HK, Rodriguez-Leyva D, Elimban V, Dent MR, Tappia PS. Subcellular remodeling may induce cardiac dysfunction in congestive heart failure. Cardiovasc Res. 2009;81: 429–38.
6. Bers DM. Calcium cycling and signaling in cardiac myocytes. Annu Rev Physiol. 2008;70:23–49.
7. Dhalla NS, Saini HK, Tappia PS, Sethi R, Mengi SA, Gupta SK. Potential role and mechanisms of subcellular remodeling in cardiac dysfunction due to ischemic heart disease. J Cardiovasc Med. 2007;8:238–50.
8. Nader M. The SLMAP/Striatin complex: an emerging regulator of normal and abnormal cardiac excitation-contraction coupling. Eur J Pharmacol. 2009;5:858.
9. Lukyanenko V, Ziman A, Lukyanenko A, Salnikov V, Lederer WJ. Functional groups of ryanodine receptors in rat ventricular cells. J Physiol. 2007;583:251–69.
10. Meissner G. Molecular regulation of cardiac ryanodine receptor ion channel. Cell Calcium. 2004;35:621–8.
11. Antos CL, Frey N, Marx SO, Reiken S, Gaburjakova M, Richardson JA, et al. Dilated cardiomyopathy and sudden death resulting from constitutive activation of protein kinase A. Circ Res. 2001;89: 997–1004.
12. Marx SO, Reiken S, Hisamatsu Y, Jayaraman T, Burkhoff D, Rosemblit N, et al. PKA phosphorylation dissociates FKBP12.6 from the calcium release channel (ryanodine receptor): defective regulation in failing hearts. Cell. 2000;101:365–76.
13. Diaz ME, Graham HK, O'neill SC, Trafford AW, Eisner DA. The control of sarcoplasmic reticulum Ca^{2+} content in cardiac muscle. Cell Calcium. 2005;38:391–6.

14. Zalk R, Lehnart SE, Marks AR. Modulation of the ryanodine receptor and intracellular calcium. Annu Rev Biochem. 2007;76:367–85.
15. Yamamoto T, Yano M, Xu X, Uchinoumi H, Tateishi H, Mochizuki M, et al. Identification of target domains of the cardiac ryanodine receptor to correct channel disorder in failing hearts. Circulation. 2008;117:762–72.
16. Yano M. Ryanodine receptor as a new therapeutic target of heart failure and lethal arrhythmia. Circ J. 2008;72:509–14.
17. Lehnart SE, Mongillo M, Bellinger A, Lindegger N, Chen BX, Hsueh W, et al. Leaky Ca^{2+} release channel/ryanodine receptor 2 causes seizures and sudden cardiac death in mice. J Clin Invest. 2008;118:2230–45.
18. Dhalla NS, Dent MR, Tappia PS, Sethi R, Barta J, Goyal RK. Subcellular remodeling as a viable target for the treatment of congestive heart failure. J Cardiovasc Pharmacol Therapeut. 2006;11:31–45.
19. Tada M, Yamada M, Kadoma M, Inui M, Ohmori F. Calcium transport by cardiac sarcoplasmic reticulum and phosphorylation of phospholamban. Mol Cell Biochem. 1982;46:73–95.
20. Toyoshima C, Nakasako M, Nomura H, Ogawa H. Crystal structure of the calcium pump of sarcoplasmic reticulum at 2.6 Å resolution. Nature. 2000;405:647–55.
21. Tada M, Yamada M, Inui M, Ohmori F. Regulation of Ca^{2+}-dependent ATPase of cardiac sarcoplasmic reticulum by cAMP- and calmodulin-dependent phosphorylation of phospholamban. Tanpakushitsu Kakusan Koso. 1982;27:2350–64.
22. James P, Inui M, Tada M, Chiesi M, Carafoli E. Nature and site of phospholamban regulation of the Ca^{2+} pump of sarcoplasmic reticulum. Nature. 1989;342:90–2.
23. Asahi M, Nakayama H, Tada M, Otsu K. Regulation of sarco(endo)plasmic reticulum Ca^{2+} adenosine triphosphatase by phospholamban and sarcolipin: implication for cardiac hypertrophy and failure. Trends Cardiovasc Med. 2003;13:152–7.
24. Babu GJ, Bhupathy P, Timofeyev V, Petrashevskaya NN, Reiser PJ, Chiamvimonvat N, et al. Ablation of sarcolipin enhances sarcoplasmic reticulum calcium transport and atrial contractility. Proc Natl Acad Sci U S A. 2007;104:17867–72.
25. Kiewitz R, Acklin C, Schafer BW, Maco B, Uhrik B, Wuytack F, et al. Ca^{2+} –dependent interaction of S100A1 with the sarcoplasmic reticulum Ca^{2+}-ATPase2a and phospholamban in the human heart. Biochem Biophys Res Commun. 2003;306:550–7.
26. Remppis A, Most P, Löffler E, Ehlermann P, Bernotat J, Pleger S, et al. The small EF-hand Ca^{2+} binding protein S100A1 increases contractility and Ca^{2+} cycling in rat cardiac myocytes. Basic Res Cardiol. 2002;97:I56–162.
27. Mercadier JJ, Lompre AM, Duc P, Boheler KR, Fraysse JB, Wisnewsky C, et al. Altered sarcoplasmic reticulum Ca^{2+}-ATPase gene expression in the human ventricle during end-stage heart failure. J Clin Invest. 1990;85:305–9.
28. del Monte F, Williams E, Lebeche D, Schmidt U, Rosenzweig A, Gwathmey JK, et al. Improvement in survival and cardiac metabolism after gene transfer of sarcoplasmic reticulum Ca^{2+}-ATPase in a rat model of heart failure. Circulation. 2001;104:1424–9.
29. Joubert F, Wilding JR, Fortin D, Domergue-Dupont V, Novotova M, Ventura-Clapier R, et al. Local energetic regulation of sarcoplasmic and myosin ATPase is differently impaired in rats with heart failure. J Physiol. 2008;586:5181–92.
30. Prasad V, Okunade GW, Miller ML, Shull GE. Phenotypes of SERCA and PMCA knockout mice. Biochem Biophys Res Commun. 2004;322:1192–203.
31. Mayosi BM, Kardos A, Davies CH, Gumedze F, Hovnanian A, Burge S, et al. Heterozygous disruption of SERCA2a is not associated with impairment of cardiac performance in humans: implications for SERCA2a as a therapeutic target in heart failure. Heart. 2006;92:105–9.
32. Moschella MC, Marks AR. Inositol 1,4,5-trisphosphate receptor expression in cardiac myocytes. J Cell Biol. 1993;120:1137–46.
33. Kockskamper J, Zima AV, Roderick HL, Pieske B, Blatter LA, Bootman MD. Emerging roles of inositol 1,4,5-trisphosphate signaling in cardiac myocytes. J Mol Cell Cardiol. 2008;45:128–47.
34. Hund TJ, Ziman AP, Lederer WJ, Mohler PJ. The cardiac IP3 receptor: uncovering the role of "the other" calcium-release channel. J Mol Cell Cardiol. 2008;45:159–61.
35. Lakatta EG, Vinogradova TM, Maltsev VA. The missing link in the mystery of normal automaticity of cardiac pacemaker cells. Ann N Y Acad Sci. 2008;1123:41–57.
36. Jiang QX, Thrower EC, Chester DW, Ehrlich BE, Sigworth FJ. Three-dimensional structure of the type 1 inositol 1,4,5-trisphosphate receptor at 24 a resolution. EMBO J. 2002;21:3575–81.
37. Ramos-Franco J, Fill M, Mignery GA. Isoform-specific function of single inositol 1,4,5-trisphosphate receptor channels. Biophys J. 1998;75:834–9.
38. Swatton JE, Morris SA, Cardy TJ, Taylor CW. Type 3 inositol trisphosphate receptors in RINm5F cells are biphasically regulated by cytosolic Ca^{2+} and mediate quantal Ca^{2+} mobilization. Biochem J. 1999;344:55–60.
39. Adkins CE, Morris SA, De SH, Sienaert I, Torok K, Taylor CW. Ca^{2+}-calmodulin inhibits Ca^{2+} release mediated by type-1, 2 and 3 inositol trisphosphate receptors. Biochem J. 2000;345:357–63.
40. Bultynck G, Sienaert I, Parys JB, Callewaert G, De SH, Boens N, et al. Pharmacology of inositol trisphosphate receptors. Pflugers Arch. 2003;445:629–42.
41. Kane C, Couch L, Terracciano CM. Excitation-contraction coupling of human induced pluripotent

stem cell-derived cardiomyocytes. Front Cell Dev Biol. 2015;3:59.

42. Yoshikane H, Nihei T, Moriyama K. Three-dimensional observation of intracellular membranous structures in dog heart muscle cells by scanning electron microscopy. J Submicrosc Cytol. 1986;18:629–36.
43. Guerrero-Hernandez A, Verkhratsky A. Calcium signalling in diabetes. Cell Calcium. 2014;56:297–301.
44. Denton RM, McCormack JG. Ca^{2+} as a second messenger within mitochondria of the heart and other tissues. Annu Rev Physiol. 1990;52:451–66.
45. Territo PR, French SA, Dunleavy MC, Evans FJ, Balaban RS. Calcium activation of heart mitochondrial oxidative phosphorylation: rapid kinetics of mVO2, NADH AND light scattering. J Biol Chem. 2001;276:2586–99.
46. Kirichok Y, Krapivinsky G, Clapham DE. The mitochondrial calcium uniporter is a highly selective ion channel. Nature. 2004;427:360–4.
47. Moreau B, Nelson C, Parekh AB. Biphasic regulation of mitochondrial Ca^{2+} uptake by cytosolic Ca^{2+} concentration. Curr Biol. 2006;16:1672–7.
48. Gunter KK, Gunter TE. Transport of calcium by mitochondria. J Bioenerg Biomembr. 1994;26:471–85.
49. Maack C, Cortassa S, Aon MA, Ganesan AN, Liu T, O'Rourke B. Elevated cytosolic Na^+ decreases mitochondrial Ca^{2+} uptake during excitation-contraction coupling and impairs energetic adaptation in cardiac myocytes. Circ Res. 2006;99:172–82.
50. Kwong JQ. The mitochondrial calcium uniporter in the heart: energetics and beyond. J Physiol. 2017;595: 3743–51.
51. Wu X, Zhang T, Bossuyt J, Li X, McKinsey TA, Dedman JR, et al. Local $InsP_3$-dependent perinuclear Ca^{2+} signaling in cardiac myocyte excitation-transcription coupling. J Clin Invest. 2006;116:675–82.
52. Gustafsson AB, Gottlieb RA. Heart mitochondria: gates of life and death. Cardiovasc Res. 2008;77: 334–43.
53. Maack C, O'Rourke B. Excitation-contraction coupling and mitochondrial energetics. Basic Res Cardiol. 2007;102:369–92.
54. Ohata H, Chacon E, Tesfai SA, Harper IS, Herman B, Lemasters JJ. Mitochondrial Ca^{2+} transients in cardiac myocytes during the excitation-contraction cycle: effects of pacing and hormonal stimulation. J Bioenerg Biomembr. 1998;30:207–22.
55. Pacher P, Csordas P, Schneider T, Hajnoczky G. Quantification of calcium signal transmission from sarco-endoplasmic reticulum to the mitochondria. J Physiol. 2000;529:553–64.
56. Cortassa S, Aon MA, Marbán E, Winslow RL, O'Rourke B. An integrated model of cardiac mitochondrial energy metabolism and calcium dynamics. Biophys J. 2003;84:2734–55.
57. Beutner G, Sharma VK, Lin L, Ryu SY, Dirksen RT, Sheu SS. Type 1 ryanodine receptor in cardiac mitochondria: transducer of excitation-metabolism coupling. Biochim Biophys Acta. 2005;1717:1–10.
58. Stanley WC, Chandler MP. Energy metabolism in the normal and failing heart: potential for therapeutic interventions. Heart Fail Rev. 2002;7:115–30.
59. Kim B, Matsuoka S. Cytoplasmic Na^+-dependent modulation of mitochondrial Ca^{2+} via electrogenic mitochondrial Na^+-Ca^{2+} exchange. J Physiol. 2008;586:1683–97.
60. Light PE, Kanji HD, Fox JE, French RJ. Distinct myoprotective roles of cardiac sarcolemmal and mitochondrial KATP channels during metabolic inhibition and recovery. FASEB J. 2001;15:2586–94.
61. Brandes R, Bers DM. Simultaneous measurements of mitochondrial NADH and Ca^{2+} during increased work in intact rat heart trabeculae. Biophys J. 2002;83:587–604.
62. Kuo TH, Zhu L, Golden K, Marsh JD, Bhattacharya SK, Liu BF. Altered Ca^{2+} homeostasis and impaired mitochondrial function in cardiomyopathy. Mol Cell Biochem. 2002;238:119–27.
63. O’Rourke B, Cortassa S, Akar F, Aon M. Mitochondrial ion channels in cardiac function and dysfunction. Novartis Found Symp. 2007;287: 140–51.
64. von Hardenberg A, Maack C. Mitochondrial therapies in heart failure. Handb Exp Pharmacol. 2017;243:491–514.
65. Cao JL, Adaniya SM, Cypress MW, Suzuki Y, Kusakari Y, Jhun BS, et al. Role of mitochondrial Ca^{2+} homeostasis in cardiac muscles. Arch Biochem Biophys. 2019;663:276–87.
66. Dewenter M, von der Lieth A, Katus HA, Backs J. Calcium signaling and transcriptional regulation in cardiomyocytes. Circ Res. 2017;121:1000–20.
67. Atar D, Backx PH, Appel MM, Gao WD, Marban E. Excitation-transcription coupling mediated by zinc influx through voltage-dependent calcium channels. J Biol Chem. 1995;270:2473–7.
68. Benitah JP, Gomez AM, Virsolvy A, Richard S. New perspectives on the key role of calcium in the progression of heart disease. J Muscle Res Cell Motil. 2003;24:275–83.
69. Hamdan M, Urien S, Le LH, Tillement JP, Morin D. Inhibition of mitochondrial carnitine palmitoyltransferase-1 by a trimetazidine derivative, S-15176. Pharmacol Res. 2001;44:99–104.
70. Mellstrom B, Savignac M, Gomez-Villafuertes R, Naranjo JR. Ca^{2+}-operated transcriptional networks: molecular mechanisms and in vivo models. Physiol Rev. 2008;88:421–49.
71. Abrenica B, Gilchrist JS. Nucleoplasmic Ca^{2+}loading is regulated by mobilization of perinuclear Ca^{2+}. Cell Calcium. 2000;28:127–36.
72. Abrenica B, Pierce GN, Gilchrist JS. Nucleoplasmic calcium regulation in rabbit aortic vascular smooth

muscle cells. Can J Physiol Pharmacol. 2003;81:301–10.

73. Echevarria W, Leite MF, Guerra MT, Zipfel WR, Nathanson MH. Regulation of calcium signals in the nucleus by a nucleoplasmic reticulum. Nat Cell Biol. 2003;5:440–6.
74. Chi TH, Crabtree GR. Perspectives: signal transduction. Inositol phosphates in the nucleus. Science. 2000;287:1937–9.
75. Zima AV, Bare DJ, Mignery GA, Blatter LA. IP3-dependent nuclear Ca^{2+} signalling in the mammalian heart. J Physiol. 2007;584:601–11.
76. Hardingham GE, Chawla S, Johnson CM, Bading H. Distinct functions of nuclear and cytoplasmic calcium in the control of gene expression. Nature. 1997;385:260–5.
77. Dolmetsch RE, Xu K, Lewis RS. Calcium oscillations increase the efficiency and specificity of gene expression. Nature. 1998;392:933–6.
78. Bkaily G, Avedanian L, Jacques D. Nuclear membrane receptors and channels as targets for drug development in cardiovascular diseases. Can J Physiol Pharmacol. 2009;87:108–19.
79. Hegyi B, Bers DM, Bossuyt J. CaMKII signaling in heart diseases: emerging role in diabetic cardiomyopathy. J Mol Cell Cardiol. 2019;127:246–59.
80. Ljubojevic S, Radulovic S, Leitinger G, Sedej S, Sacherer M, Holzer M, et al. Early remodeling of perinuclear Ca^{2+} stores and nucleoplasmic Ca^{2+} signaling during the development of hypertrophy and heart failure. Circulation. 2014;130:244–55.
81. Bkaily G, Nader M, Avedanian L, Choufani S, Jacques D, D'Orléans-Juste P. G-protein-coupled receptors, channels, and Na$^+$-H$^+$ exchanger in nuclear membranes of heart, hepatic, vascular endothelial, and smooth muscle cells. Can J Physiol Pharmacol. 2006;84:431–41.
82. Bossuyt J, Helmstadter K, Wu X, Clements-Jewery H, Haworth RS, Avkiran M, et al. Ca^{2+} /calmodulin-dependent protein kinase II delta and protein kinase D overexpression reinforce the histone deacetylase 5 redistribution in heart failure. Circ Res. 2008;102:695–702.
83. Wu H, Naya FJ, McKinsey TA, Mercer B, Shelton JM, Chin ER, et al. MEF2 responds to multiple calcium-regulated signals in the control of skeletal muscle fiber type. EMBO J. 2000;19:1963–73.
84. Zhang T, Kohlhaas M, Backs J, Mishra S, Phillips W, Dybkova N, et al. CaMKIIdelta isoforms differentially affect calcium handling but similarly regulate HDAC/MEF2 transcriptional responses. J Biol Chem. 2007;282:35078–87.
85. Pereira L, Ruiz-Hurtado G, Morel E, Laurent AC, Métrich M, Domínguez-Rodríguez A, et al. Epac enhances excitation-transcription coupling in cardiac myocytes. J Mol Cell Cardiol. 2012;52:283–91.
86. Backs J, Song K, Bezprozvannaya S, Chang S, Olson EN. CaM kinase II selectively signals to histone deacetylase 4 during cardiomyocyte hypertrophy. J Clin Invest. 2006;116:1853–64.
87. McKinsey TA, Zhang CL, Olson EN. Activation of the myocyte enhancer factor-2 transcription factor by Ca^{2+} /calmodulin-dependent protein kinase-stimulated binding of 14-3-3 to histone deacetylase 5. Proc Natl Acad Sci U S A. 2000;97:14400–5.
88. Colella M, Grisan F, Robert V, Turner JD, Thomas AP, Pozzan T. Ca^{2+} oscillation frequency decoding in cardiac cell hypertrophy: role of calcineurin/NFAT as Ca^{2+} signal integrators. Proc Natl Acad Sci U S A. 2008;105:2859–64.
89. Molkentin JD. Calcineurin-NFAT signaling regulates the cardiac hypertrophic response in coordination with the MAPKs. Cardiovasc Res. 2004;63:467–75.
90. Timmerman LA, Clipstone NA, Ho SN, Northrop JP, Crabtree GR. Rapid shuttling of NF-AT in discrimination of Ca^{2+} signals and immunosuppression. Nature. 1996;383:837–40.
91. Hallhuber M, Burkard N, Wu R, Buch MH, Engelhardt S, Hein L, et al. Inhibition of nuclear import of calcineurin prevents myocardial hypertrophy. Circ Res. 2006;99:626–35.
92. Dolmetsch RE, Lewis RS, Goodnow CC, Healy JI. Differential activation of transcription factors induced by Ca^{2+} response amplitude and duration. Nature. 1997;386:855–8.
93. Gomez-Ospina N, Tsuruta F, Barreto-Chang O, Hu L, Dolmetsch R. The C terminus of the L-type voltage-gated calcium channel Ca(V)1.2 encodes a transcription factor. Cell. 2006;127:591–606.
94. Chung HJ, Jan LY. Channeling to the nucleus. Neuron. 2006;52:937–40.
95. Bers DM. Ca^{2+}-calmodulin-dependent protein kinase II regulation of cardiac excitation- transcription coupling. Heart Rhythm. 2011;8:1101–4.
96. Ozcelikay AT, Chapman D, Elimban V, Dhalla NS. Role of intracellular Ca^{2+}-overload in inducing changes in cardiac gene expression. Curr Res Cardiol. 2014;1:13–6.

Calmodulin Kinase II Regulation of Heart Rhythm and Disease

22

Drew M. Nassal and Thomas J. Hund

Abstract

Calmodulin kinase II (CaMKII) is expressed in tissues throughout the body with essential roles in a wide variety of cellular functions from synaptic transmission in neurons to solute absorption in the epithelium to excitation–contraction coupling in cardiac myocytes. Importantly, CaMKII activity is sensitive to a variety of physiologically relevant stimuli, including intracellular Ca^{2+} and reactive oxygen species. In cardiomyocytes, CaMKII targets a host of intracellular substrates, including ion channels, Ca^{2+} cycling proteins, and transcription factors to regulate cardiac contractility, pacemaking, and electrical conduction. This chapter discusses the multiple roles of CaMKII in the heart and its emergence as an important determinant of the heart's response to both acute and chronic stress relevant to normal physiology as well as disease.

Keywords

Calmodulin kinase II · Cardiac arrhythmia · Heart failure · Ion channels

22.1 Introduction

Calmodulin kinase II (CaMKII) is a broadly expressed serine/threonine kinase that regulates critical cell functions, including synaptic transmission in neurons, solute adsorption and secretion in the epithelium, excitation–contraction coupling, and excitation–transcription coupling in cardiac myocytes [1–3]. Central to the multifunctional nature of CaMKII is its ability to detect changes in the concentration of intracellular Ca^{2+}. In the heart, CaMKII coordinates the activities of a host of intracellular substrates to regulate Ca^{2+} homeostasis, cell excitability, and gene transcription. This chapter provides an overview of our current understanding of how CaMKII modulates the heart's response to both acute and chronic stress relevant to normal physiology as well as disease, with a particular focus on cardiac conduction and pacemaking. In this section, we provide a brief review of the fundamental aspects of CaMKII biology that are important for understanding the associated pathophysiology.

22.1.1 CaMKII Structure/Function Relationship

Up to 30 CaMKII isoforms are encoded by four genes (α, β, δ, and γ), with CaMKIIα and CaMKIIβ being expressed predominantly in neurons and CaMKIIδ and CaMKIIγ showing a broader tissue distribution [4]. The major isoform

---

D. M. Nassal · T. J. Hund (✉)
The Frick Center for Heart Failure and Arrhythmia, Dorothy M. Davis Heart and Lung Research Institute, The Ohio State University Wexner Medical Center, Columbus, OH, USA
e-mail: Thomas.hund@osumc.edu

© Springer Nature Switzerland AG 2023

O. N. Tripathi et al. (eds.), *Heart Rate and Rhythm*, https://doi.org/10.1007/978-3-031-33588-4_22

in the heart is CaMKIIδ with the secondary expression of CaMKIIγ [5, 6]. In vitro studies have shown that each isoform has a unique dynamic response to Ca^{2+}/calmodulin [7]. This functional variability, combined with the heteromultimeric nature of CaMKII, allows for tissue-specific tuning of CaMKII dynamic response to changes in Ca^{2+}. In neurons, CaMKII is highly enriched in postsynaptic densities, comprising ~3% of total protein [8]. In vitro studies have shown that CaMKII can detect the frequency, amplitude, and duration of Ca^{2+} spikes in neurons [9], which allows the kinase to mediate the dependence of synaptic transmission on stimulus frequency (long-term potentiation) essential for some forms of learning and memory [10].

CaMKII is a multimeric kinase composed of 12 monomers [7, 11]. Each kinase monomer has an N-terminal catalytic domain, autoregulatory domain, and C-terminal association domain (Fig. 22.1). In its inactive state, the autoregulatory subunit binds to and inhibits the kinase catalytic domain. The binding of Ca^{2+}/calmodulin to the autoregulatory domain relieves auto-inhibition and exposes the catalytic subunit enabling the kinase to phosphorylate its substrates (Fig. 22.1). Among the many known CaMKII substrates is the kinase itself. A specific threonine residue in the autoregulatory domain (T286/287) that is exposed to the binding of Ca^{2+}/calmodulin may be phosphorylated by a neighboring active subunit ("autophosphorylation") to produce a maximally active kinase [12, 13]. Autophosphorylation also increases the affinity of the kinase for calmodulin ("trapping") and enables the kinase to remain active even upon the dissociation of Ca^{2+}/calmodulin ("autonomy") [14]. There is also a negative regulatory site (T306) in the regulatory domain that reduces CaMKII activity ("capping"), thereby providing negative feedback for the control of enzyme activity [15]. An alternative pathway for kinase activation involves oxidation at specific methionine residues (Met281 and Met282) in proximity to the autophosphorylation site in the autoregulatory domain [16]. Similar to autophosphorylation, binding of Ca^{2+}/CaM exposes critical residues in the autoregulatory domain and therefore must precede the oxidation step. Although an oxidized subunit retains activity once Ca^{2+}/calmodulin dissociates, unlike autophosphorylation, oxidation does not alter the affinity for calmodulin. Analogous to the regulation of autophosphorylation by local kinase/phosphatase activity and local concentrations of Ca^{2+}/calmodulin, oxidative activation is likely controlled by a delicate balance of oxidase/reductase activity, mitochondrial function, and local calcium signaling. Additional post-translational modifications for CaMKII have been identified including the addition of an O-linked N-acetylglucosamine (O-GlcNAc) referred to as O-glcNAcylation at Ser280 in the CaMKII regulatory domain, which disrupts its interaction with the association domain. Like autophosphorylation or oxidation, O-glcNAcylation leads to the persistent activation of CaMKII even after the dissociation of Ca^{2+}/calmodulin [17]. Lastly, autonomous activation of CaMKII may be induced by the attachment of a nitric oxide (NO) moiety to Cys290, referred to as S-nitrosylation [18]. NO donors and NO production as a consequence of β-adrenergic signaling have been shown to activate CaMKII [18–20].

22.1.2 CaMKII Subcellular Localization

CaMKII is preferentially localized to the cardiomyocyte Z-line, where it colocalizes with L-type Ca^{2+} channels and type 2 ryanodine receptors (RyR2) [21, 22]. However, CaMKII regulates proteins at multiple subcellular domains, including the intercalated disc, t-tubules, mitochondria, and nucleus [23–29] (Fig. 22.2). Thus, localization of the kinase and local regulation by Ca^{2+} and phosphatase activities are critical determinants of downstream CaMKII effects. For example, while it is known that cAMP signaling in cardiomyocytes depends on subcellular compartmentalization maintained by A-kinase anchoring proteins (AKAPs) [30], an analogous family of anchoring proteins for CaMKII has not been identified. Rather, CaMKII

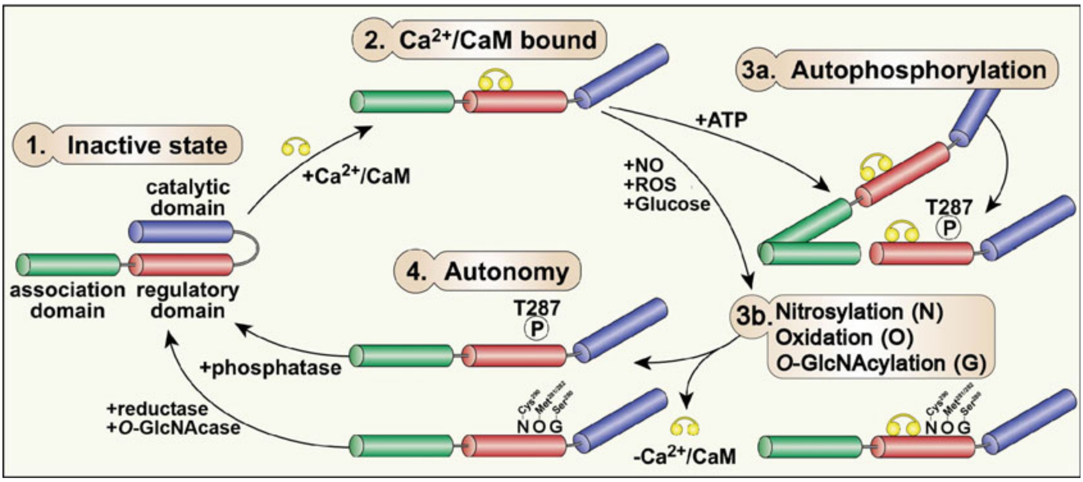
2. Ca²⁺/CaM bound
3a. Autophosphorylation
1. Inactive state
catalytic domain
association domain
regulatory domain
+Ca²⁺/CaM
+ATP
+NO
+ROS
+Glucose
T287
P
4. Autonomy
T287
P
3b. Nitrosylation (N)
Oxidation (O)
O-GlcNAcylation (G)
+phosphatase
+reductase
+O-GlcNAcase
Cys290
Met281/282
Ser280
N O G
-Ca²⁺/CaM
Cys290
Met281/282
Ser280
N O G

Fig. 22.1 Regulation of CaMKII activity by Ca^{2+}/calmodulin, autophosphorylation, and oxidation, O-GlcNAcylation, and nitrosylation. In its inactive form, the autoregulatory domain of CaMKII inhibits the catalytic domain. Binding of Ca^{2+}/calmodulin displaces the autoregulatory domain resulting in an active kinase and exposing critical residues for autophosphorylation (T287) or alternative modifications like oxidation (M281/282), O-GlcNAcylation (S280), or S-nitrosylation (C290). Autophosphorylation at the exposed T287 site by a neighboring active subunit produces a maximally active subunit that retains activity even upon dissociation of Ca^{2+}/calmodulin (autonomy). Similar autonomy is observed with oxidation at exposed M281 or M282 and other post-translational modifications in the regulatory domain. The kinase is tightly regulated by phosphatase and reductase activities

targeting sequences appear to be embedded in target proteins themselves or in accessory/scaffolding proteins. For example, CaMKII directly binds the NR2B subunit of the NMDA receptor forming a complex at postsynaptic densities to mediate long-term potentiation in neurons [31, 32]. Similarly, direct tethering of CaMKII to α_{1c} and β_{2a} subunits of the L-type Ca^{2+} channel has been shown to support CaMKII-dependent phosphorylation of the channel to facilitate channel current [33, 34]. More recently, the actin-binding structural protein β_{IV}-spectrin was found to target a subpopulation of CaMKII to the cardiomyocyte intercalated disc and axon initial segment [28]. In the heart, the β_{IV}-spectrin/CaMKII complex is essential for CaMKII-dependent phosphorylation of the cardiac Na^+ channel, $Na_V1.5$, at residue Ser571, and modulation of pathogenic late Na^+ current [28, 35, 36]. Interestingly, the common CaMKII binding domain in β_{IV}-spectrin β2a and NR2B subunits shows high homology to a portion of the CaMKII association domain.

22.2 CaMKII Regulation of Cardiac Physiology

CaMKII is a multifunctional kinase residing at the hub of an extensive signaling network in cells throughout the body, including cardiac myocytes. Furthermore, the kinase is responsive to a number of input signals relevant to normal cardiac physiology (e.g., Ca^{2+}, β-adrenergic stimulation). Thus, CaMKII is well suited to rapid modulation of cardiac function in response to physiological stress. This section describes the various roles of CaMKII in normal cardiac physiology.

22.2.1 CaMKII Regulation of Excitation–Contraction Coupling

The mechanical action of the heart depends on the coordinated release of Ca^{2+} from intracellular stores. Calcium entry through sarcolemmal voltage-gated Ca^{2+} channels triggers Ca^{2+} release

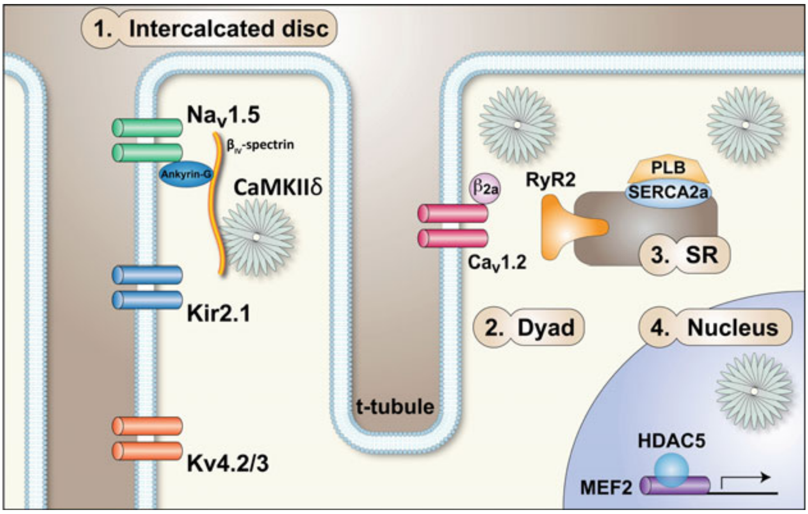

Fig. 22.2 CaMKII subcellular domains and key substrates. CaMKII targets many intracellular substrates localized to distinct subcellular domains. The cardiomyocyte intercalated disc is a specialized membrane domain important for maintaining mechanical integrity and electrical coupling between cells. CaMKII targets voltage-gated Na^+ channel, $Na_v1.5$ at the cardiomyocyte intercalated disc, through interaction with the cytoskeletal protein β_{IV}-spectrin, to regulate electrical propagation, as well as $K_v4.3$ (transient outward K^+ current, I_{to}) and Kir2.1 (inwardly rectifying K^+ current, I_{K1}) (also found at t-tubules). CaMKII regulates L-type Ca^{2+} channels (composed of $Ca_v1.2$, α2d, and β-subunits) and RyR2 SR Ca^{2+} release channels located in proximity in the cardiac dyadic space created by apposition of t-tubular and SR membranes. CaMKII regulates activity of the SR Ca^{2+} ATPase SERCA2a through direct phosphorylation of the associated inhibitory protein phospholamban (PLB). In the nucleus, CaMKII targets HDAC5, a repressor of MEF2, to regulate transcription of hypertrophic gene program

from RyR2 Ca^{2+} release channels located nearby (~10 nm) in the cisternal sarcoplasmic reticulum (SR) membrane. Close apposition of voltage-gated Ca^{2+} channels and RyR2 channels creates a dyadic space that is important for local control of Ca^{2+}-induced Ca^{2+} release in ventricular myocytes. After Ca^{2+} release, some Ca^{2+} ions are extruded from the cell by the Na^+/Ca^{2+} exchanger, but most of them are sequestered back into the SR by the SR Ca^{2+} ATPase (SERCA2a). SR Ca^{2+} ATPase activity is tightly regulated by the SERCA2a-associated protein, phospholamban (PLB). CaMKII regulates several key members involved in excitation–contraction coupling, a topic that has been thoroughly reviewed elsewhere [3, 37, 38]. Briefly, CaMKII phosphorylates the L-type Ca^{2+} channel to potentiate Ca^{2+} influx in response to repeated excitation (termed facilitation) [33, 34]. CaMKII colocalizes with and phosphorylates RyR2 to regulate channel activity, leading to increased diastolic SR Ca^{2+} leak and systolic Ca^{2+} release through an increase in the open probability of the channel [39–45]. In fact, CaMKII regulates Ca^{2+} entry and Ca^{2+} release via phosphorylation of L-type Ca^{2+} channels, Ca^{2+} release via phosphorylation of RyR2 Ca^{2+} release channels, and Ca^{2+} reuptake via phosphorylation of SERCA2a and/or PLB. Thus, CaMKII is uniquely positioned to simultaneously regulate several aspects of excitation–contraction coupling.

22.2.2 CaMKII Regulation of Cardiac Pacemaking and Conduction

The heartbeat begins as a spontaneous action potential generated from a central location in the sinoatrial node (SAN), a compact collection of specialized excitable cardiomyocytes in the right atrium [46]. The electrical signal then passes through the atria to the atrioventricular node and into the His-Purkinje system and then rapidly through the ventricles. CaMKII can regulate heart rate and rhythm by affecting cell excitability at multiple loci in this electrical activation sequence.

SAN cells possess unique structural and electrophysiological properties that facilitate spontaneous cell membrane depolarization. In fact, SAN pacemaking results from the complex coordination at the level of the single cell of both depolarizing and repolarizing currents [46, 47]. Furthermore, SAN cells have evolved an elaborate system for storing and cycling intracellular Ca^{2+}. SR Ca^{2+} load is comparable to that of ventricular myocytes [48]. Intracellular Ca^{2+} cycling is an important pathway through which SAN cells regulate spontaneous electrical activity [49]. Specifically, Ca^{2+} release hastens phase 4 depolarization of the SAN cell membrane by increasing depolarizing current via forward-mode Na^+/Ca^{2+} exchange [50, 51].

CaMKII coordinates the activities of multiple sarcolemmal and SR proteins ($Ca_v1.2$, $Ca_v1.3$, RyR2, and SERCA2a/PLB) to regulate Ca^{2+} cycling in SAN cells. Studies indicate that CaMKII mediates the fight-or-flight response of SAN activity and heart rate to β-adrenergic stimulation [48]. Specifically, transgenic mice expressing a peptide inhibitor of CaMKII (AC3-I) show a blunted heart rate response to isoproterenol both in vivo and ex vivo. Basal heart rate is unaffected in AC3-I mice or CaMKII-δ-KO mice [52], suggesting that the role of CaMKII is restricted to the fight-or-flight response. However, atrio-ventricular node conduction is altered in AC3-I mice, even under basal conditions [53]. While these observations describe the role of CaMKII in acute regulation of heart rate and rhythm, chronic activation of CaMKII has been shown to contribute to SAN dysfunction characterized by abnormal impulse formation and propagation by inducing SAN cell apoptosis [54]. These observations, in particular, highlight a critical distinction between short- and long-term consequences of CaMKII activity.

In the ventricle, CaMKII regulates cell excitability and electrical conduction via phosphorylation of voltage-gated Na^+ channels [25, 55–57]. Voltage-gated Na^+ channels (Na_v) generate the rapid upstroke of the cardiac action potential and are critical for normal electrical conduction through the heart. Na_v dysfunction caused by mutations in *SCN5A*, the gene encoding the primary cardiac Na_v α-subunit, $Na_v1.5$, has been associated with several life-threatening cardiac arrhythmia syndromes, including type 3 long QT syndrome (LQT3), Brugada syndrome, and cardiac conduction disease, as well as dilated cardiomyopathy [58, 59]. Abnormalities in $Na_v1.5$ expression and function have also been identified in common forms of acquired heart disease (e.g., heart failure and myocardial infarction) [60], where slow conduction plays an important role in arrhythmia and sudden death [61–63]. CaMKII alters Na_v channel gating consistent with Na_v channel mutations that produce combined loss-of-function/gain-of-function phenotypes (e.g., 1795insD producing combined LQT/Brugada syndrome) [25, 64]. Specifically, CaMKII overexpression has been shown to decrease channel availability while increasing the persistent, or late, current in ventricular myocytes [25, 56, 65]. CaMKII-dependent regulation of $Na_v1.5$ occurs through direct phosphorylation [28, 66, 67]. Notably, the actin-associated cytoskeletal protein $β_{IV}$-spectrin targets a subpopulation of CaMKII to $Na_v1.5$ to coordinate phosphorylation of the channel at Ser571 in the DI–DII linker [28]. CaMKII-dependent phosphorylation of $Na_v1.5$ at Ser571 has been shown to primarily increase late current in ventricular and atrial myocytes, thereby promoting action potential prolongation, dysregulation of Na^+/Ca^{2+} homeostasis, and even subsequent activation of CaMKII itself to complete an arrhythmogenic feedback loop [28, 35, 36, 68].

Several studies have identified a role for CaMKII in regulating the activities of K^+ currents essential for maintaining the resting membrane potential and action potential repolarization [69, 70]. Transgenic mice expressing the CaMKII inhibitory peptide AC3-I show decreased action potential durations and increased transient outward K^+ current, $I_{to,fast}$ (encoded by $K_v4.2/3$), and inward rectifier K^+ current, I_{K1}. At the same time, AC3-I myocytes show an increase in the

ATP-sensitive K^+ current $I_{K,ATP}$ that may contribute to increased protection from ischemia/reperfusion injury [71]. In contrast, transgenic mice overexpressing CaMKII show prolonged action potentials consistent with decreased $I_{to,fast}$ and I_{K1} [26, 27]. The mechanism for CaMKII regulation of these K^+ currents is unclear but likely involves the regulation of expression, trafficking, and/or inactivation of these channels [26, 27, 72]. For example, Kv4.2/3 have been found to form a complex with CaMKII and SAP97, a membrane-associated guanylate kinase (MAGUK protein), to regulate channel membrane expression and activity [72]. Moreover, acute CaMKII inhibition following chronic overexpression was unable to rescue I_{to} amplitude consistent with the notion of expression and trafficking changes, in addition to readily observed changes in channel kinetics [69, 70].

22.3 CaMKII Role in Disease and Arrhythmias

Mounting experimental evidence demonstrates an important role for CaMKII in cardiovascular disease and arrhythmias (Fig. 22.3). Defects in CaMKII activity and expression have been reported across a broad spectrum of etiologies and linked to pathological changes in cardiac mechanical and electrical function. In this section, we review data supporting the involvement of CaMKII in common and acquired forms of cardiac disease, the potential upstream signals leading to aberrant CaMKII signaling, and opportunities and challenges for therapeutic targeting of CaMKII.

22.3.1 CaMKII Role in Cardiac Hypertrophy and Heart Failure

CaMKII overexpression occurs in human heart failure [73, 74], and transgenic mice overexpressing CaMKIIδ develop dilated cardiomyopathy [75, 76]. Increased CaMKII activity has been linked to Ca^{2+} leak from the SR, altered gene expression, and ventricular arrhythmias in a rabbit model of heart failure [77, 78]. Several studies have provided compelling evidence that CaMKII hyperphosphorylation of RyR2 in the setting of heart failure leads to inappropriately active channels that promote diastolic Ca^{2+} leak from the SR, reduced SR Ca^{2+} content, arrhythmogenic Ca^{2+} handling events, and contractile dysfunction [76, 79–82].

Cardiac hypertrophy is the heart's adaptive response to an increase in demand imposed by multiple stress stimuli [83]. At the level of the individual cell, the hypertrophic response involves the assembly of additional sarcomeres and loss of normal sarcomeric arrangement. Importantly, hypertrophy is associated with the activation of alternative gene expression profiles. While Ca^{2+} activates multiple signal transduction pathways that regulate the expression of genes essential for cardiac growth [84], it is clear that CaMKII is a critical regulator of this hypertrophic response (excitation–transcription coupling) [85–88]. CaMKII has been shown to regulate MEF2-dependent gene transcription via phosphorylation of HDAC4/5 [24, 78], NFAT-dependent transcription via calcineurin [89], and postnatal remodeling through regulation of splicing [90]. Moreover, deletion of CaMKIIδ ($Camk2d^{-/-}$) in mice has been shown to prevent the development of cardiac hypertrophy after 3 weeks of aortic constriction [85], while another study using a different CaMKIIδ-deficient mouse showed that CaMKIIδ deletion prevented the transition from hypertrophy to overt heart failure [52]. Several groups have identified a role for CaMKII in the development of heart failure [52, 73–75]. Moreover, induced CaMKII deletion following the onset of pressure overload led to the attenuated remodeling of the hypertrophic state, indicating the direct involvement of CaMKII in driving pathologic remodeling [91]. Thus, it is clear that CaMKII activation is an important step in the heart's hypertrophic response and progression of the disease. Mechanistically, CaMKII activation has been linked to maladaptive changes in excitation–contraction coupling, including intracellular Ca^{2+} overload and SR Ca^{2+} leak that may drive remodeling changes. More recently, a role for CaMKII has emerged in

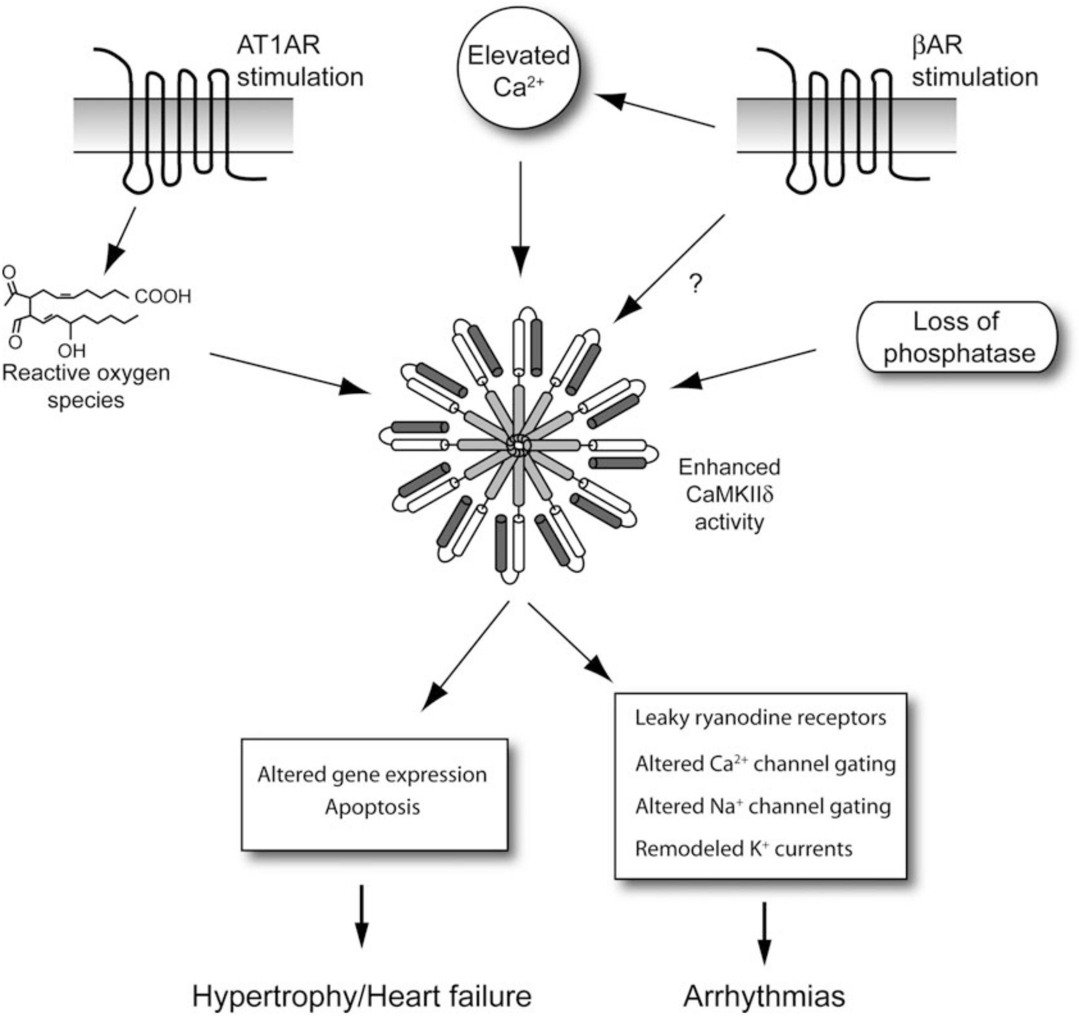
AT1AR stimulation
Elevated Ca^{2+}
βAR stimulation
COOH
O
O
OH
Reactive oxygen species
?
Loss of phosphatase
Enhanced CaMKIIδ activity
Altered gene expression
Apoptosis
Leaky ryanodine receptors
Altered Ca^{2+} channel gating
Altered Na^{+} channel gating
Remodeled K^{+} currents
Hypertrophy/Heart failure
Arrhythmias

Fig. 22.3 CaMKII dysfunction in heart disease and arrhythmias. CaMKII is a potential mediator of multiple upstream pathological stimuli, including oxidative stress, stimulation of β-adrenergic (β-AR) and angiotensin receptors (AT1AR), and decreased phosphatase activity. Excess CaMKII activity has been linked to hypertrophy and heart failure through alterations in gene transcription and apoptosis as well as arrhythmias through its effects on ion channels. Thus, CaMKII is ideally suited as a critical mediator of cardiac pathogenesis

promoting the expression of proinflammatory cytokines and chemokines in cardiomyocytes to exacerbate inflammation and cardiac dysfunction in nonischemic disease [92, 93].

22.3.2 CaMKII Role in Common Forms of Acquired Arrhythmia

CaMKII has also been implicated in remodeling (structural and electrical) and arrhythmias during myocardial ischemia and infarction [55, 94–99]. Calcium overload, β-adrenergic stimulation, acidosis, and oxidative stress are all possible upstream activators of CaMKII in ischemia and infarction [97, 99–101]. The heart undergoes dramatic structural and electrical remodeling following myocardial infarction. These changes not only help create a substrate favorable to initiating life-threatening arrhythmias but also may promote the progression of more advanced heart disease. At the cellular level, a dramatic remodeling of ion channels has been documented along with alterations in Ca^{2+} cycling and the action potential [102, 103]. Alterations in CaMKII activity and expression have been identified following myocardial infarction in several animal models of this disease [55, 94–96, 98, 99]. Studies in a large animal model of arrhythmias following myocardial infarction have shown that the levels of both autophosphorylated and oxidized CaMKII are dramatically increased in a highly localized region (infarct border zone) corresponding to the location of reentrant arrhythmias [55, 95]. Studies indicate that CaMKII also plays a role in the altered expression of inflammatory genes following myocardial infarction [98]. Consistent with a maladaptive role for CaMKII following myocardial infarction, transgenic mice expressing the CaMKII inhibitory peptide AC3-I show less structural remodeling and improved heart function following myocardial infarction compared with mice expressing the control peptide [99]. Despite these detrimental observations, however, it has also been observed that acute CaMKII activation during reperfusion following an ischemic event contributes to a significant increase in functional cardiac recovery and contractility [104–106].

A specific role for CaMKII in promoting potentially lethal arrhythmias has been identified in several animal models of heart disease [79, 107–110]. CaMKII inhibition prevents arrhythmias in transgenic mice models of hypertrophy and heart failure [107–109]. CaMKII has also been implicated in abnormal Ca^{2+} cycling and atrial arrhythmias in a transgenic model of atrial fibrillation (AF) [79] as well as in a dog model of congestive heart failure [110]. The mechanism for CaMKII-dependent arrhythmias is unclear, although CaMKII activity regulates intracellular Ca^{2+} cycling and ion channels involved in the generation of the cardiac action potential (e.g., $Ca_v1.2$, $K_v4.3$, $Na_v1.5$), providing for a number of links between CaMKII activity and arrhythmia. One likely mechanism involves secondary depolarization of the action potential during the action potential repolarization phase or diastole (afterdepolarization) [111, 112]. CaMKII activity has been implicated in the formation of afterdepolarizations in response to H_2O_2 treatment [113], aging [114], ischemia/reperfusion [115], as well as in acquired and congenital arrhythmia syndromes [35, 116–119]. It is likely that CaMKII promotes afterdepolarizations, in part, by increasing mode 2 gating of the L-type Ca^{2+} channel [120] characterized by long channel open times conducive to reactivation of the channel during action potential repolarization. CaMKII hyper-phosphorylation of RyR2 channels in the cardiac SR may also play a role by increasing the likelihood of spontaneous Ca^{2+} release [77, 79]. Finally, several studies have implicated a CaMKII-dependent increase in late Na^+ current in promoting AP prolongation and dispersion of repolarization together with intracellular Ca^{2+} overload via reverse mode Na^+/Ca^{2+} exchanger to increase arrhythmia susceptibility [36, 68, 115].

22.3.3 Pathways for Increased CaMKII Activation in Disease

CaMKII is activated by both Ca^{2+}/calmodulin and reactive oxygen species (ROS), which are tightly regulated second messengers important for the normal physiology of the heart (Fig. 22.3). However, elevations in both intracellular Ca^{2+} and ROS levels have been linked to maladaptive remodeling and arrhythmias in heart disease (e.g., heart failure). Thus, CaMKII, with both Ca^{2+}- and ROS-dependent activation pathways, is ideally suited to regulate the heart's response to insult. Increased β-adrenergic stimulation, commonly observed following myocardial infarction and in heart failure, has been shown to activate the kinase both in vitro and in vivo through elevations in Ca^{2+} [99, 121, 122]. Importantly, CaMKII has been shown to mediate apoptosis in response to isoproterenol treatment in vitro and in vivo [23, 122–125]. Neurohumoral agents such as angiotensin II play important roles in the progression of heart failure and have been shown to activate the kinase via oxidative stress [16, 125, 126]. Similarly, altered cellular metabolism and enhanced oxidative stress were found to associate with increased levels of oxidized CaMKII in the brain and heart of diabetic patients [127].

It is also important to note that CaMKII regulation results from a delicate balance between kinase and phosphatase activities. Thus, dysfunction in kinase signaling may occur through increased kinase activity or decreased phosphatase activity [128, 129]. For example, reduced expression of the regulatory subunit of the serine/threonine protein phosphatase 2A, PP2A, has been shown to cause CaMKII-dependent hyperphosphorylation of RyR2 and afterdepolarizations in rat cardiomyocytes [130]. Similarly, myocytes from mice lacking the PP2A regulatory subunit B56α show increased PP2A activity, decreased RyR2 phosphorylation, and a reduction in Ca^{2+} sparks and waves compared to wildtype [131]. Since phosphatase levels are known to change in heart disease, this may be a critical pathway for dysfunction in kinase signaling in disease. Furthermore, considering that changes in upstream CaMKII activators and phosphatases are associated with disease, it is likely that multiple pathways are involved in CaMKII dysregulation in disease.

22.3.4 CaMKII as a Therapeutic Target

Despite the profound role that CaMKII has in cardiac pathology, the development of clinical therapies around direct targeting of this signaling pathway has lagged bench-side discoveries [132]. While CaMKII inhibition has been largely effective in preclinical studies, clinical applications for these treatments are either not available or not translatable. Indeed, CaMKII is a highly ubiquitous protein with necessary physiologic functions in other tissues outside the heart, particularly the brain, where it modulates learning and memory. Therefore, significant barriers involving effects on these systems must be overcome to provide cardiac-specific inhibition for clinical application.

One of the first and most widely used inhibitors of CaMKII is KN-93 [133]. This pharmacologic inhibitor is unique because it disrupts calmodulin binding, thereby stabilizing the interaction between the enzymatic and regulatory domains and inhibiting CaMKII activation. However, this interaction is insufficient to inhibit already activated CaMKII enabled through autophosphorylation or other post-translational modifications previously discussed [134, 135]. Moreover, KN-93 has been shown to have several off-target effects, including voltage-gated K^+ channels [136–138], L-type Ca^{2+} channels [111], and inositol triphosphate receptors [139]. Despite these limitations, KN-93 has been used effectively to probe CaMKII-dependent modulation of excitation–contraction coupling, arrhythmogenic remodeling, and pathological transcriptional cascades, in vitro and in vivo. However, given its off-target effects, inhibitory actions on other kinases [140], ability to target other CaMKII isoforms [141, 142], and an IC_{50} in the μM range [111, 133], this drug is appropriate only for academic applications.

Another set of widely used CaMKII inhibitors are the molecules autocamtide-2-related inhibitory peptide (AIP) [143] and autocamtide-3-derived inhibitory peptide (AC3-I) [144]. These small peptide inhibitors are derived from the regulatory domain of CaMKII and bind to the catalytic domain to maintain the inactive conformation. AIP and AC3-I were altered to remove both the CaM-binding region and the autophosphorylation residue Thr287 to prevent displacement of the inactivated state. A natively expressed peptide inhibitor CaMKIIN has a similar mode of action by competing with the CaMKII regulatory domain [145]. Experimental refinement of this molecule has led to the development of highly potent and specific inhibitors, improving the IC_{50} to 0.4 nM [146]. Like KN-93, these molecules have successfully attenuated pathologic CaMKII signaling, leading to sustained cardiac function in HF models and the prevention of lethal cardiac arrhythmias [54, 147, 148]. However, the limited bioavailability of these peptides in vivo represents a major obstacle to translation. Namely, these molecules are essentially impenetrable to cell membranes without modifications like myristoylation and are susceptible to quick half-lives in circulation with an already limited enteral resorption [149]. Current academic applications use transgenic models that allow cells to encode these peptide sequences. As such, gene therapy approaches using viral delivery vectors represent potential strategies; however, clinical trials for such methods have not had a viable history [150].

Given these current challenges for clinical applications, paired with the academic successes provided through CaMKII inhibition, recent efforts have been made to provide a therapeutic agent for human application. These efforts have focused on designing a novel class of pharmacologic agents that is both cell permeable and targets CaMKII through ATP competition, thereby blocking its kinase activity. Among the first generation of such molecules was Scios 15b [151], and while it was never tested for its impact on pathologic cardiac remodeling, the basis of its design provided the framework for further refinement and testing. Indeed, several companies have more recently introduced similar pyrimidine-based compounds, including AS105 (Allosteros Therapeutics) [152], GS-680 (Gilead Sciences) [153], and RA306 (Sanofi R&D) [154], which have shown effective and specific CaMKII inhibition down to the low nM level with preferential targeting for the CaMKIIδ isoform. Of these, only RA306 has yet to report oral bioavailability and in vivo attenuation of pathologic remodeling in a genetic mouse model of dilated cardiomyopathy [154]. Therefore, it appears that the goal of providing a true clinical attempt for CaMKII inhibition is at last underway, and its progress will be followed with much anticipation.

Inhibiting the activity of CaMKII does not necessarily require targeting of CaMKII directly. As discussed throughout this chapter, there are a large number of intracellular CaMKII targets from ion channels, transcription factors, and Ca^{2+} handling proteins, each representing its own therapeutic opportunity. In this context, it is worth considering CaMKII targeting of $Na_v1.5$ to regulate pathogenic late Na^+ current [36]. Late Na^+ current is also a target for the antianginal agent ranolazine [155], which has been shown to reduce arrhythmogenic burden and prevent the development of heart failure in rodent and large animal studies [36, 156–160]. Unfortunately, clinical trials aimed at showing the impact of ranolazine in the incidence of atrial fibrillation, ventricular arrhythmias, and remodeling in hypertrophic cardiomyopathy have been mixed, although the hope remains that this approach will prove beneficial to specific patient subpopulations [155, 161–164]. Another example of targeting CaMKII substrates for therapeutic benefit comes from a class of compounds referred to as rycals, which stabilize RyR2 and limit Ca^{2+} leak following modification by CaMKII. Specifically, the molecule JTV519 has been shown to improve Ca^{2+} leak and cardiac function in a canine model of heart failure [165], while another compound S107 has demonstrated protection against ventricular arrhythmia and heart failure in mouse models of destabilized RyR [166]. Clearly, CaMKII has an expansive signaling network with each branch individually robust enough to impact the development of pathophysiology, providing ample opportunity for the eventual development of clinically relevant therapeutics.

22.4 Conclusions

Over the past decade, numerous studies have established a critical role for CaMKII in regulating the heart's response to injury. Central to this role is the activation of the kinase by intracellular second messengers Ca^{2+}/calmodulin and reactive oxygen species and its regulation of key proteins involved in Ca^{2+} cycling, gene transcription, and apoptosis. Thus, CaMKII is ideally suited to respond to multiple pathological stimuli and coordinate the activities of downstream effectors to alter cardiac cell function. The CaMKII signaling pathway represents a logical and highly promising therapeutic target for heart disease treatment and sudden death prevention.

Acknowledgments This work was supported by the National Institutes of Health (HL096805, HL135096, and HL134824 to TJH).

References

1. Braun AP, Schulman H. The multifunctional calcium/calmodulin-dependent protein kinase: from form to function. Annu Rev Physiol. 1995;57:417–45.
2. Bayer KU, Schulman H. CaM kinase: still inspiring at 40. Neuron. 2019;103(3):380–94.
3. Swaminathan PD, et al. Calmodulin-dependent protein kinase II: linking heart failure and arrhythmias. Circ Res. 2012;110(12):1661–77.
4. Tobimatsu T, Fujisawa H. Tissue-specific expression of four types of rat calmodulin-dependent protein kinase II mRNAs. J Biol Chem. 1989;264(30): 17907–12.
5. Edman CF, Schulman H. Identification and characterization of δ_B-CaM kinase and δ_C-CaM kinase from rat heart, two new multifunctional Ca^{2+}/calmodulin-dependent protein kinase isoforms. Biochim Biophys Acta. 1994;1221(1):89–101.
6. Kreusser MM, et al. Cardiac CaM kinase II genes delta and gamma contribute to adverse remodeling but redundantly inhibit calcineurin-induced myocardial hypertrophy. Circulation. 2014;130(15): 1262–73.
7. Gaertner TR, et al. Comparative analyses of the three-dimensional structures and enzymatic properties of α, β, γ and δ isoforms of Ca^{2+}-calmodulin-dependent protein kinase II. J Biol Chem. 2004;279(13): 12484–94.
8. Schulman H. Activity-dependent regulation of calcium/calmodulin-dependent protein kinase II localization. J Neurosci. 2004;24(39):8399–403.
9. De Koninck P, Schulman H. Sensitivity of CaM kinase II to the frequency of Ca^{2+} oscillations. Science. 1998;279(5348):227–30.
10. Lisman J, Schulman H, Cline H. The molecular basis of CaMKII function in synaptic and behavioural memory. Nat Rev Neurosci. 2002;3(3):175–90.
11. Kolodziej SJ, et al. Three-dimensional reconstructions of calcium/calmodulin-dependent (CaM) kinase IIα and truncated CaM kinase IIα reveal a unique organization for its structural core and functional domains. J Biol Chem. 2000;275 (19):14354–9.
12. Hanson PI, et al. Dual role of calmodulin in autophosphorylation of multifunctional CaM kinase may underlie decoding of calcium signals. Neuron. 1994;12(5):943–56.
13. Kuret J, Schulman H. Mechanism of autophosphorylation of the multifunctional Ca^{2+}/calmodulin-dependent protein kinase. J Biol Chem. 1985;260(10):6427–33.
14. Meyer T, et al. Calmodulin trapping by calcium-calmodulin-dependent protein kinase. Science. 1992;256(5060):1199–202.
15. Colbran RJ. Inactivation of Ca^{2+}/calmodulin-dependent protein kinase II by basal autophosphorylation. J Biol Chem. 1993;268(10):7163–70.
16. Erickson JR, et al. A dynamic pathway for calcium-independent activation of CaMKII by methionine oxidation. Cell. 2008;133(3):462–74.
17. Erickson JR, et al. Diabetic hyperglycaemia activates CaMKII and arrhythmias by O-linked glycosylation. Nature. 2013;502(7471):372–6.
18. Erickson JR, et al. S-Nitrosylation induces both autonomous activation and inhibition of calcium/calmodulin-dependent protein kinase II delta. J Biol Chem. 2015;290(42):25646–56.
19. Curran J, et al. Nitric oxide-dependent activation of CaMKII increases diastolic sarcoplasmic reticulum calcium release in cardiac myocytes in response to adrenergic stimulation. PLoS One. 2014;9(2): e87495.
20. Zhang DM, et al. Intracellular signalling mechanism responsible for modulation of sarcolemmal ATP-sensitive potassium channels by nitric oxide in ventricular cardiomyocytes. J Physiol. 2014;592(5): 971–90.
21. Ouchi J, et al. alpha1-adrenoceptor stimulation potentiates L-type Ca^{2+} current through Ca^{2+}/calmodulin-dependent PK II (CaMKII) activation in rat ventricular myocytes. Proc Natl Acad Sci U S A. 2005;102(26):9400–5.
22. Wu Y, et al. CaM kinase augments cardiac L-type Ca^{2+} current: a cellular mechanism for long Q-T arrhythmias. Am J Physiol Heart Circ Physiol. 1999;276(6 Pt 2):H2168–78.
23. Timmins JM, et al. Calcium/calmodulin-dependent protein kinase II links ER stress with Fas and mitochondrial apoptosis pathways. J Clin Invest. 2009;119(10):2925–41.
24. Wu X, et al. Local $InsP_3$-dependent perinuclear Ca^{2+} signaling in cardiac myocyte excitation-transcription coupling. J Clin Invest. 2006;116(3):675–82.
25. Wagner S, et al. Ca/calmodulin-dependent protein kinase II regulates cardiac Na channels. J Clin Invest. 2006;116(12):3127–38.
26. Li J, et al. Calmodulin kinase II inhibition shortens action potential duration by upregulation of K^+ currents. Circ Res. 2006;99(10):1092–9.
27. Wagner S, et al. Ca/calmodulin kinase II differentially modulates potassium currents. Circ Arrhythm Electrophysiol. 2009;2(3):285–94.
28. Hund TJ, et al. A betaIV spectrin/CaMKII signaling complex is essential for membrane excitability in mice. J Clin Invest. 2010;120(10):3508–19.

29. Unudurthi SD, et al. betaIV-Spectrin regulates STAT3 targeting to tune cardiac response to pressure overload. J Clin Invest. 2018;128(12):5561–72.
30. McConnachie G, Langeberg LK, Scott JD. AKAP signaling complexes: getting to the heart of the matter. Trends Mol Med. 2006;12(7):317–23.
31. Bayer KU, et al. Interaction with the NMDA receptor locks CaMKII in an active conformation. Nature. 2001;411(6839):801–5.
32. Strack S, Colbran RJ. Autophosphorylation-dependent targeting of calcium/calmodulin-dependent protein kinase II by the NR2B subunit of the N-methyl- D-aspartate receptor. J Biol Chem. 1998;273(33):20689–92.
33. Hudmon A, et al. CaMKII tethers to L-type Ca2+ channels, establishing a local and dedicated integrator of Ca2+ signals for facilitation. J Cell Biol. 2005;171 (3):537–47.
34. Grueter CE, et al. Differential regulated interactions of calcium/calmodulin-dependent protein kinase II with isoforms of voltage-gated calcium channel beta subunits. Biochemistry. 2008;47(6):1760–7.
35. Koval OM, et al. Ca^{2+}/calmodulin-dependent protein kinase II-based regulation of voltage-gated Na^+ channel in cardiac disease. Circulation. 2012;126(17): 2084–94.
36. Glynn P, et al. Voltage-gated Sodium Channel phosphorylation at Ser571 regulates late current, arrhythmia, and cardiac function in vivo. Circulation. 2015;132(7):567–77.
37. Maier LS, Bers DM. Calcium, calmodulin, and calcium-calmodulin kinase II: heartbeat to heartbeat and beyond. J Mol Cell Cardiol. 2002;34(8):919–39.
38. Anderson ME, Brown JH, Bers DM. CaMKII in myocardial hypertrophy and heart failure. J Mol Cell Cardiol. 2011;51(4):468–73.
39. Wehrens XH, et al. Ca^{2+}/calmodulin-dependent protein kinase II phosphorylation regulates the cardiac ryanodine receptor. Circ Res. 2004;94(6):e61–70.
40. Witcher DR, et al. Unique phosphorylation site on the cardiac ryanodine receptor regulates calcium channel activity. J Biol Chem. 1991;266(17):11144–52.
41. Hain J, et al. Phosphorylation modulates the function of the calcium release channel of sarcoplasmic reticulum from cardiac muscle. J Biol Chem. 1995;270 (5):2074–81.
42. Kohlhaas M, et al. Increased sarcoplasmic reticulum calcium leak but unaltered contractility by acute CaMKII overexpression in isolated rabbit cardiac myocytes. Circ Res. 2006;98(2):235–44.
43. Maier LS, et al. Transgenic CaMKIIδ_C overexpression uniquely alters cardiac myocyte Ca^{2+} handling: reduced SR Ca^{2+} load and activated SR Ca^{2+} release. Circ Res. 2003;92(8):904–11.
44. Wu Y, Colbran RJ, Anderson ME. Calmodulin kinase is a molecular switch for cardiac excitation-contraction coupling. Proc Natl Acad Sci U S A. 2001;98(5):2877–81.
45. Ferrero P, et al. Ca2+/calmodulin kinase II increases ryanodine binding and Ca2+−induced sarcoplasmic reticulum Ca2+ release kinetics during beta-adrenergic stimulation. J Mol Cell Cardiol. 2007;43 (3):281–91.
46. Dobrzynski H, Boyett MR, Anderson RH. New insights into pacemaker activity: promoting understanding of sick sinus syndrome. Circulation. 2007;115(14):1921–32.
47. Mangoni ME, Nargeot J. Genesis and regulation of the heart automaticity. Physiol Rev. 2008;88(3): 919–82.
48. Wu Y, et al. Calmodulin kinase II is required for fight or flight sinoatrial node physiology. Proc Natl Acad Sci U S A. 2009;106(14):5972–7.
49. Eisner DA, Cerbai E. Beating to time: calcium clocks, voltage clocks, and cardiac pacemaker activity. Am J Physiol Heart Circ Physiol. 2009;296(3): H561–2.
50. Bogdanov KY, Vinogradova TM, Lakatta EG. Sinoatrial nodal cell ryanodine receptor and Na^+-Ca^{2+} exchanger: molecular partners in pacemaker regulation. Circ Res. 2001;88(12):1254–8.
51. Huser J, Blatter LA, Lipsius SL. Intracellular Ca^{2+} release contributes to automaticity in cat atrial pacemaker cells. J Physiol. 2000;524(Pt 2):415–22.
52. Ling H, et al. Requirement for Ca^{2+}/calmodulin-dependent kinase II in the transition from pressure overload-induced cardiac hypertrophy to heart failure in mice. J Clin Invest. 2009;119(5):1230–40.
53. Khoo M, et al. Calmodulin kinase activity is required for normal atrioventricular nodal conduction. Heart Rhythm. 2005;2:634–40.
54. Swaminathan PD, et al. Oxidized CaMKII causes sinus node dysfunction. J Clin Invest. 2011;121: 3277–88.
55. Christensen MD, et al. Oxidized calmodulin kinase II regulates conduction following myocardial infarction: a computational analysis. PLoS Comput Biol. 2009;5(12):e1000583.
56. Aiba T, et al. Na^+ channel regulation by Ca^{2+}/calmodulin and Ca^{2+}/calmodulin-dependent protein kinase II in Guinea-pig ventricular myocytes. Cardiovasc Res. 2010;85:454–63.
57. Yoon JY, et al. Constitutive CaMKII activity regulates Na+ channel in rat ventricular myocytes. J Mol Cell Cardiol. 2009;47(4):475–84.
58. Lehnart SE, et al. Inherited arrhythmias: a National Heart, Lung, and Blood Institute and Office of Rare Diseases workshop consensus report about the diagnosis, phenotyping, molecular mechanisms, and therapeutic approaches for primary cardiomyopathies of gene mutations affecting ion channel function. Circulation. 2007;116(20):2325–45.
59. Remme CA, Wilde AA, Bezzina CR. Cardiac sodium channel overlap syndromes: different faces of SCN5A mutations. Trends Cardiovasc Med. 2008;18(3):78–87.

60. Nattel S, et al. Arrhythmogenic ion-channel remodeling in the heart: heart failure, myocardial infarction, and atrial fibrillation. Physiol Rev. 2007;87(2):425–56.
61. Saumarez RC, et al. Sudden death in noncoronary heart disease is associated with delayed paced ventricular activation. Circulation. 2003;107(20): 2595–600.
62. Wang Y, et al. Remodeling of early-phase repolarization: a mechanism of abnormal impulse conduction in heart failure. Circulation. 2006;113(15):1849–56.
63. Janse MJ, Wit AL. Electrophysiological mechanisms of ventricular arrhythmias resulting from myocardial ischemia and infarction. Physiol Rev. 1989;69(4): 1049–169.
64. Grandi E, et al. Simulation of Ca-Calmodulin-dependent protein kinase II on rabbit ventricular myocyte ion currents and action potentials. Biophys J. 2007;93 (11):3835–47.
65. Maltsev VA, et al. Modulation of late sodium current by Ca^{2+}, calmodulin, and CaMKII in normal and failing dog cardiomyocytes: similarities and differences. Am J Physiol Heart Circ Physiol. 2008;294(4):H1597–608.
66. Marionneau C, et al. Mass spectrometry-based identification of native cardiac Nav1.5 channel alpha subunit phosphorylation sites. J Proteome Res. 2012;11 (12):5994–6007.
67. Ashpole NM, et al. Ca2+/calmodulin-dependent protein kinase II (CaMKII) regulates cardiac sodium channel NaV1.5 gating by multiple phosphorylation sites. J Biol Chem. 2012;287(24):19856–69.
68. Greer-Short A, et al. Calmodulin kinase II regulates atrial myocyte late sodium current, calcium handling, and atrial arrhythmia. Heart Rhythm. 2020;17(3): 503–11.
69. Mustroph J, Maier LS, Wagner S. CaMKII regulation of cardiac K channels. Front Pharmacol. 2014;5:20.
70. Tessier S, et al. Regulation of the transient outward K^+ current by Ca^{2+}/calmodulin-dependent protein kinases II in human atrial myocytes. Circ Res. 1999;85(9):810–9.
71. Li J, et al. Calmodulin kinase II inhibition enhances ischemic preconditioning by augmenting ATP-sensitive K+ current. Channels (Austin). 2007;1(5):387–94.
72. El-Haou S, et al. Kv4 potassium channels form a tripartite complex with the anchoring protein SAP97 and CaMKII in cardiac myocytes. Circ Res. 2009;104 (6):758–69.
73. Hoch B, et al. Identification and expression of delta-isoforms of the multifunctional Ca^{2+}/calmodulin-dependent protein kinase in failing and nonfailing human myocardium. Circ Res. 1999;84(6):713–21.
74. Kirchhefer U, et al. Activity of cAMP-dependent protein kinase and Ca^{2+}/calmodulin-dependent protein kinase in failing and nonfailing human hearts. Cardiovasc Res. 1999;42(1):254–61.
75. Zhang T, et al. The cardiac-specific nuclear δ_B isoform of Ca^{2+}/calmodulin-dependent protein kinase II induces hypertrophy and dilated cardiomyopathy associated with increased protein phosphatase 2A activity. J Biol Chem. 2002;277(2):1261–7.
76. Zhang T, et al. The $delta_C$ isoform of CaMKII is activated in cardiac hypertrophy and induces dilated cardiomyopathy and heart failure. Circ Res. 2003;92 (8):912–9.
77. Ai X, et al. Ca^{2+}/calmodulin-dependent protein kinase modulates cardiac ryanodine receptor phosphorylation and sarcoplasmic reticulum Ca^{2+} leak in heart failure. Circ Res. 2005;97(12):1314–22.
78. Bossuyt J, et al. Ca^{2+}/calmodulin-dependent protein kinase IIδ and protein kinase D overexpression reinforce the histone deacetylase 5 redistribution in heart failure. Circ Res. 2008;102(6):695–702.
79. Chelu MG, et al. Calmodulin kinase II-mediated sarcoplasmic reticulum Ca2+ leak promotes atrial fibrillation in mice. J Clin Invest. 2009;119(7):1940–51.
80. McCauley MD, Wehrens XH. Ryanodine receptor phosphorylation, calcium/calmodulin-dependent protein kinase II, and life-threatening ventricular arrhythmias. Trends Cardiovasc Med. 2011;21(2): 48–51.
81. Said M, et al. Calcium-calmodulin dependent protein kinase II (CaMKII): a main signal responsible for early reperfusion arrhythmias. J Mol Cell Cardiol. 2011;51(6):936–44.
82. van Oort RJ, et al. Ryanodine receptor phosphorylation by calcium/calmodulin-dependent protein kinase II promotes life-threatening ventricular arrhythmias in mice with heart failure. Circulation. 2010;122(25): 2669–79.
83. Hunter JJ, Chien KR. Signaling pathways for cardiac hypertrophy and failure. N Engl J Med. 1999;341 (17):1276–83.
84. Frey N, McKinsey TA, Olson EN. Decoding calcium signals involved in cardiac growth and function. Nat Med. 2000;6(11):1221–7.
85. Backs J, et al. The delta isoform of CaM kinase II is required for pathological cardiac hypertrophy and remodeling after pressure overload. Proc Natl Acad Sci U S A. 2009;106(7):2342–7.
86. Ramirez MT, et al. The nuclear δ_B isoform of Ca^{2+}/calmodulin-dependent protein kinase II regulates atrial natriuretic factor gene expression in ventricular myocytes. J Biol Chem. 1997;272(49):31203–8.
87. Zhang T, Brown JH. Role of Ca^{2+}/calmodulin-dependent protein kinase II in cardiac hypertrophy and heart failure. Cardiovasc Res. 2004;63(3):476–86.
88. Zhu W, et al. Ca^{2+}/calmodulin-dependent kinase II and calcineurin play critical roles in endothelin-1-induced cardiomyocyte hypertrophy. J Biol Chem. 2000;275(20):15239–45.
89. MacDonnell SM, et al. CaMKII negatively regulates calcineurin-NFAT signaling in cardiac myocytes. Circ Res. 2009;105(4):316–25.

90. Xu X, et al. ASF/SF2-regulated CaMKIIdelta alternative splicing temporally reprograms excitation-contraction coupling in cardiac muscle. Cell. 2005;120(1):59–72.
91. Kreusser MM, et al. Inducible cardiomyocyte-specific deletion of CaM kinase II protects from pressure overload-induced heart failure. Basic Res Cardiol. 2016;111(6):65.
92. Suetomi T, Miyamoto S, Brown JH. Inflammation in nonischemic heart disease: initiation by cardiomyocyte CaMKII and NLRP3 inflammasome signaling. Am J Physiol Heart Circ Physiol. 2019;317 (5):H877–90.
93. Suetomi T, et al. Inflammation and NLRP3 Inflammasome activation initiated in response to pressure overload by Ca(2+)/Calmodulin-dependent protein kinase II delta signaling in cardiomyocytes are essential for adverse cardiac remodeling. Circulation. 2018;138(22):2530–44.
94. Currie S, Smith GL. Calcium/calmodulin-dependent protein kinase II activity is increased in sarcoplasmic reticulum from coronary artery ligated rabbit hearts. FEBS Lett. 1999;459(2):244–8.
95. Hund TJ, et al. Role of activated CaMKII in abnormal calcium homeostasis and I_{Na} remodeling after myocardial infarction: insights from mathematical modeling. J Mol Cell Cardiol. 2008;45:420–8.
96. Netticadan T, et al. Sarcoplasmic reticulum Ca^{2+}/Calmodulin-dependent protein kinase is altered in heart failure. Circ Res. 2000;86(5):596–605.
97. Said M, et al. Increased intracellular Ca^{2+} and SR Ca^{2+} load contribute to arrhythmias after acidosis in rat heart. Role of Ca^{2+}/calmodulin-dependent protein kinase II. Am J Physiol Heart Circ Physiol. 2008;295 (4):H1669–83.
98. Singh MV, et al. Ca^{2+}/calmodulin-dependent kinase II triggers cell membrane injury by inducing complement factor B gene expression in the mouse heart. J Clin Invest. 2009;119(4):986–96.
99. Zhang R, et al. Calmodulin kinase II inhibition protects against structural heart disease. Nat Med. 2005;11:409–17.
100. Damiano BP, Rosen MR. Effects of pacing on triggered activity induced by early afterdepolarizations. Circulation. 1984;69(5):1013–25.
101. Kinugawa S, et al. Treatment with dimethylthiourea prevents left ventricular remodeling and failure after experimental myocardial infarction in mice: role of oxidative stress. Circ Res. 2000;87(5):392–8.
102. Pinto JM, Boyden PA. Electrical remodeling in ischemia and infarction. Cardiovasc Res. 1999;42(2): 284–97.
103. Ursell PC, et al. Structural and electrophysiological changes in the epicardial border zone of canine myocardial infarcts during infarct healing. Circ Res. 1985;56(3):436–51.
104. DeSantiago J, Maier LS, Bers DM. Phospholamban is required for CaMKII-dependent recovery of Ca transients and SR Ca reuptake during acidosis in cardiac myocytes. J Mol Cell Cardiol. 2004;36(1): 67–74.
105. Mundina-Weilenmann C, et al. Role of phosphorylation of Thr(17) residue of phospholamban in mechanical recovery during hypercapnic acidosis. Cardiovasc Res. 2005;66(1):114–22.
106. Vila-Petroff M, et al. Ca(2+)/calmodulin-dependent protein kinase II contributes to intracellular pH recovery from acidosis via Na(+)/H(+) exchanger activation. J Mol Cell Cardiol. 2010;49(1):106–12.
107. Khoo MS, et al. Death, cardiac dysfunction, and arrhythmias are increased by calmodulin kinase II in calcineurin cardiomyopathy. Circulation. 2006;114 (13):1352–9.
108. Sag CM, et al. Calcium/Calmodulin-dependent protein kinase II contributes to cardiac Arrhythmogenesis in heart failure. Circ Heart Fail. 2009;2(6):664–75.
109. Wu Y, et al. Calmodulin kinase II and arrhythmias in a mouse model of cardiac hypertrophy. Circulation. 2002;106(10):1288–93.
110. Yeh YH, et al. Calcium-handling abnormalities underlying atrial arrhythmogenesis and contractile dysfunction in dogs with congestive heart failure. Circ Arrhythm Electrophysiol. 2008;1(2):93–102.
111. Anderson ME, et al. KN-93, an inhibitor of multifunctional Ca^{2+}/calmodulin-dependent protein kinase, decreases early afterdepolarizations in rabbit heart. J Pharmacol Exp Ther. 1998;287(3):996–1006.
112. Wu Y, Roden DM, Anderson ME. Calmodulin kinase inhibition prevents development of the arrhythmogenic transient inward current. Circ Res. 1999;84(8):906–12.
113. Xie LH, et al. Oxidative-stress-induced afterdepolarizations and calmodulin kinase II signaling. Circ Res. 2009;104(1):79–86.
114. Morita N, et al. Increased susceptibility of aged hearts to ventricular fibrillation during oxidative stress. Am J Physiol Heart Circ Physiol. 2009;297:H1594–605.
115. Howard T, et al. CaMKII-dependent late Na+ current increases electrical dispersion and arrhythmia in ischemia-reperfusion. Am J Physiol Heart Circ Physiol. 2018;315(4):H794–801.
116. Qi X, et al. The calcium/calmodulin/kinase system and arrhythmogenic afterdepolarizations in bradycardia-related acquired long-QT syndrome. Circ Arrhythm Electrophysiol. 2009;2(3):295–304.
117. Thiel WH, et al. Proarrhythmic defects in Timothy syndrome require calmodulin kinase II. Circulation. 2008;118(22):2225–34.
118. DeGrande S, et al. CaMKII inhibition rescues proarrhythmic phenotypes in the model of human ankyrin-B syndrome. Heart Rhythm. 2012;9(12): 2034–41.
119. Liu N, et al. Calmodulin kinase II inhibition prevents arrhythmias in RyR2(R4496C+/−) mice with catecholaminergic polymorphic ventricular tachycardia. J Mol Cell Cardiol. 2011;50(1):214–22.

120. Tanskanen AJ, et al. The role of stochastic and modal gating of cardiac L-type Ca2+ channels on early after-depolarizations. Biophys J. 2005;88(1):85–95.
121. Wang W, et al. Sustained beta1-adrenergic stimulation modulates cardiac contractility by Ca2+/calmodulin kinase signaling pathway. Circ Res. 2004;95(8):798–806.
122. Zhu WZ, et al. Linkage of β1-adrenergic stimulation to apoptotic heart cell death through protein kinase A-independent activation of Ca^{2+}/calmodulin kinase II. J Clin Invest. 2003;111(5):617–25.
123. Little GH, et al. Critical role of nuclear calcium/calmodulin-dependent protein kinase IIdeltaB in cardiomyocyte survival in cardiomyopathy. J Biol Chem. 2009;284(37):24857–68.
124. Yang Y, et al. Calmodulin kinase II inhibition protects against myocardial cell apoptosis in vivo. Am J Physiol Heart Circ Physiol. 2006;291(6):H3065–75.
125. Zhu W, et al. Activation of CaMKII-delta C is a common intermediate of diverse death stimuli-induced heart muscle cell apoptosis. J Biol Chem. 2007;282(14):10833–9.
126. Howe CJ, et al. Redox regulation of the calcium/calmodulin-dependent protein kinases. J Biol Chem. 2004;279(43):44573–81.
127. Luo M, et al. Diabetes increases mortality after myocardial infarction by oxidizing CaMKII. J Clin Invest. 2013;123(3):1262–74.
128. Chiba H, et al. A simulation study on the activation of cardiac CaMKII delta-isoform and its regulation by phosphatases. Biophys J. 2008;95(5):2139–49.
129. Saucerman JJ, Bers DM. Calmodulin mediates differential sensitivity of CaMKII and calcineurin to local Ca^{2+} in cardiac myocytes. Biophys J. 2008;95(10):4597–612.
130. Terentyev D, et al. miR-1 overexpression enhances Ca^{2+} release and promotes cardiac arrhythmogenesis by targeting PP2A regulatory subunit B56alpha and causing CaMKII-dependent hyperphosphorylation of RyR2. Circ Res. 2009;104(4):514–21.
131. Little SC, et al. Protein phosphatase 2A regulatory subunit B56alpha limits phosphatase activity in the heart. Sci Signal. 2015;8(386):ra72.
132. Nassal D, Gratz D, Hund TJ. Challenges and opportunities for therapeutic targeting of calmodulin kinase II in heart. Front Pharmacol. 2020;11:35.
133. Sumi M, et al. The newly synthesized selective Ca^{2+}/calmodulin dependent protein kinase II inhibitor KN-93 reduces dopamine contents in PC12h cells. Biochem Biophys Res Commun. 1991;181(3):968–75.
134. Vest RS, et al. Effective post-insult neuroprotection by a novel Ca(2+)/calmodulin-dependent protein kinase II (CaMKII) inhibitor. J Biol Chem. 2010;285(27):20675–82.
135. Buard I, et al. CaMKII “autonomy” is required for initiating but not for maintaining neuronal long-term information storage. J Neurosci. 2010;30(24):8214–20.
136. Ledoux J, Chartier D, Leblanc N. Inhibitors of calmodulin-dependent protein kinase are nonspecific blockers of voltage-dependent K+ channels in vascular myocytes. J Pharmacol Exp Ther. 1999;290(3):1165–74.
137. Rezazadeh S, Claydon TW, Fedida D, KN-93 (2-[N-(2-Hydroxyethyl)]-N-(4-methoxybenzenesulfonyl)]amino-N-(4-chlorocinnamyl)-N-methylbenzylamine), a Calcium/Calmodulin-dependent protein Kinase II inhibitor, is a direct extracellular blocker of voltage-gated potassium channels. J Pharmacol Exp Ther 2006;317(1):292–299.
138. Hegyi B, et al. KN-93 inhibits IKr in mammalian cardiomyocytes. J Mol Cell Cardiol. 2015;89(Pt B):173–6.
139. Smyth JT, et al. Inhibition of the inositol trisphosphate receptor of mouse eggs and A7r5 cells by KN-93 via a mechanism unrelated to Ca2+/calmodulin-dependent protein kinase II antagonism. J Biol Chem. 2002;277(38):35061–70.
140. Gao Y, et al. A broad activity screen in support of a chemogenomic map for kinase signalling research and drug discovery. Biochem J. 2013;451(2):313–28.
141. Mochizuki H, Ito T, Hidaka H. Purification and characterization of Ca2+/calmodulin-dependent protein kinase V from rat cerebrum. J Biol Chem. 1993;268(12):9143–7.
142. Enslen H, et al. Characterization of Ca2+/calmodulin-dependent protein kinase IV. Role in transcriptional regulation. J Biol Chem. 1994;269(22):15520–7.
143. Ishida A, et al. A novel highly specific and potent inhibitor of calmodulin-dependent protein kinase II. Biochem Biophys Res Commun. 1995;212(3):806–12.
144. Braun AP, Schulman H. A non-selective cation current activated via the multifunctional Ca(2+)-calmodulin-dependent protein kinase in human epithelial cells. J Physiol. 1995;488(Pt 1):37–55.
145. Chang BH, Mukherji S, Soderling TR. Characterization of a calmodulin kinase II inhibitor protein in brain. Proc Natl Acad Sci U S A. 1998;95(18):10890–5.
146. Coultrap SJ, Bayer KU. Improving a natural CaMKII inhibitor by random and rational design. PLoS One. 2011;6(10):e25245.
147. Joiner ML, et al. CaMKII determines mitochondrial stress responses in heart. Nature. 2012;491(7423):269–73.
148. Koval OM, et al. CaV1.2 beta-subunit coordinates CaMKII-triggered cardiomyocyte death and afterdepolarizations. Proc Natl Acad Sci U S A. 2010;107(11):4996–5000.
149. Otvos L Jr, Wade JD. Current challenges in peptide-based drug discovery. Front Chem. 2014;2:62.

150. Penny WF, Hammond HK. Randomized clinical trials of gene transfer for heart failure with reduced ejection fraction. Hum Gene Ther. 2017;28(5):378–84.
151. Mavunkel B, et al. Pyrimidine-based inhibitors of CaMKIIdelta. Bioorg Med Chem Lett. 2008;18(7):2404–8.
152. Neef S, et al. Improvement of cardiomyocyte function by a novel pyrimidine-based CaMKII-inhibitor. J Mol Cell Cardiol. 2018;115:73–81.
153. Lebek S, et al. The novel CaMKII inhibitor GS-680 reduces diastolic SR Ca leak and prevents CaMKII-dependent pro-arrhythmic activity. J Mol Cell Cardiol. 2018;118:159–68.
154. Beauverger P, et al. Reversion of cardiac dysfunction by a novel orally available calcium/calmodulin-dependent protein kinase II inhibitor, RA306, in a genetic model of dilated cardiomyopathy. Cardiovasc Res. 2020;116(2):329–38.
155. Rayner-Hartley E, Sedlak T. Ranolazine: A Contemporary Review. J Am Heart Assoc. 2016;5(3):e003196.
156. Rastogi S, et al. Ranolazine combined with enalapril or metoprolol prevents progressive LV dysfunction and remodeling in dogs with moderate heart failure. Am J Physiol Heart Circ Physiol. 2008;295(5):H2149–55.
157. Figueredo VM, et al. Improvement in left ventricular systolic and diastolic performance during ranolazine treatment in patients with stable angina. J Cardiovasc Pharmacol Ther. 2011;16(2):168–72.
158. Liang F, et al. Inhibitions of late INa and CaMKII act synergistically to prevent ATX-II-induced atrial fibrillation in isolated rat right atria. J Mol Cell Cardiol. 2016;94:122–30.
159. Ellermann C, et al. Ranolazine prevents Levosimendan-induced atrial fibrillation. Pharmacology. 2018;102(3–4):138–41.
160. Nie J, et al. Ranolazine prevents pressure overload-induced cardiac hypertrophy and heart failure by restoring aberrant Na(+) and Ca(2+) handling. J Cell Physiol. 2019;234(7):11587–601.
161. De Ferrari GM, et al. Ranolazine in the treatment of atrial fibrillation: results of the dose-ranging RAFFAELLO (Ranolazine in atrial fibrillation following an ELectricaL CardiOversion) study. Heart Rhythm. 2015;12(5):872–8.
162. Bengel P, Ahmad S, Sossalla S. Inhibition of late sodium current as an innovative antiarrhythmic strategy. Curr Heart Fail Rep. 2017;14(3):179–86.
163. Olivotto I, et al. Efficacy of Ranolazine in patients with symptomatic hypertrophic cardiomyopathy: the RESTYLE-HCM randomized, double-blind, placebo-controlled study. Circ Heart Fail. 2018;11(1):e004124.
164. Zareba W, et al. Ranolazine in high-risk patients with implanted cardioverter-defibrillators: the RAID trial. J Am Coll Cardiol. 2018;72(6):636–45.
165. Yano M, et al. FKBP12.6-mediated stabilization of calcium-release channel (ryanodine receptor) as a novel therapeutic strategy against heart failure. Circulation. 2003;107(3):477–84.
166. Bellinger AM, et al. Remodeling of ryanodine receptor complex causes "leaky" channels: a molecular mechanism for decreased exercise capacity. Proc Natl Acad Sci U S A. 2008;105(6):2198–202.

Pathways in Human Arrhythmias: Impact of Post-translational Modifications

23

Aaron D. Argall, Sara N. Koenig, and Peter J. Mohler

Abstract

The cardiac proteome has a vast number of gene products that are post-translationally modified (PTM). PTMs are essential for the regulation of normal excitation–contraction coupling. However, dysfunction in PTM may also result in aberrant cardiac excitability and potentially arrhythmia. In this chapter, we review post-translational modifications in the context of normal heart excitation–contraction coupling and in disease.

Keywords

Post-translational modifications · Cardiac arrhythmias · Phosphorylation · Cardiac rhythm

23.1 Introduction

Chemical modifications at specific residues on proteins known as post-translational modifications (PTMs) are ubiquitous aspects of cellular processing. PTMs regulate protein activity, structure, and localization depending on the presence or absence of a specific modification. These modifications include phosphorylation, methylation, acetylation, and ubiquitination to name a few. PTMs may even crosstalk with other modification sites to promote or inhibit other PTMs up- or downstream along the amino acid sequence. It is important to understand the chemical and biophysical implications PTMs assert over proteins in the normal heart. As shown in Table 23.1, most amino acid residues may be modified. In this chapter, we focus on several PTMs that regulate normal cardiac function and review protein modifications associated with aberrant cardiac excitability and arrhythmia.

23.2 Post-translational Modifications Required for Normal Cardiac Electrophysiology

Excitation–contraction coupling (ECC) is a carefully orchestrated series of events that rely on the PTM of key ion channels and cytoskeletal proteins. As shown in Fig. 23.1 and within Table 23.2, several proteins are necessary for

A. D. Argall · S. N. Koenig
The Frick Center for Heart Failure and Arrhythmia; Department of Physiology and Cell Biology, The Ohio State University Wexner Medical Center, Columbus, OH, USA

P. J. Mohler (✉)
Dorothy M. Davis Heart and Lung Research Institute; Department of Physiology & Cell Biology; Department of Internal Medicine, The Ohio State University Wexner Medical Center, Columbus, OH, USA
e-mail: peter-mohler@uiowa.edu

© Springer Nature Switzerland AG 2023

O. N. Tripathi et al. (eds.), *Heart Rate and Rhythm*, https://doi.org/10.1007/978-3-031-33588-4_23

Table 23.1 Amino acid residues that are subject to specific post-translational modifications. Except for leucine and isoleucine, many amino acids are modified in some way including phosphorylation, methylation, acetylation, ubiquitination, glycosylation, SUMOylation, and palmitoylation. More unique modifications include citrullination, hydroxylation, and myristoylation (not covered in this chapter)

Post-translation modification	Amino acid residue
Phosphorylation	Arg, Asp, Cys, Glu, His, Lys, Ser, Thr, Tyr
Methylation	Ala, Arg, Asp, Gln, Glu, Lys
Acetylation	Lys, Met, Val
Ubiquitination	Lys
Glycosylation	Arg, Asn, Cys, Pro, Ser, Thr, Tyr, Trp
SUMOylation	Lys
Palmitoylation	Cys, Gly, Ser, Thr
Citrullination	Arg
Hydroxylation	Lys, Pro, Phe
Myristoylation	Cys, Gly

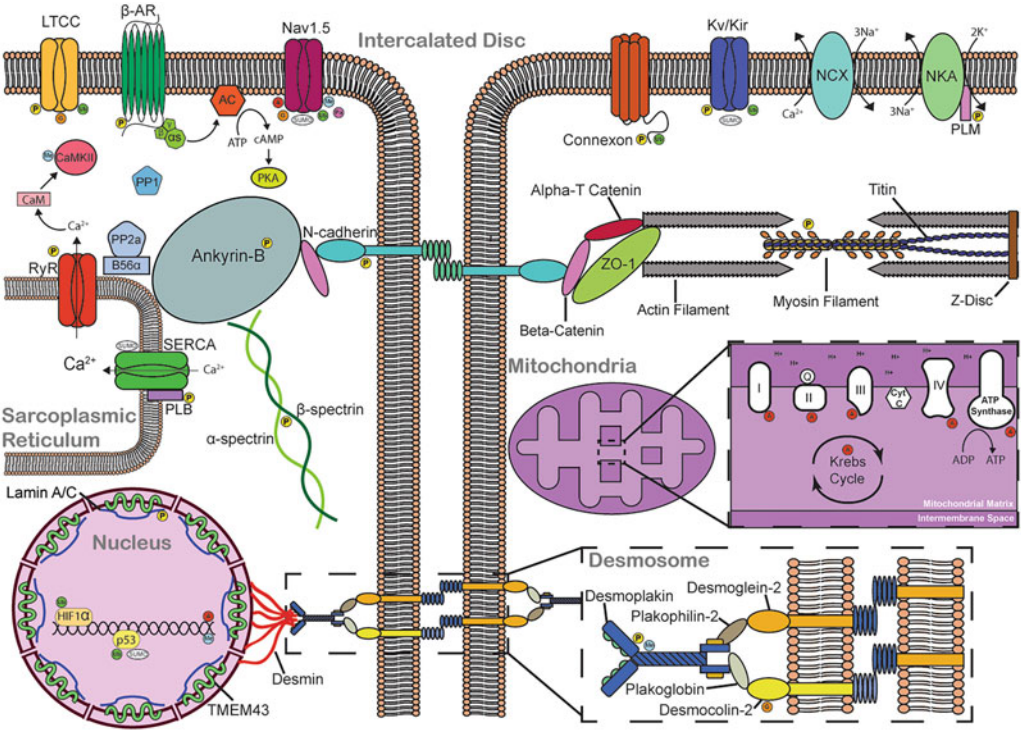
LTCC
β-AR
Nav1.5
Intercalated Disc
Kv/Kir
3Na⁺
2K⁺
NCX
NKA
Ca²⁺
3Na⁺
PLM
AC
αs
ATP
cAMP
PKA
CaMKII
PP1
CaM
Ca²⁺
Connexon
Alpha-T Catenin
Titin
PP2a
B56α
RyR
Ankyrin-B
N-cadherin
ZO-1
Actin Filament
Myosin Filament
Z-Disc
Beta-Catenin
SERCA
Ca²⁺
Ca²⁺
PLB
Mitochondria
I
II
III
Cyt C
IV
ATP Synthase
Krebs Cycle
ADP
ATP
Mitochondrial Matrix
Intermembrane Space
β-spectrin
α-spectrin
Sarcoplasmic Reticulum
Lamin A/C
Nucleus
HIF1α
p53
Desmin
TMEM43
Desmosome
Desmoplakin
Desmoglein-2
Plakophilin-2
Plakoglobin
Desmocolin-2

Fig. 23.1 Cardiac machinery responsible for normal cardiac ECC. Ion channels and transporters in the plasma membrane and sarcoplasmic reticulum facilitate ion concentration fluctuations during ECC. Cytoskeletal proteins function to traffic and position proteins within the cell and adhesion proteins act to anchor cells with one another. Every single protein and cellular process depicted is impacted by PTMs. PTMs act to alter a protein's activity, function, expression, localization, and interactions all of which during homeostasis allow for efficient cardiac contraction. In the context of arrhythmia, mutations may occur that remove a PTM site or a PTM enzyme may be aberrantly expressed causing a change in the presence of PTMs on a protein. (Adapted with permission from [1]). (yellow P—phosphorylation; light blue Me—methylation; red A—acetylation; green Ub—ubiquitination; orange G—glycosylation; white SUMO—sumoylation; pink Pa—palmitoylation)

Table 23.2 Summary of proteins involved in normal cardiac EC coupling and their respective PTMs

PTM	Enzyme	Protein	Site	Reference
Phosphorylation	PKA	RyR	S2808, S2030	[2, 3]
		LTCC and I_K channels	–	[4]
		Cardiac TnI	S23/24	[5]
		PLB	S16	[6]
		Connexins	C-terminus	[7]
	PKC	LTCC-$Ca_V1.2$ and Connexins	S1928	[8]
	PKA/PKC	I-1	T35-PKA, S67- PKC	[9–11]
		PLM	S63, S68, T69	[12, 13]
		Connexins	C-terminus	[7]
	CaMKII	RyR	S2809, S2814	[14]
		Nav1.5	S571	[15]
		PLB	T17	[16]
		TnI, LTCC, and ion channels for I_{Na}, I_{to}, and I_{K1}	–	[4]
	Akt	Connexins	C-terminus	[7, 17]
	PKG			
	CK1			
	Cdk5			
	MAPK			
	P43cdc2			
	Src	β-catenin	S33, S37, T41	[18]
	GSK3			
Methylation	PRMT1	CaMKII	R9, R275	[19]
		Desmoplakin	R2826, R2834, R2838, R2846	[20]
	PRMT3/5	$Na_V1.5$	R513, R526, R680	[21–23]
Acetylation	KATs	GAPDH	K160, K254	[24]
		Arginase-1	–	
		Malate dehydrogenase	K185, K301, K307, K314	
		NDUFA9	K175, K189, K234, K254, K328, K370	[25, 26]
	KATs/ SIRT3	Complex SDHA/SDHB	–	[27]
Ubiquitination	Nedd4–2 (E3 ligase)	KCNQ1	PY motif	[28]
		$Na_V1.5$	–	[29]
	UBE1 (E1 enzyme)			[30]
	UBA6 (E1 enzyme)			
	UBC9 (E2 enzyme)			
	Rfp2 (E3 ligase)	LTCC	K48	[31]
	MDM2 (E3 ligase)	p53	–	[32]
	Von Hippel–Lindau	HIF1-α	–	[33]
SUMOylation	SUMO-1,2,3	SERCA2a	K480, K585	[34]
		KCNK1	K274	[35]
		Kv1.5	–	[36]
	UBC9		–	
	SENP2		–	
		Kv7.2	–	[37]
Glycosylation	Oligosaccharyl-transferases	$Ca_V1.2$	N124, N299, N1359, N1410	[38]
		$Ca_V\alpha2\delta1$ subunit	N348, N468, N663, N812	[39]
		DSC2	N166, N392, N546, N629	[40]

efficient cardiac excitability, including critical proteins that make up the cytoskeleton, ion channels, and mitochondria. At every step of ECC, a protein is post-translationally modified. ECC begins either intrinsically at the pacemaker sinoatrial node or extrinsically from peripheral innervation and neurotransmitter release onto cardiomyocytes. Briefly, upon stimulation, an action potential propagates along the plasma membrane and spreads into transverse T-tubules. Voltage-gated Ca^{2+} channels open in response to this depolarizing stimulus, priming the intracellular space with rising Ca^{2+} levels. Calcium-induced calcium release then occurs whereby Ca^{2+} stores in the sarcoplasmic reticulum (SR) are released via the ryanodine receptor (RyR). Rising Ca^{2+} levels stimulate troponin C to uncover myosin-binding sites on actin to allow for myosin cross-bridge cycling to occur ultimately generating contraction of the cardiomyocyte. The electrical impulse caused by the increase in intracellular Ca^{2+} propagates between cardiomyocytes via gap junctions allowing for instantaneous and synchronous contractions throughout the heart. Ca^{2+} is then recycled back into the SR to prepare for the next ECC event. In this section, we review specific PTM events during ECC and how PTMs play a vital role in maintaining normal cardiac rhythm.

23.2.1 Phosphorylation

Protein phosphorylation is one of most common PTMs, regulating protein function and impacting nearly every cellular process. Kinases canonically phosphorylate amino acid residues including serine, threonine, tyrosine, on their hydroxyl group (-OH) via the transfer of a phosphate group ($-PO_3^{2-}$) from ATP [41]. Non-canonical phosphorylation residues include: histidine, lysine, arginine (N-linked phosphoamidate), aspartic acid and glutamic acid (carboxy O-linked acyl phosphate), and cysteine (S-linked phosphorothiolate) [42]. Phosphatases, contrastingly, hydrolyze phosphate groups from these residues, restoring their hydroxyl group and creating a free phosphate ion. Phosphorylation or dephosphorylation can activate or inhibit protein function and alter protein structure. In this section, we discuss how phosphorylation events impact protein function and crosstalk with other PTMs.

Excitation–Contraction Coupling Upon action potential stimulation via internal (SA node) or external stimuli (neurotransmitter), several key kinases, protein kinase A (PKA), calcium/calmodulin-dependent protein kinase II (CaMKII), and glycogen synthase kinase 3 (GSK3) phosphorylate downstream Ca^{2+} regulatory proteins. PKA is involved in the β-adrenergic signaling cascade where upon receptor agonist binding, the β-adrenergic receptor becomes activated and subsequently activates adenylyl cyclase. Adenylyl cyclase synthesizes cyclic AMP (cAMP) that in turn activates PKA. Activated PKA then phosphorylates several proteins including L-type calcium channel (LTCC), ryanodine receptor (RyR), phospholamban (PLB), troponin I (TnI), phospholemman (PLM), and voltage-gated delayed rectifier potassium channels responsible for I_{Kur}, I_{Ks}, and I_{Kr} [4]. PKA phosphorylation of LTCC results in an increase in $I_{Ca\text{-}L}$, whether the phosphorylation event itself is sufficient for LTCC activation or a protein–protein interaction is first required prior to phosphorylation is still being investigated [43, 44]. Regulation of LTCCs via phosphorylation have been described in the context of the mouse atrial cell line, HL-1, where PKC preferentially increased the expression of full length $Ca_v1.2$ in the plasma membrane as opposed to its truncated isoforms [8]. This increase in expression also leads to an increase in current. Through the phosphorylation of $Ca_v1.2$ at S1928, PKC was shown to control localization of LTCC to the sarcolemma. The influx of Ca^{2+} from $I_{Ca\text{-}L}$ results in calcium-induced calcium release from the SR through RyR. Phosphorylation of RyR by PKA at several residues including S2808 and S2030 activates the channel to release stored calcium from the sarcoplasmic reticulum [2, 3]. Inhibitor-1 (I-1) is an endogenous inhibitor of protein phosphatase-1 (PP1) and is differentially phosphorylated by PKA at T35 and by PKC at S67. I-1 phosphorylation at T35 activates I-1 to inhibit PP1, while S67 phosphorylation limits the activity of I-1 by releasing PP1 [9–11]. Increasing intracellular Ca^{2+} levels stimulate troponin to uncover myosin-binding sites on actin. This allows for myosin cross-bridge cycling to occur generating contraction and relaxation of the cardiomyocyte. Cardiac troponin I (cTnI) may be phosphorylated at S23/24 by several kinases and this modification regulates force contraction and relaxation [5]. Ca^{2+} is then recycled back into the SR via SR Ca^{2+}-ATPase (SERCA) to prepare for the next ECC event or pumped out of the cell via the Na/Ca exchanger. PLB in dephosphorylated state inhibits SERCA thus preventing the reuptake of cytosolic Ca^{2+} back into the SR. Once phosphorylated by PKA at S16, PLB inhibition on SERCA is removed and causes a decrease in cytosolic Ca^{2+} concentration [6]. PLM is a regulator of the Na/K ATPase. In its dephosphorylated state, PLM inhibits the Na/K pump, while phosphorylated PLM removes its inhibitory effects and allows Na/K pump activity. PLM is phosphorylated at S63 (PKC), S68 (PKA/PKC), and T69 (PKA/PKC) [12, 13].

CaMKII is activated upon an increase in intracellular Ca^{2+} levels where CaM binds cytosolic Ca^{2+}, docks to the regulatory domain of CaMKII and displaces the autoinhibitory domain. CaMKII phosphorylates RyR, PLB, TnI, LTCC, and ion channels responsible for I_{Na}, I_{to}, and I_{K1} [4]. RyR phosphorylation by CaMKII at S2809 and S2814 contributes to RyR increased Ca^{2+} sensitivity, open probability, and enhances myocyte contractility [14]. Additional RyR phosphorylation sites have been identified. Similar to the effects of PKA phosphorylation of PLB, CaMKII phosphorylation at T17 also relieves PLB inhibition on SERCA causing an increase in SR Ca^{2+} load and myocardial contraction [16].

GSK3 is expressed in two isoforms, GSK3α and GSK3β and are activated upon dephosphorylation at S21 and S9, respectively [45]. When phosphorylated, these residues have been shown to inhibit its kinase activity and are also physiologically phosphorylated at Tyr279 (GSK3α) and Tyr216 (GSK3β) [46]. GSK3 is regulated by phosphorylation via protein kinase B, i.e., Akt, and PKA [47]. PKA has been shown to physically associate with GSK3β and phosphorylates at both the S21 and S9 residues [18, 48]. GSK3 plays a primary role in regulating gene expression through its phosphorylation of β-catenin at S33, S37, and T41 [49]. β-catenin acts as a transcription factor involved in Wnt signaling to transcribe genes involved in development, proliferation, and differentiation. When β-catenin is phosphorylated at specific residues by GSK3, this leads to its degradation.

Cell Junction Gap junctions contribute to the propagation of the cardiac action potential by transmitting the wave of Ca^{2+} released from the SR to neighboring cells. Primarily linked via connexin-40 (Cx40), connexin-43 (Cx43), and connexin-45 (Cx45), these pore forming channels are uniquely regulated by phosphorylation. Connexin phosphorylation, mostly via residues on the C-terminus, controls channel stability, trafficking, and docking between two hemichannels. Phosphorylation of connexin proteins is facilitated by the following kinases: PKA, CaMKII, Akt, PKC, PKG, CK1, Cdk5, Src, MAPK, and P34cdc2 [7]. Phosphorylation of connexin hemichannels, however, is carried out uniquely by PKA, Akt, PKC, and MAPK. The presence of phosphorylation regulates gap junction turnover with a half-life ranging from 1 to 5 hrs, the homo- or heteromeric coupling between two hemichannels, and gating properties allowing for the transfer of ions and other small molecules between coupled cells [17]. Extensively reviewed by Pogoda et al., connexins and gap junction intracellular communication (GJIC) are heavily regulated by phosphorylation [49]. In the cytoplasm β-catenin, phosphorylated by GSK3 and Src, interacts with cadherins, associated with the desmosome, where its phosphorylation status regulates its affinity for cadherin binding [50].

Cytoskeleton Normal cardiac excitability is made possible not only by ion channels and gap junction proteins but also by the cytoskeleton that positions ion channels, docking proteins, and

ECC machinery appropriately. Of note, cardiac spectrins and ankyrins have been implicated in assisting with phosphorylation by acting as a platform for kinase binding. While cytoskeletal proteins are phosphorylated, ankyrins and spectrins can function to dock kinases like CaMKII near sodium channel $Na_v1.5$ and RyR2, assisting in the phosphorylation events necessary to propagate the Ca^{2+} wave [51]. Ankyrins have been shown to bind the regulatory subunit of protein phosphatase 2A (PP2A), B56α, via their spectrin-binding domain (SBD) to precisely position PP2A allowing for de-phosphorylation of RyR2 to occur in a spatial and temporal manner [52]. Associated with the cytoskeleton and desmosome, desmoplakin has been shown to be modified on its C-terminal tail by phosphorylation and methylation. There have been 68 potential phosphorylation sites identified on desmoplakin C-terminal tail, of which S2849 has been linked to regulating desmoplakin-intermediate filament (IF) interactions [53, 54]. GSK3 phosphorylates desmoplakin that promotes desmosome assembly, and its association with desmoplakin is necessary for desmoplakin-IF complex formation [20]. This processive phosphorylation is also regulated by methylation via PRMT1, explained in the next section.

23.2.2 Methylation

Protein methylation is a versatile PTM with the ability to both directly and indirectly impact cellular function. Indirect impacts of methylation may be considered in the event of epigenetics where methyl marks are attached to histone sites and an effector protein (reader) recognizes this modification to perform a specific function. Direct methylation impacts are observed in the context of ability of RNA-binding proteins to interact with RNA as well as alter the protein conformation upon methylation. Methylation is mediated by methyltransferases that use the universal methyl donor, s-adenosylmethionine (SAM), in each reaction resulting in the creation of s-adenosyl-homocysteine (SAH), and a methyl mark on the target protein. Methyl marks are linked to specific amino acid residues including arginine and lysine. Arginine methylation is carried out by protein arginine methyltransferases (PRMTs) and lysine methylation is performed by protein lysine methyltransferases (PKMTs). Arginine methylation can exist in three states, the two terminal nitrogens can have a single methyl mark (monomethylarginine), two methyl marks on a single nitrogen (asymmetric dimethylarginine), or a methyl mark on both terminal nitrogens (symmetric dimethylarginine). Similarly, lysine methylation exists in three states but contains only a single terminal nitrogen, can form mono-, di-, and trimethylated lysine residues. In contrast to methyltransferases, demethylases function to remove these methyl marks from arginines and lysines. Two families of demethylases exist: lysine-specific demethylase (LSD) and the Jumonji C (JmjC) protein families. LSD1 catalytic domain utilizes flavin adenine dinucleotide (FAD) and a lone pair of electrons from the lysine's ε-nitrogen to demethylate lysine residues during this oxidation reaction. Unique to JmjC demethylases, they require Fe^{2+} and oxygen to perform the hydroxylation reaction to remove methyl groups and can remove trimethyl marks unlike LSD1 which can only do mono- or dimethyl marks.

As methylation is involved in epigenetic and nonepigenetic mechanisms, this section will focus primarily on non-histone methylation targets associated with normal cardiac rhythm. Starting with action potential propagation, $Na_v1.5$ is post-translationally modified by arginine methylation at R513, R526, and R680 [21]. Utilizing tandem mass spectrometry methods, Beltran-Alvarez et al. [22], were the first to report that these three sites were either mono- (R513/R526) or dimethylated (R526/R680). A few years later, the same group found that PRMT3 and PRMT5 were the enzymes responsible for the arginine methylation on $Na_v1.5$ [22]. They observed that these methylation events in human embryonic kidney cells also increased $Na_v1.5$ current density by enhancing the cell surface expression of ion channels. Furthermore, they described a PTM crosstalk event between arginine methylation at R513 and serine phosphorylation at S516 on the $Na_v1.5$ channel [23]. R513 methylation decreased downstream S516 phosphorylation, while S516 phosphorylation completely blocked R513 methylation.

In 2018, Pyun et al. showed that PRMT1, a type 1 PRMT capable of asymmetric dimethylation, can regulate CaMKII activation [19]. CaMKII is primarily regulated by phosphatases which remove its activation phosphate group at T286. However, PRMTs have gained a spotlight in their aberrant expression and activity in cancer, so their role in other diseases is less known. Utilizing a cardiac-specific PRMT1 null mouse model, Pyun et al. showed unique methylation sites on CaMKII at R9 and R275 that inhibit CaMKII autophosphorylation at T286/287 [19]. They propose that PRMT1 normally regulates CaMKII activity through a methylation-phosphorylation crosstalk or steric hindrance, which then can only become activated once these methylation groups are removed. Removal of these methylation marks allows for effective CaMKII activity and promotes the phosphorylation of ECC machinery.

Methylation has also been shown to impact desmosome formation, specifically involving the protein desmoplakin. The desmosome functions as a cell–cell adhesion complex responsible for maintaining tight junctions and linking the plasma membrane adhesion molecules (cadherins) to cytoskeletal intermediate filaments (IF) [55]. The desmosome is vital for cardiac action potential propagation through the mechanical coupling of adjacent cells in concert with the electrical coupling caused by ion channel activity. PRMT1 has been shown to methylate four residues contained within the 68 phosphosite region of the desmoplakin C-terminus, R2826, R2834, R2838, and R2846 [20]. These methylation events are important for recruitment of GSK3 phosphorylation to initiate desmosome formation and help modulate desmoplakin-IF interactions vital for cytoskeletal organization—a unique example of methylation-phosphorylation crosstalk.

23.2.3 Acetylation

Protein acetylation, like methylation, has epigenetic and nonepigenetic underpinnings. Acetylation occurs when the acetyl group from acetyl coenzyme A (acetyl-CoA) is transferred to a site on a polypeptide chain. One type of acetylation is referred to as N-terminal acetylation which are catalyzed by N-terminal-acetyltransferases (NATs). The other type is known as lysine acetylation catalyzed by either histone acetyltransferases (HATs) or by lysine (K) acetyltransferases (KATs). One difference between these forms of acetylation is the fact that N-terminal-acetylation is considered irreversible while lysine acetylation is reversible. Conversely, deacetylation is performed by histone deacetylases (HDACs) and lysine deacetylases (KDACs)—a subclass called sirtuins that do not rely on acetyl-CoA but NAD+ are also considered deacetylases [56]. In this section, we will review how acetylation impacts the energetics of normal cardiac rhythm.

Focusing on the non-histone acetylation effects on normal cardiac rhythm, acetylation plays a primary role in metabolism, cellular growth, and cardiac energetics. Cardiomyocytes are one of the highest energy-demanding cells in the body comparable to neurons that rely on the precise regulation of metabolites to be processed within the electron transport chain and Krebs cycle. Briefly, glucose is converted into pyruvate in the cytoplasm where it is then transported into the mitochondria and transformed into acetyl-coenzyme A (acetyl-CoA) via pyruvate dehydrogenase (PDH). Acyl-CoA is also formed by the conversion of fatty acids within the cytosol and then transported into the mitochondria via the carnitine-acyltranslocase. Thereafter, acyl-CoA enters β-oxidation and becomes acetyl-CoA, NADH, and $FADH_2$. Acetyl-CoA coalesces from glycolysis and β-oxidation into the Krebs cycle forming more NADH and $FADH_2$. NADH

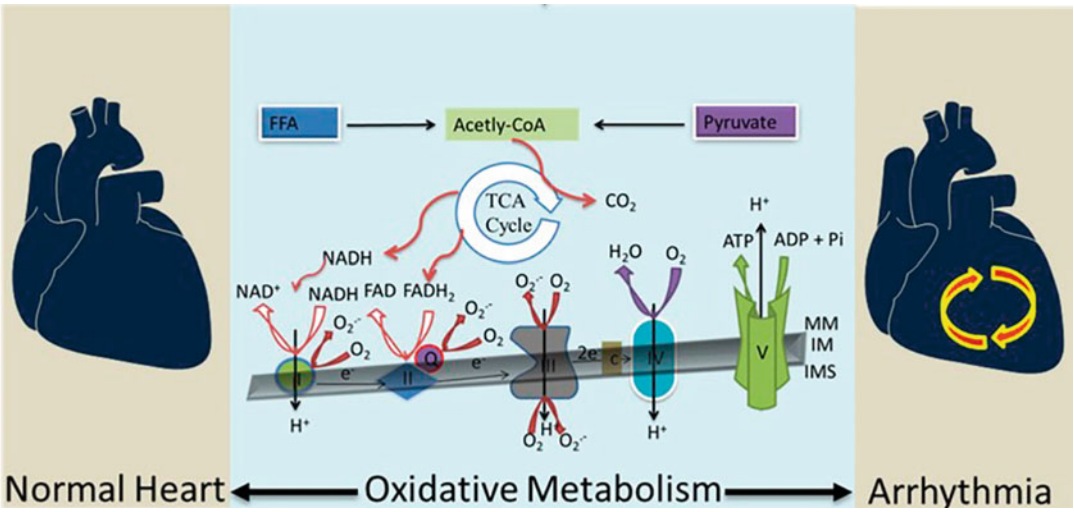

Fig. 23.2 Mitochondrial machinery involved in cardiac metabolism that can be post-translationally modified in the normal and arrhythmic heart. Acetylation is the main PTM occurring in the mitochondria where a balance between deacetylation via sirtuins and acetylation via lysine acetyltransferases regulate the oxidative metabolism within each myocyte's mitochondria. Dysfunction in this PTM regulation can lead to arrhythmias. A—acetylation. Adapted with permission [59]

enters the electron transport chain (ETC) where the ultimate by-product is the generation of ATP [57].

Normal cardiac energetics and related ECC are dependent on the precise coordination of acetylation (KATs) and deacetylation (sirtuins) [58]. At each intermediate metabolite step in the ETC and Krebs cycle, enzymes are acetylated, including GAPDH (K160, K254), arginase-1, and malate dehydrogenase (K185, K301, K307, and K314) [24]. In addition to intermediate enzymes, depicted in Fig. 23.2, protein complexes I–V involved in the ETC are also acetylated. Complex I (NADH dehydrogenase) transfers electrons from NADH to coenzyme Q_{10} and releases 4 protons into the intermembrane space. The complex I subunit NDUFA9 is known to be acetylated at several residues including: K175, K189, K234, K254, K328, and K370 [25, 26]. Complex II (succinate dehydrogenase) receives $FADH_2$ and transfers electrons to ubiquinone (Q) which delivers the electrons to complex III. Also acetylated, both subunits of complex II, SDHA and SDHB, have been shown to physically interact with SIRT3 [27]. SIRT3, highly expressed in the heart, is a mitochondrial deacetylase implicated in the regulation of NADH levels and has a direct impact on fulfilling the necessary energy requirements for synchronous cardiac contractions [60, 61]. Complex III pumps protons across the membrane and transfers electrons to cytochrome C for transport to complex IV. Complex III (cytochrome c reductase) and complex IV (cytochrome c oxidase) are also acetylated but have been less studied in the context of how acetylation impacts their regulation and SIRT3's involvement still needs to be established. Lastly, the ATP synthase (complex V) is coupled with the ETC via the proton gradient generated from complexes I, III, and IV generating ATP and H_2O. Downregulation of SIRT3 has been shown to increase acetylation of oligomycin sensitivity-conferring protein (OSCP), the δ-subunit of ATP synthase, and interact with other ATP synthase subunits [62, 63].

23.2.4 Ubiquitination

Ubiquitin is a small 8.6 kDa protein that is covalently linked to lysine residues and used as a signal for protein degradation. Two pathways utilize ubiquitin to achieve protein turnover and recycling: ubiquitin-proteasome system (UPS) and the autophagy-lysosome pathway (ALP). The UPS degrades short-lived proteins and soluble misfolded proteins, while the ALP degrades long-lived proteins, insoluble aggregates, organelles, and intracellular bacteria. Through the UPS, ubiquitin is added in a step-wise fashion via E1 (ubiquitin-activating), E2 (ubiquitin-conjugating), and E3 (ubiquitin ligase) enzymes [64]. Once a protein is polyubiquitinated, it associates with receptors Rpn10 and Rpn13 on the lid of the 26S proteasome—a complex containing the 20S regulatory complex and the 19S proteasome cap [65]. After a protein is docked to the 26S proteasome, deubiquitinating enzymes (DUBs) cleave the ubiquitin molecules from the protein, initiating the degradation of the protein into its component amino acids. The ALP also utilizes ubiquitin for degradation but involves the engulfment of large complexes via autophagosomes. The autophagosome later fuses with late endosomes and lysosomes becoming an autolysosome where lysosomal hydrolases break down the protein cargo ultimately releasing the amino acids back into the cytosol. The timely turnover of ion channels, enzymes, and contraction machinery is paramount to normal cardiac rhythm.

A primary example of ubiquitination maintaining cardiac rhythm involves the sodium channel $Na_V1.5$. $Na_v1.5$ associates with Nedd4–2, an E3 ubiquitin-protein ligase involved in the UPS, and becomes ubiquitinated leading to the internalization and eventual degradation of the channel [29]. $Na_V1.5$ is also ubiquitinated by UBE1 and UBA6, two E1 enzymes, that regulate ubiquitination through UBC9, ultimately controlling the channel's expression and current density [30]. $Ca_V1.2$, an LTCC vital to cardiac E-C coupling, comprises of α_1, $\alpha_2\delta$, and β subunits, of which the $Ca_v\beta$ has been shown to promote trafficking to the plasma membrane via inhibition of Rfp2-dependent ubiquitination at K48 [31, 66]. $Ca_V1.2$ channels lacking $Ca_V\beta$ are targeted by Rfp2, an E3 ligase, for ubiquitination before they ever leave the endoplasmic reticulum. Potassium channels including KCNQ1 are also regulated via ubiquitination through Nedd4–2. KCNQ1 ($K_V7.1$) is a voltage-gated potassium channel that forms a complex with KCNE1 to generate the delayed rectifier current I_{Ks}. At the PY motif on the C-terminal domain, Nedd4–2 associates with KCNQ1 to ubiquitinate the channel, reducing protein concentration causing a reduced membrane expression and current [28].

Transcription factor regulation is vital for gene transcription and subsequent protein translation of ECC machinery. Two transcription factors, HIF1α and p53, play versatile roles in cardiac contraction, growth, and apoptosis [67]. HIF1α (hypoxia-inducible factor 1) is a transcription factor activated during hypoxic conditions and is required to prevent the development of cardiac hypertrophy. Under normal conditions, HIF1 is hydroxylated by prolyl-4-hydroxylase domain proteins (PHDs) which then can be recognized by the ubiquitin ligase, von Hippel-Lindau. Ubiquitination of HIF1 ends when hypoxia occurs; however, HIF1's activity is repressed by p53 after sustained pressure overload resulting in hypertrophy and heart failure [33]. p53 is a major transcriptional regulator with roles in every cellular aspect (growth and apoptosis) and disease (heart failure and cancer). Ubiquitination of p53 is performed by the ubiquitin ligase murine double minute 2 (MDM2). p53 has been shown to be upregulated in patients with heart failure and its inhibition improves cardiac function by promoting angiogenesis (VEGF—a HIF1 target gene) [32, 68, 69].

23.2.5 Additional Post-translational Modifications

SUMOylation Unique and reversible, sumoylation is a PTM involving the covalent conjugation of a small ubiquitin-like modifier

(SUMO) to a lysine residue in a protein. These SUMOs can modulate a protein's subcellular localization, activity, and even provide a platform for other protein–protein interactions. UBC9 is a small ubiquitin-like modifier-conjugating enzyme E2 that ligates SUMO to a substrate. Tang et al. found that UBC9 promotes $Na_V1.5$ ubiquitination and degradation, but not SUMOylation via its interaction with Nedd4–2 [70]. Potassium channels including $K_v1.5$, KCNQ, and KCNK1 are SUMOylated substrates and are de-SUMOylated via sentrin/SUMO-specific proteases (SENPs). Specifically, de-SUMOylation of $K_v1.5$ by SENP2 causes a hyperpolarizing shift in the voltage dependence of steady-state inactivation. $K_v1.5$ also interacts with UBC9 and is modified by SUMO-1, −2, and −3 [36]. KCNQ, specifically $K_V7.2$, is de-SUMOylated by SENP2 [37]. SUMOylation of KCNK1 at K274 decreases its current [35]. Important for efficient EC coupling, SERCA2a is SUMOylated at K480 and K585 by SUMO-1 which stabilizes SERCA2a expression and activity by inhibiting its ubiquitination [34].

Glycosylation N-linked glycosylation occurs in the endoplasmic reticulum (ER) during protein trafficking and is catalyzed by oligosaccharyltransferases where glycans are added to asparagine or arginine residues on the protein backbone [71]. The addition of glycans to proteins alters their biophysical properties including folding and downstream trafficking to its appropriate cellular compartment. Other forms of glycosylation include O-linked glycosylation on serine/threonine and a lesser extent on hydroxyproline residues, C-linked glycosylation on tryptophan residues, and S-linked glycosylation on cysteine residues. $Ca_v1.2$ is essential for cardiac E-C coupling and is a target for glycosylation. Studies in *Xenopus* oocytes have shown that several $Ca_V1.2$ residues are glycosylated at asparagine residues (N124, N299, N1359, and N1410). When mutated to glutamine (Q), it was found that a double mutant in domain I (N124 and N299) caused a depolarizing shift in voltage-dependent gating while the quadruple mutant caused a strong reduction in current amplitude as a result of reduced surface expression [38]. It was later identified that four asparagine residues on $Ca_V\alpha2\delta1$ subunit (N348, N468, N663, and N812) were important glycosylation sites. Specifically, when N663 was mutated to glutamine, it reduced protein stability and channel function [39]. Another important example, but within the desmosome involves a protein responsible for cell–cell adhesion known as desmocollin-2 (DSC2). DSC2 mutations have been associated with right ventricular cardiomyopathy, and its native regulation is dependent upon appropriate trafficking in the cell. Four asparagine residues have been identified in DSC2 that are N-glycosylated (N166, N392, N546, and N629) [40]. Later it was identified in HL-1 cells that DSC2 lacking multiple N-glycosylation sites were retained within the Golgi apparatus and a loss of a single site did impact the adhesive properties of DSC2. These findings highlight the importance of N-glycosylation in normal protein trafficking in the heart [72].

23.3 Post-translational Modifications and Arrhythmia

Cardiac arrhythmias can simply be defined as an "irregular heartbeat," but the clinical manifestations and underlying genetics are quite complex. Bradycardia, or "slow heart rate," can be characterized by either: slowed SA node pacemaker activity or by impaired impulse conduction (block). Tachycardia, or "fast heart rate," can be characterized by accelerated pacemaker activity, reentry, and triggered depolarizations (afterdepolarizations). Arrhythmias may occur after any type of heart injury, through metabolic dysfunction, and by genetic underpinnings. In the arrhythmic heart, variants in ion channels and cytoskeletal proteins or aberrant expression of PTM enzymes may disrupt ECC. In this section, we review how various PTMs can promote arrhythmogenic events.

23.3.1 Phosphorylation

In human arrhythmias, primarily ion channels and some structural proteins are aberrantly phosphorylated/dephosphorylated or mutated in such a way to regulate the addition/removal of a phosphate group. For example, in the context of ischemia-reperfusion, phosphorylation by CaMKII of $Na_V1.5$ at S571 results in prolongation of AP duration, increased AP duration dispersion, and increased arrhythmia susceptibility [15].

RyR regulation through phosphorylation is responsible for SR Ca^{2+} release to promote contraction. It has been greatly debated as to which kinase, CaMKII or PKA, is the dominant player in arrhythmogenic SR Ca^{2+} leak [73]. The discrepancies between studies may be due to the animal species, type of experimental model (in vivo or in vitro) and possibly the types of reagents used during the experiments. Whichever the case, it is apparent that phosphorylation plays an important role in SR Ca^{2+} release through the RyR. For instance, upon isoproterenol administration in transgenic CaMKIIδ_c mice, there was an increased incidence of early afterdepolarizations (EADs), while after CaMKII inhibition these EADs were significantly reduced. It was also shown that Ca^{2+} spark frequency was higher in the transgenic mice as compared to WT, and when CaMKII was inhibited, the SR Ca^{2+} spark frequency significantly declined. This suggests that CaMKII phosphorylation contributes to cardiac arrhythmogenesis through an increase in SR Ca^{2+} leak [74]. Utilizing myocardium from heart failure (HF) patients, it was later discovered that CaMKII and not PKA phosphorylation of RyR2 was more significantly associated with disturbed Ca^{2+} cycling [75]. This conflicts with other studies but illustrates how different cardiac models and species may contribute to varying results.

Ankyrins have been shown to interact with kinases and phosphatases and serve as a scaffold so that their activity can spatially take place near their intended targets. An ankyrin variant Q1283H associated with stress-induced arrhythmias impacts the association of ankyrin with PP2A via its B56α subunit. This dissociation was shown to increase phosphorylation of the SR ryanodine receptor at S2814 causing abnormal Ca^{2+} dynamics and result in delayed afterdepolarization-mediated triggered activity [76]. GSK3β, β-catenin, and AnkB have recently been identified as molecular interactors. The loss of or mutations in ankyrin-B and β-catenin dysregulation are associated with arrhythmogenic cardiomyopathy [77]. Cardiac-specific deletion of AnkB resulted in aberrant β-catenin localization. Inhibition of GSK3β, which prevents β-catenin degradation, was sufficient to prevent cardiac remodeling and rescue cardiac function in these AnkB cKO mice [78].

23.3.2 Methylation

$Na_V1.5$, the cardiac sodium channel responsible for the influx of Na^+ ions to propagate the action potential, has two known variants: R526H and R260H. Not an example of a PTM inducing a pro-arrhythmic event, but rather an example of two methylation marks being removed via missense mutations. R526H is considered a loss-of-function variant associated with Brugada syndrome and R682H is a gain-of-function variant associated with Long QT type 3 syndrome. The loss of these two methylation marks suggests their functional relevance for $Na_v1.5$ channel regulation. Interestingly, an arrhythmogenic cardiomyopathy variant (R2834H) within desmoplakin decreases the number of phosphorylation sites available for GSK3 causing a disruption in appropriate desmoplakin localization [20].

23.3.3 Acetylation

As stated previously, acetylation impacts primarily proteins related to metabolism and energetics at both the epigenetic and nonepigenetic levels [79]. In the context of arrhythmia, a susceptible substrate in an injured or diseased state may be exaggerated by mitochondrial protein acetylation.

In mice with heart failure, increased acetylation of succinate dehydrogenase A (SDHA), subunit of complex I, at several lysine reduced its function within the Krebs cycle and within complex II of the ETC [80]. However, a study using a dual knockout mouse without carnitine acetyltransferase and sirtuin 3—enzymes that oppose lysine acetylation—modeling extreme mitochondrial lysine acetylation threatens the notion that hyperacetylation leads to mitochondrial dysfunction and subsequent heart failure [81]. After phenotyping and quantitative acetyl-proteomics, the double knockout mice exhibited normal bioenergetics and were not more susceptible to dysfunction.

23.3.4 Ubiquitination

In the context of atrial fibrillation (AF), autophagy activity was shown to be increased in the atria of AF patients, along with an increase in the autophagy-related gene 7 (ATG7), an E1-like activating enzyme, and microtubule-associated protein light chain 3 variant B (LC3B) [82]. This in turn caused the internalization and degradation of $Ca_v1.2$ via LC3B-positive autophagosomes leading to atrial electrical remodeling and a reduction in I_{CaL} [83]. It was also shown in this study that Rfp2, an E3 ubiquitin ligase, is upregulated and may assist in coordinating $Ca_v1.2$ channels with LC3-positive autophagosomes. In failing hearts, there is a reduction in $Ca_v1.2$ channel density in the plasma membrane [84]. A splice variant known as $Ca_v1.2_{e21\ +\ 22}$, containing exclusive exons 21 and 22, was shown to be highly expressed in hypertrophied human hearts and expressed a higher binding affinity for the $Ca_v\beta$ subunit [85]. Instead of trafficking to the plasma membrane upon $Ca_v\beta$ binding, they are retained in the endoplasmic reticulum (ER) and later degraded. The expression of this splice variant also reduced the expression of normal $Ca_v1.2$ channels by limiting $Ca_v\beta$ subunits resulting in enhanced ubiquitination and degradation of the $Ca_v1.2$ channel.

23.3.5 Additional Post-translational Modifications

Glycosylation O-linked glycosylation occurs when the enzyme O-β-(N-acetyl) glucosamine transferase (OGT) adds a β-N-acetlyglucosamine to a serine/threonine residue. Arrhythmogenesis can be initiated when CaMKII is overactive despite decreased Ca^{2+} levels. While in the context of acute hyperglycemia, Erickson et al. identified CaMKII as a target for O-GlcNAc modification at S279, whereby grants CaMKII autonomy leading to arrhythmia [86]. Due to the overlap with phosphorylation in PTM potential at serine/threonine residues, it is hypothesized that some crosstalk mechanism may occur between these two modifications. Utilizing a kinetic-based high-resolution mass spectrometry assay, Leney et al. showed that phosphorylation of three amino acids upstream of the O-GlcNAcylated site constrained O-GlcNAcylation rates due to steric hindrance between the peptide and the OGT active site. The reverse crosstalk was also shown to not occur when phosphorylation is done by a proline-directed kinase [87].

Palmitoylation S-palmitoylation is the covalent attachment of fatty acids like palmitic acid to cysteine residues of transmembrane proteins. Palmitoyltransferases are responsible for the addition of fatty acid residues onto proteins, while depalmitoylation is carried out by acyl-protein thioesterases [88]. The sodium channel $Na_v1.5$ has been shown to be a target for palmitoylation that induced a significant increase in persistent voltage-gated sodium currents, an increase similar to that of long-QT3 mutations [89]. This increase in sodium late currents may contribute to prolonged action potential duration and early afterdepolarizations which are potentially arrhythmic. It was found that $Na_v1.5$ can be palmitoylated at C981, C1176, C1178, and C1179, and mutations acquired in long QT3 or Brugada syndrome may allow for additional cysteine residues to become accessible to palmitoyltransferases.

23.4 Conclusion

The cardiac proteome has a vast number of proteins that are post-translationally modified. As our detection methods become more sophisticated and precise, the number of PTMs and the modifications of proteins in their native state will only expand. Several considerations within the cardiac PTM-ome including age of sample (mouse or patient), cardiac tissue region, cell line studied, and the protein isolation and PTM detection methods all complicate our understanding of PTMS in normal cardiac and arrhythmic states. Normal cardiac events are tightly regulated through several PTMs including phosphorylation, methylation, and acetylation. It is either through a dysfunction in post-translational processing, aberrant expression of PTM enzymes, or mutagenesis which promotes arrhythmic events to occur. Cardiac arrhythmias are complex phenomena that also rely on the ability to modify protein functions to achieve asynchronous cardiac beating. Though many studies have thoroughly explored phosphorylation and methylation, other PTMs, and their cross-regulation will quickly become more vital to our understanding of cardiac automaticity and arrhythmias.

Acknowledgments This work was supported by National Institutes of Health grants HL135754, HL134824, HL139348 and American Heart Association grant 20YVNR35490079.

References

1. Stevens TL, Wallace MJ, El Refaey M, Roberts JD, Koenig SN, Mohler PJ. Arrhythmogenic cardiomyopathy: molecular insights for improved therapeutic design. J Cardiovasc Dev Dis. 2020;7(2):21.
2. Xiao B, Zhong G, Obayashi M, Yang D, Chen K, Walsh MP, et al. Ser-2030, but not Ser-2808, is the major phosphorylation site in cardiac ryanodine receptors responding to protein kinase A activation upon β-adrenergic stimulation in normal and failing hearts. Biochem J. 2006;396(1):7–16.
3. Wehrens XHT, Lehnart SE, Reiken S, Vest JA, Wronska A, Marks AR. Ryanodine receptor/calcium release channel PKA phosphorylation: a critical mediator of heart failure progression. Proc Natl Acad Sci U S A. 2006;103(3):511–8.
4. Grandi E, Bers DM. Models of the ventricular action potential in health and disease. In: Zipes DP, Jalife J, Stevenson WG, editors. Cardiac electrophysiology: from cell to bedside. 6th ed. Philadelphia, PA: Elsevier; 2014. p. 319–30.
5. Solaro RJ, Moir AJG, Perry SV. Phosphorylation of troponin I and the inotropic effect of adrenaline in the perfused rabbit heart. Nature. 1976;262(5569):615–7.
6. Koss KL, Kranias EG. Phospholamban: a prominent regulator of myocardial contractility. Circ Res. 1996;79:1059–63.
7. Pogoda K, Kameritsch P, Retamal MA, Vega JL. Regulation of gap junction channels and hemichannels by phosphorylation and redox changes: A revision. BMC Cell Biol. 2016;17(Suppl 1):11.
8. Raifman TK, Kumar P, Haase H, Klussmann E, Dascal N, Weiss S. Protein kinase C enhances plasma membrane expression of cardiac L-type calcium channel, CaV1.2. Channels. 2017;11(6):604–15.
9. Singh A, Redden JM, Kapiloff MS, Dodge-Kafka KL. The large isoforms of A-kinase anchoring protein 18 mediate the phosphorylation of inhibitor-1 by protein kinase A and the inhibition of protein phosphatase 1 activity. Mol Pharmacol. 2011;79(3):533–40.
10. Sahin B, Shu H, Fernandez J, El-Armouche A, Molkentin JD, Nairn AC, et al. Phosphorylation of protein phosphatase inhibitor-1 by protein kinase C. J Biol Chem. 2006;281(34):24322–35.
11. Weber S, Meyer-Roxlau S, Wagner M, Dobrev D, El-Armouche A. Counteracting protein kinase activity in the heart: the multiple roles of protein phosphatases. Front Pharmacol. 2015;6:270.
12. Wypijewski KJ, Howie J, Reilly L, Tulloch LB, Aughton KL, McLatchie LM, et al. A separate pool of cardiac phospholemman that does not regulate or associate with the sodium pump: Multimers of phospholemman in ventricular muscle. J Biol Chem. 2013;288(19):13808–20.
13. Silverman BDZ, Fuller W, Eaton P, Deng J, Moorman JR, Cheung JY, et al. Serine 68 phosphorylation of phospholemman: acute isoform-specific activation of cardiac Na/K ATPase. Cardiovasc Res. 2005;65(1):93–103.
14. Wehrens XH, Lehnart SE, Reiken SR, Marks AR. Ca2+/calmodulin-dependent protein kinase II phosphorylation regulates the cardiac ryanodine receptor. Circ Res. 2004;94(6):e61–70.
15. Howard T, Greer-Short A, Satroplus T, Patel N, Nassal D, Mohler PJ, et al. CaMKII-dependent late Na+ current increases electrical dispersion and arrhythmia in ischemia-reperfusion. Am J Physiol Heart Circ Physiol. 2018;315(4):H794–801.
16. Lindemann JP, Watanabe AM. Phosphorylation of phospholamban in intact myocardium. Role of Ca2+−calmodulin-dependent mechanisms. J Biol Chem. 1985;260(7):4516–25.
17. Saffitz JE, Laing JG, Yamada KA. Connexin expression and turnover: implications for cardiac excitability. Circ Res. 2000;86:723–8.

18. Verheyen EM, Gottardi CJ. Regulation of Wnt/β-catenin signaling by protein kinases. Dev Dynam. 2010;239:34–44.
19. Pyun JH, Kim HJ, Jeong MH, Ahn BY, Vuong TA, Lee DI, et al. Cardiac specific PRMT1 ablation causes heart failure through CaMKII dysregulation. Nat Commun. 2018;9(1):5107.
20. Albrecht LV, Zhang L, Shabanowitz J, Purevjav E, Towbin JA, Hunt DF, et al. GSK3- and PRMT-1-dependent modifications of desmoplakin control desmoplakin-cytoskeleton dynamics. J Cell Biol. 2015;208(5):597–612.
21. Beltran-Alvarez P, Pagans S, Brugada R. The cardiac sodium channel is post-translationally modified by arginine methylation. J Proteome Res. 2011;10(8): 3712–9.
22. Beltran-Alvarez P, Espejo A, Schmauder R, Beltran C, Mrowka R, Linke T, et al. Protein arginine methyl transferases-3 and -5 increase cell surface expression of cardiac sodium channel. FEBS Lett. 2013;587(19): 3159–65.
23. Beltran-Alvarez P, Feixas F, Osuna S, Díaz-Hernández R, Brugada R, Pagans S. Interplay between R513 methylation and S516 phosphorylation of the cardiac voltage-gated sodium channel. Amino Acids. 2015;47(2):429–34.
24. Zhao S, Xu W, Jiang W, Yu W, Lin Y, Zhang T, et al. Regulation of cellular metabolism by protein lysine acetylation. Science. 2010;327(5968):1000–4.
25. Kim SC, Sprung R, Chen Y, Xu Y, Ball H, Pei J, et al. Substrate and functional diversity of lysine acetylation revealed by a proteomics survey. Mol Cell. 2006;23 (4):607–18.
26. Ahn BH, Kim HS, Song S, In HL, Liu J, Vassilopoulos A, et al. A role for the mitochondrial deacetylase Sirt3 in regulating energy homeostasis. Proc Natl Acad Sci U S A. 2008;105(38):14447–52.
27. Finley LWS, Haas W, Desquiret-Dumas V, Wallace DC, Procaccio V, Gygi SP, et al. Succinate dehydrogenase is a direct target of sirtuin 3 deacetylase activity. PLoS One. 2011;6(8):e23295.
28. Jespersen T, Membrez M, Nicolas CS, Pitard B, Staub O, Olesen SP, et al. The KCNQ1 potassium channel is down-regulated by ubiquitylating enzymes of the Nedd4/Nedd4-like family. Cardiovasc Res. 2007;74(1):64–74.
29. Van Bemmelen MX, Rougier JS, Gavillet B, Apothéloz F, Daidié D, Tateyama M, et al. Cardiac voltage-gated sodium channel Nav1.5 is regulated by Nedd4-2 mediated ubiquitination. Circ Res. 2004;95 (3):284–91.
30. Hu Y, Bai X, Zhang C, Chakrabarti S, Tang B, Xiong H, et al. Ubiquitination-activating enzymes UBE1 and UBA6 regulate ubiquitination and expression of cardiac sodium channel Nav1.5. Biochem J. 2020;477(9):1683–700.
31. Altier C, Garcia-Caballero A, Simms B, You H, Chen L, Walcher J, et al. The Cavβ subunit prevents RFP2-mediated ubiquitination and proteasomal degradation of L-type channels. Nature Neurosci. 2011;14(2):173–82.
32. Kubbutat MHG, Jones SN, Vousden KH. Regulation of p53 stability by Mdm2. Nature. 1997;387(6630): 299–303.
33. Sano M, Minamino T, Toko H, Miyauchi H, Orimo M, Qin Y, et al. p53-induced inhibition of Hif-1 causes cardiac dysfunction during pressure overload. Nature. 2007;446(7134):444–8.
34. Kho C, Lee A, Jeong D, Oh JG, Chaanine AH, Kizana E, et al. SUMO1-dependent modulation of SERCA2a in heart failure. Nature. 2011;477(7366): 601–6.
35. Rajan S, Plant LD, Rabin ML, Butler MH, Goldstein SAN. Sumoylation silences the plasma membrane leak K+ channel K2P1. Cell. 2005;121(1):37–47.
36. Benson MD, Li QJ, Kieckhafer K, Dudek D, Whorton MR, Sunahara RK, et al. SUMO modification regulates inactivation of the voltage-gated potassium channel Kv1.5. Proc Natl Acad Sci U S A. 2007;104 (6):1805–10.
37. Qi Y, Wang J, Bomben VC, Li DP, Chen SR, Sun H, et al. Hyper-SUMOylation of the Kv7 Potassium channel diminishes the M-current leading to seizures and sudden death. Neuron. 2014;83(5):1159–71.
38. Park HJ, Min SH, Won YJ, Lee JH. Asn-linked glycosylation contributes to surface expression and voltage-dependent gating of Cav1.2 Ca2+ channel. J Microbiol Biotechnol. 2015;25(8):1371–9.
39. Tétreault MP, Bourdin B, Briot J, Segura E, Lesage S, Fiset C, et al. Identification of glycosylation sites essential for surface expression of the CaVα2δ1 subunit and modulation of the cardiac CaV1.2 channel activity. J Biol Chem. 2016;291(9):4826–43.
40. Harrison OJ, Brasch J, Lasso G, Katsamba PS, Ahlsen G, Honig B, et al. Structural basis of adhesive binding by desmocollins and desmogleins. Proc Natl Acad Sci U S A. 2016;113(26):7160–5.
41. Ubersax JA, Ferrell JE. Mechanisms of specificity in protein phosphorylation. Nature Rev Mol Cell Biol. 2007;8:530–41.
42. Makwana MV, Muimo R, Jackson RFW. Advances in development of new tools for the study of phosphohistidine. Lab Investig [Internet]. 2018;98(3): 291–303. https://doi.org/10.1038/labinvest.2017.126.
43. Ahern BM, Satin J. The L-type calcium channel current modulation mechanism: the plot thickens and fogs. J Clin Invest. 2019;129(2):496–8.
44. Yang L, Katchman A, Kushner J, Kushnir A, Zakharov SI, Chen BX, et al. Cardiac CaV1.2 channels require β subunits for β-adrenergic–mediated modulation but not trafficking. J Clin Invest. 2019;129(2): 647–58.
45. Ali A, Hoeflich KP, Woodgett JR. Glycogen synthase kinase-3: properties, functions, and regulation. Chem Rev. 2001;101(8):2527–40.
46. Cole A, Frame S, Cohen P. Further evidence that the tyrosine phosphorylation of glycogen synthase kinase-3 (GSK3) in mammalian cells is an

autophosphorylation event. Biochem J. 2004;377(1): 249–55.

47. Sugden PH, Fuller SJ, Weiss SC, Clerk A. Glycogen synthase kinase 3 (GSK3) in the heart: a point of integration in hypertrophic signalling and a therapeutic target? A critical analysis. Br J Pharmacol. 2008;153 (Suppl 1):S137–53.
48. Fang X, Yu SX, Lu Y, Bast RC, Woodgett JR, Mills GB. Phosphorylation and inactivation of glycogen synthase kinase 3 by protein kinase A. Proc Natl Acad Sci U S A. 2000;97(22):11960–5.
49. Liu C, Li Y, Semenov M, Han C, Baeg GH, Tan Y, et al. Control of β-catenin phosphorylation/degradation by a dual-kinase mechanism. Cell. 2002;108(6): 837–47.
50. Piven OO, Winata CL. The canonical way to make a heart: β-catenin and plakoglobin in heart development and remodeling. Exp Biol Med. 2017;242:1735–45.
51. Hulsurkar M, Quick AP, Wehrens XHT. STAT3: a link between CaMKII–βIV-spectrin and maladaptive remodeling? J Clin Invest. 2018;128(12):5251–66.
52. Bhasin N, Cunha SR, Mudannayake M, Gigena MS, Rogers TB, Mohler PJ. Molecular basis for PP2A regulatory subunit B56α targeting in cardiomyocytes. Am J Physiol - Heart Circ Physiol. 2007;293(1): H109–19.
53. Beausoleil SA, Jedrychowski M, Schwartz D, Elias JE, Villén J, Li J, et al. Large-scale characterization of HeLa cell nuclear phosphoproteins. Proc Natl Acad Sci U S A. 2004;101(33):12130–5.
54. Godsel LM, Hsieh SN, Amargo EV, Bass AE, Pascoe-McGillicuddy LT, Huen AC, et al. Desmoplakin assembly dynamics in four dimensions: multiple phases differentially regulated by intermediate filaments and actin. J Cell Biol. 2005;171(6):1045–59.
55. Kottke MD, Delva E, Kowalczyk AP. The desmosome: cell science lessons from human diseases. J Cell Sci. 2006;119(5):797–806.
56. Drazic A, Myklebust LM, Ree R, Arnesen T. The world of protein acetylation. Biochim Biophys Acta - Prot Proteom. 2016;1864:1372–401.
57. Maack C, O'Rourke B. Excitation-contraction coupling and mitochondrial energetics. Bas Res Cardiol. 2007;102:369–92.
58. Parodi-Rullán RM, Chapa-Dubocq XR, Javadov S. Acetylation of mitochondrial proteins in the heart: the role of SIRT3. Front Physiol. 2018;9:1094.
59. Ezeani M. Aberrant cardiac metabolism leads to cardiac arrhythmia. Front Biosci (Schol Ed). 2020;12: 200–21.
60. Koentges C, Pfeil K, Schnick T, Wiese S, Dahlbock R, Cimolai MC, et al. SIRT3 deficiency impairs mitochondrial and contractile function in the heart. Basic Res Cardiol. 2015;110(4):1–20.
61. Dittenhafer-Reed KE, Richards AL, Fan J, Smallegan MJ, Fotuhi Siahpirani A, Kemmerer ZA, et al. SIRT3 mediates multi-tissue coupling for metabolic fuel switching. Cell Metab. 2015;21(4):637–46.
62. Wu YT, Lee HC, Liao CC, Wei YH. Regulation of mitochondrial F(o)F(1)ATPase activity by Sirt3-catalyzed deacetylation and its deficiency in human cells harboring 4977bp deletion of mitochondrial DNA. Biochim Biophys Acta Mol basis Dis. 2013;1832(1):216–27.
63. Vassilopoulos A, Pennington JD, Andresson T, Rees DM, Bosley AD, Fearnley IM, et al. SIRT3 deacetylates ATP synthase F1 complex proteins in response to nutrient-and exercise-induced stress. Antioxidants Redox Signal. 2014;21(4):551–64.
64. Kocaturk NM, Gozuacik D. Crosstalk between mammalian autophagy and the ubiquitin-proteasome system. Front Cell Dev Biol. 2018;6:128.
65. Lander GC, Estrin E, Matyskiela ME, Bashore C, Nogales E, Martin A. Complete subunit architecture of the proteasome regulatory particle. Nature. 2012;482(7384):186–91.
66. Loh KWZ, Liang MC, Soong TW, Hu Z. Regulation of cardiovascular calcium channel activity by post-translational modifications or interacting proteins. Pflugers Arch Eur J Physiol. 2020;472:653–67.
67. Pagan J, Seto T, Pagano M, Cittadini A. Role of the ubiquitin proteasome system in the heart. Circ Res. 2013;112:1046–58.
68. Chatterjee A, Mir SA, Dutta D, Mitra A, Pathak K, Sarkar S. Analysis of p53 and NF-κB signaling in modulating the cardiomyocyte fate during hypertrophy. J Cell Physiol. 2011;226(10):2543–54.
69. Tsipis A, Athanassiadou AM, Athanassiadou P, Kavantzas N, Agrogiannis G, Patsouris E. Apoptosis-related factors p53, bcl-2 and the defects of force transmission in dilated cardiomyopathy. Pathol Res Pract. 2010;206(9):625–30.
70. Tang B, Hu Y, Wang Z, Cheng C, Wang P, Liang L, et al. UBC9 regulates cardiac sodium channel Nav1.5 ubiquitination, degradation and sodium current density. J Mol Cell Cardiol. 2019;129:79–91.
71. Aebi M. N-linked protein glycosylation in the ER. Biochim Biophys Acta, Mol Cell Res. 2013;1833:2430–7.
72. Brodehl A, Stanasiuk C, Anselmetti D, Gummert J, Milting H. Incorporation of desmocollin-2 into the plasma membrane requires N-glycosylation at multiple sites. FEBS Open Bio. 2019;9(5):996–1007.
73. Dobrev D, Wehrens XHT. Role of RyR2 phosphorylation in heart failure and arrhythmias: controversies around ryanodine receptor phosphorylation in cardiac disease. Circ Res. 2014;114(8):1311–9.
74. Sag CM, Wadsack DP, Khabbazzadeh S, Abesser M, Grefe C, Neumann K, et al. Calcium/calmodulin-dependent protein kinase II contributes to cardiac arrhythmogenesis in heart failure. Circ Heart Fail. 2009;2(6):664–75.
75. Fischer TH, Herting J, Tirilomis T, Renner A, Neef S, Toischer K, et al. Ca2+/calmodulin-dependent protein kinase II and protein kinase A differentially regulate sarcoplasmic reticulum Ca2+ leak in human cardiac pathology. Circulation. 2013;128(9):970–81.

76. Zhu W, Wang C, Hu J, Wan R, Yu J, Xie J, et al. Ankyrin-B Q1283H variant linked to arrhythmias via loss of local protein phosphatase 2A activity causes ryanodine receptor hyperphosphorylation. Circulation. 2018;138(23):2682–97.
77. Garcia-Gras E, Lombardi R, Giocondo MJ, Willerson JT, Schneider MD, Khoury DS, et al. Suppression of canonical Wnt/β-catenin signaling by nuclear plakoglobin recapitulates phenotype of arrhythmogenic right ventricular cardiomyopathy. J Clin Invest. 2006;116(7):2012–21.
78. Roberts JD, Murphy NP, Hamilton RM, Lubbers ER, James CA, Kline CF, et al. Ankyrin-B dysfunction predisposes to arrhythmogenic cardiomyopathy and is amenable to therapy. J Clin Invest. 2019;129(8): 3171–84.
79. Aggarwal S, Banerjee SK, Talukdar NC, Yadav AK. Post-translational modification crosstalk and hotspots in Sirtuin interactors implicated in cardiovascular diseases. Front Genet. 2020;11:356.
80. Horton JL, Martin OJ, Lai L, Riley NM, Richards AL, Vega RB, et al. Mitochondrial protein hyperacetylation in the failing heart. JCI Insight. 2016;2(1):e84897.
81. Davidson MT, Grimsrud PA, Lai L, Draper JA, Fisher-Wellman KH, Narowski TM, et al. Extreme acetylation of the cardiac mitochondrial proteome does not promote heart failure. Circ Res. 2020;127(8): 1094–108.
82. Yuan Y, Zhao J, Yan S, Wang D, Zhang S, Yun F, et al. Autophagy: a potential novel mechanistic contributor to atrial fibrillation. Int J Cardiol. 2014;172(2): 492–4.
83. Yuan Y, Zhao J, Gong Y, Wang D, Wang X, Yun F, et al. Autophagy exacerbates electrical remodeling in atrial fibrillation by ubiquitin-dependent degradation of L-type calcium channel. Cell Death Dis. 2018;9 (9):873.
84. Goonasekera SA, Hammer K, Auger-Messier M, Bodi I, Chen X, Zhang H, et al. Decreased cardiac L-type Ca 2+channel activity induces hypertrophy and heart failure in mice. J Clin Invest. 2012;122(1): 280–90.
85. Hu Z, Wang JW, Yu D, Soon JL, De Kleijn DPV, Foo R, et al. Aberrant splicing promotes proteasomal degradation of L-type Ca v 1.2 calcium channels by competitive binding for CaV β subunits in cardiac hypertrophy. Sci Rep. 2016;6:35247.
86. Erickson JR, Pereira L, Wang L, Han G, Ferguson A, Dao K, et al. Diabetic hyperglycaemia activates CaMKII and arrhythmias by O-linked glycosylation. Nature. 2013;502(7471):372–6.
87. Leney AC, El Atmioui D, Wu W, Ovaa H, Heck AJR. Elucidating crosstalk mechanisms between phosphorylation and O-GlcNAcylation. Proc Natl Acad Sci U S A. 2017;114(35):E7255–61.
88. Zeidman R, Jackson CS, Magee AI. Protein acyl thioesterases (review). Mol Membr Biol. 2009;26: 32–41.
89. Pei Z, Xiao Y, Meng J, Hudmon A, Cummins TR. Cardiac sodium channel palmitoylation regulates channel availability and myocyte excitability with implications for arrhythmia generation. Nat Commun. 2016;7:12035.

Viral Myocarditis

24

Stefan Peischard, Huyen Tran Ho, and Guiscard Seebohm

Abstract

Virus infections are an important factor in the generation of potentially lethal cardiac disease. This chapter describes the viruses most frequently associated with human myocarditis and discusses the mechanisms involved in myocardial infection and pathogenesis. The effects of viral proteases are detrimental to cells by disrupting the integrity of mitochondria, destabilizing the cytoskeleton, impairing Ca^{2+} homeostasis, and provoking apoptotic processes. Viruses like coxsackievirus B3 may modify cardiac cellular electrophysiology by interacting with vesicular transport of ion channels, leading either to enhanced or to impaired channel protein integration into the plasma membrane. Both, the gain- or loss-of-function can be arrhythmogenic. In addition, viroporins, i.e., viral structures resembling ion channels, also contribute to increased propensity to arrhythmias following viral infection of cardiomyocytes. They conduct Ca^{2+} and thereby profoundly disrupt cellular Ca^{2+} homeostasis, induce autophagy, and promote inflammation. Last not least, healing processes lead to fibrosis, the known substrate for re-entry arrhythmias. Amongst the complex immune reactions to viral infection, activation of tumor necrosis factor alpha represents a signaling pathway which for therapeutic interventions with the aim of suppressing arrhythmias associated with viral myocarditis.

Keywords

Viral myocarditis · Enterovirus · Viroporin · Proteases · Ion channel

24.1 Introduction

Cardiac diseases and subsequent dysfunctions are the most prominent cause of death in the Western world. Consequently, huge research resources are invested, in hope of developing treatments or cures mostly for genetic heart diseases and diseases appearing due to an unhealthy lifestyle, which are most relevant for cardiac malfunctions. Since several years, viruses have been identified as agents for cardiac diseases. Virus infections turn out to be a strong factor in the generation of severe cardiac phenotypes either in combination with the mentioned aspects or as single cause. Due to the wide range of potential viral agents and complex disease patterns, detailed clinical studies on human patients are insufficient to clarify the complex network of viral infection. The use of animal models and cell systems, allow for expression of virus strains or single viral proteins

---

S. Peischard · H. T. Ho · G. Seebohm (✉)
Institute for Genetics of Heart Diseases (IfGH),
Department of Cardiovascular Medicine, University
Hospital Münster, Münster, Germany
e-mail: guiscard.seebohm@ukmuenster.de

© Springer Nature Switzerland AG 2023

O. N. Tripathi et al. (eds.), *Heart Rate and Rhythm*, https://doi.org/10.1007/978-3-031-33588-4_24

and observation in a well-controlled environment. Application of such methods leads to new findings and several general disease patterns of viral myocarditis were identified, which will be discussed in this chapter. The influence of viruses on the host cardiomyocytes is versatile and complex, changing the structure and function of many cellular organelles like the mitochondria, the contractile apparatus, membrane integrity and others, leading in total to the observed phenotypes in human patients with potentially lethal cardiac dysfunctions.

24.2 Prevalence and Incidence of Viral Myocarditis

According to the most recent Global Burden of Diseases, Injuries, and Risk Factors Study 2017 (GBD 2017) for 195 countries including around 7.4 billion humans, there are around 21 to 26 of total cases per 100,000 humans (prevalence rate) that have myocarditis and 36 to 45 new cases per 100,000 humans (incidence rate) that occurred in 2017 [1]. Myocarditis can be caused by non-infectious agents such as certain drugs, the environment, animal venoms, and diseases like autoimmune diseases as well as by infectious agents such as viruses, bacteria, fungus, spirochetes, rickettsia, protozoa, and helminthiasis. The most common cause appears to be through viruses at least in Northern America and West Europe [2].

During the early years between 1990 and the early 2000s, enteroviruses such as coxsackievirus B3 and adenoviruses were described to be the most frequent viruses to be found in myocarditis with a prevalence percentage of 14% and 23%, respectively, within myocarditis patients [3]. However, in the more recent years, studies indicated that there is a shift toward parvovirus B19 (PVB19) and human herpes virus 6 (HHV6) as the most common viruses present in myocarditis with prevalence percentages like 55.7% or 28% for parvovirus B19 and 24.1% for human herpes virus 6 [4, 5] (see also Table 24.1). But there are concerns about the relevance of parvovirus B19 in causing myocarditis as the virus can also be found in healthy participants and also with no significant difference in prevalence between the two groups [12]. It has been suggested that parvovirus B19 could only be relevant when there is a coinfection with other cardiotropic viruses such as human herpes virus 6 and enteroviruses or is dependent on the viral load. Hence, it is not clear yet, whether this virus is of pathogenic importance and whether the presence of the virus can give a clear prognosis.

24.3 Viral Infection of the Heart

Pathological infections of the cardiac system usually do not occur exclusively in humans, but are often side effects of a coinfection with other pathogens. This scenario applies to infections with, e.g., influenza, coronavirus, rhinovirus and others, in which the immune system of the patient is weakened while fighting the primary infection [13].

By fighting the main pathogen, other viruses take advantage of the situation by infecting inner organs like the cardiac system. The secondary virus, e.g., coxsackieviruses or adenoviruses, recognizes its target cell via specific surface proteins of the distinct cell. These proteins act as a hub for the virus to bind to the cell membrane and enter the cell via endocytosis. Coxsackieviruses and adenoviruses use the Coxsackievirus-Adenovirus-receptor (CAR) for host cell binding or rely on the binding to decay accelerating factor (DAF) [14]. Influenza A viruses have hemagglutinin (HA) proteins distributed around their capsid and use sialic acid-containing proteins (SA) as binding partner. In these examples, SA is an ubiquitously expressed cell-surface protein allowing the Influenza A virus to infect a huge variety of cell types including cells of the respiratory tract, leading to the common flu, or cardiac cells resulting in viral myocarditis [15, 16] In the case of adenoviruses and coxsackieviruses, the receptors CAR and DAF are expressed mostly in polarized cells like neurons and cardiomyocytes, in which CAR is located at the tight gap junctions at the cell poles. First, the virus binds to DAF, leading to a

Table 24.1 Prevalence of most common cardiotropic viruses in % in patients with diagnosed myocarditis

Number of patients in study	Year of Study	Entero-virus	Adeno-virus	Parvo-virus B19 (PVB19)	Human Herpes Virus 6 (HHV6)	Ebbstein-Bar-Virus	Cyto-megalo virus	Refer-ence
624	1988–2000	14%	23%	n.a.	n.a.	0.5%	3%	[3]
149	n.a. (sub-mitted 2003)	8%	12%	n.a.	n.a.	0%	n.a.	[6]
172	2001–2004	33%	8%	37%	11%	n.a.	n.a.	[7]
87	n.a. (sub-mitted 2005)	1%	0%	56%	18%	1%	0%	[8]
120	1992–2005	12.5%	5%	2.5%	n.a.	4%	2.5%	[9]
181	1994–2007	6.1%	2.2%	28.7%	11.0%	3.3%	n.a.	[10]
				Additional 3.9% dual infection of PVB19 and HHV6				
203	2002–2008	0%	0%	55.7%	24.1%	1%	0%	[4]
				Additional 17.2% dual infection of PVB19 and HHV6				
1098	1990–2010	0.024%	0.011%	28%	0.03%	0.012%	0.02%	[5]
112	1992–2010	0%	0%	29%	n.a.	n.a.	n.a.	[11]

clustering of several DAF proteins in the cell membrane. This clustering then leads to the activation of AbI kinase, following a restructuring of the actin cytoskeleton and a transport of the DAF-bound virus to the tight junctions of a cell [17, 18].

Here coxsackie- and adenoviruses bind with their so-called canyon region to the CAR and get internalized via caveolar endocytosis [19]. Once inside the cell, the viral particle is transported along the microtubules toward the perinuclear region via dynein molecules, where the viral genome gets uncoated [20]. Subsequently, the viral genome is transported into the nucleus through nuclear pores where it is reproduced. Additionally, viral RNA is translated by the host cell's ribosomes into functional proteins. These proteins can either be viral capsid proteins, which serve for the formation of viral progeny, or nonstructural proteins, which disrupt the host cell's function or drive correct viral assembly. These nonstructural proteins and capsid proteins share various interactions with the host cell, leading to pathologic effects, which may result in myocarditis and heart failure.

24.4 Viral Proteases

A key player in the generation of pathological phenotypes of various cell types, including cardiomyocytes, is viral proteases encoded by the viral genome. Proteases are enzymatic proteins with the ability to interact with distinct recognition sites on cellular proteins. Via hydrolysis, either in a one step or two-step reaction, the peptide bond between two amino acids in the recognition site is cleaved, leading to the degradation of the original protein [21]. Such a proteolytic cleavage may cause various outcomes for the host cell. In the case of viral myocarditis, viral proteases of enterovirus 71 (EV71) or coxsackievirus B3 (CVB3) target the cytoskeleton, the mitochondria and on translation-initiation factors as main targets for proteolytic cleavage [22]. As previous studies demonstrated there is a high priority for the cardiac virus to shut-off the host cell's cap-dependent translation and force the host cell to focus on IRES-dependent translation and thus enhance viral replication. This is achieved via proteolytic degradation of eIf4G, a main translation-initiation factor for cap-dependent translation [23, 24]. Subsequently, DAP5, a main IRES-dependent translation-initiation factor, is cleaved into DAP5-N and DAP5-C, upregulating virus expression and dysregulating mitochondrial fusion and fission proteins Bcl-2 and Bax [25]. While Bax is upregulated, the expression of Bcl-2 is inhibited. The resulting mitochondrial biogenesis imbalance leads to the release of cytochrome c and other apoptotic factors [26, 27]. Further regulated mitochondrial factors are dynamin-related protein 1 (drp1), mitochondrial fission 1 protein (fis1), and mitofusin-1 (mfn1).

The dynamin-related protein (drp1) is a mitochondrial effector protein with GTPase activity. In healthy individuals, it mediates and regulates mitochondrial fission events important, for example, for the distribution of mitochondria into daughter cells during mitosis. During viral infections, e.g., enteroviral, drp1 gets deregulated by the virus with strong effects on the host's mitochondria. Similar to Bcl-2 and Bax, the proteins drp1 and its counterpart fis1 regulate fusion and fission events in mitochondria, if their expression and activity are in correct equilibrium. In healthy patients, drp1 is located in the cytoplasm where it gets activated and transported to the mitochondria, if mitochondrial fission is necessary. In in vitro CVB3-infected cells, elevated levels of drp1 were measured in the mitochondria, leading to increased fission and fragmentation of mitochondria. Additional observations of protein expression levels revealed an upregulation of drp1 by 3.2-fold together with an upregulation of fis1 by 1.5-fold similar to drp1. The protein fis1 enhances mitochondrial fission leading to severe mitochondrial phenotypes resulting in mitochondrial dysfunction [28, 29]. Simultaneous downregulation of mfn1 by 0.7-fold hinders correct mitochondrial fusion processes exceeding severe mitochondrial fragmentation [28]. While the negative regulation of drp1, fis1 and mfn1 might be critical for sufficient ATP generation and cell death of the infected cell, this virus–host interaction might also be a valid target for drug-dependent therapy. In mice studies mvidi-1 was used as therapeutic agent to attenuate the viral effects on the mitochondrial structure. Mvidi-1 or 3-(2,4-Dichloro-5-methoxyphenyl)-2,3-dihydro-2-thioxo-4(1*H*)-quinazolinone is a potent and well-studied dynamin inhibitor selectively inhibiting mitophagy, mitochondrial division, and apoptosis caused by Dnm1 and Drp1. The application of mvidi-1 to CVB3-infected mice showed reduced weight loss induced by viral infection. Additionally, the survival rate of isolated mouse cardiomyocytes was around two times higher than in nontreated samples validated by TUNEL staining. Markers for cardiac damage, as cTNI and CK-MB decreased significantly in the serum of mvidi-1 treated mice indicating direct, positive effects of mvidi-1 on the infected cardiac system. The activity of the mitochondrial complexes SDH and COX was also significantly elevated in mvidi-1-treated mice, compared to the nontreated control group. While the SDH and COX activities did not reach the activities of noninfected mice, the activity restoration shows a huge improvement. Of note, mvidi-1 might not be sufficient to ubiquitously block all viral interactions on cardiomyocytes, but it improves the mitochondrial phenotype and increases cell survival [28]. An increased survival of cardiomyocytes during myocarditis may lead to improved recovery with less fibrosis, and hence less impairment of cardiac function.

Progressive and direct proteolysis of cellular organelles adds on to the cell's apoptosis and dysfunction. As mitochondria can be targeted by viral proteases directly, the reduction of mitochondrial activity and ATP production is a direct consequence under these conditions. Studies in mouse hearts infected with CVB3 showed significant changes in OXPHOS-complex activities and protein expression patterns, in total decreasing cellular ATP levels. The decrease in cellular ATP levels results in malfunction of ATP-dependent processes, e.g., cardiac contraction, proton gradient generation via ion-transporters, and vesicular transport [30, 31]. Additionally, proteolytic degradation of the cardiac cytoskeleton directly disrupts the contractile activity of the host's cardiomyocytes triggering the chance of arrhythmic behavior or loss of contractile function. It is reported that viral proteases degrade the sarcomeric protein dystrophin. Dystrophin is known to link sarcomeric actin with the extracellular matrix providing mechanical stability to the cardiomyocyte via dystroglycan complex (DGC). Cleavage of this complex by viral proteases disrupts cardiac cell stability and lowers the potential cardiac contraction force, which can be generated by the cell [32]. This observed pathologic effect on cells is similar to the cellular events in late-stage Duchenne muscular dystrophy (DMD) patients, with disrupted dystrophin function and dilated cardiomyopathy (DCM) [33]. This hypothesis is supported by studies in which viral proteases were expressed in cardiomyocytes carrying a mutated dystrophin variant that is inert to proteolytic cleavage. These cells maintained regular contractile function over protease expression proving the importance of dystrophin in the contractile apparatus [34].

24.5 Viral Effects on Cardiac Ion-Channels

The correct function of the human heart is driven by proper functionality of the contractile apparatus, which generates the needed force for sufficient pumping function and by the distribution and correct synchronization of several ion-channels, which control the concerted cardiac contraction. The cardiac action potential is thereby characterized by the function and correct time-dependent formation of the main currents I_{Na}, I_{to}, I_{Ca}, I_{Kr}, I_{Ks}, and I_{K1}. These currents are generated by cardiac ion-channels located in the plasma membrane of cardiac cells. The depolarizing sodium current I_{Na} is conducted by the sodium channel $\mathrm{Na_V}1.5$. Briefly after the start of the action potential Kv4.2/3 (I_{to}) limits the depolarization transiently. Additionally, there is the I_{h} current generated by HCN-channels HCN2 and HCN4 in the cardiac conduction system. The potassium currents I_{Ks}, I_{Kr} and I_{K1} are mainly carried by the channels Kv7.1/KCNE1, HERG and Kir2.1/2.2/2.3, respectively, bring about cellular repolarization. While I_{Kr} is a fast-activating current, I_{Ks}, is rather slow in comparison. Additionally, the channels Kir2.1/2.2/2.3 (I_{K1}) add to the baseline potassium transport through the cardiac cell membrane. Calcium transport over the cell membrane (I_{CaL}) is achieved via L-type calcium channels [35, 36].

The sensitive equilibrium of excitation and repolarization in cardiac cells can be partially disrupted especially during β-adrenergic stimulation by cardiac viruses like coxsackievirus B3 with potentially severe consequences for the infected patient. As viruses use membrane vesicles for intracellular replication and transport, vesicle-binding proteins, GTPases, are modulated in their activity. Studies on coxsackie viruses indicate that the vesicle-recruiting protein Rab11, which belongs to the GTPase family, shows increased activity in coxsackievirus-expressing cells. This situation leads to altered vesicle recruitment of ion-channel-containing vesicles. These vesicles, for example, Kv7.1/KCNE1-containing vesicles, are increasingly transported to the cell membrane and inserted. With increased membrane integration of Kv7.1/KCNE1, there are significantly more K^+-transporting channels in the cardiac cell membrane with potentially severely modified cardiac function. Increased K^+ efflux during cardiac action potential n leads to potentially shortened QT-intervals and to a virus-induced chronic Short-QT-syndrome similarly as documented for gain of function mutations of Kv7.1/KCNE1 channels [37]. This phenotype has arrhythmic potential and may lead to heart failure and sudden cardiac death. In vitro experiments identified the viral proteins 2A, 2 BC, 3A, and 3B as main agents for the disrupted ion-channel insertion. On the contrary, inversed observations were made for the hERG and $\mathrm{Ca_V}1.2$ channels whose virus-induced loss of function may contribute to action potential disruption as well [38]. Patients usually suffer from arrhythmia and/or sudden cardiac death due to viral infections under stress conditions, while patients under basal conditions show no signs of differing cardiac activity. Consistently, pro-arrhythmic effect of aberrantly inserted ion channels by viruses were not detected in a murine ex vivo model carried out under basal conditions lacking β-adrenergic stimulation [39]. Future experiments including β-adrenergic stimulation should clarify the viral influence on the cardiac action potential in time. In myocarditis patients, electrocardiograms often show T-wave and ST-segment changes and prolonged QRS durations most prominent during physiological stress conditions. As a consequence of reduced reserve of physiological compensatory systems, these patients decompensate typically under stress.

24.6 Viroporins

Studies on multiple types of viruses have demonstrated their ability to form structures that are functionally strikingly similar to ion channels [40, 41]. They can either selectively conduct ions such as H^+, K^+, and Ca^{2+} or nonspecific monovalent cations, i.e., Na^+ or K^+ [42]. The so-called viroporins are assumed to have five main functions beneficial for the virus: 1. virus entry, 2. virus maturation and release, 3. modulation of apoptosis, 4. disturbance of Ca^{2+} homeostasis, and 5. modulation of the resting membrane potential [42–44]. Viroporins are characteristically small, i.e., only 50 to 120 amino acids long. They possess hydrophobic regions that form amphipathic α-helical structures allowing them to insert into membranes to create transmembrane pores. They can be classified according to their number of transmembrane domains (class I or II) and according to the orientation of the N- and C-terminus to the lumen or cytosol (subclasses A and B) [43].

One of the most frequent viruses responsible for viral myocarditis and also one of the most studied, the picornavirus coxsackievirus B3, creates viroporins that conduct Ca^{2+} [45, 46]. The picornaviral viroporin, the 2B protein, is one of the best-studied Ca^{2+}-conducting viroporins so far, dating back to studies from van Kuppeveld et al. starting in 1995 [47–49]. They demonstrated that the expression of the functional 2B viroporin is not needed for the synthesis and processing of the viral polyprotein, but it was essential for viral RNA replication and facilitates release of the virus. As the 2B viroporin is a Ca^{2+} conducting viroporin, it can also destabilize the Ca^{2+} homeostasis by inserting itself into the membranes of mitochondria, plasma membrane, the endoplasmic reticulum (ER) or in sarcoplasmic reticulum (SR), and Golgi-apparatus. Studies showed that this leads to the host cell having low Ca^{2+} concentration in the ER/SR and Golgi apparatus, which function as the cell's Ca^{2+} stores and are important for Ca^{2+} signaling between organelles, and thus decreased Ca^{2+} uptake by the mitochondria. This lack of Ca^{2+} in the organelles leads to the opening of Ca^{2+}channels on the plasma membrane and therefore increasing the cytoplasmic Ca^{2+} level [45, 50–52]. This cell mechanism of Ca^{2+} channel opening to compensate the decreased ER/SR Ca^{2+} level was called capacitative calcium entry or later renamed to store-operated Ca^{2+} entry (SOCE) [53, 54].

By manipulating the Ca^{2+} homeostasis and resting membrane potentials, viruses like coxsackievirus B3 can regulate autophagy and apoptosis of the host cell to its advantage. Campanella et al. showed that apoptotic cell death is suppressed in functional 2B viroporin-expressing cells by suppressing the cell death stimuli actinomycin D and cycloheximide which in turn would activate the cell death stimulus caspase-3 [52]. The transfection of mutant 2B viroporins that should not be able to alter the Ca^{2+} homeostasis did not show any antiapoptotic effect, indicating that the perturbation of the Ca^{2+} flux between ER/ Golgi and mitochondria is most likely necessary for that effect. So far, however, it has not been clearly demonstrated how exactly the alteration of the ER-mitochondria Ca^{2+} flux affects the apoptotic signaling pathway in which actinomycin D and cyclohexamide participate. The antiapoptotic effect of 2B is apparent at the beginning of an infection, which is beneficial in the early stages of infection in order to replicate within the host cell. In later stages of infection proapoptotic pathways become more prominent that would facilitate the release of virions. It is assumed that it is due to the gradual increase of cytosolic Ca^{2+} from the ER/SR that, as previously mentioned, releases Ca^{2+} through the viroporins and extracellular Ca^{2+} [45, 55]. The endogenous pathway gets activated due to the activation of the mitochondrial apoptotic pathway and due to ER/SR stress. The mitochondrial pathway is initiated by the increase in uptake of Ca^{2+} into mitochondria, which leads to the release of cytochrome c that creates apoptosomes and ultimately leads to the activation of caspase-3 and caspase-7 [55–57]. Cathy et al. have shown that the initiation of that pathway seems to occur in a later phase after 8 h post-infection of CVB3 in vitro in HeLa cells [58, 59]. In a different study by Paloheimo et al., early apoptotic markers did not appear until 28 h post-infection in vitro in Green Monkey Kidney (GMK) cells [60]. ER/SR stress has been observed in CVB3-infected mice, and there has been a connection shown that different viroporins are causing ER/SR stress. This is possibly due to the disturbance of ER/SR calcium homeostasis and remodeling of the ER/SR membrane, by inhibiting the intracellular glycoprotein trafficking in the Golgi causing Golgi stress [27, 61].

Besides the programmed cell death apoptosis, CVB3 also regulates autophagy, the mechanism of removing components not necessary for the cell. This has been shown to enhance viral replication in CVB3 [62]. CVB3's functional viroporin 2B also plays a role in creating autophagosomes in cardiac myocytes [63, 64]. Although it is still unknown how exactly viroporin 2B induces autophagy, it has been shown for other viruses such as poliovirus and rotavirus NSP4 that their Ca^{2+} conducting viroporins and their Ca^{2+} regulation plays a pivotal role in creating autophagosomes and therefore viral replication. Removing Ca^{2+} or expression of mutant viroporins in cells inhibited autophagosome formation and decreased viral replication by 84% for NSP4. For NSP4, the viroporin was shown to induce autophagy via the Ca^{2+}/calmodulin-dependent kinase kinase-β (CaMKK-β) signaling pathway [42, 65, 66]. Thus, it is feasible that CVB3's viroporin 2B utilizes a similar mechanism to regulate and misuse the cell's autophagy to their advantage.

Viroporin 2B also affects the immune host response likely by inflammasome activation and by direct antagonism of the host immune response. Inflammasomes are part of the innate immune system and upon activation of caspase-1 which in turn activate and release of the cytokines interleukin 1β and interleukin 18 initiate pyroptosis, a special form of lytic programmed cell death [67]. An important inflammasome called NOD-like receptor family pyrin domain-containing NLRP3 was shown by Wang et al. to be activated during viral infection [68]. They also showed that inhibition of inflammasome activation in CVB3-induced myocarditis in mice alleviate some symptoms, thus this can be another drug target. NLRP3 is activated through changes in ion concentration, and it has been observed to be activated in parallel with K^+ efflux in CVB3-induced viral myocarditis [69]. Although it has not been shown for CVB3's viroporin 2B so far that 2B is the perpetrator for the activation of NLRP3, there is a possibility that it is as it has been shown in other viruses, i.e., encephalomyocarditis virus and human rhinovirus, that their viroporins stimulate the NLRP3 pathway by elevating the cytoplasmic Ca^{2+} concentration from the ER/SR and Golgi [56, 70, 71]. CVB3's viroporin 2B can also directly antagonize the host immune response by inhibiting the host cell's protein trafficking through the Golgi apparatus though CVB3's other proteins, i.e., protein 2 BC and especially 3A have been shown to inhibit protein trafficking significantly more efficiently [72]. Other mechanism of evading the host immune reaction could possibly exist but more experimental insight is required.

As the viroporin disturbs the Ca^{2+} homeostasis (see Fig. 24.1) and signaling between the organelles, it is rather likely that it also disturbs the Ca^{2+}-coupled contraction in cardiomyocytes that uses the calcium-induced calcium release mechanism (CICR) during excitation–contraction (E-C) coupling to induce contraction [73, 74].

Several cellular systems are impaired by viruses, including ion channel function and surface expression [38]. Ion channels and other electrically relevant genes are dysregulated by viruses [22]. Further, Ca^{2+}-handling and Ca^{2+}-contraction coupling and mitochondrial functions are impacted during viral infections (see Chaps. 7, 10 and 15). In addition, electrical cell–cell communications via connexins are modified by viruses ([75], see Chap. 14).

Fig. 24.1 Cardiogenic viruses interfere with cellular electrical function

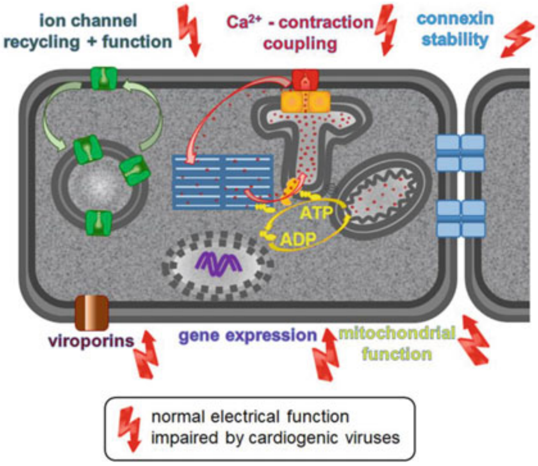
ion channel recycling + function
Ca²⁺ - contraction coupling
connexin stability
ATP
ADP
viroporins
gene expression
mitochondrial function
normal electrical function impaired by cardiogenic viruses

24.7 Immune Reactions

In the case of a viral infection of the heart, many changes in the structure and function of cardiomyocytes and associated cells take place. These changes include manipulations of the host cell by the virus on the molecular level, as previously explained, ongoing degeneration of functional cardiac tissue, fibrosis, and inflammatory responses to the viral infection induced by host molecular signaling. The viral infection of the heart, and other tissues can be divided into several phases, in which the viral effects and host–cell interactions vary tremendously.

In *phase 0*, the preinfection phase, the virus enters the target organism and in the case of myocardial viruses the blood stream. Target cells of viruses are determined by cell membrane receptor proteins like the mentioned DAF, CAR, CD45, HLA-DQ, cytokine type I interferon, and others [17, 18, 76, 77]. Binding of the virus to those structures leads to viral entry and infection of the host cell.

In the following *phase 1*, the replication phase, the viral infection has taken place and the virus starts active replication in, e.g., myocardial cells. This ongoing and exponentially rising viral replication triggers first defense and immune reactions by the host to inhibit viral spread. Thereby, the infected host inherits two types of immune responses, the innate and the adaptive immune responses. The innate immune response is classified by immune reactions generally targeting all non-belonging substances entering a host. Synchronized, the adaptive immune response recognizes the distinct type of pathogen, which entered the organism and delivers very selective and efficient counter strategies. The innate immune responses are mostly the first to occur and provide the hosts ability of a general, but fast reaction to a pathogen [78]. The adaptive immune response in contrary takes a distinct lead time and so occurs as follow-up to the innate immune response. Part of the first innate immune response are the interferons, a group of cytokines with antiviral effectivity. Interferons are produced by virus-infected cells after recognition of viral genomes in the cytoplasm. Interferons therefore lead to enhanced production of major histocompatibility complex-1 MHC-1 and proteasomes, which are helping to degrade viral proteins and mark infected cells for natural killer cells (NK cells). The activated NK cells open cellular membranes via enzymatic, perforin-mediated degradation and generate a membrane permeability for proteases, which degrade cellular organelles and induce apoptosis [79]. Released interferons activate gene transcription of antiviral proteins in neighboring cells, which gear up for an eventually upcoming viral infection. Interferons are divided into subtypes I and II with subclasses α and β, belonging to subtype I and γ forming subtype II. In experiments, interferons of type I could improve the survival rate of mice infected with enteroviruses significantly, showing the importance and effectivity of interferons in early viral defense. Of note, interferon type II did not have significant impact of viral titers and survival rate of enterovirus-infected mice [80–82].

A second defense strategy of the innate immune system is the Toll-like receptors (TLR). These receptors bind and recognize foreign and potentially pathogenic substances, like viral genomes (dsRNA, ssRNA) and proteins, and induce the expression of cytokines like interleukin-1b (IL-1b), interleukin-6 (IL-6), and interferons [83]. Those interleukins activate leukocytes, macrophages for acute pathogen defense, and T-helper cells to initiate IgG production to restore tissue homeostasis, resulting in inflammation [84, 85]. In humans, 10 different TLR's are postulated for acute recognition of pathogens of which TLR2, TLR3, TLR4, TLR7, TLR8, and TLR9 are capable to recognize a viral infection [86]. For most cardiogenic viruses, especially enteroviruses, which use dsRNA and ssRNA as genomes, TLR3, TLR7, and TLR8 possess sufficient RNA recognition sites [87]. If the TLR's fail to detect viral replication in an infected cell, a second recognition mechanism is available, that is based on the recognition of viral dsRNA's and dsRNA-intermediates. The helicases RIG-1 and MDA-5 contain a caspase activation and recruitment domain (CARD), which is opened via conformational changes in the helicase protein triggered by dsRNA binding [88, 89]. Activated CARD is able to bind to MAVS (mitochondrial antiviral signaling protein) recruiting NF-κB and interferon regulating proteins leading to the induction of various immune responses and interferon type I expression [90].

Another innate cardiac immune regulator responsive to viral infection is the JAK-STAT system, which is sensitive to IL-6-receptor activation by its ligand IL-6. The binding of IL-6 in the first place activates JAK (janus kinase)-dependent phosphorylation of the IL-6-receptor with subsequent phosphorylation and activation of STAT (signal transducers and activators of transcription). Activated STAT translocates to the nucleus and activates SOCS 1/3-expression (suppressor of cytokine signaling). Translocation of expressed SOCS 1/3 to the IL-6-receptors inhibits JAK-dependent phosphorylation of IL-6-receptors and therewith controls the duration and level of cardiac immune reactions to viral infection [91, 92]. Expression studies with SOCS 1/3 in mice support the efficiency of the antiviral feedback loop of JAK-STAT under CVB3 infections, in which SOCS 1/3-expressing mice showed improved cardiac phenotypes compared to non-SOCS-expressing controls. TNF expression additionally contributes to the inflammatory host response. Viral-induced TNF overexpression activates metalloproteinases, which degrade the extracellular matrix, including collagen, and so worsen cardiac performance as a result of a dilated phenotype [93, 94]. TNF signaling can be used as therapeutic target. Anticytokine therapies, e.g., with Enbrel® (etanercept) are based on drug binding to overexpressed TNF initiating its disposal from infected, myocardial environment. Currently, a therapeutic approach targeting TNF with Remicade® (infliximab) is undergoing clinical trial [95].

Phase 2 of viral infection follows the acute viral infection with high viral replication and inflammation and is characterized by viral genome persistence without detectable production of viral progeny. It is known that viral RNA, especially dsRNA's and dsRNA intermediates and also DNA, can last in the previously infected myocardium for months or even years [96, 97]. Very little is known about the effect of persistent viral genomes in chronic myocarditis, due to the lack of adequate samples. Studies in mice, in which a replication-restricted CVB3 cDNA was expressed in the myocardium, revealed typical phenotypes resembling DCM in human patients. This included ongoing fibrosis, hypertrophy, and degeneration of cardiomyocytes. The mortality rate due to viral genome persistence is at about 25% after 25 months after diagnosis and at 41% after 5-years [97]. Furthermore, a reactivation of viral replication may occur due to unknown environmental signals, raising the possibility of a recurrence of myocarditis years after the initial myocarditis treatment. For the viruses PVB19 and HHV-6, viral reactivation associated with new myocarditis and worsening of ventricular function was reported [98–100]. IFNβ therapy for 6-months after diagnosis increased the survival rate of chronic myocarditis patients to 92%, probably by a clear-out of persistent viral genomes from the myocardium [97].

The following *phase 3* is characterized by cardiac remodeling in reaction to overcome viral infection including wound healing, fibrosis, etc. However, migrated B-cells can produce and release autoantibodies against several host cardiac structures like β1-adrenergic receptors, cardiac myosin, cTNI, L-Type calcium channel, and others, promoting dilative cardiomyopathy [101–103]. In around 70% of viral myocarditis cases, patients recover from viral infection in regard to an intact immune system and wound healing [104]. Due to the fact that cardiomyocytes are fully differentiated, nondividing cells, wound healing is enabled by fibroblasts resulting in loss of contractile tissue. Affected regions resemble a scar-like shape and weaken the cardiac system concerning conductivity and contractile function. The scar represents an electric barrier increasing electric tissue heterogeneity and increased probability of arrhythmias.

24.8 Viral Capsids

Every virus forms a capsid to encapsulate its genetic information. Some viruses additionally possess a double lipid membrane called viral envelope around the capsid. The capsid can be made up out of multiple proteins, e.g., VP1, VP2, VP3, and VP4 for CVB3 [105]. Immunohistochemistry can be performed in myocardial samples against viral capsid proteins in order to detect viral infection [106]. Besides encapsulation, the capsid proteins also have other functions that are beneficial for the virus. Viruses use their capsids to attach to the host cell for viral entry. At the junction between VP1 and VP3, a hydrophobic pocket or “canyon” is located that can bind to different hydrophobic components. Binding of different components can either enhance the stability of the virus and therefore more resistant to uncoating or affect the binding of the virus to the host cell [107, 108]. Often, viruses need to enter the host cell’s nucleus in order to use the nuclear proteins, usually required for the host cell’s replication, for its own replication [109]. In addition, viral infections can affect several cellular functions of the cardiomyocyte (see Fig. 24.2).

CVB3’s capsid protein VP1 as well as Herpesvirus-1’s VP1–2 capsid protein and most likely also other herpesviruses such as human herpes virus-6 that is also frequently detected in patients with myocarditis have been shown to have a nuclear localization signal and with this can be imported into the nucleus [110, 111]. In addition, CVB3’s VP1 was demonstrated by Wang et al. to induce cell cycle arrest at G1 phase in the host cell in cardiomyocytes [112]. They showed that VP1 does it by upregulating heat shock protein 70 (Hsp70) which leads to downregulation of cycline E and upregulation of $p27^{Kip1}$, both regulating the cell cycle. Cell cycle arrest was shown to promote CVB3 replication.

CVB3’s VP2 also appears to play a role in viral replication. Knowlton et al. and Stadnick et al. conducted studies with point mutated VP2 and infected these mutated CVB3 in mice [113, 114]. These mice showed significantly less myocarditis and cell damage in comparison to the not mutated form implying that VP2 also plays a role in the induction/progression of myocarditis. Stadnick et al. additionally found that mutation of VP3 at the knob region leads to a decrease in virulence, as well. Stereographic imaging showed that VP2’s puff region as well as VP3’s knob region forms an epitope of the putative-binding site of DAF, thus mutations at this site can be expected to impair viral docking. In addition, Henke et al. reported that VP2 interacts with proapoptotic protein Siva that plays a role in the CD27/CD70-transduced apoptosis [115]. They showed that Siva is upregulated in CVB3 infected and apoptotic tissue areas in murine hearts, indicating that CVB3’s VP2 promotes apoptosis in myocarditis.

So far, only few studies have been conducted to illuminate the relevance of CVB3’s VP4 in

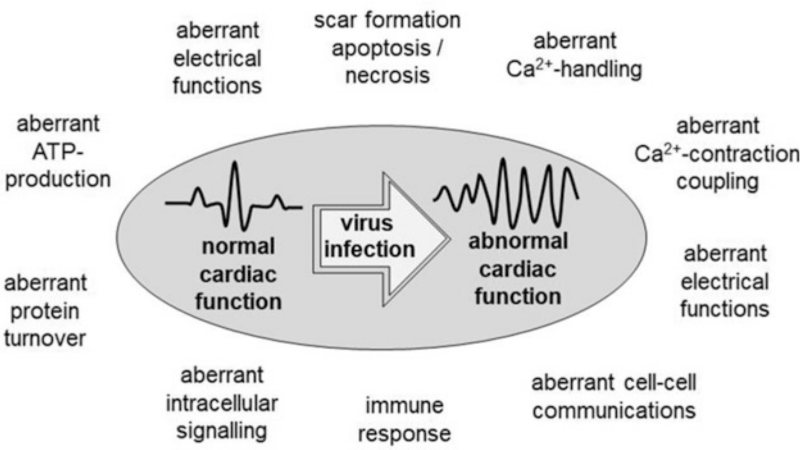
aberrant
electrical
functions
scar formation
apoptosis /
necrosis
aberrant
Ca2+-handling
aberrant
ATP-
production
aberrant
Ca2+-contraction
coupling
normal
cardiac
function
virus
infection
abnormal
cardiac
function
aberrant
electrical
functions
aberrant
protein
turnover
aberrant
intracellular
signalling
immune
response
aberrant cell-cell
communications

Fig. 24.2 Various cellular functions are dysregulated during viral myocarditis. Depicted components of cellular functions are modified during a viral infection of cardiomyocytes

myocarditis. However, it has been reported that antibodies against VP4 are produced in humans and CVB4's VP4 influences viral replication in murine pancreas [116, 117].

24.9 Diagnosis

The clinical course of a viral myocarditis is diverse and complicated, which renders a diagnosis of acute or ongoing viral myocarditis complicated. In clinical diagnosis of myocarditis, several subsets are distinguished including fulminant, chronic active, eosinophilic, and giant cell myocarditis, which are all believed to be caused by viral infection [104].

Fulminant myocarditis is characterized by multiple infection foci accompanied with necrosis and ongoing inflammation, mainly localized on the left ventricle leading to left ventricular dysfunction within 2 weeks post-infection, with migration of inflammatory B-cells, T-cells, T-helper-cells, lymphocytes, and macrophages [118].

The chronic active outcome leads to the manifestation of a restrictive cardiomyopathy within 2–4 years post-infection. This scenario is associated with progressing fibrosis and immune reactions including chronic inflammations mostly of the left ventricle [119].

Eosinophilic myocarditis usually occurs during hyper-eosinophilia, a condition in which eosinophils enter the myocardium in a high number and linger. Over weeks, these cells get degraded under the release of eosinophil-derived neurotoxin, cationic protein, major basic protein, and reactive oxygen species, leading to ongoing necrosis and fibrosis. Eosinophilic myocarditis mostly occurs in response to medications or parasites but can be caused by viruses as well. In most cases, virus-induced eosinophilic myocarditis occurs in the left ventricle [120–122].

Giant cell myocarditis is a rare disease characterized by the infiltration of big amounts of fused, multinuclear macrophages (giant cells) into the myocardium. This scenario mostly occurs in response to intense immune reactions, for example, induced by autoimmune diseases like lupus erythematosus, rheumatoid arthritis, and inflammatory bowel disease. Several studies discuss viral infections of idiopathic cases as cause for giant cell myocarditis as well. This kind of myocarditis leads to severe outcomes including congestive heart failure, heart block, inflammation, and ventricular arrhythmias with very high patient mortality within 6 months if left untreated [123, 124].

The diagnosis of viral myocarditis classically follows the Dallas criteria, a catalogue of potential observations based on immunohistochemical investigation of heart biopsies. These observations include the presence of infiltrating cells like giant cells, neutrophils, and lymphocytes, the observation of ongoing inflammation and/or necrosis and fibrosis. For detailed characterization, a second biopsy is taken after the first characterization to analyze for chronic/ongoing, resolving or resolved myocarditis [125]. The weakness about the Dallas criteria is the one-sided view on the cardiac pathology relying only on immunohistochemistry. While viral-induced inflammation and necrosis occur in infection foci, the chance of missing a representative region in a biopsy is high, which leads to a nondetection of viral influence on cardiac dysfunction. This suggestion is supported by clinical studies in which myocarditis patient biopsies were analyzed under Dallas criteria in comparison to other detection methods as PCR and HLA screening. The PCR test gives additional information about persistent viral RNA in the myocardium, while HLA is generally upregulated during viral infections. One study focused on 34 cardiac biopsy samples of patients with suspected myocarditis. In 26 samples, there was evidence for ongoing viral myocarditis diagnosed by PCR, while immunohistochemical observation only diagnosed 13 of the 26 samples as myocarditis-positive [126]. Another study focused on the detection of elevated HLA as biomarker for myocarditis. Out of 202 patients with new-onset cardiomyopathy, 84 showed elevated HLA levels, while only 54 patients were diagnosed positive under the use of the Dallas criteria [127]. These findings point out that the Dallas criteria alone are not sufficient to diagnose the wide variety of myocarditis types and subsets in patients, but that other methods as standardized PCR and HLA-screening should be added as standard diagnostic methods. Summarizing, the current diagnostic practice might fail to detect all viral infections in patients.

24.10 Conclusions

Virus infections of the heart are common and can lead to a multitude of cellular effects including markedly modified intracellular signaling, disturbed calcium handling, altered ion channel functions at the plasma membrane, mitochondrial dysfunctions, and impaired cell–cell communications. Subsequently, infected cardiomyocytes react differently in the concerted electrical action of cells within the cardiac tissue. Eventually, infected cells may undergo apoptosis or necrosis producing scars within cardiac tissues. Both functionally altered cells and tissue scars reduce cardiac performance and increase electrical heterogeneity, a well-known trigger of potentially lethal arrhythmias. Electrical and functional reserves are reduced in virus-infected hearts rendering them particularly sensitive to physiological β-adrenergic stress.

References

1. Disease GBD, Injury I, Prevalence C. Global, regional, and national incidence, prevalence, and years lived with disability for 354 diseases and injuries for 195 countries and territories, 1990-2017: a systematic analysis for the Global Burden of Disease Study 2017. Lancet. 2018;392(10159):1789–858.
2. Blauwet LA, Cooper LT. Myocarditis. Prog Cardiovasc Dis. 2010;52(4):274–88.
3. Bowles NE, Ni J, Kearney DL, Pauschinger M, Schultheiss HP, McCarthy R, et al. Detection of viruses in myocardial tissues by polymerase chain reaction. Evidence of adenovirus as a common cause of myocarditis in children and adults. J Am Coll Cardiol. 2003;42(3):466–72.
4. Grun S, Schumm J, Greulich S, Wagner A, Schneider S, Bruder O, et al. Long-term follow-up of biopsy-proven viral myocarditis: predictors of mortality and incomplete recovery. J Am Coll Cardiol. 2012;59(18):1604–15.
5. Maisch B, Alter P. Treatment options in myocarditis and inflammatory cardiomyopathy : focus on i.v. immunoglobulins. Herz. 2018;43(5):423–30.
6. Pankuweit S, Moll R, Baandrup U, Portig I, Hufnagel G, Maisch B. Prevalence of the parvovirus B19 genome in endomyocardial biopsy specimens. Hum Pathol. 2003;34(5):497–503.
7. Kuhl U, Pauschinger M, Seeberg B, Lassner D, Noutsias M, Poller W, et al. Viral persistence in the myocardium is associated with progressive cardiac dysfunction. Circulation. 2005;112(13):1965–70.
8. Mahrholdt H, Wagner A, Deluigi CC, Kispert E, Hager S, Meinhardt G, et al. Presentation, patterns of myocardial damage, and clinical course of viral myocarditis. Circulation. 2006;114(15):1581–90.
9. Caforio AL, Calabrese F, Angelini A, Tona F, Vinci A, Bottaro S, et al. A prospective study of biopsy-proven myocarditis: prognostic relevance of clinical and aetiopathogenetic features at diagnosis. Eur Heart J. 2007;28(11):1326–33.

10. Kindermann I, Kindermann M, Kandolf R, Klingel K, Bultmann B, Muller T, et al. Predictors of outcome in patients with suspected myocarditis. Circulation. 2008;118(6):639–48.
11. Nielsen TS, Hansen J, Nielsen LP, Baandrup UT, Banner J. The presence of enterovirus, adenovirus, and parvovirus B19 in myocardial tissue samples from autopsies: an evaluation of their frequencies in deceased individuals with myocarditis and in non-inflamed control hearts. Forensic Sci Med Pathol. 2014;10(3):344–50.
12. Verdonschot J, Hazebroek M, Merken J, Debing Y, Dennert R, Brunner-La Rocca HP, et al. Relevance of cardiac parvovirus B19 in myocarditis and dilated cardiomyopathy: review of the literature. Eur J Heart Fail. 2016;18(12):1430–41.
13. Magnani JW, Dec GW. Myocarditis: current trends in diagnosis and treatment. Circulation. 2006;113(6): 876–90.
14. Yajima T, Knowlton KU. Viral myocarditis: from the perspective of the virus. Circulation. 2009;119(19): 2615–24.
15. Leung HS, Li OT, Chan RW, Chan MC, Nicholls JM, Poon LL. Entry of influenza a virus with a alpha2,6-linked sialic acid binding preference requires host fibronectin. J Virol. 2012;86(19):10704–13.
16. Woodruff JF. Viral myocarditis. A review. Am J Pathol. 1980;101(2):425–84.
17. Coyne CB, Bergelson JM. Virus-induced Abl and Fyn kinase signals permit coxsackievirus entry through epithelial tight junctions. Cell. 2006;124(1): 119–31.
18. Li T, Chen X, Garbutt KC, Zhou P, Zheng N. Structure of DDB1 in complex with a paramyxovirus V protein: viral hijack of a propeller cluster in ubiquitin ligase. Cell. 2006;124(1):105–17.
19. Marchant D, Sall A, Si X, Abraham T, Wu W, Luo Z, et al. ERK MAP kinase-activated Arf6 trafficking directs coxsackievirus type B3 into an unproductive compartment during virus host-cell entry. J Gen Virol. 2009;90(Pt 4):854–62.
20. Albecka A, Laine RF, Janssen AF, Kaminski CF, Crump CM. HSV-1 glycoproteins are delivered to virus assembly sites through dynamin-dependent endocytosis. Traffic. 2016;17(1):21–39.
21. Babe LM, Craik CS. Viral proteases: evolution of diverse structural motifs to optimize function. Cell. 1997;91(4):427–30.
22. Peischard S, Ho HT, Theiss C, Strutz-Seebohm N, Seebohm G. A kidnapping story: how Coxsackievirus B3 and its host cell interact. Cell Physiol Biochem. 2019;53(1):121–40.
23. Lewis SM, Cerquozzi S, Graber TE, Ungureanu NH, Andrews M, Holcik M. The eIF4G homolog DAP5/p97 supports the translation of select mRNAs during endoplasmic reticulum stress. Nucleic Acids Res. 2008;36(1):168–78.
24. Chau DH, Yuan J, Zhang H, Cheung P, Lim T, Liu Z, et al. Coxsackievirus B3 proteases 2A and 3C induce apoptotic cell death through mitochondrial injury and cleavage of eIF4GI but not DAP5/p97/NAT1. Apoptosis. 2007;12(3):513–24.
25. Hanson PJ, Ye X, Qiu Y, Zhang HM, Hemida MG, Wang F, et al. Cleavage of DAP5 by coxsackievirus B3 2A protease facilitates viral replication and enhances apoptosis by altering translation of IRES-containing genes. Cell Death Differ. 2016;23(5): 828–40.
26. Joo CH, Hong HN, Kim EO, Im JO, Yoon SY, Ye JS, et al. Coxsackievirus B3 induces apoptosis in the early phase of murine myocarditis: a comparative analysis of cardiovirulent and noncardiovirulent strains. Intervirology. 2003;46(3):135–40.
27. Cai Z, Shen L, Ma H, Yang J, Yang D, Chen H, et al. Involvement of endoplasmic reticulum stress-mediated C/EBP homologous protein activation in Coxsackievirus B3-induced acute viral myocarditis. Circ Heart Fail. 2015;8(4):809–18.
28. Lin L, Zhang M, Yan R, Shan H, Diao J, Wei J. Inhibition of Drp1 attenuates mitochondrial damage and myocardial injury in Coxsackievirus B3 induced myocarditis. Biochem Biophys Res Commun. 2017;484(3):550–6.
29. Lackner LL, Nunnari J. Small molecule inhibitors of mitochondrial division: tools that translate basic biological research into medicine. Chem Biol. 2010;17(6):578–83.
30. Ebermann L, Wika S, Klumpe I, Hammer E, Klingel K, Lassner D, et al. The mitochondrial respiratory chain has a critical role in the antiviral process in Coxsackievirus B3-induced myocarditis. Lab Investig. 2012;92(1):125–34.
31. Xie B, Zhou JF, Lu Q, Li CJ, Chen P. Oxidative stress in patients with acute coxsackie virus myocarditis. Biomed Environ Sci. 2002;15(1):48–57.
32. Badorff C, Fichtlscherer B, Rhoads RE, Zeiher AM, Muelsch A, Dimmeler S, et al. Nitric oxide inhibits dystrophin proteolysis by coxsackieviral protease 2A through S-nitrosylation: a protective mechanism against enteroviral cardiomyopathy. Circulation. 2000;102(18):2276–81.
33. Mavrogeni S, Papavasiliou A, Spargias K, Constandoulakis P, Papadopoulos G, Karanasios E, et al. Myocardial inflammation in Duchenne muscular dystrophy as a precipitating factor for heart failure: a prospective study. BMC Neurol. 2010;10:33.
34. Badorff C, Lee GH, Lamphear BJ, Martone ME, Campbell KP, Rhoads RE, et al. Enteroviral protease 2A cleaves dystrophin: evidence of cytoskeletal disruption in an acquired cardiomyopathy. Nat Med. 1999;5(3):320–6.
35. Cranefield PF, Wit AL. Cardiac arrhythmias. Annu Rev Physiol. 1979;41:459–72.
36. Priest BT, McDermott JS. Cardiac ion channels. Channels (Austin). 2015;9(6):352–9.
37. Seebohm G, Strutz-Seebohm N, Ureche ON, Henrion U, Baltaev R, Mack AF, et al. Long QT syndrome-associated mutations in KCNQ1 and

KCNE1 subunits disrupt normal endosomal recycling of IKs channels. Circ Res. 2008;103(12):1451–7.

38. Steinke K, Sachse F, Ettischer N, Strutz-Seebohm N, Henrion U, Rohrbeck M, et al. Coxsackievirus B3 modulates cardiac ion channels. FASEB J. 2013;27 (10):4108–21.
39. Kaese S, Larbig R, Rohrbeck M, Frommeyer G, Dechering D, Olligs J, et al. Electrophysiological alterations in a murine model of chronic coxsackievirus B3 myocarditis. PLoS One. 2017;12 (6):e0180029.
40. Melton JV, Ewart GD, Weir RC, Board PG, Lee E, Gage PW. Alphavirus 6K proteins form ion channels. J Biol Chem. 2002;277(49):46923–31.
41. Ewart GD, Sutherland T, Gage PW, Cox GB. The Vpu protein of human immunodeficiency virus type 1 forms cation-selective ion channels. J Virol. 1996;70(10):7108–15.
42. Hyser JM, Estes MK. Pathophysiological consequences of calcium-conducting viroporins. Annu Rev Virol. 2015;2(1):473–96.
43. Nieva JL, Madan V, Carrasco L. Viroporins: structure and biological functions. Nat Rev Microbiol. 2012;10(8):563–74.
44. Giorda KM, Hebert DN. Viroporins customize host cells for efficient viral propagation. DNA Cell Biol. 2013;32(10):557–64.
45. van Kuppeveld FJ, Hoenderop JG, Smeets RL, Willems PH, Dijkman HB, Galama JM, et al. Coxsackievirus protein 2B modifies endoplasmic reticulum membrane and plasma membrane permeability and facilitates virus release. EMBO J. 1997;16 (12):3519–32.
46. Dennert R, Crijns HJ, Heymans S. Acute viral myocarditis. Eur Heart J. 2008;29(17):2073–82.
47. van Kuppeveld FJ, Galama JM, Zoll J, Melchers WJ. Genetic analysis of a hydrophobic domain of coxsackie B3 virus protein 2B: a moderate degree of hydrophobicity is required for a cis-acting function in viral RNA synthesis. J Virol. 1995;69(12): 7782–90.
48. van Kuppeveld FJ, Galama JM, Zoll J, van den Hurk PJ, Melchers WJ. Coxsackie B3 virus protein 2B contains cationic amphipathic helix that is required for viral RNA replication. J Virol. 1996;70(6): 3876–86.
49. van Kuppeveld FJ, van den Hurk PJ, Zoll J, Galama JM, Melchers WJ. Mutagenesis of the coxsackie B3 virus 2B/2C cleavage site: determinants of processing efficiency and effects on viral replication. J Virol. 1996;70(11):7632–40.
50. Sanchez-Martinez S, Madan V, Carrasco L, Nieva JL. Membrane-active peptides derived from picornavirus 2B viroporin. Curr Protein Pept Sci. 2012;13 (7):632–43.
51. de Jong AS, de Mattia F, Van Dommelen MM, Lanke K, Melchers WJ, Willems PH, et al. Functional analysis of picornavirus 2B proteins: effects on calcium homeostasis and intracellular protein trafficking. J Virol. 2008;82(7):3782–90.
52. Campanella M, de Jong AS, Lanke KW, Melchers WJ, Willems PH, Pinton P, et al. The coxsackievirus 2B protein suppresses apoptotic host cell responses by manipulating intracellular Ca2+ homeostasis. J Biol Chem. 2004;279(18):18440–50.
53. Putney JW Jr. A model for receptor-regulated calcium entry. Cell Calcium. 1986;7(1):1–12.
54. Putney JW Jr. Store-operated calcium channels: how do we measure them, and why do we care? Sci STKE. 2004;2004(243):pe37.
55. Zhou Y, Frey TK, Yang JJ. Viral calciomics: interplays between Ca2+ and virus. Cell Calcium. 2009;46(1):1–17.
56. Li Z, Zou Z, Jiang Z, Huang X, Liu Q. Biological function and application of picornaviral 2B protein: a new target for antiviral drug development. Viruses. 2019;11(6):510.
57. Ow YP, Green DR, Hao Z, Mak TW. Cytochrome c: functions beyond respiration. Nat Rev Mol Cell Biol. 2008;9(7):532–42.
58. Carthy CM, Yanagawa B, Luo H, Granville DJ, Yang D, Cheung P, et al. Bcl-2 and Bcl-xL overexpression inhibits cytochrome c release, activation of multiple caspases, and virus release following coxsackievirus B3 infection. Virology. 2003;313(1): 147–57.
59. Carthy CM, Granville DJ, Watson KA, Anderson DR, Wilson JE, Yang D, et al. Caspase activation and specific cleavage of substrates after coxsackievirus B3-induced cytopathic effect in HeLa cells. J Virol. 1998;72(9):7669–75.
60. Paloheimo O, Ihalainen TO, Tauriainen S, Valilehto O, Kirjavainen S, Niskanen EA, et al. Coxsackievirus B3-induced cellular protrusions: structural characteristics and functional competence. J Virol. 2011;85(13):6714–24.
61. Fung TS, Torres J, Liu DX. The emerging roles of viroporins in ER stress response and autophagy induction during virus infection. Viruses. 2015;7(6): 2834–57.
62. Wong J, Zhang J, Si X, Gao G, Mao I, McManus BM, et al. Autophagosome supports coxsackievirus B3 replication in host cells. J Virol. 2008;82(18): 9143–53.
63. Zhai X, Bai B, Yu B, Wang T, Wang H, Wang Y, et al. Coxsackievirus B3 induces Autophagic response in cardiac myocytes in vivo. Biochemistry (Mosc). 2015;80(8):1001–9.
64. Wu H, Zhai X, Chen Y, Wang R, Lin L, Chen S, et al. Protein 2B of Coxsackievirus B3 induces autophagy relying on its transmembrane hydrophobic sequences. Viruses. 2016;8(5):131.
65. Crawford SE, Hyser JM, Utama B, Estes MK. Autophagy hijacked through viroporin-activated calcium/calmodulin-dependent kinase kinase-beta signaling is required for rotavirus

replication. Proc Natl Acad Sci U S A. 2012;109(50): E3405–13.

66. Taylor MP, Kirkegaard K. Modification of cellular autophagy protein LC3 by poliovirus. J Virol. 2007;81(22):12543–53.
67. Broz P, Dixit VM. Inflammasomes: mechanism of assembly, regulation and signalling. Nat Rev Immunol. 2016;16(7):407–20.
68. Wang Y, Gao B, Xiong S. Involvement of NLRP3 inflammasome in CVB3-induced viral myocarditis. Am J Physiol Heart Circ Physiol. 2014;307(10): H1438–47.
69. Tschopp J, Schroder K. NLRP3 inflammasome activation: the convergence of multiple signalling pathways on ROS production? Nat Rev Immunol. 2010;10(3):210–5.
70. Ito M, Yanagi Y, Ichinohe T. Encephalomyocarditis virus viroporin 2B activates NLRP3 inflammasome. PLoS Pathog. 2012;8(8):e1002857.
71. Triantafilou K, Kar S, van Kuppeveld FJ, Triantafilou M. Rhinovirus-induced calcium flux triggers NLRP3 and NLRC5 activation in bronchial cells. Am J Respir Cell Mol Biol. 2013;49(6):923–34.
72. Cornell CT, Kiosses WB, Harkins S, Whitton JL. Inhibition of protein trafficking by coxsackievirus b3: multiple viral proteins target a single organelle. J Virol. 2006;80(13):6637–47.
73. Fabiato A. Calcium-induced release of calcium from the cardiac sarcoplasmic reticulum. Am J Phys. 1983;245(1):C1–14.
74. Bers DM. Cardiac excitation-contraction coupling. Nature. 2002;415(6868):198–205.
75. Zhang A, Zhang H, Wu S. Immunomodulation by atorvastatin upregulates expression of gap junction proteins in coxsackievirus B3 (CVB3)-induced myocarditis. Inflamm Res. 2010;59(4):255–62.
76. Lozano MD, Rubocki RJ, Wilson JE, McManus BM, Wisecarver JL. Human leukocyte antigen class II associations in patients with idiopathic dilated cardiomyopathy. Myocarditis Treatment Trial Investigators. J Card Fail. 1997;3(2):97–103.
77. Tchilian EZ, Gil J, Navarro ML, Fernandez-Cruz E, Chapel H, Misbah S, et al. Unusual case presentations associated with the CD45 C77G polymorphism. Clin Exp Immunol. 2006;146(3):448–54.
78. Aderem A, Ulevitch RJ. Toll-like receptors in the induction of the innate immune response. Nature. 2000;406(6797):782–7.
79. Ong S, Rose NR, Cihakova D. Natural killer cells in inflammatory heart disease. Clin Immunol. 2017;175: 26–33.
80. Karupiah G, Xie QW, Buller RM, Nathan C, Duarte C, MacMicking JD. Inhibition of viral replication by interferon-gamma-induced nitric oxide synthase. Science. 1993;261(5127):1445–8.
81. Matsumori A, Tomioka N, Kawai C. Protective effect of recombinant alpha interferon on coxsackievirus B3 myocarditis in mice. Am Heart J. 1988;115(6): 1229–32.
82. Wang YX, da Cunha V, Vincelette J, White K, Velichko S, Xu Y, et al. Antiviral and myocyte protective effects of murine interferon-beta and -{alpha} 2 in coxsackievirus B3-induced myocarditis and epicarditis in Balb/c mice. Am J Physiol Heart Circ Physiol. 2007;293(1):H69–76.
83. Medzhitov R, Preston-Hurlburt P, Janeway CA Jr. A human homologue of the drosophila toll protein signals activation of adaptive immunity. Nature. 1997;388(6640):394–7.
84. Kawano Y, Noma T, Kou K, Yoshizawa I, Yata J. Regulation of human IgG subclass production by cytokines: human IgG subclass production enhanced differentially by interleukin-6. Immunology. 1995;84 (2):278–84.
85. Arango Duque G, Descoteaux A. Macrophage cytokines: involvement in immunity and infectious diseases. Front Immunol. 2014;5:491.
86. Takeda K, Akira S. Toll-like receptors in innate immunity. Int Immunol. 2005;17(1):1–14.
87. Uematsu S, Akira S. Toll-like receptors (TLRs) and their ligands. Handb Exp Pharmacol. 2008;183:1–20.
88. Yoneyama M, Kikuchi M, Natsukawa T, Shinobu N, Imaizumi T, Miyagishi M, et al. The RNA helicase RIG-I has an essential function in double-stranded RNA-induced innate antiviral responses. Nat Immunol. 2004;5(7):730–7.
89. Yoneyama M, Kikuchi M, Matsumoto K, Imaizumi T, Miyagishi M, Taira K, et al. Shared and unique functions of the DExD/H-box helicases RIG-I, MDA5, and LGP2 in antiviral innate immunity. J Immunol. 2005;175(5):2851–8.
90. Hiscott J, Lin R, Nakhaei P, Paz S. MasterCARD: a priceless link to innate immunity. Trends Mol Med. 2006;12(2):53–6.
91. Yasukawa H, Yajima T, Duplain H, Iwatate M, Kido M, Hoshijima M, et al. The suppressor of cytokine signaling-1 (SOCS1) is a novel therapeutic target for enterovirus-induced cardiac injury. J Clin Invest. 2003;111(4):469–78.
92. Yajima T, Yasukawa H, Jeon ES, Xiong D, Dorner A, Iwatate M, et al. Innate defense mechanism against virus infection within the cardiac myocyte requiring gp130-STAT3 signaling. Circulation. 2006;114(22):2364–73.
93. Sivasubramanian N, Coker ML, Kurrelmeyer KM, MacLellan WR, DeMayo FJ, Spinale FG, et al. Left ventricular remodeling in transgenic mice with cardiac restricted overexpression of tumor necrosis factor. Circulation. 2001;104(7):826–31.
94. Hodgson DM, Zingman LV, Kane GC, Perez-Terzic-C, Bienengraeber M, Ozcan C, et al. Cellular remodeling in heart failure disrupts K(ATP) channel-dependent stress tolerance. EMBO J. 2003;22(8):1732–42.
95. Chung ES, Packer M, Lo KH, Fasanmade AA, Willerson JT, Anti TNFTACHFI. Randomized, double-blind, placebo-controlled, pilot trial of infliximab, a chimeric monoclonal antibody to

tumor necrosis factor-alpha, in patients with moderate-to-severe heart failure: results of the anti-TNF therapy against congestive heart failure (ATTACH) trial. Circulation. 2003;107(25): 3133–40.

96. Norja P, Hokynar K, Aaltonen LM, Chen R, Ranki A, Partio EK, et al. Bioportfolio: lifelong persistence of variant and prototypic erythrovirus DNA genomes in human tissue. Proc Natl Acad Sci U S A. 2006;103 (19):7450–3.
97. Kuhl U, Lassner D, von Schlippenbach J, Poller W, Schultheiss HP. Interferon-Beta improves survival in enterovirus-associated cardiomyopathy. J Am Coll Cardiol. 2012;60(14):1295–6.
98. Kuhl U, Lassner D, Dorner A, Rohde M, Escher F, Seeberg B, et al. A distinct subgroup of cardiomyopathy patients characterized by transcriptionally active cardiotropic erythrovirus and altered cardiac gene expression. Basic Res Cardiol. 2013;108(5):372.
99. Pellett PE, Ablashi DV, Ambros PF, Agut H, Caserta MT, Descamps V, et al. Chromosomally integrated human herpesvirus 6: questions and answers. Rev Med Virol. 2012;22(3):144–55.
100. Escher F, Kuhl U, Gross U, Westermann D, Poller W, Tschope C, et al. Aggravation of left ventricular dysfunction in patients with biopsy-proven cardiac human herpesvirus A and B infection. J Clin Virol. 2015;63:1–5.
101. Kaya Z, Leib C, Katus HA. Autoantibodies in heart failure and cardiac dysfunction. Circ Res. 2012;110 (1):145–58.
102. Lazzerini PE, Capecchi PL, Laghi-Pasini F, Boutjdir M. Autoimmune channelopathies as a novel mechanism in cardiac arrhythmias. Nat Rev Cardiol. 2017;14(9):521–35.
103. Kaya Z, Katus HA, Rose NR. Cardiac troponins and autoimmunity: their role in the pathogenesis of myocarditis and of heart failure. Clin Immunol. 2010;134 (1):80–8.
104. Dominguez F, Kuhl U, Pieske B, Garcia-Pavia P, Tschope C. Update on myocarditis and inflammatory cardiomyopathy: reemergence of endomyocardial biopsy. Rev Esp Cardiol (Engl Ed). 2016;69(2): 178–87.
105. Muckelbauer JK, Kremer M, Minor I, Diana G, Dutko FJ, Groarke J, et al. The structure of coxsackievirus B3 at 3.5 a resolution. Structure. 1995;3(7):653–67.
106. Andreoletti L, Leveque N, Boulagnon C, Brasselet C, Fornes P. Viral causes of human myocarditis. Arch Cardiovasc Dis. 2009;102(6–7):559–68.
107. Rombaut B, Vrijsen R, Boeye A. Comparison of arildone and 3-methylquercetin as stabilizers of poliovirus. Antiviral Res. 1985;1(Suppl 1):67–73.
108. Pevear DC, Fancher MJ, Felock PJ, Rossmann MG, Miller MS, Diana G, et al. Conformational change in the floor of the human rhinovirus canyon blocks adsorption to HeLa cell receptors. J Virol. 1989;63 (5):2002–7.
109. Cohen S, Au S, Pante N. How viruses access the nucleus. Biochim Biophys Acta. 2011;1813(9): 1634–45.
110. Wang T, Yu B, Lin L, Zhai X, Han Y, Qin Y, et al. A functional nuclear localization sequence in the VP1 capsid protein of coxsackievirus B3. Virology. 2012;433(2):513–21.
111. Abaitua F, Hollinshead M, Bolstad M, Crump CM, O'Hare P. A nuclear localization signal in herpesvirus protein VP1-2 is essential for infection via capsid routing to the nuclear pore. J Virol. 2012;86(17): 8998–9014.
112. Wang Y, Zhao S, Chen Y, Wang T, Dong C, Wo X, et al. The capsid protein VP1 of Coxsackievirus B induces cell cycle arrest by up-regulating heat shock protein 70. Front Microbiol. 2019;10:1633.
113. Knowlton KU, Jeon ES, Berkley N, Wessely R, Huber S. A mutation in the puff region of VP2 attenuates the myocarditic phenotype of an infectious cDNA of the Woodruff variant of coxsackievirus B3. J Virol. 1996;70(11):7811–8.
114. Stadnick E, Dan M, Sadeghi A, Chantler JK. Attenuating mutations in coxsackievirus B3 map to a conformational epitope that comprises the puff region of VP2 and the knob of VP3. J Virol. 2004;78(24):13987–4002.
115. Henke A, Launhardt H, Klement K, Stelzner A, Zell R, Munder T. Apoptosis in coxsackievirus B3-caused diseases: interaction between the capsid protein VP2 and the proapoptotic protein siva. J Virol. 2000;74(9):4284–90.
116. Chehadeh W, Lobert PE, Sauter P, Goffard A, Lucas B, Weill J, et al. Viral protein VP4 is a target of human antibodies enhancing coxsackievirus B4- and B3-induced synthesis of alpha interferon. J Virol. 2005;79(22):13882–91.
117. Ramsingh AI, Collins DN. A point mutation in the VP4 coding sequence of coxsackievirus B4 influences virulence. J Virol. 1995;69(11):7278–81.
118. McCarthy RE 3rd, Boehmer JP, Hruban RH, Hutchins GM, Kasper EK, Hare JM, et al. Long-term outcome of fulminant myocarditis as compared with acute (nonfulminant) myocarditis. N Engl J Med. 2000;342(10):690–5.
119. Lieberman EB, Hutchins GM, Herskowitz A, Rose NR, Baughman KL. Clinicopathologic description of myocarditis. J Am Coll Cardiol. 1991;18(7): 1617–26.
120. Burke AP, Saenger J, Mullick F, Virmani R. Hypersensitivity myocarditis. Arch Pathol Lab Med. 1991;115(8):764–9.
121. Getz MA, Subramanian R, Logemann T, Ballantyne F. Acute necrotizing eosinophilic myocarditis as a manifestation of severe hypersensitivity myocarditis. Antemortem diagnosis and successful treatment. Ann Intern Med. 1991;115(3):201–2.
122. Galiuto L, Enriquez-Sarano M, Reeder GS, Tazelaar HD, Li JT, Miller FA Jr, et al. Eosinophilic myocarditis manifesting as myocardial infarction: early

diagnosis and successful treatment. Mayo Clin Proc. 1997;72(7):603–10.

123. Cooper LT Jr, Berry GJ, Shabetai R. Idiopathic giant-cell myocarditis--natural history and treatment. Multicenter Giant Cell Myocarditis Study Group Investigators. N Engl J Med. 1997;336(26):1860–6.
124. Menghini VV, Savcenko V, Olson LJ, Tazelaar HD, Dec GW, Kao A, et al. Combined immunosuppression for the treatment of idiopathic giant cell myocarditis. Mayo Clin Proc. 1999;74(12):1221–6.
125. Aretz HT. Myocarditis: the Dallas criteria. Hum Pathol. 1987;18(6):619–24.
126. Martin AB, Webber S, Fricker FJ, Jaffe R, Demmler G, Kearney D, et al. Acute myocarditis. Rapid diagnosis by PCR in children. Circulation. 1994;90(1):330–9.
127. Wojnicz R, Nowalany-Kozielska E, Wojciechowska C, Glanowska G, Wilczewski P, Niklewski T, et al. Randomized, placebo-controlled study for immunosuppressive treatment of inflammatory dilated cardiomyopathy: two-year follow-up results. Circulation. 2001;104(1):39–45.

25 Epigenetic Influences of Air Pollution-Induced Cardiac Arrhythmias

Devin R. O'Piela, Jacob A. Grimmer, Neill A. Schwieterman,
Matthew J. Mears, Matthew W. Gorr, and Loren E. Wold

Abstract

Air pollution is a silent killer. Considered the largest environmental health risk globally, air pollution has been implicated in the development of cardiovascular and respiratory conditions as well as various cancers. Air pollution poses a serious global threat, as 91% of the world's population resides in areas that fail to meet WHO air quality guidelines. Air pollution in the form of particulate matter (PM) contributes to increased arrhythmia development. Exposure to unhealthy PM levels coupled with those suffering from arrhythmias necessitates analysis into their shared underlying causes.

Epigenetics is defined as alterations, heritable and acquired, to gene expression with preservation of the original DNA sequence. These modifications naturally occur during development but can be modified by external stimuli, ultimately resulting in differential gene expression in offspring. A handful of modifications constitute the essential pillars of this domain, often working concurrently to induce changes: DNA methylation, chromatin remodeling, histone modification, and RNA-based modifications. This chapter aims to discuss the influence of air pollution on epigenetic mechanisms and how these affect the development of cardiovascular disease, including arrhythmia development.

Keywords

Air pollution · Arrhythmia · Epigenetics · Particulate matter · Smoking · Cardiovascular disease · Heart · Epigenetics

Abbreviations

AERP	atrial effective refractory period
AF	atrial fibrillations
AHA	American Heart Association
Ang II	Angiotensin II
ARIC	Atherosclerosis Risk in Communities
CHD	chromodomain, helices, DNA-binding complexes
CpG	cytosine preceding guanosine
CTGF	connective tissue growth factor
CV	cardiovascular
DEP	diesel exhaust particles

D. R. O'Piela · N. A. Schwieterman · M. J. Mears ·
M. W. Gorr · L. E. Wold (✉)
Department of Physiology and Cell Biology, The Ohio State University College of Medicine, Columbus, OH, USA
e-mail: opiela.2@osu.edu; neill.schwieterman@osumc.edu; matthew.mears@osumc.edu; gorr.1@osu.edu; Loren.Wold@osumc.edu

J. A. Grimmer
Ohio University Heritage College of Osteopathic Medicine, Dublin, OH, USA
e-mail: jg430120@ohio.edu

© Springer Nature Switzerland AG 2023

O. N. Tripathi et al. (eds.), *Heart Rate and Rhythm*, https://doi.org/10.1007/978-3-031-33588-4_25

DNMT	DNA methyltransferase
EGC	electrocardiogram
ERK	extracellular signal-related kinase
HATs	histone acetyltransferases
HDACs	histone deacetylases
HMTs	histone methyltransferase
$HopX^{tg}$	homeodomain protein
HR	heart rate
HRV	heart rate variability
ICD	implantable cardioverter defibrillators
INO80	inositol-requiring 80 complexes
iNOS	inducible nitric oxide synthase
ISWI	imitation switch complexes
lncRNA	long noncoding RNA
MetS	metabolic syndrome
miRNAs	microRNAs
ncRNA	noncoding RNA
$PM_{0.1}$	ultrafine PM, diameter of <0.1 μm
PM_{10}	coarse PM, diameter of <10 μm
$PM_{2.5}$	fine PM, diameter of <2.5 μm
PNS	parasympathetic nervous system
pri-miRNAs	primary miRNA transcripts
RISC	RNA-induced silencing complex
ROS	reactive oxygen species
SAM	S-adenosylmethionine
sncRNAs	small noncoding RNAs
SWI/SNF	Switching defective/sucrose nonfermenting complexes
TNF	tumor necrosis factor
TSA	trichostatin A
UTR	untranslated region

25.1 Introduction: Particulate Matter and Cardiovascular Function

Environmental factors can induce profound physiological and pathophysiological consequences on the cardiovascular system [1, 2]. Obesity, stress, and air pollution, among other external stimuli, exemplify established risk factors for cardiovascular disease (CVD), which continues to be the leading cause of death in the United States. The dynamic interplay between genetics and environmental factors is complex: does one develop heart disease from obesity caused by a poor diet? Or are obese people genetically prone to developing cardiovascular disease via exposure to air pollution? Epigenetics is the balance of these dynamics via mechanisms induced by environmental triggers and those that occur during development.

Particulate matter (PM) is the sum of solid particles and liquid droplets suspended in the air. Sources of particulate matter include emissions from automobiles, smokestacks, construction sites, unpaved roads, and the black carbon and/or elemental carbon from these sources [3]. Many forms of air pollution exist alongside PM, such as carbon monoxide, ozone, oxides of nitrogen, etc. WHO estimates that PM exposure is responsible for the death of nearly seven million people annually. A number of studies have linked PM exposure to stroke, heart disease, several lung diseases, and pneumonia [4–6]. Another review by the American Heart Association (AHA) stated that CVD has resulted in over 17 million deaths annually. Of these 17 million, nearly 3.3 million were associated with exposure to ambient air pollution. The AHA has also stated that short-term exposure to PM contributed to the development of CVD and long-term exposure reduced life expectancy [5].

PM penetrates the body primarily through inhalation, where it enters the lungs and gains access to the bloodstream via alveoli. PM_{10} (coarse PM, diameter of <10 μm) has been experimentally linked, via in vivo and in vitro models, to acute and chronic CVD, whereas $PM_{2.5}$ (fine PM, diameter of <2.5 μm) and $PM_{0.1}$ (ultrafine PM, diameter of <0.1 μm) have been shown to penetrate further into the airways, alveoli, and systemic circulation, inducing the development of atherosclerosis, CVD, and provoking acute cardiac episodes and arrhythmias [7]. Recent studies of PM and CVD have demonstrated PM-induced development of cardiomyopathy, myocardial infarction, and hypertension, leading to cardiovascular (CV) dysfunction including arrhythmias, specifically tachycardia [8–11]. PM exposure is also associated with variations in heart rate (HR) in the form of tachycardia and heart rate variability (HRV). HRV, as its name states, is the variation in between heartbeats within a timeframe, measured by differences in the beat-to-beat interval. Decreased parasympathetic nervous system (PNS) activity exhibits decreased HRV, which is associated with respiratory sinus arrhythmia [12]. Furthermore, research of the underlying mechanisms of PM exposure and its proarrhythmic effects on CVD is lacking. Some studies suggest that PM affects the balance of autonomic control on the heart, increases reactive oxygen species (ROS), and changes the ability of blood to coagulate [11, 13]. This section will review the proarrhythmic effects of PM exposure and its long- and short-term effects.

25.1.1 Clinical Observations

Clinical examinations of the proarrhythmic effects of $PM_{2.5}$ have been conducted utilizing data from implantable cardioverter defibrillators (ICD), surveys, and clinical records of patients who experienced heart arrhythmias in correlation with PM concentrations recorded via satellite remote sensing, meteorological, and land-use analyses. To study the short-term effects of exposure to $PM_{2.5}$, ICDs were used to detect and record episodes of ventricular arrhythmias in a study of over 200 patients. There was a positive association between ventricular arrhythmia events and recorded PM levels; the strongest associations found over a 24-h moving average compared to the mean air pollution concentration for the calendar day and the previous day [9]. Patients with previous episodes of ventricular arrhythmias and other CVDs were more susceptible to ventricular arrhythmias correlated with PM exposure [9]. While short-term studies examine the effects of fluctuating PM emissions associated with certain occupations and shifts in weather patterns and development of CVD, long-term studies usually involve exposure of PM levels comparable to industrialized countries.

Recent studies of long-term PM exposure have demonstrated that exposure to $PM_{2.5}$ has been associated with the onset of tachycardia. An epidemiological study in China of over ten million reproductive-aged adults exposed to PM investigated this phenomenon over a span of 3 years. This study showed that 16% of participants, mean age of 28 years, were classified as having tachycardia. Older individuals (aged 40–64 years) showed a greater increase in HR than younger individuals (<30 years old) after long-term PM exposure, suggesting that older individuals may be more vulnerable to the effects of PM. This study showed a positive relationship between long-term PM exposure and tachycardia, increases in resting HR, and a 4% increase in ventricular tachycardia [14]. This work is supported by another study, which showed increases in PM by as little as 5 $\mu g/m^3$ were positively associated with HRV by 4.1% and increased diastolic blood pressure [10]. Thus, individuals exposed to prolonged elevation of PM emission are more susceptible to the development of tachycardia. Older individuals and individuals with a medical history of CVD and arrhythmia are more prone to further development and frequent episodes of arrhythmias.

As an increasingly industrialized society, where the combustion of carbon-based fuel is the primary source of PM, the findings of these epidemiological studies are concerning. If increased exposure to PM caused the development of cardiac pathological defects, a decrease in the input of PM would result in the decrease in future developments of PM-induced CVD and arrhythmia. Implementing higher industry and transportation emission standards would provide a means of limiting emitted PM; however, these standards must be implemented at a global level since air, and its associated PM levels, are not the same between cities and countries. When considering the populations that exhibited increased susceptibility to PM-induced CVD presented above, it is also crucial to further investigate what populations are more vulnerable to the effects of PM. Research focused on specific demographics (i.e., socioeconomic status, education level, race, sex, etc.), and the presence of existing disease should be conducted.

25.1.2 Experimental Studies

Variations in HR and HRV have shown mixed results when reproduced in animal studies of PM exposure. One study showed that increased exposure to concentrated air particles, analogous to PM, increased heart rate during and one hour after exposure, and caused a small increase in ventricular premature beats, though the latter was not statistically significant. These effects were short lived, which may be the result of a short exposure timeframe or the short window of observation [15].

A long-term in vivo study that investigated PM exposures comparable to those of industrialized countries demonstrated that $PM_{2.5}$ caused cardiovascular remodeling as well as various features of heart failure [16]. Long-term exposure to fine PM was shown to result in cardiac phenotypes consistent with heart failure, spontaneous arrhythmias, and increased HR. A short-term PM exposure in rats further supported these findings providing evidence that daily exposures to PM were shown to generate ROS up to two-fold of control levels [17]. ROS has been associated with increased risk of arrhythmia via several pathways as discussed below in the Underlying Mechanisms section.

Additionally, rats with metabolic syndrome (MetS) show increased susceptibility to the development of cardiac pathophysiology caused by PM exposure, including arrhythmia development. MetS rats showed altered HRV and increased HR after exposure to PM for 5 h/day over 12 days [18]. These rats, fed a high fructose diet and exposed to PM, exhibited altered cardiac electrophysiology, including a fourfold increase in atrioventricular arrhythmias, a diminished baroreflex response, and a decreased vagal influence on cardiac function, which provides another example of a population more susceptible to the development of arrhythmias. These results are similar to those from an epidemiological study in China, which found that older individuals and those afflicted with comorbidities were more susceptible to CV dysfunction after PM exposure [14].

25.1.3 Underlying Mechanisms

Recent epidemiological studies in adolescents have found that increased PM exposure caused an abnormal shift from parasympathetic control of the heart to predominant sympathetic control, associated with decreased HRV [11, 12]. As mentioned in the introduction, decreases in HRV are associated with respiratory sinus arrhythmia. Explanations for the imbalance of autonomic control of the heart may be explained by the production of ROS caused by PM exposure [19]. After long-term exposure to PM, the increase in ROS triggers ROS-dependent cell-signaling pathways, which result in an acute increase in blood pressure and a shift toward activation of the sympathetic nervous system, which results in arrhythmia.

PM exposure has also been linked to increased activity of NADPH oxidase, which generates $\bullet O_2$ upon phosphorylation of $p47^{phox}$, a subunit of NADPH, and binds to $p22^{phox}$ in the cell membrane resulting in increased ROS in the vasculature [20]. ROS in the vasculature results in the activation of inflammatory response via several pathways including focal activity, disruption of cardiac ionic currents, increased cardiac fibrosis, and impaired gap junction function [13]. Focal activity caused by ROS has been shown to prolong action potential duration, and induce early and delayed after depolarization, which facilitates arrhythmia development [13]. ROS disrupts ion currents as a result of residual Na^+ flow after the action potential peak, abnormal release, and reuptake of Ca^{2+} in the sarcoplasmic reticulum, as well as inhibiting K_{ATP} channels which prolongs action potential duration.

Other studies have suggested that exposure to PM caused an inflammatory response in the alveoli and release of cytokines, ultimately changing blood coagulation. The ultrafine PM is retained in the interstitial tissue of the lungs where an inflammatory response follows. This retention is likely due to the macrophages' inability to phagocytize ultrafine PM particles. Changes in blood coagulation have been linked to increased susceptibility to CVD event (i.e., myocardial infarction) [21]. Further research is still needed to fully understand the mechanisms of PM exposure on heart arrhythmias.

25.2 Epigenetic Modifications Overview

Epigenetic modifications are essential for normal physiological processes. However, there is clear evidence for the role of epigenetic processes in the development of cancers, cardiovascular disease, neurological, and autoimmune disorders. An increased understanding of the mechanisms that drive epigenetics could offer the missing link in developing more effective therapeutic approaches for cardiovascular disease. While epigenetic modifications can be detrimental to cardiovascular health, the epigenome possesses reversible properties that enable it to be reprogrammed. This feature has been established and applied to the development of cancer therapeutics: epigenetic drugs, termed epidrugs, are currently being developed to target the epigenetic modifications responsible for inhibiting tumor suppressor and DNA repair genes [22, 23]. Epidrugs are designed to target enzymes responsible for completing epigenetic modifications including DNA methyltransferases and histone deacetylases. By inhibiting such enzymes, epidrugs prevent unwanted silencing of genes and help to reestablish normal function within the epigenome. Thus, certain epigenetic modifications relevant in the development of disease can be reversed. Mounting evidence suggests the coupling of epigenetic drugs with chemotherapy could provide an effective treatment option for diseases such as cancers. Although still in its infancy, this research suggests that epigenetic modification may be utilized to treat cardiovascular diseases [24].

A description of each epigenetic mechanism, providing the foundation for this chapter, is depicted in Fig. 25.1. The subsequent sections will expand on the links between external stimuli, induced epigenetic modifications, and the resulting cardiac dysfunction.

25.2.1 DNA Methylation

DNA methylation, an essential epigenetic regulator in many eukaryotic organisms, occurs when a methyl (CH_3) group is covalently added to the 5-C position of a cytosine on DNA. The execution and maintenance of this modification is determined by a family of three DNA methyltransferase (DNMT) enzymes: DNMT3a, DNMT3b, and DNMT1. Common changes induced by DNA methylation include regulation of gene expression, suppression of transposable elements, genomic imprinting, and X-chromosome inactivation [25, 26]. DNA is highly methylated in vertebrates: ~60–90% of cytosine preceding guanosine (CpG) sites are methylated, with the exception of “islands” of unmethylated areas called CpG islands [27]. Methylation plays a highly regulatory role in gene expression at CpG sites; however, its role changes when CpG islands are the targets of modification.

CpG islands comprise around 1000 CpG-dense base pairs. Under normal conditions, CpG islands lack methylation [28]. These islands are nonrandom; they encompass ~1% of genomic DNA and are located at the promoter regions (5’ N-terminus) of many genes. Housekeeping genes, which act to maintain cellular function and to normalize expression values of variable genes for experimental and computational studies, are among the most common genes possessing CpG islands [29, 30]. Housekeeping gene promoter regions must remain unmethylated to ensure their constitutive expression to maintain normal cell functionality. However, when methylation within CpG islands occurs, access to DNA is decreased, blocking transcription factor binding and gene expression [28]. Methylation of CpG islands and dysregulation of prevalent methylation patterns (60–90% of CpG) potentiate an array of consequences, ranging from developmental disorders to various diseases, including CVD [27, 28, 31].

DNMT1 is the primary methyltransferase responsible for maintaining the covalent attachment between methyl groups and cytosines upon

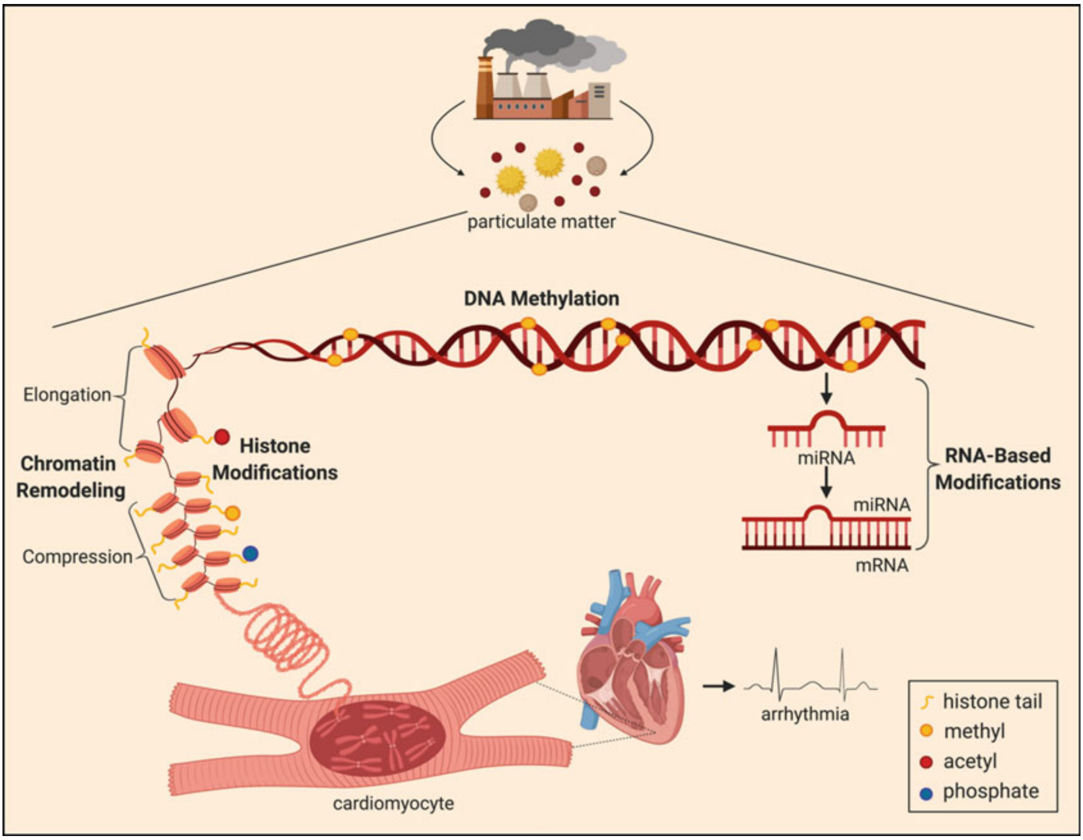
particulate matter
DNA Methylation
Elongation
Chromatin Remodeling
Compression
Histone Modifications
miRNA
miRNA
mRNA
RNA-Based Modifications
arrhythmia
cardiomyocyte
histone tail
methyl
acetyl
phosphate

Fig. 25.1 Particulate matter-induced epigenetic modifications of chromosome in cardiomyocyte including DNA methylation, histone modifications, chromatin remodeling, and RNA-based modifications and resulting dysfunction. Figure created with BioRender.com

DNA replication. DNMT1 acts to copy the parent strand methylation pattern onto the unmethylated daughter strand, transforming the double-stranded DNA from hemi-methylated to fully methylated. DNMT3a and DNMT3b (de novo methyltransferases) aid in establishing novel patterns of methylation early on in development by adding methyl groups to unmethylated CpG bases [32]. DNA methylation is vital to cell differentiation and embryonic development, and DMNT1 plays a crucial role in subsequent methylation pattern maintenance [32, 33]. Genetic knockout experiments have revealed DMNT1, DMNT2, and DMNT3 are essential to offspring viability, though DMNT2 is not directly involved in the DNA methylation process. DNMT1 inactivation resulted in embryonic lethality, and DMNT3a/DMNT3b inactivation caused death shortly after birth in mice. Reduced or disrupted patterns of these enzymatic catalysts contribute to genomic destabilization, promoting cancer, and disease development [34]. Hypermethylation of CpG island promoter regions exemplifies abnormal DNMT activity, causing transcriptional silencing effects on cellular pathways (mimicking those of mutations/deletions). Hypermethylation of DNA repair genes has also been associated with cancer and disease development [34]. Proper DNA methylation is essential to the growth, development, and maintenance of the human genome.

Methylation can be reversibly modulated by demethylation, accomplished through both an active and passive approach: demethylases are the active enzymatic agents responsible for combating the effects of malfunctioning DNMTs and methylation of CpG islands, often at promoter regions, where hyper/hypomethylation can silence gene expression and result in cancer and disease development [34]. The passive mechanism involves failure to retain methylation patterns during DNA replication and cell division. However, demethylation remains a highly uncharted concept, limiting its current application for therapeutics. Furthermore, the 5C-methyl modification is thought to be highly stable, and it has yet to be determined if breaking the carbon–carbon bond necessary to remove the methyl group from the 5-methylcytosine is possible. Still, cytidine deaminases, elongator complexes, base excision repairs, nucleotide excisions, DNA methyltransferases, and DNA glycosylases are candidate gene families and pathways suspected to play a role in the biochemical mechanisms associated with DNA demethylation [35]. With the increasing potential to reverse methylation of undesirable regions with accuracy, there is hope for detecting and treating diseases caused by epigenetic modifications by offering a directed therapeutic approach [32, 35].

25.2.2 Chromatin Remodeling

DNA is tightly packaged by wrapping around an octamer of duplicate histone proteins (H2A, H2B, H3, and H4) to form a nucleosome, which is the structural unit of the chromatin complex [36]. This system offers an effective way of housing large amounts of genetic material while dividing the genome between transcriptionally active and inactive/repressed zones [37]. Nucleosomes provide a primary means of genomic compaction and a "signaling hub" for chromatin-templated processes. During chromatin remodeling, ATP-dependent enzymes manipulate the function of nucleosomes, resulting in post-translational modifications [38]. Energy from ATP hydrolysis is used to elicit changes from nucleosome movement to destabilization or restructuring by altering associations between histones and DNA on the nucleosome [26, 39].

There are four classes of ATP-dependent chromatin remodeling complexes that are powered by ATP hydrolysis and function to slide or eject nucleosomes. The complexes manage nucleosome grouping and configuration by communicating with histone chaperones and swapping histones and histone variants [40]. The classes include switching defective/sucrose no-fermenting complexes (SWI/SNF); imitation switch complexes (ISWI); chromodomain, helicase, DNA-binding complexes (CHD); and inositol-requiring 80 complexes (INO80) [26]. The chromatin remodeling complex families contain varied levels of domains, subunits, and accessory subunits, which dictate their target specificity and role in gene expression regulation [40]. Regardless of differences in domain and subunits, the complexes serve a common purpose of altering gene expression at some capacity. Some protein complexes promote access to nucleosomal DNA, while others inhibit access by retightening and reforming the DNA-protein complexes that comprise the nucleosome [36]. The degree that chromatin is condensed modulates transcription, DNA replication, and DNA damage response. Chromatin remodeling complexes function to modulate the state of chromatin and its degree of accessibility, effectively altering gene expression [40]. Furthermore, chromatin remodeling directs protein access to DNA and plays a regulatory role in DNA damage-induced signaling pathways [41]. Irregular functionality of the ATP-dependent chromatin remodeling complexes is linked to disease development, since they are key players in fundamental cellular processes (i.e., transcription, DNA replication, and repair).

25.2.3 Histone Modifications

Histones are protein structures that organize DNA into nucleosomes as a means of packing a significant amount of genetic information into a condensed structure. Histone modifications provide a means of post-translational control of gene expression by modulating the degree of chromatin compaction. Histone modifications include phosphorylation, ubiquitination, sumoylation, acetylation, deacetylation, ADP-ribosylation, proline isomerization, deamination, methylation, and demethylation [42]. Histone acetylation refers to the introduction of an acetyl group (CH3CO) to a member of a histone tail (commonly lysine). It is the most studied modification and dysregulation that has been implicated in the development of CVD [43]. Acetylation provides greater access to chromosomal domains that are highly compacted and elicits increased access to promoter regions, ultimately activating transcription. Without acetylation, nucleosomes will continue folding into more complex and inaccessible structures. Accessibility is thus a balance of the synergistic actions between acetylation and chromatin remodeling via ATPases and methylation [44]. Histone acetyltransferases (HATs) transfer an acetyl group to histone proteins and play a crucial role in the activation of genes and transcription. Histone deacetylases (HDACs) effectively remove the acetyl group from histone tails, resulting in a reversal of DNA accessibility and an increased level of nucleosomal fiber folding, inducing repression [45]. A disruption of the balance between HAT and HDAC standard functionality can elicit cardiac pathologies, which will be discussed later in this chapter.

Histone methyltransferase (HMT) enzymes use S-adenosylmethionine (SAM) as a cofactor to catalyze the methylation of basic residues (lysines, arginines, and histidines) in histone tails. Individual residues and different residues of the same histone can be methylated to varied degrees. For example, lysine can be mono-, di-, or tri-methylated [46]. The extent of methylation affects the condition of differential gene expression, causing either activation or repression of a methylated gene [47]. Protein recruitment may cause additional chromatin folding or increased access to the DNA [36]. Demethylation refers to the reversal of methylation via removal of methyl group(s) from histone tails. Similar to histone methylation, demethylation can promote or inhibit gene activity [34]. Experimental rat models have associated heart failure development to two histone modifications: trimethylation of histone H3 on lysine-4 or lysine-9, thus revealing the implications few epigenetic modifications can have in cardiovascular disease development [48].

25.2.4 RNA-Based Modifications

The central dogma of molecular biology in which DNA is transcribed into RNA and RNA is translated into protein oversimplifies the relationship between DNA, RNA, and protein. DNA is transcribed into RNA, which can later be translated into protein; however, this is not always the case. In fact, genomic DNA is predominately transcribed into noncoding RNA (ncRNA), which fails to be translated into proteins. ncRNAs maintain a highly purposeful role in epigenetics and the evolution of disease [49]; ncRNA is divided into small noncoding RNAs (sncRNAs), which includes microRNAs (miRNAs) and long noncoding RNA (lncRNA), greater than 200 nucleotides in length [50]. miRNA—an endogenous form of sncRNA that is ~22 nucleotides long—is the most understood form of sncRNAs to date. miRNA dysregulation has been found to play a major role in the formation of cancer and disease [51–53].

The biogenesis of miRNA involves a multistep process beginning with the transcription of miRNAs into long primary transcripts (pri-miRNAs). Next, pri-miRNAs form unique precursor stem loop structures ~77 nucleotides in length (pre-miRNAs) that are cleaved by RNase III nuclease [54]. The transcripts are then exported from the nucleus to the cytoplasm and cleaved by RNase III Dicer, resulting in a final miRNA ~22 nucleotides in length [54]. Upon reaching mature form, one strand of miRNA is organized into an RNA-induced silencing complex (RISC) that can recognize and bind short fragments of mRNA [55]. The seed region of miRNA is between nucleotides 2 and 8 at the 5′ end of the strand. This region is essential for target recognition, functioning to identify the 3′ untranslated region (UTR) of the mRNA to which it binds. Targeting of 3' UTR regions is widespread, though regions such as 5' UTR or coding regions may be targeted instead. The normal function of mRNA can effectively be repressed by miRNA binding, and a single miRNA is capable of targeting several mRNAs [56]. High complementarity between the miRNA and target mRNA promotes degradation of target mRNA by a process termed RNA interference. Low complementarity yields translational inhibition of target mRNA, via induced ribosomal alterations, which is highly prevalent in human cells. The interplay between high and low complementarity and their mechanisms offers an effective way of maintaining homeostasis. In addition to interacting with mRNA, organized actions between miRNAs and other epigenetic modifications also exist [56, 57].

The descriptions above detailing each common epigenetic modification provide an overview of their properties, elucidating the highly complex and cooperative nature of epigenetic modifications and their ability to influence cellular function and genetic expression. These mechanisms apply to various systems throughout the body and can be affected by many external triggers, such as air pollution. Although epigenetic changes can induce unfavorable expression, since alterations are not at the DNA sequence level, the possibility to reverse detrimental modifications is within reach. Throughout this chapter, the relationships between epigenetics, arrhythmias, and air pollution in the form of PM exposure will be introduced. First, we will consider the connection between epigenetics and arrhythmias. We will then highlight the effect of PM on arrhythmias and the epigenome. Lastly, we will consider what role other pollutants, including traditional cigarettes, have on the development of arrhythmias.

25.3 Epigenetics as a Mechanism for Particulate Matter-Induced Cardiovascular Disease

25.3.1 Role of DNA Methylation in Arrhythmogenesis

Abnormal patterns of DNA methylation have been closely associated with many CVDs, such as arrhythmias [58]. Parental atrial fibrillation (AF) is a risk factor for arrhythmia development, indicating a genetic component [59, 60]. A variety of remodeling changes, such as fibrosis and signaling pathways, lead to physiological changes and cardiac disease conditions, in which AF is a common endpoint [60–62]. Additionally, regulation of extracellular matrix proteins, which cause fibrosis that leads to arrhythmias, has been shown to be regulated by DNA methylation [63]. Fibrosis slows the electrical function by jeopardizing the electrical impulse propagation. There are some discrepancies in the literature concerning the uniformity of methylation across the atrium of the heart. Methylation was largely found to be conserved across atrial tissue of coronary bypass surgery patients where after surgery 25% of the patients developed AF, which contrasts starkly with another study involving induced heart failure in rats that found CpG islands to be hypermethylated in the atria with fibrillation [64, 65]. The link between DNA methylation and gene expression in heart disease needs to be further studied before it can be a predictive indicator of gene expression in human populations [66]. DNA methylation has been shown, however, to play a central role in the maintenance of cardiac fibrosis, which contributes to the pathogenesis of AF [62, 63].

SERCA2a, an ATPase that plays an important role in transporting calcium into the sarcoplasmic reticulum, contains CpG islands in the promoter region of its gene [67]. When the expression of SERCA2a is altered, calcium handling becomes abnormal, a lower expression leads to less capacity for calcium handling, leading to a change in contractility and arrhythmia [67]. The methylation of the SERCA2a promoter region is affected by DNMT levels. In one study, DNMT levels in HL-1 cardiomyocytes were increased after introduction of tumor necrosis factor alpha (TNF-α), leading to an enhancement in methylation of SERCA2a, reducing its expression [67]. Activity of SERCA2a and phospholamban can imperatively influence the calcium handling leading to potential risk to developing an arrhythmia as well as heart failure [68]. When cardiac fibrosis was induced via isoproterenol injections in rats, DNMT3a was found to silence RASSF1A via extracellular signal related kinase (ERK1/2) upregulation, which caused increased fibroblast proliferation [69]. Inhibition of this methylation may be a novel treatment for impaired heart function and arrhythmogenesis [67].

The homeobox gene Pitx2c plays a role in AF, and contains CpG islands in its promoter region, allowing it to be silenced through methylation [65]. Heart failure induces Pitx2c promotor hypermethylation, in part due to increased levels of DNMT1, which decreases the protein levels of Pitx2c [65]. Pitx2c promotor methylation in HL-1 cells (atrial cell line) and DNMT are increased when treated with Angiotensin II (Ang II), thereby downregulating the protein levels of Pitx2c and Kir2.1 [65]. When cultured with the Ang II receptor blocker losartan, the effects of hypermethylation on Pitx2c expression in HL-1 cells that had been treated with Ang II is reduced [65]. Thus, Losartan may be beneficial for blocking Ang II receptors which may be a novel therapeutic target [65]. Pitx2c regulates expression of the sodium channel subunit $\mathrm{Na_v}1.5$; as well as rectifier channels KCNA3, KCNC4, and Kir2.1; all of these potassium channels play a role in contractility. A study of both mouse and human atria samples that had atrial arrhythmias found Pitx2c to exhibit increased methylation [70]. Dysregulation of Pitx2c promotes susceptibility to AF by modifying calcium handling, altering function of melanocytes, (melanin producing cells that are found in the valves and septum of the heart among other areas of the body) and changing cell-to-cell communication [70].

SUR1 and SUR2 are two gene subunits that form ATP sensitive potassium channels in cardiac myocytes that combine with Kir6.2, a major potassium channel subunit, whose expression is also susceptible to DNA methylation [71]. By using RNAzol on HL-1 cells cultured from atrial myocytes, it was shown that SUR2 can be silenced by CpG methylation, ultimately leading to changes in $\mathrm{K_{ATP}}$ density and composition, and may eventually lead to dysfunction in the heart [71]. Bisulfate sequencing on these same HL-1 cells has shown that SUR2 is much more prone to methylation versus SUR1 (57.6% vs 0.14%) at CpG sites within their promotor regions [71]. Investigated as a potential treatment, decitabine caused a decrease in SUR1 and increased the unmethylated fraction of SUR2 mRNA and CpG island expression [71]. More avenues to study these epigenetic changes are needed to explore this multi-faceted function, as the targeted silencing of gene expression can imbalance the structural proteins compromising overall function.

25.3.2 Role of DNA Histone Modifications in Arrhythmogenesis

HDACs are another way in which expression can change epigenetically via post-translational modification. Alteration of HDAC enzymes may cause DNA to be less accessible to transcription factors. Reduced DNA transcription can lead to a range of arrhythmogenic diseases, including long QT syndrome, Brugada syndrome, short QT syndrome, catecholaminergic polymorphic ventricular tachycardia, and arrhythmogenic right ventricular cardiomyopathy [72]. Knockout of HDAC1 and HDAC2 in a mouse model resulted in neonatal lethality, which severely altered growth and function of the hearts by upregulating calcium channel subunits, resulting in cardiac arrhythmias among other cardiac defects [73]. Much like DNA methylation, histone deacetylases are epigenetic modulators and can influence cell proteostasis, prompting investigation of the role of HDACs in the structural remodeling associated with AF and potential therapeutics to abate AF.

HDACs are vital to calcium homeostasis; AF patients have CaMKII-hyperphosphorylated ryanodine receptors, causing sarcoplasmic reticulum leak, sodium-calcium exchanger overactivation, and delayed after-polarizations [74]. In cardiomyocytes found in the pulmonary vein, the use of MPTOE014 (an HDAC inhibitor) modulated the regulatory proteins for calcium homeostasis, helping negate AF inducibility [75]. Tachypacing, (induced rapid pacing) of HL-1 atrial cardiomyocytes resulted in deacetylation, depolymerization, and degradation of α-tubulin by calpain [76]. HDAC6 activated by the tachypacing, leads to this imbalance in α-tubulin which modifies the microtubule structure in cardiomyocytes causing contractile dysfunction [76]. Additionally, inhibition of HDAC6 via tubastatin A was protective in a dog model of AF, suggesting that the TDAC domain of HDAC6 is a potential upstream target to reduce cardiomyocyte remodeling and protect α-tubulin proteostasis [76]. Inhibiting a targeted HDAC may help regulate natural levels of DNA transcription as a means to inhibit adverse cardiac remodeling.

Histone deacetylase inhibitors have been examined as a therapeutic target of fibrosis in chronic conditions. The HDAC inhibitor mocetinostat was shown to be antifibrotic in the hearts of rats with myocardial infarctions, where HDAC1 and HDAC2 were upregulated via left anterior descending coronary artery occlusion [77]. Valproate, an anticonvulsant drug, impairs HDAC6 and HDAC8 when elevated by cardiac hypertrophy, making it a possible inhibitor to treat or prevent cardiac dysfunction [78]. HDAC inhibitors trichostatin A (TSA), valporic acid, and SK-7041 partially reversed hypertrophy in a rat model [78]. In primary mouse myocytes, TSA inhibits Ang-II-induced cardiac hypertrophy response [70]. TSA has also been shown to reduce cardiac hypertrophy in a mouse model of heart failure [79]. In another mouse model, mice with overexpression of homeodomain protein (HopX^{tg}), which induces cardiac hypertrophy through HDAC activity, saw reduced atrial arrhythmia after TSA treatment [80]. It also normalized size distribution, expression of connexin40, and Angiotension II levels between wild type and HopX^{tg} mutant mice [80]. Thus, HDAC inhibition has its therapeutic uses in reversing connexin40 remodeling, atrial fibrosis, and atrial arrhythmia vulnerability where hypertrophy is present.

25.3.3 Role of miRNA Reprogramming in Arrhythmogenesis

Studies have demonstrated a clear impact of miRNAs on arrhythmogenesis by regulating gene expression related to AF. Many recent studies have investigated the functions of how miRNA contribute to the genesis of AFs and have been implicated largely in fibrosis and ion channel remodeling, two of the main mechanisms that lead to AF [81]. miRNA may be used as therapeutic target or biomarker for AF. Some miRNAs (miRNA1, miRNA133, miRNA208, and miRNA499) are capable of reprogramming fibroblasts, both in vivo and in vitro, to become cardiac myocyte-like [82]. Many fibrosis-regulating miRNA bind to profibrotic targets [83]. Most atrial fibrosis promoting miRNA are down-regulated in AF conditions, except miRNA-21, which is up-regulated [83].

The table below has a list of the known miRNAs and their likely role in altering heart function, potentially contributing to arrhythmia development. Many miRNAs contribute to electrical and structural remodeling in the heart; miRNA1, miRNA26, miRNA106b-25 cluster, miRNA-133, miRNA 208, miRNA328, and miRNA499 all up- or down-regulate genes that affect electrical remodeling. MiRNA21, miRNA26, miRNA29b, miRNA30, miRNA499, and miRNA 590 play a role in dysregulating genes that lead to structural remodeling. In vivo manipulation of miRNA has been investigated in AF: miRNA1, miRNA21, miRNA26, miRNA29b, and miRNA328 have all been manipulated in either mouse, rat, dog, or rabbit and have been shown to reduce atrial remodeling and fibrillation [62]. Looking into the miRNA that lead to AF can give clues to what may be triggering the onset, and potentially how to abate the disease therapeutically. The Table 25.1 outlines the miRNA that have been found to be linked to AF regulation. miRNA targets for expression and the consequences associated with their dysregulation are also presented.

25.4 Particulate Matter and the Epigenome

The reactive, pro-oxidant nature of PM makes it a prime target for environmentally caused changes to the epigenome. As PM enters the body, it has the ability to readily interact with cell populations

Table 25.1 AF-associated miRNAs and corresponding regulatory targets

miRNA	Target of Regulation	Alterations
miRNA 1	Suppresses expression of KCNJ2, KCNE1, KCNB2, GJA1 [62], expression of CACNB2 is lower in control settings, regulates Kir2.1	• Repesses phosphate proteins • Reduced in atrial fibrillation • Shorter atrial effective refractory period (AERP) • Decreases intracellular Ca2+ concentration • Electrical remodeling, upregulates/increases I_{K1}*
miRNA 21	CACNA1C, CACNB2, SPRY1 [62]	• Increased mi-RNA 21 correlates positively with atrial collagen content • Reduces expression of Spry1 and increases expression of connective tissue growth factor (CTGF), lysyl oxidase, and Rac1-GTPase • Profibrotic inhibition prevents fibrosis. Increased in AF when knocked down. Reduces promotion and suppresses AF
miRNA 26	Represses KCNJ2 [84], Kir2.1, IK1 TRPC3 [84, 85]	• Represses Kir2.1 protein • Causes TRPC3-dependent enhancement of fibroblast proliferation and differentiation • Downregulation of miRNA26 increases expression of KCNJ2/I_{K1} in fibroblasts and cardiomyocytes [84] • TRPC overexpression allows for greater Ca^{2+} entry [84, 85]
miRNA 29	COL1A1, COL3A1, FBN	• Targets extracellular matrix proteins [62] • mi-RNA 29 expression is decreased in plasma from AF patients • Negatively regulated by TNF-β [62] • Targets collagen and fibronectin [86] • Suppression enhances collagen production [86]
miRNA 30	Inversely related to CTGF, targets CTGF [86]	• Higher levels of mi-RNA 30 has less collagen production; downregulated in AF
miRNA 106	Loss of mi-RNA 106 enhances RyR2 (ryanodine receptor type 2), mi-RNA 106b-25 suppresses gene TBx3, required for sinoatrial node development	• Increased RyR2 protein, total Ca2+ leak in sarcoplasmic reticulum, and spark frequency
miRNA 122	Caspase 3, Bcl-x [87]	• Associated with cardiomyocyte apoptosis [87]
miRNA 133	Modulate post transcriptional expression of HCN4 gene expression, downregulated in atrial fibrillation, targets CTGF [86]	• Higher amounts reduces collagen • Targets TNF-β [62] • Targets collagen 1 [70]
miRNA 146	Negative inflammation regulator	• Upregulated with collagen in AF patients
miRNA 150	Regulates genes implicated in atrial remodeling	• Downregulated in patients with AF • Increases post ablation
miRNA 206	Autonomic nerve remodeling	• Overexpression increases ROS levels in vitro and in vivo
miRNA 328	KCNN3, CACNA1C,p and CACNA1B [62]	• Elevated in AF patients, atrial remodeling • Knockdown restores Cav1.2 and CavB1 expressions [62] • Electrical remodeling, reduction of L-type Ca^{2+} current and shortening and density
miRNA 499	KCNN3	• Upregulated in the AF atria • Downregulated SK3 protein expression

(continued)

Table 25.1 (continued)

miRNA	Target of Regulation	Alterations
		• Inhibitors upregulate SK3, downregulated in human atrial AF patients
miRNA 590	TGF-βR2	• Antifibrotic • Targets TNF-β [62]

from the lung, blood, and vasculature. How PM affects these cells and its relevance to human health is under investigation at the cellular level, in animal-based research, and in clinical cohorts. The highlight of current clinical investigations is based primarily upon the fact that interactions with PM causes changes in the epigenetic layout. Primary evidence for this involves repeated-element methylation and methylation of specific genes during PM exposure. However, emerging work is centered around the adult origins of developmental disease hypothesis. This hypothesis stipulates that the insults (e.g. PM exposure) that occur during germ cell or in utero development affect phenotypes at adulthood, indicating that epigenetic modifications may play an important role.

25.4.1 In Vivo Modifications to the Epigenome

As the ability for real-time PM exposure monitoring in human subjects is limited, many studies have utilized clinical cohorts and examined the significance of local PM levels on epigenetic markers using patient data. Altered methylation of repeated elements have been correlated with PM or PM markers in several of these studies. Decreased methylation of long interspersed nuclear element −1 (*LINE-1*), which comprises approximately 17% of the human genome, has been positively associated with black carbon and SO_4 levels [88–90], and blood levels for several persistent organic pollutants [91]. Similarly, hypomethylation of the transposable element *Alu* has been found to be associated with PM and its constituents [37, 38, 41], confirming the presence of global changes to the epigenome in humans exposed to PM. How such changes contribute to disease severity, alter development, and change the genetic makeup of offspring is currently under investigation.

Additional studies have examined altered epigenetic modification and function of specific genes with PM exposure. PM exposure in a cohort of children was negatively associated with inducible nitric oxide synthase (iNOS) promoter methylation [92], which was also found in a cohort of foundry workers, where the *NOS2A* gene had decreased expression following three days of work [93]. This decrease in iNOS promoter methlyation was also found to be PM-associated and was suggested to be of functional relevance in respiratory outcomes due to increased expression after PM exposure [94]. Correlation of PM levels with methylation of specific genes have also been found including *Foxp3* [95], *TLR-2, ICAM-1* [90], and *TLR4* [96]. One study found PM to be associated with genes in the MAPK pathway, but not the Nf-κB pathway [97], demonstrating that PM can cause specific, nonglobal changes to the epigenome. As to whether these changes are adaptations to organic pollutants providing protection or are damaging and contributing to the phenotype found with PM exposure remains undetermined.

25.4.2 Germline and In Utero Exposure to PM

The Barker hypothesis, or the developmental origins of adult disease hypothesis, was initiated with the observation that those born following periods of in utero stress, such as famine, and thus had reduced birth weight, are at a greater risk for heart disease later in life [98]. Data therein thus implies fetal genetic imprinting, and thus epigenetics is a clear candidate for these outcomes. How PM affects the developmental timeline, and if there are relevant cardiac effects, is thus a target of important study.

Determining how PM affects the developing human and what changes manifest during adulthood are by nature very difficult, thus several studies in animals have been used to further understand the biology and mechanism. Mice were exposed during pregnancy to a relevant level of PM, and then removed from exposure at birth; resulting pups from these mice compared to pups from dams exposed to filtered air had reduced cardiac output, cardiac electrical remodeling and alterations in gene expression of deacetylases and DNA methyltransferases at adulthood [8]. These mice were born with reduced bodyweight and had an impaired cardiac phenotype merely from exposure to PM in utero. Continuing work is also indicating a germline effect, as preconception exposure of mice to PM has been found to cause a decrease in cardiac function of male offspring [99], perhaps due to the fact that hypermethylation of sperm DNA has been shown to occur after PM exposure [100]. Indeed, pups from mice undergoing transplacental exposure of diesel exhaust particles (DEP) have been found to have genetic deletions [101], adding to the evidence that PM causes gene-level alterations during development.

25.5 Cigarette Smoke and Arrhythmogenic Potential

Several conditions exhibit arrhythmogenic potential including heart failure, endocarditis, heart valve disease, diabetes, and asthma. Furthermore, lifestyles such as consuming alcohol may impact the likelihood of developing arrhythmias [102]. Epidemiological studies examining traditional cigarette smoking demonstrate mixed results on arrhythmogenic risk potential; however, many in the scientific community posit cigarette smoking as a risk factor. The epidemiological evidence linking PM with increased CVD and respiratory disease incidence has been widely published and accepted [103]. Cigarette smoke is comprised of thousands of chemicals, including PM, that are carcinogenic and include tar, benzene, formaldehyde, and arsenic. While the chemical profile of cigarette smoke contains several similar compounds found in PM, key differences arise in the source and concentration of particles. Automobile emissions, industrial wastes, agricultural practices, and roadside dust are all sources of ambient PM. Therefore, due to regional differences in the production of these pollutants, PM profiles are variable and difficult to characterize. Cigarette usage also bears the risk of complications caused by nicotine, an addictive substance associated with many acute cardiovascular responses [104–107]. Cigarette smoke, however, has a much more consistent compound profile allowing for more standardized and replicable studies. Here, we compare cigarette smoke-induced arrhythmogenesis to particulate matter induced arrhythmia.

25.5.1 Epidemiology of Atrial Fibrillation and Cigarette Smoking

AF has been the focus of many population-based studies of smoking. These large analyses have produced varying results, complicating our understanding of the role of smoking on AF. The Atherosclerosis Risk in Communities study (ARIC) analyzed participants over an average follow-up period of 13.1 years. In this study, current smokers exhibited a 2.05 relative risk score of developing AF compared to those who never smoked [108]. Benefits to smoking cessation were found. While those who ceased cigarette use still had a relative risk score of 1.32 compared to never smokers, this score is considerably lower than current smokers [108]. Similar trends in data are seen in the Rotterdam and Hordaland studies as both show an increased risk of AF for current smokers [109, 110], however, these studies resulted in different conclusions on the incidence of AF in former smokers. Interestingly, the Rotterdam study found no benefit for former smokers [109] as the relative risk of AF development was nearly identical between former and current smokers. In contrast, the Hordaland study observed former smokers carried no increased risk for AF [111], thus suggesting substantial benefits for cessation. These studies outlined the adverse association of smoking behavior and AF; however, questions regarding the potential benefits of cessation on arrhythmogenesis must be understood more clearly.

Contradictory to the above correlation between smoking and AF, several notable studies of similar design demonstrated no significant risk of AF with smoking habits. In a cohort of 15,000 men and women, current or former smoking status was not found to correlate with higher incidence of AF [110]. In a retrospective analysis of the Framingham Heart Study, this result was further solidified, as no correlation was found between smoking and AF [112]. However, cardiac disease traditionally related to smoking was linked to AF development through a 10-year risk assessment, thus suggesting that any arrhythmogenic potential due to smoking may require long-term exposures to first establish conditions such as heart failure or ventricular hypertrophy. Additionally, the Manitoba Follow-up Study showed similar findings [112, 113]. These results are significant since they question the association of smoking behavior and AF development. Therefore, further studies are warranted to understand the potential correlation and identify whether smoking directly or indirectly leads to AF.

25.5.2 Epidemiology of Ventricular Arrhythmogenesis and Cigarette Smoking

Ventricular arrhythmias have also been associated with traditional cigarette usage. Several studies have analyzed electrocardiogram (ECG) recordings of chronic heavy smokers and never smokers and found altered ventricular repolarizations with changes in electrocardiographic T wave ($T_{p\text{-}e}$) to QT ratios ($T_{p\text{-}e}$/QT), an index of arrhythmogenesis and predictor of future arrhythmia [114]. In an echocardiographic analysis of healthy male and female subjects (24 smokers and 23 nonsmokers), chronic smoking was found to correlate with prolonged $T_{p\text{-}e}$ interval and increases to $T_{p\text{-}e}$/QT ratio and $T_{p\text{-}e}$/QTc ratio [115]. These ECG markers indicate global cardiac electrical dysfunction, a possible pathophysiological mechanism that can be targeted for therapeutic development. The evidence for altered electrical instability in arrhythmogenesis was further confirmed by a large study revealing similar results. Comparing 121 smokers to 70 control subjects, the authors found increases in the following intervals of smokers: QTd, cQTd, $T_{p\text{-}e}$, $cT_{p\text{-}e}$ [116]. Additionally, $T_{p\text{-}e}$/QT and $T_{p\text{-}e}$/QTc ratios were significantly increased in smokers compared to nonsmokers [116]. The large body of evidence examining the relationship between smoking, ECG abnormalities, and arrhythmogenesis thus provides a clear framework for clinicians to treat and monitor arrhythmia in the early stages of disease.

25.5.3 Nicotine Exposure on Molecular Mechanisms Associated with Arrhythmogenesis

The most widely studied constituent of tobacco smoke is nicotine, an addictive substance that acts on nicotinic acetylcholine receptors. The hemodynamic responses to nicotine exposure, regardless of the route of administration (intravenous, nasal spray, and ingestion), have been characterized by increases in heart rate and blood pressure [117, 118]. Since the type of nicotine exposure does not significantly impact the effects of nicotine on the body, studies investigating molecular mechanisms altered by nicotine can be easily translated to other exposures. The implications of adverse cardiovascular responses thus extend clinically to the many nicotine delivery products that exist such as cigarettes, e-cigarettes, and nicotine replacement therapy.

In a case–control study examining the role of nicotine on fibrosis, atrial tissue slices from patients (both smokers and nonsmokers) undergoing elective coronary artery bypass grafting were studied for fibrosis [119]. In this analysis, the authors found that pack years, a unit of measurement in cigarette smoke research to identify tobacco exposure, was the only parameter associated with the magnitude of fibrosis [119]. Furthermore, the authors exposed cultured atrial tissue to increasing doses of nicotine and found an increase in collagen III mRNA expression [119]. Fibrosis changes the composition of atrial tissue and subsequently alters cardiomyocyte electrophysiology, leading to atrial arrhythmias like AF [120]. To find a molecular pathway for nicotine-induced fibrosis, researchers analyzed canine atrial fibroblasts incubated with nicotine for 24 hours. These fibroblasts demonstrated an increase in collagen production and upregulation of TGF-β1 and TGF-βRII via downregulation of miR133 and miR590 [121]. The resulting response is an increase in CTGF signaling, a known fibrotic mechanism [121]. In addition to induced cardiac remodeling, nicotine has been shown to directly interact with potassium ion channels. In a study assessing the pharmacologic effects of nicotine on A-type K^+ channels in dog ventricular cardiomyocytes, it was discovered that nicotine is a potent blocker of the outward K_V4 current [122]. This interaction delays cardiomyocyte repolarization by inhibiting the outward flow of potassium and may contribute to arrhythmogenesis. Nicotine has also been shown to alter sodium current expression in rabbits following in utero exposure. Using a device to continually deliver nicotine subcutaneously, similar to nicotine replacement therapy, researchers found an increase in the I_{Na} amplitude of offspring due to upregulated $Na_V1.5$ [123]. Continuing to understand the role of in utero nicotine exposure and its impact on sodium currents, the same group investigated sodium channel response following isoproterenol stimulation, an agonist of β-adrenergic receptors. They found that isoproterenol did not affect I_{Na}, suggesting myocyte dysfunction in response to sympathetic activity [124]. This data, paired with alterations in potassium ion flow, shows the potential for nicotine to induce arrhythmogenesis via directly impairing the electrical signaling in the heart. Pharmacological analysis must be further investigated for additional ion channels affected by nicotine to understand changes in cardiac electrical currents. Additionally, since many new nicotine products have entered the market in recent years (e-cigarettes and nicotine replacement therapy), it is imperative to understand the variety of adverse alterations that nicotine may induce on the cardiovascular system.

25.6 Conclusion

Mounting evidence suggests that global cardiac fibrosis, a preclinical factor associated with arrhythmogenesis, is induced through adverse epigenetic alterations. Analyses of changes in several epigenetic pathways (DNMTs, HDACs, and miRNAs) provide a framework for potential areas of focus. Changes in specific targets due to these mechanisms have previously shown increased fibrosis of cardiac tissue, which creates an environment conducive to development of arrhythmias. However, the precise progression from fibrosis to arrhythmic phenotype is unknown since both cardiac fibrosis and arrhythmia may exist independently of one another.

PM, a pollutant known to be associated with CVD development and mortality, has been shown to alter the epigenome in several experimental models. Research has demonstrated that DNA methylation, particularly hypomethylation, of many genes related to oxidative stress and immune function is changed due to PM exposure. Whether these modifications are adverse or protective adaptations has yet to be discovered. Transient elevations in regional PM concentration correlate with higher incidence of ventricular arrhythmia and overall CVD events. Interestingly, sustained exposure over a long period of time leads to tachycardia. Therefore, the public health implications of PM exposure must not be ignored. Further study into the mechanisms of acute and long-term PM exposure is an important topic, especially in areas where transient changes in PM concentration are common.

Cardiac arrhythmias occur via alterations in the normal conduction sequence of a heartbeat, including tachycardia, bradycardia, or irregular/erratic patterns. Clinically, these conditions can range from life-threatening occurrences to harmless transient episodes. This variation in presentation has caused difficulties in identifying precise pathological mechanisms of arrhythmogenesis. In this chapter, we have discussed how epigenetics is a promising target for arrhythmogenesis research, and how the use of environmental triggers has contributed to our understanding of arrhythmogenesis via epigenetic mechanisms. Elucidating these precise mechanisms will provide targets for epigenetic treatments that are currently being investigated in many diseases including cancer, cardiovascular, neurological, and metabolic diseases.

References

1. Tanwar V, Katapadi A, Adelstein JM, Grimmer JA, Wold LE. Cardiac pathophysiology in response to environmental stress: a current review. Curr Opin Physiol. 2018;1:198–205.
2. Gorr MW, Falvo MJ, Wold LE. Air pollution and other environmental modulators of cardiac function. Compr Physiol. 2017;7(4):1479–95.
3. Particulate Matter (PM) Basics [Internet]. EPA. Environmental Protection Agency; [cited 2021Sep23]. Available from: https://www.epa.gov/pm-pollution/particulate-matter-pm-basics
4. Shimizu Y. 9 out of 10 people worldwide breathe polluted air, but more countries are taking action [Internet]. World Health Organization. World Health Organization; 2018 [cited 2021 Sep 23]. 2018. Available from: https://www.who.int/news-room/detail/02-05-2018-9-out-of-10-people-worldwide-breathe-polluted-air-but-more-countries-are-taking-action
5. Brook RD, Franklin B, Cascio W, Hong Y, Howard G, Lipsett M, et al. Air pollution and cardiovascular disease: a statement for healthcare professionals from the expert panel on population and prevention science of the American Heart Association. Circulation. 2004;109(21):2655–71.
6. Goswami A, Barman J, Rajput K, Lakhlani HN. Behaviour study of particulate matter and chemical composition with different combustion strategies. SAE Technical Paper Series. 2013;
7. Franklin BA, Brook R, Arden PC. Air pollution and cardiovascular disease. Curr Probl Cardiol. 2015;40 (5):207–38.
8. Tanwar V, Gorr MW, Velten M, Eichenseer CM, Long VP, Bonilla IM, et al. In utero particulate matter exposure produces heart failure, electrical remodeling, and epigenetic changes at adulthood. J Am Heart Assoc. 2017;6(4):e005796.
9. Rich DQ, Schwartz J, Mittleman MA, Link M, Luttmann-Gibson H, Catalano PJ, et al. Association of short-term ambient air pollution concentrations and ventricular arrhythmias. Am J Epidemiol. 2005;161(12):1123–32.
10. Cole-Hunter T, de Nazelle A, Donaire-Gonzalez D, Kubesch N, Carrasco-Turigas G, Matt F, et al. Estimated effects of air pollution and space-time-activity on cardiopulmonary outcomes in healthy adults: a repeated measures study. Environ Int. 2018;111:247–59.
11. Miller JG, Gillette JS, Manczak EM, Kircanski K, Gotlib IH. Fine particle air pollution and physiological reactivity to social stress in adolescence: the moderating role of anxiety and depression. Psychosom Med. 2019;81(7):641–8.
12. Billman GE. The LF/HF ratio does not accurately measure cardiac sympatho-vagal balance. Front Physiol. 2013;4:4.
13. Sovari AA. Cellular and molecular mechanisms of arrhythmia by oxidative stress. Cardiol Res Pract. 2016;2016:1–7.
14. Xie X, Wang Y, Yang Y, Xu J, Zhang Y, Tang W, et al. Long-term exposure to fine particulate matter and tachycardia and heart rate: results from 10 million reproductive-age adults in China. Environ Pollut. 2018;242:1371–8.
15. Wellenius GA. Cardiac effects of carbon monoxide and ambient particles in a rat model of myocardial infarction. Toxicol Sci. 2004;80(2):367–76.
16. Wold LE, Ying Z, Hutchinson KR, Velten M, Gorr MW, Velten C, et al. Cardiovascular remodeling in response to long-term exposure to fine particulate matter air pollution. Circulation: Heart Fail. 2012;5 (4):452–61.
17. Gurgueira SA, Lawrence J, Coull B, Murthy GG, González-Flecha B. Rapid increases in the steady-state concentration of reactive oxygen species in the lungs and heart after particulate air pollution inhalation. Environ Health Perspect. 2002;110(8):749–55.
18. Carll AP, Crespo SM, Filho MS, Zati DH, Coull BA, Diaz EA, et al. Inhaled ambient-level traffic-derived particulates decrease cardiac vagal influence and baroreflexes and increase arrhythmia in a rat model of metabolic syndrome. Part Fibre Toxicol. 2017;14 (1):16.
19. Brook RD, Rajagopalan S, Pope CA, Brook JR, Bhatnagar A, Diez-Roux AV, et al. Particulate matter air pollution and cardiovascular disease. Circulation. 2010;121(21):2331–78.
20. Ying Z, Kampfrath T, Thurston G, Farrar B, Lippmann M, Wang A, et al. Ambient particulates alter vascular function through induction of reactive

oxygen and nitrogen species. Toxicol Sci. 2009;111 (1):80–8.

21. Seaton A, Godden D, MacNee W, Donaldson K. Particulate air pollution and acute health effects. Lancet. 1995;345(8943):176–8.
22. Fragale A, Romagnoli G, Licursi V, Buoncervello M, Del Vecchio G, Giuliani C, et al. Antitumor effects of epidrug/IFNA combination driven by modulated gene signatures in both colorectal cancer and dendritic cells. Cancer Immunol Res. 2017;5(7):604–16.
23. Nebbioso A, Carafa V, Benedetti R, Altucci L. Trials with 'epigenetic' drugs: an update. Mol Oncol. 2012;6(6):657–82.
24. Miranda Furtado CL, Dos Santos Luciano MC, Silva Santos RD, Furtado GP, Moraes MO, Pessoa C. Epidrugs: targeting epigenetic marks in cancer treatment. Epigenetics. 2019;14(12):1164–76.
25. Chen T. Mechanistic and functional links between histone methylation and DNA methylation. Progr Mol Biol Translat Sci. 2011;101:335–48.
26. Duygu B, Poels EM, Costa Martins PA. Genetics and epigenetics of arrhythmia and heart failure. Front Genetics. 2013;4:219.
27. Ng H-H, Adrian B. DNA methylation and chromatin modification. Curr Op Gen Develop. 1999;9(2): 158–63.
28. Moore LD, Le T, Fan G. DNA methylation and its basic function. Neuropsychopharmacology. 2012;38 (1):23–38.
29. Caiafa P, Zampieri M. DNA methylation and chromatin structure: the puzzling CPG Islands. J Cell Biochem. 2005;94(2):257–65.
30. Eisenberg E, Levanon EY. Human housekeeping genes, revisited. Trends Genet. 2013;29(10):569–74.
31. Foy J-P, Pickering CR, Papadimitrakopoulou VA, Jelinek J, Lin SH, William WN, et al. New DNA methylation markers and global DNA hypomethylation are associated with oral cancer development. Cancer Prevent Res. 2015;8(11): 1027–35.
32. Nakao M. Epigenetics: interaction of DNA methylation and chromatin. Gene. 2001;278(1–2):25–31.
33. Phillips T. The role of methylation in gene expression [Internet]. Nature news. Nature Publishing Group; [cited 2021Sep23]. Available from: https://www.nature.com/scitable/topicpage/the-role-of-methylation-in-gene-expression-1070/
34. Jin B, Robertson KD. DNA methyltransferases, DNA damage repair, and cancer. Exp Med Biol. 2013;754: 3–29.
35. Carey N, Marques CJ, Reik W. DNA demethylases: a new epigenetic frontier in drug discovery. Drug Disc Today. 2011;16(15–16):683–90.
36. Alberts B, Johnson A, Lewis J, Morgan D, Raff MC, Roberts K, et al. Chromosomal DNA and its packaging in the chromatin fiber. In: Molecular biology of the cell. 4th ed. New York, NY: Garland Science; 2002.
37. Narlikar GJ, Sundaramoorthy R, Owen-Hughes T. Mechanisms and functions of ATP-dependent chromatin-remodeling enzymes. Cell. 2013;154(3): 490–503.
38. McGinty RK, Tan S. Nucleosome structure and function. Chem Rev. 2014;115(6):2255–73.
39. Dong J, Gao Z, Liu S, Li G, Yang Z, Huang H, et al. Slide, the protein interacting domain of imitation switch remodelers, binds DDT-domain proteins of different subfamilies in chromatin remodeling complexes. J Integ Plant Biol. 2013;55(10):928–37.
40. Aydin ÖZ, Vermeulen W, Lans H. ISWI chromatin remodeling complexes in the DNA damage response. Cell Cycle. 2014;13(19):3016–25.
41. Luijsterburg MS, van Attikum H. Chromatin and the DNA damage response: the cancer connection. Mol Oncol. 2011;5(4):349–67.
42. Zhang P, Torres K, Liu X, Liu C-gong E, Pollock R. An overview of chromatin-regulating proteins in cells. Curr Prot Pept Sci. 2016;17(5):401–10.
43. Wang Y, Miao X, Liu Y, Li F, Liu Q, Sun J, et al. Dysregulation of histone acetyltransferases and deacetylases in cardiovascular diseases. Oxidative Med Cell Longev. 2014;2014:1.
44. Fry CJ, Peterson CL. Chromatin remodeling enzymes: Who's on first? Curr Bio. 2001;11(5): R185–97.
45. Eberharter A, Becker PB. Histone acetylation: a switch between repressive and permissive chromatin. EMBO Rep. 2002;3(3):224–9.
46. Greer EL, Shi Y. Histone methylation: a dynamic mark in health, disease and inheritance. Nature Rev Genet. 2012;13(5):343–57.
47. Santos-Rosa H, Schneider R, Bannister AJ, Sherriff J, Bernstein BE, Emre NC, et al. Active genes are tri-methylated at K4 of histone H3. Nature. 2002;419(6905):407–11.
48. Kaneda R, Takada S, Yamashita Y, Choi YL, Nonaka-Sarukawa M, Soda M, et al. Genome-wide histone methylation profile for heart failure. Genes Cells. 2009;14(1):69–77.
49. Diamantopoulos MA, Tsiakanikas P, Scorilas A. Non-coding RNAs: the riddle of the transcriptome and their perspectives in cancer. Ann Transl Med. 2018;6(12):241.
50. Hombach S, Kretz M. Non-coding RNAs: classification, biology and functioning. Adv Exp Med Biol. 2016;937:3–17.
51. Peng Y, Croce CM. The role of microRNAs in human cancer. Signal Transduct Target Ther. 2016;1:15004.
52. Calin GA, Dumitru CD, Shimizu M, Bichi R, Zupo S, Noch E, et al. Frequent deletions and down-regulation of micro- RNA genes miR15 and miR16 at 13q14 in chronic lymphocytic leukemia. Proc Natl Acad Sci U S A. 2002;99(24):15524–9.
53. Klein U, Lia M, Crespo M, Siegel R, Shen Q, Mo T, et al. The DLEU2/miR-15a/16-1 cluster controls B cell proliferation and its deletion leads to chronic

lymphocytic leukemia. Cancer Cell. 2010;17(1):28–40.

54. Lee Y, Ahn C, Han J, Choi H, Kim J, Yim J, et al. The nuclear RNase III Drosha initiates microrna processing. Nature. 2003;425(6956):415–9.
55. Meltzer PS. Small RNAs with big impacts. Nature. 2005;435(7043):745–6.
56. Bianchi M, Renzini A, Adamo S, Moresi V. Coordinated actions of microRNAs with other epigenetic factors regulate skeletal muscle development and adaptation. Internat J Mol Sc. 2017;18(4):840.
57. Ferguson LR. RNA silencing: mechanism, biology and responses to environmental stress. Mutation Res. 2011;714(1–2):93–4.
58. Zhi H, Ning S, Li X, Li Y, Wu W, Li X. A novel reannotation strategy for dissecting DNA methylation patterns of human long intergenic non-coding RNAs in cancers. Nucleic Acids Res. 2014;42(13):8258–70.
59. Fox CS, Parise H, D'Agostino RB, Lloyd-Jones DM, Vasan RS, Wang TJ, et al. Parental atrial fibrillation as a risk factor for atrial fibrillation in offspring. J Am Med Assoc. 2004;291(23):2851–5.
60. Ellinor PT, Shin JT, Moore RK, Yoerger DM, MacRae CA. Locus for atrial fibrillation maps to chromosome 6q14–16. Circulation. 2003;107(23):2880–3.
61. Wakili R, Voigt N, Kääb S, Dobrev D, Nattel S. Recent advances in the molecular pathophysiology of atrial fibrillation. J Clin Invest. 2011;121(8):2955–68.
62. Nattel S, Harada M. Atrial remodeling and atrial fibrillation. J Am Coll Cardiol. 2014;63(22):2335–45.
63. Tao H, Yang J-J, Shi K-H, Deng Z-Y, Li J. DNA methylation in cardiac fibrosis: new advances and perspectives. Toxicology. 2014;323:125–9.
64. Ma B, Wilker EH, Willis-Owen SA, Byun H-M, Wong KC, Motta V, et al. Predicting DNA methylation level across human tissues. Nucleic Acids Res. 2014;42(6):3515–28.
65. Kao Y-H, Chen Y-C, Chung C-C, Lien G-S, Chen S-A, Kuo C-C, et al. Heart failure and angiotensin II modulate atrial Pitx2c promotor methylation. Clin Exp Pharmacol Physiol. 2013;40(6):379–84.
66. Zhong H, Kim S, Zhi D, Cui X. Predicting gene expression using DNA methylation in three human populations. PeerJ. 2019;7:e6757.
67. Kao Y-H, Chen Y-C, Cheng C-C, Lee T-I, Chen Y-J, Chen S-A. Tumor necrosis factor-α decreases sarcoplasmic reticulum Ca2+-ATPase expressions via the promoter methylation in cardiomyocytes. Crit Care Med. 2010;38(1):217–22.
68. Frank KF, Bölck B, Brixius K, Kranias EG, Schwinger RH. Modulation of SERCA: implications for the failing human heart. Basic Res Cardiol. 2002;97(Suppl 1):I72-8.
69. Tao H, Yang J-J, Chen Z-W, Xu S-S, Zhou X, Zhan H-Y, et al. DNMT3A silencing RASSF1A promotes cardiac fibrosis through upregulation of ERK1/2. Toxicology. 2014;323:42–50.
70. Kirchhof P, Kahr PC, Kaese S, Piccini I, Vokshi I, Scheld H-H, et al. PITX2C is expressed in the adult left atrium, and reducing Pitx2c expression promotes atrial fibrillation inducibility and complex changes in gene expression. Circulation: Cardiovasc Genet. 2011;4(2):123–33.
71. Fatima N, Schooley JF, Claycomb WC, Flagg TP. Promoter DNA methylation regulates murine SUR1 (ABCC8) and SUR2 (ABCC9) expression in HL-1 cardiomyocytes. PLoS One. 2012;7:e41533.
72. Monteforte N, Napolitano C, Priori SG. Genetics and arrhythmias: diagnostic and prognostic applications. Revist Españ Cardiol (English Edition). 2012;65(3):278–86.
73. Montgomery RL, Davis CA, Potthoff MJ, Haberland M, Fielitz J, Qi X, et al. Histone deacetylases 1 and 2 redundantly regulate cardiac morphogenesis, growth, and contractility. Genes Dev. 2007;21(14):1790–802.
74. Terentyev D, Belevych AE, Terentyeva R, Martin MM, Malana GE, Kuhn DE, et al. miR-1 overexpression enhances Ca2+ release and promotes cardiac arrhythmogenesis by targeting PP2A regulatory subunit B56alpha and causing CaMKII-dependent hyperphosphorylation of RyR2. Circ Res. 2009;104(4):514–21.
75. Lkhagva B, Chang S-L, Chen Y-C, Kao Y-H, Lin Y-K, Chiu CT-H, et al. Histone deacetylase inhibition reduces pulmonary vein arrhythmogenesis through calcium regulation. Internat. J Cardiol. 2014;177(3):982–9.
76. Zhang D, Wu C-T, Qi XY, Meijering RAM, Hoogstra-Berends F, Tadevosyan A, et al. Activation of histone deacetylase-6 induces contractile dysfunction through derailment of α-tubulin proteostasis in experimental and human atrial fibrillation. Circulation. 2014;129(3):346–58.
77. Nural-Guvener HF, Zakharova L, Nimlos J, Popovic S, Mastroeni D, Gaballa MA. HDAC class I inhibitor, Mocetinostat, reverses cardiac fibrosis in heart failure and diminishes CD90+ cardiac myofibroblast activation. Fibrogenesis Tissue Repair. 2014;7:10.
78. Kee HJ, Bae EH, Park S, Lee KE, Suh SH, Kim SW, et al. HDAC inhibition suppresses cardiac hypertrophy and fibrosis in DOCA-salt hypertensive rats via regulation of HDAC6/HDAC8 enzyme activity. Kidney Blood Press Res. 2013;37(4–5):229–39.
79. Kook H, Lepore JJ, Gitler AD, Lu MM, Wing-Man Yung W, Mackay J, et al. Cardiac hypertrophy and histone deacetylase–dependent transcriptional repression mediated by the atypical homeodomain protein Hop. J Clin Invest. 2003;112(6):863–71.
80. Iyer A, Chan V, Brown L. The DOCA-salt hypertensive rat as a model of cardiovascular oxidative and inflammatory stress. Curr Cardiol Rev. 2010;6(4):291–7.

81. van den Berg NW, Kawasaki M, Berger WR, Neefs J, Meulendijks E, Tijsen AJ, et al. MicroRNAs in atrial fibrillation: from expression signatures to functional implications. Cardiovasc Drugs Ther. 2017;31(3): 345–65.
82. Jayawardena TM, Finch EA, Zhang L, Zhang H, Hodgkinson CP, Pratt RE, et al. MicroRNA induced cardiac reprogramming in vivo evidence for mature cardiac myocytes and improved cardiac function. Circ Res. 2015;116(3):418–24.
83. Nattel S. Molecular and cellular mechanisms of atrial fibrosis in atrial fibrillation. JACC: Clin Electrophysiol. 2017;3(5):425–35.
84. Luo X, Pan Z, Shan H, Xiao J, Sun X, Wang N, et al. MicroRNA-26 governs profibrillatory inward-rectifier potassium current changes in atrial fibrillation. J Clin Invest. 2013;123(5):1939–51.
85. Qi X-Y, Huang H, Ordog B, Luo X, Naud P, Sun Y, et al. Fibroblast inward-rectifier potassium current upregulation in profibrillatory atrial remodeling. Circ Res. 2015;116(5):836–45.
86. Duisters RF, Tijsen AJ, Schroen B, Leenders JJ, Lentink V, van der Made I, et al. miR-133 and miR-30 regulate connective tissue growth factor: implications for a role of microRNAs in myocardial matrix remodeling. Circ Res. 2009;104(2):170–8.
87. Zhang X, Jing W. Upregulation of miR-122 is associated with cardiomyocyte apoptosis in atrial fibrillation. Mol Med Rep. 2018;18(2):1745–51.
88. Baccarelli A, Wright RO, Bollati V, Tarantini L, Litonjua AA, Suh HH, et al. Rapid DNA methylation changes after exposure to traffic particles. Am J Resp Crit Care Med. 2009;179(7):572–8.
89. Madrigano J, Baccarelli A, Mittleman MA, Wright RO, Sparrow D, Vokonas PS, et al. Prolonged exposure to particulate pollution, genes associated with glutathione pathways, and DNA methylation in a cohort of older men. Environ Health Perspect. 2011;119(7):977–82.
90. Bind M-A, Baccarelli A, Zanobetti A, Tarantini L, Suh H, Vokonas P, et al. Air pollution and markers of coagulation, inflammation, and endothelial function. Epidemiology. 2012;23(2):332–40.
91. Rusiecki JA, Baccarelli A, Bollati V, Tarantini L, Moore LE, Bonefeld-Jorgensen EC. Global DNA hypomethylation is associated with high serum-persistent organic pollutants in Greenlandic inuit. Environ Health Perspect. 2008;116(11):1547–52.
92. Salam MT, Byun H-M, Lurmann F, Breton CV, Wang X, Eckel SP, et al. Genetic and epigenetic variations in inducible nitric oxide synthase promoter, particulate pollution, and exhaled nitric oxide levels in children. J Aller Clin Immunol. 2012;129 (1):232.
93. Tarantini L, Bonzini M, Apostoli P, Pegoraro V, Bollati V, Marinelli B, et al. Effects of particulate matter on genomic DNA methylation content and inos promoter methylation. Environ Health Perspect. 2009;117(2):217–22.
94. Breton CV, Salam MT, Wang X, Byun H-M, Siegmund KD, Gilliland FD. Particulate matter, DNA methylation in nitric oxide synthase, and childhood respiratory disease. Environ Health Perspect. 2012;120(9):1320–6.
95. Nadeau K, McDonald-Hyman C, Noth EM, Pratt B, Hammond SK, Balmes J, et al. Ambient air pollution impairs regulatory T-cell function in asthma. J Aller Clin Immunol. 2010;126(4):845.
96. Bellavia A, Urch B, Speck M, Brook RD, Scott JA, Albetti B, et al. DNA hypomethylation, ambient particulate matter, and increased blood pressure: findings from controlled human exposure experiments. J Am Heart Assoc. 2013;2(3):e000212.
97. Carmona JJ, Sofer T, Hutchinson J, Cantone L, Coull B, Maity A, et al. Short-term airborne particulate matter exposure alters the epigenetic landscape of human genes associated with the mitogen-activated protein kinase network: a cross-sectional study. Environ Health. 2014;13:1.
98. Barker DJP. The fetal origins of coronary heart disease. Eur Heart J. 1997;18(6):883–4.
99. Tanwar V, Adelstein JM, Grimmer JA, Youtz DJ, Katapadi A, Sugar BP, et al. Preconception exposure to fine particulate matter leads to cardiac dysfunction in adult male offspring. J Am Heart Assoc. 2018;7 (24):e010797.
100. Yauk C, Polyzos A, Rowan-Carroll A, Somers CM, Godschalk RW, Van Schooten FJ, et al. Germ-line mutations, DNA damage, and global hypermethylation in mice exposed to particulate air pollution in an urban/industrial location. Proc Natl Acad Sci U S A. 2008;105(2):605–10.
101. Reliene R, Hlavacova A, Mahadevan B, Baird WM, Schiestl RH. Diesel exhaust particles cause increased levels of DNA deletions after transplacental exposure in mice. Mutat Res. 2005;570(2):245–52.
102. George A, Figueredo VM. Alcohol and arrhythmias: a comprehensive review. J Cardiovasc Med. 2010;11 (4):221–8.
103. Dominici F, Peng RD, Bell ML, Pham L, McDermott A, Zeger SL, et al. Fine particulate air pollution and hospital admission for cardiovascular and respiratory diseases. J Am Med Ass. 2006;295 (10):1127.
104. Benowitz NL, Gourlay SG. Cardiovascular toxicity of nicotine: implications for nicotine replacement therapy. J Am Coll Cardiol. 1997;29(7):1422–31.
105. Kerr DMI, Brooksbank KJM, Taylor RG, Pinel K, Rios FJ, Touyz RM, et al. Acute effects of electronic and tobacco cigarettes on vascular and respiratory function in healthy volunteers: a cross-over study. J Hyperten. 2019;37(1):154–66.
106. Akbarzadeh MA, Yazdani S, Ghaidari ME, Asadpour-Piranfar M, Bahrololoumi-Bafruee N, Golabchi A, et al. Acute effects of smoking on QT dispersion in healthy males. ARYA Atherosclerosis. 2014;10:89–93.

107. Alshehri AM, Azoz AM, Shaheen HA, Farrag YA, Khalifa MA, Youssef A. Acute effects of cigarette smoking on the cardiac diastolic functions. J Saudi Heart Assoc. 2013;25(3):173–9.
108. Chamberlain AM, Agarwal SK, Folsom AR, Duval S, Soliman EZ, Ambrose M, et al. Smoking and incidence of atrial fibrillation: results from the atherosclerosis risk in communities (ARIC) study. Heart Rhythm. 2011;8(8):1160–6.
109. Heeringa J, Kors JA, Hofman A, van Rooij FJA, Witteman JCM. Cigarette smoking and risk of atrial fibrillation: the Rotterdam Study. Am Heart J. 2008;156(6):1163–9.
110. Stewart S. Population prevalence, incidence, and predictors of atrial fibrillation in the Renfrew/Paisley study. Heart. 2001;86(5):516–21.
111. Zuo H, Nygård O, Vollset SE, Ueland PM, Ulvik A, Midttun Ø, et al. Smoking, plasma cotinine and risk of atrial fibrillation: the Hordaland Health Study. J Int Med. 2017;283(1):73–82.
112. Schnabel RB, Sullivan LM, Levy D, Pencina MJ, Massaro JM, D'Agostino RB, et al. Development of a risk score for atrial fibrillation (Framingham Heart Study): a community-based cohort study. Lancet. 2009;373(9665):739–45.
113. Krahn AD, Manfreda J, Tate RB, Mathewson FAL, Cuddy TE. The natural history of atrial fibrillation: incidence, risk factors, and prognosis in the Manitoba follow-up study. Am J Med. 1995;98(5):476–84.
114. Gupta P, Patel C, Patel H, Narayanaswamy S, Malhotra B, Green JT, et al. TP-E/Qt ratio as an index of arrhythmogenesis. J Electrocardiol. 2008;41(6):567–74.
115. İlgenli T, Tokatlı A, Akpınar O, Kılıçaslan F. The effects of cigarette smoking on the TP-e interval, TP-E/qt ratio and TP-E/QTC ratio. Adv Clin Exp Med. 2015;24(6):973–8.
116. Taşolar H, Ballı M, Bayramoğlu A, Otlu YÖ, Çetin M, Altun B, et al. Effect of smoking on TP-e interval, TP-e/QT and TP-e/qtc ratios as indices of ventricular arrhythmogenesis. Heart Lung Circ. 2014;23(9):827–32.
117. Felber Dietrich D, Schwartz J, Schindler C, Gaspoz J-M, Barthelemy J-C, Tschopp J-M, et al. Effects of passive smoking on heart rate variability, heart rate and blood pressure: an observational study. International J Epidemiol. 2007;36(4):834–40.
118. Pope CA, Eatough DJ, Gold DR, Pang Y, Nielsen KR, Nath P, et al. Acute exposure to environmental tobacco smoke and heart rate variability. Environ Health Perspect. 2001;109(7):711–6.
119. Goette A, Lendeckel U, Kuchenbecker A, Bukowska A, Peters B, Klein HU, et al. Cigarette smoking induces atrial fibrosis in humans via nicotine. Heart. 2007;93(9):1056–63.
120. Burstein B, Nattel S. Atrial fibrosis: mechanisms and clinical relevance in atrial fibrillation. J Am Coll Cardiol. 2008;51(8):802–9.
121. Shan H, Zhang Y, Lu Y, Zhang Y, Pan Z, Cai B, et al. Downregulation of miR-133 and miR-590 contributes to nicotine-induced atrial remodelling in canines. Cardiovasc Res. 2009;83(3):465–72.
122. Wang H, Shi H, Zhang L, Pourrier M, Yang B, Nattel S, et al. Nicotine is a potent blocker of the cardiac A-type K+ channels. Circulation. 2000;102 (10):1165–71.
123. Ton AT, Biet M, Delabre J-F, Morin N, Dumaine R. In-utero exposure to nicotine alters the development of the rabbit cardiac conduction system and provides a potential mechanism for sudden infant death syndrome. Arch Toxicol. 2017;91(12): 3947–60.
124. Biet M, Ton AT, Delabre J-F, Morin N, Dumaine R. In utero exposure to nicotine abolishes the postnatal response of the cardiac sodium current to isoproterenol in newborn rabbit atrium. Heart Rhythm. 2019;16(4):494–501.

Part V

Mechanisms of Inherited Arrhythmia

The Short QT Syndrome

26

Jules C. Hancox, Mark J. McPate, Aziza El Harchi,
Andrew S. Butler, Yihong Zhang, Dominic G. Whittaker,
Christopher E. Dempsey, Harry J. Witchel, Ismail Adeniran,
Alan G. Stuart, and Henggui Zhang

Abstract

The short QT syndrome (SQTS) is characterised by abbreviated QT intervals on the electrocardiogram and by an increased risk of atrial and ventricular arrhythmias and of sudden death. Gain-of-function mutations to three potassium channel genes: *KCNH2, KCNQ1* and *KCNJ2* are responsible for distinct forms of SQTS (SQT1, SQT2 and SQT3, respectively), whilst loss-of-function mutations to the L-type calcium channel genes *CACNB2b*, *CACNA1C* and *CACNA2D1* give rise to abbreviated QT intervals accompanied by ST-segment elevation and a combined short QT-Brugada phenotype. Mutations to *SCN5A, SCN10A, SLC4A3* and *SLC22A5* have also been associated with abbreviated QT intervals. Shortened effective refractory periods and altered transmural dispersion of repolarisation are implicated in increased ventricular arrhythmia risk. Current treatment focuses on implantable defibrillators to protect against fatal ventricular arrhythmia. There is also evidence that Class 1a antiarrhythmic drugs may be beneficial in restoring QT intervals towards normal and decreasing arrhythmia risk.

Keywords

Brugada syndrome · Transmural dispersion of repolarisation · Gain of function mutations · Potassium channels · Carnitine deficiency · Class 1a antiarrhythmics

---

J. C. Hancox (✉)
School of Physiology, Pharmacology and Neuroscience, School of Biomedical Sciences, University Walk, Bristol, UK

Biological Physics Group, School of Physics and Astronomy, University of Manchester, Manchester, UK
e-mail: jules.hancox@bristol.ac.uk

M. J. McPate · A. El Harchi · A. S. Butler · Y. Zhang
School of Physiology, Pharmacology and Neuroscience, School of Biomedical Sciences, University Walk, Bristol, UK

D. G. Whittaker
Biological Physics Group, School of Physics and Astronomy, University of Manchester, Manchester, UK

School of Mathematical Sciences, University of Nottingham, Mathematical Sciences Building, University Park, Nottingham, UK

C. E. Dempsey
School of Biochemistry, School of Biomedical Sciences, University Walk, Bristol, UK

H. J. Witchel
Medical Research Building, Brighton and Sussex Medical School, University of Sussex, Brighton, UK

I. Adeniran · H. Zhang
Biological Physics Group, School of Physics and Astronomy, University of Manchester, Manchester, UK

A. G. Stuart
National Institute for Health Research (NIHR), Cardiovascular Biomedical Research Centre, Congenital Heart Unit, Bristol Heart Institute, Bristol, UK

© Springer Nature Switzerland AG 2023
O. N. Tripathi et al. (eds.), *Heart Rate and Rhythm*, https://doi.org/10.1007/978-3-031-33588-4_26

26.1 Introduction: The Genetic Short QT Syndrome as a Distinct Clinical Entity

The relationship between abnormally long QT intervals and increased arrhythmia risk is well-established. Rate corrected QT (QT_c) intervals of >440–460 ms (in males and females respectively) are considered to be prolonged, with values of 500 ms or greater being specifically associated with arrhythmias, in particular the polymorphic ventricular tachycardia *torsades de pointes* [1]. Pathological QT_c interval prolongation (the ‘long QT syndrome’; LQTS) can be due to genetic ‘channelopathies’ or be ‘acquired’ as a result of ion channel remodelling in a disease state such as heart failure, or caused by ion channel blocking effects of clinically used cardiac and non-cardiac drugs.

A number of factors unrelated to ion channel gene mutations can lead to QT interval shortening; these include catecholamines, acetylcholine, hypercalcemia, and hyperthermia [2]. Anabolic steroid use is also associated with shortened QT intervals [3–5] to the extent that it has been suggested that QT_c interval shortening may be a reliable marker of steroid abuse in bodybuilders and strength-athletes [5, 6]. QT interval shortening can be seen on patient ECGs following digitalis administration [7–9]. Cardiac glycosides shorten ventricular repolarisation, at least in part because the combined rise in intracellular Na^+ and Ca^{2+} following glycoside exposure can promote outward Na^+-Ca^{2+} exchange current during the action potential (AP) plateau [10]; they can also lead to augmented K^+ conductance [11]. Although glycoside-related arrhythmogenesis is strongly associated with after-depolarisations linked to sodium/calcium overload [12], ventricular refractory period shortening has also been reported [13], which could predispose to re-entrant arrhythmia and, thereby, influence ventricular arrhythmia risk [2].

By comparison with the LQTS, short QT syndrome (SQTS) as a *genetic* cardiac channelopathy is a comparatively young clinical entity. The SQTS is typically characterised by abnormally short QT intervals on the electrocardiogram, together with changes to T-wave morphology (tall, peaked T waves), poor rate adaptation of the QT interval and an increased risk of atrial and ventricular arrhythmias and of sudden death [14–18]. The first published description of SQTS with a familial link as a distinct clinical syndrome was by Gussak and colleagues in 2000 [19]. Three members of the same family had QT intervals of <300 ms over the resting heart rate range, the youngest of whom presented with episodes of syncope and paroxysmal atrial fibrillation (AF), whilst similar ECG changes were noted for an unrelated individual who suffered sudden death [19]. A distinction was made between the idiopathic form of SQT, in which QT interval shortening was independent of heart rate, and a deceleration-dependent form likely to result from excessive vagal stimulation [19–21]. Since that initial study, pathological QT interval shortening associated with increased arrhythmia risk has been linked to mutations in a number of cardiac ion channel and transporter genes (reviewed in [22, 23]). It is notable that short QT intervals appear to be rare in the general population, with a prevalence of QT_c intervals of <320 ms of ~0.1% [24, 25]. In a paediatric cohort, the reported prevalence was 0.05% and although the median QT interval was observed to be shorter in females, there was a male preponderance in those with a QTc interval < 340 ms [26]. However, congenital SQTS has high lethality with cardiac arrest often the first manifestation of the condition [27]. Diagnostic criteria for congenital SQTS have been proposed that combine patient and family history together with clinical electrophysiology measurements (rate corrected QT interval and J_{point} to T_{peak}) [28].

The European Society of Cardiology (ESC) has proposed that a positive diagnosis of SQTS can be made with a QT_c interval of ≤340 ms [29], or with a longer QT_c interval of ≤360 ms, if there is evidence also of one or more of: a familial history of SQTS; a confirmed pathogenic mutation; a family history of sudden death below 40 years of age; survival from ventricular tachycardia (VT) or fibrillation (VF) in the absence of structural heart disease [29]. The ability to make a positive diagnosis based on clinical phenotype is important, because the yield of successful gene culprits from genotyping suspected SQTS cases is low (less than 25–30%) [22, 28]. As discussed elsewhere [23], "spot" ECG measurements may be insufficient to diagnose SQTS, because surface ECG abnormalities may be intermittent [30, 31]; thus, 24 hour Holter monitoring or repeated ECGs during hospitalization may be preferable [30, 31]. It has also been shown that the rate correction formula used may influence the derived QT_c value and so clinical QT interval measurements at a low/resting rate are likely to be of particular value [32]. Indeed, the poor rate adaptation of the QT interval in genetic forms of SQTS means that abbreviated QT intervals of SQTS patients are likely more readily to be detected at lower than at faster heart rates [33, 34].

The principal aim of this chapter is to provide an overview of the evidence that links specific gene mutations to altered ion channel and transporter function that leads to accelerated repolarisation and, thereby, the SQTS. Mechanisms of arrhythmogenesis and treatment will also be considered.

26.2 SQT1 and KCNH2

KCNH2 (also known as "*hERG*" – *human Ether-à-go-go Related Gene* [35]) mediates the α-subunit of the rapid delayed rectifier K+ current, I_{Kr} channel [36, 37], which plays a critical role in ventricular AP repolarisation (Fig. 26.1) and setting the QT interval of the electrocardiogram [38–41]. Loss-of-function mutations of I_{Kr} are responsible for the LQT2 form of the long QT syndrome, whilst unique structural features of the *KCNH2*-encoded subunit render the channel uniquely susceptible to pharmacological blockade, underlying the acquired form of the LQTS [38–42]. These aspects of hERG channel function are covered in detail in Chap. 11 of this volume.

hERG mutations were first identified as a genetic cause for SQTS through candidate gene screening of three families, two of which had affected members who exhibited *hERG* mutations [43]. Members of both families exhibited QT_C intervals of <300 ms, episodes of both atrial and ventricular arrhythmias and there were incidences of sudden death in patients without cardiac structural abnormalities [43]. One family showed cases of severe arrhythmia and sudden death in the first year of life [43]. On genetic screening, members of the two families exhibited distinct mutations at the same nucleotide position (1764) of *KCNH2*. Thus, in one family there was a C→ G substitution and in the second there was a C→ A substitution; however, these led to a common amino-acid substitution in the *KCNH2* product, the 'hERG' K^+ channel (Kv11.1), with an asparagine → lysine switch at residue 588 (N588K) [43]. A subsequent independent study identified another family with the C1764G nucleotide and N588K amino-acid substitution [44]. Affected individuals exhibited short QT intervals (between 225 and 240 ms over the normal heart rate range), paroxysmal AF, short atrial and ventricular refractory periods and AF and ventricular fibrillation (VF) that was inducible on programmed electrical stimulation [44].

One feature of hERG current (I_{hERG}) /I_{Kr} kinetics that is of key importance to the channel's contribution to ventricular repolarisation is the presence of fast, voltage-dependent inactivation that limits current flow at positive voltages and leads to an area of negative slope in the current–voltage (I-V) relation [36, 37, 45, 46]; this normally limits the channel's contribution to repolarisation immediately after the peak of the AP (see Figure 26.1 and [46–49]). Conformational changes at the outer mouth of the channel underlie this rapid inactivation [40, 41, 45, 50]. The N588 residue identified in SQT1 patients resides in the S5-Pore (S5-P) linker region of the channel, and this region has also been implicated in hERG's rapid inactivation process (*e.g* [51–53]). In the original study identifying the basis of SQT1, N588K-hERG was expressed both with and without the putative hERG accessory subunit KCNE2 (MiRP1; [54]) and, when compared with WT hERG at ambient temperature, N588K-hERG appeared not to rectify at positive voltages [43]. Measurements of I_{hERG} using the 'AP clamp' technique showed that this mutation led

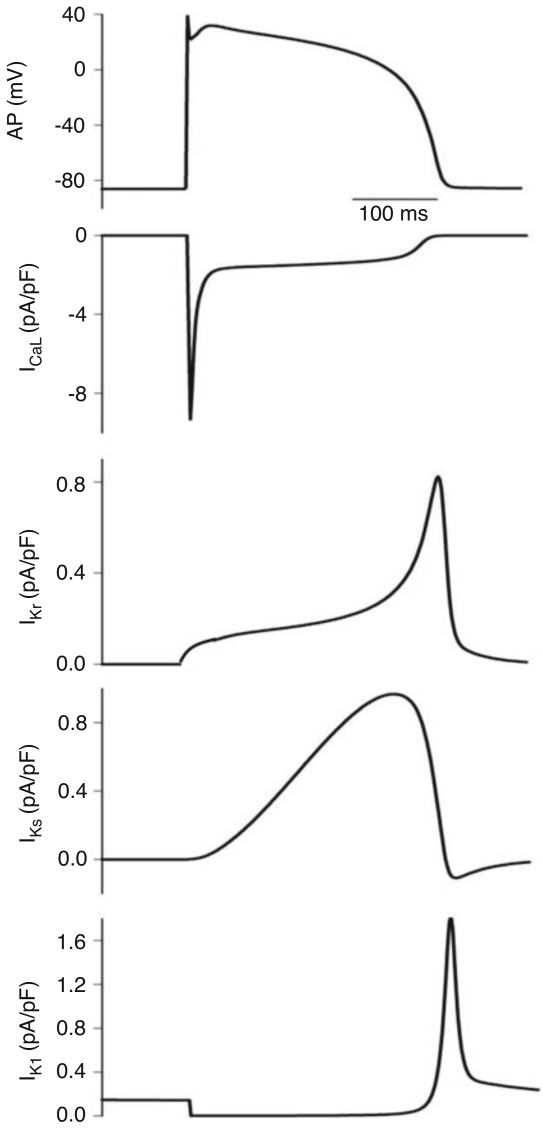

Fig. 26.1 Schematic diagram showing the normal profiles during the ventricular AP of repolarising and depolarising currents that have been implicated in SQTS variants 1–6. The depolarising current shown is L-type Ca current ($I_{Ca,L}$), whilst in terms of repolarising currents both rapid and slow sub-types of delayed rectifier K^+ current (I_{Kr} and I_{Ks}, respectively) and the inwardly rectifying K^+ current I_{K1} are shown. *CACNA1C and CACNB2b* encode $I_{Ca,L}$ subunits, whilst *KCNH2* and *KCNQ1*, respectively, encode I_{Kr} and I_{Ks} pore-forming subunits

to increased current early during the ventricular AP plateau. Collectively, the cellular electrophysiological data from this study led to the suggestion that the N588K mutation results in a loss of hERG channel inactivation [43]. Subsequent detailed kinetic studies conducted at both ambient [55] and physiological [56] temperatures showed that inactivation of I_{hERG} was in fact not eliminated by the N588K mutation, but rather was positive shifted (by ~ + 60 to +90 mV); this was accompanied by a modest increase in the Na^+/K^+ permeability ratio [55, 56]. These alterations to function occur both when the major hERG ‘1a’ isoform is studied alone [55, 56] and when hERG 1a is co-expressed together with the shorter hERG 1b isoform [57] (heteromeric hERG 1a/1b has recently been proposed to recapitulate native I_{Kr} more closely than hERG 1a alone [58–60]). Interestingly, although hERG 1a and 1b differ only in that the latter has a truncated N-terminus, and this might not be anticipated to influence the effect on channel function of a mutation in the S5-Pore linker, in our hands the inactivation-attenuating effect of the N588K mutation actually appeared to be greater for hERG 1a/1b heteromeric channels than for hERG 1a alone [57]. AP clamp measurements at 37 °C showed augmented I_{hERG} during both atrial and ventricular AP waveforms, with peak repolarising current occurring earlier during the AP [61]. This is consistent with SQT1 leading to abbreviation of atrial as well as ventricular repolarisation, and with reports of shortened atrial effective refractory period (ERP) and incidence of AF in SQT1 patients [43, 44]. It is noteworthy that a second hERG mutation, S631A located in the channel pore, which produces a similar attenuated inactivation phenotype to that produced by N588K [50, 62], has been associated with SQTS and arrhythmogenic syncope [63]. The S631A mutation produces comparable effects on hERG during ventricular repolarisation to those reported for N588K [48, 64]. The N588K hERG mutation is the second most commonly identified mutation (18.5%) in successfully genotyped SQTS [65].

The most commonly occurring clinical SQTS variant thus far identified is the T618I hERG mutation, which residue lies in the pore loop of the hERG channel; it accounts for 25.9% of genotyped probands [65]. It was first reported in members of a Chinese family with a mean QT_c interval of <320 ms and a history of sudden death [66]. Electrophysiological investigation showed abbreviated ERP and provocation of ventricular arrhythmia with programmed electrical stimulation [66]. This mutation has now been reported in unrelated families from different geographical regions (Europe, USA, Canada, China, and Japan) [65], with a mean QT_c interval for probands and other carriers of 313 ms, poor rate adaptation of the QT_c interval, tall peaked T-waves, no gender preference in terms of carriers and 100% penetrance. T618I carriers resemble those with the N588K mutation in that they are susceptible to ventricular arrhythmia; however, in contrast to the situation for N588K hERG, no reported T618I probands or carriers have experienced AF (cf 60% probands for N588K hERG) [65]. The basis for this difference is not clear. In vitro electrophysiological analyses have reported positively shifted I_{hERG} inactivation with the T618I mutation, albeit to a more modest extent than seen for the N588K or S631A mutations [66, 67]. However, not all studies of T618I have reported an inactivation voltage shift and a negative shift in voltage-dependent activation and faster activation time course have also been suggested [65]. Differences in experimental conditions between studies may have contributed to these different observations [22].

Additional *KCNH2* mutations have also been implicated in QT interval shortening. The S5 domain I560T mutation was found in a 64 year old man with paroxysmal AF and atrial flutter was diagnosed with SQTS (QT_c interval of 319 ms and peaked T waves on the precordial leads) and a family history of sudden death [68]. In vitro analysis has shown that this mutation produces a moderate attenuation of I_{hERG} inactivation with acceleration of activation and slowing of deactivation at some membrane potentials [68, 69]. A *KCNH2* mutation to the N terminus of the hERG protein was identified in a young male who had experienced syncope whilst driving [30]. His minimal QT_c interval was 366 ms and his QT interval showed poor rate adaptation during exercise-testing [30]. Genetic screening identified an N-terminal glutamate to aspartate mutation (D50E) in hERG [30]. An arginine → histidine mutation (R1135H) was identified in a 34-year-old male with a QT_C interval of 329 ms and Brugada-type features on his ECG [70]. His brother had a non-documented arrhythmia and moderately shortened QT interval (QT_c of 377 ms), whilst his mother had not reported episodes of arrhythmia, but had bradycardia and a QT_c interval of 379 ms. All three were heterozygous for the R1135H mutation [70]. In vitro investigation of R1135H hERG identified a slowing of I_{hERG} deactivation [70]. This is a distinct kinetic change from the inactivation modification of other hERG mutations, but has been shown in simulations to be able to lead both to shortened repolarisation and, potentially, also to Brugada-like ECG changes [71]. Interestingly, other hERG mutations (R164C and W927G) have been reported with ST segment elevation associated with moderate shortening of the QT_c interval (respectively 342 and 350 ms) [72]; this is consistent with some potential for overlap between SQTS and Brugada phenotypes [23].

Potential mechanisms of arrhythmogenesis and the treatment of SQT1 are considered in Sects. 26.10 and 26.11 of this chapter.

26.3 SQT2 and *KCNQ1*

SQT2 is associated with *KCNQ1* mutations [73, 74]. The *KCNQ1* product (also called KCNQ1 or Kv7.1; previous nomenclature KvLQT1) combines with KCNE1 (minK) to produce the cardiac I_{Ks} channel [75, 76]. I_{Ks} contributes to ventricular repolarisation over the AP plateau phase (Fig. 26.1) and constitutes an important 'repolarisation reserve' when I_{Kr} is reduced [39, 77, 78]. The importance of KCNQ1 to ventricular function is illustrated by the fact that loss-of-function KCNQ1 mutations give rise to the LQT1 form of long QT syndrome [39, 42, 77]. The SQT2 variant of SQTS was first reported for a 70-year-old male resuscitated from VF [73], with no evident abnormalities on physical examination, but with a short QT_c interval of 302 ms. Genetic analysis showed no abnormalities in *KCNH2, KCNE1* or *KCNE2*, but revealed a G→C substitution at nucleotide 919 of *KCNQ1*. This led to a single amino-acid substitution (V307L) in the pore helix of the KCNQ1 channel protein [73]. In vitro electrophysiological analysis revealed that the V307L mutation resulted in a negative-shift in the voltage-dependence of activation of recombinant 'I_{Ks}' channels incorporating mutant KCNQ1 subunits. The time course of current activation was also faster for mutant than for WT channels [73]. Incorporation of these changes to I_{Ks} into a human ventricular AP model led to AP shortening [73] and QT interval shortening [79]. Subsequent detailed modelling at cell and tissue levels indicates significant effects of the V307L mutation under both homozygotic and heterozygotic conditions on APD across the ventricular wall and to marked shortening of ventricular effective refractory period [80].

The second SQT2 KCNQ1 mutation was found in a baby girl delivered at 38 weeks following bradycardia and irregular rhythm in utero [74]. Once born, her heart rate (in the range of 60 beats per min) was markedly bradycardic for a neonate, whilst her ECG exhibited a QT interval of 280 ms, and irregular rhythm with no P or F waves [74]. Genetic analysis revealed a G→A substitution at nucleotide 421 which resulted in a valine to methionine substitution at position 141 (V141M) in the S1 domain of the KCNQ1 channel protein; the mutation was absent in the girl's parents and therefore it represented a de novo mutation in the infant [74]. When expressed with KCNE1, the V141M KCNQ1 mutation led to an instantaneous current component that was absent for WT KCNQ1 [74]. Incorporation of the changes to KCNQ1 + KCNE1 with the V141M mutation into a human ventricular cell model led to AP shortening, whilst its incorporation into a rabbit SAN cell model (which may approximate though not necessarily recapitulate precisely human pacemaking) arrested spontaneous activity [74]. Interestingly, the affected residue in this form of SQT2 lies immediately adjacent to a residue (S140) mutation to which (S140G) is implicated in one form of familial AF [81]. Subsequent work has suggested that both of these KCNQ1 mutations lead to a marked negative shift in the voltage dependence of I_{Ks} and to a profound slowing of current deactivation [82]. The R259H KCNQ1 mutation was identified in a family in which a 20 year old male had experienced an aborted cardiac arrest [83]. He had a QT_c interval of 310 ms, whilst that of his mother was 300 ms (she had experienced paroxysmal VT). In vitro analysis showed increased current magnitude, faster activation and slower deactivation of KCNQ1 + KCNE1 currents carried by channels incorporating the R259H KCNQ1 mutation [83]. The F279I mutation was found in the son of a 37-year-old male who had died suddenly. The son's QT_c interval was 356 ms (shortening to 350 ms on exercise), with prominent T waves on precordial leads V_1-V_4 [84]. In biophysical and biochemical analyses the F279I mutation produced a gain of function by impairing the interaction between KCNQ1 and KCNE and producing a negative voltage-shift in current activation and acceleration of activation kinetics [84]. It is worth noting that in a comparison of SQT2 and non-SQT2 patients, Harrell and colleagues have reported a higher incidence of sinus bradycardia and AF in SQT2 than non-SQT2 patients [68].

26.4 SQT3 and *KCNJ2*

The SQT3 variant of the SQTS was reported in 2005 for a 5-year-old child who exhibited an abnormal ECG during a routine clinical examination [79]. Although asymptomatic, her QT_c interval was 315 ms and showed a narrow and peaked T wave. Her mother's ECG did not exhibit abnormalities, but that of her father had a QT_c interval of 320 ms and he had a history of palpitations and presyncopal events [79]. On genetic analysis no mutations were found in *KCNH2* or *KCNQ1*, but both father and daughter exhibited a single base pair substitution (G514A) in *KCNJ2* [79]. This resulted in an aspartate → asparagine (D → N) amino-acid substitution at position 172 of the Kir2.1 K^+ channel protein.

Kir2.1 is a member of the family of inward rectifiers (Kir2.1, 2.2 and 2.3) responsible for the inwardly rectifying K^+ channel current I_{K1} [39]. I_{K1} contributes to maintaining the negative resting potential of atrial and ventricular myocytes and outward I_{K1} is important for the AP terminal repolarisation phase (Fig. 26.1 [39, 85, 86]. Kir2.1 is expressed in both human atrial and ventricular tissue [87]. Its importance to ventricular repolarisation is illustrated by the fact that loss-of-function Kir2.1 mutations underlie Andersen's syndrome [88, 89], whilst familial AF has been associated with the V93I gain-of-function Kir2.1 mutation [90]. The D172 residue is located in the ion conduction pathway of the channel and had previously been implicated in the binding of polyamines and Mg^{2+} ions that gives rise to the inward rectification of Kir2.1 current [91]. The D172N mutation, presumably by impairing this process, leads to an increase in outward Kir2.1 current accompanied by a modest rightward voltage-shift of peak outward current [79, 91, 92]. Co-expression of WT and D172N channels, to mimic the heterozygous state of the SQT3 proband, results in an increase in outward Kir2.1 current that is intermediate between WT and D172N Kir2.1 when expressed alone [79, 92]. Incorporation of the kinetic changes to I_{K1} predicted from the Kir2.1 D172N into a ventricular AP model led to AP shortening and steeper restitution of AP duration, whilst incorporation into a 1D tissue strand could replicate the changes to T wave morphology seen in the SQT3 proband [79]. The subsequent use of the AP clamp technique in in vitro experiments on heterozygous WT-D172N Kir2.1 channels has provided direct evidence for increased I_{K1} during the terminal repolarisation phase of ventricular APs [92] and has also shown the potential for the mutation to affect the contribution of I_{K1} to atrial repolarisation [92].

The M301K Kir2.1 mutation was identified in an 8 year old girl with a QT_c interval of 194 ms who had AF and a family history of perinatal death of her sister [93]. AF and VF were inducible during evaluation with right heart catheterization [93]. The mutation is located in the C-terminus at a highly conserved position and was absent in 400 control alleles. In cellular electrophysiological analysis, M301K did not produce functional channels on its own, but when co-expressed with wild-type channels the mutation substantially reduced Kir2.1 current rectification over a range of voltages [93]. This would increase a contribution of I_{K1} to repolarisation over a wider range of voltages than is normally the case and thereby account for a greater QT_c shortening than seen with the D172N mutation [93]. The E299V mutant was found in an 11 year old boy who had experienced AF since the age of 8 and who had a markedly abbreviated QT interval (close to 200 ms over a wide range of rates) [94]. This mutation also transpires markedly to impair rectification of Kir2.1 current and in ventricular and atrial simulations produces markedly abbreviated repolarisation [94, 95]. The K346T mutation was identified in monozygotic 9-year-old twins with a mixed SQTS (QT_c of 331 ms) and autism-epilepsy phenotype [96]. When expressed in mammalian (HEK 293) cells, the mutation exerted qualitatively similar effects on outward current to those seen earlier for the D172N mutation; it also decreased Kir2.1 protein ubiquitination and degradation, thus increasing channel protein stability [96].

26.5 SQT4–SQT6

SQT4 and SQT5 can be distinguished from the primary mutations identified for the SQT1–3 variants of SQTS in that: (i) they involve loss of functions to channel subunits of an ion channel involved in membrane potential depolarisation (L-type calcium current; see Fig. 26.1) rather than repolarisation (to *CACNA1C* for SQT4 and *CACNB2b* for SQT5); (ii) a mixed Brugada-SQT phenotype is present, which is unsurprising given that the mutations came to light from genetic screening of patients with Brugada syndrome [97]. When the clinical phenotype and underlying mutations were first published, this was in the context of presenting a novel clinical entity [97]. However, given that QT interval abbreviation was a marked feature of the ECG, it is appropriate to include some consideration of the identified genotypes in the context of the SQTS. Of 82 probands with Brugada syndrome 7 were found to have mutations in the genes responsible for the α and β_{2b} subunits of the L-type Ca^{2+} channel, 3 of whom exhibited moderately shortened QT_c intervals ($\leq$ 360 ms). One, a 2-year-old male with a QT_c interval of 330 ms and ajmaline-inducible ST segment elevation, presented with aborted sudden cardiac death (SCD) and had a brother who was also symptomatic. The other relatives (in all, a total of 6 from 10) exhibited ECG abnormalities, including tall peaked T waves. On genetic analysis, the proband exhibited a heterozygous C1442T change in *CACNB2b* that led to a serine → leucine substitution (S481L) in the β_{2b} subunit [97]. The second patient, a 41-year-old male, had a QT_c interval of 300 ms and presented with AF. His brother had died suddenly at 45. Programmed electrical stimulation was able to elicit monomorphic ventricular tachycardia. An A→G substitution (A1468G) led to a glycine → arginine substitution (G490R) in the *CACNA1C* product, that was also present in his two daughters [97]. The third patient, a 44-year-old male, had prominent ST segment elevation and a QT_c interval of 360 ms; his mother had SCD at 48 years of age, while his father had no known medical problems. He had a heterozygous C→T transition at position 116 of *CACNA1C*, leading to an alanine → valine amino-acid substitution (A39V) in the gene product [97]. Co-expression of the relevant mutant α/β subunit with its WT partner led to marked current suppression for each of the observed mutations [97]. Confocal microscopy showed that the A39V $Ca_v1.2$ mutation was associated with marked perinuclear as opposed to membrane staining, suggestive of impaired trafficking, whilst the G490R $Ca_v1.2$ and S481L $Ca_{v\beta2b}$ mutations did not appear to impair channel trafficking. A G5918C mutation to *CACNA1C*, leading to R1973P in $Ca_v1.2$ has been found in a family with early repolarisation and SQTS; this mutation produced a marked reduction in $Ca_v1.2$ current [98, 99]. Additional mutations to desmin (*DES*) and myopalladin (*MYPN*) were also detected, consistent with severe left ventricular hypertrophy in the proband and hypertrophic cardiomyopathy as well as early repolarisation/SQTS in this family [98, 99]. The R1977Q $Ca_v1.2$ mutation was identified in a patient with a QT_c of 316 ms as part of an analysis of a group of 73 SQTS patients [27].

The S755T substitution in the *CACNA2D1* encoded $Ca_v\alpha_2\delta$-1 subunit was found in a 17-year-old female patient who had experienced sudden loss of consciousness and VF. Once hospitalized, her QT_c interval was found to be 329 ms and AF and VT could be provoked by programmed electric stimulation. Comparison of ionic currents between wild-type and mutant $Ca_v\alpha_2\delta$-1 subunit co-expression with $Ca_v1.2\alpha1$ and $Ca_v\beta_{2b}$ showed the mutant to result in markedly smaller currents, without obvious effects on channel protein expression [100].

26.6 SQT7

SCN5A has been linked to a mixed Brugada/SQTS phenotype through the R689H mutation [101]. A 40-year-old male with the mutation was found to have a Brugada-like ECG and abbreviated QT interval (320 ms at a rate of 71 beats/minute). His father had died suddenly at age 39. In vitro patch clamp analysis showed that the R689H mutation resulted in a loss of $Na_v1.5$ channel function [101]. The situation in respect of this mutation is not straightforward, however, as it had previously been associated with *long* QT phenotype and a separate study suggested it could increase the late component of Na current (I_{Na}) [102]. Consequently, the precise phenotype (or phenotypes) possible with this mutation [22] is open to question.

26.7 SQT8

In 2017, SQTS was linked for the first time to a defective ion transporter [103]. Genetic analysis of two unrelated families with an SQTS phenotype revealed a missense mutation (R370H) in the AE3 anion transporter, which is encoded by the *SLC4A3* gene [103]. This mutation resulted in reduced surface expression of the AE3 transporter and reduced bicarbonate transport. Knock-down of the analogous gene (*slc4a3*) in zebrafish embryos abbreviated repolarisation and increased intracellular pH of zebrafish hearts, whilst increasing intracellular pH and reducing intracellular chloride ion concentration abbreviated rabbit ventricular repolarisation [103]. Thus, AE3 transporter dysfunction has been causally linked to a SQTS phenotype [103], though the precise mechanism through which the observed changes lead to accelerated repolarisation requires further study [23].

26.8 SQT9

A recent case has raised the possibility of a role for *SCN10A* in QT_c interval shortening [104]. A 47-year-old women died suddenly with J wave syndrome, associated with an abbreviated QT_c interval of 303 ms. Genetic analysis revealed a G805V mutation to *SCN10A*-encoded $Na_v1.8$. The patient had been treated for rheumatoid arthritis with etoricoxib and the authors of the report of this case suggested potential for a pharmacogenomic component, as prostaglandin E2 influences $Na_v1.8$ trafficking and this could have been altered by etoricoxib [104]. Biophysical and trafficking analysis is needed to demonstrate whether or not the G805V mutation has a loss-of-function effect that can account for repolarisation abnormalities seen in this case.

26.9 Primary Carnitine Deficiency as a Cause of QT Interval Shortening

Primary carnitine deficiency (PCD) is an inherited condition in which patients exhibit low intracellular and plasma carnitine and reduced renal carnitine reabsorption. Mutations to *SLC22A5* result in malfunction of the OCTN2 sodium-dependent carnitine transporter; in turn, this leads to impaired oxidation of long chain fatty acids (LCFCs) and accumulation in the cell cytosol [105, 106]. PCD leads to impaired cardiac metabolism and is associated with a progressive cardiomyopathy and increased arrhythmia risk [107]. Increasing evidence suggests that some PCD patients can exhibit an SQTS phenotype [108–111] and work on a small animal model of PCD has shown a causal link between carnitine deficiency and abbreviated repolarisation [108], although the underlying ionic basis for this has yet to be elucidated. Though rare, PCD should be considered as a potential cause of SQTS, particularly when cardiomyopathy is present [23, 109].

Currently identified ion channel mutations associated with the SQTS and their functional consequences are summarised in Table 26.1.

Table 26.1 List of known SQTS variants

SQTS subtype	*Gene* and gene product	Channel or transporter (subunit)	Mutation (amino acid change)	Gain/Loss of function
SQT1	*KCNH2* (hERG)	I_{Kr} (α [pore-forming] sub-unit)	N588K R1135H E50D I560T T618I S631A	Gain of function Gain of function Gain of function Gain of function Gain of function Gain of function
SQT2	*KCNQ1* (KCNQ1/ KvLQT1)	I_{Ks} (α sub-unit)	V307L V141M R259H F279I	Gain of function Gain of function Gain of function Gain of function
SQT3	*KCNJ2* (Kir2.1)	I_{K1}	D172N M301K E299V K346T	Gain of function Gain of function Gain of function Gain of function
SQT4	*CACNA1C* ($Ca_V1.2$)	L-type I_{Ca} (α subunit)	A39V G490R R1973P R1977Q	Loss of function Loss of function Loss of function Loss of function
SQT5	*CACNB2b* ($β_{2b}$ subunit)	L-type I_{Ca} ($β_{2b}$ subunit)	S481L	Loss of function
SQT6	*CACNA2D1*	L-type I_{Ca} (α2δ1 subunit)	S755T	Loss of function
SQT7	*SCN5A*	I_{Na} (canonical α subunit)	R689H	Putative loss of function
SQT8	*SLC4A3*	Anion exchanger AE3	R370H	Loss of function
SQT9	*SCN10A*	I_{Na} (noncanonical α subunit)	G805V	Presumed loss of function (functional data required)
Other				
Primary carnitine deficiency	*SLC22A5*	OCTN2	W62X ♂ + R471 ♀ R471 + null R289*	Loss of function

26.10 Mechanisms of Arrhythmogenesis

Given the evidence for dangerous ventricular arrhythmia and sudden death in SQT families [16, 33], it is of some importance that mechanisms of arrhythmogenesis in the syndrome are understood. Shortened atrial and ventricular refractory periods of SQTS patients [16, 33] might be anticipated to increase the risk of re-entrant arrhythmia and work on experimental and in silico SQTS models bears this out. Insight into the effect of ventricular AP shortening in facilitating an arrhythmogenic substrate has come from experiments using the K_{ATP} channel activator pinacidil on canine ventricular wedge preparations. Although this model does not correspond precisely to SQTS channel gene mutations, it reproduces QT interval shortening and demonstrates increased maximal transmural dispersion of repolarisation (TDR) and susceptibility to polymorphic ventricular tachycardia [112]. Subsequent use of an I_{Kr}-activating compound (PD-118057) in experiments with the ventricular wedge preparation has shown QT interval shortening, increased TDR and effective refractory period (ERP) abbreviation, and susceptibility to evoked arrhythmia [113]. In intact rabbit hearts, pinacidil use has

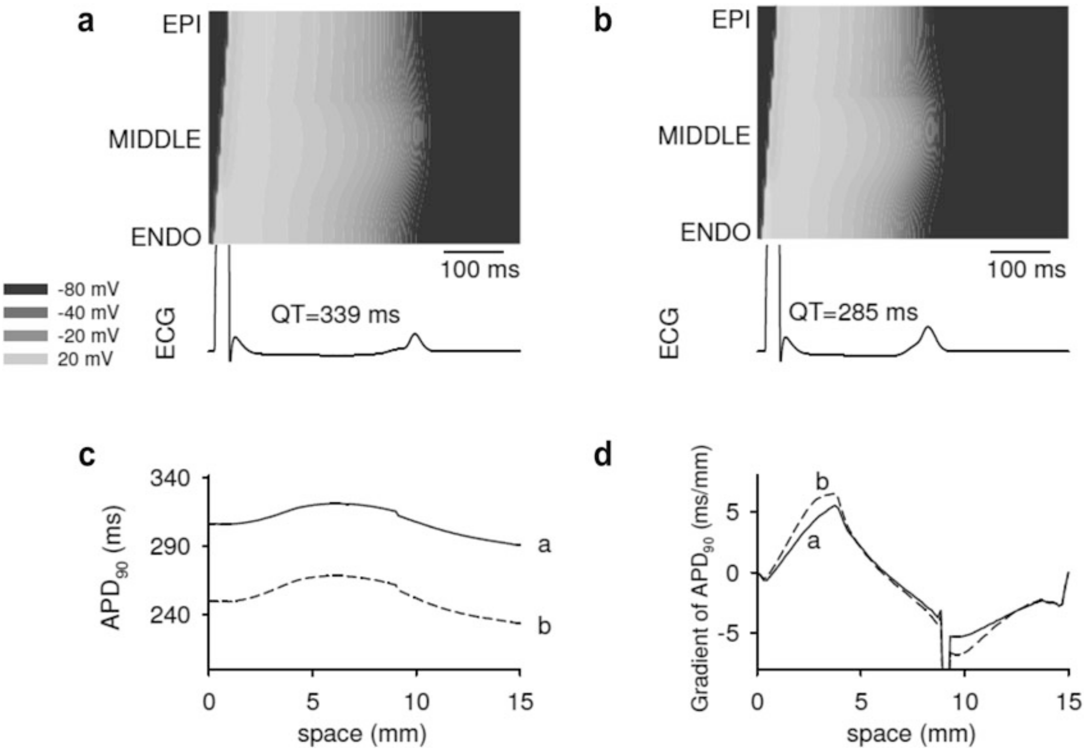

Fig. 26.2 (**a** & **b**): Space-time plot of computed AP propagation and the pseudo-ECG and reconstructed QT intervals for WT (**a**) and heterozygous V307L-KCNQ1 mutant (**b**) conditions in I_{Ks}-linked SQT2. The membrane potential of cells along the 1D strand is mapped into grey spectrum ranging from black for −100 mV to bright for +50 mV (see grey-scale key). Space runs vertically from the ENDO end at the bottom to the EPI end at the top. Time runs horizontally (left to right). (**c**): Spatial distribution of action potential duration at 90% repolarisation (APD_{90}) on 1D transmural strand in WT (marked by a) and heterozygous V307L KCNQ1 mutant (marked by b) conditions; (**d**): spatial gradient of APD_{90} on 1D transmural strand in WT (marked by a) and heterozygous mutant (marked by b) conditions. For further information on simulated SQT2 see [80]

been shown to produce abbreviation of the QT interval and dispersion of repolarisation [114].

Computer simulations that mimic the prominent kinetic changes to I_{Kr}, I_{Ks} and I_{K1} of the major SQT1–3 mutations have shown accelerated repolarisation convincingly at cell and tissue levels (e.g [74, 79, 80, 94, 95, 115–124]). In early simulations changes to T-wave morphology were more accurately reproduced for SQT2 [80] and SQT3 [79] variants than for SQT1 [115, 116]. At the single cell level AP shortening in simulated SQT1 and SQT2 is heterogeneous, with midmyocardial AP repolarisation more greatly affected than that in epi- or endo-cardial cells [80, 115, 116]. Using a combination of cellular, 1D and 2D tissue simulations to study SQT2 we were able to reproduce QT interval shortening and altered T-wave amplitude (Fig. 26.2a, b), by incorporating kinetic changes to I_{Ks} to match those observed for V307L KCNQ1 + KCNE1 [73, 80]. Maximal transmural voltage heterogeneity (δV) during APs was augmented, associated with augmented heterogeneity of AP duration (Fig. 26.2c, d) and ERP. In ventricular tissue models, the vulnerable window for unidirectional conduction block was increased and re-entrant arrhythmias facilitated in simulations of the V307L mutant [80]. Subsequent incorporation of further experimental features of V307L [125] into Markov chain models recapitulating wild-type and V307L conditions (both under heterozygotic and homozygotic conditions) has allowed recapitulation of re-entry in 3D human ventricle models [121], whilst in silico comparison of V307L and V141M mutations have shown the more pervasive effects of the V141M mutation led to marked sinus bradycardia, whilst both mutations facilitated AF [122].

Simulated AP shortening has been shown to be accompanied by altered AP restitution (e.g [79, 115]). AP voltage-clamp experiments and simulations have shown that, in the case of SQT1, there is a markedly smaller effect of the N588K hERG mutation on I_{hERG} during Purkinje fibre APs than during ventricular APs [55, 57, 61]. This is attributable to differences in AP morphology between the two cell types and may lead to increased heterogeneity between ventricular and Purkinje fibre repolarisation in SQT1, which could feasibly contribute to prominent U-waves seen in some SQTS patients [55, 57, 61]. One simulation study has suggested that hERG gating defects due to the N588K mutation might facilitate early after-depolarisations in SQT1 [117], with reduced hERG 'tail currents' [126] and altered response to 'premature' stimuli in vitro [61]. Our simulation work, using Markov-based formulations of the N588K hERG mutation reproduced increased T wave height seen in SQT1 when a transmural asymmetry of I_{Kr} expression was incorporated into the wild-type and mutant simulations [118]. These simulations also highlighted localized increases in ventricular transmural δV with the N588K mutation [118]. Such heterogeneity together with reduced substrate size required to sustain re-entry facilitates re-entry in both 2D and 3D tissue models [118, 123]. Our incorporation of the N588K hERG mutation in an electromechanically coupled ventricular model showed a reduction in the intracellular Ca^{2+} transient and contraction in the SQT1 condition, with a lesser effect of the SQT3 D172N mutation [120]. These in silico results anticipated later patient findings from Doppler imaging and speckle tracking echocardiography that found reduced left ventricular contraction and increased mechanical dispersion in SQTS compared to control subjects [127].

The first genetic animal model of the SQTS was the *reggae* zebrafish mutant, which exhibits a gain-of-function zERG (zebrafish-erg) mutation to the zERG channel voltage sensor region that can be linked causally to abbreviated repolarisation and cardiac fibrillation [128]. Recently, a transgenic SQT1 rabbit model has been developed that incorporates the N588K mutant [129]. The model shows abbreviation of the QT interval and of atrial and ventricular refractory periods, and it displays decreased slope of the QT-RR relationship. Whilst these features are reminiscent of the human clinical phenotype, tall T waves seen in SQT1 patients were not evident [129] and, as recently highlighted [130], in contrast with patient and in silico data systolic function was not affected, though diastolic relaxation was enhanced. One notable finding in this transgenic model was the presence of some ionic current remodelling: I_{K1} was reduced, whilst I_{Ks} was slightly increased [129]. Human induced pluripotent stem-cell (hiPSC) derived cardiomyocytes (hiPSC-CMs) with the N588K and T618I mutations have been made and demonstrate a causal relationship between the presence of these gain-of-function mutations and abbreviated repolarisation [131, 132]. In addition to abbreviated repolarisation and increased I_{Kr} density, N588K hiPSC-CMs showed abnormal Ca^{2+} transients and arrhythmic activity. mRNA for hERG, *CACNA1C* and subunits of the transient outward K^+ channel were upregulated in N588K hiPSC-CMs, but interestingly those for subunits of I_{K1} and I_{Ks} (*KCNJ2* and *KCNQ1*) were not [131]. Thus, ion channel remodelling in the hiPSC-CM line in response to the N588K mutation appears to differ from that in the transgenic rabbit [130]. 2D sheets of N588K-hiPSC-CMs have also been studied and show abbreviated repolarisation and effective refractory period as expected [133]. Optical mapping has also shown increased inducibility of spiral waves and allowed their quantification in N588K hERG expressing hiPSC-CM sheets [133]. There is striking agreement between arrhythmogenic mechanisms observed in this preparation and those seen in earlier computational modelling [130]. T618I hiPSC-CMs show both abbreviated action potentials and increased action potential variability compared to both controls and gene-corrected hiPSC-CMs [132]. They also show an altered gene expression profile [132]. The mechanism and significance of this remains to be established.

26.11 Treatment

Due to the risk of fatal ventricular arrhythmia, the primary treatment for SQTS patients is the use of implantable cardioverter defibrillator devices (ICDs; [16, 33, 134, 135]). However, the marked changes to T wave morphology present in many patients means that there is an inherent risk in ICD use of inappropriate shock delivery, due to T wave over-sensing [16, 17, 33, 134]. Although this risk can be mitigated by ICD reprogramming [134], ICD use does not, per se, restore normal QT interval duration or rate dependence; also some patients (e.g. very young infants) may not be suitable for ICD implantation. Consequently (adjunct) pharmacotherapeutic options may be desirable that can restore QT intervals towards normal and protect against arrhythmia generation [16, 22, 33, 136, 137].

In the initial study that identified SQT1, pharmacological treatment with the class III antiarrhythmic drug sotalol was attempted, but this failed to restore a normal QT interval [43]. In vitro experiments in the same study showed that N588K-hERG was less sensitive to inhibition by D-sotalol than was WT hERG. A subsequent study tested a number of drugs on a sample of six SQTS patients; the drugs investigated included the class Ic antiarrhythmic drug flecainide, the class Ia agent hydroquinidine and the class III agents sotalol and ibutilide [138]. Of these agents, only hydroquinidine produced substantial QT interval lengthening and it also prolonged ventricular effective refractory period and protected against induced VF [138]. A subsequent comparison of quinidine and sotalol showed that, at ambient temperature, the IC_{50} for I_{hERG} current by sotalol was increased 20-fold by the N588K mutation whereas that for quinidine was only increased by 5.8 fold [139]. Quinidine also restored towards normal the heart rate adaptation of the QT interval of SQT1 patients [139].

High potency hERG inhibition appears to depend, directly or indirectly, on hERG channel inactivation [41, 140–144]. The greater effectiveness of quinidine than of sotalol against SQT1 and N588K-hERG channels was suggested to reflect the fact that quinidine's ability to inhibit hERG is comparatively insensitive to inactivation of the channel [14, 43, 139]. We investigated another class Ia antiarrhythmic agent, disopyramide, finding that the I_{hERG} blocking potency of this agent was also little-affected by the N588K hERG mutation (an IC_{50} 1.5 fold that of WT hERG compared to 3.5 fold that for quinidine [145] see also Fig. 26.3a). In direct comparison, the high affinity Class III inhibitor E-4031 showed a $>$ 11-fold change in IC_{50} [145]. Disopyramide was subsequently tested in a pilot study on two SQT1 patients and found to exert beneficial effects on QT interval, rate dependence and ventricular ERP [146]. Quinidine but not sotalol application to hiPSC-CMs with the N588K hERG mutation prolonged action potential duration [131], whilst when they were applied to N588K-expressing hiPSC-CM sheets both quinidine and disopyramide, but not sotalol, normalised action potential duration and suppressed arrhythmia induction [133]. This corresponds well to patient data. Our recent simulation work indicates that beneficial effects of quinidine and disopyramide on the QT interval in N588K-linked SQT1 are attributable to I_{Kr} block, whilst prolongation of the abbreviated ERP is attributable to effects on both I_{Kr} and I_{Na} [123, 124]. This finding is consistent with data from perfused canine right atrial preparations showing that combined I_{Kr} and I_{Na} block was necessary to prolong both action potential duration and ERP [147]. Disopyramide and quinidine have also been observed to be effective in vitro against the T618I and S631A hERG mutations [64, 66, 67, 144, 148, 149], whilst quinidine is also effective against the I560T hERG mutation ([69]; Fig. 26.3b). Ajmaline, mexiletine and ivabradine have recently been reported to prolong

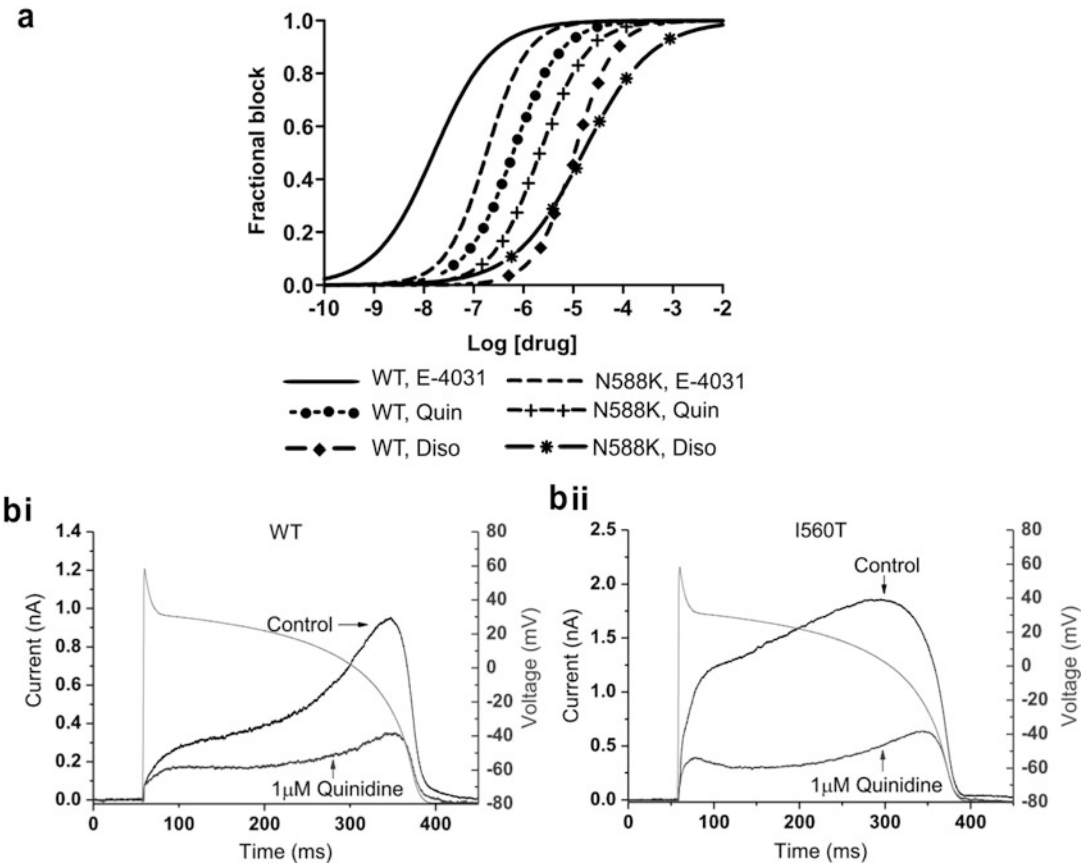

Fig. 26.3 In vitro pharmacology of SQT1. (**a**) Comparative pharmacology of WT and N588K hERG. Figure shows concentration–response relations for inhibition by three drugs of WT and N588K (SQT1) hERG currents recorded from hERG-expressing Chinese Hamster Ovary cells. Half-maximal inhibitory (IC_{50}) values for inhibition by E-4031, quinidine and disopyramide are as follows, E-4031: WT 16 nM, SQT1 183 nM; quinidine: WT 0.62 μM, SQT1 2.2 μM; disopyramide: WT 10.7 μM, SQT1 15.8 μM. E-4031 is included as a methanesulphonanilide, structurally related to sotalol, for which the N588K mutation markedly affected inhibitory potency. Note that symbols do not denote plotted data points; rather, the concentration response relations have been plotted as continuous lines, and some line types incorporate symbols to help differentiate between the different plots. For further information see [145]. (**b**) Quinidine is effective against the I560T hERG mutation. Panels show action potential (AP) voltage commands overlaid with corresponding wild-type (WT; Bi) or I560T (Bii) hERG current (I_{hERG}) elicited using AP voltage clamp. 1 μM quinidine was effective in reducing I_{hERG} magnitude in each case, indicating that it retains its hERG-blocking effect in the presence of the I560T mutation. Reproduced from [69] under a Creative Commons (CC BY) license

the duration of action potentials from iPSC-CMs from an SQT1 patient [150].

The potential for I_{Kr} block to delay repolarisation in non-SQT1 forms of SQTS is illustrated by the effectiveness of I_{Kr} inhibition in pinacidil (K_{ATP}) models of SQTS [112, 151, 152] and our in silico simulations of effects of I_{Kr} block in SQT3 [95]. Calcium channel-related SQTS/Brugada syndrome has been reported to be responsive to quinidine [97]. Indeed, the ability of hydroquinidine to protect against life-threatening arrhythmic events in the SQTS is not restricted to SQT1 [153], and long-term follow-up of both adult and paediatric cohorts with SQTS suggest that quinidine/hydroquinidine can be beneficial across different SQTS variants

[154–156]. Disopyramide has also been reported to be beneficial in a patient with SQTS of unknown genotype [157].

Although the notion of genotype-specific pharmacology for the SQTS is an attractive concept [136], selective I_{Ks} inhibition is at present only a theoretical treatment for SQT2 as there are no selective I_{Ks} inhibitors in clinical use [22]. However, in vitro and in silico data indicate the potential for an I_{Ks}-based strategy [121, 125]. The effectiveness of the strategy would likely differ between mutations and drug interaction sites, illustrated by the fact that the V307L KCNQ1 SQT2 mutation has been shown to attenuate the blocking potency of the I_{Ks}-inhibitor chromanol 293B [158]. Experimental data with chloroquine and the pentamidine analogue PA-3 and SQT3 simulation data suggest some potential for an I_{K1} inhibition-based approach (on its own, or coupled with I_{Kr} block) in SQT3 [22, 92, 95, 159–161]. Perhaps the most striking example of a genotype-specific treatment is for PCD [110]. Patients with PCD and abbreviated ventricular repolarisation respond to dietary carnitine supplementation with QT interval lengthening [108–110]; thus, early successful identification and genotyping of PCD could result in a dietary intervention that could reduce the need for pharmacological intervention.

26.12 Conclusions

Twenty years after the report of familial idiopathic short QT intervals by Gussak and colleagues [19], a lot has been learned about the SQTS. Highly abbreviated QT_C intervals are rare in the normal population [24, 162–164], and genetic SQTS, though dangerous, is uncommon. Whilst multiple genes have been implicated in the SQTS (Table 26.1), a recent analysis of 32 SQTS variants in the literature concluded that only those in *hERG (KCNH2)*, *KCNQ1* and *KCNJ2* have a conclusive pathogenic role [165]. However, in our view, it would be premature to restrict genetic screening for SQTS to these genes for several reasons. First, screening patients against known candidate SQTS genes has had only limited success, with a genetic cause not identified in the majority of cases [15, 22, 28, 33]. This indicates that there is still much to learn about clinically relevant modifiers of cardiac repolarisation; moreover, mutations to other genes will need to be identified to have a more complete understanding of the basis of QT interval shortening [23]. Second, the identification of genetic variants that produce a mixed Brugada/SQTS phenotype raises the possibility of a continuum of abbreviated repolarisation phenotypes that, from a physiological perspective at least, may not readily conform to distinct boundaries between disorders. Similarly, the fact that PCD can produce a SQTS phenotype together with cardiomyopathy [110] highlights the fact that SQTS need not always occur in structurally normal hearts. Thus, an inclusive approach to considering genetic causes of QT interval abbreviation may be the one which is most consistent with underlying (patho)physiology. The potential value of whole exome sequencing for resolving genetic causes of SQTS is exemplified by the discovery of a loss-of-function mutation to *SLC4A3*-encoded AE3 ([103] and Sect. 26.7). The future increased use of such an approach, where targeted screening fails, may shed further light on this fascinating and sometimes elusive syndrome.

Acknowledgement The authors work on the short QT syndrome has been funded by the British Heart Foundation (PG 04/090, PG 06/139, PG 06/147, FS 08/021; FS/14/5/30533, PG/17/89/33414, PG/15/106/31915, PG/19/26/34302) and SADS (Sudden Arrhythmic Death Syndrome) UK.

References

1. Yap YG, Camm AJ. Drug induced QT prolongation and torsades de pointes. Heart. 2003;89:1363–72.
2. Garberoglio L, Giustetto C, Wolpert C, Gaita F. Is acquired short QT due to digitalis intoxication responsible for malignant ventricular arrhythmias? J Electrocardiol. 2007;40(1):43–6.
3. Bidoggia H, Maciel JP, Capalozza N, Mosca S, Blaksley EJ, Valverde E, et al. Sex differences on the electrocardiographic pattern of cardiac repolarization: possible role of testosterone. Am Heart J. 2000;140(4):678–83.

4. Charbit B, Christin-Maitre S, Demolis JL, Soustre E, Young J, Funck-Brentano C. Effects of testosterone on ventricular repolarization in hypogonadic men. Am J Cardiol. 2009;103(6):887–90.
5. Bigi MA, Aslani A, Aslani A. Short QT interval: a novel predictor of androgen abuse in strength trained athletes. Ann Noninvasive Electrocardiol. 2009;14 (1):35–9.
6. Hancox JC, Choisy SC, James AF. Short QT interval linked to androgen misuse: wider significance and possible basis. Ann Noninvasive Electrocardiol. 2009;14(3):311–2.
7. Cheng TO. Digitalis administration: an underappreciated but common cause of short QT interval. Circulation. 2004;109(9):e152.
8. Hachimi-Idrissi S, Corne L, Maes V, Ramet J. Gitaloxin poisoning in a child. Intensive Care Med. 1996;22(12):1442–4.
9. Jowett NI. Foxglove poisoning. Hosp Med. 2002;63 (12):758–9.
10. Levi AJ. A role for Na/Ca exchange in the action potential shortening caused by strophanthidin in Guinea-pig ventricular myocytes. Cardiovasc Res. 1993;27:471–81.
11. Bassingthwaighte JB, Fry CH, McGuigan JA. Relationship between internal calcium and outward current in mammalian ventricular muscle; a mechanism for the control of the action potential duration? J Physiol. 1976;262(1):15–37.
12. Levi AJ, Dalton GR, Hancox JC, Mitcheson JS, Issberner J, Bates JA, et al. Role of intracellular sodium overload in the genesis of cardiac arrhythmias. J Cardiovas Electrophys. 1997;8:700–21.
13. Gomes JA, Dhatt MS, Akhtar M, Carambas CR, Rubenson DS, Damato AN. Effects of digitalis on ventricular myocardial and His-Purkinje refractoriness and reentry in man. Am J Cardiol. 1978;42 (6):931–8.
14. Gaita F, Giustetto C, Bianchi F, Wolpert C, Schimpf R, Riccardi R, et al. Short QT syndrome: a familial cause of sudden death. Circulation. 2003;108:965–70.
15. Giustetto C, Di MF, Wolpert C, Borggrefe M, Schimpf R, Sbragia P, et al. Short QT syndrome: clinical findings and diagnostic-therapeutic implications. Eur Heart J. 2006;27(20):2440–7.
16. Schimpf R, Wolpert C, Gaita F, Giustetto C, Borggrefe M. Short QT syndrome. Cardiovasc Res. 2005;67(3):357–66.
17. Anttonen O, Junttila J, Giustetto C, Gaita F, Linna E, Karsikas M, et al. T-wave morphology in short QT syndrome. Ann Noninvasive Electrocardiol. 2009;14 (3):262–7.
18. McPate MJ, Witchel HJ, Hancox JC. Short QT syndrome. Futur Cardiol. 2006;2:293–301.
19. Gussak I, Brugada P, Brugada J, Wright RS, Kopecky SI, Chaitman BR, et al. Idiopathic short QT interval: a new clinical syndrome? Cardiology. 2000;94:99–102.
20. Gussak I, Brugada P, Brugada J, Antzelevitch C, Osbakken M, Bjerregaard P. ECG phenomenon of idiopathic and paradoxical short QT intervals. Card Electrophysiol Rev. 2002;6:49–53.
21. Gussak I, Liebl N, Nouri S, Bjerregaard P, Zimmerman F, Chaitman BR. Deceleration-dependent shortening of the QT interval: a new electrocardiographic phenomenon? Clin Cardiol. 1999;22(2):124–6.
22. Hancox JC, Whittaker DG, Du C, Stuart AG, Zhang H. Emerging therapeutic targets in the short QT syndrome. Expert Opin Ther Targets. 2018;22(5): 439–51.
23. Hancox JC, Whittaker DG, Zhang H, Stuart AG. Learning from studying very rare cardiac conditions: the example of short QT syndrome. J Congenit Cardiol. 2019;3(3):1–15. https://doi.org/10.1186/s40949-019-0024-7.
24. Anttonen O, Junttila MJ, Rissanen H, Reunanen A, Viitasalo M, Huikuri HV. Prevalence and prognostic significance of short QT interval in a middle-aged Finnish population. Circulation. 2007;116(7): 714–20.
25. Dhutia H, Malhotra A, Parpia S, Gabus V, Finocchiaro G, Mellor G, et al. The prevalence and significance of a short QT interval in 18,825 low-risk individuals including athletes. Br J Sports Med. 2016;50(2):124–9.
26. Guerrier K, Kwiatkowski D, Czosek RJ, Spar DS, Anderson JB, Knilans TK. Short QT interval prevalence and clinical outcomes in a pediatric population. Circ Arrhythm Electrophysiol. 2015;8(6):1460–4.
27. Mazzanti A, Kanthan A, Monteforte N, Memmi M, Bloise R, Novelli V, et al. Novel insight into the natural history of short QT syndrome. J Am Coll Cardiol. 2014;63(13):1300–8.
28. Gollob MH, Redpath CJ, Roberts JD. The short QT syndrome: proposed diagnostic criteria. J Am Coll Cardiol. 2011;57(7):802–12.
29. Priori SG, Blomstrom-Lundqvist C, Mazzanti A, Blom N, Borggrefe M, Camm J, et al. 2015 ESC guidelines for the management of patients with ventricular arrhythmias and the prevention of sudden cardiac death: the task force for the management of patients with ventricular arrhythmias and the prevention of sudden cardiac death of the European Society of Cardiology (ESC). Endorsed by: Association for European Paediatric and Congenital Cardiology (AEPC). Eur Heart J. 2015;36(41):2793–867.
30. Redpath CJ, Green MS, Birnie DH, Gollob MH. Rapid genetic testing facilitating the diagnosis of short QT syndrome. Can J Cardiol. 2009;25(4): e133–5.
31. Terlemez S, Cil E, Kula S, Oguz AD, Tunaoglu FS. A diagnosis that escapes our attention: Short QT syndrome. Gazi Med J. 2018;29(3):246–8.

32. Providencia R, Karim N, Srinivasan N, Honarbakhsh S, Vidigal Ferreira MJ, Goncalves L, et al. Impact of QTc formulae in the prevalence of short corrected QT interval and impact on probability and diagnosis of short QT syndrome. Heart. 2018;104(6):502–8.
33. Maury P, Extramiana F, Sbragia P, Giustetto C, Schimpf R, Duparc A, et al. Short QT syndrome. Update on a recent entity. Arch Cardiovasc Dis. 2008;101(11–12):779–86.
34. Wolpert C, Schimpf R, Veltmann C, Giustetto C, Gaita F, Borggrefe M. Clinical characteristics and treatment of short QT syndrome. Expert Rev Cardiovasc Ther. 2005;3(4):611–7.
35. Warmke JW, Ganetzky B. A family of potassium channel genes related to *eag* in *Drosophila* and mammals. Proc Natl Acad Sci U S A. 1994;91: 3438–42.
36. Sanguinetti MC, Jiang C, Curran ME, Keating MT. A mechanistic link between an inherited and an acquired cardiac arrhythmia: HERG encodes the I_{Kr} potassium channel. Cell. 1995;81:299–307.
37. Trudeau MC, Warmke JW, Ganetzky B, Robertson GA. HERG, an inward rectifier in the voltage-gated potassium channel family. Science. 1995;269:92–5.
38. Witchel HJ, Hancox JC. Familial and acquired long QT syndrome and the cardiac rapid delayed rectifier potassium channel. Clin Exp Pharmacol Physiol. 2000;27:753–66.
39. Tamargo J, Caballero R, Gomez R, Valenzuela C, Delpon E. Pharmacology of cardiac potassium channels. Cardiovasc Res. 2004;62(1):9–33.
40. Sanguinetti MC, Tristani-Firouzi M. hERG potassium channels and cardiac arrhythmia. Nature. 2006;440(7083):463–9.
41. Hancox JC, McPate MJ, El Harchi A, Zhang YH. The hERG potassium channel and hERG screening for drug-induced torsades de pointes. Pharmacol Ther. 2008;119:118–32.
42. Modell SM, Lehmann MH. The long QT syndrome family of cardiac ion channelopathies: a HuGE review. Genet Med. 2006;8(3):143–55.
43. Brugada R, Hong K, Dumaine R, Cordeiro J, Gaita F, Borggrefe M, et al. Sudden death associated with short-QT syndrome linked to mutations in HERG. Circulation. 2004;109:30–5.
44. Hong K, Bjeerregaard P, Gussak I, Brugada R. Short QT syndrome and atrial fibrillation caused by mutation in KCNH2. J Cardiovas Electophysiol. 2005;16: 394–6.
45. Smith PL, Baukrowitz T, Yellen G. The inward rectification mechanism of the HERG cardiac potassium channel. Nature. 1996;379(6568):833–6.
46. Spector PS, Curran ME, Zou A, Keating MT, Sanguinetti MC. Fast inactivation causes rectification of the I_{Kr} channel. J Gen Physiol. 1996;107:611–9.
47. Hancox JC, Levi AJ, Witchel HJ. Time course and voltage dependence of expressed HERG current compared with native 'rapid' delayed rectifier K current during the cardiac ventricular action potential. Pflugers Archiv - Eur J Physiol. 1998;436:843–53.
48. Hancox JC, Witchel HJ, Varghese A. Alteration of HERG current profile during the cardiac ventricular action potential, following a pore mutation. Biochem Biophys Res Comm. 1998;253:719–24.
49. Zhou Z, Gong Q, Ye B, Fan Z, Makielski JC, Robertson GA, et al. Properties of HERG channels stably expressed in HEK 293 cells studied at physiological temperature. Biophys J. 1998;74:230–41.
50. Schoenherr R, Heinemann SH. Molecular determinants for activation and inactivation of HERG, a human inward rectifier potassium channel. J Physiol. 1996;493(3):635–42.
51. Liu J, Zhang M, Jiang M, Tseng GN. Structural and functional role of the extracellular S5-P linker in the HERG potassium channel. J Gen Physiol. 2002;120: 723–37.
52. Jiang M, Zhang M, Maslennikov IV, Liu J, Wu DM, Korolkova YV, et al. Dynamic conformational changes of extracellular S5-P linkers in the hERG channel. J Physiol. 2005;569:75–89.
53. Clarke CE, Hill AP, Zhao J, Kondo M, Subbiah RN, Campbell TJ, et al. Effect of S5P alpha-helix charge mutants on inactivation of hERG K^+ channels. J Physiol. 2006;573:291–304.
54. Abbott GW, Sesti F, Splawski I, Buck M, Lehmann MH, Timothy KW, et al. MiRP1 forms I_{Kr} potassium channels with HERG and is associated with cardiac arrhythmia. Cell. 1999;97:175–87.
55. Cordeiro JM, Brugada R, Wu YS, Hong K, Dumaine R. Modulation of I_{Kr} inactivation by mutation N588K in KCNH2: a link to arrhythmogenesis in short QT syndrome. Cardiovasc Res. 2005;67:498–509.
56. McPate MJ, Duncan RS, Milnes JT, Witchel HJ, Hancox JC. The N588K-HERG K^+ channel mutation in the 'short QT syndrome': mechanism of gain-in-function determined at 37°C. Biochem Biophys Res Comm. 2005;334:441–9.
57. McPate MJ, Zhang H, Cordeiro JM, Dempsey CE, Witchel HJ, Hancox JC. hERG1a/1b heteromeric currents exhibit amplified attenuation of inactivation in variant 1 short QT syndrome. Biochem Biophys Res Commun. 2009;386(1):111–7.
58. Jones EM, Roti EC, Wang J, Robertson GA. Cardiac I_{Kr} channels minimally comprise hERG 1a and 1b subunits. J Biol Chem. 2004;279:44690–4.
59. Sale H, Wang J, O'Hara TJ, Tester DJ, Phartiyal P, He JQ, et al. Physiological properties of hERG 1a/1b heteromeric currents and a hERG 1b-specific mutation associated with long-QT syndrome. Circ Res. 2008;103(7):e81–95.
60. Jones DK, Liu F, Vaidyanathan R, Eckhardt LL, Trudeau MC, Robertson GA. hERG 1b is critical for human cardiac repolarization. Proc Natl Acad Sci U S A. 2014;111(50):18073–7.
61. McPate MJ, Zhang H, Ideniran I, Cordeiro JM, Witchel HJ, Hancox JC. Comparative effects of the short QT N588K mutation at 37°C on hERG K^+

channel current during ventricular, Purkinje fibre and atrial action potentials: an action potential clamp study. J Physiol Pharmacol. 2009;60:23–41.

62. Zou A, Curran ME, Keating MT, Sanguinetti MC. Single HERG delayed rectifier K^+ channels expressed in Xenopus oocytes. Am J Phys. 1997;272:H1309–14.
63. Akdis D, Saguner AM, Medeiros-Domingo A, Schaller A, Balmer C, Steffel J, et al. Multiple clinical profiles of families with the short QT syndrome. Europace. 2018;20(FI1):f113–21.
64. Butler A, Zhang Y, Stuart AG, Dempsey CE, Hancox JC. Action potential clamp characterization of the S631A hERG mutation associated with short QT syndrome. Physiol Rep. 2018;6(17):e13845.
65. Hu D, Li Y, Zhang J, Pfeiffer R, Gollob MH, Healey J, et al. The phenotypic spectrum of a mutation hotspot responsible for the short QT syndrome. JACC Clin Electrophysiol. 2017;3(7):727–43.
66. Sun Y, Quan XQ, Fromme S, Cox RH, Zhang P, Zhang L, et al. A novel mutation in the KCNH2 gene associated with short QT syndrome. J Mol Cell Cardiol. 2011 Mar;50(3):433–41.
67. El Harchi A, Melgari D, Zhang YH, Zhang H, Hancox JC. Action potential clamp and pharmacology of the variant 1 Short QT syndrome T618I hERG K^+ channel. PLoS One. 2012;7(12):e52451.
68. Harrell DT, Ashihara T, Ishikawa T, Tominaga I, Mazzanti A, Takahashi K, et al. Genotype-dependent differences in age of manifestation and arrhythmia complications in short QT syndrome. Int J Cardiol. 2015;190:393–402.
69. Butler A, Zhang Y, Stuart AG, Dempsey CE, Hancox JC. Functional and pharmacological characterization of an S5 domain hERG mutation associated with short QT syndrome. Heliyon. 2019;5(4):e01429.
70. Itoh H, Sakaguchi T, Ashihara T, Ding WG, Nagaoka I, Oka Y, et al. A novel KCNH2 mutation as a modifier for short QT interval. Int J Cardiol. 2009;137:83–5.
71. Wilders R, Verkerk AO. Role of the R1135H KCNH2 mutation in Brugada syndrome. Int J Cardiol. 2010;144:149–51.
72. Wang QI, Ohno S, Ding WG, Fukuyama M, Miyamoto A, Itoh H, et al. Gain-of-function KCNH2 mutations in patients with Brugada syndrome. J Cardiovasc Electrophysiol. 2014;25(5): 522–30.
73. Bellocq C, van Ginneken AC, Bezzina CR, Alders M, Escande D, Mannens MM, et al. Mutation in the KCNQ1 gene leading to the short QT-interval syndrome. Circulation. 2004;109(20):2394–7.
74. Hong K, Piper DR, Valdecantos AD, Brugada J, Oliva A, Burashnikov E, et al. De novo KCNQ1 mutation responsible for atrial fibrillation and short QT syndrome in utero. Cardiovasc Res. 2005;68(3): 433–40.
75. Barhanin J, Lesage F, Guillemare E, Fink M, Lazdunski M, Romey G. KvLQT1 and IsK (minK) proteins associate to form the I_{Ks} cardiac potassium current. Nature. 1996;384:78–80.
76. Sanguinetti MC, Curran ME, Zou A, Shen J, Spector PS, Atkinson DL, et al. Coassembly of KvLQT1 and minK (IsK) proteins to form cardiac I_{Ks} potassium channel. Nature. 1996;384:80–3.
77. Roden DM, Lazzara R, Rosen MR, Schwartz PJ, Towbin JA, Vincent M, et al. Multiple mechanisms in the long-QT syndrome. Current knowledge, gaps and future directions. Circulation. 1996;94:1996–2012.
78. Jost N, Virag L, Bitay M, Takacs J, Lengyel C, Biliczki P, et al. Restricting excessive cardiac action potential and QT prolongation: a vital role for I_{Ks} in human ventricular muscle. Circulation. 2005;112: 1392–9.
79. Priori SG, Pandit SV, Rivolta I, Berenfeld O, Ronchetti E, Dhamoon A, et al. A novel form of short QT syndrome (SQT3) is caused by a mutation in the KCNJ2 gene. Circ Res. 2005;96(7):800–7.
80. Zhang H, Kharche S, Holden AV, Hancox JC. Repolarisation and vulnerability to re-entry in the human heart with short QT syndrome arising from KCNQ1 mutation--a simulation study. Prog Biophys Mol Biol. 2008;96(1–3):112–31.
81. Chen YH, Xu SJ, Bendahhou S, Wang XL, Wang Y, Xu WY, et al. KCNQ1 gain-of-function mutation in familial atrial fibrillation. Science. 2003;299(5604): 251–4.
82. Restier L, Cheng L, Sanguinetti MC. Mechanisms by which atrial fibrillation-associated mutations in the S1 domain of KCNQ1 slow deactivation of I_{Ks} channels. J Physiol. 2008;586(Pt 17):4179–91.
83. Wu ZJ, Huang Y, Fu YC, Zhao XJ, Zhu C, Zhang Y, et al. Characterization of a Chinese KCNQ1 mutation (R259H) that shortens repolarization and causes short QT syndrome 2. J Geriatr Cardiol. 2015;12(4): 394–401.
84. Moreno C, Oliveras A, Bartolucci C, Munoz C, Salar E, et al. A new KCNQ1 mutation at the S5 segment that impairs its association with KCNE1 is responsible for short QT syndrome. Cardiovasc Res. 2015;107(4):613–23.
85. Shimoni Y, Clark RB, Giles WR. Role of an inwardly rectifying potassium current in rabbit ventricular action potential. J Physiol. 1992;448:709–27.
86. Mitcheson JS, Hancox JC. An investigation of the role played by the E-4031-sensitive (rapid delayed rectifier) potassium current in isolated rabbit atrioventricular nodal and ventricular myocytes. Pflugers Archiv - Eur J Physiol. 1999;438:843–50.
87. Gaborit N, Le BS, Szuts V, Varro A, Escande D, Nattel S, et al. Regional and tissue specific transcript signatures of ion channel genes in the non-diseased human heart. J Physiol. 2007;582(Pt 2):675–93.
88. Plaster NM, Tawil R, Tristani-Firouzi M, Canun S, Bendahhou S, Tsunoda A, et al. Mutations in Kir2.1 cause the developmental and episodic electrical

phenotypes of Andersen's syndrome. Cell. 2001;105 (4):511–9.
89. Tristani-Firouzi M, Jensen JL, Donaldson MR, Sansone V, Meola G, Hahn A, et al. Functional and clinical characterization of KCNJ2 mutations associated with LQT7 (Andersen syndrome). J Clin Invest. 2002;110(3):381–8.
90. Xia M, Jin Q, Bendahhou S, He Y, Larroque MM, Chen Y, et al. A Kir2.1 gain-of-function mutation underlies familial atrial fibrillation. Biochem Biophys Res Commun. 2005;332(4):1012–9.
91. Abrams CJ, Davies NW, Shelton PA, Stanfield PR. The role of a single aspartate residue in ionic selectivity and block of a murine inward rectifier K^+ channel Kir2.1. J Physiol. 1996;493(Pt 3):643–9.
92. El Harchi A, McPate MJ, Zhang YH, Zhang H, Hancox JC. Action potential clamp and chloroquine sensitivity of mutant Kir2.1 channels responsible for variant 3 short QT syndrome. J Mol Cell Cardiol. 2009;137:83–5.
93. Hattori T, Makiyama T, Akao M, Ehara E, Ohno S, Iguchi M, et al. A novel gain-of-function KCNJ2 mutation associated with short-QT syndrome impairs inward rectification of Kir2.1 currents. Cardiovasc Res. 2012;93(4):666–73.
94. Deo M, Ruan Y, Pandit SV, Shah K, Berenfeld O, Blaufox A, et al. KCNJ2 mutation in short QT syndrome 3 results in atrial fibrillation and ventricular proarrhythmia. Proc Natl Acad Sci U S A. 2013;110: 4291–6.
95. Whittaker DG, Ni H, Harchi AE, Hancox JC, Zhang H. Atrial arrhythmogenicity of KCNJ2 mutations in short QT syndrome: insights from virtual human atria. PLoS Comput Biol. 2017;13(6):e1005593.
96. Ambrosini E, Sicca F, Brignone MS, D'Adamo MC, Napolitano C, Servettini I, et al. Genetically induced dysfunctions of Kir2.1 channels: implications for short QT3 syndrome and autism-epilepsy phenotype. Hum Mol Genet. 2014;23(18):4875–86.
97. Antzelevitch C, Pollevick GD, Cordeiro JM, Casis O, Sanguinetti MC, Aizawa Y, et al. Loss-of-function mutations in the cardiac calcium channel underlie a new clinical entity characterized by ST-segment elevation, short QT intervals, and sudden cardiac death. Circulation. 2007;115(4):442–9.
98. Chen Y, Barajas-Martinez H, Zhu D, Wang X, Chen C, Zhuang R, et al. Novel trigenic CACNA1C/DES/MYPN mutations in a family of hypertrophic cardiomyopathy with early repolarization and short QT syndrome. J Transl Med. 2017;15 (1):78.
99. Chen Y, Barajas-Martinez H, Zhu D, Wang X, Chen C, Zhuang R, et al. Erratum to: novel trigenic CACNA1C/DES/MYPN mutations in a family of hypertrophic cardiomyopathy with early repolarization and short QT syndrome. J Transl Med. 2017;15 (1):101.
100. Templin C, Ghadri JR, Rougier JS, Baumer A, Kaplan V, Albesa M, et al. Identification of a novel loss-of-function calcium channel gene mutation in short QT syndrome (SQTS6). Eur Heart J. 2011;32 (9):1077–88.
101. Hong K, Hu J, Yu J, Brugada R. Concomitant Brugada-like and short QT electrocardiogram linked to SCN5A mutation. Eur J Hum Genet. 2012;20(11): 1189–92.
102. Sottas V, Rougier JS, Jousset F, Kucera JP, Shestak A, Makarov LM, et al. Characterization of 2 genetic variants of Na(v) 1.5-arginine 689 found in patients with cardiac arrhythmias. J Cardiovasc Electrophysiol. 2013;24(9):1037–46.
103. Thorsen K, Dam VS, Kjaer-Sorensen K, Pedersen LN, Skeberdis VA, Jurevicius J, et al. Loss-of-activity-mutation in the cardiac chloride-bicarbonate exchanger AE3 causes short QT syndrome. Nat Commun. 2017;8(1):1696.
104. Di SG, Palumbo P, Castellana S, Mastroianno S, Biagini T, Palumbo O, et al. Sudden cardiac death in J wave syndrome with short QT associated to a novel mutation in Nav 1.8 coding gene *SCN10A*: first case report for a possible pharmacogenomic role. J Electrocardiol. 2018;51(5):809–13.
105. Tamai I, Ohashi R, Nezu J, Yabuuchi H, Oku A, Shimane M, et al. Molecular and functional identification of sodium ion-dependent, high affinity human carnitine transporter OCTN2. J Biol Chem. 1998;273 (32):20378–82.
106. Iwata D, Kato Y, Wakayama T, Sai Y, Kubo Y, Iseki S, et al. Involvement of carnitine/organic cation transporter OCTN2 (SLC22A5) in distribution of its substrate carnitine to the heart. Drug Metab Pharmacokinet. 2008;23(3):207–15.
107. Fu L, Huang M, Chen S. Primary carnitine deficiency and cardiomyopathy. Korean Circ J. 2013;43(12): 785–92.
108. Roussel J, Labarthe F, Thireau J, Ferro F, Farah C, Roy J, et al. Carnitine deficiency induces a short QT syndrome. Heart Rhythm. 2016;13(1):165–74.
109. Perin F, Rodriguez-Vazquez Del Rey MDM, Carreras-Blesa C, Rrabal-Fernandez L, Jimenez-Jaimez J, Tercedor L. Dilated cardiomyopathy with short QT interval suggests primary carnitine deficiency. Rev Esp Cardiol (Engl Ed). 2018;71:1074–5.
110. Hancox JC. Primary carnitine deficiency as a potential cause of short QT syndrome. Cardiovasc Res Med. 2018;2(1):10–2.
111. Gelinas R, Leach E, Horvath G, Laksman Z. Molecular autopsy implicates primary carnitine deficiency in sudden unexplained death and reversible short QT syndrome. Can J Cardiol. 2019;35(9): 1256e1–2.
112. Extramiana F, Antzelevitch C. Amplified transmural dispersion of repolarization as the basis for arrhythmogenesis in a canine ventricular-wedge model of short-QT syndrome. Circulation. 2004;110 (24):3661–6.
113. Patel C, Antzelevitch C. Cellular basis for arrhythmogenesis in an experimental model of the

SQT1 form of the short QT syndrome. Heart Rhythm. 2008;5(4):585–90.

114. Milberg P, Tegelkamp R, Osada N, Schimpf R, Wolpert C, Breithardt G, et al. Reduction of dispersion of repolarization and prolongation of postrepolarization refractoriness explain the antiarrhythmic effects of quinidine in a model of short QT syndrome. J Cardiovasc Electrophysiol. 2007;18(6):658–64.

115. Zhang H, Hancox JC. In silico study of action potential and QT interval shortening due to loss of inactivation of the cardiac rapid delayed rectifier potassium current. Biochem Biophys Res Commun. 2004;322(2):693–9.

116. Weiss DL, Seemann G, Sachse FB, Dossel O. Modelling of short QT syndrome in a heterogeneous model of the human ventricular wall. Europace. 2005;7(Suppl 2):105–17.

117. Itoh H, Horie M, Ito M, Imoto K. Arrhythmogenesis in the short-QT syndrome associated with combined HERG channel gating defects: a simulation study. Circ J. 2006;70(4):502–8.

118. Adeniran I, McPate MJ, Witchel HJ, Hancox JC, Zhang H. Increased vulnerability of human ventricle to re-entrant excitation in hERG-linked variant 1 short QT syndrome. PLoS Comput Biol. 2011;7(12):e1002313.

119. Adeniran I, El Harchi A, Hancox JC, Zhang H. Proarrhythmia in KCNJ2-linked short QT syndrome: insights from modelling. Cardiovasc Res. 2012;94(1):66–76.

120. Adeniran I, Hancox JC, Zhang H. In silico investigation of the short QT syndrome, using human ventricle models incorporating electromechanical coupling. Front Physiol. 2013;4:166.

121. Adeniran I, Whittaker DG, El Harchi A, Hancox JC, Zhang H. In silico investigation of a KCNQ1 mutation associated with short QT syndrome. Sci Rep. 2017;7(1):8469.

122. Whittaker DG, Colman MA, Ni H, Hancox JC, Zhang H. Human atrial Arrhythmogenesis and sinus bradycardia in KCNQ1-linked short QT syndrome: insights from computational modelling. Front Physiol. 2018;9:1402. https://doi.org/10.3389/fphys.2018.01402.

123. Whittaker DG, Ni H, Benson AP, Hancox JC, Zhang H. Computational analysis of the mode of action of Disopyramide and quinidine on hERG-linked short QT syndrome in human ventricles. Front Physiol. 2017;8:759.

124. Whittaker DG, Hancox JC, Zhang H. In silico assessment of pharmacotherapy for human atrial patho-electrophysiology associated with hERG-linked short QT syndrome. Front Physiol. 2018;9:1888.

125. El Harchi A, McPate MJ, Zhang YH, Zhang H, Hancox JC. Action potential clamp and mefloquine sensitivity of recombinant I_{Ks} channels incorporating the V307L KCNQ1 mutation. J Physiol Pharmacol. 2010;61(2):123–31.

126. Grunnet M, Diness TG, Hansen RS, Olesen SP. Biophysical characterization of the short QT mutation hERG-N588K reveals a mixed gain-and loss-of-function. Cell Physiol Biochem. 2008;22(5–6):611–24.

127. Frea S, Giustetto C, Capriolo M, Scrocco C, Fornengo C, Benedetto S, et al. New echocardiographic insights in short QT syndrome: more than a channellopathy? Heart Rhythm. 2015;12:2095–105.

128. Hassel D, Scholz EP, Trano N, Friedrich O, Just S, Meder B, et al. Deficient zebrafish ether-a-go-go-related gene channel gating causes short-QT syndrome in zebrafish reggae mutants. Circulation. 2008;117(7):866–75.

129. Odening KE, Bodi I, Franke G, Rieke R, Ryan de MA, Perez-Feliz S, et al. Transgenic short-QT syndrome 1 rabbits mimic the human disease phenotype with QT/action potential duration shortening in the atria and ventricles and increased ventricular tachycardia/ventricular fibrillation inducibility. Eur Heart J. 2019;40:842–53.

130. Hancox JC, Zhang Y, Du C, Zhang H. Complementarity between Arrhythmia Mechanisms Found in Silico and in genetic models of N588K-hERG linked short QT syndrome. J Integr Cardiol Open Access. 2020;3(1):1–4. https://doi.org/10.31487/j.JICOA.2020.01.13.

131. El-Battrawy I, Lan H, Cyganek L, Zhao Z, Li X, Buljubasic F, et al. Modeling short QT syndrome using human-induced pluripotent stem cell-derived cardiomyocytes. J Am Heart Assoc. 2018;7(7):e007394.

132. Guo F, Sun Y, Wang X, Wang H, Gong T, Chen X, et al. Patient specific and gene corrected induced pluripotent stem-cell derived cardiomyocytes elucidate single cell phenotype of short QT syndrome. Circ Res. 2018;124:66–78.

133. Shinnawi R, Shaheen N, Huber I, Shiti A, Arbel G, Gepstein A, et al. Modeling reentry in the short QT syndrome with human-induced pluripotent stem cell-derived cardiac cell sheets. J Am Coll Cardiol. 2019;73(18):2310–24.

134. Schimpf R, Wolpert C, Bianchi F, Giustetto C, Gaita F, Bauersfeld U, et al. Congenital short QT syndrome and implantable cardioverter defibrillator treatment: inherent risk for inappropriate shock delivery. J Cardiovasc Electrophysiol. 2003;14(12):1273–7.

135. Schimpf R, Bauersfeld U, Gaita F, Wolpert C. Short QT syndrome: successful prevention of sudden cardiac death in an adolescent by implantable cardioverter-defibrillator treatment for primary prophylaxis. Heart Rhythm. 2005;2(4):416–7.

136. Bjerregaard P, Jahangir A, Gussak I. Targeted therapy for short QT syndrome. Expert Opin Ther Targets. 2006;10(3):393–400.

137. Duncan RS, McPate MJ, Ridley JM, Gao Z, James AF, Leishman DJ, et al. Inhibition of the HERG

potassium channel by the tricyclic antidepressant doxepin. Biochem Pharmacol. 2007;74:425–37.

138. Gaita F, Giustetto C, Bianchi F, Schimpf R, Haissaguerre M, Calo L, et al. Short QT syndrome: pharmacological treatment. J Am Coll Cardiol. 2004;43:1494–9.
139. Wolpert C, Schimpf R, Giustetto C, Antzelevitch C, Cordeiro JM, Dumaine R, et al. Further insights into the effect of quinidine in short QT syndrome caused by a mutation in HERG. J Cardiovas Electophysiol. 2005;16:54–8.
140. Weerapura M, Hebert TE, Nattel S. Dofetilide block involves interactions with open and inactivated states of HERG channels. Pflugers Arch. 2002;443:520–31.
141. Chen J, Seebohm G, Sanguinetti MC. Position of aromatic residues in the S6 domain, not inactivation, dictates cisapride sensitivity of HERG and eag potassium channels. Proc Natl Acad Sci U S A. 2002;99: 12329–33.
142. Witchel HJ. The hERG potassium channel as a therapeutic target. Expert Opin Ther Targets. 2007;11(3): 321–36.
143. Perrin MJ, Kuchel PW, Campbell TJ, Vandenberg JI. Drug binding to the inactivated state is necessary but not sufficient for high-affinity binding to human ether-à-go-go-related gene channels. Mol Pharmacol. 2008;74:1443–52.
144. McPate MJ, Duncan RS, Hancox JC, Witchel HJ. Pharmacology of the short QT syndrome N588K-hERG K^+ channel mutation: differential impact on selected class I and class III antiarrhythmic drugs. Br J Pharmacol. 2008;155:957–66.
145. McPate MJ, Duncan RS, Witchel HJ, Hancox JC. Disopyramide is an effective inhibitor of mutant HERG K+ channels involved in variant 1 short QT syndrome. J Mol Cell Cardiol. 2006;41:563–6.
146. Schimpf R, Veltmann C, Giustetto C, Gaita F, Borgreffe M, Wolpert C. In vivo effects of mutant HERG K^+ channel inhibition by disopyramide in patients with a short QT-1 syndrome: a pilot study. J Cardiovas Electophysiol. 2007;18:1157–60.
147. Nof E, Burashnikov A, Antzelevitch C. Cellular basis for atrial fibrillation in an experimental model of short QT1: implications for a pharmacological approach to therapy. Heart Rhythm. 2010;7(2): 251–7.
148. Lees-Miller JP, Duan Y, Teng GQ, Duff HJ. Molecular determinant of high affinity dofetilide binding to HERG1 expressed in Xenopus oocytes: involvement of S6 sites. Mol Pharmacol. 2000;57: 367–74.
149. Paul AA, Witchel HJ, Hancox JC. Inhibition of HERG potassium channel current by the Class 1a antiarrhythmic agent disopyramide. Biochem Biophys Res Comm. 2001;280:1243–50.
150. Zhao Z, Li X, El-Battrawy I, Lan H, Zhong R, Xu Q, et al. Drug testing in human-induced pluripotent stem cell-derived cardiomyocytes from a patient with short QT syndrome type 1. Clin Pharmacol Ther. 2019;106 (3):642–51.
151. Frommeyer G, Weller J, Ellermann C, Kaese S, Kochhauser S, Lange PS, et al. Antiarrhythmic properties of ivabradine in an experimental model of Short-QT- syndrome. Clin Exp Pharmacol Physiol. 2017;44:941–5.
152. Frommeyer G, Ellermann C, Dechering DG, Kochhauser S, Bogeholz N, Guner F, et al. Ranolazine and Vernakalant prevent ventricular arrhythmias in an experimental whole-heart model of short QT syndrome. J Cardiovasc Electrophysiol. 2016;27:1214–9.
153. Mazzanti A, Maragna R, Vacanti G, Kostopoulou A, Marino M, Monteforte N, et al. Hydroquinidine prevents life-threatening arrhythmic events in patients with short QT syndrome. J Am Coll Cardiol. 2017;70(24):3010–5.
154. Giustetto C, Schimpf R, Mazzanti A, Scrocco C, Maury P, Anttonen O, et al. Long-term follow-up of patients with short QT syndrome. J Am Coll Cardiol. 2011;58(6):587–95.
155. Villafane J, Atallah J, Gollob MH, Maury P, Wolpert C, Gebauer R, et al. Long-term follow-up of a pediatric cohort with short QT syndrome. J Am Coll Cardiol. 2013;61(11):1183–91.
156. El-Battrawy I, Besler J, Liebe V, Schimpf R, Tulumen E, Rudic B, et al. Long-term follow-up of patients with short QT syndrome: clinical profile and outcome. J Am Heart Assoc. 2018;7(23):e010073.
157. Mizobuchi M, Enjoji Y, Yamamoto R, Ono T, Funatsu A, Kambayashi D, et al. Nifekalant and disopyramide in a patient with short QT syndrome: evaluation of pharmacological effects and electrophysiological properties. Pace - Pacing Clin Electrophysiol. 2008;31:1229–32.
158. Lerche C, Bruhova I, Lerche H, Steinmeyer K, Wei AD, Strutz-Seebohm N, et al. Chromanol 293B binding in KCNQ1 (Kv7.1) channels involves electrostatic interactions with a potassium ion in the selectivity filter. Mol Pharmacol. 2007;71(6): 1503–11.
159. Lopez-Izquierdo A, Ponce-Balbuena D, Ferrer T, Sachse FB, Tristani-Firouzi M, Sanchez-Chapula JA. Chloroquine blocks a mutant Kir2.1 channel responsible for short QT syndrome and normalizes repolarization properties in silico. Cell Physiol Biochem. 2009;24(3–4):153–60.
160. Luo C, Wang K, Zhang H. Modelling the effects of chloroquine on KCNJ2-linked short QT syndrome. Oncotarget. 2017;8(63):106511–26.
161. Ji Y, Veldhuis MG, Zandvoort J, Romunde FL, Houtman MJC, Duran K, et al. PA-6 inhibits inward rectifier currents carried by V93I and D172N gain-of-function KIR2.1 channels, but increases channel protein expression. J Biomed Sci. 2017;24(1):44. https://doi.org/10.1186/s12929-017-0352-x.
162. Gallagher MM, Magliano G, Yap YG, Padula M, Morgia V, Postorino C, et al. Distribution and prognostic significance of QT intervals in the lowest half centile in 12,012 apparently healthy persons. Am J Cardiol. 2006;98(7):933–5.

163. Reinig MG, Engel TR. The shortage of short QT intervals. Chest. 2007;132(1):246–9.
164. Kobza R, Roos M, Niggli B, Abacherli R, Lupi GA, Frey F, et al. Prevalence of long and short QT in a young population of 41,767 predominantly male Swiss conscripts. Heart Rhythm. 2009;6(5):652–7.
165. Campuzano O, Fernandez-Falgueras A, Lemus X, Sarquella-Brugada G, Cesar S, Coll M, et al. Short QT syndrome: a comprehensive genetic interpretation and clinical translation of rare variants. J Clin Med. 2019;8(7):1035. https://doi.org/10.3390/jcm8071035.

Defects in Ankyrin-based Protein Targeting Pathways in Human Arrhythmia

27

Emma K. Dudley, Holly C. Sucharski, Sara N. Koenig, and Peter J. Mohler

Abstract

Ion channels and transporters regulate transmembrane electrochemical gradients to control cardiomyocyte depolarization/repolarization and cell excitability. Ion channel and transporter function depend on proper expression and localization within specific cellular membrane domains. Ankyrins are a family of proteins that are widely expressed in vertebrate tissues including the heart. Ankyrin-based cellular pathways are critical for ion channel and transporter membrane targeting in ventricular cardiomyocytes, atrial myocytes, and sinoatrial node cells, revealing their essential role in proper cardiac function. Moreover, findings in both mice and humans associate altered function in ankyrin-B with a variety of phenotypes, including fatal ventricular arrhythmias, ankyrin-B syndrome (distinct from long QT syndrome), atrial fibrillation, sinus node disease, sudden cardiac death, and arrhythmogenic right ventricular cardiomyopathy. While the molecular mechanisms of ankyrin-associated diseases remain to be clarified, it is posited that disruptions in ankyrin-based pathways have a range of distinct molecular repercussions such as altering typical calcium handling dynamics in excitable cells and possibly interfering with the Wnt/β-catenin signaling. In addition to *ANK2*-associated cardiac disease, dysfunction in ankyrin-G-based cellular pathways for voltage-gated Na_v channel targeting and regulation has also been associated with human arrhythmia. This chapter will focus on the cell biology of cardiac ankyrins in human arrhythmias.

Keywords

Ankyrin · Arrhythmia · Sinus node dysfunction · Ion channel · Na/Ca exchanger · Na/K ATPase · Long QT syndrome · Spectrin · $Na_v1.5$ · Sarcoplasmic reticulum · Transverse tubule · Sudden death · Genetics · Transporter

27.1 Introduction

Ankyrins are a family of adaptor proteins responsible for the organization of membrane-associated, cytoskeletal, and signaling proteins at specialized membrane domains. Ankyrins were first identified in 1978 as a key structural

---

Emma K. Dudley and Holly C. Sucharski contributed equally with all other contributors.

E. K. Dudley · H. C. Sucharski · S. N. Koenig · P. J. Mohler (✉)
Dorothy M. Davis Heart and Lung Research Institute, Columbus, OH, USA

Departments of Physiology and Cell Biology and Internal Medicine, Division of Cardiovascular Medicine, Frick Center for Heart Failure and Arrhythmia Research, The Ohio State University College of Medicine and Wexner Medical Center, Columbus, OH, USA
e-mail: peter.mohler@osumc.edu

© Springer Nature Switzerland AG 2023

O. N. Tripathi et al. (eds.), *Heart Rate and Rhythm*, https://doi.org/10.1007/978-3-031-33588-4_27

component of the erythrocyte membrane cytoskeleton [1]. Nearly a decade later, ankyrin defects were first linked with human hereditary spherocytosis due to the disruption of membrane surface tension of erythrocytes [2, 3]. Ankyrin proteins have since been shown to coordinate the physiological roles of a host of cell types including Purkinje neurons, epithelial cells, and pancreatic beta cells [4–7]. In the past twenty years, ankyrin function in excitable cardiomyocytes has been widely explored and continues to pose as a fruitful area of study in the underpinnings of cardiac physiology and pathology [8, 9].

Ankyrin polypeptides are derived from three human genes and exhibit divergent, nonoverlapping functions. Ankyrin-R polypeptides, encoded by *ANK1* on human chromosome 8p11, are the prototypic ankyrins first characterized from the erythrocyte cytoskeleton [10]. *ANK1* gene products are also expressed in neurons and muscle [11]. Ankyrin-B, encoded by *ANK2* on human chromosome 4q25–27, is expressed in most cell types including the brain and heart, where it regulates the spatial-temporal dynamics of cardiac function via the targeting of key ion handling proteins such as Na^+/Ca^{2+} exchanger (NCX) and Na^+/K^+-ATPase (NKA) [12, 13]. Ankyrin-G is encoded by *ANK3* on human chromosome 10q21. Similar to ankyrin-B, *ANK3* gene products are expressed in most vertebrate cells [14, 15]. Ankyrin-G, however, is expressed at the intercalated disc and t-tubules in ventricular cardiomyocytes and possesses select binding partners in the heart. For example, ankyrin-G is required for the specific targeting of the cardiac voltage-gated sodium channel ($Na_v1.5$) [8, 9].

In the heart, ventricular cardiomyocytes primarily express one isoform of ankyrin-B (220 kD ankyrin-B), and ankyrin-G (190 kD ankyrin-G) [16]. Splicing of ankyrin genes results in a spectrum of structurally- and functionally diverse polypeptides ranging in size from 26 to 480 kD. Small ankyrin isoforms lacking large regions of a canonical ankyrin may be localized to specialized membrane sites including the Golgi apparatus, lysosomes, and sarcoplasmic reticulum (SR) [8]. Ankyrin-B isoforms have been identified in the heart, where they exhibit distinct functions based upon their binding profiles. Specifically, 188kD ankyrin-B isoform acts to regulate NCX expression, whereas the 212 kD splice variant binds obscurin for proper formation at the M-line in cardiomyocytes [17]. In the brain, a 440-kD giant ankyrin-B splice variant has also recently been implicated in autism [18]. The 220 kD ankyrin-B is primarily localized to the M-line, transverse tubule (T-Tubule), and Z-line membranes and is to function as a cellular adaptor for targeting specific ion channels/transporters to t-tubule/sarcoplasmic reticulum membrane. Ankyrin-B targets Na^+/K^+-ATPase (NKA), inositol 1,4,5 trisphosphate receptor (IP_3R), and Na^+/Ca^{2+} exchanger (NCX) to specific membrane sites [8] (Fig. 27.1). Canonical ankyrin-G (190 kD) is localized at both ventricular cardiomyocyte intercalated disc and t-tubule membrane domains. Ankyrin-G isoforms also display importance in proper neuronal structure and function, where the giant 480-kD isoform plays an integral role in the arrangement of the axon initial segment (AIS) in the brain [19].

Canonical ankyrins (190–220 kD) are comprised of four distinct structural domains including a membrane-binding domain (MBD) of 24 *ANK* repeats, a spectrin-binding domain (SBD), a death domain (DD), and a C-terminal domain (CTD) (Fig. 27.1). The ankyrin MBD is distinguished by its alpha-helical structure [4, 20] and interacts with a host of diverse membrane proteins including ion channels, transporters, pumps, and cell adhesion molecules including NKA, voltage-gated Na^+ and K^+ channels, NCX, IP_3R, the anion exchanger, CD44, and E-cadherin [21, 22]. In fact, microdomains within the ankyrin MBD may allow for the formation of large homomeric and heteromeric protein complexes to orchestrate large structural and signaling complexes essential for proper cardiac rhythm [8].

While the ankyrin SBD has been shown to have critical roles in linking ankyrin-associated membrane proteins with the spectrin- and actin-based cytoskeleton [23], this large domain interacts with key signaling proteins. For example, the SBD of ankyrin-B interacts with the

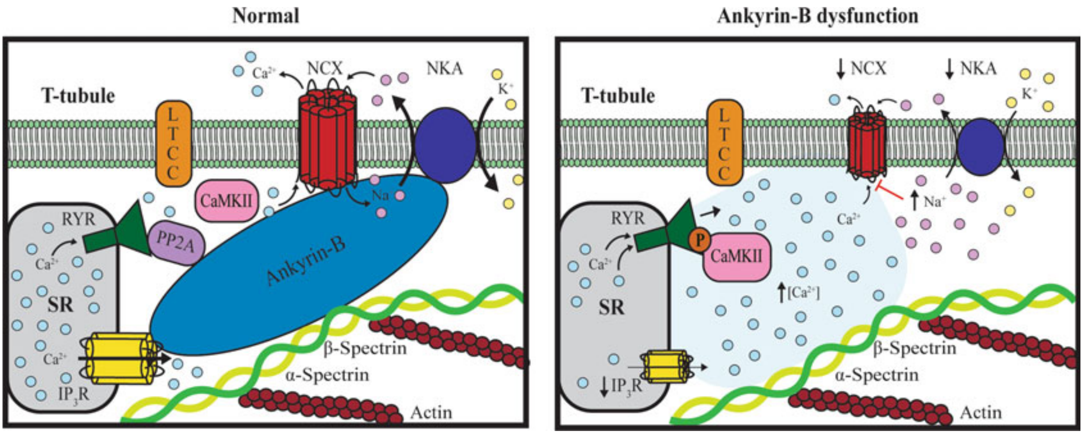

Fig. 27.1 Ankyrin-B membrane domains associated with protein complexes in the cardiomyocyte. Ankyrins are comprised of four major structural domains including the membrane-binding domain (MBD), the spectrin-binding domain (SBD), the C-terminal domain (CTD), and the death domain (DD). Together, the CTD and DD comprise the regulatory domain. Ankyrin-B targets cardiac ion channels and transporters (Na^+/K^+-ATPase, Na^+/Ca^{2+} exchanger, IP_3R), key structural proteins (β-spectrin, obscurin, β-catenin), and signaling molecules (PP2A)

targeting subunit (B56α) of the protein phosphatase 2A (PP2A) protein complex, facilitating its interaction with the ryanodine receptor (RYR) [24]. In fact, loss of ankyrin-B impairs PP2A targeting to specific membrane domains in ventricular cardiomyocytes which may alter local signaling and calcium handling in the cardiomyocyte [24]. The ankyrin SBD is the site of select human *ANK2* loss-of-function variants associated with arrhythmia which is likely attributed to alterations in RYR phosphorylation from reduced PP2A activity [25].

The ankyrin DD and CTD comprise the ankyrin regulatory domain (RD) that mediates both ankyrin intramolecular interactions as well as with proteins including obscurin, the MBD, and HSP40 in ankyrin-B [26–28]. In fact, ankyrin-B interacts with the large Rho-GEF, obscurin, and is critical for the subcellular localization of PP2A in cardiomyocytes [24]. In addition, the ankyrin RD modulates intramolecular interactions that may serve an autoregulatory function (Fig. 27.1). For example, the ankyrin-B DD is thought to allow for auto-inhibition via direct interaction with a specific region of the SBD [29]. Furthermore, inter-domain interactions between the ankyrin-B MBD and CTD have been shown to regulate intermolecular interactions that confer isoform-specific functionality [8]. Finally, although the ankyrin DD and CTD tend to be highly divergent, multiple human *ANK2* loss-of-function arrhythmia variants have been identified in the RD, and further supports a critical role for this ankyrin region in normal cardiac function [8, 25].

27.2 Ankyrin Dysfunction in Human Arrhythmia

Since the early 2000s, links between ankyrin dysfunction and human cardiac disease have been continuously identified, solidifying the importance of ankyrin polypeptides in healthy cardiac function. The next sections will review the association of human cardiac disease and ankyrin-based cellular pathways.

27.2.1 Ankyrin-B Dysfunction in Human Ventricular Arrhythmia

Long QT syndrome (LQTS) is a heterogeneous group of inherited arrhythmias characterized by prolonged QT_C intervals on the electrocardiogram (ECG) and increased likelihood for sudden death [30]. Variants in the three genes (*KCNQ1*, *KCNH2*, and *SCN5A*) account for the majority of clinical LQTS cases [31]. The atypical, type 4 long QT syndrome (type 4 LQTS) was described first by Schott et al in 1995 in a large French kindred with a complex cardiac phenotype including sinus bradycardia, abnormal heart rate variability, atrial fibrillation, long QT interval, and sudden cardiac death [32]. Specifically, an *ANK2* missense variant was identified in the affected individuals and resulted in the substitution of glycine for a highly conserved glutamic acid at residue 1425 (E1425G) near the C-terminus of the SBD [8]. Today, based on additional clinical data, we no longer refer to *ANK2* as a "long QT" associated gene. Instead, we now refer to this as "ankyrin-B syndrome". It is likely that both environmental determinants and secondary genetic variants dictate the phenotype in ankyrin-B-associated disease, as familial ankyrin-B syndrome often presents with incomplete penetrance and phenotypic variability.

Recently, rare *ANK2* variants have also been associated with cases of arrhythmogenic right ventricular cardiomyopathy (ARVC), a disease that is typically associated with desmosomal protein variants. Roberts et al identified ARVC in a male proband harboring an AnkB-p.Glu1458Gly variant. The group went on to screen another ARVC family, where an AnkB-p.Met1988Thr variant was found to segregate with disease. Notably, cardiac tissue exhibited clear signs of ankyrin dysfunction, with altered NCX and ankyrin-B targeting. While desmosomal structure appeared normal in cardiac tissue from ARVC probands, β-catenin expression at the intercalated disc was significantly altered. Binding studies revealed a novel interaction between ankyrin-B and β-catenin, presenting a distinct pathway of ARVC pathogenesis and a possible therapeutic option for ARVC through upregulation of the β-catenin/Wnt signaling pathway [33].

To date, distinct *ANK2* loss-of-function variants have been identified in patient populations associated with a range of cardiovascular disease and clinical severity [8, 25, 33, 34]. At the cellular level, *ANK2* variants have been identified that demonstrate loss-of-function activity for ankyrin-B in cardiomyocytes [8]. The clinical phenotypes associated with these variants range from no obvious symptoms to sudden death. In fact, different variants result in different degrees of ankyrin-B loss of function in vitro that correlate with the clinical severity [8].

The clinical phenotypes in individuals heterozygous for *ANK2* variants include severe bradycardia, idiopathic ventricular fibrillation, atrial fibrillation, and polyphasic T waves on the ECG [8]. Interestingly, prolongation of the QT interval is not a consistent finding in individuals heterozygous for ankyrin-B loss of function, giving rise to the name "ankyrin-B syndrome" instead of LQT4 syndrome. However, despite inconsistencies in QT_c, individuals heterozygous for ankyrin-B loss-of-function variants may be susceptible to arrhythmias [8].

27.2.2 Ankyrin-B Dysfunction and Human Sinus Node Disease

In addition to association with severe ventricular arrhythmias, ankyrin-B plays an unexpected, but important role in regulation of sinoatrial node (SAN) automaticity [8]. Sinus node dysfunction (SND) is a highly prevalent condition affecting individuals of all ages but is more common with increasing age [35]. This common clinical identity leads to bradycardia and syncope and accounts for approximately half of pacemaker implantations in the United States [36]. SND has been thought to be mostly caused by fibrous tissue replacing the nodal tissue, although the etiology of the disease is far from being fully understood [37]. Work on familial forms of this disease has elucidated single gene defects associated with ion channels [38–40]. Two families with severe and highly penetrant SND were mapped to the general *ANK2* locus. In one family, affected individuals carried the E1425G *ANK2* variant. In a second family, affected individuals were carriers of a mutual haplotype at the *ANK2* locus although to date, no variant has been identified [8]. Ankyrin-related SND has furthermore been studied in a single proband demonstrating concomitant SND, prolonged QT_c, and atrial fibrillation [41]. The molecular mechanisms underlying SND due to ankyrin-B dysfunction are unknown. Based on the spectrum of cardiac phenotypes displayed by carriers of different polymorphisms, the molecular phenotype is likely to be complex involving multiple protein partners in the sinus node cell. In summary, ankyrin dysfunction represents a distinct collection of cardiovascular illnesses including sick sinus syndrome with bradycardia, ventricular arrhythmias, and risk of sudden death.

27.2.3 Physiological and Cellular Roles of Ankyrin-B in the Ventricle

Ankyrin-$B^{+/-}$ mice have served as a robust tool for elucidating the role of ankyrin-B in human arrhythmia. Ankyrin-B homozygous knock-out mice die shortly after birth [13]; however, ankyrin-$B^{+/-}$ mice are viable and display a number of cardiac phenotypes similar to individuals heterozygous for the ankyrin-B E1425G variant. Specifically, ankyrin-$B^{+/-}$ mice display significant bradycardia and exhibit a high degree of heart rate variability compared to wild-type mice. Similar to many patients with ankyrin-B syndrome, ankyrin-$B^{+/-}$ mice display significant QT_c prolongation and episodes of intermittent isorhythmic atrioventricular dissociation compared to wild-type littermates [8]. Select individuals harboring the ankyrin-B E1425G loss of function variant have experienced sudden death following physical exertion [8]. Likewise, ankyrin-$B^{+/-}$ mice but not wild-type littermates subjected to exercise followed by epinephrine injection are predisposed to sudden death [8]. In summary, ankyrin-$B^{+/-}$ mice, similar to patients with human ankyrin-B syndrome, display severe bradycardia, prolonged QT interval, heart rate variability, syncope, polymorphic ventricular arrhythmia, and sudden cardiac death in response to catecholaminergic stimulation.

Cardiac-specific murine models have been utilized to further characterize ankyrin-B loss-of-function mutations. Roberts et al. selectively knocked out cardiac ankyrin-B using a Cre/LoxP system under the direction of the αMHC promoter. These mice demonstrate both structural and electrical phenotypes, including decreased ejection fraction, decreased fractional shortening, sinus bradycardia, VT and trigamy upon catecholamine challenge, and premature death. This phenotype is notably in line with symptoms from human ARVC patients with *ANK2* variants, elucidating a critical link between ankyrin function and cardiac structure [33].

Studies in isolated ankyrin-$B^{+/-}$ cardiomyocytes have provided important information regarding the underlying ionic mechanism for arrhythmias in ankyrin-B-deficient mice and human patients with ankyrin-B mutations. Reduced expression of ankyrin-B in ankyrin-$B^{+/-}$ ventricular cardiomyocytes results in reduced expression and abnormal localization of ankyrin-B-associated proteins including Na^+/K^+-ATPase, Na^+/Ca^{2+} exchanger, and IP_3 receptor (Fig. 27.2) [8]. Decreased ankyrin-B function results in a reduced Na^+/Ca^{2+} exchange activity through direct and indirect mechanisms. Reduced Na^+/K^+-ATPase activity increases cytosolic Na^+ concentration, that inhibits the activity of Ca^{2+} export via the Na^+/Ca^{2+} exchanger, similar to the activity of digitalis [42]. In addition, reduced ankyrin-B function directly alters the membrane expression and localization of the Na^+/Ca^{2+} exchanger [8]. This likely further reduces extracellular Ca^{2+} export via the Na^+/Ca^{2+} exchanger, resulting in elevated SR Ca^{2+} stores and increased propensity for spontaneous Ca^{2+} release. Indeed, new models of ankyrin-$B^{+/-}$ cardiomyocytes predict an increase in Ca^{2+} sparks due to the uncoupling of Na^+/Ca^{2+} exchanger from the Na^+/K^+-ATPase, which subsequently induce ionic imbalances that could underlie arrhythmia (Fig. 27.2) [43]. Furthermore, ankyrin-$B^{+/-}$ cells display elevated SR Ca^{2+} stores and catecholamine-induced afterdepolarizations that may result in extrasystoles and even arrhythmia at the level of the whole heart [8].

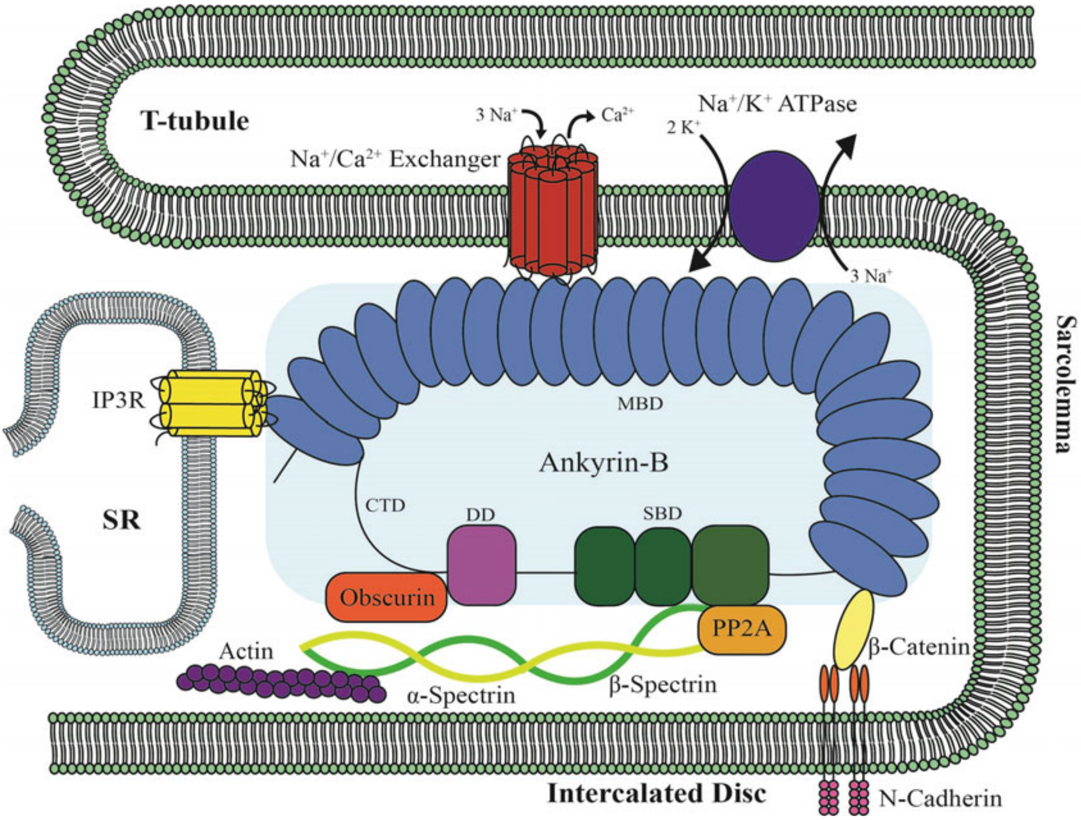

Fig. 27.2 Mechanism for Ankyrin-B-based arrhythmias. Comparison of cardiomyocyte signaling changes with loss of ankyrin-B and wild-type ankyrin-B. Deficiency of ankyrin-B has been shown to decrease the expression and normal localization of Na/K ATPase (NKA), Na/Ca exchanger (NCX), and IP_3R, ultimately resulting in altered SR calcium load. The decrease in expression and localization of NKA results in a Na^+ accumulation that prevents exchange of Ca^{2+} through NCX. Also, the altered ankyrin-B dependent-targeting of PP2A disrupts the PP2A/CaMKII balance favoring RYR hyperphosphorylation and leading to increased Ca^{2+} in the cytoplasm. At the tissue level, these cellular events support arrhythmia particularly in response to catecholamines

27.2.4 Physiological and Cellular Roles of Ankyrin-B in the Sinus Node

In addition to the ventricle, dysfunction in ankyrin-B protein targeting leads to loss of cytosolic Ca^{2+} regulation in the sinoatrial node [8]. Precise handling of cytosolic Ca^{2+} is essential for normal SAN function and thus electrical automaticity of the SAN [44]. Ankyrin-B is expressed in SAN cells and is necessary for the localization and membrane expression of the voltage-gated Ca^{2+} channel, $Ca_v1.3$, in addition to the Na^+/Ca^{2+} exchanger, Na^+/K^+-ATPase and IP_3 receptor [8]. Action potential rate reduction and increased rate variability in ankyrin-$B^{+/-}$ SAN cells were observed compared to wild type (WT) cells [8]. Previous studies have reported a similar cellular phenotype and spontaneous SAN arrhythmias in mice lacking $Ca_v1.3$ [45]. I_{NCX} has also been shown to be important for SAN automaticity. Specifically, Na^+/Ca^{2+} exchanger knockout mice die before birth with significant heart rate defects [46, 47]. These data suggest that defects in ankyrin-$B^{+/-}$ mouse SAN automaticity may be in large part due to loss of ankyrin-B targeting of $Ca_v1.3$ and Na^+/Ca^{2+} exchanger.

Finally, in addition to sinus node disease and ventricular arrhythmias, individuals carrying

ANK2 variants may display atrial fibrillation [8, 41]. The molecular basis for atrial fibrillation associated with ankyrin dysfunction is currently unknown. However, based on findings in other cardiac excitable cell types, it is logical to postulate that loss of ankyrin targeting of key membrane and signaling proteins may represent the underlying cause. The link between ankyrin dysfunction and human atrial fibrillation is an exciting and obvious future direction for the field.

27.2.5 Ankyrin-G Dysfunction and Human Brugada Syndrome

Ankyrin-G is vital for the organization of functionally related proteins at the cardiac intercalated disc through the facilitation of Na^+ channel targeting [8]. Experiments from cerebellar-specific ankyrin-G knockout mice reveal that ankyrin-G deficiency results in abnormal expression and localization of neuronal Na_v channels [48]. Biochemical experiments demonstrate that, through direct binding, ankyrin-G and $Na_v1.5$ colocalize at the intercalated disc and T-tubule membranes of ventricular cardiomyocytes, where ankyrin-G expression is required for $Na_v1.5$ targeting [8]. As a result of deficient targeting, Na^+ current is reduced in ankyrin-G conditional knock out mice and reduced to nonexistent in ankyrin-G null myocytes. Moreover, $Na_v1.5$ recruitment is an exclusive function of ankyrin-G, as ankyrin-B-deficient cardiomyocytes do not display significant loss of $Na_v1.5$ expression [8]. Makara et al identified that ankyrin-G is necessary for targeting of calcium/calmodulin-dependent protein kinase II (CaMKII), a known regulator of $Na_v1.5$, to the intercalated disc in cardiac-specific ankyrin-G−/− mice [9]. These mice also display loss of βIV spectrin as well as alterations to plakophilin-2, suggesting that recruitment of $Na_v1.5$ by ankyrin-G permits the formation of larger signaling structures at the intercalated disc. Importantly, these ankyrin-G cKO mice exhibit a range of electrical irregularities, including bradycardia and QRS prolongation [8]. Ankyrin-G has also been shown to recruit both K_{ATP} and Na^+ channels to the intercalated disc in rats, where ankyrin-G and not ankyrin-B colocalizes with these ion channels [49]. In the context of the whole heart, decreased Na^+ current may reduce membrane excitability, resulting in slow and discontinuous conduction favorable to the initiation and maintenance of arrhythmias [50].

The Brugada syndrome, first described in 1992, is an autosomal-dominant potentially fatal cardiac arrhythmia characterized by ST segment elevation in the right precordial leads, right bundle branch block and T wave inversions on the ECG [51]. Affected individuals are at high risk of death as a result of ventricular tachycardia or fibrillation despite having structurally normal hearts [51]. Typically, the syndrome manifests itself in adulthood, though cases have been reported in children and in the elderly [52]. Variants in the *SCN5A* gene that encodes for $Na_v1.5$ are associated with a host of Brugada syndrome cases [53]. Specifically, *SCN5A*-associated variants are hypothesized to affect the biophysical properties of the sodium channel resulting in reduced, or inconsistent inward I_{Na}. Recent work demonstrates a link between ankyrin-G, $Na_v1.5$, and the Brugada syndrome. Specifically, *SCN5A* variants that block association of $Na_v1.5$ with ankyrin-G have been associated with human Brugada syndrome probands [8]. In fact, $Na_v1.5$ E1053K that blocks ankyrin-G-association is ineffectively targeted to the cardiomyocyte intercalated disc consistent with reduced I_{Na} and the Brugada syndrome phenotype associated with this variant [54]. Together, these findings illustrate a key role for ankyrin-G in myocyte ion channel targeting to the intercalated disc. Moreover, these studies demonstrate that dysfunction of the ankyrin-G-based protein targeting pathway may result in defects in normal physiology and human disease.

In addition to its role as a targeting protein, ankyrin-G serves as a structural component in various cell types. In epithelial cells, ankyrin-G directly interacts with a cell adhesion protein, E-cadherin, and is required for its localization to the lateral membrane [5, 55]. This interaction is critical for maintaining cell–cell adhesion. N-cadherin, found in both neural and cardiac tissues, may also interact with ankyrin-G in vivo [5, 55]. Inappropriate N-cadherin expression at the intercalated disc in cardiomyocytes may disrupt mechanical adhesion and electrical communication between cells and predispose the heart to arrhythmias [56, 57]. These observations further suggest the critical importance of ankyrin-G as a component of cell adhesion assemblies as well as in channel and transporter targeting. The potential role of ankyrin-G for protein organization at the myocyte intercalated disc is an important future direction for the field.

27.3 Conclusion

Cardiac ankyrin polypeptides have been recognized as key components in targeting transporters and ion channels in the cardiomyocyte. Ankyrin-B-based targeting pathways are essential for handling cytosolic calcium and thus play a major role in the normal physiology of excitable cells. Dysfunction in cardiac ankyrins is associated with several clinically relevant arrhythmias as well as sick sinus syndrome, bradycardia, atrial fibrillation, ventricular arrhythmias, arrhythmogenic cardiomyopathy, and risk of sudden death. Similarly, defects in ankyrin-G-based pathways in cardiomyocytes are associated with a Brugada syndrome-like phenotype, an autosomal-dominant disease associated with sudden death. These points further underline the importance of ankyrins in normal cardiovascular function. However, while these findings illustrate the importance of cardiac ankyrins, there is a great deal still unknown. In fact, as ankyrins organize a host of key signaling, ion transport, and structural components of the myocyte, these molecules may ultimately represent an unexpected, but potentially powerful therapeutic target for modulation of cellular excitability in cardiac rhythm disorders.

References

1. Bennett V. Purification of an active proteolytic fragment of the membrane attachment site for human erythrocyte spectrin. J Biol Chem. 1978;253(7):2292–9.
2. Eber SW, Gonzalez JM, Lux ML, Scarpa AL, Tse WT, Dornwell M, et al. Ankyrin-1 mutations are a major cause of dominant and recessive hereditary spherocytosis. Nat Genet. 1996;13(2):214–8.
3. Palek J. Hereditary elliptocytosis, spherocytosis and related disorders: consequences of a deficiency or a mutation of membrane skeletal proteins. Blood Rev. 1987;1(3):147–68.
4. Bennett V, Baines AJ. Spectrin and ankyrin-based pathways: metazoan inventions for integrating cells into tissues. Physiol Rev. 2001;81(3):1353–92.
5. Kizhatil K, Bennett V. Lateral membrane biogenesis in human bronchial epithelial cells requires 190-kDa Ankyrin-G. J Biol Chem. 2004;279(16):16706–14.
6. Kizhatil K, Sandhu NK, Peachey NS, Bennett V. Ankyrin-B is required for coordinated expression of beta-2-spectrin, the Na/K-ATPase and the Na/Ca exchanger in the inner segment of rod photoreceptors. Exper Eye Rs. 2009;88(1):57–64.
7. Kizhatil K, Yoon W, Mohler PJ, Davis LH, Hoffman JA, Bennett V. Ankyrin-G and beta2-Spectrin collaborate in biogenesis of lateral membrane of human bronchial epithelial cells. J Biol Chem. 2007;282(3):2029–37.
8. Curran J, Mohler PJ. Alternative paradigms for ion channelopathies: disorders of ion channel membrane trafficking and posttranslational modification. Annu Rev Physiol. 2015;77:505–24.
9. Makara MA, Curran J, Lubbers ER, Murphy NP, Little SC, Musa H, et al. Novel mechanistic roles for Ankyrin-G in cardiac remodeling and heart failure. JACC Basic Transl Sci. 2018;3(5):675–89.
10. Lambert S, Yu H, Prchal JT, Lawler J, Ruff P, Speicher D, et al. cDNA sequence for human erythrocyte ankyrin. Proc Natl Acad Sci U S A. 1990;87(5):1730–4.
11. Lambert S, Bennett V. Postmitotic expression of ankyrinR and beta R-spectrin in discrete neuronal populations of the rat brain. J Neurosci. 1993;13(9):3725–35.
12. Otto E, Kunimoto M, McLaughlin T, Bennett V. Isolation and characterization of cDNAs encoding human brain ankyrins reveal a family of alternatively spliced genes. J Cell Biol. 1991;114(2):241–53.
13. Scotland P, Zhou D, Benveniste H, Bennett V. Nervous system defects of AnkyrinB (−/−) mice suggest functional overlap between the cell adhesion molecule L1 and 440-kD AnkyrinB in premyelinated axons. J Cell Biol. 1998;143(5):1305–15.
14. Kordeli E, Lambert S, Bennett V, Ankyrin G. A new ankyrin gene with neural-specific isoforms localized at the axonal initial segment and node of Ranvier. J Biol Chem. 1995;270(5):2352–9.
15. Kordeli E, Ludosky MA, Deprette C, Frappier T, Cartaud J. AnkyrinG is associated with the postsynaptic membrane and the sarcoplasmic reticulum in the skeletal muscle fiber. J Cell Sci. 1998;111(Pt 15):2197–207.

16. Tuvia S, Buhusi M, Davis L, Reedy M, Bennett V. Ankyrin-B is required for intracellular sorting of structurally diverse Ca2+ homeostasis proteins. J Cell Biol. 1999;147(5):995–1008.
17. Wu HC, Yamankurt G, Luo J, Subramaniam J, Hashmi SS, Hu H, et al. Identification and characterization of two ankyrin-B isoforms in mammalian heart. Cardiovasc Res. 2015;107(4):466–77.
18. Kunimoto M, Otto E, Bennett V. A new 440-kD isoform is the major ankyrin in neonatal rat brain. J Cell Biol. 1991;115(5):1319–31.
19. Jenkins PM, Kim N, Jones SL, Tseng WC, Svitkina TM, Yin HH, et al. Giant ankyrin-G: a critical innovation in vertebrate evolution of fast and integrated neuronal signaling. Proc Natl Acad Sci U S A. 2015;112(4):957–64.
20. Michaely P, Tomchick DR, Machius M, Anderson RGW. Crystal structure of a 12 ANK repeat stack from human ankyrinR. EMBO J. 2002;21(23): 6387–96.
21. Li ZP, Burke EP, Frank JS, Bennett V, Philipson KD. The cardiac Na+-Ca2+ exchanger binds to the cytoskeletal protein ankyrin. J Biol Chem. 1993;268 (16):11489–91.
22. Malhotra JD, Kazen-Gillespie K, Hortsch M, Isom LL. Sodium channel beta subunits mediate homophilic cell adhesion and recruit ankyrin to points of cell-cell contact. J Biol Chem. 2000;275(15):11383–8.
23. Bennett V, Stenbuck PJ. Identification and partial purification of ankyrin, the high affinity membrane attachment site for human erythrocyte spectrin. J Biol Chem. 1979;254(7):2533–41.
24. Curran J, Mohler PJ. Coordinating electrical activity of the heart: ankyrin polypeptides in human cardiac disease. Expert Opin Ther Targets. 2011;15(7):789–801.
25. Zhu W, Wang C, Hu J, Wan R, Yu J, Xie J, et al. Ankyrin-B Q1283H variant linked to arrhythmias via loss of local protein phosphatase 2A activity causes ryanodine receptor hyperphosphorylation. Circulation. 2018;138(23):2682–97.
26. Kontrogianni-Konstantopoulos A, Catino DH, Strong JC, Sutter S, Borisov AB, Pumplin DW, et al. Obscurin modulates the assembly and organization of sarcomeres and the sarcoplasmic reticulum. FASEB J. 2006;20(12):2102–11.
27. Hall TG, Bennett V. Regulatory domains of erythrocyte ankyrin. J Biol Chem. 1987;262(22):10537–45.
28. Davis LH, Davis JQ, Bennett V. Ankyrin regulation: an alternatively spliced segment of the regulatory domain functions as an intramolecular modulator. J Biol Chem. 1992;267(26):18966–72.
29. Wang C, Yu C, Ye F, Wei Z, Zhang M. Structure of the ZU5-ZU5-UPA-DD tandem of ankyrin-B reveals interaction surfaces necessary for ankyrin function. Proc Natl Acad Sci U S A. 2012;109(13):4822–7.
30. Moss AJ, Schwartz PJ, Crampton RS, Locati E, Carleen E. The long QT syndrome: a prospective international study. Circulation. 1985;71(1):17–21.
31. Splawski I, Shen J, Timothy KW, Lehmann MH, Priori S, Robinson JL, et al. Spectrum of mutations in long-QT syndrome genes. KVLQT1, HERG, SCN5A, KCNE1, and KCNE2. Circulation. 2000;102(10):1178–85.
32. Schott JJ, Charpentier F, Peltier S, Foley P, Drouin E, Bouhour JB, et al. Mapping of a gene for long QT syndrome to chromosome 4q25-27. Am J Human Genet. 1995;57(5):1114–22.
33. Roberts JD, Murphy NP, Hamilton RM, Lubbers ER, James CA, Kline CF, et al. Ankyrin-B dysfunction predisposes to arrhythmogenic cardiomyopathy and is amenable to therapy. J Clin Invest. 2019;129(8): 3171–84.
34. Derbala MH, Guo AS, Mohler PJ, Smith SA. The role of betaII spectrin in cardiac health and disease. Life Sci. 2018;192:278–85.
35. Rubenstein JJ, Schulman CL, Yurchak PM, DeSanctis RW. Clinical spectrum of the sick sinus syndrome. Circulation. 1972;46(1):5–13.
36. Adan V, Crown LA. Diagnosis and treatment of sick sinus syndrome. Am Fam Phys. 2003;67(8):1725–32.
37. Demoulin JC, Kulbertus HE. Histopathological correlates of sinoatrial disease. Br Heart J. 1978;40 (12):1384–9.
38. Benson DW, Wang DW, Dyment M, Knilans TK, Fish FA, Strieper MJ, et al. Congenital sick sinus syndrome caused by recessive mutations in the cardiac sodium channel gene (SCN5A). J Clin Invest. 2003;112(7): 1019–28.
39. Smits JP, Koopmann TT, Wilders R, Veldkamp MW, Opthof T, Bhuiyan ZA, et al. A mutation in the human cardiac sodium channel (E161K) contributes to sick sinus syndrome, conduction disease and Brugada syndrome in two families. J Mol Cell Cardiol. 2005;38(6): 969–81.
40. Ueda K, Nakamura K, Hayashi T, Inagaki N, Takahashi M, Arimura T, et al. Functional characterization of a trafficking-defective HCN4 mutation, D553N, associated with cardiac arrhythmia. J Biol Chem. 2004;279(26):27194–8.
41. Robaei D, Ford T, Ooi S-Y. Ankyrin-B syndrome: a case of sinus node dysfunction, atrial fibrillation and prolonged QT in a young adult. Heart Lung Circ. 2015;24(2):e31–e4.
42. Akera T, Brody TM. The role of Na+,K+-ATPase in the inotropic action of digitalis. Pharmacol Rev. 1977;29(3):187–220.
43. Chu L, Greenstein JL, Winslow RL. Na+ microdomains and sparks: role in cardiac excitation-contraction coupling and arrhythmias in ankyrin-B deficiency. J Mol Cell Cardiol. 2019;128:145–57.
44. Kodama I, Nikmaram MR, Boyett MR, Suzuki R, Honjo H, Owen JM. Regional differences in the role of the Ca2+ and Na+ currents in pacemaker activity in the sinoatrial node. Am J Phys. 1997;272(6 Pt 2): H2793–806.
45. Mangoni ME, Couette B, Bourinet E, Platzer J, Reimer D, Striessnig J, et al. Functional role of L-type Cav1.3 Ca2+ channels in cardiac pacemaker activity. Proc Natl Acad Sci U S A. 2003;100(9): 5543–8.

46. Bogdanov KY, Maltsev VA, Vinogradova TM, Lyashkov AE, Spurgeon HA, Stern MD, et al. Membrane potential fluctuations resulting from submembrane Ca2+ releases in rabbit sinoatrial nodal cells impart an exponential phase to the late diastolic depolarization that controls their chronotropic state. Circ Res. 2006;99(9):979–87.
47. Wakimoto K, Kobayashi K, Kuro OM, Yao A, Iwamoto T, Yanaka N, et al. Targeted disruption of Na+/Ca2+ exchanger gene leads to cardiomyocyte apoptosis and defects in heartbeat. J Biol Chem. 2000;275(47):36991–8.
48. Zhou D, Lambert S, Malen PL, Carpenter S, Boland LM, Bennett V. AnkyrinG is required for clustering of voltage-gated Na channels at axon initial segments and for normal action potential firing. J Cell Biol. 1998;143(5):1295–304.
49. Yang HQ, Perez-Hernandez M, Sanchez-Alonso J, Shevchuk A, Gorelik J, Rothenberg E, et al. Ankyrin-G mediates targeting of both Na(+) and KATP channels to the rat cardiac intercalated disc. elife. 2020;9:e52373.
50. Shaw RM, Rudy Y. Ionic mechanisms of propagation in cardiac tissue. Roles of the sodium and L-type calcium currents during reduced excitability and decreased gap junction coupling. Circ Res. 1997;81(5):727–41.
51. Brugada P, Brugada J. Right bundle branch block, persistent ST segment elevation and sudden cardiac death: a distinct clinical and electrocardiographic syndrome. A multicenter report. J Am Coll Cardiol. 1992;20(6):1391–6.
52. Antzelevitch C, Brugada P, Borggrefe M, Brugada J, Brugada R, Corrado D, et al. Brugada syndrome: report of the second consensus conference. Heart Rhythm. 2005;2(4):429–40.
53. Smits JP, Eckardt L, Probst V, Bezzina CR, Schott JJ, Remme CA, et al. Genotype-phenotype relationship in Brugada syndrome: electrocardiographic features differentiate SCN5A-related patients from non-SCN5A-related patients. J Am Coll Cardiol. 2002;40(2):350–6.
54. Priori SG, Napolitano C, Gasparini M, Pappone C, Bella PD, Giordano U, et al. Natural history of Brugada syndrome. Circulation. 2002;105(11):1342–7.
55. Kizhatil K, Davis JQ, Davis L, Hoffman J, Hogan BL, Bennett V. Ankyrin-G is a molecular partner of E-cadherin in epithelial cells and early embryos. J Biol Chem. 2007;282(36):26552–61.
56. Li J, Levin MD, Xiong Y, Petrenko N, Patel VV, Radice GL. N-cadherin haploinsufficiency affects cardiac gap junctions and arrhythmic susceptibility. J Mol Cell Cardiol. 2008;44(3):597–606.
57. Li J, Patel VV, Kostetskii I, Xiong Y, Chu AF, Jacobson JT, et al. Cardiac-specific loss of N-cadherin leads to alteration in connexins with conduction slowing and arrhythmogenesis. Circ Res. 2005;97(5):474–81.

Part VI

Novel Antiarrhythmic Approaches

28

Ion Channels as Drug Targets in Atrial Fibrillation

Ursula Ravens and Rémi Peyronnet

Abstract

Atrial fibrillation is triggered when an abnormal electrical impulse encounters a substrate that allows initiation of re-entry. The arrhythmia has a strong tendency to become persistent due to structural and electrical remodeling. Currently available antiarrhythmic drugs are not sufficiently effective and are burdened by cardiac and extracardiac side effects that may offset their therapeutic benefits. Detailed knowledge about the mechanisms leading to generation and maintenance of arrhythmias may lead to the discovery of new targets for pharmacological interventions. These could include atria-selective ion channels (e.g., Nav1.5 ($I_{Na,}$), Kv1.5 (I_{Kur}), Kir3.1/3.4 ($I_{K,ACh}$), TASK-1 (I_{TASK-1}), and SK ($I_{K,Ca}$) channels, pathology-selective ion channels (constitutively active Kir3.x, TRP channels), ischemia-uncoupled gap junctions, proteins related to malfunctioning intracellular Ca^{2+} homeostasis (e.g., "leaky" ryanodine receptors, overactive Na^+,Ca^{2+} exchanger), or risk factors for arrhythmias ("upstream" therapies). In this chapter, ion channels as drug targets for atrial fibrillation will be discussed in the context of the remodeled atria.

Keywords

Atrial fibrillation · Electrical and structural remodeling · Atria-selective drugs · Nonconventional cardiac ion channels

28.1 Introduction

Atrial fibrillation (AF) is initiated when abnormal focal electrical activity encounters a suitable substrate that allows re-entry propagation. AF is often associated with cardiovascular disease, especially hypertension, heart failure, valve disease, coronary artery disease or non-cardiac disease such as diabetes, obesity, inflammatory disease, and old age, alcohol consumption, and physical inactivity are risk factors [1]. Nevertheless, about one-third of the patients have so-called "lone" AF without known underlying heart disease. Current pharmacological therapy is often

---

U. Ravens (✉)
Department of Pharmacology and Toxicology, Medical Faculty Carl Gustav Carus, Dresden University of Technology, Dresden, Germany

Institute for Experimental Cardiovascular Medicine, University Heart Center Freiburg • Bad Krozingen, Freiburg, Germany

Faculty of Medicine, University of Freiburg, Freiburg, Germany
e-mail: ursula.ravens@tu-dresden.de; ursula.ravens@uniklinik-freiburg.de

R. Peyronnet
Institute for Experimental Cardiovascular Medicine, University Heart Center Freiburg • Bad Krozingen, Freiburg, Germany

Faculty of Medicine, University of Freiburg, Freiburg, Germany

© Springer Nature Switzerland AG 2023

O. N. Tripathi et al. (eds.), *Heart Rate and Rhythm*, https://doi.org/10.1007/978-3-031-33588-4_28

ineffective and has many side effects, so that new drugs are highly wanted. A brief outline of the atrial action potential, the electrophysiological mechanisms of AF and the accompanying remodeling processes will provide the conceptual framework that has led to new drug development.

28.1.1 The Atrial Action Potential

During the cardiac action potential distinct ion channels open and close in a voltage- and time-dependent manner producing depolarizing (inward) and repolarizing (outward) currents (see Fig. 28.1). The resting membrane potential is mainly determined by the inwardly rectifying K^+ currents I_{K1}, $I_{K,Ach,}$ and $I_{K,ATP}$, in combination with electrogenic ion transporters and exchangers. The upstroke of the action potential is due to the rapidly activating and inactivating Na^+ current I_{Na}. The plateau phase is maintained by a delicate balance of depolarizing Ca^{2+} influx (L-type Ca^{2+} current $I_{Ca,L}$) and repolarizing K^+ currents. The latter include the transient outward current I_{to}, the ultrarapidly activating, outwardly rectifying current I_{Kur}, the rapidly activating, dendrotoxin-senstive outward current $I_{Kv1.1}$, the rapidly and the slowly activating delayed rectifier current I_{Kr} and I_{Ks}, the background inward rectifier I_{K1}, the acetylcholine-activated inward rectifier $I_{K,Ach}$, the 'leak' current via TASK-1 channels, $I_{TASK\text{-}1}$, and the Ca^{2+}-activated outward current I_{SK}. Among these potassium channels, I_{Kur}, $I_{K,Ach}$, $I_{TASK\text{-}1,}$ and I_{SK} are expressed mainly in the atria with almost no expression in the healthy ventricles and are therefore considered as atria-selective.

28.1.2 Electrophysiological Background of AF

Ectopic pacemaker activity, often originating in the orifices of the pulmonary veins, or individual extrasystoles developing at any site within the atria, are typical triggers for AF, which must meet a substrate that will support re-entrant activity. Re-entry occurs when an excitation wavefront returns to its origin and encounters tissue that is no longer refractory. The circulating wave can initiate further excitatory waves in the surrounding tissue at its own high frequency thereby maintaining AF ("leading circle theory", [4]). Short refractoriness and slow conduction will increase the likelihood of re-entry. Conversely, prolonged refractoriness and enhanced conduction terminate reentry because the wavefront is extinguished when reaching tissue still in the refractory state. Re-entry can also be conceived as a spiral wave where the wavefront is rotating around a central core ("rotor theory of AF," [5]). The rotor will turn faster and in a more stable position the higher the excitability and the shorter the refractory period ("stabilization of rotor"). Reduction of excitability and prolongation of refractoriness slow down and enlarge the rotor so that it is more likely to collapse.

Instabilities of the membrane potential either at the action potential plateau or resting level are referred to as early and delayed after depolarizations (EAD, DAD) that can serve as triggers or substrates for ectopic activity. During critical prolongation of the AP plateau phase, inactivated Na^+ and/or Ca^{2+} channels may re-open providing the extra depolarizing current for EAD. In the atria EAD may provide a trigger for initiating AF, and in the ventricles, EAD can lead to torsades de pointes arrhythmia or even fibrillation; DAD are typically observed under conditions of sarcoplasmic reticulum (SR) Ca^{2+} overload [6] or abnormal SR Ca^{2+} release [7, 8]. Physiologically, cellular excitation triggers Ca^{2+} release from the SR via Ca^{2+} release channels. This Ca^{2+} is pumped back into the SR during diastole. High Ca^{2+} load of the SR causes spontaneous Ca^{2+} release without prior excitation. The resulting cytosolic Ca^{2+} increase activates the plasmalemmal Na^+/Ca^{2+}-exchanger that produces the transient inward current underlying DAD (see Chap. 13 by Tóth and Varró).

The autonomic nervous system regulates heart rate and rhythm and malfunction of either sympathetic or vagal tone can generate and maintain arrhythmia. In particular, AF can be promoted by adrenergic as well as cholinergic mechanisms

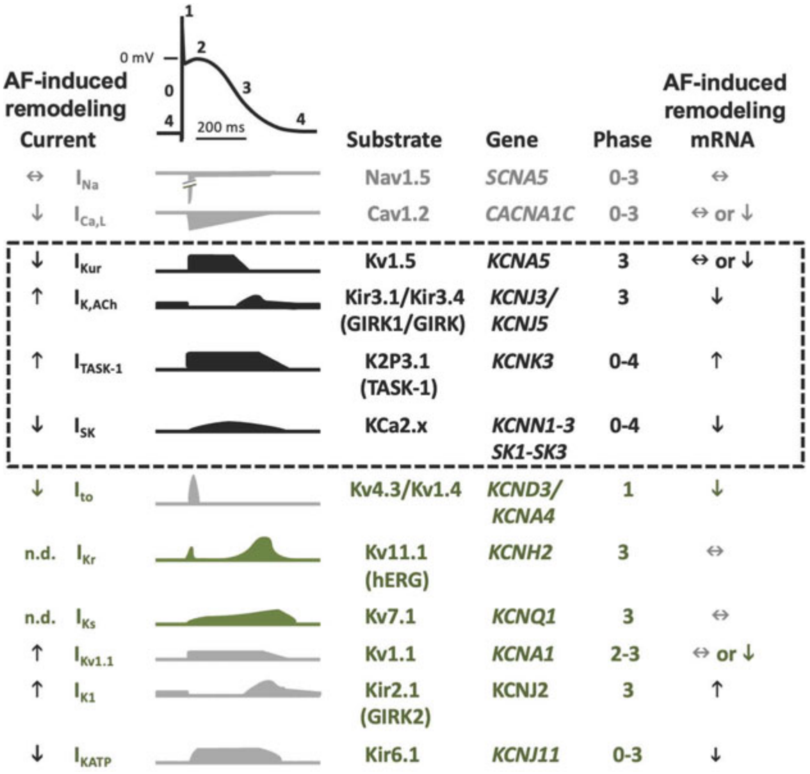
0 mV
1
2
3
0
4
4
200 ms
AF-induced remodeling Current
Substrate
Gene
Phase
AF-induced remodeling mRNA
⇔ I_{Na} Nav1.5 SCNA5 0-3 ⇔
↓ $I_{Ca,L}$ Cav1.2 CACNA1C 0-3 ⇔ or ↓
↓ I_{Kur} Kv1.5 KCNA5 3 ⇔ or ↓
↑ $I_{K,ACh}$ Kir3.1/Kir3.4 (GIRK1/GIRK) KCNJ3/ KCNJ5 3 ↓
↑ I_{TASK-1} K2P3.1 (TASK-1) KCNK3 0-4 ↑
↓ I_{SK} KCa2.x KCNN1-3 SK1-SK3 0-4 ↓
↓ I_{to} Kv4.3/Kv1.4 KCND3/ KCNA4 1 ↓
n.d. I_{Kr} Kv11.1 (hERG) KCNH2 3 ⇔
n.d. I_{Ks} Kv7.1 KCNQ1 3 ⇔
↑ $I_{Kv1.1}$ Kv1.1 KCNA1 2-3 ⇔ or ↓
↑ I_{K1} Kir2.1 (GIRK2) KCNJ2 3 ↑
↓ I_{KATP} Kir6.1 KCNJ11 0-3 ↓

Fig. 28.1 Typical shape of an atrial action potential from a patient in sinus rhythm and schematic of the underlying currents and ion channels, as well as their remodeling in permanent AF. Changes due to AF-induced electrical remodeling are indicated by the arrows. n.d., not determined. The dotted frames emphasize "atria-selective" outward currents considered not to be present in the ventricles (but see [2] for SK channels). Modified from The Sicilian gambit (1991) [3]. GIRK, G-protein-activated inwardly rectifying K^+ channel; TASK, TWIK (tandem of P domains in a weak inward-rectifying K^+ channel)–related acid-sensitive K^+ channel; SK, Ca^{2+}-activated K^+ channel of small conductance; hERG, human ether-a-go-go related gene channel

[9–11]. Adrenergic stimulation is an effective trigger of arrhythmias via enhancing EAD and DADs with little effect on arrhythmia maintenance. Conversely, cholinergic mechanisms are important both as a trigger and contributor to the maintenance of AF [12].

28.1.3 Electrical and Structural Remodeling in AF

Patients with familial AF have been studied for genetic causes of the arrhythmia. In the past decade, many mutations were found in genes encoding for cardiac ion channels that are involved in familial AF [13]. Most known mutations in genes encoding for K^+ channel proteins associated with familial AF suggest that gain of function (I_{Kr}, I_{Ks}, I_{K1}) represents the arrhythmogenic risk, but also loss of function has been reported [14]. In addition, gene polymorphisms may enhance susceptibility to AF without causing the arrhythmia. Recent epigenetic studies of human left atrial tissue have identified gene networks that underlie AF [15].

Atrial fibrillation has a strong tendency to become persistent when the arrhythmic episodes last longer [16]. This characteristic property of AF is thought to be due to profound structural and electrical alterations ("remodeling"), caused by a plethora of malfunctions including disturbed intracellular calcium handling [17–19]. Electrical remodeling is characterized by shortening of the atrial refractory period and the inability of the cardiac action potential to adapt to increased frequency [20]. Reduced refractoriness supports multiple wavelet re-entry and periodic activity of sustained, high-frequency functional re-entry sources known as "rotors," which are thought to contribute to sustained AF [21]. The high rate of electrical activity during AF imposes an enormous Ca^{2+} load on the myocardial cells that compromises cellular Ca^{2+} homeostasis [22]. As a consequence, multiple cellular functions are altered including stability of membrane potential, regulation of proteins by phosphorylation or nitrosylation, and changes in gene expression of ion channels.

Remodeled action potentials in long-lasting permanent AF have a short triangular shape [20], and the underlying cellular mechanisms for atrial electrical remodeling have been reviewed in depth elsewhere [18]; compare Fig. 28.1). Briefly, $I_{Ca,L}$ is reduced [23] probably due to altered channel phosphorylation [24], although some authors also found decreased expression of mRNA [25]. I_{to} and $I_{K,ACh}$ are also diminished in amplitude, and this is associated with a decline in mRNA for the ion-conducting α-subunits Kv4.3 and Kir3.1/Kir3.4, respectively. TASK-1 is upregulated in AF [26], and SK-2 and SK-3 are downregulated [27]. The delayed rectifier currents I_{Kr} and I_{Ks} have not been determined, while data on I_{Kur} are conflicting, with reports of no change or downregulation of current, mRNA and protein of the pore-forming α-subunit Kv1.5. Current amplitude of background inward rectifier I_{K1} and mRNA for Kir2.1/Kir2.3 are upregulated [28], while $I_{K,ATP}$ is downregulated [29, 30]. These findings raise the question, whether atrial remodeling will leave the—in control conditions—atria-selective channels I_{Kur}, $I_{K,Ach,}$ and $I_{K,Ca}$ in a sufficiently intact state of function for them to serve as useful drug targets.

Atrial fibrillation also induces structural and ultrastructural changes in atrial tissue for which the term "structural remodeling" has been coined [31]. High-frequency, uncoordinated atrial activation during AF leads to an increase in local angiotensin synthesis, oxidative injury of atrial myocytes, inflammation, altered cell metabolism, restructuring of extracellular matrix, uncoupling of gap junctions, hypertrophy, and fibrosis, all of which can provide a "morphologic substrate" for maintenance of AF [32–34]. Therefore, drugs that interfere with these mechanisms ('upstream therapy') may prevent structural remodeling.

28.2 Current Drug Treatment of AF

Unlike ventricular fibrillation, AF is not immediately life threatening although mortality is increased largely due to associated stroke [35]. Therefore, stroke prevention by suitable anticoagulation is part of standard therapy [1]. By intuition, rhythm control would be the optimal therapeutic goal in AF; however, rate control was shown to be equivalent with respect to mortality [36]. Suppression of atrial triggers and prolongation of atrial refractory period should terminate AF and hence support rhythm control, whereas rate control involves prolongation of atrioventricular nodal refractoriness and slowing of atrioventricular nodal conduction by different classes of drugs like β-blockers, calcium channel blockers, or amiodarone.

Currently available antiarrhythmic drugs for treatment of AF—perhaps with exception of amiodarone—are not sufficiently effective, and all are burdened by cardiac and extracardiac side effects that may offset their therapeutic benefits. Treatment of AF with class I agents according to the classification of Vaughan Williams [37] is limited by negative inotropic effects and by ventricular proarrhythmic effects particularly in patients with ischemic heart disease and severe left ventricular dysfunction [38]. Interestingly, the two theories of re-entry, i.e., "leading circle" and "rotors," will result in opposite consequences of drug-induced Na^+ channel block on re-entry. According to the leading circle theory, reduced conduction velocity due to block of Na^+ channels facilitates re-entry. Re-entrant rotors, on the other hand, are destabilized by reduced excitability due to Na^+ channel block. This antiarrhythmic effect is therapeutically exploited when using class I antiarrhythmic drugs (flecainide, propafenone) for conversion of AF to sinus rhythm.

Class III drugs (sotalol, dofetilide) suppress re-entry by prolongation of action potential duration and refractoriness, but may induce EADs and torsades de pointes arrhythmias not only in the atria but also in the ventricles. The risk for torsades de pointes and sudden cardiac death may be particularly high with agents directed toward selective block of individual K^+ channels, e.g., hERG channels [39]. In fact, it is not clear whether targeting an individual ion channel may be a good idea in the first place, given the antiarrhythmic efficacy of the multiple ion channel blocker amiodarone, although this drug is discriminated by serious extracardiac side effects.

The concept of "upstream therapy" comprises angiotensin-converting enzyme inhibitors, angiotensin-receptor blockers, aldosterone antagonists, statins, and omega-3 polyunsaturated fatty acids, although the effectivity of some of these agents remains controversial [40].

28.3 Novel Approaches

Given the chronic character of AF, new drugs must meet high standards regarding efficacy and safety. As outlined above, combinations of block of different ion channels may produce the most favorable electrophysiological profile. The benzofuran derivate dronedarone blocks I_{Na}, $I_{Ca,L}$, I_{to}, I_{Kr}, I_{Ks}, $I_{K,Ach}$, and β_1-adrenoceptors, but lacks the iodine moiety that may be responsible for the pulmonary, thyroid, hepatic, and ocular toxicity of amiodarone. Dronedarone is supposed to have fewer side effects, but also less efficacy [41]. Another strategy is to develop drugs with high selectivity for atrial versus ventricular myocardium (see below). Table 28.1 contains selected examples of putative atria-selective drugs that have either been approved or are still in clinical trials.

28.3.1 Atria-Selective Drugs

Sodium channel blockers will exhibit selectivity for atrial over ventricular tissue when a number of pre-requisites are met: The drugs must bind preferentially to inactivated rather than open or closed channels and have rapid dissociation kinetics during rest. Ranolazine and amiodarone fulfill these conditions and are considered to be "atria-selective" Na^+ channel blockers [42]. Atrial selectivity is due, in this setting, to the differences in electrophysiological properties between atria and ventricles. In atria, the resting membrane potential is more depolarized than in ventricle and the potential for half-maximum inactivation of I_{Na} is about 10 mV more negative. Therefore, in atria fewer channels fully recover during diastole but remain in the inactivated, drug-binding state. If the affinity of a Na^+ channel blocker is higher for inactivated than for resting channels, the drug is preferentially bound to inactivated channels—as predominant in atria—and released from channels in the resting state. The latter condition is met in the ventricles where a larger fraction of Na^+ channels recovers from inactivation during diastole and hence allows drug to dissociate. In addition, there is a disease-specific component of atrial selectivity, due to the high atrial rate in AF that further enhances block of Na^+ channels [43]. In the case of vernakalant, which also blocks inactivated Na^+ channels and has rapid dissociation kinetics [44], atrial selectivity is further supported by block of atria-selective $I_{K,ACh}$ [45] and I_{Kur} [46] (see below). Vernakalant is approved for intravenous conversion of AF to sinus rhythm.

The cardiac Na^+ current consists of two components, a rapidly activating and inactivating "peak" current $I_{Na,P}$ and a "late" current $I_{Na,L}$. In ventricular cardiomyocytes of normal donor and explanted failing human hearts this $I_{Na,L}$ has been characterized by an ultraslow, voltage-independent inactivation, and reactivation [47]. I_{NaL} is increased in ischemia, hypertrophy, and heart failure [48] and is likely to contribute to heart failure-associated action potential prolongation and beat-to-beat variability, since block of I_{NaL} with ranolazine shortens action potentials in heart failure myocytes and eliminates early after depolarizations [49]. Amiodarone also blocks I_{NaL} in heart failure [50]. Notably, several drugs that display atrial selectivity as outlined above also block $I_{Na,L}$

Table 28.1 Atria-selective antiarrhythmic drugs

Current → Channel	Drugs (blockers)	Clinical approval/trials
Cardiac Na^+ current → Nav1.5	Ranolazine, amiodarone, vernakalant	Currently in clinical use
Ultrarapidly activating K^+ current I_{Kur} → Kv1.5	XEN-D0103 / S66913	Not effective in clinical trials
Acetylcholine-activated inwardly rectifying K^+ current $I_{K,ACh}$ → Kir3.1/Kir3.4	Tertiapin-Q AZD2927 XAF-1407 NTC-801/BMS914392	Not effective in clinical trials; Sinus bradycardia
Background "leak" current → TASK-1	Doxapram	Clinical trial currently ongoing
Ca^{2+}-activated K^+ current I_{KCa} (small conductance channels) → SK	UCL 1684 UCL 1848	Tests in large animal models of AF are ongoing

[51], which may counteract the block of I_{Kr} and hence provide protection against excessive ventricular action potential prolongation when these drugs are used in patients. In human atrial cardiomyocytes, $I_{Na,L}$ has been associated with AF [52], although the evidence for this is equivocal [53].

The ultrarapidly activating K^+ current I_{Kur} is detected only in the atria but not in the ventricle, allowing atria-selective drug targeting. Indeed, many drug companies have developed selective I_{Kur} blockers that prolong atrial action potential duration and hence the effective refractory period, without producing ventricular action potential prolongation that may deteriorate into torsades de pointes arrhythmias [54]. AF-induced remodeling decreases I_{Kur} amplitude and may alter I_{Kur} sensitivity towards block [55], casting some doubt on whether further reducing I_{Kur} might be useful. On the other hand, one might argue that block of this current supports the process of adaptation to the arrhythmia. Despite promising preclinical data in human atrial tissue from patients in sinus rhythm and AF [56, 57], clinical trials failed to provide evidence for a reduction in AF burden [58] or for any other clinically meaningful effect [59].

Block of the atria-selective acetylcholine-activated inwardly rectifying K^+ current $I_{K,ACh}$ could be useful in vagally induced AF; however, selective $I_{K,ACh}$ blockers may produce undue sinus bradycardia. Interestingly, the multichannel blocker dronedarone is 100 times more potent in blocking $I_{K,ACh}$ than its precursor compound amiodarone [41, 60]. We and others have previously reported that $I_{K,ACh}$ develops constitutive activity during AF-induced electrical remodeling [61–63]. In cell-attached single channel recording, current flow through I_{K1} and $I_{K,ACh}$ channels can be distinguished by their distinct gating behavior and single channel conductance. Constitutive activity of $I_{K,ACh}$ provides not only an atria-selective but also a pathology-selective drug target. In dogs, a corresponding constitutively active $I_{K,ACh}$-like current is upregulated in response to atrial tachypacing and block of this current by the highly selective $I_{K,ACh}$ blocker tertiapin-Q resulted in prolongation of action potential duration and suppression of inducible AF episodes [61].

In humans, $I_{K,ACh}$ is conducted via Kir3.1 and Kir3.4, which associate in heteromeres with a predominant stoichiometry of 2:2. Homomers of Kir3.4 but not of Kir3.1 are also functional [64]. Interestingly, the properties of $I_{K,ACh}$ in cells that overexpress Kir3.4 are similar to the AF-induced $I_{K,ACh}$, i.e., channels exhibit constitutive activity in the absence of any ligand [65]. The clinically tested $I_{K,ACh}$ blocker AZD2927, though effectively restoring sinus rhythm in a dog model of AF, does not prolong left atrial effective refractory period in man [66]; and BMS914392 (*alias* NTC-801) is ineffective in reducing AF burden in patients with paroxysmal AF [67]. These drugs may have lacked clinical efficacy because of their selectivity towards

Kir3.1/Kir3.4 heteromers. Recent experiments in large animals (horse, goat) demonstrated that tachypacing-induced AF was successfully converted to sinus rhythm with the novel $I_{K,ACh}$ inhibitor XAF-1407 which blocks both Kir3.1/Kir3.4 and Kir3.4/Kir3.4 channels, suggesting that block of homomers of Kir3.4 might be required for efficacy against AF [68, 69].

Many antiarrhythmic drugs block ligand-activated $I_{K,ACh}$ in a concentration-dependent manner with no difference in potency between atrial cardiomyocytes from sinus rhythm or AF [70]. It is presently not known, whether block of constitutively active $I_{K,ACh}$ contributes to clinical therapeutic efficacy in converting AF and maintaining sinus rhythm.

The two-pore-domain potassium (K2P) channels belong to a large family of background "leak" channels that are highly regulated and control excitability, stabilize membrane potential below firing threshold and shorten effective refractory period [71, 72]. They are robustly expressed in the cardiovascular system and are involved in multiple physiological functions, including cardioprotection, regulation of cardiac rhythm, and mechanical stress sensing [73]. Block of these K^+ background channels prolongs action potential duration in human atria from patients in permanent AF, where upregulation of K2P3.1 (TASK-1) and increase in current have recently been reported [26]. Since TASK-1 is more abundant in human atria than ventricles [74, 75], this channel may serve as an atria-selective drug target for treating AF. In fact, many antiarrhythmic drugs also block TASK-1, as for instance amiodarone [76], carvedilol [77], or several Kv1.5 channel blockers [78]. In pig models of AF, the TASK-1 blocker doxapram (A293) facilitates conversion in paroxysmal AF [79] and can be employed for rhythm control in permanent AF [80]. This antiarrhythmic principle is currently being tested in a clinical trial (Doxapram conversion to sinus rhythm "DOCTOS" study, EudraCT No:2018–002979-17, Protocol-Code: K620).

Upon the first description of Ca^{2+}-activated K^+ channels with small conductance (SK) in mouse and human hearts, it was instantaneously suggested that they might serve as atria-selective drug targets for pharmacological intervention in AF [81]. All three SK channel isoforms (SK1–3) are more prominently expressed in human atria than ventricles under control conditions [27, 82]. In genetically engineered mice, increase in SK2 abbreviates atrial action potentials [83], while loss of SK2 function prolongs action potential duration and induces EAD [84]. The critical role of cardiac SK channels in cardiac excitability has been expertly reviewed elsewhere [85].

Most research groups report downregulation of SK2 and/or SK3 expression in atrial tissue from patients in permanent AF [27, 82, 86], but upregulation has also been found [87]. In heart failure—a condition often associated with AF [88]—SK channel blockers prolong action potential duration also in ventricular cardiomyocytes, suggesting that SK channels may lose their atria-selectivity due to upregulation of SK channels [2, 89, 90]. Despite this limitation, preclinical testing of SK channel pore blockers (e.g., UCL1684 or UCL 1848) and modulators decreasing Ca^{2+} sensitivity (e.g., NS8593; AP30663) in large animal models of AF are ongoing [91–93], as recently summarized by Heijman et al. [doi: 10.1161/CIRCRESAHA.122.321858].

28.3.2 Non Atria-Selective K^+ Channels

The proarrhythmic potential of blockers targeting the classic non atria-selective K^+ channels has been discussed above. Here, Kv1.1 channels deserve special mention, because they were originally considered as neurospecific [94, 95] and only recently associated also with the heart [96]. Genetic knockout or pharmacological suppression with the selective blocker dendrotoxin prolongs murine atrial and ventricular action potentials and enhances susceptibility to arrhythmias [96–98]. Moreover, dendrotoxin-sensitive K^+ current contributes to action potential shortening in human, and despite unaltered mRNA expression, protein levels are increased in AF [99]. Apparently, Kv1.1 is not atria-selective because there is also robust expression in human ventricle [98]. It is presently not known whether or not Kv1.1 will play a role as a putative antiarrhythmic drug target [100].

28.3.3 Ion Channels with Unknown Potential as Drug Targets

The transient receptor potential (TRP) channels of the canonical family (TRPC) have been recognized to contribute to abnormal Ca^{2+} influx under pathophysiological conditions such as hypertrophy (for recent review see [101]). TRPC1 and TRPC3 are expressed in human atrial myocytes from patients with diseased hearts, and protein expression of TRPC3 is increased in AF patients. Further details on TRPC channels are summarized in the Chap. 12 by Alvarez and Alvarez-Collazo.

The transient inward current underlying DAD is carried by the Na^{+}/Ca^{2+} exchanger, but in addition, a Ca^{2+}-activated nonselective cation current may also contribute to DADs in human atrial myocytes [102], whereas contributions of a Ca^{2+}-activated Cl^{-} current seem unlikely because these currents are absent in human atria [103]. Detailed electrophysiological analysis of Ca^{2+}-activated nonselective cation channels in freshly isolated human atrial myocytes revealed striking resemblance to the properties of TRP channels of the melastatin family TRPM4b and TRMP5 [102], suggesting that these channels might indeed be involved in Ca^{2+} overload induced arrhythmogenesis [104, 105].

Mechanical stretch is a cause of spontaneous electrical activity [106] and arrhythmia. Mechanosensors such as stretch-activated ion channels have been detected in the heart many decades ago [107–110], but their identification in cardiac cells is still ongoing [111]. Interestingly, in ventricular myocytes, TRPC6 channel activity is modulated by cell deformation [112]. Stretch-activated channels are likely to be involved in AF because the enhancement of susceptibility to AF by acute atrial dilation can be suppressed in isolated heart experiments with GsMTx4, a selective blocker of cation nonselective stretch-activated channels, isolated from tarantula venom [113]. TREK-1 is a member of the K2P family of K^{+} channels widely expressed in the cardiovascular system and activated by stretch [114]. The role of TREK-1 has been intensively investigated with respect to cardiac arrhythmia [115]. In patients with AF and normal ventricular function, atrial expression level of TREK-1 is not affected [26], but it is downregulated in patients with AF and concomitant heart failure [116].

Piezo1 channels are cation nonselective stretch-activated channels [117] that have recently been identified in mouse cardiomyocytes ([111] and human atrial non-cardiomyocytes [118–120]. Based on results obtained on cardiac-specific knockout or overexpression of Piezo1 in mice, the channel is proposed to play a crucial role in the control of cardiac mechanical activity by modulating mechanically induced Ca^{2+} and reactive oxygen species (ROS) signaling. In addition, Piezo1 expression is shown to be upregulated in pathological conditions (i.e., doxorubicin-induced dilated cardiomyopathy) and its cardiac-specific overexpression (knockin mouse model) induces severe heart failure and arrhythmias. In light of these findings, investigating the presence and function of Piezo1 in atrial cardiomyocytes represents an exciting next step.

Taken together, modulation of stretch-activated channels as an antiarrhythmic target is worth of further investigation [121], although atria-selective model drugs are not known.

28.3.4 Other Mechanisms

Facilitating conduction via gap junctions is an important new antiarrhythmic principle in both ventricular and atrial arrhythmias [122]. The antiarrhythmic peptide AAP10 [123, 124] and the stable analogon rotigaptide (ZIP123) [125] improved intercellular coupling and prevented ischemia-induced slowing of conduction. Though rotigaptide-enhanced conduction in various AF models, the arrhythmia was only suppressed in the ischemic substrate [126].

Enhancing instead of blocking K^{+} channel activity in order to stabilize the resting membrane potential, especially in patients with long QT syndrome, could also be a useful antiarrhythmic principle. Indeed, several drug companies are at present investigating HERG channel openers for their general antiarrhythmic potential [127].

28.4 Conclusion

Increased knowledge of the pathophysiology of AF-induced electrical remodeling has led to development of atrial-selective drugs. Unfortunately, such selectivity present in control conditions may disappear with the development of heart diseases, such as AF. Exploration of the inverse approach—identification of targets that become atria-selective upon AF—and new putative antiarrhythmic concepts directed at previously neglected ion channels (K2P, TRP), gap junctions, proteins involved in Ca^{2+} homeostasis, neurohormones, and receptor systems may lead to new drugs with the expected level of efficacy and safety.

Acknowledgments The authors thank Peter Kohl for critical reading of this chapter. UR and RP are affiliated with SFB1425, funded by the German Research Foundation (DFG #422681845). UR is member of the Atrial Fibrillation NETwork (AFNET), Münster, Germany.

References

1. Hindricks G, Potpara T, Dagres N, Arbelo E, Bax JJ, Blomström-Lundqvist C, et al. 2020 ESC guidelines for the diagnosis and management of atrial fibrillation developed in collaboration with the European Association for Cardio-Thoracic Surgery (EACTS). Eur Heart J. 2021;42:373–498. https://doi.org/10.1093/eurheartj/ehaa612.
2. Darkow E, Nguyen TT, Stolina M, Kari FA, Schmidt C, Wiedmann F, et al. Small conductance Ca2+−activated K+ (SK) channel mRNA expression in human atrial and ventricular tissue: comparison between donor, atrial fibrillation and heart failure tissue. Front Physiol. 2021;12:650964. https://doi.org/10.3389/fphys.2021.650964.
3. The Sicilian Gambit. A new approach to the classification of antiarrhythmic drugs based on their actions on arrhythmogenic mechanisms. Task Force of the Working Group on Arrhythmias of the European Society of Cardiology. Circulation. 1991;84:1831–51. https://doi.org/10.1161/01.cir.84.4.1831.
4. Allessie MA, Bonke FI, Schopman FJ. Circus movement in rabbit atrial muscle as a mechanism of tachycardia. III. The "leading circle" concept: a new model of circus movement in cardiac tissue without the involvement of an anatomical obstacle. Circ Res. 1977;41:9–18. https://doi.org/10.1161/01.res.41.1.9.
5. Vaquero M, Calvo D, Jalife J. Cardiac fibrillation: from ion channels to rotors in the human heart. Heart Rhythm. 2008;5:872–9. https://doi.org/10.1016/j.hrthm.2008.02.034.
6. Bers DM. Sarcoplasmic reticulum Ca release in intact ventricular myocytes. Front Biosci. 2002;7:d1697–711.
7. Dobrev D, Nattel S. Calcium handling abnormalities in atrial fibrillation as a target for innovative therapeutics. J Cardiovasc Pharmacol. 2008;52:293–9. https://doi.org/10.1097/FJC.0b013e318171924d.
8. Vest JA, Wehrens XH, Reiken SR, Lehnart SE, Dobrev D, Chandra P, et al. Defective cardiac ryanodine receptor regulation during atrial fibrillation. Circulation. 2005;111:2025–32. https://doi.org/10.1161/01.CIR.0000162461.67140.4C.
9. Workman AJ. Cardiac adrenergic control and atrial fibrillation. Naunyn Schmiedeberg's Arch Pharmacol. 2010;381:235–49. https://doi.org/10.1007/s00210-009-0474-0.
10. Rattanawong P, Kewcharoen J, Srivathsan K, Shen WK, et al. Drug therapy for vagally-mediated atrial fibrillation and sympatho-vagal balance in the genesis of atrial fibrillation: a review of the current literature. J Atr Fibrillation. 2020;13:2410. https://doi.org/10.4022/jafib.2410.
11. Bettoni M, Zimmermann M. Autonomic tone variations before the onset of paroxysmal atrial fibrillation. Circulation. 2002;105:2753–9. https://doi.org/10.1161/01.cir.0000018443.44005.d8.
12. Liu L, Nattel S. Differing sympathetic and vagal effects on atrial fibrillation in dogs: role of refractoriness heterogeneity. Am J Phys. 1997;273:H805–16. https://doi.org/10.1152/ajpheart.1997.273.2.H805.
13. Feghaly J, Zakka P, London B, MacRae CA, Refaat MM. Genetics of atrial fibrillation. J Am Heart Assoc. 2018;7:e009884. https://doi.org/10.1161/jaha.118.009884.
14. Olson EN. Gene regulatory networks in the evolution and development of the heart. Science. 2006;313:1922–7. https://doi.org/10.1126/science.1132292.
15. Hall AW, Chaffin M, Roselli C, Lin H, Lubitz SA, Bianchi V, et al. Epigenetic analyses of human left atrial tissue identifies gene networks underlying atrial fibrillation. Circ Genom Precis Med. 2020;13:e003085. https://doi.org/10.1161/circgen.120.003085.
16. Wijffels MC, Kirchhof CJ, Dorland R, Allessie MA. Atrial fibrillation begets atrial fibrillation. A study in awake chronically instrumented goats. Circulation. 1995;92:1954–68.

17. Lenaerts I, Bito V, Heinzel FR, Driesen RB, Holemans P, D'Hooge J, et al. Ultrastructural and functional remodeling of the coupling between Ca2+ influx and sarcoplasmic reticulum Ca2+ release in right atrial myocytes from experimental persistent atrial fibrillation. Circ Res. 2009;105:876–85. https://doi.org/10.1161/circresaha.109.206276.
18. Nattel S, Maguy A, Le Bouter S, Yeh YH. Arrhythmogenic ion-channel remodeling in the heart: heart failure, myocardial infarction, and atrial fibrillation. Physiol Rev. 2007;87:425–56. https://doi.org/10.1152/physrev.00014.2006.
19. Liu T, Xiong F, Qi XY, Xiao J, Villeneuve L, Abu-Taha I, et al. Altered calcium handling produces reentry-promoting action potential alternans in atrial fibrillation-remodeled hearts. JCI Insight. 2020;5:e133754. https://doi.org/10.1172/jci.insight.133754.
20. Dobrev D, Ravens U. Remodeling of cardiomyocyte ion channels in human atrial fibrillation. Basic Res Cardiol. 2003;98:137–48. https://doi.org/10.1007/s00395-003-0409-8.
21. Pandit SV, Berenfeld O, Anumonwo JM, Zaritski RM, Kneller J, Nattel S, et al. Ionic determinants of functional reentry in a 2-D model of human atrial cells during simulated chronic atrial fibrillation. Biophys J. 2005;88:3806–21. https://doi.org/10.1529/biophysj.105.060459.
22. Dobrev D. Atrial Ca2+ signaling in atrial fibrillation as an antiarrhythmic drug target. Naunyn Schmiedeberg's Arch Pharmacol. 2010;381:195–206. https://doi.org/10.1007/s00210-009-0457-1.
23. Van Wagoner DR, Pond AL, Lamorgese M, Rossie SS, McCarthy PM, Nerbonne JM. Atrial L-type Ca2+ currents and human atrial fibrillation. Circ Res. 1999;85:428–36. https://doi.org/10.1161/01.res.85.5.428.
24. Christ T, Boknik P, Wohrl S, Wettwer E, Graf EM, Bosch RF, et al. L-type Ca2+ current downregulation in chronic human atrial fibrillation is associated with increased activity of protein phosphatases. Circulation. 2004;110:2651–7. https://doi.org/10.1161/01.CIR.0000145659.80212.6A.
25. Lai LP, Su MJ, Lin JL, Lin FY, Tsai CH, Chen YS, et al. Down-regulation of L-type calcium channel and sarcoplasmic reticular Ca(2+)-ATPase mRNA in human atrial fibrillation without significant change in the mRNA of ryanodine receptor, calsequestrin and phospholamban: an insight into the mechanism of atrial electrical remodeling. J Am Coll Cardiol. 1999;33:1231–7. https://doi.org/10.1016/s0735-1097(99)00008-x.
26. Schmidt C, Wiedmann F, Voigt N, Zhou XB, Heijman J, Lang S, et al. Upregulation of K(2P)3.1 K+ current causes action potential shortening in patients with chronic atrial fibrillation. Circulation. 2015;132:82–92. https://doi.org/10.1161/CIRCULATIONAHA.114.012657.
27. Skibsbye L, Poulet C, Diness JG, Bentzen BH, Yuan L, Kappert U, et al. Small-conductance calcium-activated potassium (SK) channels contribute to action potential repolarization in human atria. Cardiovasc Res. 2014;103:156–67. https://doi.org/10.1093/cvr/cvu121.
28. Dobrev D, Graf E, Wettwer E, Himmel HM, Hala O, Doerfel C, et al. Molecular basis of downregulation of G-protein-coupled inward rectifying K(+) current I(K,ACh) in chronic human atrial fibrillation: decrease in GIRK4 mRNA correlates with reduced I(K,ACh) and muscarinic receptor-mediated shortening of action potentials. Circulation. 2001;104:2551–7.
29. Brundel BJ, Van Gelder IC, Henning RH, Tuinenburg AE, Wietses M, Grandjean JG, et al. Alterations in potassium channel gene expression in atria of patients with persistent and paroxysmal atrial fibrillation: differential regulation of protein and mRNA levels for K+ channels. J Am Coll Cardiol. 2001;37:926–32. https://doi.org/10.1016/s0735-1097(00)01195-5.
30. Balana B, Dobrev D, Wettwer E, Christ T, Knaut M, Ravens U. Decreased ATP-sensitive K(+) current density during chronic human atrial fibrillation. J Mol Cell Cardiol. 2003;35:1399–405.
31. Ausma J, Wijffels M, Thone F, Wouters L, Allessie M, Borgers M. Structural changes of atrial myocardium due to sustained atrial fibrillation in the goat. Circulation. 1997;96:3157–63. https://doi.org/10.1161/01.cir.96.9.3157.
32. Goette A, Lendeckel U. Tachycardia-induced remodeling: atria and ventricles take a different route. Cardiovasc Res. 2004;63:194–5. https://doi.org/10.1016/j.cardiores.2004.05.005.
33. Li D, Fareh S, Leung TK, Nattel S. Promotion of atrial fibrillation by heart failure in dogs: atrial remodeling of a different sort. Circulation. 1999;100:87–95.
34. Harada M, Nattel S. Implications of inflammation and fibrosis in atrial fibrillation pathophysiology. Card Electrophysiol Clin. 2021;13:25–35. https://doi.org/10.1016/j.ccep.2020.11.002.
35. Tsang TS, Miyasaka Y, Barnes ME, Gersh BJ. Epidemiological profile of atrial fibrillation: a contemporary perspective. Prog Cardiovasc Dis. 2005;48:1–8. https://doi.org/10.1016/j.pcad.2005.06.001.
36. Wyse DG, Waldo AL, DiMarco JP, Domanski MJ, Rosenberg Y, Schron EB, et al. A comparison of rate control and rhythm control in patients with atrial fibrillation. N Engl J Med. 2002;347:1825–33. https://doi.org/10.1056/NEJMoa021328.
37. Vaughan Williams EM. A classification of antiarrhythmic actions reassessed after a decade of new drugs. J Clin Pharmacol. 1984;24:129–47.
38. Echt DS, Liebson PR, Mitchell LB, Peters RW, Obias-Manno D, Barker AH, et al. Mortality and morbidity in patients receiving encainide, flecainide, or placebo. The cardiac arrhythmia suppression trial. N Engl J Med. 1991;324:781–8. https://doi.org/10.1056/nejm199103213241201.

39. Sanguinetti MC, Tristani-Firouzi M. hERG potassium channels and cardiac arrhythmia. Nature. 2006;440:463–9. https://doi.org/10.1038/nature04710.
40. Savelieva I, Kourliouros A, Camm J. Primary and secondary prevention of atrial fibrillation with statins and polyunsaturated fatty acids: review of evidence and clinical relevance. Naunyn Schmiedeberg's Arch Pharmacol. 2010;381:1–13. https://doi.org/10.1007/s00210-009-0468-y.
41. Patel C, Yan GX, Kowey PR. Dronedarone Circulation. 2009;120:636–44. https://doi.org/10.1161/circulationaha.109.858027.
42. Antzelevitch C, Burashnikov A. Atrial-selective sodium channel block as a novel strategy for the management of atrial fibrillation. J Electrocardiol. 2009;42:543–8. https://doi.org/10.1016/j.jelectrocard.2009.07.007.
43. Burashnikov A, Di Diego JM, Zygmunt AC, Belardinelli L, Antzelevitch C. Atrium-selective sodium channel block as a strategy for suppression of atrial fibrillation: differences in sodium channel inactivation between atria and ventricles and the role of ranolazine. Circulation. 2007;116:1449–57. https://doi.org/10.1161/circulationaha.107.704890.
44. Fedida D. Vernakalant (RSD1235): a novel, atrial-selective antifibrillatory agent. Expert Opin Investig Drugs. 2007;16:519–32. https://doi.org/10.1517/13543784.16.4.519.
45. Fedida D, Orth PM, Chen JY, Lin S, Plouvier B, Jung G, et al. The mechanism of atrial antiarrhythmic action of RSD1235. J Cardiovasc Electrophysiol. 2005;16:1227–38. https://doi.org/10.1111/j.1540-8167.2005.50028.x.
46. Kozlowski D, Budrejko S, Lip GY, Mikhailidis DP, Rysz J, Raczak G, et al. Vernakalant hydrochloride for the treatment of atrial fibrillation. Expert Opin Investig Drugs. 2009;18:1929–37. https://doi.org/10.1517/13543780903386246.
47. Maltsev VA, Sabbah HN, Higgins RS, Silverman N, Lesch M, Undrovinas AI. Novel, ultraslow inactivating sodium current in human ventricular cardiomyocytes. Circulation. 1998;98:2545–52. https://doi.org/10.1161/01.cir.98.23.2545.
48. Valdivia CR, Chu WW, Pu J, Foell JD, Haworth RA, Wolff MR, et al. Increased late sodium current in myocytes from a canine heart failure model and from failing human heart. J Mol Cell Cardiol. 2005;38:475–83. https://doi.org/10.1016/j.yjmcc.2004.12.012.
49. Undrovinas AI, Belardinelli L, Undrovinas NA, Sabbah HN. Ranolazine improves abnormal repolarization and contraction in left ventricular myocytes of dogs with heart failure by inhibiting late sodium current. J Cardiovasc Electrophysiol. 2006;17(Suppl 1):S169–s177. https://doi.org/10.1111/j.1540-8167.2006.00401.x.
50. Maltsev VA, Sabbah HN, Undrovinas AI. Late sodium current is a novel target for amiodarone: studies in failing human myocardium. J Mol Cell Cardiol. 2001;33:923–32. https://doi.org/10.1006/jmcc.2001.1355.
51. Persson F, Andersson B, Duker G, Jacobson I, Carlsson L. Functional effects of the late sodium current inhibition by AZD7009 and lidocaine in rabbit isolated atrial and ventricular tissue and Purkinje fibre. Eur J Pharmacol. 2007;558:133–43. https://doi.org/10.1016/j.ejphar.2006.11.040.
52. Sossalla S, Kallmeyer B, Wagner S, Mazur M, Maurer U, Toischer K, et al. Altered Na(+) currents in atrial fibrillation effects of ranolazine on arrhythmias and contractility in human atrial myocardium. J Am Coll Cardiol. 2010;55:2330–42. https://doi.org/10.1016/j.jacc.2009.12.055.
53. Poulet C, Wettwer E, Grunnet M, Jespersen T, Fabritz L, Matschke K, et al. Late sodium current in human atrial cardiomyocytes from patients in sinus rhythm and atrial fibrillation. PLoS One. 2015;10:e0131432. https://doi.org/10.1371/journal.pone.0131432.
54. Ford JW, Milnes JT. New drugs targeting the cardiac ultra-rapid delayed-rectifier current (IKur): rationale, pharmacology and evidence for potential therapeutic value. J Cardiovasc Pharmacol. 2008;52:105–20. https://doi.org/10.1097/FJC.0b013e3181719b0c.
55. Christ T, Wettwer E, Voigt N, Hala O, Radicke S, Matschke K, et al. Pathology-specific effects of the IKur/Ito/IK,ACh blocker AVE0118 on ion channels in human chronic atrial fibrillation. Br J Pharmacol. 2008;154:1619–30. https://doi.org/10.1038/bjp.2008.209.
56. Loose S, Mueller J, Wettwer E, Knaut M, Ford J, Milnes J, et al. Effects of IKur blocker MK-0448 on human right atrial action potentials from patients in sinus rhythm and in permanent atrial fibrillation. Front Pharmacol. 2014;5:26. https://doi.org/10.3389/fphar.2014.00026.
57. Ford J, Milnes J, El Haou S, Wettwer E, Loose S, Matschke K, et al. The positive frequency-dependent electrophysiological effects of the IKur inhibitor XEN-D0103 are desirable for the treatment of atrial fibrillation. Heart Rhythm. 2016;13:555–64. https://doi.org/10.1016/j.hrthm.2015.10.003.
58. Shunmugam SR, Sugihara C, Freemantle N, Round P, Furniss S, Sulke N. A double-blind, randomised, placebo-controlled, cross-over study assessing the use of XEN-D0103 in patients with paroxysmal atrial fibrillation and implanted pacemakers allowing continuous beat-to-beat monitoring of drug efficacy. J Interv Card Electrophysiol. 2018;51:191–7. https://doi.org/10.1007/s10840-018-0318-2.
59. Camm AJ, Dorian P, Hohnloser SH, Kowey PR, Tyl B, Ni Y, et al. A randomized, double-blind, placebo-controlled trial assessing the efficacy of S66913 in patients with paroxysmal atrial fibrillation. Eur Heart J Cardiovasc Pharmacother. 2019;5:21–8. https://doi.org/10.1093/ehjcvp/pvy022.

60. Guillemare E, Marion A, Nisato D, Gautier P. Inhibitory effects of dronedarone on muscarinic K+ current in Guinea pig atrial cells. J Cardiovasc Pharmacol. 2000;36:802–5. https://doi.org/10.1097/00005344-200012000-00017.
61. Cha TJ, Ehrlich JR, Chartier D, Qi XY, Xiao L, Nattel S. Kir3-based inward rectifier potassium current: potential role in atrial tachycardia remodeling effects on atrial repolarization and arrhythmias. Circulation. 2006;113:1730–7. https://doi.org/10.1161/CIRCULATIONAHA.105.561738.
62. Dobrev D, Friedrich A, Voigt N, Jost N, Wettwer E, Christ T, et al. The G protein-gated potassium current I(K,ACh) is constitutively active in patients with chronic atrial fibrillation. Circulation. 2005;112:3697–706. https://doi.org/10.1161/CIRCULATIONAHA.105.575332.
63. Voigt N, Friedrich A, Bock M, Wettwer E, Christ T, Knaut M, et al. Differential phosphorylation-dependent regulation of constitutively active and muscarinic receptor-activated IK,ACh channels in patients with chronic atrial fibrillation. Cardiovasc Res. 2007;74:426–37. https://doi.org/10.1016/j.cardiores.2007.02.009.
64. Silverman SK, Lester HA, Dougherty DA. Subunit stoichiometry of a heteromultimeric G protein-coupled inward-rectifier K+ channel. J Biol Chem. 1996;271:30524–8.
65. El-Haou S, Ford JW, Milnes JT. Novel K+ channel targets in atrial fibrillation drug development--where are we? J Cardiovasc Pharmacol. 2015;66:412–31. https://doi.org/10.1097/FJC.0000000000000277.
66. Walfridsson H, Anfinsen OG, Berggren A, Frison L, Jensen S, Linhardt G, et al. Is the acetylcholine-regulated inwardly rectifying potassium current a viable antiarrhythmic target? Translational discrepancies of AZD2927 and A7071 in dogs and humans. Europace. 2015;17:473–82. https://doi.org/10.1093/europace/euu192.
67. Podd SJ, Freemantle N, Furniss SS, Sulke N. First clinical trial of specific IKACh blocker shows no reduction in atrial fibrillation burden in patients with paroxysmal atrial fibrillation: pacemaker assessment of BMS 914392 in patients with paroxysmal atrial fibrillation. Europace. 2016;18:340–6. https://doi.org/10.1093/europace/euv263.
68. Fenner MF, Carstensen H, Nissen SD, Hesselkilde EM, Lunddahl CS, Jensen MAH, Loft-Andersen AV, et al. Effect of selective I(K,ACh) inhibition by XAF-1407 in an equine model of tachypacing-induced persistent atrial fibrillation. Br J Pharmacol. 2020;177:3778–94. https://doi.org/10.1111/bph.15100.
69. Sobota V, Gatta G, van Hunnik A, van Tuijn I, Kuiper M, Milnes J, et al. The acetylcholine-activated potassium current inhibitor XAF-1407 terminates persistent atrial fibrillation in goats. Front Pharmacol. 2020;11:608410. https://doi.org/10.3389/fphar.2020.608410.
70. Voigt N, Rozmaritsa N, Trausch A, Zimniak T, Christ T, Wettwer E, et al. Inhibition of IK,ACh current may contribute to clinical efficacy of class I and class III antiarrhythmic drugs in patients with atrial fibrillation. Naunyn Schmiedeberg's Arch Pharmacol. 2010;381:251–9. https://doi.org/10.1007/s00210-009-0452-6.
71. Goldstein SA, Bockenhauer D, O'Kelly I, Zilberberg N. Potassium leak channels and the KCNK family of two-P-domain subunits. Nat Rev Neurosci. 2001;2:175–84. https://doi.org/10.1038/35058574.
72. Gierten J, Ficker E, Bloehs R, Schlomer K, Kathofer S, Scholz E, et al. Regulation of two-pore-domain (K2P) potassium leak channels by the tyrosine kinase inhibitor genistein. Br J Pharmacol. 2008;154:1680–90. https://doi.org/10.1038/bjp.2008.213.
73. Abraham DM, Lee TE, Watson LJ, Mao L, Chandok GS, Wang HG, et al. The two-pore-domain potassium channel TREK-1 mediates cardiac fibrosis and diastolic dysfunction. J Clin Invest. 2018;128(11):4843–55. https://doi.org/10.1172/jci95945.
74. Ellinghaus P, Scheubel RJ, Dobrev D, Ravens U, Holtz J, Huetter J, et al. Comparing the global mRNA expression profile of human atrial and ventricular myocardium with high-density oligonucleotide arrays. J Thorac Cardiovasc Surg. 2005;129:1383–90. https://doi.org/10.1016/j.jtcvs.2004.08.031.
75. Limberg SH, Netter MF, Rolfes C, Rinne S, Schlichthorl G, Zuzarte M, et al. TASK-1 channels may modulate action potential duration of human atrial cardiomyocytes. Cell Physiol Biochem. 2011;28:613–24. https://doi.org/10.1159/000335757.
76. Gierten J, Ficker E, Bloehs R, Schweizer PA, Zitron E, Scholz E, et al. The human cardiac K2P3.1 (TASK-1) potassium leak channel is a molecular target for the class III antiarrhythmic drug amiodarone. Naunyn Schmiedeberg's Arch Pharmacol. 2010;381:261–70. https://doi.org/10.1007/s00210-009-0454-4.
77. Staudacher K, Staudacher I, Ficker E, Seyler C, Gierten J, Kisselbach J, et al. Carvedilol targets human K2P 3.1 (TASK1) K+ leak channels. Br J Pharmacol. 2011;163:1099–110. https://doi.org/10.1111/j.1476-5381.2011.01319.x.
78. Kiper AK, Rinne S, Rolfes C, Ramirez D, Seebohm G, Netter MF, et al. Kv1.5 blockers preferentially inhibit TASK-1 channels: TASK-1 as a target against atrial fibrillation and obstructive sleep apnea? Pflugers Arch. 2015;467:1081–90. https://doi.org/10.1007/s00424-014-1665-1.
79. Wiedmann F, Kiper AK, Bedoya M, Ratte A, Rinne S, Kraft M, et al. Identification of the A293 (AVE1231) binding bite in the cardiac two-pore-domain potassium channel TASK-1: a common low affinity antiarrhythmic drug binding site. Cell Physiol

Biochem. 2019;52:1223–35. https://doi.org/10.33594/000000083.

80. Wiedmann F, Beyersdorf C, Zhou XB, Kraft M, Foerster KI, El-Battrawy I, et al. The experimental TASK-1 potassium channel inhibitor A293 can be employed for rhythm control of persistent atrial fibrillation in a translational large animal model. Front Physiol. 2020;11:629421. https://doi.org/10.3389/fphys.2020.629421.
81. Xu Y, Tuteja D, Zhang Z, Xu D, Zhang Y, Rodriguez J, et al. Molecular identification and functional roles of a Ca(2+)-activated K+ channel in human and mouse hearts. J Biol Chem. 2003;278: 49085–94. https://doi.org/10.1074/jbc.M307508200.
82. Yu T, Deng C, Wu R, Guo H, Zheng S, Yu X, et al. Decreased expression of small-conductance Ca2+−activated K+ channels SK1 and SK2 in human chronic atrial fibrillation. Life Sci. 2012;90:219–27. https://doi.org/10.1016/j.lfs.2011.11.008.
83. Ozgen N, Dun W, Sosunov EA, Anyukhovsky EP, Hirose M, Duffy HS, et al. Early electrical remodeling in rabbit pulmonary vein results from trafficking of intracellular SK2 channels to membrane sites. Cardiovasc Res. 2007;75:758–69. https://doi.org/10.1016/j.cardiores.2007.05.008.
84. Li Y, Díaz ME, Eisner DA, O'Neill S. The effects of membrane potential, SR Ca2+ content and RyR responsiveness on systolic Ca2+ alternans in rat ventricular myocytes. J Physiol. 2009;587:1283–92. https://doi.org/10.1113/jphysiol.2008.164368.
85. Zhang XD, Thai PN, Lieu DK, Chiamvimonvat N. Cardiac small-conductance calcium-activated potassium channels in health and disease. Pflugers Arch. 2021;473:477–89. https://doi.org/10.1007/s00424-021-02535-0.
86. Ling TY, Wang XL, Chai Q, Lau TW, Koestler CM, Park SJ, et al. Regulation of the SK3 channel by microRNA-499--potential role in atrial fibrillation. Heart Rhythm. 2013;10:1001–9. https://doi.org/10.1016/j.hrthm.2013.03.005.
87. Zhou X, Sun Q, Voigt N, Heijman J, Lang S, Nattel S, et al. Contributions of small-conductance Ca2+−activated K+ channels to shortening of action potential duration in human chronicatrial fibrillation. Clin Res Cardiol. 2014;103:V859.
88. Santhanakrishnan R, Wang N, Larson MG, Magnani JW, McManus DD, Lubitz SA, et al. Atrial fibrillation begets heart failure and vice versa: Temporal associations and differences in preserved versus reduced ejection fraction. Circulation. 2016;133: 484–92. https://doi.org/10.1161/circulationaha.115.018614.
89. Chang PC, Hsieh YC, Hsueh CH, Weiss JN, Lin SF, Chen PS. Apamin induces early afterdepolarizations and torsades de pointes ventricular arrhythmia from failing rabbit ventricles exhibiting secondary rises in intracellular calcium. Heart Rhythm. 2013;10:1516–24. https://doi.org/10.1016/j.hrthm.2013.07.003.
90. Bonilla IM, Long VP 3rd, Vargas-Pinto P, Wright P, Belevych A, Lou Q, et al. Calcium-activated potassium current modulates ventricular repolarization in chronic heart failure. PLoS One. 2014;9:e108824. https://doi.org/10.1371/journal.pone.0108824.
91. Haugaard MM, Hesselkilde EZ, Pehrson S, Carstensen H, Flethoj M, Praestegaard KF, et al. Pharmacologic inhibition of small-conductance calcium-activated potassium (SK) channels by NS8593 reveals atrial antiarrhythmic potential in horses. Heart Rhythm. 2015;12:825–35. https://doi.org/10.1016/j.hrthm.2014.12.028.
92. Diness JG, Kirchhoff JE, Speerschneider T, Abildgaard L, Edvardsson N, Sorensen US, et al. The KCa2 channel inhibitor AP30663 selectively increases atrial refractoriness, converts vernakalant-resistant atrial fibrillation and prevents ts reinduction in conscious pigs. Front Pharmacol. 2020;11:159. https://doi.org/10.3389/fphar.2020.00159.
93. Bentzen BH, Bomholtz SH, Simó-Vicens R, Folkersen L, Abildgaard L, Speerschneider T, et al. Mechanisms of action of the KCa2-negative modulator AP30663, a novel compound in development for treatment of atrial fibrillation in man. Front Pharmacol. 2020;11:610. https://doi.org/10.3389/fphar.2020.00610.
94. Smart SL, Lopantsev V, Zhang CL, Robbins CA, Wang H, Chiu SY, et al. Deletion of the K(V)1.1 potassium channel causes epilepsy in mice. Neuron. 1998;20:809–19. https://doi.org/10.1016/s0896-6273(00)81018-1.
95. Robbins CA, Tempel BL. Kv1.1 and Kv1.2: similar channels, different seizure models. Epilepsia. 2012;53(Suppl 1):134–41. https://doi.org/10.1111/j.1528-1167.2012.03484.x.
96. Glasscock E, Yoo JW, Chen TT, Klassen TL, Noebels JL. Kv1.1 potassium channel deficiency reveals brain-driven cardiac dysfunction as a candidate mechanism for sudden unexplained death in epilepsy. J Neurosci. 2010;30:5167–75. https://doi.org/10.1523/jneurosci.5591-09.2010.
97. Si M, Trosclair K, Hamilton KA, Glasscock E. Genetic ablation or pharmacological inhibition of Kv1.1 potassium channel subunits impairs atrial repolarization in mice. Am J Physiol Cell Physiol. 2019;316:C154–61. https://doi.org/10.1152/ajpcell.00335.2018.
98. Trosclair K, Si M, Watts M, Gautier NM, Voigt N, Traylor J, et al. Kv1.1 potassium channel subunit deficiency alters ventricular arrhythmia susceptibility, contractility, and repolarization. Physiol Rep. 2021;9:e14702. https://doi.org/10.14814/phy2.14702.
99. Glasscock E, Voigt N, McCauley MD, Sun Q, Li N, Chiang DY, et al. Expression and function of Kv1.1 potassium channels in human atria from patients with atrial fibrillation. Basic Res Cardiol. 2015;110:505. https://doi.org/10.1007/s00395-015-0505-6.

100. Voigt N, Dobrev D. Atrial-selective potassium channel blockers. Card Electrophysiol Clin. 2016;8:411–21. https://doi.org/10.1016/j.ccep.2016.02.005.
101. Nishida M, Kurose H. Roles of TRP channels in the development of cardiac hypertrophy. Naunyn Schmiedeberg's Arch Pharmacol. 2008;378:395–406. https://doi.org/10.1007/s00210-008-0321-8.
102. Guinamard R, Chatelier A, Demion M, Potreau D, Patri S, Rahmati M, et al. Functional characterization of a Ca(2+)-activated non-selective cation channel in human atrial cardiomyocytes. J Physiol. 2004;558:75–83. https://doi.org/10.1113/jphysiol.2004.063974.
103. Köster OF, Szigeti GP, Beuckelmann DJ. Characterization of a [Ca2+]i-dependent current in human atrial and ventricular cardiomyocytes in the absence of Na+ and K+. Cardiovasc Res. 1999;41:175–87. https://doi.org/10.1016/s0008-6363(98)00202-8.
104. Guinamard R, Demion M, Magaud C, Potreau D, Bois P. Functional expression of the TRPM4 cationic current in ventricular cardiomyocytes from spontaneously hypertensive rats. Hypertension. 2006;48:587–94. https://doi.org/10.1161/01.HYP.0000237864.65019.a5.
105. Peyronnet R, Nerbonne JM, Kohl P. Cardiac mechano-gated ion channels and arrhythmias. Circ Res. 2016;118:311–29. https://doi.org/10.1161/CIRCRESAHA.115.305043.
106. Kaufmann R, Theophile U. Autonomously promoted extension effect in Purkinje fibers, papillary muscles and trabeculae carneae of rhesus monkeys. Pflugers Arch Gesamte Physiol Menschen Tiere. 1997;297:174–89.
107. Kim D. Novel cation-selective mechanosensitive ion channel in the atrial cell membrane. Circ Res. 1993;72:225–31.
108. Craelius W, Chen V, El-Sherif N. Stretch activated ion channels in ventricular myocytes. Biosci Rep. 1988;8:407–14. https://doi.org/10.1007/bf01121637.
109. Kelly D, Mackenzie L, Hunter P, Smaill B, Saint DA. Gene expression of stretch-activated channels and mechanoelectric feedback in the heart. Clin Exp Pharmacol Physiol. 2006;33:642–8. https://doi.org/10.1111/j.1440-1681.2006.04392.x.
110. Schmidt C, Peyronnet R. Voltage-gated and stretch-activated potassium channels in the human heart : pathophysiological and clinical significance. Herzschrittmacherther Elektrophysiol. 2018;29:36–42. https://doi.org/10.1007/s00399-017-0541-z.
111. Jiang F, Yin K, Wu K, Zhang M, Wang S, Cheng H, et al. The mechano-sensitive Piezo1 channel mediates heart mechano-chemo transduction. Nat Commun. 2021;12:869. https://doi.org/10.1038/s41467-021-21178-4.
112. Dyachenko V, Husse B, Rueckschloss U, Isenberg G. Mechanical deformation of ventricular myocytes modulates both TRPC6 and Kir2.3 channels. Cell Calcium. 2009;45:38–54. https://doi.org/10.1016/j.ceca.2008.06.003.
113. Bode F, Sachs F, Franz MR. Tarantula peptide inhibits atrial fibrillation. Nature. 2001;409:35–6. https://doi.org/10.1038/35051165.
114. Wiedmann F, Rinné S, Donner B, Decher N, Katus HA, Schmidt C. Mechanosensitive TREK-1 two-pore-domain potassium (K(2P)) channels in the cardiovascular system. Prog Biophys Mol Biol. 2021;159:126–35. https://doi.org/10.1016/j.pbiomolbio.2020.05.007.
115. Decher N, Kiper AK, Rinne S. Stretch-activated potassium currents in the heart: focus on TREK-1 and arrhythmias. Prog Biophys Mol Biol. 2017;130:223–32. https://doi.org/10.1016/j.pbiomolbio.2017.05.005.
116. Lugenbiel P, Wenz F, Syren P, Geschwill P, Govorov K, Seyler C, et al. TREK-1 (K(2P)2.1) K(+) channels are suppressed in patients with atrial fibrillation and heart failure and provide therapeutic targets for rhythm control. Basic Res Cardiol. 2017;112:8. https://doi.org/10.1007/s00395-016-0597-7.
117. Coste B, Mathur J, Schmidt M, Earley TJ, Ranade S, Petrus MJ, et al. Piezo1 and Piezo2 are essential components of distinct mechanically activated cation channels. Science. 2010;330:55–60. https://doi.org/10.1126/science.1193270.
118. Klesen A, Jakob D, Emig R, Kohl P, Ravens U, Peyronnet R. Cardiac fibroblasts : active players in (atrial) electrophysiology? Herzschrittmacherther Elektrophysiol. 2018;29:62–9. https://doi.org/10.1007/s00399-018-0553-3.
119. Blythe NM, Muraki K, Ludlow MJ, Stylianidis V, Gilbert HTJ, Evans EL, et al. Mechanically activated Piezo1 channels of cardiac fibroblasts stimulate p38 mitogen-activated protein kinase activity and interleukin-6 secretion. J Biol Chem. 2019;294(46):17395–408. https://doi.org/10.1074/jbc.RA119.009167.
120. Emig R, Knodt W, Krussig MJ, Zgierski-Johnston CM, Gorka O, Groß O, et al. Piezo1 channels contribute to the regulation of human atrial fibroblast mechanical properties and matrix stiffness sensing. Cell. 2021;10:10. https://doi.org/10.3390/cells10030663.
121. Quinn TA, Kohl P. Cardiac Mechano-electric coupling: acute effects of mechanical stimulation on heart rate and rhythm. Physiol Rev. 2021;101(1):37–92. https://doi.org/10.1152/physrev.00036.2019.
122. Dhein S, Hagen A, Jozwiak J, Dietze A, Garbade J, Barten M, et al. Improving cardiac gap junction communication as a new antiarrhythmic mechanism: the action of antiarrhythmic peptides. Naunyn Schmiedeberg's Arch Pharmacol. 2010;381:221–34. https://doi.org/10.1007/s00210-009-0473-1.
123. Easton JA, Petersen JS, Martin PE. The anti-arrhythmic peptide AAP10 remodels Cx43 and Cx40 expression and function. Naunyn

Schmiedeberg's Arch Pharmacol. 2009;380:11–24. https://doi.org/10.1007/s00210-009-0411-2.

124. Jozwiak J, Dhein S. Local effects and mechanisms of antiarrhythmic peptide AAP10 in acute regional myocardial ischemia: electrophysiological and molecular findings. Naunyn Schmiedeberg's Arch Pharmacol. 2008;378:459–70. https://doi.org/10.1007/s00210-008-0317-4.

125. Clarke TC, Thomas D, Petersen JS, Evans WH, Martin PE. The antiarrhythmic peptide rotigaptide (ZP123) increases gap junction intercellular communication in cardiac myocytes and HeLa cells expressing connexin 43. Br J Pharmacol. 2006;147:486–95. https://doi.org/10.1038/sj.bjp.0706631.

126. Shiroshita-Takeshita A, Sakabe M, Haugan K, Hennan JK, Nattel S. Model-dependent effects of the gap junction conduction-enhancing antiarrhythmic peptide rotigaptide (ZP123) on experimental atrial fibrillation in dogs. Circulation. 2007;115:310–8. https://doi.org/10.1161/circulationaha.106.665547.

127. Seebohm G. Activators of cation channels: potential in treatment of channelopathies. Mol Pharmacol. 2005;67:585–8. https://doi.org/10.1124/mol.104.010173.

K Channel Openers as New Antiarrhythmic Agents

29

Nathalie Strutz-Seebohm and Guiscard Seebohm

Abstract

Cardiac cation channels are membrane proteins that provide controlled ion passage through cellular membranes to allow electrical control of the cardiac cell. In a variety of channelopathies, ion channel function is reduced and activators of cation channels are promising candidates to regain channel function in acquired or inherited channelopathies. Shortage in cation channel activators prevented testing of efficiency of activators in a variety of indications. This shortage could be overcome by modern optimized drug screening methods but increasing knowledge about cation channel activator binding and action might enable us in the future to use in silico-guided drug design of channel modulators. New compounds will enable us to increase our understanding in cation channel modulation and to test the concept of channel activation as a clinically relevant principle in the treatment of cardiac channelopathies.

Keywords

Arrhythmia · Drug · Heart · Channel · Therapy · Agonist

29.1 Introduction

Ion channels are membrane integral proteins that allow controlled passage of ion through cellular membranes. Cation-selective channels play key roles in physiological processes such as control of ion homeostasis, cell volume, vesicle trafficking, neuro transmitter/hormone secretion, and electrical control of excitable tissues. The importance of cation channels in the treatment of diverse diseases is also amplified by the fact that many therapeutic drugs mediate their effects by targeting the cation channel proteins. Potassium selective channels are the most genetically and functionally diverse of all cation channels. Starting with the first cloned potassium selective ion channel from *Drosophila,* Shaker, several hundred potassium channel genes have been identified in the human genome. The number of functionally distinct channels in native tissues is further increased by heteromultimeric co-assembly of potassium channel α-subunits with other α- and β-subunits and other modifications such as alternative splicing of mRNAs, glycosylation, sumoylation, and phosphorylation. In the light of the broad range of physiological roles of cation channels, it is not

N. Strutz-Seebohm (✉)
AG Rezeptorstruktur und Funktion, IfGH - Abteilung Zelluläre Elektrophysiologie und Molekularbiologie, Westfälische Wilhelms-Universität Münster, Münster, Germany
e-mail: Nathalie.Strutz-Seebohm@ukmuenster.de

G. Seebohm
IfGH - Abteilung Zelluläre Elektrophysiologie und Molekularbiologie, Westfälische Wilhelms-Universität Münster, Münster, Germany

© Springer Nature Switzerland AG 2023

O. N. Tripathi et al. (eds.), *Heart Rate and Rhythm*, https://doi.org/10.1007/978-3-031-33588-4_29

surprising that channel impairment results in a variety of pathophysiological conditions. The following text will give an overview of molecular details and availability of potassium channel modulators and try to address their potential as anti-arrhythmic drugs.

29.2 Acquired and Inherited Alterations of the ECG Morphology

Channels might lose or gain function as a result of mutations in the promotor or coding region of a gene. Much less understood are the effects by genetic variations and chemical modifications (e.g. DNA methylation) in the noncoding region of ion channel loci. Further, alteration of channel function might result from regulatory derangements or by autoantibodies. The diseases based on altered ion channel function are called channelopathies and include Bartter's syndrome type 2 (KCNJ1, Kir1.1 or RomK) [1], persistent hyperinsulinaemic hypoglycaemia of infancy (Kir 6.2 and Sur) [2, 3], and episodic ataxia type 1 (KCNA1 or Kv1.1) [4]. Cardiac arrhythmia can be caused by structural alterations of the heart as a result of, e.g., aging or/and viral infection with the picorna virus, coxsacki virus B3, parvovirus B19, or SARS-Cov-2. In these contexts, age-related or cardiomyopathic dilatative responses lead to altered cardiac geometry, increase in fibroblasts and altered gene expression, and the function of ion channels. The changes in cardiac geometry and increase in fibroblasts are still very difficult to address pharmacologically leaving ion channels as preferential targets for clinically relevant drug development.

Less common but still clinically relevant are genetics-based ion channel defects. The inherited long QT syndrome (iLQTS) is a disorder which can occur by mutations in the coding region of the cardiac Na^+-channel (SCN5A, LQT syndrome 3) [5] or ankyrin-B (LQTS4) [6]. However, in most cases of LQTS, the potassium channel α-subunits KCNQ1 (LQTS1) and HERG (human ether-a-go-go-related gene, LQTS2) or their β-subunits (KCNE1, 2; LQT 5, 6) are affected. Further 10 LQT syndromes that may be less common have been described [7, 8]. In total, the current number of inherited LQTS sums up to 17 (LQTS1–17).

A second group of patients develops LQTS as response to clinically used drugs. This type of LQTS is called acquired LQTS (aLQTS) or drug-induced LQTS and is far more common than the inherited forms of LQTS. Drugs associated with increased risk of aLQTS include antiarrhythmics (dofetilide, ibutilide, procainamide, quinidine, sotalol, amiodarone, and disopyramide), psychoactive drugs (chlorpromazine, droperidol, haloperidol, levomethadyl, mesoridazine, methadone, pimozide, and thioridazine), antimalaria drugs (halofantrine, chloroquine), antibiotics (clarithromycine, erythromycine, and sparfloxazine), and others. A more complete list of drugs with risk of prolonging the QT interval and inducing *torsade-de-pointes* arrhythmias (QT drug list by Risk Groups) are available at http://www.torsades.org/medical-pros/drug-lists/drug-lists.htm. Most of the listed drugs are highly potent HERG blockers. However, some drugs in the list are KCNQ1/KCNE1-blockers as well. The iLQTS-associated KCNQ1/KCNE1 and HERG/KCNE2 channel mutations cause a decrease in net ventricular repolarizing current I_K by reducing potassium currents through "loss of function" mechanisms, whereas the aLQTS is the result of I_K-blockade. Thus, the reduced repolarizing I_K in both cases results in lengthened action potentials, reduced repolarization reserve, increased Ca^{2+}-inflow, increased likelihood of early after depolarizations (EAD), and prolongation of the QT interval in the electrocardiogram (ECG), predisposing affected individuals to syncope, seizures, aborted cardiac arrests and sometimes sudden cardiac death. Treatment for inherited LQTS includes invasive and cost-intensive therapies like high thoracic left sympathectomy and implantation of a cardioverter-defibrillator [9]. These invasive treatments are not favoured by patients and especially in children they are problematic. A more targeted approach is possible but limited to the case of LQT3: Using

Na^+-channel inhibitors to counteract the pathophysiological channel activity, which is the basis of this form of LQTS. The primary drug therapy of LQTS is the blockade of β-adrenergic receptors which was shown to be beneficial in some symptomatic LQTS patients [10, 11]. However, about 20–35% of LQTS patients presented as β-blocker therapy resistant [12, 13]. These high-risk patients still have breakthrough cardiac events like aborted cardiac arrest, syncope, and even sudden death even at ongoing β-blocker therapy. The failure rate of β-blocker therapy might be higher in patients carrying mutations in the potassium channel gene HERG than in the sodium channel gene encoding SCN5A as indicated by, e.g., the patient study by Chatrath et al. [14]. The standard therapies have considerably reduced mortality in inherited LQTS. Not well established is relevance of the life style for the LQTS phenotype. Currently, a clinical study with the goal to determine how lifestyle and exercise influence the well-being of individuals with and long QT syndrome (LQTS). This "*Lifestyle and Exercise in the Long QT Syndrome*" (*LIVE-LQTS*) by the Stanford University Medical Center will contribute to a better understanding of the handling of LQTS.

The aLQTS forces discontinuation of drug application and prevents usage of certain drugs in predisposed patients. This can be highly problematic if the iLQTS-causing drug is vital to the patient in a different clinical context. Thus, there exists a well-recognized need for improved treatments of both, iLQTS and aLQTS.

29.3 Pharmacological Inhibition of Cardiac Potassium Channels

It should be noted that block of I_{Kr} or I_{Ks} could be beneficial under special conditions and therefore highly selective blockade of I_{Kr} channels or I_{Ks} channels were considered as promising antiarrhythmic approaches and several companies developed selective blockers [15, 16]. Indeed, some of the most effective antiarrhythmic drugs, amiodarone, and its newly released (less effective) analog dronedarone, have several ion channel targets including I_{Kr} channels. The block of I_{Kr} channels is regarded a severe problem for pharmaceutical compounds intended for clinical trials and testing for I_{Kr} blockade has become an integral part of drug development and safety pharmacology. The inhibition of I_{Ks} has been identified as a potential problem of clinically useful drugs as well and testing for I_{Ks} blockade may become a further step of drug development and safety pharmacology [17]. The situation is complicated because the aLQTS might not always be apparent. During aLQTS and iLQTS, a drug-activating I_K will be beneficial.

HERG channels somehow act as "black hole-like super-absorber" for many drugs on the market: Many small hydrophobic drugs with aromatic ring systems and a central cationic charge target and thereby inhibit I_{Kr} channels. For some time, it has remained elusive why so many drugs bind to and block the HERG channel. Then, roughly two decades ago Mitcheson et al. [18] determined the putative binding site of the highly potent I_{Kr} inhibitors MK-499, cisapride, and terfenadine. The main determinants for the "sticky" binding site for highly potent blockers are aromatic residues pointing towards the central cavity. These aromatic residues allow hydrophobic and/or pi-stacking interactions with lipophilic and aromatic constituents of the respective drug molecules [19]. Meanwhile, reasonably reliable pharmacophore models exist that allow for virtual screening to prevent I_{Kr}-mediated iLQTS [20]. However, proposed binding modes differ in their orientations and interpretations on the role of key residues in the channel. Knowing that many clinically relevant drugs contain aromatic ring systems combined with an amine and are lipophilic to favor membrane passage the high incidence of interactions of the I_{Kr} channels with drugs becomes interpretable.

Currently, especially the pharmaceutic industry aims to combine pharmacophore modeling of I_{Kr} inhibitors with structural constraints for the I_{Kr} channel pore derived from homology to the known potassium channel structures [21] with the goal to generate in silico tools for the prediction of potential I_{Kr} inhibitors. Recently, there have been successful optimization strategies to avoid off-target interactions with hERG [20]. In any case, for acute aLQTS, a drug counteracting the I_{Kr} block would be highly desirable.

29.4 Impaired Channel Function Can Cause Cardiac Arrhythmia

Cardiac arrhythmia results from altered electrical substrate. These alterations include the heterogeneity of functional tissue caused by ischemia/infarction, virus/bacteria infection or the substitution of injured cardiomyocytes by fibroblasts as age- or infection-associated event. Further, the breakdown of ion channel functional gradients (e.g., I_{to}), impaired cell–cell contacts with altered Connexin 40, 43, and 45 function or dysbalanced ion fluxes within cardiomyocytes may lead to changes in the electrical properties of cardiac tissue which favor generation of ectopic foci and subsequent potentially lethal cardiac arrhythmias. One key point in understanding arrhythmias is the concerted function of ion channels in the myocyte. Concludingly, arrhythmia can be regarded as primary (altered function of ion channel protein by mutation) or secondary (altered functions of ion channels as a secondary event) channelopathy.

Channelopathies mainly result from a loss of channel function and disrupted balance of ion fluxes in tissues. Therefore, an attractive approach to treat channelopathies is to activate ion channels to regain channel function and re-establish balance of ion fluxes. In cardiac tissue, the concerted action of cation fluxes allows for the generation of the typical action potentials and the tightly controlled calcium influx. Loss of function (or gain of function) mutations in cation channels lead to "dissonance in the ion channel concert" accompanied by different action potential shape, changed timing and amplitude of ion fluxes, and often cardiac arrhythmias. An example for loss of function in delayed rectifier potassium currents causes the afore-mentioned lengthened ventricular action potential with increased QT interval and increased risk of *torsade-de-pointes* arrhythmia.

29.5 Activation of Potassium Channels

Channel activation may be achieved by augmentation of channel currents without marked alterations of kinetics. Activators that act by hastening activation, slowing deactivation, and/or alter voltage dependence are termed "gating modifiers". The macroscopic current ($I_{macroscopic}$) flowing through a homogenous population of ion channels is described by the formula: $I_{macroscopic} = I_{single\ channel} * n * p_o$, whereas $I_{single\ channel}$ describes the single channel conductance, n determines the number of active channel, and p_o—the open probability of the channels. Compounds that increase currents by augmenting $I_{macroscopic}$ currents are often called pure agonists. Increased macroscopic currents $I_{macroscopic}$ by changes in the so-called "micro-gating" describe the increase of mean open time p_0. Recently, studies on pharmacological manipulation of I_{Kr} channel trafficking suggest that in future compounds that facilitate I_{Kr} channel exocytosis may become available. Compounds acting like this will increase the number of functional channels in the plasma membrane to increase macroscopic channel current $I_{macroscopic}$. The discrimination among the exact action of a compound is complex and can be best addressed by single-channel analysis in combination with measurements of macroscopic currents and surface ion channel protein detection. Indeed, without being able to exclude the possibility that a "pure" agonist acts as a gating modifier of the micro-gating it may be questioned if it should be called a "pure agonist" but rather less-defined "agonist." The situation is even more complicated as partial agonists exert both agonism and antagonism. The specific context of agonism/antagonism varies and can be concentration-dependent and/or state-dependent.

To test the potential clinical benefit of activating cation channels as clinical approach to treat cardiac arrhythmias, specific agonist compounds are needed. In many cases, the lack of agonist molecules with different modes of action has compromised testing this hypothesis.

Only a limited, but increasing number of highly potent and selective cation channel activators are known [22]. Several of these activators like 1-EBIO, stilbenes, rottlerin, and fernemates are not specific and of relatively low potency. Commonly, these agonist molecules are relatively small, hydrophobic and rich in aromatic rings (Fig. 29.1). Examples of cation channel agonists are:

- a variety of K_{ATP}-channel agonists (BMS-180448, cromakalim, celikalim, diazoxide, JTV-506, KR-30450, lemakalim, levosimendan, minoxidil sulfate, nicorandil, P1075, pinacidil, rilmakalim, SKP-450, WAY-133537, Y 26763, ZD6169, and ZM-244085); several classes of Ca^{2+}-activated K^+-channel (BK and SK) activators (BMS-204352, chlorzoxazone, zoxazolamine, DHS-I, 1-EBIO/DC-EBIO, maxiKdiol, NS304/analogs, BRL-55834, and NS11021);
- some KCNQ activator classes (BMS-204352/MaxiPost, retigabine, meclofenamic acid, fernemates, R-L3, stilbenes, ICA-27243, benzo(d)isoxazole, salicylate analogues, 3-aminoquinazolin-one, 2-acrylthiazol), ML277, quercetin, PBA, gintonin, rottlerin, ω6- and ω9–polyunsaturated fatty acids, CP1, phosphatidylinositol 4,5-bisphosphate ($PI(4,5)P_2$);
- I_{Kr} agonists (RPR260243, RD-307243, A-935142, NS1643, and NS3623);
  - the KCNK-agonist riluzole,
  - the GIRK channel agonist flupirtine;
  - the Kv4.3 channel agonist NS5806;

Some cation channel agonists hold the potential of clinical applicability: The K_{ATP}-channel activators are clinically used as antihypertensive drugs and to stimulate hair re-growth. K_{ATP}-channel agonists are discussed in context of asthma, hyperactive bladder disorder treatment and mitochondria-linked arrhythmias. Increasing resting membrane stabilization by K_{ATP}-channel opening was proposed to be beneficial in LQTS [23, 24]. The L-type Ca^{2+} channel opener Bay K 8644 remained a tool for basic research and has been tested for its potential in verapamil intoxication [25]. The KCNQ channels form the classical M-channels and the activators retigabine, R-L3, ML277, quercetin, PBA, gintonin, rottlerin, ω6- and ω9–polyunsaturated fatty acids, CP1, phosphatidylinositol 4,5-bisphosphate ($PI(4,5)P_2$) and BMS-204352 could become important in the treatment of incontinence, high blood pressure, epilepsy or cardiac arrhythmia [26–38]. BK-channel activators could be relevant in treatment of stroke, hypertension and overactive bladder disorders [39]. The activation of KCNK channels by riluzole exerts significant anti-seizure properties [40] and could be of use as antiarrhythmic drugs as well. Other possible indications for specific channel openers are reviewed [41, 42]. Thus, cation channel activators are still relatively rare but hold a broad variety of potential applications including administration as antiarrhythmics.

29.6 In Vitro and In Vivo Effects of Potassium Channel Activators

In 1998 the first highly potent selective KCNQ1/KCNE1 activator R-L3 was published [35]. R-L3 acts as a gating modifier by mildly slowing channel activation but dramatically decreasing the rate of channel deactivation. In addition, the compound increases macroscopic current amplitudes by a mechanism independent of the kinetic effects [43]. R-L3 shortens action potential duration, suppresses early afterdepolarisations in ventricular myocytes isolated from hypertrophied rabbit hearts. In addition, R-L3 reverses action potential lengthening and therewith suppresses early afterdepolarizations in myocytes treated with the I_{Kr} blocker dofetilide [44] (Fig. 29.2). The I_{Kr} inhibition by dofetilide mimicks iLQTS and thus these experiments suggests that R-L3 may be beneficial in some forms of iLQT and aLQTS. In 2004 Kang et al. [45] characterized the first known I_{Kr} channel activator, RPR260243. The compound markedly slows I_{Kr} channel deactivation thereby enhancing net I_{Kr} currents. RPR260243 increases the energy barrier for open state to closed state transitions. The slowing of deactivation identifies this compound as a gating modifier similar to R-L3. RPR260243

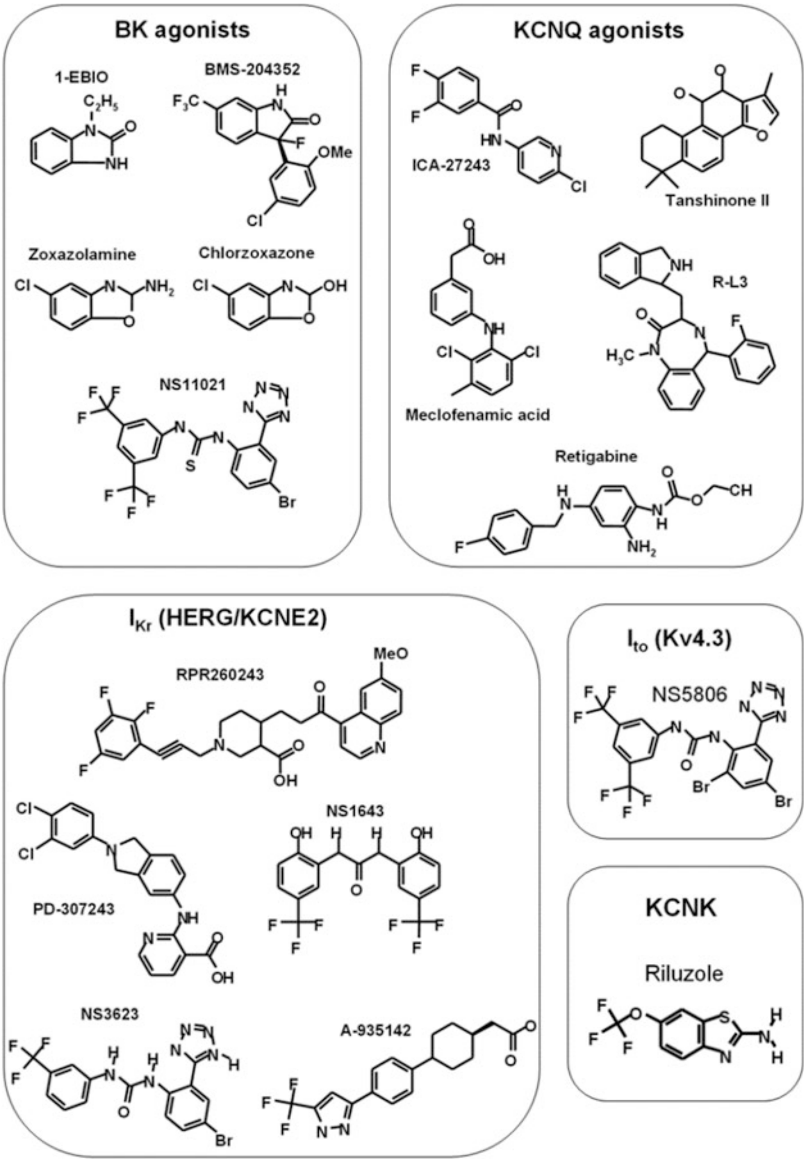
BK agonists
1-EBIO
BMS-204352
Zoxazolamine
Chlorzoxazone
NS11021
KCNQ agonists
ICA-27243
Tanshinone II
Meclofenamic acid
R-L3
Retigabine
I_{Kr} (HERG/KCNE2)
RPR260243
PD-307243
NS1643
NS3623
A-935142
I_{to} (Kv4.3)
NS5806
KCNK
Riluzole

Fig. 29.1 Structures of exemplary potassium channel agonists

functionally counteracts blockade by dofetilide in the Langendorff heart model. Therefore, these experiments strongly suggest that both, activation of cardiac I_{Kr} and/or I_{Ks} may act as QT interval shortening mechanisms suited for the normalization of QT in forms of iLQT and the 17 aLQTS. R-L3 has the potential to activate most of the LQTS associated mutant channels. However, one mutation disrupted the activating effect probably by disrupting the R-L3 binding site [43]. These data provided proof of principle of the concept that the combined knowledge of an inherited gene variant in an ion channel gene and the binding site of a drug in the respective channel could be used to predict a possible drug resistance by mutational disruption of the molecular binding site in the ion channel protein.

The first I_{to} agonist published was NS5806 [46]. However, the compound recapitulated the electrocardiographic and proarrhythmic manifestations of Brugada syndrome in isolated canine ventricular myocytes. In canine ventricular

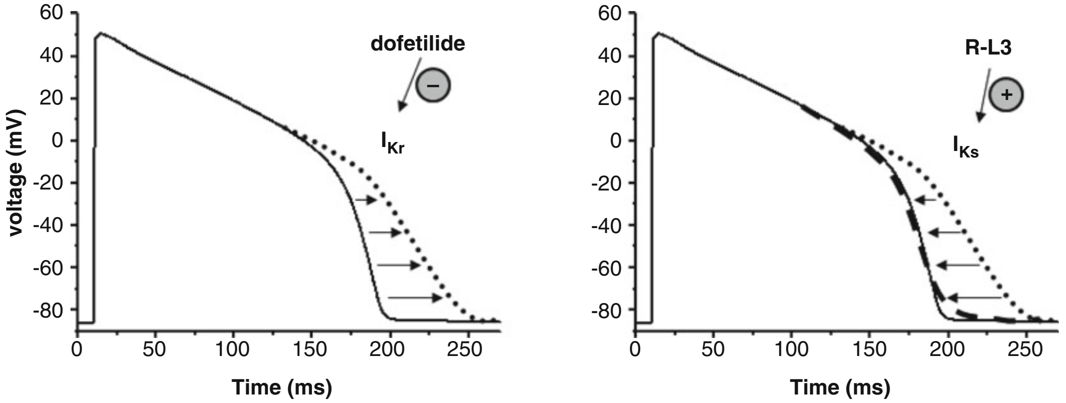

Fig. 29.2 Dofetilide inhibition of I_{Kr} channels induced action potential lengthening, which can be reversed by activation of I_{Ks} by R-L3

wedge preparations, NS5806 increased epicardial phase 1 and notch amplitude of the action potential and led to the development of phase 2 re-entry and polymorphic ventricular tachycardia. These data suggested that I_{to} activation is not suited for the development of an antiarrhythmic agent. Rather, these data might strengthen the arguments for a pharmacological I_{to} inhibition as an antiarrhythmic approach. Indeed, pharmaceutical companies aim to identify and test I_{to} inhibitors.

29.7 The Structural Basis of Channel Activation

The pharmaceutical industry searches for ion channel modulators using high throughput screening methods and huge compound libraries. Robust assays can easily screen 10,000–100,000 compounds per day on a single target. However, only a limited set of cation channel activators lead scaffolds have been reported so far. Why is it more difficult to discover activators? A glimpse of an idea arises when studying data on interactions of cation channel agonists with their specific binding site(s) on the respective cation channel. In the last 20 years the data available on ion channel modulator binding sites has grown so that such study is now feasible. The variety of K_{ATP}-channel activators might arise from the fact that all K_{ATP}-channel activators bind to one of two binding sites in the sulfonylurea subunit of the channel and that this subunit provides a relatively easily accessible drug target. Thus, these compounds do not bind to the pore-forming subunit Kir6.1/2 which is homologous in cation channels. BK channel agonists mostly bind to calmodulin in the BK channel protein complex to increase the calcium sensitivity of the channels. Thus, also these agonists do not bind to the channel forming subunit. However, as calmodulin is an integral part in several multi-protein complexes drugs acting like the BK agonists could be expected to exert pharmacological side effects when systemically administered. Therefore, compounds binding to the channel forming subunit promise greater selectivity. (S)-(−)Bay K 8644 binds to and interacts with the S5-S6 pore module of L-type Ca channels [47–49].

The identification of the binding site of an agonist for a cardiac voltage-dependent potassium channel with relative high resolution was a pioneering step into understanding agonist-pore interactions. Alanine-scanning methods combined with 3D-modelling techniques were used to determine the putative binding site of the benzodiazepine R-L3 that activates KCNQ1 channels [43]. The binding site is located deep in the potassium channel protein among pore helix, S5, S6 and possibly S4. Theoretically, this position and the small size of the binding pocket might allow only closely related chemicals to enter and bind to this position. This may be a desired prerequisite for the generation of selective drug candidates. If substances have to bind to sites deep inside channel proteins as recently shown by Sun and MacKinnon for BAY K 8644 [36] and R-L3, then even minor structural changes in the agonist scaffold could disrupt correct binding and the chemical optimization process might be relatively challenging. However, the chemical optimization process should generate sufficient selectivity towards closely related ion channel proteins. In line with this idea, retigabine, a first-generation drug candidate as an anti-epileptic, does not target cardiac I_{Ks} channels (KCNQ1) but the closely related neuronal homologous (KCNQ2–5) channels [50–55]. On the other hand R-L3 activates the cardiac I_{Ks} channels (KCNQ1) but not the neuronal KCNQ2/3 channels [35]. The binding site of retigabine could be localized to the lower S5-S6 region below the pore helix and adjacent to the neighboring channel subunit [50, 53, 55, 56]. Finally, the compound CP1 has been described to overlap with its binding site with that of PI(4,5)P_2 and to mimic the action of the native lipid PI(4,5)P_2 [29]. Comparing the binding sites of the described activators it becomes obvious that there exist several interaction sites for KCNQ channel agonists (Fig. 29.3). These putative binding sites suggest strict molecular requirements for the compounds to be ligands for the specific agonist binding pocket. These molecular constraints determine size (volume), geometry, chemical nature (hydrophobicity, aromaticity) and dynamics of the compound. Meanwhile, several KCNQ channel agonists have been reported. Based on functional and structural data on compounds like CP1, R-L3, polyunsaturated fatty acids, PI(4,5)P_2, and retigabine the binding sites of these compounds could be assessed at reasonable to good resolution [26, 29, 36].

The size and chemical nature of the agonists suggest a scheme in which MaxiPost and Benzo(d)isoxazole may bind to the R-L3 site and retigabine analogues, 2-arythiazole and 3-aminoquinazoline-one may target the retigabine binding site. CP1 might bind to a site close to PI(4,5)P_2, and polyunsaturated fatty acids bind in the region of the outer leaflet region (Fig. 29.3). Common to these compounds is that they bind to and stabilize the open channel structure kinetically favoring open channel function. This feature might prove helpful when in silico screening is applied. Compounds that virtually bind to binding pockets existing only in the open state, structural models but not closed-state target models might represent potential gating modulators with activating profile.

29.8 The Quest for Potassium Channel Activators

Often agonists are identified by accident when screening for compounds intended for other targets. Possibly, there is a technical problem not addressed by modern screening techniques: Pharmaceutical companies screen for lead structures. Then they modify these leads to explore the structure in detail to find the molecule with the best combination of EC_{50}, bioavailability, selectivity and drug stability. This concept works well for binding sites on the surface or in relatively large cavities. An example is the search for small molecule cation channel blockers for which the preferential binding site is the large central cavity of cation channels (Fig. 29.4). Thus, in the conventional screen lead structures and analogs binding to surface accessible binding sites are preferentially identified. Therefore, it is not surprising that agonists are often found randomly when working with compounds intended for distinct targets but not by systematic screens for channel activators. For example, I_{Ks} antagonists with a lead benzodiazepine scaffold were searched for by MSD and by accident the I_{Ks} agonist R-L7 was identified. More recently, novel screening approaches have been used to identify channel activators. Often automated patch-clamp techniques have been used to identify ion channel activators rather than commonly voltage dependent-fluorescence in cell-based assays that are well suited to screen for identification of channel blockers. A combination of in silico

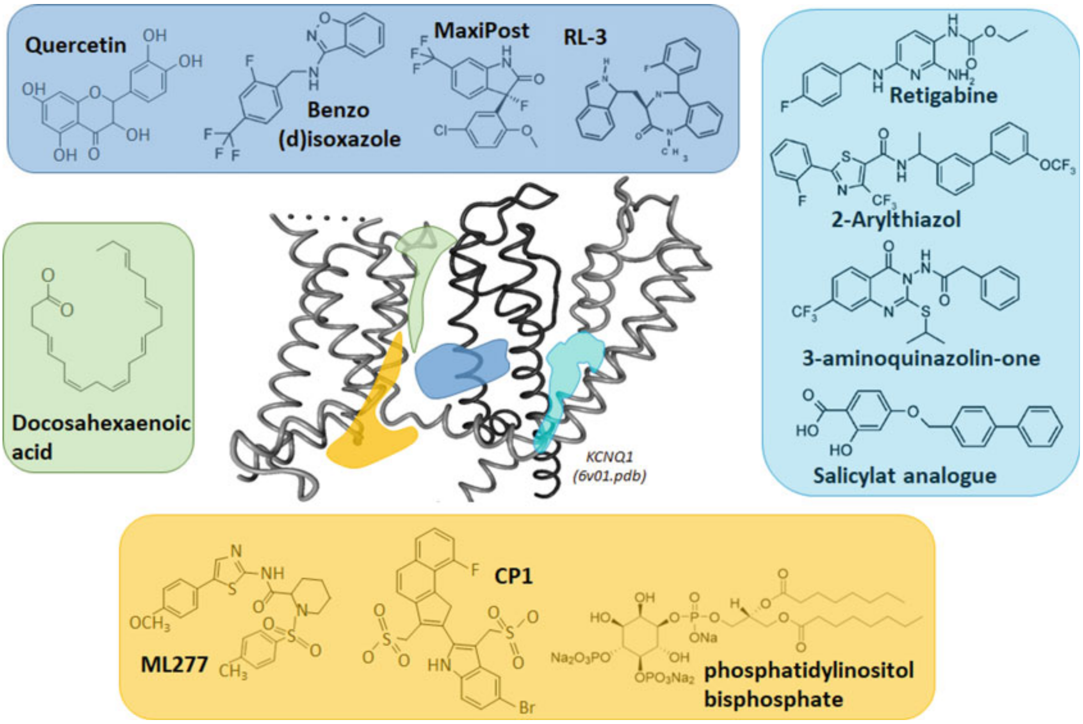
Quercetin
Benzo (d)isoxazole
MaxiPost
RL-3
Retigabine
2-Arylthiazol
3-aminoquinazolin-one
Salicylat analogue
Docosahexaenoic acid
KCNQ1 (6v01.pdb)
ML277
CP1
phosphatidylinositol bisphosphate

Fig. 29.3 Structure and putative discrete binding sites of four classes of KCNQ channel agonists. The binding sites have been shown in silico, indirectly experimentally or via Cryo-EM

screening methods combined with automated patch clamp or automated TEVC proved effective. The electrophysiological methods used to be relatively slow [57], but recent technical advances increased the throughput dramatically. This is the basis for more direct assays with sufficiently high sensitivity. Gathering of structural data and functional modification of channel features by drugs

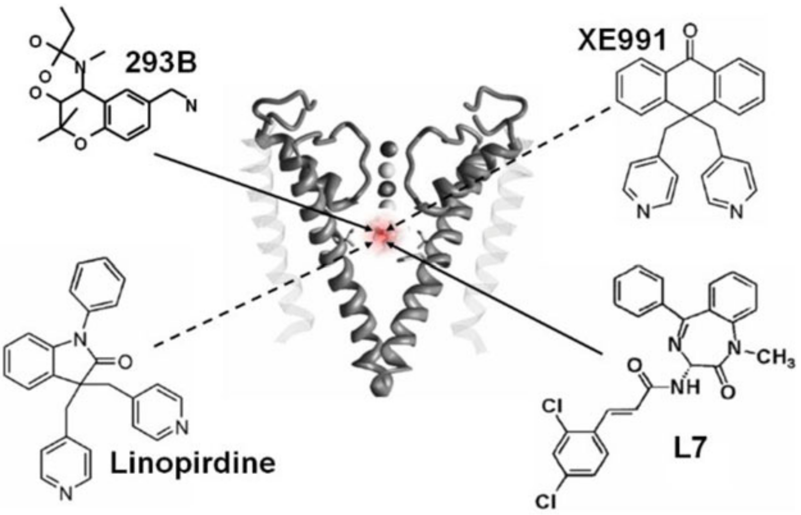
293B
XE991
Linopirdine
L7

Fig. 29.4 Structure and putative binding site in the central cavity of I_{Ks} (KCNQ1/KCNE1) channel inhibitors. The binding sites of 293B and L7 have been shown experimentally

will allow us to use computer-aided approaches for putative channel activators in future. Such in silico approaches could be combined with high-resolution electrophysiological screening methods.

29.9 Conclusion

In summary, activators of cation channels are promising candidates to regain channel function in acquired or inherited cardiac channelopathies like LQTS. Novel drug screening methods have provided activators with varying functional activity. Functional testing as pharmacological agents in clinical context is now within reach. An extended knowledge about cation channel activator binding and action might enable us to apply in silico guided drug design of cation channel agonists. The new potent cation channel activators will enable us to test the concept of ion channel activation as a clinically relevant principle in cardiac arrhythmias disorders.

References

1. Derst C, Konrad M, Kockerling A, Karolyi L, Deschenes G, Daut J, et al. Mutations in the ROMK gene in antenatal Bartter syndrome are associated with impaired K+ channel function. Biochem Bioph Res Co. 1997;230:641–5.
2. Nestorowicz A, Wilson BA, Schoor KP, Inoue H, Glaser B, Landau H, et al. Mutations in the sulfonylurea receptor gene are associated with familial hyperinsulinism in Ashkenazi Jews. Hum Mol Genet. 1996;5:1813–22.
3. Thomas PM, Cote GJ, Wohllk N, Haddad B, Mathew PM, Rabl W, et al. Mutations in the sulfonylurea receptor gene in familial persistent Hyperinsulinemic hypoglycemia of infancy. Science. 1995;268:426–9.
4. Adelman JP, Bond CT, Pessia M, Maylie J. Episodic ataxia results from voltage-dependent potassium channels with altered functions. Neuron. 1995;15: 1449–54.
5. Wang Q, Shen JX, Splawski I, Atkinson D, Li ZZ, Robinson JL, et al. Scn5a mutations associated with an inherited cardiac-arrhythmia. Long Qt Syndrome Cell. 1995;80:805–11.
6. Mohler PJ, Schott JJ, Gramolini AO, Dilly KW, Guatimosim S, duBell WH, et al. Ankyrin-B mutation causes type 4 long-QT cardiac arrhythmia and sudden cardiac death. Nature. 2003;421:634–9.
7. Priori SG, Wilde AA, Horie M, Cho Y, Behr ER, Berul C, et al. HRS/EHRA/APHRS expert consensus statement on the diagnosis and management of patients with inherited primary arrhythmia syndromes: document endorsed by HRS, EHRA, and APHRS in may 2013 and by ACCF, AHA, PACES, and AEPC in June 2013. Heart Rhythm. 2013;10:1932–63.
8. Skinner JR, Winbo A, Abrams D, Vohra J, Wilde AA. Channelopathies that lead to sudden cardiac death: Clinical and genetic aspects. Heart Lung Circ. 2019;28:22–30.
9. Schwartz PJ, Priori SG, Dumaine R, Napolitano C, Antzelevitch C, Stramba-Badiale M, et al. A molecular link between the sudden infant death syndrome and the long-QT syndrome. New Engl J Med. 2000;343:262–7.
10. Schwartz PJ, Periti M, Malliani A. Long Q-T syndrome. Am Heart J. 1975;89:378–90.
11. Ward OC. A new familial cardiac syndrome in children. J Irish Med Assoc. 1964;54:103–6.
12. Ackerman MJ. The long QT syndrome: ion channel diseases of the heart. Mayo Clin Proc. 1998;73:250–69.
13. Moss AJ, Zareba W, Hall WJ, Schwartz PJ, Crampton RS, Benhorin J, et al. Effectiveness and limitations of beta-blocker therapy in congenital long-QT syndrome. Circulation. 2000;101:616–23.
14. Chatrath R, Bell CM, Ackerman MJ. Beta-blocker therapy failures in symptomatic probands with genotyped long-QT syndrome. Pediatr Cardiol. 2004;25:459–65.
15. Gerlach U. Blockers of the slowly delayed rectifier potassium IKs channel: potential antiarrhythmic agents. Curr Med Chem Cardiovasc Hematol Agents. 2003;1:243–52.
16. Lee K, Park JY, Ryu PD, Kwon LS, Kim HY. IKr channel blockers: novel antiarrhythmic agents. Curr Med Chem Cardiovasc Hematol Agents. 2003;1:203–23.
17. Towart R, Linders JT, Hermans AN, Rohrbacher J, van der Linde HJ, Ercken M, et al. Blockade of the I (Ks) potassium channel: an overlooked cardiovascular liability in drug safety screening? J Pharmacol Toxicol Methods. 2009;60:1–10.
18. Mitcheson JS, Chen J, Lin M, Culberson C, Sanguinetti MC. A structural basis for drug-induced long QT syndrome. Proc Natl Acad Sci U S A. 2000;97:12329–33.
19. Chen J, Seebohm G, Sanguinetti MC. Position of aromatic residues in the S6 domain, not inactivation, dictates cisapride sensitivity of HERG and eag potassium channels. Proc Natl Acad Sci U S A. 2002;99: 12461–6.
20. Kalyaanamoorthy S, Barakat KH. Development of safe drugs: the hERG challenge. Med Res Rev. 2018;38:525–55.
21. Bains W, Basman A, White C. HERG binding specificity and binding site structure: evidence from a

fragment-based evolutionary computing SAR study. Prog Biophys Mol Biol. 2004;86:205–33.

22. Seebohm G. Activators of cation channels: potential in treatment of channelopathies. Mol Pharmacol. 2005;67:585–8.
23. Shimizu W, Antzelevitch C. Effects of a K(+) channel opener to reduce transmural dispersion of repolarization and prevent torsade de pointes in LQT1, LQT2, and LQT3 models of the long-QT syndrome. Circulation. 2000;102:706–12.
24. Tan HL, Alings M, Van Olden RW, Wilde AA. Long-term (subacute) potassium treatment in congenital HERG-related long QT syndrome (LQTS2). J Cardiovasc Electrophysiol. 1999;10:229–33.
25. Magdalan J. New treatment methods in verapamil poisoning: experimental studies. Pol J Pharmacol. 2003;55:425–32.
26. Bohannon BM, Perez ME, Liin SI, Larsson HP. Omega-6 and omega-9 polyunsaturated fatty acids with double bonds near the carboxyl head have the highest affinity and largest effects on the cardiac I-Ks potassium channel. Acta Physiol. 2019;225: e13186.
27. Choi SH, Lee BH, Kim HJ, Jung SW, Kim HS, Shin HC, et al. Ginseng Gintonin activates the human cardiac delayed rectifier K+ channel: involvement of Ca2+/calmodulin binding sites. Mol Cells. 2014;37: 656–63.
28. De Silva AM, Manville RW, Abbott GW. Deconstruction of an African folk medicine uncovers a novel molecular strategy for therapeutic potassium channel activation. Sci Adv. 2018;4:4.
29. Liu YF, Xu XJ, Gao JY, Naffaa MM, Liang HW, Shi JY, et al. A PIP2 substitute mediates voltage sensor-pore coupling in KCNQ activation. Commun Biol. 2020;3:3.
30. Lubke M, Schreiber JA, Quoc TL, Korber F, Muller J, Sivanathan S, et al. Rottlerin: structure modifications and KCNQ1/KCNE1 Ion Channel activity. ChemMedChem. 2020;15:1078–88.
31. Manville RW, Abbott GW. Cilantro leaf harbors a potent potassium channel-activating anticonvulsant. FASEB J. 2019;33:11349–63.
32. Matschke V, Piccini I, Schubert J, Wrobel E, Lang F, Matschke J, et al. The natural plant product Rottlerin activates Kv7.1/KCNE1 channels. Cell Physiol Biochem. 2016;40:1549–58.
33. Mruk K, Kobertz WR. Discovery of a novel activator of KCNQ1-KCNE1 K+ channel complexes. PLoS One. 2009;4:4.
34. Redford KE, Abbott GW. The ubiquitous flavonoid quercetin is an atypical KCNQ potassium channel activator. Commun Biol. 2020;3:3.
35. Salata JJ, Jurkiewicz NK, Wang JX, Evans BE, Orme HT, Sanguinetti MC. A novel benzodiazepine that activates cardiac slow delayed rectifier K+ currents. Mol Pharmacol. 1998;54:220–30.
36. Hockerman GH, Peterson BZ, Johnson BD, Catterall WA. Molecular determinants of drug binding and action on L-type calcium channels. Annu Rev Pharmacol Toxicol. 1997;37:361-96. doi: 10.1146/annurev.pharmtox.37.1.361. PMID: 9131258
37. Yu H, Lin Z, Mattmann ME, Zou B, Terrenoire C, Zhang H, et al. Dynamic subunit stoichiometry confers a progressive continuum of pharmacological sensitivity by KCNQ potassium channels. Proc Natl Acad Sci U S A. 2013;110:8732–7.
38. Zheng YM, Zhu XJ, Zhou PZ, Lan X, Xu HY, Li M, et al. Hexachlorophene is a potent KCNQ1/KCNE1 Potassium Channel activator which rescues LQTs mutants. PLoS One. 2012;7:7.
39. Malysz J, Buckner SA, Daza AV, Milicic I, Perez-Medrano A, Gopalakrishnan M. Functional characterization of large conductance calcium-activated K+ channel openers in bladder and vascular smooth muscle. Naunyn Schmiedeberg's Arch Pharmacol. 2004;369:481–9.
40. Borowicz KK, Swiader M, Drelewska E, Czuczwar SJ. Interactions between riluzole and conventional antiepileptic drugs - a comparison of results obtained in the subthreshold method and isobolographic analysis. J Neural Transm. 2004;111:1511–22.
41. Cooper EC, Jan LY. Ion channel genes and human neurological disease: recent progress, prospects, and challenges. Proc Natl Acad Sci U S A. 1999;96:4759–66.
42. Lawson K, Dunne MJ. Peripheral channelopathies as targets for potassium channel openers. Expert Opin Inv Drug. 2001;10:1345–59.
43. Seebohm G, Pusch M, Chen J, Sanguinetti MC. Pharmacological activation of normal and arrhythmia-associated mutant KCNQ1 potassium channels. Circ Res. 2003;93:941–7.
44. Xu X, Salata JJ, Wang J, Wu Y, Yan GX, Liu T, et al. Increasing I(Ks) corrects abnormal repolarization in rabbit models of acquired LQT2 and ventricular hypertrophy. Am J Physiol Heart Circ Physiol. 2002;283: H664–70.
45. Kang JS, Chen XL, Wang HG, Ji JZ, Cheng H, Incardona J, et al. Discovery of a small molecule activator of the human ether-a-go-go-related gene (HERG) cardiac K+ channel. Mol Pharmacol. 2005;67:827–36.
46. Calloe K, Soltysinska E, Jespersen T, Lundby A, Antzelevitch C, Olesen SP, et al. Differential effects of the transient outward K+ current activator NS5806 in the canine left ventricle. J Mol Cell Cardiol. 2010;48:191–200.
47. Yamaguchi S, Zhorov BS, Yoshioka K, Nagao T, Ichijo H, Adachi-Akahane S. Key roles of Phe1112 and Ser1115 in the pore-forming IIIS5-S6 linker of L-type Ca2+ channel alpha1C subunit (CaV 1.2) in binding of dihydropyridines and action of Ca2+ channel agonists. Mol Pharmacol. 2003;64:235–48.
48. Zhao YY, Huang GXY, Wu JP, Wu QR, Gao S, Yan Z, et al. Molecular basis for ligand modulation of a mammalian voltage-gated Ca2+ channel. Cell. 2019;177:1495.

49. Zhorov BS, Folkman EV, Ananthanarayanan VS. Homology model of dihydropyridine receptor: implications for L-type ca(2+) channel modulation by agonists and antagonists. Arch Biochem Biophys. 2001;393:22–41.
50. Lange W, Geissendorfer J, Schenzer A, Grotzinger J, Seebohm G, Friedrich T, et al. Refinement of the binding site and mode of action of the anticonvulsant Retigabine on KCNQ K+ channels. Mol Pharmacol. 2009;75:272–80.
51. Main MJ, Cryan JE, Dupere JRB, Cox B, Clare JJ, Burbidge SA. Modulation of KCNQ2/3 potassium channels by the novel anticonvulsant retigabine. Mol Pharmacol. 2000;58:253–62.
52. Rundfeldt C, Netzer R. The novel anticonvulsant retigabine activates M-currents in Chinese hamster ovary-cells tranfected with human KCNQ2/3 subunits. Neurosci Lett. 2000;282:73–6.
53. Schenzer A, Friedrich T, Pusch M, Saftig P, Jentsch TJ, Grotzinger J, et al. Molecular determinants of KCNQ (K(V)7) K+ channel sensitivity to the anticonvulsant retigabine. J Neurosci. 2005;25:5051–60.
54. Wickenden AD, Yu W, Zou A, Jegla T, Wagoner PK. Retigabine, a novel anti-convulsant, enhances activation of KCNQ2/Q3 potassium channels. Mol Pharmacol. 2000;58:591–600.
55. Wuttke TV, Seebohm G, Bail S, Maljevic S, Lerche H. The new anticonvulsant retigabine favors voltage-dependent opening of the Kv7.2 (KCNQ2) channel by binding to its activation gate. Mol Pharmacol. 2005;67:1009–17.
56. Li X, Zhang QS, Guo PP, Fu J, Mei LH, Lv DS, et al. Molecular basis for ligand activation of the human KCNQ2 channel. Cell Res. 2021;31(1):52–61.
57. Xu J, Wang XB, Ensign B, Li M, Wu L, Guia A, et al. Ion-channel assay technologies: quo vadis? Drug Discov Today. 2001;6:1278–87.

Index

A
Acidosis, 16, 286, 296–298, 301, 311, 316–318, 323, 449
Actinomycin D, 480
Action potential (AP), 3–7, 9, 11–13, 16, 19, 28, 29, 31–36, 38, 39, 44–47, 50–52, 54, 55, 57–59, 64, 65, 74, 75, 89–93, 95, 97–103, 112, 113, 116, 134–140, 142, 143, 156, 158–164, 168, 169, 171–175, 178, 195, 203, 205, 210, 211, 228, 233–236, 238–240, 243, 255–258, 268, 278, 279, 284–286, 294–298, 300, 310, 311, 314, 316, 317, 329, 332–335, 360, 362, 366, 367, 369, 379, 380, 382, 387, 399–401, 405–407, 411, 412, 420, 446–448, 450, 462–465, 469, 470, 518–523, 526–530, 544, 552–557, 568, 570, 571, 573
  AP upstroke velocity, 316
Acute ischemia-reperfusion injury, 301–302
Adenosine 5′-triphoshate (ATP), 277
Agonist, 46, 80, 94, 101, 159, 171, 196, 203, 228, 236, 279, 281, 286, 300, 406, 411, 412, 418, 462, 508, 570–574
Air pollution, 494, 495, 501
A-kinase anchoring proteins, 444
Alternans, 209–210
Angiotensin II, 297
Angiotensin-converting enzymes, 431
Anisotropic conduction, 318
Anisotropy, 315–316
Ankyrins, 15, 277, 279, 409, 464, 469, 539
  Ankyrin-B, 241, 331
Anrep effect, 335
Antiarrhythmic drug, 7, 12, 18, 19, 263, 529, 554, 556–558
Antiarrhythmic peptide 10 (AAP10), 317, 321, 322, 558
Apoptosis, 480
Arrhythmias, 4, 40, 65, 93, 118, 132, 172, 188, 228, 255, 277, 293, 311, 360, 377, 401, 417, 431, 447, 460, 479, 495, 518, 541, 552, 568
  re-entrant arrhythmia, 317
  Torsades de Pointes (TdP) arrhythmia, 255
Arrhythmogenesis, 9, 16, 18, 138, 139, 188–189, 191, 195, 196, 211, 242, 280, 287, 296, 297, 300, 305, 316–321, 323, 352, 377, 387–390, 469, 470, 501–503, 506–509, 518, 519, 522, 526–529, 558
Arrhythmogenic right ventricular cardiomyopathy, 195–196
Atrial dilation, 240, 558
Atrial fibrillation (AF), 10–18, 72, 78, 114, 121, 123–125, 141, 188–194, 197–202, 209–211, 228–230, 236, 237, 239–243, 258, 293, 300, 310, 316, 319, 323, 366, 417, 419, 450, 452, 470, 501–508, 518, 519, 521–524, 528, 542, 543, 545, 546, 551–559
Atria-selective drugs, 555–557
Atrio-ventricular block, 379
Autoantibodies, 238, 484
  anti-Ro/SSA autoantibodies, 238
  Ca^{2+} channel autoantibodies (CC-AAbs), 238
  cardiac troponin I autoantibodies, 238
Autoimmune congenital heart block (ACHB), 238
Automaticity, 30, 37, 50, 55, 64, 71, 77, 79, 89, 90, 93–95, 98–101, 103, 104, 116, 118, 121, 123, 124, 126, 190, 192, 193, 195, 228, 280, 293, 294, 299, 317, 379, 471, 542, 544
Autonomic, 46, 65–67, 71, 79, 97, 99–101, 103, 110, 112, 114, 119, 121, 123, 124, 136, 151–154, 156, 157, 159, 164, 166, 168–170, 175, 177, 179, 180, 187–211, 406, 495, 496, 504, 552
Autonomic innervation of the heart, 153–157
Autonomic nervous system, 151
Autonomic neuromodulatory interventions (ANIs), 196–205, 210, 211
Autonomic neurotransmitters, 65, 188–192
Autophagy, 480
  autophagosome, 481
  autophagy-lysosome pathway (ALP), 467
Autoregulation, 131, 143, 231, 335–336

B
Background current, 33, 35, 60, 380
Bainbridge response, 132
Barker hypothesis, 505
β-adrenergic signaling, 462
β-adrenergic stimulation, 54, 233, 242, 243, 337, 364, 419, 423, 433, 445, 447, 449, 450, 479
β-adrenoceptors, 331
β-catenin, 463
Biophysical model, 27

© Springer Nature Switzerland AG 2023

O. N. Tripathi et al. (eds.), *Heart Rate and Rhythm*, https://doi.org/10.1007/978-3-031-33588-4

Bradycardia, 141
Bridging-integrator-1, 348
Brugada syndrome (BrS), 206, 207, 278

C
Ca^{2+}-and Na^{+}-activated K channels (K$_{Ca}$/K$_{Na}$), 11–12
Ca^{2+}-calmodulin-dependent kinase II (CaMKII), 337
Ca^{2+} handling proteins, 116, 124, 141, 239, 429, 430
Ca^{2+} homeostasis, 71, 408, 481, 502
Ca^{2+}-induced Ca^{2+} release (CICR), 233, 294, 329, 481
Calcium (Ca^{2+}), 8, 30, 46, 64, 90, 119, 132, 178, 188, 228, 294, 329, 347, 399, 418, 444, 462, 479, 501, 518, 541, 553, 570
Calcium paradox, 302
Calcium transient, 90, 92, 93, 97, 100, 101
  systolic Ca^{2+} transient, 329
Calmodulin (CaM), 230
Calmodulin kinase II (CaMKII), 9, 18, 94–97, 103, 235, 243, 407, 418, 420, 431, 436, 437, 461, 463, 465, 469, 470, 544, 545
Calsequestrin, 400
CamKII inhibitor KN-93, 337
Capacitive coupling, 314
Cap-dependent translation, 477
  eIf4G, 477
Cardiac arrhythmia, 8, 9, 12, 13, 40, 94, 137, 140, 141, 190, 228, 230, 234, 235, 238–240, 242, 255–267, 284, 293–294, 297–303, 311, 316, 360, 364, 367, 370, 377, 378, 396, 422, 447, 452, 468, 471, 502, 509, 545, 558, 568, 570, 571, 576
Cardiac disease, 78, 79, 114, 121, 152, 236, 240, 243, 278, 297, 310, 316, 323, 419, 433, 475, 501, 507, 541
Cardiac ganglia, 154, 155, 158, 163
Cardiac glycosides, 266, 300, 334–335, 419, 421, 422, 518
Cardiac muscle, 282, 329, 331, 332, 385, 421, 423, 430, 432, 433, 435
Cardiac rhythm, 10, 11, 16–18, 27, 38, 40, 77, 78, 80, 234–237, 240, 286, 360, 377, 462, 464, 465, 467, 540, 546, 557
Cardiac rhythm disturbances, 243
Cardiomyocyte, 18, 55, 71, 95, 110, 134, 159, 188, 228, 256, 277, 294, 310, 347, 360, 379, 408, 416, 429, 444, 462, 476, 498, 528, 540, 555, 570
Cardiotoxicity screening, 360, 367–368, 370
Cardiovascular disease (CVD), 152, 448, 494–497, 500–503, 506, 508
Cariporide, 304, 420
Carnitine deficiency, 525, 526
Ca^{2+} spark, 400
Caspase activation and recruitment domain (CARD), 483
Catecholaminergic polymorphic ventricular tachycardia (CPVT), 234, 298, 334
Caveolae, 331, 350
  caveolar endocytosis, 477
  caveolin-3, 331, 348
Cervical sympathetic denervation, 189
Channel, 4, 28, 34, 43, 64, 90, 111, 132, 158, 193, 228, 255, 276, 293, 310, 331, 348, 360, 378, 399, 416, 429, 444, 459, 479, 496, 518, 540, 556, 567
Channelrhodopsins (ChR), 176, 360, 362
Choline acetyltransferase, 164
Class Ia antiarrhythmics, 529
Class III antiarrhythmics, 199, 255, 256, 263, 529, 555
Commotio cordis, 137
Computational modelling, 135, 136, 140, 368–370, 528
Conductance, 4, 11, 13, 16, 28, 29, 35, 36, 44–46, 48, 50, 55, 58, 59, 102, 116, 117, 202, 204, 228, 257, 259, 268, 278, 281, 284–286, 310, 311, 313, 316–318, 321, 322, 338, 378, 381–385, 518, 553, 556, 557, 570
Conduction failure, 316
Conduction pathways, 39, 111–117, 120, 267, 523
Conduction velocity, 310
Congenital abnormality, 235, 293
Connexins, 17, 102, 103, 111, 116, 117, 127, 199, 311–313, 318–320, 323, 437, 461, 463, 481, 570
Contraction, 3, 5, 16, 17, 34, 72, 73, 97, 131–133, 137, 139, 141, 172, 310, 318, 329, 333, 336, 348, 351, 352, 354, 360, 367–369, 378, 380, 399–401, 415–418, 430, 433, 460, 462, 463, 466, 467, 479, 481, 528
Coxsackievirus-Adenovirus-receptor (CAR), 476
C3SD peptide, 339
Current source/sink ratio, 311
Cyclic nucleotide-regulated (CNG) channels, 14–15
Cycloheximide, 480
Cytokines, 482
  interferon, 482

D
Dallas criteria, 485
Danegaptide, 322
Decay accelerating factor (DAF), 476
Decitabine, 502
Deep-learning, 378, 393
Defibrillation, 137
Delayed afterdepolarization (DAD), 16, 190, 282, 294, 298, 300, 303–305, 379, 401, 404, 552, 553, 558
Desmosome, 463–465, 468
Detubulation, 332
Diabetes, 506, 551
Diacylglycerol (DAG), 277
Diastolic Ca^{2+} leak, 299
Diastolic depolarization (DD), 4, 7, 14, 44–46, 48, 51–56, 58, 64, 65, 74–77, 89–94, 97, 99, 101, 112, 113, 116, 278, 305
Dilated cardiomyopathy (DCM), 238, 277, 483
Drugs, 5, 43, 74, 94, 121, 189, 228, 256, 278, 303, 313, 362, 379, 412, 417, 451, 476, 497, 518, 552, 568
  isoproterenol, 508
  mibefradil, 9, 228, 404
  norepinephrine, 302
  verapamil, 228

Dyads, 330
Dysferlin, 348
Dystrophin, 478

E
Early afterdepolarizations (EAD), 16, 190, 233, 235, 238, 243, 278, 282, 284, 294, 298, 300, 303–305, 378, 379, 381, 387–392, 396, 469, 552, 553, 555, 557, 568
Early-repolarization syndrome (ERS), 228
Electrical and structural remodeling, 205, 503, 553–554
Electron transport chain (ETC), 466
Electrophysiological remodeling, 242
Emergence, 90, 102
Endothelin-1, 302
Enterovirus, 476, 477, 483
Ephaptic coupling, 314, 317
Epidrugs, 497
Epigenetic, 39, 71–72, 464, 465, 469, 494, 497–503, 505, 506, 508, 509, 553
Excitation-contraction coupling (ECC), 132, 133, 143, 228, 279, 280, 348, 399–401, 410, 417, 459, 460, 462, 463, 465–468, 481
Excitation-metabolism coupling, 435
Excitation-transcription coupling, 438

F
Fibroblasts, 79, 80, 110, 119, 136, 138, 279, 318, 360, 369, 379, 383, 390, 396, 484, 502–504, 508, 568, 570
Frank-Starling mechanism, 335
Funny current (I_f), 14, 30–33, 37, 40, 46, 63–80, 91–93, 97, 101, 116, 193, 234, 239, 278, 303
  TRPC channel blocker SKF-96365, 281

G
Gain of function mutations, 8, 237, 258, 269, 479, 528
Gap junction single channel conductance, 311
Gap junction uncoupling, 317
Gap junctions, 310
Genetics, 76–79, 121, 124, 176, 178, 180, 210, 229, 232, 235–237, 240, 243, 276, 383, 400, 422, 452, 468, 475, 484, 494, 498, 499, 501, 505, 506, 518–519, 521–525, 528, 531, 553, 557, 568
Glycocalyx, 330
Glycogen synthase kinase 3 (GSK3), 462

H
Heart, 3, 28, 63, 92, 112, 131, 152, 188, 228, 256, 277, 293, 310, 338, 347, 360, 377, 399, 415, 430, 443, 459, 475, 494, 518, 540, 551, 568
Heart failure (HF), 9–11, 14–18, 72, 75, 118, 119, 121, 125, 126, 132, 133, 137, 190, 195, 196, 199, 202, 204–211, 228–230, 240–243, 277, 280, 293, 294, 296, 299–302, 305, 316, 319–321, 323, 333, 338–340, 352, 355, 377, 378, 419, 421–423, 430–432, 434, 436, 437, 447–452, 467, 469, 470, 477, 479, 485, 496, 500–503, 506, 507, 518, 551, 555, 557, 558
Heart rate variability (HRV), 494
Hemichannels, 311
Histone acetyltransferases (HATs), 465
Histone deacetylases (HDACs), 465
Human ether-a-go-go-related gene (hERG), 11, 69, 229, 234, 236, 256, 257, 262, 266, 519–521, 526, 528–531, 553, 555, 559, 568–570
Hyperpolarization-activated cyclic nucleotide-gated (HCN) channels, 66
Hypertrophic obstructive cardiomyopathy (HOCM), 320

I
Ignition, 92, 93, 100, 101, 103
Immune system disease, 235, 238
Impulse conduction, 17, 294, 300, 378, 468
Induced pluripotent stem cell-derived cardiomyocytes, 433
Infarcted heart, 278, 401, 404–406, 408–410, 412
Inflammasome, 481
  NOD-like receptor family pyrin domain-containing NLRP3, 481
Inflammatory cytokines, 238
Inositol trisphosphate receptor (IP3R), 17, 430, 438
Inotropic agents, 329–341
Intercalated disks, 311
Intracardiac nervous system, 152
Intracellular Ca^{2+} handling, 133, 142, 298, 299, 412, 429
Inward Ca^{2+} current (I_{Ca}), 8, 9, 55, 58, 123, 333, 335–339, 380, 479, 526
Inwardly rectifying K channels (2TM), 12–14
Inward rectifier K^+ current I_{K1}, 479
Ion channels, 4, 35, 43, 71, 90, 116, 132, 158, 210, 230, 276, 360, 378, 401, 437, 449, 459, 479, 508, 518, 540, 553, 567
Ionic currents, 4, 6, 7, 19, 28–30, 35, 37, 43–45, 60, 64, 93, 256, 260, 281, 282, 380–382, 406, 412, 496, 524, 528
Ionic inhomogeneities, 384, 385, 396
IRES-dependent translation, 477
  DAP5, 477
Ischemia, 14, 17, 18, 121, 169, 172, 188–191, 196, 202, 205, 277–279, 282, 294, 297–299, 301, 303, 304, 311, 313, 316–319, 322, 323, 379, 419, 420, 448–450, 555, 570
  ischemia-reperfusion injury, 298
Ischemic cardiomyopathy (ICM), 238

J
JAK-STAT system, 483
J-wave syndromes, 236

K
KCNH2, 11, 234, 256–258, 266, 269, 519–523, 526, 531, 542
Kinases, 240, 281, 297, 337, 407, 420, 431, 451, 462–464, 469
Kv1.1, 10
Kv11.1, 234, 255–267, 367, 519
  Kv11.1 activators, 266, 268

Kv11.1 blocker, 264–266
  bepridil, 264
  dofetilide, 264
  E-4031, 264
  MK-499, 264

L

Late Na^+ current, 367, 445
Lateralization, 316, 318–320
Lead potential, 35, 45, 46
Leak K channels (K_{2P}/4 TM), 12
Lipid rafts, 313
Lipophilic membrane dye (di-8-ANEPPS), 349
Long QT syndrome (LQTS), 4, 8, 188, 189, 192, 202, 203, 229, 234–237, 240, 255–258, 263, 266, 269, 331, 367, 408, 518, 519, 522, 541, 542, 568, 569, 571, 572, 576
L-type Ca^{2+} channel (LTCC), 34, 44, 228, 277, 294, 329, 399–401, 404, 412, 416, 419, 423, 429, 436
  distal C-terminus, 233
  inactivation, 228
  proximal C-terminus, 233
Lysine (K) acetyltransferases (KATs), 465
Lysine deacetylases (KDACs), 465

M

Major histocompatibility complex-1 (MHC-1), 482
Mathematical model, 34, 44, 48, 53, 55, 58, 60, 135, 377–396, 407
Mechanical stretch, 277
Mechano-electric coupling, 132
Mechano-electric feedback, 16, 132, 133, 279
Mechanosensing, 350
Membrane curvature, 348
Metabolic syndrome (MetS), 496
Methyl-β-cyclodextrin (MBCD), 332
MicroRNAs (miRs), 240
Mitochondria, 6, 18, 97, 295, 301, 348, 430, 433–435, 444, 462, 465, 466, 476–478, 480, 571
  dynamin-related protein (drp1), 478
  mitochondrial fission, 478
  mitochondrial fusion, 478
  mvidi-1 (dynamin inhibitor), 478
Mitochondrial and nuclear channels, 18
Mitogen-activated protein kinases, 420
Molecular landscape, 118–119
Myocardial biopsies, 485
Myocytes, 4, 6–8, 12–18, 45, 50, 53, 54, 64, 65, 67, 69, 71–75, 77, 79, 80, 93, 95, 134, 136, 143, 153, 167, 170, 178, 205, 233, 238–243, 255–258, 277, 279, 280, 286, 296, 297, 300, 318, 322, 329–341, 348, 350, 351, 360, 366–368, 370, 379, 383, 396, 400, 401, 405–407, 409–412, 418, 423, 432, 433, 436, 437, 443, 445–447, 451, 463, 466, 481, 502, 503, 508, 523, 545, 546, 554, 555, 558, 570–572

N

$Na_v1.5$, 4, 7, 234, 331, 333, 367, 445–447, 450, 452, 461, 464, 465, 467–470, 479, 502, 508, 525, 540, 545, 556
Na/Ca exchanger (NCX), 31, 33, 90, 92–94, 97, 99–101, 103, 234, 276, 277, 282, 286, 294–296, 301, 303, 330, 331, 334, 335, 399, 400, 408, 409, 411, 412, 416, 417, 419–423, 430, 431, 433, 434, 436, 437, 540, 542, 544
  KB-R7943, 303
  NCX1, forward mode, 294
  NCX1 inhibitors, 303
  NCX1, reverse mode, 294
  ORM-11372, 303
  SEA-0400, 303
  YM-244769, 303
NADPH oxidase, 496
Na^+-H^+ exchanger (NHE), 294, 296, 303, 334, 416, 417, 419, 420, 423, 436
  cariporide, 304
  NHE1 inhibitors, 303
  HOE 694, 304
Na^+-K^+ ATPase (NKA), 93, 294, 416–419, 421, 423, 433, 437, 463, 544
Near-infrared optical mapping (NIOM), 112–114, 118, 123, 125
Neuroanatomy, 157, 165, 170, 176, 180
Neuro-cardiac axis, 191, 196, 211
Neurocardiogenic syncope, 191–192
Neurocardiology, 152
Neuronal heart rate control, 156
Neuropeptide Y, 164
Nicotine, 506, 507
Nitric oxide, 164
Nonselective cationic channels, 276
N-terminal-acetyltransferases (NATs), 465
Nucleus, 6, 18, 152, 153, 171, 232, 338, 404, 422, 430, 435, 437, 444, 446, 477, 483, 484, 500

O

Optical defibrillation, 366–367
Optical pacing, 366, 368
Optogenetics, 176, 210–211, 359–370
Osmotic shock, 332

P

Pacemaker action potentials, 116
Pacemaker activity, 4, 9, 15, 17, 18, 31, 33, 34, 43, 47, 55, 60, 72–74, 76, 80, 119, 240, 299, 468, 552
Pacemaking, 9, 34, 37, 63–66, 73, 76, 79, 80, 89–104, 118, 119, 121, 125, 126, 135, 276, 303, 443, 446–448, 522
Parasympathetic and sympathetic efferent neurons, 153
Parasympathetic neurons, 192
Particulate matter (PM), 5, 494–497, 501, 503–506, 508, 509
Passive cable properties, 313
Periostin, 121
Phospholamban (PLB), 329, 404
Phosphorylation, 8, 9, 64, 67, 94–101, 103, 229, 233, 235, 239, 241–243, 295, 297, 299, 311, 313, 316, 317, 322, 337, 404, 417–423, 431, 432, 434, 436, 437, 445–448, 451, 459, 460, 462–465, 469–471, 483, 496, 499, 541, 554, 567

Physiome project, 38, 39
Pitx2c, 502
Plasmalemmal Ca^{2+} ATPase (PMCA), 330, 335
Plasma membrane Ca^{2+}-ATPase (PMCA), 295
Postganglionic neurons, 153–155, 164, 166–170, 201
Post-translational modification (PTM), 444, 445, 451, 459–471
Postural orthostatic tachycardia syndrome, 193
Potassium channel, 9, 28, 118, 139, 202, 204, 268, 314, 318, 350, 462, 467, 468, 502, 552, 567–576
Potassium channel blocker, 557
Precordial thump (PT), 141, 142
Preganglionic neurons, 153
Premature ventricular contractions (PVCs), 196, 378, 379, 390–393, 396
Proteases, 422, 477–479, 482
Proteasome, 482
Protein arginine methyltransferases (PRMTs), 464
Protein kinase A (PKA), 8, 15, 16, 94–95, 97, 98, 103, 233, 238, 243, 278, 310, 311, 313, 314, 337–340, 407, 417–419, 421, 431, 432, 461–463, 469
Protein kinase A inhibitor H-89, 337
Protein kinase C, 322
Purinergic receptors, 276, 281, 284
Purkinje cells, 28, 366, 400–404, 412

Q
QT intervals, 4, 195, 236, 239, 255–258, 263, 266, 518, 519, 521–529, 531, 542, 543, 568, 570, 572

R
Rapid delayed rectifier K^+ current (I_{Kr}), 11, 29, 34, 35, 44, 46, 51, 53, 59, 60, 93, 255–259, 263, 266, 462, 479, 519, 520, 522, 527–531, 552, 554, 556, 569–571
Rate, 3, 33, 55, 65, 90, 119, 132, 156, 188, 240, 255, 294, 336, 351, 360, 378, 400, 416, 432, 447, 468, 476, 495, 518, 552, 569
Reactive oxygen species (ROS), 299, 495, 496
  free oxygen radicals, 302
Recovery from block, 264
Regulation, 4, 14, 17, 67–72, 79, 94, 98–99, 112, 119, 123, 126, 127, 142, 199, 204, 206, 231, 235, 236, 241, 243, 257, 278, 279, 295–297, 305, 310–313, 330, 332, 334–340, 350, 408, 416, 419–421, 423, 430, 433, 435–437, 444–448, 451, 452, 462, 465–469, 478, 481, 497, 499, 501, 503, 505, 542, 544, 554, 557
Release channel, 17, 90, 93, 399, 400, 404, 446
Renal denervation, 200–201
Repolarization reserve, 233, 300
Respiratory sinus arrhythmia, 132
RGK protein Rad, 242
Romano-Ward syndrome, 257
Rotigaptide, 317, 322
Ryanodine receptor channels (RyR), 17
Ryanodine receptors, 6, 53, 90, 116, 233, 234, 277, 329, 417, 429, 430, 435, 438, 444, 462, 469, 502, 504, 541
  orphaned RyRs, 242

S
Safety factor of propagation, 316
SAN compartmentation, 110, 116, 118, 119, 123, 126, 127
SAN extracellular matrix, 119–121
Sarcolemma (SL), 4, 6, 12–14, 16–18, 98, 279, 284, 329–336, 338–340, 404, 405, 416, 417, 419–423, 429–431, 433, 435, 437, 438
Sarcolemmal Ca^{2+}-pump ATPase, 416, 423
Sarcolipin, 432
Sarcoplasmic/endoplasmic reticulum Ca^{2+}-ATPase (SERCA), 90, 92, 96, 97, 99, 100, 277, 295, 329, 330, 335, 337, 338, 404, 417, 422, 430, 432, 433, 463
Sarcoplasmic reticulum (SR), 4, 6, 17, 18, 53–55, 90, 92, 94–97, 99, 100, 112, 114, 121, 123, 126, 127, 233, 239, 277, 282, 284, 294, 295, 297–301, 313, 319, 329, 331, 333–336, 338, 339, 347–349, 352, 354, 399–401, 404, 407, 410–412, 416–418, 423, 429–437, 446–448, 450, 462, 463, 469, 540, 543, 544, 552
Scaffolding protein, 331
Scroll wave, 378
Sex hormones, 71
Short QT syndrome (SQTS), 229, 234, 236, 237, 258, 267–269, 417, 518–531
Sinoatrial node, 34, 38, 63, 68, 73, 89, 103, 104, 110–127, 132, 163, 165, 166, 177, 229, 237, 278, 446, 462, 504, 542, 544
Sinoatrial node dysfunction and deafness syndrome (SANDDS), 237
Sinus node dysfunction (SND), 77, 112, 116, 118, 119, 121–127, 542
Sinus node pacemaker, 74, 303
Sirtuins, 465
Slowly activating outward rectifier current I_{Ks}, 479
Small ubiquitin-like modifier (SUMO), 467
Smoking, 506–507
Sodium-calcium-exchanger, 502
Sodium channels, 4, 117, 118, 125, 310, 314, 362, 400, 464, 467, 469, 470, 540, 545, 555
Sodium homeostasis, 296, 447
Source-sink problem, 316
Spectrin, 545
Spinal cord stimulation, 201–202
Spiral wave, 378
SR inositol trisphosphate receptor channels, 18
Store-operated Ca^{2+} channel (SOCC), 416–418
Store-operated Ca^{2+} entry (SOCE), 280, 336, 480
Stretch-activated channels (SAC), 16, 172, 279, 558
Sudden cardiac death, 233
Sudden death, 203, 377, 417, 447, 518, 519, 521, 526, 542, 543, 546, 569
Suramin, 282
Sympathetic nervous system, 496
Sympathetic neurons, 201
Synchronization, 91, 99, 101, 102, 379, 479

T
Tachycardia, 137
Therapy, 98, 104, 124–127, 141, 142, 152, 153, 181, 191, 197, 199, 202–206, 208–210, 352, 366, 370, 431, 433, 434, 452, 478, 484, 507, 508, 551, 554, 555, 569
Thyroid hormone (TH), 71, 314
Timothy syndrome, 235
Toll-like receptors (TLR), 483
Torsades de Pointes tachycardia, 233
Tragus stimulation, 199–200
Transient inward current (I_{ti}), 16, 54, 294, 295, 298, 302, 400, 552, 558
Transient receptor potential channels (TRP), 15
Transmural dispersion of repolarisation (TDR), 526
Transporter, 6, 7, 18, 43–45, 48, 50, 59, 90, 93, 98, 164, 208, 276, 286, 295, 296, 302, 305, 330, 332–336, 409, 412, 423, 429, 437, 518, 519, 525, 526, 540, 541, 546
Trapping, 264
T-tubules, 6–8, 11, 16, 17, 53, 232, 242, 243, 330–341, 347–355, 399, 409, 416, 429, 444, 446, 462, 540, 545
  atrial cells, 351
  contraction-induced deformation, 352
  deformation dynamics, 354
  electron tomography, 353
  electrotonic conduction, 350
  lipid fingerprint, 351
  luminal content, 351
T-type Ca^{2+} channels, 228
  mibefradil, 228
Tyrosine hydroxylase, 164

U
Ubiquitin-proteasome system (UPS), 467

V
Vagus nerve stimulation, 191
Vasoactive intestinal polypeptide, 164
Ventricular arrhythmia, 9, 11, 12, 16, 65, 188–192, 195–197, 199, 201–205, 207, 208, 211, 237–239, 242, 243, 255, 263, 281, 299–304, 317, 320, 362, 365, 369, 378, 401, 432, 433, 448, 452, 495, 507, 508, 518, 519, 521, 526, 529, 541–544, 546
Ventricular cell, 34–35, 45, 100, 137, 399, 412, 522
Ventricular fibrillation (VF), 15, 138–142, 188–192, 194–196, 203, 205–207, 209, 210, 236, 237, 255–258, 266, 284, 285, 317, 321, 323, 378, 379, 393, 396, 518, 519, 522–524, 529
Viral myocarditis, 475–486
Viroporin, 480–481
Voltage-dependent calcium channels, 235
  high-voltage activated channels, 228
  low-voltage activated channels, 228
Voltage-gated channels, 4–11, 118, 228, 231, 280, 314, 331, 416, 419, 445–447, 462, 467, 470, 540, 544
Voltage clamp experiments, 30

W
Window currents, 233